

# *Handbook of Machining with Grinding Wheels*



Ioan D. Marinescu  
Mike Hitchiner  
Eckart Uhlmann  
W. Brian Rowe  
Ichiro Inasaki

# **Handbook of Machining with Grinding Wheels**

# MANUFACTURING ENGINEERING AND MATERIALS PROCESSING

A Series of Reference Books and Textbooks

SERIES EDITOR

**Geoffrey Boothroyd**

*Boothroyd Dewhurst, Inc.*

*Wakefield, Rhode Island*

1. Computers in Manufacturing, *U. Rembold, M. Seth, and J. S. Weinstein*
2. Cold Rolling of Steel, *William L. Roberts*
3. Strengthening of Ceramics: Treatments, Tests, and Design Applications, *Harry P. Kirchner*
4. Metal Forming: The Application of Limit Analysis, *Betzalel Avitzur*
5. Improving Productivity by Classification, Coding, and Data Base Standardization: The Key to Maximizing CAD/CAM and Group Technology, *William F. Hyde*
6. Automatic Assembly, *Geoffrey Boothroyd, Corrado Poli, and Laurence E. Murch*
7. Manufacturing Engineering Processes, *Leo Alting*
8. Modern Ceramic Engineering: Properties, Processing, and Use in Design, *David W. Richerson*
9. Interface Technology for Computer-Controlled Manufacturing Processes, *Ulrich Rembold, Karl Armbruster, and Wolfgang Ülzmann*
10. Hot Rolling of Steel, *William L. Roberts*
11. Adhesives in Manufacturing, *edited by Gerald L. Schneberger*
12. Understanding the Manufacturing Process: Key to Successful CAD/CAM Implementation, *Joseph Harrington, Jr.*
13. Industrial Materials Science and Engineering, *edited by Lawrence E. Murr*
14. Lubricants and Lubrication in Metalworking Operations, *Elliot S. Nachtman and Serope Kalpakjian*
15. Manufacturing Engineering: An Introduction to the Basic Functions, *John P. Tanner*
16. Computer-Integrated Manufacturing Technology and Systems, *Ulrich Rembold, Christian Blume, and Ruediger Dillman*
17. Connections in Electronic Assemblies, *Anthony J. Bilotta*
18. Automation for Press Feed Operations: Applications and Economics, *Edward Walker*
19. Nontraditional Manufacturing Processes, *Gary F. Benedict*
20. Programmable Controllers for Factory Automation, *David G. Johnson*
21. Printed Circuit Assembly Manufacturing, *Fred W. Kear*
22. Manufacturing High Technology Handbook, *edited by Donatas Tijunelis and Keith E. McKee*

23. Factory Information Systems: Design and Implementation for CIM Management and Control, *John Gaylor*
24. Flat Processing of Steel, *William L. Roberts*
25. Soldering for Electronic Assemblies, *Leo P. Lambert*
26. Flexible Manufacturing Systems in Practice: Applications, Design, and Simulation, *Joseph Talavage and Roger G. Hannam*
27. Flexible Manufacturing Systems: Benefits for the Low Inventory Factory, *John E. Lenz*
28. Fundamentals of Machining and Machine Tools: Second Edition, *Geoffrey Boothroyd and Winston A. Knight*
29. Computer-Automated Process Planning for World-Class Manufacturing, *James Nolen*
30. Steel-Rolling Technology: Theory and Practice, *Vladimir B. Ginzburg*
31. Computer Integrated Electronics Manufacturing and Testing, *Jack Arabian*
32. In-Process Measurement and Control, *Stephan D. Murphy*
33. Assembly Line Design: Methodology and Applications, *We-Min Chow*
34. Robot Technology and Applications, *edited by Ulrich Rembold*
35. Mechanical Deburring and Surface Finishing Technology, *Alfred F. Scheider*
36. Manufacturing Engineering: An Introduction to the Basic Functions, Second Edition, Revised and Expanded, *John P. Tanner*
37. Assembly Automation and Product Design, *Geoffrey Boothroyd*
38. Hybrid Assemblies and Multichip Modules, *Fred W. Kear*
39. High-Quality Steel Rolling: Theory and Practice, *Vladimir B. Ginzburg*
40. Manufacturing Engineering Processes: Second Edition, Revised and Expanded, *Leo Alting*
41. Metalworking Fluids, *edited by Jerry P. Byers*
42. Coordinate Measuring Machines and Systems, *edited by John A. Bosch*
43. Arc Welding Automation, *Howard B. Cary*
44. Facilities Planning and Materials Handling: Methods and Requirements, *Vijay S. Sheth*
45. Continuous Flow Manufacturing: Quality in Design and Processes, *Pierre C. Guerindon*
46. Laser Materials Processing, *edited by Leonard Migliore*
47. Re-Engineering the Manufacturing System: Applying the Theory of Constraints, *Robert E. Stein*
48. Handbook of Manufacturing Engineering, *edited by Jack M. Walker*
49. Metal Cutting Theory and Practice, *David A. Stephenson and John S. Agapiou*
50. Manufacturing Process Design and Optimization, *Robert F. Rhyder*
51. Statistical Process Control in Manufacturing Practice, *Fred W. Kear*
52. Measurement of Geometric Tolerances in Manufacturing, *James D. Meadows*
53. Machining of Ceramics and Composites, *edited by Said Jahanmir, M. Ramulu, and Philip Koshy*
54. Introduction to Manufacturing Processes and Materials, *Robert C. Creese*

55. Computer-Aided Fixture Design, *Yiming (Kevin) Rong and Yaoxiang (Stephens) Zhu*
56. Understanding and Applying Machine Vision: Second Edition, Revised and Expanded, *Nello Zuech*
57. Flat Rolling Fundamentals, *Vladimir B. Ginzburg and Robert Ballas*
58. Product Design for Manufacture and Assembly: Second Edition, Revised and Expanded, *Geoffrey Boothroyd, Peter Dewhurst, and Winston A. Knight*
59. Process Modeling in Composites Manufacturing, *edited by Suresh G. Advani and E. Murat Sozer*
60. Integrated Product Design and Manufacturing Using Geometric Dimensioning and Tolerancing, *Robert Campbell*
61. Handbook of Induction Heating, *edited by Valery I. Rudnev, Don Loveless, Raymond Cook and Micah Black*
62. Re-Engineering the Manufacturing System: Applying the Theory of Constraints, Second Edition, *Robert Stein*
63. Manufacturing: Design, Production, Automation, and Integration, *Beno Benhabib*
64. Rod and Bar Rolling: Theory and Applications, *Youngseog Lee*
65. Metallurgical Design of Flat Rolled Steels, *Vladimir B. Ginzburg*
66. Assembly Automation and Product Design: Second Edition, *Geoffrey Boothroyd*
67. Roll Forming Handbook, *edited by George T. Halmos*
68. Metal Cutting Theory and Practice: Second Edition, *David A. Stephenson and John S. Agapiou*
69. Fundamentals of Machining and Machine Tools: Third Edition, *Geoffrey Boothroyd and Winston A. Knight*
70. Manufacturing Optimization Through Intelligent Techniques, *R. Saravanan*
71. Metalworking Fluids: Second Edition, *Jerry P. Byers*
72. Handbook of Machining with Grinding Wheels, *Ioan D. Marinescu, Mike Hitchiner, Eckart Uhlmann, W. Brian Rowe, and Ichiro Inasaki*

# **Handbook of Machining with Grinding Wheels**

**Ioan D. Marinescu  
Mike Hitchiner  
Eckart Uhlmann  
W. Brian Rowe  
Ichiro Inasaki**



**CRC Press**

Taylor & Francis Group

Boca Raton London New York

---

CRC Press is an imprint of the  
Taylor & Francis Group, an informa business

CRC Press  
Taylor & Francis Group  
6000 Broken Sound Parkway NW, Suite 300  
Boca Raton, FL 33487-2742

© 2007 by Taylor & Francis Group, LLC  
CRC Press is an imprint of Taylor & Francis Group, an Informa business

No claim to original U.S. Government works  
Printed in the United States of America on acid-free paper  
10 9 8 7 6 5 4 3 2 1

International Standard Book Number-10: 1-57444-671-1 (Hardcover)  
International Standard Book Number-13: 978-1-57444-671-5 (Hardcover)

This book contains information obtained from authentic and highly regarded sources. Reprinted material is quoted with permission, and sources are indicated. A wide variety of references are listed. Reasonable efforts have been made to publish reliable data and information, but the author and the publisher cannot assume responsibility for the validity of all materials or for the consequences of their use.

No part of this book may be reprinted, reproduced, transmitted, or utilized in any form by any electronic, mechanical, or other means, now known or hereafter invented, including photocopying, microfilming, and recording, or in any information storage or retrieval system, without written permission from the publishers.

For permission to photocopy or use material electronically from this work, please access [www.copyright.com](http://www.copyright.com) (<http://www.copyright.com/>) or contact the Copyright Clearance Center, Inc. (CCC) 222 Rosewood Drive, Danvers, MA 01923, 978-750-8400. CCC is a not-for-profit organization that provides licenses and registration for a variety of users. For organizations that have been granted a photocopy license by the CCC, a separate system of payment has been arranged.

**Trademark Notice:** Product or corporate names may be trademarks or registered trademarks, and are used only for identification and explanation without intent to infringe.

**Visit the Taylor & Francis Web site at**  
**<http://www.taylorandfrancis.com>**

**and the CRC Press Web site at**  
**<http://www.crcpress.com>**

---

# Preface

Grinding, once considered primarily a finishing operation involving low rates of removal, has evolved as a major competitor to cutting, as the term “abrasive machining” suggests. This is what Milton Shaw, the man who is considered the great pioneer and father of American grinding, said about 10 years ago. Shaw led the development of grinding in the United States over the last 50 years.

We named this book *Handbook of Machining with Grinding Wheels* because the borders between grinding and other operations such as superfinishing, lapping, polishing, and flat honing are no longer distinct. Machining with grinding wheels extends from high-removal rate processes into the domains of ultra-high accuracy and superfinishing. This book aims to explore some of the new “transition operations,” and for this reason we chose this title.

This book presents a wide range of abrasive machining technology in fundamental and application terms. The emphasis is on why things happen as they do, rather than a how-to-do-it approach. The topics covered in this book cover a range of abrasive machining processes with grinding wheels, making this probably the most complete book regarding all kinds of grinding operations.

The aim of this book is to present a unified approach to machining with grinding wheels that will be useful in solving new grinding problems of the future. It should be of value to engineers and technicians involved in solving problems in industry and to those doing research on machining with grinding wheels in universities and research organizations.

The team of authors are famous researchers who have devoted their entire lives doing research in this field and who are still actively contributing to new research and development. The authors represent a large region of the world where abrasive machining with grinding wheels are most advanced: United States, Great Britain, Japan, and Germany. I thank my co-authors for taking time from their busy activities to write and review this book over a period of 2 years.

All the co-authors are my long-time friends, and with some of them, I have previously published or we are still in the process of finishing other books. Here is a short presentation of them.

Professor Brian Rowe is considered the world father of Centerless Grinding in addition to other notable research concerning grinding aspects: thermal and dynamic aspects, fluid-film bearings, etc. He established a great laboratory and school in manufacturing processes at Liverpool John Moores University. As an emeritus professor, Brian is busier than before retirement. As he is a native English speaker, he spent a lot of time polishing our English in order to have a unitary book. I thank him for similar great work on our previous book, *Tribology of Abrasive Machining Processes*.

Professor Ichiro Inasaki is the leading figure in Grinding in Japan. As dean of the Graduate School of Science and Technology at Keio University, he developed a great laboratory with outstanding research activities. His “intelligent grinding wheel” is featured in the Noritake Museum and represents one of his best accomplishments and contributions. He led the International Institution for Production Engineering Research in 2004/2005 as the president and was granted several awards including an SME award. Ichiro-san and I have written two books: *Handbook of Ceramic Grinding and Polishing*, and *Tribology of Abrasive Machining Processes*.

Professor Eckart Uhlmann is professor and director of the Institute for Machine-Tools and Management at Technical University of Berlin. Dr. Uhlmann received this chaired professorship after a very successful industrial career with Hermes Abrasive in Germany. His main research is on one of these transition processes: grinding with lapping kinematics. As the head of his institute, one of the largest in Germany, he holds the leading position in research on all aspects of abrasive machining with grinding wheels. A future book with Dr. Uhlmann will be also published this year, *Handbook of Lapping and Polishing/CMP*.



Dr. Mike Hitchiner is manager of Precision Technology at Saint-Gobain Abrasives, the largest grinding wheel company in the world. Mike has devoted all his life to research, development, and practical application of grinding processes. He started this activity during his Ph.D. studies at the University of Oxford in England, and today he is considered “Mr. CBN Grinding” by the precision-grinding industry. He has brought an important industrial perspective to this book, as well as hundreds of applications.

As the leading author, my own experience in abrasive-machining research complements and widely extends the experience of the other authors across industrial and fundamental areas of investigation. My researches have particularly focused on new and challenging techniques of abrasive machining particularly for new materials. I have been fortunate to have studied the latest technologies developed in countries across the world firsthand and contributed to developing new techniques for application in industry and in research.

The main purpose of this book is to present abrasive-machining processes as a science more than an art. Research and development on abrasive-machining processes have greatly increased the level of science compared to 25 years ago when many aspects of abrasive machining processes still depended largely on the expertise of individual technicians, engineers, and scientists.

The book has two parts: “The Basic Process of Grinding” and “Application of Grinding Processes.” This structure allows us to present more about *understanding of grinding behavior* in the first part and more about *industrial application* in the second part.

**Ioan D. Marinescu**

*Toledo, 2006*

---

# The Authors

**Ioan D. Marinescu** is a professor of mechanical, industrial, and manufacturing engineering at the University of Toledo. He is also the director of the Precision Micro-Machining Center of the College of Engineering ([www.eng.utoledo.edu/pmmc](http://www.eng.utoledo.edu/pmmc)) of the same university. He has a Ph.D. in manufacturing processes, an honorary doctorate from University of Iashi, Romania, and is a member of numerous international professional organizations: JSPE, SME, ASME, ASPE, CIRP, IDA, ASAT, and NAMRI.

Professor Marinescu is author of more than 15 books and over 300 technical and scientific papers. He has given lectures and workshops in more than 40 countries around the world. Also, he is the executive director and cofounder of the American Society for Abrasive Technology.

Ten years ago, Dr. Marinescu founded his own company, Advanced Manufacturing Solutions Co., LLC, a company that specializes in consulting, R&D, manufacturing, and trade ([www.interams.com](http://www.interams.com)). He is the president and CEO of this company.

**Mike Hitchiner** obtained his doctorate in 1982 at the University of Oxford for research in grinding and machining with cubic boron nitride (CBN) and diamonds. After another 3 years of university research in diamonds and CBN, he joined Saint-Gobain Abrasives (SGA) and its affiliate companies in 1985. He worked initially on conventional abrasive grain manufacture and advanced ceramics before becoming R&D manager for vitrified CBN in Europe in 1987. In 1989, he joined Universal Superabrasives (SGA) as technology manager for vitrified CBN for the U.S. market. More recently, he has broadened his responsibilities as the technology manager for precision grinding applications for North America, as well as projects throughout Asia and Europe.

**Eckart Uhlmann** is the director of the Fraunhofer-Institute for Production Systems and Design Technology IPK and professor of machine tools and manufacturing technology at the Institute for Machine Tools and Factory Management of the Technical University in Berlin, Germany. He received his doctorate in engineering on “Creep Feed Grinding of High-Strength Ceramic Materials.” Prior to his academic career, he served several years as vice-president and director of research and development at Hermes Schleifmittel GmbH & Co., Hamburg, Germany. In addition to being a consultant for various German and international companies, Dr. Uhlmann holds many professional memberships, including the Berlin Wissenschaftskommission, the Verein Deutscher Ingenieure, and the International Institution for Production Engineering Research. He also holds an honorary doctorate from Kolej Universiti Teknikal Kebangsaan, Malaysia.

**W. Brian Rowe** gained 6 years of experience with Austin Motor Company, Birmingham, England, and another 6 years with Wickman Machine Tools, Coventry, England. He studied at the University of Aston in Birmingham earning an honors degree in mechanical and production engineering in 1961. He earned a Ph.D. for research on the mechanics of centerless grinding at Manchester University in 1964 and became a doctor of science in 1976 for his wider research on tribology. He became the head of mechanical engineering in 1973 at Liverpool Polytechnic (later to become Liverpool John Moores University) and eventually became assistant rector responsible for corporate academic development, strategic planning, and for development of research. In 1992, he relinquished his administrative responsibilities in order to focus on research. As director of the Advanced Manufacturing Technology Research Laboratory (AMTREL), he built up a significant team of researchers that worked closely with industry in the United Kingdom. AMTREL has made

contributions across a wide spectrum of machine tool technologies particularly in relation to grinding and grinding-machine design. He has supervised more than 40 Ph.D.s who have gone on to influence manufacturing developments around the world. He thanks them for their contributions in making his career highly rewarding. He has jointly published with them more than 250 scientific papers, patents, and books including *Design of Hydrostatic and Hybrid Bearings* in 1982 and *Tribology of Abrasive Machining Processes* in 2004.

**Ichiro Inasaki**, Dean of the Faculty of Science and Technology, Keio University, has been dedicated to research work in manufacturing engineering and machine tool technologies. He completed his doctorates at Keio University in 1969 and honorary Dr.-Ing. at Hanover University, Germany, in 1999. He serves as fellow of the Japan Society of Mechanical Engineers, the Japan Society of Precision Engineering, and the Society of Manufacturing Engineers, and served as president for CIRP between 2004 and 2005. As a positive part of his career, he has undertaken a role as editor of international journals including the *International Journal for Manufacturing Science and Production*, *Machining Science and Technology*, *International Journal of Production Engineering and Computers*, *Journal of Engineering Manufacture (IMechE)*, and *Journal of Nanotechnology and Precision Engineering* for years to date.

His achievements and contributions to the world manufacturing engineering industries deserve appreciation and recognition, and awards were conferred on him by the Japan Society of Mechanical Engineers in 1969, 1987, 1997, and 1999, the Japan Society for Precision Engineering in 1992 and 2005, the Japan Society for Abrasive Technology in 1980 and 1998, the Japanese Society of Tribologists in 2003, and the Society of Manufacturing Engineers (F. W. Taylor Research Medal) in 2005. His dedicated efforts have been condensed in books, publications in journals, and more than 300 papers in the field of manufacturing engineering.

---

# Contents

## Part I

The Basic Process of Grinding.....	1
------------------------------------	---

<b>Chapter 1</b> Introduction.....	3
------------------------------------	---

1.1 From Craft to Science .....	3
1.2 Basic Uses of Grinding .....	4
1.2.1 High Accuracy Required .....	4
1.2.2 High Removal Rate Required .....	4
1.2.3 Machining of Hard Materials.....	4
1.3 Elements of the Grinding System.....	4
1.3.1 The Basic Grinding Process.....	4
1.3.2 Four Basic Grinding Operations .....	5
1.4 The Importance of the Abrasive.....	6
1.5 Grinding Wheels for a Purpose.....	7
1.6 Problem-Solving .....	7
1.6.1 Part I .....	7
1.6.2 Part II.....	8
References .....	8

<b>Chapter 2</b> Grinding Parameters.....	9
-------------------------------------------	---

2.1 Introduction.....	9
2.1.1 Wheel Life .....	9
2.1.2 Redress Life.....	10
2.1.3 Cycle Time .....	10
2.2 Process Parameters .....	11
2.2.1 Uncut Chip Thickness or Grain Penetration Depth.....	11
2.2.2 Wheel Speed.....	11
2.2.3 Work Speed .....	11
2.2.4 Depth of Cut.....	11
2.2.5 Equivalent Wheel Diameter .....	11
2.2.6 Active Grit Density .....	12
2.2.7 Grit Shape Factor .....	12
2.2.8 Force per Grit .....	12
2.2.9 Specific Grinding Energy .....	12
2.2.10 Specific Removal Rate .....	12
2.2.11 Grinding Power .....	13
2.2.12 Tangential Grinding Force.....	14
2.2.13 Normal Grinding Force .....	14
2.2.14 Coefficient of Grinding .....	14
2.2.15 Surface Roughness .....	15
2.2.16 $R_T$ Roughness.....	15
2.2.17 $R_A$ Roughness.....	15

2.2.18	$R_z$ Roughness.....	15
2.2.19	Material or Bearing Ratio.....	15
2.2.20	Peak Count.....	15
2.2.21	Comparison of Roughness Classes.....	15
2.2.22	Factors That Affect Roughness Measurements.....	15
2.2.23	Roughness Specifications on Drawings.....	16
2.2.24	Stock Removal Parameter.....	17
2.2.25	Decay Constant $\tau$ .....	17
2.2.26	G-Ratio.....	17
2.2.27	P-Ratio.....	18
2.2.28	Contact Length.....	18
2.2.29	Geometric Contact Length.....	18
2.2.30	Real Contact Length.....	18
2.3	Grinding Temperatures.....	18
2.3.1	Surface Temperature $T$ .....	18
2.3.2	Maximum Workpiece Surface Temperature.....	19
2.3.3	The $C_{\max}$ Factor.....	19
2.3.4	The Transient Thermal Property $\beta_w$ .....	19
2.3.5	Workpiece Partition Ratio $R_w$ .....	19
2.3.6	Effect of Grinding Variables on Temperature.....	19
2.3.7	Heat Convection by Coolant and Chips.....	20
2.3.8	Control of Thermal Damage.....	20
Appendix 2.1	Drawing Form and Profile Tolerancing.....	21
References	.....	21
<b>Chapter 3 Material Removal Mechanisms.....</b>		<b>23</b>
3.1	Significance.....	23
3.1.1	Introduction.....	23
3.1.2	Defining Basic Behavior.....	23
3.2	Grinding Wheel Topography.....	24
3.2.1	Introduction.....	24
3.2.2	Specification of Single Cutting Edges.....	24
3.3	Determination of Grinding Wheel Topography.....	25
3.3.1	Introduction.....	25
3.3.2	Static Methods.....	25
3.3.3	Dynamic Methods.....	26
3.3.4	Kinematic Simulation Methods.....	26
3.3.5	Measurement of Grinding Wheel Topography.....	27
3.3.6	Roughness Measures.....	27
3.3.7	Qualitative Assessment.....	28
3.3.8	Counting Methods.....	28
3.3.9	Piezo and Thermoelectric Measurements.....	28
3.3.10	Photoelectric Method.....	28
3.3.11	Mirror Workpiece Method.....	28
3.3.12	Workpiece Penetration Method.....	28
3.4	Kinematics of the Cutting Edge Engagement.....	29
3.5	Fundamental Removal Mechanisms.....	31
3.5.1	Microplowing, Chipping, and Breaking.....	31
3.6	Material Removal in Grinding of Ductile Materials.....	32
3.7	Surface Formation in Grinding of Brittle-Hard Materials.....	35

3.7.1	Indentation Tests.....	35
3.7.2	Scratch and Grinding Behavior of Brittle-Hard Materials.....	35
3.7.2.1	Fine-Grained Materials.....	36
3.7.2.2	Coarse-Grained Materials.....	36
3.8	Energy Transformation.....	41
	References.....	42
<b>Chapter 4</b>	<b>Grinding Wheels.....</b>	<b>45</b>
4.1	Introduction.....	45
4.1.1	Developments in Productivity.....	45
4.1.2	System Development.....	45
4.1.3	Conventional and Superabrasive Wheel Design.....	45
4.2	Wheel Shape Specification.....	46
4.2.1	Basic Shapes.....	46
4.2.2	Hole Tolerances.....	48
4.2.3	Side and Diameter Tolerances.....	49
4.3	Wheel Balance.....	49
4.3.1	Introduction to Wheel Balance.....	49
4.3.2	Static and Dynamic Unbalance.....	50
4.3.3	Automatic Wheel Balancers.....	52
4.3.4	Dynamic Balancing in Two Planes.....	52
4.3.5	Coolant Unbalance.....	53
4.4	Design of High-Speed Wheels.....	54
4.4.1	Trend toward Higher Speeds.....	54
4.4.2	How Wheels Fail.....	54
4.4.3	Hoop Stress and Radial Stress.....	54
4.4.4	Reinforced Wheels.....	55
4.4.5	Segmented Wheels.....	56
4.4.6	Segment Design.....	56
4.4.7	Abrasive Layer Depth.....	57
4.4.8	Recent Development of High-Speed Conventional Wheels.....	58
4.4.9	Safety of Segmented Wheel Designs.....	59
4.4.10	Speed Rating of Grinding Wheels.....	60
4.5	Bond Life.....	61
4.6	Wheel Mount Design.....	61
4.6.1	A Conventional Wheel Mount.....	62
4.6.2	Use of Blotters.....	62
4.6.3	Clamping Forces.....	62
4.6.3.1	Clamping Force to Compensate for the Weight of the Wheel.....	62
4.6.3.2	Clamping Force for Unbalance of the Wheel.....	63
4.6.3.3	Clamping Force for Motor Power Surge.....	63
4.6.3.4	Clamping Force for Reaction of Wheel to Workpiece.....	63
4.6.4	High-Speed Wheel Mounts.....	64
4.6.5	The Single-Piece Wheel Hub.....	64
4.6.6	Direct Mounting on the Spindle.....	64
4.6.7	CFRP Wheel Hubs.....	66
4.6.8	Electroplated Wheels.....	66
4.6.9	Aluminum Hubs.....	68
4.6.10	Junker Bayonet Style Mounts.....	68

4.6.11	HSK Hollow Taper Mount .....	68
4.6.12	Titanium Hub Design .....	70
4.7	Wheel Design and Chatter Suppression .....	71
4.7.1	The Role of Damping .....	71
4.7.2	Forced and Self-Excited Vibrations .....	71
4.7.2.1	Forced Vibrations .....	71
4.7.2.2	Self-Excited Vibration .....	71
4.7.3	Damped Wheel Designs and Wheel Compliance .....	72
4.7.4	Wheel Frequency and Chatter .....	73
4.7.5	Summary .....	73
	References .....	73

**Chapter 5 The Nature of the Abrasive .....** 75

5.1	Introduction .....	75
5.2	Silicon Carbide .....	75
5.2.1	Development of SiC .....	75
5.2.2	Manufacture of SiC .....	75
5.2.3	Hardness of SiC .....	75
5.3	Alumina (Alox)-Based Abrasives .....	76
5.4	Electrofused Alumina Abrasives .....	76
5.4.1	Manufacture .....	76
5.4.2	Brown Alumina .....	77
5.4.3	White Alumina .....	77
5.4.4	Alloying Additives .....	78
5.4.5	Pink Alumina .....	78
5.4.6	Ruby Alumina .....	79
5.4.7	Zirconia-Alumina .....	79
5.4.8	Single Crystal White Alumina .....	79
5.4.9	Postfusion Processing Methods .....	79
5.4.10	Postfusion Heat Treatment .....	79
5.4.11	Postfusion Coatings .....	79
5.5	Chemical Precipitation and/or Sintering of Alumina .....	79
5.5.1	Importance of Crystal Size .....	79
5.5.2	Microcrystalline Grits .....	80
5.5.3	Seeded Gel Abrasive .....	80
5.5.4	Application of SG Abrasives .....	80
5.5.5	Sol Gel Abrasives .....	80
5.5.6	Comparison of SG and Cubitron Abrasives .....	81
5.5.7	Extruded SG Abrasive .....	81
5.5.8	Future Trends for Conventional Abrasives .....	82
5.6	Diamond Abrasives .....	82
5.6.1	Natural and Synthetic Diamonds .....	82
5.6.2	Origin of Diamond .....	83
5.6.3	Production Costs .....	83
5.6.4	Three Forms of Carbon .....	84
5.6.5	The Shape and Structure of Diamond .....	85
5.6.6	Production of Synthetic Diamond .....	85
5.6.7	Controlling Stone Morphology .....	85
5.6.8	Diamond Quality Measures .....	86

5.6.9	Diamond Coatings.....	86
5.6.10	Polycrystalline Diamond (PCD).....	87
5.6.11	Diamond Produced by Chemical Vapor Deposition (CVD).....	88
5.6.12	Structure of CVD Diamond.....	88
5.6.13	Development of Large Synthetic Diamond Crystals.....	88
5.6.14	Demand for Natural Diamond.....	89
5.6.15	Forms of Natural Diamond.....	89
5.6.16	Hardness of Diamond.....	89
5.6.17	Wear Resistance of Diamond.....	90
5.6.18	Strength of Diamond.....	90
5.6.19	Chemical Properties of Diamond.....	90
5.6.20	Thermal Stability of Diamond.....	91
5.6.21	Chemical Affinity of Diamond.....	92
5.6.22	Effects of Chemical Affinity in Manufacture.....	92
5.6.23	Effects of Chemical Affinity in Grinding.....	92
5.6.24	Grinding Steels and Cast Irons with Diamond.....	92
5.6.25	Thermal Properties.....	92
5.7	CBN.....	93
5.7.1	Development of CBN.....	93
5.7.2	Shape and Structure of CBN.....	93
5.7.3	Types of CBN Grains.....	94
5.7.4	Microcrystalline CBN.....	95
5.7.5	Sources and Costs of CBN.....	95
5.7.6	Wurtzitic Boron Nitride.....	95
5.7.7	Hardness of CBN.....	96
5.7.8	Wear Resistance of CBN.....	96
5.7.9	Thermal and Chemical Stability of CBN.....	97
5.7.10	Effect of Coolant on CBN.....	97
5.7.11	Effect of Reactivity with Workpiece Constituents.....	98
5.7.12	Thermal Properties of CBN.....	98
5.8	Grain Size Distributions.....	98
5.8.1	The ANSI Standard.....	98
5.8.2	The FEPA Standard.....	99
5.8.3	Comparison of FEPA and ANSI Standards.....	99
5.8.4	US Grit Size Number.....	99
5.9	Future Grain Developments.....	99
5.10	Postscript.....	99
	References.....	100
<b>Chapter 6 Specification of the Bond.....</b>		<b>103</b>
6.1	Introduction.....	103
6.2	Single-Layer Wheels.....	103
6.3	Electroplated (EP) Single-Layer Wheels.....	103
6.3.1	Structure of an EP Layer.....	103
6.3.2	Product Accuracy.....	103
6.3.3	Wear Resistance of the Bond.....	103
6.3.4	Grit Size and Form Accuracy.....	104
6.3.5	Wheel Wear Effects in Grinding.....	104
6.3.6	Grit Size and Form-Holding Capability.....	105
6.3.7	Wheel Break-In Period.....	105



6.3.8	Summary of Variables Affecting Wheel Performance .....	107
6.3.9	Effect of Coolant on Plated Wheels .....	107
6.3.10	Reuse of Plated Wheels .....	107
6.4	Brazed Single-Layer Wheels.....	107
6.5	Vitrified Bond Wheels for Conventional Wheels .....	108
6.5.1	Application of Vitrified Bonds.....	108
6.5.2	Fabrication of Vitrified Bonds .....	108
6.5.3	Structure and Grade of Conventional Vitrified Wheels.....	109
6.5.4	Mixture Proportions .....	110
6.5.5	Structure Number.....	110
6.5.6	Grade of Conventional Vitrified Wheels .....	110
6.5.7	Fracture Wear Mode of Vitrified Wheels .....	111
6.5.8	High Porosity Vitrified Wheels.....	112
6.5.9	Multiple Pore Size Distributions .....	113
6.5.10	Ultrahigh Porosity Vitrified Wheels .....	113
6.5.11	Combining Grade and Structure .....	113
6.5.12	Lubricated Vitrified Wheels .....	113
6.6	Vitrified Bonds for Diamond Wheels .....	114
6.6.1	Introduction .....	114
6.6.2	Hard Work Materials.....	114
6.6.3	Low Chemical Bonding.....	114
6.6.4	High Grinding Forces .....	114
6.6.5	Diamond Reactivity with Air at High Temperatures .....	114
6.6.6	Porous Vitrified Diamond Bonds.....	115
6.7	Vitrified Bonds for CBN .....	115
6.7.1	Introduction .....	115
6.7.2	Requirements for Vitrified CBN Bonds .....	116
6.7.3	CBN Wheel Structures.....	116
6.7.4	Grades of CBN Wheels .....	116
6.7.5	Firing Temperature.....	116
6.7.6	Thermal Stress.....	118
6.7.7	Bond Mix for Quality .....	118
6.8	Resin Bond Wheels .....	118
6.9	Plastic Bonds .....	119
6.10	Phenolic Resin Bonds .....	119
6.10.1	Introduction .....	119
6.10.2	Controlled Force Systems.....	119
6.10.3	Abrasive Size .....	120
6.10.4	Benefits of Resilience .....	120
6.10.5	Phenolic Resin Bonds for Superabrasive Wheels .....	121
6.10.6	Wheel Marking Systems for Resin Bonds.....	121
6.11	Polyimide Resin Bonds .....	121
6.11.1	Introduction .....	121
6.11.2	Cost Developments and Implications .....	121
6.11.3	Induced Porosity Polyimide.....	121
6.12	Metal Bonds .....	122
6.12.1	Introduction .....	122
6.12.2	Bronze Alloy Bonds.....	122
6.12.3	Porous Metal Bonds.....	122
6.12.4	Crush-Dressing.....	122
6.12.5	High-Porosity Impregnated Metal Bonds.....	124

6.13 Other Bond Systems.....	124
6.13.1 Rubber.....	124
6.13.2 Shellac.....	124
6.13.3 Silicate.....	124
References.....	124

**Chapter 7 Dressing.....127**

7.1 Introduction.....	127
7.2 Traverse Dressing of Conventional Vitrified Wheels with Stationary Tools .....	127
7.2.1 Nomenclature .....	127
7.2.2 Single-Point Diamonds .....	128
7.2.3 Diamond Size.....	128
7.2.4 Scaif Angle.....	129
7.2.5 Cooling.....	129
7.2.6 Dressed Topography.....	130
7.2.7 Dressing Feed and Overlap Ratio.....	130
7.2.8 Dressing Depth.....	131
7.2.9 Dressing Forces.....	131
7.2.10 Dressing Tool Wear.....	131
7.2.11 Rotationally Adjustable Tools.....	132
7.2.12 Profile Dressing Tools.....	132
7.2.13 Synthetic Needle Diamonds .....	133
7.2.14 Natural Long Diamond Blade Tools .....	134
7.2.15 Grit and Cluster Tools.....	135
7.2.16 Form Blocks.....	135
7.3 Traverse Dressing of Superabrasive Wheels with Stationary Tools.....	137
7.3.1 Introduction .....	137
7.3.2 Jig Grinding.....	137
7.3.3 Toolroom Grinding .....	137
7.4 Uniaxial Traverse Dressing of Conventional Wheels with Rotary Diamond Tools .....	138
7.4.1 Introduction .....	138
7.4.2 Crush or Dressing Speed Ratio .....	138
7.4.3 Single-Ring Diamond and Matrix Diamond Discs .....	139
7.4.4 Dressing Conditions for Disc Dressers .....	140
7.4.5 Synthetic Diamond Discs .....	141
7.4.6 Sintered and Impregnated Rolls .....	141
7.4.7 Direct-Plated Diamond Rolls.....	141
7.4.8 Cup-Shaped Tools .....	141
7.5 Uniaxial Traverse Dressing of Vitrified CBN Wheels with Rotary Diamond Tools .....	142
7.5.1 Introduction .....	142
7.5.2 Dressing Depth.....	142
7.5.3 Crush Ratio .....	143
7.5.4 The Dressing Affected Layer.....	143
7.5.5 Touch Dressing .....	144
7.5.6 Truer Design for Touch Dressing .....	147
7.5.7 Impregnated Truers .....	147
7.5.8 Traverse Rotary Truers Using Needle Diamonds .....	149
7.6 Cross-Axis Traverse Dressing with Diamond Discs .....	149
7.6.1 Introduction .....	149
7.6.2 Traverse Rate.....	150

7.7	Diamond Form-Roll Dressing .....	150
7.7.1	Manufacture and Design .....	150
7.7.2	Reverse Plating .....	153
7.7.3	Infiltrated Rolls .....	153
7.7.4	Reverse Plated Rolls .....	154
7.7.5	Dress Parameters for Form Rolls .....	154
7.7.6	Dress Parameters for Form CBN Wheels .....	158
7.7.7	Handling Diamond Rolls .....	159
7.8	Truing and Conditioning of Superabrasive Wheels .....	160
	References .....	165
<b>Chapter 8 Grinding Dynamics .....</b>		<b>167</b>
8.1	Introduction .....	167
8.1.1	Loss of Accuracy and Productivity .....	167
8.1.2	A Need for Chatter Suppression .....	167
8.2	Forced and Regenerative Vibrations .....	167
8.2.1	Introduction .....	167
8.2.2	Forced Vibration .....	168
8.2.3	Regenerative Vibration .....	168
8.3	The Effect of Workpiece Velocity .....	168
8.4	Geometrical Interference between Grinding Wheel and Workpiece .....	170
8.5	Vibration Behavior of Various Grinding Operations .....	170
8.6	Regenerative Self-Excited Vibrations .....	172
8.6.1	Modeling of Dynamic Grinding Processes .....	172
8.6.2	Grinding Stiffness and Grinding Damping .....	172
8.6.3	Contact Stiffness .....	174
8.6.4	Dynamic Compliance of the Mechanical System .....	175
8.6.5	Stability Analysis .....	176
8.7	Suppression of Grinding Vibrations .....	178
8.7.1	Suppression of Forced Vibrations .....	178
8.7.2	Suppression of Self-Excited Chatter Vibrations .....	179
8.8	Conclusions .....	183
	References .....	184
<b>Chapter 9 Grinding Wheel Wear .....</b>		<b>185</b>
9.1	Three Types of Wheel Wear .....	185
9.1.1	Introduction .....	185
9.2	Wheel Wear Mechanisms .....	185
9.2.1	Abrasive Wheel Wear .....	185
9.2.2	Adhesive Wheel Wear .....	185
9.2.3	Tribochemical Wheel Wear .....	186
9.2.4	Surface Disruptions .....	186
9.2.5	Diffusion .....	186
9.3	Wear of the Abrasive Grains .....	186
9.3.1	Types of Grain Wear .....	186
9.3.2	A Combined Wear Process .....	186
9.3.3	Grain Hardness and Temperature .....	187
9.3.4	Magnitude of the Stress Impulses .....	187
9.3.5	Growth of Grain Flats .....	187

9.3.6	Grain Splintering .....	188
9.3.7	Grain Break-Out .....	189
9.3.8	Bond Softening .....	189
9.3.9	Effect of Single Grain Forces .....	189
9.3.10	Wear by Deposition .....	191
9.4	Bond Wear .....	191
9.4.1	Introduction .....	191
9.4.2	Balancing Grain and Bond Wear .....	191
9.5	Assessment of Wheel Wear .....	192
9.5.1	Microtopography .....	192
9.5.2	Profile Wear .....	192
	References .....	193
 <b>Chapter 10</b> Coolants .....		195
10.1	Introduction .....	195
10.2	Basic Properties of Grinding Fluids .....	195
10.2.1	Basic Properties .....	195
10.2.2	Basic Requirements .....	195
10.2.3	Secondary Requirements .....	195
10.3	Types of Grinding Fluids .....	196
10.4	Base Materials .....	197
10.4.1	Introduction .....	197
10.4.2	Water-Based and Oil-Based Fluids .....	198
10.4.3	Rinsing Capacity .....	198
10.4.4	Lubricating Capability .....	199
10.5	Additives .....	199
10.6	Application Results .....	201
10.7	Environmental Aspects .....	201
10.8	The Supply System .....	201
10.8.1	Introduction .....	201
10.8.2	Alternative Cooling Lubricant Systems .....	202
10.8.3	Fluid Supply System Requirements .....	202
10.9	Grinding Fluid Nozzles .....	203
10.9.1	Basic Types of Nozzle System .....	203
10.9.2	The Jet Nozzle .....	204
10.9.3	The Shoe Nozzle .....	204
10.9.4	Through-the-Wheel Supply .....	205
10.9.5	Minimum Quantity Lubrication Nozzles .....	205
10.9.6	Auxiliary Nozzles .....	206
10.10	Influence of the Grinding Fluid in Grinding .....	206
10.10.1	Conventional Grinding .....	206
10.10.2	Influence of the Fluid in Grinding Brittle-Hard Materials .....	207
10.10.3	High-Speed and High-Performance Grinding .....	209
	References .....	213
 <b>Chapter 11</b> Monitoring of Grinding Processes .....		217
11.1	The Need for Process Monitoring .....	217
11.1.1	Introduction .....	217
11.1.2	The Need for Sensors .....	217

11.1.3	Process Optimization .....	217
11.1.4	Grinding Wheel Wear.....	217
11.2	Sensors for Monitoring Process Variables.....	218
11.2.1	Introduction .....	218
11.2.2	Force Sensors .....	219
11.2.3	Power Measurement.....	222
11.2.4	Acceleration Sensors .....	223
11.2.5	AE Systems .....	223
11.2.6	Temperature Sensors .....	226
11.3	Sensor for Monitoring the Grinding Wheel .....	228
11.3.1	Introduction .....	228
11.3.2	Sensors for Macrogeometrical Quantities .....	230
11.3.3	Sensors for Microgeometrical Quantities .....	230
11.4	Sensors for Monitoring the Workpiece.....	233
11.4.1	Introduction .....	233
11.4.2	Contact-Based Workpiece Sensors for Macrogeometry.....	233
11.4.3	Contact-Based Workpiece Sensors for Microgeometry .....	234
11.4.4	Contact-Based Workpiece Sensors for Surface Integrity .....	235
11.4.5	Noncontact-Based Workpiece Sensors .....	237
11.5	Sensors for Peripheral Systems .....	240
11.5.1	Introduction .....	240
11.5.2	Sensors for Monitoring of the Conditioning Process.....	240
11.5.3	Sensors for Coolant Supply Monitoring.....	242
	References .....	244

**Chapter 12** Economics of Grinding .....247

12.1	Introduction .....	247
12.2	A Grinding Cost Comparison Based on an Available Grinding Machine .....	247
12.2.1	Introduction .....	247
12.2.2	Aeroengine Shroud Grinding Example .....	247
12.3	A Cost Comparison Including Capital Investment .....	249
12.3.1	Introduction .....	249
12.3.2	Automotive Camlobe Grinding Example .....	249
12.4	Cost Comparison Including Tooling.....	250
12.4.1	Introduction .....	250
12.4.2	Effect of Tooling Costs in Camlobe Grinding .....	250
12.5	Grinding as a Replacement for Other Processes.....	251
12.5.1	Introduction .....	251
12.5.2	Fine Grinding as a Replacement for Lapping.....	251
12.5.3	High-Speed Grinding with Electroplated CBN Wheels to Replace Turn Broaching .....	252
12.6	Multitasking Machines for Hard-Turning with Grinding .....	252
12.7	Summary .....	253
	References .....	253

**Part II**

Application of Grinding Processes .....	255
-----------------------------------------	-----

<b>Chapter 13</b>	<b>Grinding of Ductile Materials</b>	257
13.1	Introduction	257
13.1.1	Grindability	257
13.1.2	Effect of Chip Form	257
13.1.3	Chemical Reactivity	257
13.2	Cast Irons	258
13.2.1	Gray Cast Iron	258
13.2.2	White Cast Iron	258
13.2.3	Malleable Cast Iron	259
13.2.4	Nodular or Ductile Cast Iron	259
13.3	Steels	259
13.3.1	Plain Carbon Steels	259
13.3.2	Alloy Steels	260
13.3.3	Tool Steels	260
13.3.4	Stainless Steels	262
13.4	Heat-Resistant Superalloys	263
13.4.1	Precipitation-Hardened Iron-Based Alloys	264
13.4.2	Nickel-Based Alloys	264
13.4.3	Cobalt-Based Alloys	264
13.4.4	Titanium	264
	References	265

<b>Chapter 14</b>	<b>Grinding of Ceramics</b>	267
14.1	Introduction	267
14.1.1	Use of Ceramic Materials	267
14.1.2	Machining Hard Ceramics	267
14.1.3	Wheel-Dressing Requirements	267
14.1.4	ELID Grinding	268
14.1.5	Advantages of ELID	268
14.2	Background on Ceramic Materials	268
14.2.1	History	268
14.2.2	Structure	268
14.2.3	Ceramic Groups	269
14.2.4	Ceramic Product Groups	269
14.2.5	Application of ZTA Ceramics	270
14.2.6	Grinding of Ceramics	270
14.3	Diamond Wheels for Grinding Ceramics	271
14.3.1	The Type of Diamond Abrasive	271
14.3.2	Types of Diamond Wheel	271
14.3.3	Wheel Truing and Dressing	273
14.4	Physics of Grinding Ceramics	274
14.5	ELID Grinding of Ceramics	278
14.5.1	Mechanism of ELID Grinding Technique	278
14.5.2	Research Studies on ELID	280
14.5.3	Summary on ELID Grinding	282
	References	282

<b>Chapter 15</b>	<b>Grinding Machine Technology</b>	<b>285</b>
15.1	The Machine Base	285
15.1.1	Introduction	285
15.1.2	Cast Iron Bases	285
15.1.3	Reuse of Cast Bases	285
15.1.4	Welded Bases	285
15.1.5	Damping in Machine Tools	287
15.1.6	Large Mass Bases	287
15.1.7	Tuned Mass Dampers	287
15.1.8	Composite Material Bases	287
15.1.9	Granite Bases	288
15.2	Foundations	288
15.3	Guideways	290
15.3.1	Introduction	290
15.3.2	Definition of Axes	290
15.4	Slideway Configurations	290
15.4.1	Introduction	290
15.4.2	The Flat and Vee Way	291
15.4.3	The Double Vee Slideway	291
15.4.4	Dovetail Slideway	291
15.4.5	Plain Slideway Materials	293
15.5	Hydrostatic Slideways	294
15.5.1	Hydrostatic Bearing Principle	294
15.5.2	Plane-Pad Hydrostatic Slideway Configurations	294
15.5.3	Plane-Pad Hydrostatic Flowrate	294
15.5.4	Hydrostatic Slideway Materials and Manufacture	294
15.5.5	Round Hydrostatic Slideways	295
15.5.6	Diaphragm-Controlled Hydrostatic Slideways	295
15.5.7	Self-Compensating Hydrostatic Slideways	296
15.6	Recirculating Rolling Element Slideways	297
15.7	Linear Axis Drives and Motion Control	299
15.7.1	Introduction	299
15.7.2	Hydraulic Drives	299
15.7.3	Electrohydraulic Drives	299
15.7.4	Ac Servo- and Ballscrew Drives	299
15.8	Elements of AC Servodrive Ballscrew Systems	299
15.8.1	The Ballscrew	299
15.8.2	The Ballnut	301
15.8.3	AC Servomotors	302
15.8.4	Encoders	303
15.8.5	Resolvers	305
15.9	Linear Motor Drive Systems	305
15.9.1	Introduction	305
15.9.2	A Linear Motor System	305
15.9.3	Laser Interferometer Encoders for Linear Motor Drives	306
15.10	Spindle Motors and Grinding Wheel Drives	307
15.11	Drive Arrangements for Large Conventional Wheels	307
15.11.1	Rolling Element Spindle Bearings for Large Wheels	307
15.11.2	Hydrodynamic Spindle Bearings for Large Wheels	309
15.11.3	Hydrostatic Spindle Bearings for Large Wheels	310

15.12	Drive Arrangements for Small Wheel Spindle Units .....	312
15.12.1	Introduction .....	312
15.12.2	Rolling Bearing Spindles with Belt Drive for Small Wheels .....	312
15.12.3	High-Speed Spindles for Small Wheels .....	313
15.12.3.1	Direct Drive Motors .....	313
15.12.3.2	Dynamic Balancing of High-Speed Spindles .....	313
15.12.3.3	Oil-Mist Lubrication for High-Speed Spindles .....	313
15.12.3.4	Adjustment of Bearing Preload for High-Speed Spindles .....	313
15.12.4	Use of Ceramic Balls for High-Speed Spindles.....	314
15.12.5	Liquid Cooled High-Speed Spindles .....	314
15.12.6	Floating Rear Bearing for High-Speed Spindles.....	314
15.13	Spindles for High-Speed Grinding.....	315
15.13.1	Introduction .....	315
15.13.2	Spindle Bearings for High-Speed Grinding of Hardened Steel.....	315
15.13.3	Spindle Bearings for HEDG .....	315
15.13.4	Spindle Cooling for High-Speed Grinding.....	315
15.13.5	Spindle Bearings for Very Small High-Precision High-Speed Wheels .....	316
15.13.6	Active Magnetic Bearings for High-Speed Wheels .....	316
15.14	Miscellaneous Wheel Spindles and Drives.....	316
15.14.1	Hydraulic Spindle Drives.....	316
15.14.2	Air Motors and Bearings .....	316
15.15	Rotary Dressing Systems .....	317
15.15.1	Pneumatic Drives .....	317
15.15.2	Hydraulic Drives .....	317
15.15.3	Electric Drives .....	318
15.16	Power and Stiffness Requirements for Rotary Dressers.....	319
15.17	Rotary Dressing Spindle Examples.....	320
15.17.1	Introduction .....	320
15.17.2	DFW-ACI Air-Driven Spindle .....	320
15.17.3	ECI Hydraulic Spindle .....	320
15.17.4	DFW-HI Heavy-Duty Hydraulic Spindle for Internal Grinders .....	321
15.17.5	DFW-HO Five-Eighths Heavy-Duty Hydraulic Spindle Typically Used for Centerless Wheels.....	322
15.17.6	DFW-HO Variable-Speed Hydraulic Dresser .....	322
15.17.7	DFW-HHD Hydraulic Heavy-Duty Plunge Dresser .....	322
15.17.8	DFW-HTG Heavy-Duty Hydraulic Spindle .....	322
15.17.9	DFW-NTG Belt-Drive Spindle .....	324
15.17.10	DFW-VF44 AC Servo HF Spindle .....	325
15.17.11	DFS-VS8 DC Servo Variable-Speed Dresser .....	325
15.18	Dressing Infeed Systems .....	325
15.18.1	Introduction .....	325
15.18.2	Single Hydraulically Driven Carrier.....	326
15.18.3	Mini Double-Barrel Infeed .....	327
15.18.4	Double-Barrel Infeed Carrier.....	327
15.18.5	Double-Barrel Plunge-Form Dresser .....	328
15.18.6	Triple-Barrel Infeed Carrier with Hydraulic-Mechanical Compensator.....	329
15.18.7	Stepping Motor Carrier.....	329
15.18.8	Stepping Motor Carrier for a Cylindrical Grinder.....	329
15.18.9	Combination Stepper Motor and DC Traverse Motor .....	331
15.18.10	Plunge-Roll Infeed System for a Creep-Feed Grinder.....	331



15.18.11 Servomotor Infeed and Double-Barrel Carrier Dresser .....	331
15.18.12 Two-Axis CNC Profile Dresser .....	332
References .....	336

**Chapter 16 Surface Grinding .....** 341

16.1 Types of Surface Grinding Process .....	341
16.2 Basics of Reciprocating Grinding .....	341
16.2.1 Process Characterization .....	341
16.2.1.1 Real Depth of Cut .....	341
16.2.1.2 Speed Ratio .....	343
16.2.1.3 Specific Removal Rate .....	343
16.2.1.4 Upcut and Downcut Grinding .....	343
16.2.1.5 Nonproductive Time .....	343
16.2.2 Influences of Grinding Parameters on Grinding Performance .....	343
16.2.2.1 The Influence of Cutting Speed (Wheel Speed) .....	343
16.2.2.2 The Influence of Feedrate (Workspeed) .....	344
16.2.2.3 The Influence of Infeed .....	344
16.2.2.4 The Influence of the Interrupted Cut .....	344
16.2.2.5 Reciprocating Grinding without Cross-Feed .....	345
16.2.2.6 Multiple Small Parts .....	345
16.2.3 Economics .....	346
16.3 Basics of Creep Grinding .....	346
16.3.1 Introduction .....	346
16.3.2 Process Characterization .....	346
16.3.3 High-Efficiency Deep Grinding .....	347
16.3.4 The Influence of the Set Parameters in Creep Feed Grinding .....	348
16.3.4.1 The Influence of Cutting Speed $v_c$ .....	348
16.3.4.2 The Influence of Infeed, $a_e$ , and Feedrate, $v_{fr}$ .....	348
16.3.4.3 The Influence of Dressing Conditions .....	348
16.3.4.4 The Influence of Grinding Wheel Specification .....	348
16.3.4.5 The Influence of Up- and Down-Cut Grinding .....	349
16.3.4.6 Process .....	349
16.3.4.7 Work Results .....	351
16.3.4.8 Grinding Wheels .....	351
16.3.4.9 Grinding Wheel Wear .....	351
16.3.5 Requirements for Creep Feed Grinding Machines .....	352
16.3.6 Typical Applications .....	352
16.3.7 Economics of Creep Feed Grinding .....	353
16.4 Basics of Speed-Stroke Grinding .....	353
16.5 Successful Application of Creep Feed Grinding .....	356
16.5.1 Creep Feed Grinding with Vitrified Wheels Containing Alox and Silicon Carbide .....	356
16.5.2 Coolant Application in CF Grinding .....	356
16.5.2.1 Film Boiling .....	356
16.5.2.2 Coolant Delivery System .....	356
16.5.3 Continuous Dress Creep Feed .....	364
16.5.3.1 The Viper Process .....	364
16.5.4 Creep Feed Grinding with CBN .....	366
16.5.4.1 Electroplated CBN .....	368

16.5.4.2	Vitrified CBN .....	370
16.5.4.3	Process Selection .....	371
16.6	Face Grinding .....	381
16.6.1	Introduction .....	381
16.6.2	Rough Grinding with Segmented Wheels .....	383
16.6.3	Rough Machining/Finish Grinding .....	387
16.6.4	Single-Sided Face Grinding on Small-Surface Grinders .....	387
16.6.5	High-Precision Single-Sided Disc Grinding .....	387
16.6.6	Double-Disc Grinding .....	390
16.7	Fine Grinding .....	401
16.7.1	Principles and Limitations of Lapping .....	401
16.7.2	Double-Sided Fine Grinding .....	403
16.7.3	Comparison of Fine Grinding with Double-Disc Grinding .....	406
Appendix 16.1	Lapping Kinematics .....	407
A16.1.1	Introduction .....	407
A16.1.2	Kinematical Fundamentals .....	408
A16.1.3	Analysis of Path Types and Velocities .....	408
A16.1.4	Kinematic Possibilities of Machines .....	410
References	.....	412

## **Chapter 17** External Cylindrical Grinding .....

17.1	The Basic Process .....	417
17.1.1	Introduction .....	417
17.1.2	Work Drives .....	417
17.1.3	The Tailstock .....	417
17.1.4	Wheel Speeds .....	418
17.1.5	Stock Removal .....	419
17.1.6	Angle-Approach Grinding .....	420
17.1.7	Combined Infeed with Traverse .....	420
17.2	High-Speed Grinding .....	421
17.2.1	Introduction .....	421
17.2.2	Energy and Temperatures in High-Speed Grinding .....	421
17.2.2.1	The $C_{\max}$ Factor .....	422
17.2.2.2	Peclet Number $L$ and Workspeed .....	423
17.2.2.3	Contact Angle $\phi$ .....	423
17.2.2.4	Heat Convection by Coolant and Chips .....	424
17.2.3	Coolant Drag and Nozzle Design in High-Speed Grinding .....	428
17.2.4	Maximum Removal Rates .....	429
17.2.5	Peel Grinding .....	430
17.3	Automotive Camlobe Grinding .....	431
17.4	Punch Grinding .....	439
17.5	Crankshaft Grinding .....	442
17.6	Roll Grinding .....	447
References	.....	450

## **Chapter 18** Internal Grinding .....

18.1	Introduction .....	453
18.2	The Internal Grinding Process .....	453

18.3	Abrasive Type.....	455
18.3.1	Grain Selection.....	455
18.3.2	Impact on Grind Configuration.....	456
18.3.4	Quill Designs for CBN .....	457
18.4	Process Parameters.....	458
18.4.1	Wheel Speed .....	458
18.4.2	Workspeed .....	459
18.4.3	Oscillation .....	459
18.4.4	Incoming Part Quality.....	459
18.4.5	Dressing.....	459
18.4.6	Grinding Cycles .....	461
18.4.7	Automatic Compensation of Process Variations .....	462
18.5	Machine Tool Selection .....	466
18.5.1	Introduction .....	466
18.5.2	Fuel Injection .....	467
18.5.3	Automotive Components (Lifters, Tappets, UJ Cups, Plain Bearings).....	468
18.5.4	Machine Layout .....	468
18.5.5	Wheel Speeds.....	468
18.5.6	Work-Spindle Runout.....	468
18.5.7	Work-Loading Mechanisms .....	469
18.5.8	Coolant .....	469
18.5.9	Gauging .....	469
18.5.10	Flexible Multipurpose Grinders .....	470
18.6	Troubleshooting.....	474
	References .....	476
 <b>Chapter 19</b> Centerless Grinding.....		479
19.1	The Importance of Centerless Grinding .....	479
19.2	Basic Process.....	480
19.2.1	External Centerless Grinding.....	480
19.2.2	Approximate Guide to Work-Height .....	480
19.2.3	Internal Centerless Grinding .....	481
19.2.4	Shoe Centerless Grinding .....	481
19.2.5	Roundness and Rounding Geometry .....	481
19.2.6	System Interactions .....	484
19.3	Basic Relationships.....	485
19.3.1	Depth of Cut.....	485
19.3.2	Removal Rate .....	485
19.3.3	Power.....	485
19.3.4	Specific Energy .....	486
19.3.5	Contact Length.....	486
	19.3.5.1 Geometric Contact Length .....	486
	19.3.5.2 Dynamic Contact Length .....	486
19.3.6	Equivalent Grinding Wheel Diameter .....	487
19.3.7	Equivalent Chip Thickness .....	487
19.3.8	Grinding Ratio.....	487
19.4	Feed Processes .....	487
19.4.1	Plunge Feed.....	487
19.4.2	Through-Feed .....	489

19.5	Centerless Wheels and Dressing Geometry .....	490
19.5.1	The Grinding Wheel.....	490
19.5.2	Grinding Wheel Dressing.....	490
19.5.3	The Control Wheel.....	491
19.5.4	Control Wheel Dressing.....	492
	19.5.4.1    Dressing Geometry .....	492
	19.5.4.2    Control Wheel Runout.....	493
19.6	The Workrest .....	493
19.7	Speed Control.....	494
19.7.1	Spinning Out of Control .....	494
19.7.2	Failure to Turn.....	495
19.8	Machine Structure .....	496
19.8.1	The Basic Machine Elements .....	496
19.8.2	The Grinding Force Loop .....	496
19.8.3	Structural Layout.....	498
	19.8.3.1    Low Workspeeds.....	499
	19.8.3.2    High Workspeeds .....	499
19.8.4	Spindle Bearings .....	499
19.9	High Removal Rate Grinding .....	501
19.9.1	Introduction .....	501
19.9.2	Routes to High Removal Rate .....	502
	19.9.2.1    Increasing the Number of Active Grits .....	502
	19.9.2.2    Increasing Removal Rate per Grit.....	502
	19.9.2.3    Longer Redress Life .....	502
	19.9.2.4    Improved Abrasive.....	502
	19.9.2.5    Grinding Trials.....	503
	19.9.2.6    Improved Grinding Machines and Auxiliary Equipment .....	503
19.9.3	Process Limits .....	504
	19.9.3.1    Effect of Infeed Rate .....	504
	19.9.3.2    Effect of Wheel Speed.....	505
	19.9.3.3    Effect of Workspeed .....	505
19.9.4	Specific Energy as a Measure of Efficiency.....	506
19.10	Economic Evaluation of Conventional and CBN Wheels .....	506
19.10.1	Introduction .....	506
19.10.2	Cost Relationships.....	507
19.10.3	Wheel Cost/Part.....	507
19.10.4	Labor Cost/Part .....	507
19.10.5	Machine Cost/Part .....	509
19.10.6	Total Variable Cost/Part .....	509
19.10.7	Experiment Design.....	510
	19.10.7.1    Stage 1. Basic Trials.....	510
	19.10.7.2    Stage 2. Select Best Conditions and Confirm .....	510
	19.10.7.3    Stage 3. Cost Comparisons .....	511
19.10.8	Machine Conditions and Cost Factors.....	512
19.10.9	Materials, Grinding Wheels, and Grinding Variables .....	512
	19.10.9.1    AISI 52100 Steel .....	512
	19.10.9.2    Inconel 718 Trials.....	513
19.10.10	Direct-Effect Charts .....	514
19.10.11	Redress Life and Cost Comparisons.....	515
	19.10.11.1    AISI 52100.....	515
	19.10.11.2    Inconel 718 .....	515

19.10.12	Effects of Redress Life .....	515
19.10.13	Economic Conclusions .....	516
19.11	The Mechanics of Rounding .....	516
19.11.1	Avoiding Convenient Waviness.....	516
19.11.1.1	Rules for Convenient Waviness.....	517
19.11.2	Theory of the Formation of the Workpiece Profile.....	518
19.11.3	Workpiece Movements .....	519
19.11.4	The Machining-Elasticity Parameter .....	521
19.11.5	The Basic Equation for Rounding .....	522
19.11.6	Simulation.....	523
19.11.7	Roundness Experiments and Comparison with Simulation .....	525
19.12	Vibration Stability .....	527
19.12.1	Definitions .....	527
19.12.1.1	Marginal Stability .....	527
19.12.1.2	A Stable System .....	527
19.12.1.3	An Unstable System .....	527
19.12.1.4	Chatter.....	527
19.12.1.5	Forced Vibration .....	528
19.12.2	A Model of the Dynamic System .....	528
19.12.3	Nyquist Test for Stability .....	530
19.12.4	The Depth of Cut Function.....	530
19.12.5	The Geometric Function .....	531
19.12.6	Machine and Wheel Compliances .....	534
19.12.6.1	Static Compliance.....	534
19.12.6.2	Dynamic Compliances.....	535
19.12.6.3	Added Static Compliance.....	536
19.13	Dynamic Stability .....	537
19.13.1	Threshold Conditions .....	537
19.13.2	Dynamic Stability Charts .....	539
19.13.3	Up Boundaries.....	539
19.13.4	Down Boundaries .....	540
19.14	Avoiding Critical Frequencies .....	541
19.14.1	Vibration Frequencies at Threshold Conditions .....	541
19.14.2	Selection of Work Rotational Speed.....	541
19.14.3	Selection of Grinding Wheel Rotational Speed .....	542
19.14.4	Selection of Dresser Speed .....	542
19.14.5	Speed Rules .....	542
19.15	Summary and Recommendations for Rounding .....	543
19.16	Process Control .....	543
	References .....	546

**Chapter 20** Ultrasonic Assisted Grinding .....549

20.1	Introduction .....	549
20.2	Ultrasonic Technology and Process Variants.....	549
20.3	Ultrasonic-Assisted Grinding with Workpiece Excitation .....	552
20.4	Peripheral Grinding with Radial Ultrasonic Assistance.....	552
20.5	Peripheral Grinding with Axial Ultrasonic Assistance .....	555
20.6	Ultrasonic-Assisted Grinding with Excitation of the Wheel .....	557
20.6.1	Ultrasonic-Assisted Cross-Peripheral Grinding.....	557
20.6.2	Ultrasonic-Assisted Face Grinding .....	558

20.7 Summary .....	561
References .....	562
<b>Appendix 1:</b> Glossary .....	563
<b>Appendix 2:</b> Notation and Use of SI Units.....	591
Use of Units .....	591
Examples of Correct and Incorrect Practice .....	591
Factors for Conversion between SI Units and British Units (Values Rounded) .....	592
<b>Index</b> .....	593



# *Part I*

---

## *The Basic Process of Grinding*





---

# 1 Introduction

## 1.1 FROM CRAFT TO SCIENCE

Grinding has been employed in manufacturing for more than 100 years, although the earliest practice can be traced back to neolithic times [Woodbury 1959]. The lack of machine tool technology meant that primitive operations were mostly limited to simple hand-held operations. An early device for dressing a sandstone grinding wheel was patented by Altzschner in 1860 [Woodbury 1959].

The 20th century saw the burgeoning of grinding as a modern process. Seminal publications by Alden and Guest started the process of bringing the art of grinding into a scientific basis [Alden 1914, Guest 1915].

Grinding is a machining process that employs an abrasive grinding wheel rotating at high speed to remove material from a softer material. In modern industry, grinding technology is highly developed according to particular product and process requirements. Modern machine tools may be inexpensive machines with a simple reciprocating table, or they may be expensive machines. Many grinding machines combine computer-controlled feed-drives and slide-way motions, allowing complex shapes to be manufactured free from manual intervention. Modern systems will usually incorporate algorithms to compensate for wheel and dressing tool wear processes. Programmable controls may also allow fast push-button set-up. Monitoring sensors and intelligent control introduce the potential for a degree of self-optimization [Rowe et al. 1994, 1999].

Faster grinding wheel speeds and improved grinding wheel technology have allowed greatly increased removal rates. Grinding wheel speeds have increased by two to ten times over the last century. Removal rates have increased by a similar factor and in some cases by even more. Removal rates of 30 mm<sup>3</sup>/mm/s were considered fast 50 years ago, whereas today, specific removal rates of 300 mm<sup>3</sup>/mm/s are increasingly reported for easy-to-grind materials. In some cases, removal rates exceed 1,000 mm<sup>3</sup>/mm/s. Depths of cut have increased by up to 1,000 times values possible 50 years ago. This was achieved through the introduction of creep-feed and high-efficiency deep grinding technology.

Advances in productivity have relied on increasing sophistication in the application of abrasives. The range of abrasives employed in grinding wheels has increased with the introduction of new ceramic abrasives based on sol gel technology, the development of superabrasive cubic boron nitride (CBN), and diamond abrasives based on natural and synthetic diamond.

New grinding fluids and methods of delivering grinding fluid have also been an essential part in achieving higher removal rates while maintaining quality. Developments include high-velocity jets, shoe nozzles, factory-centralized delivery systems, neat mineral oils, synthetic oils, vegetable ester oils, and new additives. Minimum quantity lubrication provides an alternative to flood and jet delivery aimed at environment-friendly manufacturing.

Grinding is not a process without its share of problems. Problems experienced may include thermal damage, rough surfaces, vibrations, chatter, wheel glazing, and rapid wheel wear. Overcoming these problems quickly and efficiently is helped by a correct understanding of the interplay of factors in grinding. Commonly encountered problems are analyzed in succeeding chapters to show how parameters can be optimized and grinding quality improved.

Grinding dynamics and the sources of vibration problems are explained and different approaches to avoiding vibrations are explored. Some of the techniques described may be surprising to some practitioners. For example, it is shown that increased flexibility of the grinding wheel can be an advantage for vibration suppression.

Attitudes to costs have changed over the years. Buying the cheapest grinding wheels has given way to evaluation of system costs including labor, equipment, and nonproductive time. Examples are included in Chapters 12 and 19 to show how systematic analysis can greatly increase productivity and quality while reducing cost per part. Often the key to reducing costs is to reduce nonproductive time.

## 1.2 BASIC USES OF GRINDING

Grinding is a key technology for production of advanced products and surfaces in a wide range of industries. Grinding is usually employed where one or more of the following factors apply.

### 1.2.1 HIGH ACCURACY REQUIRED

Grinding processes are mostly used to produce high-quality parts to high accuracy and to close tolerances. Examples range from very large parts, such as machine tool slide-ways to small parts, such as contact lenses, needles, electronic components, silicon wafers, and rolling bearings.

### 1.2.2 HIGH REMOVAL RATE REQUIRED

Grinding processes are also used for high removal rate. A typical example is high-removal-rate grinding for the flutes of hardened twist drills. The flutes are ground into solid round bars in one fast operation. Twist drills are produced in very large quantities at high speeds explaining why grinding is a key process for low costs, high production rates, and high quality.

### 1.2.3 MACHINING OF HARD MATERIALS

While accuracy and surface-texture requirements are common reasons for selecting abrasive processes, there is another reason. Abrasive processes are the natural choice for machining and finishing very hard materials and hardened surfaces. In many cases, grinding is the only practical way of machining some hard materials. The ability to machine hard material has become more and more important with the increasing application of brittle ceramics and other hard materials such as those used in aerospace engines.

## 1.3 ELEMENTS OF THE GRINDING SYSTEM

### 1.3.1 THE BASIC GRINDING PROCESS

Figure 1.1 illustrates a surface-grinding operation. Six basic elements are involved: the grinding machine, the grinding wheel, the workpiece, the grinding fluid, the atmosphere, and the grinding

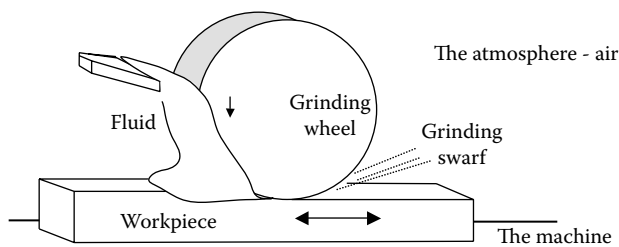


FIGURE 1.1 The six basic elements involved in surface grinding.

swarf. In addition, there is the need for a dressing device to prepare the grinding wheel. The grinding wheel machines the workpiece, although inevitably the workpiece wears the grinding wheel.

Grinding swarf is produced from the workpiece material and is mixed with a residue of grinding fluid and worn particles from the abrasive grains of the wheel. The swarf is not necessarily valueless but has to be disposed of or recycled.

The grinding fluid is required to lubricate the process to reduce friction and wear of the grinding wheel. It is also required to cool the process, the workpiece, and the machine to prevent thermal damage to the workpiece and improve accuracy by limiting thermal expansion of both workpiece and machine. The grinding fluid also transports swarf away from the grinding zone.

The atmosphere plays an important role in grinding most metals by reducing friction. Newly formed metal surfaces at high temperature are highly reactive leading to oxides that can help to lubricate the process. It is usual to emphasize physical aspects of grinding, but chemical and thermal aspects play an extremely important role that is easily overlooked.

The machine tool provides static and dynamic constraint on displacements between the tool and the workpiece. The machine tool stiffness is therefore vital for achievement of tolerances for geometry, size, roughness, and waviness. Vibration behavior of the machine also affects fracture and wear behavior of the abrasive grains.

To summarize, the main elements of an abrasive machining system are [Marinescu et al. 2004]:

The workpiece material, shape, hardness, speed, stiffness, thermal, and chemical properties

The abrasive tool, structure, hardness, speed, stiffness, thermal, and chemical properties, grain size, and bonding

The geometry and motions governing the engagement between the abrasive tool and the workpiece (kinematics)

The process fluid, flowrate, velocity, pressure, physical, chemical, and thermal properties

The atmospheric environment

The machine, accuracy, stiffness, temperature stability, vibrations

### 1.3.2 FOUR BASIC GRINDING OPERATIONS

Four basic grinding processes are illustrated in Figure 1.2. The figure shows examples of peripheral grinding of flat surfaces and cylindrical surfaces. The figure also shows examples of face grinding of nonrotational flat surfaces and face grinding of rotational flat surfaces. Face grinding of rotational flat surfaces can be carried out on a cylindrical grinding machine and may therefore be simply termed cylindrical face grinding.

Figure 1.1 introduces common terms with four basic operations. A distinction is drawn between grinding with the face of the grinding wheel, known as face grinding, and grinding with the periphery of the wheel, known as peripheral grinding. Surface grinding usually refers to grinding flat or profiled surfaces with a linear motion. Cylindrical grinding refers to grinding a rotating workpiece. Cylindrical grinding may be performed internally or externally. A full description of grinding operations commonly employed is rather more complex and is described in other chapters.

In practice, the range of possible grinding processes is large and includes a number of profile-generating operations, profile-copying operations, slitting, and grooving. Profiling processes include grinding of spiral flutes, screw threads, spur gears, and helical gears using methods similar to gear cutting, shaping, planing, or hobbing with cutting tools. There are other processes suitable for grinding crankshafts, cam plates, rotary cams, and ball joints. Terminology for these different processes can be confusing. The International Academy for Production Engineering (CIRP) has published a number of terms and definitions [CIRP 2005]. Details of CIRP publications can be found on the Internet at [www.cirp.net](http://www.cirp.net). Further details of process classification are given in Chapter 3 and later chapters dealing with applications.

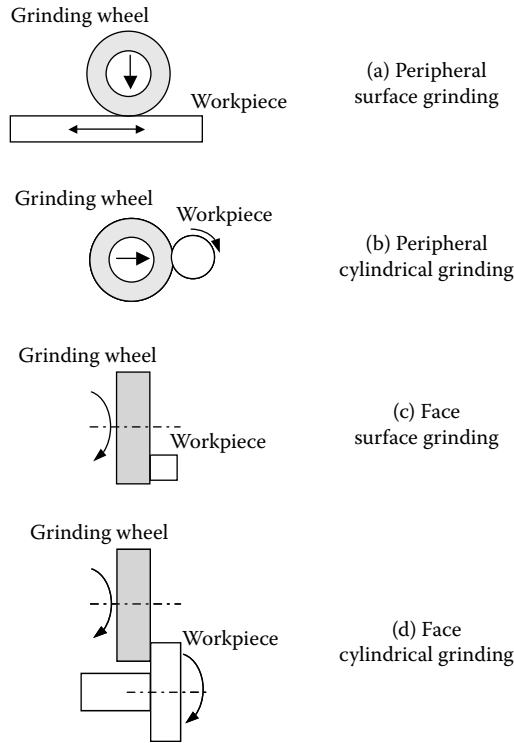


**FIGURE 1.2** Examples of four basic grinding operations using straight wheels.

## 1.4 THE IMPORTANCE OF THE ABRASIVE

The importance of the abrasive cannot be overemphasized. The enormous differences in typical hardness values of abrasive grains are illustrated in Table 1.1 [after De Beers]. A value for a typical M2 tool steel is given for comparison. The values given are approximate since variations can arise due to the particular form, composition, and directionality of the abrasive.

In grinding, it is essential that the abrasive grain is harder than the workpiece at the point of interaction. This means that the grain must be harder than the workpiece at the temperature of the interaction. Since these temperatures of short duration can be very high, the abrasive grains must retain hot hardness. This is true in all abrasive processes, without exception, since if the workpiece is harder than the grain, it is the grain that suffers most wear.

**TABLE 1.1**  
**Typical Hardness of Abrasive Grain Materials**  
**at Ambient Temperatures**

	Units (GPa)
Diamond	56–102
Cubic boron nitride	42–46
Silicon carbide	~ 24
Aluminium oxide	~ 21

*Source:* From De Beers, 1983. With permission.

The hardness of the abrasive is substantially reduced at typical contact temperatures between a grain and a workpiece. At 1,000°C, the hardness of most abrasives is approximately halved. CBN retains its hardness better than most abrasives, which makes it a wear-resistant material. Fortunately, the hardness of the workpiece is also reduced. As can be seen from Table 1.1, the abrasive grains are at least one order of magnitude harder than hardened steel.

The behavior of an abrasive depends not only on hardness but on wear mode. Depending on if wear progresses by attritious wear, microfracture, or macrofracture determines if the process remains stable or if problems will progressively develop through wheel blunting or wheel breakdown. This range of alternatives means that productivity is improved when grinding wheels are best suited for the particular grinding purpose.

## 1.5 GRINDING WHEELS FOR A PURPOSE

Grinding wheels vary enormously in design according to the purpose for which the wheel is to be used. Apart from the variety of abrasives already mentioned, there is the variety of bonds employed including plastic, resinoid, vitrified, metal bonds, and plated wheels.

There is scope for engineering bond properties to achieve strength and wear behavior suited to the particular abrasive within each class of bond. The bond must hold the abrasive until wear makes the abrasive too inefficient as a cutting tool. In addition, the porosity of the wheel must be sufficient for fluid transport and chip clearance. However, porosity affects grit-retention strength and so the wheel must be correctly engineered for the workpiece material and the removal-rate regime.

A grinding wheel is bonded and engineered according to the particular process requirement. A general-purpose wheel will give greatly inferior removal rates and economics compared to an optimized wheel for the particular product. This may be relatively unimportant in a toolroom dealing with various tools of similar material. However, wheel selection and optimization become critical for large-scale repeated batches of aerospace and automotive parts. In such cases, the process engineer should adopt a systematic approach to problem-solving and work closely with the grinding wheel and machine tool manufacturers.

## 1.6 PROBLEM-SOLVING

Few readers have time and fortitude to read a handbook from beginning to end. Although much could be learned from such an approach, readers are encouraged to cherry-pick their way through the most appropriate chapters. Readers are mostly busy people who want to solve a problem. The handbook is therefore structured to allow individual areas of interest to be pursued without necessarily reading chapters consecutively.

### 1.6.1 PART I

The 12 chapters in Part I cover the principles of grinding. This part includes all aspects that relate to grinding generally. Topics include basic grinding parameters, grinding wheels and grinding wheel structure, and wheel-dressing processes used for preparing wheels for grinding and used for restoring grinding efficiency. Further chapters include vibrations, wheel-wear mechanisms, coolants, process monitoring, and grinding costs. Principles are explained as directly as possible and references are given to further sources of information. For example, some readers may wish to explore the science and tribology of grinding more deeply [Marinescu et al. 2004]. Tribology is the science of friction, lubrication, and wear [DES (Jost) Report 1966]. The tribology of abrasive machining processes brings together the branches of science at the core of grinding and grinding wheel behavior.

## 1.6.2 PART II

The 8 chapters in Part II explore applications of grinding. Part II covers grinding of conventional ductile materials, grinding of brittle-hard materials, grinding machine technology and rotary dressers, surface grinding, external cylindrical grinding, internal cylindrical grinding, centerless grinding, and ultrasonically assisted grinding. A particular emphasis is placed on developments in technology that can lead to improved part quality, higher productivity, and lower costs.

The authors draw on industrial and research experience, and give numerous references to scientific publications and trade brochures where appropriate. Readers will find the references to the various manufacturers of machine tools, auxiliary equipment, and abrasives a useful starting point for sourcing suppliers. The references to scientific publications provide an indication of the wide scope of research and development in this field around the world.

## REFERENCES

- Alden, G. I. 1914. "Operation of Grinding Wheels in Machine Grinding." *Trans. Am. Soc. Mech. Eng.* 36, 451–460.
- CIRP (International Institution for Production Engineering). 2005. *Dictionary of Production Engineering II—Material Removal Processes*, Springer, New York.
- De Beers Industrial Diamond Division, 1983. "Abrasive Boron Nitride—The Family of Choice," Cooley, B.A. and Juchem, H.O., *Diamond and CBN Grit Products*, De Beers, UK.
- DES (Jost) Report. 1966. "Lubrication (Tribology) Education and Research." Her Majesty's Stationery Office, London.
- Guest, J. J. 1915. *Grinding Machinery*. Edward Arnold, London.
- Marinescu, I. D., Rowe, W. B., Dimitrov, B., and Inasaki, I. 2004. *Tribology of Abrasive Machining Processes*. William Andrew Publishing, Norwich, NY.
- Rowe, W. B., Li, Y., Inasaki, I., and Malkin, S. 1994. "Applications of Artificial Intelligence in Grinding." *Ann. Int. Inst. Prod. Eng. Res.* Keynote Paper 43, 2, 521–532.
- Rowe, W. B., Statham, C., Liverton, J., and Moruzzi, J. 1999. "An Open CNC Interface for Grinding Machines." *Int. J. Manuf. Sci. Tech.* 1, 1, 17–23.
- Woodbury, R. S. 1959. *History of the Grinding Machine*. The Technology Press, MIT, Cambridge, MA.

---

# 2 Grinding Parameters

## 2.1 INTRODUCTION

Grinding, in comparison to turning or milling, is often considered somewhat of a “black art” where wheel life and cycle times cannot be determined from standard tables and charts. Certainly precision grinding, being a finishing process with chip formation at submicron dimensions occurring by extrusion created at cutting edges with extreme negative rake angles, is prone to process variability such as chatter, system instability, coolant inconsistency, etc. Nevertheless, with grinding equipment in a competent state of repair, performance can be controlled and predicted within an acceptable range. Importantly, rules and guidelines are readily available to the end user to modify a process to allow for system changes. It is also essential to ensure surface quality of the parts produced. These objectives are balanced through an analysis of costs as described in subsequent chapters on economics and on centerless grinding. The importance of the grinding parameters presented below is to provide an understanding of how process adjustments change wheel performance, cycle time, and part quality.

Probably the best way for an end user to ensure a reliable and predictable process is to develop it with the machine tool builder, wheel maker, and other tooling suppliers at the time of the machine purchase using actual production parts. This then combines the best of the benefits from controlled laboratory testing with real components without production pressures, resulting in a baseline against which all future development work or process deterioration can be monitored.

The number of grinding parameters that an end user needs to understand is actually quite limited. The key factors are generally associated with either wheel life, cycle time, or part quality. The purpose of this discussion is to define various parameters that relate to wheel life, cycle time, and part quality and to demonstrate how these parameters may be used to understand and improve the grinding process. In most cases, the author has avoided the derivations of the formulae, providing instead the final equation. Derivations and more detailed discussion can be found in publications such as Marinescu et al. [2004] or Malkin [1989].

### 2.1.1 WHEEL LIFE

The statement that a process can be controlled “within an acceptable range” requires some definition. A recent study by Hitchiner and McSpadden (2005) investigated the process variability of various vitrified cubic boron nitride (CBN) processes as part of a larger program to develop improved wheel technology. They showed that under “ideal” conditions repeatability of wheel life within  $\pm 15\%$  or better could be achieved. However, variability associated with just wheel grade from one wheel to another ( $\pm 1\%$  porosity), all within the standard limits of a commercial specification, made the process less repeatable and increased the variability to  $\pm 25\%$ . In the field, for example, in a high-production internal-grinding operation with 20 machines, the average monthly wheel life was tightly maintained within  $\pm 5\%$ . However, these average values obscured an actual individual wheel life variability of  $\pm 100\%$ ! Of these, wheels with very low or zero life were associated with setup problems while the large variability at the high end of wheel life was associated with machine-to-machine variables such as coolant pressure, spindle condition, or gauging errors. A process apparently in control based on monthly usage numbers was actually quite the opposite (Figure 2.1 and Figure 2.2).

Wheel makers and machine tool builders are usually in the best position to make predictions as to wheel performance. Predictions are based on either laboratory tests or past experience on comparable applications. Laboratory tests tend to reproduce ideal conditions but can make little



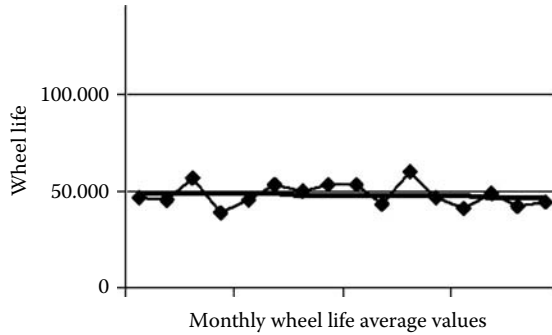


**FIGURE 2.1** Monthly average wheel life values for high-production internal grinding operation.

allowance for a deficiency in fixturing or coolant, etc. In fact, the author witnessed a situation where the laboratory results and the actual field wheel life differed by a factor of 40. The loss of wheel life in the field was caused by vibration from poor part clamping and wheel bond erosion from excessively high coolant pressure. Laboratory data were able to inform the end user that there was a major problem and provide evidence to search for the solution.

**2.1.2 REDRESS LIFE**

In practice, the end user seeks to reduce cycle time for part production as a route to reducing costs and increasing production throughput. The number of parts produced per dress is critical for economic production [Rowe, Ebbrell, and Morgan 2004]. For parts produced in large batches, redress life can be given as the number of parts per dress  $n_d$ . If redress has to take place for every part produced, the cost of grinding is greatly increased. Long redress life depends on having the correct grinding wheel for the grinding conditions and also on the dressing process. Dressing parameters are discussed further in the chapter on dressing.

**2.1.3 CYCLE TIME**

Cycle time is usually defined as the average total time to grind a part. For a batch of  $n_b$  parts produced in a total time  $t_b$ , the cycle time is

$$t_c = \frac{t_b}{n_b}$$

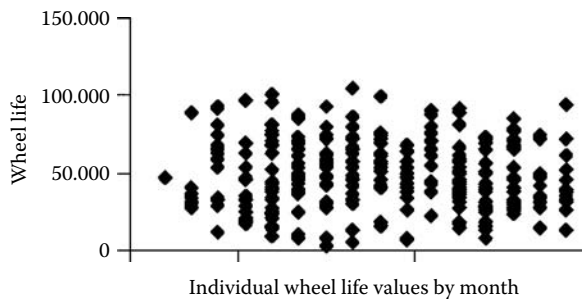


**FIGURE 2.2** Individual wheel life values over same period as Figure 2.1.

The cycle time, therefore, depends on the dressing time, as well as the grinding time, and the loading and unloading time.

## 2.2 PROCESS PARAMETERS

### 2.2.1 UNCUT CHIP THICKNESS OR GRAIN PENETRATION DEPTH

The starting point for any discussion on grinding parameters is “uncut chip thickness,”  $h_{cu}$ , as this provides the basis for predictions of roughness, power, and wear [Shaw 1996]. Uncut chip calculations are typically based on representations of the material removed in the grind process as a long, slender, triangular shape with a mean thickness,  $h_{cu}$ . However, a more practical way of looking at this parameter is to think of  $h_{cu}$  as representing the depth of abrasive grit penetration into the work material. In fact, this parameter is often termed the grain penetration depth. The magnitude of  $h_{cu}$  may be calculated from the various standard parameters for grinding and the surface morphology of the wheel.

$$h_{cu} = \sqrt{\frac{V_w}{V_s} \cdot \frac{1}{C \cdot r} \sqrt{\frac{a_e}{d_e}}} \quad h_{cu} \ll a_e$$

where  $v_s$  = wheel speed,  $v_w$  = work speed,  $a_e$  = depth of cut,  $d_e$  = equivalent wheel diameter,  $C$  = active grit density, and  $r$  = grit cutting point shape factor.

Other useful measures of grain penetration include equivalent chip thickness  $h_{eq} = a_e \cdot v_w / v_s$ . However, equivalent chip thickness takes no account of the spacing of the grains in the wheel surface.

### 2.2.2 WHEEL SPEED

Wheel speed,  $v_s$ , is given in either meters/second (m/s) or surface feet per minute (sfpm). To convert the former to the latter, use a rule of thumb multiplication factor of approximately 200 (or 196.85 to be precise).

### 2.2.3 WORK SPEED

Work speed,  $v_w$ , is a term most typically applied to cylindrical grinding; equivalent terms for surface grinding are either traverse speed or table speed.

### 2.2.4 DEPTH OF CUT

Depth of cut,  $a_e$ , is the depth of work material removed per revolution or table pass.

### 2.2.5 EQUIVALENT WHEEL DIAMETER

Equivalent wheel diameter,  $d_e$ , is a parameter that takes into account the conformity of the wheel and the workpiece in cylindrical grinding and gives the equivalent wheel diameter for the same contact length in a surface grinding application (i.e.,  $d_e \rightarrow d_s$  as  $d_w \rightarrow \infty$ ). The plus sign is for external cylindrical grinding, while the negative sign is for internal cylindrical grinding.

$$d_e = \frac{d_s \times d_w}{d_s \pm d_w} \quad \begin{array}{l} d_w = \text{workpiece part diameter} \\ d_s = \text{wheel diameter} \end{array}$$

### 2.2.6 ACTIVE GRIT DENSITY

Active grit density,  $C$ , is the number of active cutting points per unit area on the wheel surface.

### 2.2.7 GRIT SHAPE FACTOR

Grit shape factor,  $r$ , is the ratio of chip width to chip thickness. In most discussions of precision grinding, the product  $C \cdot r$  is considered as a single factor that can be somewhat affected by dress conditions; but under stable grinding conditions, that is, with a fixed or limited range of dress conditions, can be considered as a constant for a given wheel specification.

There are several key parameters that research has shown to be directly dependent on  $h_{cu}$ :

$$f_g \propto h_{cu}^{1.7} \propto \left\{ \frac{v_w}{v_s} \cdot \frac{1}{C \cdot r} \cdot \sqrt{\frac{a_e}{d_e}} \right\}^{0.85}$$

### 2.2.8 FORCE PER GRIT

Grit retention is directly related to the forces experienced by the grit and these forces increase with uncut chip thickness. It can be seen that for a constant stock removal rate ( $a_e \cdot v_w$ ) forces are lower at large depth of cut and low table speed. Hence, a softer grade might be used for creep feed rather than for reciprocated surface grinding. A softer grade has a better self-sharpening action and reduces grinding forces.

Wheel wear can accelerate as a wheel diameter gets smaller and force/grit increases.

### 2.2.9 SPECIFIC GRINDING ENERGY

Specific grinding energy,  $e_c$  (or  $u$  in older publications), is the energy that must be expended to remove a unit volume of workpiece material. The units are usually  $\text{J}/\text{mm}^3$  or  $\text{in.}\cdot\text{lb}/\text{in.}^3$ ; conversion from metric to English requires a multiplication factor of  $1.45 \times 10^5$ . Analysis of the energy to create chips leads to the following relationship between  $e_c$  and  $h_{cu}$ :

$$e_c \propto \frac{1}{h_{cu}^n} \propto \sqrt{\frac{v_s}{v_w} \cdot C \cdot r} \cdot \sqrt{\frac{d_e}{a_e}}$$

where  $n = 1$  for precision grinding. The relationship is logical insofar as it takes more energy to make smaller chips, but is valid only so long as chip formation is the dominant source. In general terms, for precision grinding of hardened steel, the surface roughness will follow a trend rather like that shown in Figure 2.3 as a function of specific energy (see below).

Hahn [1962] and Malkin [1989] show that in many cases, especially in fine grinding or low metal removal rates, significant energy is consumed by rubbing and ploughing. Under these circumstances specific energy,  $e_c$ , varies with removal rate,  $Q'$ , as illustrated in Figure 2.3.

### 2.2.10 SPECIFIC REMOVAL RATE

Specific removal rate,  $Q'$  or  $Q'_w$ , is defined as the metal removal rate of the workpiece per unit width of wheel contact,  $Q' = a_e \cdot v_w$ . The units are either  $\text{mm}^3/\text{mm}/\text{s}$  or  $\text{in.}^3/\text{in.}/\text{min}$ . To convert from the former to the latter requires a rule of thumb multiplication factor of approximately 0.1 (or 0.1075 to be precise).

For very low values of  $Q'$ , rubbing and ploughing dominate, but as  $Q'$  increases so does the proportion of energy consumed in chip formation. More to the point, the energy consumed by rubbing and ploughing remains constant, thereby becoming a smaller proportion of the total energy

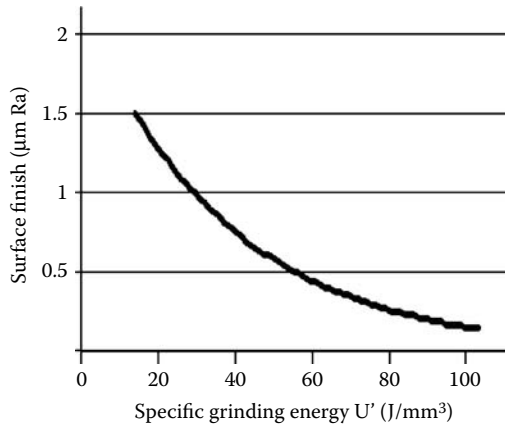


FIGURE 2.3 Example of the relationship between surface roughness and specific grinding energy for a fixed  $Q'$ .

consumed as stock removal rates increase. Precision grinding for the steels illustrated in Figure 2.4 gives specific energy values of 60–30 J/mm<sup>3</sup>, of which about 20 J/mm<sup>3</sup> is associated with chip formation.

Chip formation dominates in high removal-rate precision applications such as camlobe grinding or peel grinding with vitrified CBN or rough grinding with plated CBN. Under these circumstances

$$e_c \propto \frac{1}{h_{cu}}$$

is a good predictor of performance.

### 2.2.11 GRINDING POWER

Grinding power,  $P$ , can be estimated from the specific grinding energy,  $e_c$ , using the equation

$$P = e_c \cdot Q' \cdot b_w$$

where  $b_w$  is the width of grind.

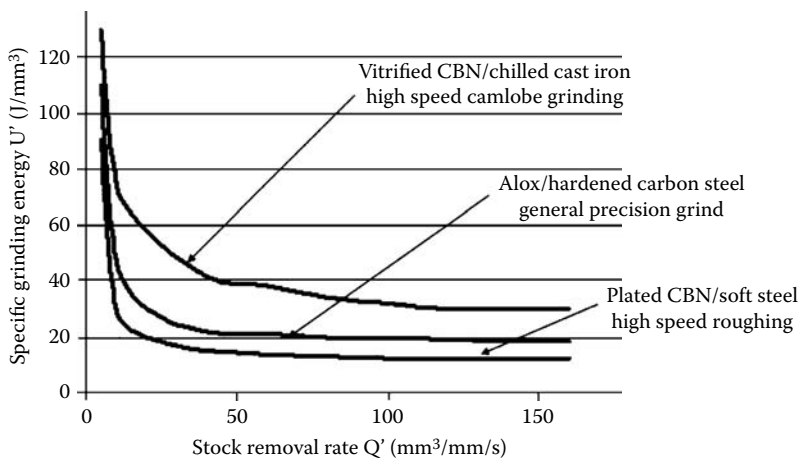


FIGURE 2.4 Examples of specific grinding energy  $U'$  trends versus stock removal rate  $Q'$ .

### 2.2.12 TANGENTIAL GRINDING FORCE

Tangential grinding force,  $F_t$ , may then be calculated from

$$F_t = \frac{P}{v_s} = \frac{e_c \cdot Q' \cdot b_w}{v_s}$$

### 2.2.13 NORMAL GRINDING FORCE

Normal grinding force,  $F_n$ , is related to the tangential grinding force by the coefficient of grinding, a parameter defined in a similar way to friction coefficient.

### 2.2.14 COEFFICIENT OF GRINDING

Coefficient of grinding is  $\mu$ , where

$$\mu = \frac{F_t}{F_n}$$

The value for  $\mu$  can vary from as little as 0.2 for low stock removal applications for grinding hard steels and ceramics to as high as 0.8 in very high stock removal applications such as peel grinding, or grinding soft steels or gray cast iron. Coolant can also have a major impact on the value as a result of the hydrodynamic pressure created by high wheel speeds. The effect is particularly noticeable with high-viscosity straight oils. Typical precision-grinding applications on steels have values of  $\mu$  in the range of 0.25–0.5.

Since tangential force can be readily calculated from power but not from normal force, knowledge of  $\mu$  is particularly useful to calculate required system stiffness, work holding requirements, chuck stiffness, etc. Figure 2.5 plots general values for  $\mu$  as a function of material classes and hardness. For most precision production grinding processes with hardened steel or cast iron it can be seen that  $\mu$  tends to a value of about 0.3. Note, however, that these numbers are for flat profile wheels in a straight plunge mode. If a profile is added to a wheel or the angle of approach is changed from  $90^\circ$ , then allowance must be made for increased normal forces and for side forces.

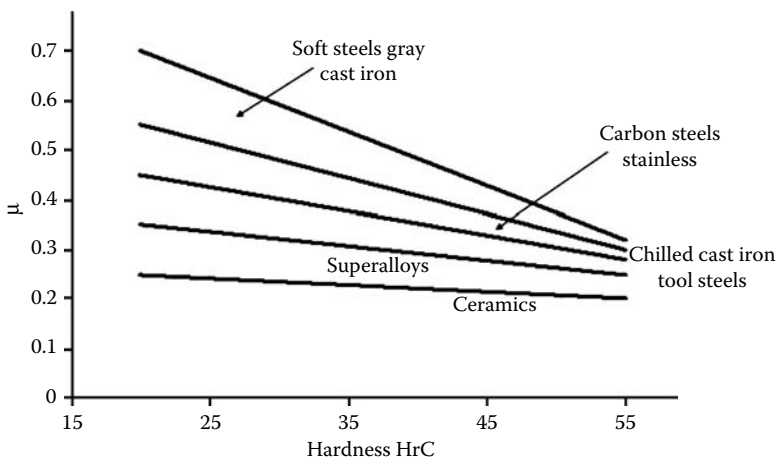


FIGURE 2.5  $\mu(F_t/F_n)$  for major material types in precision grinding.

### 2.2.15 SURFACE ROUGHNESS

Surface roughness, not surprisingly, is closely related to uncut chip thickness.

$$R_t \propto \frac{h_{cu}^{4/3}}{a_e^{1/3}}$$

$$\approx \left( \frac{v_w}{v_s} \cdot \frac{1}{C \cdot r \cdot \sqrt{d_e}} \right)^{2/3}$$

### 2.2.16 $R_t$ ROUGHNESS

$R_t$  roughness is the SI parameter for maximum surface roughness, the maximum difference between peak height and valley depth within the sampling length. As a first approximation,  $R_t$  is independent of depth of cut but is dependent on  $v_w$ ,  $v_s$ ,  $C \cdot r$ , and  $d_e$ . The relationship between surface roughness and specific grinding energy can also be readily obtained by direct substitution.

$R_t$  is but one of several measures of surface roughness. Two other common roughness standards are  $R_a$  roughness and  $R_z$  roughness.

### 2.2.17 $R_a$ ROUGHNESS

$R_a$  roughness is the arithmetic average of all profile ordinates from a mean line within a sampling length after filtering out form deviations.

### 2.2.18 $R_z$ ROUGHNESS

$R_z$  roughness is the arithmetic average of maximum peak-to-valley readings over five adjacent individual samplings lengths.  $R_t$  and  $R_z$  values are much larger than  $R_a$  roughness values for measurements from the same surface.

Two other parameters related to surfaces, especially those used for rubbing contact, are defined as follows:

### 2.2.19 MATERIAL OR BEARING RATIO

Material or bearing ratio,  $t_p$ , is the proportion of bearing surface at a depth  $p$  below the highest peak.

### 2.2.20 PEAK COUNT

Peak count,  $P_c$ , is the number of local peaks that project through a given band height.  $t_p$  is less for grinding than for other operations such as honing, although it can be improved to some extent by a two-stage rough-and-finish grind with wheels of very different grit size.  $P_c$  can be controlled somewhat by adjusting dress parameters.

### 2.2.21 COMPARISON OF ROUGHNESS CLASSES

Comparison of various international surface roughness systems is given in Table 2.1.

### 2.2.22 FACTORS THAT AFFECT ROUGHNESS MEASUREMENTS

Relative values between different roughness systems will vary by up to 20% depending on the metal-cutting process by which they were generated. Even when considering just grinding, the abrasive type can alter the ratio of  $R_z$  to  $R_a$ , CBN often giving a higher ratio to alumina. This

**TABLE 2.1**  
**Guideline Comparisons of International Surface Finish Systems**

Ra ( $\mu\text{m}$ )	Rt ( $\mu\text{m}$ )	Rz ( $\mu\text{m}$ )	RMS ( $\mu\text{in.}$ )	CLA ( $\mu\text{in.}$ )	PVA ( $\mu\text{in.}$ )	Roughness Class France ( $\mu\text{m}$ )	Renault R France ( $\mu\text{m}$ )	Citreon b France ( $\mu\text{m}$ )	Citreon V France ( $\mu\text{m}$ )	Roughness Class China	Quality Class Russia
0.025	0.2	0.16	1.12	1	6.3	12C	0.13	0.08	0.15	N1	12
0.05	0.3	0.32	2.2	2	12	11C	0.25	0.15	0.3	N2	11
0.06	0.5	0.38	2.7	2.4	16	11B	0.3	0.18	0.36	N2	11
0.08	0.6	0.5	3.6	3.2	20	11A	0.4	0.24	0.48	N2/N3	11
0.1	0.8	0.63	4.5	4	25	10C	0.5	0.3	0.6	N3	10
0.12	1	0.75	5.3	5	32	10B	0.6	0.37	0.73	N3	10
0.16	1.25	1	7.1	6.3	40	10A	0.8	0.48	0.97	N3/N4	10
0.2	1.5	1.25	9	8	50	9C	1	0.61	1.22	N4	9
0.25	2	1.6	11.2	10	63	9B	1.25	0.76	1.52	N4	9
0.31	2.5	2	14	12.5	80	9A	1.6	0.95	1.8	N4/N5	9
0.4	3.2	2.5	18	16	100	8C	2	1.2	2.4	N5	8
0.5	4	3.2	22.4	20	125	8B	2.5	1.5	3	N5	8
0.63	5	4	28	25	160	8A	3.2	1.9	3.8	N5/N6	8
0.8	6.3	5	35.5	31.5	200	7C	4	2.4	4.8	N6	7
1	8	6.3	45	40	250	7B	5	3	6	N6	7
1.25	10	8	56	50	320	7A	6.3	3.8	7.6	N6/N7	7
1.6	12.5	10	71	63	400	6C	8	4.7	9.4	N7	

difference also shows up cosmetically when looking visually at surfaces ground with alumina or CBN. When changing from lapping to fine grinding, the change in appearance of the finish can be dramatic, changing from a matt-pitted surface to a shiny but scratched surface, both of which have comparable surface roughness values. The type of grinding process will also affect the appearance in terms of the grind line pattern. For example, in face grinding of a shoulder using, for example, a 2A2 or 6A2 wheel, the grind gives a cross-hatch appearance as in Figure 2.6(a). In angle approach grinding, the face is produced with line contact and the lines are concentric with the journal diameter as in Figure 2.6(b).

### 2.2.23 ROUGHNESS SPECIFICATIONS ON DRAWINGS

Common roughness specifications (marks) on part drawings are shown in Figure 2.7. This gives both the current standard practice, especially in Europe, and the older machining marks still seen

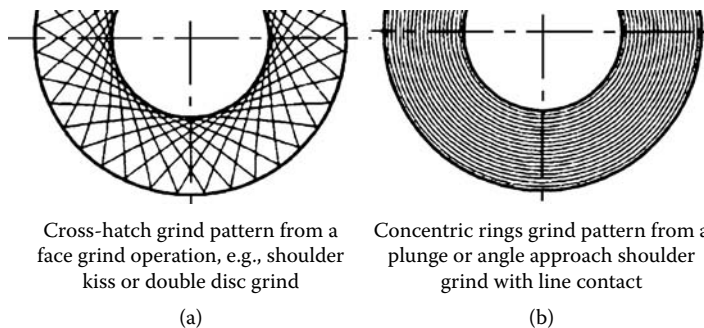


**FIGURE 2.6** Comparison of grind pattern from (a) face and (b) angle approach line contact grinding.

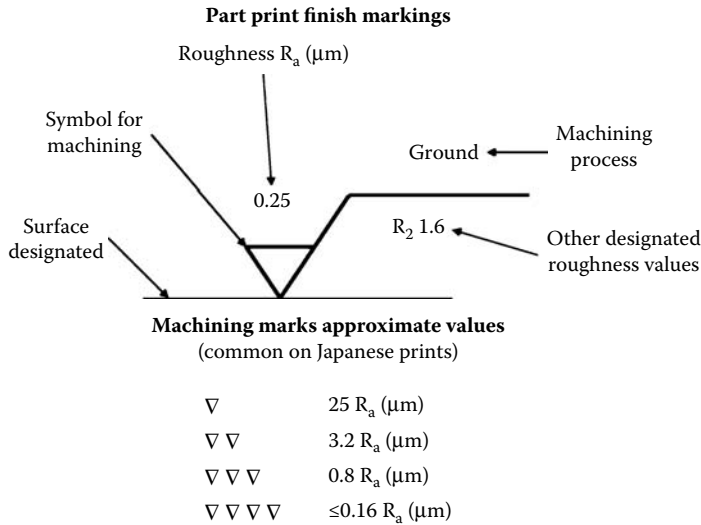


**FIGURE 2.7** Print markings for surface finish.

especially on Japanese drawings. One (∇) or two (∇) marks are indicative of a turning or milling operation, but three (∇) or four (∇) marks are indicative of the requirement to grind or even lap.

Two other force-related factors are of particular interest to end users with low stiffness systems such as internal grinding. The first is stock removal parameter  $\Lambda$ .

**2.2.24 STOCK REMOVAL PARAMETER**

$\Lambda$  is defined as the ratio between stock removal rate and normal force:

$$\Lambda = \frac{Q'}{F_n}$$

$\Lambda$  is an indicator of the sharpness of the wheel, but is limited by the fact that it must be defined for each wheel speed and removal rate. The second factor is decay constant  $\tau$ .

**2.2.25 DECAY CONSTANT  $\tau$**

When the infeed reaches its final feed point, the grinding force  $F$  will change with time  $t$  as the system relaxes according to the equation

$$F = F_0 e^{-t/\tau}$$

$F_t$  and power are directly related; therefore  $\tau$  can be determined from a log plot of the decay in power during spark-out. After  $3\tau$  virtually all grinding has ceased, preventing any improvement in part tolerance, while roughness, as shown above, will not improve further. Consequently, spark-out times in internal grinding should be limited to no more than  $3\tau$ .

**2.2.26 G-RATIO**

G-ratio is used as the primary measure of wheel wear. This is defined as

$$\text{G-ratio} = \frac{\text{Volume of material ground per unit wheel width}}{\text{Volume of wheel worn per unit wheel width}}$$



G-ratio is dimensionless with values that can vary from  $<1$  for some soft alox creep feed vitrified wheels to as high as 100,000 for vitrified CBN wheels. G-ratio will fall linearly with increases in  $Q'$  accelerating to an exponential drop as the maximum metal removal rate for the wheel structure is reached.

### 2.2.27 P-RATIO

P-ratio is a closely related index that has started to be used as an alternative to G-ratio for plated superabrasive wheels.

$$\text{P-ratio} = \text{Volume of metal ground per unit area of wheel surface}$$

This allows for the fact that it is hard to define a wear depth on a plated wheel. P-ratio usually has the dimensions of  $(\text{mm}^3/\text{mm}^2)$ . For high-speed high stock-removal applications in oil-cooled grinding crankshafts, for example, P-ratio values have reached 25,000  $\text{mm}^3/\text{mm}^2$ . Since the usable layer depth on a plated wheel is only at most about 0.1 mm, a P value of 25,000 mm corresponds to a G-ratio greater than or equal to 250,000.

### 2.2.28 CONTACT LENGTH

$l_c$  is the length of the grinding contact zone and is the length over which the heat input to the workpiece is spread. The contact length is approximately equal to the geometric contact length for rigid metal bond wheels.

### 2.2.29 GEOMETRIC CONTACT LENGTH

$$l_c \approx l_g = \sqrt{a_e \cdot d_e}$$

### 2.2.30 REAL CONTACT LENGTH

The real contact length is typically twice this value for more elastic vitrified wheels. Marinescu et al. [2004] show that

$$l_c = \sqrt{l_g^2 + l_f^2}$$

where

$$l_f^2 = \frac{8 \cdot R_r^2 \cdot F'_n \cdot d_e}{\pi \cdot E^*}$$

gives the contribution to the contact length due to elastic deflection between the abrasive and the workpiece due to the normal grinding force. This deflection is increased for rough surfaces such as an abrasive wheel. A typical value for the roughness factor is  $R_r \approx 5$ . The combined elastic modulus for the workpiece and abrasive materials is given by

$$\frac{1}{E^*} = \frac{1 - \nu_1^2}{E_1} + \frac{1 - \nu_2^2}{E_2}$$

## 2.3 GRINDING TEMPERATURES

### 2.3.1 SURFACE TEMPERATURE $T$

Prediction of grinding temperatures and the avoidance of burn are critical to grinding quality. Numerous calculations modeling the partition of heat between the elements in the grind zone have been developed over the last 50 years. Maximum temperature of the workpiece is usually based on an

original paper by Jaeger [1942] and on the principles of moving heat sources described by Carslaw and Jaeger [1959]. Heat partitioning is described in depth by Marinescu et al. [2004]. The following simple version suffices to illustrate the key factors governing maximum surface temperature.

### 2.3.2 MAXIMUM WORKPIECE SURFACE TEMPERATURE

The maximum surface temperature depends on the grinding power ( $F'_t \cdot v_s$ ), the grinding speeds, and material parameters.

$$T_{\max} = C_{\max} \cdot R_w \cdot \frac{F'_t \cdot v_s}{\beta_w} \cdot \sqrt{\frac{1}{v_w \cdot l_c}}$$

where the thermal parameters that affect grinding temperature are the  $C_{\max}$  factor, the transient thermal property,  $\beta_w$ , and the workpiece partition ratio,  $R_w$ .

### 2.3.3 THE $C_{\max}$ FACTOR

This is a constant that gives the maximum temperature. The value is approximately equal to 1 for conventional grinding. The value is reduced for deep grinding. Rowe and Jin [2001] give charts of  $C$  values for maximum temperature and for finish surface temperature.

### 2.3.4 THE TRANSIENT THERMAL PROPERTY $\beta_w$

The transient thermal property of  $\beta_w$  of the workpiece material is given by

$$\beta_w = \sqrt{k \cdot \rho \cdot c}$$

where  $k$  = thermal conductivity,  $\rho$  = density, and  $c$  = heat capacity.

### 2.3.5 WORKPIECE PARTITION RATIO $R_w$

Workpiece partition ratio  $R_w$  is the proportion of the grinding energy that is conducted into the workpiece. The work partition ratio is a complex function of the wheel grain conductivity and sharpness and of the workpiece thermal property. Ignoring, for the present, coolant convection and convection by the grinding chips,  $R_w$  approximates to  $R_{ws}$ . Hahn [1962] modeled heat transfer between a sliding grain and a workpiece. It can be shown that

$$R_{ws} = \left( 1 + \frac{k_g}{\beta_w \cdot \sqrt{r_0 \cdot v_s}} \right)^{-1}$$

$k_g$  is the thermal conductivity of the abrasive grain and  $r_0$  is the contact radius of the grain.  $R_{ws}$  is relatively insensitive to variations of  $r_0$ . Typically,  $R_{ws}$  for conventional grinding varies between 0.7 and 0.9 for vitrified wheels and between 0.4 and 0.6 for CBN wheels.

### 2.3.6 EFFECT OF GRINDING VARIABLES ON TEMPERATURE

The temperature equation for conventional grinding can, therefore, be very approximately reduced for a given wheel/work/machine configuration to

$$T_{\max} \propto \sqrt{a_e \cdot v_s \cdot C \cdot r}$$

from which it follows that increasing the wheel speed, increasing the depth of cut, or increasing the number of active cutting edges (e.g., by dull dressing) will increase the surface temperatures. Further discussion of temperatures generated when grinding at very high wheel speeds is made in a later chapter.

### 2.3.7 HEAT CONVECTION BY COOLANT AND CHIPS

A note of caution should be sounded for deep grinding where the long contact length allows substantial convective cooling from the grinding coolant. Also in high-rate grinding with low specific energy, the heat taken away by the grinding chips reduces maximum temperature very substantially [Rowe and Jin 2001].

Allowance can be made for convective cooling by subtracting the heat taken away by the coolant and chips as described by Rowe and Jin [2001]. Allowance for convective cooling is essential for creep grinding as shown by Andrew, Howes, and Pearce [1985]. It has also been found important for other high-efficiency deep-grinding processes as employed for drill flute grinding, crankshaft grinding, and cutoff grinding. If allowance is not made for convective cooling the temperatures are very greatly overestimated.

The maximum temperature equation modified to allow for convective cooling has the form

$$T_{\max} = \frac{F'_t v_s - \rho \cdot c \cdot T_{mp} \cdot a_e \cdot v_w}{\frac{\beta_w \sqrt{v_w l_c}}{R_w C_{\max}} + \frac{2}{3} \cdot h_f \cdot l_c}$$

where  $T_{mp}$  is a temperature approaching the melting point of the workpiece material. For steels, the material is very soft at 1,400°C and this temperature gives a reasonable estimate for the chip convection term.

$h_f$  is the coolant convection coefficient that applies as long as the maximum temperature does not cause the fluid to burn out in the grinding zone. If burnout occurs, the convection coefficient is assumed to be zero. Burnout is a common condition in grinding but should be avoided in creep grinding and for low-stress grinding. Values estimated for convection coefficient when grinding with efficient fluid delivery are 290,000 W/m<sup>2</sup>K for emulsions and 23,000 W/m<sup>2</sup>K for oil.

### 2.3.8 CONTROL OF THERMAL DAMAGE

An increasingly popular approach to control thermal damage has been developed by Malkin [1989] with literature examples of its application in industry by General Motors on cast iron [Meyer 2001], with Bell Helicopter on hardened steel, and [Stephenson et al. 2001] on Inconel to impose a limit on grinding temperatures. Malkin [1989] provides the maximum allowable specific grinding energy for a given maximum temperature rise as

$$e_c = A + C \cdot T_{\max} \cdot (d_e^{1/4} \cdot a_e^{-3/4} \cdot v_w^{-1/2})$$

$A$  and  $C$  are constants based on the thermal conductivity and diffusivity properties of the workpiece and wheel. A series of tests are made for different values of  $a_e$ ,  $v_w$ , and  $d_e$  and the workpieces analyzed for burn. Plotting these on a graph of  $e_c$  against  $d_e^{1/4} a_e^{-3/4} v_w^{-1/2}$  establishes the slope  $CT_{\max}$  and intercept  $A$ .

The method is illustrated schematically in Figure 2.8. In an industrial situation, a power-meter is used to monitor specific energy values. If the specific energy values exceed the threshold level for burn, it is necessary to take corrective action to the process. This can mean redressing the wheel or making some other process change such as reducing the depth of cut, increasing the workspeed, or using a different grinding wheel.

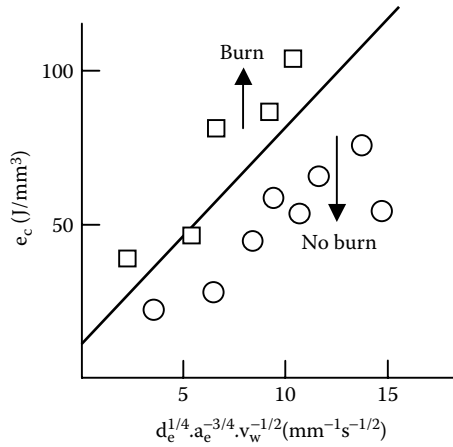


FIGURE 2.8. Specific energy values below the threshold avoid burn. Specific energy values above the threshold cause burn.

APPENDIX 2.1 DRAWING FORM AND PROFILE TOLERANCING

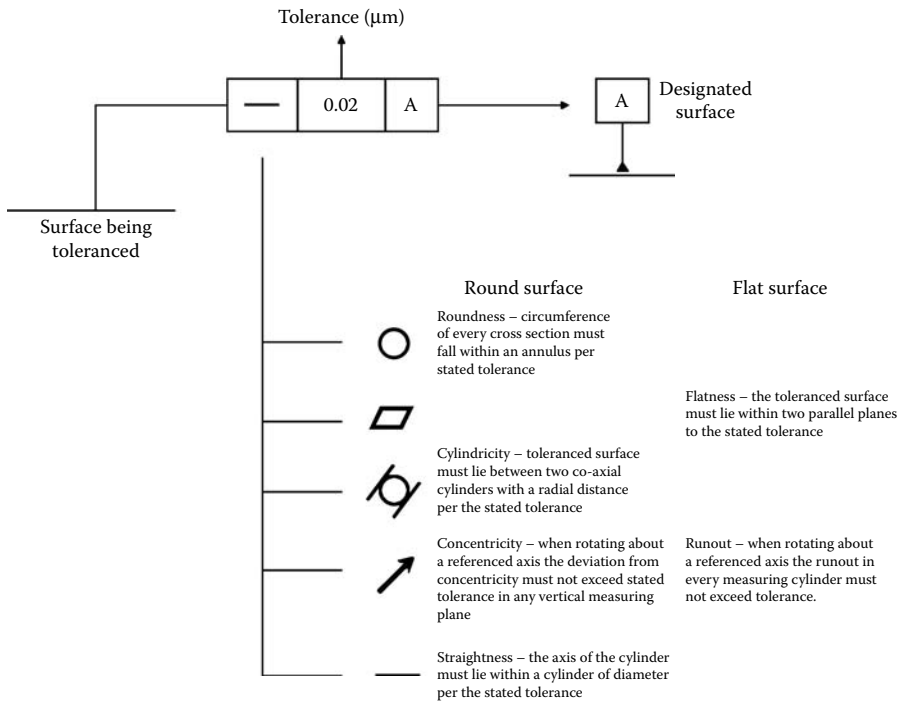


FIGURE A2.1 Examples of form and position tolerances.

REFERENCES

Andrew, C., Howes, T. D., and Pearce, T. R. A. 1985. *Creep Feed Grinding*. Holt, Rinehart and Winston, New York.  
 Carslaw, H. S. and Jaeger, J. C. 1959. *Conduction of Heat in Solids*. Oxford Science Publications, Oxford University Press, Oxford.  
 Hahn, R. S. 1962. "On the Nature of the Grinding Process." *Proceedings of the 3rd Machine Tool Design & Research Conference*. Pergamon Press, Oxford, p. 129.

- Hitchiner, M.P. and McSpadden, S.B. 2005. "Evaluation of Factors Controlling CBN Abrasive Selection for Vitriified Bonded Wheels." *Ann. CIRP*. 54, 1, G.3.
- Jaeger, J.C. 1942. "Moving Sources of Heat and the Temperature at Sliding Contacts." *Proceedings of the Royal Society of New South Wales*. 76, 203.
- King, R. I and Hahn, R. S. 1986. *Handbook of Modern Grinding Technology*. Chapman & Hall, London.
- Malkin, S. 1989. *Grinding Technology Book*. Ellis Horwood, New York.
- Marinescu, I. D., Rowe, W. B., Dimitrov, B., and Inasaki, I. 2004. *Tribology of Abrasive Machining Processes*. William Andrew Publishing, Norwich, NY.
- Meyer, J. E. 2001. "Specific Grinding Energy Causing Thermal Damage in Helicopter Gear Steels." SME 4th International Machining & Grinding Conference.
- Rowe, W. B. and Jin, T. 2001. "Temperatures in High Efficiency Deep Grinding (HEDG)." *Ann. Int. Inst. Prod. Eng.* 50, 1, 205–208.
- Rowe, W. B., Ebbrell, S., and Morgan, M. N. 2004. "Process Requirements for Precision Grinding." *Ann. Int. Inst. Prod. Eng.* 44, 1, 12–13.
- Shaw, M. C. 1996. *Principles of Abrasives Processing*, Oxford Science Series. Clarendon Press, Oxford.
- Stephenson, D. J. et al. 2001. "Burn Threshold Studies for Superabrasive Grinding Using Electroplated CBN Wheels." SME 4th International Machining & Grinding Conference.

---

# 3 Material Removal Mechanisms

## 3.1 SIGNIFICANCE

### 3.1.1 INTRODUCTION

Knowledge of the basic principles of a process is a prerequisite for its effective improvement and optimization. During grinding, surface formation is one of the basic mechanisms. In the case of cutting with geometrically defined cutting edges, a singular engagement of the cutting edge defines the removal mechanism. The consequent removal mechanisms can be directly observed by means of modern investigation methods.

In the case of grinding, the investigation of removal mechanisms is complicated due to many different factors. The first problem is posed by the specification of the tool. The abrasive grains are three-dimensional and statistically distributed in the volume of the grinding wheel. The geometry of the single cutting edges is complex. Moreover, there is a partially simultaneous engagement of the cutting edges involved in the process. The surface formation is the sum of these interdependent cutting edge engagements, which are distributed stochastically. Furthermore, the chip formation during grinding takes place within a range of a few microns. The small chip sizes make the observation even more difficult.

### 3.1.2 DEFINING BASIC BEHAVIOR

In spite of the complexity, some statements can be made on the removal mechanisms, surface formation, and the wear behavior during grinding. Analogy tests and theoretical considerations on the basis of the results of physical and chemical investigations are used for this purpose. In the past few years, chip and surface formation have been modeled with the help of high-performance computers and enhanced simulation processes.

- Indentation tests—In analogy tests, the engagement of the cutting edge in the material surface is investigated first. The advantage of this method is that single cutting edges can be investigated before and after the process, and their geometry is known. With the help of so-called indentation tests with singular cutting edges, the material behavior to a static stress can be observed without the influence of the movement components typical for grinding. On the basis of these indentation tests, elastic and plastic behavior as well as crack formation can be observed in the case of brittle-hard materials at the moment the cutting edge penetrates the material.
- Scratch tests—A further method is the investigation of the removal mechanisms during scratching with single cutting edges, which allows the accurate examination of the geometry and the wear of the cutting edges. Contrary to the indentation tests, there is chip formation during this test method. Furthermore, the influence of different cooling lubricants can be investigated.
- Cutting edge geometry—A further prerequisite of a comprehensive understanding of the material removal during grinding is the geometrical specification of the single cutting edges. This mainly takes place in analogy to the geometrical relations at geometrically defined cutting edges.

- **Thermal and mechanical properties**—The thermal and mechanical characteristics of the active partners of the grinding process also have a significant influence. Heat is generated in the working zone through friction. This contact zone temperature influences the mechanical characteristics of the workpiece as well as of the tool.
- **Surface modification**—As a result of the removal mechanisms, the subsurface of the machined workpiece is influenced by the grinding wheel due to the mechanical stress. Residual stresses develop depending on the specification of the machined workpiece material. These stresses can have a positive effect on component characteristics; hence, they are in some cases specifically induced. Due to the mechanical stresses, cracks or structural and phase changes may occur on the subsurface that have a negative effect on the component characteristics.

This shows the complexity of the mechanisms of surface formation during grinding. The better the surface formation is known, the more specifically and accurately the process parameters, the tool specification, and the choice of an eligible cooling lubricant can be optimized.

## 3.2 GRINDING WHEEL TOPOGRAPHY

### 3.2.1 INTRODUCTION

In the case of grinding, the cutting process is the sum of singular microscopic cutting processes, whose temporal and local superposition leads to a macroscopic material removal. As a consequence, the cause-and-effect principle of grinding can only be described on the basis of the cutting behavior of the individual abrasive grains [Sawluk 1964]. The most important parameter is the number of the currently engaged cutting edges [Kassen 1969]. An exact determination of the geometrical engagement conditions of the single cutting edges, however, is not possible for manufacturing processes like grinding or honing. Due to the stochastic distribution of the geometrically not defined cutting edges, their position and shape cannot be exactly determined.

Therefore, the position, number, and shape of the abrasive grains are analyzed statistically and related to the process kinematics and geometry to achieve a specification of the engagement conditions of the abrasive grain. Thus, grinding results can be related to events at the effective area of grinding contact for particular input values of machine and workpiece parameters and other specifications of the process. The main cutting parameters of the removal process are the theoretical chip thickness, length, and engagement angle. Knowing the overall relations between input values, cutting and chip values, as well as process output values, the behavior of the process can be cohesively described and used to improve the set-up of the machining process. This implies a wheel specification suitable for the grinding situation and the choice of parameters leading to an economical grinding process.

Different authors have described the material removal mechanisms of diverse grinding processes. Thereby, a distinction is made between topography, uncut chip thickness, grinding force, grinding energy, surface, and temperature models in relation to different basic models [Kurrein 1927, Pahlitzsch and Helmerdig 1943, Reichenbach et al. 1956, Kassen 1969, Werner 1971, Inasaki, Chen, and Jung 1989, Malyshev, Levin, and Kovalev 1990, Lierath et al. 1990, Toenshoff et al. 1992, Paulmann 1990, Marinescu et al. 2004].

### 3.2.2 SPECIFICATION OF SINGLE CUTTING EDGES

The geometry of single cutting edges may be described statistically by measurement of cutting edge profiles. The depiction of the form of a cutting edge of an abrasive grain represents the average of all measured geometries. The main characteristic of the cutting edges acting during grinding is the clearly negative rake angle (Figure 3.1).

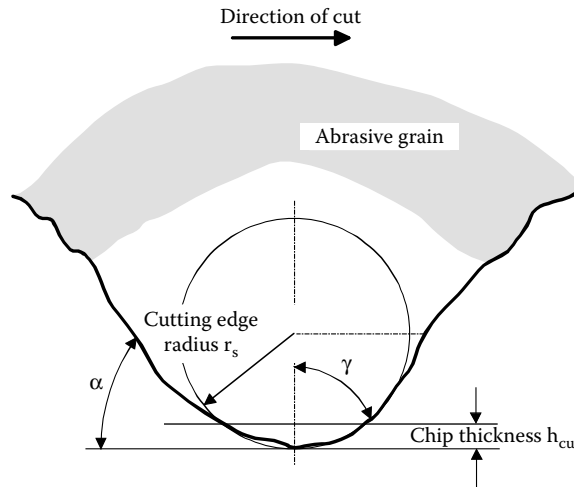


**FIGURE 3.1** Average shape and analytic description of a cutting edge. (From Koenig and Klocke 1996. With permission.)

### 3.3 DETERMINATION OF GRINDING WHEEL TOPOGRAPHY

#### 3.3.1 INTRODUCTION

The determination of the grinding wheel topography can be divided into static, kinematic, and dynamic methods [Bruecher 1996]:

- Static methods—All abrasive grains on the surface of the grinding tool are considered. The kinematics of the grinding process is not taken into account.
- Dynamic methods—In this process, the number of actual abrasive grain engagements are measured. The active cutting edge number is the totality of cutting edges involved in the cutting process.
- Kinematic methods—Kinematic methods combine the effects of the kinematics of the process with the statically determined grain distribution for the specification of microkinematics at the single grain, that is, for the determination of cutting parameters.

#### 3.3.2 STATIC METHODS

If static assessment methods are used, basically all cutting edges in the cutting area are included in the topography analysis. There is no distinction, whether a cutting edge of the grinding process is actively involved or not in the cutting process. Static processes are independent of the grinding conditions [Shaw and Komanduri 1977; Verkerk 1977].

Figure 3.2 shows a schematic section of a cutting surface of a grinding wheel. All abrasive grains protruding from the bond have cutting edges—the so-called static cutting edges. Since grains usually have more than one cutting edge, the distance between the static cutting edges does not correspond to the average statistical grain separation on the grinding wheel. Therefore, instead of the distance between the static cutting edges, the number of cutting edges is specified per unit length, that is, the static cutting edge number  $S_{stat}$ , the cutting edge density per surface unit  $N_{stat}$ , or the number per unit volume of the cutting area  $C_{stat}$  [Daude 1966, Lortz 1975, Kaiser 1977, Shaw and Komanduri 1977, Verkerk 1977, Rohde 1985, Treffert 1995, Marinescu et al. 2004].



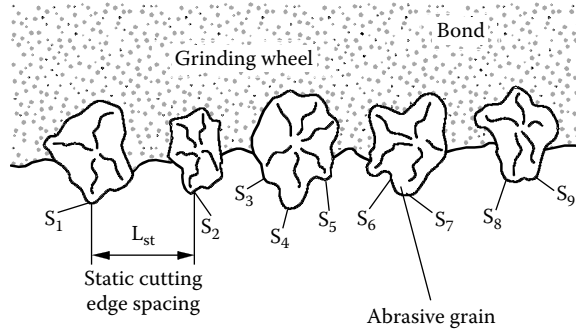


FIGURE 3.2 Static cutting edges. (From Koenig and Klocke 1996. With permission.)

### 3.3.3 DYNAMIC METHODS

In contrast to static methods, dynamic methods depend on the grinding conditions. Giving consideration to the grinding process, the parameters, and the geometrical engagement conditions, information is obtained about which areas of the effective surface of the grinding wheel are actually involved in the process [Verkerk 1977, Gaertner 1982].

Figure 3.3 shows some of the existing cutting edges actively involved in the process. The number and density of the active cutting edges  $S_{act}$  and  $C_{act}$  are therefore smaller than those of the static cutting edges  $S_{stat}$  and  $C_{stat}$ . Their value is mainly determined by the geometric and kinematic parameters. As a result of constant wheel wear and of the consequent topography changes of the wheel, the cutting edge density has continually changing values.

### 3.3.4 KINEMATIC SIMULATION METHODS

In the kinematic approach, the process kinematics is additionally taken into account for the specification of the effective cutting area. On the basis of the kinematically determined cutting edge number, the trajectories of the single grains are reproduced when considering the grinding

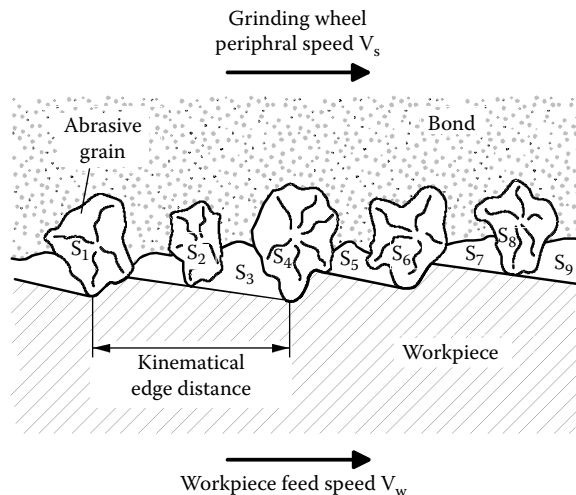


FIGURE 3.3 Kinematic cutting edges. (From Koenig and Klocke 1996. With permission.)

Methods for the determination of the grinding wheel topography			
Static method	Dynamic method		Kinematical method
Post-process	In-process	Post-process	Post-process
Carbon paper method -static cutting edge nr. $N_S$	Piezoelectr. method -act. cutting edge nr. $N_{Sact}$	Photoelectr. method -act. cutting edge nr. $N_{Sact}$	Profile method, kinematical simulation of the process -kin. cutting edge number $N_{Skin}$
Microscop. method a. grinding wheel b. print -qual. impression -stat. cutting edge nr. $N_S$ cutting edge density $C_S$	Thermoelectr. method -act. cutting edge nr. $N_{Sact}$	Scratching-method -act. cutting edge nr. $N_{Sact}$	
Profile method -surface parameters ( $R_Z, R_p, R_K, R_{VK}, R_{PK}$ ) -stat. cutting edge nr. $N_S$ cutting edge density $C_S$	Transition resistance -act. bond ridge	Reproduction method -spec. s. roughness ( $R_{tb}$ ) -end s. rough. ( $R_{taus}$ ) -effective s. rough. ( $R_{tw}$ )	

FIGURE 3.4 Methods for characterizing topography of grinding wheels. (From Bruecher 1996. With permission.)

process, the setting parameters, and the geometrical engagement conditions [Lortz 1975, Gaertner 1982, Steffens 1983, Bouzakis and Karachaliou 1988, Stuckenholz 1988, Treffert 1995].

### 3.3.5 MEASUREMENT OF GRINDING WHEEL TOPOGRAPHY

Figure 3.4 summarizes different methods for measuring the topography of grinding wheels. In the case of the carbon paper method, white paper and carbon paper are put between the grinding wheel and a slightly conical, polished plastic ring. The grinding wheel topography is reproduced on the white paper by rolling the grinding wheel on the plastic ring. Due to the conical shape of the ring, the measurement of the cutting edge distribution is expected to be dependent on the cutting area depth [Nakayama 1973].

### 3.3.6 ROUGHNESS MEASURES

Various surface parameters,  $R_Z, R_K, R_{VK},$  and  $R_{PK}$ , are available as measures of topography and, in particular, the maximum profile height,  $R_p$ , is useful due to its integrating character for the specification of the grinding wheel topography [Schleich 1982, Werner and Kentner 1987, Warnecke and Spiegel 1990, Uhlmann 1994, Bohlheim 1995]. A further value derived from static methods is the static cutting edge number per length or surface unit  $N'_S$  or  $N_S$  [Daude 1966, Lortz 1975, Kaiser 1977, Shaw and Komanduri 1977, Verkerk 1977, Rohde 1985, Treffert 1995]. The cutting edges are determined on the basis of the envelope curve of the effective area of the grinding wheels, which is defined by the external cutting edges. With increasing depth, the cutting edges penetrate equidistant intersection surfaces or lines. Similar to a material ratio curve, a frequency curve of the static cutting edge numbers is formed depending on the cutting edge depth  $z_S$ .

### 3.3.7 QUALITATIVE ASSESSMENT

SEM, optical, and stereo-microscopic images are used for the qualitative evaluation of wear processes [Schleich 1982, Stuckenholz 1988, Dennis and Schmieden 1989, Warnecke and Spiegel 1990, Wobker 1992, Uhlmann 1994, Marinescu et al. 2004].

### 3.3.8 COUNTING METHODS

Microscopic processes can, however, also be used to make quantitative statements on the state of the grinding wheel effective area. For this purpose, grains or different wear characteristics were statically counted [Buettner 1968, Bohlheim 1995]. The measurements are either carried out directly on the grinding wheel surface or indirectly on a print of the surface.

### 3.3.9 PIEZO AND THERMOELECTRIC MEASUREMENTS

Piezoelectric and thermoelectric processes for the determination of the active cutting edge number are based on the measurement of force signals or temperature peaks of single active cutting edges [Daude 1966, Kaiser 1977, Shaw and Komanduri 1977, Verkerk 1977, Damlos 1985]. The piezoelectric process is only applicable for small contact surfaces, since it has to be ensured that no more than one cutting edge is engaged in the contact zone at any time. Small samples of a width of circa 0.3 mm [Kaiser 1977] are ground with relatively small feed. In the thermoelectric process, a thermocouple wire of a small diameter is divided by a thin insulating layer from the surrounding material within the workpiece. Every active cutting edge or bond ridge destroys the insulating layer and creates a thermocouple junction through plastic deformation. This leads to the emission of a measurable thermoelectric voltage signal from which a corresponding temperature can be established. Therefore, the material has to be electrically conductive and sufficiently ductile. Hence, this process cannot be applied to ceramics [Shaw and Komanduri 1977]. A contact resistance measurement can be applied for diamond and cubic boron nitride (CBN) grinding wheels with an electrically conducting bond for the purpose of distinguishing between active cutting edges and active bond ridges [Kaiser 1977].

### 3.3.10 PHOTOELECTRIC METHOD

Photoelectric methods according to the scattered light principle are based on light reflected by the cutting area and collected using a radiation detector. In this method, the scattered light distribution and the duration and number of light impulses in the direction of the regular direct reflection are evaluated [Werner 1994].

### 3.3.11 MIRROR WORKPIECE METHOD

The topography of the grinding wheel can be depicted in a control workpiece. For this purpose, a mirroring workpiece angled diagonally to the grinding direction is ground once. Counting the scratch marks, a conclusion can be drawn to the number of active cutting edges per unit surface area. Since the scratch marks of successive cutting edges might overlap each other, it is not possible to determine the overall number of engaged cutting edges [Shaw and Komanduri 1977, Verkerk 1977].

### 3.3.12 WORKPIECE PENETRATION METHOD

A further method is the penetration of a thin steel plate or a stationary workpiece by the effective area of the grinding wheel. The roughness profile of the ground test piece results from the overlapping of the profiles of the cutting edges active in the removal process. The roughnesses of the test pieces are called specific surface roughness,  $R_{ts}$ , end surface roughness,  $R_{taus}$ , or effective surface roughness,  $R_{tw}$  [Karatzoglu 1973, Saljé 1975, Fruehling 1976, Weinert 1976, Jacobs 1980,

Gaertner 1982, Rohde 1985, Stukenholz 1988]. These processes are suitable for a comparative assessment of the cutting edge topographies. It is, however, not possible to make any statements on the shape and number of cutting edges [Lortz 1975, Werner 1994].

### 3.4 KINEMATICS OF THE CUTTING EDGE ENGAGEMENT

In order to compare a variety of grinding processes, it is necessary to define general and comparable process parameters. With these parameters, different processes can be compared with each other allowing an efficient optimization of the process. The most important grinding parameters are the geometric contact length,  $l_g$ , chip length,  $l_{cu}$ , and the chip thickness,  $h_{cu}$ .

The kinematics and the contact conditions of different grinding processes are represented in Figure 3.5. They constitute the basis of many process parameters.

Neglecting the elastic deformation of the active partners of the grinding process, the grinding wheel penetrates the workpiece with the real depth of cut,  $a_e$ . The arc contact length is defined by the geometric contact length,  $l_g$ :

$$l_g = \sqrt{a_e \cdot d_{eq}} \quad (3.1)$$

For the same depth of cut values, different contact lengths result in the case of cylindrical and surface grinding. The equivalent wheel diameter  $d_{eq}$  is a calculation method of representing geometric contact length independent of the grinding process, where

$$d_{eq} = \frac{d_w \cdot d_s}{d_w + d_s} \quad (3.2)$$

applies to the equivalent grinding wheel diameter in external cylindrical grinding. In the case of internal cylindrical grinding, the equivalent grinding wheel diameter is:

$$d_{eq} = \frac{d_w \cdot d_s}{d_w - d_s} \quad (3.3)$$

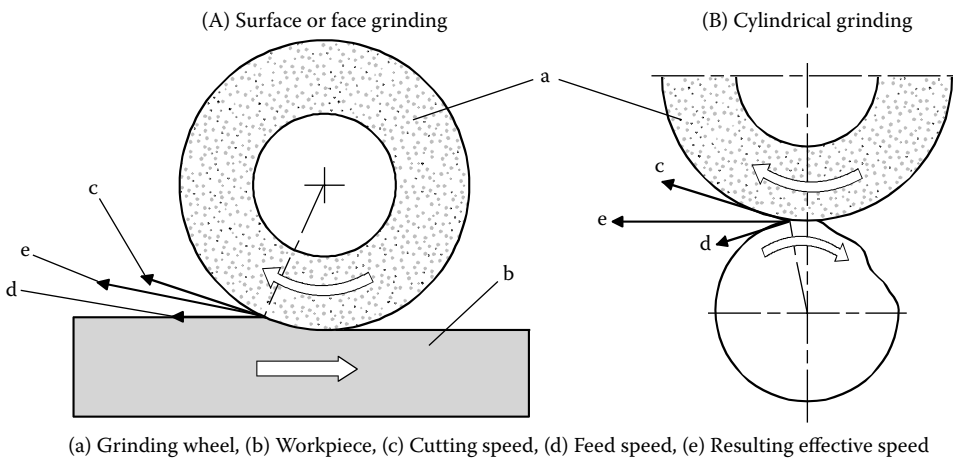


FIGURE 3.5 Contact conditions for different peripheral grinding processes.

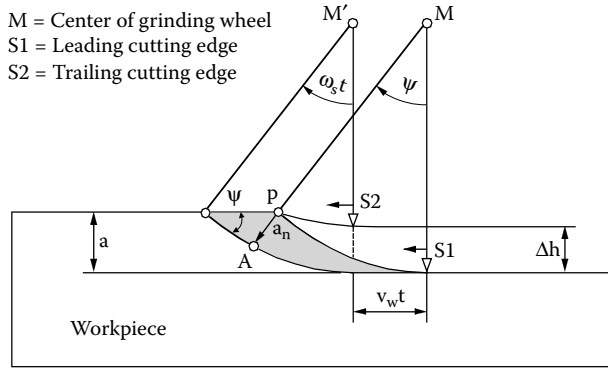


FIGURE 3.6 Contact conditions for two cutting edges.

The equivalent grinding wheel diameter  $d_{eq}$  indicates the diameter of the grinding wheel, which has the same contact length in surface grinding. Thus, the equivalent grinding wheel diameter corresponds to the actual grinding wheel diameter in surface grinding.

The movement of the wheel relative to the workpiece is put in related to the speed quotient  $q$ . In up-grinding, it is negative:

$$q = \pm \frac{v_s}{v_f} \tag{3.4}$$

In peripheral grinding with rotating grinding tools, the cutting edges move on orthocycloidal paths due to the interference of the speed components.

Figure 3.6 demonstrates the paths of two successive cutting edges. Both points have the same radial distance from the wheel center. The path the center travels between the two engagements of the wheel results from the feed movement and the time required.

The cutting edge engagement and the resulting uncut chip parameters depend on the statistical average of the cutting edges distributed on the grinding tool. The equation

$$h_{cu} = k \left[ \frac{l}{C_1} \right]^\alpha \left[ \frac{v_f}{v_c} \right]^\beta \left[ \frac{a_e}{d_{eq}} \right]^\gamma \tag{3.5}$$

relates the maximum uncut chip thickness  $h_{cu}$  to the cutting edge distribution, the grinding parameters, and the geometric values [Kassen 1969]. The mean maximum uncut chip cross-sectional area  $\bar{Q}_{max}$  is a further characteristic parameter of the grinding process. Like the maximum uncut chip thickness  $h_{cu}$ , it depends on the parameters, the cutting edge distribution, and the geometry of the active partners of the grinding process. The mean maximum uncut chip cross-sectional area  $\bar{Q}_{max}$  is calculated from

$$\bar{Q}_{max} = \frac{2}{A_N} (C_1)^{-\beta} \left( \frac{v_f}{v_c} \right)^{1-\alpha} \left( \frac{a_e}{d_{eq}} \right)^{1-\frac{\alpha}{2}} \tag{3.6}$$

On the basis of these values, a theoretical assessment can be made of the grinding process. There is a direct relation between the cutting parameters and the resulting surface quality. Equations (3.5) and (3.6) lead to the conclusion that the surface quality improves with increasing cutting velocity and grinding wheel diameter. With increasing feed speed and higher depth of cut, however, the surface quality decreases.

The value of the uncut chip parameters, however, are only applicable to a real grinding process to a limited extent, since the kinematic relations were only derived for idealized engagement conditions [Marinescu et al. 2004]. The cutting process is not a simple geometric process; there are also plastic and elastoplastic processes in real grinding so that chip formation is different from the geometric theory. It is for this reason that experiments are indispensable to gain knowledge and understanding about the material removal mechanisms.

## 3.5 FUNDAMENTAL REMOVAL MECHANISMS

### 3.5.1 MICROFLOWING, CHIPPING, AND BREAKING

The removal process during the engagement of an abrasive cutting edge on the surface of a workpiece mainly depends on the physical properties between the active partners. A basic distinction can be made between three different mechanisms: microflowing, microchipping, and microbreaking (Figure 3.7).

In microflowing, there is a continual plastic, or elastoplastic, material deformation toward the trace border with negligible material loss. In real processes, the simultaneous impact of several abrasive particles or the repeated impact of one abrasive particle leads to material failure at the border of the traces. Ideal microchipping provokes chip formation. The chip volume equals the volume of the evolving trace. Microflowing and microchipping mainly occur during the machining of ductile materials. The relation between microflowing and microcutting basically depends on the prevailing conditions such as the matching of the active partners of the grinding process, grinding parameters, and cutting edge geometry.

Microbreaking occurs in case of crack formation and spreading. The volume of a chip removed can be several times higher than the volume of the trace. Microbreaking mostly occurs during the machining of brittle-hard materials such as glass, ceramics, and silicon.

Hence, the mechanisms of surface formation during grinding consist of these three basic processes. Which of them predominates strongly depends on the workpiece material. Therefore, material removal mechanisms will be presented in Section 3.6 for ductile materials on one hand, and for brittle-hard materials on the other.

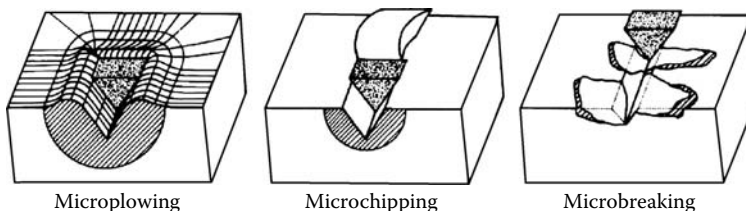


**FIGURE 3.7** Physical interaction between abrasive particles and the workpiece surface. (From Zum 1987. With permission.)

### 3.6 MATERIAL REMOVAL IN GRINDING OF DUCTILE MATERIALS

During grinding, the cutting edge of the grain penetrates the workpiece on a very flat path causing plastic flow of the material after a very short phase of elastic deformation. Since the angle between cutting edge contour and workpiece surface is very small due to the cutting edge rounding, no chip is formed initially. The workpiece material is only thrust aside, forms material outbursts or side ridges, and flows to the flank underneath the cutting edge [Koenig and Klocke 1996]. Figure 3.8 shows the chip formation during grinding of ductile materials.

Only if the cutting edge penetrates the workpiece to a depth that the undeformed chip thickness,  $h_{cu}$ , equals the so-called critical cutting depth,  $T_{\mu}$ , does the actual chip formation begin. Since displacement processes and chip formation occur simultaneously in the further process, it is crucial for the efficiency of the material removal how much of the uncut chip thickness,  $h_{cu}$ , is actually removed as chip, and what the effective chip thickness,  $h_{cueff}$ , is.

Grof [1977] has further differentiated the chip formation process during the machining of ductile materials with high cutting velocities. On the basis of experiments, he determined altogether six phases of singular chip formation during grinding (Figure 3.9). In the first quarter of the contact length (phase 1), the engaging abrasive grain first makes a groove, causing plastic and elastic deformation in the material, which is then thrust aside from the groove. The surface is presumed to consolidate during this contact phase [Werner 1971] without chip formation.

Through the further advance of the cutting edge (phase 2), a flow chip is removed with a nearly parallelogram-shaped cross section. This chip is compressed and bent in dependence of the pore space. Due to the large point angle of a cutting edge, the chip is very flat and offers a big surface for heat discharge through radiation and convection. In case of small infeeds or feeds, the working contact ends in the third phase, forming almost exclusively thread-shaped chips.

In case of large infeeds and feeds, the cutting edge penetrates the material deeper. This leads to a distinctive shear zone at approximately three fourths of the maximum engagement length resulting in strong heat development (phase 3). The strong material accumulation through the high pressure causes an increase of the contact zone temperature. Due to the small effective surface of the cooling lubricant, this heat cannot be discharged. This leads to a melting of the formed chip above the plastic state.

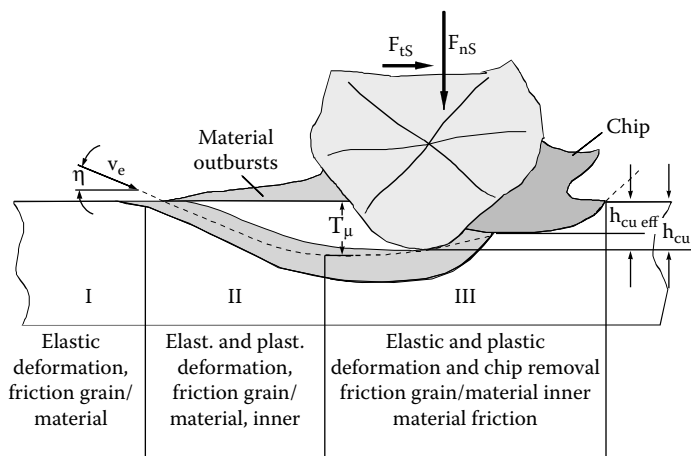
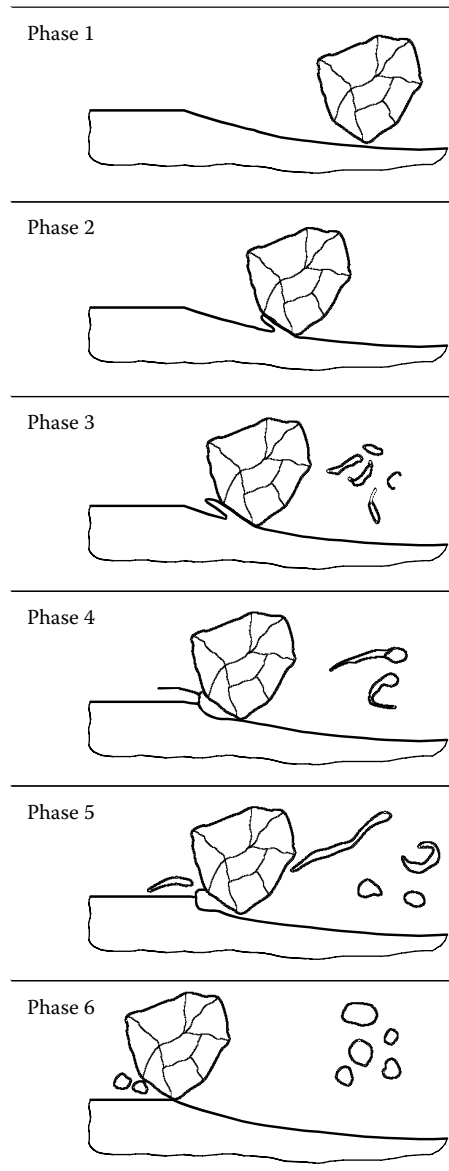


FIGURE 3.8 Removal process during the machining of ductile materials. (From Koenig and Klocke 1996. With permission.)



**FIGURE 3.9** Removal process during the machining with high cutting speeds. (From Grof 1977. With permission.)

If the cutting edge engagement is terminated in this phase, tadpole-shaped chips are formed (phase 4). If the engagement takes place along the entire contact length, the whole material is liquefied in the pore space after the thread-shaped chip falls off (phase 5).

Due to the surface tension, the molten chip becomes spherical after leaving the contact surface. This takes place in a zone where there is none or only a small amount of cooling lubricant (phase 6). The fact of sphere formation has been observed by other researchers as well [Hughes 1974, Marinescu et al. 2004].

A further model of cutting edge engagement has been presented by Stephens [1983]. The cutting edge engagement can be ideally considered as an even-yielding process. In this model, the contact zone is divided into layers that are arranged parallel to the movement axis. The material starts



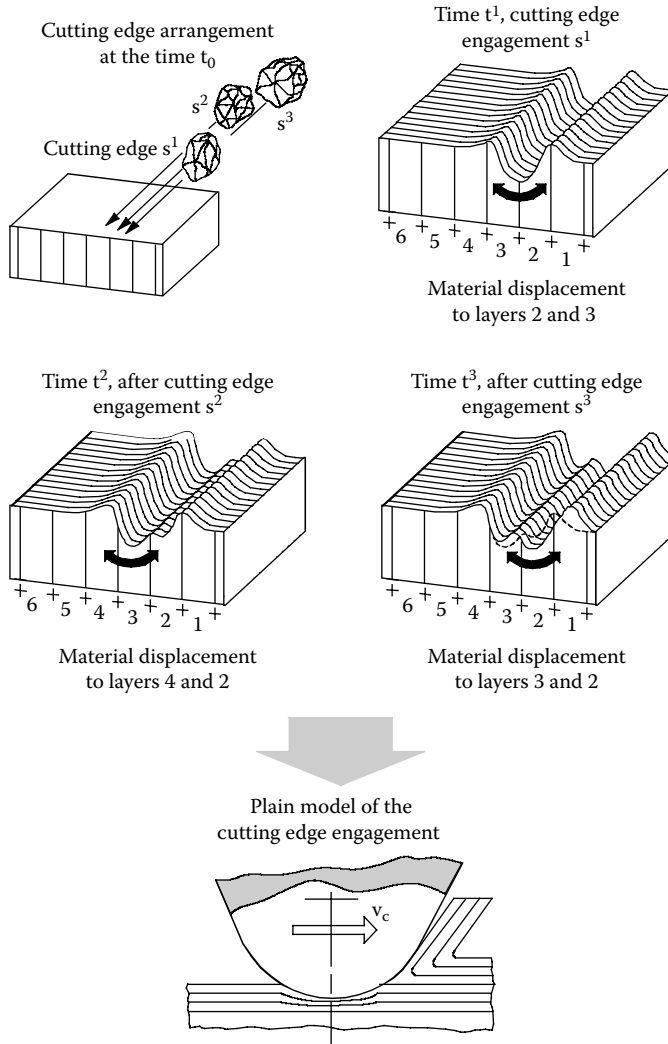


**FIGURE 3.10** Idealization of the cutting edge engagement through plain yielding. (From Steffens 1983. With permission.)

to yield in different directions at the cutting edge engagement. Thus, the individual layers are thrust aside at the point of engagement of the first cutting edge. When successive cutting edges engage, these areas are removed or thrust aside anew. Through these processes, the number of kinematic cutting edges increases partially in a subarea. Since these changes are statistically distributed to the whole surface, there is overall no material accumulation.

The description shown in Figure 3.10 can serve as a model for the alternative description of a layer as an interaction of all displacement processes. A further prerequisite for the application of slip line theory is the knowledge of the rheological properties of the material, which is supposed to be inelastic ideal plastic.

On the basis of these theoretical considerations and experimental investigations, statements can be made on the friction conditions, which are decisively influenced by the lubrication [Koenig, Steffens, and Yegenoglu 1981, Steffens 1983, Vits 1985]. If the friction is increased, the critical cutting depth decreases, which is additionally influenced by the radius of the cutting edge of the

grain [Koenig et al. 1981, Steffens 1983]. Improved lubrication increases the plastic deformation toward a higher critical cutting depth. Thus, there is a reduction of friction between the active partners. With constant uncut chip thickness,  $h_{cu}$ , the effective chip thickness,  $h_{c_{eff}}$  (thickness of the formed chip), decreases simultaneously with a reduction of friction [Steffens 1983, Vits 1985].

### 3.7 SURFACE FORMATION IN GRINDING OF BRITTLE-HARD MATERIALS

#### 3.7.1 INDENTATION TESTS

Fundamental mechanisms of crack formation and spreading in the case of brittle-hard materials were carried out by Lawn and Wilshaw [1975]. The stressing of a ceramic surface with a cutting edge causes hydrostatic compression stress around a core area in the subsurface of the workpiece. This leads to a plastic deformation of the material (Figure 3.11a). If a certain boundary stress is exceeded, a radial crack develops below the plastically deformed zone (Figure 3.11b), which expands with increasing stress (Figure 3.11c).

After discharge, the radial crack closes in the initial phase (Figure 3.11d). During a further reduction of the stress state, axial stresses occur around the plastically deformed zone leading to lateral cracks below the surface (Figure 3.11e). The lateral cracks grow with decreasing stress. This growth can continue up to the surface of the material after complete discharge (Figure 3.11f) leading to the break-off of material particles, which form a slab around the indentation zone [Lawn and Wilshaw 1975].

#### 3.7.2 SCRATCH AND GRINDING BEHAVIOR OF BRITTLE-HARD MATERIALS

Despite the low ductility, elastoplastic deformations occur as removal mechanisms alongside brittle fracture during the grinding of brittle-hard materials (Figure 3.12). Thereby, material removal through brittle fracture is based on the induction of microcracks. Ductile behavior of brittle-hard materials during grinding can be derived from the presumption that, below a threshold of boundary chip thickness defined by a critical stress, the converted energy is insufficient for crack formation and the material is plastically deformed [Bifano et al. 1987, Komanduri and Ramamohan 1994]. It is supposed, however, that cracks that do not reach the surface are also formed under these conditions.

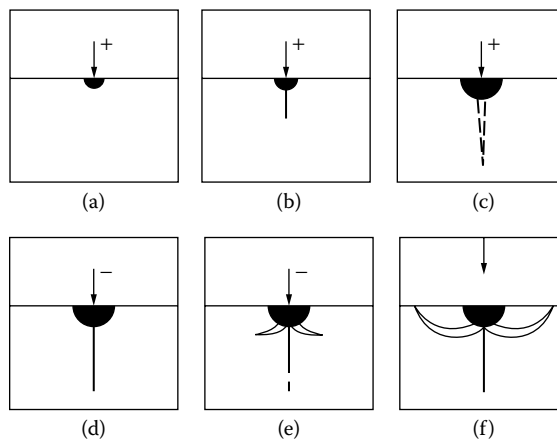


**FIGURE 3.11** Mechanisms of crack spread in case of punctual stress. (From Lawn and Wilshaw 1975. With permission.)

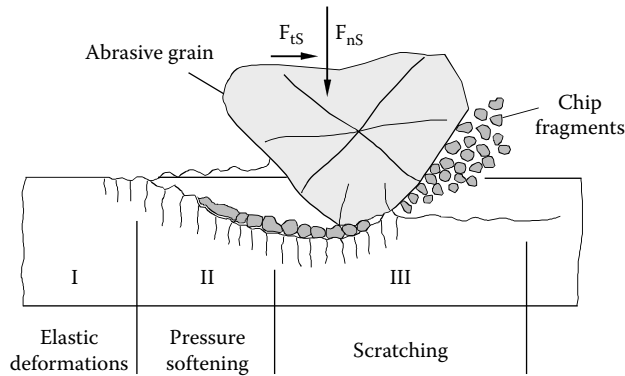


**FIGURE 3.12** Material removal process in machining of brittle-hard materials. (From Saljé and Moehlen 1987. With permission.)

Thus, not only the amount of stress, defined by the uncut chip thickness, is responsible for the occurrence of plastic deformations, but also the above-mentioned hydrostatic compression stress below the cutting edge [Komanduri and Ramamohan 1994, Shaw 1995]. The transition from mainly ductile material removal to brittle friction is decisively determined by uncut chip thickness at the single grain by grain shape and by material properties. Large cutting edge radii promote plastic material behavior and shift the boundary of the commencing brittle friction to larger engagement depths. As a consequence, Hertzian contact stresses occur below the cutting edge, which cause hydrostatic stress countering the formation of cracks [Uhlmann 1994].

Roth [1995] investigated removal mechanisms during the grinding of aluminum oxide ceramics. He observed the influence of different grain sizes of the material as well as different diamond geometries on the material removal processes.

### 3.7.2.1 Fine-Grained Materials

When a scratching tool enters a fine-grained material, an entry section is formed by pure plastic deformation. The length of the entry section strongly depends on the corner radius of the diamond. If the material-specific shear stress is exceeded due to increasing scratching depth, a permanent deformation occurs thrusting aside the material and causing bulgings along the scratched groove. The base of the scratch and the flanks are even and cover a thin layer of plastically deformed material (Figure 3.13a).

Different scratches occur in the material from a critical scratch depth on with the boundary condition linked to it. Along with lateral crack systems observed during penetration tests, a median crack occurs through a succession of semi-elliptical radial cracks at the base that runs vertically to the surface in the direction of the scratch. Similar scratch structures were observed during Vickers indentation tests. Also, V-shaped cracks are formed vertically to the surface and spread. The aperture angle is between  $40^\circ$  and  $60^\circ$  and grows with the increasing distance from the scratch. Obviously, they are crack structures that develop due to the shear stress of the tangential scratching force (shear scratches). If lateral cracks grow until the V-shaped cracks extend vertically to the surface, whole material particles break off on both sides of the scratch.

### 3.7.2.2 Coarse-Grained Materials

In the case of coarse-grained materials, the removal processes take place in a different way. A sharp diamond plastically divides the grains in the structure under high energy input. With increasing infeed cracks develop mainly along the grain boundary. This is accompanied by intercrystalline failure, which leads to a break-off of grains near to the surface (Figure 3.13b).

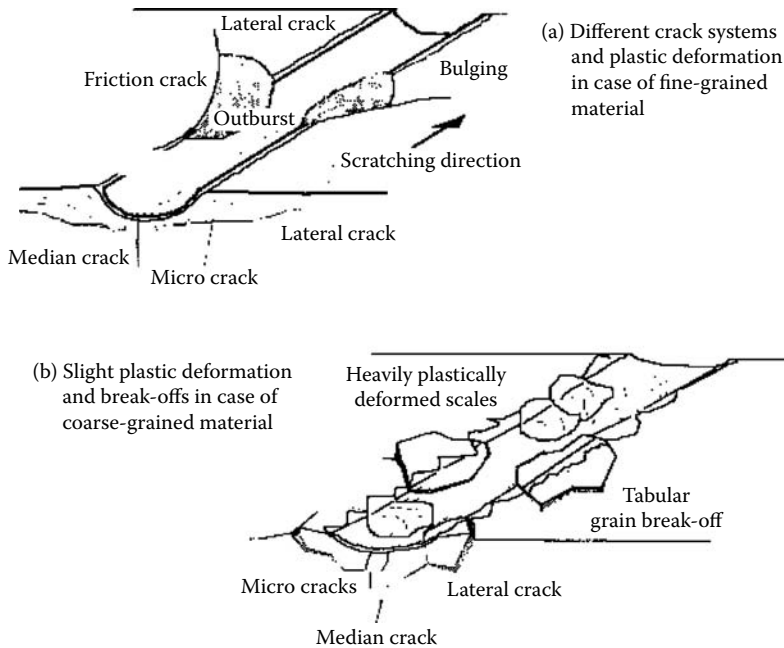


**FIGURE 3.13** Material removal mechanisms during the scratching of aluminum oxide. (From Roth 1995. With permission.)

In the case of blunt scratching grains, however, strong plastic deformations occur deeper, since the maxima of the shear stresses grow. Thin, strongly deformed flakes occur on the workpiece surface. Through the extremely negative rake angle, the material is pushed forward and “extruded,” not provoking ductile material removal. The stress increases with further growing infeed until the stability is exceeded at the grain boundaries and the top grain layer breaks off in the form of whole plates (Figure 3.13b).

On the basis of scratch tests and transmission electron microscopic (TEM) structure analyses, Uhlmann assembles the mechanisms of surface formation during ceramic grinding [Uhlmann 1994]. Surface formation can be divided into three types of mechanisms:

- Primary mechanisms, which act during the penetration of the cutting edges into the material
- Secondary mechanisms, which occur through the discharge by the first cutting edge and the multiple stress by successive cutting edges
- Tertiary mechanisms, which prevent the spread of cracks in the case of materials with a high glass phase ratio.

The individual mechanisms are summarized in Table 3.1.

These material-removal processes also occur during the machining of glass. For the industrial application of optical glass, however, the conditions must allow a ductile surface formation. Thus, the development of an extensive crack system on the surface can be prevented. Figure 3.14 summarizes the conditions for a model of ductile grinding of glass on the basis of scratch tests. According to this, a flattened blunt grain has to penetrate the material with a very small, single uncut chip thickness. The single uncut chip thickness has to be below the critical chip depth, allowing an almost crack-free surface of glass materials.

**TABLE 3.1**  
**Mechanisms of Surface Formation [Uhlmann 1994]**

<b>Surface Formation</b>	
<b>Primary Mechanisms</b>	
Mechanical Stress	Thermal Stress
Material condensation	Plastification or melting of the material or material phases
Formation of obstructions	Ductile removal of material in front of the cutting edge (chip formation)
Crack induction	
Brittle break-off of particles in front of and alongside the cutting edge (particle formation)	
<b>Secondary Mechanisms</b>	
Mechanical Stress	Thermal Stress
Break-off of particles behind and alongside the cutting edge	Crack spread through thermal stresses due to temperature gradients
Induction of deep-lying cracks	Induction of deep-lying cracks
Spread of deep-lying cracks through multiple stress of successive cutting edges	Blistering of ceramic particles after crack spread toward the workpiece surface
Break-off of particles after crack spread toward the workpiece surface	
<b>Tertiary Mechanisms</b>	
Thermal Stress	
Crack stopping effects at thermally plastified grain boundary phases	
Crack diversion at partially plastified grain boundary conditions in surface-near areas	

Monocrystal silicon is the most frequently applied substrate material in microsystems technology. The full range of physical properties of the material can only be exploited by a high degree of purity, homogeneity, and crystal perfection. However, machining wafers induce damage in the subsurface and its monocrystal structure. Therefore, the subsurface damage has to be removed by polishing and etching prior to the processing of the electronic structures on the wafer front side. A concerted implementation of ductile material removal for the grinding process represents a possibility to improve the surface and subsurface quality as well as the economic efficiency of the entire process chain for wafer production [Holz 1994, Menz 1997, Kerstan et al. 1998, Tricard et al. 1998, Lehnicke 1999, Tönshoff and Lehnicke 1999, Klocke, Gerent, and Pähler 2000].

In grinding, surface formation mechanisms can be classified as ductile and brittle mechanisms. In brittle surface formation, microcracks and microcrack spread are generated in the subsurface by tensile stresses caused by the engagement of the abrasive grains of the grinding wheel into the surface of the wafer [Cook and Pharr 1990, Lawn 1993, Holz 1994, Menz 1997, Brinksmeier et al. 1998, Lehnicke 1999, Tönshoff and Lehnicke 1999]. In ductile surface formation, the induced tensile stresses are insufficient to cause microcracks or crack propagation. The induced shear stress strength causes deformation and movement of dislocations that promote ductile material behavior (Figure 3.14). This leads to better surface qualities and smaller depths of subsurface damage [Lawn 1993, Menz 1997, Brinksmeier et al. 1998, Kerstan et al. 1998, Tönshoff and Lehnicke 1999]. However, the basic mechanisms of ductile material removal are not known. It is further controversial whether chip formation is actually taking place or whether brittle-effective mechanisms continue to cause chips, through which the grooves on the surface are covered by plastified material. In this case, the surface seems to be formed in a ductile mode. The subsurface below would nevertheless be severely damaged by microcracks.

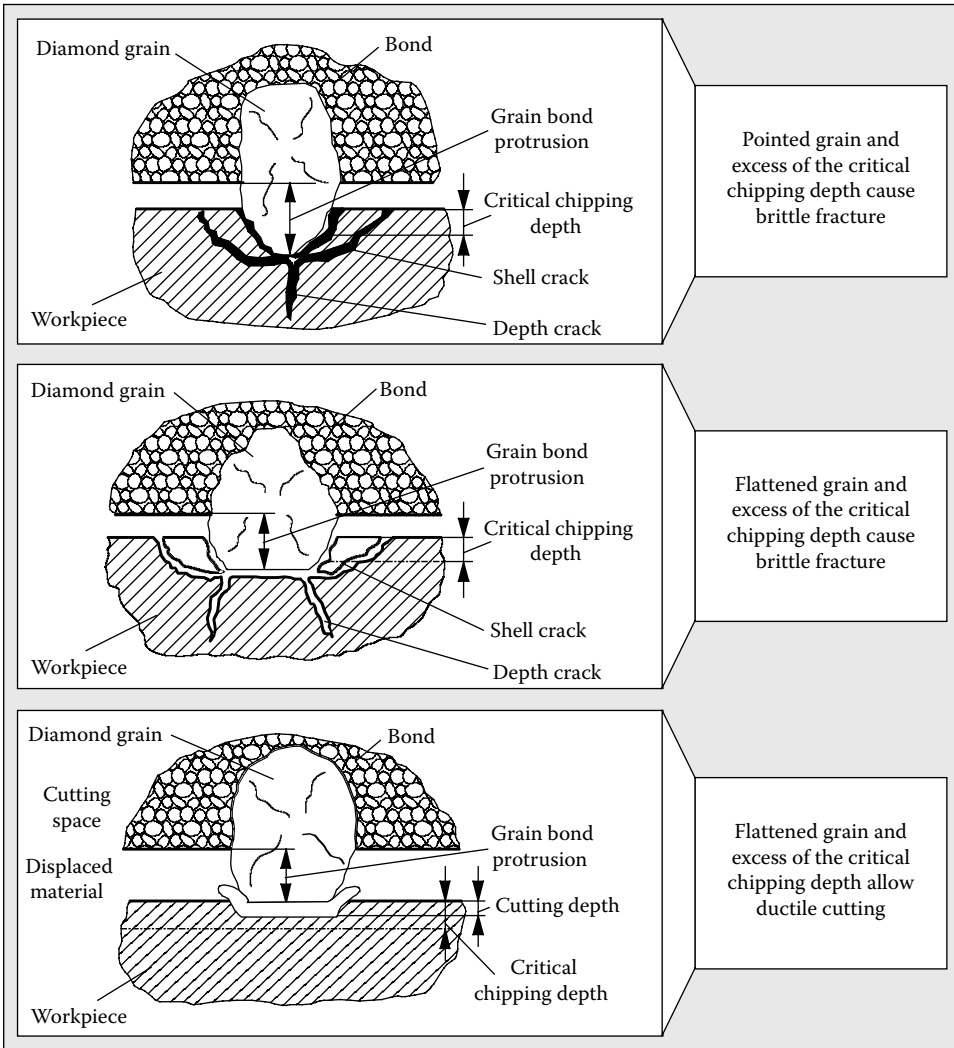


**FIGURE 3.14** Theoretical prerequisites for ductile grinding of optical glass. (From Koch 1991. With permission.)

The mode, size, and shape of the subsurface microcrack system depend on the induced contact stresses during the engagement of the abrasive grain. The contact stress field is basically determined by the geometry of the indenter and the modulus of elasticity, hardness, and fracture toughness of the indenter and the workpiece material [Lawn 1993]. In the case of monocrystal silicon as workpiece material, the anisotropy of these properties, as well as the position of the slip system, is also decisive. The formation of such microcrack systems was frequently investigated in analogy tests with several brittle-hard materials such as silicon [Cook and Pharr 1990, Holz 1994].

The transition of elastoductile to mainly brittle surface formation can be classified into four different scratching morphologies (Figure 3.15). The individual areas of the scratches were identified and marked under the microscope. To provide a three-dimensional image, the transition areas between the areas of different scratch morphologies were measured at a length of 1 mm. Then the scratch depths were determined on the individual profiles.

Knowing the material removal mechanisms during the machining of silicon, it is possible to realize a damage-poor process with the adequate settings and tools during the grinding of semiconductors.

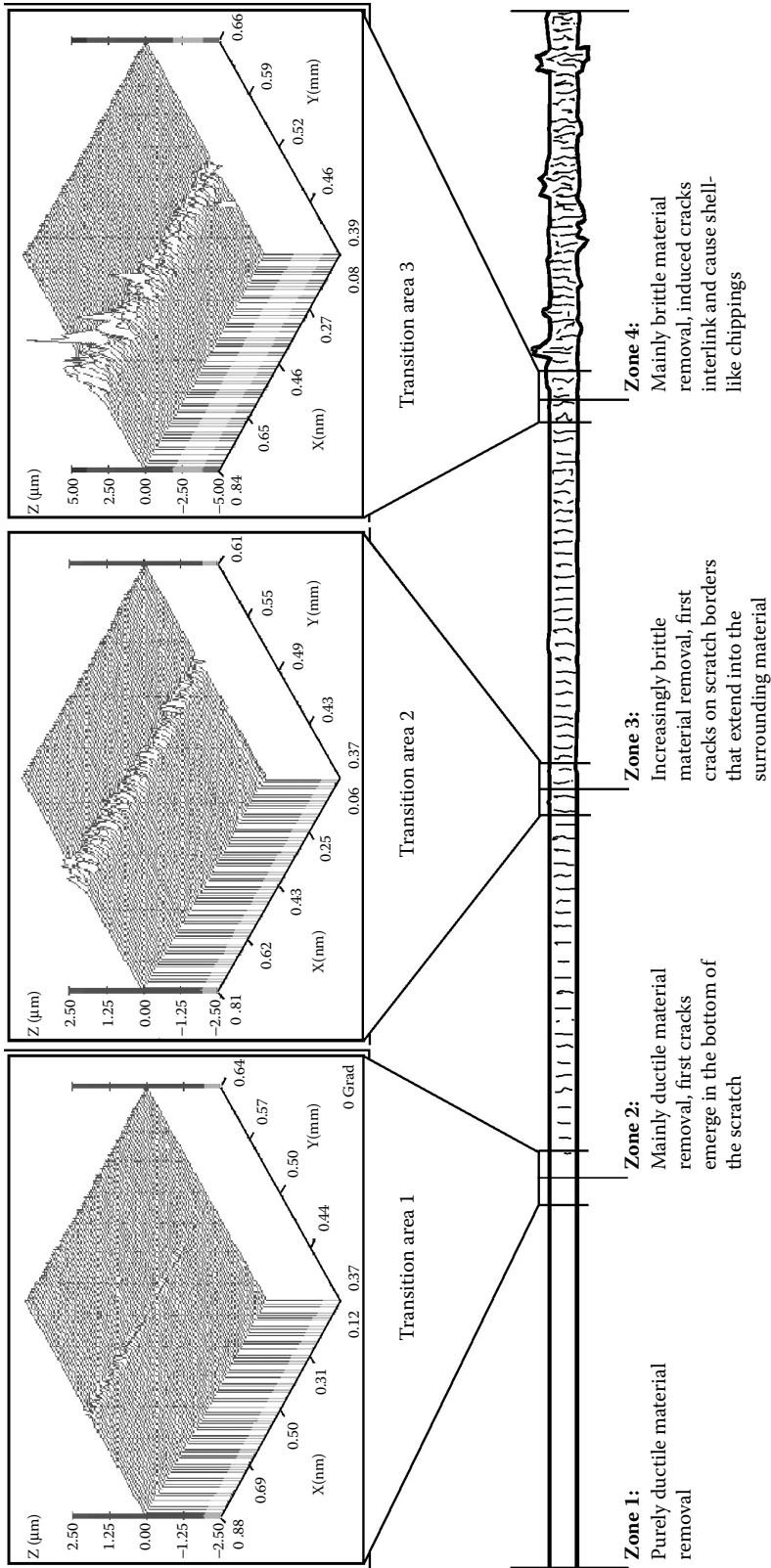


**FIGURE 3.15** Classification of scratch marks in four morphological zones and three transition areas characterizing the change from purely ductile to mainly brittle surface formation.

This damage-poor grinding process is necessary to shorten the whole process chain and to decrease machining costs.

### 3.8 ENERGY TRANSFORMATION

Mechanical energy is introduced into the grinding process by relative movement between the tool and the workpiece (Figure 3.16). This energy is mainly transformed into heat in an energy transformation process, leading to temperature increase in the contact zone. The transformation of mechanical energy into thermal energy takes place through friction and deformation processes [Grof 1977, Lowin 1980]. External friction processes between abrasive grain and workpiece surface as well as between chip and abrasive grain are partly responsible for the heat development during grinding. However, heat also develops as a result of internal friction through displacement processes and plastic deformations [Grof 1977, Lowin 1980, Marinescu et al. 2004].

Heat development and heat flow during the grinding of brittle-hard materials differ decisively from the process in the machining of ductile materials (Figure 3.17). Heat development in the case of ceramics has been investigated in many studies. Due to the relatively poor heat conductivity of ceramics and, in contrast, to a very high heat conductivity of diamond as a grinding agent, a big percentage of the heat flow to the tool and a considerably smaller heat flow to the workpiece was observed [Wobker 1992, Uhlmann 1994].

The following energy transformation processes occur during the grinding of ceramics [Uhlmann 1994]:

- Energy from retained dislocations (plastic surface areas) after particle removal
- Deformation energy at the workpiece surface (plastic scratch marks with a bulging at the edge)
- Elastic excess energy from the extension of existing microcracks during particle removal
- Elastic energy from microscopic surface areas returning in the initial position
- Friction work between diamond cutting edge and workpiece surface

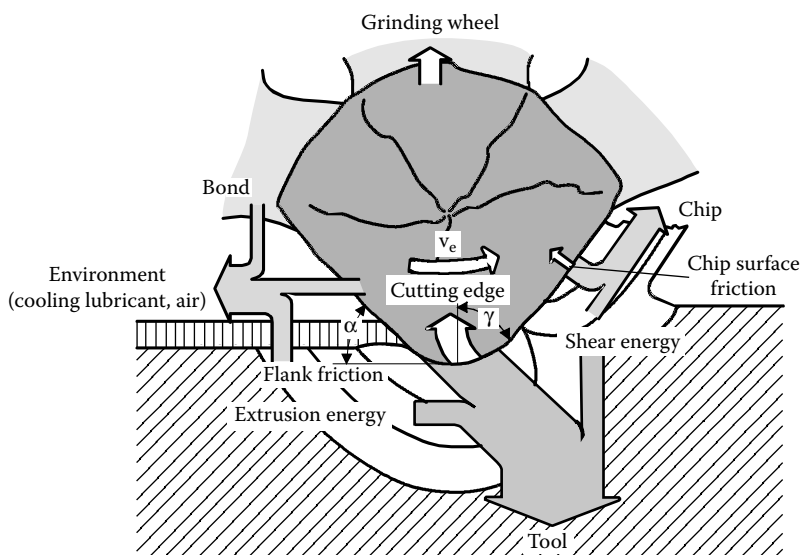


FIGURE 3.16 Heat flow during the grinding of metallic materials. (From Koenig and Klocke 1996. With permission.)



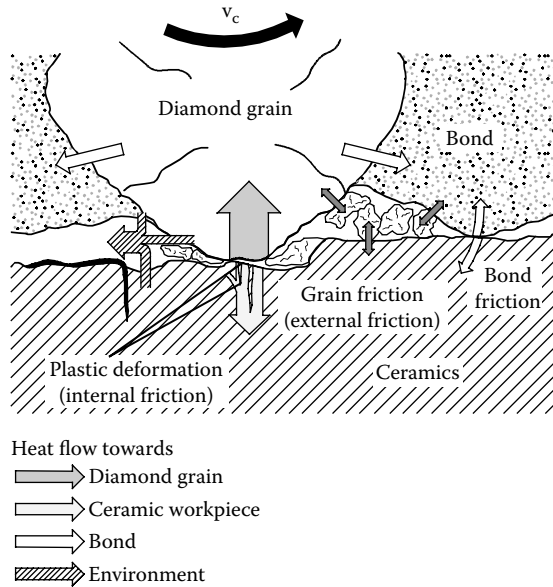


FIGURE 3.17 Heat flow during the grinding of ceramics. (From Uhlmann 1994. With permission.)

- Friction work between ceramic particles (workpiece surface as well as ceramic particles) and diamond cutting edge
- Friction work between bond and workpiece surface

The use of cooling lubricant influences the heat development and the heat flow. The lubricant reduces the friction between the active partners entailing smaller heat development. The cooling mainly takes place through the water ratio in the cooling lubricant. Through the cooling effect, the percentage of conducted heat increases.

## REFERENCES

- Bifano, T. et al. 1987. "Precision Machining of Ceramic Materials, Vortrag anläßl." Intersociety Symposium on Machining of Advanced Ceramic Materials and Components, Westerville, OH.
- Bohlheim, W. 1995. "Verfahren zur Charakterisierung der Topografie von Diamantschleifscheiben." *IDR* 29, 2.
- Bouzakis, K.-D. and Karachaliou, C. 1988. "Erfassung der Spanungsgeometrie und der Zerspankraftkomponenten beim Flachsleifen aufgrund einer Dreidimensionalen Beschreibung der Schleifscheibentopographie." *Fortschr.-Ber. VDI Reihe 2 Nr. 165*, VDI, Düsseldorf.
- Brinksmeier, E., Preuß, W., Riemer, O., and Malz, R. 1988. "Ductile to Brittle Transition Investigated by Plunge-Cut Experiments in Monocrystalline Silicon." *Proceedings of the ASPE Spring Topical Meeting on Silicon Machining*.
- Bruecher, T. 1996. "Kühlschmierung beim Schleifen keramischer Werkstoffe." Ph.D. dissertation, Technische Universität, Berlin.
- Buettner, A. 1968. "Das Schleifen sprödharter Werkstoffe mit Diamant-Topfscheiben unter besonderer Berücksichtigung des Tiefschleifens." Dr. Ing. dissertation, Technische Universität, Hannover.
- Cook, R. F. and Pharr, G. M. 1990. "Direct Observation and Analysis of Indentation Cracking in Glasses and Ceramics." *J. Am. Ceram. Soc.* 73, 4.
- Damlos, H.-H. 1985. "Prozessablauf und Schleifergebnisse beim Tief- und Pendelschleifen von Profilen." *Fortschr.-Ber. VDI, Reihe 2, Nr. 88*, VDI-Verlag, Düsseldorf.
- Daude, O. 1966. *Untersuchung des Schleifprozesses*. Dr. Ing. dissertation, RWTH, Aachen.

- Dennis, P. and van Schmieden, W. 1989. "Abdruckverfahren zur Dokumentation von Verschleißvorgängen." VDI-Z 131, 1, S. 72–75.
- Fruehling, R. 1976. "Topographische Gestalt des Schleifscheiben-Schneidenraumes und Werkstückrauhtiefe beim Außenrund-Einsteichschleifen." Dr. Ing. dissertation, TU Braunschweig.
- Gaertner, W. 1982. "Untersuchungen zum Abrichten von Diamant- und Bornitridschleifscheiben." Dr. Ing. dissertation, Technische Universität Hannover.
- Grof, H. E. 1977. "Beitrag zur Klärung des Trennvorgangs beim Schleifen von Metallen." Dr. Ing. dissertation, TU München.
- Holz, B. 1994. "Oberflächenqualität und Randzonenbeeinflussung beim Planschleifen einkristalliner Siliciumscheiben." Produktionstechnik – Berlin, Forschungsberichte für die Praxis, Bd. 143, Hrsg.: Prof. Dr. H. C. Mult. Dr. Ing, G. Spur. München, Wien, Hanser.
- Hughes, F. H. 1974. "Wärme im Schleifprozess – ein Vergleich zwischen Diamant- und konventionellen Schleifmitteln." *IDR* 8, 2.
- Inasaki, C., Chen, C., and Jung, Y. 1989. "Surface, Cylindrical and Internal Grinding of Advanced Ceramics. Grinding Fundamentals and Applications." *Trans. ASME* 39, S. 201–211.
- Jacobs, U. 1980. "Beitrag zum Einsatz von Schleifscheiben mit kubisch-kristallinem Bornitrid als Schneidstoff." Dr. Ing. dissertation, TU Braunschweig.
- Kaiser, M. 1977. "Tiefschleifen von Hartmetall." *Fertigungstechnische Berichte*, Bd. 9, Hrsg.: H. K. Tönshoff, Gräfelfing, Resch.
- Karatzoglou, K. 1973. "Auswirkungen der Schneidflächenbeschaffenheit und der Einstellbedingungen auf das Schleifergebnis beim Flach-Einsteichschleifen." Dr. Ing. dissertation, TU Braunschweig.
- Kassen, G. 1969. "Beschreibung der elementaren Kinematik des Schleifvorganges." Dissertation, RWTH, Aachen.
- Kerstan, M., Ehlert, A., Huber, A., Helmreich, D., Beinert, J., and Doell, W. 1998. "Ultraprecision Grinding and Single Point Diamond Turning of Silicon Wafers and Their Characterisation." *Proceedings of the ASPE Spring Topical Meeting on Silicon Machining, Camel-by-the-Sea, CA*.
- Klocke, F., Gerent, O., and Pähler, D. 2000. "Effiziente Prozesskette zur Waferfertigung." *ZwF* 95, 3.
- Koch, E. N. 1991. "Technologie zum Schleifen asphärischer optischer Linsen." Dissertation, RWTH, Aachen.
- Koenig, W., Steffens, K., and Yegenoglu, K. 1981. "Modellversuche zur Erfassung der Wechselwirkung zwischen Reibbedingungen und Stofffluss." *Industrie Anzeiger*. 103, 35.
- Koenig, W. and Klocke, F. 1996. *Fertigungsverfahren Band 2. Schleifen, Honen, Läppen*. 3. Auflage, VDI-Verlag GmbH, Düsseldorf.
- Komanduri, R. and Ramamohan, T. R. 1994. "On the Mechanisms of Material Removal in Fine Grinding and Polishing of Advanced Ceramics and Glasses, in *Advancement of Intelligence Production*. The Japan Society for Precision Engineering, Elsevier Science, Amsterdam.
- Kurrein, M. 1927. "Die Bearbeitbarkeit der Metalle im Zusammenhang mit der Festigkeitsprüfung." *Werkstattstechnik*. 21, S. 612–621.
- Lawn, B. and Wilshaw, R. 1975. "Review Indentation Fracture: Principles and Applications." *J. Mat. Sci.* 10.
- Lawn, B. 1993. *Fracture of Brittle Solids*, 2nd ed., Cambridge University Press, New York.
- Lehnicke, S. 1999. *Rotationsschleifen von Silizium-Wafern*. Fortschritt-Berichte VDI, Reihe 2, Nr. 534, VDI-Verlag, Düsseldorf.
- Lierath, F., Jankowski, R., Schneckel, S., and Bage, T. 1990. "Prozessmodelle zur Qualitätssteigerung von Arbeitssabläufen in der Feinbearbeitung." Tagungsband zum 6. Intern. Braunschweiger Feinbearbeitungskolloquium.
- Lortz, W. 1975. "Schleifscheibentopographie und Spanbildungsmechanismus beim Schleifen." Dr. Ing. dissertation, RWTH, Aachen.
- Lowin, R. 1980. "Schleiftemperaturen und ihre Auswirkungen im Werkstück." Dissertation, RWTH, Aachen.
- Malyshev, V., Levin, B., and Kovalev, A. 1990. *Grinding with Ultrasonic Cleaning and Dressing of Abrasive Wheels*. 61, 9, Stanki I Instrument, Moscow 22–26.
- Marinescu, I. D., Rowe, W. B., Dimitrov, B., and Inasaki, I. 2004. *Tribology of Abrasive Machining Processes*. William Andrew Publishing, Norwich, NY.
- Menz, C. 1997. *Randzonenanalyse bearbeiteter Siliziumoberflächen*. Fortschritt-Berichte VDI, Reihe 2, Nr. 431, VDI-Verlag, Düsseldorf.
- Nakayama, K. 1973. "Taper Print Method for the Measurement of Grinding Wheel Surface." *Bull. Japan Soc. Prec. Eng.* 7, 2.
- Pahlitzsch, G. and Helmerdig, H. 1943. "Bestimmung und Bedeutung der Spandicke beim Schleifen." *Werkstattstechnik*. 11/12, S. 397–399.

- Paulmann, R. 1990. "Grundlagen zu einem Verfahrensvergleich." *Jahrbuch Schleifen, Honen, Läppen und Polieren*. 56, Ausgabe, Vulkann-Verlag, Essen.
- Reichenbach, G. S., Mayer, I. E., Kalpakcioglu, S., and Shaw, M. C. 1956. "The Role of Chip Thickness in Grinding." *Trans. ASME* 18, S, 847–850.
- Rohde, G. 1985. "Beitrag zum Verhalten von keramisch-gebundenen Schleifscheiben im Abricht- und Schleifprozess." Dr. Ing. dissertation, TU Braunschweig.
- Roth, P. 1995. *Abtrennmechanismen beim Schleifen von Aluminiumoxidkeramik*. Fortschr.-Ber. VDI, Reihe 2, Nr. 335, VDI-Verlag, Düsseldorf.
- Saljé, E. 1975. "Die Wirkrautiefe als Kenngröße des Schleifprozesses." *Jahrbuch der Schleif-, Hon-, Läpp- und Poliertechnik und der Oberflächenbearbeitung*, 47, Ausgabe, Vulkan, Essen, S, 23–35.
- Saljé, E. and Moehlen, H. 1987. "Prozessoptimierung beim Schleifen keramischer Werkstoffe, Industrie Diamanten Rundschau." *IDR* 21, 4.
- Sawluk, W. 1964. "Flachschleifen von oxydkeramischen Werkstoffen mit Diamant-Topfscheiben." Dissertation, Technische Hochschule Braunschweig.
- Schleich, H. 1982. "Schärfen von Bornitridschleifscheiben." Dr. Ing. dissertation, RWTH, Aachen.
- Shaw, M. C. and Komanduri, R. 1977. "The Role of Stylus Curvature in Grinding Wheel Surface Characterization." *Ann. CIRP* 25, 1.
- Shaw, M. C. 1995. "Cutting and Grinding of Difficult Materials." Technical paper presented at the Abrasive Engineering Society, Ceramic Industry Manufacturing Conference and Exposition, Pittsburgh, PA.
- Steffens, K. 1983. *Thermomechanik des Schleifens*. Fortschr.-Ber. VDI, Reihe 2, Nr. 65, VDI-Verlag, Düsseldorf.
- Stuckenholz, B. 1988. "Das Abrichten von CBN-Schleifscheiben mit kleinen Abrichtzustellungen." Dr. Ing. dissertation, RWTH, Aachen.
- Toenshoff, H. K., Peters, J., Inasaki, I., and Paul, T. 1992. "Modelling and Simulation of Grinding Processes." *Ann. CIRP* 41, 2, 677–688.
- Tönshoff, H. K. and Lehnicke, S. 1999. "Subsurface Damage Reduction of Ground Silicon Wafers." Proceedings of Euspen, Bremen, Germany.
- Treffert, C. 1995. "Hochgeschwindigkeitsschleifen mit galvanisch gebundenen CBN-Schleifscheiben." Berichte aus der Produktionstechnik, Bd. 4/95, Aachen, Shaker.
- Tricard, M., Kassir, S., Herron, P., and Pei, Z. J. 1998. "New Abrasive Trends in Manufacturing of Silicon Wafers." Proceedings of the ASPE Annual Meeting, Indianapolis, IN.
- Uhlmann, E. 1994. "Tiefschleifen hochfester keramischer Werkstoffe." *Produktionstech—Berlin, Forschungsber für die Praxis*, Bd. 129, Hrsg.: Prof. Dr. H. C. Mult. Dr. Ing. G. Spur, München, Wien, Hanser.
- Verkerk, J. 1977. "Final Report Concerning CIRP Cooperative Work on the Characterization of Grinding Wheel Topography." *Ann. CIRP* 26, 2.
- Vits, R. 1985. "Technologische Aspekte der Kühlschmierung beim Schleifen." Dr. Ing. dissertation, RWTH, Aachen.
- Warnecke, G. and Spiegel, P. 1990. "Abrichten kunstharzgebundener CBN- und Diamantschleifscheiben." *IDR* 24, 4, S, 229–235.
- Weinert, K. 1976. "Die zeitliche Änderung des Schleifscheibenzustandes beim Außenrund-Einsteichschleifen." Dr. Ing. dissertation, TU Braunschweig.
- Werner, F. 1994. *Hochgeschwindigkeitstriangulation zur Verschleißdiagnose an Schleifwerkzeugen*. Fortschr.-Ber. VDI, Reihe 8, Nr. 429, VDI-Verlag, Düsseldorf.
- Werner, G. 1971. "Kinematik und Mechanik des Schleifprozesses." Dissertation RWTH, Aachen.
- Werner, G. and Kenter, M. 1987. "Work Material Removal and Wheel Wear Mechanisms in Grinding of Polycrystalline Diamond Compacts." Vortrag anläßl. Intersociety Symposium on Machining of Advanced Ceramic Materials and Components, Westerville, OH.
- Wobker, H. G. 1992. *Schleifen keramischer Schneidstoffe*. Fortschr.-Ber. VDI, Reihe 2, Nr. 237, VDI-Verlag, Düsseldorf.
- Zum Gar, K.-H. 1987. "Grundlagen des Verschleißes." VDI Berichte Nr. 600.3: Metallische und Nichtmetallische Werkstoffe und ihre Verarbeitungsverfahren im Vergleich, VDI-Verlag, Düsseldorf.

---

# 4 Grinding Wheels

## 4.1 INTRODUCTION

### 4.1.1 DEVELOPMENTS IN PRODUCTIVITY

Huge increases in productivity have been achieved in recent decades due to advances in grinding wheel technology. These increases have only been possible by parallel developments in the machines and auxiliary equipment employed since the greatest gains have been from the grinding system.

Grinding wheels operating at low wheel speeds employed in the early twentieth century have progressed to advanced conventional abrasives and superabrasives operating at high wheel speeds in the present era. Over this period, material removal rates have increased for some grinding processes by a staggering 10 to 100 times. The grinding wheel technology that made such advances possible primarily involved the development of new abrasives as described in Chapter 5. In this chapter, mechanical design aspects of wheel design are introduced that affect grinding quality, performance, and safety. Essential information is given on wheel design for high-speed operation including design of segmented wheels.

### 4.1.2 SYSTEM DEVELOPMENT

New abrasives require new ways of working that reflect in new designs of grinding wheel assembly, truing, dressing, and conditioning techniques, coolant delivery and coolant formulation, and finally, new designs of machines capable of high wheel speeds and capable of delivering higher power to the grinding wheel. A variety of wheel designs have developed to cope with differing product geometries.

However, two other considerations gave rise to a new approach to wheel design:

- High wheel speeds must be designed for much greater wheel strength.
- Expensive, but hard-wearing, diamond and cubic boron nitride (CBN) superabrasives only need thin layers of abrasive to achieve a long wheel life.

### 4.1.3 CONVENTIONAL AND SUPERABRASIVE WHEEL DESIGN

In the next few chapters, the distinction will be made repeatedly between operation with conventional abrasives such as alumina and silicon carbide and operation with superabrasives such as CBN and diamond. The wheel designs tend to be distinctly different. One reason is the expense of the raw materials used for diamond and CBN superabrasives. Another reason is that these materials, especially CBN, tend to call for higher wheel speeds to take advantage of the potential for increased production rate and long wheel life. The higher speeds also drive the difference in wheel design.

The following sections provide essential information on basic dimensions and geometry of grinding wheels in these two categories. Figure 4.1 and Figure 4.2 contrast the difference in wheel design at the two extremes between a conventional wheel and an electroplated superabrasive wheel. In-between these two extremes lies a range of wheel designs including high-speed segmented designs as described below.

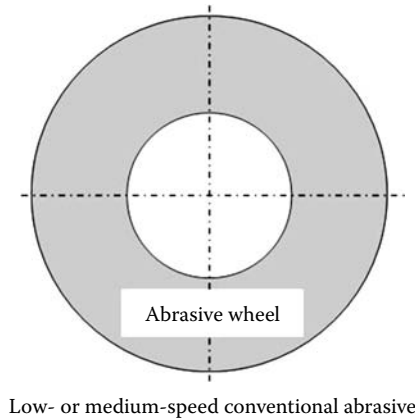


**FIGURE 4.1** Conventional abrasive wheel.

## 4.2 WHEEL SHAPE SPECIFICATION

### 4.2.1 BASIC SHAPES

Grinding wheels come in a variety of shapes and sizes. Standard International wheel shapes and examples for conventional and superabrasive wheels are given in Table 4.1 and Table 4.2. Wheel dimensions are usually expressed as diameter ( $D$ )  $\times$  thickness ( $T$ )  $\times$  hole ( $H$ ). For superabrasives the layer thickness ( $X$ ) is added afterward. Conventional wheels are typically sold as standard stock sizes although they can be cut to size and bushed in the bore to order. They also can be pre-profiled for certain applications such as worm gear grinding. Many superabrasive wheels, especially resin bond, also come in standard stock sizes but many are custom built, often with complex premolded profiled layers. The cost of this is readily offset against the savings in abrasive and initial dress time.

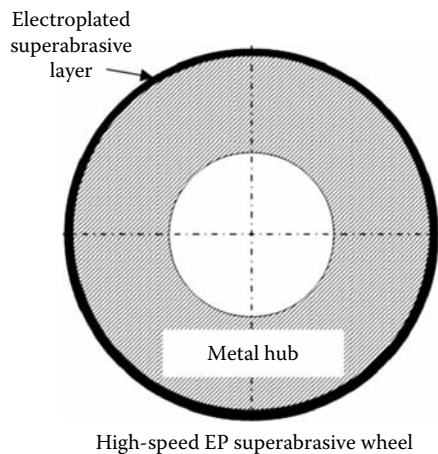
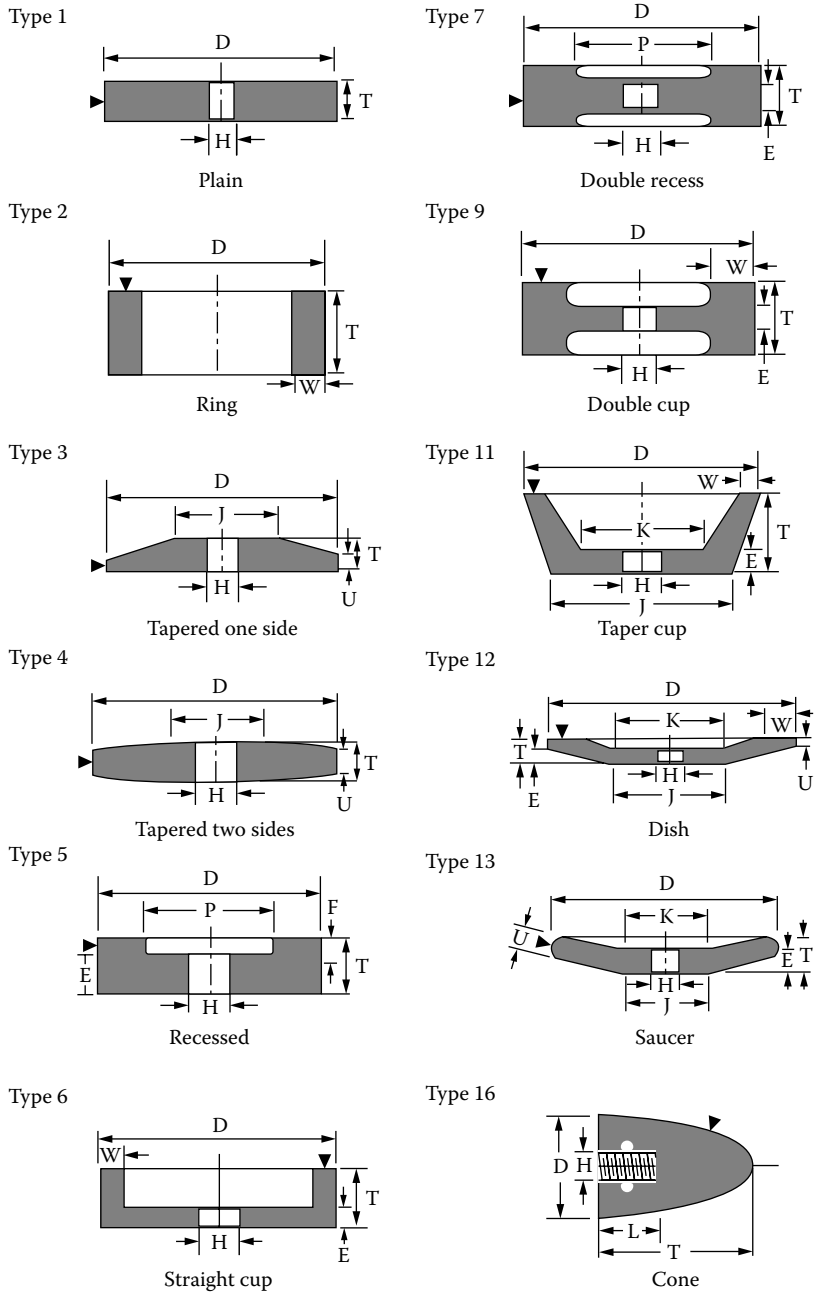


**FIGURE 4.2** High-speed CBN wheel.

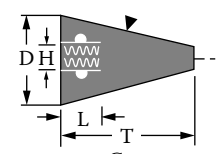
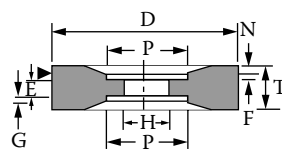
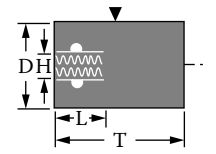
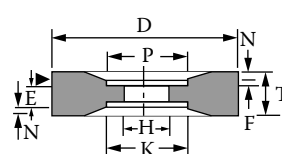
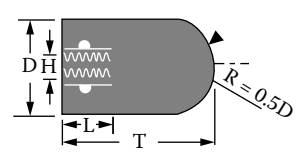
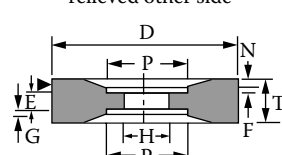
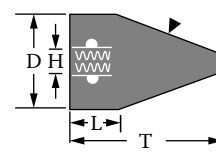
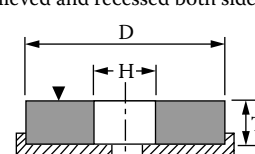
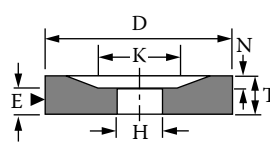
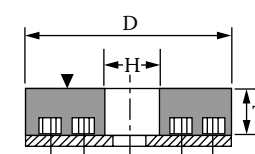
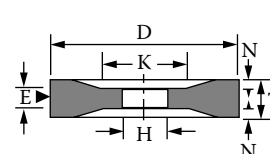
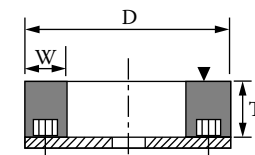
**TABLE 4.1**  
**International Standard Shapes for Conventional Wheels**



Conventional roughing wheels	H13 bore fit
Conventional precision wheels	H11 bore fit
Standard superabrasive wheels	H7 bore fit
High-speed CBN wheels	H6-H4 bore fits

(continued)

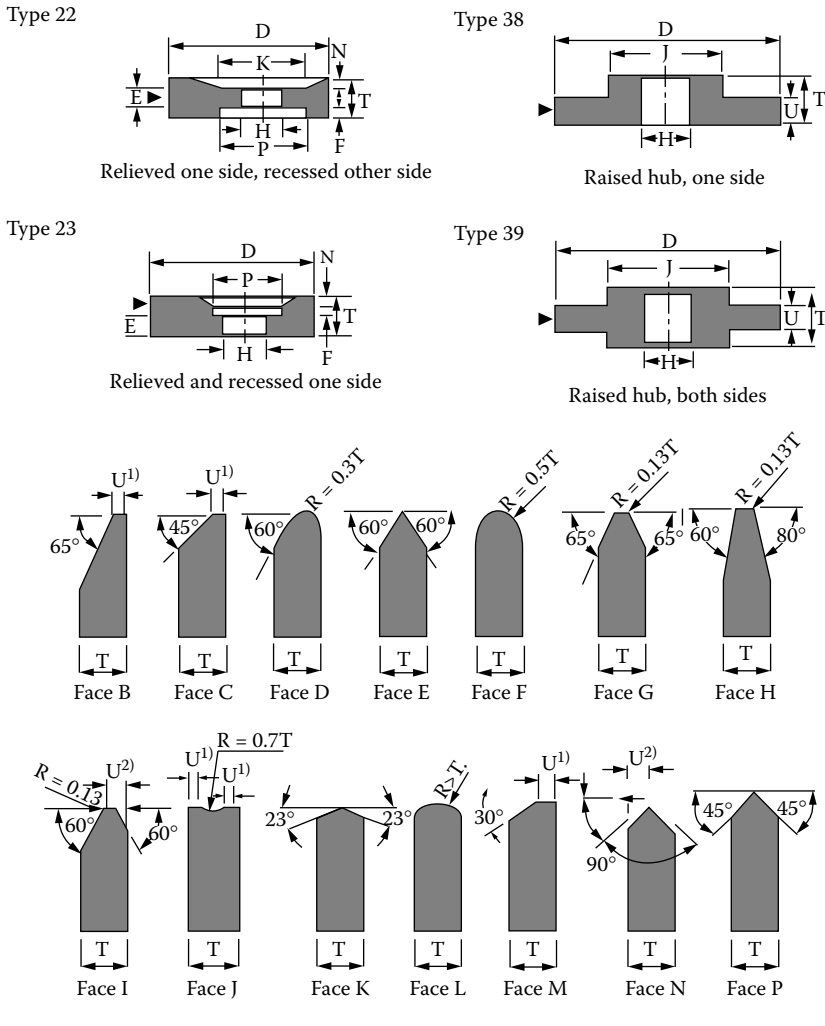
**TABLE 4.1 (CONTINUED)**  
**International Standard Shapes for Conventional Wheels**

<p>Type 17</p>  <p>Cone</p>	<p>Type 24</p>  <p>Relieved and recessed one side, recessed other side</p>
<p>Type 18</p>  <p>Plug</p>	<p>Type 25</p>  <p>Relieved and recessed one side, relieved other side</p>
<p>Type 18R</p>  <p>Plug</p>	<p>Type 26</p>  <p>Relieved and recessed both sides</p>
<p>Type 19</p>  <p>Cone</p>	<p>Type 35</p>  <p>Plated disc</p>
<p>Type 20</p>  <p>Relieved one side</p>	<p>Type 36</p>  <p>Inserted nut disc</p>
<p>Type 21</p>  <p>Relieved two sides</p>	<p>Type 37</p>  <p>Inserted nut ring</p>

### 4.2.2 HOLE TOLERANCES

Wheel dimensional tolerancing is very dependent on application and supplier. Some typical manufacturer's guidelines are given below. Conventional cored wheels should not have a tight fit for fear of cracking due to thermal expansion differentials with the steel wheel mounts. On the other hand, steel-cored superabrasives for high speed require the best possible running truth to eliminate problems of chatter and vibration. Tolerances based on bore diameters are given in Table 4.3.

**TABLE 4.1 (CONTINUED)**  
**International Standard Shapes for Conventional Wheels**



**4.2.3 SIDE AND DIAMETER TOLERANCES**

Side and outer diameter runout of wheels varies from one manufacturer to another and depends on application. For superabrasive wheels, the following tolerances are recommended (Table 4.4).

Outer diameter tolerances may be considerably more open, as long as running truth is maintained.

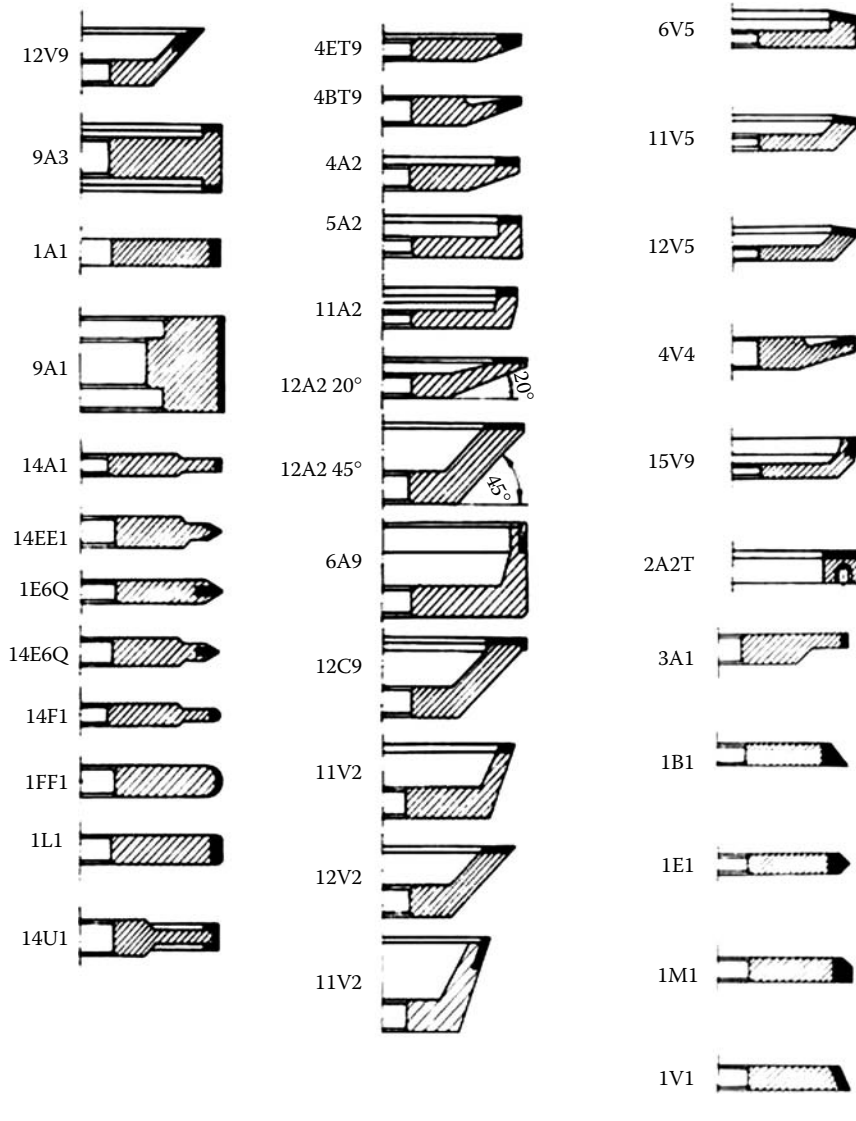
**4.3 WHEEL BALANCE**

**4.3.1 INTRODUCTION TO WHEEL BALANCE**

Balance is closely associated with runout. As the degree of unbalance force increases, runout will also increase. Balance tolerances depend on application. The Japanese JIS B4131 code gives the following balance tolerances in terms of center of gravity displacement  $g$  (Table 4.5). For high



**TABLE 4.2**  
**Superabrasive Wheel Shape Examples**



speed, the balance requirements are significantly more stringent than those shown in Table 4.5. For camshaft grinding, a high-speed CBN wheel of 14 diameter weighing 25 lb operating at 5,000 rpm must be balanced to <0.015 oz in order to prevent visual chatter even when used on a grinder with a high stiffness hydrostatic spindle. This is equivalent to  $g = 0.4$ , which is almost an order of magnitude tighter than current standards.

**4.3.2 STATIC AND DYNAMIC UNBALANCE**

“Static” unbalance is the term employed for unbalance within a single plane. Balancing of static unbalance may be performed either at zero speed or at running speed. Wheels are initially balanced statically off the machine but more frequently balanced at a fixed running speed. A confusion of terms

**TABLE 4.3**  
**Standard Fits for Wheel Bore Tolerancing<sup>a</sup>**

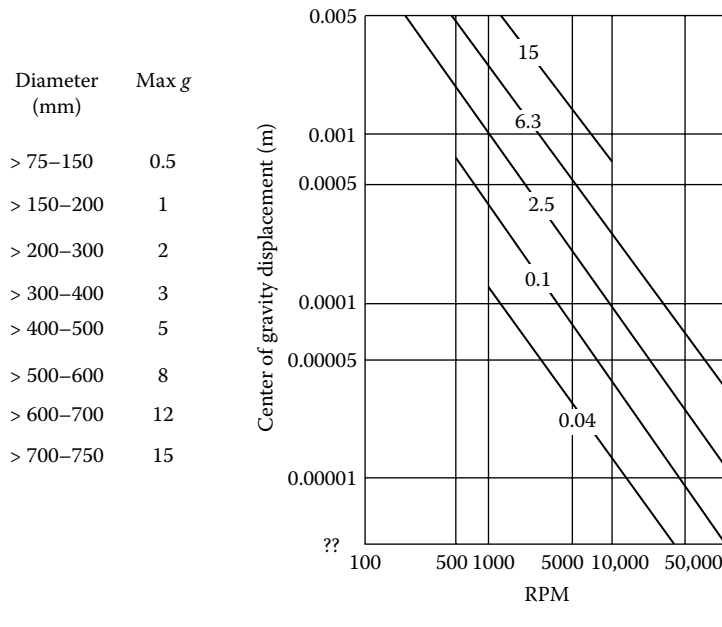
Bore Diameter (mm)	H4 Upper Limit (μm)	H5 Upper Limit (μm)	H6 Upper Limit (μm)	H7 Upper Limit (μm)	H11 Upper Limit (μm)	H13 Upper Limit (μm)
>3–6	4	5	8	12	75	180
>6–10	4	6	9	15	90	220
>10–18	5	8	11	18	110	270
>18–30	6	9	13	21	130	330
>30–40	7	11	16	25	160	390
>40–50	7	11	16	25	160	390
>50–65	8	13	19	30	190	460
>65–80	8	13	19	30	190	460
>80–100	10	15	22	35	220	540
>100–120	10	15	22	35	220	540
>120–140	12	18	25	40	250	630
>140–160	12	18	25	40	250	630
>160–180	12	18	25	40	250	630
>180–200	14	20	29	46	290	720
>200–225	14	20	29	46	290	720
>225–250	14	20	29	46	290	720
>250–280	16	23	32	52	320	810
>280–315	16	23	32	52	320	810
>315–355	18	25	36	57	360	890
>355–400	18	25	36	57	360	890
>400–450	20	27	40	63	400	970
>450–500	20	27	40	63	400	970

<sup>a</sup>Lower limit nominal (0).

**TABLE 4.4**  
**Side Runout Tolerances for Superabrasive Wheels**

Wheel Diameter (mm)	Standard Superabrasive Wheels (μm)	High-Speed CBN (μm)
<250	20	5
250–400	30	10
400–600	50	15
600–750	70	20

**TABLE 4.5**  
**Japanese JIS B4131 Specification for Wheel Balance Tolerances**



is easily caused. Balancing at speed is often incorrectly called dynamic balancing, although strictly, the term “dynamic” balancing means balancing in two or more planes to avoid a conical gyration.

### 4.3.3 AUTOMATIC WHEEL BALANCERS

Chatter is visible down to displacements of 10  $\mu\text{m}$ . Achieving displacements below this, even with the most sophisticated hydrostatic wheel bearings, is becoming increasingly more of a challenge as wheel speeds increase. For regular hydrodynamic or ball-bearing-based spindles, some form of dynamic balancer mounted to the machine is essential.

Automatic balancers are mounted on the spindle nose and function by adjusting the position of eccentric weights. Older systems actually pumped chlorofluorocarbon (CFC) gas from one chamber to another, but these have been phased out for environmental reasons. A separate sensor is employed to detect the level of vibration. The wheel guarding may need to be altered to allow a wheel balancer to be accommodated in an older machine. Wheel balancers are standard on the majority of new cylindrical grinders.

Figure 4.3 shows an automatic balancing device incorporated within a conventional wheel mounting arrangement.

The response times of automatic balancers have managed to keep pace with higher speed requirements and many can operate at 10,000 rpm or higher. The range has expanded to cover not only large cylindrical wheel applications, but smaller wheels down to 6 in. for use on multitasking machining centers. Others have the vibration sensor built into the balance head and can also be used as a crash protection and acoustic dress sensor.

### 4.3.4 DYNAMIC BALANCING IN TWO PLANES

Most recently, automatic balancers have been developed for dynamic balancing in two planes for compensation of long wheels such as for through-feed centerless grinding or for complete wheel/spindle/motor assemblies.

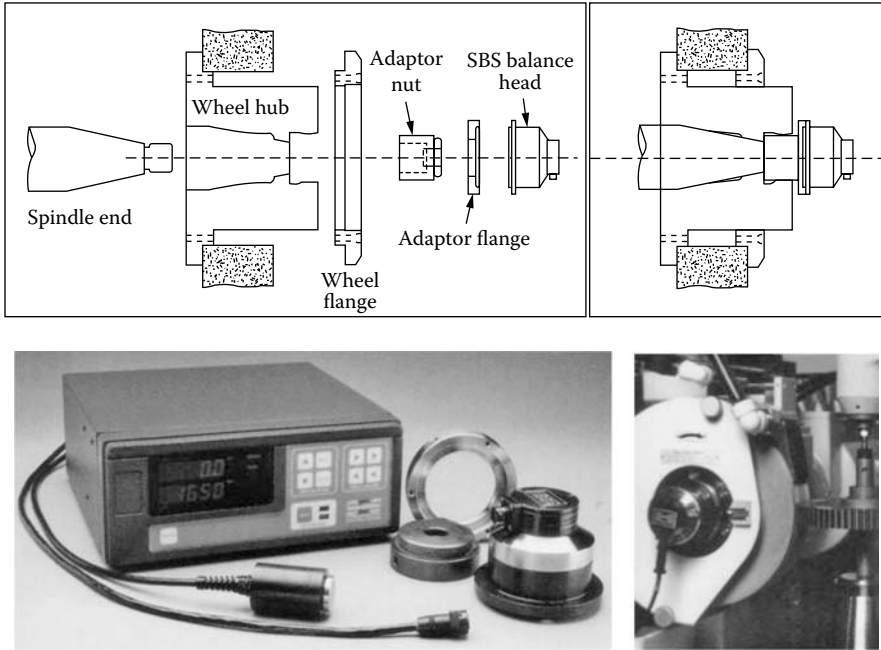


FIGURE 4.3 Automatic wheel balancer. (Courtesy of SBS, Schmidt Industries. With permission.)

### 4.3.5 COOLANT UNBALANCE

Coolant is a key factor for maintaining balance. A grinding wheel can absorb a considerable quantity of coolant (e.g., 220# WA 1A1 wheel can hold up to 16 wt%). When spun, the coolant is not released instantaneously but may take several minutes or even hours depending on its viscosity. This can be seen in Figure 4.4, which shows the rate of loss of retained coolant in a

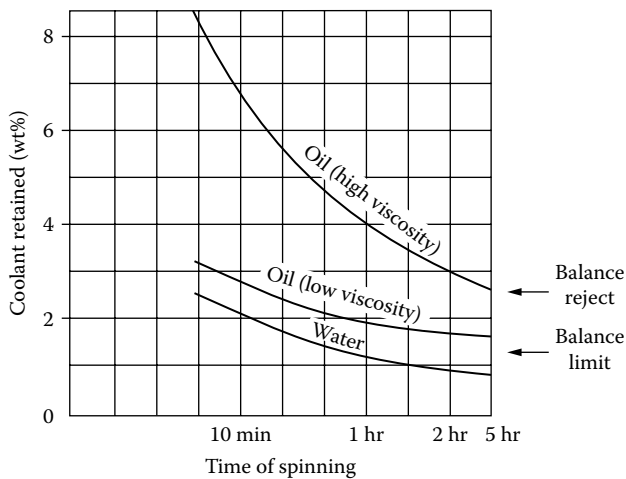


FIGURE 4.4 Coolant retention in a spinning grinding wheel as a function of time.

12 in.  $\times$  1/2 in. WA 220# 1A1 wheel spun at 48 m/s. The primary problem arises when coolant is allowed to drip on a stationary wheel or a stationary wheel is allowed to drain vertically. This will throw the wheel into an unbalanced condition when next used. The effect is unlikely to cause actual wheel failure, although it can happen. However, coolant unbalance will generate prolonged problems of vibration and chatter even when constantly dressing the wheel. It is also an issue with vitrified CBN wheels at high-enough wheel speed (>60 m/s) even though the porous layer may only be a few millimeters thick.

## 4.4 DESIGN OF HIGH-SPEED WHEELS

### 4.4.1 TREND TOWARD HIGHER SPEEDS

Vitrified CBN wheel speeds have risen significantly in the last 10 years. In 1980, 60 m/s was considered high speed; by 1990, 80 m/s was becoming common in production; by 1995, the speed reached 120 m/s; and then by 2000, the speed was 160 m/s. At the time of this writing several machines for vitrified wheels have been reported entering production for grinding cast iron at 200 m/s. Speeds of up to 500 m/s have been reported experimentally with plated CBN [Koenig and Ferlemann 1991]. Such wheel speeds place increased safety demands on both the wheel maker and machine tool builder.

Conventional vitrified bonded wheels generally default to a maximum wheel speed of 23 to 35 m/s depending on bond strength and wheel shape. Certain exceptions exist; thread and flute grinding wheels tend to operate at 40 to 60 m/s and internal wheels up to 42 m/s. (A full list is given in ANSIB7.1 2000 Table 23.)

### 4.4.2 HOW WHEELS FAIL

To achieve higher speeds requires an understanding of how wheels fail. Vitrified bonds are brittle, elastic materials that will fail catastrophically when the localized stresses exceed material strength. Stresses occur from clamping of the wheel, grinding forces, acceleration and deceleration forces on starting, stopping, or changing speed, wheel unbalance, or thermal stresses. However, under normal and proper handling and use of the wheel, the greatest factor is the centrifugal stresses due to constant rotation at operating speed.

### 4.4.3 HOOP STRESS AND RADIAL STRESS

The stresses and displacements created in a monolithic grinding wheel can be readily calculated from the classic equations for linear elasticity. The radial displacement  $U$  is given by

$$r^2 \cdot \frac{d^2U}{dr^2} + r \cdot \frac{dU}{dr} - U + \frac{r}{h} \cdot \frac{dh}{dr} \cdot \left[ r \cdot \frac{dU}{dr} + U \cdot v \right] = - \frac{1-v^2}{E} \cdot \rho \cdot \omega^2 \cdot r^3$$

This can be solved using finite difference approximations to give radial displacements at any radius of the wheel. The circumferential or hoop stress and radial stress equations are given by the following, where it is assumed the wheel outer diameter is >10 times wheel thickness.

$$\sigma_{\theta\theta} = \frac{E}{(1-v^2)} \cdot \left[ \frac{U}{r} + v \cdot \frac{dU}{dr} \right] \quad \sigma_{rr} = \frac{E}{(1-v^2)} \cdot \left[ \frac{dU}{dr} + v \cdot \frac{U}{r} \right]$$

The solutions to these equations are given by Barlow and Rowe [1983], Barlow et al. [1995], and Barlow, Jackson, and Hitchiner [1996] as

$$U = \frac{r}{E} \left[ (1-\nu) \cdot C_1 - (1+\nu) \cdot \frac{C_2}{r^2} - \frac{(1-\nu^2)}{8} \cdot \rho \cdot \omega^2 \cdot r^2 \right]$$

$$\sigma_{rr} = C_1 + \frac{C_2}{r^2} - \frac{3+\nu}{8} \cdot \rho \cdot \omega^2 \cdot r^2$$

$$\sigma_{\sigma\sigma} = C_1 - \frac{C_2}{r^2} - \frac{1+3\nu}{8} \rho \omega^2 \cdot r^2$$

The constants  $C_1$  and  $C_2$  are subject to the appropriate boundary conditions:

- Radial stress at the periphery of the wheel is zero.
- Free radial displacement at the bore.

The second boundary condition concerns the displacement of the bore and depends on the level of clamping of the wheel. It is usual in the design of wheels to assume the worst-case situation, which is free radial displacement, as this gives the highest level of circumferential stress. The maximum hoop stress occurs at the bore. In this case, the radial stress is zero.

Full constraint at the bore leads to zero displacement but the radial stress is now nonzero. Figure 4.5 gives an example of the stress distribution for the two extremes.

#### 4.4.4 REINFORCED WHEELS

Wheel failure, in line with this analysis, occurs from cracks generated at or near the bore where the stress is highest. The failure is catastrophic with conventional wheels. Typically four or five large,

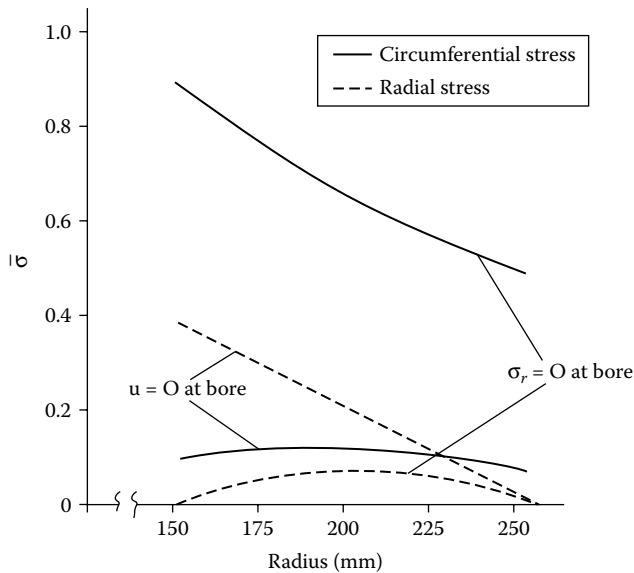


**FIGURE 4.5** Normalized stress distribution across a rotating grinding wheel for both free spinning and constrained wheels. (From Barlow 1983. With permission.)

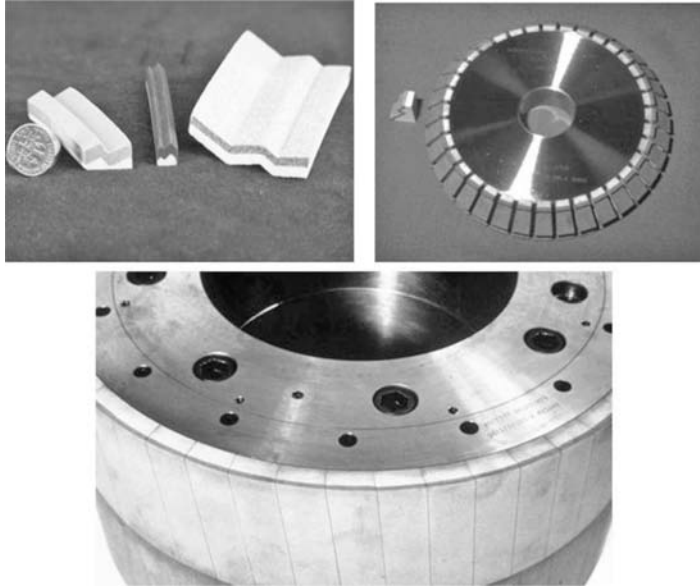


**FIGURE 4.6** Segmented vitrified CBN wheels and molded segment cross sections. (Courtesy of Saint-Gobain Abrasives. With permission.)

highly dangerous pieces are flung out. To increase the burst speed either the overall strength of the bond must be increased (e.g., finer grit size, lower porosity, better processing methods must be applied to eliminate large flaws), or the strength must be increased where the stress is highest. For conventional wheels this has often been achieved with a two-component vitrified structure where the inner portion is higher strength, although not necessarily suitable for grinding.

For vitrified CBN wheels higher speeds are achieved by substituting the inner section of the wheel with a higher strength material such as aluminum, carbon fiber reinforced plastic (CFRP), and especially steel.

#### 4.4.5 SEGMENTED WHEELS

Wheel manufacture of a high-speed segmented wheel consists of epoxy bonding or cementing a ring of vitrified CBN segments to steel core as shown in Figure 4.6.

The segmented design serves several purposes. First, it produces a much more consistent product than a continuous or monolithic structure because of the limited movements required in pressing segments of such small volume. This is especially true when, as in the examples shown above, a conventional backing (white) layer is added behind the CBN to allow the use of the full layer of the abrasive layer. This gives both a better consistency in grinding and a higher Weibull number for strength consistency. Second, it allows a wheel to be repaired in the event of being damaged, providing a considerable cost saving for an expensive CBN wheel. Third, and very important, the segments provide stress relief, acting as “expansion joints” as wheel speed increases and the steel core expands due to centrifugal force.

#### 4.4.6 SEGMENT DESIGN

Trying to model segmented wheels using the traditional laws of elasticity has proved difficult because of complex effects within and around the adhesive layer. Finite element analysis (FEA)-based models are now more common with much of the groundwork having been done by Barlow et al. [1995, 1996].

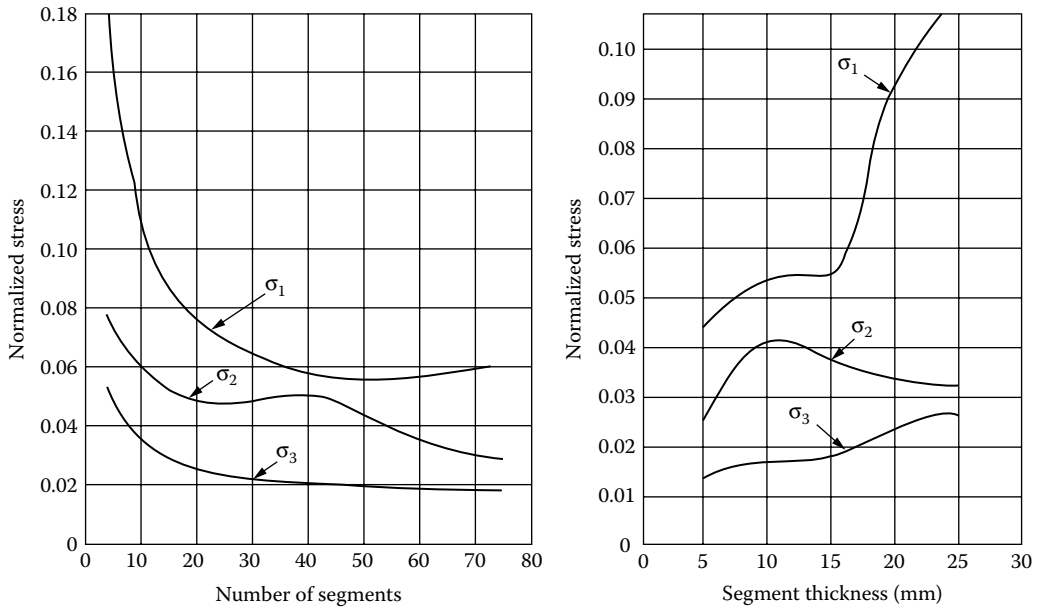


**FIGURE 4.7** Maximum stress levels in a rotating segmented wheel as a function of segment number and abrasive thickness.

Both hoop stresses and radial stresses can lead to wheel failure. Hoop stress is dependent on the expansion of the core and the segment length. Radial stress is dependent on both the expansion of the core, but also, more importantly, on the mass and, therefore, thickness of the segment. Figure 4.7 plots the principal stresses of a 20-in.-diameter aluminum body wheel (12-in. bore) as a function of segment number and abrasive layer thickness.  $\sigma_1$  is the maximum principal stress,  $\sigma_2$  is the minimum principal stress, and  $\sigma_3$  is axial or out-of-plane stress. As can be seen, there is an optimum number of segments, 35, in the example below. Higher segment numbers give rise to additional stresses at the joint edges because as the wheel expands in a radial direction it must contract in the axial direction.

#### 4.4.7 ABRASIVE LAYER DEPTH

For thin segments, the major stress is circumferential, but for thicker segments the dominant stress shifts to radial. For this reason, an abrasive layer thickness of 10 mm maximum is typical for a high-speed wheel. This immediately places limitations on profile forms allowed. The key factor is the mass of the segment, and its impact on radial stress is also important when considering the effect of wheel radius on burst speed. As the wheel radius is reduced, the centripetal force ( $mv^2/r$ ) must increase which will directly increase the radial stress. Figure 4.8 plots burst speed as a function of wheel radius for various abrasive layer depths. Ideally, the calculated burst speed should be at least twice the maximum recommended operating speed. For the 5-mm CBN layer the burst speed levels off at 320 m/s because this was the calculated burst speed for the steel core used in the example. The most striking factor about this graph is that the burst speed drops rapidly as the wheel diameter is reduced. For a wheel diameter of 6 in., the maximum recommended wheel speed would be only 100 m/s based on the particular bond strength used in the example. The value employed is believed typical of current CBN technology. Not surprisingly, therefore, high-speed wheels operating in the range of 100 to 200 m/s tend to be >12 in. diameter with flat or shallow forms.



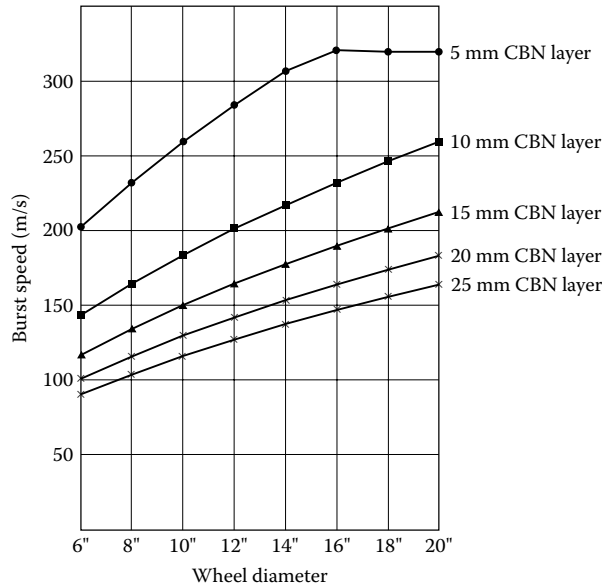


**FIGURE 4.8** Segmented wheel burst speed as a function of wheel diameter and abrasive thickness (for defined vitrified bond strength).

#### 4.4.8 RECENT DEVELOPMENT OF HIGH-SPEED CONVENTIONAL WHEELS

Segmental wheel research first began with conventional wheels in the 1970s as part of an effort to evaluate the effect of high speed [Yamamoto 1972, Anon 1979, Abdel-Alim, Hannam, and Hinduja 1980]. However, the labor-intensive manufacturing costs were not competitive for the economic gains in productivity possible at that time. However, the recent development of ultrahigh porosity specifications (and therefore low-density) using extruded SG abrasives has allowed the development of wheels with thick layers of conventional abrasive capable of operation at up to 180 m/s. An example is illustrated in Figure 4.9.

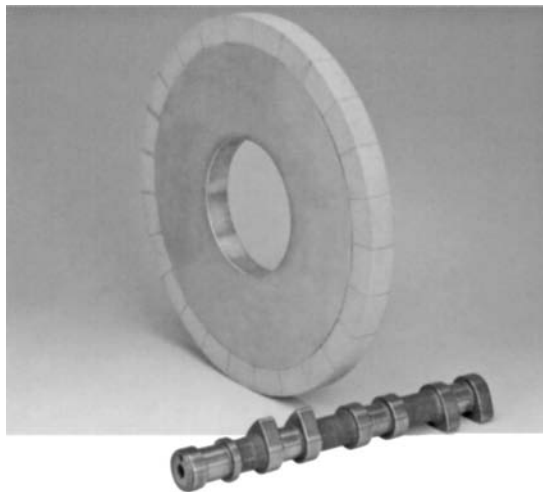


**FIGURE 4.9** Segmented vitrified Optimos Altos wheel containing needle-shaped ceramic (TG2) abrasive rated for 180 m/s. (Courtesy of Saint-Gobain Abrasives. With permission.)

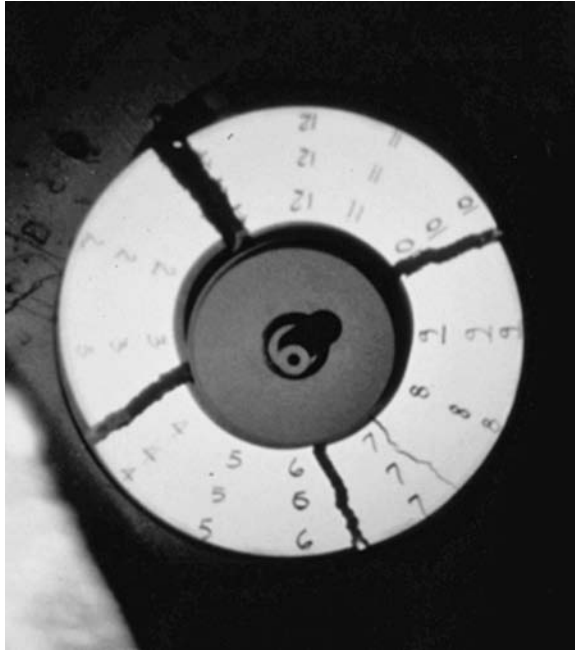


**FIGURE 4.10** Solid wheel failure at 90 m/s (monolithic alox body).

#### 4.4.9 SAFETY OF SEGMENTED WHEEL DESIGNS

The last and most important benefit of segmental designs is safety. The two high-speed photographs compare the failure of a conventional wheel (Figure 4.10) with a high-speed segmental wheel (Figure 4.11). The failure in the latter can just be seen between segments 11 and 12.

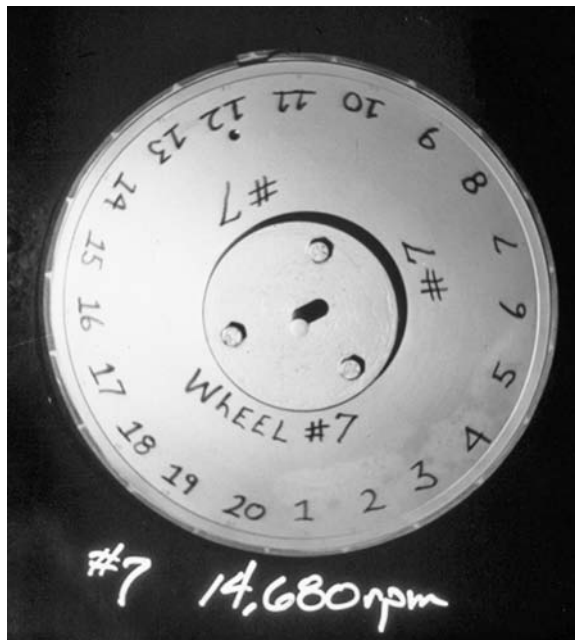


**FIGURE 4.11** Segmental wheel failure at 255 m/s (steel core).

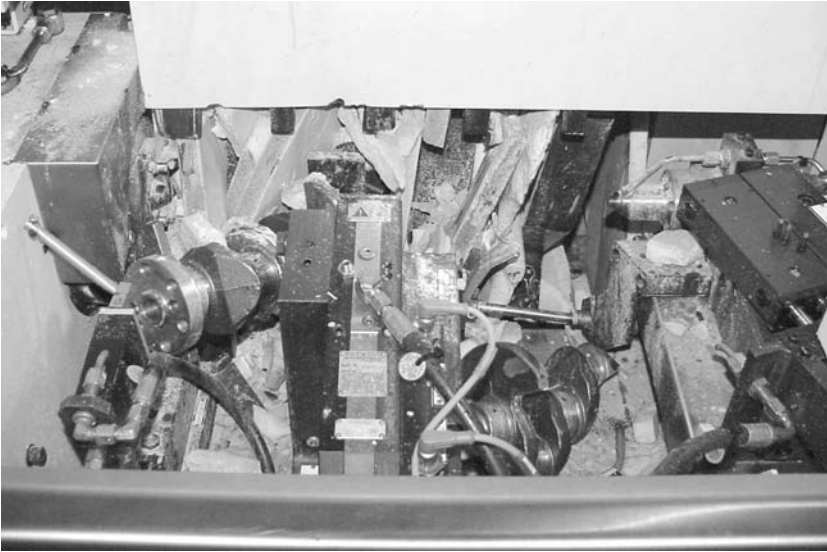


**FIGURE 4.12** Wheel failure in a multiwheel cylindrical grinding operation.

The major difference in the two failures is the energy release. The results of a failure in a large conventional wheel can be extremely destructive for the machine tool, as illustrated in the photograph (Figure 4.12) showing the aftermath of a multiwheel crankshaft journal wheel set failure. With this level of energy released, the situation is potentially very dangerous, costly, and time-consuming even when well guarded. By comparison the energy released by a segment failure, and the level of damage accompanying it, are very small. Any failure though is still unacceptable to the wheel maker or end user.

Figure 4.13 compares the energy release in wheel failure for a quadrant of a conventional wheel compared with the energy release for a segment of a segmented wheel.

#### **4.4.10 SPEED RATING OF GRINDING WHEELS**

Wheels are speed tested by overspinning the wheel by a factor prescribed by the appropriate safety code for the country of use. In the U.S., ANSI B7.1 specifies that all wheels must be spin tested with an overspeed factor of 1.5 times the operating speed. The theory behind this reverts back to conventional wheel research where the 1.5 factor was proposed to detect preexisting flaws that might otherwise cause fatigue failure in the presence of moisture or water-based coolants during the expected life of the wheel [Grinding Wheel Institute (GWI) 1983]. In Germany, for the highest speed wheels, the DSA 104 code requires the wheel design be tested to withstand 3 times the operating stress. This gives an overspeed factor of  $\sqrt{3}$  or 1.71. However, all production wheels must be tested at only 1.1 times the operating speed. This code was due to the result of research in Germany that indicated that high overspeed factors could induce flaws that could themselves lead to failure. This discrepancy in the safety laws has a major impact on transfer of technology in the context of the global economy [Service 1991, 1993, 1996]. The author has seen numerous examples of machine tools imported into the United States with incorrect spin test factors. In other countries with imported machine tools but no official safety code for wheel speed testing, the factor reverts back to the process as specified by the particular machine tool builder with the associated machine guarding on which the wheel is run.

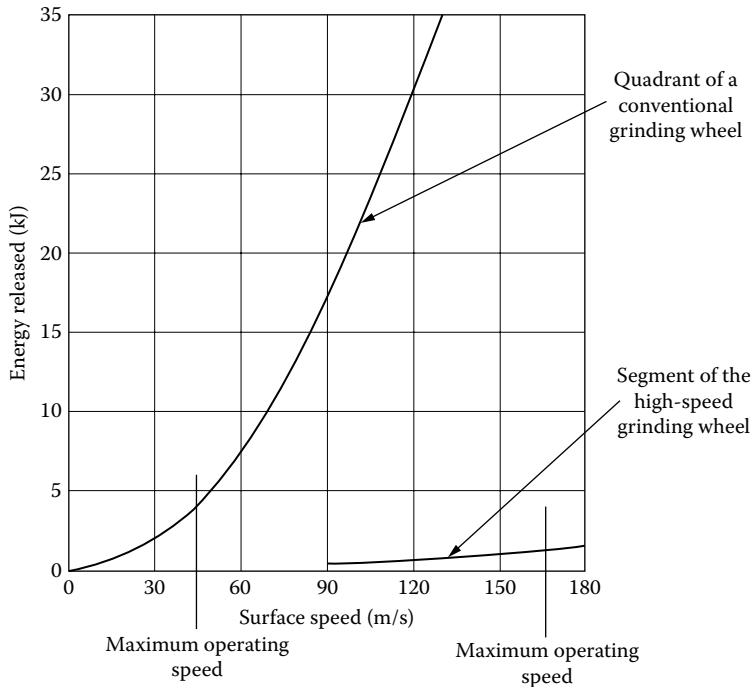


**FIGURE 4.13** Energy release comparison for a conventional alox wheel with a steel-cored segmented wheel.

Wheel makers must obey the safety codes of the appropriate country but they must also ensure above and beyond that the wheels are safe to the best of their abilities. For the SGA brands the author has been associated with, the wheels are spin-tested at  $1.5 \times$  operating speed for the U.S. market per the ANSI standards, but the wheels are designed and tested to  $>2 \times$  burst speed. For example, the wheel photographed in Figure 4.11 had a theoretical burst speed of 252 m/s. Seven wheels were tested and all failed at speeds between 255 and 273 m/s. As expected, failure occurred in the abrasive layer immediately adjacent to the epoxy bond where the stress in the abrasive was highest [Hitchiner 1991].

#### 4.5 BOND LIFE

Spin testing in itself however is not sufficient. Higher stresses actually occur in the epoxy bond than in the bond. Fortunately, the bond strength of epoxy is about ten times greater than the abrasive. However, epoxy is prone to attack by moisture and coolant and will weaken over time. Efforts have been made to seal the bond from the coolant [Kunihito et al. 1991], but these are generally ineffective and the wheel maker must have life data for his particular bonding agent in coolant. Since wheels may have a life of several years on the machine with spares held in stock for a comparable time, these data take considerable time to accrue. Currently, Saint-Gobain Abrasives recommends a maximum life of 3 years on the machine or 5 years total including appropriate storage without re-spin testing.

#### 4.6 WHEEL MOUNT DESIGN

Holding the abrasive section together on the wheel body has already been discussed. A second problem is how to hold the wheel body on the machine spindle.

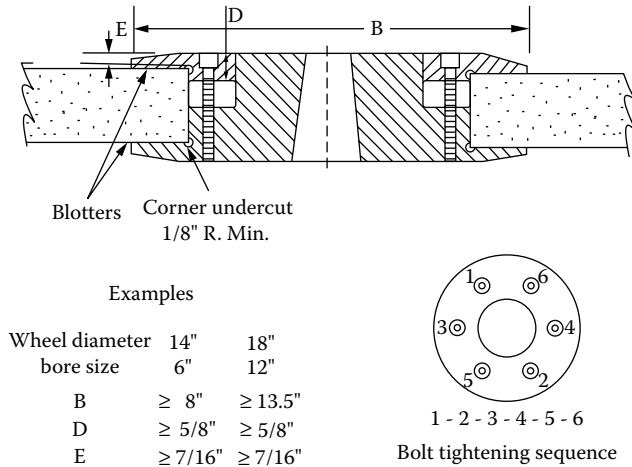


FIGURE 4.14 Flange design for conventional wheels and bolt-tightening sequence.

Centrifugal forces cause the wheel to expand radially both on the outer diameter *and* the bore. It, therefore, must also *contract* axially. The problem is, therefore, to prevent movement of the wheel on the hub either by minimizing bore expansion/contraction and/or by maintaining sufficient clamping pressure on the wheel to resist torsional slippage.

**4.6.1 A CONVENTIONAL WHEEL MOUNT**

An example of a conventional wheel mount [ANSI B7.1 1988, Figure 43] is shown in Figure 4.14.

**4.6.2 USE OF BLOTTERS**

Blotters are required for conventional wheels to equalize the variations in pressure due to the effects of microasperities in the grit structure of the vitrified body. Failure to incorporate compressible blotters gives rise to local stress concentrations that are very dangerous. The blotters are made of either paper or plastic (polyester) with a thickness of typically 0.015 in.

**4.6.3 CLAMPING FORCES**

The flanges are fixed together with a series of bolts, six in the example above, that are torqued to ≤20 ft.lb in the sequence shown unless otherwise recommended. Overall clamping pressures must be kept to <1000 psi and usually are considerably below this value.

Optimum torque values can lead to lower rotational stresses and higher burst speeds. Barlow et al. [1995] carried out FEA analysis of clamping pressures and the effect on wheel stresses. An example showing the reduction in maximum radial stress is shown in Figure 4.15.

However, overtorquing causes distortion of the flange leading to a high-stress peak that can readily exceed 2000 psi and lead to wheel failure [Meyer 1996]. De Vicq [1979] recommended using tapered flange contact faces to compensate. Unfortunately, this is impractical except for dedicated machines and the accuracy of torquing methods is not always sufficient to ensure correct flange deflection.

In the absence of any significant axial contraction, it is relatively straightforward to calculate clamping forces required to prevent rotational slippage [Menard 1983].

**4.6.3.1 Clamping Force to Compensate for the Weight of the Wheel**

$$F_m = M_s g / \mu_b$$

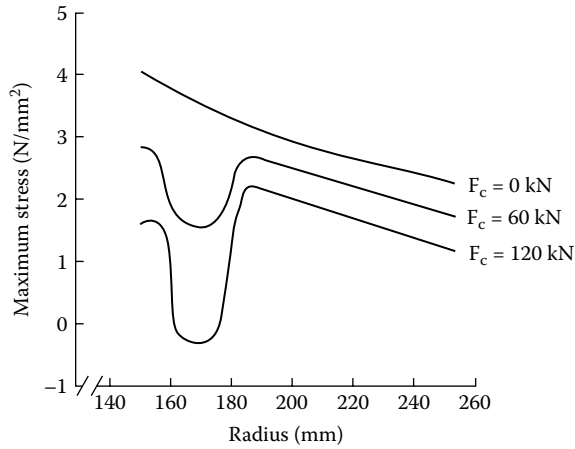


**FIGURE 4.15** Effect of clamping force from a 175-mm-radius flange on wheel stress.

where

$M_s$  = mass of the wheel

$\mu_b$  = coefficient of friction for the blotter

paper blotter = 0.25

plastic blotter = 0.15 [De Vicq 1979]

#### 4.6.3.2 Clamping Force for Unbalance of the Wheel

$$F_u = \delta v_s^2 / r_s^2 \mu_b$$

where

$\delta$  = unbalance (force . distance)

$v_s$  = wheel speed

$r_s$  = wheel radius

#### 4.6.3.3 Clamping Force for Motor Power Surge

It is assumed that electric motors can develop a surge torque of 2.5 times their rated torque before stalling.

$$F_s = 2.5 P_{sp} r_f / v_s \mu_b r_s$$

where

$r_f$  = flange average radius

$P_{sp}$  = spindle motor power

#### 4.6.3.4 Clamping Force for Reaction of Wheel to Workpiece

Again assume a motor surge capability of 2.5:

$$F_n = 2.5 P_{sp} / v_s \mu_b \mu_g$$

**TABLE 4.6**  
**Dimensional Changes in a High-Speed Rotating Steel Cored Wheel**

Body Shape	Outer Diameter Expansion	Inner Diameter Expansion	Axial Contraction
1A1 plain	47 $\mu\text{m}$	29 $\mu\text{m}$	3 $\mu\text{m}$
3A1 stepped body	164 $\mu\text{m}$	13 $\mu\text{m}$	3 $\mu\text{m}$
1-pc hub plain	41 $\mu\text{m}$	9 $\mu\text{m}$	5 $\mu\text{m}$
1-pc turbine profile	35 $\mu\text{m}$	14 $\mu\text{m}$	6 $\mu\text{m}$

where

$\mu_g$  = coefficient of grinding (0.4 typical)

In addition to these forces there will be effects of accidental vibration and shocks, possible compression of the blotters, and the increased clamping force required as the wheel wears when holding constant surface footage. Practical experience leads to another factor 2 on forces. Total clamping force required becomes

$$F_{total} = 2(F_m + F_u + F_s + F_n)$$

When the number of bolts is known, tables are available giving torque/load values for the required clamping force. Calculations then need to be made to determine the flange deflection.

#### 4.6.4 HIGH-SPEED WHEEL MOUNTS

With high-speed steel-cored wheels the need for blotters is eliminated. Clamping is, therefore, steel on steel and not prone to the same brittle failure from stress risers. Nevertheless, there is the uncertainty on wheel contraction and its effect on clamping. One solution is to eliminate the flanges entirely. Landis (Waynesboro, Pennsylvania) developed a one-piece wheel hub where the entire wheel body and tapered mount are a single piece of steel with the vitrified CBN segments bonded onto the periphery [Pflager 1997].

FEA analysis was carried out on a range of steel-cored wheel shapes as shown in Figure 4.16 based on 500 mm diameter  $\times$  20 mm o.d. face running at 6,000 rpm (157 m/s).

#### 4.6.5 THE SINGLE-PIECE WHEEL HUB

The straight one-piece hub was found to give the minimum level of bore expansion and is the design currently used in production. The “turbine” or parabolic profile minimizes outer diameter (o.d.) expansion but at the expense of some additional bore (i.d.) expansion. It is also considerably more expensive to machine. This one-piece design concept (Figure 4.17) has proved extremely successful in the crankshaft pin grinding and camshaft lobe grinding industries for speeds in the range of 60 to 120 m/s. It has eliminated the need for automatic balancers and allows fast change overtimes for lean manufacturing with minimal or no redress requirements.

#### 4.6.6 DIRECT MOUNTING ON THE SPINDLE

Nevertheless, the design still has problems with bore expansion albeit now directed to a movement on a keyed tapered arbor. For the very highest wheel speeds, OEMs and wheel makers are designing

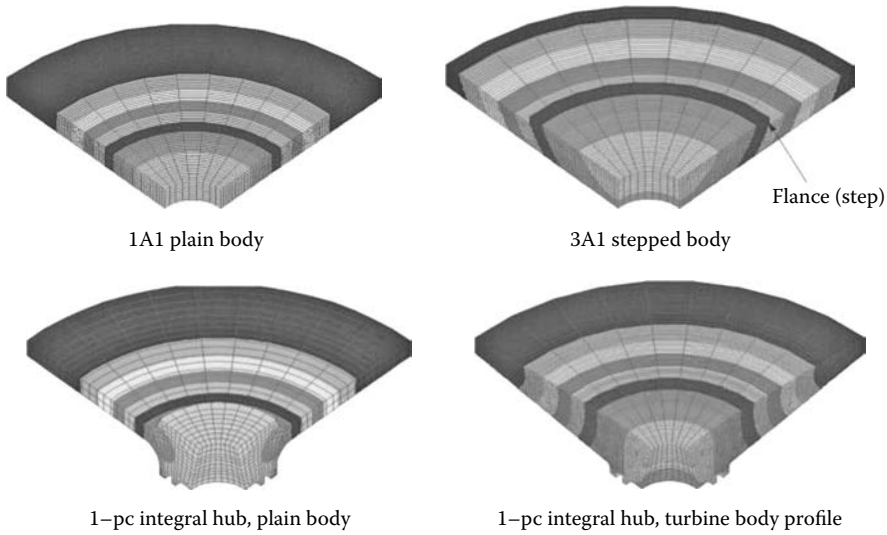


**FIGURE 4.16** Optimization of hub design for minimal bore and diameter expansion.

wheels to bolt directly to the motor spindle. Several examples for both vitrified and plated CBN wheels are shown later.

Figure 4.18 shows a typical steel-cored wheel for grinding camshafts at speeds up to 160 m/s. This particular example was made by TVMK for operation on a TMW camlobe grinder. The wheel has a small 40-mm hole governed partly by the motor spindle shaft size, but also allows a bore tolerance of  $\pm 2.5 \mu\text{m}$  to be practically achieved. There are a large number of bolts (10) to hold the wheel thus allowing a high clamping force to be achieved. Since the wheel face is flat and flush to the spindle there is no flange distortion. The bolt circle diameter is also small (68 mm), which minimizes problems from motor surge leading to slippage during start-up. The body is twice as wide as the CBN section and tapered down toward the outer diameter. This reduces the bore

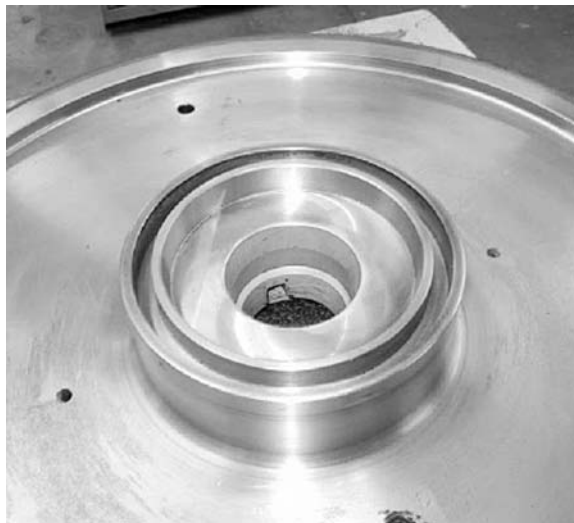


**FIGURE 4.17** Example of one-piece integral hub design.



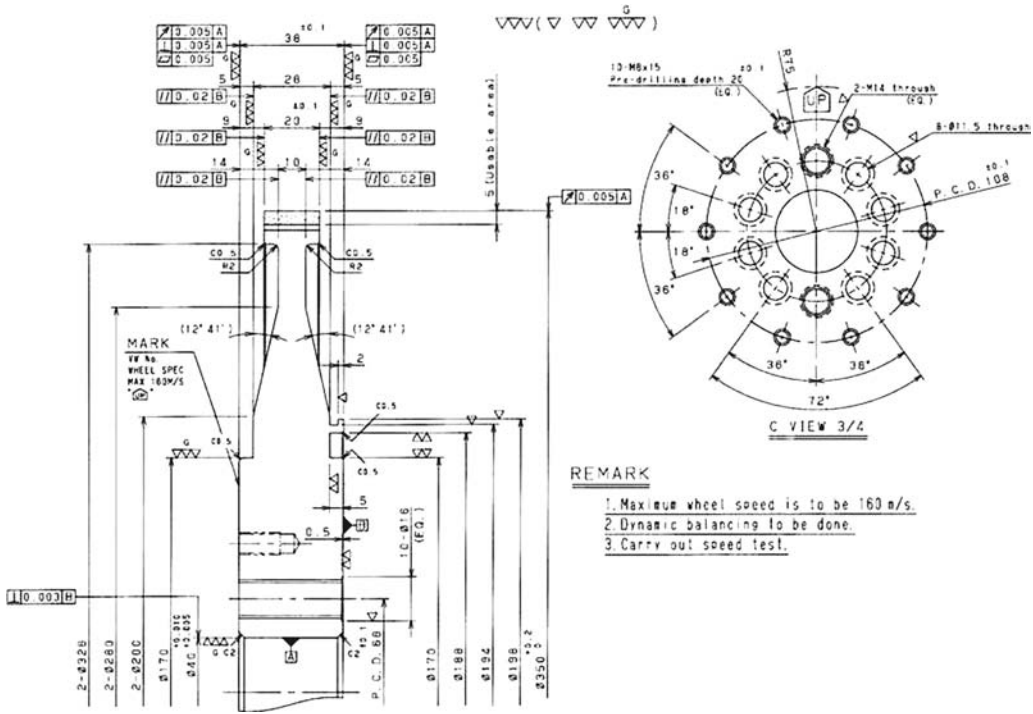


FIGURE 4.18 Steel-cored vitrified CBN wheel for grinding camshafts at 160 m/s.

expansion without creating some of the stress distortions seen with the 3A1 shape above. The vitrified CBN layer depth is 5 mm with a total layer of abrasive of about 6.5 mm.

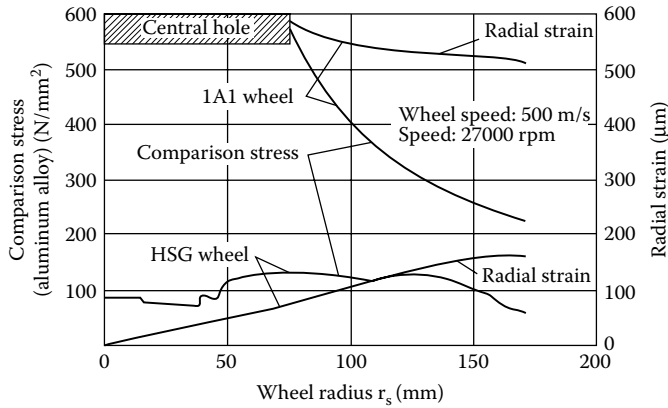
#### 4.6.7 CFRP WHEEL HUBS

The current limit for steel-cored vitrified CBN wheels due to stresses in the abrasive layer from core expansion is considered to be 200 m/s. This will vary somewhat depending on the particular bond and layer depth. However, for speeds of 160 m/s and greater the steel is sometimes replaced with a material of comparable elastic modulus but one third the density, namely, carbon fiber reinforced plastic (CFRP) or even titanium. This reduces wheel expansion by a factor of 3. Several wheel suppliers offer high-speed wheels with CFRP hubs in their literature. However, the cores are expensive if provided with the appropriate carbon fiber (CF) reinforcement level. CFRP hubs with lower CF content are available for lower wheel speeds that offer purely weight benefits. The primary problem with mounting a carbon fiber center is that the fibers are layered mats with a high Young's Modulus in the radial direction but a low compressive modulus axially. Either a steel flange ring is required for the bolt heads to lock against or steel inserts must be added into countersunk bolt holes.

#### 4.6.8 ELECTROPLATED WHEELS

Electroplated CBN wheels have been developed for considerably higher wheel speeds than vitrified CBN. The plated layer can withstand greater expansion of the hub. Research was reported as early as 1991 by Koenig and Ferlemann [1991] at 500 m/s using Winter wheels, while Tyrolit recently also offered a similar product design rated for 440 m/s in its literature.

The wheel design described by Koenig and Ferlemann (Figure 4.19) has several novel features including the use of lightweight aluminum alloy for the hub material, a lack of a bore hole to further reduce radial stress, and an optimized wheel body profile based on turbine blade research to give the



Stress and strain equalization of a 1A1 wheel compared to an optimized wheel

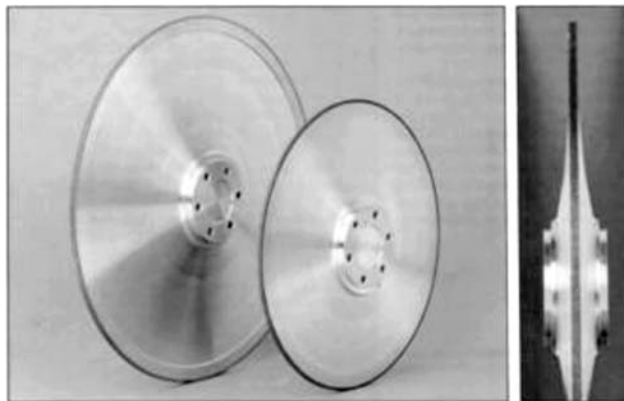
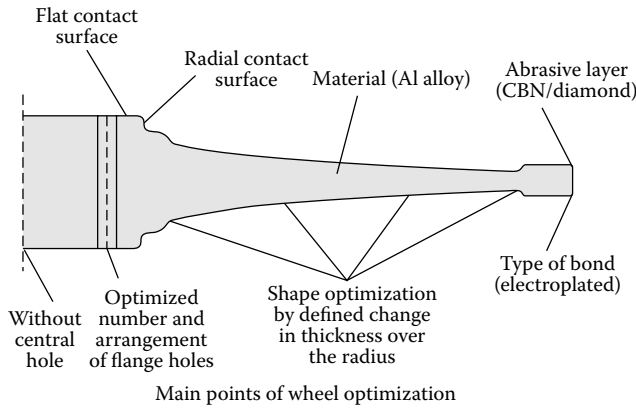


**FIGURE 4.19** Optimized wheel shapes for high-speed plated CBN. (From Koenig and Ferlemann 1991. With permission.)

minimum wheel mass for uniform strength. Although this technology has been available for 10 years, there are only a limited number of machines in actual production running over 200 m/s. The radial expansion at 500 m/s is about 160 µm! A plated CBN layer can withstand the expansion at high speed, but the expansion is rarely perfectly uniform. Even a 1% difference due to any anisotropy in the hub material will lead to regenerative chatter and performance issues well before the expected life of the wheel.

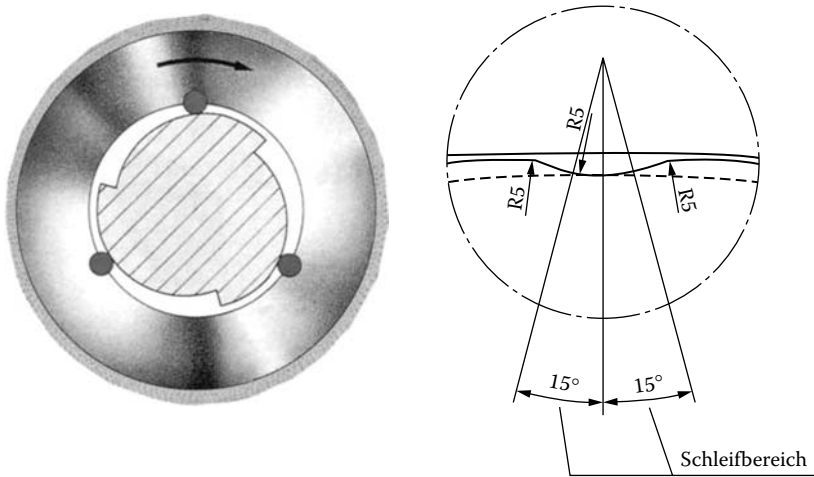


FIGURE 4.20 Junker patented bayonet style mount systems for high-speed wheels.

#### 4.6.9 ALUMINUM HUBS

Aircraft grade aluminum alloys are used as hub materials for some high-speed vitrified CBN. The obvious attraction is the lower density relative to steel. Various grades are available with tensile strengths of 120 to 140 kpsi. However, they have higher thermal expansion and appear to give more size and stability problems.

#### 4.6.10 JUNKER BAYONET STYLE MOUNTS

Other methods have been developed to compensate for bore expansion. Erwin Junker Maschinenfabrik developed a patented bayonet-style cam and follower three-point type mount. Various forms of the design are shown in Figure 4.20. The first consists of three roller bearings inserted into the bore, the second is the later, more common, version consisting of a hardened steel ring insert with three preformed raised areas as detailed. The design assures  $<1.25 \mu\text{m}$  runout repeatability at speeds up to 140 m/s [Junker n.d. 1992].

#### 4.6.11 HSK HOLLOW TAPER MOUNT

Another method is the incorporation of the increasingly popular HSK tool holder shank. The HSK system was developed in the late 1980s at Aachen T.H., Germany as a hollow tapered shaft capable of handling high-speed machining. It became a shank standard in 1993 with the issuance in Germany of DIN 69893 for the hollow 1:10 taper shank together with DIN 69063 for the spindle receiver.

This system has seen a rapid growth, especially in Europe, as a replacement to the various 7:24 steep taper shanks known as the CAT or V-flange taper in the United States (ASME-B5.10-1994), the SK taper in Germany (DIN69871), and the BT taper in Japan (JISC-B-6339/BT.JISC). These tapers previously dominated the CNC milling industry.

The HSK system actually consists of a family of shank sizes from 25 to 160-mm flange diameter and designs from A thru F, of which the HSK-A is the most common for grinding applications with flange diameters from 80 to 125 mm. Muller-Held [1998] reported that the HSK system could limit maximum position deviations to  $0.3 \mu\text{m}$  compared with  $2 \mu\text{m}$  for an SK taper. Lewis [1996] reported it was 3 times more accurate in the X and Y planes and 400 times better in the Z axis. Bending stiffness was 7 times better, while the short length of the taper allowed faster tool change times. The important detail, however, for this discussion is the fact that the design has a *hollow* taper that expands under centrifugal load to aid the maintenance of contact. However, Aoyama and

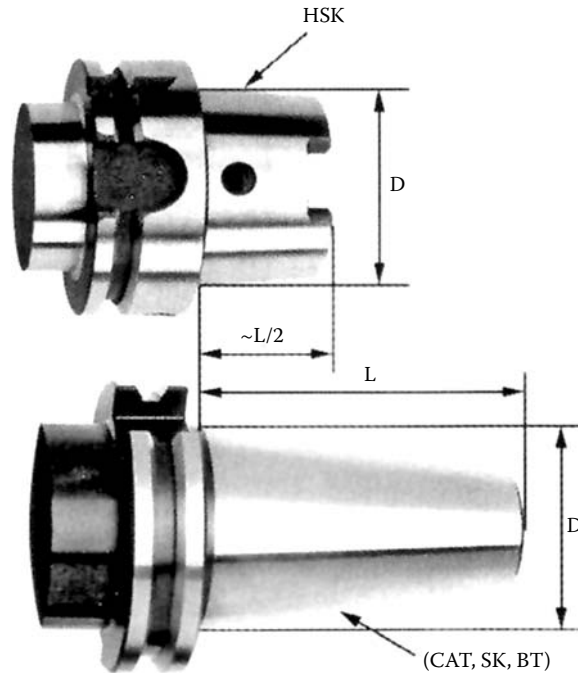


**FIGURE 4.21** Comparison of the HSK mount with earlier CAT and other taper systems.

Inasaki [2001] reported that radial stiffness reduces with increased rotational speed but is still far superior to any other taper mounting system.

The HSK wheel mount system has been widely adopted for hybrid grinding/metal cutting machines. Regular 1A1 style-plated wheels have been routinely run at up to 140 m/s on HSK taper arbors. At least one research machine has been built using a one-piece hub design incorporating HSK

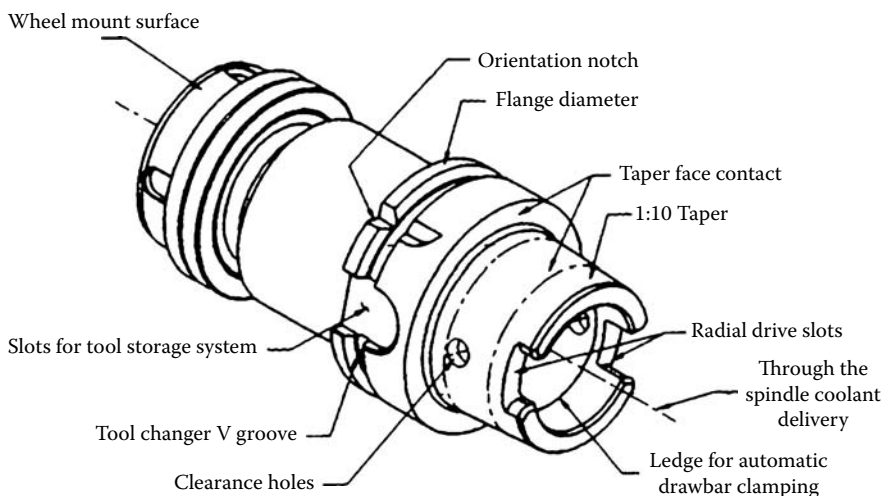


**FIGURE 4.22** Elements of a typical HSK tool mount for automatic tool changing.

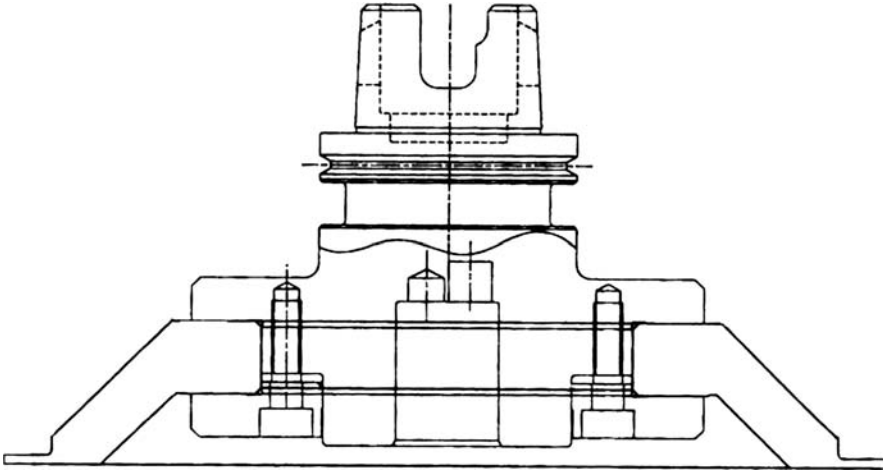


**FIGURE 4.23** Plated CBN groove grinding wheel mounted on HSK adaptor.

mounting for use up to 250 m/s. Currently the primary hesitation in broader adoption of this technique is the cost, availability, and delivery due to the limited number of capable high-precision manufacturing sources.

#### 4.6.12 TITANIUM HUB DESIGN

As a final note, Ramesh [2001] reported using titanium flanges as a wheel mount option in a thesis on high-speed spindle design and grinding. This design is shown in Figure 4.24.

The wheels are made with steel cores and without a center hole being held by titanium flanges clamping to shoulders on the wheel. Titanium has comparable strength to high tensile steel but has one third the density. It is, therefore, expected that the wheel core will try to expand more than the flanges at high speeds and therefore the radial clamping will increase.

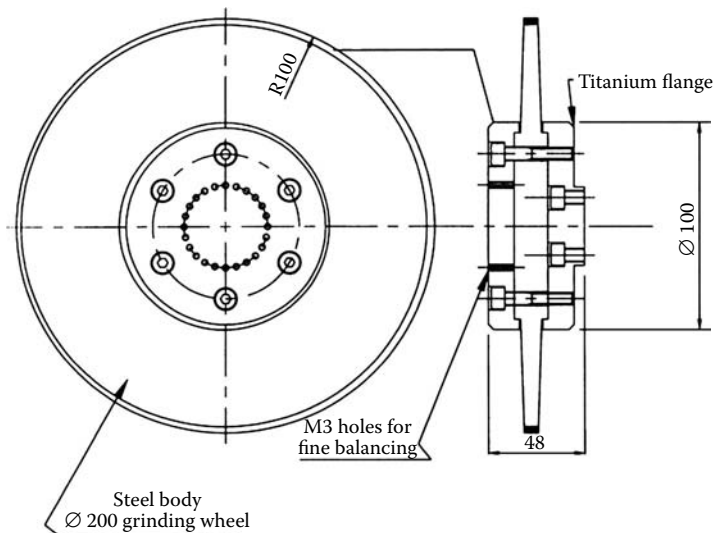


**FIGURE 4.24** Mount method for high-speed wheels using titanium flanges. (From Ramesh 2001. With permission.)

## 4.7 WHEEL DESIGN AND CHATTER SUPPRESSION

Chatter is an ever-present problem in grinding. Many claims have been made that the design of the wheel, especially regarding the use of hub materials with high *damping* characteristics used in conjunction with superabrasive wheels, can suppress its occurrence [Broetz 2001, Tyrolit 2001]. The reality is much more complicated and requires a brief discussion of the sources of vibration and chatter in grinding.

### 4.7.1 THE ROLE OF DAMPING

The basic equation for motion of a single-degree-of-freedom system is given by

$$x''(t) + 2\zeta\omega_n x'(t) + \omega_n^2 x(t) = F(t)$$

where

$$\begin{aligned}\zeta &= \text{damping factor} \\ \omega_n &= \text{natural frequency}\end{aligned}$$

In the absence of damping, energy is exchanged without loss during the course of motion at particular natural frequencies and the amplitude of vibration will build over time depending on the rate of input of energy. Damping absorbs energy either through internal friction of the particular material or more often in joints and seams. Prediction of the damping of a machine is not possible although damping in a particular mode of vibration may be determined empirically by use of a hammer test and measuring the decay rate. Damping is related to decay rate according to

$$\delta = (2\pi\zeta)/(1-\zeta^2)^{1/2} = \text{logarithmic decrement}$$

### 4.7.2 FORCED AND SELF-EXCITED VIBRATIONS

The source of the energy that creates vibration can be either external leading to forced vibration or inherent in the instability of the grind process leading to self-excited vibration.

#### 4.7.2.1 Forced Vibrations

Forced vibrations can be eliminated in three ways. First is to eliminate the energy at its source. Wheels, motors, belts, and workpieces should all be balanced as should the three-phase power supply. Ultra-precision bearings and ball screws should be used and properly maintained in work and wheel spindles and slides. Second, the grinder should be insulated from sources of vibration such as hydraulic and coolant pumps, and vibrations carried through the foundations. Third, where resonances cannot be eliminated the machine dynamics must be modified. Where a particularly prominent frequency exists in, for example, a motor or cantilevered member, tuned mass dampers consisting of a weight with a damped spring can be fitted at the point where the vibration needs to be reduced. This may often consist of a weight attached to the member via a rubber sheet sandwiched between. The sizes of the mass, spring, and damper are selected so that the mass oscillates out of phase with the driving frequency and, hence, dissipates energy. A relatively small-tuned mass can have a large effect in reducing vibration amplitude.

#### 4.7.2.2 Self-Excited Vibration

Self-excited chatter occurs only during grinding and the amplitude of vibration climbs with time. A small perturbation due to instability in the system causes a regular variation in grinding forces

that in turn creates an uneven level of wear around the wheel. The process is thus regenerative. There are several methods available for suppressing this form of chatter.

First, the system stiffness and damping can be increased. Second, the grinding conditions can be continuously varied by changing the work speed, wheel speed, work support compliance, or by periodically disengaging the wheel from the workpiece. For example, Gallemaers, Yegenoglu, and Vatovez [1986] reported that by periodically varying the work speed to prevent lobe buildup on the wheel, they could increase the grind (G) ratio by up to 40% and productivity (by extending the time between dresses) by up to 300%. Third, the stiffness of the contact area can be reduced to shift the state of the system more toward a stable grinding configuration [Snoeys 1968]. Fourth is the use of various filter effects to reduce the wavelength to less than the contact width. The work speed can be slowed to the point the chatter lines merge. Alternatively, and more interesting, the frequency of the chatter can be increased to the point that the grinding process itself acts as a filter to absorb the vibration energy. For this reason, the natural frequency of wheels is targeted at >500 Hz or ideally >1,000 Hz.

#### 4.7.3 DAMPED WHEEL DESIGNS AND WHEEL COMPLIANCE

It is interesting to note that most scientific studies on “damped” wheel designs are based on suppressing self-excited chatter. Furthermore, they all use hub materials that not only have good damping characteristics, but are also considerably more compliant and lightweight than “standard” hub materials such as steel. As the following examples illustrate, it is not only damping that is important for reducing vibrations. Reducing stiffness at the wheel contact has a similar effect. The analysis of chatter with added compliance at the wheel contact is given in the chapter on centerless grinding. Sexton, Howes, and Stone [1982] reported excellent results in reducing chatter when grinding steel with resin CBN wheels by the use of a “Retimet” nickel foam hub material with a radial stiffness of 0.5 N/ $\mu\text{m}\cdot\text{mm}$ . This was compared with values of 4 to 10 N/ $\mu\text{m}\cdot\text{mm}$  for standard phenolic (Bakelite) or aluminum-filled phenolic hubs. McFarland, Bailey, and Howes [1999] used polypropylene with a radial stiffness of 1.56 N/ $\mu\text{m}\cdot\text{mm}$  and natural frequency of 1,169 Hz. This was compared to a radial stiffness for an aluminum hub of 24 N/ $\mu\text{m}\cdot\text{mm}$ . Warnecke and Barth [1999] compared the performance of a resin-bonded diamond wheel on a flexible phenolic aluminum composite hub with a similar bond on an aluminum hub grinding SiN and demonstrated an improvement in life of over 70%. FEA analysis of the contact zone revealed over twice the radial deflection with the flexible hub. It would appear that compliance in the hub can be transferred through a resin superabrasive layer and can significantly increase contact width. See also Zitt and Warnecke [1996].

In 1989, Frost carried out an internal study for Unicorn (Saint-Gobain Abrasives) to evaluate the impact of the higher stiffness of vitrified CBN bonds on the centerless grinding process. The following radial contact stiffness values were obtained for conventional and CBN vitrified specifications:

47A100 L6YMRAA	0.06 N/ $\mu\text{m}\cdot\text{mm}$
5B46 P50 VSS	0.78 N/ $\mu\text{m}\cdot\text{mm}$
5B76 P50 VSS	0.31 N/ $\mu\text{m}\cdot\text{mm}$

The compliance of the CBN bonds were an order of magnitude greater than the conventional bond and approached or exceeded that of the hub materials described above. It would, therefore, be expected that as with the example earlier of resin-bonded diamond wheels, flexible hubs with radial stiffness values of the order of 0.5 N/ $\mu\text{m}\cdot\text{mm}$  could increase the contact width in the grind zone for wheels with a thin vitrified CBN layer. Further analysis of the effect of wheel compliance on chatter in centerless grinding is given in Chapter 19.

#### 4.7.4 WHEEL FREQUENCY AND CHATTER

The effect of wheel frequency on chatter was experienced first-hand by the author while developing a process for grinding large-diameter thin-walled casings with vitrified CBN. The project was initially prone to extreme chatter and noise. Maximizing the stiffness and nodal frequency of a steel-cored wheel by reducing the diameter by 30% and then doubling the body width increased wheel life by an order of magnitude and reduced noise by >20 dB. However, subsequently changing the hub material from steel to CFRP of comparable stiffness but one third the density further doubled wheel life. CFRP would have provided some additional damping but also significantly increased the natural frequency of the wheel due to its low density.

#### 4.7.5 SUMMARY

In conclusion, lightweight flexible hubs can provide benefit in grinding by limiting self-excited chatter generation with superabrasive wheels. Damping may also be an issue, but hub compliance and frequency responses are more likely to be the controlling factors. The concept is unlikely to be effective where significant forced vibration is present, although it is sometimes difficult to differentiate the two.

Compliance is much higher in conventional wheels. The effect on contact width for suppressing chatter is particularly pronounced when using plastic bonds for camshaft grinding or shellac bonds for roll grinding. Some benefit is even seen using rubber inserts in the bores of vitrified alox wheels for roll grinding. Even with resin diamond wheels, Busch [1970] was able to show a 300% improvement in life merely by placing a rubber sleeve between the wheel and flange to increase compliance.

Further research is likely to be focused on this aspect of wheel design as superabrasive technology targets applications such as roll and centerless grinding. It should be noted that efforts have been published regarding commercial product introducing microelasticity into vitrified diamond and CBN bonds [Graf 1992]. A more comprehensive review of the whole subject of grinding chatter excluding centerless grinding is given by Inasaki, Karpuschewski, and Lee [2001].

## REFERENCES

- Abdel-Alim, A., Hannam, R. G., and Hinduja, S. 1980. "A Feasibility Analysis of a Novel Form of High Speed Grinding Wheel." 21<sup>st</sup> International Machine Tool Design & Research Conference, Swansea.
- Anon. 1979. "High-Speed Plunge Grinding." *Mfg. Eng.* June 9, 67–69.
- Aoyama, T. and Inasaki, I. 2001. "Performance of HSK Tool Interfaces under High Rotational Speed." *Ann. CIRP* 50, M09.
- Barlow, N. and Rowe, W. B. 1983. "Discussion of Stresses in Plain and Reinforced Cylindrical Grinding Wheels." *Int. J. Mach. Tool Design Res.* 23, 2/3, 153–160.
- Barlow, N., Jackson, M. J., Mills, B., and Rowe, W. B. 1995. "Optimum Clamping of CBN and Conventional Vitreous-Bonded Cylindrical Grinding Wheels." *Int. J. Mach. Tools & Manuf.* 35, 1, 119–132.
- Barlow, N., Jackson, M. J., and Hitchiner, M. P. 1996. "Mechanical Design of High-Speed Vitrified CBN Grinding Wheels, Manufacturing Engineering: 2000 and Beyond." IMEC Conference, Proceedings. D. Marinescu, Ed., p. 568–570.
- Broetz, A. 2001. "Innovative Grinding Tools Increase the Productivity in Mass Production: Grinding of Crankshafts and Camshafts with Al<sub>2</sub>O<sub>3</sub> and CBN Grinding Wheels." Precision Grinding & Finishing in the Global Economy, Oak Brook, IL, Jan. 10, Conference, Proceedings. Gorham.
- Busch, D. M. 1970. "Machine Vibrations and Their Effect on the Diamond Wheel." *IDR* 30/360, 447–453.
- De Vicq, A. N. 1979. *An Investigation of Some Important Factors Affecting the Clamping of Grinding Wheels under Loose Flanges*. Machine Tool Industry Research Assoc., August, Macclesfield, U.K.
- Frost, M. 1989. "An Evaluation of Two Experimental CBN Wheels for Use in Centerless Grinding." Project report for Unicorn Industries, University of Bristol.



- Gallemaers, J. P., Yegenoglu, K., and Vatovez, C. 1986. "Optimizing Grinding Efficiency with Large Diameter CBN Wheels, SME86-644." International Grinding Conference.
- Graf, W. 1992. "CBN- und Diamantschleifscheiben mit mikroelastischer Keramikbindung." VSI-Z-Special Werkzeuge.
- Grinding Wheel Institute (GWI), 1983, *Fatigue Proof Test Procedure for Vitrified Grinding Wheels*. Grinding Wheel Institute.
- Hitchiner, M. P. 1991. "Systems Approach to Production Grinding with Vitrified CBN." SME 1991, Superabrasives Conference Proceedings.
- Inasaki, I., Karpuschewski, B., and Lee, H. S. 2001. "Grinding Chatter – Origin and Suppression." *Ann. CIRP*, keynote paper 50, 2.
- Junker Group International, commercial company presentation.
- Junker Maschinen. 1992. *A New Era in the Field of O.D. Grinding*. Trade brochure.
- Koenig, W. and Ferlemann, F. 1991. "CBN Grinding at Five Hundred m/s." *IDR* 2, 72–79.
- Kunihito et al. 1991. "Segmented Grinding Wheel." *EP*. 433 692 A2, June 26.
- McFarland, D. M., Bailey, G. E., and Howes, T. D. 1999. "The Design and Analysis of a Polypropylene Hub CBN Wheel to Suppress Grinding Chatter." *Trans. ASME* 121, Feb, 28–31.
- Menard, J. C. 1983. "Document WG6-4E, Calculations Based on Studies Conducted in 1963 at the Technical High School of Hannover, Germany." Private communication 5/3/1983.
- Meyer, R. 1996. "Safe Clamping of Cylindrical Grinding Wheels." Consultant for ANSI B7.1 code. Private communication 2/12/96.
- Muller-Held, B. 1998. "Development of a Repeatable Tool-Holder Based on a Statically Deterministic Coupling." MIT/RWTH Aachen project report, Feb.
- Pflager, W. W. 1997. "Finite Element Analysis of Various Wheel Configurations at 160 m/sec." Landis Internal Report, Sept. 23.
- Ramesh, K. 2001. *Towards Grinding Efficiency Improvement Using a New Oil-Air Mist Lubricated Spindle*. Ph.D. thesis, Nanyang Technical University, Singapore, May.
- Service, T. 1991. "Safe at Any Speed." *Cutting Tool Eng.* June, 99–101.
- Service, T. 1993. "Rethinking Grinding Wheel Standards." *Cutting Tool Eng.* Dec, 26–29.
- Service, T. 1996. "Superabrasive Safety." *Cutting Tool Eng.* June, 22–27.
- Sexton, J., Howes, T. D., and Stone, B. J. 1982. "The Use of Increased Wheel Flexibility to Improve Chatter Performance in Grinding." *Proc. Inst. Mech. Eng.* 1, 196, 291–300.
- Snoeys, R. 1968. *Cause and Control of Chatter Vibration in Grinding Operations*. Technical Society for Tool and Manufacturing Engineers.
- Tyrolit, S. S. 2001. "Grinding Disk Comprises an Intermediate Vibration Damping Ring Which Is Made as a Separate Part of Impregnated High-Strength Fibers, and Is Glued to the Central Carrier Body and/or the Grinding Ring." U.S. Patent DE 20102684.
- Warnecke, G. and Barth, C. 1999. "Optimization of the Dynamic Behavior of Grinding Wheels for Grinding of Hard and Brittle Materials Using the Finite Element Method." *Ann. CIRP*.
- Yamamoto, A. 1972. A Design of Reinforced Grinding Wheels. *Bull. JSPE* 6, 4, 127–128.
- Zitt, U. and Warnecke, G. 1996. "The Influence of a New Hub Material Concept on Process Behavior and Work Result in High Performance Grinding Processes with CBN." *Abrasives Magazine* April/May, 16–24.

---

# 5 The Nature of the Abrasive

## 5.1 INTRODUCTION

Modern grinding abrasives mainly fall into one of two groups, namely,

- Conventional abrasives based either on silicon carbide (SiC) or aluminum oxide (Al<sub>2</sub>O<sub>3</sub>), and
- Superabrasives based either on diamond or cubic boron nitride (CBN).

The division into two groups is based on a dramatic difference in hardness of the grains leading to very different wheel wear characteristics and grinding strategies. The division is also based on cost; wheels made using superabrasives are typically 10 to 100 times more expensive.

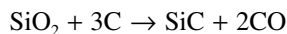
## 5.2 SILICON CARBIDE

### 5.2.1 DEVELOPMENT OF SiC

SiC was first synthesized in 1891 by Dr. E. G. Acheson, who gave it the trade name “Carborundum.” It was initially produced in only small quantities and sold for \$0.40/ct or \$880/lb as a substitute for diamond powder for lapping precious stones. In its time, it might well have been described as the first synthetic “superabrasive,” certainly compared to the natural emery and corundum minerals then otherwise available. However, once a commercially viable process of manufacturing was determined, its price fell precipitously, and by 1938 it sold for \$0.10/lb [Heywood 1938]. Today the material costs about \$0.80/lb.

### 5.2.2 MANUFACTURE OF SiC

SiC is manufactured in an Acheson resistance heating furnace through the reaction of silica sand and coke at a temperature of around 2,400°C. The overall reaction is described by the equation



A large carbon resistor rod is placed on a bed of raw materials to which a heavy current is applied. The raw material also includes sawdust to add porosity to help release the CO, and salt to remove iron impurities. The whole process takes about 36 hours and yields 10 to 50 tons of product. From the time it is formed, the SiC remains a solid as no melting occurs (SiC sublimates at 2,700°C). After cooling, the SiC is sorted by color; from green SiC, which is 99% pure, to black SiC, which is 97% pure. It is then crushed and sized as described for alumina below.

### 5.2.3 HARDNESS OF SiC

SiC has a Knoop hardness of about 2,500 to 2,800 and is very friable. The impurities within the black grade increase the toughness somewhat but the resulting grain is still significantly more friable than alumina. Above 750°C, SiC shows a chemical reactivity toward metals with an affinity for carbon, such as iron and nickel. This limits its use to grinding hard, nonferrous metals. SiC also reacts with boron oxide and sodium silicate, common constituents of vitrified wheel bonds [Viernekes 1987].

### 5.3 ALUMINA (ALOX)-BASED ABRASIVES

Alumina-based abrasives are derived either from a traditional route of electrofusion, or more recently by chemical precipitation and/or sintering. Unlike SiC, alumina is available in a large range of grades because it allows substitution of other oxides in a solid solution, and defect content can be much more readily controlled. The following description of alumina-based abrasives is classified into electrofused alumina abrasives and chemically precipitated or sintered alumina abrasives.

### 5.4 ELECTROFUSED ALUMINA ABRASIVES

#### 5.4.1 MANUFACTURE

The most common raw material for electrofused alumina is bauxite, which, depending on source, contains 85 to 90% alumina, 2 to 5% TiO<sub>2</sub>, and up to 10% of iron oxide, silica, and basic oxides. The bauxite is fused in an electric-arc furnace at 2,600°C using a process demonstrated by Charles Jacobs in 1897 but first brought to commercial viability under the name “alundum” with the introduction of the Higgins furnace by Aldus C. Higgins of the Norton Company in 1904 (Figure 5.1) [Tymeson 1953].

A Higgins furnace consists of a thin metal shell on a heavy metal hearth. A wall of water running over the outside of the shell is sufficient to maintain the shell integrity. A bed of crushed and calcined bauxite (mixed with some coke and iron to remove impurities) is poured into the bottom of the furnace and a carbon starter rod is laid on it. Two or three large vertical carbon rods are then brought down to touch and a heavy current is applied. The starter rod is rapidly consumed but the heat generated melts the bauxite, which then becomes an electrolyte. Bauxite is added continually over the next several hours to build up the volume of melt to as much as 20 tonnes. Current flow is controlled by adjusting the height of the electrodes which are eventually consumed in the process.

Perhaps the most surprising feature of the process is the fact that a thin, water-cooled steel shell is sufficient to contain the process. This is indicative of the low thermal conductivity of



**FIGURE 5.1** Higgins-type electric arc furnace for fusion processes of alumina and zirconia. (Courtesy of Saint-Gobain Abrasives. With permission.)

alumina, a factor that is also significant for its grinding performance as will be described in later sections. The alumina forms a solid insulating crust next to the steel. After the fusion is complete, the furnace is either left to cool or, with more modern furnaces typical of those currently in use in the United States, the melt is poured onto a water-cooled steel hearth to better control microstructure.

Once cooled, the alumina is broken up and passed through a series of hammer, beater, crush, roller, and/or ball mills to reduce it to the required grain size. The type of crush process also controls the grain shape, producing either blocky or thin splintered grains. After milling, the product is sieved to the appropriate sizes down to about 40  $\mu\text{m}$  (400#).

#### 5.4.2 BROWN ALUMINA

The resultant abrasive is called brown alumina and contains typically 3%  $\text{TiO}_2$ . It has a Knoop hardness of 2,090 and a medium friability. Increasing the  $\text{TiO}_2$  content increases the toughness but reduces hardness. Although termed brown, the high temperature furnacing in air required in subsequent vitrified wheel manufacture turns the brown alumina grains a gray-blue color due to further oxidation of the  $\text{TiO}_2$ .

#### 5.4.3 WHITE ALUMINA

Electrofused alumina is also made using low-soda Bayer Process alumina that is >99% pure. The resulting grain is one of the hardest, but most friable, of the alumina abrasive family providing a cool-cutting action especially suitable for precision grinding in vitrified bonds. Also, its low sodium content deters wheel breakdown from coolant attack when used in resin bonds.

White alumina is the most popular grade for micron-sized abrasives in part because the crushing process concentrates impurities in the fines when processing other alumina grades. To produce micron sizes, the alumina is further ball-milled or vibro-milled after crushing and then traditionally separated into sizes using an elutriation process. This is achieved by passing a slurry of the abrasive and water through a series of vertical columns. The width of the columns is adjusted to produce a progressively slower vertical flow velocity from column to column. Heavier abrasive settles out in the faster flowing columns while the lighter particles are carried over to the next. The process is effective down to about 5  $\mu\text{m}$  and is also used for micron-sizing SiC. More recently, air classification has also been adopted.



FIGURE 5.2 Pouring of molten alumina. (From Wellborn 1994. With permission.)

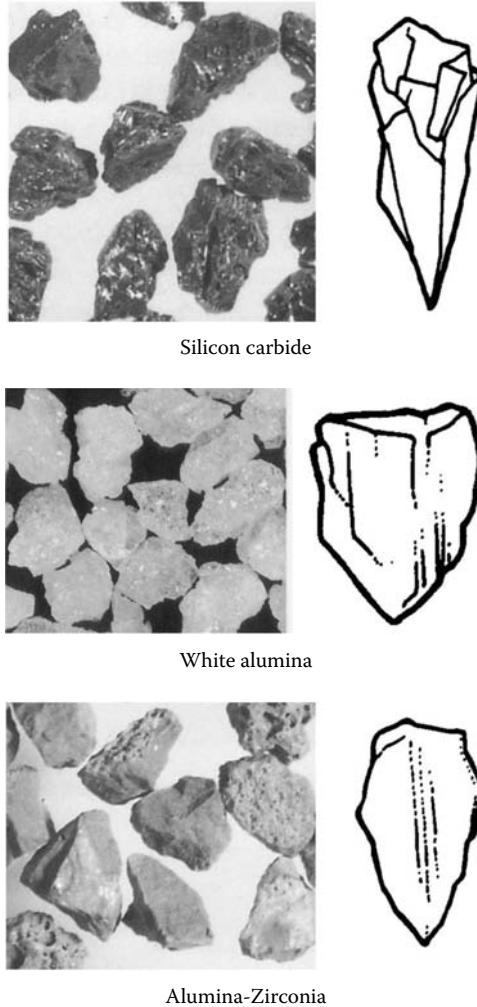


**FIGURE 5.3** Examples of SiC, fused alumina, and fused alumina-zirconia grain types.

Not surprisingly, since electrofused technology has been available for 100 years, many variations of the process exist both in terms of starting compositions and processing routes. Some examples are illustrated in Figure 5.3.

#### 5.4.4 ALLOYING ADDITIVES

Additives are employed to modify the properties of alumina as described below. Examples of additives include chromium oxide, titanium oxide, zirconium oxide, and vanadium oxide.

#### 5.4.5 PINK ALUMINA

The addition of chromium oxide produces pink alumina. White alumina is alloyed with <0.5% chrome oxide to give the distinctive pink hue of pink alumina. The resulting grain is slightly harder than white alumina, while addition of a small amount of  $\text{TiO}_2$  increases its toughness. The resultant product is a medium-sized grain available in elongated, or blocky, but sharp, shapes.

#### 5.4.6 RUBY ALUMINA

Ruby alumina has a higher chrome oxide content of 3% and is more friable than pink alumina. The grains are blocky, sharp-edged, and extremely cool cutting making them popular for tool room and dry grind application on steels (e.g., ice skate sharpening). Vanadium oxide has also been used as an additive giving a distinctive green hue.

#### 5.4.7 ZIRCONIA-ALUMINA

Zirconia is added to alumina to refine the grain structure and produce a tough abrasive. At least three different zirconia-alumina compositions are used in grinding wheels:

- 75% Alox, 25% ZrO<sub>2</sub>
- 60% Alox, 40% ZrO<sub>2</sub>
- 65% Alox, 30%ZrO<sub>2</sub>, 5%TiO<sub>2</sub>

Manufacture usually includes rapid solidification to enhance the nature of the grain structure. The resulting abrasives are fine grain, extremely tough, and give excellent life in medium to heavy stock removal applications such as billet grinding in foundries.

#### 5.4.8 SINGLE CRYSTAL WHITE ALUMINA

Grain growth is closely controlled in a sulphide matrix. The alumina is separated out by acid leaching without crushing. The grain shape is nodular, which aids bond retention, while the elimination of crushing reduces mechanical defects from processing.

#### 5.4.9 POSTFUSION PROCESSING METHODS

As mentioned above, the type of particle reduction method can greatly affect the resulting grain shape. Impact crushers like hammer mills will create a blocky shape, while roll crushers will cause more splintering. It is further possible using electrostatic forces to separate sharp shapes from blocky grains to provide grades of the same composition but very different cutting action.

#### 5.4.10 POSTFUSION HEAT TREATMENT

The performance of an abrasive can also be altered by heat treatment, particularly for brown alumina. The grit is heated to 1,100°C to 1,300°C, depending on grit size, in order to anneal cracks and flaws created by the crushing process. This can enhance toughness by 25 to 40%.

#### 5.4.11 POSTFUSION COATINGS

Finally, several coating processes exist to improve bonding of the grains in the grinding wheel. Red iron oxide is applied at high temperature to increase surface area for better bonding in resin cutoff wheels. Silane is applied for some resin bond wheel applications to repel coolant infiltration between bond and abrasive grit and thus protect the resin bond.

### 5.5 CHEMICAL PRECIPITATION AND/OR SINTERING OF ALUMINA

#### 5.5.1 IMPORTANCE OF CRYSTAL SIZE

A limitation of the electrofusion route is that the resulting abrasive crystal structure is very large; an abrasive grain may consist of only one to three crystals. Consequently, when grain fracture

occurs, the resulting particle loss may be a large proportion of the whole grain. This results in inefficient grit use. One way to avoid this is to dramatically reduce the crystallite size.

### 5.5.2 MICROCRYSTALLINE GRITS

The earliest grades of microcrystalline grits were produced in 1963 (U.S. Patent 3,079,243) by compacting a fine-grain bauxite slurry, granulating to the desired grit size, and sintering at 1,500°C. The grain shape and aspect ratio could even be controlled by extruding the slurry.

### 5.5.3 SEEDED GEL ABRASIVE

The most significant development, however, probably since the invention of the Higgins furnace, was the release in 1986 of SG (seeded gel) abrasive by The Norton Company (U.S. Patents 4,312,827 1982; 4,623,364 1986). This abrasive was a natural outcome of the wave of technology sweeping the ceramics industry at that time to develop high strength engineering ceramics using chemical precipitation methods. In fact, this class of abrasives is commonly termed “ceramic.” SG is produced by a chemical process whereby MgO is first precipitated to create 50-nm-sized alumina-magnesia spinel seed crystals in a precursor of boehmite. The resulting gel is dried, granulated to size, and sintered at 1,200°C. The grains produced are composed of a single-phase  $\alpha$ -alumina structure with a crystallite size of about 0.2  $\mu\text{m}$ . Again, defects from crushing are avoided; the resulting abrasive is unusually tough but self-sharpening because fracture now occurs at the micron level.

### 5.5.4 APPLICATION OF SG ABRASIVES

As with all new technologies, it took significant time and application knowledge to understand how to apply SG. The abrasive was so tough that it had to be blended with regular fused abrasive at levels as low as 5% to avoid excessive grinding forces. Typical blends are now

- 5SG (50%)
- 3SG (30%)
- 1SG (10%)

These blended abrasive grades can increase wheel life by up to a factor of 10 over regular fused abrasives although manufacturing costs are also higher.

The grain shape can also be controlled to surprising extremes by the granulation processes adopted. The shape can be varied from the very blocky to the very elongated as illustrated in Figure 5.4.

### 5.5.5 SOL GEL ABRASIVES

In 1981, actually prior to the introduction of SG, 3M Company introduced a sol-gel abrasive material they called Cubitron for use in coated abrasive fiber discs. This was again a submicron chemically precipitated and sintered material, but unlike SG, was a multiphase composite structure that did not use seed grains to control crystallite size. The value of the material for grinding wheel applications was not recognized until after the introduction of SG. After protracted patent litigation and settlement with Norton, Cubitron is now used by most other wheel makers. In the manufacture of Cubitron, alumina is coprecipitated with various modifiers such as magnesia, yttria, lanthana, and neodymia to control microstructural strength and surface morphology upon subsequent sintering. For example, one of the most popular materials, Cubitron 321, has a microstructure that contains submicron platelet inclusions, which act as reinforcements somewhat similar to a whisker-reinforced ceramic [Bange and Orf 1998].

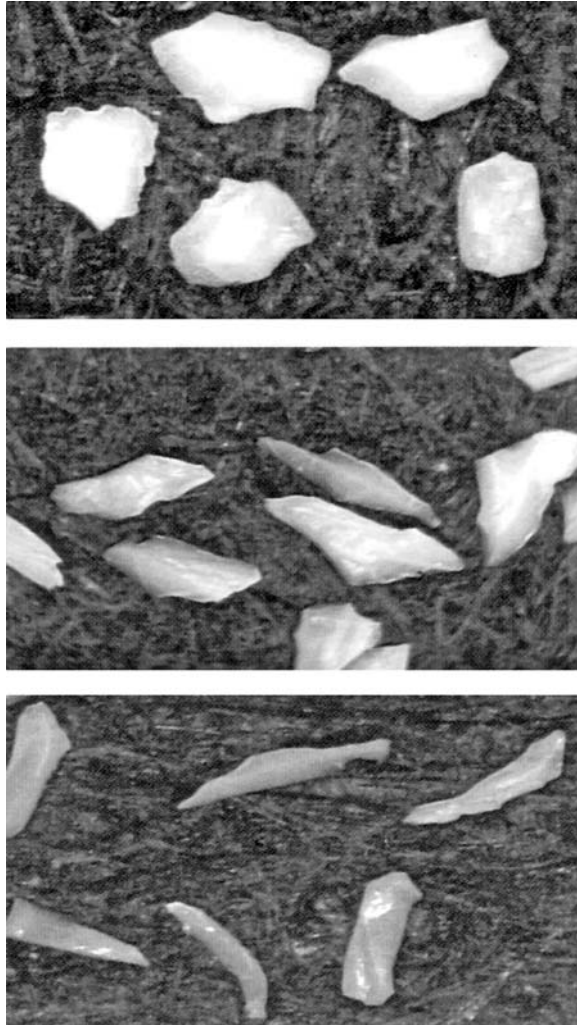


**FIGURE 5.4** Examples of seeded gel abrasive grain shapes. (Courtesy of Saint-Gobain Abrasives. With permission.)

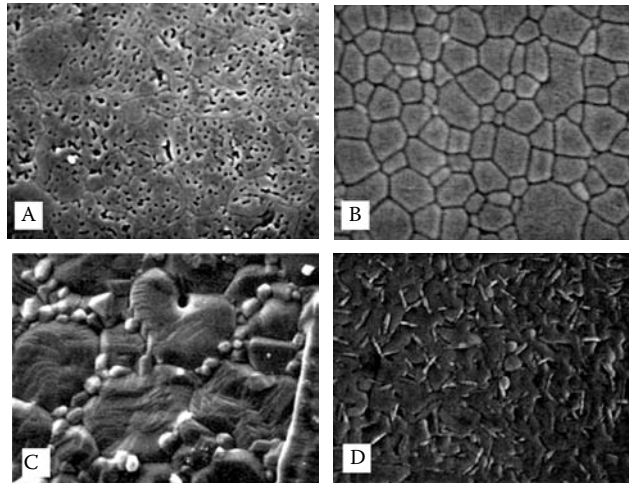
### 5.5.6 COMPARISON OF SG AND CUBITRON ABRASIVES

Direct comparison of the performance of SG and Cubitron is difficult because the grain is merely one component of the grinding wheel. SG is harder (21 GPa) than Cubitron (19 GPa). Anecdotal evidence in the field suggests that wheels made from SG give longer life but Cubitron is freer-cutting. This can make Cubitron the preferred grain in some applications but, from a cost/performance point of view, it is, therefore, also currently more prone to challenge from a well-engineered (i.e., shape-selected) fused grain that is the product of a lower cost, mature technology.

### 5.5.7 EXTRUDED SG ABRASIVE

SG grain shape can also be controlled by extrusion. Norton has taken this concept to an extreme and in 1999 introduced TG and TG2 (extruded SG) grains in products called Targa and ALTOS. TG grain had an aspect ratio of 4:1, while TG2 had an aspect ratio of 8:1. TG2 grains have the appearance of rods or “worms” due to these high aspect ratios. The resulting natural packing





- A – Unseeded pure alumina-sintered gel with large uncontrolled grain growth
- B – Norton SG alumina with controlled microstructure
- C – Unseeded sintered alumina gel with magnesia additions
- D – 3M cubitron 321 with magnesia and rare earth oxide additions

**FIGURE 5.5** Examples of ceramic grain processing microstructures.

characteristics of these shapes in a grinding wheel result in a high-strength, lightweight structure with porosity levels as high as 70% or even greater. The grains touch each other at only a few points where bond also concentrates like “spot welds.” The product offers potential for both higher stock removal rates and higher wheel speeds due to the strength and density of the resulting wheel body [Klocke, Mueller, and Englehorn 2000].

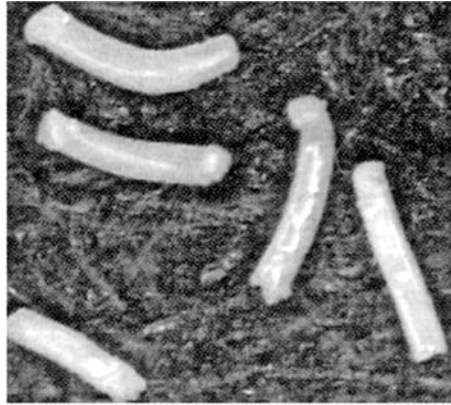
### 5.5.8 FUTURE TRENDS FOR CONVENTIONAL ABRASIVES

With time, it is expected that SG, TG/TG2, Cubitron, and other emerging chemical precipitation/sintering processes will increasingly dominate the conventional abrasive market. The production of electrofused product is likely to shift more and more from traditional manufacturing sites with good availability of electricity, such as around the Great Lakes of the United States and Norway, to lower cost, growing economies such as China and Brazil.

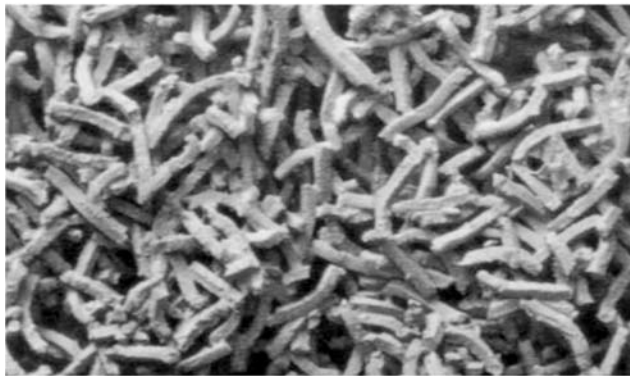
## 5.6 DIAMOND ABRASIVES

### 5.6.1 NATURAL AND SYNTHETIC DIAMONDS

Diamond holds a unique place in the grinding industry. Being the hardest material known it is not only the abrasive choice for grinding the hardest, most difficult materials, but also it is the only material that can truly address all abrasive wheels effectively. Diamond is the only wheel abrasive that is still obtained from natural sources. Although synthetic diamond dominates in wheel manufacture, natural diamond is preferred for dressing tools and form rolls. Diamond materials are also used increasingly as wear surfaces for applications such as end stops and work-rest blades on grinding machines. In these types of applications, diamond can give 20 to 50 times the life of tungsten carbide.



Loose grain appearance



Wheel structural appearance

**FIGURE 5.6** Norton TG2 abrasive grain and Altos Wheel Structure. (From Norton 1999a, 1999b. With permission.)

### 5.6.2 ORIGIN OF DIAMOND

Diamond is created by the application of extreme high temperatures and pressures to graphite. Such conditions occur naturally at depths of 120 miles in the upper mantle or in heavy meteorite impacts. Diamond is mined from Kimberlite pipes that are the remnant of small volcanic fissures typically 2 to 50 m in diameter where magma has welled up in the past. Major producing areas of the world include South Africa, West Africa (Angola, Tanzania, Zaire, Sierra Leone), South America (Brazil, Venezuela), India, Russia (Ural Mountains), Western Australia, and most recently Canada. Each area, and even each individual pipe, will produce diamonds with distinct characteristics.

### 5.6.3 PRODUCTION COSTS

Production costs are high, with 13 million tons of ore, on average, processed to produce 1 ton of diamonds. Much of this cost is supported by the demand for diamonds by the jewelry trade. Since World War II, the output of industrial grade diamond has been far outstripped by demand. This spurred the development of synthetic diamond programs initiated in the late 1940s and 1950s [Maillard 1980].

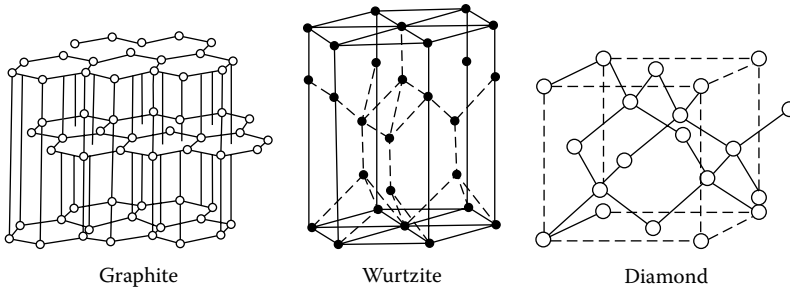


FIGURE 5.7 Common structures of carbon.

### 5.6.4 THREE FORMS OF CARBON

The stable form of carbon at room temperature and pressure is graphite, where the carbon atoms are arranged in a layered structure. Within the layer, atoms are positioned in a hexagonal lattice. Each carbon atom is bonded to three others in the same plane with the strong  $sp^2$  covalent bonding required for a high hardness material. However, bonding between the layers is weak, being generated from Van de Waals forces only, and results in easy slippage and low friction. (In fact, pure graphite is highly abrasive because, although there is low friction between the layers, the edges of individual sheets have dangling bonds that are highly reactive. It is only the presence of water vapor in the air or dopants added to the graphite that neutralizes these sites and makes graphite a low-friction surface). Diamond, which is meta-stable at room temperature and pressure, has a cubic arrangement of atoms with pure  $sp^3$  covalent bonding with each carbon atom bonded to four other carbon atoms. There is also an intermediate material called wurtzite or hexagonal diamond where the hexagonal layer structure of graphite has been distorted above and below the layer planes but not quite to the full cubic structure. The material is nevertheless almost as hard as the cubic form.

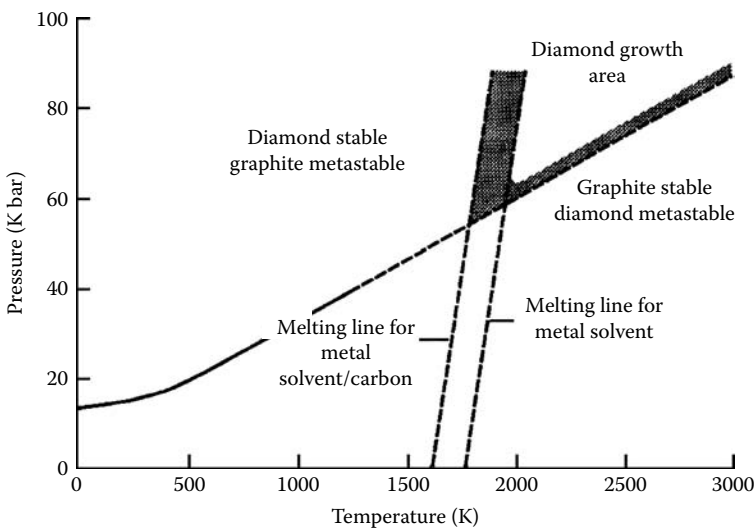


FIGURE 5.8 Phase diagram for carbon.

### 5.6.5 THE SHAPE AND STRUCTURE OF DIAMOND

The principal crystallographic planes of diamond are the cubic (100), dodecahedron (011), and octahedron (111). The relative rates of growth on these planes are governed by the temperature and pressure conditions, together with the chemical environment during both growth and, in the case of natural diamond, possible dissolution during its travel to the earth's surface. This, in turn, governs the diamond stone shape and morphology.

The phase diagram for diamond/graphite is shown in Figure 5.8.

### 5.6.6 PRODUCTION OF SYNTHETIC DIAMOND

The direct conversion of graphite to diamond requires temperatures of 2,500 K and pressures of >100 Kbar. Creating these conditions was the first hurdle to producing man-made diamonds. The General Electric Company (GE) achieved this through the invention of a high-pressure/temperature gasket called the "belt" and announced the first synthesis of diamond in 1955. Somewhat to their surprise, it was then announced that a Swedish company, ASEA, had secretly made diamonds 2 years previously using a more complicated six-anvil press. ASEA had not announced the fact because they were seeking to make gems and did not consider the small brown stones they produced the culmination of their program! De Beers announced their ability to synthesize diamonds shortly after GE in 1958.

The key to manufacture was the discovery that a metal solvent such as nickel or cobalt could reduce the temperature and pressure requirements to manageable levels. Graphite has a higher solubility in nickel than diamond has; therefore, at the high-process temperatures and pressures the graphite dissolves in the molten nickel and diamond then precipitates out. The higher the temperatures, the faster is the precipitation rate and the greater the number of nucleation sites. The earliest diamonds were grown fast at high temperatures and had weak, angular shapes with a mosaic structure. This material was released by GE under the trade name RVG, for "Resin Vitrified Grinding" wheels. Most of the early patents on diamond synthesis have now expired and competition from emerging economies has driven down the price of this type of material to as little as \$400/lb, although quality and consistency from these sources are still often sometimes questionable.

### 5.6.7 CONTROLLING STONE MORPHOLOGY

By controlling the growth conditions, especially time and nucleation density, it is possible to grow much higher quality stones with well-defined crystal forms: cubic at low temperature, cubo-octahedra at intermediate temperatures, and octahedra at the highest temperatures. The diagram for growth morphologies of diamond is shown in Figure 5.9.

The characteristic shape of good-quality natural stones is octahedral, but the toughest stone shape is cubo-octahedral. Unlike in nature, this can be grown consistently by manipulation of the synthesis process. This has led to a range of synthetic diamond grades typified by the MBG series from GE and the PremaDia series from De Beers [1999], which are the abrasives of choice for saws used in the stone and construction industry and for glass grinding wheels.

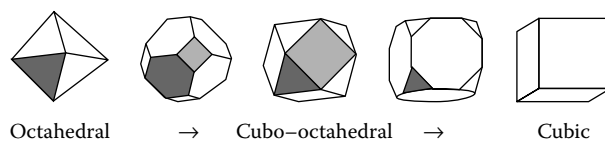


FIGURE 5.9 Growth morphologies of diamond.

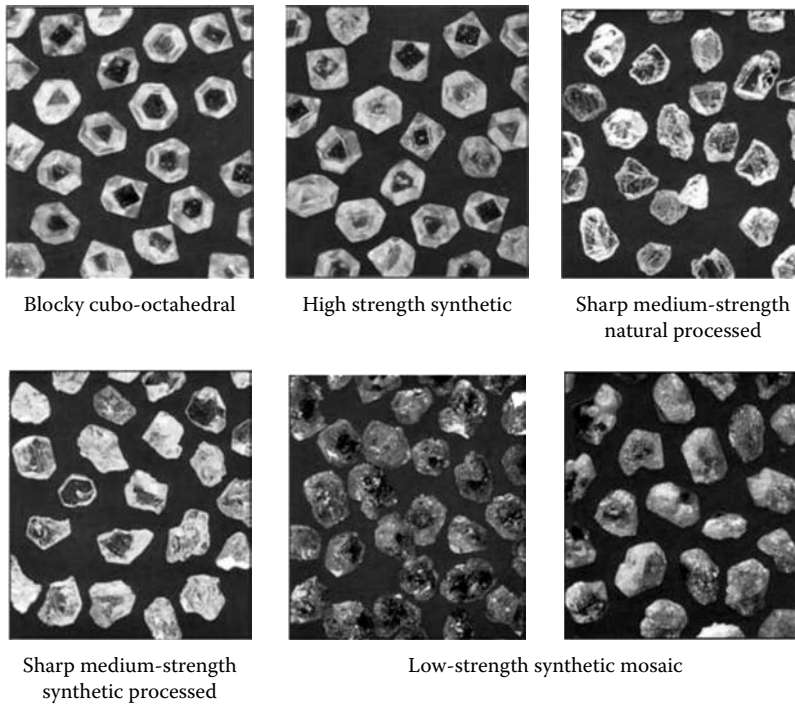


FIGURE 5.10 Typical diamond grit shapes, morphologies, and coatings. (From De Beers.)

### 5.6.8 DIAMOND QUALITY MEASURES

The quality and price of the diamond abrasive grain grade is governed both by the consistency of shape and the level of entrapped solvent in the stones. Since most of the blockiest abrasive is used in metal bonds processed at high temperatures, the differential thermal expansion of metal inclusions in the diamond can lead to reduced strength or even fracture. Other applications require weaker phenolic or polyimide resin bonds processed at much lower temperatures and use more angular, less thermally stable diamonds. Grit manufacturers, therefore, characterize their full range of diamond grades by room temperature toughness (TI), thermal toughness after heating at, for example, 1,000°C (TTI), and shape (blocky, sharp, or mosaic). Included in the midrange, sharp grades are both crushed natural as well as synthetic materials.

### 5.6.9 DIAMOND COATINGS

Diamond coatings are common. One range includes thick layers or claddings of electroplated nickel, electroless Ni-P, copper, or silver at up to 60%wt. The coatings behave as heat sinks, while increasing bond strength and keeping abrasive fragments from escaping. Electroplated nickel, for example, produces a spiky surface that provides an excellent anchor for phenolic bonds when grinding wet. Copper and silver bonds are used more for dry grinding, especially with polyimide bonds, where the higher thermal conductivity outweighs the lower strength of the coating [Jakobuss 1999]. Attention should be paid to wheel Material Data Safety Sheets (MSDS) to confirm chemical composition to ensure any coating used does not present a contaminant problem. For example, silver contamination may be a problem in grinding of titanium alloys.

Coatings can also be applied at the micron level either as a wetting agent or as a passive layer to reduce diamond reactivity with the particular bond. Titanium is coated on diamonds used in nickel-, cobalt-, or iron-based bonds to limit graphitization of the diamond while wetting the

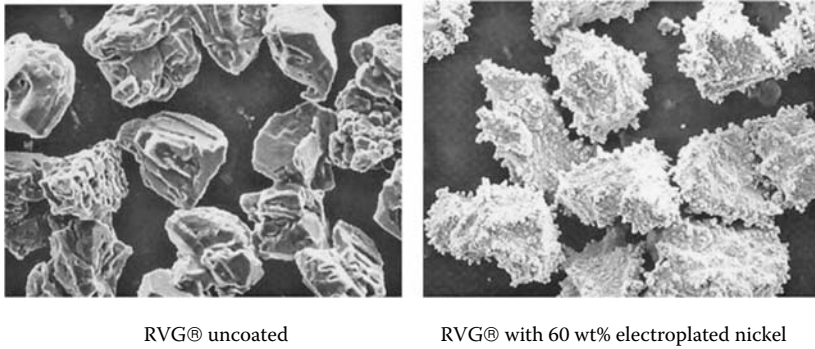


**FIGURE 5.11** Effect of coating on surface morphology of diamond grain. (From GE superabrasives. With permission.)

diamond surface. Chromium is coated on diamonds used in bronze- or WC-based bonds to enhance chemical bonding and reactivity of the diamond and bond constituents.

Finally, for electroplated bonds, the diamonds are acid etched to remove any surface nodules of metal solvent that would distort the plating electrical potential on the wheel surface leading to uneven nickel plating or even nodule formation. It also creates a slightly rougher surface to aid mechanical bonding.

### 5.6.10 POLYCRYSTALLINE DIAMOND (PCD)

Since 1960, several other methods of growing diamond have been developed. In 1970, DuPont launched a polycrystalline material produced by the sudden heat and pressure of an explosive shock. The material was wurtzitic in nature and produced mainly at micron particle sizes suitable more for lapping and polishing than grinding or as a precursor for PCD monolithic material.

In 1970, PCD (Poly Crystalline Diamond) blanks were introduced that consisted of a fine grain sintered diamond structure bonded to a tungsten carbide substrate. The material was produced by the action of high temperatures and pressures on a diamond powder mixed with a metal solvent to promote intergrain growth. Since it contained a high level of metal binder it could be readily fabricated in various shapes using electrodischarge machining (EDM) technology. Although not used in grinding wheels, it is popular as reinforcement in form dress rolls and for wear surfaces on grinding machines. Its primary use, though, is in cutting tools.

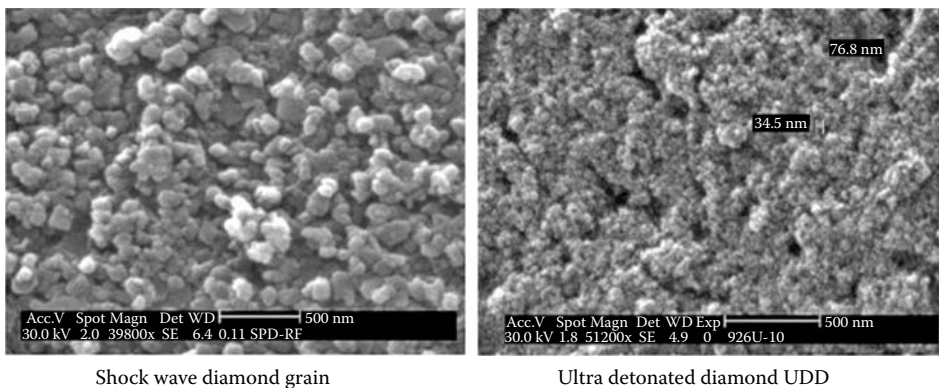


**FIGURE 5.12** Examples of shock wave-produced diamond grains. (From Saint Gobain Ceramics. With permission.)

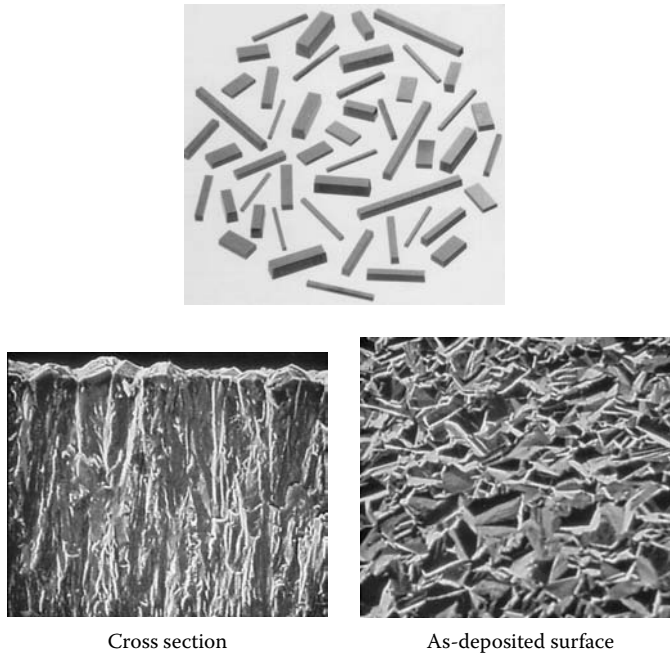


**FIGURE 5.13** Chemical vapor deposition, diamond samples, and microstructure. (From Gigel 1994. With permission.)

### 5.6.11 DIAMOND PRODUCED BY CHEMICAL VAPOR DEPOSITION (CVD)

In 1976, reports began to come out of Russia of diamond crystals being produced at low pressures through Chemical Vapor Deposition. This was treated with some skepticism in the West even though Russia had a long history of solid research on diamond. However, within 5 years, Japan was also reporting rapid growth of diamond by CVD at low pressures and the product finally became available in commercial quantities by about 1992. The process involves reacting a carbonaceous gas in the presence of hydrogen atoms in near vacuum to form the diamond phase on an appropriate substrate. Energy is provided in the form of hot filaments or plasmas at  $>800^{\circ}\text{C}$  to dissociate the carbon and hydrogen into atoms. The hydrogen interacts with the carbon and prevents any possibility of graphite forming while promoting diamond growth on the substrate. The resulting layer can form to a thickness of  $>1$  mm.

### 5.6.12 STRUCTURE OF CVD DIAMOND

CVD diamond forms as a fine crystalline columnar structure. There is a certain amount of preferred crystallographic orientation exhibited; more so than, for example, PCD, but far less than in single crystal diamond. Wear characteristics are therefore much less sensitive to orientation in a tool. Again, the CVD diamond is not used as an abrasive but is proving very promising when fabricated in the form of needle-shaped rods for use in dressing tools and rolls. Fabrication with CVD is slightly more difficult as it contains no metal solvents to aid EDM wire cutting and diamond wetting also appears more difficult and must be compensated for by the use of an appropriate coating.

### 5.6.13 DEVELOPMENT OF LARGE SYNTHETIC DIAMOND CRYSTALS

In the last 10 years, increasing effort has been placed on growing large synthetic diamond crystals at high temperatures and pressures. The big limitation has always been that press time and hence

cost goes up exponentially with diamond size. The largest saw grade diamonds are typically 30 to 40#. The production of larger stones in high volume, suitable for tool and form-roll dressing applications, is not yet cost-competitive with natural diamond. However, there has recently proved to be an exception to this, namely, the introduction, first by Sumitomo, of needle diamond rods produced by the slicing up of large synthetic diamonds. The rods are typically less than 1 mm in cross section by 2 to 5 mm long (similar in dimensions to the CVD diamond rods discussed above) but orientated along the principal crystallographic planes to allow optimized wear and fracture characteristics when orientated in a dressing tool. Several companies now supply a similar product.

#### **5.6.14 DEMAND FOR NATURAL DIAMOND**

Even with the dramatic growth in synthetic diamond, the demand by industry for natural diamond has not declined. If anything, the real cost of natural diamond has actually increased especially for higher quality stones. The demand for diamonds for jewelry is such that premium stones used in the 1950s for single-point diamonds are now more likely to be used in engagement rings; while very small gem quality stones once considered too small for jewelry and used in profiling dressing discs, are now being cut and lapped in countries such as India. With this type of economic pressure it is not surprising that the diamonds used by industry are those rejected by the gem trade because of color, shape, size, crystal defects such as twins or naats, or excessive inclusion levels; or are the processed fragments from, for example, cleaving gems. Although significant quantities of processed material are still used in grinding wheel applications, it is the larger stones used in single-point and form-roll dressing tools that are of most significance. Here the quality of the end product depends on the reliability of the diamond source and of the ability of the tool maker to sort diamonds according to requirements. The highest quality stones will be virgin as-mined material. Lower quality stones may have been processed by crushing and/or ball-milling, or even reclaimed from old form dressing rolls or drill bits where they had previously been subjected to high temperatures or severe conditions.

#### **5.6.15 FORMS OF NATURAL DIAMOND**

Natural diamond grows predominantly as the octahedral form that provides several sharp points optimal for single-point diamond tools. It also occurs in a long-stone form, created by the partial dissolution of the octahedral form as it ascended to the Earth's surface. These are used in dressing tools such as the Fliesen blade developed by Ernst Winter & Son. It should be noted, though, that long-stone shapes are also produced by crushing and ball-milling of diamond fragments; these will have introduced flaws which significantly reduce strength and life. The old adage of "you get what you pay for" is very pertinent in the diamond tool business!

Twinned diamond stones called maacles also occur regularly in nature. These are typically triangular in shape. The twinned zone down the center of the triangle is the most wear-resistant surface known and maacles are used both in dressing chisels as well as reinforcements in the most demanding form-roll applications.

#### **5.6.16 HARDNESS OF DIAMOND**

The hardness of diamond is a difficult property to define for two reasons. First, hardness is a measure of plastic deformation but diamond does not plastically deform at room temperature. Second, hardness is measured using a diamond indenter. Measuring hardness in this case is, therefore, akin to measuring the hardness of soft butter with an indenter made of hard butter! Fortunately, the hardness of diamond is quite sensitive to orientation and using a Knoop indenter; a distorted pyramid with a long diagonal seven times the short diagonal, orientated in the hardest



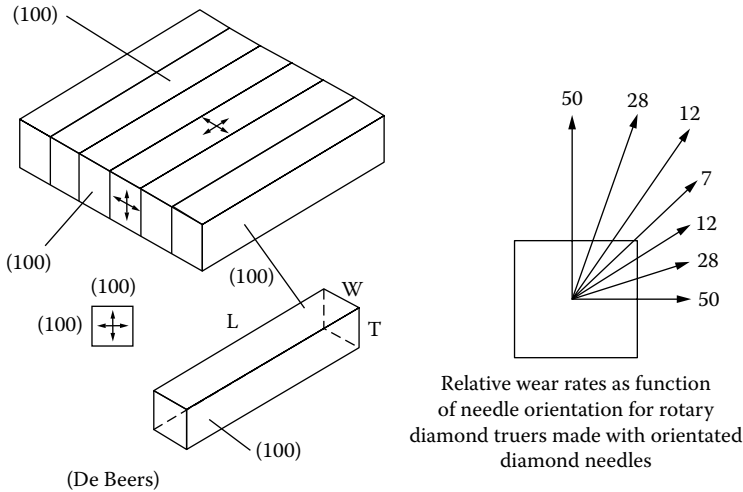


**FIGURE 5.14** Monocrystal diamond needles cut with controlled crystallographic orientation for enhanced repeatability and life in dressing tools. (From De Beers 1993. With permission.)

direction, gives somewhat repeatable results. The following hardness values have been obtained [Field 1983]:

- (001) plane. [110] direction. 10,400 kg/mm<sup>2</sup>
- (001) plane. [100] direction. 5,700 kg/mm<sup>2</sup>
- (111) plane. [111] direction. 9,000 kg/mm<sup>2</sup>

### 5.6.17 WEAR RESISTANCE OF DIAMOND

More important than hardness is mechanical wear resistance. This is also a difficult property to pin down because it is so dependent on load, material, hardness, speed, and so on. Wilks and Wilks [1972] showed that when abrading diamond with diamond abrasive, wear resistance increases with hardness but the differences between orientations are far more extreme. For example, on the cube plane, the wear resistance between the [100] and the [110] directions varies by a factor of 7.5, giving good correlation with wear data of needle diamonds reported in Figure 5.14. In other planes, the differences were as great as a factor 40, sometimes with only relatively small changes in angle. Not surprisingly, diamond gem lappers often speak of diamond having “grain”-like wood. Factors regarding the wear resistance of diamond on other materials in a machining process such as grinding, however, must include *all* possible attritious wear processes including thermal and chemical.

### 5.6.18 STRENGTH OF DIAMOND

Diamond is very hard and brittle. It can be readily cleaved along its four (111) planes. Its measured strength varies widely due in part to the nature of the tests, but also because it is heavily dependent on the level of defects, inclusions, and impurities present. Not surprisingly, small diamonds (with smaller defects) give higher values for strength than larger diamonds. The compressive strength of top-quality synthetic diamond (100#) grit has been measured at 1,000 kg.mm<sup>-2</sup>.

### 5.6.19 CHEMICAL PROPERTIES OF DIAMOND

The diamond lattice is surprisingly pure, as the only other elements known to be incorporated are nitrogen and boron. Nitrogen is present in synthetic diamonds at up to 500 parts per million in

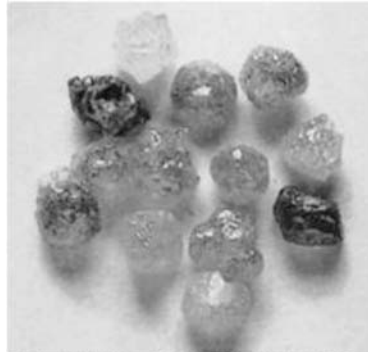
single substitutional sites and gives the stones their characteristic yellow/green color. Over an extended time at high temperature and pressure, the nitrogen migrates and forms aggregates, and the diamond becomes the colorless stone found in nature. Synthetic diamond contains up to 10% included metal solvents, while natural diamond usually contains inclusions of the minerals in which it was grown (e.g., olivine, garnet, and spinels).

**5.6.20 THERMAL STABILITY OF DIAMOND**

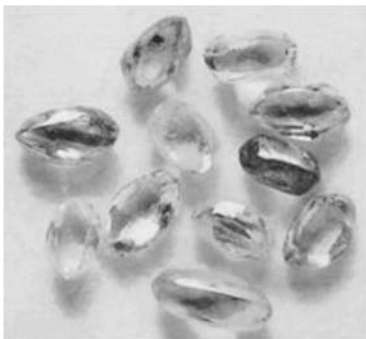
Diamond is metastable at room temperatures and pressures and it will convert to graphite given a suitable catalyst or sufficient energy. In a vacuum or in inert gas, diamond remains unchanged up



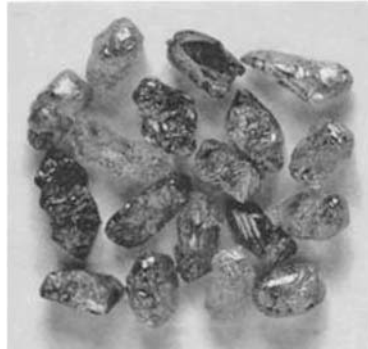
Premium dressing stones



Lower quality/processed dressing stones



Premium long stones



Lower quality/processed long stones



Maacles



Ballas

**FIGURE 5.15** Natural industrial Diamonds. (From Henri Polak Diamond Corp. 1979. With permission.)

to 1,500°C; in the presence of oxygen it will begin to degrade at 650°C. This factor plays a significant role in how wheels and tools are processed in manufacturing.

### 5.6.21 CHEMICAL AFFINITY OF DIAMOND

Diamond is readily susceptible to chemical degradation from carbide formers, such as tungsten, tantalum, titanium, and zirconium, and true solvents of carbon, which include iron, cobalt, manganese, nickel, chromium, and the Group VIII platinum and palladium metals.

### 5.6.22 EFFECTS OF CHEMICAL AFFINITY IN MANUFACTURE

This chemical affinity can be both a benefit and a curse. It is a benefit in the manufacture of wheels and tools where the reactivity can lead to increased wetting and, therefore, higher bond strengths in metal bonds. For diamond tool manufacture, the reactant is often part of a more complex eutectic alloy (e.g., copper-silver, copper-silver-indium, or copper-tin) in order to minimize processing temperature, disperse and control the active metal reactivity, and/or allow simplified processing in air. Alternatively, tools are vacuum brazed. For metal-bonded wheels, higher temperatures and more wear-resistant alloy bonds are used but fired in inert atmospheres.

### 5.6.23 EFFECTS OF CHEMICAL AFFINITY IN GRINDING

The reactivity of diamond with transition metals such as nickel and iron is a major limitation to the use of diamond as an abrasive for machining and grinding these materials. Thornton and Wilks [1978, 1979] showed that certainly in single-point turning of mild steel with diamond, chemical wear was excessive and exceeded abrasive mechanical wear by a factor of  $10^4$ . Hitchiner and Wilks [1987] showed that difference when turning nickel was  $>10^5$ . Turning pearlitic cast iron, however, the wear rate was only  $10^2$  greater. Furthermore, the wear on pearlitic cast iron was actually 20 times less than that measured using CBN tools. Much less effect was seen on ferritic cast iron, which unlike the former material contained little free carbon; in this case, diamond wear increased by a factor of 10 when turning workpieces of comparable hardness.

### 5.6.24 GRINDING STEELS AND CAST IRONS WITH DIAMOND

It is generally considered, as the before-mentioned results imply, that chemical-thermal degradation of the diamond prevents it being used as an abrasive for steels and nickel-based alloys, but that under certain circumstances free graphite in some cast irons can reduce the reaction between diamond and iron to an acceptable level. For example, in honing of automotive cast iron cylinder bores, which is performed at very similar speeds (2 m/s) and cut rates to that used in the turning experiments mentioned above, diamond is still the abrasive of choice outperforming CBN by a factor of 10. However, at the higher speeds (80 m/s typical) and temperatures of cylindrical grinding of cast iron camshafts, the reverse is the case.

### 5.6.25 THERMAL PROPERTIES

Diamond has the highest thermal conductivity of any material with a value of 600 to 2,000 W/mK at room temperature, falling to 70 W/mK at 700°C. These values are 40 times greater than the thermal conductivity of alumina. Much is written in the literature of the high thermal conductivity of both diamond and CBN, and the resulting benefits of lower grinding temperatures and reduced thermal stresses. Despite an extremely high thermal conductivity, if the heat capacity of the material is low it will simply get hot quickly! Thermal models for moving heat sources, as shown by Jaeger [1942], employ a composite transient thermal property. The transient thermal property is  $\beta = \sqrt{k \cdot \rho \cdot c}$ , where  $k$  is the thermal conductivity,  $\rho$  is the density, and  $c$  is the thermal heat capacity.

The value of  $\beta$  for diamond is  $6 \times 10^4$  W/m K compared to 0.3 to  $1.5 \times 10^4$  W/m K for most ceramics, including alumina and SiC, and for steels. Copper has a value of  $3.7 \times 10^4$  W/m K due in part to a much higher heat capacity than that of diamond. This may explain its benefit as a cladding material and wheel filler material.

Steady-state conditions are quickly established during the grain contact time in grinding. This is because the heat source does not move relative to the grain. The situation is similar to rubbing a finger across a carpet. It is the carpet that sees the moving heat source and stays cool, rather than the finger that sees a constant heat source and gets hot! In grinding, the abrasive grain is like the finger and the workpiece is like the carpet. In this case, it is the thermal conductivity of the grain that governs the heat conducted by the grain rather than the transient thermal property [Rowe et al. 1996]. For nonsteady conduction, a time-constant correction is given by Rowe and Black [Marinescu et al. 2004, Chapter 6]. The application of thermal properties to calculation of temperatures is discussed in more detail in Chapter 17 on external cylindrical grinding.

The coefficient of linear thermal expansion of diamond is  $1.5 \times 10^{-6}/\text{K}$  at  $100^\circ\text{C}$  increasing to  $4.8 \times 10^{-6}/\text{K}$  at  $900^\circ\text{C}$ . The values are significant for bonded wheel manufacturers who must try to match thermal expansion characteristics of bond and grit throughout the firing cycle.

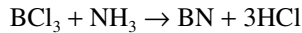
For further details on the properties of diamond, see Field [1979, 1983].

## 5.7 CBN

### 5.7.1 DEVELOPMENT OF CBN

CBN is the final and most recent of the four major abrasive types, and the second hardest superabrasive after diamond. Trade names include Borazon (from GE who first synthesized it commercially), Amborite and Amber Boron Nitride (after De Beers), or in Russian literature as Elbor, Cubonite, or  $\beta$ -BN.

Boron nitride at room temperatures and pressures is made using the reaction:



The resulting product is a white slippery substance with a hexagonal layered atomic structure called HBN (or  $\alpha$ -BN) similar to graphite but with alternating nitrogen and boron atoms. Nitrogen and boron lie on either side of carbon in the periodic table, and it was postulated that high temperatures and pressures could convert HBN to a cubic structure similar to diamond. This was first shown to be the case by a group of scientists under Wentdorf at GE in 1957. The first commercial product was released 12 years later in 1969.

Both the cubic (CBN) and wurtzitic (WBN or  $\gamma$ -BN) forms are created at comparable pressures and temperatures to those for carbon. Again, the key to successful synthesis was the selection of a suitable solvent to reduce conditions to a more manageable level. The chemistry of BN was quite different to carbon; for example, bonding was not pure  $sp^3$  but 25% ionic, and BN did not show the same affinity for transition metals. The successful solvent/catalyst turned out to be any one of a large number of metal nitrides, borides, or oxide compounds of which the earliest commercial one used (probably with some additional doping) was  $\text{Li}_3\text{N}$ . This allowed economic yields at 60 kbar,  $1,600^\circ\text{C}$ , and <15-min cycle times.

### 5.7.2 SHAPE AND STRUCTURE OF CBN

As with diamond crystal growth, CBN grain shape is governed by the relative growth rates on the octahedral (111) and cubic planes. However, the (111) planes dominate and, because of the presence of both B and N in the lattice, some (111) planes are positive terminated by B atoms and some are negative terminated by N atoms. In general, B (111) plane growth dominates and the resulting

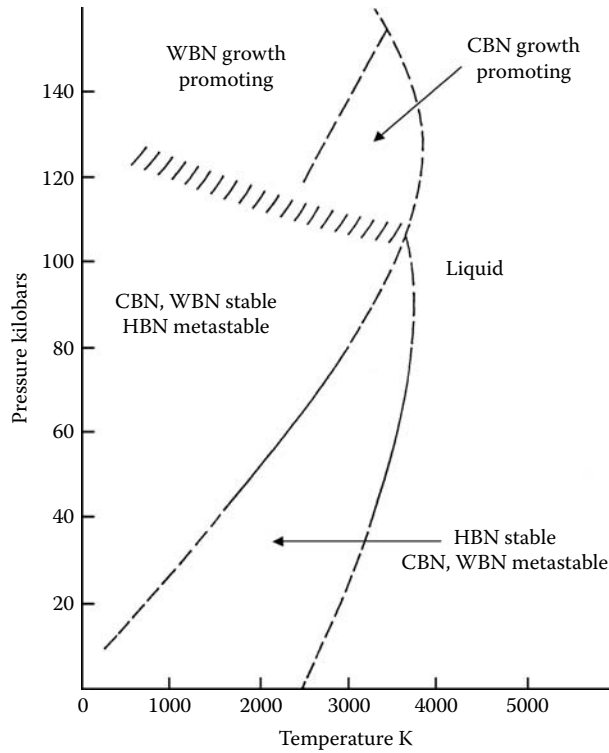


FIGURE 5.16 Phase diagram for cubic boron nitride.

crystal morphology is a truncated tetrahedron. Twinned plates and octahedra are also common. The morphology can be driven toward the octahedral or cubo-octahedral morphologies by further doping and/or careful control of the pressure-temperature conditions.

### 5.7.3 TYPES OF CBN GRAINS

As with diamond, CBN grain grades are most commonly characterized by toughness and by shape. Toughness is measured both at room temperatures and at temperatures up to >1,000°C comparable to those used in wheel manufacture, the values being expressed in terms of a toughness index (TI) and thermal toughness index (TTI). The details of the measurement methods are normally proprietary but, in general, grains of a known screened-size distribution are treated to a series of impacts and then rescreened. The fraction of grain remaining on the screen is a measure of the toughness. For TTI measurements, the grains may be heated in a vacuum or a controlled atmosphere or even mixed with the wheel bond material, which is subsequently leached out. TI and TTI are both strongly influenced by doping and impurity levels. Additional degradation of the grain within the wheel bond during manufacture can also occur due to the presence of surface flaws that may be opened up by penetration of bond.

The surface roughness of CBN is a more pronounced and critical factor than for diamond in terms of factors influencing grinding wheel performance. A rough angular morphology provides a better, mechanical anchor. Of the examples illustrated in Figure 5.17, GE Type 1 abrasive is a relatively weak irregular crystal. The coated version GE Type II abrasive used in resin bonds has a simple nickel-plated cladding. However, GE 400 abrasive is a tougher grain with a similar shape

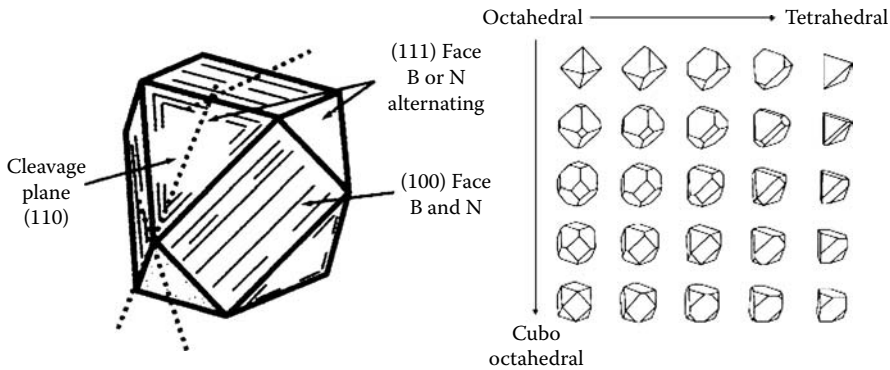


**FIGURE 5.17** Cubic boron nitride crystal growth planes and morphology. (After Bailey and Juchem, De Beers 1998. With permission.)

but with much smoother, flaw-free faces. The coated version GE 420 is, therefore, first coated with a thin layer of titanium to create a chemically bonded roughened surface to which the nickel cladding can be better anchored.

Only a relatively few grades of CBN are tough and blocky with crystal morphologies shifted away from tetrahedral growth. The standard example is GE 500 used primarily in electroplated wheels. De Beers also has material, ABN 600, where the morphology has been driven toward the cubo-octahedral.

#### 5.7.4 MICROCRYSTALLINE CBN

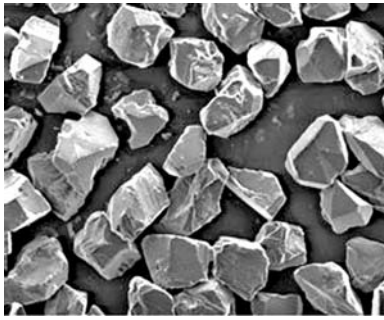
Interestingly, GE also developed a grit-type GE 550 that is a microcrystalline product; this could be considered the “SG” of CBN grains. It is extremely tough and blocky and wears by microfracturing. However, just like SG grains, it also generates high grinding forces and is, therefore, limited to use in the strongest bonds, such as bronze metal, for high force/grit applications, especially honing. It has also been used in limited quantities in plated applications. One problem with its microcrystalline nature is that the surface of GE 550 is much more chemically reactive with vitrified bonds.

#### 5.7.5 SOURCES AND COSTS OF CBN

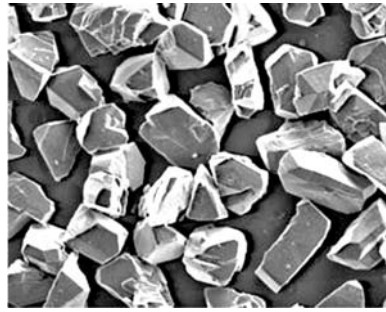
The manufacture of CBN has been dominated by GE in the United States, by De Beers from locations in Europe and South Africa, and by Showa Denko, Iljin, and Tomei from the Far East. Russia and Romania have also been producing CBN for over 30 years, and, more recently, China has rapidly become an extremely important player. Historically, consistency has been in question with materials from some of these latter sources but with intermediate companies such as ABC Abrasives (Saint-Gobain Ceramics) controlling the QC aspects of the materials to the end user, they are becoming a very real low-cost alternative to traditional suppliers. It is, therefore, expected that CBN prices will be driven down over the next decade offering major new opportunities and applications for CBN technology. Currently, CBN costs are of the order of \$1,500 to \$5,000/lb or at least three to four times that of the cheapest synthetic diamond.

#### 5.7.6 WURTZITIC BORON NITRIDE

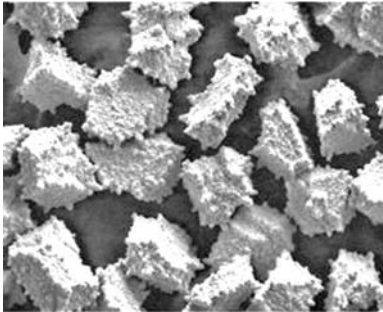
As with carbon, wurtzitic boron nitride (WBN) has also been produced by explosive shock methods. Reports of commercial quantities of the material began appearing about 1970 [Nippon Oil and Fats 1981],



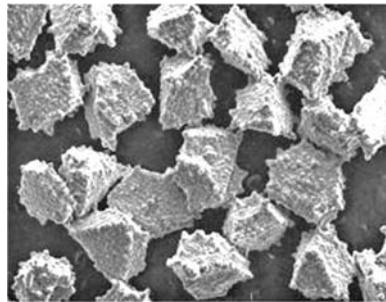
GE type 1 weak, sharp, monocrystal



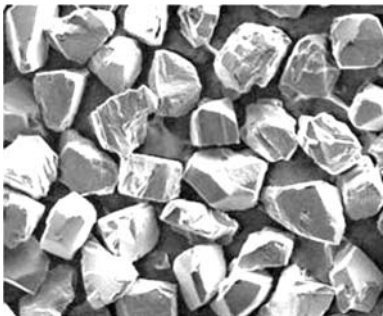
GE 400 tough, sharp, monocrystal



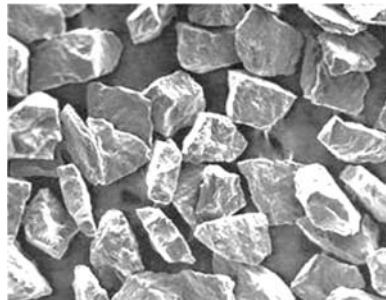
GE type II (Ge type 1 60% Ni coated)



GE 420 (GE 400 Ti bonded, 60% Ni coated)



GE 500 tough, blocky, monocrystal



GE 500 very tough, microcrystalline

**FIGURE 5.18** Examples of cubic boron nitride grain types and morphologies. (From General Electric 1998. With permission.)

but its use has again been focused more on cutting tool inserts with partial conversion of the WBN to CBN, and this does not appear to have impacted the abrasive market.

### 5.7.7 HARDNESS OF CBN

The hardness of CBN at room temperature is approximately  $4,500 \text{ kg/mm}^2$ . This is about half as hard as diamond and twice as hard as conventional abrasives.

### 5.7.8 WEAR RESISTANCE OF CBN

The differences in abrasion resistance are much more extreme. A hardness factor of 2 can translate into a factor of  $100 > 1,000$  in abrasion resistance depending on the abrading material. The author

**TABLE 5.1**  
**Mechanical Properties of Typical Alumina and SiC Abrasives**

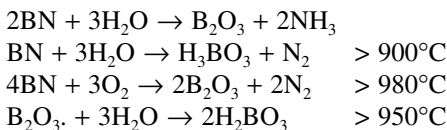
Abrasive	Hardness Knoop	Relative Toughness	Shape/Morphology	Applications
Green SiC	2840	1.60	Sharp/angular/glassy	Carbide/ceramics/precision
Black SiC	2680	1.75	Sharp/angular/glassy	Cast iron/ceramics/ductile nonferrous metals
Ruby Alox	2260	1.55	Blocky/sharp-edged	Hss and high-alloy steel
White Alox	2120	1.75	Fractured facets/sharp	Precision ferrous
Brown Alox	2040	2.80	Blocky/faceted	General purpose
Alox/10% ZrO	1960	9.15	Blocky/rounded	Heavy-duty grinding
Alox/40% ZrO	1460	12.65	Blocky/rounded	Heavy-duty snagging
Sintered Alox	1370	15.40	Blocky/rounded/smooth	Foundry billets/ingots

remembers, as a research student under Wilks, when the first CBN samples were supplied for abrasion-resistance measurements using the same technique used for measuring the wear resistance of diamond. The CBN was so soft in comparison to diamond that it was impossible to obtain a value on the same wear scale. As with diamond, the key is the total wear resistance to all attritious-wear processes.

Like diamond, CBN is brittle, but it differs in having six (110) rather than four (111) cleavage planes. This gives a more controlled breakdown of the grit especially for the truncated tetrahedral shape of typical CBN grains. The grain toughness is generally much less than that of blocky cubo-octahedral diamonds. This, combined with its lower hardness, provides the very useful advantage that CBN wheels can be dressed successfully by diamond (rotary) tools.

### 5.7.9 THERMAL AND CHEMICAL STABILITY OF CBN

CBN is thermally stable in nitrogen or vacuum to at least 1,500°C. In air or oxygen, CBN forms a passive layer of B<sub>2</sub>O<sub>3</sub> on the surface, which prevents further oxidation up to 1,300°C. However, this layer is reactive with water, or more accurately high temperature steam at 900°C, and will allow further oxidation of the CBN grains following the reactions [Carius 1989, Yang, Kim, and Kim 1993]



### 5.7.10 EFFECT OF COOLANT ON CBN

Reactivity has been associated with reduced wheel life when grinding in water-based coolants compared with straight-oil coolants. However, the importance of this reaction is not clear-cut as water also inflicts a much higher thermal shock to the crystal as it is heat cycled through the grinding zone. Regardless of root cause, the effect is dramatic as illustrated in Table 5.2, which gives comparative life values for surface grinding with CBN wheels [Carius 2001].

CBN is also reactive toward alkali oxides—not surprising in light of their use as solvents and catalysts in CBN synthesis! The B<sub>2</sub>O<sub>3</sub> layer is particularly prone to attack or dissolution by basic oxides such as Na<sub>2</sub>O by the reaction





**TABLE 5.2**  
**Effect of Coolant Type on CBN Wheel**  
**Performance**

Workpiece	Synthetic Light Duty 2%	Soluble Heavy Duty 10%	Straight Oil
M2	X	1.7X	5X
M50	X	4X	16X
T15	X	1.7X	3X
D2	X	1.3X	11X
52–100	X	10X	14X
410 SS	X	25X	44X
IN 718	X	8X	50X

Such oxides are common constituents of vitrified bonds and the reactivity can become extreme at temperatures above 900°C affecting processing temperatures for wheels [Yang, Kim, and Kim 1993].

#### 5.7.11 EFFECT OF REACTIVITY WITH WORKPIECE CONSTITUENTS

CBN does not show any significant reactivity or wetting by transition metals such as iron, nickel, cobalt, or molybdenum until temperatures reach in excess of 1,300°C. This is reflected in a low rate of wear when grinding these materials with CBN abrasive in comparison with wear of diamond abrasive. CBN does show marked wetting by aluminum at only 1050°C and also with titanium. As demonstrated in wetting studies of low temperature silver–titanium eutectics, CBN reacts readily at 1,000°C to form  $TiB_2$  and  $TiN$  [Benko 1995]. This provides an explanation of why in grinding aerospace titanium alloys such as Ti-6Al-4V, CBN wheels wear typically five times faster than diamond wheels [Kumar 1990]. By comparison, the wear rate using the alternative of SiC abrasive is 40 times greater than CBN. This is a further example of the need to consider the combined effects of the mechanical, chemical, and thermal wear processes as much as abrasive cost.

Pure, stoichiometrically balanced CBN material is colorless, although commercial grades are either a black or an amber color depending on the level and type of dopants present. The black color is believed to be due to an excess (doping) of boron.

#### 5.7.12 THERMAL PROPERTIES OF CBN

The thermal conductivity of CBN is almost as high as that of diamond. At room temperature, thermal conductivity is 200 to 1,300 W/mK, and the transient thermal property  $\beta = 2.0 \times 10^4$  to  $4.8 \times 10^4$  J/m<sup>2</sup>sK. The thermal expansion of CBN is about 20% higher than diamond.

### 5.8 GRAIN SIZE DISTRIBUTIONS

Several national and international standards define particle size distributions of abrasive grains. All are based on sizing by sieving in the sizes typical of most regular grinding applications.

#### 5.8.1 THE ANSI STANDARD

In the case of the ANSI standard [B74.16 1995], mesh size is defined by a pair of numbers that corresponds to sieves with particular mesh sizes. The lower number gives the number of meshes per linear inch through which the grain can only just fall, while staying on the surface of the sieve with the next highest number of meshes which is the higher number.

### 5.8.2 THE FEPA STANDARD

FEPA [ISO R 565–1990, also DIN 848-1988] gives the grit size in microns of the larger mesh hole size through which the grit will just pass.

### 5.8.3 COMPARISON OF FEPA AND ANSI STANDARDS

The FEPA and ANSI sizing standards are closely related; FEPA has a tighter limit for oversize and undersize (5 to 12%) but no medium nominal particle size. ANSI has somewhat more open limits for oversize and undersize (8 to 15%) but a targeted midpoint grit dimension. FEPA is more attuned to the superabrasive industry, especially in Europe, and may be further size-controlled by the wheel maker; ANSI is more attuned to conventional wheels and, in many cases, may be further broadened by mixing two or three adjacent sizes. In tests, no discernable difference could be seen between wheels made using grain to the FEPA or ANSI size distribution [Hitchiner and McSpadden 2004]. A major attraction of working with the FEPA system is that it provides a measure of the actual size of the grain (in microns), whereas with the ANSI system the mesh size increases with the numbers of wires in the sieve mesh and, therefore, becomes larger as the grain size becomes smaller.

### 5.8.4 US GRIT SIZE NUMBER

There is also a system called US grit size number with a single number that does not quite correlate with either the upper or lower ANSI grit size number. This has created considerable confusion especially when using a single number in a specification. A FEPA grit size of 64 could be equivalent to a 280, 230, or 270 US grit size depending on the wheel manufacturer's particular coding system. This can readily lead to error of one grit size when selecting wheel specifications unless the code system is well defined. Table 5.3 gives the nearest equivalents for each system.

## 5.9 FUTURE GRAIN DEVELOPMENTS

Research is accelerating both in existing alumina-based grain technology and in new ultra-hard materials. In the group of ceramic-processed alumina materials, Saint-Gobain released SG in 1986 [U.S. Patent 4,623,364] followed by extruded SG in 1991 [U.S. Patent 5,009,676]. More recently in 1993, Treibacher released an alumina material with hard filler additives [U.S. Patent 5,194,073]. Electrofused technology has also advanced. Pechiney produced an Al-O-N grain (Abral) produced by the cofusion of alumina and AlON followed by slow solidification. It offered much higher thermal corrosion resistance relative to regular alumina while also having constant self-sharpening characteristics akin to ceramic-processed materials but softer acting [Roquefeuil 2001].

New materials have also been announced with hardness approaching CBN and diamond. Iowa State University announced in 2000 an Al-Mg-B material with a hardness value comparable to CBN [U.S. Patent 6,099,605]. Dow Chemical patented in 2000 an Al-C-N material with a hardness value close to diamond [U.S. Patent 6,042,627]. In 1992, the University of California patented some  $-C_3N_4$  and  $-C_3N_4$  materials that may actually be harder than diamond [U.S. Patent 5,110,679]. Whether any of these materials eventually proves to have useful abrasive properties and can be produced in commercial quantities has yet to be seen. Nevertheless, there will undoubtedly be considerable advances in abrasive materials in the coming years.

## 5.10 POSTSCRIPT

In the short time since this chapter was first prepared the superabrasives market has seen dramatic change. GE Superabrasives is no longer owned by GE and has been renamed Diamond Innovations. De Beers has moved much of its European manufacturing to South Africa and renamed its Industrial

**TABLE 5.3**  
**Particle Size Comparisons**

FEPA Designation	ISO R 5665—1990 Aperture Range (µm)	ANSI Grit Size	US Grit Number	Japanese (JIS) Size	Particles Per Carat
		<b>Standard</b>			
1181	1,180/1,000	16/18			
1001	1,000/850	18/20			
851	850/710	20/25			
711	710/600	25/30			
601	600/500	30/35			
501	500/425	35/40		35	
426	425/355	40/45			
356	355/300	45/50			
301	300/250	50/60	50	50	2,000
251	250/212	60/70	60		
213	212/180	70/80	80		
181	180/150	80/100	100	80	10,000
151	150/125	100/120	120	100	17,000
126	125/106	120/140	150	120	21,000
107	106/90	140/170	180	140	49,000
91	90/75	170/200	220	170	88,000
76	75/63	200/230	240	200	140,000
64	63/53	230/270	280	230	250,000
54	53/45	270/325	320	270	280,000
46	45/38	325/400	400	325	660,000
<b>Wide range</b>					
1182	1,180/850	16/20			33
892	850/600	20/30		20	
602	600/425	30/40		30	282
502	500/355	35/45			
427	425/300	40/50		40	770
252	250/180	60/80		60	3,000

Division, Element 6. Chinese manufacturers, as of 2005, have increased their superabrasive grain capacity to over 4 billion carats/annum creating a market excess and further driving down prices. It is expected that in the coming years this will accelerate the conversion of large production wheels from alox to CBN grain for high production applications such as through-feed centerless and plunge grinding. It will also ensure the continuance of the ongoing battle between the competing technologies of hard turning and grinding.

## REFERENCES

- Bailey, M. W. and Juchem, H. O. 1993. "The Advantages of CBN Grinding: Low Cutting Forces and Improved Workpiece Integrity." *IDR* Pt. 3, 83–89.
- Bange, D. W. and Orf, N. 1998. "Sol Gel Abrasive Makes Headway." *Tooling & Production* March, 82–84.
- Benko, E. 1995. "Wettability Studies of Cubic Boron Nitride by Silver-Titanium." *Ceramics International* 21, 303–307.
- Carius, A. C. 1989. "Modern Grinding Technology." *SME* Novi, MI 10/10/1989.

- Carius, A. C. 2001. "CBN Abrasives and the Grindability of PM Materials." Precision Grinding & Finishing in the Global Economy – 2001 Conference Proceedings. Gorham, 10/1/2001, Oak Brook, IL.
- De Beers Industrial Diamond Division. 1993. *Monocrystal Diamond Product Range*. Commercial brochure.
- De Beers Industrial Diamond Division. 1999. *Premadia Diamond Abrasives*. Commercial brochure.
- DiCorletto, J. 2001. "Innovations in Abrasive Products for Precision Grinding," Precision Grinding & Finishing in the Global Economy – 2001 Conference Proceedings. Gorham, 10/1/2001, Oak Brook, IL.
- DeVries, R. C. 1972. *Cubic Boron Nitride: Handbook of Properties*. GE Report #72CRD178, June.
- Field, J. E. 1979. *The Properties of Diamond*. Academic Press, London.
- Field, J. E. 1983. "Diamond – Properties and Definitions." Cavendish Lab.
- General Electric Superabrasives. 1998. "Understanding the Vitreous Bonded Borazon CBN System." General Electric Borazon CBN Product Selection Guide. Commercial brochure.
- Gigel, P. 1994. *Finer Points* 6, 3, 12–18.
- Henri, Polak Diamond Corp. 1979. Commercial brochure.
- Heywood, J. 1938. *Grinding Wheels and Their Uses*. Penton Co.
- Hitchiner, M. P. and McSpadden, S. 2004. "Evaluation of Factors Controlling CBN Abrasive Selection for Vitrified Bonded Wheels." *Advances in Abrasive Technology*. VI Trans Tech Publ. Ltd., pp. 267–272.
- Hitchiner, M. P. and Wilks, J. 1984. "Factors Affecting Chemical Wear during Machining." *Wear* 93, 63–80.
- Hitchiner, M.P. and Wilks, J. 1987. "Some Remarks on the Chemical Wear of Diamond and CBN during Turning and Grinding," *Wear*, 114, 327–338.
- Jaeger, J. C. 1942. *Proc. R. Soc. New South Wales* 76.
- Jakobuss, M. 1999. "Influence of Diamond and Coating Selection on Resin Bond Grinding Wheel Performance." Precision Grinding Conference. Chicago, IL, June 15–17.
- Klocke, F., Mueller, N., and Englehorn. 2000. *Abrasive Magazine* June/July, 24–27.
- Kumar, K. V. 1990. SME 4th International Grinding Conference. Dearborn, MI, MR90-505.
- Maillard, R., Ed. 1980. *Diamonds – Myth, Magic and Reality*. Crown Publ., New York.
- Marinescu, I., Rowe, W. B., Dimitrov, B., and Inasaki, I. 2004. *Tribology of Abrasive Machining Processes*. William Andrew Publishing, Norwich, NY.
- Nippon Oil and Fats Co. Ltd. 1981. "WURZIN (wBN) Tool." Commercial document.
- Norton, S. A. 1999a. "Project Optimos – Grind in the Fast Lane." Commercial brochure.
- Norton, S. A. 1999b. "Project Altos." Commercial brochure.
- Roquefeuil, F. 2001. "ABRAL: A New Electrofused Alon Grain for Precision Grinding." Precision Grinding & Finishing in the Global Economy – 2001 Conference Proceedings. Gorham, 10/1/2001, Oak Brook, IL.
- Rowe, W. B., Morgan, M. N., Black, S. C. E., and Mills, B. 1996. "A Simplified Approach to Thermal Damage in Grinding." *Ann. CIRP* 45, 1, 299–302.
- Thornton, A. G. and Wilks, J. 1978. "Clean Surface Reactions between Diamond and Steel." *Nature* 8/24/78, 792–793.
- Thornton, A. G. and Wilks, J. 1979. "Tool Wear and Solid State Reactions during Machining." *Wear* 53, 165.
- Tymeson, M. M. 1953. *The Norton Story*. Norton Co., Worcester, MA.
- Viernekes, N. 1987. "CBN Ceramic-Bonded Abrasive Wheels for Semi-Automated Grinding Processes." *Wälzlagertechnik* 1, 30–34.
- Wellborn, W. 1994. "Modern Abrasive Recipes." *Cutting Tool Engineering* April, 42–47.
- Wilks, E. M. and Wilks, J. 1972. "The Resistance of Diamond to Abrasion." *J. Phys. D: Appl. Phys.* 5, 1902–1919.
- Yang, J., Kim, D., and Kim, H. 1993. "Effect of Glass Composition on the Strength of Vitreous Bonded c-BN Grinding Wheels." *Ceramics Int.* 19, 87–92.



---

# 6 Specification of the Bond

## 6.1 INTRODUCTION

Wheel bond systems can be divided into two types: those holding a single layer of abrasive grain to a solid steel core, and those providing a consumable layer many grains thick with the abrasive held within the bond. The latter may be mounted on a resilient core or produced as a solid monolithic structure from the bore to the outer diameter. This chapter deals with the different types of bonding structures employed in grinding wheel design and the effects on wheel performance.

## 6.2 SINGLE-LAYER WHEELS

Single-layer wheels are generally limited to superabrasives because of the economics of wheel life. They can be subdivided into electroplated wheels fabricated at essentially room temperatures, and brazed wheels fabricated at temperatures as high as 1,000°C. The following discussion applies in general to plated cubic boron nitrides (CBN) and to plated diamond wheels, although in practice CBN dominates the precision grinding market and is the central focus below.

## 6.3 ELECTROPLATED (EP) SINGLE-LAYER WHEELS

### 6.3.1 STRUCTURE OF AN EP LAYER

Electroplated wheels consist of a single layer of superabrasive grains bonded to a precision-machined steel blank using nickel deposited by an electroplating or occasionally electroless plating process. The plating depth is controlled to leave about 50% of the abrasive exposed (Figure 6.1).

### 6.3.2 PRODUCT ACCURACY

The accuracy and repeatability of the process is dependent on many factors. The blank must be machined to a high accuracy, and the surface prepared appropriately and balanced; ideally, blank-profile tolerances are maintained to within 2  $\mu\text{m}$  and wheel runout maintained to within 5  $\mu\text{m}$  [McClellan 1999]. The abrasive is generally resized to provide a tighter size distribution than that used in other bond systems. This is to avoid any high spots and better control grain aspect ratio. The abrasive is applied to the blank by various proprietary methods to produce an even and controlled-density distribution. For tight tolerance applications or reduced surface roughness the wheel may also be postconditioned (also termed “dressing,” “truing,” or “shaving”) where an amount equivalent to approximately 5 to 7% of the grit size is removed to produce a well-defined grit protrusion height above the plating. With good control of plate thickness this helps to control and/or define a usable layer depth.

### 6.3.3 WEAR RESISTANCE OF THE BOND

The hardness, or more accurately the wear resistance of the nickel, is controlled by changes to the bath chemistry. Nitride coating, similar to coatings used on cutting tools, has been reported to further improve the wear resistance of the nickel, but data have been mixed indicating that performance parameters are not yet understood [Julien 1994, Bush 1993]. Solid lubricant coatings of the wheel surface have also been reported to increase life.

**TABLE 6.1**  
**Direct Plating Grit Size Allowances**

FEPA	US Mesh	Form Allowance (in.)	Form Allowance ( $\mu\text{m}$ )	Surface Concentration (ct/in. <sup>2</sup> )	Surface Concentration (ct/cm <sup>2</sup> )
B854	20/30#	.0370"	940		
B602	30/40#	.0260"	660	2.34	0.363
B427	40/50#	.0180"	455	1.8	0.279
B301	50/60#	.0130"	330	1.5	0.233
B252	60/80#	.0110"	280	1.4	0.217
B181	80/100#	.0080"	203	1.14	0.177
B151	100/120#	.0066"	168	1	0.155
B126	120/140#	.0056"	142	0.8	0.124
B107	140/170#	.0046"	117	0.67	0.104
B91	170/200#	.0039"	99	0.56	0.087
B76	200/230#	.0034"	86	0.47	0.073
B64	230/270#	.0030"	76	0.4	0.062
B54	270/325#	.0026"	66	0.33	0.051
B46	325/400#	.0023"	58	0.28	0.043

### 6.3.4 GRIT SIZE AND FORM ACCURACY

The size of the grit must be allowed for when machining the required form in the blank. This will be different to the nominal grit size and dependent on the aspect ratio of the particular grit type. For example, Table 6.1 gives standard values for GE 500 abrasive with an aspect ratio of 1.4.

### 6.3.5 WHEEL WEAR EFFECTS IN GRINDING

One major attraction of plated wheels is the fact that they do not require dressing and, therefore, eliminate the need for an expensive diamond form-roll and dressing system. However, plated wheels present challenges to the end user due to the effects of wheel wear. Figure 6.2 illustrates changes in grinding power, workpiece roughness, and wheel wear with time for a typical precision-plated wheel when CBN grinding aerospace alloys. Initially, the surface roughness is high as only the very tips of the grits are cutting. The power then rises rapidly together with an associated rapid rate of wheel wear and a drop in roughness. The process tends to stabilize, with wear flat formation

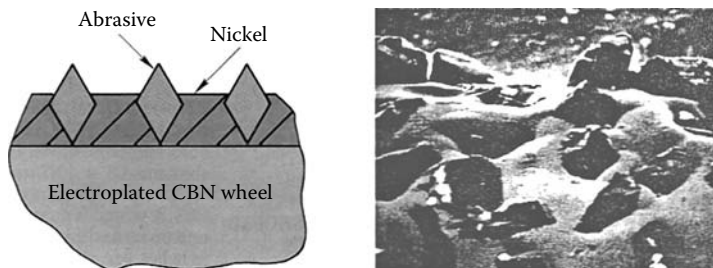


**FIGURE 6.1** Schematic of an electroplated cubic boron nitride wheel section and the appearance of the actual surface of such a wheel.

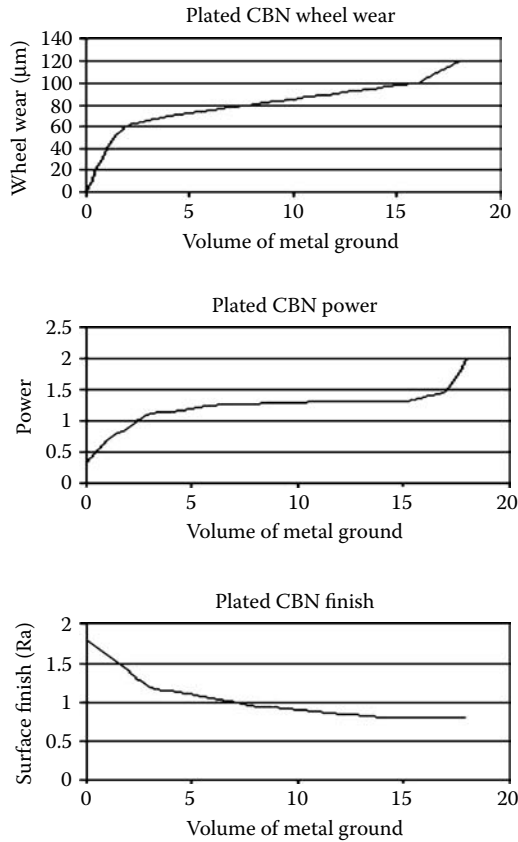


FIGURE 6.2 Typical performance characteristics of plated wheels (B126 grit size).

being balanced by fracture, unless the grinding conditions are too aggressive. This leads to a much more protracted period of time when the rates of change of all three variables are reduced by up to a factor 10. Failure occurs when power levels finally become so high that burn occurs, or the plating and grain are stripped from the core. This latter effect is particularly concerning because in most cases it cannot yet be detected in advance or predicted easily except by empirical data from production life values from several wheels.

**6.3.6 GRIT SIZE AND FORM-HOLDING CAPABILITY**

Table 6.2 and Table 6.3 give values for typical form-holding capabilities and roughness as a function of grit size for standard precision-plated and postplated conditioned wheels. Roughness values will vary somewhat depending on workpiece hardness. The values indicated are those for grinding aerospace alloys in the hardness range 30 to 50 Hrc using CBN abrasive.

**6.3.7 WHEEL BREAK-IN PERIOD**

The phenomenon of a break-in period associated with a high rate of wear of a new wheel is particularly important when trying to hold tolerances of <.001" (25 μm). Table 6.2 and Table 6.3 give the break-in depth for both precision and conditioned wheels. As can be seen with conditioning



**TABLE 6.2**  
**Standard Precision-Plated Wheel Form Capabilities**

Grit Size FEPA	Grit Size US Mesh	Minimum Radius (mm)	Precision Allowance Blank ( $\mu\text{m}$ )	Precision Tolerances ( $\pm\mu\text{m}$ )	Precision Roughness (Ra)	Precision Break-In Depth ( $\mu\text{m}$ )
B852	20/30	2	920	100		
B602	30/40	1.5	650	90		
B501	35/40	1.3	650	80		
B427	40/50	1	500	60	160	63
B301	50/60	0.8	400	40	125	
B252	60/80	0.7	290	30	85	40
B213	70/80	0.6	260	30	75	
B181	80/100	0.5	220	30	63	35
B151	100/120	0.4	190	30	38	
B126	120/140	0.3	165	25	35	
B107	140/170	0.26	140	25	32	
B91	170/200	0.23	130	25	32	20
B76	200/230	0.2	100	25	28	
B64	230/270	0.18	90	20	25	
B54	270/325	0.15	75	20	22	
B46	325/400	0.12	65	20	20	10

of the wheel surface to remove the tips of the grits, it is possible to virtually eliminate the break-in period. Although conditioning can double the price of the wheel when trying to hold tolerances of  $<.0005''$  ( $12\ \mu\text{m}$ ), it can be easily justified by increasing wheel life by an order of magnitude.

**TABLE 6.3**  
**Conditioned Plated Wheel Form Capabilities**

FEPA	Grit Size US Mesh	Min Radius Capability (mm)	Condition Allowance Blank ( $\mu\text{m}$ )	Condition Tolerances ( $\pm\mu\text{m}$ )	Condition Roughness (Ra)	Condition Break-In Depth ( $\mu\text{m}$ )
B852	20/30	2	850	10		$<5$
B602	30/40	1.5	600	10		$<5$
B501	35/40	1.3	600	10		$<5$
B427	40/50	1	450	8	80	$<5$
B301	50/60	0.8	360	6	70	$<5$
B252	60/80	0.7	250–280	5	60	$<5$
B213	70/80	0.6	240–250	5	50	$<5$
B181	80/100	0.5	200	5	40	$<5$
B151	100/120	0.4	165	5	32	$<5$
B126	120/140	0.3	140–150	5	28	$<5$
B107	140/170	0.26	110	5	25	$<5$
B91	170/200	0.23	95	5	22	$<5$
B76	200/230	0.2	80	5	NA	$<5$
B64	230/270	0.18	70	4	NA	$<5$
B54	270/325	0.15	60	4	NA	$<5$
B46	325/400	0.12	50	3	NA	$<5$

### 6.3.8 SUMMARY OF VARIABLES AFFECTING WHEEL PERFORMANCE

The number of variables for a given wheel specification that can make a significant impact on performance is quite limited. The plating thickness is held within a narrow band. The homogeneity of the plating is controlled by the plating rate and anode design. Care should be taken to avoid nodule formation especially around tight radii. Such areas are also the most prone to wear; this can be reduced by the use of electroless nickel-phosphorus for increased strength, evenness of plating, and maximum plate hardness. The biggest variable is the grit itself and how it wears under the prevailing grinding conditions. If the grit is too weak, then fracture and rapid wheel wear occur. If the grit is too tough, wear flats build up and burn ensues.

### 6.3.9 EFFECT OF COOLANT ON PLATED WHEELS

Another major factor is coolant. When grinding aerospace alloys with CBN in oil, the high lubricity of the coolant ensures a slow but steady buildup of wear flats. The lubricity of water-based coolant is much lower, thus causing more rapid wear of the grain tips. However, water has much higher thermal conductivity than oil and induces thermal shock in the abrasive leading to weakening and fracture. When used wheels are examined, it is found that those used for grinding in oil may have lasted several times longer than those used in water, yet they still have a high proportion of their layer depth remaining. Similar wheels used for grinding in water may have worn completely down to the nickel substrate. One conclusion, therefore, is to use a tougher grit when grinding in water but a slightly weaker grit in oil. An alternate method would be to reduce the surface concentration of CBN when grinding in oil.

It should be noted that in most production applications with plated CBN, oil coolant is required to obtain the necessary life to make a plated process competitive over alternate methods. Plated CBN, in particular, has proved extremely cost effective in aircraft engine subcontractors with low-batch volumes of parts requiring profile tolerances in the .0004" to .002" range as well as high-speed rough grinding of camshafts and crankshafts.

### 6.3.10 REUSE OF PLATED WHEELS

Used plated wheels are generally returned to the manufacturer for strip and replat. The saving is typically about 40% and with care, the steel core can be reused five to six times.

## 6.4 BRAZED SINGLE-LAYER WHEELS

Electroplating is a low-temperature process (<100°C) in which the plating holds the abrasive mechanically. Consequently, the plating depth required to anchor the abrasive needs to be at least 50% of the abrasive height. An alternative process is to chemically bond the CBN to the steel hub by brazing using a relatively high-temperature metal alloy system based on, for example, Ni/Cr with trade names such as MSL (metal single layer) from Saint-Gobain Abrasives [Peterman n.d., Chattopadhyay 1990, Lowder and Evans 1994]. Use of a chemical bonding method allows a much greater exposure of the abrasive and, hence, an increased usable layer depth. It also gives greater chip clearance and lower grinding forces. However, brazing occurs at temperatures up to 1,000°C and that can degrade the grit toughness and distort steel blanks. Braze also wicks up around the grit placing it under tensile stress upon cooling and thus further weakening it. Consequently, the use of brazed wheels tends to be for high stock removal roughing operations of materials such as fiberglass, brake rotors and exhaust manifolds, or applications with form tolerances >0.002" (50 µm). For a schematic of a brazed CBN wheel section and the appearance of the actual surface of such a wheel, see Figure 6.3.

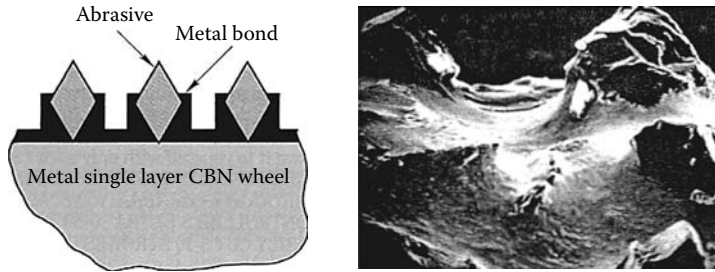


**FIGURE 6.3** Schematic of brazed cubic boron nitride wheel section and appearance of the actual surface of such a wheel.

## 6.5 VITRIFIED BOND WHEELS FOR CONVENTIONAL WHEELS

### 6.5.1 APPLICATION OF VITRIFIED BONDS

Vitrified bond alumina wheels represent nearly half of all conventional wheels and are employed for the great majority of precision high-production grinding applications. Vitrified superabrasive technology, especially for CBN, is the fastest growing sector of the precision grinding market but is still less than 20% of the market total.

### 6.5.2 FABRICATION OF VITRIFIED BONDS

Vitrified bonds are essentially glasses made from high-temperature sintering of powdered glass frits, clays, and chemical fluxes such as feldspar and borax. The attractions of vitrified bonds are their high-temperature stability, brittleness, rigidity, and their ability to support high levels of porosity in the wheel structure. The mixture of frits, clays, and fluxes are blended with abrasive and a binder such as dextrin and water. The mixture is pressed in a mold usually at room temperatures. The binder imparts sufficient green strength for the molded body to be mechanically handled

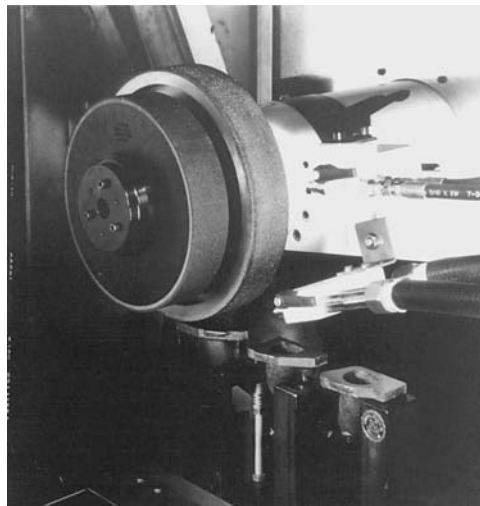
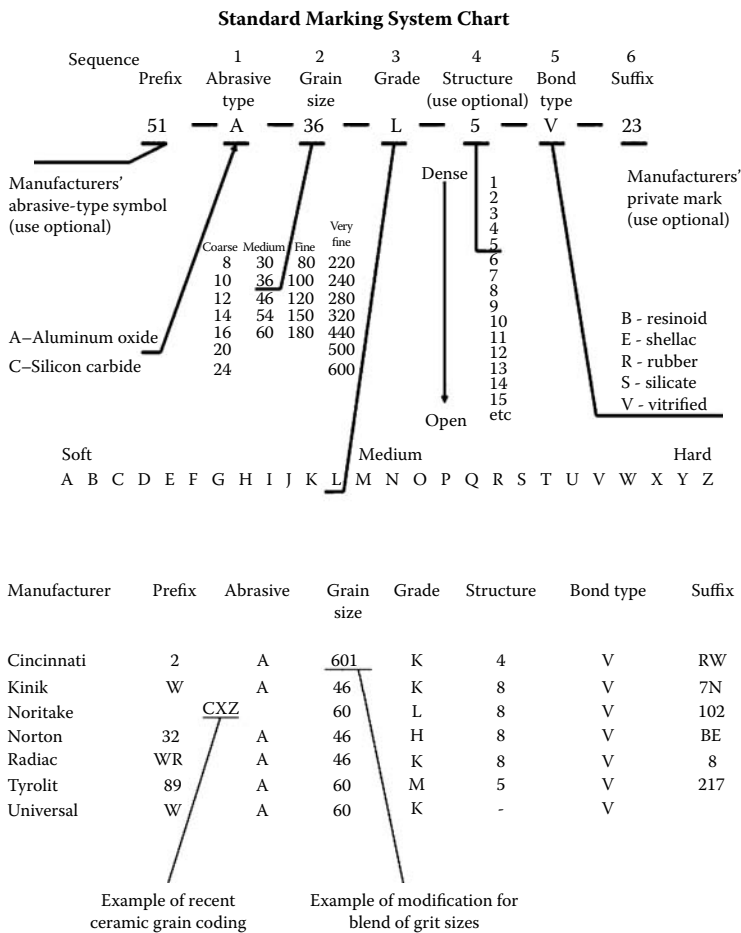


**FIGURE 6.4** Roughing and finishing of exhaust manifolds using metal single-layer and vitrified cubic boron nitride wheels. (Photo courtesy of Campbell Grinders. With permission.)

**TABLE 6.4**  
**Commercial Examples of Wheel Designations**



to a kiln where it is fired under a well-controlled temperature/time cycle in the range of 600 to 1,300°C depending on the abrasive and glass formulation. The frit provides the actual glass for vitrification, the clays are incorporated to provide green strength up to the sintering temperature, while the fluxes control/modify the surface tension at the abrasive grain–bond interface. Clays and flux additions, therefore, control the amount of shrinkage, which, except for the very hardest of wheel grades, is kept to a minimum. It should also be noted that the pressing stage in wheel manufacture, which is done either to a fixed pressure or fixed volume, provides a controlled volume of porosity after firing.

Some typical conventional vitrified wheel specifications are given in Table 6.4 that comply with standard coding practice.

### 6.5.3 STRUCTURE AND GRADE OF CONVENTIONAL VITRIFIED WHEELS

In addition to the grit type and size discussed above, it can be seen that two other factors are key to the wheel specification: *Grade* or hardness designated by a letter, and *Structure*, which is designated by a number.

#### 6.5.4 MIXTURE PROPORTIONS

To understand how these factors relate to the physical properties of the wheel, first consider how loose abrasive grains pack together under pressure. If grains with a standard size distribution are poured into a container and tamped down, they will occupy about 50% by volume. It will also be noticed that each grain is in contact with its neighbors resulting in an extremely strong and rigid configuration. Now consider the effect of adding the vitrified bond to this configuration. The bond is initially a fine powder and fills the interstices between the grains. Upon sintering, the bond becomes like a viscous liquid that wets and coats the grains. There is usually actual diffusion of oxides across the grain boundary resulting in chemical as well as physical bonding. If, for example, 10% by volume of a vitrified bond had been added, then a porosity of 40% would remain. The size and shape of individual pores are governed by the size and shape of the grains. The percentage of abrasive that can be packed into a given volume can be increased to greater than 60% by broadening the grain size distribution. The volume of abrasive can also be reduced to as low as 30% while maintaining mutual grain contact by changing the shape of the abrasive. For example, long, needle-shaped (high-aspect ratio) abrasive grains have a much lower packing density than standard grain [DiCorletto 2001].

#### 6.5.5 STRUCTURE NUMBER

However, consider the situation where the grit volume of a standard grit distribution is now reduced from 50%. The most obvious effect is that immediately some of the grains stop being in contact. The integrity and strength of the whole can now only be maintained in the presence of the bond that fills the gaps created between the grains and provides the strength and support. These points are called bond posts and become critical to the overall strength and performance of the wheel. As the grit volume is further reduced, the bond posts become longer and the structure becomes weaker. Not surprisingly, therefore, the abrasive volume percent is a critical factor and is designated by the wheel manufacturers as *Structure Number*. For example, Coes [1971] gives the following association between grit structure number and abrasive percent for Norton brand wheels:

Structure number	0	1	2	3	4	5	6	7	8
Abrasive volume percent	68	64	60	58	56	54	52	50	48

Kinik [n.d.] reported for their brand of wheels that structure number is related to abrasive volume by:

Structure number	0	1	2	3	4	5	6	7	8	9	10	11	12	13	14
Abrasive volume percent	62	60	58	56	54	52	50	48	46	44	42	40	38	36	34

Each supplier uses slightly different notation and most are not generally reported for competitive reasons.

#### 6.5.6 GRADE OF CONVENTIONAL VITRIFIED WHEELS

With the abrasive volume defined, the remaining volume is shared between the bond and porosity. The bond bridges can obviously be strengthened by increasing the amount of bond to make them thicker. The greater the amount of bond present, the lower the porosity and the harder the wheel will act. The actual definition of *Grade* will again vary from supplier to supplier. For some it is simply a direct correlation to porosity; for others it is a more-complicated combination of porosity

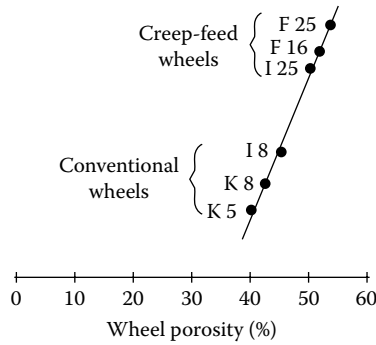


FIGURE 6.5 Porosity for various Norton grade/structure combinations. (Engineer et al. 1992. With permission.)

percent, P, and structure number, S. Malkin [1989] gives one supplier’s system where the grade letter is correlated according to

$$\text{Grade} \propto 43.75 - 0.75P + 0.5S$$

This definition is designed to make grinding performance characteristics relate to grade (e.g., burn, dressing forces, power, etc.) so that grinding performance changes more predictably from one grade letter to the next.

The interplay can also be seen in Figure 6.5 which gives the porosity level for various Norton grade letter/structure number combinations.

More formally, vitrified bond systems are described by ternary phase diagrams that map the allowed bond/grain/porosity combinations as shown in the example in Figure 6.6 [DiCorletto 2001].

### 6.5.7 FRACTURE WEAR MODE OF VITRIFIED WHEELS

In addition to the size of the bond-bridge, the fracture mode is also critical. The bond must be strong enough to hold the grains under normal grinding conditions, but under higher stress it must allow the grain to fracture in a controlled way. The bond should not be so strong relative to the grit strength that the abrasive glazes and leads to burn.

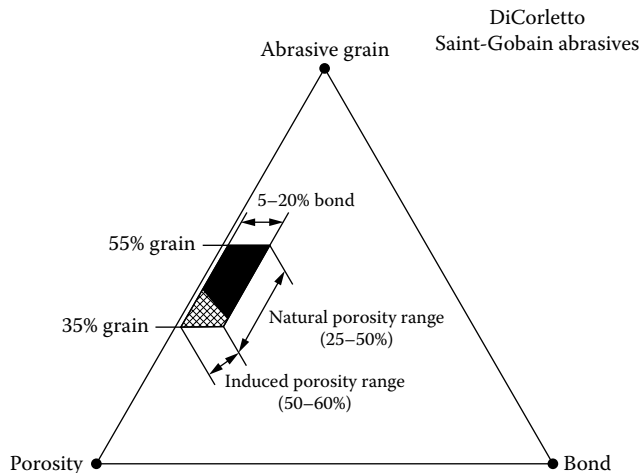
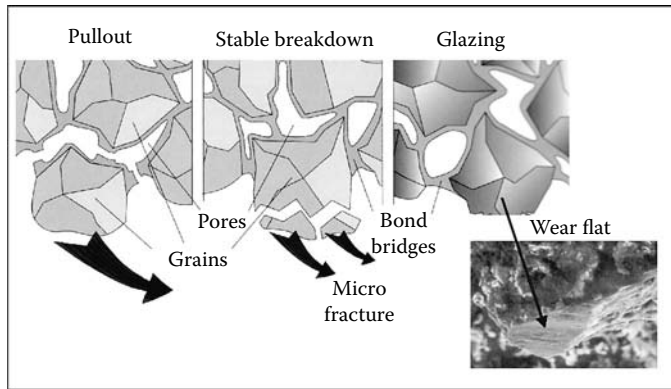


FIGURE 6.6 Ternary phase diagram showing operating range for alox vitrified bond systems.



**FIGURE 6.7** Pullout, stable breakdown, and glazing regimes in grinding. (Based on a drawing by Rappold 2002. With permission.)

One method to regulate this is by adding fine quartz or other particles to the bond to control crack propagation. Another is to recrystallize the glass creating nucleation centers that act in a similar fashion.

### 6.5.8 HIGH POROSITY VITRIFIED WHEELS

The primary attraction for producing wheels with high structure numbers is to allow the highest levels of porosity to be produced while still maintaining structural integrity. This provides for very good coolant access and chip clearance in the grinding process. However, it is very difficult to maintain green strength and the integrity of the pores during manufacture of the wheel without additives to act as structural supports or “pore formers.” These are typically either hollow particles such as bubble alumina, glass beads, or mullite, which remain an integral part of the wheel structure but break open at the grinding surface, or fugitive materials such as naphthalene, sawdust, or crushed walnut shells that burn out in the firing process. Hollow particles maintain a strong and coherent wheel structure, while fugitive fillers leave a structure with a high permeability that allows coolant to be carried deep into the wheel. Fugitive pore formers also allow a great flexibility in the shape and size of the pore as shown in Figure 6.8 below. In particular, pore formers allow pore sizes much greater than the grit size to be readily induced.

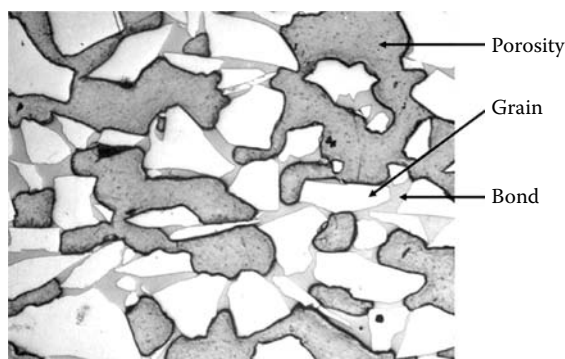


**FIGURE 6.8** Polished surface of an induced porosity vitrified wheel structure. (Resin has been used to infiltrate the pores for sample preparation.)

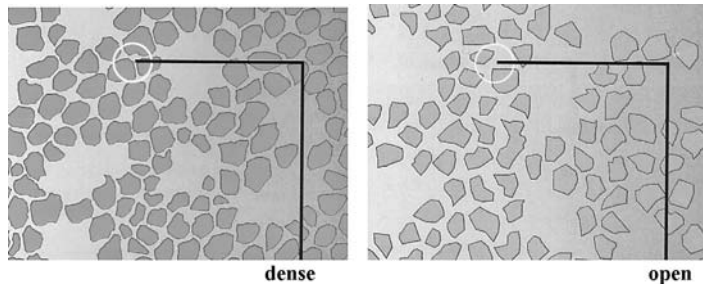


**FIGURE 6.9** Comparison of regular induced porosity wheels and Poros 2 dual structure wheels.

### 6.5.9 MULTIPLE PORE SIZE DISTRIBUTIONS

Wheel manufacturers such as Universal Grinding Wheel (Saint-Gobain Abrasives) have taken this concept further, and produced wheels with multiple pore former size distributions to create both macroporosity for high permeability and microporosity for controlled fracture of the bond. This type of wheel, with trade names such as Poros 2, has proved very effective for creep-feed grinding where coolant delivery into the grinding contact zone is critical for avoidance of burn (Figure 6.9).

### 6.5.10 ULTRAHIGH POROSITY VITRIFIED WHEELS

The introduction of extruded Seeded Gel needle-shaped grains has provided another opportunity for creating extremely porous *and* permeable structures. The natural packing density of grains with an aspect ratio of 8:1 is about 30% by volume. Norton (Saint-Gobain Abrasives) has recently developed a product called Altos with a totally interlinked porosity as high as 65 to 70%. The structure contains only a few percent of bond, but is, nevertheless, very strong because the bond migrates and sinters at the contact points between grains acting analogous to “spot welds.” The high-structural permeability allows prodigious amounts of coolant to be carried into the grind zone. This type of wheel gives probably the highest stock removal rates of any vitrified wheel, higher even than those possible with vitrified CBN, together with excellent G-ratios for a conventional abrasive. It is, therefore, finding major opportunities for grinding difficult burn-sensitive materials such as nickel-based alloys for the aerospace and land-based power generation industries.

### 6.5.11 COMBINING GRADE AND STRUCTURE

In very broad terms, wheel grades E thru I are considered soft and are usually used with high-structure numbers (11 to 20 with induced porosity) for creep-feed and burn-sensitive applications. Grades J through M are considered medium grade, usually used with lower-structure numbers for steels and regular cylindrical and internal grinding. Very hard wheels are produced for applications such as ball-bearing grinding. These wheels are X or Z grade and can contain as little as 2% porosity. Specifications of this hardness are produced by either hot pressing or by oversintering such that the bond fills all the pores. In this type of application, structural numbers can vary from 8 to >24. Their use is limited to relatively few specialist applications such as the grinding of ball bearings.

### 6.5.12 LUBRICATED VITRIFIED WHEELS

The pores may also be filled with lubricants such as sulfur, wax, or resin by impregnating regular wheel structures after firing. Sulfur, a good high-temperature extreme pressure (EP) lubricant, is common in the bearing industry for internal wheels although it is becoming less popular due to environmental issues.



## 6.6 VITRIFIED BONDS FOR DIAMOND WHEELS

### 6.6.1 INTRODUCTION

A number of considerations must be taken into account when selecting vitrified bond for diamond that places different demands relative to conventional wheels. These are primarily the effects of:

- Hard work materials
- Low chemical bonding
- High grinding forces
- Reactivity with air at high temperatures

These considerations are discussed as follows.

### 6.6.2 HARD WORK MATERIALS

Materials ground with diamond tend to be hard, nonmetallic, brittle materials. Therefore, there are limited issues with wheels loading up with grinding debris and wheel porosity can be relatively low. On the other hand, hard workpiece debris is likely to cause much greater bond erosion than other work materials. Therefore, either the bond erosion resistance must be higher or, more practically, a lot more bond must be used.

### 6.6.3 LOW CHEMICAL BONDING

Diamond does not show significant chemical bonding with components in a vitrified bond. The bond must, therefore, rely primarily on mechanical bonding sometimes enhanced with various diamond grain coatings either to improve wetting or mechanical anchorage.

### 6.6.4 HIGH GRINDING FORCES

Grinding forces with diamond can be very high and efforts are made to limit the forces by reducing the number of cutting points by significantly lowering the volume of diamond from 50%. This introduces the term *Concentration*, which is a measure of the volume of superabrasive per unit volume of wheel. Two hundred concentration is equivalent to 8.8 ct/cm<sup>3</sup> by weight or 50% by volume. Most diamond wheels are typically 12 to 100 concentration.

### 6.5.5 DIAMOND REACTIVITY WITH AIR AT HIGH TEMPERATURES

Diamond reacts with air at temperatures above 650°C. Therefore, the wheels must either be fired at low temperatures, or in an inert, or reducing, atmosphere. Very low temperature bonds, however,

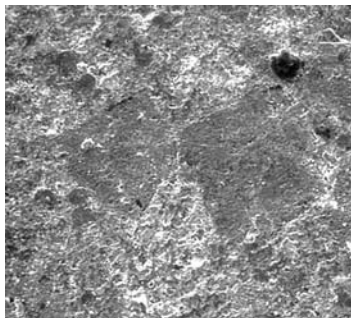


**FIGURE 6.10** Hot pressed fully densified vitrified diamond bond structure.

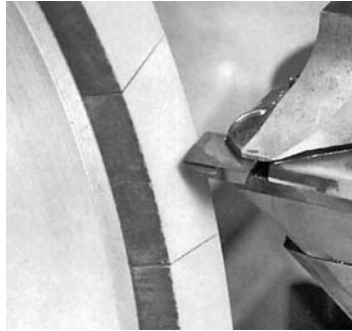


**FIGURE 6.11** Typical application for a porous vitrified fine grain diamond structure wheel—grinding of polycrystalline diamond inserts.

were traditionally very prone to dissolution in water. That limited shelf life made air firing unattractive. A simple method was, therefore, developed to manufacture wheels at higher temperatures by hot pressing using graphite molds. The graphite generated a reducing carbon-rich atmosphere locally. Since the mold strength was low, the bond had to be heated above regular sintering temperatures to limit pressing pressures. Consequently, the bonds fully densified with <2% open porosity. Pockets could be generated in the wheel by adding soft lubricant materials such as graphite or hexagonal boron nitride that wears rapidly on exposure at the grinding surface; fugitive fillers were also added to burn out during firing. Nevertheless, the wheels had a major limitation: their bond content was so high they could not be automatically dressed using diamond tools. As such, they fell into the same category as metal and resin bonds (see later) that had to be trued and then subsequently conditioned. This structure has been standard for many years and used extensively in applications such as double disc and Poly Crystalline Diamond (PCD) grinding, although recently it is being superseded by newer technologies.

## 6.6.6 POROUS VITRIFIED DIAMOND BONDS

In the last 10 years there has been a revolution in the development of porous cold-pressed vitrified diamond bonds driven by the increased use of PCD and carbide for cutting tools and the growth of engineering ceramics. Vitrified diamond bonds, much used in conjunction with micron sizes of diamond grit, are employed for edge grinding of PCD and polycrystalline boron nitride (PCBN) cutting tools, thread grinding of carbide taps and drills, and fine grinding and centerless grinding of ceramics, for example, seals and some diesel engine applications. A number of these bonds are just starting to be dressed automatically with rotary diamond dressers on the grinder without subsequent conditioning.

## 6.7 VITRIFIED BONDS FOR CBN

### 6.7.1 INTRODUCTION

When CBN was introduced into the market in 1969, its cost naturally lent itself to being processed by wheel makers that knew how to handle expensive abrasive – namely, diamond wheel makers – using the dense hot-pressed vitrified systems described above. Unfortunately, these had none of the properties, such as chip clearance and dressability, required for high-production grinding of steels where CBN would prove to be most suited.

Furthermore, vitrified bonds used by conventional wheel makers were so reactive that they literally dissolved all the CBN into the bond by converting it into boric oxide. Grit suppliers tried

to counter this by producing CBN grains with thin titanium coatings on them. Unsurprisingly, it took 10 years and numerous false starts before porous vitrified bonds with the capability of being dressed automatically were finally presented to the market. While some manufacturers still pursued hot-pressed bonds with high fugitive or other filler content [Li 1995], the majority developed controlled reactivity cold-pressed bonds using methods common to processing of conventional vitrified wheels. Just as with conventional abrasives, it was possible to modify the bond formulations to obtain just sufficient reactivity and diffusion to create strong wetting and bonding.

### 6.7.2 REQUIREMENTS FOR VITRIFIED CBN BONDS

The demands of vitrified bonds for CBN differ again from those for either conventional or diamond bonds. Typical wheel supplier specifications, in compliance with standard coding practice, are shown in Table 6.5. The wheel specification format is dictated by the standard practices of the diamond wheel industry. As such, the hardness is expressed as a grade letter but wheel structure is often not given, or described in only the vaguest of terms. As with vitrified diamond, concentration plays a key role in controlling the number of cutting points on the wheel face. Concentrations for CBN wheels, however, tend to be higher than in diamond wheels at up to 200 conc (50% by volume) especially for internal and many cylindrical grinding applications. This limits the structural number to a relatively narrow range.

### 6.7.3 CBN WHEEL STRUCTURES

Typical porous vitrified CBN wheel structures are shown in Figure 6.12. In many ways, the sequence of photographs represents the development of CBN bonds over the last 30 years. The initial wheels were very dense structures with porosity levels of the order of 20%. With the high cost of CBN, performance was focused on achieving maximum possible wheel life. With the development of cylindrical grinding applications for burn-sensitive hardened steels in the 1980s, the porosity levels rose to 30%. More recently, with the rapid expansion of CBN into aerospace and creep-feed applications, porosity levels have risen to the order of 40%. Further development in this area appears key to several wheel makers, for example, Noichl [n.d].

### 6.7.4 GRADES OF CBN WHEELS

A comparison with porosity levels in Figure 6.8 shows clearly that the grade of CBN wheel for a given application, even with the development of higher porosity structures, is much denser than for conventional wheels. This is hardly surprising as CBN is so expensive it must be held for a much greater period of time, even if higher levels of wear flats are created. This is possible because of the high diffusivity of CBN relative to both alox and most workpiece materials. A number of wheel manufacturers do try to mark up CBN wheel grades to be close to those of conventional wheels for the purpose of helping end users more familiar with conventional wheels specify a given wheel for an application. However, it must be understood that usually dressing forces will be much higher because of the grain hardness and because of the additional bond, while hydrodynamic forces from the coolant will also be higher because of the lower porosity. This will place additional challenges on the system stiffness and create a need for new strategies for achieving part tolerances. Some relief is becoming available in terms of higher strength bonds that allow porosity levels to shift back toward those of alox wheels again, but this is often counteracted by higher working wheel speeds.

### 6.7.5 FIRING TEMPERATURE

The actual glass bonds and manufacturing techniques used for vitrified CBN wheels are highly proprietary and there is rapid development still in progress. General Electric (GE) in 1988, for

**TABLE 6.5**  
**Commercial Examples of Vitrified CBN Wheel Specifications**

<p style="text-align: center;"><b>Cincinnati Milacron</b></p> <p style="text-align: center;">2BN    150    R    100    VHA    1/16</p> <p>Grit type    Grit sizes    Grades    Concentration    Bonds    Depth of CBN</p> <p>2BN    60 thru 320    P,R,T,U    100-125-150    VHA    1/16</p> <p>2BN    60 thru 320    P,R    100-125-150    VHC</p> <p style="text-align: center;"><b>DWH</b></p> <p style="text-align: center;">V    B 20/30    C50    CB1    15 B10    AL</p> <p>↑    ↑    ↑    ↑    ↑    ↑</p> <p>Bond    Grit size    Concentration C    Grit type    DWH bond    AL</p> <p>Others, e.g., inbedding in %, blank material</p> <p>E=Electroplated, R=Resin, V=Vitrified, M=Metal</p> <p style="text-align: center;"><b>Krebs &amp; Reidel</b></p> <p style="text-align: center;">2B    91    X    10    V    6236    175</p> <p>Grit CBN type    Grit size    Hardness    Matrix    Bond vitrified    Bond identification number    Concentration</p>	<p style="text-align: center;"><b>Meister</b></p> <p style="text-align: center;">CB5    270    2    D    84    55</p> <p>CBN type    Grit size    Grade    Density    Concentration    V Bonding No</p> <p>Fine    US mesh    FEPA    D dense    34 medium    55</p> <p>Coarse    00    B252    8 soft    O open    64</p> <p>P induced porosity    84 high</p> <p style="text-align: center;"><b>Noritake</b></p> <p style="text-align: center;">80    L    200    V    N1    305 × 20 × 127    3X</p> <p>CB Abrasive    Grit size    Grade    Concentration    Bond type    Mfes record    Wheel size    CBN thickness</p> <p>CB CBM    00 coarse    ?    25    ?    N1    (diameter) ×    3X</p> <p>16000 ?    T    220    N3    (thickness) ×    (hole) mm</p> <p style="text-align: center;"><b>Osaka Diamond</b></p> <p style="text-align: center;">BN    230    J    100    V1    3.0</p> <p>Grain size    Bond hardness    Concentration    Bond matrix    Layer thickness</p> <p>00-1000    D, E, G, J, N    50-200    V1 thru V5 (hard)-(soft)</p> <p style="text-align: center;"><b>Tyrolit</b></p> <p style="text-align: center;">7B    230    P    100    V    735</p> <p>Type of grain    Grain size    Grade    Concentration    Bond    Internal symbol</p> <p style="text-align: center;"><b>Efes (FAG)</b></p> <p style="text-align: center;">Example 853 B64 P 8 V7153 C192</p> <p style="text-align: center;">(1) (2) (3) (4) (5) (6)</p> <p>(1) Abrasive type (B = CBN)                  (2) Grit size (µm)                  (3) Grade                  (4) Structure                  (5) Vitrified bond                  (6) Concentration</p> <p style="text-align: center;"><b>TVMK (Toyoda Van moppes)</b></p> <p style="text-align: center;">Example B 200 N 150 V BA -3.0</p> <p style="text-align: center;">(1) (2) (3) (4) (5) (6) (7)</p> <p>(1) - Grit type                  (2) - Grit size (US mesh)                  (3) - Hardness (grade)                  (4) - Concentration                  (5) - Bond type                  (6) - Bond feature                  (7) - Layer depth (mm)</p> <p style="text-align: center;"><b>Unicorn (universal)</b></p> <p style="text-align: center;">Example 1B 126 M 150 V SS</p> <p style="text-align: center;">(1) (2) (3) (4) (5) (6)</p> <p>(1) - Grit type                  (2) - Grit size (µm)                  (3) - Grade                  (4) - Concentration                  (5) - Vitrified bond                  (6) - Bond system</p>
	<p style="text-align: center;"><b>Osaka Diamond</b></p> <p style="text-align: center;">430AXXXXXX    400    - 5 - 2 -    M126 -    VR100N    H = 320</p> <p>Order No.    Diameter    Layer width    Layer depth    Grit size    Bond and concentration    Diameter of hole</p> <p style="text-align: center;"><b>Norton</b></p> <p style="text-align: center;">Example 1B 220/1 J 175 VX322C</p> <p style="text-align: center;">(1) (2) (3) (4) (5)</p> <p>(1) Grit type                  (2) Grit size                  (3) Grade                  (4) Concentration                  (5) Vitrified bond system</p> <p style="text-align: center;"><b>Unicorn (Indimant)</b></p> <p style="text-align: center;">Example 49 B126 V36 W2J6V G 1M</p> <p style="text-align: center;">(1) (2) (3) (4) (5) (6)</p> <p>(1) - Grit type                  (2) - Grit size (µm)                  (3) - Concentration (V36 = 150 conc)                  (4) - Vitrified bond system                  (5) - Grade                  (6) - Internal coding</p> <p style="text-align: center;"><b>Winter</b></p> <p style="text-align: center;">Example B 64 VSS 34 26 G A18C V360</p> <p style="text-align: center;">(1) (2) (3) (4) (5) (6) (7) (8)</p> <p>(1) - Grit type                  (2) - Grit size (µm)                  (5) - Vitrified bond system                  (3) - Structure                  (6) - Bond code                  (6) - Grade                  (4) - Mfg codes                  (5) - Concentration (V360 = 150 conc)</p>

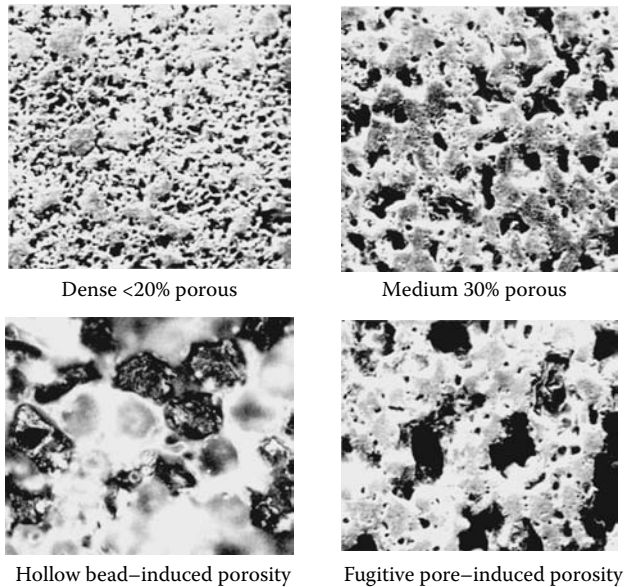


**FIGURE 6.12** Vitrified cubic boron nitride wheel structures (polished surfaces).

example, recommended that bonds with CBN should not be fired at temperatures over 700°C [General Electric 1988]. Yet, Yang [1998] subsequently found the optimum firing temperature to be 950°C for a nominally identical bond composition.

### 6.7.6 THERMAL STRESS

An important factor is to match thermal expansion characteristics of the glass with the abrasive [e.g., Balson 1976], or to optimize the relative stress developed between bond and grain in the sintering process. Yang et al. [1976] reported this could be readily optimized by adjustments to minor alkali additives, primarily sodium oxide.

### 6.7.7 BOND MIX FOR QUALITY

As with bonds for conventional abrasives, bond strength can be improved by the introduction of microinclusions for crack deflection either in the raw materials or by recrystallization of the glass [Valenti et al. 1992]. With the far greater demand for life placed on CBN vitrified bonds and the narrower working range of grades available, quality control of composition and particle size of the incoming raw materials and the firing cycles used to sinter the bonds are critical. It has very often been process resilience, as demonstrated by batch-to-batch consistency in the finished wheels that has separated a good wheel specification from a poor one.

## 6.8 RESIN BOND WHEELS

Resin covers a broad range of organic bonds fabricated by hot pressing at relatively low temperatures, and characterized by the soft nature of cutting action, low temperature resistance, and structural compliance. The softest bonds may not even be pressed but merely mixed in liquid form with abrasive and allowed to cure. Concepts of grade and structure are very different to vitrified bonds. There is no interlocked structure with bond bridges (because there is minimal porosity), but rather an analogy would be to compare the grains to currants in a currant bun! Retention is dependent

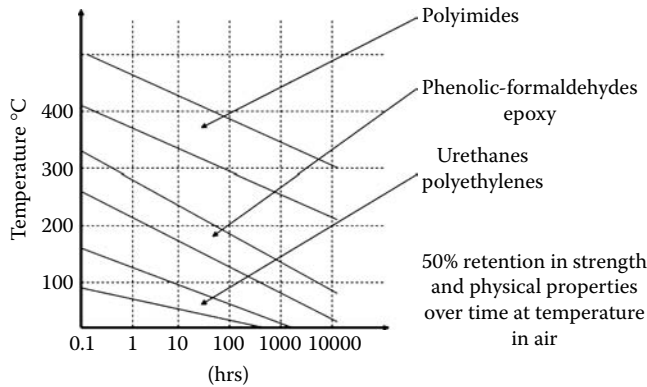


**FIGURE 6.13** Temperature/time properties of resins.

on the localized strength and resilience of the bond surrounding the grain and very sensitive to localized temperatures created in the grind zone and the chemical environment. For example, the bond is susceptible to attack by alkali components in coolants.

Resin bonds can be divided into three classes based on strength/temperature resistance (Figure 6.13). These are plastic, phenolic resin, and polyimide resin.

## 6.9 PLASTIC BONDS

Plastic bonds provide the softest wheels made using epoxy- or urethane-type bonds. Plastic wheels, used with conventional abrasives, are popular for double disc and cylindrical grinding. At one time, prior to the introduction of vitrified CBN, these were the primary wheels for grinding hardened steel camshafts because they gave both a very soft grinding action and a compliance that helped inhibit the generation of chatter. They are still popular in the knife industry and in job shops for grinding burn-sensitive steels. Manufacturing costs and cycle times are low so pricing is attractive and delivery times can be very fast.

For superabrasive wheels, plastic bonds appear limited to ultrafine grinding applications using micron diamond grain for the glass and ceramics industries. Again, its compliance offers an advantage of finer surface finish capabilities but wheel life is limited.

## 6.10 PHENOLIC RESIN BONDS

### 6.10.1 INTRODUCTION

Phenolic bonds represent the largest market segment for conventional grinding wheels after vitrified bonds, and dominate the rough-grinding sector of the industry for snagging and cutoff applications. The bonds consist of thermosetting resins and plasticizers, which are cured around 150 to 200°C. The bond type was originally known as “Bakelite” and for this reason still retains the letter “B” in most wheel specifications. Grade or hardness is controlled to some extent by the plasticizer and use of fillers.

### 6.10.2 CONTROLLED FORCE SYSTEMS

Unlike vitrified wheels, most resin wheels are used under controlled pressure, that is, controlled force rather than fixed infeed systems, and very often at high speed.

**TABLE 6.6**  
**Standard Pressure Ranges for Conventional Resin Bond Cutoff**  
**Wheels**

Operation	Pressure Range	Abrasive Size
Portable grinder	10–25 lbf	16–36#
Floorstand	25–100 lbf	12–20#
Swing frame	100–200 lbf	10–16#
Remote control machine	200–2000 lbf	8–14#
Pressure-controlled grinding [Coes 1971]		

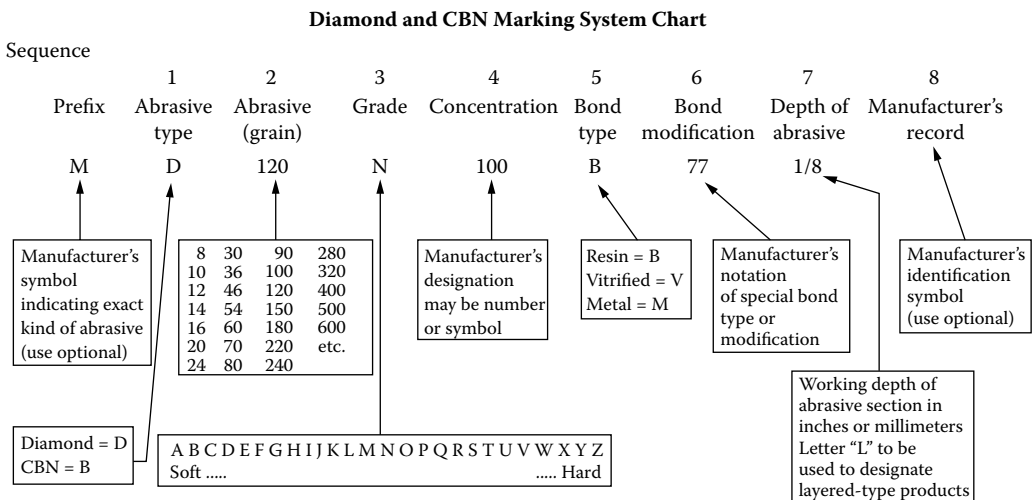
**6.10.3 ABRASIVE SIZE**

Abrasive size is usually used to control recommended grade. Finer grit wheels remove material faster for a given pressure, but wear faster, and are used to avoid the excessive porosity that would be required in a coarse wheel to get cutting action. Porosity reduces burst speed and allows grits to be easily torn out. With available pressures, coarser grit sizes can be used (Table 6.6). Glass fibers are also added to reinforce cutoff wheels for higher burst strength.

**6.10.4 BENEFITS OF RESILIENCE**

Resin bonds are also used for precision applications where its resilience provides benefits of withstanding interrupted cuts and better corner retention. One such area is flute grinding of steel drills where the wheel must maintain a sharp corner and resist significant side forces. There have been enormous improvements in life and removal rates over the last 10 years with the introduction of SG and most recently TG abrasives. Some are capable of grinding at  $Q' > 100$  mm<sup>3</sup>/mm/s while still producing several drills between dresses. This is one example where advances in conventional engineered abrasives are competing very successfully with emerging CBN technologies.

**TABLE 6.7**  
**ANSI Standard Marking Systems for Superabrasive Wheels**



### **6.10.5 PHENOLIC RESIN BONDS FOR SUPERABRASIVE WHEELS**

For superabrasive wheels, phenolic resin bonds represent the earliest, and most popular, bond type particularly for diamond wheels and especially for tool-room applications. The bonds were originally developed for diamond with the introduction of carbide tooling in the 1940s. Their resilience made them optimal for maintaining tight radii while withstanding the impact of interrupted cuts typical of drill, hob, and broach grinding. To prevent localized temperature rise, the abrasive is typically metal coated to act as a heat sink to dissipate the heat. In addition, high volumes of copper or other metal fillers may be used to increase thermal conductivity and heat dissipation.

Not surprisingly, phenolic resin bonds were quickly adopted with the introduction of CBN in 1969, and phenolic resin bonds predominate for the steel tool industry [Craig 1991].

### **6.10.6 WHEEL MARKING SYSTEMS FOR RESIN BONDS**

Because the basic technology is so mature, the number of wheel makers is too numerous to list. However, the marking system for wheels is covered by standards such as ANSI B74-13 shown later for the United States or JIS B 4131 for Japan [Koeper 1994].

Many wheel makers are located close to specific markets to provide quick turnaround. Alternatively, many are sourced from low-cost manufacturing countries. The key to gaining a commercial advantage in this type of competitive environment is application knowledge either by the end user developing a strong database and constant training, or using the knowledge of the larger wheel makers with strong engineering support.

## **6.11 POLYIMIDE RESIN BONDS**

### **6.11.1 INTRODUCTION**

Polyimide resin was developed by DuPont in the 1960s originally as a high-temperature lacquer for electrical insulation. By the mid 1970s, it had been developed as a cross-linked resin for grinding wheels giving far higher strength, thermal resistance, and lower elongation than conventional phenolic bonds. The product was licensed to Universal Diamond Products (Saint-Gobain Abrasives) and sold under the trade name of Univel, where it came to dominate the high-production carbide grinding business especially for flute grinding. Polyimide has five to ten times the toughness of phenolic bonds and can withstand temperatures of 300°C for 20 times longer. Its resilience also allows it to maintain a corner radius at higher removal rates or for longer times than phenolic resin (Figure 6.14).

### **6.11.2 COST DEVELOPMENTS AND IMPLICATIONS**

Polyimide bonds, for reason of cost, are limited to superabrasives and are most effective with diamond abrasives on carbide. Because the wheels are so tough, they will highlight any weakness in the machine such as spindle play or backlash in the infeed system. They also require a spindle power of at least 7.5 kW/cm linear contact width (25 hp/in.).

In the past few years, with the expiry of various patents, alternate sources for polyimide resin have become available. They are significantly less expensive than the Du Pont-based process but, to date, have not quite matched the performance. However, the price/performance ratio is still very attractive making polyimide resin bonds cost-competitive relative to phenolic resin bonds in a broader range of applications.

### **6.11.3 INDUCED POROSITY POLYIMIDE**

In some applications, the Univel product has proved so tough in comparison to regular phenolic bonds that induced porosity techniques from vitrified bond technology have been used to improve the cutting action.



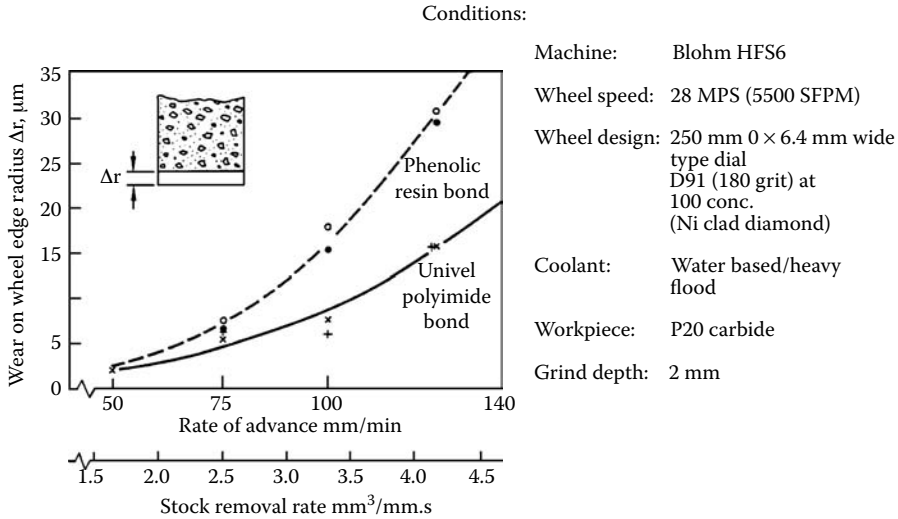


FIGURE 6.14 Comparison of the performance of phenolic and polyimide bonds.

## 6.12 METAL BONDS

### 6.12.1 INTRODUCTION

Metal represents the toughest and most wear-resilient of bond materials and is almost exclusively used with superabrasives. Much of this is for stone and construction, glass grinding, and honing. As such, metal is the largest user of synthetic industrial diamonds, but falls outside the scope of this book as it is often used for roughing operations.

### 6.12.2 BRONZE ALLOY BONDS

Metal bonds for production grinding tend to be based on bronze in the copper-tin alloy range of 85:15 to 60:40 with various fillers and other small alloy components. Metal bonds are the most resilient and wear resistant of any of the bonds discussed, but also create the highest grinding forces and the most problems in dressing. Their use has been limited to thin wheels for dicing and cutoff, profile grinding, fine grinding at low speeds, and high-speed contour or peel grinding. This latter process is dependent on maintaining a well-defined point on the wheel and, therefore, the maximum wheel life. However, in many cases involving CBN, metal has been replaced by vitrified bond, even at the sacrifice of wheel life, in order to improve the ease of dressing.

### 6.12.3 POROUS METAL BONDS

Metal bronze bonds become more brittle as the tin content is increased. In the 1980s, brittle metal bond systems began to emerge with sufficient porosity that profiles could be formed in the wheel automatically by crush dressing using steel or carbide form rolls.

### 6.12.4 CRUSH-DRESSING

Bonds suitable for crush-dressing, sold under trade names such as Crushform, developed by Van Moppes-IDP (Saint-Gobain Abrasives) [Daniel 1983, Barnard 1985, 1989], were of particular

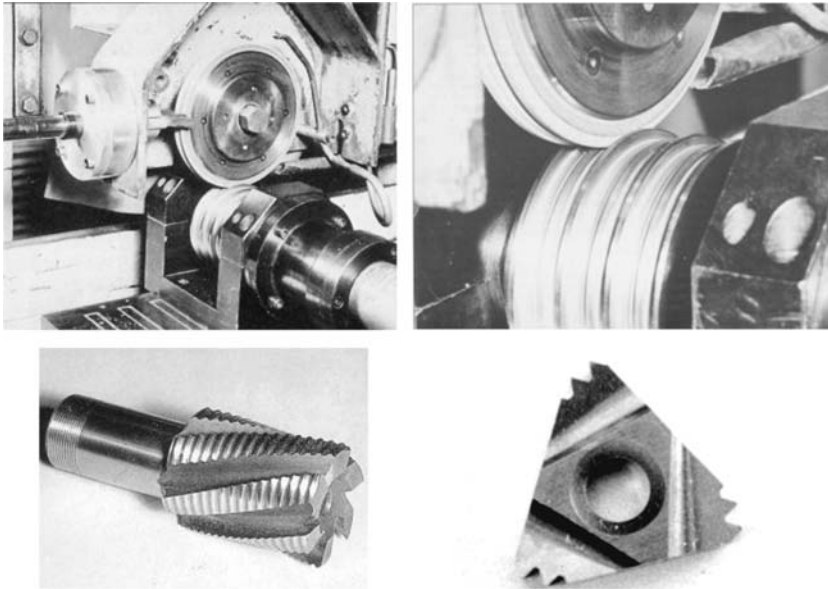


**FIGURE 6.15** “Crush-form” dressing of porous metal bond diamond wheel for form grinding of carbide tools. (Courtesy of Saint-Gobain Abrasives. With permission.)

interest to the carbide tool insert market. However, there were some problems with this type of wheel. The dress process did not leave the wheel in a free-cutting state and, therefore, the surface had to be subsequently conditioned using dressing sticks or brushes. This was readily resolved as shown in Figure 6.15. Note the horizontal brush infeed in the top left picture.

The bigger problem, however, was the extreme forces generated in dressing. Where the use of crushable metal bond wheels has been successful, such as at OSG Corporation in Japan [Yoshimi and

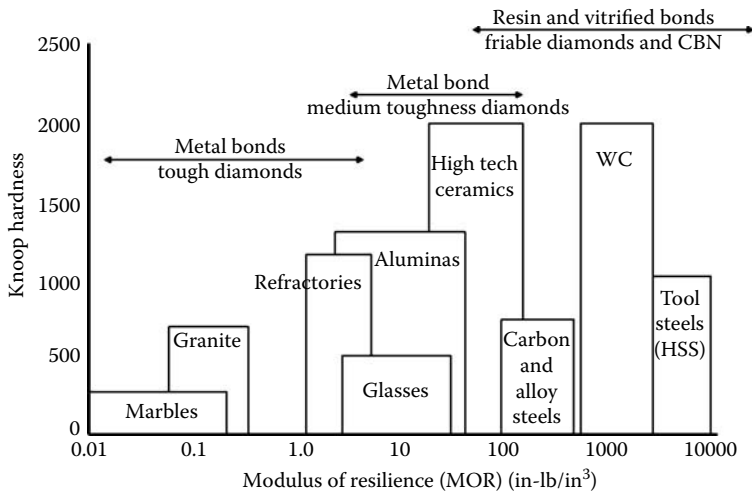


**FIGURE 6.16** Superabrasive bond and grain selection as a function of workpiece resilience. (Based on Jakobuss 1999. With permission.)

Oshita 1986], special high-stiffness grinders have had to be built specifically for their use. As such, the use of crushable metal bonds has been limited awaiting advances in standard production machine tool stiffness. Vitrified technology has been substituted in most cases [Pung 2001], although new advances in more user-friendly porous metal bond technology such as Scepter from Norton (Saint-Gobain Abrasives) is creating renewed interest [McSpadden et al. 1999].

### 6.12.5 HIGH-POROSITY IMPREGNATED METAL BONDS

The concept of a porous, brittle metal bond has been taken further by increasing the porosity level to the point of having interconnected porosity in a sintered metal skeleton and vacuum impregnating the pores with resin. This is sold under trade names such as Resimet from Van Moppes (Saint-Gobain Abrasives). This type of bond has been extremely successful for dry grinding applications on tool steels and carbide. It is freer cutting and gives longer life than resin, requires no conditioning, while the metal bond component offers an excellent heat sink.

## 6.13 OTHER BOND SYSTEMS

There are several older traditional bond systems used with conventional abrasives. These include the following.

### 6.13.1 RUBBER

Rubber bonds introduced in the 1860s are still used extensively for regulating wheels for centerless grinding and some reinforced grades for wet cutoff grinding. Manufacturing is becoming an increasing problem for environmental reasons, and alternatives, such as epoxy, are being substituted where possible.

### 6.13.2 SHELLAC

Shellac- or “elastic”-bonded wheels were first made in 1880, and, due to a combination of elasticity and resilience, probably represent the best wheel for producing fine, chatter-free finishes for grinding of steel rolls for the cold strip steel mills and paper industries. Shellac comes from fluid exuded by insects onto themselves as they swarm cassum or lac trees in India. As such, it is highly variable both in availability and properties depending on the weather conditions and species. On occasion, a single wheel maker can consume 10% of the entire world’s production. Not surprisingly, many wheel makers have sought alternative solutions to grinding applications.

### 6.13.3 SILICATE

Silicate bonds were first produced around 1870 by mixing wet soda of silicate with abrasive, tamping in a mold, drying, and baking. It is still popular in certain parts of the world by reason of its simplicity and low cost of manufacture. The wheels are generally used for large face wheels.

## REFERENCES

- Balson, P. C. 1976. “Vitreous Bonded Cubic Boron Nitride Abrasive Article.” U.S. Patent 3,986,847. 10/19/1976.
- Barnard, J. M. 1985. “Creep Feed Grinding Using Crushform and Dressable Superabrasive Wheels.” Superabrasives '85 SME Conference, Chicago, IL, MR85-292.
- Barnard, J. M. 1989. “Crushable CBN and Diamond Wheels.” Part 1. *IDR* 1, 1–34; “Crushable Wheels—Case Histories.” Part 2. *IDR* 4, 176–178.

- Bush, J. 1993. "Advanced Plated CBN Grinding Technology." IDA Diamond & CBN Ultrahard Materials Conference, Windsor, Canada.
- Chattopadhyay, A.K. et al. 1990. "On Performance of Chemically Bonded Single-Layer CBN Grinding Wheel." *Ann. CIRP* 39, 1, 309–312.
- Coes, L. Jr. 1971. *Applied Mineralogy I—Abrasives*. Springer-Verlag, New York.
- Craig, P. 1991. "The Age of Resin Isn't History." *Cutting Tool Eng.* June, 94–97.
- Daniel, P. 1983. "'Crushform' Wheels Can Be Formed in Your Plant." *IDR* 6.
- DiCorletto, J. 2001. "Innovations in Abrasive Products for Precision Grinding." Precision Grinding & Finishing in the Global Economy—2001 Conference Proceedings. Gorham, 10/1/2001, Oak Brook, IL.
- Engineer, F. et al. 1992. "Experimental Measurement of Fluid Flow through the Grinding Zone." *J. Eng. Ind.* 114, 61–66.
- GE Superabrasives. 1988. "Understanding the Vitreous Bonded Borazon CBN System." General Electric Borazon ® CBN Product Selection Guide. Commercial brochure.
- Jakobuss, M. 1999. "Influence of Diamond and Coating Selection on Resin Bond Grinding Wheel Performance." Precision Grinding Conference. Chicago, IL, June 15–17.
- Julien, D.L. 1994. "Titanium Nitride and Titanium Carbide Coated Grinding Tools and Method Thereof." U.S. Patent 5,308,367, 5/3/94.
- Kinik. n.d. "Grinding Wheels Catalog #100E." Trade catalog.
- Koepfer, C. 1994. "Grit, Glue—Technology Tool." *Modern Machine Shop*.
- Li, R. 1995. "Improved Vitrified Abrasive Bodies." WO Patent WO 95/19871, 7/27/95.
- Lowder, J.T. and Evans, R.W. 1994. "Process for Making Monolayer Superabrasive Tools." U.S. Patent 5,511,718, 11/4/94. (See also U.S. 3,894,673 and U.S. 4,018,576.)
- Malkin, S. 1989. *Grinding Technology*. Ellis Horwood, Chichester, UK.
- McClew, D. 1999. "Technical and Economic Considerations of Grinding Aerospace Alloys with Electroplated CBN Superabrasive Wheels." Precision Grinding '99. Gorham Int. Chicago.
- McSpadden, S. B. et al. 1999. "Performance Study of Scepter™ Metal Bond Diamond Grinding Wheel." Precision Grinding Conference. Chicago, IL.
- Noichl, H. n.d. "What Is Required to Make a Grinding Wheel Specification Work?" IGT Grinding Forum, University of Bristol.
- Peterman, L. n.d. "ATI Techview PBS® vs. Electroplating." Trade paper.
- Pung, R. 2001. "Enhancing Quality and Productivity with Vitrified Superabrasive Products." Precision Grinding & Finishing in the Global Economy 2001. Gorham Int. 10/1/2001, Oak Brook, IL.
- Rappold, Winterthur, 2002. "Cylindrical Grinding." Trade brochure. Rappold – Winterthur 02/2002 #136551.00.
- Valenti et al. 1992. "Glass-Ceramic Bonding in Alumina/CBN Abrasive Systems." *J. Mat. Sci.* 27, 4145–4150.
- Yang, J. 1998. "The Change in Porosity during the Fabrication of Vitreous Bonded CBN Tools." *K. Korean Ceram. Soc.* 35, 9, 988–994.
- Yang, J. et al. 1993. "Effect of Glass Composition on the Strength of Vitreous Bonded c-BN Grinding Wheels." *Ceram. Int.* 19, 87–92.
- Yoshimi, R. and Ohshita, H. 1986. "Crush-Formable CBN Wheels Ease Form Grinding of End Mills." Machine and Tool Blue Book.



---

# 7 Dressing

## 7.1 INTRODUCTION

Understanding the procedures and mechanisms of dressing grinding wheels is critical to obtaining optimum performance in grinding. The available dressing methods are numerous and confusing – even the basic terminology varies from one manual or paper to another. For the purposes of this discussion, the following terms will be used:

- **Truing:** Creating a round wheel concentric to the axis of wheel rotation, and generating, if necessary, a particular profile on the wheel face. It is also to clean out any metal embedded or “loaded” in the wheel face. A further function is to obtain a new set of sharp cutting edges on the grains at the cutting surfaces.
- **Conditioning:** Preferential removal of bond from around the abrasive grits.
- **Dressing:** Truing the wheel and conditioning the surface sufficient for the wheel to cut at the required performance level.

Many people use the term dressing to mean conditioning, but with most of the high-production grinding occurring today, truing and conditioning are simultaneous processes and are referred to in combination as dressing. In Europe, conditioning can mean dressing or truing, sharpening can mean conditioning, and profiling can be used for truing [Pricken 1999].

All wheels require dressing with the exception of electroplated wheels, although even here they may be occasionally trued initially 10 to 20  $\mu\text{m}$  or occasionally conditioned lightly with a dressing stick to remove loaded metal. The focus of this chapter, however, is on bonded wheels, especially vitrified. These bonds are popular because their porous, crushable bonds allow dressing in a single automatic operation.

Dressing processes for conventional wheels can be divided into two distinct classes:

- Dressing with stationary diamond tools
- Dressing with rotary diamond truers that offer much longer tool life

The simplest to begin with are stationary tool processes.

## 7.2 TRAVERSE DRESSING OF CONVENTIONAL VITRIFIED WHEELS WITH STATIONARY TOOLS

### 7.2.1 NOMENCLATURE

The terminology for the various parameters involved in dressing is as follows:

- $a_d$  = dressing depth of cut (or dress infeed amount) per pass
- $b_d$  = effective contact width of the dressing tool
- $n_s$  = grinding wheel rpm
- $f_d$  = axial tool traverse across grinding wheel surface, feed/rev
- $U_d$  = dressing overlap ratio
- $v_{fd}$  = axial tool traverse feed velocity

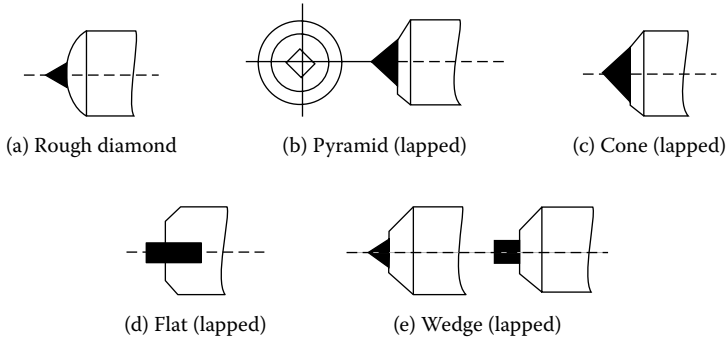


FIGURE 7.1 Standard single-point diamond shape.

### 7.2.2 SINGLE-POINT DIAMONDS

The simplest tool is the single-point diamond. Typical designs of the diamond are shown in Figure 7.1, Figure 7.2, and Figure 7.3. The majority of tools are A-shaped with the corner of rough unlapped diamonds. In general, these corners are well-enough defined for repeatable dress action for flat wheel forms. The diamond is buried in a metal matrix with about one third of the diamond exposed. High-quality diamonds tend to have up to four usable points and the tools can be returned to the toolmaker for resetting. Although the initial cost is higher, this is usually the most cost-effective choice unless tools are being abused. In this case, much lower quality throw-away tools are recommended. The diamond weight can vary from a standard 1/2 ct up to 2 ct for aggressive or heavy dressing.

### DIAMOND SIZE

General recommendations for diamond size are based on wheel size as in Table 7.1.

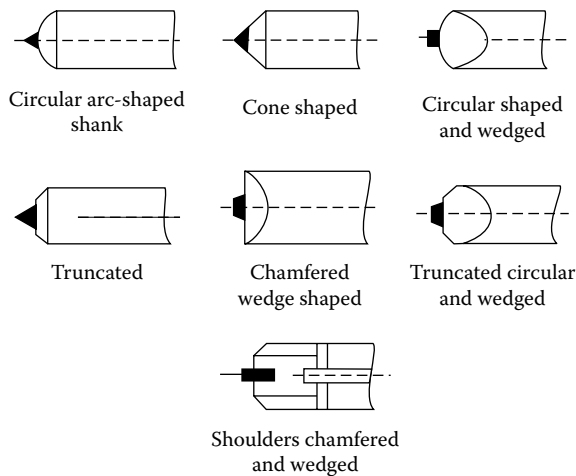


FIGURE 7.2 Standard single-point diamond top-end shapes of tool shanks.

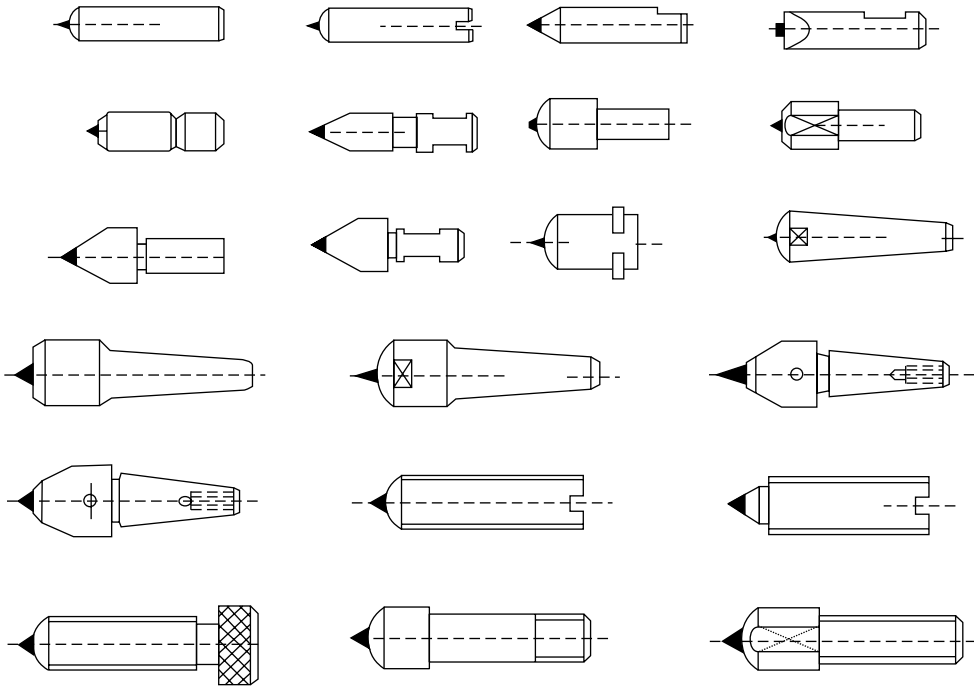


FIGURE 7.3 Standard single-point tool shank shapes.

### 7.2.4 SCAIF ANGLE

The diamond is mounted in a holder and held at a scaif angle against the wheel rotation and with the traverse motion as illustrated in Figure 7.4. The single point cuts a thread across the face of the wheel fracturing or dislodging grains and bond leaving a fresh topography on the wheel surface (Figure 7.5).

### 7.2.5 COOLING

Copious coolant should be applied as the diamond is heat sensitive and the tool holder should have its own coolant nozzle. The coolant supply must be turned on before commencing a dressing pass. If the coolant is turned on during a pass, the diamond may be damaged by severe thermal shock.

**TABLE 7.1**  
**Single-Point Diamond Size**  
**Recommendations for Single-Point Tools**  
**Based on Wheel Diameter**

Up to 3"	1/5 Carat
3" to 7"	1/4 Carat
8" to 10"	1/3 Carat
11" to 14"	1/2 Carat
15" to 20"	3/4 Carat
Over 20"	1 Carat



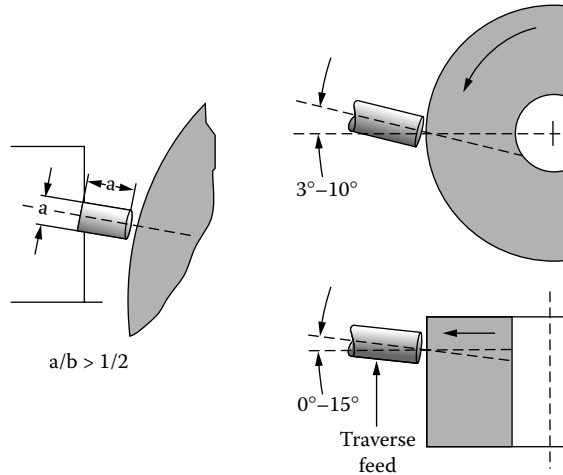


FIGURE 7.4 Dressing configuration using single-point diamonds. (From Rappold 2002. With permission.)

### 7.2.6 DRESSED TOPOGRAPHY

The resulting roughness is governed, in simplistic terms, by the height of profile  $\delta$  resulting from the overlap of the tool radius from one rotation of the wheel to the next. This height should always be less than the dress depth in order to avoid noncleanup of the wheel surface at each pass and a resulting poor appearance in the ground part. The value for  $\delta$  is controlled by the traverse rate, depth of cut, and tool radius. Significant research has been carried out to predict surface topography from tool profiles and wheel/tool interaction kinetics (e.g., Torrance and Badger [2000]).

### 7.2.7 DRESSING FEED AND OVERLAP RATIO

Grinding engineers employ empirical approximations and guidelines to determine dressing feedrate. Depending on the dressing depth, the tool is assigned an effective cutting width,  $b_d$ , which is assumed is swept out on the wheel each revolution. An overlap ratio,  $U_d$ , is then assigned for each type of operation and allows the axial dressing feedrate,  $v_{fd}$ , to be determined.

$$U_d = b_d / f_d = b_d \cdot n_s / v_{fd}$$

For typical single-point dressing, dressing width,  $b_d$ , is about 0.5 to 1.0 mm and the following values for overlap ratio,  $U_d$ , may be used for general applications. These values are applicable to all traverse dressing operations.

- Rough grinding  $U_d = 2-3$
- Medium grinding  $U_d = 3-4$
- Finish grinding  $U_d = 6-8$

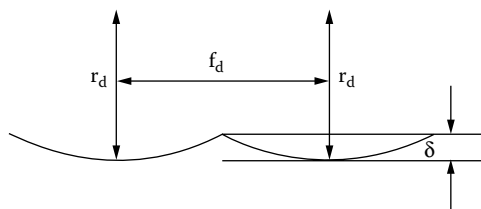


FIGURE 7.5 Dress profile generated by single-point tool.

**TABLE 7.2**  
**Grit Size Values for Calculating Dress Traverse Rates**

FEPA Designation Standard	ANSI Grit Size	US Grit Number	Average Size (mm)	Average Size (in.)
301	50/60	50	0.3	0.012
251	60/70	60	0.25	0.01
213	70/80	80	0.225	0.009
181	80/100	100	0.175	0.007
151	100/120	120	0.15	0.006
126	120/140	150	0.125	0.005
107	140/170	180	0.1	0.004
91	170/200	220	0.0875	0.0035
76	200/230	240	0.075	0.003
64	230/270	280	0.0625	0.0025
54	270/325	320	0.045	0.0018

In practice, many problems are caused by setting the dressing feedrate too slow. This is equivalent to assigning a value of overlap ratio that is far too high. The result is rapid wear of the diamond and damage to the abrasive grains in the wheel. The grinding forces will be too high and the wheel will soon need redressing.

An alternative method, since the grinding severity is based on grit size in the wheel, is to set the effective contact width/rev to half the average abrasive grit size (Table 7.1).

### 7.2.8 DRESSING DEPTH

Depth of cut will also control roughness. However, the maximum dress depth should be kept under 30  $\mu\text{m}$  for regular alumina wheels, after which the only change is increased tool wear. For seeded gel-type abrasives, the maximum dress depth should be under 20  $\mu\text{m}$ . The minimum dress amount will depend on machine accuracy and stability, wheel wear, finish, etc., but may be as low as 2  $\mu\text{m}$ .

### 7.2.9 DRESSING FORCES

For a typical K grade, conventional wheel dressing forces with single-point diamonds are typically in the range of 30 to 80 N normal to the wheel with a cutting force coefficient of about 0.25. Although these forces are lower than in other tools to be discussed later, the tool should, nevertheless, be well clamped in the holder and not overextended. Note the requirement  $a/b > 1/2$  in Figure 7.4.

### 7.2.10 DRESSING TOOL WEAR

Single-point tools wear relatively quickly compared with multipoint dressing tools. A tool is typically worn out when the wear flat at the tip exceeds about 0.6 mm. One advantage of having the tool tilted to the axis of the wheel is that the tool can be rotated in the holder to keep the tip sharp. Caution should be applied, however, in that standard commercial tools often do not have the tool accurately centered in the holder. This can cause the operator to continually chase size after each rotation. The result is that the tool does not get rotated but rather is thrown away!

As the dressing tool wears, it loses its sharpness. This can affect the grinding process in a number of ways. Grinding forces and power may be reduced due to the dislodgement of abrasive grains and severe grain fracture using a blunt diamond as shown in Figure 7.6. However, this is not necessarily good news. Workpiece roughness is greatly increased and the grinding process becomes more variable as a dressing tool wears. This is the opposite of the requirement for close

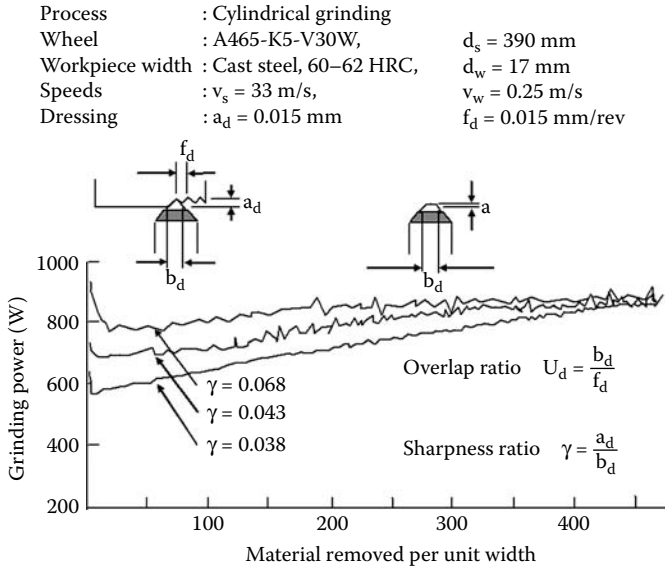


**FIGURE 7.6** Effect of dressing tool wear on grinding power and grinding wheel wear. (After Chen 1995. With permission.)

control of tolerances [Chen 1995, Marinescu et al. 2004]. There is also increased risk of dressing chatter with dressing tool wear. This is due to vibration of the diamond while dressing and leads to very poor wheel topography and chatter marks.

**7.2.11 ROTATIONALLY ADJUSTABLE TOOLS**

Tools are available called “Rotoheads” or Norton’s “U-dex-it” that are specifically designed so that the head can be rotated without loosening the tool in the holder. The diamond is centrally positioned in the holder to within 25  $\mu$ m.

**7.2.12 PROFILE DRESSING TOOLS**

For profiling applications, chisel-shaped tools with well-defined radii are used. These are used on profile dressing units such as Diaform, which were traditionally pantograph-based, although now more often use 2-axis computer numerical control (CNC) motion.

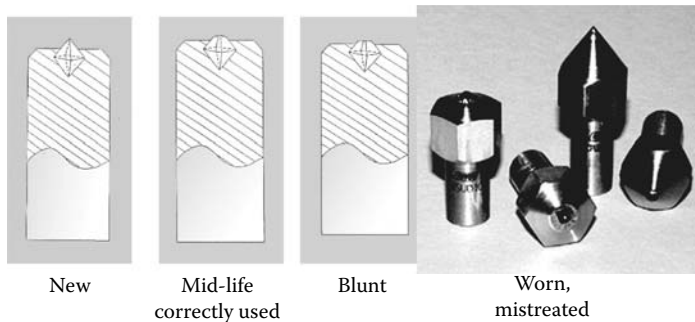


**FIGURE 7.7** Problems in tool wear due to poor tool monitoring. (From Saint-Gobain Abrasives. With permission.)

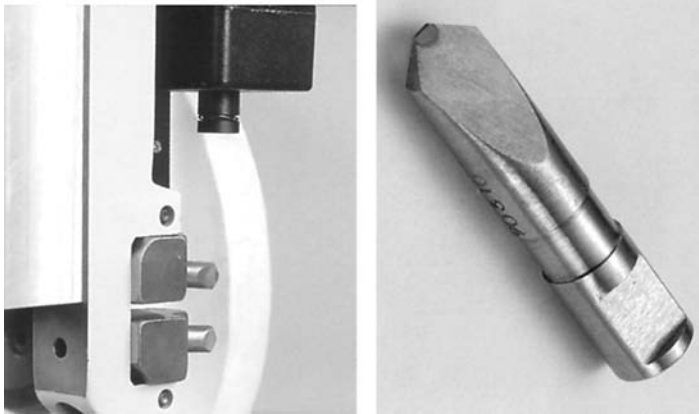


FIGURE 7.8 Diamond blades for Diaform wheel traverse profiling.

### 7.2.13 SYNTHETIC NEEDLE DIAMONDS

The wear of single-point diamonds in profile dressing leads to problems with changing dress conditions because of the increasing cross section of the flat generated. The introduction of synthetic needle diamonds provides a solution in the form of a constant cross section. This type of tool has seen increasing usage as a replacement for higher quality single points. They are used both as a single stone but also more commonly as a blade tool with up to four stones in a row. When specifying the diamond stone size,  $b_d$  is assumed to be the width of the diamond. This will vary somewhat based on the orientation of the stones, which will also affect finish.

Few guidelines have been published for the use of stationary tools for generating profiles on the wheel face. The Winterthur Company [Winterthur 1998] recommends that 0.6-mm stones be used for abrasive grit sizes <80/100#, and 0.8-mm stones for coarser wheels with an overlap ratio,  $U_d$ , value of 4. The number of stones used is dependent on the wheel diameter and width. Typically two stones are used for wheels <4 in., three stones for <20 in., and four stones for >20 in. The Noritake Company [Noritake n.d.] gave the following recommendations based on wheel surface area and wheel grit size (Table 7.3).

By offsetting the position of the stones, it is possible to use this type of blade dresser for dressing simple profiles such as angle-head wheels. The tool should be prelapped to the appropriate angle to limit break-in times.

**TABLE 7.3**  
**Recommendations for Stationary Dressing Tools**  
**Using Needle Diamonds**

Wheel Diameter × Wheel Width (in. <sup>2</sup> )	Number of Stones	Abrasive Grit Size	Needle Diamond Face Width (in. × 10 <sup>-3</sup> )
<5	1	36# to 60#	36 to 44
>5 to <20	2	60# to 120#	24 to 36
>20 to <60	3	120# to 150#	20 to 24
>60 to >120	4	150# +	16 to 20
>120	5		

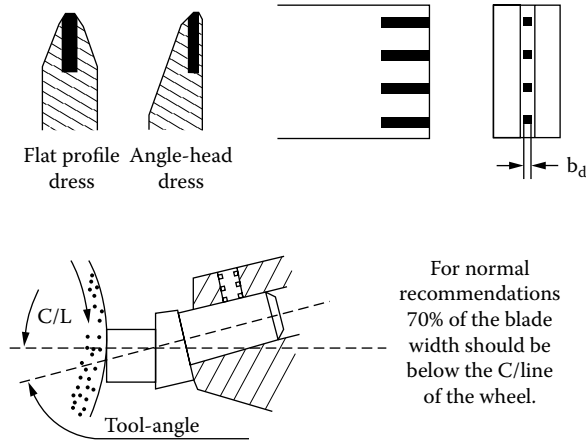


FIGURE 7.9 Needle diamond dressing blades and application. (From Unicorn n.d. With permission.)

7.2.14 NATURAL LONG DIAMOND BLADE TOOLS

Prior to the introduction of synthetic needles natural long stones were used. These have trade names such as the Fliesen tool from Winter (Saint-Gobain Abrasives). Some tools of this style have multiple layers of diamonds to maximize tool life, but care needs to be taken in their design to avoid changes in dress behavior when transitioning from one layer to another.

Blade tools have double the truing forces of single-point diamonds (50 to 150 N depending on wheel grade and grit size) but can handle depths of cut up to 50  $\mu\text{m}$  for roughing of regular abrasive. For ceramic-type abrasives, the maximum dress depth is 25 to 20  $\mu\text{m}$ .  $b_d$  is typically 0.75 to 1.0 mm. As with single points, the tools should be biased by up to 30° in the direction of traverse (Figure 7.10 and Figure 7.11).

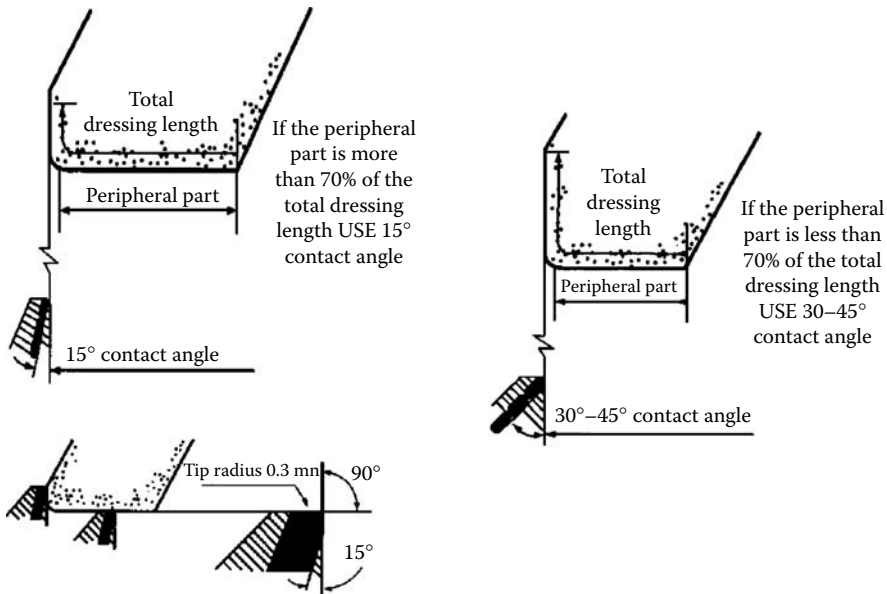


FIGURE 7.10 Application of needle blade tools for angle-head wheel dressing. (Courtesy of Saint-Gobain Abrasives. With permission.)

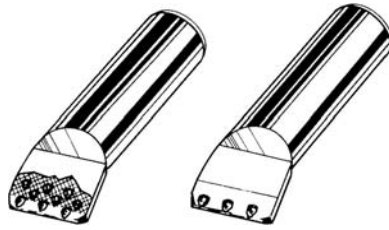


FIGURE 7.11 Examples of blade tools with natural long stones.

### 7.2.15 GRIT AND CLUSTER TOOLS

Finally, for the roughest dressing of large cylindrical or centerless wheels there are grit tools and cluster impregnated tools (Figure 7.12).

Grit tools represent the most cost-effective dressing tool for the commonest applications using straight wheels. Clusters consist of a single layer of five to seven large natural diamonds semiexposed on a round flat surface held in a sintered metal matrix. As with other tools, they are inclined up to  $15^\circ$  with the tool center line intersecting the wheel center line. Their large head diameter results in fast traverse rates for reduced dress cycle times relative to other tools.

Grit tools consist of a consumable layer of diamond grains held in a highly wear-resistant sintered metal matrix. The tools wear progressively over time exposing new grains. Diamond size selection is governed by the abrasive grain size in the wheel, while the tool width,  $b_d$  (and length,  $L$ ), are dictated by the diameter and width of the wheel (Table 7.4). Note that the tool now consists of a random collection of diamond-cutting points whose action will depend on their exposure during any point in the life of the tool. Also the tool will wear a radius to the shape of the wheel. Overall, the process is not as consistent as a single point but in most cases acceptable and offset by the fact the tools are cheap, easy to make, and long lasting. Dressing forces with grit tools, however, must be respected; forces are typically five to eight times greater than those for single-point diamonds. The tool must, therefore, be clamped extremely rigidly with little or no overhang. Minimum dress depth is  $10\ \mu\text{m}$  because of the relatively dull dress action. They can handle dress depths up to  $125\ \mu\text{m}$  dressing conventional alumina wheels and  $50$  to  $25\ \mu\text{m}$  with ceramic-type abrasives.

### 7.2.16 FORM BLOCKS

In addition to the stationary tools for traverse dressing, full forms can be dressed simultaneously using form blocks. These are blocks that have a layer of diamond either sintered or directly plated and molded to the form required in the wheel. They are used especially in surface grinding where the block is set on the table at the same height as the finished ground height. The reciprocating

**TABLE 7.4**  
**Grit Tool Recommendations for Conventional Wheels**

Diamond Grit Size	Abrasive Grit Size	Type	$b_d$	L	Application
18/20	46#	round	$1/4''$	N/A	small toolroom
20/25	54#	round	$3/8''$	N/A	medium toolroom
20/30	60#	block	$1/4''$	$1/2''$	$<20''\ \phi \times <10''$ wide
20/30	80#	block	$1/4''$	$3/4''$	$>20''\ \phi \times <10''$ wide
30/40	100#	block	$3/8''$	$1/2''$	$<20''\ \phi \times >10''$ wide
40/50	120#	block	$3/8''$	$3/4''$	$>20''\ \phi \times >10''$ wide

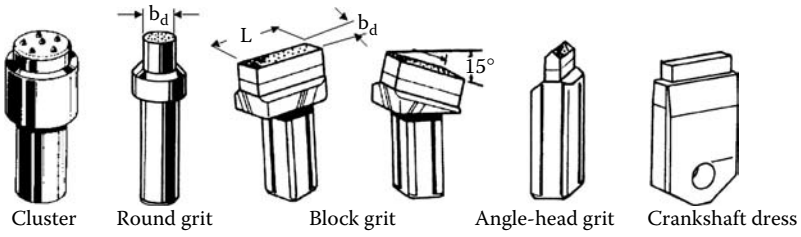


FIGURE 7.12 Examples of standard cluster and grit tool configurations.

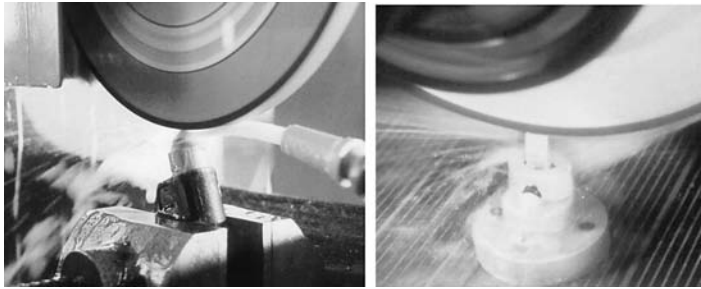


FIGURE 7.13 Single-point and blade-tool dressing. Note copious use of coolant. (From Pricken 1999. With permission.)

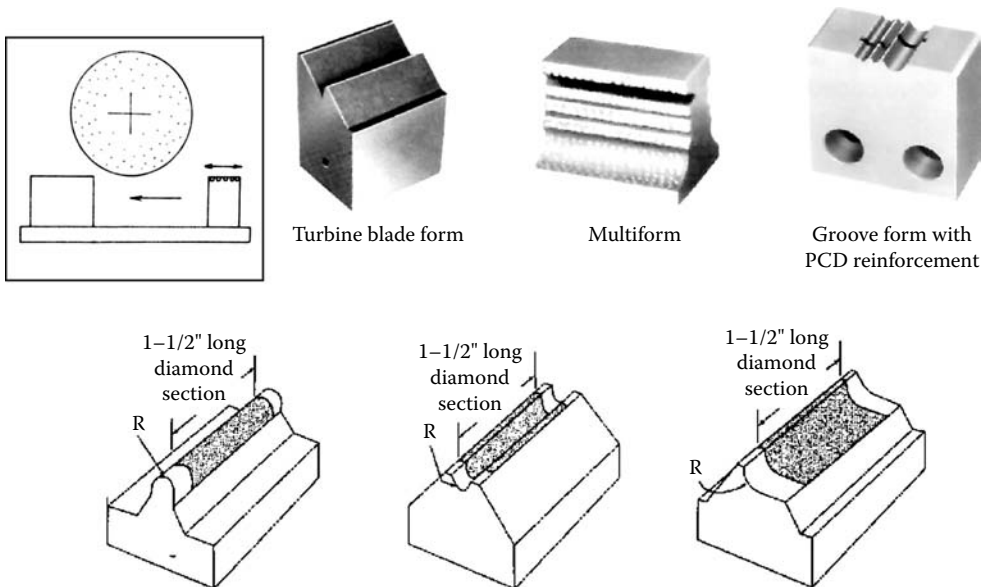


FIGURE 7.14 Examples of block dressers for profile dressing alox wheels: (a) [TVMK 1992 (with permission)]; (b) [Engis 1996 (with permission)].

stroke length is adjusted so that it dresses the wheel before finish grind. The blocks are either molded to the full form required or supplied as standard shapes for flexibility in toolroom applications. Dimensional form accuracies can be held to  $\pm 5 \mu\text{m}$ ; minimum radius capability is  $75 \mu\text{m}$  (Figure 7.14).

## 7.3 TRAVERSE DRESSING OF SUPERABRASIVE WHEELS WITH STATIONARY TOOLS

### 7.3.1 INTRODUCTION

Perhaps the most widely sought after, but as yet unavailable, stationary tool is the one that can dress high-performance vitrified cubic boron nitride (CBN) wheels. The problem is that single-point and needle diamonds wear much too quickly for most superabrasive wheels at the speeds the wheels must operate. Grit tools leave the wheels too dull and create too much pressure. There are a couple of exceptions, however: dressing small and/or low concentration wheels.

### 7.3.2 JIG GRINDING

Jig grinding, such as on Moore jig grinders, uses a range of CBN and diamond wheels. The process has a relatively low stock-removal requirement because most applications are still performed dry and the wheels must be mounted on long quills to get deep into, for example, mold cavities. The wheel spindle is usually pneumatically driven and can be slowed to a few hundred rpm for dressing, making the wheel act extremely soft. Using small diameter, high-porosity wheels, the author has even had acceptable life with single-point diamond tools dressing dry (although this would not be the optimum process, it can do a job).

### 7.3.3 TOOLROOM GRINDING

The other area is again in the toolroom targeted at grinding steels such as D2, A2, and M2 on low-power reciprocating surface grinders. Several wheel makers have produced products such as Memox from Noritake, CBLite from Norton (Saint-Gobain Abrasives), and Vitrazon TR from Universal (Saint-Gobain Abrasives) that are low-concentration vitrified CBN wheels with relatively high porosity. At low stock-removal rates typical of a surface grind operation ( $Q'_w \leq 1 \text{ mm}^3/\text{mm/s}$ ), they can still achieve a G-ratio of 500 to 1,000. The attraction of this type of wheel is that it can remove material at a rate as fast or faster than that of a conventional wheel, since in most cases the process is limited more by spindle power and machine stiffness, while an unskilled operator can set a grinder up to remove a given depth of stock without having to compensate repeatedly for wheel wear. This type of wheel has been dressed with single points, but more often grit tools and needle diamond blade tools. The following recommendations are found in the trade literature:

- Depth of cut per pass should be kept in the range of 2 to 5  $\mu\text{m}$ . Dressing forces may be as high as 100 N so rigid tool support is again critical.
- Resin CBN and diamond wheels can be trued with similar small grit tools (or “nibs”) to those used for vitrified CBN. Carius [1984] reports that diamond form blocks are also used to dress resin CBN wheels. The author is not aware of any reports yet using needle diamond blades, although it is to be expected. However, these wheels need to be subsequently conditioned, which is discussed in a separate section below. Vitrified diamond wheels, if containing a high porosity, may also be trued with diamond nibs. Dense hot-pressed wheels, however, must be trued and conditioned with conventional abrasive wheels and blocks.



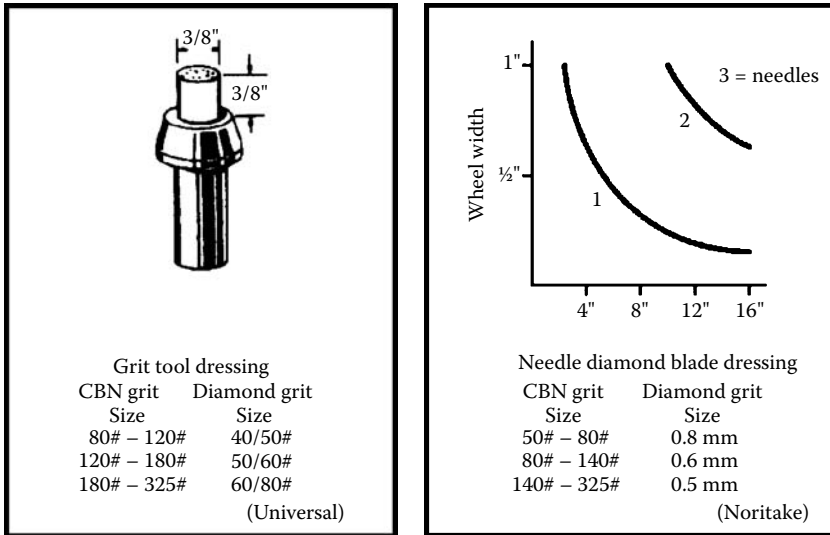


FIGURE 7.15 Grit tool and needle blade tool recommendations for dressing low concentration vitrified cubic boron nitride wheels.

## 7.4 UNIAXIAL TRAVERSE DRESSING OF CONVENTIONAL WHEELS WITH ROTARY DIAMOND TOOLS

### 7.4.1 INTRODUCTION

Rotary diamond tools were the industry's answer to life issues with stationary tools and are in many ways the rotary equivalents to single points, blades, grit tools, and form blocks. A rotary diamond tool (also called "truer," "dresser," or "roll") consists of a disc with diamond in some form held on the periphery driven on a powered spindle. Life is significantly enhanced because of the 100-fold increase in diamond now available. However, the rotary motion also provides additional benefits in terms of dressing action. In particular, the relative speed of the dressing roll to the wheel, known as the dressing speed ratio or sometimes as the crush ratio, has a major impact on the conditioning action occurring during dressing. The simplest method we will consider is uniaxial dressing, where the axis of the wheel and the dresser spindle are parallel.

### 7.4.2 CRUSH OR DRESSING SPEED RATIO

As indicated in Figure 7.16, all the parameters used for stationary tools are still important. In addition, there is the crush ratio defined as the surface speed ratio of the roll to the wheel or  $q_d = v_d/v_s$ .

Schmitt [1968] produced the seminal study on the effect of crush ratio on conditioning of conventional vitrified wheels. The work was focused on plunge dressing with formed diamond rolls that will be discussed below. However, the research clearly illustrated the effect of crush ratio on finish and dressing forces, as shown in the trend graphs in Figure 7.17.

More recently Takagi and Liu [1996] have studied the effect of crush ratio by analyzing the velocity vector of the impact between the diamond in the roll and the abrasive grains and assigning a "truer penetration angle  $\theta$ ." When  $\theta$  is small or negative the force is essentially shear and grain wear is attritious, but as the crush ratio ( $q_d$ ) approaches +1 the force becomes increasingly compressive and leads to large-scale crushing of grain and bond.

Crush ratio must be considered a key parameter in dressing. For a uni-directional (+ve) crush ratio the finish and forces change significantly over the range of +0.4 to +0.8. However, the dressing

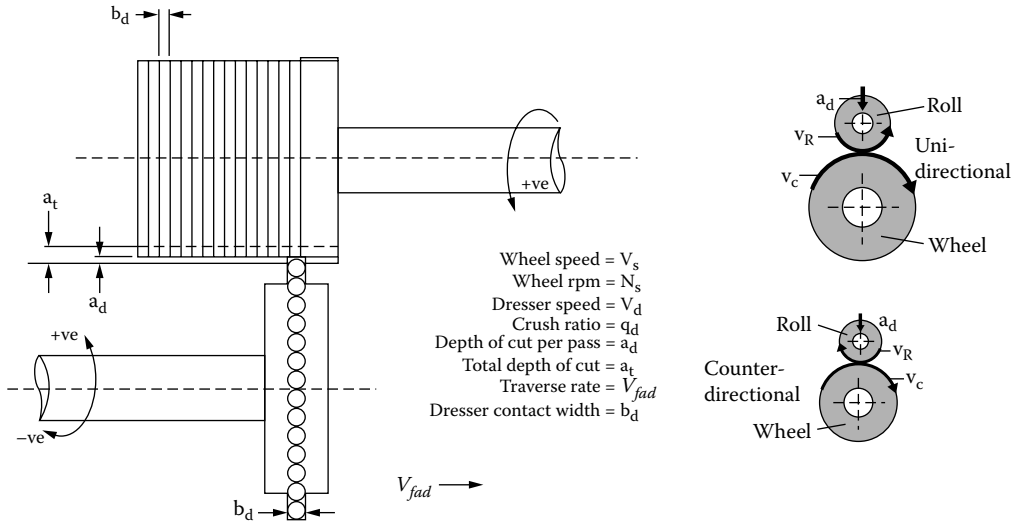


FIGURE 7.16 Dress parameters for uniaxial traverse dressing.

forces also increase dramatically leading to higher roll wear, stiffer machine requirements, and higher torque dresser motors. Diamond truer wear climbs so dramatically that it is usually recommended not to exceed +0.8. For most conventional wheel applications with traverse dressing, the wheel and machine characteristics, especially dresser designs, are such that most applications run counter-directional (-ve) operating in the range of -0.4 to -0.8. Also, the depths of cut taken can usually generate by contact geometry alone the required finish in spite of a lack of crush action. The situation, however, is rather different for CBN or form-roll dressing as described in the subsequent sections.

Rotary dressing introduces both increased flexibility and increased potential for problems. The diamond disc is now rotating, introducing balance issues and the potential for chatter and a resulting “orange-peel” appearance to the ground surface. Fractional multiples of the roll/wheel rpm can induce chatter and should be avoided. These are not just simple ratios such as 1:2 or 1:3 but can be as subtle as, for example, 7:13 or 5:11. Small adjustments in wheel or roll rpm can have a major impact on the quality of the ground surface.

7.4.3 SINGLE-RING DIAMOND AND MATRIX DIAMOND DISCS

The rotary diamond differs from a stationary tool in that it is not cutting a continuous thread in the wheel, but, consisting as it does of a ring of exposed diamond points, it is cutting a series of

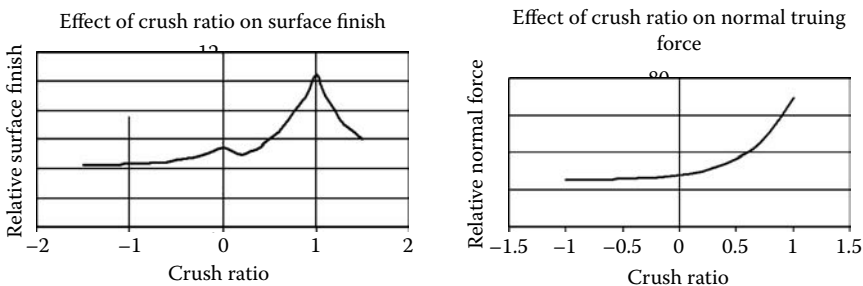
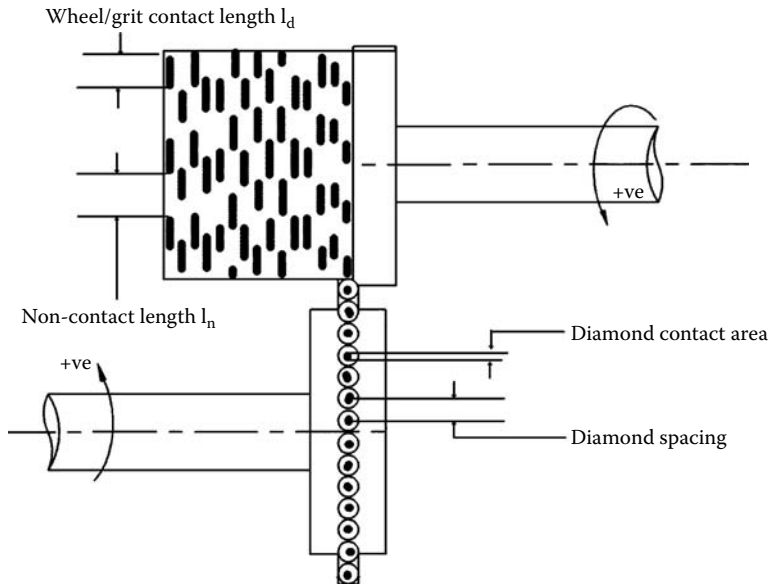


FIGURE 7.17 Effect of dressing speed ratio on surface roughness and dressing force.



**FIGURE 7.18** Wheel surface appearance generated by a single diamond ring rotary truer traversing with an overlap factor of one.

“divets” out of the grinding wheel. For a truing disc with a single ring of diamonds, the overlap factor,  $U_d$ , is dependent on the diamond spacing in order to ensure complete cleanup of the wheel face (Figure 7.18).

Also, for a well-defined spacing of diamonds, if a stone is missing or misplaced it can set up repetitive patterns on the face of the wheel, which transfers to the ground surface. The truer designs to be discussed below, therefore, fall into two categories: those with a series of accurately spaced diamonds akin to a rotary blade dresser, and truers with a totally random distribution of diamonds in a metal matrix akin to rotary grit tools.

Disc dressers are the rotary equivalent of the blade tool. They contain a ring of diamond held in a sintered or brazed matrix, and lapped to a precise form. Traditionally, the diamonds were high-quality long natural stones, but are now being replaced in many cases by polycrystalline diamond (PCD) and more recently chemical vapor deposition materials. Companies such as Dr. Kaiser and Precidia (Saint-Gobain Abrasives) have specialized in their manufacture. Typical roll tolerances and a range of forms as given by Dr. Kaiser are shown below (Figure 7.19 and Figure 7.20).

The use of this type of roll is reserved for the highest precision operations with tight finish requirements  $<0.4$  Ra. The rolls are expensive but can hold radii as small as  $200 \mu\text{m}$  for  $>10^\circ$  included angle and  $100 \mu\text{m}$  for  $>30^\circ$  included angle. Larger radii are held to  $\pm 10 \mu\text{m}$  allowing a precise value to be entered into a CNC control to generate an accurate wheel profile.

#### 7.4.4 DRESSING CONDITIONS FOR DISC DRESSERS

Traverse rates should be calculated from actual geometry of the disc. For discs of a given tip radius,  $r$ , and depth of dress,  $a_d$ , simple geometry gives the effective contact width as  $b_d = 2[(2r - a_d)a_d]^{1/2}$ . The same rules for overlap factor,  $U_d$ , as a function of  $b_d$  apply as for stationary tools. Dress infeed amounts should be limited to the range of 5 to  $20 \mu\text{m}$ . Truing forces are low and, for the small-radii discs, comparable to single-point dressing. Consequently, the dresser spindle motors require relatively modest power ( $<0.2$  KW) and stiffness requirements resulting in compact units that can be readily fitted or retrofitted to the grinder.

### 7.4.5 SYNTHETIC DIAMOND DISCS

Synthetic diamond discs are expensive but the initial outlay can be compensated for by the fact that if wear is properly monitored before becoming catastrophic, the discs can be relapped up to 40 times [Dr. Kaiser n.d.].

### 7.4.6 SINTERED AND IMPREGNATED ROLLS

Less expensive are sintered, impregnated, or “infiltrated” rolls, which consist of a molded layer of diamond abrasive grains. These will contain a random distribution of diamonds. The rolls tend to be of a relatively large radius  $< 1/8$  in., which may be relapped two to three times, or a flat profile with a consumable layer of 2 to 5 mm.

### 7.4.7 DIRECT-PLATED DIAMOND ROLLS

Another low-cost, throw-away alternative for some applications is direct-plated diamond with similar profiles to sintered rolls.

### 7.4.8 CUP-SHAPED TOOLS

Cup shapes, as well as discs, are used as illustrated by the example in Figure 7.19. A cup-shaped tool is used tilted to the wheel face at an angle usually defined more by space availability for the



FIGURE 7.19 Examples of various traverse diamond truer designs. (From SGA. With permission.)

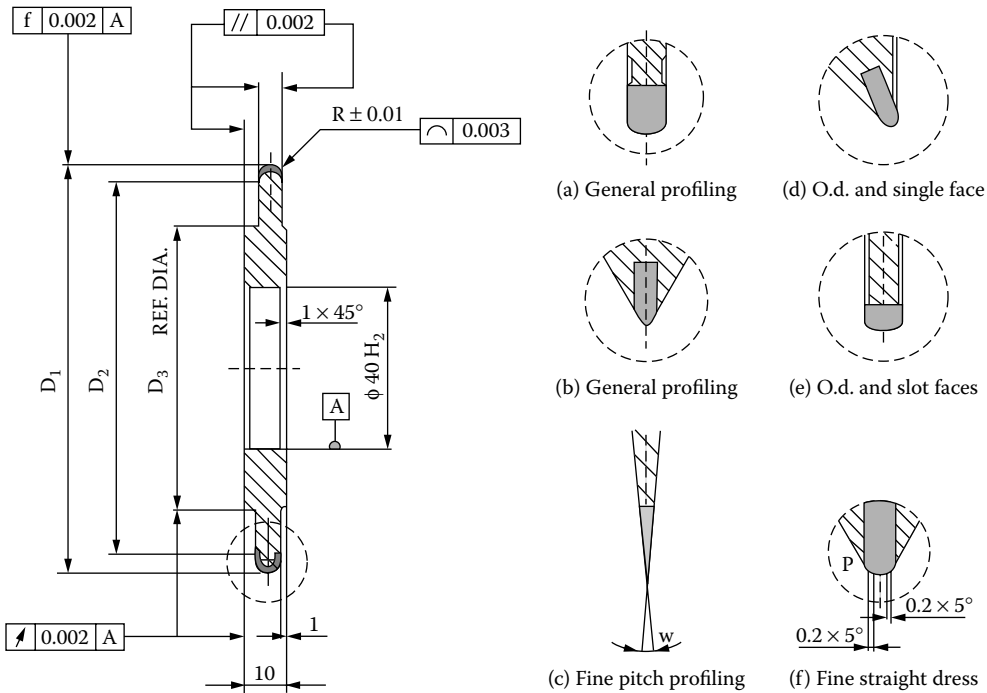


**FIGURE 7.20** Diamond traversing rotary discs with defined contact geometry. (From Kaiser n.d. With permission.)

motor than by the optimum dress geometry. Cups are either used where space is confined, such as in internal grinding, or where an outer diameter and face must be dressed. The other situation for their use is with low-torque dresser motors (see later). In the case of sintered cups, the tilt angle is prelapped in the face of the cup to avoid break-in issues.

## 7.5 UNIAXIAL TRAVERSE DRESSING OF VITRIFIED CBN WHEELS WITH ROTARY DIAMOND TOOLS

### 7.5.1 INTRODUCTION

The rules for dressing vitrified CBN wheels are similar in many ways to those described for conventional wheels. The same concepts of crush ratio, traverse rates, effective contact width, and depth of cut apply. The changes that must be made to the dressing conditions relate to the greater hardness, toughness, and cost of the abrasive, and the greater hardness of the bond.

### 7.5.2 DRESSING DEPTH

First and foremost, the depth of cut per pass with CBN is greatly reduced. This is, in large part, an economic requirement and the effect of this is to reduce the maximum surface roughness due to geometric effect from the truer. That, combined with the harder wheel grade, makes a higher crush ratio necessary and a more aggressive truer design to compensate. Whereas most conventional wheel applications run with a negative crush ratio, CBN is generally dressed with a crush ratio of +0.4 to +0.8. The only exceptions to these are where dressing is expressly required to lower finish to a minimal value, or because of a lack of dresser spindle motor torque.

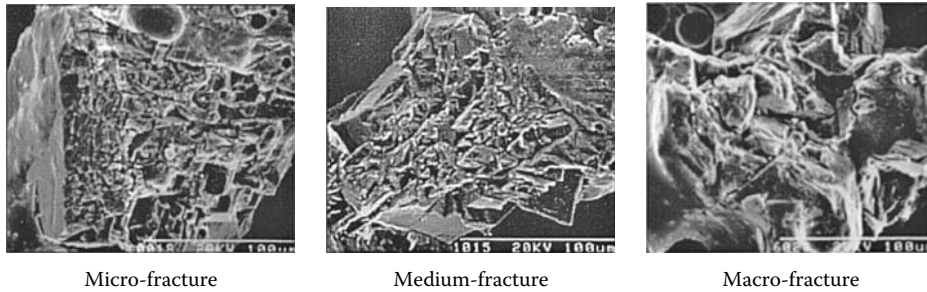


**FIGURE 7.21** Fracture modes of 80# GE type 1 abrasive. (From Ishikawa and Kumar 1991. With permission.)

### 7.5.3 CRUSH RATIO

Crush ratio can have a profound effect on the dressing action. Ishikawa and Kumar [1991] reported a study on dressing of vitrified bonded wheels containing coarse grade 80# GE 1 abrasive. They distinguished between three forms of grit fracture: “micro,” “medium,” and “macro” as illustrated in the micrographs in Figure 7.21. It was determined that at a modest  $q_d = +0.2$ , there was a definite shift from predominantly a microfracture regime at  $a_d = 1 \mu\text{m}$  to a macrofracture regime at  $a_d = 3 \mu\text{m}$ ; changes to  $a_d$  as small as  $0.5 \mu\text{m}$  had a significant impact on grind power and finish. Microfracture led to a high surface abrasive concentration and, therefore, a higher wheel life, but also relatively high grinding forces; macrofracture with its lower surface concentration of sharper abrasives led to lower wheel life but lower grinding energy. As the crush ratio was increased from  $+0.2$  to  $+0.8$ , the level of macrofracture increased dramatically to dominate the process accompanied by increased bond loss. This result is important because coarse grade GE 1 abrasive was the workhorse of cylindrical grinding and it, therefore, defined the required dressing infeed accuracy and crush ratio requirements for the earliest grinders designed specifically for vitrified CBN.

These results are specific to a particular grade and size of CBN that is relatively easy to fracture. It is, therefore, to be expected that a tougher grade of CBN, or blockier shape or finer grit size would require either a higher crush ratio and/or deeper depth of cut to achieve the same degree of grit fracture. Evidence for this is suggested in the work by Takagi and Liu [1996] who found that when dressing much tougher 80# GE 500 abrasive at  $5 \mu\text{m}$  depth of cut, microfracture still dominated at  $q_d = 0.5$ ; only at  $q_d = 0.9$  was this replaced by macrofracture.

With the introduction of several new, generally tougher, but sharper, grades of CBN within the last few years, further investigation of dressing characteristics as a function of grit size, morphology, toughness, wheel speed, and vitrified bond strength is badly needed.

### 7.5.4 THE DRESSING AFFECTED LAYER

The other effect of very fine dress infeed depths is related to the fact that the dress depth becomes comparable to or significantly less than the depth to which the surface of the wheel has been affected by previous grinding. The surface of any grinding wheel is significantly modified compared to its bulk structure. The dressing process fractures and removes abrasive particles and bond to reduce the surface concentration of both.

Yokogawa and Yonekura [1983] were the first to describe this affected layer, which they termed “Tsukidashiryō,” also known as “Active Surface Roughness”; this can vary in depth from a few microns to over 30. For most medium- to high-stock removal applications, once grinding begins the abrasive metal chips will wear the bond preferentially and further increase the affected depth (Figure 7.22). This effect is accompanied by a drop in grinding forces and a rise in surface roughness and is most striking for the first few parts after dress. Figure 7.23 illustrates the expected trend for



FIGURE 7.22 Concept of “active surface roughness.”

various crush ratio parameters based on Jakobuss and Webster [1996]. In many cases, the CBN abrasive is virtually unaffected by the grinding process and changes in grinding parameters and wear is entirely the result of bond wear leading to the grits finally falling out [Williams and Yazdzik 1993]. For this reason, wheel wear often becomes very unstable after 10 to 20  $\mu\text{m}$  depending on grit size.

### 7.5.5 TOUCH DRESSING

When dressing a conventional wheel, a similar break in period occurs but is generally too rapid to be observed, and the dress infeed amount is such that most or all of the layer affected by grinding is removed and a fresh surface layer is created each dress. This is not so for CBN where the dress depth,  $a_d$ , is only 3  $\mu\text{m}$  or less for the reasons discussed above. This is known as “touch dressing.” A brand new wheel straight after the first dress will have its shallowest affected depth, which will increase with grinding. A CBN wheel is most likely to cause burn grinding the very first part after a new wheel dress. For the second dress, if too little material is removed, the parts/dress achieved

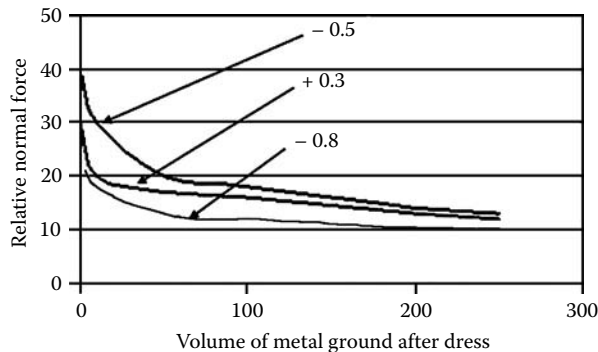


FIGURE 7.23 Effect of crush ratio on normal grinding forces.

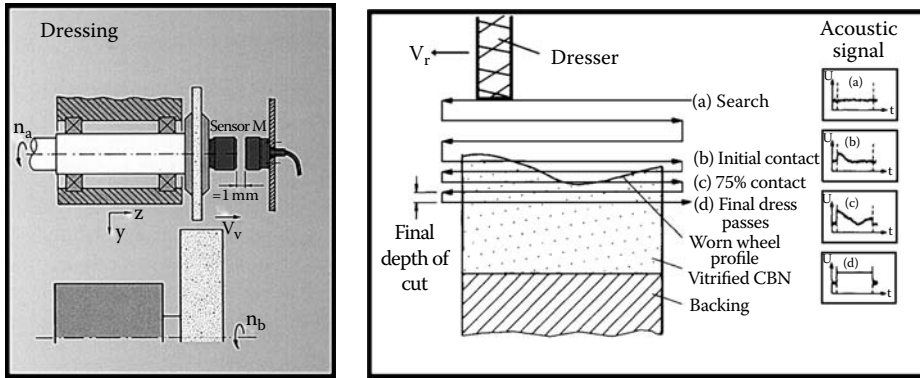


FIGURE 7.24 Acoustic sensor dressing strategy. (After Dittel 1996. With permission.)

will be reduced, whereas if too much is removed, the surface returns to that of a new wheel. In general, a balance has to be struck dependent on the particular grinding process in question. What is clear is that not only is the dress depth of cut per pass important governed by the fracture characteristics of the abrasive, but the total depth of cut is also critical governed by the active surface roughness. Many cylindrical applications with vitrified CBN are set up to make a given number of dress passes at a dress depth,  $a_d$ , of 0.5 to 3  $\mu\text{m}$ . Furthermore, they are optimized by making changes as small as 0.5  $\mu\text{m}$  in  $a_d$ .

Achieving this level of accuracy obviously requires machine tools that are accurate enough to infeed at this small an increment. CBN-capable grinders have mechanical slide systems with ac servo/ballscrews or linear motors with an infeed resolution of 0.1  $\mu\text{m}$ . Even with this level of accuracy, however, there is still the problem of thermal stability, which can cause positional errors of the diamond relative to the wheel of up to 100  $\mu\text{m}$ . In the 1980s, therefore, techniques were developed to detect the contact of the dresser with the wheel. By far the most sensitive and reliable to date are those based on acoustics. Sensors have been developed by several companies capable of detecting a dress depth of cut of  $<0.25 \mu\text{m}$ . The systems detect and filter sound in the frequency range of 50 to 400 KHz adjustable for different grit sizes and wheel speeds. A major limitation on the signal/noise ratio (S/N ratio) has been bearing noise from the spindle and a number of strategies have been developed to minimize this problem. These include mounting the sensor adjacent to the dresser and using hydraulic fluid as an acoustic coupling, the use of coolant as an acoustic coupler, mounting a sensor/transmitter on the dresser head, or by mounting the sensor on the wheel head. The typical method of use is illustrated in Figure 7.24.

A dress procedure using an acoustic sensor is detailed in Figure 7.24.

- The dresser is initially set back a safe distance from the wheel, typically 50 to 100  $\mu\text{m}$ , and multiple passes at dress depth of 5 to 10  $\mu\text{m}$ /pass are made in a search mode. The infeed amount is generally governed by cycle time issues, that is, making the fewest number of passes.
- On first contact with the worn wheel surface, the infeed amount drops to 2 to 5  $\mu\text{m}$ /pass.
- At 75% full-face contact (i.e., signal above a preset trip level) the wheel drops into the final dress depth/pass.
- A preset number of passes are made at final infeed,  $a_d$ . The signal from the sensor should be a solid line.

The accuracy of the process is actually governed more by the infeed amount per pass during the initial search stage and is usually a compromise with cycle time issues. A value must also be



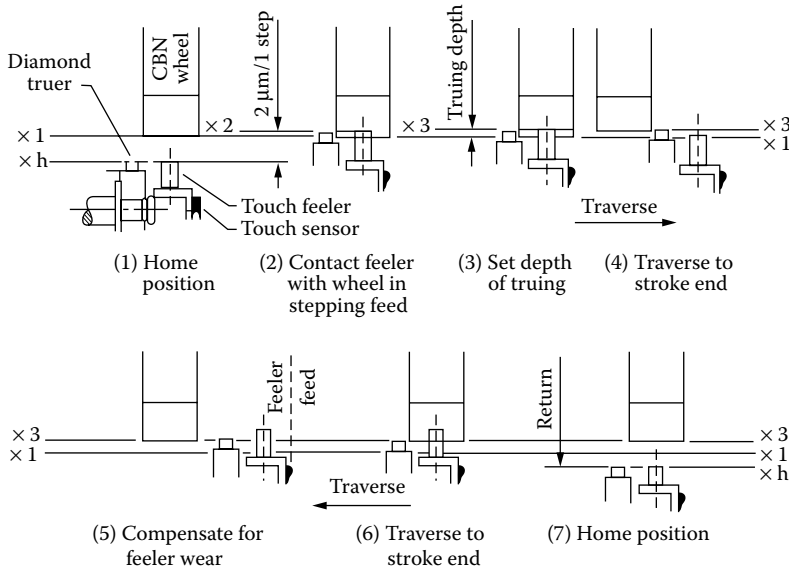


**FIGURE 7.25** Toyoda Machine Works strategy for acoustic emission-enhanced rotary dressing. (From Suzuki 1984. With permission.)

entered into the machine control unit to compensate for truer wear that can be as much as 20% of the assumed dress amount. This value must be determined empirically by monitoring part size changes or by physically measuring the wheel with a pie tape every 50 dresses.

The gap distance between the sensor transmitter and pickup is very sensitive to position and needs to be recalibrated periodically as it can move when changing the diamond roll. More recently, this issue has been remedied by inserting the sensor and pickup internally within the spindle shaft. This method is now commonplace in high-production precision grinding.

Suzuki [1984] was one of the first to report the use of acoustic sensors for dressing CBN wheels for actual production applications, where he used it to true resin CBN wheels to grind camshafts before vitrified CBN was widely available. The technology was then transferred to the first vitrified CBN-capable camlobe grinders, the Model GCH 32 from Toyoda Machine Works (TMW). Suzuki overcame the problem of dresser spindle bearing noise by isolating the (Marposs) acoustic sensor a short distance away from the dresser and having a separate touch feeler (steel pin on a spring) attached to it to touch the wheel. The pin was plunge fed into the wheel at 2-μm increments. After the diamond trued the wheel, the feeler retouched the wheel to calibrate the relative position of feeler and diamond. (See Figure 7.25 for Toyoda Machine Works strategy for acoustic emission-enhanced rotary dressing.)

Since the feeler and the dresser were close together, it was assumed that thermal movements would not create significant errors. A value was required in the machine control to compensate for diamond wear and pin wear in order to keep track of wheel diameter. The primary variance in the dress amount was the pin wear that was governed by the infeed increment of 2 μm. The sensor proved extremely repeatable although prone initially to false signals from the presence of coolant. This was resolved by carrying out the actual touch-sensing portion of the cycle dry. The system has been very successful for camshaft and crankshaft grinding and is functioning on several hundred machines worldwide [Hitchiner 1997].

Since all high-speed vitrified CBN wheels are segmented, they are especially prone to slight changes in shape with wheel speed. Dressing should ALWAYS, therefore, be carried out at the same wheel speed as for grinding for operating speeds, >50 m/s, to avoid chatter.

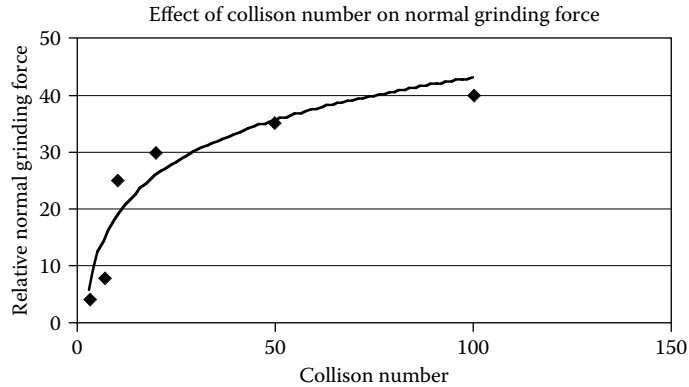


**FIGURE 7.26** Effect of collision number in dressing on grinding force.

### 7.5.6 TRUER DESIGN FOR TOUCH DRESSING

Attention must also be paid to the diamond truer design. As CBN is so much harder than conventional abrasive, the truer will wear much more per dress. This makes profiling truers with precisely lapped geometries uneconomic for most applications. Certainly for all flat form dressing applications, a truer with a consumable diamond layer is required.

### 7.5.7 IMPREGNATED TRUERS

An obvious solution, based on conventional wheel experience, would be to use an impregnated truer. The difficulty is that these truers are designed such that the matrix wears just enough to keep the diamond exposed. Conventional wheels create a lot of abrasive swarf, which erodes the matrix, but little diamond wear. In contrast, CBN wheels create little swarf and, hence, matrix wear, but cause a much higher degree of diamond attritious wear. Consequently, the matrix must be somewhat less wear resistant for CBN applications but still retain the diamond.

The width of a regular impregnated truer is also a problem in light of the discussion regarding grit fracture before. An impregnated truer will have an effective contact width,  $b_d$ , many times wider than the diamond size and so will have diamond grains dispersed randomly throughout. Consequently, during dressing, if we picture the situation illustrated in Figure 7.18 but now with a much wider width, some CBN grains may be hit several times while others remain untouched. The first hit will be at the full truing depth and fracture the CBN grit but the following grains will be at a much shallower depth and merely glaze it again. The total number of hits is termed the “collision number.” The effect is very apparent in Figure 7.26, which plots the effect of collision number on normal grinding force under a range of dressing and grinding conditions [Brinksmeier and Çinar 1995]. A single ring of diamond grains is clearly the best option.

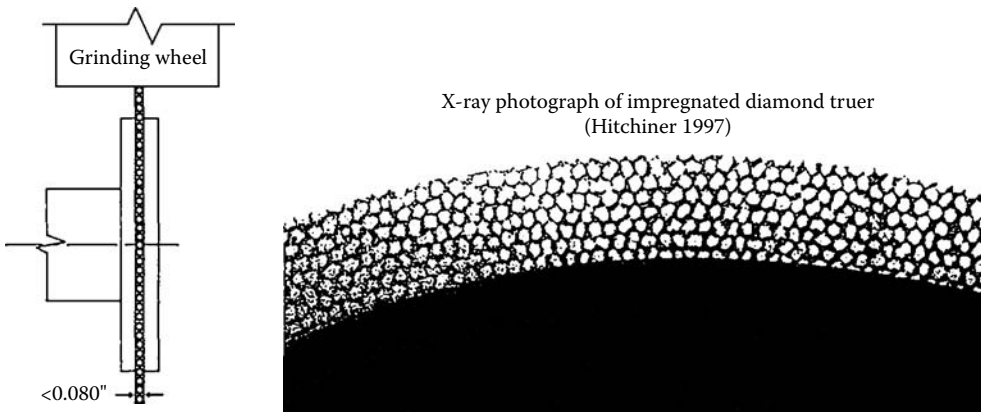
It is possible to estimate the equivalent of this single layer, and multiples thereof, for various truer contact widths and diamond grit sizes of impregnated truers as a function of diamond concentration.

Although these guidelines have worked well for general applications, there was a need for a sharper dress for burn-sensitive materials and aggressive removal rates. Several solutions have been developed—some proprietary, several covered by patents.

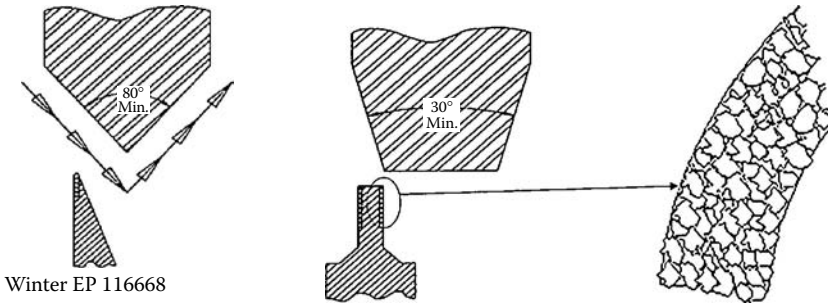
Most of these consist of a compact or single layer of diamond. For example, Hitchiner [1997] reported an impregnated layer of diamond sandwiched between two steel side plates for support. Although the overall width is 0.080, the actual diamond layer is only about a grain thick. Figure 7.27 shows an X-ray photograph through a truer showing the individual diamonds. The design is suitable primarily for dressing of flat profiles. Winter EP 116668 (Saint-Gobain Abrasives) patented a truer

**TABLE 7.5**  
**Recommendations for Impregnated Diamond Truer Compositions**

Diamond Size	Concentration for 1 mm Contact Width			To Dress
	Sharp	Medium	Dull	
D501	100	150	—	B181–B151
D301	80	125	160	B126–B91
D181	60	90	120	B91–B64
D126	47	75	95	B76–B54
D91	35	43	72	B46



Plated diamond truer for vitrified CBN



**Bonded profiling roller (BPR)**

Matrix bonds with diamond so that diamond retention isn't dependent upon metal pocket

- Allowing higher concentration
- Allowing minimal included angles

Constant thickness of diamond section eliminates need to re-lap

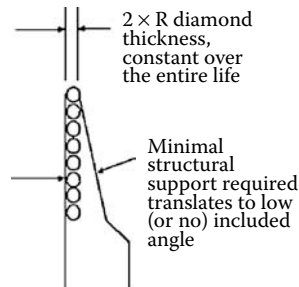


**FIGURE 7.27** Strategies for aggressively dressing vitrified superabrasive wheels. (Courtesy of Saint-Gobain Abrasives. With permission.)

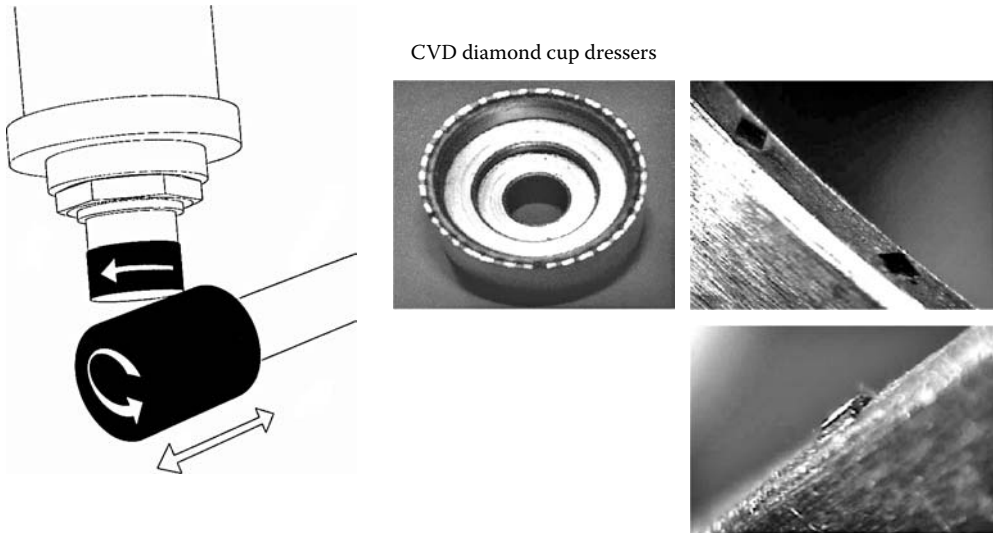


**FIGURE 7.28** Needle (“prismatic”) diamond dressing cup design and application.

design based on holding the diamond to the side of a steel support by direct plating. This method allows simple contouring in addition to dressing flat profiles. Finally Norton [1983] (Saint-Gobain Abrasives) developed a method called BPR, or bonded profile roller, using the brazed plated process to produce a truer which is only a diamond grain wide. This maintains a constant tip radius as it wears and can be used for quite complex profiling.

### 7.5.8 TRAVERSE ROTARY TRUERS USING NEEDLE DIAMONDS

Finally, there are truers based on the use of needle diamond blocks. These give probably the most consistent, effective dress of any truer design for dressing of flat profiles. For these to function correctly, the diamond must be above the level of the matrix in which it is held. This limits their usable depth to about 0.5 mm without significant fracturing occurring. However, they can be re-exposed two to three times. As with any tool, there is a balance between initial tool cost and overall cost.

Total truing force with these styles of dresser is of the order of 2 to 10 N for typical cylindrical grinding conditions to  $<2$  N for internal grinding. (See Figure 7.28 for needle diamond dressing cup design and application.)

## 7.6 CROSS-AXIS TRAVERSE DRESSING WITH DIAMOND DISCS

### 7.6.1 INTRODUCTION

Cross-axis dressing has often been considered a poorer dressing method. It has historically been applied to situations such as the retrofitting of older internal grinders from single-point diamond to rotary dressing where space does not allow a large-enough dresser spindle motor for the required torque to operate in a uniaxial orientation, or it is simply impossible to orientate the dresser spindle otherwise, as typified by Figure 7.29. The axis of the dresser is orientated at  $90^\circ$  to the wheel axis. The method has also been attempted to profile dress conventional wheels for grinding crankpins with blend radii and sidewall grinding, but the slightest error in height position relative to the wheel center results in poor surface quality on the part.

The process, however, has been revisited for dressing vitrified CBN wheels using the styles of dressers indicated above.

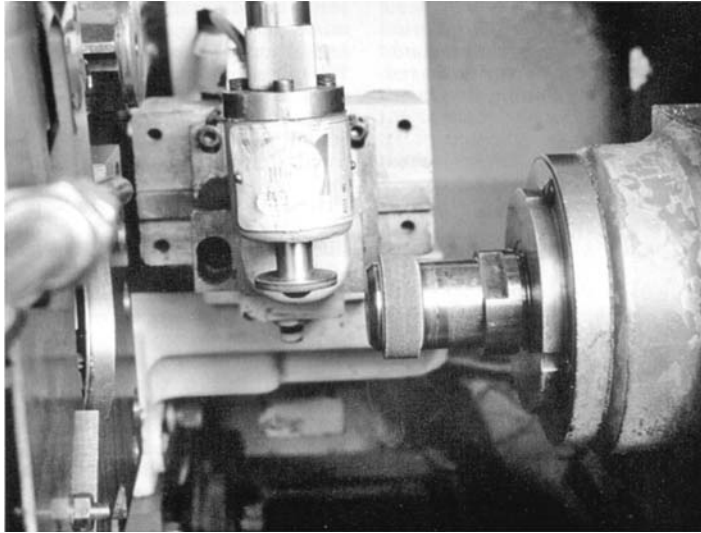


FIGURE 7.29 Cross-axis dressing of an internal vitrified cubic boron nitride wheel.

## 7.6.2 TRAVERSE RATE

The dress action produces only shear so it is never as effective as uniaxial dressing with a high +ve crush ratio. The traverse rate is dependent on dressing disc diameter,  $\phi_d$ , and depth of cut,  $a_d$ . Simple geometry gives an optimum traverse rate of

$$v_{fad} \approx 1.5 N_s (\phi_d a_d)^{1/2}$$

where  $N_s$  is the wheel rpm.

Hence, the process is, to a first approximation, independent of CBN or diamond grit size or dresser rpm. Dressers developed for uniaxial dressing also work well for cross-axis dressing, particularly the thin impregnated diamond disc design described above. The most successful application of cross-axis dressing to date has come from CNC profile grinding for applications such as punch grinding and high-speed contour grinding. An example of this is shown in Figure 7.30, which is a photograph of a Weldon (Weldon Solutions, York, PA) high-speed grinder tooled for cylindrical profile grinding at 130 m/s. The acoustic sensor is mounted in the wheel head and monitors the dress process and the grind process, as well as adding crash protection. The dresser touches on the outer diameter (o.d.) and face at the start of the dress sequence to determine wheel position in x and z planes and compensate for thermal movement.

Cross-axis dressing is the most cost-effective method of profile dressing where the contour allows its use. One additional benefit is that it gives clearance to dress profiles of over 180°. This allows, for example, back-angle relief to be dressed on the sides of a 1A1R shape wheel when high-speed contour grinding shaft diameters with shoulders.

## 7.7 DIAMOND FORM-ROLL DRESSING

### 7.7.1 MANUFACTURE AND DESIGN

Traverse dressing of profiles, especially with the required frequency when using conventional wheels, has a major limitation: cycle time. Modern high-production, precision grinding relies on

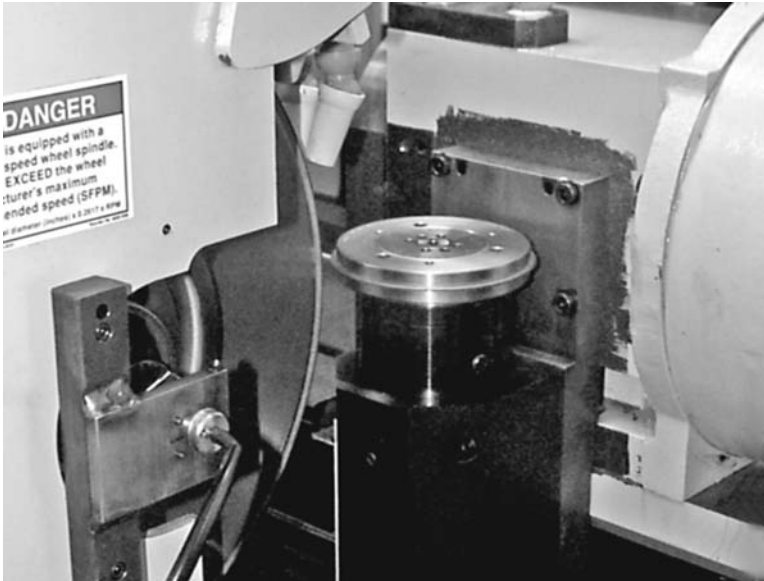


**FIGURE 7.30** Cross-axis dressing on a Weldon 1632 high-speed grinder equipped with ac servoelectric dresser and wheel spindle-mounted acoustic emissions sensor. (From Weldon. With permission.)

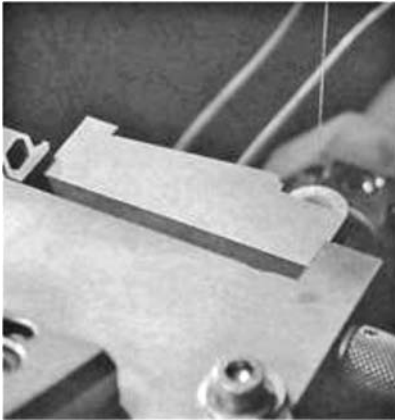
rapid dress times achieved by plunging a truer coated with diamond conforming to the required profile. Rotary form truers or rolls can be classified into two common categories:

- RPC rolls, or Reverse Plated Construction, produced by a precision electroforming process
- Infiltrated rolls produced by high temperature furnacing

It is important that the end user understands the manufacture and properties of each type of roll in order to select the best product for the application. Usage in the market is split about 50:50 between the two. There are many general usage recommendations but there is little regarding the specifics of manufacturing for proprietary reasons. One source has published a series of photographs to illustrate their process that can give insight (Figure 7.31) [TVMK n.d.]

After design of the required form and any modifications required for final shape correction in the mold, the profile is cut on the inside of a mold. In the example shown below, the form is first generating an electrodischarge machining–wire-cut form tool, which is then plunged into a graphite-based material making up the mold. Other proprietary mold materials and CNC machine processing methods are used depending on the particular manufacturer. Diamonds are then tacked onto the cut surface of the mold. “Hand-set” rolls have diamonds placed in very specific patterns to control finish. Traditionally these have been set laboriously by hand (Figure 7.31b and Figure 7.32), although automated robotic techniques are now reported as shown in Figure 7.31c.

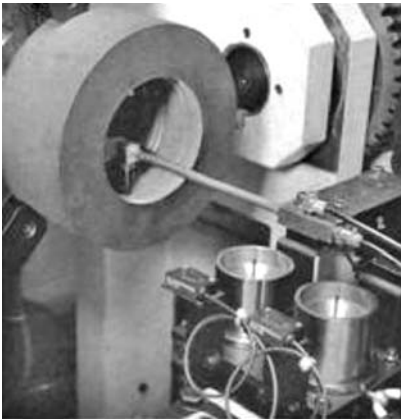
Alternatively, a high density of diamond is packed onto the face either by pouring or, for higher densities, by centrifuging. Handset patterns are used for low-force applications or rough-finish requirements. High density or “random set” diamond rolls are used on stiff dressing systems for maximum roll life. Dresser spindle stiffness issues tend to limit roll-form widths for this latter style to about 6 on most grinders. In the case of sintered rolls, very often the diamond is premixed with the metal (tungsten-iron) powder prior to packing to give a diamond section thickness of approximately 1.5 mm [Decker 1993].



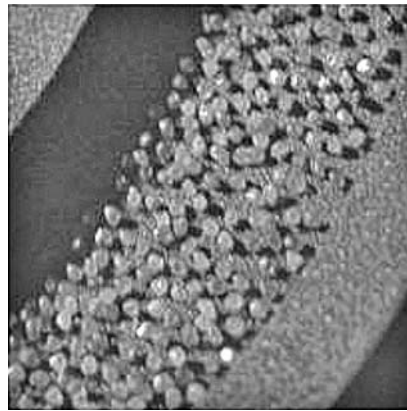
(a) Formtool



(b) Handsetting diamond



(c) Robotic setting diamonds



(d) Diamonds set in mold



(e) Profile inspection visual



(f) Profile inspection electronic

**FIGURE 7.31** Aspects of diamond roll manufacturing. (Courtesy of TVMK. With permission.)

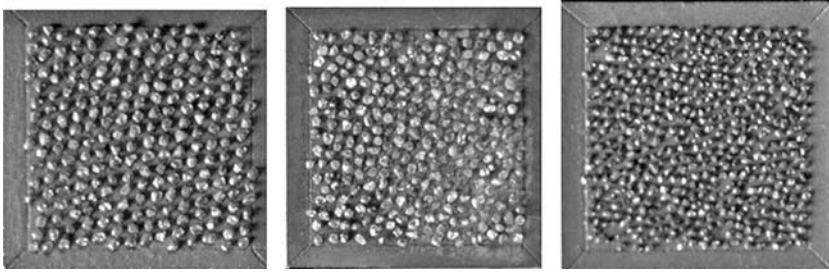


**FIGURE 7.32** Examples of reference handset diamond roll pattern blocks.

In addition to the regular stones, which run in size from 18/20# to 40/50#, additional evenly spaced stones (maacles, long stones, PCD, etc.) are often added to reinforce profile areas of weakness such as tight radii.

Processing can now take one of two routes.

### 7.7.2 REVERSE PLATING

For RPC rolls, the coated mold is placed in a nickel-plating tank and a shell of nickel is allowed to build up around the diamond. The plating process can take up to a month in order to avoid internal stresses or gassing, and to allow the contour to be faithfully followed. After this time, a steel core is fitted using a low-temperature alloy to attach it and the mold broken open. The whole process occurs at or relatively close to room temperature, which minimizes distortion. However, the shell is thin and does not take a lot of abuse. For infiltrated rolls, the core is fitted prior to processing and a tungsten-iron-based powder is packed between the core and the diamonds. The whole is then furnaceed at several hundred °C. The process is much quicker than plating, but the higher temperatures cause greater distortion and form error.

After mold break-out, the bore is ground concentric to the o.d. with  $\pm 2 \mu\text{m}$ . Depending on the required tolerances, most rolls are then lapped where necessary to correct profile errors and reinforce key areas. Modern processing methods are such that RPC rolls do not necessarily require lapping in many instances to produce the required form tolerances. Certainly the lower processing temperatures result in low distortion. Therefore the amount of and variation in lap, and hence, consistency of performance from one roll to another, is less. However, lapping, accompanied by some mechanical or chemical exposure of the diamond, is often critical to control the diamond surface density throughout the profile.

After lapping, the roll is balanced, and a coupon cut to confirm profile. Standard tolerances on profiles are typically 40% to 70% of that allowed on the component. The process is capable of  $2 \mu\text{m}$  on geometrical form tolerances,  $\pm 2 \mu\text{m}$  on lengths. Angular tolerances are held to  $\pm 2 \text{ min}$ . Tighter tolerances are achievable, down to  $0.75 \mu\text{m}$  on radial profiles for the bearing industry. Tolerancing has become so tight in recent years that it is often necessary for the roll maker to buy the same model of profile inspection equipment as used by the customer in order to get correlation in inspection.

### 7.7.3 INFILTRATED ROLLS

Infiltrated rolls are used for operations requiring fast roll deliveries and for abusive applications, especially where operator skill levels are a concern. The tough tungsten-iron construction can take more impact abuse than the thin nickel shell of the reverse plated roll design. Infiltrated rolls are also used for roughing applications using sparse handset diamond patterns. The tough matrix of the infiltrated roll can better withstand erosion between the diamonds by the loosened abrasive grains. For this reason, silicon carbide wheels are most often dressed with infiltrated rolls.



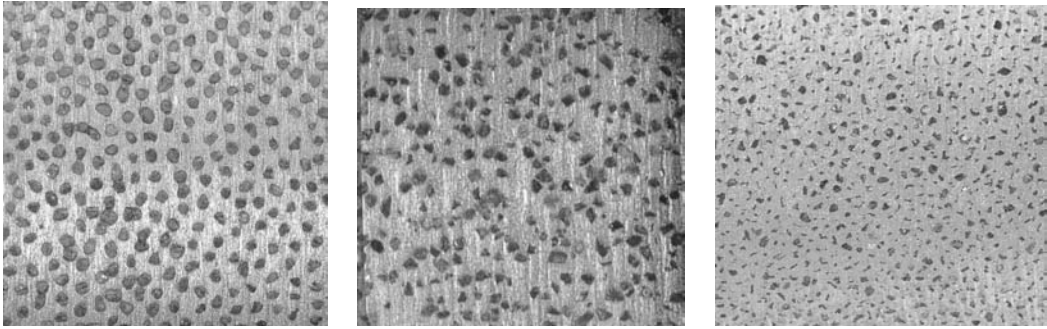


**FIGURE 7.33** Surface appearance of typical diamond roll constructions.

#### 7.7.4 REVERSE PLATED ROLLS

Reverse-plated rolls are used for finishing operations, for maximum roll life under good process control, and for applications with good system stiffness. Reverse-plated rolls will generally have high-density random diamond coverage to protect the matrix from erosion.

The diamond concentration can vary over the roll depending on the profile. For example, for profiles with a shallow angle to the axis of plunge where heat from rubbing is an issue, the concentration can be cut significantly in the case of handset rolls or by adding diamond-free areas (Figure 7.34). Similarly, for groove grinding, multiple roll assemblies may be used to provide diamond-free areas to eliminate burn (Figure 7.35).

#### 7.7.5 DRESS PARAMETERS FOR FORM ROLLS

This discussion will consider first the dressing of conventional abrasive wheels with form diamond rolls. This can then be extrapolated to include vitrified CBN. The dressing process entails plunging the roll into the wheel at a fixed infeed rate in mm/min or mm/rev of wheel at a fixed crush ratio followed by a fixed dwell time. The infeed rate per rev is analogous to dress depth per pass in



**FIGURE 7.34** Diamond-free areas on shoulder of reverse-plated roll.

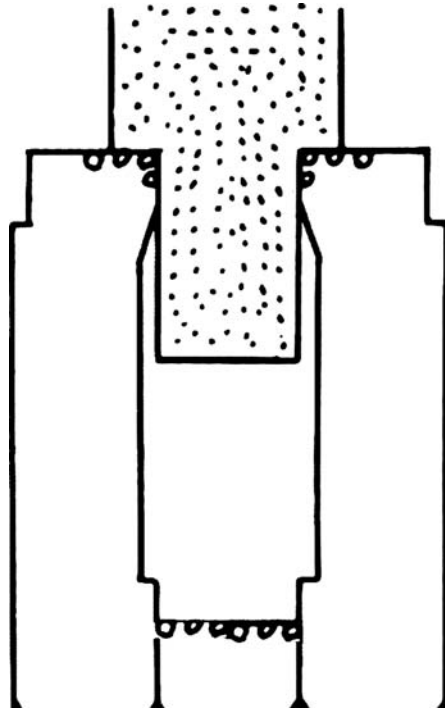


**FIGURE 7.35** Three-piece diamond roll set for groove grinding. The wheel continues to plunge to lower diamond surface.

traverse dressing. The crush ratio has a direct analogy with traverse dressing principles while the dwell time can perhaps be related to overlap factor, that is, number of turns of the wheel that the roll is in contact at the end of the infeed cycle.

The dress infeed can be one of three configurations as shown in Figure 7.36. For the first, the axes for the roll, wheel, and workpiece are all parallel. This is the easiest for checking the form accuracy and designing the roll. However, the grind is likely to be prone to burn and corner breakdown when grinding surfaces that are perpendicular to the component axis. This can be relieved to some extent as described before by reducing diamond concentration, but is still far from ideal. The second is an angle approach: the roll axis and wheel axis are no longer parallel in order to optimize the angle of approach of the roll

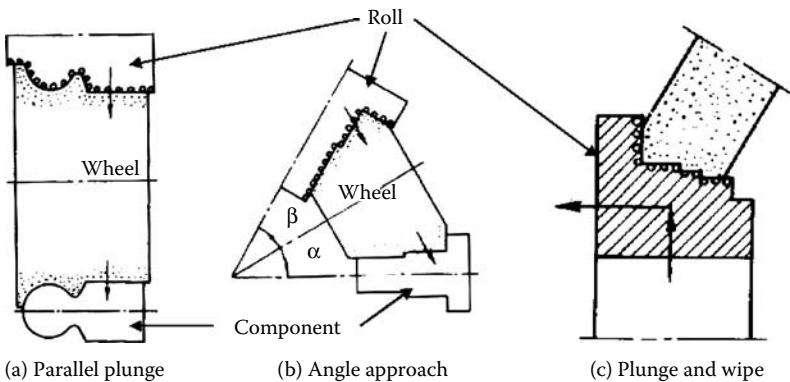


**FIGURE 7.36** Dress methods for diamond form rolls.

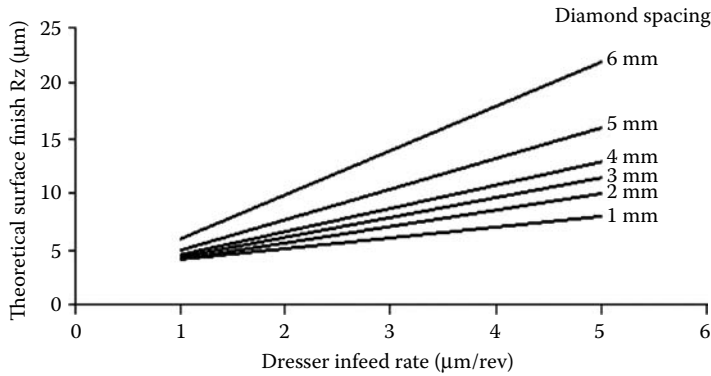


FIGURE 7.37 Theoretical surface roughness as a function of diamond spacing.

to minimize burn. Finally, the third approach is a combination of angle approach followed by a traverse movement or “wipe.” This is usually done to minimize dressing resistance especially where the dresser spindle might otherwise be laboring. It also improves surface finish and gives longer roll life. This discussion will be focused on parallel plunge approach.

Plunge dressing may be discontinuous occurring after a given number of parts, or performed continuously throughout the grinding cycle. This is very common in surface form grinding with heavy cuts where it is known as “Continuous Dress Creep Feed” or CDCF.

- Dressing depth for form rolls. The depth of cut in plunge dressing with alox wheels is typically  $>5 \mu\text{m/rev}$ , which is 25 to 50% less than in most traverse dressing operations. The surface finish and cutting action are, therefore, more dependent on the design of the roll. Rezeal et al. [n.d.] presented the effect of diamond spacing on surface finish under continuous dress conditions as shown in Figure 7.37. The results illustrate that diamond spacing and dress depth both have a significant influence.

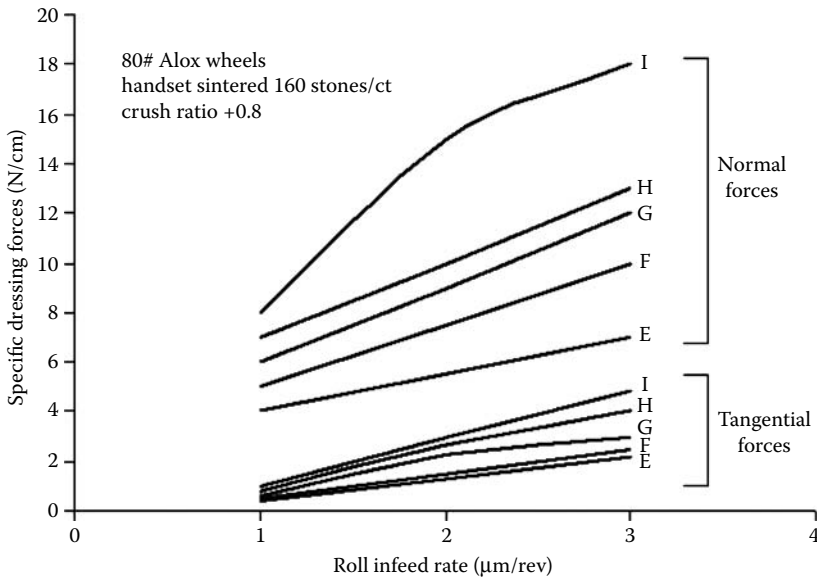
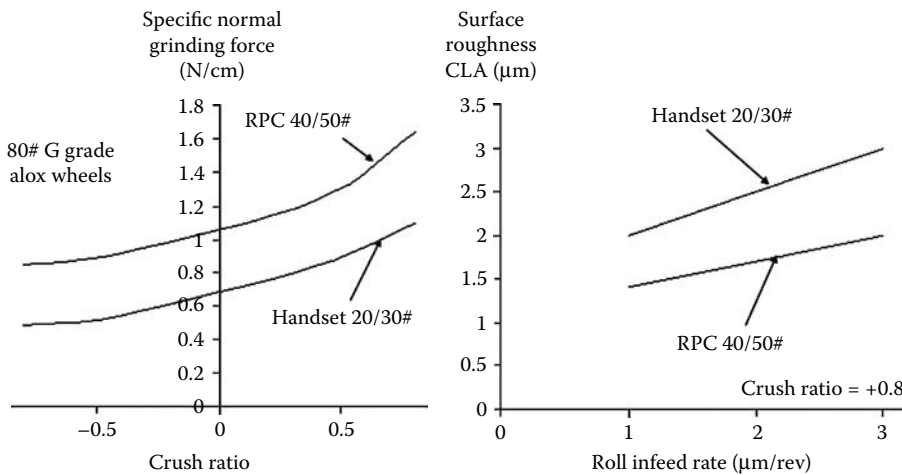


FIGURE 7.38 Forces in plunge roll dressing of alox wheels.

**TABLE 7.6**  
**Typical Diamond Coverage Values for Diamond Form Rolls**

Diamond Size	Diamonds/Carat	Diamond Coverage (ct/cm <sup>2</sup> )		
		Dense	Medium	Sparse
18/20#	110	2.3	2.0	1.6
20/25#	140	2.1	1.8	1.5
25/30#	250	1.7	1.5	1.3
30/35#	360	1.5	1.3	1.1
35/40#	615	1.2	1.0	0.8
40/45#	1,225	0.9	0.7	0.5

- Diamond spacing from rolls. Diamond spacing is rarely, if ever, defined as such by roll makers. Instead, the roll print will have a diamond size and ct/cms to define surface coverage. Diamond spacing can be estimated from these values; it can be readily shown that diamond spacings are, in fact, all significantly less than 1 mm, suggesting the dress infeed per rev plays a more critical role. The dress infeed per rev is limited by the system stiffness, wheel grade, and dresser spindle power.
- Dressing forces for form rolls. Rezeal et al. [n.d.] compared the dressing forces for handset coarse sintered rolls with reverse-plated fine-mesh synthetic diamond rolls and found the latter dressed with up to twice the force (Figure 7.39). The dressing force coefficient was about 0.2. These values can be used to calculate dresser motor capacity. However, caution should be used when designing equipment for unidirectional dressing as considerably more motor power is required to resist the force from a roll speeding up driven by the wheel (up to a factor 3!), than that required for opposing a given force in counterdirectional dressing. Also, the values given above are for flat forms; at least an additional factor 2 must be assumed for deep profiles.



**FIGURE 7.39** Effect of roll manufacturing method and diamond size on grinding forces and surface roughness.

- Infeed rate for form rolls. For a noncontinuous dress on a typical alox wheel, the infeed rate will be in the range of 0.2 to 2  $\mu\text{m}/\text{rev}$  depending on the machine stiffness. After the infeed of the machine axes has been completed, there will be a programmed dwell period while the system relaxes. For a standard production grinder, this should occur within 0.5 s. Pahlitzsch and Schmidt [1969] reported that surface roughness reached a minimum value after 80 to 150 revolutions of the wheel at dwell on the roll. This provides the end user with a working range of dwell times. Excessive dwell times should be avoided to prevent premature roll wear and the development of chatter.

Available information on the plunge roll dressing of vitrified CBN wheels is sparse although growing rapidly as a production technique. The primary applications for this process are in the aerospace industry using relatively porous wheels <6 wide, and in the fuel injection and bearing industries using narrow (<1) wide wheels. In both cases, the limitations are in the machine and spindle stiffnesses.

### 7.7.6 DRESS PARAMETERS FOR FORM CBN WHEELS

Hitchiner [1998, 1999] gives typical parameters for dressing of CBN wheels for grinding aircraft blades and vanes. Crush ratio values of +0.6 to +0.8 are used as for conventional wheels but infeed rates are limited to 0.1 to 0.25 mm/min or 0.03 to 0.20  $\mu\text{m}/\text{rev}$ , which are 10 times less than for conventional wheels. On stiff, purpose-designed machines, the dwell time is kept to a minimum, that is, zero dwell time is programmed in the CNC control, while the actual value is limited by the machine control response and inertia, which is perhaps 0.1 s. For a modern stiff grinder, the relaxation time is as little as 0.35 s, while for older, weaker grinders a dwell time of up to 2 s has been necessary to generate a round wheel. More comment is made on this in the discussion on dressing spindles (Chapter 15).

Efforts have been made to employ acoustic sensors for touch dressing. Care has to be taken to allow for the fact that contact has to be resolved in two planes. The dressing arrangement in Figure 7.40 was presented by Landis (Waynesboro, PA) at the IMTS (Tool Show) in Chicago in 1996 for dressing vitrified CBN angle-approach wheels. The acoustic sensor is mounted to the left

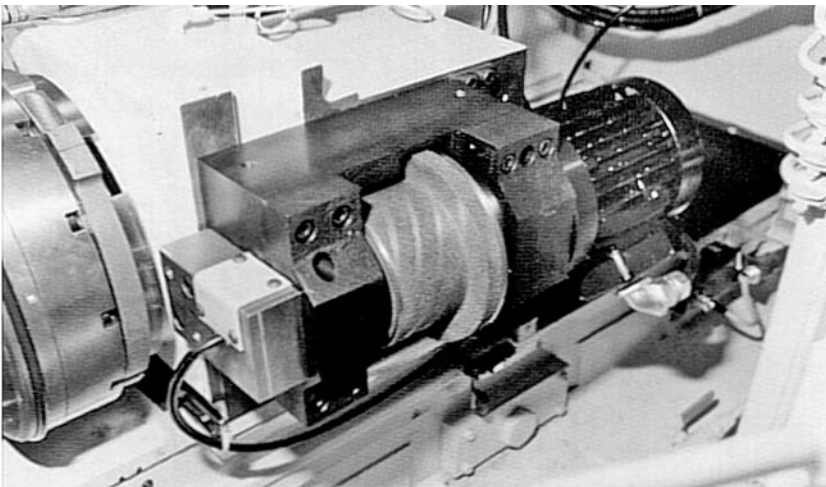


**FIGURE 7.40** Landis 2SE with form-roll dressing arrangement for vitrified cubic boron nitride. (Courtesy of Landis, Waynesboro, PA. With permission.)

of the diamond roll with diamond-free areas to relieve dressing pressure. The roll shape provided two orthogonal planes on which to touch the wheel. An alternative approach on more complicated forms is to have a wheel edge and side from which to touch.

Issues with system relaxation times and programmed dwell times, whether it is with conventional or CBN abrasive, inevitably lead to situations where the wheel has less than ideal sharpness. To overcome this, several methods have been applied to give a very brief period of contact. These rely upon sweeping the roll past the wheel in a sliding motion analogous to using a stationary block dresser. The method, with the dresser mounted on a linear slide, has been used on, for example, matrix grinders for ballnut grinding for the last 30 years. An alternative method is to have the dresser spindle mounted on a swing arm. The technique had advantages of offering the minimum contact time, but field reports suggest stability problems rough dressing conventional wheels. A problem with this approach is that numerous spark-out passes must be made to ensure the entire wheel face has been contacted and to eliminate chatter. This then becomes analogous to traverse dressing with a wide impregnated roll. Certain parts of the wheel are hit numerous times while other areas could go almost untouched.

### 7.7.7 HANDLING DIAMOND ROLLS

Diamond rolls are high-precision tools and must be treated as such. The following are recommended procedures for assembling a roll on a spindle shaft:

- Standard roll/spindle assembly tolerances. Standard toleranced assemblies refer to rolls with bore tolerances of 2.5 to 7  $\mu\text{m}$  over nominal mounting on shafts with nominal to 2.5  $\mu\text{m}$  undersize, giving an average “loose” fit of 5  $\mu\text{m}$ . The shaft itself should have a runout condition of  $\leq 1.25 \mu\text{m}$  truth in running (T.I.R.), and after assembly in the spindle bearings of  $\leq 2.5 \mu\text{m}$  T.I.R.
- Diamond rolls should be mounted in a clean environment removed from the production area by a person properly trained to deal with the tolerance level involved.
- A fine grit oilstone should be rubbed lightly on the end faces of the diamond roll and any spacers to ensure that there are no burrs or raised metal due to previous handling.
- A film of gauge oil should be sprayed in the bores and then wiped clean with a lint-free cloth to ensure the absence of dust or grit before assembling.
- The shaft should be treated as step c.
- Carefully align the diamond roll bore to the shaft. It is critical that the roll be started in a straight fashion. Otherwise, the roll can jam on the shaft before engaging the full bore. A slight lead of 5  $\mu\text{m}$  over 40 mm is extremely helpful. The diamond roll should slide down the shaft with minimal pressure until it bottoms out.
- An aid to ease of assembly is to place the roll in warm water (40°C to 60°C) to minimally expand the bore and ease assembly. DO NOT use a hot plate or hot air gun as this will distort the roll or, in the case of reverse plated rolls, melt the alloy holding the diamond layer to the core.
- Never force the diamond roll onto the shaft if unable to assemble. Inspect the bore and shaft for actual size or inspect for “raised” metal contact.
- Complete mounting by assembling clamping nut or mounting screws, using care not to overtighten, to approximately 130 N.m (100 ft.lb) on nut or 4 N.m (3 ft.lb) on typical 10-32 screw.
- Inspect assembly for runout by rotating in bearings before mounting in machine (if possible). Runout condition should not exceed 5  $\mu\text{m}$  T.I.R. on diamond rolls using diamond free, indicating bands at ends of roll.

For disassembly, the roll should again be removed from the shaft in a clean environment, away from the production area. The shaft end and diamond roll end faces should be wiped clean to

prevent dirt becoming trapped during removal and scoring the shaft or roll bore. If proper assembly procedure was followed, removal should be accomplished by simply sliding diamond rolls off shaft. Never force the roll especially by the use of hammers of any kind.

- Line-fit roll/spindle assembly tolerances. Line-fit toleranced assemblies refer to rolls with bore tolerances of nominal to  $-2.5\ \mu\text{m}$  under nominal mounting on shafts with nominal to  $2.5\ \mu\text{m}$  undersize, giving an average fit of zero or linefit. The shaft itself should have a runout condition of  $\leq 1.25\ \mu\text{m}$  T.I.R., and after assembly in the spindle bearings of  $\leq 2\ \mu\text{m}$  T.I.R.
- It is generally recommended that the roll manufacturer assemble and disassemble line-fit rolls. It is mandatory that the assembly be carried out in a clean environment, preferably temperature controlled, by trained individuals.
- A fine grit oilstone should be rubbed lightly on the end faces of the diamond roll and any spacers to ensure there are no burrs or raised metal due to previous handling.
- A film of gauge oil should be sprayed in the bores and then wiped clean with a lint free cloth to ensure the absence of grit before assembling.
- Chill the shaft for approximately 30 minutes using cold tap water or ice packs to contract the mating diameter. Warm the diamond roll in hot water ( $65^\circ\text{C}$  max) for 2 to 5 min to minimally expand the bore.
- Quickly, but carefully, align the diamond roll bore in the shaft and slide the roll down until bottomed out.
- Turn the roll slowly on the shaft, maintaining a downward pressure, until temperature is equalized and the diamond roll becomes immovable.
- Complete mounting by assembling clamping nut (using care not to overtighten) to approximately 130 N.m (100 ft.lb). Locking screws are not recommended because of the lack of time to accurately align the bolt pattern.
- Inspect assembly for runout by rotating in the bearing assembly before mounting in the machine (if possible). Runout should not exceed  $2.5\ \mu\text{m}$  T.I.R. on the diamond rolls using the diamond-free indicating diameters at the ends of roll.

For disassembly, the roll should again be removed from the shaft in a clean environment, away from the production area. The shaft end and diamond roll end faces should be wiped clean to prevent dirt becoming trapped during removal and scoring the shaft or roll bore. Cool assembly in cold tap water or with ice packs for 30 min, then run hot water over the diamond roll only before quickly removing the diamond roll assembly. Never force the roll, especially by the use of hammers of any kind.

## 7.8 TRUING AND CONDITIONING OF SUPERABRASIVE WHEELS

Nonporous superabrasive cannot, in general, be dressed with diamond tooling. Truing can be performed for some softer CBN bonds, such as resin, using diamond nibs or rotary diamond traversing discs, but, in general, most wheels are trued and conditioned using conventional abrasive blocks or wheels. In the case of diamond, this can sometimes be completed in one operation to be effectively a dress process. Otherwise, two separate grades of conventional abrasive are chosen: the first is with a comparable or larger grit size to true the wheel, the second with a grit size half that of the superabrasive to condition the wheel by eroding the bond only. The processes can be carried out wet or dry and, in general, coolant is used only if used in grinding.

In its simplest form, the dressing arrangement is simply to feed dressing sticks into the wheel (cylindrical or cutter grind applications) or pass the wheel over the block (surface grind applications). Alternatively, a mechanical or electrical brake truer device is used (Figure 7.41).

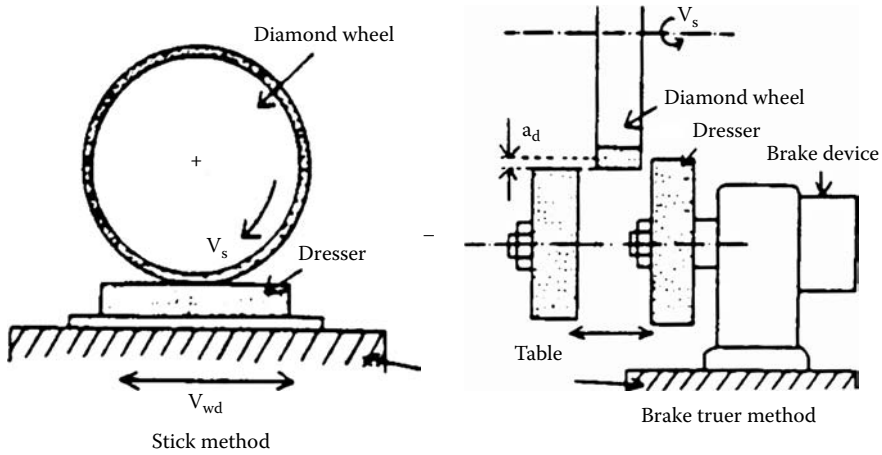


FIGURE 7.41 Conditioning processes with abrasive stick and wheel. (From Inasaki 1989. With permission.)

On the simpler mechanical version, the dressing wheel is driven by the grinding wheel. The brake truer contains a set of weights that move out centrifugally as the rotational speed increases until they brake by making contact with the inner wall of the unit. This allows a speed differential to be maintained between dressing and grinding wheel (Figure 7.42). The electric version merely has an a.c. motor instead to regulate speed and is used for small, thin, or fine-mesh wheels that provide insufficient torque to drive the mechanical version. When using the brake truer, infeed rates can start up to 50 to 75  $\mu\text{m}/\text{pass}$  at 2 m/min for roughing depending on the wheel grade before bringing the infeed amounts down for final flatness.

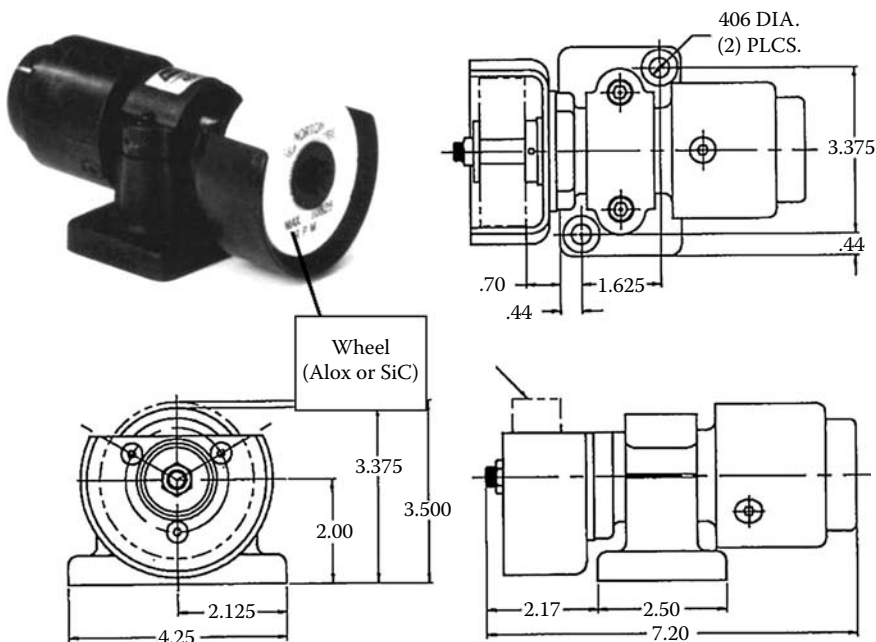


FIGURE 7.42 Brake truer device. (From Norton 1993. With permission.)



**TABLE 7.7**  
**Recommended Dressing Wheel Grades for Truing with Brake Truer Devices**

Abrasive	Bond	Grit Size	Operation	Wet	Dry
Diamond	Resin	80#–120#	DRESS	WA60L	GC60L
		150#–320#	DRESS	WA120L	GC60L
		400#–800#	DRESS	WA325L	GC60L
	Metal	80#–120#	DRESS	WA46N-R	GC46N-R
		150#–320#	DRESS	WS80N-R	GC80N-R
		400#–800#	DRESS	WA230N-R	GC230N-R
	Vitrified	80#–120#	DRESS	WA80N	GC80N
		150#–320#	DRESS	WA150N	GC150N
		400#–800#	DRESS	WA400N	GC400N
CBN	Resin	80#–120#	TRUE	GC60J-N	GC60J-N
		150#–320#	TRUE	GC120J-N	GC120J-N
		400#–800#	TRUE	GC325J-N	GC325J-N
	Metal	80#–120#	CONDITION	WA220G	WA220G
		150#–320	CONDITION	WA400G	WA400G
		400#–800#	CONDITION	WA800G	WA800G
		80#–120#	TRUE	WA46J-N	GC46J-N
		150#–320#	TRUE	WA80J-N	GC80J-N
		400#–800	TRUE	WA230J-N	GC230J-N
	Vitrified	80#–120#	CONDITION	WA220G	WA220G
		150#–320#	CONDITION	WA400G	WA400G
		400#–800#	CONDITION	WA800G	WA800G
		80#–120#	TRUE	WA80N	GC80N
		150#–320#	TRUE	WA150N	GC150N
		400#–800#	TRUE	WA400N	GC400N
Metal	80#–120#	CONDITION	WA220G	WA220G	
	150#–320	CONDITION	WA400G	WA400G	
	400#–800#	CONDITION	WA800G	WA800G	

Source: Compiled from several sources, especially Diamant Boart America [1991].

Traditional dressing, truing, and conditioning grades of stones for both diamond and CBN resin wheels are given in Table 7.7. Also, recent developments in engineered ceramic grains indicate much higher removal rates and, hence, shorter dress times for both truing and conditioning may be achievable using these grains in conditioning wheels and blocks. However, this has not yet been well documented.

Dressing of diamond wheels over 300 mm in diameter can be especially time consuming. One method to reduce dress time for cylindrical grinding applications is to use the work drive as a dresser motor and mount the dresser wheel in a fixture or arbor driven between centers. The diamond wheel speed should be about 25 m/s while the dresser wheel should be at one third this speed running unidirectional. Traverse rates should be about 0.1 m/min with infeed depths of 15 to 25  $\mu\text{m}$ . After truing with a SiC wheel, the diamond surface should be conditioned with white alox sticks.

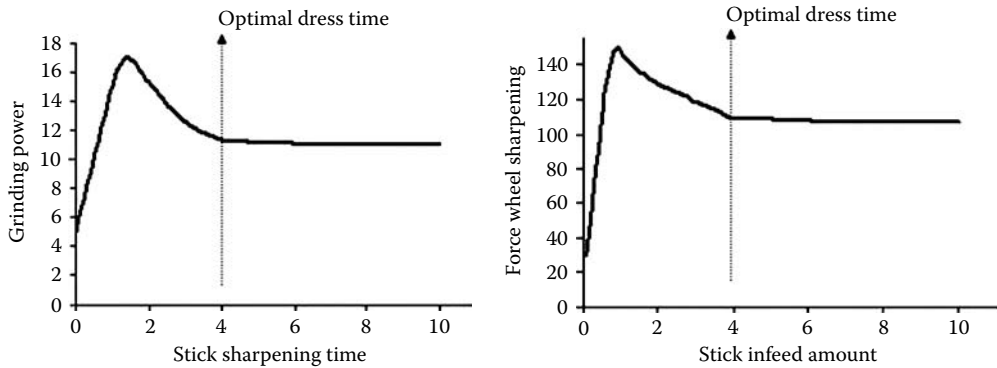


FIGURE 7.43 Optimization of stick dressing by monitoring stick pressure and initial grinding forces.

There was considerable interest and research into stick infeed methods for conditioning cylindrical CBN wheels in the 1980s and early 1990s prior to the optimization of vitrified CBN rotary truing methods and establishment of functional grinding parameters for high-production grinding. For example, Juchem [1993] reported data conditioning resin-bonded CBN with white alumina sticks. At a constant infeed rate, it was found that the initial grinding force after dress increased initially with dress time, then fell to a steady-state value. Optimal dress conditions with the minimum of wheel wear occurred when the forces just reach this steady-state condition. At this point, the bond was optimally eroded without overexposing the abrasive grains (Figure 7.43).

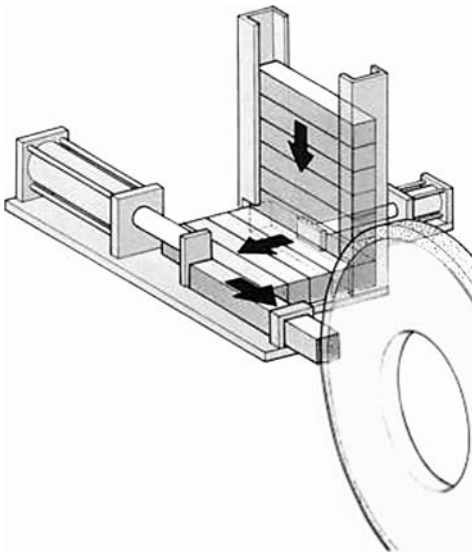
Materials for conditioning wheels are not limited to conventional abrasives. Soft mild steel and molybdenum are both used in thrufeed centerless grinding for conditioning resin diamond wheels. The material is fed as bars through the grinder generating long stringy chips that erode the resin matrix.

An alternative is to treat the surface of the wheel with slurry containing loose abrasive grain. Several systems exist where the surface is blasted directly with a high-pressure slurry jet [Kataoka et al. 1992] or fed between a steel roll and a wheel [Hanard 1985].

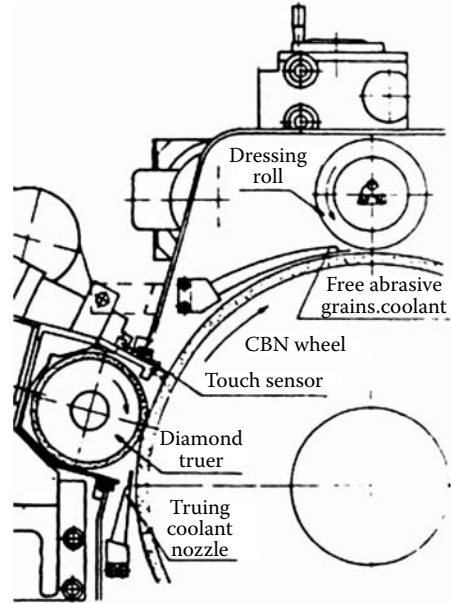
The first CBN cam grinders used resin CBN wheels (Figure 7.44), which were trued with a rotary diamond and then conditioned with either an alumina stick (Fortuna) or with slurry fed between the wheel and a crush roll (TMW). The process was extremely cost effective from the aspect of abrasive cost/part. The only problem was the conditioning process because it was hard to control relative to the simpler dressing process required with the vitrified CBN wheel technology that superseded it [Renaud and Hitchiner 1991].

Conditioning with the correct block grade produces a very well-exposed abrasive wheel surface, and even for vitrified CBN this can be greater than by simply rotary diamond dressing. One area this is critical for is low stock removal applications such as finish double-disc grinding [Hitchiner et al. 2001] Chen describes how to open up a vitrified CBN wheel surface by grinding and “touch dressing” and how to avoid the problem of closing up the wheel surface by dressing too deep [Chen, Rowe, and Cai 2002]. Problems experienced when dressing techniques for conventional vitrified abrasive are employed for vitrified CBN include: high grinding forces, rapid consumption of the abrasive layer, poor grinding results, and shortened redress life.

Koyo Machine offers a range of vertical spindle double-disc grinders designed specifically around the use of superabrasive wheels for finish grinding of tight tolerance components for, for example, the fuel injection, hydraulic pump, gear, and ceramics industries. Double-disc grinding is characterized by low chip loads and high normal forces due to the high contact area of the wheels. Consequently, with CBN there is little grit pullout and fracturing or bond erosion and the abrasive grains glaze giving progressively lower finishes and higher forces until either flatness is lost or



Stick infeed mechanism on fortuna camlobe grinder



Truing and conditioning resin bond CBN with diamond truer and free abrasive slurry on a TMW GCB7 camlobe grinder

FIGURE 7.44 Examples of conditioning processes on early cubic boron nitride-capable camlobe grinders.

burn occurs. The more exposed the abrasive the longer the time between dresses. The machines, therefore, use a rotary block dressing method where white alumina blocks are passed between the wheels. This also makes the machines flexible to use resin, even metal, as well as vitrified bond wheels. (See Figure 7.45.)

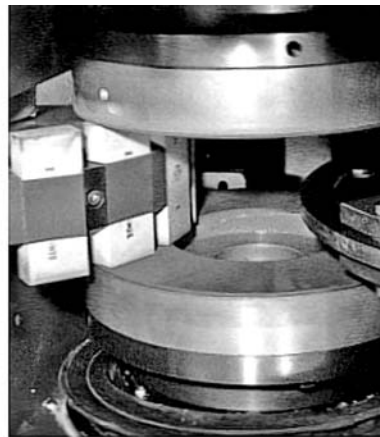
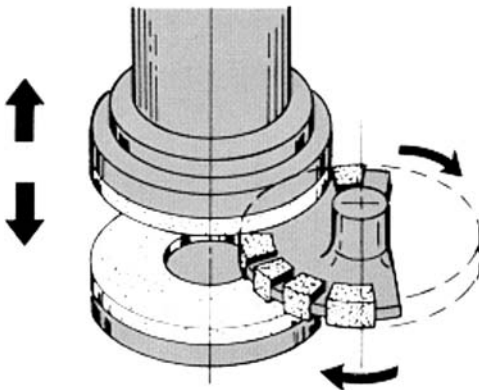


FIGURE 7.45 Koyo block truing/conditioning process for superabrasive double-disc wheels. (Courtesy of Koyo Machine USA, Novi, MI. With permission.)

## REFERENCES

- Brinksmeier and Çınar. 1995. "Characterization of Dressing Processes by Determination of the Collision Number of the Abrasive Grits." *Ann. CIRP* 44, 1, 299–304.
- Carius, A. C. 1984. "Preliminaries to Success – Preparation of Grinding Wheels Containing CBN." SME Technical Paper MR84-547.
- Chen, X. 1995. *Strategy for Selection of Grinding Wheel Dressing Conditions*. John Moores University, Liverpool, U.K.
- Chen, X., Rowe, W. B., and Cai, R. 2002. "Precision Grinding Using CBN Wheels." *Int. J. Mach. Tools & Manuf.* 42, 585–593.
- Decker, D. B. 1993. "Truing and Dressing Grinding Wheels with Rotary Dressers." *Finer Points* 5, 4, 6–10.
- Diamant Boart America. 1991. "5214 Universal Truing and Dressing Unit—Instruction and Operation Manual."
- Dittel, W. 1996. "Acoustic Control Systems." Trade brochure, Walter Dittel GmbH.
- Dr. Kaiser n.d. "High-Precision Diamond Profile Rolls." Trade brochure.
- Edwards, D. 1987. "Dressing for CBN." *Modern Machine Shop* SMD 81-593.
- Engis Corporation. 1996. "Superabrasive." Trade catalog, Engis Corporation.
- Fortuna. 1991. "Automated Camshaft Grinding." Trade brochure, Werke.
- Hanard, M. R. 1985. "Production Grinding of Cam Lobes with CBN." SME Conference Proceedings. "Superabrasives '85," pp. 4-1–4-11.
- Hitchiner, M. P. 1997. "Camshaft Lobe Grinding and the Development of Vitrified CBN Technology." *Abrasives Mag.* Aug/Sept, pp. 12–18.
- Hitchiner, M. P. 1998. "Dressing of Vitrified CBN Wheels for Production Grinding." Ultrahard Materials Technical Conference. May 28, 1998, Windsor, Ont.
- Hitchiner, M. P. 1999. "Grinding of Aerospace Alloys with Vitrified CBN." *Abrasives Mag.* Dec/Jan, pp. 25–35.
- Hitchiner, M. P., Willey, B., and Ardelt, A. 2001. "Developments in Flat Grinding with Superabrasives." Precision Grinding & Finishing in the Global Economy – 2001 Conf Proc. Gorham 11/1/2001, Oak Brook, IL.
- Inasaki, I. 1989. "Dressing of Resinoid Bonded Diamond Grinding Wheels." *Ann. CIRP* 38, 1, 315–318.
- Ishikawa, T. and Kumar, K. 1991. "Conditioning of Vitrified CBN Superabrasive Wheels." Superabrasives '91 Conference Proceedings SME. June 11–13, Chicago.
- Jakobuss, M. and Webster, J. 1996. "Optimizing the Truing and Dressing of Vitrified-Bond CBN Grinding Wheels." *Abrasives Mag.* Aug/Sept, p. 23.
- Juchem, H. O. 1993. "Conditioning of Ultrahard Abrasive Grinding Tools." *Finer Points* 5, 4, 21–27.
- Kataoka, S. et al. 1992. "Dressing Method and Apparatus for Super Abrasive Grinding Wheel." U.S. Patent 5,168,671. 12/8/1992.
- Marinescu, I., Rowe, W. B., Dimitrov, B., and Inasaki, I. 2004. "Tribology of Abrasive Machining Processes." William Andrew Publishing, Norwich, New York.
- Mindek, R. 1992. "Improved Rotary Disc Truing of Hot-Pressed CBN Grinding Wheels." MSc thesis, University of Connecticut.
- Noritake. n.d. "LL-Dresser." Trade brochure.
- Norton, Abrasives 1993. "Superabrasive Truing and Dressing Devices." Catalog 118.
- Pahlitzsch, G. and Schmidt, R. 1969. "Wirkung von Korngröße und -konzentration beim Abrichten von Schleifscheiben mit diamantbestückten Rollen." *wt-Zeitschrift für industrielle Fertigung*, 59, Jahrgang, Heft 4 Seite 158–161.
- Pricken, W. 1999. "Dressing of Vitrified Bond Wheels with CVDRESS and MONODRESS." *IDR* 3, 99, 225–231.
- Rappold. 2002. "Cylindrical Grinding." Rappold –Winterthur. Trade brochure. 02/2002 #136551.00.
- Renaud, W. and Hitchiner, M. P. 1991. "The Development of Camshaft Lobe Grinding with Vitrified CBN." SME Conference Proceedings. "Superabrasives '91" MR91-163.
- Rezeal, S. M., Pearce, T. R. A., and Howes, T. D. n.d. "Comparison of Hand-Set and Reverse Plated Diamond Rollers under Continuous Dressing Conditions." *IGT* University of Bristol, U.K.
- Schmitt, R. 1968. "Truing of Grinding Wheels with Diamond Studded Rollers." Dissertation, TU Braunschweig.
- Suzuki, I. 1984. "Development of Camshafts and Crankshafts Grinding Technology Using Vitrified CBN Wheels." SME MR84-526.

- Takagi, J. and Liu, M. 1996. "Fracture Characteristics of Grain Cutting Edges of CBN Wheel in Truing Operation." *J. Mater. Proc. Tech.* 62, 396–402.
- Torrance, A. A. and Badger, J. A. 2000. "The Relation between the Traverse Dressing of Vitrified Grinding Wheels and Their Performance." *Int. J. Machine Tools & Manuf.* 40, 1787–1811.
- TVMK. 1992. "Products Guide." Toyoda Trade Brochure. Van Moppes Ltd.
- TVMK. n.d. "Proposal & Creation Toyoda Van Moppoes Ltd Company Guidance." Trade brochure.
- Unicorn International. n.d. "D25 Tool Selection Guide for Anglehead Grinding Machine." Trade brochure.
- Universal Superabrasives. 1994. "Diamond Dressing Tools." Trade brochure.
- Unno and Yokogawa. 1989. Patent EP 0,426,173. Toyoda. 10/31/89.
- Williams, J. and Yazdzik, Y. 1993. In-Process Dressing Characteristics of Vitrified Bonded CBN Grinding Wheels." *J. Eng. Gas Turbines & Power Trans ASME* 115, 1, 200–204.
- WINTER. Principle and mode of operation of WINTER diamond from roller. Patent No. EP 116668.
- Winterthur Corporation. 1998. "Precision Grinding Wheels." Trade brochure.
- Yokogawa and Unno. 1994. "Dressing Performance of Prismatic Monocrystalline Diamond Dresser." *JSPE* 60, 6, 803–807.
- Yokogawa and Yonekura. 1983. "Effects of 'Tsukidashiryō' of Resin Bonded Borazon CBN Wheels on Grinding Performance." *Bull. JSPE* 17, 2, 113–118.

---

# 8 Grinding Dynamics

## 8.1 INTRODUCTION

### 8.1.1 LOSS OF ACCURACY AND PRODUCTIVITY

Vibrations can cause serious problems in grinding processes leading to loss of machining accuracy and loss of productivity. Of the various types of vibration, chatter vibration is one of the most crucial ones because it reduces form accuracy as well as increasing surface roughness of the ground parts. Form accuracy and low surface roughness are two of the main targets to be attained by grinding. In addition, productivity is lost because material removal rate has to be reduced as a way of suppressing chatter. A great deal of research has been conducted that is aimed at achieving a clear understanding of the mechanism of chatter vibration and consequently at developing practical suppression methods.

### 8.1.2 A NEED FOR CHATTER SUPPRESSION

The ultimate aim of research on grinding chatter is to develop practical methods for suppressing chatter vibrations while maintaining high productivity. While there have been some proposals from research laboratories to meet this requirement, few have been successfully applied in industry. Thanks to significant developments in sensing and control technologies available today, it seems that the necessary tools for developing methods of suppressing chatter vibrations are being provided.

## 8.2 FORCED AND REGENERATIVE VIBRATIONS

### 8.2.1 INTRODUCTION

There are basically two types of vibration in grinding processes: forced vibrations and self-excited vibrations (Figure 8.1).

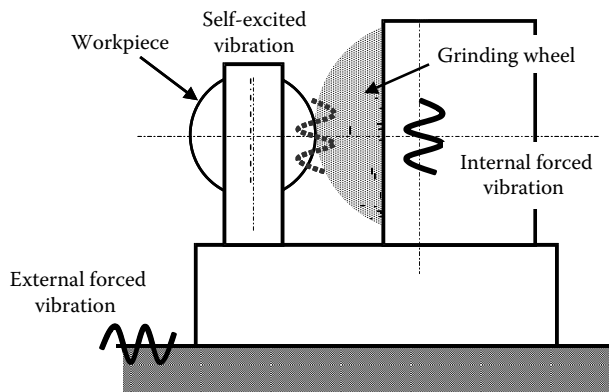


FIGURE 8.1 Chatter vibrations in grinding.

### 8.2.2 FORCED VIBRATION

Out-of-balance and eccentricity of the grinding wheel are the main causes of forced vibrations [Inasaki and Yonetsu 1969, Gawlak 1984]. The wheel, as a source of vibration, can be relatively easily identified through frequency measurement. The main concern with wheel-induced vibration is how to eliminate out-of-balance and wheel runout. There are a number of other sources of forced vibration such as vibration from hydraulic devices integrated into a grinding machine and from floor vibration, which are sometimes more difficult to locate and suppress successfully.

### 8.2.3 REGENERATIVE VIBRATION

A great deal of effort has been made to understand the mechanisms of self-excited chatter vibration in grinding. There are various conceivable reasons for process instability, for example, gyroscopically induced vibration of the grinding wheels [Hahn 1963]. The regenerative effect is considered to be a major cause of self-excited vibration in grinding. Regenerative vibration is similar to the self-excited vibration experienced in cutting processes [Inasaki, Yonetsu, and Shimizu 1974]. Due to the rotational motion of the workpiece during the material removal process, the waves generated on the workpiece surface, caused by the relative vibration between the grinding wheel and the workpiece, results in a change of depth of cut after one revolution of the workpiece. The phase shift between the surface waves (outer modulation) and the current relative vibration (inner modulation) makes the process unstable when a certain condition is satisfied. A characteristic feature of grinding chatter is, however, that such regenerative effect possibly exists on both the workpiece and the grinding wheel surfaces [Gurney 1965, Inasaki 1975]. This fact makes self-excited grinding chatter quite a complicated phenomenon. We can make a distinction between the two types of regenerative vibration as follows:

- Work-regenerative chatter. The waves generated on the workpiece surface through the regenerative effect grow quite rapidly; therefore, this type of chatter vibration is regarded as one of the constraints when the set-up parameters are determined.
- Wheel-regenerative chatter. On the other hand, waves generated on the grinding wheel surface grow rather slowly due to higher wear resistance of the grinding wheels; therefore, this type of chatter is a determinant for wheel life. When the vibration amplitude builds up to a certain critical limit, it is considered that the grinding wheel has reached the end of its re-dress life and those waves should be removed through truing and dressing.

## 8.3 THE EFFECT OF WORKPIECE VELOCITY

The development of regenerative chatter amplitude in cylindrical grinding is schematically illustrated in Figure 8.2. When the workpiece velocity is extremely high, of the order of some 10 m/min, or the chatter frequency is low, vibration with large amplitude can be observed at the beginning of grinding even if a newly dressed grinding wheel is used. In addition, significant chatter marks can be observed with the naked eye on the workpiece surface suggesting that the work-regenerative effect is the main reason for this vibration.

The occurrence of this chatter is significantly influenced by the combination of set-up parameters as shown in Figure 8.3 [Sugihara, Inasaki, and Yonetsu 1980a]. To the contrary, when the workpiece velocity is decreased to the order of some m/min, or chatter frequency is high, vibration cannot be detected at the beginning of grinding. However, the amplitude increases gradually as the grinding time advances. In this case, the chatter marks are not easily seen with the naked eye on the ground surface. However, the surface roughness perpendicular to the grinding direction deteriorates a lot. The

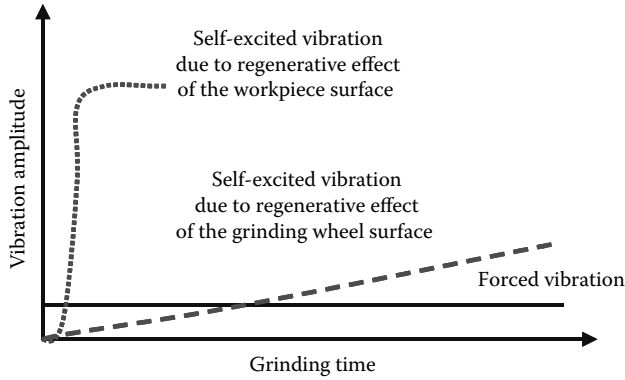


FIGURE 8.2 Vibration phenomena in grinding.

rate of amplitude increase is affected by the combination of set-up parameters and the type of grinding wheel used. The chatter frequency, which is closely related to the natural frequency of the mechanical system, and the workpiece velocity have a dominant effect on the occurrence of two different types of regenerative chatter vibration. Furthermore, it can be generally said that grinding processes are, in most cases, unstable in terms of the grinding wheel regenerative chatter [Inasaki et al. 1974]. In other words, the speed of the vibration development is a matter of concern with respect to this type of chatter.

Other important factors to be taken into account in terms of grinding chatter are the elastic deformation of the grinding wheel [Brown, Saito, and Shaw 1971, Inasaki 1975] and the geometrical interference between the grinding wheel and the workpiece [Rowe and Barash 1964]. The influence of the former factor on the stability will be discussed in Section 8.4.

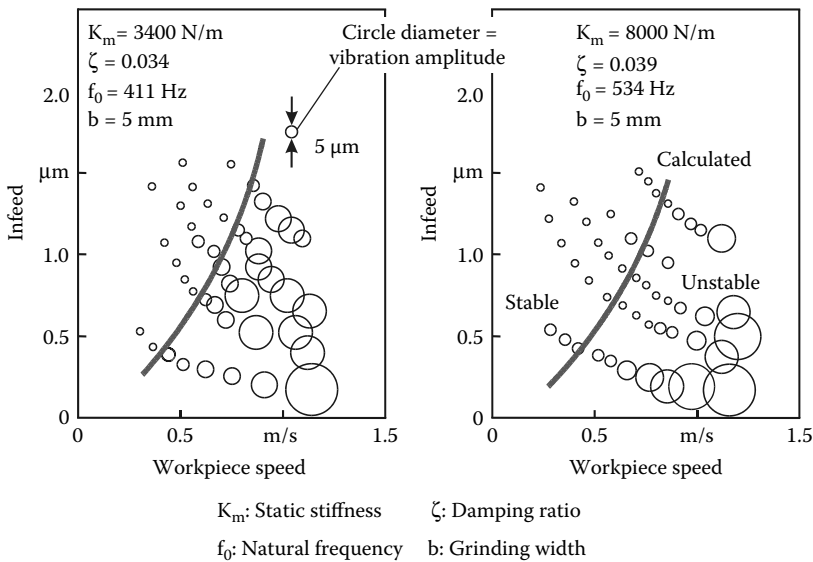


FIGURE 8.3 Vibration instability in grinding.



## 8.4 GEOMETRICAL INTERFERENCE BETWEEN GRINDING WHEEL AND WORKPIECE

The waves generated on the workpiece as well as on the grinding wheel surfaces are the envelope of the relative vibration between them. To start with, the waves generated on the workpiece surface will be considered. In this case, the waves are the envelope of the periphery of the grinding wheel. As far as the following conditions are satisfied, the amplitudes of the relative vibration and the waves generated on the workpiece surface are identical: low vibration frequency, small relative amplitude, and low workpiece velocity. However, once the critical limit, determined with the above-mentioned parameters, is exceeded, the amplitude of waves generated on the workpiece surface becomes smaller than that of the relative vibration. In other words, the envelope curve is attenuated.

Assuming that the amplitude of the relative vibration and the waves are  $y$  and  $a_w$ , respectively, the following relationship can be derived:

$$\begin{aligned}
 G_{e0} &= \frac{a_w}{y} \\
 &= \frac{1}{2} \left( 1 - \cos \sqrt{\frac{y_{cr}}{y}} \pi \right) \quad \text{for } \frac{y_{cr}}{y} < 1 \\
 &= 1 \quad \text{for } \frac{y_{cr}}{y} \geq 1
 \end{aligned} \tag{8.1}$$

where

$$y_{cr} = \frac{v_w^2}{\omega^2} \frac{2(d_w \pm d_s)}{d_w d_s} \tag{8.2}$$

is a critical amplitude,  $v_w$  is the workpiece speed,  $\omega$  is the angular chatter frequency,  $d_w$  is the workpiece diameter, and  $d_s$  is the grinding wheel diameter. The plus sign in Equation 8.2 is for cylindrical external grinding, the minus sign for internal grinding, and  $d_w = \infty$  for surface grinding. When  $y_{cr} < y$  the amplitude of waves becomes smaller than that of the relative vibration. Otherwise, both amplitudes are identical. As for the waves generated on the grinding wheel, the critical amplitude can be obtained by replacing the workpiece speed  $v_w$  with the grinding wheel speed  $v_s$ . Therefore, the critical amplitude is much larger for the waves generated on the grinding wheel because the wheel speed is much higher than the workpiece speed.

The calculated results from Equation 8.1 are given in Figure 8.4 [Inasaki 1975]. The geometrical interference is a strong nonlinear term in the grinding dynamics [Inasaki et al. 1974]. It is clear from Equations 8.1 and 8.2 that waves with large amplitude and higher frequency cannot be generated on the workpiece surface because the critical amplitude becomes small.

## 8.5 VIBRATION BEHAVIOR OF VARIOUS GRINDING OPERATIONS

The vibration behavior in cylindrical, internal, and surface grinding processes differ in significant ways [Inasaki 1977a]. In the case of internal and surface grinding, the chatter frequency is, in most cases, related to the natural frequency of the grinding wheel spindle system because the

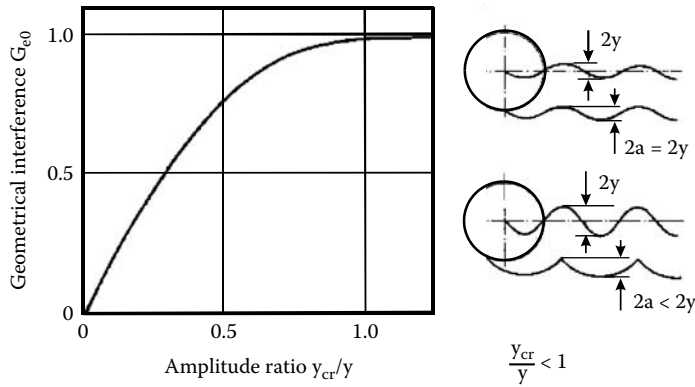
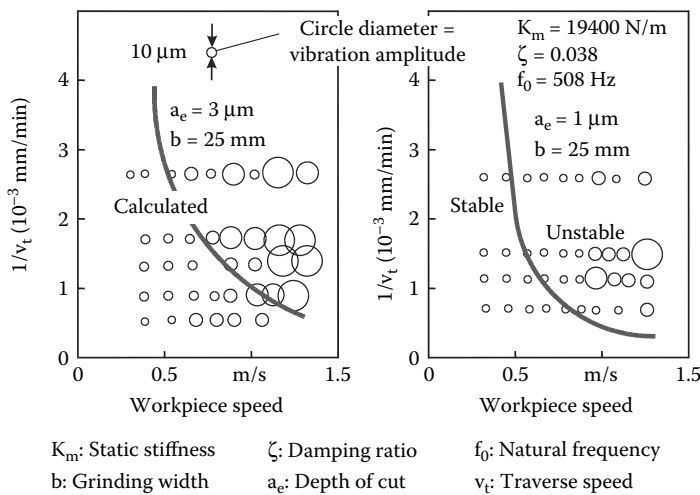


FIGURE 8.4 Geometrical interference.

dynamic stiffness of internal grinding spindles is often lower than that of the workpiece system. This is not the case, however, for cylindrical grinding. In this latter case, the dynamic stiffness of the workpiece system is usually lower than that of the grinding wheel spindle system. In addition, chatter vibration caused by the regenerative effect on the workpiece surface seems to be difficult to develop in surface grinding. This is due to the fact that the phase shift between the inner and the outer modulation is not necessarily constant because of the uncertainty in the workpiece reciprocating motions.

There are two types of grinding operations: plunge grinding and traverse grinding. The stability analysis becomes much more complex for the traverse grinding process because the different contact condition between the grinding wheel and the workpiece should be taken into consideration along the wheel width [Shimizu, Inasaki, and Yonetsu 1978]. Figure 8.5 shows an example of the stability limit in cylindrical traverse grinding [Sugihara et al. 1980b].



$K_m$ : Static stiffness       $\zeta$ : Damping ratio       $f_0$ : Natural frequency  
 $b$ : Grinding width       $a_e$ : Depth of cut       $v_t$ : Traverse speed

FIGURE 8.5 Stability limit in cylindrical traverse grinding.

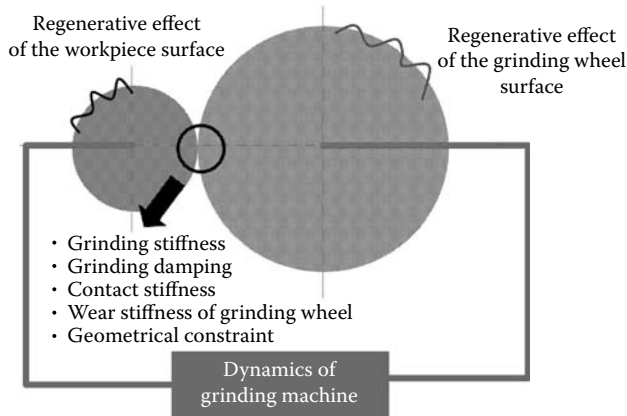


FIGURE 8.6 Factors affecting grinding dynamics.

## 8.6 REGENERATIVE SELF-EXCITED VIBRATIONS

### 8.6.1 MODELING OF DYNAMIC GRINDING PROCESSES

A mathematical model of dynamic grinding process can be established taking the factors shown in Figure 8.6 into account. The characteristic parameters in grinding dynamics, which are not generally necessary to consider in cutting dynamics, are the contact stiffness of the grinding wheel and the grinding damping. A comprehensive block diagram for representing the dynamic grinding process becomes very complex. Therefore, the process is divided into two extreme cases: the dynamic grinding process model for work-regenerative chatter and the model for the wheel-regenerative chatter. This simplification can be made possible by taking the geometrical interference into account. When the condition  $y_{cr}/y \geq 1$  in Equation 8.1 is satisfied, only the work-regenerative effect need be considered and hence the grinding wheel regenerative effect can be ignored. This is due to the following two reasons:

1. The work-regenerative effect has a large effect on the process stability.
2. The development of grinding wheel regeneration is much slower than that of workpiece regeneration.

On the other hand, for the case of  $y_{cr}/y \ll 1$ , the workpiece regenerative effect can be ignored because the amplitude of waves generated on the workpiece surface is much smaller than the amplitude of the relative vibration. However, the regenerative effect on the grinding wheel surface must be considered in the stability analysis.

Based on the above simplification, the block diagrams for the dynamic grinding process are depicted as shown in Figure 8.7 and Figure 8.8 for the workpiece regenerative chatter and for the grinding wheel regenerative chatter, respectively [Inasaki 1977b].

### 8.6.2 GRINDING STIFFNESS AND GRINDING DAMPING

A simplified linear dynamic grinding system can be represented by masses, springs, and elements. Based on the following simple grinding force model, which says that the normal grinding force  $F_n$  is proportional to the material removal rate damping

$$F_n = \lambda b \left( \frac{v_w}{v_s} a \right)^\epsilon \quad (8.3)$$

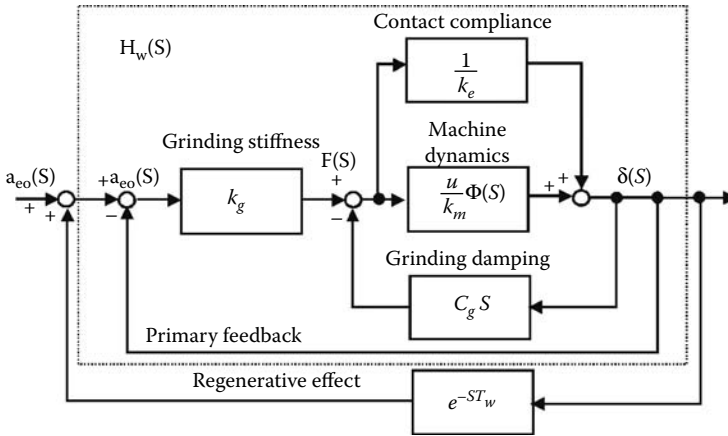


FIGURE 8.7 Block diagram for workpiece regenerative chatter.

the dynamic grinding force model can be derived as [Inasaki 1977a]

$$F_n(t) = k_g a(t) + c_g x(t) \tag{8.4}$$

where

$$k_g = \lambda \epsilon b \frac{v_w}{v_s} \left( \frac{v_w}{v_s} a \right)^{\epsilon-1} \tag{8.5}$$

$$c_g = \lambda \epsilon b \frac{1}{v_s} \left( \frac{v_w}{v_s} a \right)^{\epsilon-1} \sqrt{a / \left( \frac{1}{d_s} \pm \frac{1}{d_w} \right)} \tag{8.6}$$

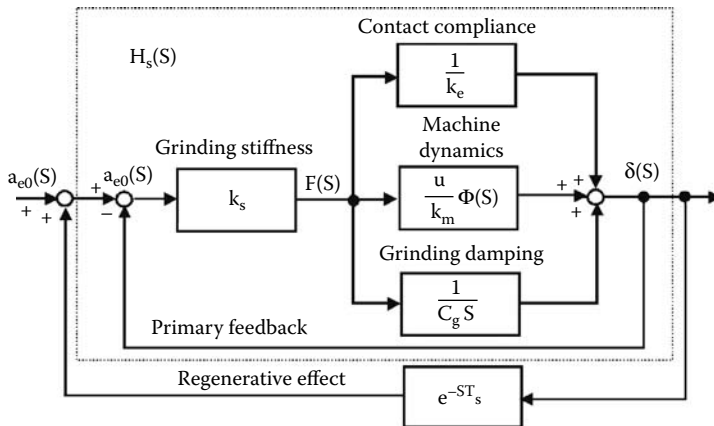


FIGURE 8.8 Block diagram for grinding wheel regenerative chatter.

where  $\lambda$  is constant,  $b$  is grinding width,  $v_w$  is workpiece speed,  $v_s$  is grinding speed,  $a$  is wheel depth of cut,  $\varepsilon$  is exponent, and  $x$  is mutual approach speed between grinding wheel and workpiece. The plus sign in the denominator is for external cylindrical grinding, the minus sign for internal grinding, and  $d_w = \infty$  for surface grinding.

$k_g$ , given by Equation 8.5, is the grinding stiffness, which is the coefficient between the grinding force and the depth of cut.  $c_g$ , given by Equation 8.6, is the grinding damping, which is the coefficient between the grinding force and the mutual approach speed between the grinding wheel and the workpiece. The grinding damping increases in proportion to the length of the contact between the wheel and the workpiece. Generally speaking, the grinding system becomes less stable as the grinding stiffness increases, while increase of grinding damping makes the system more stable.

In order to analyze chatter vibration caused by the grinding wheel regenerative effect, the grinding stiffness given by Equation 8.5 should be replaced with the wear stiffness of the grinding wheel. As a first-order approximation, the wear stiffness is obtained as

$$k_s = k_g G \frac{v_s}{v_w} \quad (8.7)$$

where  $G$  is the grinding ratio. Taking practical values of the grinding ratio and the speed ratio into account, it is confirmed that the wear stiffness of the grinding wheel is much higher than the grinding stiffness. Therefore, as far as the analysis of the chatter vibration caused by the workpiece regenerative effect is concerned, the wear stiffness of the grinding wheel can be assumed to be infinite.

### 8.6.3 CONTACT STIFFNESS

A characteristic feature of grinding dynamics is that the elastic deformation of the grinding wheel is too large to be neglected and, furthermore, it has a significant influence on the process stability. The contact stiffness of the grinding wheel is defined as the relationship between the normal compressive force  $F_n$  and the elastic deformation of the grinding wheel  $\delta$  induced at the contact zone. Some models have been proposed for theoretically calculating the elastic deformation of grinding wheels by applying the Hertzian elastic contact theorem (Figure 8.9 and Figure 8.10)

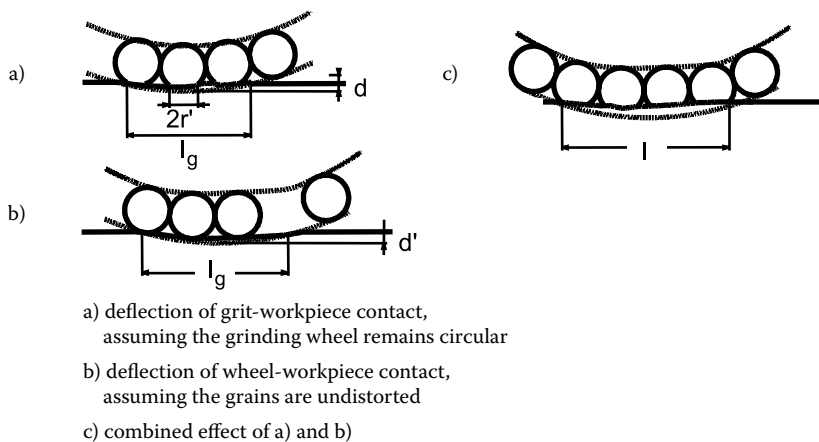


FIGURE 8.9 A deformation model for the grinding wheel. (Source: Brown.)

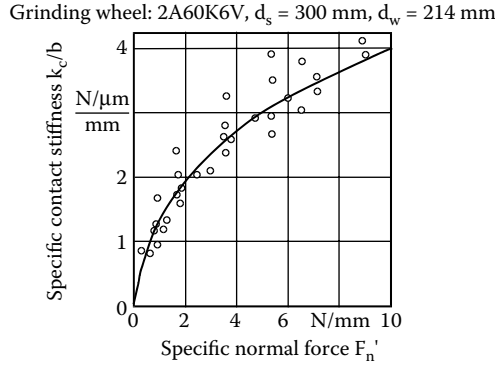


FIGURE 8.10 Specific contact stiffness of the grinding wheel.

[Brown et al. 1971, Inasaki 1975]. According to those analyses, it is suggested that the deformation  $\delta$  is given by following equation:

$$\delta = F_n^\rho \tag{8.8}$$

where  $0 < \rho < 1$ .

Therefore, the contact stiffness obtained through differentiating Equation 8.8

$$k_c = \frac{dF_n}{d\delta} \tag{8.9}$$

has a nonlinear characteristic of the hard-spring type. By combining Equations 8.3 and 8.9, the contact stiffness can be expressed as a function of the grinding set-up parameters. For example, the increase of the speed ratio  $v_w/v_s$  and the depth of cut results in an increase of the contact stiffness.

The contact stiffness has also been experimentally investigated [Inasaki 1977a, Younis 1972]. Of course, an increase of grinding wheel hardness corresponds to an increase of the contact stiffness.

### 8.6.4 DYNAMIC COMPLIANCE OF THE MECHANICAL SYSTEM

The dynamic compliance of the mechanical system, which consists of the workpiece, the grinding wheel, and the grinding machine, is represented by

$$\Omega(j\omega) = \frac{u}{k_m} \Phi(j\omega) \tag{8.10}$$

and

$$u = \cos \alpha \cos(\alpha - \beta) \tag{8.11}$$

where  $\alpha$  is the angle between the direction of the depth of cut and the direction of the natural frequency mode of the mechanical system,  $\beta$  is the angle between the direction of the depth of cut and the direction of the resultant grinding force,  $k_m$  is the static stiffness of the mechanical system, and  $\Phi(j\omega)$  is the nondimensional dynamic compliance.

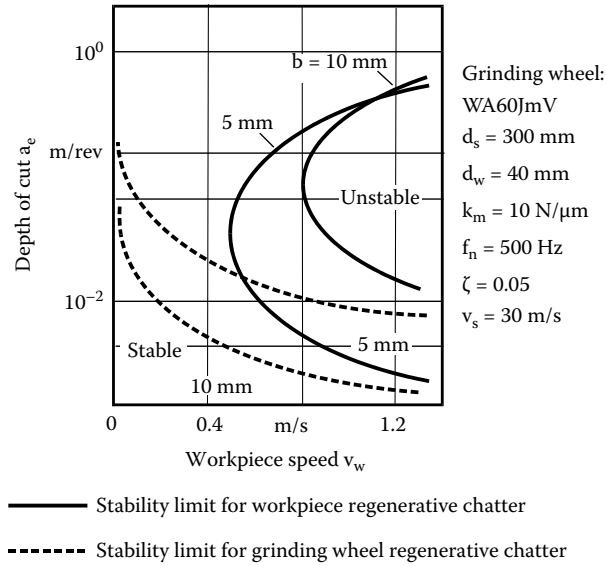


FIGURE 8.11 Stability limit for grinding chatter.

The practical grinding machine has many degrees of freedom; however, in most cases the model is simplified as having a single degree of freedom in the theoretical investigation. It is important to notice that the orientation factor  $u$  has a significant influence on the resultant dynamic compliance.

### 8.6.5 STABILITY ANALYSIS

The stability limit of the self-excited chatter vibration in plunge grinding can be obtained by substituting  $s = j\omega$  into the characteristic equations based on Figure 8.7 and Figure 8.8. Influence of the depth of cut, the workpiece speed, and the grinding width on the stability limit is illustrated in Figure 8.11 [Inasaki 1977a] for chatter vibration of both types: the regenerative effect on the workpiece surface and the regenerative effect on the grinding wheel surface. With respect to the former type of chatter vibration, absolute stability can be attained when the workpiece velocity is sufficiently low. On the other hand, the latter type of chatter vibration has a large area of instability, that is, most practical grinding conditions exist in the unstable region. Therefore, as far as the chatter vibration caused by the regenerative effect on the grinding wheel surface is concerned, it is necessary to know the increase speed of the vibration amplitude.

The positive real part of the roots of the characteristic equation is the index for the rate of increase of the vibration amplitude, while the imaginary part indicates the chatter frequency. Some calculated examples of the roots distribution are shown in Figure 8.12 and Figure 8.13 [Inasaki 1977a]. The important results deduced from those figures are

- The increased rate of vibration amplitude for the wheel regenerative chatter is much slower than that of the workpiece regeneration type.
- The roots exist with the constant interval of  $1/T_s$  or  $1/T_w$  in the imaginary axis, where  $T_s$  and  $T_w$  are the rotational period of the grinding wheel and the workpiece, respectively. This result explains the fact that the chatter vibration observed is accompanied by an amplitude modulation.
- The chatter frequency is always higher than the natural frequency of the mechanical system.

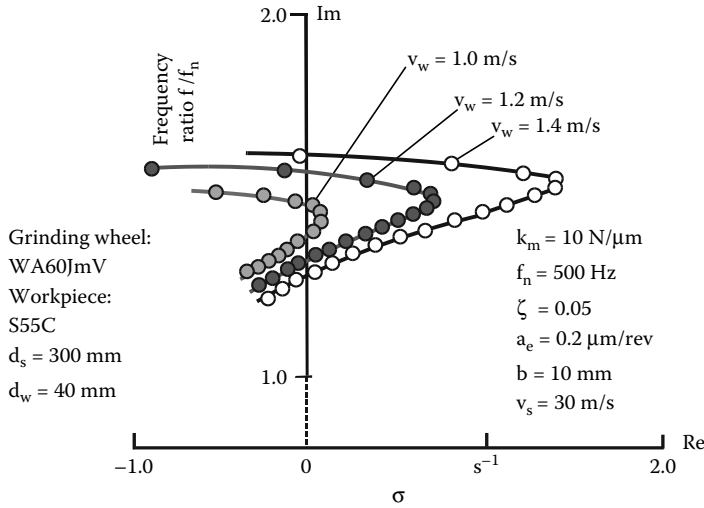


FIGURE 8.12 Roots of workpiece regenerative chatter.

Figure 8.14 shows the calculated results of the positive real parts for the grinding wheel regenerative chatter. It is assumed here that the instability occurs at the frequency that gives the maximum positive real part. From this result, the following conclusions are deduced:

- The development of chatter vibration becomes faster with larger depth of cut, larger grinding width, lower workpiece speed, and higher grinding wheel speed. With respect to the effect of depth of cut, however, it is necessary from the practical point of view to consider the increase of vibration amplitude against the amount of cumulative material removed. The calculated result shows that a larger amount of material can be removed before the grinding wheel comes to the end of its redress life with larger depth of cut.

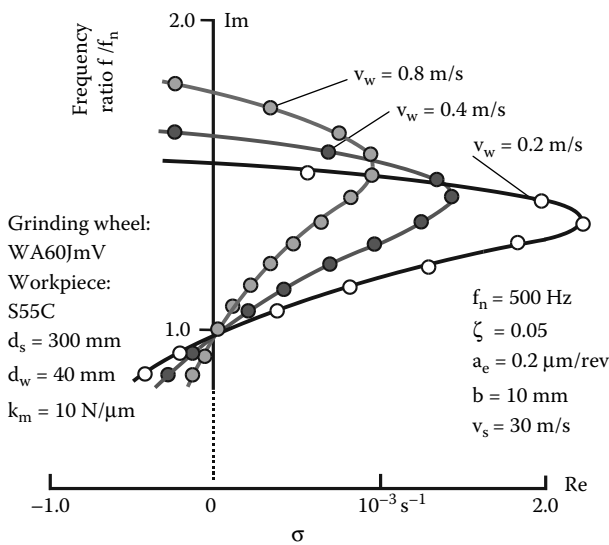


FIGURE 8.13 Roots of grinding wheel regenerative chatter.



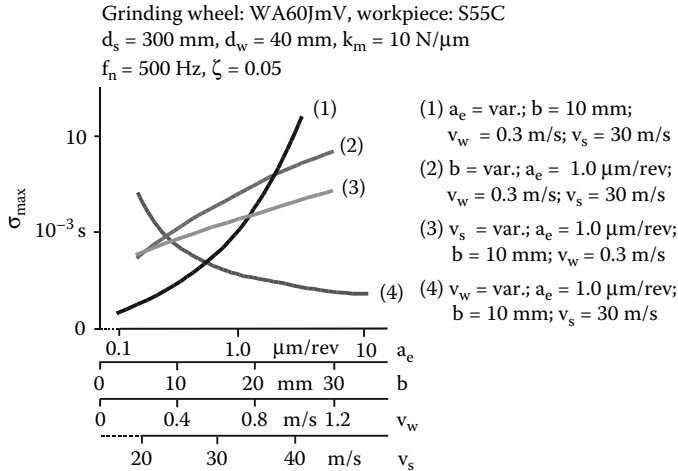


FIGURE 8.14 Parameter-related rate of increase of the chatter amplitude.

- The rate of increase in vibration amplitude decreases with a decrease in the contact stiffness and increase in the wear stiffness of the grinding wheel. This result means that the influence of the grinding wheel hardness is complex. An increase of stiffness and damping in the mechanical system reduces the rate of chatter development.

A similar analysis can be conducted for internal as well as surface grinding [Inasaki 1977a].

The stability analysis of traverse grinding is much more complex than that of the plunge grinding. However, some theoretical and experimental investigations have been conducted for the workpiece regenerative chatter in cylindrical grinding [Shimuzu et al. 1978]. Important conclusions were

- The process tends to be unstable under the condition of lower traverse speed, higher workpiece speed, larger grinding wheel width, and smaller depth of cut.
- Chatter frequency increases with increases of traverse speed, grinding wheel width, depth of cut, and workpiece speed.

## 8.7 SUPPRESSION OF GRINDING VIBRATIONS

In order to suppress vibrations in grinding, it is necessary to identify whether it is forced vibration or self-excited vibration. Figure 8.2 provides a possibility for identifying the type of vibration in grinding. If the vibration is detected while the machine idles, it is forced vibration. Vibrations with higher frequency than the grinding wheel rotational frequency are, in most cases, regenerative chatter. Vibration observed at the beginning of grinding, just after dressing, is more likely to be workpiece regenerative chatter. Grinding wheel regenerative chatter appears after a considerable time of grinding.

### 8.7.1 SUPPRESSION OF FORCED VIBRATIONS

The most significant source of forced vibration in grinding is unbalance of the grinding wheel. In order to suppress the adverse effect of forced vibration on the grinding process, unbalance of the grinding wheel should be detected using a vibration sensor, followed by balancing the grinding wheel [Kaliszer 1963, Trmal and Kaliszer 1976, Gawlak 1984]. Figure 8.15 shows an example of a balancing method based on liquid injection into a wheel flange pocket [Horiuchi and Kojima 1986]. Elimination of unbalance of the grinding wheel is essential to meet the requirement of higher grinding accuracy.

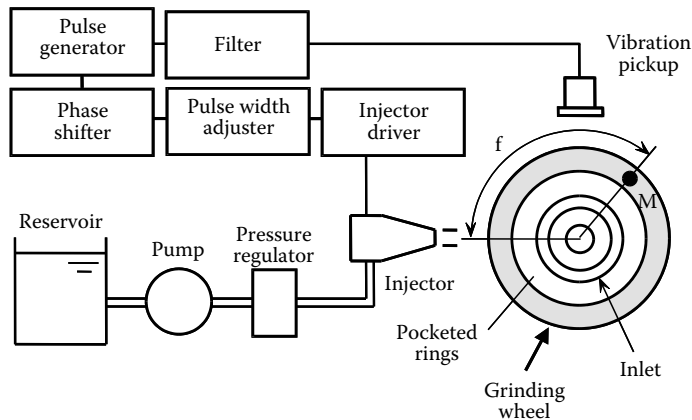


FIGURE 8.15 Automatic balancer for grinding wheels.

Eccentricity of the grinding wheel is another significant source of forced vibration. This can be eliminated through truing the grinding wheel; however, truing and balancing should be repeated alternatively several times in order to completely eliminate the vibration source because truing possibly generates an additional unbalance in the grinding wheel.

Sources of forced vibration can usually be located through frequency analysis of the vibrations. For example, forced vibrations caused by unbalance and eccentricity of the grinding wheel have a frequency component that corresponds to the wheel rotational frequency.

### 8.7.2 SUPPRESSION OF SELF-EXCITED CHATTER VIBRATIONS

The ultimate goal of research is to develop practical means for suppressing vibrations. Based on understanding of the chatter principle, a number of practical methods have been proposed. The methods can be categorized into one of three strategies shown in Figure 8.16:

- Modification of the grinding conditions,
- Increase of the dynamic stiffness of the mechanical system, and
- Disturbing the regenerative effect.

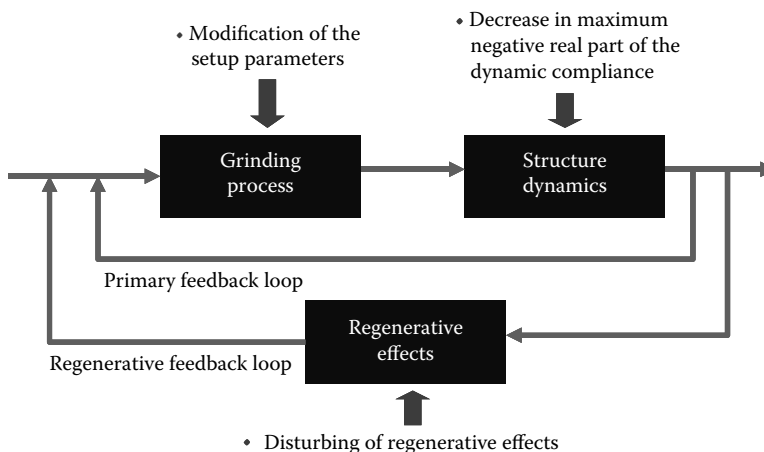
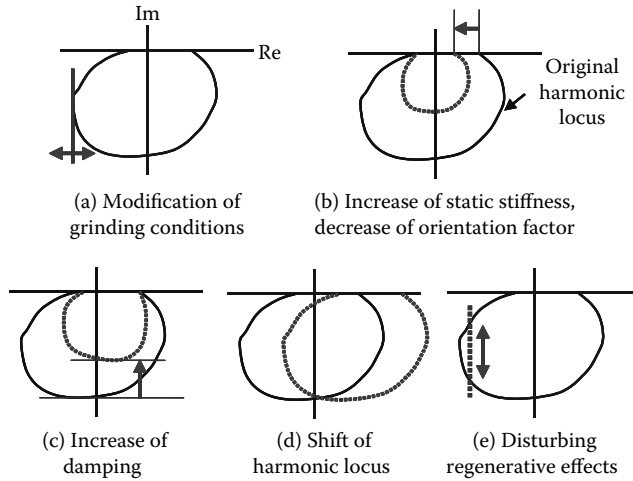


FIGURE 8.16 Principles of suppression of regenerative chatter.



**FIGURE 8.17** Strategies for suppressing regenerative chatter.

Figure 8.16 represents a block diagram of the simplified dynamic grinding system that consists of the grinding stiffness, the mechanical system, and the regenerative feedback loop. The block diagram is valid for workpiece regenerative chatter.

A stability analysis based on the dynamic model depicted in Figure 8.16 can be achieved as shown in Figure 8.17. The dynamic compliances of the mechanical system are represented by vector loci on the complex planes, while straight lines parallel to the imaginary axes represent the material removal process. Instability occurs when both lines have intersections. Based on those representations, methods for suppressing the regenerative chatter vibration can be further categorized as follows:

1. Modification of grinding conditions (Figure 8.17a)
2. Increase of the dynamic stiffness of the mechanical system
  - a. Increase of the static stiffness (Figure 8.17b)
  - b. Decrease of the orientation factor (Figure 8.17b)
  - c. Increase of the damping (Figure 8.17c)
3. Shifting the vector locus of the dynamic compliance to positive real part (Figure 8.17d)
4. Disturbing the regenerative effect (Figure 8.17e)

With respect to Method 1, decrease of the grinding stiffness is the most straightforward because it results in shifting the line parallel to the imaginary axis to the left and, consequently, the intersections of both lines can be avoided. Decrease of the grinding width and the workpiece speed meets this requirement (Figure 8.11).

Increase of the static stiffness or decrease of the orientation factor is effective for shrinking the vector loci and consequently for improving the dynamic performance of the grinding machines (Method 2.a and Method 2.b). Figure 8.18 shows an influence of the orientation factor on the stability [Inasaki et al. 1974]. In this series of grinding tests, the cross section of the workpiece center was modified from circular to rectangular and its orientation angle was changed. Interestingly, the critical limit in terms of grinding width changes depending on the orientation angle of the workpiece center. Influence of the static stiffness and the orientation factor on the stability is significant; therefore, it is worthwhile to take this effect into account at the design stage of a grinding machine.

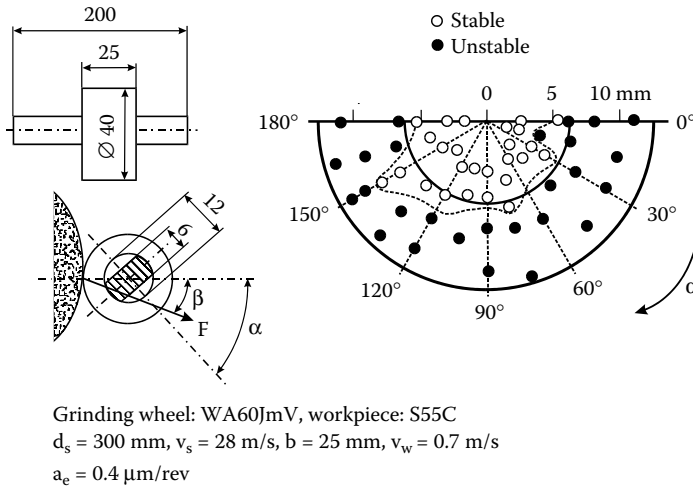


FIGURE 8.18 Influence of the orientation factor on chatter stability.

Another strategy for improving the dynamic performance of the mechanical system is to increase the damping by adding some kinds of dampers. Methods are divided into two kinds: application of passive [Tönshoff and Grosebruch 1988] and active dampers. Figure 8.19 shows an example of passive damper application [Hong, Nakano, and Kato 1990]. In this case, the damper is attached to the wheel head of the cylindrical grinding machine. Passive dampers are effective only when they are optimally tuned to the main mechanical system and the vibration characteristic of the mechanical system does not change significantly during the operation. However, application of active dampers is more flexible and can cope with a change in the vibration characteristics of the mechanical system. Figure 8.20 shows an example of the active damper application [Weck and Brecher 2001].

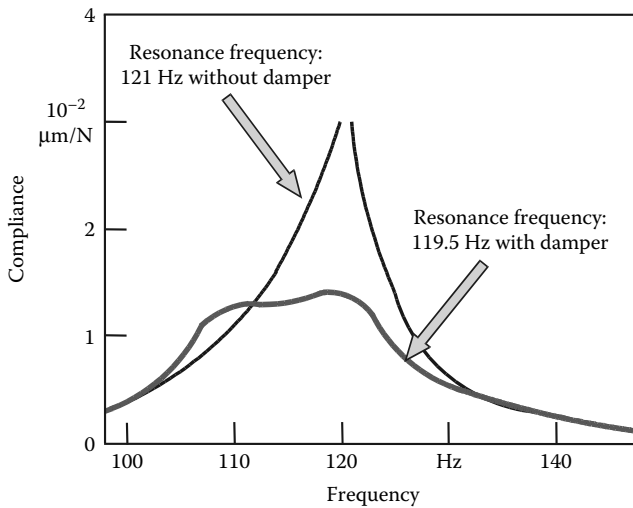


FIGURE 8.19 Effect of a passive damper for reducing structure compliance.

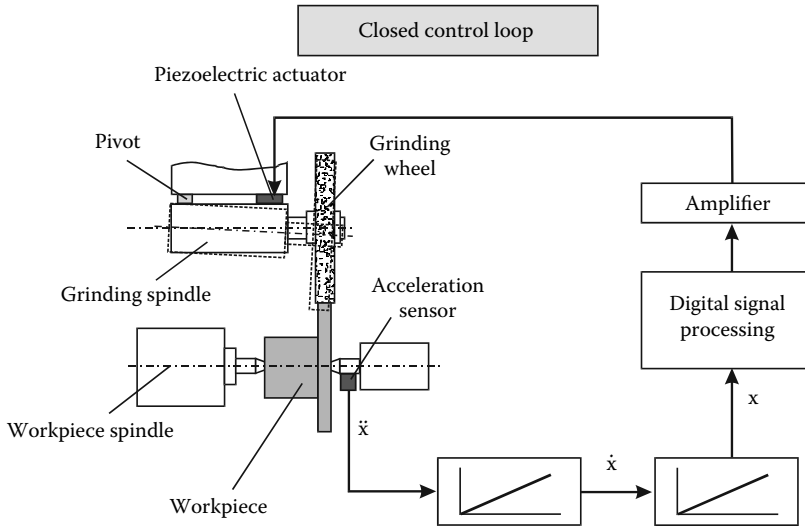


FIGURE 8.20 Application of an active damper in plunge outer diameter grinding.

Shifting the vector locus to the right on the complex plane, Method 3 can be achieved by adding a spring element between the workpiece and the grinding wheel. It is essential here to add only the spring element without any additional mass to the system. The resultant vector locus after the attachment of the spring element  $k_a$  is

$$\Omega(j\omega) = \frac{1}{k_a} + \frac{u}{k_m} \Phi(j\omega) \tag{8.12}$$

This idea for suppressing the chatter vibration can be realized to some extent by decreasing the contact stiffness of the grinding wheel [Sexton and Stone 1981]. Figure 8.21 shows an example of the grinding wheel modified to meet the idea.

A practical method for suppressing self-excited vibration is to intentionally disturb the phase shift between the inner and the outer modulation (Method 4). This idea can be put into practice by periodically varying the rotational speed of either the workpiece or the grinding wheel. The former method is effective for suppressing workpiece regenerative chatter [Inasaki 1977b] while the latter one is effective for suppressing grinding wheel regenerative chatter [Hoshi et al. 1986]. Figure 8.22

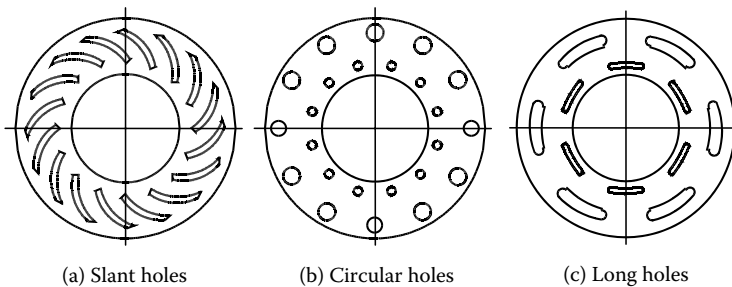
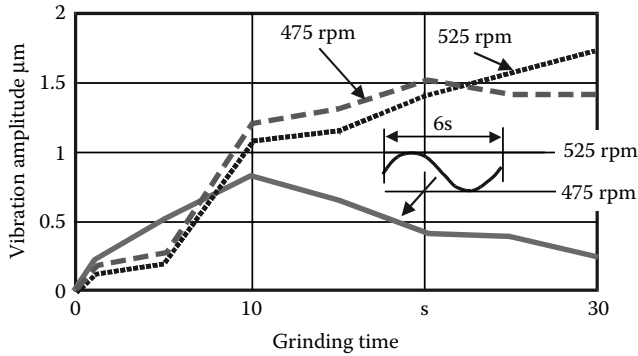


FIGURE 8.21 Flexible grinding wheel for suppressing chatter vibration.



Grinding wheel: WA60JmV, workpiece: S55C,  
 $d_s = 300 \text{ mm}$ ,  $d_w = 40 \text{ mm}$ ,  $k_m = 12 \text{ N}/\mu\text{m}$   
 $f_n = 575 \text{ Hz}$ ,  $\zeta = 0.052$ ,  $v_s = 30 \text{ m/s}$ ,  $b = 25 \text{ mm}$ ,  
 $v_w \approx 2.15 \text{ m/s}$

FIGURE 8.22 Chatter suppression by varying workpiece rotational speed.

and Figure 8.23 show the effect of varying the workpiece rotational speed and the grinding wheel rotational speed, respectively. The methods introduced here are effective and practical; however, the applications are restricted to rough grinding because varying the rotational speed may have some adverse effect on the surface quality of the ground parts.

### 8.8 CONCLUSIONS

From the theoretical point of view, it can be said that the mechanism of self-excited chatter vibration in grinding has been made clear. Self-excited chatter is a result of regenerative effects on both the workpiece and the grinding wheel surfaces. A full description of chatter is, however, complex. This is mainly due to the difficulty of identifying the required dynamic characteristics of the process, of the grinding machine, and of the grinding wheel. In addition, those characteristics are likely to change during the grinding process. Taking those difficulties into account, it is considered that a

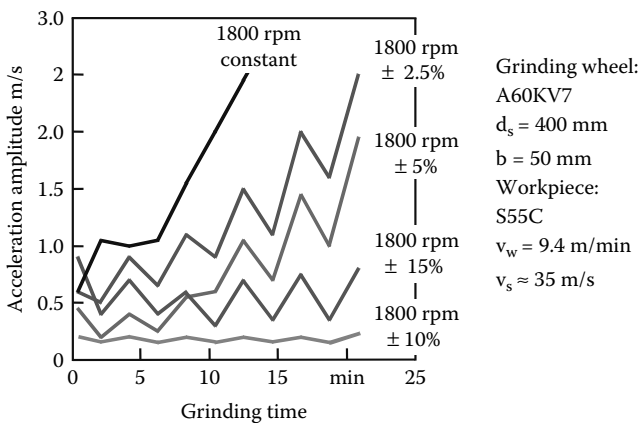


FIGURE 8.23 Chatter suppression by varying grinding wheel speed.

sophisticated chatter suppression system is required that consists of monitoring and control of chatter to meet the requirement for precision grinding processes. Advanced sensors and actuators available today are generally expected to make the achievement of chatter control possible. For the roughing process, however, periodical change of the grinding wheel rotational speed as well as workpiece rotational speed appears to be a practical solution. It is also desirable to give a higher compliance to the grinding wheel surface. With respect to grinding machine design, it is essential to increase stiffness and damping in order to achieve high dynamic stability.

## References

- Brown, R. H., Saito, K., and Shaw, M. C. 1971. "Local Elastic Deflections in Grinding." *Ann. CIRP* 19, 105–113.
- Gawlak, G. 1984. "Some Problems Connected with Balancing of Grinding Wheels." *J. Eng. Ind.* 106, 233–236.
- Gurney, J. P. 1965. "An Analysis of Surface Wave Instability in Grinding." *J. Mech. Eng. Sci.* 7, 2, 198–209.
- Hahn, R. S. 1963. "Grinding Chatter – Causes and Cures." *The Tool and Manufacturing Engineer* Sept, 74–78.
- Hong, S. K., Nakano, Y., and Kato, H. 1990. "Improvement of Dynamic Characteristics of Cylindrical Grinding Machines by Means of Dynamic Dampers." Proceedings of the 1st International Conference on New Manufacturing Technology, Chiba (Japan).
- Horiuchi, O. and Kojima, H. 1986. "A New Liquid-injection Type Automatic Balancer for the Grinding Wheel" (in Japanese). *JSPE* 52, 2, 713–718.
- Hoshi, T., Matsumoto, S., Mitsui, S., Horiuchi, O., and Koumoto, Y. 1986. "Suppression of Wheel-Regenerative Grinding Vibration by Alternating Wheel Speed" (in Japanese). *JSPE* 52, 10, 1802–1807.
- Inasaki, I. 1975. "Ratterschwingungen beim Außen-rund-Einsteichschleifen." *Werkstatt Betrieb*. 108, 6, 341–346.
- Inasaki, I. 1977a. "Regenerative Chatter in Grinding." Proceedings of the 18th MTDR Conference.
- Inasaki, I. 1977b. "Selbsterregte Ratterschwingungen beim Schleifen, Methoden zu ihrer Unterdrückung." *Werkstatt Betrieb*. 110, 8, 521–524.
- Inasaki, I. and Yonetsu, S. 1969. "Forced Vibrations during Surface Grinding." *Bull. JSME* 12, 50, 385–391.
- Inasaki, I., Yonetsu, S., and Shimizu, T. 1974. "Selbst-erregte Schwingungen beim Aussenrundeinsteichschleifen." *Ann. CIRP* 23, 1, 117–118.
- Kaliszer, H. 1963. "Accuracy of Balancing Grinding Wheels by Using Gravitational and Centrifugal Methods." Proceedings of the 4th International MTDR Conference. Advances in MTDR.
- Rowe, W. B. and Barash, M. M. 1964. "Computer Method for Investigating the Inherent Accuracy of Centerless Grinding." *Int. J. Mach. Tool Design Res.* 4, 91–116.
- Sexton, J. S. and Stone, B. J. 1981. "The Development of an Ultrahard Abrasive Grinding Wheel Which Suppresses Chatter." *Ann. CIRP* 30, 1, 215–218.
- Shimizu, T., Inasaki, I., and Yonetsu, S. 1978. "Regenerative Chatter during Cylindrical Traverse Grinding." *Bull. JSME* 21, 152, 317–323.
- Sugihara, K., Inasaki, I., and Yonetsu, S. 1980a. "Stability Limit of Regenerative Chatter in Cylindrical Plunge Grinding – A Proposal of the Practical Stability Limit Equation" (in Japanese). *JSPE* 46, 2, 201–206.
- Sugihara, K., Inasaki, I., and Yonetsu, S. 1980b. "Stability Limit of Regressive Chatter in Cylindrical Traverse Grinding" (in Japanese). *JSPE* 46, 3, 305–310.
- Tönshoff, H. K. and Gosebruch, H. 1988. "Verstellbarer passiver Dämpfer für Schwingungen in Außenrundschleifmaschinen." *VDI-Z* 130, 5, 57–60.
- Trmal, G. and Kaliszer, H. 1976. "Adaptively Controlled Fully Automatic Balancing System." Proceedings of the 17th International MTDR Conference.
- Weck, M. and Brecher, C. 2001. "The Essential Difference of the Chatter Phenomena between Processes with Defined and Undefined Cutting Edges." Technical Presentation in CIRP-STC "G," Paris, January.
- Younis, M. A. 1972. "Theoretische und praktische Untersuchung des Ratterverhaltens beim Außen-rundschleifen." *Industrie-Anzeiger* 94, 59, 1461–1465.

---

# 9 Grinding Wheel Wear

## 9.1 THREE TYPES OF WHEEL WEAR

### 9.1.1 INTRODUCTION

As a result of process forces during grinding, a grinding wheel is subject to modification by a process of wheel wear. Wear leads to changed process conditions and quality deviations in the component. Figure 9.1 shows three different types of grinding wheel wear: profile deviation, roundness deviation, and changes in grinding wheel sharpness.

In plunge grinding, where the wheel profile is reproduced in the ground component, profile deviations lead to workpiece shape defects. In the case of longitudinal grinding, profile deviations lead to screw thread undercuts. Roundness deviations make the machine system vibrate by dynamic alternating forces, which cause chatter marks to be machined on the component.

Loss of grinding wheel sharpness leads to higher grinding forces, which may entail dynamic and thermal deflections between the grinding wheel and workpiece, as well as uncontrolled grinding processes leading to chatter marks on the component. Finally, there will be shape and position errors, as well as dimensional deviations on the component. These modifications of the grinding wheel in the course of the grinding process are due to wear and result from microscopic changes in the abrasive grains and alterations in the chip space.

## 9.2 WHEEL WEAR MECHANISMS

Wheel wear results from material loss at the wheel surface, which can be traced back to mechanical contact between the wheel moving relative to the workpiece or any other body such as the dressing tool. Wear effects can be ascribed to the following main mechanisms: abrasion, adhesion, tribochemical reactions, surface disruption, and diffusion [DIN 50320 1979, DIN 50323 1988].

### 9.2.1 ABRASIVE WHEEL WEAR

As a prerequisite of abrasive wear, the surface of one of the two interacting partners of the abrasive process must be penetrated and a tangential movement must take place between them. The result is plastic and elastic deformations with groove and chip formation in the microrange. Grooving wear dominates, when hard workpiece material particles or loose particles of grain in the contact zone lead to surface changes in the wheel [Engelhorn 2002].

### 9.2.2 ADHESIVE WHEEL WEAR

Adhesion wear is based on an atomic bond at a microcontact surface between the active partners of the wear process through microwelding. This bond is very strong, which means that shearing through the relative movement of the active parts takes place at a different place than that of the original microcontact surface. Chemical adhesion is based on atomic interaction through thermally induced diffusion processes. In contrast, in mechanical adhesion, the surfaces of the active parts are engaged in the microrange, while high temperatures lead to surface deformation [Telle 1993].



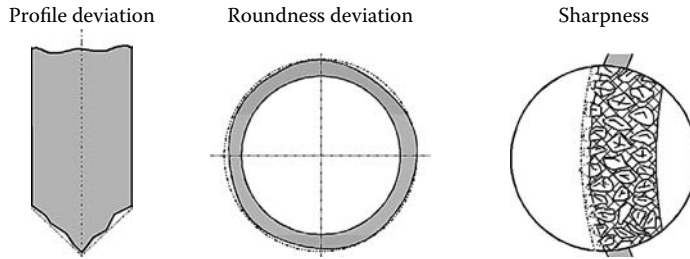


FIGURE 9.1 Types of grinding wheel wear.

### 9.2.3 TRIBOCHEMICAL WHEEL WEAR

In the case of tribochemical wear, chemical reactions take place either between the active partners of the wear process or with the surrounding environmental medium. These chemical reactions cause changes in the boundary layer properties, which lead to adhesion of reaction products on the abrasive grain and to grain damage. Factors of a tribochemical reaction are chemical affinity between the active partners and ambient conditions such as temperature, pressure, and concentration.

### 9.2.4 SURFACE DISRUPTIONS

Surface disruptions can be traced back to mechanical thermal alternating pressures opening up grain boundaries and cleavage planes. This leads to structure changes, fatigue, cracks, and separation of single particles causing breakage and cutting material failure [Zum Gahr 1987, Telle 1993].

### 9.2.5 DIFFUSION

Prerequisites of diffusion processes in the working zone are the adequate activation energy and a sufficient chemical potential of the active partners. The diffusion accounts for a thermal activation of single atoms, which, as a result, change places. This causes material loss, and impurity atoms are inserted into the grain surface, which might lead to a loss of hardness. Surface diffusion processes can be divided into intercrystalline diffusion along the grain boundaries and transcristalline diffusion into the grain volume.

## 9.3 WEAR OF THE ABRASIVE GRAINS

### 9.3.1 TYPES OF GRAIN WEAR

Overlap between the above-mentioned wear mechanisms leads to changes in the abrasive grain. These wear types are depicted in Figure 9.2. They basically can be divided into

- Flattening
- Microcrystalline grain splintering
- Partial grain break-off, and
- Total grain break-off

### 9.3.2 A COMBINED WEAR PROCESS

The strength of the particular wear process depends on the process parameters and on the grain and bond properties. The character of the wear process is governed by contributions from thermal and mechanical wear, which are determined by machining parameters, cooling and lubrication conditions, and process kinematics. Grinding wheel properties are determined by the stability and

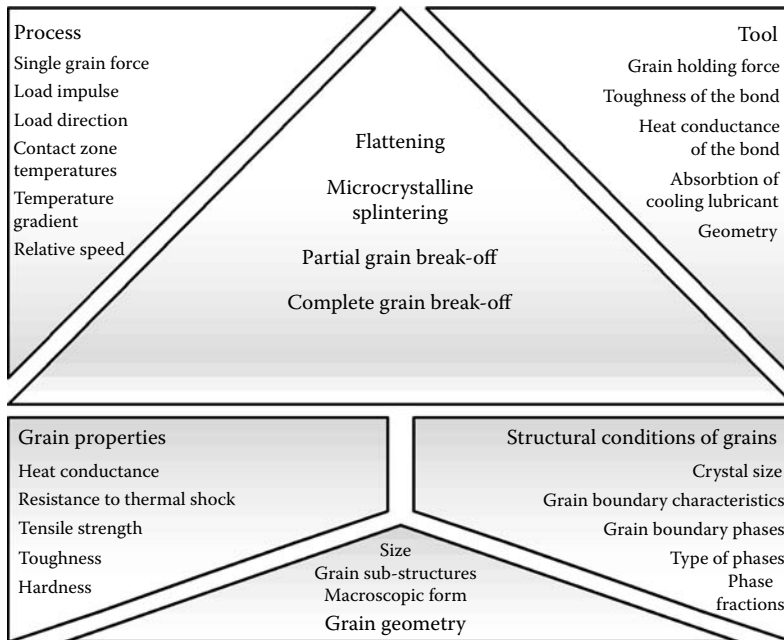


**FIGURE 9.2** Influences on grain wear. (From Anon. 2003a. With permission.)

thermal diffusivity of the grinding wheel bond. Additionally, the basic porosity of the bond has a crucial influence on lubricant absorption and thus on the thermal conditions within the working zone. The abrasive grains of the abrasive medium differ in terms of hardness, tensile strength, and ductility. The fracture and splintering behavior can thereby be controlled by screening procedures during abrasive manufacture and the synthesis process [Juchem and Martin 1989, Jackson and Hayden 1993, Uhlmann and Stark 1997].

### 9.3.3 GRAIN HARDNESS AND TEMPERATURE

Hardness of the abrasive grains also depends on the process conditions. Figure 9.3 shows the hardness of polycrystalline sintered corundum grains with changing process temperature. With increasing temperature, abrasive grain hardness declines. At 800°C, it is approximately 25% compared to room temperature. The wear resistance of the grains depends not only on the hardness at ambient temperature, but more importantly on the hardness at the operating contact temperatures.

### 9.3.4 MAGNITUDE OF THE STRESS IMPULSES

The strength of the grain wear process is related to the magnitude of the stress impulses of the abrasive interactions. As an example, Figure 9.4 shows the abrasive grains of a D126 St50 grinding wheel with a concentration of C90 during grinding silicon carbide. In the left part of the image, the wear is typified by a wear flat developed on the grain. By increasing the magnitude of the stress impulses by superposing an ultrasonic oscillation, the wear process can be changed leading to splintering under otherwise similar process conditions, thus generating new sharp grain cutting edges.

### 9.3.5 GROWTH OF GRAIN FLATS

Reasons for the flattening of single grains are the above-mentioned mechanisms of abrasion, adhesion, corrosion, and diffusion. Flats only develop at the grain tip area at low single-grain forces

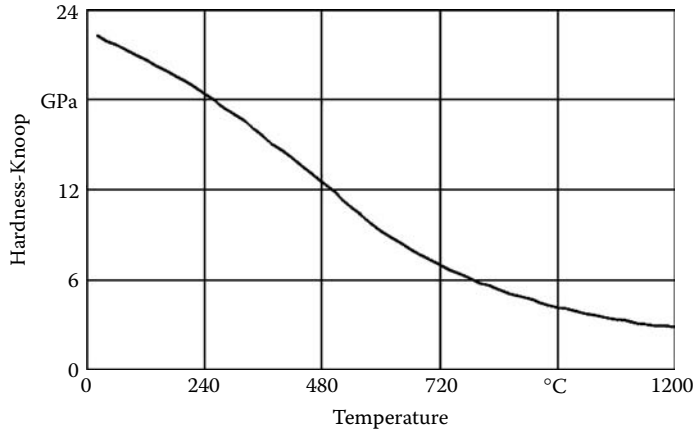


**FIGURE 9.3** Hardness against temperature in polycrystalline sintered corundum abrasive grains. (From Anon. 2003c. With permission.)

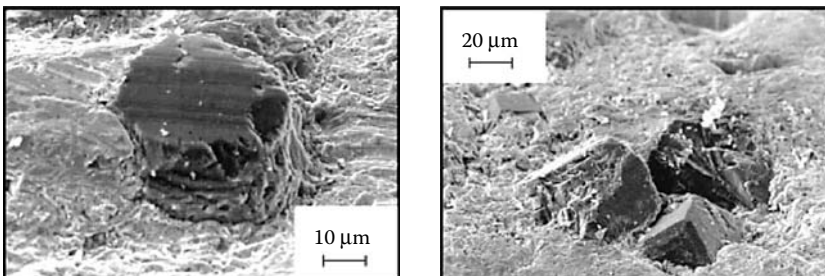
and high process temperatures. Hence, the grinding wheel specification must be adjusted for the process conditions. A grinding wheel specified for reciprocating grinding cannot be sensibly used in other fields of application. Therefore, if the wheel is used in deep feed grinding or in internal cylindrical grinding, grain flats may be increased due to decreased single-grain forces and increased process temperatures [Uhlmann and Stark 1997].

Figure 9.5 shows a model of a D126 C100 grinding wheel surface in a topography section of  $1 \times 1 \text{ mm}^2$ . The topography is depicted first for flattened grains and second for process conditions with normal splintering behavior. All other characteristics of the grinding wheel remain unchanged.

A clear change of parameters can be seen in the tip area. Flattening can only be verified by these parameters. The high material rate in the tip area leads to a high reduced groove depth,  $R_{pk}$ , and to a high tip surface  $A_1$  on the flattened grain. The parameters of the groove area are not affected by flattening.

### 9.3.6 GRAIN SPLINTERING

A further grain wear type is microcrystalline grain splintering. This wear type is caused by microcracks resulting from mechanical and thermal tensions. These microcracks lead to a microfracture, or even to partial grain break-off.



**FIGURE 9.4** Grain splintering and flattening. (From Uhlmann and Daus 2000. With permission.)

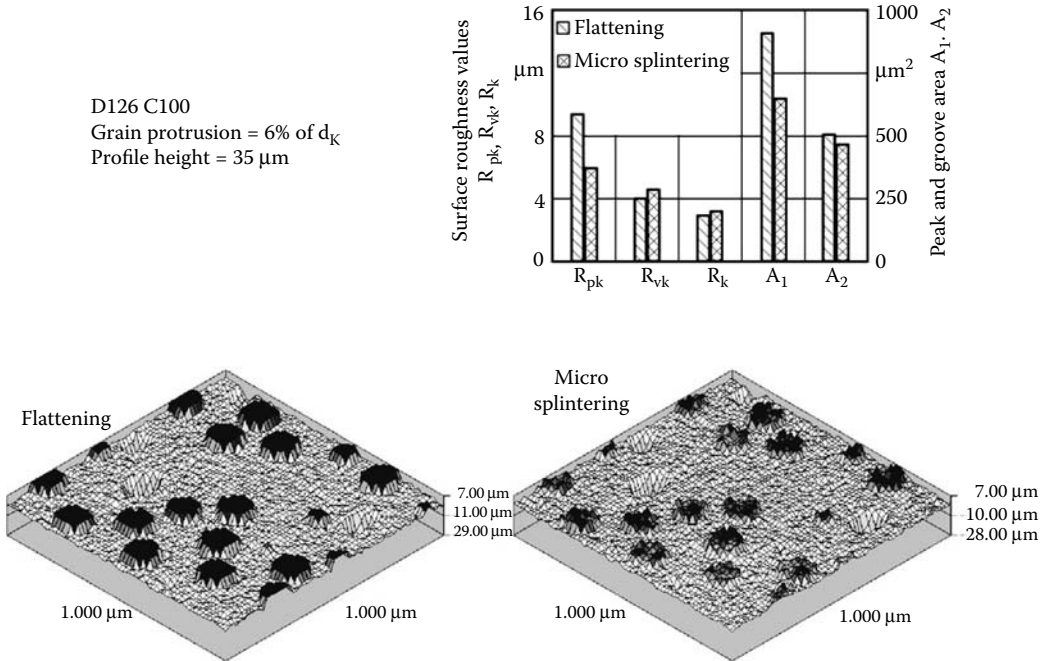


FIGURE 9.5 Influence of grain flattening on the grinding wheel topography.

### 9.3.7 GRAIN BREAK-OUT

In the case of total grain break-off, whole abrasive grains are detached from the bond. The reason is a mechanical overstress of the bond due to excessive grain protrusions, as well as by excessive process temperatures. In these cases, the grain retention forces are smaller than the process forces. If a grinding wheel bond is subject to thermal overstress, especially in the case of a resin bond, the bond might soften. It is also possible for the decomposition temperature of the binding material to be reached. The grain break-off force decreases with a growing grain protrusion [Yegenoglu 1986].

### 9.3.8 BOND SOFTENING

Figure 9.6 shows two grinding wheel topographies, the right one showing a cumulative grain break-off due to increasing bond softening. At constant bond wear, this leads to a deeper embedding of the abrasive grain. The result in the present case is a decreasing number of cutting edges and increased stress on the surrounding grains. If bond wear increases due to bond softening, this leads to increased radial wear of the wheel.

Figure 9.6 also shows the parameters of the grinding wheel topography. It clearly can be seen how the groove parameters  $A_2$  and  $R_{vk}$  grow with increasing grain break-off.

### 9.3.9 EFFECT OF SINGLE GRAIN FORCES

Wear occurs on the basis of single-grain forces and process temperatures [Marinescu et al. 2004]. Continuously sharp grain cutting edges are favorable for the grinding process and for a high grinding ratio,  $G$ . This requires microcrystalline grain splintering.

Wear types depend on the thermal mechanical grain stress. Figure 9.7 presents the qualitative depiction of grain flat growth, microcrystalline splintering, partial grain break-off, and total grain break-off against the thermal and mechanical grain stress.

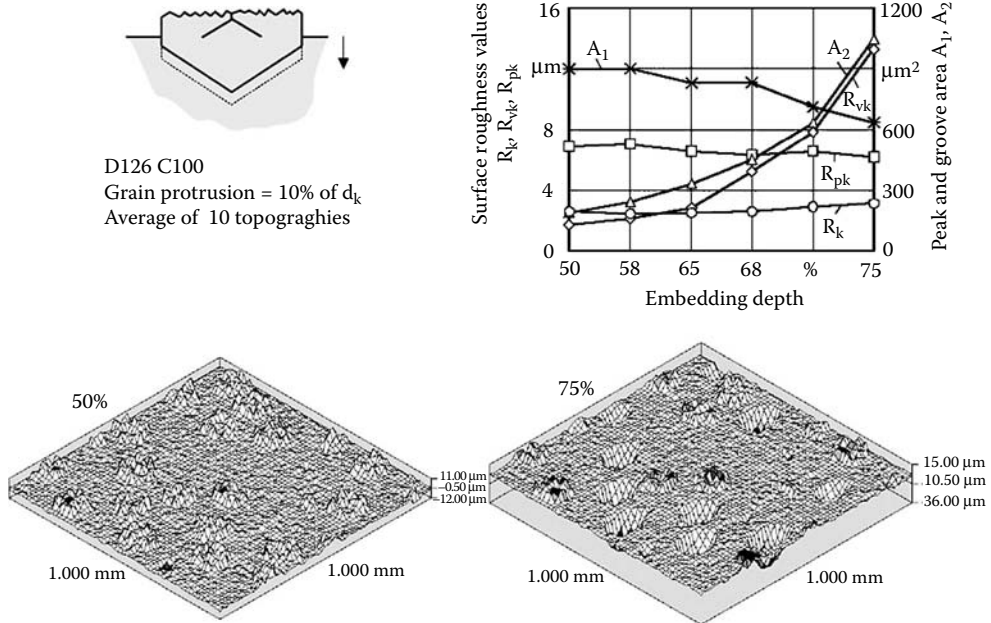


FIGURE 9.6 Topography behavior with increasing grain break-off.

To achieve the desired microcrystalline grain splintering, an initial force is necessary that depends on the grain properties as well as on the grain structure. If this initial force is not achieved, the wear type shifts to grain flattening. If the initial force is exceeded, the wear mechanism shifts over partial grain break-off to total grain break-off. Through the selection of the grain specification and by changing the grinding material concentration and bond structure, the grinding wheel can be adjusted to the desired single grain forces achieving the necessary initial force for microsplintering.

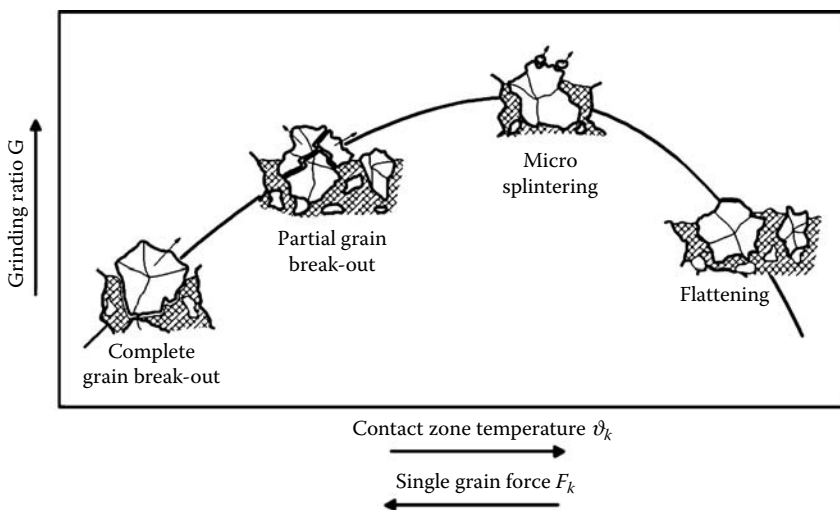


FIGURE 9.7 Strength of wear type against the process conditions. (From Uhlmann and Stark 1997. With permission.)

### 9.3.10 WEAR BY DEPOSITION

Besides the above-mentioned wear types, wear by deposition may also occur. Workpiece material residues are deposited under high pressure in the chip space, where they are held by undercut. Since these depositions are built up over several cutting edges, no cutting is possible any more with these grains [Lauer-Schmaltz 1979].

## 9.4 BOND WEAR

### 9.4.1 INTRODUCTION

Not only the abrasive grain, but also the grinding wheel bond is increasingly subject to wear. The reason is abrasion by ground material particles, which have an abrasive effect on the binding material. With increasing wear, the bond is set back. In the case of long-chipping materials, this bond damage may occur at the grain cutting edges through the flowing chip, whereas in the case of short-chipping materials, wear occurs through a lapping process in the chip space.

For efficient grinding, new multilayer grinding wheels usually have a grain protrusion of 20% to 30% of the nominal grain diameter. This grain protrusion is necessary for the cutting process to evacuate the removed material volume and to let the cooling lubricant reach the active area.

### 9.4.2 BALANCING GRAIN AND BOND WEAR

Constant process conditions require constant grain protrusion above the bond level. This implies a uniform grain and bond wear. Besides the specification of grain and bond, the application criteria are decisive for the wear balance. A balance occurs in the so-called self-sharpening range, when blunt grains constantly detach from the bond giving way to succeeding sharp grains as new cutting edges in the grinding process. Thus, the grinding wheel is constantly ready to work; see Figure 9.8 [Warnecke et al. 1994, Anon. 2003a].

If the grinding wheel is badly adjusted, the grain and bond wear are unbalanced. If the bond wear is too low compared to the grain wear, the grinding layer becomes blunt with insufficient grain protrusion. The process behavior is characterized by high process forces with thermal and mechanical overstress. This results in thermal damage and chatter marks on the component.

If bond wear is excessive in a super-sharp grinding wheel, the embedded depth of the grains decreases and the grain-holding forces with it. The result is excessive radial wear of the grinding wheel, which makes the process uneconomic. Hence, the ideal bond is not that with the lowest wear, but the one with the best adjustment to grain wear.

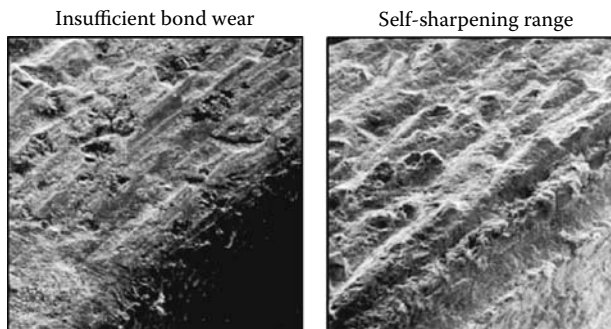


**FIGURE 9.8** Grinding layer of a cubic boron nitride grinding wheel with resin bond with too low bond wear and in the self-sharpening range. (From Anon. 2003a. With permission.)

Grinding with continuous in-process sharpening has been developed as a reaction to topographic changes in the grinding wheel during the process leading to nonstationary process behavior. This technology allows for machining processes, which, under conventional process conditions, lead to system overstress. Moreover, a specific control of the parameter level is possible for nearly all grinding tasks [Spur 1989, Tio 1990, Carlsburg 1993, Liebe 1996].

## 9.5 ASSESSMENT OF WHEEL WEAR

### 9.5.1 MICROTOPOGRAPHY

The current microtopography of the grinding tool can be judged directly by measurement or reproduction, or indirectly by analyzing the process effects or the work result. The best-known methods for a direct judgment of the grinding wheel topography are the measurement of the tool surface by gauging, for example, by laser triangulation or by profile method, or making imprints for a judgment under the microscope. The direct methods known today have the disadvantage that they can only be realized by intervening into the process disturbing the thermal balance [Brinksmeier and Werner 1992, Tönshoff 1998, Warnecke 2000, Marinescu et al. 2004].

### 9.5.2 PROFILE WEAR

Through its varying size and strength at the profile edges of the grinding wheel during the process, increasing microwear leads to an increase in macrowear. These profile deviations entail quality deviations on the component. It is especially at the exposed profile tips of the grinding wheel where the process stress is the highest and edge rounding occurs. Figure 9.9 shows the profile wear of a D126 C50 diamond grinding wheel with resin bond grinding an SSiC-ceramic. The grinding wheel profile angle is  $\alpha_s = 45^\circ$ .

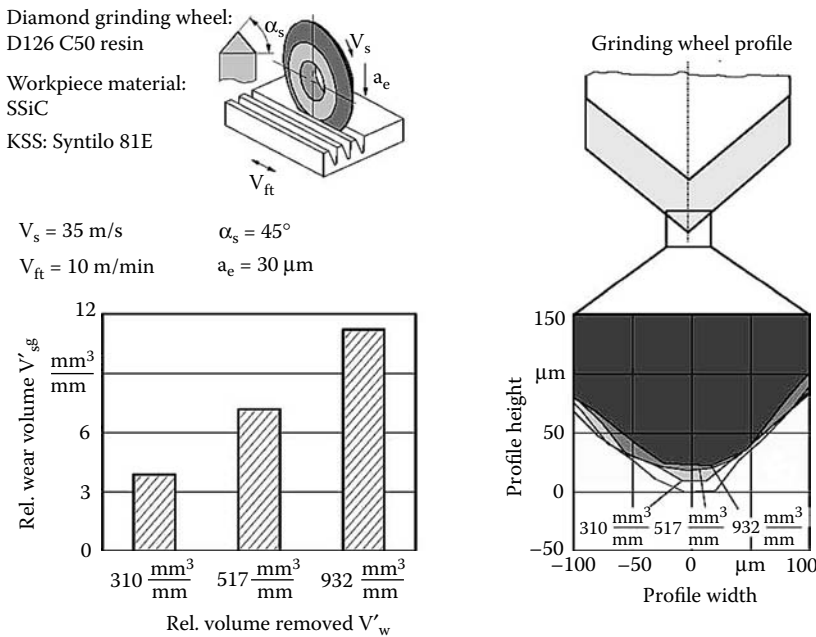


FIGURE 9.9 Profile wear of a diamond grinding wheel with resin bond machining silicon carbide.

The right-hand part of the image shows the increasing edge rounding in the course of the process. In this range, the wear volume of the grinding wheel profile also increases. The loss of grinding wheel volume, observable as the difference between the grinding wheel volume in the newly profiled state and that after the subsequent profiling, is characteristic for the wheel life up to the total consumption of the grinding layer. It is composed of the volume worn in the grinding process and that removed during dressing. Since the grinding wheel re-obtains the required shape in the profile dressing process, the maximum radial wear can be determined for the radial loss. The loss volume can be calculated by multiplying this sum by the geometry parameters of the grinding wheel. Finally, the dressing volume can be calculated by knowing the other two volumes. It gives information on the required regeneration effort of the profile in the profile dressing process, representing a decisive cost factor especially when using superabrasive grinding wheels [Malkin 1989, Liebe 1996, Klocke et al.1997].

## REFERENCES

- Anon. 2003a. Diamant- und CBN-Schleifscheiben. Firmeninformation der Fa. Winter & Sohn GmbH, Norderstedt, [www.winter-diamantwerkz-saint-gobain.de](http://www.winter-diamantwerkz-saint-gobain.de).
- Anon. 2003b. Hermes Schleifkörper. Firmeninformation der Fa. Hermes Schleifmittel GmbH, Hamburg, [www.hermes-schleifmittel.de](http://www.hermes-schleifmittel.de).
- Anon. 2003c. Firmeninformation der Fa. Hermes Schleifmittel GmbH, Hamburg.
- Brinksmeier, E. and Werner, F. 1992. "Monitoring of Grinding Wheel Wear." 42nd General Assembly of CIRP, Aix-en-Provence, F, Aug. 23 to 29, *Ann. CIRP* 41.
- Cartsburg, H. 1993. "Hartbearbeitung keramischer Verbundwerkstoffe." Ph.D. thesis, TU Berlin. Hanser, München.
- DIN 50320. 1979. "Verschleiß, Begriffe, Systemanalyse von Verschleißvorgängen, Gliederung des Verschleißgebietes." Beuth Verlag, Berlin.
- DIN 50323. 1988 and 1993. "Tribologie; Verschleiß, Begriffe." Teil 1 Nov. 1988, Teil 2 (Entwurf) Nov. 1993, Deutscher Normenausschuss. Beuth Verlag, Berlin.
- Engelhorn, R. 2002. "Verschleißmerkmale und Schleifeinsatzverhalten zweiphasig verstärkter Sol-Gel-Korunde." Ph.D. thesis, RWTH Aachen.
- Jackson, W. E. and Hayden, S. C. 1993. "Quantifiable Diamond Characterization Techniques: Shape and Compressive Fracture Strength." Proc. Diamond & CBN Ultrahard Materials Symposium. Windsor, Canada.
- Juchem, H. O. and Martin, J. S. 1989. "Verbrauch an Diamant- und CBN-Körnungen steigt stetig." *IDR* 23, 2.
- Klocke, F., Hegener, G., and Muckli, J. 1997. "Innovative Schleifwerkzeuge sichern Wettbewerbsvorteile." VDI-2, vol. 139, 7–8, Springer VDI Verlag, Düsseldorf, Germany.
- Lauer-Schmaltz, H. 1979. "Zusatzung von Schleifscheiben." Ph.D. thesis, RWTH Aachen.
- Liebe, I. 1996. "Auswahl und Konditionierung von Werkzeugen für das Außenrund-Profilerschleifen technischer Keramiken." Ph.D. thesis, TU-Berlin.
- Malkin, S. 1989. *Grinding Technology*. Ellis Horwood, New York.
- Marinescu, I. D., Rowe, W. B., Dimitrov, B., and Inasaki, I. 2004. *Tribology of Abrasive Machining Processes*. William Andrew Publishing, Norwich, NY.
- Spur, G. 1989. *Keramikbearbeitung - Schleifen, Honen, Läppen, Abtragen*. Hanser, München.
- Telle, R. 1993. Werkstoffentwicklung und Materialverhalten moderner Schneidkeramiken, in *Werkzeuge für die moderne Fertigung*; Hrsg.: W. Bartz, Technische Akademie Esslingen, vol. 370, Expert Verlag.
- Tio, T. H. 1990. "Pendelplanschleifen nichtoxidischer Keramiken." Ph.D. thesis, Verlag Hanser, TU-Berlin.
- Tönshoff, H., Karpuschewski, B., Andrae, P., and Türich, A. 1998. "Grinding Performance of Superhard Abrasive Wheels – Final Report Concerning CIRP-Co-Operative Work in STG G." *Ann. CIRP* 47, 2.
- Uhlmann, E. 1994. "Tiefschleifen hochfester keramischer Werkstoffe." Ph.D. thesis, München: Hanser, TU-Berlin.
- Uhlmann, E. 1996. "Entwicklungsstand von Hochleistungsschleifwerkzeugen mit mikrokristalliner Aluminiumoxidschleifkörnung." Proc. 8. Int. Braunschweiger Feinbearbeitungskolloquium. 24–26/04.



- Uhlmann, E. and Daus, N. 2000. "Ultrasonic Assisted Face Grinding and Cross-Peripheral Grinding of Ceramics." Proceedings of the 7th International Symposium. Cer. Mat.Com. Eng. Goslar, 19–21/06.
- Uhlmann, E. and Stark, C. 1997. "Potentiale von Schleifwerkzeugen mit mikrokristalliner Aluminiumoxidkörnung." Beitrag 58. Jahrbuch Schleifen, Honen, Läppen und Polieren.
- Warnecke, G. 2000. Zuverlässige Hochleistungskeramik. Abschlussbericht zum BMBF-Verbundprojekt "Prozesssicherheit und Reproduzierbarkeit in der Prozesskette keramischer Bauteile." Kaiserlautern.
- Warnecke, G., Hollstein, T., König, W., Spur, G., and Tönshoff, H.-K. 1994. Schleifen von Hochleistungskeramik — Werkstoff, Anwendung, Bearbeitung, Qualität. zugl. Abschlußbericht BMFT Verbundprojekt "Schleifen von Hochleistungskeramik." Verlag TÜV Rheinland, Köln.
- Yegenoglu, K. 1986. "Berechnung von Topographiekenngößen zur Auslegung von CBN-Schleifprozessen." Ph.D. thesis. RWTH Aachen.
- Zum Gahr, K.-H. 1987. *Microstructure and Wear of Materials*. Elsevier Science, Amsterdam.

---

# 10 Coolants

## 10.1 INTRODUCTION

Coolant is a term generally used to describe grinding fluids used for cooling and lubrication in grinding. The main purpose of a grinding fluid is to minimize mechanical, thermal, and chemical impact between the active partners of the abrasion process. The lubricating effect of a grinding fluid reduces friction between the abrasive grains and the workpiece, as well as between the bond and the workpiece. A second requirement of a grinding fluid is direct cooling of the grinding contact zone through the absorption and transportation of the heat generated in the grinding process. Other functions of a grinding fluid are the evacuation of chips from the contact zone, bulk cooling of the workpiece and the grinding machine, and corrosion protection [König and Klocke 1996, Marinescu et al. 2004].

## 10.2 BASIC PROPERTIES OF GRINDING FLUIDS

### 10.2.1 BASIC PROPERTIES

The selection of a grinding fluid is of crucial significance for the achievement of favorable cooling and lubricating conditions. Type, base oil, additives, and concentration of the fluid are all important for the efficiency of cooling and lubrication. Cooling and lubrication requirements are met in different ways by every particular grinding fluid. Depending on the contact conditions in the process, the cooling and lubricating properties of the applied grinding fluid have a substantial impact on the process and on the work result.

### 10.2.2 BASIC REQUIREMENTS

The basic requirements of a grinding fluid are good lubrication, good cooling and flushing performance, and high corrosion protection.

### 10.2.3 SECONDARY REQUIREMENTS

Secondary requirements are economic and efficient operation, operational stability (long life), and environmental protection.

It is imperative for grinding fluids to be compatible with environmental and human health, as well as being reliable in operation. Additional requirements of the fluid are

- Easily filtered and recycled
- The residual film is easily removed from the workpiece, grinding wheel, and machine
- Provides solid particle transport for swarf removal
- Inhibits foaming and mist formation
- Exhibits low flammability
- Exhibits good compatibility with the materials of the machine tool system

In the case of water composite fluids, mixing behavior and emulsifiability must be considered (Table 10.1).

**TABLE 10.1**  
**Important Properties of Cooling Lubricants**

Usage Properties	
Functional Properties	Operational Behavior
Lubrication effect (pressure absorption capacity)	Human and environmental compatibility (toxicity, odor, skin compatibility)
Cooling effect	Resistance to aging and bacteria (stability)
Flushing effect (cleaning, chip transport)	Filterability, recycleability, mixing behavior, emulsifiability
Corrosion protection	Washability, residual behavior, solid particle transport capability
	Foam, fog behavior, inflammability
	Compatibility with different materials

*Source:* From Brücher, 1996. With permission.

The functional properties and the operational behavior of cooling lubricants are significantly influenced by physical-chemical properties. Thermal capacity and conductivity, evaporation heat, and viscosity are affected by the quantitative ratios of the base materials used. Additionally, the performance of a cooling lubricant can be adjusted by the addition of active substances and additives.

### 10.3 TYPES OF GRINDING FLUIDS

Grinding fluids are commercially available with different property profiles to meet the requirements of specific machining tasks. DIN 51 385 divides grinding fluids into

- Water-immiscible
- Water-miscible
- Water composite fluids

The more general fields of application of cooling lubricants are cutting and partial forming processes [DIN 51 385].

**Water-immiscible cooling lubricants** are generally not mixed with water for any application [DIN 51 385].

**Water-miscible cooling lubricants** are emulsifiable, emulsifying, or water-soluble concentrates, to which water is added before use.

**Water-composite cooling lubricants** are ready-for-use composites of water-miscible cooling lubricants with water. Within the group of water-miscible cooling lubricants, DIN 51 385 subdivides:

- Oil-in-water emulsions
- Water-in-oil emulsions
- Cooling lubricant solutions

For cutting, mainly oil-in-water emulsions and solutions are used, whereas water-in-oil emulsions are less common [Eckhardt 1983].

There are differences within the group of water-immiscible cooling lubricants according to the fraction and the type of the active substances contained [Bartz 1978, VDI-Richtlinie 3396 1983]. Classification within the group of water-miscible cooling lubricants is carried out according to the

content of active substances or to droplet size in rough disperse and fine disperse emulsions, as well as in fine colloidal, micellar, and molecular disperse solutions [Bartz 1978, VDI-Richtlinie 3396 1983].

The group of water-immiscible cooling lubricants also comprises natural and synthetic hydrocarbons such as mineral oils or poly- $\alpha$ -olefins, synthetic and vegetable ester, as well as water- and oil-soluble polymers such as polyglycols or composites of these substances [König et al. 1993]. To improve their lubricating properties and their pressure absorption capacity, either chemically active Extreme Pressure (EP), substances, or polar agents binding the lubricating film can be added to the base oils. Furthermore, water-immiscible and water composite cooling lubricants may contain corrosion, foam, and oxidation inhibitors or anti-fog additives [VDI-Richtlinie 3396 1983, Korff 1991, König et al. 1993].

Oil-in-water-emulsions are mainly stable disperse composites of water and mineral oil or esters, which contain finely dispersed oil droplets in a water phase [König et al. 1993]. The appropriate concentration of cooling lubricant emulsions must be determined for every single case of application depending on the corrosion protection capacity of the emulsions and on the cutting conditions. Conventional emulsion concentrations for grinding are in the range of 2% to 6% [Eckhardt 1983], or in special cases up to 20% [Klocke 1982]. Oil and water can be amalgamated with the help of bipolar surface-active substances. These substances favorably dissolve at the interface of the oil and water phase of an emulsion reducing the surface tension. Emulsifiers thus reduce the natural striving of the disperse phase to minimize the surface area [Mang 1983, Spur 1983, Möller and Boor 1986, König et al. 1993, Kassack 1994]. Through the variation of the emulsifier content or of the emulsifier type, different grades of dispersion can be set. Water-miscible solutions are made of completely water-soluble inorganic (e.g., water-soluble salts) or organic (e.g., polyglycols, boron acid amide) active agents for the improvement of corrosion protection and wetting capability, and are free of mineral oil [Bartelt and Studt 1992, Möller & Boor 1986, König et al. 1993]. Usually, cooling lubricant solutions are used as emulsions in low concentration [Eckhardt 1983]. Water composite cooling lubricants contain EP-additives, polar active agents, stabilizers, solution agents, preservatives, and corrosion and foam inhibitors in order to improve their functional properties [Bartz 1978, Spur 1983, VDI-Richtlinie 3396 1983, Möller and Boor 1986, König et al. 1993].

## 10.4 BASE MATERIALS

### 10.4.1 INTRODUCTION

In many cases, mineral oils are used as the base material for cooling lubricants. Mineral oil bases consist of hydrocarbons with mostly paraffinic, naphthenic, or aromatic structures. Depending on the fraction of the paraffins, naphthenes, and condiments, a distinction can be made between paraffin-based, naphthene-based, and mixed base oils [Mang 1983, Möller and Boor 1986]. The main advantages of paraffinic base oils in cooling lubricants are good viscosity-temperature behavior, high aging resistance, small affinity to evaporation, high flashpoint, and low toxicity. In contrast to paraffin-based mineral oils, the advantages of naphthene-based oils are their good resistance to cold, better thermal stability, higher moistening capacity, and active agent solubility [Möller and Boor 1986, Pfeiffer et al. 1993]. Extracted and deparaffined solvent-rafines or hydrocrack oils are gaining even more importance due to a lower condiment ratio, less mist generation, and high resistance to aging [König et al. 1993, Kassack 1994]. Also, synthetically produced poly- $\alpha$ -olefins, polyglycols, and esters are increasingly used, which, in contrast to mineral oils, have higher viscosity indices, a lower affinity to evaporation, longer service life as a result of high thermal stability, and/or resistance to oxidation and high human compatibility. Additionally, esters have especially good lubricating characteristics [Mang 1983, König et al. 1993, Pfeiffer 1993, Kassack 1994]. General values of the kinematic viscosity of cutting and grinding oils are in the range of  $\nu = 2.0$  to 45 mm<sup>2</sup>/s at 40°C [Mang 1983].

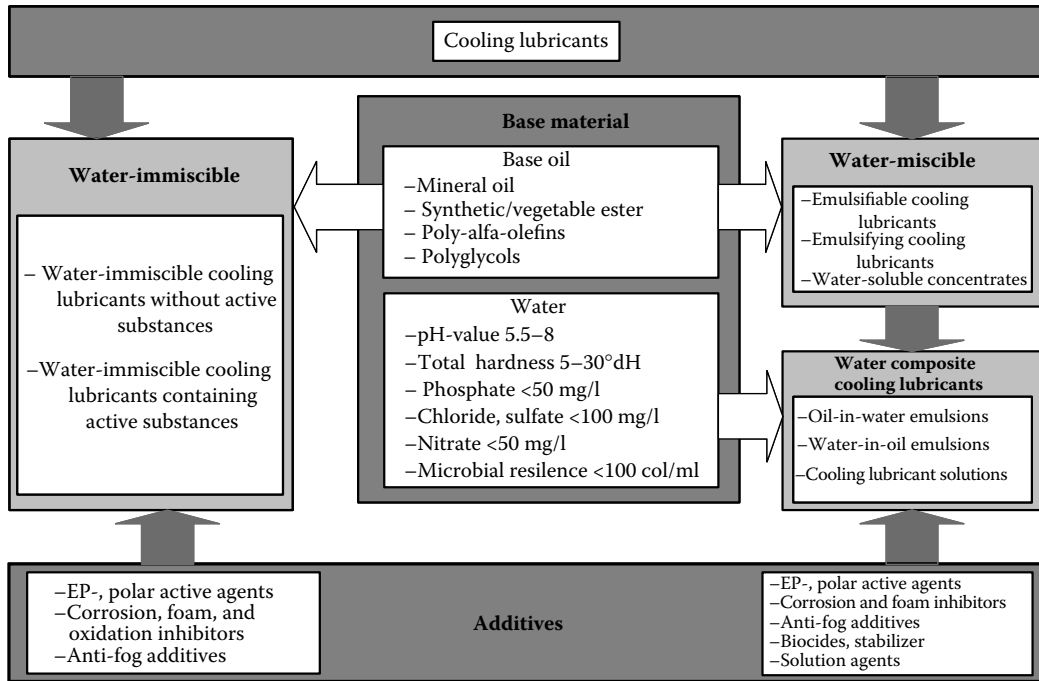


FIGURE 10.1 Classification and composition of cooling lubricants. (From Brücher 1996. With permission.)

#### 10.4.2 WATER-BASED AND OIL-BASED FLUIDS

In addition to the concentrates, water composite cooling lubricants contain a high percentage of water. The properties of this cooling lubricant group are, therefore, crucially influenced by the quality of the mixing water used, upon which special requirements must be placed concerning the nitrate, chloride, sulphate, and phosphate content, total hardness, pH-value, and the microbial resilience (Figure 10.1) [Möller and Boor 1986, Leiseder 1991, König et al. 1993, Pfeiffer 1993].

The most important base materials of water-immiscible and water composite cooling lubricants (water and mineral oil) have fundamentally differing thermal physical properties (Table 10.2). Hence, the capacity of a cooling lubricant to carry away thermal energy from the grinding process through heat absorption strongly depends on its water or mineral oil content. The cooling effect of cooling lubricants is, first of all, defined by their heat conductivity, evaporation heat, specific heat, and wetting capacity. Due to their high water fraction, cooling lubricant solutions are characterized by an efficient cooling effect. Compared to water-immiscible cooling lubricants, oil-in-water emulsions have a good cooling effect, too, which decreases in favor of a higher lubricating effect if the oil fraction is increased [Zwingmann 1979, König 1980, Eckhardt 1983, VDI-Richtlinie 3396 1983]. The cooling effect of water-immiscible cooling lubricants is also strongly influenced by viscosity. Low-viscosity cooling lubricants penetrate tight gaps much faster and are, therefore, better at dissipating heat.

#### 10.4.3 RINSING CAPACITY

The rinsing or washing capability of cooling lubricants depends on viscosity and wetting capacity. The surface tension against air is a measure of the wetting capacity of liquids. At a surface tension against air of approximately  $\sigma_o = 30$  mN/m, the wetting capacity of mineral oil is superior to water. Through the addition of detergents, however, the surface tension of water of approximately  $\sigma_o = 72$  mN/m can be reduced to  $\sigma_o = 30$  mN/m, too [Zwingmann 1960]. Generally, with decreasing

**TABLE 10.2**  
**Physical Properties of Water and Mineral Oil**

	Water	Mineral Oil
Density $\rho$ at 20°C in kg/m <sup>3</sup>	998.2	ca. 870
Specific heat $c_p$ at 20°C in J/gK	4.2	1.9
Heat conductivity $\lambda$ at 20°C in W/mK	0.58	0.14
Evaporation heat $\Delta h_v$ at 40°C in J/g	2,260	210
Kinematical viscosity $\nu$ at 40°C in mm <sup>2</sup> /s	0.6	approx. 2.0–45
Surface tension $\sigma_0$ against air in mN/m	73	30

*Source:* From Mang 1983, VDI-Richtlinie 3396 1983, Möller and Boor 1986.  
With permission.

viscosity, water-immiscible cooling lubricants exhibit better washing capability [Mang 1983, Spur 1983]. Due to the low viscosity, water-miscible cooling lubricants show a superior rinsing capacity compared to water-immiscible products [Spur 1983].

#### 10.4.4 LUBRICATING CAPABILITY

The lubricating capacity of a cooling lubricant first of all depends on the additives it contains. Also, viscosity influences the lubricating capacity of water-immiscible and water-miscible cooling lubricants. The kinematic viscosity of mineral oil is 15 times higher than that of water, and grinding oils generally have a better lubricating capacity than water composite cooling lubricants [Kohblanck 1956, Zwingmann 1979]. The lubricating effect of oil-in-water emulsions depends on the oil fraction it contains and increases with a larger percentage of oil. Since cooling lubricant solutions are free of mineral oil, they have a poorer lubricating capacity than emulsions [Eckhardt 1983]. Due to the high temperatures and pressures in the contact zone, the pressure absorption capacity of water and mineral oil is not sufficient concerning the formation of a stable lubricating film. For this reason, additives are added to state-of-the-art cooling lubricants to improve the lubricating properties.

#### 10.5 ADDITIVES

An important group of cooling lubricant additives are polar additives, whose molecules contain polar groups (Figure 10.2). Polar additives are mostly unsaturated hydrocarbon compounds such as fatty acids, fatty alcohol, and fatty acid esters. Due to their polarity, these agents firmly deposit on the workpiece surface and form an adhering lubricating film. Additionally, there are cases where chemical reactions occur between the material and the cooling lubricant additive developing metallic soaps acting as highly viscous, plastic lubricating films. Due to the low melting point of these metallic soaps of approximately 150°C, the impact of polar additives decreases with higher temperatures [Zwingmann 1979, König 1980, Spur 1983, VDI-Richtlinie 3396 1983, Korff 1991, König et al. 1993, Kassack 1994]. A further group of active agents are the so-called EP additives, which consist of phosphor and sulphur compounds. Additives previously used containing chlorine are barely applied nowadays due to ecological and physiological reasons [König et al. 1993, Kassack 1994]. EP additives generate metal phosphates or sulphides in the contact zone through chemical reactions with the workpiece surface. They act as solid lubricating layers with high pressure resistance and low shear strength. The minimum temperature necessary for the occurrence of this reaction depends on the used agent. Phosphor additives have a temperature range of approximately 50°C to 850°C, while sulfur-containing additives are active between approximately 500°C and 1,000°C [Keyser 1974, Zwingmann 1979, König 1980, Zimmermann 1982, Spur 1983, Kassack 1994]. To cover

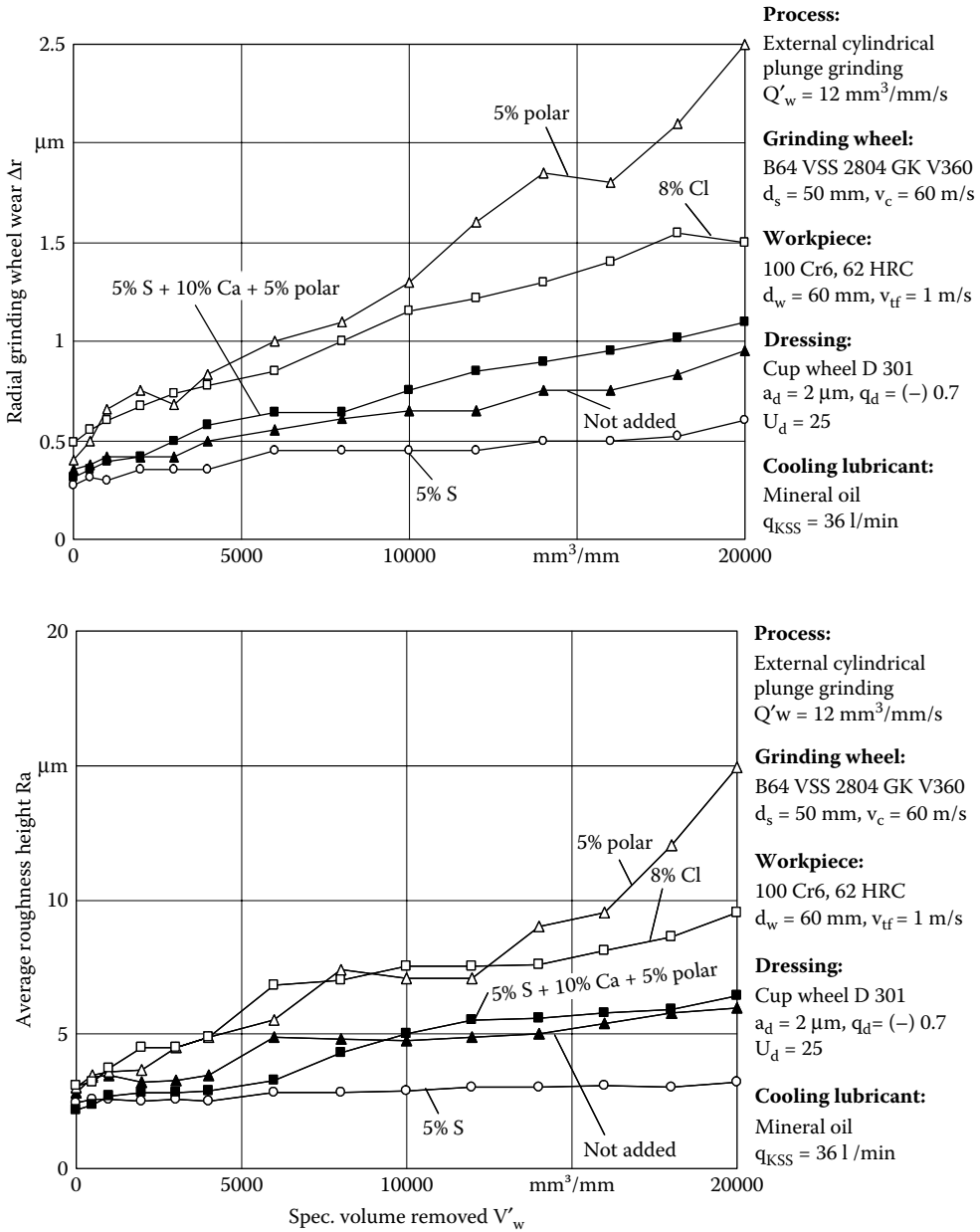


**FIGURE 10.2** Influence of different additives on the grinding wheel wear and surface quality during cylindrical grinding. (From Heuer 1992. With permission.)

a wide temperature range, EP additives that act at high temperatures are combined with polar additives that act at lower temperatures in the cutting process of metals. As an example, sulphur substrates on a fatty oil basis are often used in metal working [Korff 1991, Kassack 1994].

Other cooling lubricant additives are added to avoid corrosion through adsorption on the workpiece surface or chemical reactions with the faces of the workpiece. Alcanolamines and carbon or boron acids are often used as corrosion inhibitors. Due to the nitrosamines problem, sodium nitrides are no longer used as corrosion protection additives. Boron compounds in water composite

cooling lubricants are widely used as corrosion protection additives because of an additional protection against bacterial infection. The preservatives used in water composite products for the control of microorganisms, bacteria, and fungus growth are toxic and cannot be considered harmless in physiological terms. Alongside boron acids, the most important groups of these agents are formaldehyde-separators, phenols, and N/S heterocycles. In order to avoid foaming, poly-silicons and acrylates are added that have low surface tension and make foam quickly collapse. Antifog additives are mainly polymethacrylates and olefin copolymers, which lead to a recombination of the aerosol to fluid droplets causing the fog to condense near the point of its origin [Möller and Boor 1986, Korff 1991, König et al. 1993, Pfeiffer 1993, Kassack 1994].

## 10.6 APPLICATION RESULTS

Tangential grinding force and grinding power can be minimized and generated heat reduced by reducing friction using a cooling lubricant with a strong lubricating effect [Howes 1990, Brinksmeier 1991a]. Successful cooling leads to quick heat dissipation keeping the active partners below a critical temperature. However, the shear resistance of the workpiece material is increased through the cooling of the active zone, again causing an increase in the process forces [Brinksmeier 1991a]. Depending on its cooling and lubricating performance, the cooling lubricant has a significant influence on the achievable material removal rate, grinding forces, grinding temperature, and on grinding wheel wear. Beyond the influence on process parameters, achievable surface quality and subsurface characteristics crucially depend on the cooling lubricant used. It has also been reported that clogging of the grinding wheel depends on the type of cooling lubricant [Khudobin 1969, Tawakoli 1990]. Against this background, a specific selection and adaptation of the cooling lubricant is necessary for a particular machining task.

## 10.7 ENVIRONMENTAL ASPECTS

Increasing public awareness toward environmental protection, new ecological legal conditions as well as increasing disposal costs have led to new approaches in manufacturing for grinding fluids. It has been recognized that inappropriate disposal and landfilling of cooling lubricants represent a serious hazard since deposition has a significant impact on the air, soil, and ground water. Moreover, dioxins are emitted to the environment. The “Act of Closed Substance Cycle Waste Management and Ensuring Environmentally Compatible Waste Disposal,” which became effective in 1996 in Germany, focuses on the protection of natural resources through the avoidance and recycling of waste. Production is required by law to take place with a minimum input and first of all with a minimum consumption of resources emitting a minimum of harmful substances [Brinksmeier 1993]. Hence the entire cooling lubricant system represents a key starting point for an ecoefficient design of the grinding process. Grinding fluid is fed in large amounts to the grinding machine and large quantities of abrasive slurry are generated in the fluid supply system.

Ecological and health aspects are resulting in a more frequent application of dry machining or of so-called “Minimum Quantity Lubrication” systems. Increasing demands for improved product quality and economic grinding of parts, and a minimum amount of grinding fluid, represent contradictory requirements [Klocke and Gerschwiler 1996, Heinzel 1999, Weinert 1999].

## 10.8 THE SUPPLY SYSTEM

### 10.8.1 INTRODUCTION

The design of a supply system and the selection of the feed parameters must meet the specific technological demands of the grinding process. Since the cooling of the grinding process primarily depends on cooling lubricant supply to the contact zone, secondary cooling effects play only a



minor role, hence the percentage of the cooling lubricant amount acting in the contact zone has to be set to a technologically required minimum.

### 10.8.2 ALTERNATIVE COOLING LUBRICANT SYSTEMS

The amount of cooling lubricant required can be reduced by the use of alternative cooling lubricants. It has been shown that good grinding results can be achieved by using liquid nitrogen linked to minimum lubrication. Compared to grinding with oil, surface qualities are slightly poorer, but wear of the grinding wheel is much lower. The lubrication of the grinding process with solid graphite is a further possibility. In this case, machining forces are similar to those in grinding with a grinding fluid. If solid graphite lubrication is linked to dry machining, considerably lower process forces were found, first of all, in the case of increased feed rates.

Besides the design of the supply system, the use of alternative cooling lubricants, and the reduction of the cooling lubricant quantity, there is a further potential for optimization of the entire cooling system, including the whole life cycle of the cooling lubricant. Since cooling lubricants are designed for a particular machining task, the complex process of downstream cleaning and processing is not considered. Only cleaning of the filter system is included in the design. In this case, slurry in the filter system can be processed and a large part of the substances it contains can be recycled [Brinskmeier 1991a].

It is possible that the entire process will be integrated within the grinding machine in the future. After start-up, the grinding machine will be able to process a large part of the used cooling lubricant and refeed it to the process. Furthermore, residual material derived from the chip particles and abrasive residuals can be refeed to the production process.

### 10.8.3 FLUID SUPPLY SYSTEM REQUIREMENTS

The cooling lubricant supply system is required to accomplish several different tasks during the machining process as well as during auxiliary process time or even during the off-state of the grinding machine. First of all, it has to provide an uninterrupted flow of cooling lubricant to the active zone. Moreover it is required to store and transport the cooling lubricant maintaining a constant quality and temperature and with a sufficient quantity to execute the job of cooling, lubricating, flushing, and chip transport. In addition to economic requirements related to investment costs or maintenance cost, a number of further requirements must be met including operating safety especially when using oil as cooling lubricant [König et al. 1993, Brücher 1996, König and Klocke 1996].

In an industrial environment, it is a common approach to install a central or group circulation system that supplies a number of machine tools using the same cooling lubricant. These systems require the specification of a single cooling lubricant for all processes supplied but reduce the complexity for cleaning, cooling, controlling and supply of the fluid, and, in addition, reduce the circulating volume of the cooling lubricant [Brücher 1996].

Centralized systems are composed of components transporting the fluid to the process (pumps, pipes, nozzles, measurement and control devices, mixing devices), a return system (channels, pipes, pumps), maintenance devices (filters, reservoirs, monitoring devices), and equipment for swarf treatment (conveyor, chip crusher, centrifuges, cleaning nozzles). Design of a cooling lubricant supply system strongly depends on the required flow and pressure of the fluid leaving the nozzle at the contact zone. By applying a particular nozzle form, its positioning and the required fluid pressure determine the total volume of cooling lubricant to be supplied. Additionally, the volume stored in the feed and return pipes, the volume contained in filter and tempering devices, a minimum reserve volume, and, if necessary, an additional volume for foam discharging have to be taken into account [VDI-Richtlinie 3035 1997].

Although cooling lubricant supply systems are often designed for either water-miscible or water-immiscible cooling lubricants, the application of both types and many different specifications

of cooling lubricants during the life span of a machine has become an increasing demand by industry. This needs to be incorporated into the material choice for a cooling lubricant supply system where it is generally recommended to avoid zinc-plated steel pipes or nonferrous fittings. In order to prevent the degradation of cooling lubricant or corrosion of machine components, the compatibility of all materials used has to be ensured especially in terms of a fluid that changes its physical and chemical properties over the course of time. Tanks for fresh and used fluid are required to store the entire cooling lubricant volume of the supply system in case of a machine stoppage that leads to the fluid all flowing back into those tanks due to a gravitation-controlled piping system. Because of long distances between machine tools and central tanks, it is often necessary to install a separate backflow tank at each machine. Furthermore, the design of each tank should prevent the deposition of any solid residuals or backflow of fluid and offer a facility to empty the tank completely [VDI-Richtlinie 3035 1997].

Depending on volume flow, fluid pressure, and contamination of the fluid, a variety of different pumps can be used. A crucial feature of all types is the sealing of the pump shaft against the contaminated cooling lubricant, which is presently done by axial face seals made of tungsten carbide including special CVD or PVD coatings. To minimize pressure drop, the supply pump should be placed as close as possible to the delivery nozzles. The cross section of the connected piping system must be adjusted to the particular flow conditions in order to avoid cavitation, which normally limits the flow velocity in suction pipes to 1.5 m/s and in pressure pipes to 2.5 m/s [VDI-Richtlinie 3035 1997].

Grinding swarf contaminates the grinding fluid and degrades the grinding operation itself and the lifetime of the fluid if accumulated in the fluid. Cleaning and conditioning of the fluid is accomplished by a number of different methods and principles. Chemical, biological, and, above all, mechanical contamination can be eliminated by sedimentation, filtering, centrifugation, and magnetic tape separators depending on the required degree of purity. Sedimentation is a reasonable method for coarse cleaning of the fluid but in finish grinding, a stage cleaning process using several different filter principles is recommended. The most common filters used are tape filters and candle filters, both requiring a change and disposal of the filter within a fixed period of time. In addition to a very clean cooling lubricant, it is crucial for high-speed grinding applications and finish grinding operations to have the fluid supplied at a precisely controlled temperature. The grinding heat needs to be dissipated while passing through the fluid supply system. The fluid needs to dwell long enough in the supply system to allow heat dissipation or must be removed in an extra cooling system [Tawakoli 1990, Brücher 1996, König and Klocke 1996, VDI-Richtlinie 3035 1997].

It is essential in all grinding applications to control the fluid pressure or volume flow. With regard to safety of the grinding process, an automatic machine stop is essential to cope with an unplanned pressure drop or significant flow reduction. Furthermore, it is desirable to check and control the quality of the supplied fluid by measuring the pH-value or electrical conductivity. In grinding with water-immiscible cooling lubricants, the mist generated in combination with high process temperatures and glowing chips flying away from the contact zone poses an explosion hazard. Therefore, safety devices such as blowback flaps and fire extinguishers need to be installed. For grinding with minimum lubrication systems, separate technical regulations take effect [Tawakoli 1990, VDI-Richtlinie 3035 1997].

## **10.9 GRINDING FLUID NOZZLES**

### **10.9.1 BASIC TYPES OF NOZZLE SYSTEM**

The performance and characteristics of the cooling lubricant nozzle for the supply liquid lubricant have a major influence on the grinding result. A number of different nozzles have been developed in order to meet the requirements of various applications. Some of these nozzles are described in

greater detail in Chapters 16 on surface grinding and Chapter 17 on cylindrical grinding. Generally, there are three ways to distinguish between types of nozzle systems [Heinzel 1999]:

- By function (flooding, not flooding)
- By focusing (free jet nozzle, point nozzle, swell nozzle, spray nozzle)
- By nozzle geometry (squeezed pipe, needle nozzle, shoe nozzle)

The primary task of all nozzles is the distribution of lubricants to the active zone. The nozzle carries out this task through focusing and directing the lubricant jet as well as accelerating the liquid. Investigations show a positive effect on the cooling performance by focusing the lubricant jet, associated with minimizing the turbulence of the flow by a sharp-edged exit of the nozzle or an extended parallel outlet of the nozzle. Additionally a minimum flow velocity must be generated, that is, by reducing the cross-sectional area at the nozzle outlet for wetting the wheel surface with cooling lubricant. The main obstacle to overcome for wetting the entire grinding wheel surface prior to its entry into the contact zone is a rotating air cushion around the grinding wheel [Marinescu et al. 2004]. Due to friction between the rough wheel surface and its surrounding atmosphere, a rotating air cushion is generated. The rotating air stream causes a permanent air flow away from the grinding wheel especially at high cutting speeds preventing grinding fluid from reaching the contact zone [Tawakoli 1990, Treffert 1995, Brücher 1996, Heinzel 1999, Beck 2001].

In order to breach the rotating air cushion by the cooling lubricant itself, a significant amount of kinetic energy has to be spent. The primary cooling lubricant nozzle can be used applying a higher flow rate and a higher flow velocity, which consumes more lubricant and significantly reduces the overall economic efficiency of the whole supply system. Another solution is to use a second nozzle in a radial direction to the wheel in front of the inlet of the actual cooling lubricant nozzle. Further improvement can be achieved by employing one nozzle for the peripheral surface and two additional nozzles for the side faces of the grinding wheel. In terms of an optimized design of the entire supply system, it is recommended to use a close-fitting housing for the grinding wheel.

Air guide plates closely aligned to the wheel surface are widely used to deflect the rotating air cushion away from the grinding wheel. Precise alignment and readjustment to a changing wheel profile or diameter are required [Tawakoli 1990, Brücher 1996, Heinzel 1999].

### 10.9.2 THE JET NOZZLE

At present, the most common type of cooling lubricant nozzle is the free jet nozzle aimed at flooding the entire contact zone. Being rather simple in design, this nozzle type is oriented in the tangential direction to the grinding wheel. In addition, the nozzle outlet should be positioned very close to contact zone. By varying the volume flow, the flow pressure, and the outlet cross-sectional area, the flow velocity can be matched to the peripheral velocity of the grinding wheel, being a prerequisite for maximizing the volume flow through the contact zone. However, it is only the minor part of the lubricant used that enters the contact zone since the maximum flow through the contact zone is geometrically limited by the pore space of the grinding wheel or the grinding layer. The geometry of the free jet nozzle is independent from the wheel profile or its dimensions, which makes this nozzle type relatively flexible in application. A tangential nozzle with a small width is referred to as a point nozzle, whereas the combination of several point nozzles is called a needle or multipoint nozzle [Heinzel 1999].

### 10.9.3 THE SHOE NOZZLE

An alternative nozzle design combining elements for deflecting the rotating air cushion with a highly effective distribution of the cooling lubricant to the contact zone is the so-called shoe nozzle. This nozzle type fits exactly to the wheel profile and encloses the grinding wheel on three sides.

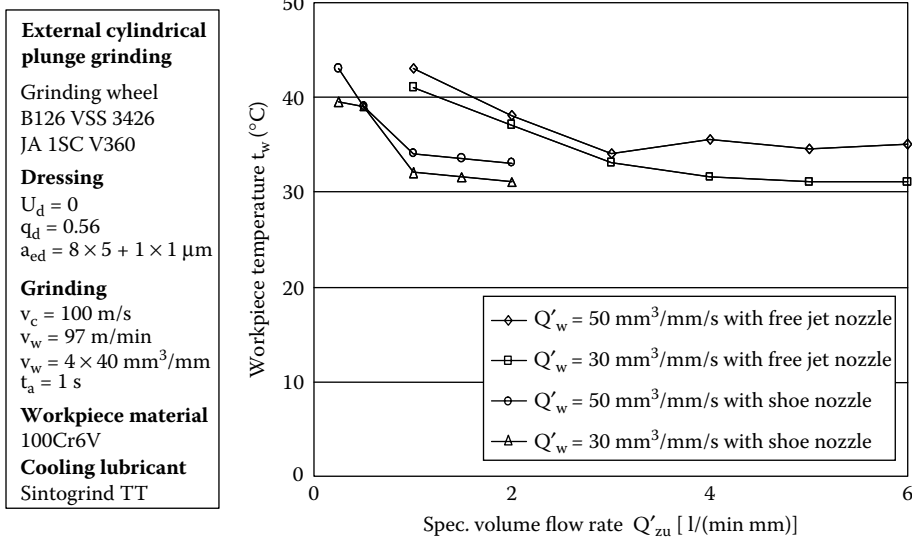


**FIGURE 10.3** Workpiece temperature versus specific volume flow rate of the cooling lubricant for a shoe nozzle. (From Beck 2000. With permission.)

The rotating air cushion is deflected at the nozzle inlet allowing the complete wetting of the wheel surface with lubricant at the inner chamber of the shoe nozzle. The rotation of the grinding wheel itself accelerates the fluid to circumferential velocity. The total amount of cooling lubricant supplied can be limited to the volume necessary to fill the whole pore space of the wheel surface because a further supply shows an insignificant effect on the work result (Figure 10.3). The nozzle geometry is determined by the grinding wheel profile and an adjustment to a changing wheel diameter is required; hence, there is only a limited flexibility in the application of those nozzles. Several investigations prove the capability of this nozzle form to reduce the wheel wear as well as the thermal degradation of the boundary layer with a less required flow rate of the lubricant [Tawakoli 1990, Heinzl 1999, Beck 2000].

#### 10.9.4 THROUGH-THE-WHEEL SUPPLY

A slightly different concept of lubricant distribution is the supply of cooling lubricant from the interior of the grinding wheel or the grinding layer. The fluid is fed into a chamber of the wheel body allowing the centrifugal force to distribute it through radial channels to the grinding layer. Through pores or gaps in the grinding layer, the cooling lubricant is directly provided to the active zone. The technical complexity of this solution has so far prevented a broad application. Alternatively, a porous grinding wheel can be infiltrated by fluid supplied from a conventional external cooling nozzle, which will leave the wheel inside the contact zone due to the centrifugal force [Tawakoli 1990, Heinzl 1999].

#### 10.9.5 MINIMUM QUANTITY LUBRICATION NOZZLES

Minimum quantity lubrication (MQL) is aimed at reducing the amount of lubricant used for a grinding application. MQL nozzles have been the topic of several research projects. With the assistance of pressurized air, a mist of cooling lubricant is sprayed onto the surface of the grinding wheel. Ideally, only a thin film of fluid covers the wheel surface prior to its entry into the contact zone. Investigations concerning MQL report an increase in grinding force, wheel wear, workpiece surface roughness, and onset of grinding burn at lower material removal rates in contrast to

conventional fluid supply systems. Furthermore, secondary functions of the fluid such as chip transport or cooling of the grinding machine have to be carried out through additional devices. However, certain grinding operations using a minimum quantity lubrication show some potential for applications in an industrial environment such as rough grinding with plated metal bond cubic boron nitride (CBN) wheels [Heinzel 1999, Weinert 1999].

### 10.9.6 AUXILIARY NOZZLES

In addition to the nozzle supplying cooling lubricant to the contact zone, it is recommended to use auxiliary nozzles in radial direction to the grinding wheel. Their task is to remove chips and other loading from the wheel surface as well as to extinguish sparks or glowing chip particles. The effectiveness of these measures depends more on the fluid pressure than on the volume flow. It could be seen that there is a significant reduction in surface roughness of the ground workpieces by applying two more of those cleaning nozzles [Vits 1985, König and Klocke 1996].

## 10.10 INFLUENCE OF THE GRINDING FLUID IN GRINDING

### 10.10.1 CONVENTIONAL GRINDING

In comparison to dry grinding and grinding with emulsions, lower temperatures were measured in grinding with oil [Dederichs 1972]. The capacity of the cooling lubricant to discharge heat from the contact zone can be affected by the occurrence of film boiling of the fluid in the contact zone, leading to an abrupt overheating of the workpiece and to thermal damage. Face grinding of steel with a water-based fluid showed that, with a rising subsurface temperature caused by an increase in depth of cut, the cooling lubricant increasingly evaporates above a depth of cut of  $a_e = 35 \mu\text{m}$  and temperatures in excess of  $100^\circ\text{C}$  leading to similar grinding temperatures as in dry grinding. There is a similar effect during grinding with oil, but, at a higher critical temperature in excess of  $300^\circ\text{C}$  [Yatsui and Tsukada 1983, Howes, Neailey, and Harrison 1987, Howes 1990, Brinksmeier 1991a, Marinescu et al. 2004]. Thus, in many cases, it appears to be more effective to reduce the grinding heat generated by using a grinding fluid with a good lubricating effect than to absorb an increased amount of heat with the help of a grinding fluid of a high specific heat capacity [Klocke 1982].

In addition to a superior material-removal rate and surface quality, wear of the grinding wheels and the tangential grinding forces are lower when grinding metals with grinding oils than in the case of grinding with water composite fluids. No uniform tendencies of the normal grinding force could be observed comparing the use of grinding oils and water composite fluids [Zwingmann 1960; Gühring 1967; Keyser 1970; Sperling 1971; Peters and Aereus 1976; Oates, Bezer, and Balfour 1977; Polyanskov and Khudobin 1979; Tönshoff and Jürgenharke 1979; König 1980; Althaus 1982; Zimmermann 1982; Ott 1985; Vits 1985; Holtz and Sauren 1988; Kersch 1988; Carus 1989; Brinksmeier 1991a, b; Heuer 1991, 1992; Ott 1991; Böschke 1993; Treffert 1995; Webster 1995; Heinzel 1999; Marinescu et al. 2004].

In external grinding of roller bearing steel 100Cr6 (62 HRC) with CBN grinding wheels, pure grinding oil gave lower wear than 5% emulsion, with improved surface quality and lower tangential forces. Higher wear of CBN grinding wheels with water composite fluids is often traced back to hydrolytic wear. Model tests, where CBN grains were heated up to  $1,000^\circ\text{C}$ , showed grain-edge rounding, etching of the grain surface, and a loss of weight as a result of a chemical reaction between boron nitride and water leading to the development of boron acid and ammonia. Such wear behavior, however, could not be observed under practical daily grinding conditions. Generally, it is found that chemical wear in grinding with CBN grinding wheels using solutions or emulsions is of secondary significance [Triemel 1976, Heuer 1991]. Lower normal forces occurred using emulsion in external cylindrical grinding of 100Cr6 with CBN grinding wheels, at removal rates

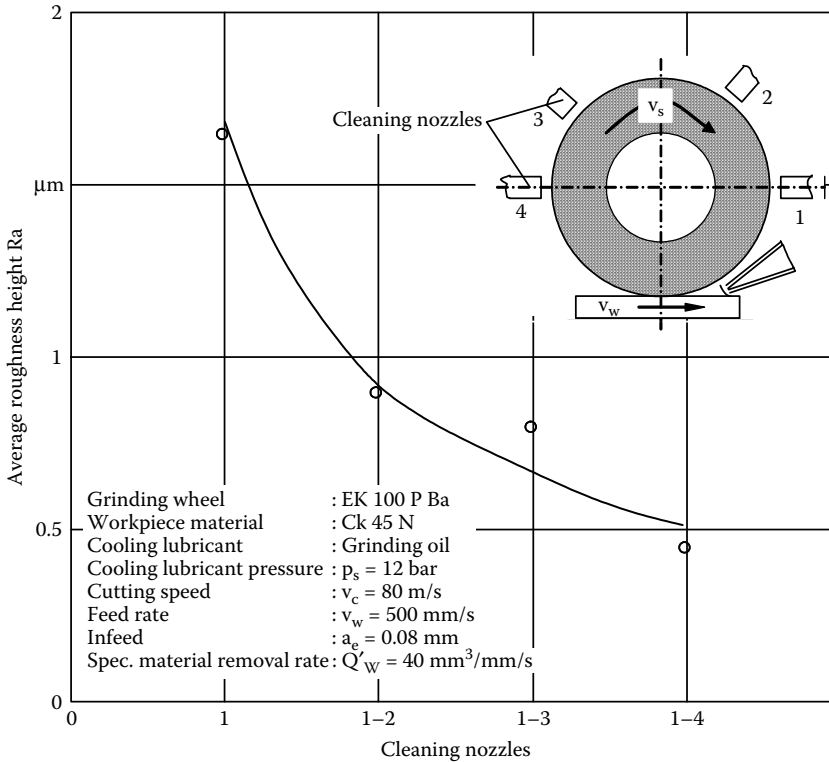


**FIGURE 10.4** Influence of arrangement and number of cleaning nozzle on surface quality during surface grinding. (From König 1996. With permission.)

of  $\dot{Q}'_w = 2.0$  mm<sup>3</sup>/mm/s and 12.0 mm<sup>3</sup>/mm/s, and a cutting speed of  $v_c = 60$  m/s, leading to equivalent chip thickness,  $h_{eq} = 0.03$  to  $0.2$  μm. This was traced back to greater bond wear due to increased friction between chips and bond, causing grain break-out and, consequently, a reduction of the cutting edge number. In contrast, CBN grains remain fixed in the bond for a longer time when grinding with oil and, despite lower friction, the grains show increasing flattening with grinding time (Figure 10.4) [Heuer 1991, 1992].

Similar results were found in internal cylindrical grinding of hardened 100Cr6 steel (Figure 10.5). In this case, the normal cutting forces as well as the tangential force component are eventually higher using oil than with water composite cooling lubricants, whereas in external cylindrical grinding a decrease in tangential cutting force is observable. Furthermore, higher G-ratio and better surface quality are achieved with grinding oil [Tönshoff and Jurgensharke 1979, Althaus 1982].

### 10.10.2 INFLUENCE OF THE FLUID IN GRINDING BRITTLE-HARD MATERIALS

Despite the fundamentally different material-removal mechanisms, conclusions relating to fluids for brittle-hard materials are similar to those for ductile materials. In the case of reciprocating face grinding of ceramic materials with diamond grinding wheels, there are advantages concerning surface quality and process behavior if grinding oil is used in contrast to water composites. While the use of water composite fluids is characterized by an increase of the normal force during the grinding of Al<sub>2</sub>O<sub>3</sub> and HPSN, lubrication with grinding oil showed a process behavior with low and nearly constant normal grinding forces up to a specific material-removal volume of  $V'_w = 780$  mm<sup>3</sup>/mm. Furthermore, there is lower radial wear of the grinding wheel during the grinding of these ceramics with grinding oil [Tio and Bruecher 1988, Brücher 1993, Spur 1993]. The obvious differences in the topography

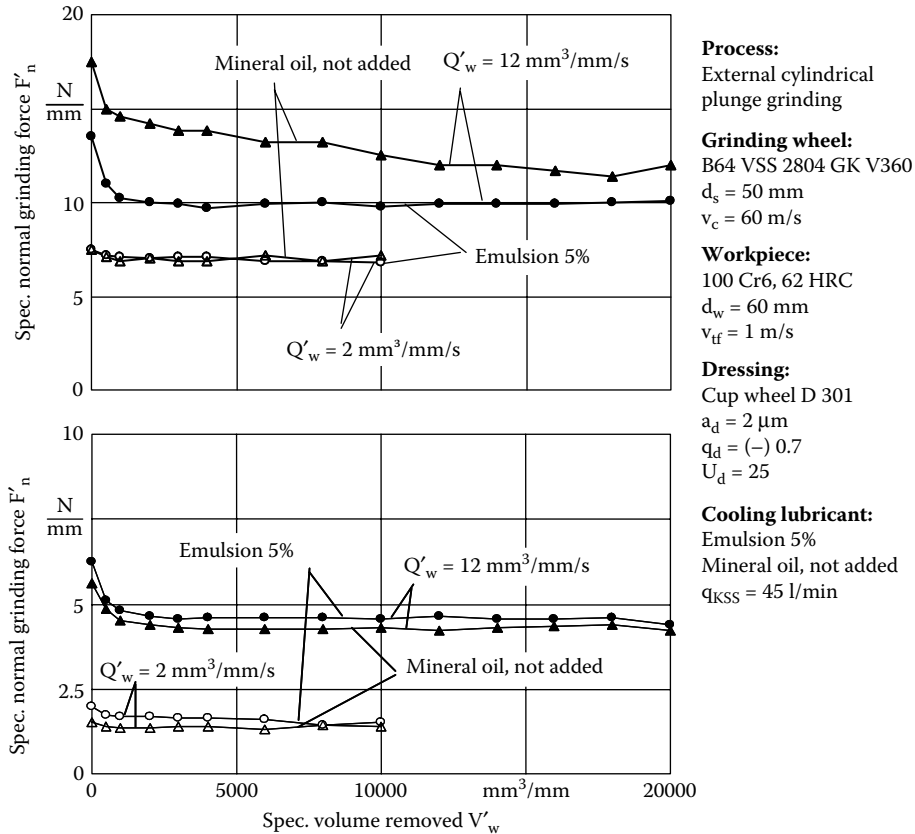


**FIGURE 10.5** Influence of different cooling lubricants on grinding forces during cylindrical grinding. (From Heuer 1992. With permission.)

of the  $Al_2O_3$  surfaces ground with grinding oil and emulsions suggest a considerable influence of the grinding fluid on the chip-formation mechanisms. In contrast to the surfaces ground with grinding oil, there are hardly any directional grinding marks on surfaces ground with water composite fluids [Tio 1988, Roth and Wobker 1991, Wobker 1992, Brucher 1993].

These findings are also confirmed for the face grinding of an aluminum oxide reinforced with 10%  $ZrO_2$ . Different surface structures are generated depending on the grinding fluid and nearly constant normal and tangential grinding forces occur. Moreover, the grinding wheel wear is lower if grinding oil is used [Brinksmeier 1991a, Heuer 1991, Roth and Wobker 1991, Wobker 1992]. In contrast, if petroleum or petroleum fog was used for cooling and lubrication in the face grinding of different oxide ceramic materials in further research projects, lower normal forces occurred than with emulsion, emulsion fog, or compressed air. The lowest tangential force and the lowest wear, however, were measured in grinding with emulsion and emulsion fog. The surface quality achieved was almost independent of the grinding fluid in these investigations [Sawluk 1964]. Grinding of HPSN and  $Al_2O_3/TiC$  gave different results. In these cases, higher normal forces were measured with grinding oil than with water composite fluids. This was explained by elevated thermal stress of the grinding wheel. Wear of the grinding wheel was also lower with these materials if water-immiscible fluids were used [Brinksmeier 1991a, Heuer 1991, Roth and Wobker 1991, Wobker 1992].

There are hardly any differences between water composite grinding fluids of different compositions in terms of grinding forces during face grinding with axial feed of  $\text{Al}_2\text{O}_3 + 10\% \text{ZrO}_2$ , HPSN, and  $\text{Al}_2\text{O}_3/\text{TiC}$ . Wear of the grinding wheel was, however, lower with emulsion than with a solution irrespective of the material [Wobker 1992]. Friction and wear tests using a four-ball tester with hexadecanen (C16H18) and different additives showed a significant reduction of the friction value and of the wear coefficient in the case of the friction pairs  $\text{Al}_2\text{O}_3/\text{Al}_2\text{O}_3$  and  $\text{ZrO}_2/\text{ZrO}_2$ . The most obvious influence in the case of these pairs was shown after the addition of 0.1 mol% zinc-dialkyldithiophosphate. In the case of the friction pairs  $\text{SiC}/\text{SiC}$  and  $\text{Si}_3\text{N}_4/\text{Si}_3\text{N}_4$ , the influence of the additives was smaller. While marginally smaller friction and wear coefficients were observed in the case of the silicon nitride tool under addition of zinc-dialkyldithiophosphate, too, no change of the friction and wear parameters was detected in the case of silicon carbide [Bartelt and Studt 1992]. The effects of an addition of fatty acids of different chain lengths were analyzed in sliding wear tests with hexadecan lubrication within the scope of other investigations. Fatty acids with six or more carbon atoms proved to be good lubrication additives. This effect is due to thicker adsorption layers [Studt 1987].

In the case of grinding spectacle lenses, superior cutting performance was achieved by using grinding oil although the surface quality was poorer [Pfau 1987]. The use of light grinding oil is better in the cutoff grinding of glass. Although the use of petroleum would lead to a service life increase of up to 10% to 15%, this fluid is not used due to the fire hazard. In contrast, when face grinding glass blocks with diamond cup wheels, a 3% to 5% synthetic water composite fluid is used instead of oil [Seifarth 1987]. In the case of cutoff grinding of hard stone, studies show that grinding oil leads to a reduction of grinding forces and of tool wear. Furthermore, a higher surface quality can be expected if grinding oil is used. Wear tests on the grains of diamond grinding wheels indicate increased grain wear through grain flattening and splintering, while the highest number of damaged grains was observed in cutoff grinding with grinding oil [Tönshoff and Schulze 1980]. Investigation of the grinding of concentric circular grooves in marble showed only a minor influence of the composition of water composite fluid [Gerhäuser and Laika 1977].

Investigations carried out at the IWF defined the minimum volume flow required in the contact zone for grinding different ceramic materials (Figure 10.6). Supplying this specific contact zone volume flow, grinding wheel wear reaches a minimum. A further increase of the volume flow leads to negligible further reduction of wear with clearly increased resistance against the supply of the cooling lubricant. Hence, this minimum contact zone volume flow is a significant design criterion for the design of the coolant supply system [Brücher 1996].

### 10.10.3 HIGH-SPEED AND HIGH-PERFORMANCE GRINDING

In the case of high-speed grinding of hardened 100Cr6 steel with electroplated CBN grinding wheels, the use of grinding oil instead of water composite grinding fluids leads to a reduction of wear. At a cutting speed of  $v_c = 140 \text{ m/s}$  and material removal rates  $Q'_w = 2.0 \text{ mm}^3/\text{mm/s}$  and  $80.0 \text{ mm}^3/\text{mm/s}$ , normal as well as tangential force components reduced when grinding in oil. The roughness of the ground surface is slightly higher with oil in contrast to different emulsions. The reason for the positive result in terms of surface quality in grinding with emulsions is an accelerated wear of the grains, which leads to an increase of the active cutting edge number and chip thickness on the electroplated grinding wheel used [Treffert 1995]. In high-speed grinding of materials of different hardnesses with CBN wheels, up to 50% higher grinding ratios were achieved with grinding oil in contrast to a synthetic solution and an emulsion. However, the advantages achievable with grinding oil increased with a decreasing material hardness [Kersch 1988].

In the case of high-performance grinding of Ck45N steel with conventional corundum grinding wheels, the use of grinding oil at a cutting speed of  $v_c = 60 \text{ m/s}$  led to an increase of the achievable cutting performance by approximately 200% in contrast to an emulsion where the performance was limited by the occurrence of burn marks. At the same time, smaller normal forces and surface roughnesses were observed at an equal material removal rate [Gühning 1967].



**Profiling with SiC-roller  
Sweep sharpening  
with corundum stone:**

$v_{cds} = 20 \text{ m/s}$   
 $Q'_{ds} = 0.5 \text{ mm}^3/\text{mm/s}$   
 (D126-100)  
 $Q'_{ds} = 2.5 \text{ mm}^3/\text{mm/s}$   
 (D126 K+)

**Grinding parameters:**

$v_c = 35 \text{ m/s}$   
 $v_{ft} = 10 \text{ m/min}$   
 $Q'_w = 5.0 \text{ mm}^3/\text{mm/s}$   
 $V'_w = 780 \text{ mm}^3/\text{mm}$

**Cooling lubricant:**

Solution Syntilo 81 (4%)  
 $\vartheta = 20^\circ\text{C}$   
 $\alpha_{DKS} = 15^\circ$ , tangential  
 IDKS = 65 mm

**Free jet and  
flooding nozzles:**  
 $p = 0.2\text{--}10.0 \text{ bar}$

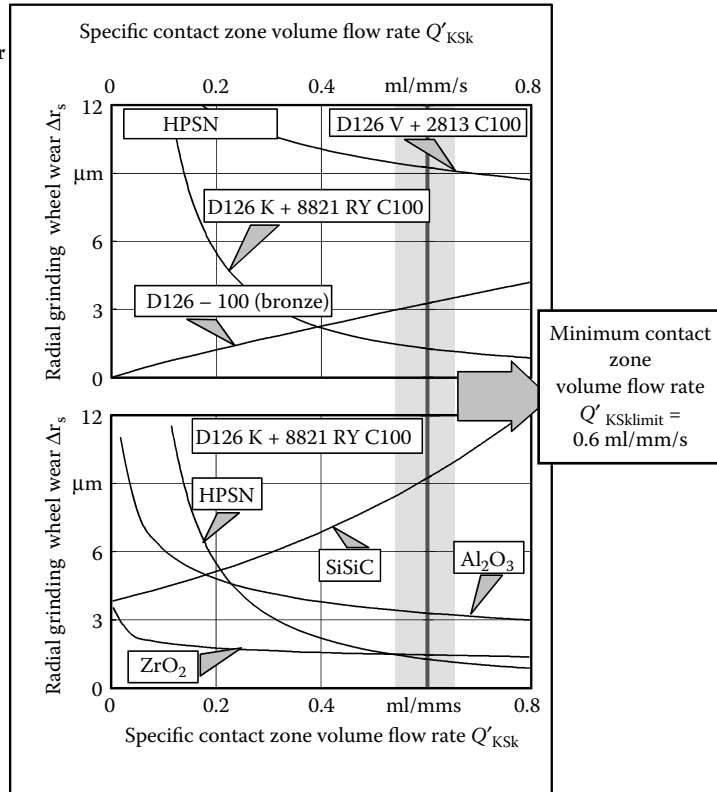


**FIGURE 10.6** Determination of a minimum contact zone flow rate for different grinding conditions (From Brücher 1996. With permission.)

During the external cylindrical plunge grinding of Ck45N and 100Cr6 with corundum grinding wheels, lower tangential grinding forces and a lower grinding wheel wear were stated when grinding oils were used, independently of the material removal rate. The normal component of the grinding force, too, exhibits lower values during the grinding of the mentioned materials at elevated material removal rates above  $Q'_w = 3.0 \text{ mm}^3/\text{mm/s}$  with oil instead of water composite fluids. In the case of grinding with lower material removal rates, the normal force level for both materials is higher with oils than with different emulsions. The reason is higher grain-related normal forces and a higher number of kinematic cutting edges due to increased plastic deformation. This effect is much stronger in the case of the ductile material Ck45N than in the case of 100Cr6. Due to a wear-related leveling of the grinding wheels surface, grinding with poor lubricants entails an increase in the number of active cutting edges at low removal rates. As a result, normal forces arising from water or oil-based fluids become equal at an increasing chip volume and at a specific material removal rate below  $Q'_w = 3.0 \text{ mm}^3/\text{mm/s}$ .

Furthermore, better surface quality was achieved in grinding with oil at specific material removal rates of  $Q'_w > 3.0 \text{ mm}^3/\text{mm/s}$  in the case of both materials (Figure 10.7). A large uncut chip thickness causes excessive cutting-edge stresses leading to intensive self-sharpening of the wheel surface through grain breakage. In the case of water composite fluids, the sharpening of the grinding wheel is clearer due to increased friction. As a consequence, the cutting edge number is lower leading to a poorer surface quality. In the case of low material-removal rates, an inverse tendency can be observed at the beginning of the grinding process. In this range, which is characterized by small uncut chip thicknesses and increased grain flattening, greater friction during grinding with solutions

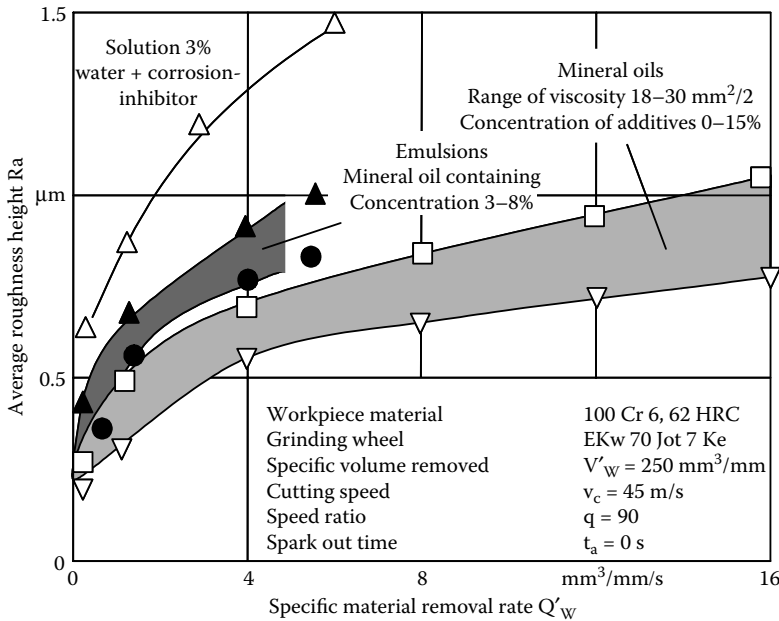


**FIGURE 10.7** Influence of different types of cooling lubricants on surface quality during surface grinding. (From Vits 1985. With permission.)

and emulsions initially leads to increased blunting of the grains and thus to higher cutting edge numbers, which, in turn, results in better surface quality. After the grinding-in phase, which leads to a balance of grain flattening, splintering, and break-out, a lower roughness of the surface can be observed if ground with oil [Vits 1985].

If water composite fluids are used, process behavior strongly depends on the composition and the concentration, which also influence the cooling and lubricating properties [Bock 1993]. In grinding of tempered steel, the specific grinding energy increases with a rising water fraction and with the use of solutions instead of emulsions [Dederichs 1972, Vits 1985]. When emulsions were used for internal grinding of ball-bearing steel 100Cr6 with vitrified bond CBN grinding wheels, work results were improved at concentrations between 2% and 10% with increasing concentrate or oil content [Althaus 1982]. In the case of thread grinding with plated and resinoid bond grinding wheels, reduced grinding wheel wear, lower grinding forces, and superior surface quality were found with increase in the emulsion concentration. The disadvantages of solutions with a low concentration in terms of the grinding wheel wear demonstrated by the flank angle enlargement cannot be compensated, even by higher volume flow [Klocke 1982]. Using conventional grinding wheels to grind steel, little influence of the concentration of water composite fluids was found. In fact, smaller normal and tangential forces, superior surface qualities, and less wear were found with water composite fluids containing mineral oil. However, there was no clear influence of concentration on process or work-result parameters within the group of emulsions [Vits 1985]. In the majority of cases of grinding metallic materials, superior lubricating properties of emulsions with increased concentration dominate over the better cooling characteristics of solutions or mineral oils containing emulsions of lower concentrations. In some cases, optima could be observed in terms of the target parameters such as grinding wheel wear, surface quality, and power input using water composite fluids of an intermediate concentration [Peters and Aerens 1976, Oates et al. 1977]. Investigations showed a maximum G-ratio during the grinding of steel with CBN grinding wheels and a completely synthetic fluid solution simultaneously with minimum power input and surface roughness at a concentration of 4% [Oates et al. 1977].

In contrast, performance of water-immiscible fluids strongly depends on the viscosity. Decreased oil viscosity leads to poorer lubrication and increased viscosity to poorer cooling; the best results can be expected from grinding oils with medium viscosity. This conclusion was reached, comparing grinding oils for internal cylindrical grinding with viscosities of  $\nu = 12 \text{ mm}^2/\text{s}$ ,  $48 \text{ mm}^2/\text{s}$ ,  $220 \text{ mm}^2/\text{s}$ , and  $432 \text{ mm}^2/\text{s}$  at  $20^\circ\text{C}$ . Oil of a viscosity of  $\nu = 48 \text{ mm}^2/\text{s}$  had the highest grinding ratio. A viscosity increase of  $\nu = 18 \text{ mm}^2/\text{s}$  to  $30 \text{ mm}^2/\text{s}$  linked to a cutting speed of  $v_c = 45 \text{ m/s}$  and grinding wheels of corundum [Vits 1985], as well as of  $\nu = 7 \text{ mm}^2/\text{s}$  to  $25 \text{ mm}^2/\text{s}$  at a cutting speed of  $v_c = 90 \text{ m/s}$  using CBN tools [Treffert 1995], had only a marginal effect on the grinding forces and on the surface quality during external cylindrical grinding of ball bearing steel. In grinding with corundum wheels, increased viscosity, however, leads to a change of the grinding wheel wear. While low wear values were measured when a more ductile oil was used, this tendency was reversed due to a progressive wear increase, typical for this oil, from a specific material removal rate of  $Q'_w = 12 \text{ mm}^3/\text{mm/s}$ . The reason for this is that the highly viscous oil does not penetrate the grinding wheel structure to the same extent leading to a lower cooling effect and to higher grinding temperatures. Additionally, it has a poor rinsing capacity, leading to clogging of the grinding wheel [Vits 1985].

Beyond the mentioned parameters, the efficiency of water composite as well as of water-immiscible fluids can be affected by additives forming a lubricating film. Since the effect of the so-called EP additives is based on chemical reactions with the workpiece material taking place under defined temperatures, and the stability of the products of reaction depends on a certain temperature, the influence of cooling lubricant additives on the grinding process and on the work result crucially depends on the machined material and on the process conditions [Ott 1991]. Therefore, no general statements on the efficiency of single additives can be derived from the present investigations. In many cases, however, an additive adapted to the machining task improves the grinding process and the work result [Nee 1979; Klocke 1982; Vits 1985; Carius 1989; Brinksmeier 1991b; Heuer 1991, 1992; Spur et al. 1995b]. During the grinding of nickel-based alloys with CBN grinding wheels, for instance, grinding forces were reduced and burning and chatter marks avoided through the addition of sulfur additives into an ester-base product [Spur 1995b]. In the case of external cylindrical grinding of 100Cr6, the addition of 5% sulfured fatty acid ester and the addition of polar components or chlorine paraffins in contrast to the unalloyed base oil led to the lowest grinding wheel wear and to the best surface quality [Heuer 1991, 1992].

Beyond the parameters of the grinding process and of the surface quality, the condition of the ground subsurface plays a key role in the assessment of the effectiveness of different grinding fluids. Althaus (1982) reported higher compressive residual stress at process start after grinding with oil than with emulsion using residual stress as a criterion for the assessment of the subsurface state in internal grinding of 100Cr6 steel at a cutting speed of  $v_c = 30 \text{ m/s}$  and a specific material removal rate of  $Q'_w = 1.0 \text{ mm}^3/\text{mm/s}$  with conventional corundum wheels as well as with vitrified CBN tools. With increasing material removal, the compressive residual stress, however, increases even more with water composite fluids exceeding the residual stress level of the subsurface ground with oil [Althaus 1982]. Those results are contrary to findings of novel research projects, which observed compressive residual stress when emulsions were used for external cylindrical grinding of the same material with a cutting speed of  $v_c = 60 \text{ m/s}$  and a specific material removal rate of  $Q'_w = 12.0 \text{ mm}^3/\text{mm/s}$  independently of the volume removed. This relation is interpreted by Brinksmeier [1991b] and Heuer [1992] against the background of the grind-in behavior of vitrified CBN grinding wheels. According to this, the grind-in process decelerated through reduced friction due to grinding with oil and leads to smaller chip spaces and to a higher thermal stress of the subsurface, reflected in a stress level shifted to tensile residual stress. If there are identical grinding wheel topographies, equal compressive residual stress is measured for water composite and water-immiscible fluids, although a higher specific grinding energy is absorbed from the process if an emulsion is used due to the higher friction. This effect is compensated by the better cooling effect of this fluid. The differences from the results of Althaus can be explained by the much lower

material removal rate. Thus, due to sufficient chip space in the grinding wheel surface, the grind-in of the grinding wheel is insignificant [Brinksmeier 1991b]. Other investigations report on an unfavorable effect on the microhardness gradient normal to the surface during grinding with emulsion, characterized by the formation of a soft membrane. In this case, oil could avoid a negative influence on the subsurface [Flaischlen 1977]. Vits, too, reported a smaller depth of the affected zone after grinding 100Cr6 with grinding oils than with water composite fluids [Vits 1985].

The results listed in this chapter illustrate the need to be aware of the complexity of the tribochemical and tribomechanical influences in grinding. For further reading on the tribology of abrasive machining processes, the reader is referred to the book by Marinescu, Rowe, Dimitrov, and Inasaki [2004].

## REFERENCES

- Althaus, P.-G. 1982. "Leistungssteigerung beim Innenschleifen durch kubisches Bornitrid (CBN) und neue Maschinenkonzeptionen." Ph.D. thesis, Universität Hannover.
- Bartelt, G. and Studt, P. 1992. "The Effect of Selected Oil Additives on Sliding Friction and Wear of Ceramic/Ceramic Couples Lubricated with Hexadecane." Proceedings of the 5th Nordic Symposium on Tribologie, Helsinki, Finland.
- Bartz, W. J. 1978. "Wirtschaftliches Zerspanen durch Kühlschmierstoffe." Teil I und II, *wt-Z. industrielle Fertigung*, 8, 471.
- Beck, T. 2001. "Kühlschmierstoffeinsatz beim Schleifen mit CBN." Ph.D. thesis, RWTH Aachen.
- Bock, R. 1993. "Umweltfreundliche Kühlschmierstoffe." *Jahrbuch "Schleifen, Honen, Läppen und Polieren."* 57, 63, Vulkan.
- Böschke, K. 1993. "Der Kühlschmierstoff als Werkstoff." *wt-Werkstattstechnik*, vol. 3, Springer Verlag, Düsseldorf, Germany.
- Brinksmeier, E. 1991a. "Aufgaben der Kühlschmierstoffe bei spanender Bearbeitung." Proc. "Kühlschmierstoffe in der spanenden Fertigung." des dt. Industrieforums f. Tech. (DIF), Frankfurt.
- Brinksmeier, E. 1991b. *Prozess- und Werkstückqualität in der Feinbearbeitung*. Fortschrittberichte VDI, Reihe 2, Nr. 234, VDI-Verlag, Düsseldorf.
- Brinksmeier, E. and Schneider, C. 1993. "Bausteine für umweltverträgliche Feinbearbeitungsprozesse." Proc. 7. Braunschweiger Feinbearbeitungskolloquium, "Hohe Prozesssicherheit, hohe Leistung, hohe Präzision."
- Brücher, T. 1993. "Kühlschmierung – ein wesentlicher Faktor für wirtschaftliche Schleifbearbeitung." Proc. "Wirtschaftliche Schleifverfahren," des dt. Industrieforums f. Technologie (DIF), Ratingen.
- Brücher, T. 1996. "Kühlschmierung beim Schleifen keramischer Werkstoffe." Ph.D. thesis, Technische Universität Berlin.
- Carius, A. C. 1989. "Effects of Grinding Fluid Type and Delivery on CBN Wheel Performance." SME, *Modern Grinding Technologie*, Detroit, MI.
- Dederichs, M. 1972. "Untersuchung der Wärmebeeinflussung des Werkstücks beim Flachsleifen." Ph.D. thesis, RWTH Aachen.
- DIN 51 385. 1981. *Kühlschmierstoff – Begriffe*. Berlin, Beuth.
- Eckhardt, F. 1983. "Kühlschmierstoffe für die spanende Metallbearbeitung." Teil 1–11, *TZ für Metallbearbeitung*.
- Flaischlen, E. 1977. "Maßnahmen zur Vermeidung von thermischer Oberflächenschäden beim Schleifen – Beispiel aus der Praxis." *Jahrbuch "Schleifen, Honen, Läppen und Polieren."* 48, 151, Vulkan.
- Gerhäuser, W. and Laika, K. 1977. "Einflussgrößen auf den Verschleiß von Diamantwerkzeugen bei der Gesteinsbearbeitung." *Jahrbuch "Schleifen, Honen, Läppen und Polieren."* 48, 341, Vulkan.
- Gühring, K. 1967. "Hochleistungsschleifen." Ph.D. thesis, RWTH Aachen.
- Heinzel, C. 1999. "Methoden zur Untersuchung und Optimierung der Kühlschmierung beim Schleifen." Ph.D. thesis, Universität Bremen.
- Heuer, W. 1991. "Potentiale der Kühlschmierung beim Schleifen mit hochharten Schleifstoffen." Proc. "Kühlschmierstoffe in der spanenden Fertigung." des deutschen Industrieforums f. Techn. (DIF), Frankfurt.

- Heuer, W. 1992. *Außenrundscheifen mit kleinen keramisch gebundenen CBN-Schleifscheiben*. Fortschrittberichte VDI, Reihe 2, Nr. 270.
- Holz, R. and Sauren, J. 1988. *Schleifen mit Diamant und CBN*. Hrsg.: Ernst Wint er & Sohn GmbH & Co., Hamburg.
- Howes, T. D. 1990. "Assessment of the Cooling Lubricative Properties of Grinding Fluids." *Ann. CIRP* 39, 1, 313.
- Howes, T.D., Neailey, K., and Harrison, J. 1987. "Fluid Film Bioling in Shallow Cut Grinding." *Ann. CIRP* 36, 1, 223.
- Kassack, J. F. 1994. "Einfluss von Kühlschmierstoff-Additiven auf Werkzeugverschleiß, Zerspankraft und Bauteilqualität." Ph.D. thesis, RWTH Aachen.
- Kersch, H.-W. 1988. "Einfluss des Kühlschmierstoffes beim Hochgeschwindigkeitsschleifen mit CBN." *Werkstatt und Betrieb*. 12, 979.
- Keyser, W. 1970. "Kühlschmierung beim Schleifen." *IDR* 3, 158.
- Keyser, W. 1974. "Kühlschmiermittel für die Feinstbearbeitung von Oberflächen." *Jahrbuch "Schleifen, Honen, Läppen und Polieren"* 46, Ausgabe.
- Khudobin, L. V. 1969. "Cutting Fluids and Its Effect on Grinding Wheel Clogging." *Mach. Tooling* 4, 54.
- Klocke, F. 1982. *Gewindeschleifen mit Bornitridschleifscheiben*. Produktionstech. – Berlin, Forschungsber. Für die Praxis, Bd. 30, Hanser Verlag.
- Klocke, F. and Gerschwiler, K. 1996. *Trockenbearbeitung-Grundlagen*. Grenzen, Perspektiven, VDI-Berichte Nr. 1240.
- Kohblanck, G. 1956. *Kühlen und Schmierungen in der Zerspantechnik*. Teil 1 und 2 Fertigungstechnik 5 und 4, 152, 205.
- König, W. 1980. *Fertigungsverfahren*. Bd. 2, VDI-Verlag, Düsseldorf.
- König, W. and Klocke, F. 1996. *Fertigungsverfahren Band 2 – Schleifen, Honen, Läppen*. Düsseldorf: VDI-Verlag.
- König, W. et al. 1993. "Kühlschmierstoff – Eine ökologische Herausforderung an die Fertigungstechnik." *Wettbewerbsfaktor Produktionstechnik*. Sonderausgabe für AWK, VDI-Verlag, Düsseldorf.
- Korff, J. 1991. "Additive für Kühlschmierstoffe." Proc. "Kühlschmierstoffe in der spanenden Fertigung." des deutschen Industrieforums f. Techn. (DIF), Frankfurt, 21–22, Oktober.
- Leiseder, M. L. 1991. *Metalworking Fluids*. Landsberg: Verlag moderne Industrie.
- Mang, T. 1983. *Die Schmierung in der Metallbearbeitung*. Vogel Verlag, Würzburg.
- Marinescu, I. D. and Webster, J. A. 1983. "Tribo Technological Aspects of Brittle Materials Grinding." *Transactions of the 5th International Grinding Conference*, Cincinnati, OH.
- Marinescu, I., Rowe, W. B., Dimitrov, B., and Inasaki, I. 2004. *Tribology of Abrasive Machining Processes*. William Andrew Publishing, Norwich, NY.
- Möller, U. J. and Boor, U. 1986. *Schmierstoffe im Betrieb*. VDI-Verlag, Düsseldorf.
- Müller, J. 1985. "Anforderungen an wassermischbare bzw. wassergemischte Kühlschmierstoffe – Theorie und Praxis." *Sonderdruck aus: Tribologie und Schmierungstechnik* 4, 222.
- Nee, A. Y. C. 1979. "The Effect of Grinding Fluid Additives on Diamond Abrasive Wheel Efficiency." *Int. J. Mach. Tool Des. Res.* 19, 21.
- Oates, P. D., Bezer, H. J., and Balfour, A. M. 1977. "Bewertung von Kühlschmierstoffen für die Verwendung mit AMBER BORON NITRIDE – Schleifmitteln." *IDR* 4, 221.
- Ott, H. W. 1985. "Kühlschmierungen – Voraussetzung für kostengünstiges Schleifen und Abrichten." Proc. "Schleifen als qualitätsbestimmende Endbearbeitung." des VDI Bildungswerkes, Düsseldorf.
- Ott, H. W. 1991. "Kühlschmierstoffzusammensetzung und Prozessgrößen beim Schleifen." Proc. "Kühlschmierstoffe in der spanenden Fertigung." des deutschen Industrieforums f. Techn. (DIF), Frankfurt.
- Peters, J. and Aereus, R. 1976. "An Objective Method for Evaluating Grinding Coolants." *Ann. CIRP* 25, 1, 247.
- Pfau, A. 1987. "Stand der Technik in der Bearbeitung von Brillengläsern." *Diamant Information M4*, De Beers Industrial Diamond Division, April.
- Pfeiffer, W. et al. 1993. "Kühlschmierstoffe – Umgang, Messung, Beurteilung." Schutzmaßnahmen, BIA-Report 3, 91.
- Polyanskov, Y. V. and Khudobin, L. V. 1979. "The Effect of Coolant on the Surface Finish of a Ground Surface in Sparking-Out." *Russ. Eng. J.* 5, 46.
- Roth, P. and Wobker, H.-G. 1991. "Schleifbearbeitung keramischer Werkstoffe." *Sprechsaal* 4, 254.

- Sawluk, W. 1964. "Flachschleifen von oxidkeramischen Werkstoffen mit Topfscheiben." Ph.D. thesis, TH Braunschweig.
- Schrimpf, H. 1978. "Volumenminimierung und Funktionsoptimierung der Sammelbehälter von Schmierömlaufanlagen." *Schmiertechnik und Tribologie* 06, 206.
- Seifarth, M. 1987. "Bearbeitung von optischem Glas mit Diamantwerkzeugen." *Diamant Information M4*, De Beers Industrial Diamond Division, April.
- Sperling, F. 1971. "Optimales Kühlschmiermittel beim Schleifen." *Ind. Anzeiger* 87, 2150.
- Spur, G. 1983. "Kühlschmierstoffe für die Metallzerspanung." *Lehrblätter/Fertigungstechnik, Zwf* 12, 585–586.
- Spur, G. 1993. "Werkstoffspezifische Schleiftechnologie – Schlüssel für erhöhte Prozessfähigkeit in der Keramikbearbeitung." *Jahrbuch "Schleifen, Honen, Läppen und Polieren,"* 57, Ausgabe, 335.
- Spur, G., Niewelt, W., and Meier, A. 1995. "Schleifen von Superlegierungen für Gasturbinen – Einfluss des Kühlschmierstoffs auf das Arbeitsergebnis." *Zwf* 6, 311.
- Studt, P. 1987. "Influence of Lubrication Oil Additives on Friction of Ceramics under Conditions of Boundary Lubrication." *Wear* 115, 185.
- Tawakoli, T. 1990. "Hochleistungs-Flachschleifen, Technologie." *Verfahrensplanung und wirtschaftlicher Einsatz*, VDI-Verlag.
- Tawakoli, T. 1993. "Anforderungen an Kühlschmierstoffanlagen beim Hochleistungsschleifen." *Ind. Diamanten Rundschau* 1, 34.
- Tio, T. H. and Brücher, T. 1988. "Kühlschmierung bei der Schleifbearbeitung keramischer Werkstoffe." Proc. Arbeitskreises "Keramikbearbeitung," Produktionstechnisches Zentrum Berlin.
- Tönshoff, H. K. and Jürgenharke, B. 1979. "Innenschleifen kleiner Bohrungen." *Jahrbuch "Schleifen, Honen, Läppen und Polieren,"* 49, Ausgabe.
- Tönshoff, H. K. and Schulze, R. 1980. "Einfluss des Kühlmittels bei der Bearbeitung von Hartgestein." *IDR* 1, 19.
- Treffert, C. 1995. *Hochgeschwindigkeitsschleifen mit galvanisch gebundenen CBN-Schleifscheiben*. Berichte aus der Produktionstechnik, Bd. 4/49.
- Triemel, J. 1976. "Schleifen mit Bornitrid." *Fertigungstechnische Berichte*. Bd. 6.
- VDI-Richtlinie 3035. 1997. *Anforderungen an Werkzeugmaschinen, Fertigungsanlagen und periphere Einrichtungen beim Einsatz von Kühlschmierstoffen*. Düsseldorf: VDI-Verlag, September.
- VDI-Richtlinie 3396. 1983. *Kühlschmierstoffe für spanende Fertigungsverfahren*. Düsseldorf, VDI-Verlag.
- Vits, R. 1985. "Technologische Aspekte der Kühlschmierung beim Schleifen." Ph.D. thesis, RWTH Aachen.
- Webster, J. 1995. "Selection of Coolant Type and Application Technique in Grinding." Proceedings of Supergrind '95 "Developments in Grinding," Storrs, CT.
- Weinert, K. 1999. *Trockenbearbeitung und Minimalmengenschmierung*. Springer Verlag, New York.
- Wiggenhauser, R. 1994. "Ganzheitlich.Umweltgerechtes Auslegen der Peripherie von Zahnrad-Profilschleifmaschinen." *Maschinenmarkt Würzburg* 100, 35, 38.
- Wobker, H.-G. 1992. *Schleifen keramischer Schneidstoffe*. Fortschrittberichte VDI, Reihe 2, Nr. 237.
- Yatsui, H. and Tsukada, S. 1983. "Influence of Fluid Type on Wet Grinding Temperature." *Bull. Japan Soc. Prec. Eng.* 2, 133.
- Zimmermann, D. 1982. "Kühlschmierstoffe für die Feinbearbeitung." *tz für Metallbearbeitung* 4, 16.
- Zwingmann, G. 1960. *Schmier- und Kühlflüssigkeiten bei der Feinbearbeitung*. Schriftenreihe Feinbearbeitung, DEVA, Stuttgart.
- Zwingmann, G. 1979. "Kühlschmierstoffe für die spanende Metallbearbeitung." Teil 1 und 2. *Werkstatt und Betrieb* 6, 409, 483.



---

# 11 Monitoring of Grinding Processes

## 11.1 THE NEED FOR PROCESS MONITORING

### 11.1.1 INTRODUCTION

The behavior of any grinding process is very complex. There are a large number of input variables and the whole process is transient, that is, the mechanisms change with time. The general need for a monitoring system is expressed by Figure 11.1.

### 11.1.2 THE NEED FOR SENSORS

An essential feature of any monitoring system is that there are sensors that can detect whether the process is running normally or abnormally. A monitoring system in an automatic grinding machine is incorporated into a control system. The system has to be able to correct the machine operational settings so that a near-optimal condition can be restored if the system is running abnormally or even in a suboptimal state.

Sensor systems for a grinding process should be capable of detecting any malfunctions in the process with high reliability so that the production of substandard parts can be minimized. Some major quality issues in the grinding process are the occurrence of chatter vibration, grinding burn, and surface roughness deterioration. Quality problems have to be identified in order to maintain the desired workpiece quality.

### 11.1.3 PROCESS OPTIMIZATION

In addition to quality detection, another important task of the monitoring system is to provide useful information for optimizing the grinding process in terms of total grinding time or total grinding cost. Optimization of the process can possibly be achieved if degradation of the process behavior can be tracked by the monitoring system. The information obtained with a sensor system can be used also to establish databases as part of an intelligent system [Rowe et al. 1994, Tönshoff, Friemuth, and Becker 2002].

### 11.1.4 GRINDING WHEEL WEAR

An important aspect of a grinding process is grinding wheel performance. The grinding wheel should be properly selected and conditioned to meet the requirements of the parts. Grinding wheel performance may change significantly during the grinding process, which makes it difficult to predict process behavior in advance. Conditioning of the grinding wheel surface is necessary before grinding starts. It becomes necessary as well after the wheel has reached the end of its redress life to restore the wheel configuration and the surface topography to the initial state. Therefore, sufficient sensor systems are required to minimize the additional machining time, to assure the desired grinding wheel topography is maintained, and to minimize wasted abrasive material during conditioning.



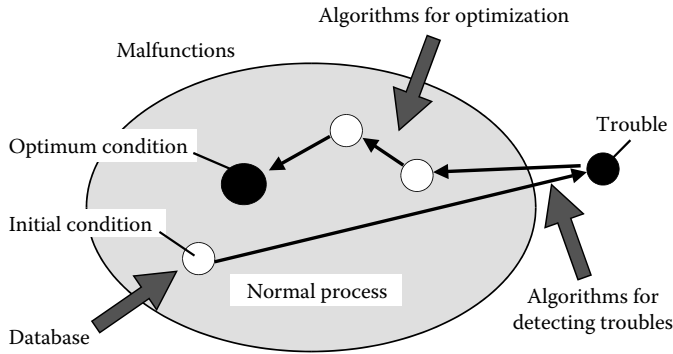


FIGURE 11.1 Role of a monitoring system for grinding.

## 11.2 SENSORS FOR MONITORING PROCESS VARIABLES

### 11.2.1 INTRODUCTION

As with all manufacturing processes, ideally, the variables of greatest interest are measured directly as close to their origin as possible. Grinding processes are affected by a large number of input variables that each influence the resulting output quantities. Brinksmeier [1991] proposed a systematic approach to distinguish between different types of quantities to describe a manufacturing process precisely [Marinescu et al. 2004].

The most common sensors to be used in either the industrial or the research environment are for force, power, and acoustic emission (AE) [Byrne et al. 1995]. Figure 11.2 shows the setup for the most popular integration of sensor systems in either surface or outer diameter grinding. Sensors mainly have to detect grinding performance during the period of intermittent contact between the grinding wheel and workpiece. Only during this limited interaction can many process quantities be detected.

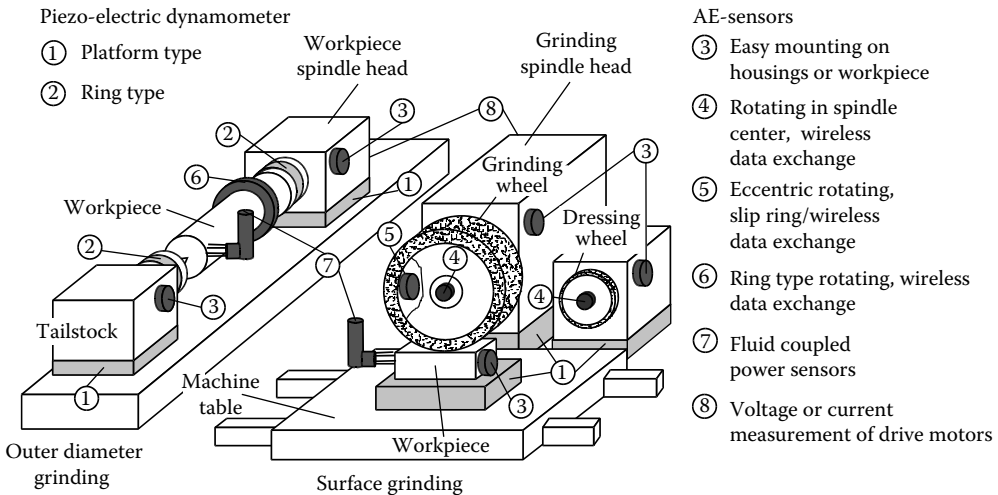


FIGURE 11.2 Possible mounting positions of force, acoustic emissions, and power sensors.

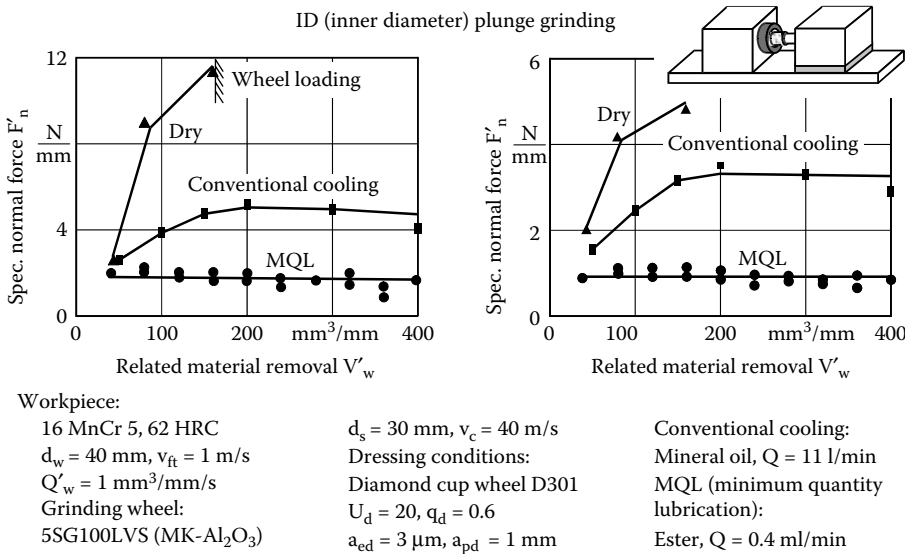


FIGURE 11.3 Grinding forces measurement with platform dynamometer.

11.2.2 FORCE SENSORS

The first attempts to measure grinding forces go back to the early 1950s and were based on strain gauges. Although the system performed well to achieve substantial data on grinding, the most important disadvantage of this approach was the significant reduction of the total stiffness during grinding. Thus research was done to develop alternative systems. With the introduction of piezo-electric quartz force transducers a satisfactory solution was found. In Figure 11.2, different locations are shown for mounting a force platform. In surface grinding, the platform is most often mounted on the machine table to carry the workpiece. In inner (ID) or outer diameter (OD) grinding this solution is not available due to the rotation of the workpiece. In this case, either the whole grinding spindle head is mounted on a platform or the workpiece spindle head and sometimes also the tailstock are put on a platform [Karpuschewski 2001].

Figure 11.3 shows an example of force measurement with the spindle head on a platform during ID plunge grinding. In this case, the results are used to investigate the influence of coolant supply systems while grinding case-hardened steel. The force measurements give a clear view that it is not possible to grind without coolant using the chosen grinding wheel due to wheel loading and, respectively, high normal and tangential forces. But it is also seen that there is a high potential for minimum quantity lubrication (MQL) with very constant force levels over the registered related material removal [Brunner 1998].

For OD grinding, it is also possible to use ring-type piezo-electric dynamometers. With each ring, again, all three perpendicular force components can be measured; they are mounted under preload behind the nonrotating center points. To complete possible mounting positions of dynamometers in grinding machines, also the dressing forces can be monitored by the use of piezo-electric dynamometers, for example, the spindle head of rotating dressers can be mounted on a platform. Besides these general solutions, many special setups have been used for nonconventional grinding processes like ID cut-off grinding of silicon wafers or ID grinding of long small bores with rod-shaped tools.

Force measurements can also be used to get information about the surface integrity state of a workpiece. The tangential force is the more important component, because the multiplication of tangential force and cutting speed results in the grinding power  $P_c$  as shown in Figure 11.4 for OD plunge grinding. If this grinding power is referred to the zone of contact, the specific grinding

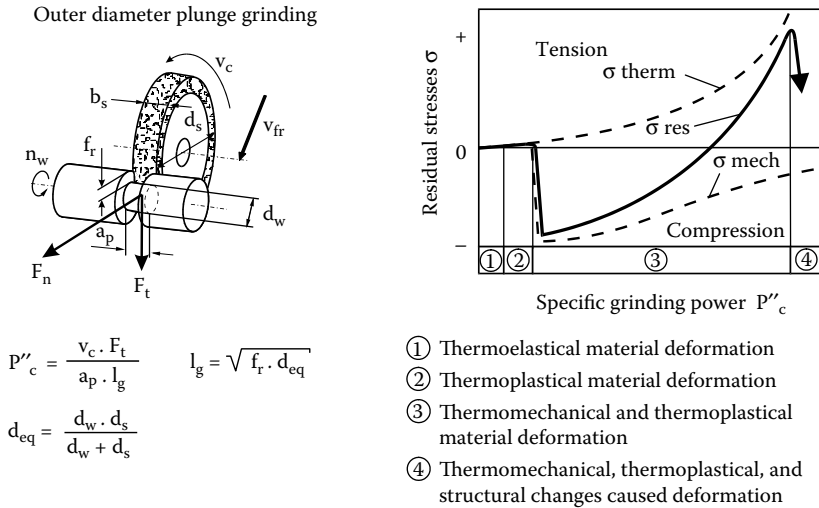


**FIGURE 11.4** Residual stress determination depending on grinding power.

power  $P_c$  can be calculated. Grinding power can be used to estimate the heat generation during grinding [Brinksmeier 1991, Karpuschewski 1995, Marinescu et al. 2004].

On the right-hand side of Figure 11.4, the residual stress change at the surface of a ground-hardened steel workpiece is schematically shown for increasing specific grinding power [Brinksmeier 1991]. The effects of thermal and mechanical loads interact with each other. At the beginning, only small thermally induced residual stresses due to external friction are likely to occur. With the beginning of plastic deformations, a steep increase of compressive residual stresses can be registered. With rising specific grinding power and thus higher temperatures in the contact zone the mechanical influence decreases while the thermal load becomes dominant.

At very high levels of  $P_c$  structural changes might disturb the further tensile residual stress rise. Rehardening layers are likely to occur, drastically reducing tensile residual stresses [Karpuschewski 1995]. Figure 11.5 shows representative structure surveys, Vickers microhardness depths, and residual

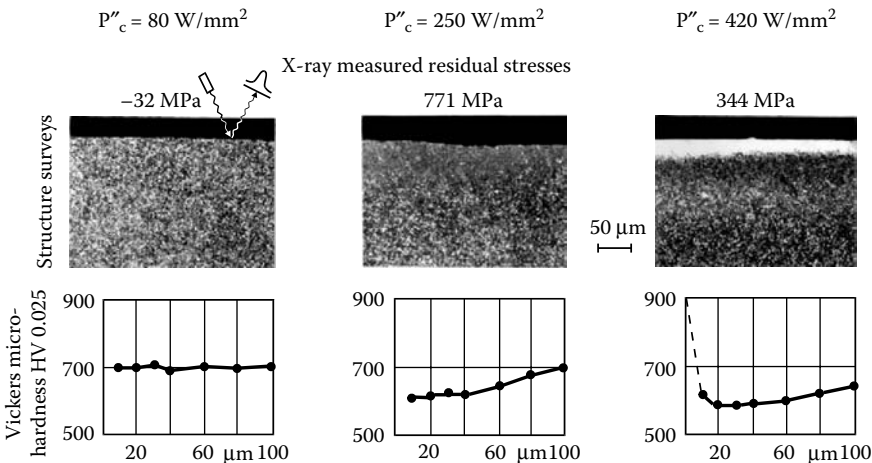


**FIGURE 11.5** Influence of the specific grinding power on surface integrity of 16 MnCr 5.

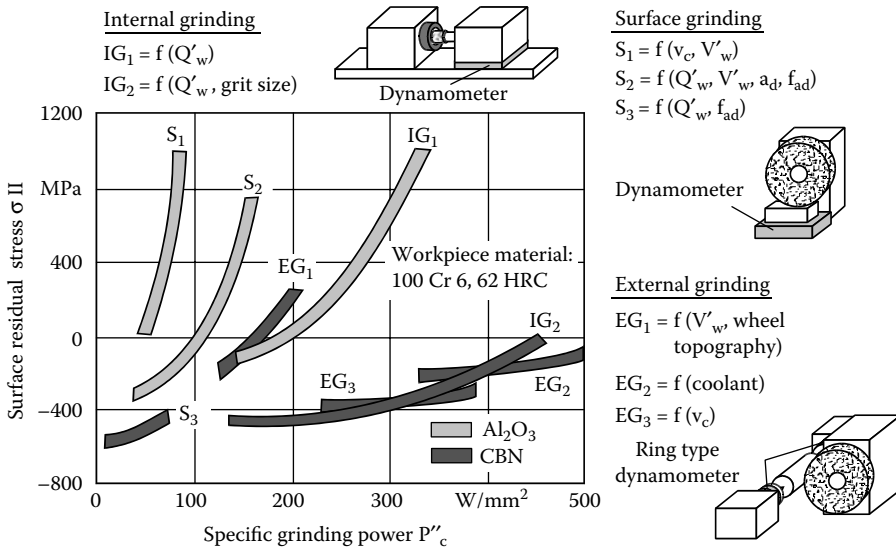


FIGURE 11.6 Set of different thermal transfer functions based on force measurement.

stress measurements of different plunge-cut ground workpieces made of case-hardened steel. The specific grinding power as the main characteristic was varied through the increase of the specific material removal rate  $Q'_w$ . Brinksmeier analyzed a large variety of different grinding processes to establish an empirical model for the correlation between the specific grinding power based on force measurement and the X-ray-calculated residual stress states [Brinksmeier 1991]. Figure 11.6 shows so-called thermal transfer functions for different grinding operations on ball bearing steel. The results reveal that it is possible to generate compressive residual stresses with any grinding operation as long as the specific grinding power is small enough. For higher values of  $P_c$ , there is a clear tendency toward tensile residual stresses. The superior behavior of cubic boron nitride (CBN) grinding wheels compared to conventional abrasives is obvious, because this abrasive has a much better thermal conductivity and is thus able to remove more heat from the zone of contact.

Recent fundamental investigations of grinding efficiency and thermal damage have highlighted the importance of specific energy in grinding [Rowe and Jin 2001]. Specific energy is the energy per unit volume of material removed usually quoted in joules/cubic millimeter. Specific energy can be calculated by dividing the grinding power by the material removal rate.

$$e_c = \frac{F_t v_s}{a_e v_w}$$

Specific energy is an inverse measure of grinding efficiency. Low specific energy represents high removal rate with low consumption of energy. Table 11.1 clearly demonstrates that low specific energy gives rise to lower temperatures than high specific energy. Table 11.1 shows a measurement where the lowest temperature was recorded at the highest removal rate. This is the opposite of normal expectation and is simply a result of low specific energy. For this reason there is an increasing trend toward monitoring specific energy as a measure of the health of grinding processes. If the specific energy increases with time, it probably means the grinding wheel needs redressing.

The specific energy is conveniently computed from a grinding force sensor or from a power sensor. Power sensing is dealt with in the next section.

**TABLE 11.1**  
**Effect of Specific Energy and Removal Rate on Grinding Temperature**

Depth of cut, mm		0.407	0.98	0.92	0.96
Wheel diameter, mm		173	173	173	170
Workspeed, m/s		0.2	0.2	0.25	0.3
Contact length, mm		8.37	13.0	12.6	12.8
Peclet number		45	70	85	103
Removal rate, mm <sup>2</sup> /s		81	196	230	288
Total heat flux, $q_t = P_c/b_w l_c$	W/mm <sup>2</sup>	165	200	238	248
Flux to chips, $q_{ch}$	W/mm <sup>2</sup>	79	122	149	184
Net heat flux, $q_t - q_{ch}$	W/mm <sup>2</sup>	85.8	78	89	64
Predicted, $T_{max} - wet$	°C	238	224	249	172
Predicted, $t_{max} - dry$	°C	1180	1290	1280	823
Measured, $T_{max} - msd$	°C	1250	1350	1050	180
Specific energy	J/mm <sup>3</sup>	17.0	13.3	13.0	11

The results also show that it is not possible to predict the residual stress state only based on the specific grinding power without knowing the corresponding transfer function. The variations in the heat distribution due to different grinding wheel characteristics, process kinematics, and parameters are too widely spread. But nevertheless it can be clearly stated that a force measurement especially of the tangential force is a well-suited method to control the surface integrity state of ground workpieces.

The application of dynamometers can be regarded as state of the art. But also wire strain gauges are still in use. For example, force measurement in face grinding of inserts is not possible with a piezo-electric system due to limited space. In this case, an integration of wire strain gauges with a telemetric wireless data exchange was successfully applied [Friemuth 1999, Karpuschewski 2001].

### 11.2.3 POWER MEASUREMENT

The measurement of power consumption of a grinding spindle drive can be regarded as technically simple, but the evidence of this process quantity is definitely limited. The amount of power used for the material removal process is always only a fraction of the total power consumption. Nevertheless, power monitoring is widely used in industrial applications by defining specific thresholds to avoid any overload of the whole machine tool due to bearing wear or any errors from operators or automatic handling systems. In grinding, power monitoring is a popular method to avoid thermal damage of the workpiece. The main reason is the easy installation without influencing the working space of the machine tool and the relatively low costs. However, different investigations have clearly shown that the dynamic response of a power sensor at the main spindle is limited.

A typical result is shown in Figure 11.7 for a grinding process on spiral bevel ring gears, introducing a vitreous bond CBN grinding wheel for this complex operation. The cone-shaped grinding wheel with a metal core is fed to the workpiece made of case-hardened steel with a 6-axis CNC grinding machine; the process is called flare-cup grinding. Monitoring of the grinding power revealed a constant moderate increase over the material removal,  $V'_w$ . At a specific material removal of 8,100 mm<sup>3</sup>/mm, which corresponds to a number of 27 ground ring gears, grinding burn was detected for the first time by nital etching. The macro- and microgeometry of the 28th workpiece was still within the tolerances, so the tool life criterion was the surface integrity state. After conditioning the grinding wheel with a diamond form roll, the process can be continued. The grinding burn limit fixed by this test was proven in further succeeding investigations. For this type of medium, or even large-scale production in the automotive industry using grinding wheels with

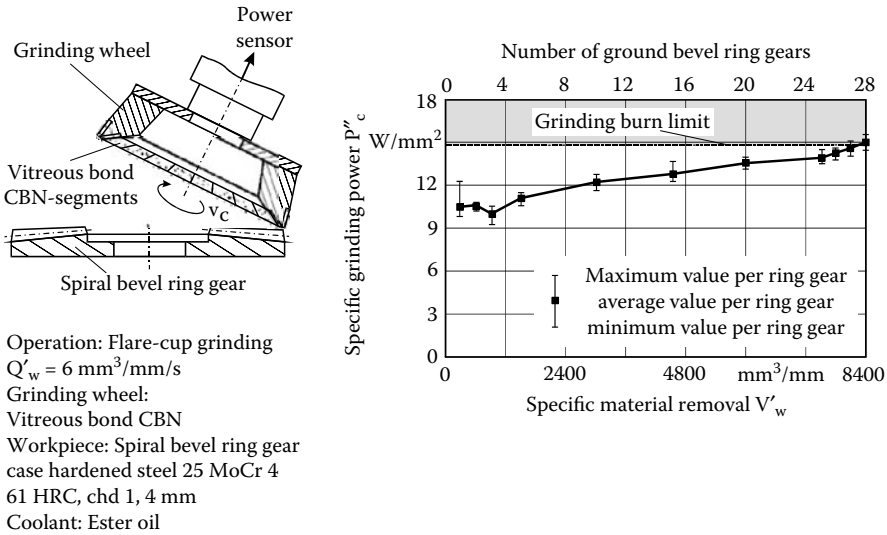


FIGURE 11.7 Power monitoring in spiral bevel gear grinding to avoid grinding burn.

a long lifetime, this power monitoring is a very effective way to avoid thermal damage of the workpiece and also to get rid of the environmentally harmful etching process.

These results reveal that power monitoring can be a suitable sensor technique to avoid surface integrity changes during grinding. The most promising application is seen for superabrasives, because the slow wear increase of the grinding wheel can be clearly determined with this dynamically limited method.

### 11.2.4 ACCELERATION SENSORS

In abrasive processes, the major application for acceleration sensors is related to balancing systems for grinding wheels. Especially large grinding wheels without a metal core may have a significant unbalance at the circumference. With the aid of acceleration sensors, the vibrations generated by this unbalance are monitored during the rotation of the grinding wheel at cutting speed. Different systems are in use to compensate this unbalance, for example, hydro compensators using coolant to fill different chambers in the flange or mechanical balancing heads, which move small weights to specific positions. Although these systems are generally activated at the beginning of a shift, they are able to monitor the change of the balance state during grinding and can continuously compensate the unbalance.

### 11.2.5 AE SYSTEMS

The application of AE sensors has become very popular in all kinds of machining processes over the last decade. A large variety of sensors specially designed for monitoring purposes have been introduced on the market. They combine some of the most urgent requirements for sensor systems like relatively low costs, no negative influence on the stiffness of the machine tool, easy to mount, and even capable of transmitting signals from rotating parts.

First results on AEs were published in the 1950s in tensile tests. Since then decades have passed until this approach was first used to monitor manufacturing processes. The mechanisms leading to AE are mainly deformations through dislocations and distorted lattice planes, twin formation of polycrystalline structures, phase transitions, friction, crack formation, and propagation. Due to these different mechanisms, AE appears either as a burst-type signal or as a continuous

emission. The grinding process is characterized by the simultaneous contact of many different cutting edges randomly shaped with the workpiece surface. Every single contact of a grain generates a stress pulse in the workpiece. During operation, the properties of the single grain and their overall distribution on the circumference of the grinding wheel change due to the occurrence of wear. Thus many different sources of AE have to be considered in the grinding process. The single pulse is a combination of the impact of the grain with the workpiece material and its fracture behavior, of wear of the individual abrasive, as well as wear of the bond material. Even the structure of the workpiece material may change due to thermal overload during grinding. A change from austenite to martensite structures in ferrous materials also generates AE, although the energy content is significantly lower compared to the other sources.

Different types of signal evaluation can be applied to the AE-sensor output. The most important quantities are root-mean-square value, raw AE signals, and frequency analysis. The time domain course of the root-mean-square value  $U_{AE,RMS}$  contains essential information about the process condition [Inasaki 1991, Byrne et al. 1995]. This value can be regarded as a physical quantity for the intensity of the acoustic signal. It is directly related to the load of the material, thus making this value attractive for any kind of monitoring. However, it has to be regarded as an average statistical value, because most often a low-pass filter is applied. If short transient effects like single grit contacts are to be revealed, the raw AE signal without any filtering is more attractive. Evaluation in the frequency domain is used to identify dominant patterns, which can be related to specific process conditions like chatter.

Possible positions of AE-sensors in grinding are shown in Figure 11.2. The spindle drive units, the grinding wheel, or the workpiece can be equipped with a sensor. In addition, fluid-coupled sensors may be used without any direct mechanical contact to one of the mentioned components.

In Figure 11.8, the correlation between the surface roughness of a ground workpiece and the root-mean-square value of the AE-signal is shown [Meyen 1991]. A three-step outer diameter plunge grinding process with a conventional corundum grinding wheel was supervised. It is obvious that for a dressing overlap of  $U_d = 2$ , the coarse grinding wheel topography generated leads to a high initial surface roughness of  $R_z = 5 \mu\text{m}$ . Due to continuous wear of the grains the roughness increases as more material is removed. For the finer dressing overlap of  $U_d = 10$ , a smaller initial

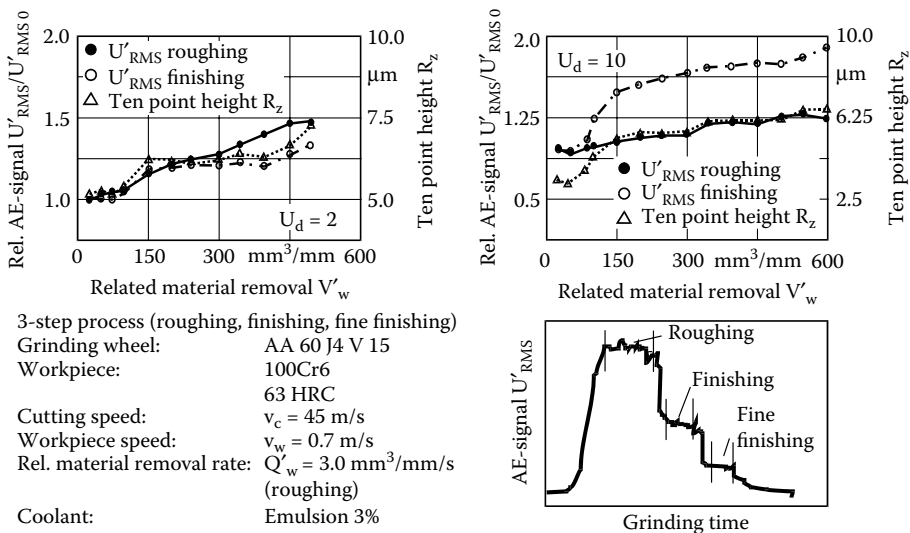
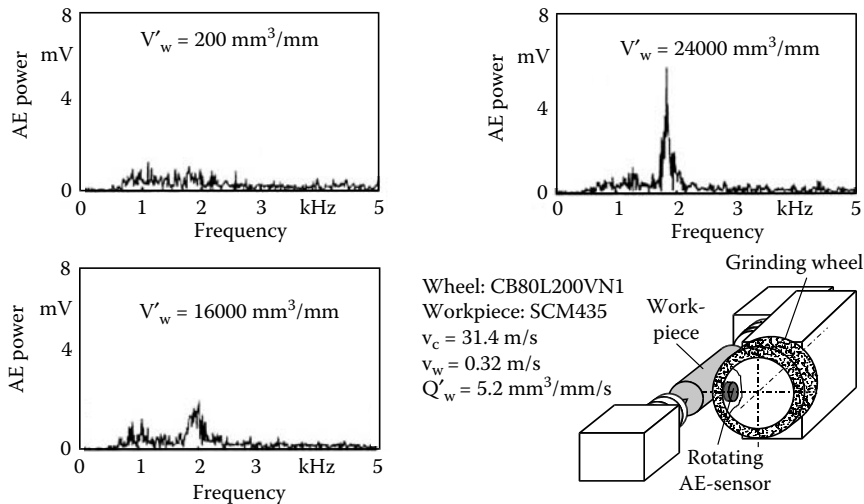


FIGURE 11.8 Correlation between surface roughness and the acoustic emissions-root mean square signal.



**FIGURE 11.9** Acoustic emission frequency analysis for chatter detection in grinding.

roughness with a significant increase can be seen for the first parts followed by a decreasing tendency. This tendency of the surface roughness is also represented by the AE-signal. Higher dressing overlaps lead to more cutting edges thus resulting in a higher AE activity. The sensitivity of the fine finishing AE-signal is higher, because the final roughness is mainly determined in this process step. Meyen has shown in many other tests that a monitoring of the grinding process with AE is possible.

Besides these time domain analyses, the AE-signal can be investigated in the frequency domain. Effects like wear or chatter vibration have different influence on the frequency spectrum, thus it should be possible to separate these effects. Figure 11.9 shows the result of a frequency analysis of the AE-signal in outer diameter plunge grinding with a vitreous bond CBN grinding wheel [Wakuda et al. 1993]. As a very special feature, the AE sensor is mounted in the grinding wheel core and the signals are transferred via a slip ring to the evaluation computer; thus grinding, as well as dressing operations, can be monitored. The results reveal that no significant peak can be seen after dressing and first grinding tests. Only after a long grinding time do specific frequency components emerge from the spectrum, which gain constant rising power during the continuation of the test. The detected frequency is identical with the chatter frequency, which could be stated by additional measurements. The AE-signals were used as input data for a neural network to automatically identify the occurrence of any chatter vibrations in grinding [Wakuda et al. 1993].

From the very first beginning of AE application in grinding, attempts were made to correlate the signal to the occurrence of grinding burn. The works of Klumpen [1994] and Saxler [1997] are directly related to the possibility of grinding burn detection with AE sensors. They made a systematic approach to identify dominant influences on the AE signal during grinding.

One fundamental result was that all process variations, which finally generate grinding burn, including increasing material removal rate or infeed or reduced coolant supply, lead to an increase of AE. Klumpen [1994] could only identify grinding burn by applying a frequency analysis of the AE signal to determine the inclination of the integral differences. This must be regarded as a major disadvantage because a frequency analysis is usually performed after grinding. This conclusion may change, of course, with the increasing availability of modern fast data signal-processing computer devices. Saxler concentrated on the AE signal in the time domain.



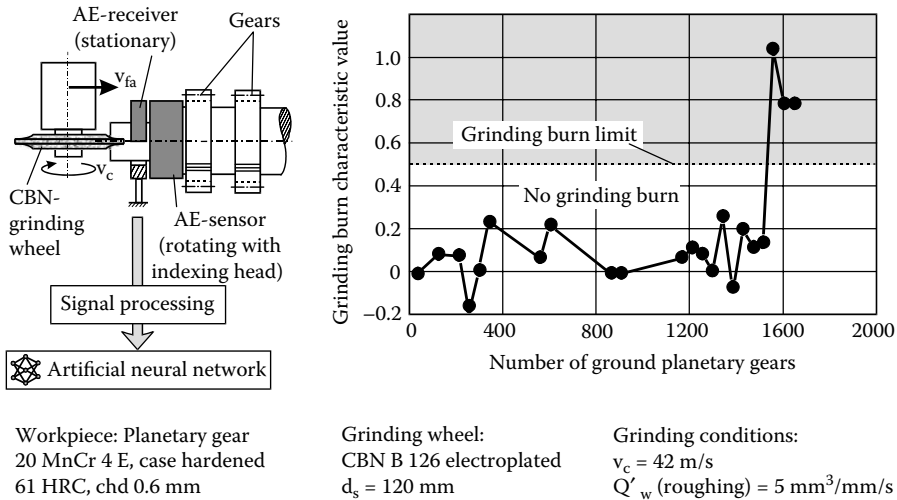


**FIGURE 11.10** Grinding burn detection with acoustic emission.

The major result of the work by Klumpen [1994] is shown in Figure 11.10. Based on his investigations and theoretical considerations, he concludes that the AE sensor must be mounted on the workpiece to be most sensitive to grinding burn detection. This is, of course, a major drawback for practical applications. An industrial test was conducted during gear grinding of planetary gears with an electroplated CBN-grinding wheel. The sensor was installed at the hydroexpansion clamping mandrel instead of one of a set of five gears. The sensor can rotate with the indexing head. The signals are wireless transferred to the stationary receiver. With the aid of artificial neural networks, Klumpen was able to achieve a dimensionless grinding burn characteristic value from the AE values of different frequency ranges in the time domain. Thus an in-process detection of workpiece surface integrity changes became possible. The high efforts for training of the artificial neural network and the problems related to the sensor mounting at the workpiece side must be seen as limiting factors for a wider industrial application. However, the results have clearly shown that AE systems can be regarded as suitable process quantity sensors in grinding to monitor surface integrity changes.

### 11.2.6 TEMPERATURE SENSORS

In any grinding process mechanical, thermal, and even chemical effects are usually superimposed in the zone of contact. Grinding in any variation is generating a significant amount of heat that may cause a deterioration of the dimensional accuracy of the workpiece, an undesirable change of the surface integrity, or lead to increased wear of the wheel. Figure 11.11 shows the most popular temperature measurement devices. The preferred method for temperature measurement in grinding is the use of thermocouples. The second metal in a thermocouple can be the workpiece material itself; this setup is called the single-wire or single-pole method. A further distinction is made according to the type of insulation. A permanent insulation of the thin wire or foil from the workpiece by use of sheet mica is known as open circuit. The insulation is interrupted by the individual abrasive grains; thus, measurements can be repeated or process conditions varied until the wire is worn or damaged. Many authors used this setup. Also the grinding wheel can be equipped with the thin wire or a thermo foil if the insulation properties of abrasive and bond material are sufficient. In the closed circuit type, a permanent contact of the thermal wire and the workpiece by welding or brazing is achieved. The most important advantage of this method is the possibility to measure temperatures in different distances from the zone of contact until the thermocouple is finally exposed

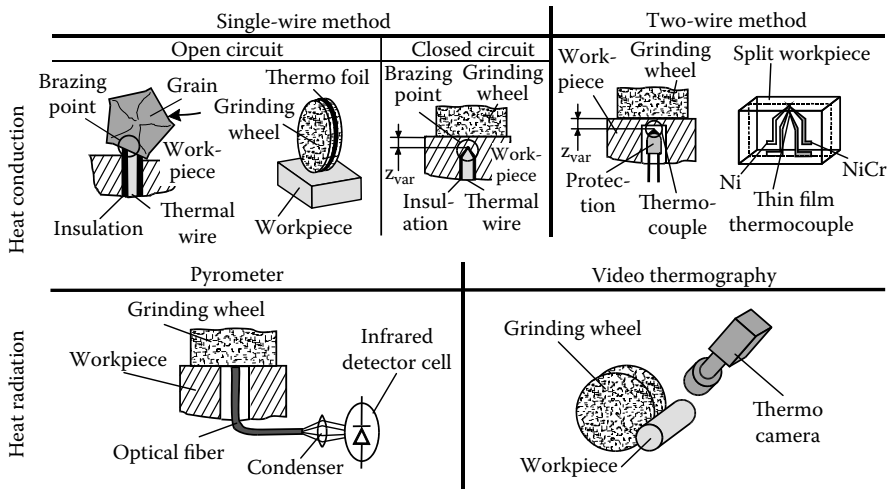


FIGURE 11.11 Temperature measurement systems in grinding.

at the surface. For the single-wire method, it is necessary to calibrate the thermocouple for every different workpiece material. This disadvantage is overcome by the use of standardized thermocouples where the two different materials are assembled in a ready-for-use system with sufficient protection. A large variety of sizes and material combinations are available for a wide range of technical purposes.

With this two-wire method it is again possible to measure the temperatures at different distances from the zone of contact. This approach can be regarded as most popular for temperature measurement in grinding. One disadvantage of the double-pole technique is that the depth of the thermocouple junction is much larger than it is for the single-pole technique. This has the effect that the temperature reading is averaged over a greater depth below the surface in a region where there is a steep temperature gradient.

Recent advances in application of thin-film single-pole and double-pole thermocouples offer considerable advantages of accuracy and of giving a direct temperature reading at the contact zone [Marinescu et al. 2004, Batako, Rowe, and Morgan 2005].

Thin film grindable thermocouples are a special case of the single-wire and two-wire methods [Lierse 1998, Batako et al. 2005]. An advantage of the thin-film method is an extremely small contact depth to resolve temperatures in a small area at the contact surface and the possibility to measure a temperature profile for every single test depending on the number of evaporated thermocouples in simultaneous use. Batako et al. found that a thin, but wide, single-pole thermocouple greatly increases the probability of maintaining a continuous temperature signal throughout the passage through the grinding contact zone.

Temperature measurements using thin-film thermocouples are shown in Figure 11.12 in grinding  $Al_2O_3$  ceramic with a resin-bonded diamond grinding wheel [Lierse 1998]. Obviously, the set grinding conditions have a significant influence on the generation of heat in the zone of contact. The heat penetration time is of major importance. In deep grinding with very small tangential feed speed, high temperatures are registered, whereas higher tangential feed speeds in pendulum grinding lead to a significant temperature reduction. As expected the avoidance of coolant leads to higher temperatures compared to a use of mineral oil. However, in any case, either for single or two-wire methods, the major disadvantage is the high effort to carry out these measurements. Due to the necessity to install the thermocouple as close to the zone of contact as possible, it is always a technique where either grinding wheel or workpiece has to be specially prepared. Thus, all these

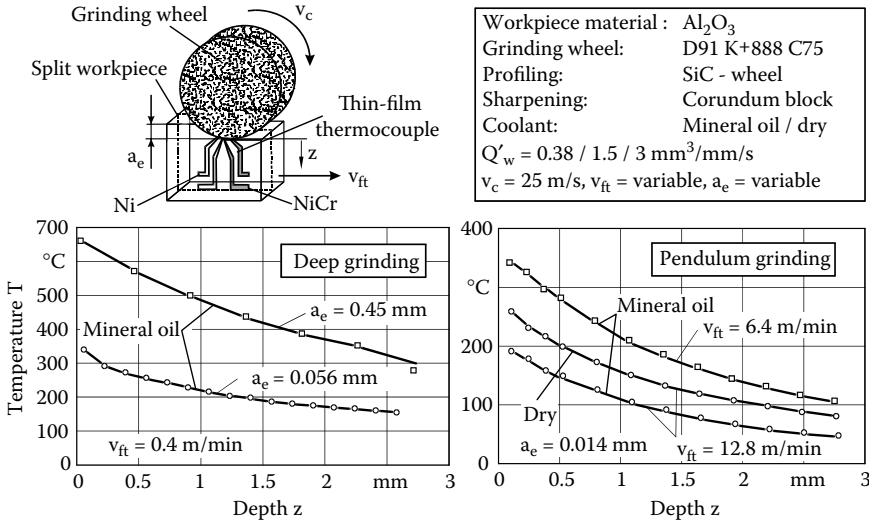


FIGURE 11.12 Grinding temperature measurement with thin-film thermocouples.

methods are only used in fundamental research; an industrial use for monitoring is not possible due to the partial destruction of major components.

Besides these heat conduction–based methods the second group of usable techniques is related to heat radiation. Infrared radiation techniques were used to investigate the temperature of grinding wheel and chips. By the use of a special infrared radiation pyrometer, with the radiation transmitted through optical fiber, it is even possible to measure the temperature of working grains of the grinding wheel just after cutting [Ueda, Hosokawa, and Yamamoto 1985]. Also, the use of coolant was possible and could be evaluated. In any case, these radiation-based systems need a careful calibration, taking into account the properties of the material to be investigated, the optical fiber characteristics, and the sensitivity of the detector cell. However, again for most of the investigations a preparation of the workpiece was necessary as shown in Figure 11.11 (bottom left).

A second heat radiation–based method uses thermography. For this type of measurement, the use of coolants is always a severe problem because the initial radiation generated in the zone of contact is significantly reduced in the mist or direct flow of the coolant until it is detected in the camera. Thus, the major application of this technique was limited to dry machining. Brunner [1998] was able to use a high-speed video thermography system for OD-grinding of steel to investigate the potential of dry or MQL grinding [Karpuschewski 2001].

## 11.3 SENSOR FOR MONITORING THE GRINDING WHEEL

### 11.3.1 INTRODUCTION

The grinding wheel state is of substantial importance for the quality of the grinding results. The wheel condition can be described by the characteristics of the grains. Wear can lead to flattening, breakage, and even pullout of whole grains. Moreover, the number of cutting edges and the ratio of active/passive grains are of importance. Also, the bond of the grinding wheel is subject to wear. Due to its hardness and composition, the bond significantly influences the wear and variation of the grain distribution. Wheel loading, when it occurs, generates negative effects due to insufficient chip removal and coolant supply.

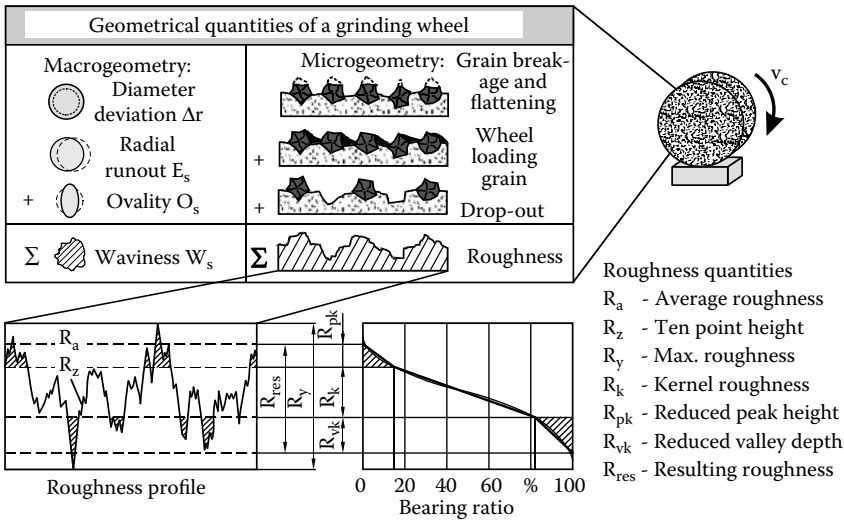


FIGURE 11.13 Geometrical quantities of a grinding wheel.

All these effects can be summarized as aspects of wheel topography, which changes during the wheel life between two dressing cycles. As a result, the diameter of the grinding wheel reduces with wear. In most cases, dressing cycles have to be carried out without any information about the actual wheel wear. Commonly, grinding wheels are dressed without reaching the end of acceptable wheel life in order to prevent workpiece damages, for example, workpiece burn. Figure 11.13 gives an overview about different geometrical quality features concerning the redress life of grinding wheels. As a rule, the different types of wheel wear are divided into macroscopic and microscopic features. Many attempts have been made to describe the surface topography of a grinding wheel and to correlate the quantities to the result on the workpiece.

In Figure 11.14, methods are introduced that are suitable for dynamic measurement of the grinding wheel. Most of the systems are not able to detect all micro- and macrogeometrical quantities, but can only be used for special purposes.

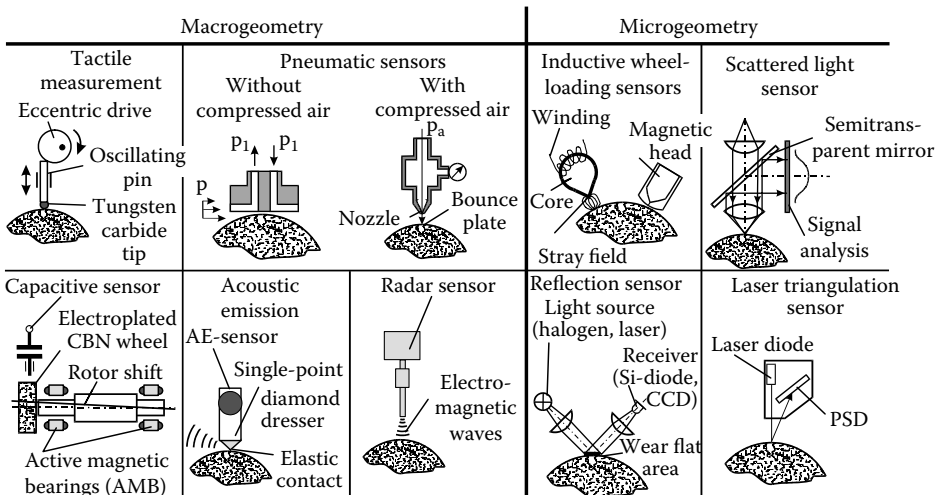


FIGURE 11.14 Sensors for grinding wheel topography measurement.

### 11.3.2 SENSORS FOR MACROGEOMETRICAL QUANTITIES

The majority of sensors are capable of measuring the macrogeometrical features. Any kind of mechanical contact of a sensor with the rotating grinding wheel causes serious problems because the abrasives always tend to grind the material of the touching element. Only by realizing short touching pulses with small touching forces and by using a very hard tip material like tungsten carbide is it possible to achieve satisfactory results. Another group of sensors for the measurement of grinding wheels is based on pneumatic systems. Although this method is, in principle, unable to detect microgeometrical features of a grinding wheel due to the nozzle diameter of 1 mm or more, the method is able to determine macrogeometry. A distinction should be made between systems that employ a compressed air supply or those that do not. The latter responds to airflow around the rotating grinding wheel. The results obtained reveal a dependence of the airflow on the distance of the sensor to the surface, on the circumferential speed, and to some extent on the topography of the grinding wheel. The method with a compressed air supply is based on the nozzle-bounce plate principle, with the grinding wheel being the bounce plate. These systems are capable of measuring the distance changes related to radial wear with a resolution of 0.2  $\mu\text{m}$ . This feature, comparatively easy setup, and moderate costs are the main reasons that pneumatic sensors have already found acceptance in industrial application.

Another possibility to register the macrogeometry of a grinding wheel was reported by Westkämper and Klyk [1993]. In high-speed ID grinding with CBN wheels, a spindle with active magnetic bearings (AMB) was used to achieve the necessary circumferential speed of 200 m/s with small-diameter wheels. These spindles have the opportunity to shift the rotor from rotation around the geometrical center axis to the main axis of inertia to compensate any unbalance. It is necessary to use balancing planes especially if electroplated CBN wheels are used without the possibility of dressing. To measure the runout of these, grinding wheels on the abrasive layer at the very high circumferential speed capacitive sensors have shown the best performance.

Also AE can be used to determine the macrogeometry of the grinding wheel. Oliveira, Dornfeld, and Winter [1994] proposed a system consisting of a single-point diamond dresser equipped with an AE sensor to detect the position of the grinding wheel surface. AE signals can be obtained without physical contact of the dresser and the wheel due to turbulence. In total, three different contact conditions can be distinguished including noncontact, elastic contact, and brittle contact.

Another principle used to determine radial wheel wear is based on a miniature radar sensor [Westkämper and Hoffmeister 1997]. The radar technique is well known from speed as well as traffic control with a maximum accuracy in the centimeter range. The sensor used for grinding works on an interferometric principle. With an emitting frequency of 94 GHz and a wavelength of  $\lambda = 3.18$  mm, this sensor has a measuring range of 1 mm and a resolution of 1  $\mu\text{m}$ . Main advantages are the robustness against any dust, mist, or coolant particles and the possibility to measure on any solid surface. The sensor was used in surface grinding of turbine blades with continuous dressing (CD). A control loop was established to detect and control the radial wear of the grinding wheel, taking into account the infeed of the dressing wheel.

### 11.3.3 SENSORS FOR MICROGEOMETRICAL QUANTITIES

The loading of a grinding wheel with conductive metallic particles is a special type of microgeometrical wear that can be detected using sensors based on inductive phenomena. The sensor consists of a high permeability core and a winding. It is positioned a short distance from the surface. The metallic particles generate a change of impedance, which can be further processed to determine the state of wheel loading. Also, a conventional magnetic tape recorder head may be used to detect the presence and relative size of ferrous particles in the surface layer of a grinding wheel. Due to the fact that only this special type of wear in grinding of metallic materials can be detected, these sensors did not reach practical application.

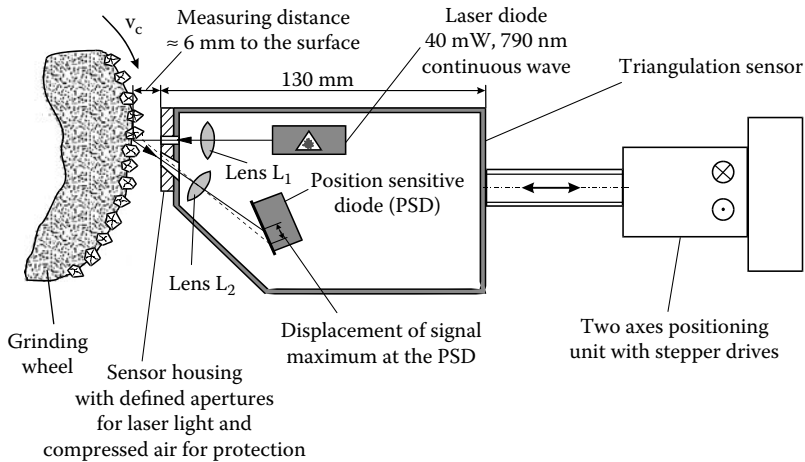


**FIGURE 11.15** Measurement principle of a laser triangulation system.

The limitations of all techniques introduced so far drive attention toward optical methods. Optical methods are promising because of their frequency range and independence of the surface material. A scattered light sensor was used to determine the reflected light from the grinding wheel surface by using CCD arrays. Gotou and Touge [1996] adopted the principle with a silicon diode as a receiver and using a laser source. Grinding wheels in wet-type grinding at 30 m/s could be measured. It was stated that the wear flat areas are registered by the output signal and that these areas change during grinding.

The optical method with the highest technical level so far is based on laser triangulation. Figure 11.15 shows the basic elements, which are a laser diode with 40-mW continuous wave (c.w.) power and a position-sensitive detector (PSD) with amplifier and two lenses [Tönshoff, Karpuschewski, and Werner 1993]. The laser diode emits monochromatic laser light of 790-nm wavelength focused by lens,  $L_1$ , on the grinding wheel surface. The scattered reflected light is collected by lens,  $L_2$ , and focused on the PSD. If the distance to the sensor changes, the position of the reflected and focused light on the PSD also changes. The sensor is mounted to a two-axes stepper drive unit to be moved in normal direction to the grinding wheel surface and in axial direction to make measurements on different traces on the grinding wheel circumference. This sensor system was intensively tested in laboratory environment and in industrial application. For the determination of macrogeometrical quantities such as radial runout, no practical limitations exist. The maximum surface speed may even exceed 300 m/s.

Figure 11.16 shows the result of an investigation in outer diameter plunge grinding of ball bearing steel with a corundum grinding wheel. In dependence of three different material removal rates, the change of the radial runout as function of the material removal at 30 m/s is documented. For the smallest material removal rate, no change is detectable from the initial value after dressing. However, for increasing material removal rates of  $Q'_w = 1,0 \text{ mm}^3/\text{mm/s}$ , respectively,  $2,0 \text{ mm}^3/\text{mm/s}$ , the radial runout is rising after a specific material removal. In the latter cases, the increasing radial runout leads to chatter vibrations with visible marks on the workpiece surface. Obviously the system is capable of detecting significant macrogeometric changes due to wear of the grinding wheel.

For microgeometrical measurements, the investigations have revealed that the maximum speed of the grinding wheel should not exceed 20 m/s based on hardware and software limitations. This means that, for most applications, the grinding wheel has to be decelerated for the measurement. This major drawback is limiting the practical field of application. For conventional abrasives with relatively short dressing intervals, an economic use of this type of microgeometrical monitoring is

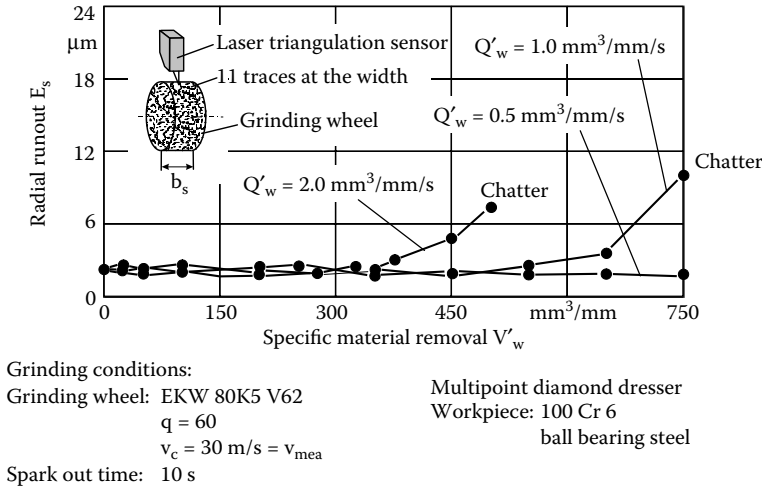


FIGURE 11.16 Optical macrogeometrical grinding wheel topography measurement.

not possible if the wheel has to be decelerated. The most interesting application for this sensor is seen in the monitoring of superabrasives, especially CBN-grinding wheels. This sensor system was intensively tested during profile grinding of gears with an electroplated CBN-grinding wheel [Regent 1999]. The measurement was done on the involute profile of the grinding wheel on 10 traces during the workpiece changing time at a measurement speed of  $v_{\text{mea}} = 10 \text{ m/s}$ .

Figure 11.17 (left) shows the setup of the investigation. On the right-hand side, a result of this sensor application is presented. The measured quantity is the reduced peak height,  $R_{pk}$ , deduced from the bearing ratio curve, which can be used to describe the change of the grinding wheel topography at the grain tips.

As shown, the change in Trace 3 can be clearly correlated with the occurrence of grinding burn, which was confirmed by nital etching and succeeding metallographical and X-ray inspection.

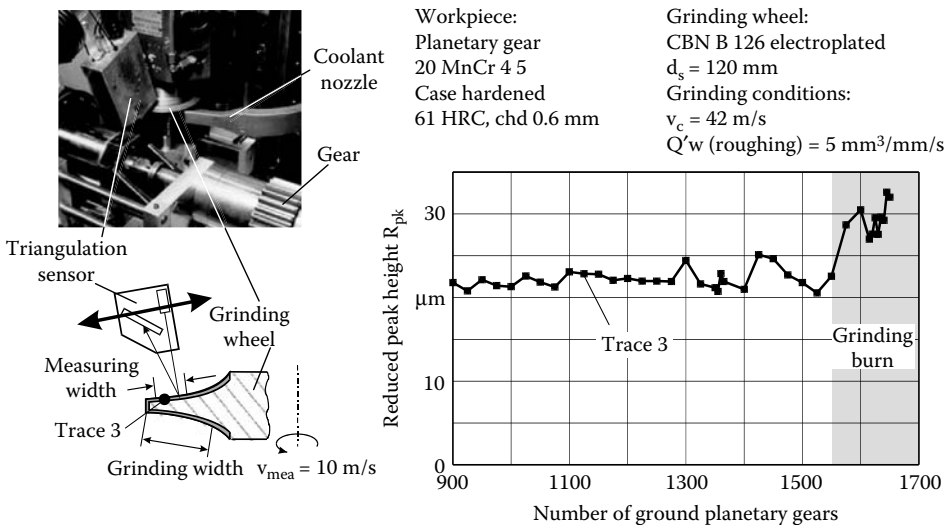


FIGURE 11.17 Grinding burn identification using a laser triangulation sensor.

Although this result is very promising, some problems have to be taken into consideration. Measurements, as well as simulations, have revealed that it is not possible to correlate the sensor roughness results definitely to a specific wear pattern. In real applications, there are always several types of wear, for example, grain flattening and loading, that cannot be separated by the measuring quantities.

The examples shown for grinding wheel sensors reveal that the majority of systems are related to macrogeometrical features. Many attempts have been made to establish optical systems for the measurement of microgeometrical quantities. The overall limitation for these techniques will always be the hostile conditions in the working space of a grinding machine with coolant and process residues in direct contact with the object to be measured. In many cases it is thus preferable to directly measure the manufactured workpiece.

## 11.4 SENSORS FOR MONITORING THE WORKPIECE

### 11.4.1 INTRODUCTION

Two essential quality aspects determine the result of a grinding process on the workpiece. On the one hand, the geometrical quality demands have to be fulfilled. These are dimension, shape, and waviness as essential macrogeometrical quantities. The roughness condition is the main microgeometrical quantity. However, increasing attention is also paid to the surface integrity state of a ground workpiece because of its significant influence on the functional behavior. The physical properties are characterized by the change in hardness and residual stresses on the surface and in subsurface layers, by changes in the structure, and the likely occurrence of cracks. All geometrical quantities can be determined by using laboratory reference measuring devices. For macrogeometrical properties, any kind of contacting systems are used, for example, 3D-coordinate measuring machines, contour stylus instruments, or gauges. Roughness measurement is usually performed with stylus instruments giving standardized values, but optical systems are also applied in some cases.

### 11.4.2 CONTACT-BASED WORKPIECE SENSORS FOR MACROGEOMETRY

The determination of macrogeometrical properties of workpieces during manufacturing is the most common application of sensors in abrasive processes, especially grinding. For decades, contacting sensors have been in use to determine the dimensional change of workpieces during manufacturing. A large variation of in-process gauges for any kind of operation is available. In ID or OD grinding, the measuring systems can either be comparator or absolute measuring heads with the capability of automatic adjustment to different part diameters. The contacting tips are usually made of tungsten carbide, combining the advantages of wear resistance, moderate costs, and sufficient frictional behavior. If constant access to the interesting dimension during grinding is possible, these gauges are often used as a signal source for adaptive control (AC) systems. The conventional technique for measuring round parts rotating around their rotational axis can be regarded as state of the art. The majority of automatically operating grinding machines are equipped with these systems. In a survey of contacting sensors for workpiece macrogeometry in Figure 11.18 (left), a more complex measurement setup is shown. Due to the development of new drives and control systems for grinding machines a continuous path-controlled grinding of crankshafts has now become possible [Tönshoff et al. 1998].

The crankshaft is clamped only once in the main axis of the journals. For machining the pins, the grinding wheel moves back and forth during rotation of the crankshaft around the main axis to generate a cylindrical surface on the pin. An in-process measurement device for the pin diameter has to follow this movement. A first prototype system is installed in a crankshaft grinding machine. The gauge is mounted to the grinding wheel head and moves back and forth together with the grinding wheel.



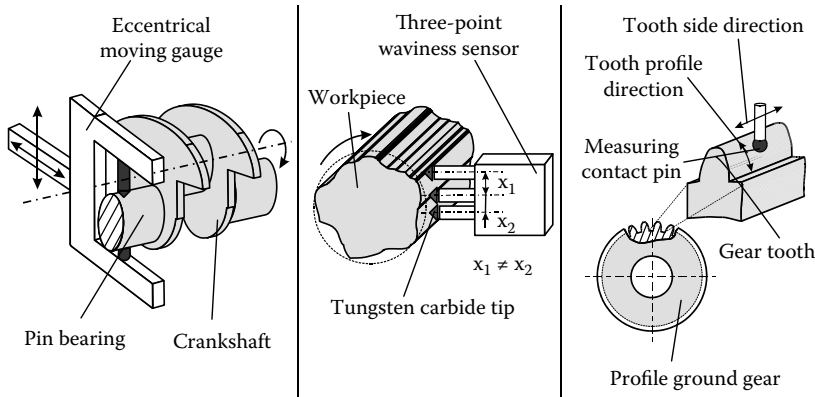


FIGURE 11.18 Contact sensor systems for workpiece macrogeometry.

The detection of waviness on the circumference of rotationally symmetric parts in grinding is more complex due to the demand for a significantly higher scanning frequency. Foth [1989] has developed a system with three contacting pins at nonconstant distances to detect the development of waviness on workpieces during grinding as a result of, for example, regenerative chatter (Figure 11.18, middle). Only by using this setup was it possible to identify the real workpiece shape, taking into account the vibration of the workpiece center during rotation.

The last example of contact-based macrogeometry measurement in a machine tool is related to gear grinding (Figure 11.18, right). Especially for manufacturing of small batch sizes or single components of high value it is essential to fulfill the “first part good part” philosophy. For these reasons several gear-grinding machine tool builders have decided to integrate an intelligent measuring head in their machines to be able to measure the characteristic quantities of a gear including, for example, flank modification, pitch, or root fillet. Usually a measurement is done after rough grinding, before the grinding wheel is changed or redressed for the finish operation. Sometimes, the initial state before grinding is checked to compensate large deviations resulting from distortions due to heat treatment. Of course, the measurement can only be done if the manufacturing process is interrupted, but still the main advantage is significant time saved. Any removal of the part from the grinding machine tool for checking on an additional gear-measuring machine will take a longer time. Also, the problem of precision losses due to rechucking is not valid because the workpiece is rough machined, measured, and finished in the same setup. These arguments are generally true for any kind of high-value parts with small batch sizes and complex grinding operations. Thus, it is not surprising that also in the field of aircraft engine manufacturing new radial grinding machines are equipped with the same kind of touch probe system in the working space.

### 11.4.3 CONTACT-BASED WORKPIECE SENSORS FOR MICROGEOMETRY

The determination of microgeometrical quantities on a moving workpiece by using contacting sensor systems is a challenging task. A permanent contact of any stylus to the surface is not possible because the dynamic demands are much too high. Only intermittent contacts can be used to generate a signal, which should be proportional to the roughness. Saljé [1979] introduced a sensor based on a damped mass spring element. The surface of the fast-moving workpiece stimulates self-oscillations of the sensing element, which are correlated to the roughness. Also, rotating roughness sensors for OD grinding have been tested, but in the end, because of limitations including wear and speed, the idea of contacting the surface for roughness measurement has not led to industrial success [Karpuschewski 2001].

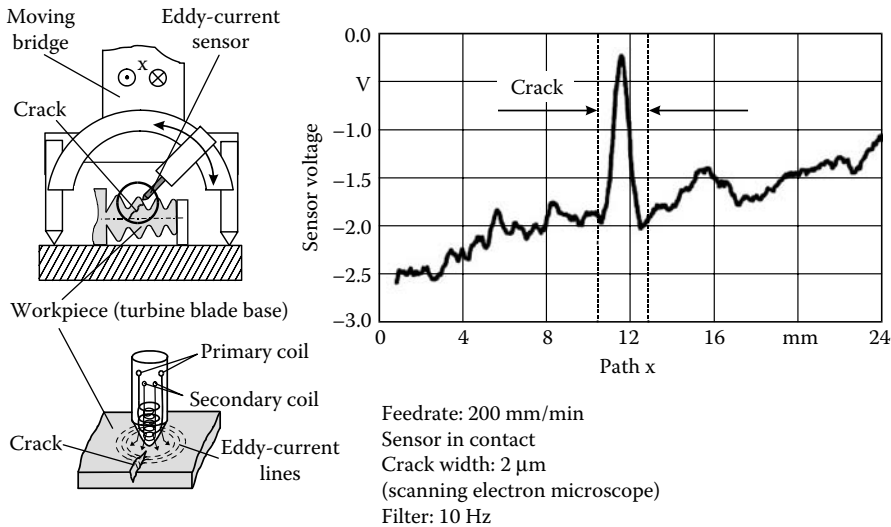


FIGURE 11.19 Eddy-current crack detection after surface grinding of turbine blades.

#### 11.4.4 CONTACT-BASED WORKPIECE SENSORS FOR SURFACE INTEGRITY

The best way to investigate the influence of any cutting or grinding process on the physical properties of the machined workpiece would be to directly measure on the generated surface. Until now only very few sensors are available to meet this demand. Two techniques are explained that have the highest potential for this purpose.

The principle of eddy-current measurement for crack detection is based on the fact that cracks at the workpiece surface will disturb the eddy-current lines, which are in the measuring area of a coil with alternating-current excitation. The feedback to the exciting field leads to changes of the impedance for coils with only one winding, respectively, to a change of the signal voltage for sensors with two separated primary and secondary windings. All kinds of conductive materials can be tested. The penetration depth is determined by the excitation frequency. Conductivity, as well as permeability of the workpiece, can be investigated. In grinding, an eddy-current sensor was introduced to monitor the occurrence of cracks.

In Figure 11.19 (left), the setup for this eddy-current-based measurement is shown, and is used for the determination of cracks generated during profile surface grinding of turbine blade roots [Lange 1996]. Figure 11.19 (right) shows the result of such a measurement. The crack was investigated afterward with the aid of a scanning electron microscope and had a width of 2  $\mu\text{m}$ .

The eddy-current sensor could clearly determine this crack with a contact measurement. This size has to be regarded as the minimum resolution of the sensor. In any case, the sensor must be positioned in a perpendicular direction to the surface because any tilting is reducing the sensitivity. Thus, an additional shift option was implemented in the moving bridge. The results prove the suitability of eddy-current sensors for crack detection on turbine blade materials. Although the measurement speed was smaller than the grinding table speed, a check in the grinding machine may still be acceptable because of the high safety demand on these workpieces.

The second possibility to detect changes of the physical properties on machined surfaces of ferrous materials is based on micromagnetic techniques. Residual stresses, hardness values, and the structure in subsurface layers influence the magnetic domains of ferromagnetic materials. Any magnetization change can be measured with the so-called Barkhausen noise. The existence of compressive stress in ferromagnetic materials reduces the intensity of the Barkhausen noise whereas tensile stresses will increase the signal [Karpuschewski 1995]. In addition to these stress-sensitive

properties, the hardness and structure state of the workpiece also influence the Barkhausen noise. To separate the different material characteristics of a ground workpiece, different quantities deduced from the Barkhausen noise signal must be taken into consideration. The most important quantities deduced from the signal are the maximum amplitude of the Barkhausen noise,  $M_{max}$ , and the coercivity,  $H_{cM}$ . In any case, the measurement time is very short and amounts to only a few seconds, which is one of the major advantages of this technique. This so-called two-parameter micromagnetic set-up was further improved by adding modules for the measurement of the incremental permeability, the harmonics of the exciting field, and eddy-currents [Regent 1999]. The major aim of this multiparameter system was to further separate the influence of the initial material properties from the changes due to machining operations.

A detailed investigation of the potential of the two-parameter micromagnetic approach was employed to characterize surface integrity states of workpieces with different heat treatments [Karpuschewski 1995]. Afterward, this technique was transferred to practical application. Figure 11.20 (left) shows the results of a large industrial test on planetary gears ground with electroplated CBN grinding wheels [Regent 1999]. It is essential to adapt the sensor geometry to the geometrical situation on the workpiece. In this case, the critical area to be tested was on the tooth flanks, thus the sensor had to be adapted to the module of the gear. In Figure 11.20 (right), the results over the lifetime of an electroplated wheel are shown. The Barkhausen noise amplitude is corrected to consider slight changes of the excitation field. It can be seen that all gears where grinding burn was identified by nital etching were also recognized with the micromagnetic setup. However, gears with high  $M_{max, corr}$  values appear, which do not show any damage in nital etching. A possible explanation for this deviation is the different penetration depth of the methods. Nital etching gives only information about the very top layer of the workpiece. Any subsurface damage cannot be registered. Micromagnetic measurements can also reveal that damage depending on the frequency range.

The major challenge is to exactly identify the grinding burn limit. It has to be mentioned further that the measuring time required to scan all flanks of one gear is significantly higher than the

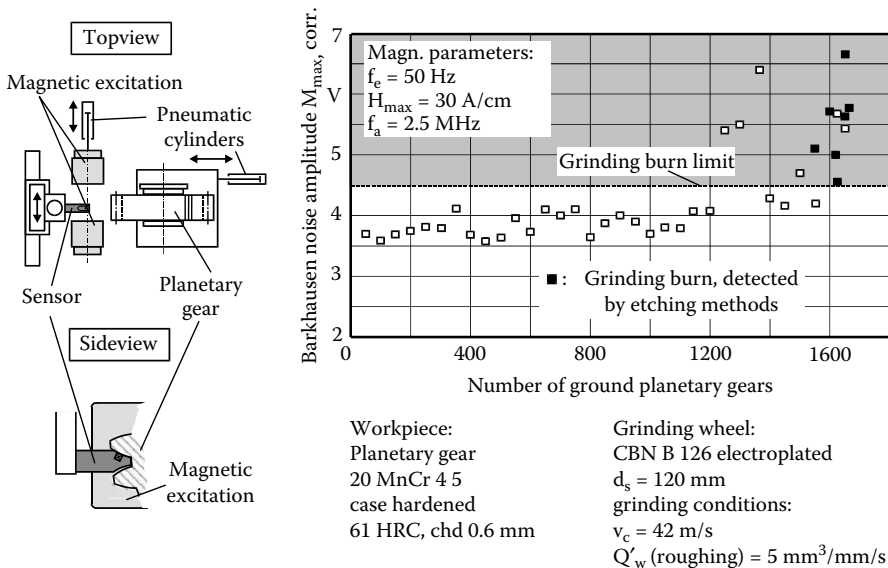
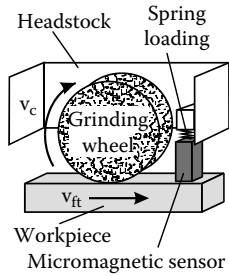


FIGURE 11.20 Micromagnetic surface integrity characterization of ground planetary gears.



Grinding wheel:  
 HKW 80 K4 VT  
 Workpiece material:  
 16 MnCr 5, case hardened  
 62 HRC, chd 1.0 mm  
 Grinding conditions:  
 $v_c = 25 \text{ m/s}$ ,  $Q'_w = 1.5 \text{ mm}^3/\text{mm/s}$   
 $v_{ft} = v_{mea} = 3 \text{ m/min}$   
 Coolant: Emulsion 5%

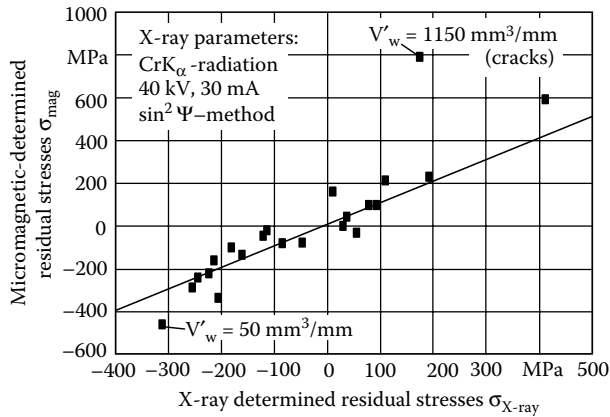


FIGURE 11.21 Micromagnetic in-process measurement of surface integrity during grinding.

grinding time. With intelligent strategies or increased number of sensors in parallel use, this time can be shortened for a suitable random testing. A total automated measurement is possible. Thus, the very inaccurate and environmentally hazardous etching can be replaced by this technology [Karpuschewski 2001].

Furthermore, in the laboratory, the first tests for in-process measurements of surface integrity changes based on this micromagnetic sensing were conducted for outer diameter and surface grinding [Tönshoff et al. 1998, Regent 1999]. In Figure 11.21, the first results of this approach during surface grinding of steel are presented. The sensor with integrated excitation is moving on the surface behind the grinding wheel at the chosen table speed of 8 m/min. Permanent contact is assured by spring loading. The X-ray measurement is done on one point of the ground surface, and the micromagnetic result represents the average over the whole workpiece length. The deviations in the area of compressive residual stresses and low-tensile residual stresses are less than 100 MPa, and only in areas of significant damage with tensile stresses higher than 200 MPa do the deviations increase. This can be explained by the occurrence of cracks after grinding due to the high thermal load on the workpiece.

Although further investigations on the wear resistance of the sensor head, on long-term coolant influence, maximum workpiece speed, geometrical restrictions, and other parameters have to be conducted, this sensor seems to offer the possibility of in-process workpiece surface integrity measurement for the first time.

### 11.4.5 NONCONTACT-BASED WORKPIECE SENSORS

All the mentioned restrictions of contacting sensor systems on the workpiece surface gave a significant push to develop noncontact sensors. As for grinding wheels again, optical systems seem to have a high potential. In Figure 11.22, different optical systems as well as two other noncontacting sensor principles are introduced.

A laser-scanner is shown as a very fast optical system to measure macrogeometrical quantities. The scanner transmitter contains primarily the beam-emitting HeNe-laser, a rotating polygonal mirror, and a collimating lens for paralleling the diffused-laser beam. The setup of the scanner receiver contains a collective lens and a photo diode. The electronic evaluation unit counts the time, and the photo diode

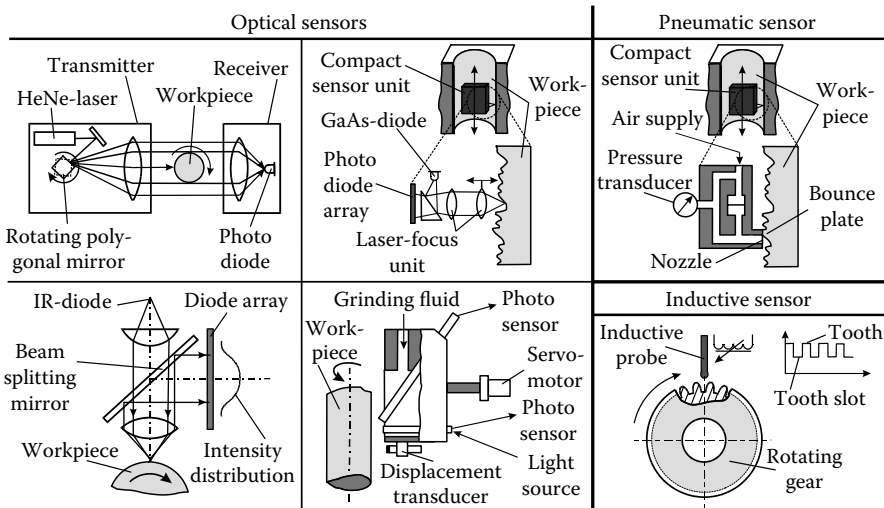


FIGURE 11.22 Noncontact sensor systems for workpiece quality characterization.

is covered by the shadow of the object. The diameter is a function of the speed of the polygonal mirror and the time the laser beam does not reach the covered photo diode. Conicity can be evaluated by an axial shifting of the workpiece. On principle, this optical measurement cannot be performed during the application of coolant. For a detailed workpiece characterization, a setup with a laser-scanner outside of the working space of the grinding machine is preferred. A flexible measurement cell incorporating a laser-scanner was introduced for the determination of macrogeometrical properties [Tönshoff, Brinksmeier, and Karpuschewski 1990]. The system was able to automatically measure the desired quantities within grinding time, and the information was fed back to the grinding machine control unit.

For the determination of macro- and microgeometrical quantities, a different optical system has to be applied. The basis of a scattered light sensor for the measurement of both roughness and waviness is the angular deflection of nearly normal incident rays. The setup of a scattered light sensor is shown in Figure 11.22 (bottom left). A beam-splitting mirror guides the reflected light to an array of diodes. A commercially available system was introduced in the 1980s [Brodthmann, Gast, and Thurn 1984] and used in a wide range of tests. The optical roughness measurement quantity of this system is called scattering value,  $S_N$ , and is deduced from the intensity distribution. In different tests, the scattered light sensor was directly mounted in the working space of the grinding machine to measure the workpiece roughness. A compressed-air barrier protected the optical system. In all investigations, they tried to establish a correlation between optical and stylus roughness measurements.

It is possible to obtain a close relationship while grinding or honing with constant process parameters [von See 1989, König and Klumpen 1993] (Figure 11.23). This restriction is indispensable because a change of input variables like dressing conditions or tool specification may lead to workpieces with the same stylus roughness values,  $R_a$  or  $R_z$ , but different optical scattering values,  $S_N$ . If a quantitative roughness characterization referring to stylus values is demanded, a time-consuming calibration will always be necessary. As shown in Figure 11.23, the measuring direction has to be clearly defined to achieve the desired correlation. A second limitation is seen in the sensitivity of the system. The scattered light sensor is able to determine differences in high-quality surfaces, but for roughness states of ten-point height  $R_z > 5.0 \mu\text{m}$ , the scattering value,  $S_N$ , is reaching its saturation with a decreasing accuracy already starting at  $R_z = 3.0 \mu\text{m}$  [von See 1989]. Thus, some relevant grinding or honing operations cannot be supervised by this sensor system.

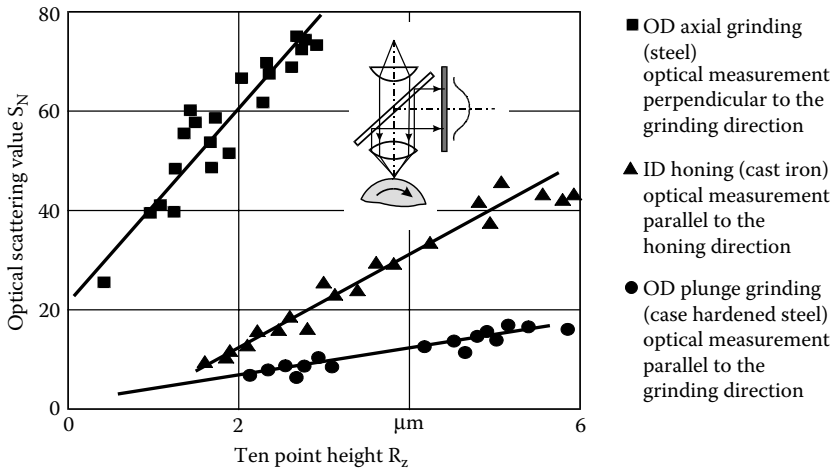


FIGURE 11.23 Different correlation curves for an optical scattered light sensor.

A different optical sensor is based on a laser diode [Westkämper et al. 1992] (Figure 11.22, top middle). The sensor is equipped with a gallium-arsenide diode, which is commonly used in a CD player. With a lens system, the beam is focused on the surface and the reflected light is registered on an array of four photo diodes. This system can be used as an autofocus system; with the signal from the four diodes the focus-lens is moved until the best position for minimum diameter is reached. The correlation of the obtained optical average roughness,  $R_{a,opt}$ , to the stylus reference measurement is shown in Figure 11.24 (left).

An almost linear dependence of the two different roughness quantities could be found, but this is much too slow to use the system for any in-process measurement. By using the focus-error signal of the four diodes without moving the lens, it is possible to increase the measurement speed significantly. Another optical approach for in-process roughness measurement is based on the use of optical fiber sensors [Inasaki 1985a]. The workpiece surface is illuminated through fiber optics and the intensity

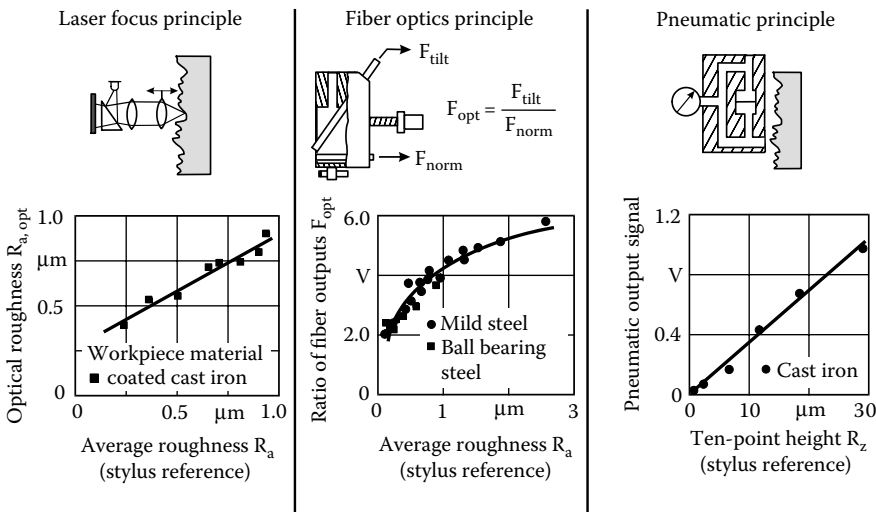


FIGURE 11.24 Correlation curves for different workpiece roughness sensors.

of the reflected light is detected and evaluated (Figure 11.24, middle). The latter setup was chosen to increase the sensitivity of the sensor system. The photo sensor in normal direction will register less intensity, whereas the inclined photo sensor will detect more intensity with larger light scattering due to increased roughness. The ratio of both photo sensors is related to roughness changes. A second advantage of the setup with two fiber optics despite the increased sensitivity is the achieved independence of the workpiece material. Coolant is flowing around the whole sensor head to make measurement possible during grinding. It is essential to keep the coolant as clean as possible during operation because the reflection conditions are definitely influenced by the filtering state of the fluid. This is the major drawback of the sensor system because the coolant quality is not likely to be stable in production. Besides these mentioned systems some other optical techniques for online measurement of surface topography have been proposed, for example, speckle patterns. Although the measurement speed may allow installing these systems in the production line surrounding, it is not realistic to use it as a sensor in the machine tool working space.

In summary, because of all the problems related to coolant supply, it must be stated that these conditions do not allow using optical systems during grinding as reliable and robust industrial sensors. Only optical sensor applications measuring in interruptions of coolant supply either in the working space of the machine tool or in the direct surrounding have gained importance in industrial production.

In addition to optical sensors, two other principles are used for noncontact workpiece characterization. A pneumatic sensor, as shown in Figure 11.22 (top right), was designed and used for the measurement of cylinder surfaces. The measurement is based on the already-mentioned nozzle-bounce plate principle. A correlation to stylus measurements is possible (Figure 11.24, right). Main advantages of this system are the small size, the robustness against impurities and coolant, and the fact that an area and not a trace is evaluated. So, on principle, any movement of the sensor during measurement is not necessary.

The last system to be introduced as a noncontact workpiece sensor is based on an inductive sensor. The sensor is used in gear grinding machines to identify the exact position of tooth and tooth slot at the circumference of the premachined and usually heat-treated gear (Figure 11.22, bottom right). The gear is rotating at high speed and the obtained signal is evaluated in the control unit of the grinding machine. This signal is used to index the gear in relation to the grinding wheel to define its precise position [Karpuschewski 2001].

## 11.5 SENSORS FOR PERIPHERAL SYSTEMS

### 11.5.1 INTRODUCTION

Primary motion between tool and workpiece characterizes the grinding process, but also supporting processes and systems are of major importance. In this chapter, basically the monitoring of the conditioning process and the coolant supply will be discussed.

### 11.5.2 SENSORS FOR MONITORING OF THE CONDITIONING PROCESS

The condition of the grinding wheel is a very decisive factor for satisfactory grinding results. Thus, the grinding wheel has to be prepared for the grinding by using a suitable conditioning technology. The major problem in any conditioning operation is the possible difference between nominal and real conditioning infeed. There are four main reasons for these deviations. The unknown radial grinding wheel wear after removal of a specific workpiece material volume must be regarded as a significant factor. Also, the changing relative position of grinding wheel and conditioning tool because of thermal expansion of machine components is relevant. As a third reason, infeed errors related to friction of the guide-ways or control accuracy have to be considered, although their influence is declining in modern grinding machines. The last reason to mention is the wear of the

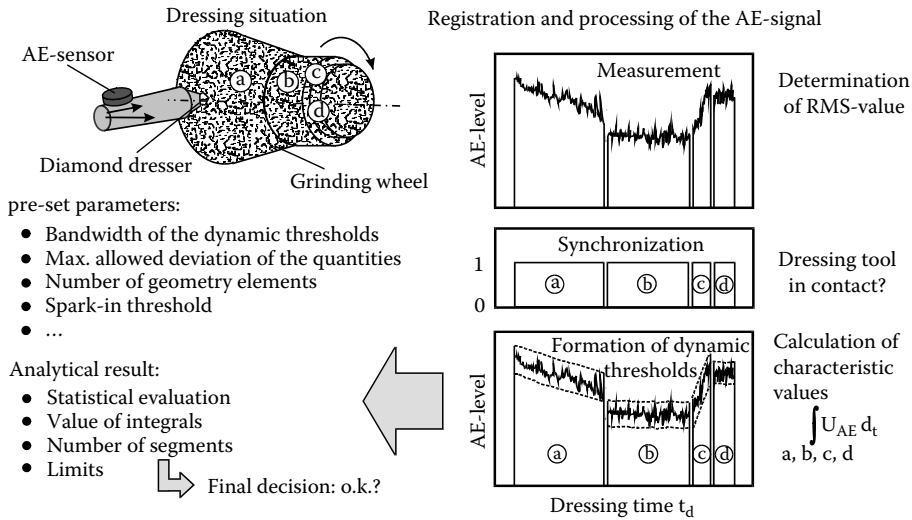


FIGURE 11.25 Dressing diagnosis for random grinding wheel profiles with acoustic emissions signals.

conditioning tool, which is, of course, dependent on the individual type of tool. The first wear effects for rotating dressers may be noticeable only after regular use for several weeks.

Because of the immense importance of the grinding wheel topography, the monitoring of the conditioning operation has been the subject for research for many decades. In the early 1980s it was first used as an AE-based system for the monitoring of the dressing operation. At that time, the work was concentrated on dressing of conventional grinding wheels with a static single-point diamond wheels. It was possible to detect first contact of the dresser and the grinding wheel and the AE intensity could be used to determine the real dressing infeed in dependence of dressing feedrate and grinding-wheel speed. The dressing feed speed could be identified by the AE signal [Inasaki 1985b]. In addition, it was stated that the AE signal reacts significantly faster to the first contact of the dressing tool and grinding wheel compared to monitoring by means of the spindle power.

The limitation to straight cylindrical profiles was overcome by Meyen [1991] who developed a system capable of detecting dressing errors on any complex grinding wheel profile (Figure 11.25). The strategy comprises the determination of a sliding average value with static and dynamic thresholds for every single dressing stroke. The different geometry elements are identified and the currently measured AE signal is compared to the reference curve, which has to be defined in advance. With the calculation of further statistical quantities like standard deviation or mean signal inclination, it is possible to identify the typical dressing errors in case of exceeding the thresholds.

As a consequent next step, AE systems were tested for conditioning operations of superabrasives such as CBN [e.g., Heuer 1992, Wakuda et al. 1993]. The high hardness and wear resistance of these grinding wheels require a different conditioning strategy and monitoring accuracy compared to conventional abrasives.

The conditioning intervals due to the superior wear resistance can amount up to several hours. The dressing infeed should be limited to a range between 0.5  $\mu\text{m}$  and 5  $\mu\text{m}$  instead of 20  $\mu\text{m}$  to 100  $\mu\text{m}$  for conventional wheels in order to save wheel costs. Especially for vitreous-bonded CBN grinding wheels, it was proposed to use very small dressing infeeds more frequently in order to avoid an additional sharpening. This strategy known as “touch dressing” revealed the strong demand to establish reliable contact detection and a monitoring system for dressing of superabrasives. In most of the cases, rotating dressing tools are used. The schematic setup of a conditioning system with a rotary cup wheel, which is often used on internal grinding machines, is shown in Figure 11.26.



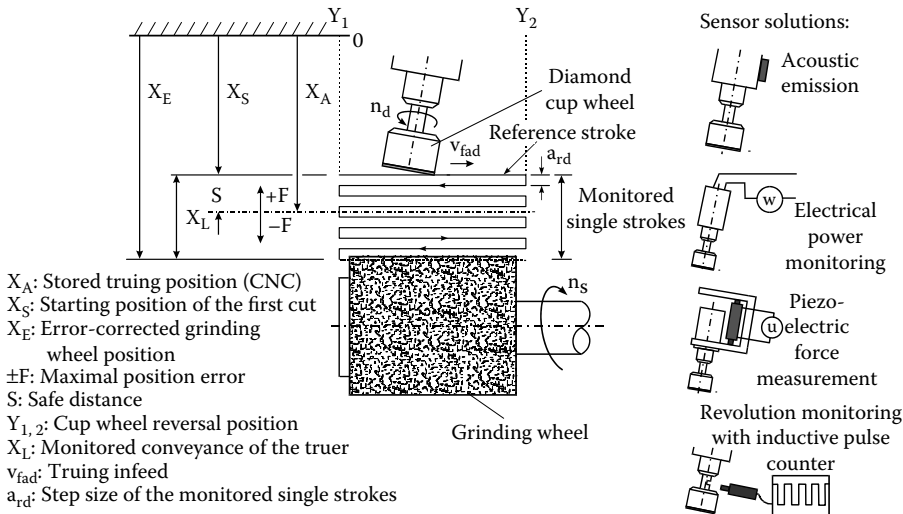


FIGURE 11.26 Dressing monitoring with rotating diamond tools.

The conditioning cycle consists of four stages: fast approach, contact detection, defined infeed, and new initiation. Besides AE techniques, other methods have also been tested. Heuer [1992] additionally investigated the possibility of using either the required power of the dressing tool spindle or a piezoelectric force measurement for monitoring. The latter technique was available because a piezoelectric actuator was installed as a high precision positioning system for the infeed of the dressing tool.

A further technique for contact detection was introduced by Tönshoff, Falkenburg, and Mohlfeld [1995]. The measurement of the rotational speed change of the high frequency dressing spindle, which gives a maximum number of revolutions of  $60,000 \text{ min}^{-1}$ , was used to determine not only the first contact, but also the whole dressing process. After contact detection of any of the mentioned systems, the conditioning program is continued until the desired number of strokes and infeed is reached. Depending on the type of system, it is possible to monitor the course of the signal over the whole width of the grinding wheel.

The use of AE sensors for contact detection of the conditioning, respectively, dressing operation can be regarded as state of the art. Many different systems are available. New grinding machine tools with self-rotating conditioning tools are usually equipped with an AE system already in the delivery state.

### 11.5.3 SENSORS FOR COOLANT SUPPLY MONITORING

In almost all grinding processes, coolants are used to reduce heat and to provide sufficient lubrication. These are the main functions of any coolant supply. Furthermore, the removal of chips and process residues from the workspace of the machine tool, the protection of surfaces, and human compatibility should be provided. Modern coolant compositions also try to fulfill the contradictory demands of long-term stability and biological recycling ability.

With the wider use of superabrasives such as CBN and the possibility of high-speed grinding and high-efficiency deep grinding, more attention has been paid to the coolant supply. Coolant pressure and flow rate measured with a simple flowmeter in the coolant supply tube before the nozzle are often part of the parameter descriptions. Different authors have also worked on the influence of different nozzle designs [e.g., Heuer 1992]. In most cases, the influence of different supply options including conventional flooding nozzles, shoe, spot jet, or spray nozzles or even

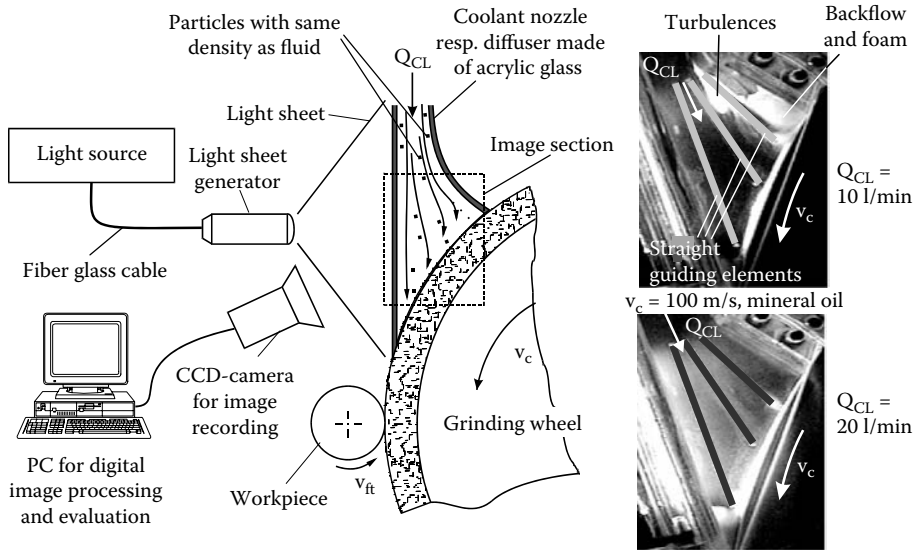


FIGURE 11.27 Flow behavior monitoring by means of Particle-Image-Velocimetry.

internal supply through the grinding wheel is described by using the previously mentioned process quantities such as forces or temperature [Heinzel 1999].

Besides the technological demands, the environmental aspects of manufacturing get significantly more attention. The last mentioned point especially has led attention toward a detailed investigation of coolant supply and the possibility to reduce or avoid coolants in grinding completely [Karpuschewski, Brunner, and Falkenburg 1997]. Brinksmeier, Heinzel, and Wittmann [1999] and Heinzel [1999] made a very systematic approach to investigate the coolant-related influences and to optimize the relevant parameters and designs. A special flow-visualization technique was used for the development of a suitable shoe nozzle design (Figure 11.27). Tracer particles with almost the same density are added to the transparent fluid. All interesting parts of the nozzle are made from acrylic glass and a CCD-camera is recording the flow images perpendicular to the light sheet plane. Although only a qualitative result is available, this technique offers the possibility to systematically study and improve the whole design of coolant nozzles. As an example, Figure 11.27 (right) shows the flow behavior of a nozzle with straight guiding elements at two different flowrates.

The coolant is mineral oil and the grinding wheel is rotating at a speed of 100 m/s. For the smaller flowrate of 10 l/min, inhomogeneous flow behavior can be observed. Turbulences, backflow, and foam between top- and center-guiding elements and at the entry side of the grinding wheel are visible. A doubling of the flowrate leads to steady flow behavior.

Besides this use of an optical monitoring method to optimize the design of coolant nozzles, a special sensor installation for pressure and force investigations was introduced [Heinzel 1999]. The force measurement is done by an already-discussed piezoelectric dynamometer. During grinding, only the total normal force can be registered by this instrument. The idea is to separate the normal force component used for cutting, friction, and deformation from the component that is resulting from the buildup of the hydrostatic pressure between grinding wheel and workpiece, and because of the impact of the coolant flow on the surfaces. For this purpose, an additional pressure sensor is integrated in the workpiece carrier, allowing measurement of the pressure course over a grinding path through a bore in the workpiece. In Figure 11.28 results of this sensor configuration are shown [Heinzel 1999].

The left part shows a result of the pressure measurement in dependence of different depths of cut. It is shown that with increasing infeed the maximum of the pressure distribution is shifted in

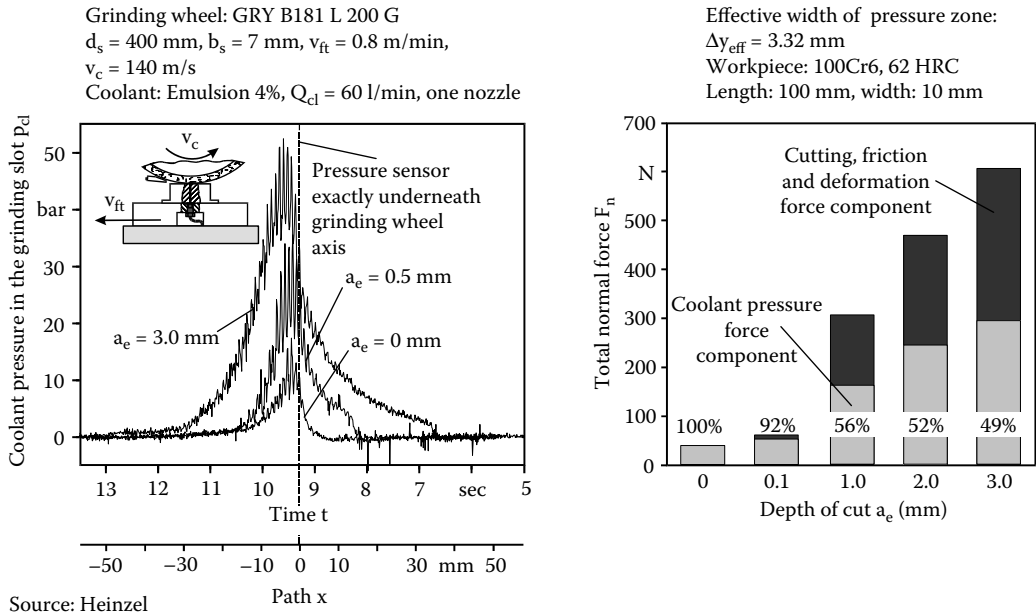


**FIGURE 11.28** Coolant supply monitoring with pressure sensor and dynamometer.

front of the contact zone, which can be explained by the geometry of the generated slot. Higher infeed leads to a geometrical boundary in front of the contact zone and results in a rise of the dynamic pressure. If the measured pressure distribution is numerically integrated over the corresponding workpiece surface, the coolant pressure force component can be determined taking some assumptions for the calculation into consideration.

The right side of Figure 11.28 shows results of this combined calculation and measurement. A path with no infeed is already leading to a normal force of 34 N, only generated by the coolant pressure. With increasing depth of cut the amount of this force component is, of course, reduced. Almost half of the normal force is attributed to the coolant pressure, even under deep grinding conditions of  $a_e = 3$  mm.

This described method is suitable to investigate the influence of different coolant compositions. The efficiency of additives can be evaluated especially if the coolant pressure force component is known and can be subtracted from the total normal force to emphasize the effect on the cutting, friction, and deformation component.

The use of special sensor systems for coolant-supply investigations is a relative new field of activities. First results have shown that these sensors can contribute to a better understanding of the complex thermomechanical interaction in the zone of contact. Also, direct industrial improvements such as coolant nozzle optimization or additive efficiency evaluations for grinding can be performed. Thus a further improvement of the monitoring techniques is desirable.

## REFERENCES

- Batako, A. D., Rowe, W. B., and Morgan, M. N. 2005. "Temperature Measurement in Grinding." *Int. J. Mach. Tools Manu.* (Elsevier) 45, 11, 1231–1245.
- Brinksmeier, E. 1991. *Prozess- und Werkstückqualität in der Feinbearbeitung*. Habilitationsschrift, Universität Hannover.

- Brinksmeier, E., Heinzl, C., and Wittmann, M. 1999. "Friction, Cooling and Lubrication in Grinding." *Ann. CIRP* 48, 2, 581–598.
- Brodthmann, R., Gast, T., and Thurn, G. 1984. "An Optical Instrument for Measuring the Surface Roughness in Production Control." *Ann. CIRP* 33, 1, 403–406.
- Brunner, G. 1998. "Schleifen mit mikrokristallinem Aluminiumoxid." Ph.D. dissertation, Universität Hannover.
- Byrne, G. et al. 1995. "Tool Condition Monitoring (TCM): The Status of Research and Industrial Application." *Ann. CIRP* 44, 2, 541–567.
- Foth, M. 1989. "Erkennen und Mindern von Werkstückwelligkeiten während des Außenrundschleifens." Ph.D. dissertation, Universität Hannover.
- Friemuth, T. 1999. "Schleifen hartstoffverstärkter keramischer Werkzeuge." Ph.D. dissertation, Universität Hannover.
- Gotou, E. and Touge, M. 1996. "Monitoring Wear of Abrasive Grains." *Jour. Mater. Process. Technol.* 62, 408–414.
- Heinzl, C. 1999. "Methoden zur Untersuchung und Optimierung der Kühlschmierung beim Schleifen." Ph.D. dissertation, Universität Bremen.
- Heuer, W. 1992. "Außenrundsleifen mit kleinen keramisch gebundenen CBN-Schleifscheiben." Ph.D. dissertation, Universität Hannover.
- Inasaki, I. 1985a. "In-Process Measurement of Surface Roughness during Cylindrical Grinding Process." *Precis. Eng.* 7, 2, 73–76.
- Inasaki, I. 1985b. "Monitoring of Dressing and Grinding Processes with Acoustic Emission Signals." *Ann. CIRP* 34, 1, 277–280.
- Inasaki, I. 1991. "Monitoring and Optimization of Internal Grinding Process." *Ann. CIRP* 40, 1, 359–362.
- Karpuschewski, B. 1995. "Mikromagnetische Randzonenanalyse geschliffener einsatzgehärteter Bauteile." Ph.D. dissertation, Universität Hannover.
- Karpuschewski, B. 2001. Sensoren zur Prozeßüberwachung beim Spanen, Habilitationsschrift, Universität Hannover.
- Karpuschewski, B., Brunner, G., and Falkenberg, Y. 1997. "Strategien zur Reduzierung des Kühlschmierstoffverbrauchs beim Schleifen, Jahrbuch Schleifen, Honen, Läppen und Polieren." Vulkan-Verlag Essen, 58. Ausgabe.
- Klumpen, T. "Acoustic Emission (AE) beim Schleifen, Grundlagen und Möglichkeiten der Schleifbranddetektion." Ph.D. dissertation, RWTH Aachen 1994.
- König, W. and Klumpen, T. 1993. "Angepaßte Überwachungsstrategien und Sensorkonzepte – der Schlüssel für eine hohe Prozeßsicherheit, 7." Internationales Braunschweiger Feinbearbeitungskolloquium, 2.-4.
- Lange, D. 1996. "Sensoren zur Prozeßüberwachung und Qualitätsprüfung, 8." Internationales Braunschweiger Feinbearbeitungskolloquium 24.–26.4.
- Lierse, T. 1998. "Mechanische und thermische Wirkungen beim Schleifen keramischer Werkstoffe." Ph.D. dissertation, Universität Hannover.
- Marinescu, I., Rowe, W. B., Dimitrov, B., and Inasaki, I. 2004. *Tribology of Abrasive Machining Processes*. William Andrew Publishing, Norwich, NY.
- Meyen, H. P. 1991. "Acoustic Emission (AE) – Mikroseismik im Schleifprozeß." Ph.D. dissertation, RWTH Aachen.
- Oliveira, G. J., Dornfeld, D. A., and Winter, B. 1994. "Dimensional Characterization of Grinding Wheel Surface through Acoustic Emission." *Ann. CIRP* 43, 1, 291–294.
- Regent, C. 1999. "Prozeßsicherheit beim Schleifen." Ph.D. dissertation, Universität Hannover.
- Rowe, W. B. and Jin, T. 2001. "Temperatures in High Efficiency Deep Grinding." *Ann. CIRP* 50, 1, 205–208.
- Rowe, W. B., Li, Y., Inasaki, I., and Malkin, S. 2004. "Applications of Artificial Intelligence in Grinding." Keynote Paper. *Ann. CIRP* 43, 2, 521–532.
- Saljé, E. 1979. "Roughness Measuring Device for Controlling Grinding Processes." *Ann. CIRP* 28, 1, 189–191.
- Saxler, W. 1997. "Erkennung von Schleifbrand durch Schallemissionsanalyse." Ph.D. dissertation, RWTH Aachen.
- Tönshoff, H. K., Brinksmeier, E., and Karpuschewski, B. 1990. "Information System for Quality Control in Grinding." Paper MR90-503, 4th International Grinding Conference, Dearborn, MI.
- Tönshoff, H. K., Karpuschewski, B., and Werner, F. 1993. Fast Sensor Systems for the Diagnosis of Grinding Wheel and Workpiece. MR93-369. 5th International Grinding Conference, Cincinnati, OH.
- Tönshoff, H. K., Falkenberg, Y., and Mohlfeld, A. 1995. "Touch-dressing – Konditionieren von keramisch gebundenen CBN-Schleifscheiben." *IDR* 1, 43–48.

- Tönshoff, H. K. et al. 1998. "Grinding Process Achievements and Their Consequences on Machine Tools – Challenges and Opportunities." *Ann. CIRP* 47, 2, 651–668.
- Tönshoff, H. K., Friemuth, T., and Becker, J. C. 2002. "Process Monitoring in Grinding." *Ann. CIRP* 51, 2.
- Ueda, T., Hosokawa, A. and Yamamoto, A. 1985. "Studies on Temperature of Abrasive Grains in Grinding – Application of Infrared Radiation Pyrometer." *J. Eng. Ind. Trans. ASME* 107, 127–133.
- von See, M. 1989. "Optimierung von Honprozessen auf der Basis von Modellversuchen und betrachtungen." Ph.D. dissertation, TU Braunschweig.
- Wakuda, M. et al. 1993. "Monitoring of the Grinding Process with an AE Sensor Integrated CBN Wheel." *J. Adv. Autom. Technol.* 5, 4, 179–184.
- Westkämper, E. and Hoffmeister, H.-W. 1997. *Prozeßintegrierte Qualitätsprüfung beim Profilschleifen hochbeanspruchter Triebwerksbauteile, Arbeits- und Ergebnisbericht 1995–97 des Sonderforschungsbereiches 326*. Universität Hannover und TU Braunschweig.
- Westkämper, E. and Kappmeyer, G. 1992. "Prozeßintegrierte Qualitätsprüfung beim Honen zylindrischer Bauteile." Seminar des Sonderforschungsbereiches 326, Universität Hannover und TU Braunschweig.
- Westkämper, E. and Klyk, M. 1993. "High-Speed I.D. Grinding with CBN Wheels." *Prod. Eng.* I, 1, 31–36.

---

# 12 Economics of Grinding

## 12.1 INTRODUCTION

The right way of evaluating grinding costs is key to achieving maximum profitability in grinding. Old attitudes of treating abrasive cost, or even total perishable tooling costs, as a single measure of a process are completely misleading and unacceptable.

Models for evaluating “total grinding costs” came to the forefront in the early 1990s with the emergence of cubic boron nitride (CBN) for grinding automotive and aeroengine components. Abrasives costs with CBN, at that time, were often two or three times higher than with conventional abrasives but the reduction in labor costs and scrap produced far higher overall cost savings. Several models are available for costing. One model is given in Chapter 19 with respect to centerless and cylindrical grinding processes [Rowe, Ebbrell, and Morgan 2004]. The following cost analysis gives a clear picture of all the costs involved in a decision involving the comparison of two proposed methods.

## 12.2 A GRINDING COST COMPARISON BASED ON AN AVAILABLE GRINDING MACHINE

### 12.2.1 INTRODUCTION

If similar machines are to be employed or if the grinding machines are readily available for production, the problem of making cost comparisons between two processes is simplified. [English, Nolan, and Ratterman [1991] and Carius [1999] and presented the worksheet in Table 12.1 for costing purposes.

Table 12.1 shows the main process costs that enter into a comparison between two processes as required by a process engineer in decision-making, ignoring the capital cost involved in setting up a grinding facility. It has to be emphasized that these costs depend on the efficiency of the process itself. In other words, it is necessary to carry out grinding trials to determine cycle time, number of parts per dress, and so on before the costs can be established. An example of the investigation required in order to establish costs per part in Table 12.1 are given in Chapter 19. An example of the implications and benefits of the costing approach are given here.

### 12.2.2 AEROENGINE SHROUD GRINDING EXAMPLE

The application illustrated in Figure 12.1 is the internal grinding of large aeroengine shroud assemblies for aircraft engines. Traditionally, the part was ground using seeded gel (SG) abrasive, but the SG process was replaced by a vitrified CBN wheel that reduced grind cycle time by 50%. The greatest time saving was achieved by the elimination of the need to dress several times for each component ground. Relevant costs are given in Table 12.2.

Cost items 1 to 4 are tooling costs and illustrate that the switch to CBN abrasive created a negative impact on grinding costs of \$12.11. However, the increased productivity, items 5 to 8, had a positive impact on labor cost alone of \$179.44. Also, the quality improvement as a result of the very low wheel-wear rate using the superabrasive yielded an even greater cost saving of \$399 by

**TABLE 12.1**  
**Total Manufacturing Cost Calculation Worksheet**

1.	Total manpower overhead cost/part	\$/part
2.	Total wheel cost/part	\$/part
3.	Total wheel change cost/part	\$/part
4.	Total dresser roll cost/part	\$/part
5.	Total dresser roll change cost/part	\$/part
6.	Total maintenance labor cost/part	\$/part
7.	Total scrap cost/part	\$/part
8.	Total coolant cost/part	\$/part
9.	Total coolant filter cost/part	\$/part
10.	Total coolant disposal cost/part	\$/part
11.	Total inspection cost/part	\$/part
	<b>Total grinding cost</b>	<b>\$/part</b>

**TABLE 12.2**  
**Cost Calculation for Internal Profile Grinding of Aeroengine Shroud Assembly**

	Alox	CBN	Impact of CBN
1.	Wheel cost/part	\$10.00	\$28.74
2.	Dresser roll cost/part	\$7.44	\$3.15
3.	Coolant cost/part	\$5.56	\$2.46
4.	Filter cost/part	\$2.00	\$0.88
			-\$12.11
5.	Labor/part	\$247.77	\$123.85
6.	Wheel change/part	\$30.00	\$0.62
7.	Diamond roll change/part	\$0.20	\$0.19
8.	Maintenance/part	\$62.81	\$36.75
			+\$179.44
9.	Scrap	\$440.48	\$48.68
10.	Inspection cost/part	\$22.50	\$14.40
			+\$399.90
11.	Coolant disposal cost/part	\$0.65	\$0.29
			+\$0.36
	<b>Total grinding costs per part</b>	<b>\$829.48</b>	<b>\$260.01</b>

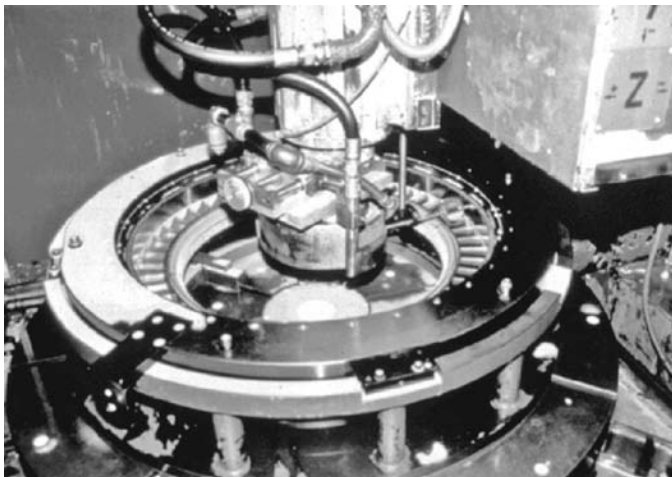


**FIGURE 12.1** Internal profile grinding of aeroengine turbine shroud assembly. (From GE Superabrasives. With permission.)

the elimination of scrap. Finally, there was also a modest environmental benefit of \$0.36 in terms of reduced coolant-disposal costs. Converting from a conventional wheel with a G-ratio of 1 to a CBN wheel with a G-ratio of 1,000 effectively halved the amount of swarf in the coolant stream. Furthermore, the filtered swarf was much cleaner and, therefore, easier to recycle.

In summary, a change of process from traditional wisdom considering abrasive cost alone would have had a negative impact of \$18.74/part. In fact, the change of process reduced total manufacturing cost by \$569.47/part.

## 12.3 A COST COMPARISON INCLUDING CAPITAL INVESTMENT

### 12.3.1 INTRODUCTION

Total in-process costs may be only half the analysis. For new processes, consideration needs to be given to balance capital equipment costs against operating costs.

### 12.3.2 AUTOMOTIVE CAMLOBE GRINDING EXAMPLE

An example of this was the introduction in the late 1980s of CBN to grinding camshafts. After the initial installation, which was instigated because it was the only viable method of generating a particular profile on the camlobe, the abrasive cost was found to be 50% higher using CBN. However, the productivity was found to be about 30% higher than a typical alumina wheel-based process. This had a major impact on the number of grinders required on a later new installation even when the profile issues were not present.

An example is shown in Table 12.3. A new installation required six less grinders and each machine was actually less expensive. So, even taking the most negative view of the process by considering abrasive cost only, for an increase in abrasive cost of \$90K/annum, a capital equipment cost saving of \$5.3M was achieved. Furthermore, since this was a relatively new technology, significant process costs were likely to be recuperated through future process optimization.

Dramatic process improvement was, in fact, proven to be the case. Figure 12.2 illustrates the improvement in abrasive cost alone over 8 years at the first CBN installation for grinding camshafts in North America.

**TABLE 12.3**  
**Capital Equipment Investment Versus Production**  
**Abrasive Costs for a High Production Camshaft**  
**Manufacturing Line<sup>a</sup>**

	Alox	CBN
Number of machines	22	16
Cost/machine	\$750K	\$700K
Capital equipment cost	\$16.5M	\$11.2M
<b>Capital investment savings</b>		<b>\$5.3M</b>
<b>Annual abrasive cost</b>	<b>\$180K</b>	<b>\$270K</b>

<sup>a</sup>Production requirements = 750,000 parts/annum.



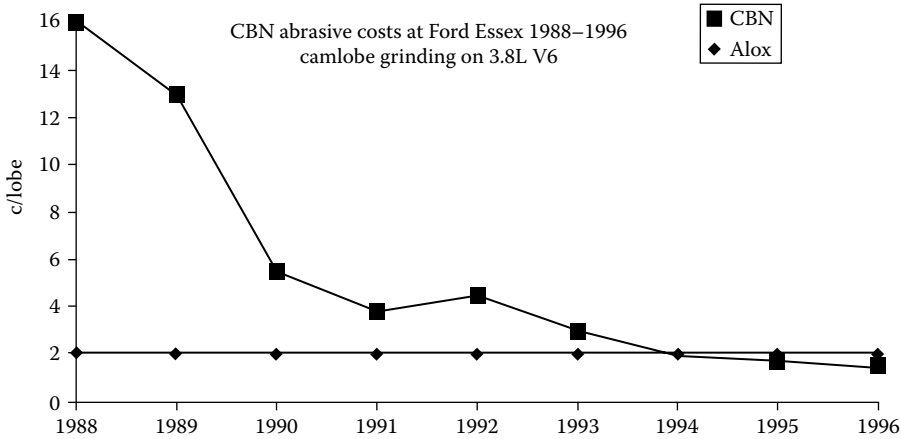


**FIGURE 12.2** Abrasive cost improvement in camshaft lobe grinding 1988 to 1996. (From Renaud and Hitchiner 1995. With permissions.)

## 12.4 COST COMPARISON INCLUDING TOOLING

### 12.4.1 INTRODUCTION

With better understanding of new technologies such as this, it is often possible to push productivity considerably further. The example described before, based on grinder technology that is now 15 years old, had a cycle time of about 6 min limited by burn. On the latest grinders with much more sophisticated CNC controls, higher wheel speeds and faster linear motor technology, it is possible to grind camshafts up to 50% faster, albeit with higher abrasive cost initially. Capital equipment is very expensive and industry is trying to drive up their return on investment by limiting such expenditures. A project engineer must, therefore, weigh up carefully capital against process costs. The following example shows how more expensive tooling can bring down costs.

### 12.4.2 EFFECT OF TOOLING COSTS IN CAMLOBE GRINDING

Consider the example of a camlobe grinding operation at a high production automotive engine plant as shown in Table 12.4.

**TABLE 12.4**  
**Comparison of Capital Equipment Costs Versus Tooling Costs for Various Production Rates**

Camlobe grinding of automotive camshafts			
Production requirement = 1,000,000 cams/annum			
Machine cost with gantry loading, installation, etc. = \$1M			
Production rates			
		10/hr @ \$0.25/camshaft	
		15/hr @ \$0.40/camshaft	
		20/hr @ \$0.60/camshaft	
Cycle Time	Grinders	Capital Cost	Tooling Cost
6 min	25	\$25M	\$250K/annum
4 min	17	\$17M	\$400K/annum
3 min	13	\$13M	\$600K/annum

For an increase in tooling costs of \$350K per annum, a capital cost saving of \$12M can be achieved. Again past history would indicate that processing costs would be further reduced over the expected life of the grinders and would be a primary focus for future cost savings from both process optimization and competition between tooling suppliers.

## 12.5 GRINDING AS A REPLACEMENT FOR OTHER PROCESSES

### 12.5.1 INTRODUCTION

With the rapid advances in metalworking technology, it is now necessary, when selecting new machines, to go back to the basic fundamentals of processing a part. An analysis of capital and processing costs may well indicate that the traditional metal-cutting process for producing a given part may not be the most cost effective. Grinding has recently successfully replaced such processes as lapping and broaching, while grinding itself has been replaced on many occasions by hard turning. Machine tool builders are combining metal-cutting processes, converting machines for one process to another, or reducing costs by adopting commonality of machine components. At the same time, tighter environmental and quality demands and the “Just-In-Time” approach to manufacturing can make historic processing methods obsolete. Some examples are described below.

### 12.5.2 FINE GRINDING AS A REPLACEMENT FOR LAPPING

Grinding of flat components by processes such as double-disc grinding has traditionally been limited to achievable flatness tolerances of about a micron. To obtain flatnesses of the order of 0.2  $\mu\text{m}$  to 0.6  $\mu\text{m}$  (1–2 light bands) demanded for seals, fuel injection, automotive transmission, and pump components has required lapping. This is a slow, batch process carried out on large cast iron tables up to 3 m in diameter using free abrasive slurries. Lapping is very dirty and requires an expensive postlap cleaning process. However, the kinematics of some lappers is quite sophisticated as described later in this handbook. Machine tool builders have, therefore, combined lapping kinematics with fixed superabrasive grinding wheels to reduce cycle time by up to a factor of 10.

An example of a comparison of the cost of lapping and fine grinding is shown in Table 12.5 grinding PM steel parts on a Peter Wolters double-sided grinder with vitrified CBN pellet wheels [Hitchiner 2002].

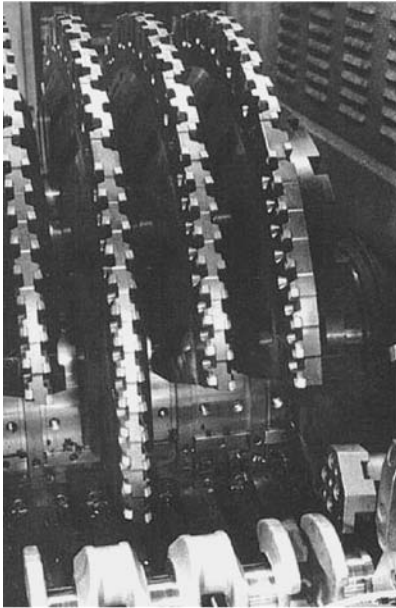
The greater savings come not from the actual grinding process but from the elimination of the subsequent cleaning process required after lapping (Table 12.5).

---

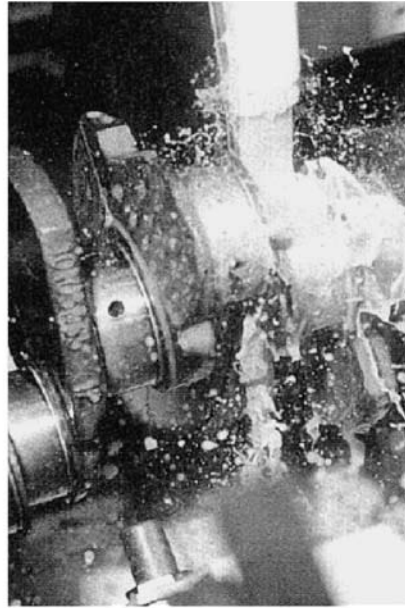
**TABLE 12.5**  
**Comparative Example of Lapping and Fine Grinding Costs**

Input	Lapping Cost/Part	Grinding Cost/Part
Labor/machine cost	\$0.60	\$0.25
Abrasive costs	\$0.08	\$0.25
Plate cost (lapping)	\$0.01	\$0.00
Cleaning cost	\$0.34	\$0.00
<b>Total</b>	<b>\$1.03</b>	<b>\$0.50</b>

---



**Turn broaching**



**High-speed grinding with electroplated CBN wheels**

**FIGURE 12.3** Illustrative examples of turn broaching and grinding of crank pins. (Courtesy of Landis, Wayneboro, PA. With permission.)

### **12.5.3 HIGH-SPEED GRINDING WITH ELECTROPLATED CBN WHEELS TO REPLACE TURN BROACHING**

Traditionally, crankshaft journals are roughed from a forging using turn broaches. The majority of stock is present in the sidewall and undercut at the edges of the journal where it takes a heavy toll on tool insert life. Insert resetting can take several hours using expensive specialized equipment. Current high-speed grinding technology using electroplated CBN wheels in oil coolant was able to process the part in half the time of a turn broach at comparable or lower tooling costs. See illustrative examples in Figure 12.3. A crank grinder costs the same as a turn broach, effectively halving the capital equipment costs while eliminating the labor and capital costs of tool insert resetting.

## **12.6 MULTITASKING MACHINES FOR HARD-TURNING WITH GRINDING**

Hard turning can remove stock much faster and with lower forces than regular grinding processes but it cannot hold quite the tolerances and finishes of grinding. However, when combined in a single machine with a single chucking the two processes can enhance each other. The photographs in Figure 12.4 show an operation to process two inner diameters and the faces of a hardened steel transmission gear component. The process was originally envisioned as being processed entirely by a single grinding wheel with an estimated cycle time of 4 min. The critical surfaces were the inner diameters. The problem, however, was the grinding of the top face due to quill deflection resulting in a cycle time of 10 min. However, the addition of a turning bar for hard turning the top face reduced the cycle time to 3 min to exceed end-user expectations while still maintaining very acceptable quality.

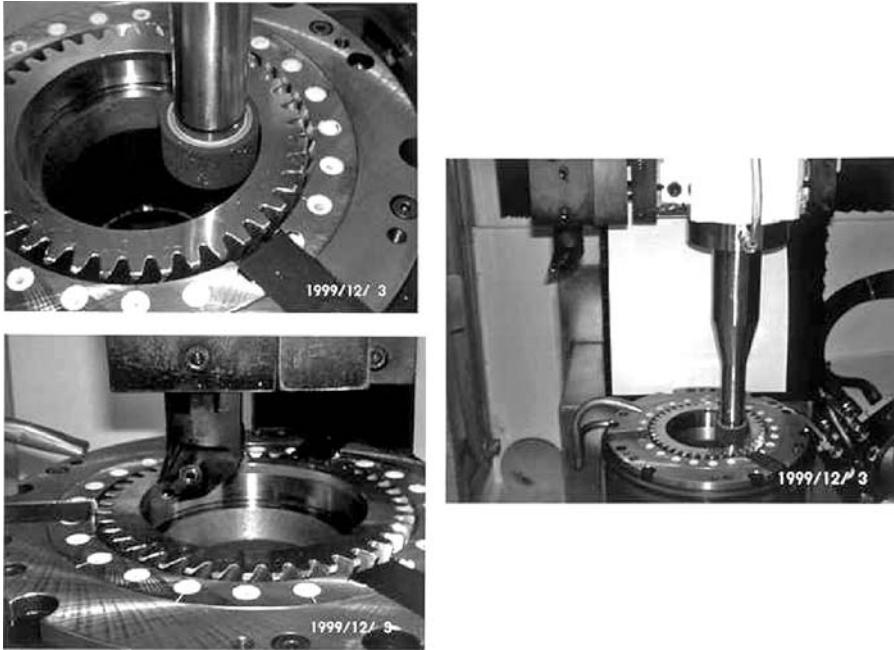


**FIGURE 12.4** Multitasking machine for grinding and hard-turning. (Courtesy of Campbell Grinders. With permission.)

## 12.7 SUMMARY

Close attention must be paid to the *entire* cost of a given manufacturing process. On very few occasions, the abrasive cost alone for a given operation governs the processing route. Continual advances in machine tool, wheel, and coolant technology, together with ever-greater demands for productivity, quality, and environmental considerations, demand that the manufacturing engineer review all options available each time an opportunity for new equipment arises. Careful consideration should be given to emerging technologies, global sourcing (if backed up with adequate local technical support), and fundamental university and corporate research.

## REFERENCES

- Carius, A. 1999. "Systems View of Grinding Costs Reveals Dramatic Cost Saving Opportunities." *MAN* p. 6.
- English, W., Nolan, T. C., and Ratterman, E. 1991. "Hidden Aspects of Superabrasive Economics." *Superabrasives 91*, SME Conference Proceedings, Chicago, IL.
- Hitchiner, M. 2002. "The Growth of Micro Grinding Technology Using Bonded Superabrasive Wheels." MR02-289, IMTS 2002, SME Conference, Chicago, IL, September 4–11.
- Renaud, W. and Hitchiner, M. 1995. "The Development of Camshaft Lobe Grinding with Vitrified CBN." MR95-163, SME 1st International Machining & Grinding Conference.
- Rowe, W. B., Ebbrell, S., and Morgan, M. N. 2004. "Process Requirements for Precision Engineering." *Ann. CIRP* 53, 1, 255–258.



## *Part II*

---

### *Application of Grinding Processes*



---

# 13 Grinding of Ductile Materials

## 13.1 INTRODUCTION

### 13.1.1 GRINDABILITY

Workpiece material composition and condition control all aspects of the grinding process. As ever greater demands are placed on productivity and quality, it becomes critical that the engineer understands the metallurgy of the materials being ground and their impact on the grinding process. Grindability is the term used to describe the ease of grinding a given workpiece material, and is akin to the term “machinability” used in milling and turning. Machinability, a more familiar term to engineers, is usually judged by four criteria: tool life, tool forces and power consumption, surface quality (including roughness, integrity, and burrs), and chip form. Comparable criteria exist for grindability; namely, G-ratio, Stock Removal Parameter  $\Lambda$ , surface quality (including roughness, surface residual stress, and burrs), and chip form. In broad terms, an easy-to-machine material is usually easy to grind especially when judged in terms of tool life and power.

### 13.1.2 EFFECT OF CHIP FORM

However, major deviations can arise when the influence of the chip form is considered. Machining involves using a tool of defined geometry to produce uniform chips of the order of 100  $\mu\text{m}$  to 1,500  $\mu\text{m}$  in thickness. By contrast, grinding is carried out with a random array of cutting-point shapes, generally with a high negative rake angle and random spacings and heights: chip thickness varies from  $<1 \mu\text{m}$  to no more than 50  $\mu\text{m}$  even for the most aggressive of rough grinding. An easy-to-machine material would be judged more for the ease of handling and disposal of its chips. A material that produces long stringy chips would be given a poor rating as would one that produced a fine, discontinuous chip. The ideal chip would be a nicely broken chip of a half or full turn of the normal chip helix. In grinding, the greater factor is loading, or the imbedding of metal into the face of the wheel, especially from a long, stringy chip, and a short, discontinuous chip is preferred. Chip breakers can change machining chip form while high-pressure coolant jets reduce built-up edge on tool inserts. Similarly, optimized grind geometry, for example, small  $d_e$  values, combined with high-pressure coolant scrubbers can minimize loading. Under these conditions grindability and machinability based on tool life or cutting energy or the rate of increase in cutting energy become more in step being based on the mechanical properties of the work material.

### 13.1.3 CHEMICAL REACTIVITY

Chemical reactivity between a particular workpiece and abrasive material can affect these trends. Diamond is chemically reactive to most transition metals, cubic boron nitride (CBN) is reactive with titanium, while SiC is reactive to titanium, iron, or cobalt. These properties can reduce wheel life by 10 to  $10^4$  times from expected values based on their relative mechanical properties. Small amounts of additives such as lead in steel or copper in porous powdered metal components will improve machinability by allowing a more continuous chip formation, but in doing so reduce grindability due to increased wheel loading.



## 13.2 CAST IRONS

Iron or “ferrous” alloys are the most ubiquitous metals in industry today. They include numerous classes of cast iron, carbon steels, tool, alloy and stainless steels, as well as exotic materials for the aerospace, nuclear, and medical industries. In their oldest and simplest forms, iron alloys depend on their carbon content and composition. Cast iron contains carbon in excess of the solubility limit in the austenite phase. It is used mainly to pour sand castings because of its excellent flow properties that make it ideal for complex cast shapes. It is most commonly found in automotive engine manufacture (blocks, manifolds, cranks, small cams). Cast iron is generally very brittle compared to steel and incompatible with most forming operations such as drawing or forging.

The properties of cast iron (Figure 13.1) depend heavily on how the carbon is distributed.

### 13.2.1 GRAY CAST IRON

Gray cast iron is so called because it gives a gray fracture due to the presence of flake graphite. Its grindability is very good, in either the soft ferritic phase or the harder pearlitic phase, as the graphite disrupts the metal flow to produce very short chips. It is relatively abrasive, especially in the pearlitic phase, requiring either a hard alox wheel grade or preferably the use of CBN.

### 13.2.2 WHITE CAST IRON

White cast iron is an extremely hard alloy produced by rapid cooling of the casting to combine all the carbon with iron to form cementite. When chipped, the fractured surface appears silvery white. White iron has no ductility and is thus incapable of handling bend or twist loads. It is used for its extreme abrasion resistance as rolls in mills or rock crushers. White iron is very heat sensitive and prone to cracking. It is usually ground with free-cutting silicon carbide abrasive wheels but recently white iron has begun to be ground with vitrified CBN in some applications.

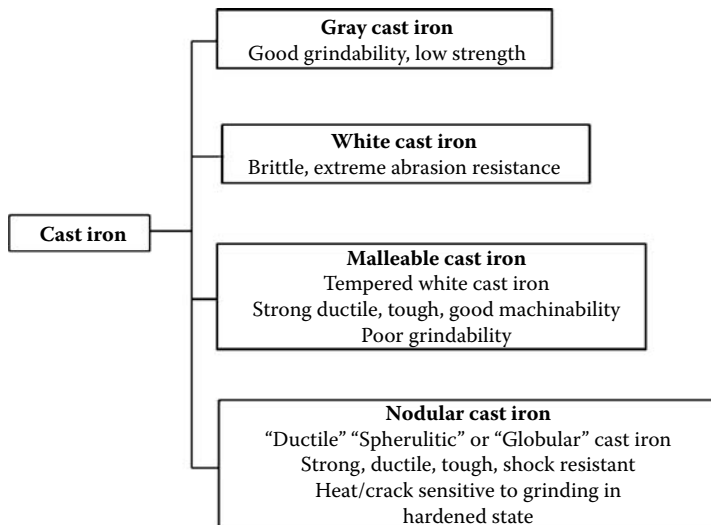


FIGURE 13.1 Classes and properties of cast iron.

### 13.2.3 MALLEABLE CAST IRON

Malleable cast iron is produced by controlled annealing of white iron to produce round graphite nodules. The material is ductile, tough, and has good machinability, but grindability is lessened by a tendency for wheel loading.

### 13.2.4 NODULAR OR DUCTILE CAST IRON

Nodular ductile cast iron has the carbon in the form of round graphite nodules but now also alloyed with numerous other elements such as silicon and magnesium. In this form, it is frequently used in automotive applications such as camshafts, crankshafts, and cylinder heads. The surface of the casting can be “chilled” by rapidly cooling it next to a metal chiller creating a hardened layer of white cast iron up to 55 HRC hardness under a softer, more ductile substrate. Again, a range of alloying elements is added to control the depth and hardness of this chilled layer. Chilled cast iron is particularly common in camshaft manufacture. Due to the highly abrasive nature of this layer combined with high productivity requirements and heat-sensitive nature of the material, chilled cast iron for this type of precision application is ground almost exclusively with CBN.

## 13.3 STEELS

Steels are differentiated from cast iron in part by the level of carbon. Cast iron has typically 1.7 to 4.5% carbon while steels have only 0.05% to 1.5% carbon. The versatility of steel is evidenced by the enormous range of grades available selected for their processing, mechanical, electrical, magnetic, and corrosion-resistance properties. The major families of steel types are listed in Figure 13.2.

### 13.3.1 PLAIN CARBON STEELS

The simplest, and cheapest, steels are plain carbon steels having no other alloying element. As the carbon content is increased, the ductility is reduced while the maximum hardness is increased up to about 63 HRC (Figure 13.3). Plain carbon steels are identified in the AISI or SAE four digit code system by 10xx where the 10 identifies the material as plain steel; the values for xx indicate the carbon content where, for example, 1050 steel is 0.50% carbon.

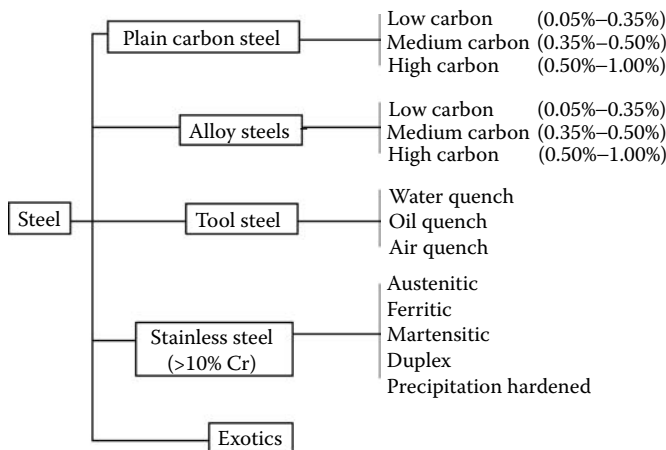
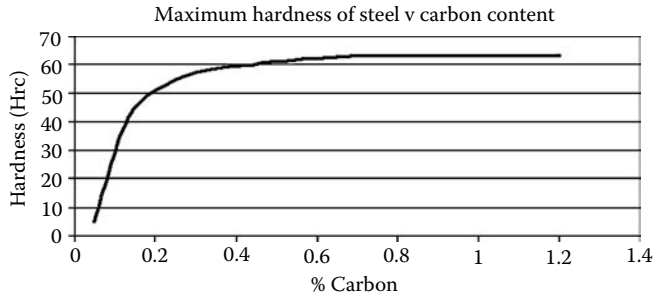


FIGURE 13.2 Major families of steel types.



**FIGURE 13.3** Effect of carbon content on maximum hardness of plain steel.

1050 steel is probably the mainstay of many industries including the automotive and bearing. It is easy to grind using fused alox or ceramic abrasive wheels and able to take a good case-hardening depth without stress cracks. Case-hardening is achieved by a carburizing process to drive carbon into the surface layer followed by quenching. This results in a surface layer of depth 1 mm with a hardness value up to 63 Hrc for maximum wear resistance on a softer more ductile core for toughness. Steels with higher carbon content, for example, 1080, are used where greater hardening depths might be required. Certain industries and applications such as internal grinding of small bearings and camlobe grinding of automotive camshafts have in part or almost totally converted to CBN and this will continue as machine, wheel, and processing technology improves. Even cylindrical grinding of 1050 steel in the soft state is now in production with vitrified CBN.

### 13.3.2 ALLOY STEELS

Alloy steels are carbon steels with additional alloying elements to enhance their physical properties or improve their machinability. Typical alloy steel types, including the AISI codes, are given in Table 13.1. Physical property improvements include through-hardenableity, toughness, tensile strength, and wear resistance. Alloying elements adjust grain size that can adversely affect machinability or improve grindability. The alloying elements also form hard carbide particles in the grain structure, which are highly abrasive and cause increased wheel grain wear. Martensitic structures in particular, having high tensile strength and low elongation, produce short chips and cause high abrasion wear levels in the grinding wheel leading manufacturers toward increased usage of CBN.

### 13.3.3 TOOL STEELS

The impact of the carbide level becomes most extreme with tool steels, so named for their heat, abrasion, and shock resistance, dimensional stability in heat treatment, and cutting ability. All of these contain one or more of the alloy elements chromium, tungsten, molybdenum, and vanadium, and have special heat treatment processes to control grain structure (Table 13.2). The resultant material can have hardness values up to 67 Hrc. The primary carbides of interest here are  $M_6C$  carbides of molybdenum and tungsten, and  $MC$  carbides from vanadium. Essentially the carbides provide the wear resistance while the softer metal matrix provides toughness. These carbide particles are very hard [Badger 2003].

Tool steels are extremely difficult to grind with conventional wheels. The  $MC$  carbides exceed the hardness of alox grains (Table 13.3). Indeed in the 1960s prior to the introduction of CBN, some toolrooms would use resin-bonded wheels containing very friable diamond as an alternative to SiC or alox wheels. Interesting to note, grain wear is not only due to the amount of carbide present, but also due to the size of the carbide particles. This is of particular interest when considering the grinding of workpieces made using powder-metal (PM) technology.

**TABLE 13.1**  
**AISI Steel Grade Identification and Effect of Alloy Type**

<b>AISI Steel Grade Identification Using First Two Digits</b>	
10xx/11xx <sup>a</sup>	Carbon only
13xx	Manganese
23xx/25xx	Nickel
31xx/33xx/303xx	Nickel chromium
40xx/44xx	Manganese molybdenum
41xx	Chromium molybdenum
43xx/47xx/81xx/86xx/ 93xx/94xx/98xx	Nickel chromium molybdenum
46xx/48xx	Nickel molybdenum
50xx/51xx/501xx/511xx/ 521xx/514xx/515xx	Chromium
61xx	Chromium vanadium
92xx	Silicon manganese
<b>Impact of alloy elements</b>	
Manganese	Mechanical strength, improved heat treat depth
Nickel	Improved toughness
Molybdenum	Improved high temperature hardness and corrosion resistance
Chromium	Improved hardening and corrosion resistance
Vanadium	Improved hardness and toughness, fine grain control
Silicon	Improved tempered hardness
<sup>a</sup> xx identifies the amount of carbon present, for example, xx = 50 is 0.50% carbon.	

Powder-metal parts are pressed to shape in a die, then sintered in a furnace at temperatures around 2,000°F (1,100°C). The powder does not melt so it never fully densifies. Mechanical bonds formed during pressing transform into metallurgical bonds during sintering. A major advantage of using PM is the ability to produce complex shapes to near-net shape. Typically the PM process

**TABLE 13.2**  
**Categories of Tool Steel<sup>a</sup>**

<b>Category</b>	<b>Description</b>
W	Water hardening
O	Oil hardening
A	Air hardening
D	Oil and air hardening (chromium)
S	Shock resistant
H	Hot working
M	High-speed (molybdenum)
T	High-speed (tungsten)
L and F	Special purpose
P	Mold-marking

<sup>a</sup>Uses: arbors, broaches, machine centers, chasers, cutting tools, dies, form & lathe tools, reamers, blades, rolls, taps, vise jaws, and wrenches. Aerospace bearings (M50).

**TABLE 13.3**  
**Comparison of the Hardness of**  
**Tool Steel Carbides to Abrasive**  
**Grains**

Constituent	Hardness (Knoop)
Matrix	800
M <sub>6</sub> C carbide	1,600
MC carbide	2,800
Alox grain	2,100
CBN grain	4,700

can control lengths to within 0.003 to 0.005 in. (75 to 125  $\mu\text{m}$ ). Since the structures do not fully densify, they contain pores between the grains. Machining of PM parts is, therefore, quite difficult because it consists of machining a series of interrupted cuts at the microscopic level resulting in high abrasive tool wear and chipping. The porosity also reduces heat conduction and drives more heat into the chip. All these factors, which adversely affect machinability, are a benefit for grindability, and PM technology, contrary to popular belief, may actually have increased the need for grinding as a precision finishing process.

Another benefit of PM technology is that it allows the control of the grain size of the carbides in tool steels. Badger [2003] reported that although the PM tool steel ASP2060 contained 15% MC carbide, it had only slightly poorer grindability based on G-ratio assessments than M2 steel containing only 2% carbide content. PM steels with comparable carbide content to those produced by conventional forging and heat treatment processes had up to 10 times the grindability based on G-ratio assessments as shown in Figure 13.4 and Figure 13.5.

It should be noted as a caveat that each PM application must be considered individually as there are enormous variations in composition, particle hardness, apparent hardness, porosity, and pore fillers. It is not uncommon to have a material with an apparent hardness of only 30 Hrc but a particle hardness of 60 Hrc.

### 13.3.4 STAINLESS STEELS

The last group of alloys is the stainless steels defined as steels containing more than 10% chromium. These are designed first and foremost to resist oxidation where they are used in the food, medical, petroleum, and chemical industries. In addition, some precipitation-hardened stainless steels are

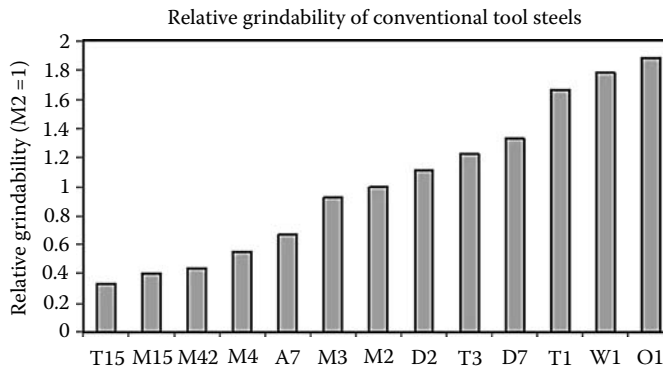


**FIGURE 13.4** Relative grindability of conventionally produced tool steels.

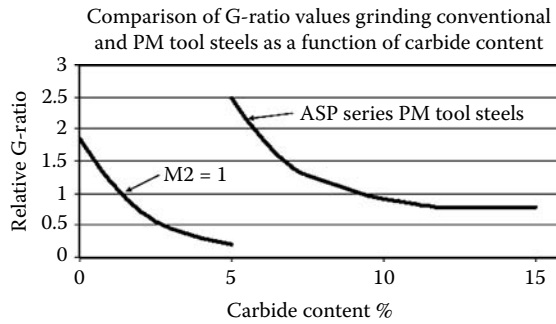


**FIGURE 13.5** Comparison of the grindability of tool steels, based on carbide content, made by conventional and powder-metal methods.

designed to withstand high temperatures, bringing them into the lower end of the range of heat-resistant alloys used in the aerospace industries. They are characterized by producing long chips when ground and a tendency to cause loading. They also will work-harden producing high grinding forces and wheel wear. Currently most applications are ground using the more advanced ceramic such as SG- or TG-type grains or regular alox grains in continuous dress creep feed (CDCF) grinding.

Precipitation-hardened steels lead into the final and most difficult of material groups to grind in the high-production manufacturing arena.

### 13.4 HEAT-RESISTANT SUPERALLOYS

Heat-resistant superalloys (HRSA) are based on high levels of nickel, chromium, and/or cobalt. In many cases, iron, as an alloying element, may be almost or entirely absent. These are the workhorses

Heat-resistant super alloys Aero- and land-based engine alloys operating (650–980)°C	
Iron-based precipitation hardened (withstand ≤ 670°C)	Incoloy 909 30HrC 40.4% Fe, 37.5% Ni A-286 30HrC 55.9% Fe, 25.5% Ni, 15% Cr Greek ascology 30HrC 80% Fe, 2% Ni, 13% Cr
Nickel-based cast, wrought, & precipitation hardened (blades, vanes, shafts, nozzles)	Inconel 718 43HrC 52.5% Ni, 19% Cr, 19% Fe Inconel 738 37HrC 60.5% Ni, 16% Cr, 9.5% Co Inconel 939 40HrC 49.6% Ni, 22% Cr, 10% Co, Rene 108 59% Ni, 8.3% Cr, 10% Co, 10% W, Waspalloy 58% Ni, 19% Cr, 13.5% Co Hastelloy X <8HrC 47% Ni, 22% Cr, 18% Fe, 9% Mo
Cobalt-based wrought & cast (afterburners, vanes, also nuclear reactors and medical implants)	Haynes 25 30HrC 51% Co, 20% Cr, 10% Co, 1% W Stellite 31 56% Co, 25.5% Cr, 10.5% Ni

**FIGURE 13.6** Major classes and examples of heat-resistant superalloys.

of the aerospace engine and land-based power generation industries. Their superior ability to retain strength and corrosion resistance at high temperatures allows their use in turbine vanes and blades, and after-burners that operate at temperatures up to 980°C. For major classes and examples of heat-resistant superalloys, see Figure 13.6.

### 13.4.1 PRECIPITATION-HARDENED IRON-BASED ALLOYS

The lowest class of HRSA materials is the precipitation-hardened iron-based alloys discussed before.

### 13.4.2 NICKEL-BASED ALLOYS

The second, and most prolific, group of alloys is the nickel-based superalloys. These are used extensively for blades, vanes, buckets, shrouds, shafts, nozzles, honeycomb, and rotors. The raw material may be supplied as a forging, casting, or as bar stock depending on the application. Blades and vanes, for example, are supplied as castings, usually hollow to reduce weight. Because the grindability is so poor and hence grinding costs high, casting suppliers have improved their technology dramatically over the last decade to produce near-net shapes and reduce grinding processes from ones requiring CDCF grinding to remove up to 10 mm of stock to finish grind processes removing as little as a tenth of this. Some blades are even produced as directionally solidified single crystals to maximize the strength in a particular direction. The material may also be supplied after various heat treatments including annealing, solution treatment, and aging. Many basic material grades may have several levels of heat treatment, each of which significantly affecting its grindability. Nevertheless, all nickel-based alloys share the following properties that make their grindability “difficult”:

- High strength, including dynamic shear strength, retains at the high temperatures seen in grinding.
- Poor thermal conductivity.
- Material structure contains hard carbide for wear resistance and crack arrest.
- Material work hardens during chip formation.
- Extreme sensitivity to heat damage; the so-called “white layer” is very detrimental to component strength in an industry where safety is paramount.

The grindability of nickel-based alloys based on G-ratio and surface quality of chip form is perhaps a twentieth that of carbon steels or gray cast iron; based on stock removal parameter, grindability is about a third. CBN and advanced ceramic grains are becoming increasingly dominant for grinding both nickel- and cobalt-based materials.

### 13.4.3 COBALT-BASED ALLOYS

The third group of alloys is cobalt based. These alloys display the best high-temperature corrosion resistance but have the lowest grindability and are the most expensive. They are, therefore, used in just the hottest part of the engine. However, one area where expense is not so important and where strength and corrosion resistance are critical is in the medical industry where wrought and cast cobalt-chromium alloys are becoming common for implants such as knee and hip joints. They are strengthened by solid-solution elements and the presence of carbides, and experience the same problems in grindability as the aerospace industry. Plated CBN and extruded ceramic grain are common for this type of application.

### 13.4.4 TITANIUM

Figure 13.7 gives typical values for the relative grindability of many of the material types described above. These numbers are dependent on advances in the various abrasive and wheel bond technology

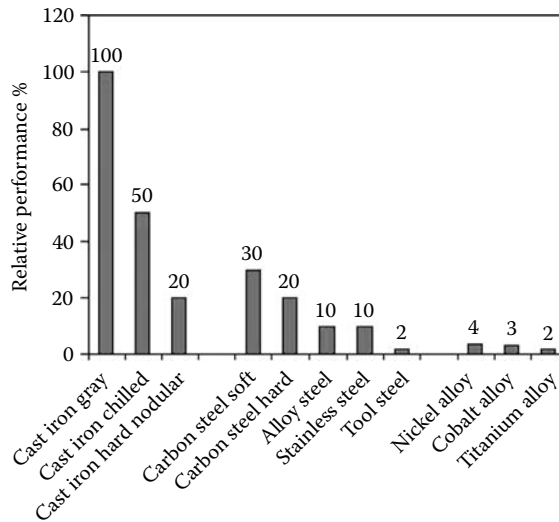


**FIGURE 13.7** Relative grindability by material type.

and on the type of application. With the growth of CBN technology, the grindability of hard steel and chilled iron has increased significantly. Similarly, recent developments in extruded ceramic grain technology may raise the grindability of nickel- and cobalt-based alloys based on G-ratio and stock removal parameter from those shown. Titanium alloys are also included in Figure 13.7. Titanium is problematic because it is chemically reactive with CBN limiting the application of superabrasives; it is also reactive with alumina. Some success has been reported using plated diamond [Kumar 1990] to grind aerospace-grade titanium alloys, but most applications still use porous SiC wheels. On the other hand, the machinability of titanium remains better than nickel- or cobalt-based alloys based on chip form and surface quality, and in many cases should be considered as a better alternative to grinding.

## REFERENCES

- Badger, J. A. 2003. "Grindability of High-Speed Steel." *Abrasives Mag.* Dec–Mar, 16–19.
- Kumar, K. V. 1990. "Superabrasive Grinding of Titanium Alloys." SME Conference Proceedings, Paper MR90-505.





---

# 14 Grinding of Ceramics

## 14.1 INTRODUCTION

This chapter discusses factors affecting the grinding of the new generation of hard engineering ceramics. Particular attention is drawn to effects on predressing time and surface quality. Electrolytic in-Process Dressing (ELID) grinding is introduced as an exciting new process used for machining a range of very hard materials and, in particular, for machining ceramics.

### 14.1.1 USE OF CERAMIC MATERIALS

Ceramic materials are used in engineering where there are demanding requirements for particular material properties. These may include requirements such as unusually high heat resistance, unusually high wear and corrosion resistance, low specific weight, or unusual electrical properties. Noticeable examples include ceramic bearings for high speeds in the machine tool industry and electronic components for the computer industry.

It is possible to engineer ceramic materials for high density and high strength. Developments in ceramic materials have greatly increased the range of engineering applications in recent decades. Zirconia, for example, is a modern material that is very tough and, apart from the obvious use for jewelry, is finding increasing engineering use for wear resistance. Hard silicon nitride ceramics also offer a way to overcome the greatest disadvantage of traditional ceramics: that being their brittleness. Ceramic-ceramic composites have further increased the range of properties that can be achieved.

### 14.1.2 MACHINING HARD CERAMICS

Abrasive machining is practically the only successful method for machining these hard and brittle materials. Superabrasive grinding wheels with diamonds are generally employed due to the extreme hardness of some ceramics. The combination of high hardness and strength, however, causes considerable wear on the diamond abrasive itself with effect on the geometric accuracy of the grinding wheel, the protrusion height of individual grains (cutting edges), and the distribution pattern of active cutting edges. Therefore, careful preparation of the wheel prior to grinding is essential.

### 14.1.3 WHEEL-DRESSING REQUIREMENTS

Surface conditioning of a grinding wheel generally includes the two requirements of truing and dressing. Dressing replaces worn (dulled) cutting edges with sharp edges by fracturing the worn grains and regenerates a wheel face loaded with swarf by removing a layer from the face with a dressing tool. Dressing a superabrasive wheel is much more difficult than dressing a conventional wheel and is not always possible. A special process known as ELID was introduced to allow the grinding of hard ceramics and is discussed in more detail in this chapter.

The necessity for dressing increases costs in grinding. In addition, the loss of abrasive particles from the wheel surface is expensive due to the high cost of superabrasive wheels and the associated loss of wheel life. Consequently, it is very important to use superabrasive wheels effectively to minimize waste of the wheel as well as to reduce dressing time.

#### 14.1.4 ELID GRINDING

The new ELID technique has attracted special interest because it eliminates conventional dressing times while improving the quality of ground surfaces. In ELID grinding, the grinding wheel is connected to a positive electrode and a negative electrode is mounted in proximity to the wheel with a gap of 0.1 to 0.3 mm. During predressing or grinding, a power source provides a pulsed direct current.

The gap is filled with an electrolyte grinding fluid to obtain an electrochemical action. The direct current pulse ionizes and removes conductive bond material. As the action proceeds, the surface of the wheel becomes coated with a nonconducting layer such as iron oxide or hydroxide. The nonconducting layer has the effect of preventing excessive electrolytic action. The rate of electrolytic action is an essential aspect of process control to ensure adequate protrusion of the grains while avoiding excessive wheel wear.

#### 14.1.5 ADVANTAGES OF ELID

Advantages of ELID include:

- Elimination of dressing time by in-process dressing.
- Elimination of the need for conventional dressing tools and, hence, reduced dressing costs.
- Elimination of physical or mechanical damage to the dressed grains.
- A significant reduction in normal grinding force with ELID grinding compared with conventional grinding.
- Extremely smooth surfaces can be achieved by use of ultrafine abrasives.
- High precision parts can be achieved with excellent process efficiency.

### 14.2 BACKGROUND ON CERAMIC MATERIALS

#### 14.2.1 HISTORY

The word ceramic can be traced back to the Greek term *keramos*, meaning “a potter” or “pottery.” *Keramos*, in turn, is related to an older Sanskrit root meaning “to burn.” Thus, the early Greeks used the term to mean, “burned stuff” or “burned earth” when referring to products obtained through the action of fire upon earthy materials (The American Ceramic Society) [Marinescu, Toenshoff, and Inasaki 2001].

#### 14.2.2 STRUCTURE

The structure of ceramic crystals is among the most complex of all materials, containing various elements of different sizes. The bonding between these atoms is generally covalent (electron sharing, hence, strong bonds) and ionic (primary bonding between oppositely charged ions, thus, strong bonds). These bonds are much stronger than metallic bonds. Consequently, hardness and thermal and electrical resistance of ceramics may be significantly higher than those of metals [Inasaki 1998].

The properties of ceramics products are dependent on the chemical composition and atomic and microscale structure. Compositions of ceramic products vary widely, and both oxide and nonoxide materials are commonly used. In recent times, the composition, grain structure, and also the distribution and structure of porosity have been more carefully controlled to achieve greater product performance and reliability [Inasaki 1998].

### 14.2.3 CERAMIC GROUPS

Ceramics are classified in the following subgroups [Marinescu et al. 2001]:

- Oxides (alumina, zirconia, and partially stabilized zirconia)
- Carbides (tungsten and titanium used for cutting tools, silicon carbide used as abrasives in grinding wheels)
- Nitrides (cubic boron nitride [CBN], titanium nitride, and silicon nitride)
- Sialon (silicon nitride with various additions of aluminum oxide, yttrium oxide, and titanium carbide)
- Cermets (ceramics bonded with a metallic phase)
- Silicates are products of the reaction of silica with oxides of aluminum, magnesium, calcium, potassium, sodium, and iron such as clay, asbestos, mica, and silicate glasses.

### 14.2.4 CERAMIC PRODUCT GROUPS

Table 14.1 presents typical examples of products obtained by ceramic powder processing. Nowadays, ceramic-ceramic composites are used for many engineering applications. Development of ceramic-ceramic composites is largely due to improvements in microstructure of reinforced ceramics such as  $\text{Al}_2\text{O}_3 + \text{TiC}$ ,  $\text{Al}_2\text{O}_3 + \text{ZrO}_2$ ,  $\text{ZrO}_2 + \text{Al}_2\text{O}_3$ , and whisker-reinforced ceramics such as  $\text{Al}_2\text{O}_3 + \text{SiCw}$ ,  $\text{Si}_3\text{N}_4 + \text{SiCw}$ , etc. Among these,  $\text{Al}_2\text{O}_3 + \text{ZrO}_2$  and  $\text{ZrO}_2 + \text{Al}_2\text{O}_3$  are referred to as toughened ceramics, which have widened the scope of application of oxide ceramics.

One of the main oxide ceramics is alumina, also called corundum. Emery is also a widely used oxide ceramic. It has high hardness and moderate strength. Aluminum oxide is almost totally manufactured synthetically in order to control quality.

---

**TABLE 14.1**  
**Products Obtained by Ceramic Powder Processing [Malkin 1989]**

Group of Applications	Products Obtained by Ceramic Powder Processing
Electronics	Substrates, chip carriers, electronic packaging Capacitors, inductors, resistors, electrical insulation Transducers, electrodes, igniters
Advanced structural materials	Cutting tools, wear-resistant inserts Engine components Resistant coatings Dental and orthopedic prostheses High-efficiency lamps
Chemical processing components	Ion exchange media Emission control components Catalyst supports Liquid and gas filters
Refractory structures	Refractory lining in furnaces Regenerators Crucibles Heating elements
Construction materials	Tile structural clay products Cement, concrete
Institutional and domestic products	Hotel china and dinnerware Bathroom fixtures Decorative fixtures and household items

*Source:* From Malkin 1989. With permission.

---

Synthetic aluminum oxide, first made in 1893, is used for applications such as electrical and thermal insulation and as cutting tools and abrasives [Ruhle 1985].

Zirconia (zirconium oxide,  $ZrO_2$ ) has high toughness, high resistance to thermal shock, wear, and corrosion, low thermal conductivity, and a low friction coefficient when paired with many materials [Green and Hannink 1989].

Zirconia-toughened alumina (ZTA) is a ceramic system obtained as a result of the transformation toughening of  $ZrO_2$  in a constrained matrix of  $Al_2O_3$ . One field of application for ZTA due to excellent wear behavior is the application for cutting tools. In recent decades ceramic cutting tools have made a strong impact in manufacturing.

#### 14.2.5 APPLICATION OF ZTA CERAMICS

The enhanced strength and toughness of ZTA ceramics have made these materials more widely applicable and more productive than plain ceramics and cermets for machining steels and cast irons. ZTA ceramics can be used as cutting tool inserts for metal cutting applications [Sornakumar and Gopalakrishnan 1995].

Cutting inserts are made by sintering followed by grinding and lapping. During the sintering process, ceramics are subject to volumetric shrinkage and as a result cannot meet the requirements for form and size accuracy without further machining. To meet these demands, machining by grinding, lapping, honing, or polishing with diamonds is necessary.

The performance of ZTA cutting inserts is strongly influenced by the grinding process. The active faces of the inserts should be smooth, without cracks, and the cutting edges should be free of chips. ELID grinding can provide a solution to these requirements such that dimensional accuracy and surface quality are achieved and even surpassed with a considerable increase in productivity [Marinescu and Ohmori 1999, Ohmori and Li 2000a].

The ELID grinding technique was recently developed in Japan and there is an increased tendency to apply it for grinding hard and brittle materials [Bandyopadhyay 1996, Ohmori and Li 2000a]. However, there are still insufficiently explored areas that make industrialists hesitant in adopting the method. Very little experimentation on ELID grinding has been conducted in the United States until very recently. The need for further practical information provides the motivation for further research.

#### 14.2.6 GRINDING OF CERAMICS

The characteristics of grinding advanced ceramics are very different from the ones for metals and research is still ongoing for a more comprehensive understanding and a better control of grinding parameters. Figure 14.1 presents the factors affecting the grinding process [Marinescu and Ohmori 1999].

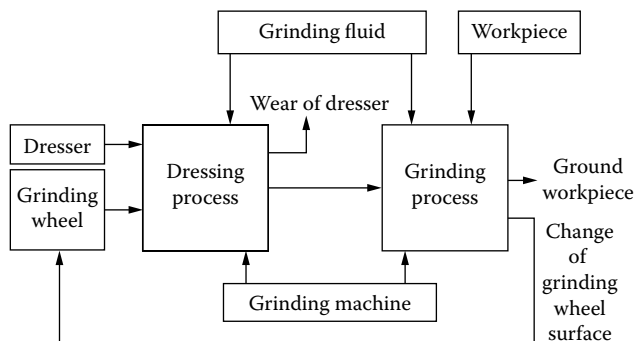


FIGURE 14.1 Factors affecting the grinding process. (From Marinescu and Ohmiri 1999. With permission.)

Due to the fact that ceramics are brittle and have high hardness they are best ground using diamond-grinding wheels [Marinescu et al. 2001].

## 14.3 DIAMOND WHEELS FOR GRINDING CERAMICS

### 14.3.1 THE TYPE OF DIAMOND ABRASIVE

Diamonds, used for grinding ceramics, are mainly synthetic diamonds. The synthesis process permits control of diamond characteristics generating either blocky grit shapes with very high impact strength, or friable grits with low-impact strength. Diamonds are also classified by grit size and grit size distribution. The grit system can be used to control the desired working result within a wide range [Carius 2002].

The abrasive grains employed for ELID grinding usually consist of synthetic diamond. Diamond is the most efficient superabrasive material used for grinding all sorts of hard, nonmetallic materials. Depending on the materials to be ground, different strength and wear characteristics are required for the diamond used. For best economic performance, the abrasive grain formulation must be matched with a correct bond formulation.

The main property of diamond is its hardness (10 on Mohs hardness scale). Not only do different diamonds have appreciably different structures and mechanical properties, but also different parts of the same stone may differ appreciably.

The characteristics of diamond are

- Material pure carbon (C)
- Atomic weight 12
- Melting point 3,700 K

Diamond has the following properties:

- Behaves more like a nonmetal
- Is an electrical insulator but conducts heat very well
- Is truly stable only at high pressures
- Crystals form in the area of pressure and temperature where diamond is stable.

For ELID grinding, the grinding wheel is normally a metal-bonded diamond wheel. This structure presents a very different challenge for dressing compared with a vitrified diamond wheel or a resin-bond diamond wheel or even an electroplated diamond wheel.

### 14.3.2 TYPES OF DIAMOND WHEEL

Basically, a grinding wheel has three components: abrasive, bond, and core. Figure 14.2 presents the three components of a superabrasive diamond or CBN wheel [Inasaki 1998].

In general application, diamond wheels can be resin, metal, or vitrified bond. Wheels can be classified according to the bond material as either [Marinescu et al. 2001] monolayer-electroplated wheels or multilayer wheels, which include resin bonded, vitrified bonded, and metal bonded.

Resin bonds have been widely used for diamond wheels for many years and offer the particular feature of structural flexibility. Phenolic resins and their derivatives are still the most commonly used bond types. Resin-bonded wheels are relatively easy to use in a wide range of applications typically in the conventional grinding of cemented carbides.

Vitrified bond diamond wheels have steadily become a more important market segment of the diamond tool market for conventional grinding. They are relatively easy to profile and maintain their shape. A further advantage of this type of wheel is that porosity can be introduced into the bond in a controlled manner. This allows extra chip clearance volume on the wheel surface and space for the improved transport of coolant into the grinding zone [Marinescu et al. 2001].

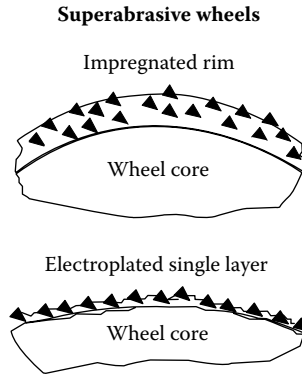


**FIGURE 14.2** Abrasive system, bond system, and core system for a superabrasive wheel. (a) Impregnated rim, (b) electroplated single layer. (From Marinescu et al. 2001. With permission.)

Two basic techniques are available for the production of vitrified bond diamond wheels: hot pressing, and cold pressing followed by free firing. Each method is designed for different application areas. Hot-pressed wheels are normally used for grinding diamond, as in the manufacture of both polycrystalline diamond cutting tools and natural diamond tools such as hardness-testing indenters. Cold-pressed tools, which have inbuilt porosity, are used in deep grinding of advanced ceramic materials and cemented carbides.

Metal bond wheels are used for applications such as grinding of glass, stone, ceramics, semi-conductors, and plastics.

For ELID grinding a cast-iron metal bond is normally used. Cast iron provides the necessary electrical conductivity. Figure 14.3 shows types of diamonds for metal bonded wheels [Carius 2002]. The strong, relatively hard, and inelastic metal bond requires diamond products with properties that are correctly matched to those of the bond. This type of tool is less tolerant of an unsuitable grit selection than other bond systems. The main feature of metal bonds is that the diamond is rigidly retained in the bond. Metal bonds provide very high abrasive resistance to the small detritus that occurs when machining short chipping materials. The wheel is manufactured by sintering at a high temperature.

The diamond layer in a wheel can be laid on different core materials. The diamond wheel is adapted for the specific machining operation. The nature of the core material is important in the machining of brittle ceramics and permits adaptation of the wheel with respect to vibration behavior and thermal conductivity [Marinescu et al. 2001].

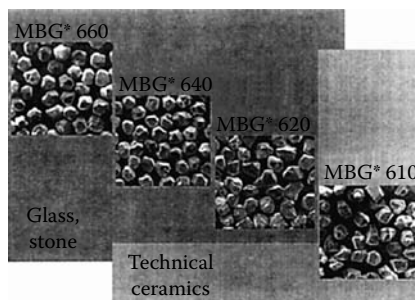


**FIGURE 14.3** Diamonds for metal bonded wheels. (From Carius 2002. With permission.)

When machining ceramic materials, it is important to minimize external vibration sources because of the brittle nature of these materials. The grinding wheel must be prepared and conditioned to reduce runout error, clamping error, and grinding wheel unbalance. Keeping the weight of the grinding wheel low helps to minimize vibrations.

### 14.3.3 WHEEL TRUING AND DRESSING

The actual cutting edges and points on abrasive grains at the wheel active surface are microcutting tools that interact with the workpiece material. The spatial distribution of abrasive grains over the wheel surface and their morphology comprise the grinding wheel topography.

The grinding wheel topography and the macroscopic wheel shape are initially generated by conditioning the wheel before grinding and periodically during the course of grinding. Wheel preparation generally includes truing and dressing. Truing usually refers to removal of material from the cutting surface of a grinding wheel so that the spinning wheel runs true with minimum runout from its macroscopic shape, although truing may also include profiling of the wheel to a particular shape [Marinescu et al. 2001].

Dressing is the process of conditioning of the wheel surface so as to achieve a certain grinding behavior. Generally dressing is the process of conditioning worn grains on the surface of a grinding wheel in order to produce sharp new grains and truing out-of-round wheels. Dressing is necessary when excessive attritious wear dulls the wheel or when the wheel becomes loaded. Dulling of the wheel is known as glazing because of the shiny appearance of the wheel surface. Loading occurs when the pores on the surface of the wheel become filled or clogged with chips.

Pregrinding preparation of superabrasive wheels usually involves two distinct processes: truing and dressing. Most superabrasive wheels are trued and dressed, with the exception of electroplated wheels, which may only require “cleaning” or “touching up” with an abrasive stick. One popular truing method for diamond wheels utilizes a vitrified green (friable) silicon carbide grinding wheel mounted on a brake-controlled truing device. The truing wheel is operated as if it cylindrically traverse grinds the grinding wheel. The axes of the dressing wheel and grinding wheel are parallel to each other, as in Figure 14.4.

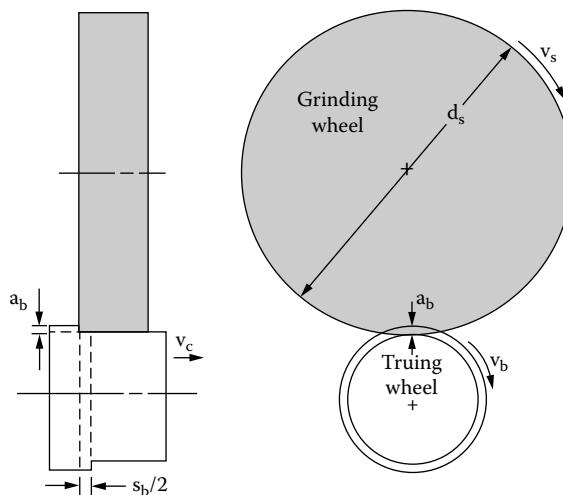


**FIGURE 14.4** Brake-controlled truing arrangement for peripheral wheels. (From Kalpakjian 1997. With permission.)



Other types of wheels (e.g., cup wheels) use a similar device. The depth increment  $a_b$  might be between 10 and 20  $\mu\text{m}$  after each traverse across the wheel face with a cross-feed velocity,  $v_c$ , corresponding to a lead of  $s_b = 0.1$  to 0.2 mm per grinding wheel revolution.

Numerous other truing methods utilizing diamond tools, similar to those applied to conventional abrasive wheels, have been tried with diamond wheels, but with limited success. Diamond truing of diamond wheels removes wheel material much faster than silicon carbide truing, but there is a danger of damage both to the truing tool and wheel. Truing with single-point and multipoint diamond tools may also necessitate excessive wheel loss, and the truing tool wears out rapidly [Kalpakjian 1997].

After truing, dressing of superabrasive wheels is usually accomplished by in-feeding a fine-grained vitrified abrasive stick into the wheel surface either manually or with a holding device. Again, there is a danger of damage to the abrasive grains with excessive use of an abrasive stick.

The decisive factors for grinding behavior include grit type, grit size, and concentration, but also specification of the bond system and conditioning of the grinding layer. The interplay between wear processes on the grit and on the bond affects both grinding behavior and workpiece quality. Metal bond wheels in particular react strongly to differences in dressing [Malkin 1989].

These operations for superabrasive wheels (truing and dressing) should be avoided as much as possible because they require production workflow to be interrupted. Some of the advantages of using superabrasives can be canceled if the dressing time is excessive. A further consideration is the loss of expensive abrasive particles from the wheel surface due to the dressing process. This can be important since initial superabrasive wheel cost may be several times the cost of conventional wheels. Consequently, it is very important for effective utilization of superabrasive wheels to avoid wasting wheel material due to dressing as well as to reduce dressing time.

#### 14.4 PHYSICS OF GRINDING CERAMICS

The material-removal rates in grinding of ceramics vary widely depending on the application (Figure 14.5). With recent advances toward understanding of the mechanics of grinding ceramics, it is possible to achieve material-removal rates comparable to that in metal grinding. However, current practice achieves only about a tenth of these material-removal rates.

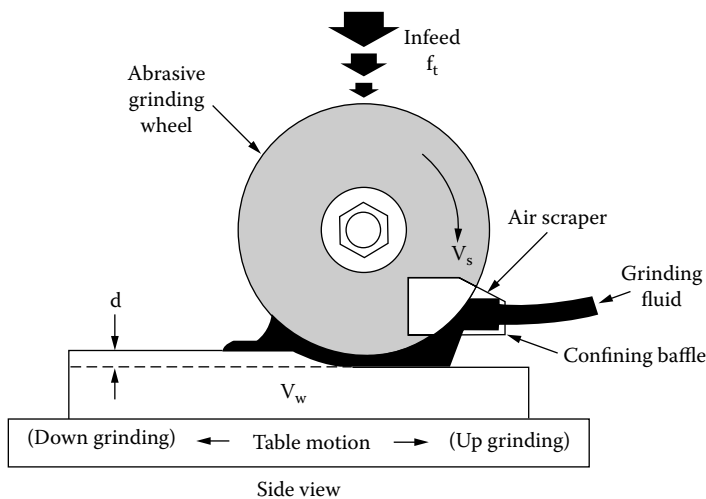


FIGURE 14.5 Schematic of surface grinding. (From Malkin 1989. With permission.)

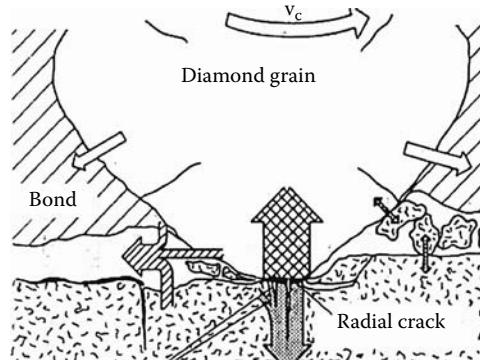


FIGURE 14.6 Surface contact. (From Uhlmann 1998. With permission.)

One model of chip formation is based on the Hertzian surface pressure of two bodies in contact with each other, where the stresses and deformations produce microcracks, which cause breakdown of the ceramic grains so that brittle material erosion takes place (Figure 14.6 and Figure 14.7) [Marinescu et al. 2001].

Ceramic materials are more brittle than metallic materials and show very little plastic deformation under load up to the point of fracture. For this reason, it might be expected that the mechanism of abrasive machining of ceramic materials would mainly involve brittle fracture. Microscopic examination of high-density polycrystalline alumina surfaces ground with diamond shows fractured areas that are consistent with a brittle fracture mechanism. However, evidence of plastic flow with striations along the grinding direction is also observed. This would

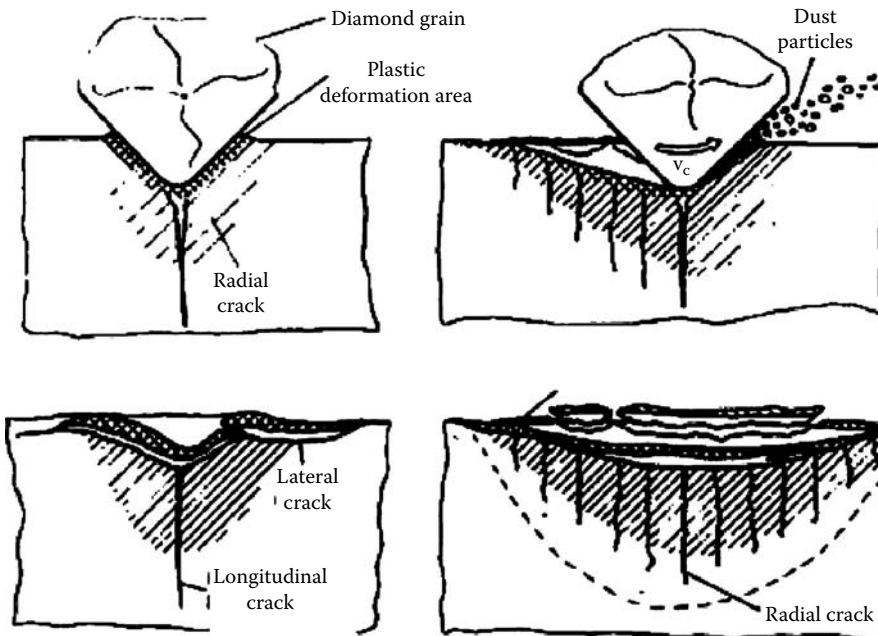


FIGURE 14.7 Phenomena of surface deformations for diamond on ceramic. (From Uhlmann 1998. With permission.)

suggest that both flow and fracture play an important role in the grinding process for ceramics [Bifano 1998].

Another model is based on the assumption that ceramic material is softened by higher local temperatures at the cutting points, thus becoming plastically deformable, and can, therefore, be machined in a similar manner to other materials. Ductile-regime grinding has been used to describe the material-removal mechanisms in grinding of ceramics under suitable conditions. A transition from brittle to ductile mode material removal at smaller cutting depths can be argued purely from considerations of necessary material-removal energy. Specifically, for lower machining depths of cut, it can be shown that plastic flow is a more energetically favorable material-removal process than fracture. The limiting depth at which a brittle-ductile transition occurs is a function of the intrinsic material properties governing plastic deformation and fracture [Bifano 1998].

Ductile mode grinding enhances surface quality, but is very slow and costly. One possible method of promoting ductile flow and achieving removal rates is by using high peripheral wheel speeds. Higher wheel speeds reduce the uncut chip thickness and result in a smaller force per grit, increased ductile flow, and decreased strength degradation. The reduction in surface fracture and apparent increase in flow may be associated with glassy phase formation at elevated grinding temperatures [Bifano 1998].

A combination of the two modes, brittle and ductile, depending on the type of ceramic and the machining conditions is probably involved in reality. The transition is decided by the size of plastically deformed layer caused by the interference between the material and the tool.

Figure 14.8a and Figure 14.8b provide a comparison between ground surface finishes of silicon nitride in brittle mode grinding and of zirconium oxide in ductile mode grinding. Figure 14.8a shows the result of brittle mode grinding [Ohmori and Li 2000b].

Brittle materials exhibit discontinuous failure phenomena. Ductile mode grinding (Figure 14.8b) is superior to brittle mode grinding with respect to both geometrical accuracy and surface integrity. The ductile regime grinding hypothesis of Bifano states that, for any material, if the dimensional scale of material removal is small enough, then plastic flow of the material will take place without fracture. The nature of the material does not affect ductile chip formation.

The term semiductile grinding is used for the brittle-ductile transition process in grinding of ceramics. The transition from a brittle to a ductile mode during the machining of brittle materials is described in terms of energy balance between the strain energy and the surface energy. Another interpretation of ductile transition phenomena is based on cleavage fracture due to presence of defects. The critical values of a cleavage and plastic deformation are affected by the density of defects/dislocations in the work material. Since the density of defects is not so large in brittle materials, the critical value of a fracture depends on size of the stress field [Ngoi and Sreejith 2000].

The mechanism of material removal with abrasive cutting edges on the wheel surface is basically the same as with cutting tools. The size of chips removed in grinding is, however, much smaller than the case of cutting providing better surface finish and machining accuracy. The order of chip thickness in grinding is far less than 0.1 mm, whereas it is larger than 0.1 mm in cutting.

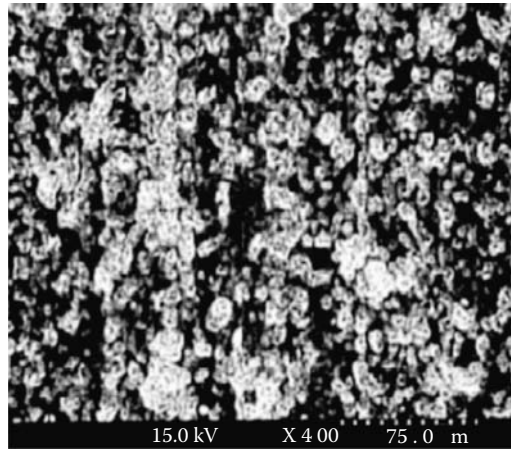
The average cross-sectional area of chips,  $A_{cu}$ , in grinding can be estimated as follows for surface grinding (Figure 14.9) [Marinescu et al. 2001].

The material removal rate is  $Q$ , where  $b$  is the grinding width,  $v_w$  is the workpiece speed, and  $a_e$  is the depth of cut.

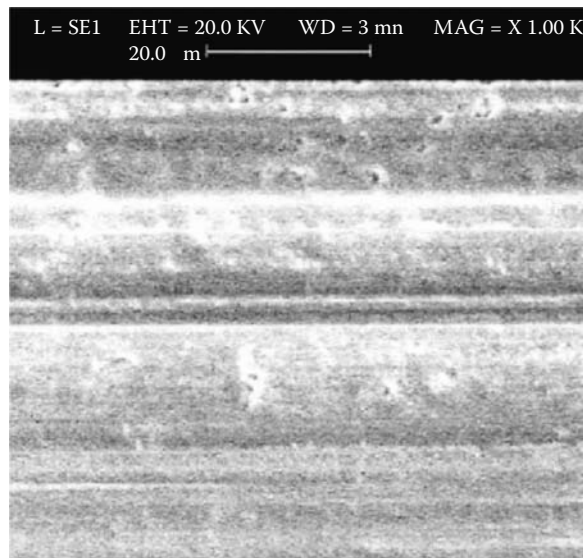
$$Q = b.v_w.a_e \quad (2.1)$$

The number of chips produced per unit time,  $N$ , is given by

$$N = C.b.v_s \quad (2.2)$$



(a)



(b)

**FIGURE 14.8** Grinding in brittle mode and ductile mode. (a) Brittle mode grinding of  $\text{Si}_3\text{N}_4$ . (b) Ductile mode grinding of  $\text{ZrO}_2$ . (From Zhang et al. 2003. With permission.)

Assume that each cutting edge on the wheel surface produces a chip, where  $v_s$  is the grinding wheel surface speed and  $C$  is the number of cutting edges per unit area on the wheel surface. The average chip volume  $V_{cu}$  is

$$V_{cu} = \frac{Q}{N} = \frac{v_w \cdot a_e}{C \cdot v_s} \quad (2.3)$$

The chip length is given by

$$l_g = \sqrt{a_e d_s} \quad (2.4)$$

where  $d_s$  is the wheel diameter.

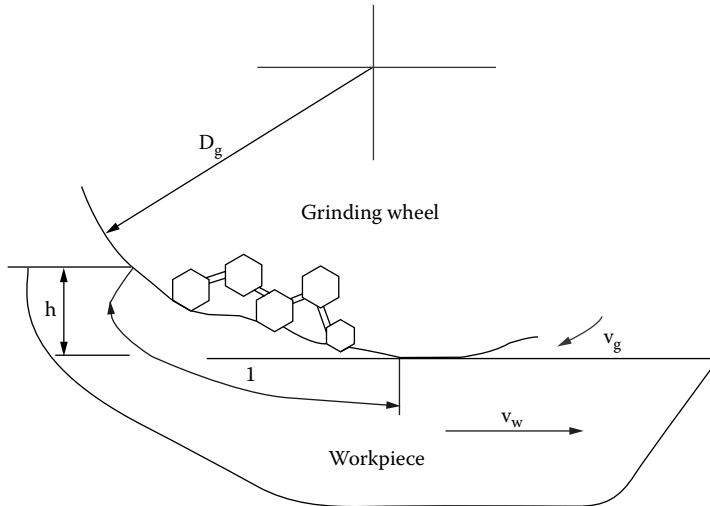


FIGURE 14.9 Parameters in surface grinding. (From Marinescu et al. 2001. With permission.)

The average cross-sectional area of chips is [Green and Hannink 1989]

$$A_{cu} = \frac{V_{cu}}{l_g} = \frac{v_w}{C \cdot v_s} \sqrt{\frac{a_e}{d_s}} \quad (2.5)$$

$A_{cu}$  is increased through increase of work speed or depth of cut. This increases the cutting force acting on each cutting edge and results in breakage or dislodgement of the abrasive from the bond. This phenomenon is called “self-sharpening” [Marinescu et al. 2001]. The surface roughness of the workpiece, however, deteriorates.

Conversely,  $A_{cu}$  is decreased through increase of wheelspeed and attritious wear of cutting edges becomes more significant. In this case, heat generation increases while surface roughness becomes smaller.

## 14.5 ELID GRINDING OF CERAMICS

### 14.5.1 MECHANISM OF ELID GRINDING TECHNIQUE

ELID is a new technique that uses electrolysis to remove bond material. The application of this dressing technique during the course of a grinding process allows chips and debris to be removed easily and allows grindability to be maintained over a long period of time. Various applications of ELID grinding have been developed. With ELID dressing, it was possible to realize mirror grinding with various types of systems using existing machine tools such as [Ohmori and Itoh 1998, Ohmori and Li 2000a]:

- Surface grinders
- Rotary surface grinders
- Turning centers
- Infeed grinders
- Lap grinding machines

The ELID system consists of a negative electrode, a brush, a power supply, a metal-bonded wheel, and an electrolytic grinding fluid (Figure 14.10).

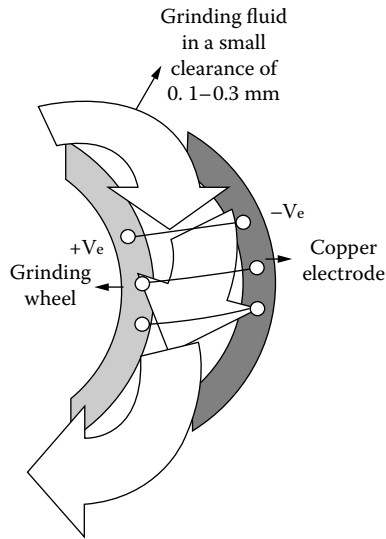


**FIGURE 14.10** The phenomenon of electrolysis in-between grinding wheel and a copper electrode.

The wheel is made the anode of the power supply through the application of a brush smoothly contacting the surface. The cathode is placed in proximity to the wheel surface. The power supply transforms an alternating current into direct current as necessary for electrolysis. Generally, ELID must be applied to a wheel, which has been trued to run concentric to the spindle axis. The shape of the wheel is profiled to the required geometry and dull abrasives are fractured. Before commencement of grinding it is necessary to perform a predressing operation because it is necessary to have diamond grains exposed above the level of the bond. Truing of the grinding wheel is, therefore, required for the following reasons [Ohmori and Itoh 1998, Ohmori and Li 2000a]:

- The wheel must be concentric to the spindle axis.
- The wheel profile must have the correct geometry.
- Dull abrasives need to be fractured.

After truing, an ELID predressing operation on the diamond wheel is necessary to

- Expose diamond grains above the bond level (sharpening)
- Provide chip clearance

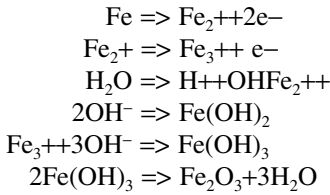
Diamond grains protrude from the wheel surface after predressing of the wheel.

The ELID process is performed in the following three steps [Marinescu and Ohmori 1999]:

1. Precision truing of the grinding wheel carried out by the electrodischarge truing technique
2. Predressing of the grinding wheel by electrolysis
3. Grinding with ELID

The cast-iron bond material of the grinding wheel is electrically conductive. Power is supplied to the metal bond through a brush that contacts the wheel. A copper electrode forms the cathode and a current is provided through the electrolyte in the gap between the anode and the cathode.

Electrolysis occurs at the gap between the metal bond and the electrode. The cast iron is ionized into  $\text{Fe}_2^+$  [Ohmori and Li 2000b]:



The above chemical reactions show that the ionized Fe forms hydroxides, and these substances change into oxides such as  $\text{Fe}_2\text{O}_3$ , which form an insulating layer. The electroconductivity of the wheel surface is reduced due to the growth of the insulating layer. After the oxide layer is formed and prepressing is completed, ELID grinding can be performed [Ohmori and Itoh 1998].

Due to grinding, the oxide layer is removed when the wheel touches the workpiece. The thickness of the oxide layer is decreased and electroconductivity increases again. The metal bond is removed by electrolysis and transformed into a further oxide layer. The result is new sharp edges protruding from the surface of the wheel. This means that electrolytic in-process dressing is performed at the same time as grinding. The mechanism of ELID is shown in Figure 14.11.

#### 14.5.2 RESEARCH STUDIES ON ELID

ELID grinding technique was used for the first time in Japan at the Riken Laboratories. The pioneers of this technique are Dr. Hitoshi Ohmori and Prof. Takeo Nakagawa. Dr. Ohmori's new method is a result of the development over several years of the combined grinding and dressing technique for hard and brittle materials in an effort to effectively utilize cast-iron fiber-bonded wheels that are considered to be the toughest among all metal-bonded wheels. Nakagawa found one solution for the efficient machining of the ceramics is to use a cast iron-bonded diamond grinding wheel mounted on a rigid numerically controlled grinding machine. A cast iron-bonded wheel is a metal-bonded wheel of very high strength. It gives a low wear rate, and a high grinding ratio even at a low grinding speed [Green and Hannink 1989, Ohmori and Itoh 1998, Ohmori and Li 2000b]. Ohmori and Li [2000a], at the Institute of Physical and Chemical Research (RIKEN), successfully applied the ELID to grind hard materials components and studied the possibility to apply this new technique for surface grinding, centerless grinding, and double-sided grinding. Efficient and precise ELID grinding was successfully carried out on  $\text{Si}_3\text{N}_4$  and  $\text{ZrO}_2$ , titanium carbide, and sialon. Mirror surfaces were achieved using the ELID technique, the best surface roughness and precision being obtained with a #4000 diamond wheel using through-feed grinding. Marinescu and Ohmori [1999], from the Abrasive Micro-Machining Laboratory, Toledo, performed ELID centerless grinding on different types of ceramics at RIKEN Laboratories in collaboration with the ELID Grinding Project Team from Tokyo. The following conclusions were obtained:

- Stable, efficient, and precision grinding for ceramic components has been achieved by mirror grinding with ELID technique.
- Efficient and precision truing by the electrodischarge method for metal-bonded grinding wheels for centerless grinding can be achieved.
- Good ground surface roughness and accuracy are offered with #4000 metal-bonded grinding wheel by through-feed grinding for  $\text{ZrO}_2$  optical fiber ferrules [Marinescu and Ohmori 1999].

Lee [2000], at Pusan National University, Korea, proposed a dressing system controlled by computer for ultra precision grinding of STD-11, die steel. The superabrasive wheel is CBN 12000.

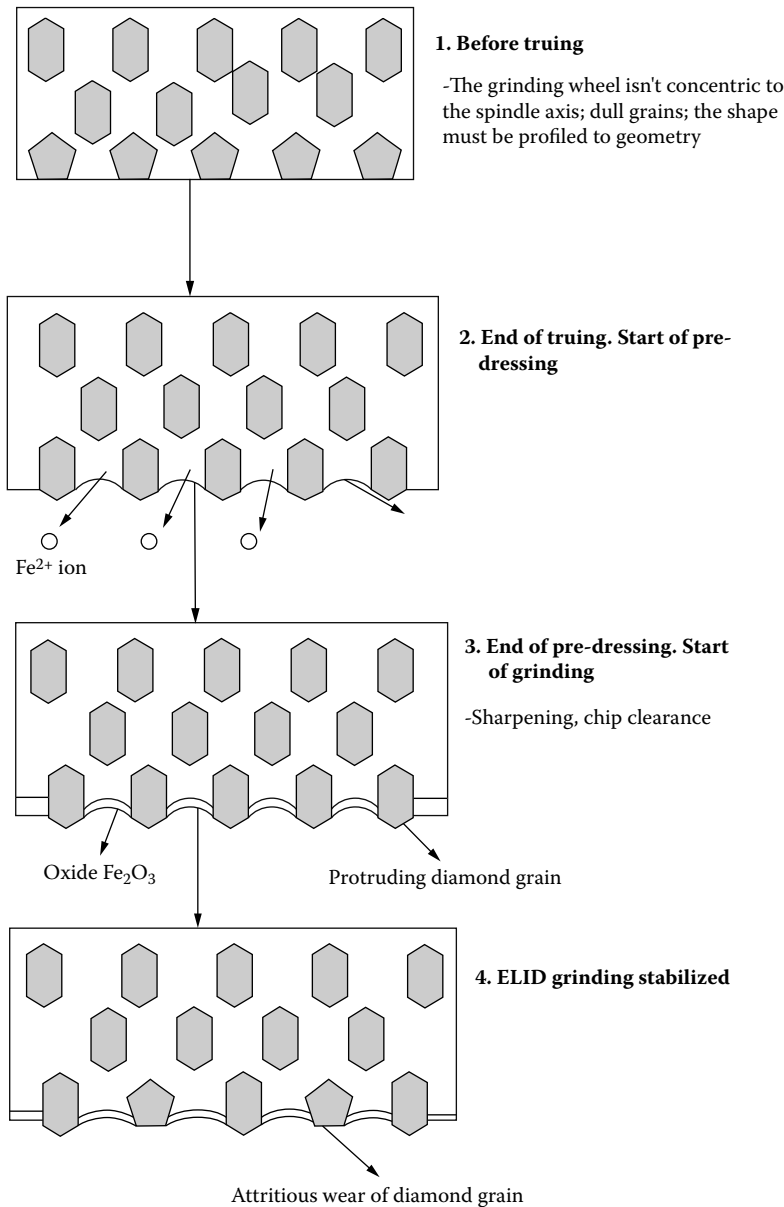


**FIGURE 14.11** Mechanism of electrolytic in-process dressing.

Bandyopadhyay [1996] performed ELID grinding experiments for Oak Ridge National Laboratory at Riken Laboratories under the supervision of Dr. H. Ohmori during two summers at Riken. Part I of his research addressed basic aspects of ELID grinding affecting the rate of material removal, the normal forces developed during grinding, and the conditions that improve the ratio of the material removed to that of abrasive consumed. Part II of the report addressed the effects of ELID grinding on the bending strength of silicon nitride.

Hong and Li [2000] studied theoretical aspects of ELID at the University of Rochester, New York. They studied the anodic metal matrix removal rate in ELID. The electric field or current density distribution around a diamond particle embedded in a metal anode during ELID was



calculated for the two-dimensional case of a long diamond particle, without a particle and with some protrusion. The mathematical model and the assumptions are presented in two recent articles in the *Journal of Applied Physics*.

### 14.5.3 SUMMARY ON ELID GRINDING

ELID grinding is a new technique and has given good results for machining hard silicon nitride and zirconia. This grinding technique is highly recommended for machining ceramics. However, up to this time, no published research could be found related to ELID grinding of ZTA ceramics.

The possibility of implementing this method in different types of grinding processes and for different concentrations of diamond in the grinding wheel has been demonstrated experimentally. Some characteristics related to surface finish are available. However, the influence of the grinding regime (rotational speed, depth of cut, and feed) on the surface roughness has been insufficiently explored.

A mathematical model of the anodic metal matrix removal rate in ELID has been developed. This theoretical approach, however, has not yet been applied to the modeling of the predressing time.

### REFERENCES

- Bandyopadhyay, B. P. 1996. "Application of Electrolytic In Process Dressing for High Efficiency Grinding of Ceramics Parts." Oak Ridge National Laboratory report, Research activities 1995–1996, ORNL/SUB/96-SV716/1.
- Bifano, T. G. 1998. "Ductile Regime Grinding of Brittle Materials." Ph.D. dissertation, North Carolina University.
- Bifano, T. G., Dow, T. A., and Scattergood, R. O. 1998. "Ductile-Regime Grinding: A New Technology for Machining Brittle Materials." Intersociety Symposium on Machining of Advanced Ceramic Materials and Components, ASME, New York.
- Carius, A. 2002. "Characteristics of Superabrasive Diamond and CBN Micron Powders." GE Superabrasives, Superabrasive Certification Course, University of Toledo, May–October.
- Green, D. J. and Hannink, R. H. J. 1989. "Transformation Toughening of Ceramics." CRC Press, Boca Raton, FL.
- Hong, C. J. and Li, M. 2000. "Anodic Metal Matrix Removal Rate in Electrolytic In-Process Dressing. Part I: Two-Dimensional Modeling." *J. Appl. Phys.* 87, 6, 3151–3158. "Part II: Protrusion Effect and Three-Dimensional Modeling," pp. 3159–3164.
- Inasaki, I. 1998. "Fluid Film in the Grinding Arc of Contact." Contribution at January CIRP Meeting, Paris, 27–31.
- Kalpajian, S. 1997. *Manufacturing Processes for Engineering Materials*. Third edition, Addison-Wesley.
- Koenig, W. and Popp, M. 1988. "Precision Machining of Advanced Ceramics—A Challenge in Production Technology." Proceedings of the International Congress for Ultraprecision Technology, May, Aachen FRG.
- Lee, E. S. 2000. "The Effect of Optimum In Process Electrolytic Dressing in the Ultra Precision Grinding of Die Steel by a Superabrasive Wheel." *Int. J. Adv. Manuf. Technol.* 16, 814–821.
- Malkin, S. 1989. "Grinding Technology. Theory and Applications of Machining with Abrasives." Ellis Norwood Ltd., U.K.
- Marinescu, I. and Ohmori, H. 1999. "ELID Grinding of Ceramic Materials." *Finishing of Advanced Ceramics, Ceramic Transactions*, 102.
- Marinescu, I., Toenshoff, H., and Inasaki, I. 2001. *Handbook of Ceramic Grinding and Polishing*. Noyes Publications, William Andrew Publishing, Norwick, NY.
- Ngoi, B. K. A. and Sreejith, P. S. 2000. "Ductile Regime Finish Machining—A Review." *Int. J. Adv. Manuf. Technol.* 16, 547–550.
- Ohmori, H. and Itoh, N. 1998. "Performances on Mirror Surface Grinding with ELID for Efficient Fabrication of Precision Cylindrical Components of Hard Materials." *Int. Jpn. Soc. Prec. Eng.* 32, 5, 1451–1457.

- Ohmori, H. and Li, W. 2000a. "Efficient and Precision Grinding of Small Hard and Brittle Cylindrical Parts by the Centerless Grinding Process Combined with Electro-Discharge Truing and Electrolytic In-process Dressing." *J. Mat. Proc. Technol.* 98, 321–327.
- Ohmori, H. and Li, W. 2000b. "Fine Cylindrical Machining Technique for Hard Material Components by Centerless Grinding Process Combined with Electro-Discharge Truing and Electrolytic In-Process Dressing." *Finishing of Advanced Ceramics, Ceramic Transactions.*
- Ruhle, M. 1985. "Ceramic Microstructures and Properties." *J. Vac. Sci. Technol.* A3, 749–756.
- Sornakumar, T. and Gopalakrishnan, M. V. 1995. "Development of Alumina and Ce-TTZ Ceramic-Ceramic Composite (ZTA) Cutting Tool." *Int. J. Refract. Met. Hard Mater.* 13, 375–378.
- Uhlmann, E. 1998. "Technological and Ecological Aspects of Cooling Lubrication during Grinding of Ultrahard Materials." Ultrahard Materials Technical Conference, Conference Papers.
- Zhang, B., Bheng, X. L., Tokura, H. and Yoshikawa, H. M. 2003. "Grinding Induced Damage in Ceramics." *J. Mater. Process. Technol.* 132, 353–364.



---

# 15 Grinding Machine Technology

A detailed discussion of machine tool design is beyond the scope of this book. The following sections highlight some important features in the design and construction of grinding machines and their elements. For a more detailed discussion, there are publications dedicated to this field such as Slocum [1992].

## 15.1 THE MACHINE BASE

### 15.1.1 INTRODUCTION

The machine base of a grinder is the most fundamental element on which all the active and passive assemblies are carried. It must be rigid, yet deform elastically, must inhibit vibration, survive in a hostile shop environment, and be thermally stable or at least have predictable thermal properties. Construction is usually based either on a casting or weldments, and selection is generally based on cost and/or application.

### 15.1.2 CAST IRON BASES

Class 40 cast iron (40,000 psi tensile strength) is the traditional material and still viewed by many original equipment manufacturers (OEMs) as the best material for a machine tool base. Castings have a good stiffness-to-weight ratio and good damping qualities. The material is inexpensive and easy to mold in required shapes to include coolant ways and runoffs, hydraulic and electrical conduit holes, and honeycombing to further improve weight/stiffness ratio.

Some problems with castings are that they require a pattern and that they must be stress-relieved; both of which can be very expensive for larger forms. High-production grinders produced in volume, and/or designed to a common base, can absorb these costs. Custom or one-off grinder manufacturers are usually forced to use less expensive alternatives.

### 15.1.3 REUSE OF CAST BASES

The desire for stable cast-iron bases has led to a whole industry of machine tool builders who are referred to as “remanufacturers.” These builders take an old machine tool, strip it down to the cast-iron base that has become extremely stable over its lifetime, and essentially reassemble the grinder using all the latest components of current grinding technology. This should not be confused with “retrofits” of electrical, hydraulic, or lubrication updates to a machine, or a “rebuild,” which is the reworking of particular parts of a grinder to bring it up, at best, to the original OEM specification.

### 15.1.4 WELDED BASES

Where cast iron is impracticable from a cost point of view several alternatives are used normally based around welded steel. This material has a higher modulus and strength than cast iron so machine tool builders will weld steel sections together with ribbing to provide additional stiffness. Weld joints add some vibration damping and each additional rib weld will also add mass where required. Nevertheless simple steel weldments have considerably less damping

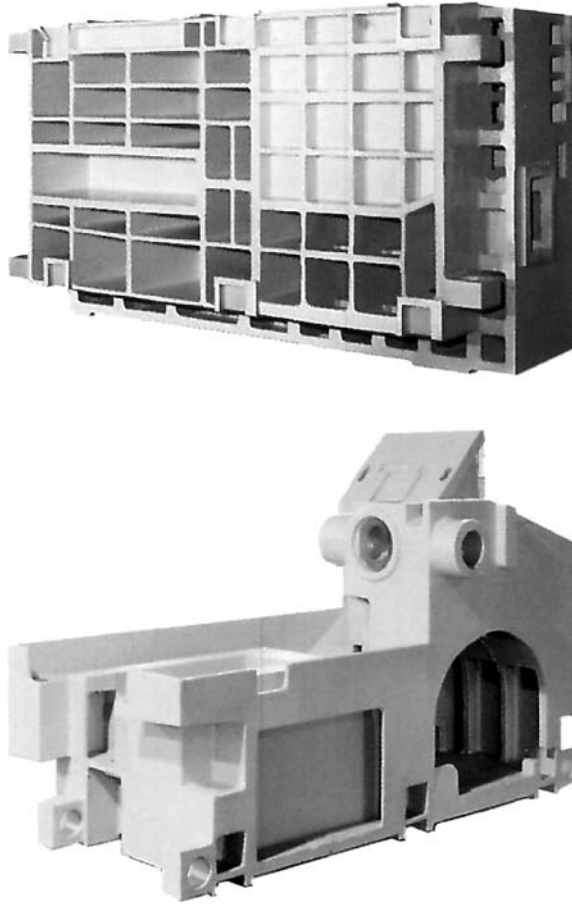


**FIGURE 15.1** Goldcrown centerless grinder base casting: side and underside views. (Courtesy of Landis, Waynesboro, PA. With permission.)

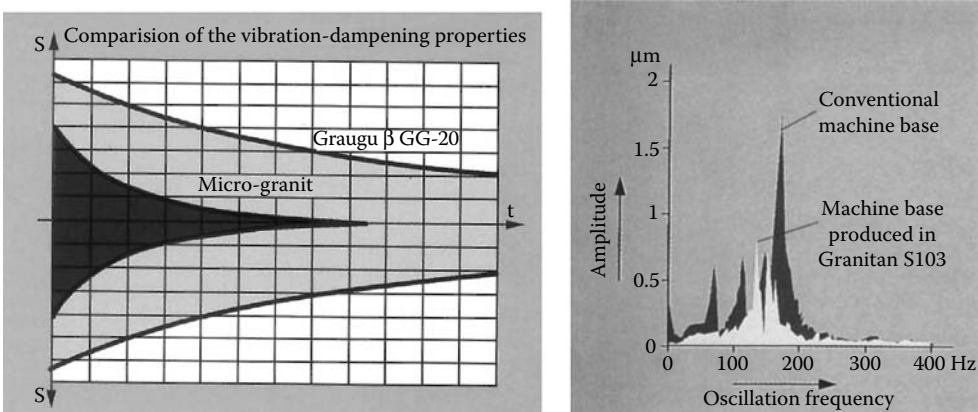


**FIGURE 15.2** Damping improvements of polymer matrices relative to cast iron. (From Elb 1997, Studer n.d. With permission.)

ability than cast iron. This can be improved slightly by pumping coolant through ducting, which also aids thermal stability.

### **15.1.5 DAMPING IN MACHINE TOOLS**

Most machine tools are lightly damped [Tobias 1965]. Typically, the damping ratio is approximately 0.05 to 0.15. Damping in a machine tool derives mainly from sliding joints and bearings. Significant damping also arises from screwed and bolted joints. The reason that damping arises from joints is because dissipation of vibration energy requires irreversible strains to take place on a continual basis. Irreversible strains or friction, as it is more commonly known, occurs through plastic and viscous shear mechanisms and not through elastic deflections from which the vibration energy is recovered. Frictional dissipation occurs mainly in joints and only in a minor way by deflections within the body of a casting. It is for this reason that the main structural elements provide only a minor contribution to the total damping of a machine. In order to introduce damping into a structure, it is necessary to engineer the distribution of mass, structural stiffness, friction, and movement within the design.

### **15.1.6 LARGE MASS BASES**

One approach to design of a machine base is to make it truly massive. An example is the use of a solid granite base described later in this chapter. This makes the machine base very rigid and minimizes distortion of the base when subjected to a rocking motion. Most machines exhibit rocking behavior in the frequency range 20 to 35 Hz as described by Tobias [1965]. The rocking motion has to be minimized by careful attention to the foundation and mounting on the foundation. From a vibration viewpoint, a massive base reduces the rocking frequency to a low value. This has the advantage that it tends to isolate the rocking vibration from the higher frequency modes of the machine. A massive and rigid base, therefore, inhibits vibration of the whole machine assembly rather than contributing toward it.

### **15.1.7 TUNED MASS DAMPERS**

A particular vibration can be substantially reduced by addition of a spring-mounted mass tuned to have the same resonant frequency as the unwanted vibration. The additional mass required can be less than one fifth the size of the mass requiring to be damped [Den Hartog 1956]. For example, if the rocking frequency of the base is of particular concern, a mass suspended on springs within the base and tuned to the appropriate frequency will greatly reduce the amplitude of vibration for a relatively low cost. This principle was employed in a 508-m-high tower in Taipei to eliminate sway of the building. A large steel ball weighing approximately 600 tonnes was suspended internally at the top of the tower. It has also been used very successfully for damping of long wheel spindles for grinding of landing gear, and for eliminating resonances when plunge roll dressing of wide vitrified cubic boron nitride (CBN) wheels.

### **15.1.8 COMPOSITE MATERIAL BASES**

Builders have sought alternative means of providing improved damping. One method is the use of a polymer matrix composite made using crushed concrete, granite, or quartz with trade names such as Granitan S103 [Studer n.d.], Mineralit [Emag 1998], and Micro-Granite [Elb 1997]. The materials have significantly greater damping characteristics than steel or even cast iron. They can be cast into almost any shape, do not require aging or annealing, are one third the density of cast iron, and can support rails and slideways if inserts are used to anchor them. They are used either as fillers in weldment structures or as monolithic bases [Drake 2000]. In the latter case, foam cores may be added to improve the weight/strength ratio. With appropriate design, a monolithic polymer structure,

**TABLE 15.1**  
**Properties of Polymer Concrete Compared with Cast Iron**

Material Property	ITW Philadelphia's Polymer Concrete Compared with Class 40 Cast Iron	
	ITW Concrete	Class 40 Cast Iron
Compressive Strength (PSI)	20,000	130,000
Tensile Strength (PSI)	2,000	40,000
Compressive Modulus (PSI)	4.2E6	15.0E6
Coefficient of Thermal Expansion (IN/INF)	6.8E-6	6.7E-6
Thermal Conductivity (BTU/FT-HR-F)	91.2	1,300

particularly for a low load-bearing application, can have the same stiffness as cast iron but much greater damping. Perhaps the optimum use of polymers, however, is as used in the Viking centerless grinder [Viking 1998] where epoxy-granite is used as a filler material in a nodular cast-iron base, thus gaining the best of both worlds.

It should be noted when designing machine bases that polymer matrices are not as strong as cast iron and have a much lower thermal conductivity. Arnone [1997] provides the following data for one particular grade of polymer concrete (Table 15.1).

An example of a company that has made significant effort to improve on a standard weldment is Weldon Solutions (York, PA) [Weldon 1991, 1994, 1998]. This machine tool builder makes both standard cylindrical grinders and custom machines with unique base shapes. In earlier efforts to improve damping, they used expansive concrete as filler in a welded steel base. This proved quite effective but added significantly to the weight of the base. More critically the thermal expansion mismatch could cause structural bowing. Weldon, therefore, worked jointly with Dr. A. Slocum of Massachusetts Institute of Technology to develop a more thermally stable system based on internal viscous damping [Hallum 1994, Weldon 1994]. The "Shear Damper" base consists of a series of stiff steel tubes wrapped with a highly viscous polymer tape. The tubes are suspended within the base weldment leaving a 3 to 5 mm gap with the walls. This gap is injected with an epoxy material constraining the viscous layer such that its only movement is in shear that dissipates vibration energy.

The beauty of this method is that it decouples the damping and stiffness functions of the structure and is broad frequency-based unlike, for example, a tuned mass damper. The internal tubes can also act as conduits for coolant or other fluids to control the base temperature (Figure 15.3 and Figure 15.4).

### 15.1.9 GRANITE BASES

For grinders where thermal stability is absolutely critical, an alternative approach is to use solid granite as used for inspection tables. Tschudin [n.d.] reports using Granitline, a natural quarried granite, for the bases of high-precision centerless grinders. Buderus [1998] also reports using a natural granite bed for its combination grinding/hard-turning centers that has both higher static stiffness and better damping characteristics than a typical cast-iron base. The use of solid granite illustrates the application of the massive base principle discussed above.

## 15.2 FOUNDATIONS

Floor construction is a critical consideration when installing a new grinder. It must first and foremost be capable of supporting the weight without deforming. It should also absorb shock and isolate the machine from adjacent machine noise. The principles of vibration isolation of machines are described in detail by Den Hartog [1956]. For light machines, a sealed concrete floor 150 mm to

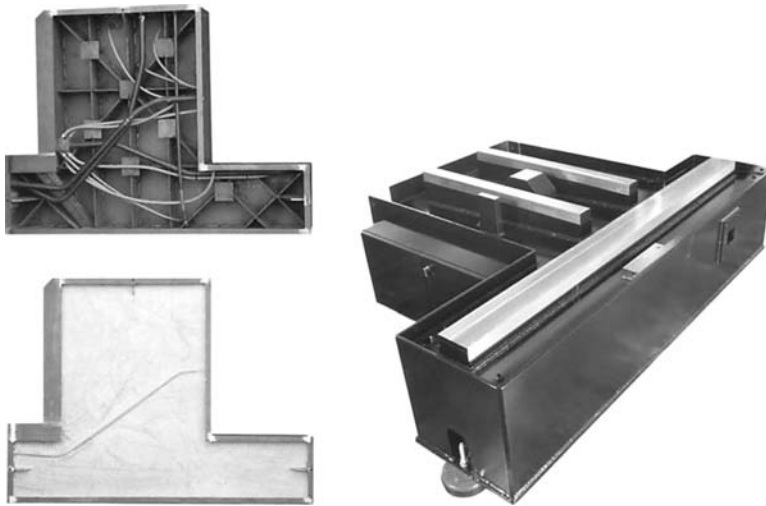


**FIGURE 15.3** Construction steps in a polymer concrete-filled steel base weldment. (Courtesy of Weldon Solutions. With permission.)

200 mm thick is usually sufficient in combination with elastic pads on the machine. Larger grinders will require an independent thick cast slab that may have to be isolated from the factory floor by shock-isolation elements. Because these slabs are made of concrete, which are slow to react to changes in temperature and, therefore, liable to warping, good temperature control of the factory is recommended. Many grinder bases, such as the one in Figure 15.3, are designed with 3-point floor support that allows, assuming the base has sufficient stiffness, for leveling of the grinder on uneven floors. However, with care of installation, a 5-point mount is actually more desirable in eliminating vibration modes especially from rocking or reversal of machine axes on machines such as reciprocating surface grinders [Yoshida 2000].

A machine table that reciprocates creates substantial inertia forces during the reversal of motion. A reciprocating surface grinder, unless anchored to the foundation, tends to “walk” across the floor.

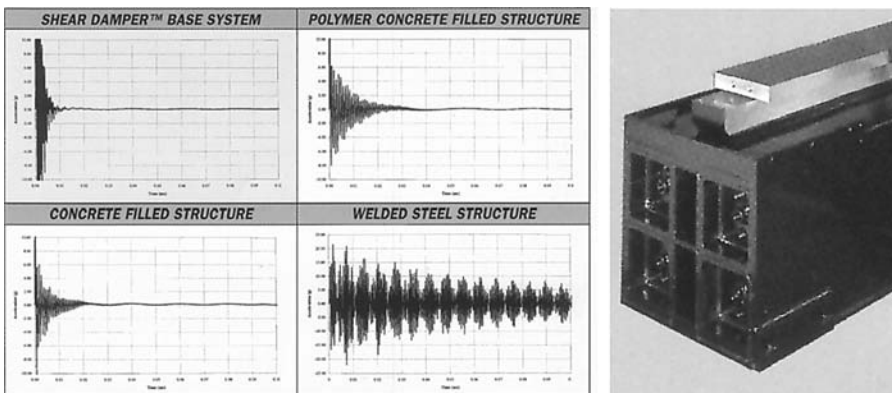


**FIGURE 15.4** Frequency response of various Weldon machine base constructions. (From Weldon 1994. With permission.)



This can be avoided by using anchor bolts sunk into the foundation. Provision must be included for leveling the machine on the foundations and also for vibration damping.

## 15.3 GUIDEWAYS

### 15.3.1 INTRODUCTION

Guideways are the elements or surfaces that carry and guide the moving elements such as work-piece holder/drives and wheel and dresser heads. Guideways can be divided into two categories—sliding and rolling element. Guideways of either type are often known simply as slideways. Their selection is dependent on many factors such as speed, acceleration, range of motion, accuracy and repeatability, stiffness, damping characteristics, thermal stability, weight, load capacity, slip-stick characteristics, ease of manufacturing, and cost including support equipment such as hydraulic pumps, chillers, filters, etc. In many cases, the choice is also dependent on which machine axis is involved and it is, therefore, opportune at this point to define the primary machine axes as defined by International Machine Tool Standards [Smith 1993], and some examples for the more common grinder types.

### 15.3.2 DEFINITION OF AXES

- X-axis—The horizontal axis of motion parallel to the work-holding surface
- Y-axis—The axis of motion perpendicular to both the X- and Z-axes
- Z-axis—The axis of motion parallel to the principal spindle of the machine
- A-axis—The axis of rotary motion of a machine tool member about the X-axis
- B-axis—The axis of rotary motion of a machine tool about the Y-axis
- C-axis—The axis of rotary motion of a machine tool about the Z-axis

Additional linear axes follow sequentially backward through the alphabet; for example, dressing axes tend to be U and V, while rotary axes follow sequentially forward through the alphabet. Axes carrying in-line probes are also given letters generally out of sequence. After the three principal axes, labeling varies from one machine tool builder to another.

Misalignments in a system lead to the following types of error in slide motion (Figure 15.5).

## 15.4 SLIDEWAY CONFIGURATIONS

### 15.4.1 INTRODUCTION

Slideways traditionally refer to a range of linear sliding contact guideways based on square, T, or flat and V cross sections. In recent decades, the advent of NC and CNC machines has led to rolling element slideways for ease of positional control.

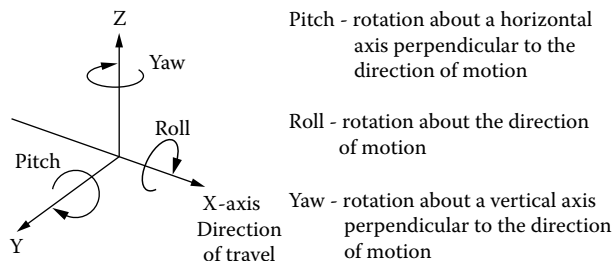


**FIGURE 15.5** Axis error definitions in machine tool technology.

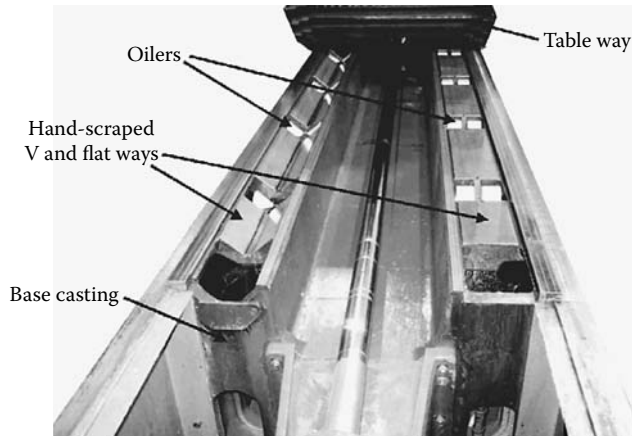


**FIGURE 15.6** Flat and Vee slideway on a Favretto slideway grinder.

### 15.4.2 THE FLAT AND VEE WAY

The simplest load-bearing arrangement is the “Flat and Vee” slideway. This uses gravity to preload the bearing configuration. It is considered by many machine tool builders as the optimum configuration for horizontal axes on large grinders under heavy, but even, downward loading. The path accuracy can be  $<1 \mu\text{m}$  and wear of the slide is self-compensating [Waldrich Siegen 1996]. Under uneven or changing load, it is prone to yaw errors. It is most commonly seen still on large surface grinders, for example, bed grinding or on cylindrical roll grinders that handle workpieces up to 10 tons or more. Figure 15.6 shows a photograph of the Flat and Vee way on a Favretto slideway grinder. The bearing surfaces are hand-scraped for good bearing contact and oil retention. The upper and lower surfaces are kept lubricated by oilers that consist of a series of rollers semisubmerged in small oil reservoirs. The method is simple and eliminates the need for hydraulic pumps and plumbing. Alternatively, oil is supplied under pressure from an external pump and fed through oil lubrication channels.

### 15.4.3 THE DOUBLE VEE SLIDEWAY

A variation on the Flat and Vee is the Double Vee slideway. This again depends on gravity for its preload and is self-compensating for wear. However, it can handle changes in the load position with much less yaw error. The major difficulty with this slideway design is in the manufacture, especially over any significant length. For this reason, it is most often used on short stroke axes such as the Z-axis on small manual and NC surface grinders, for example [Acer n.d.], or as the example in Figure 15.7 [Kent n.d.].

### 15.4.4 DOVETAIL SLIDEWAY

Other designs of slideway cross sections do not have the luxury of using gravity for preload and have to incorporate some form of constraint or box. The standard Tee-shaped slideway is shown in Figure 15.8 [Slocum 1992].

Preloading must now be achieved by gibs that are held in place by torqued setscrews. This leads to problems with backlash over time as the gibs wear. This particular design is more common in machining centers and mills where it can provide excellent damping at relatively low cost.

Plain constrained slideways offer probably the greatest stiffness and damping of any guideway system. It is perhaps not surprising that the Viking centerless grinder (Landis, Waynesboro, PA), which was designed specifically around maximizing its stiffness at 3 Mlbf/in., uses dovetail plain slideways.

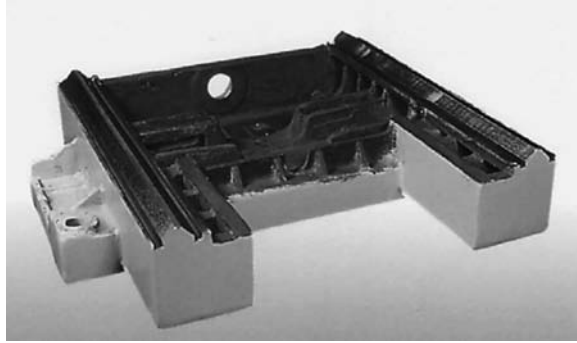


FIGURE 15.7 Example of Double Vee slideway. (From Kent n.d. With permission.)

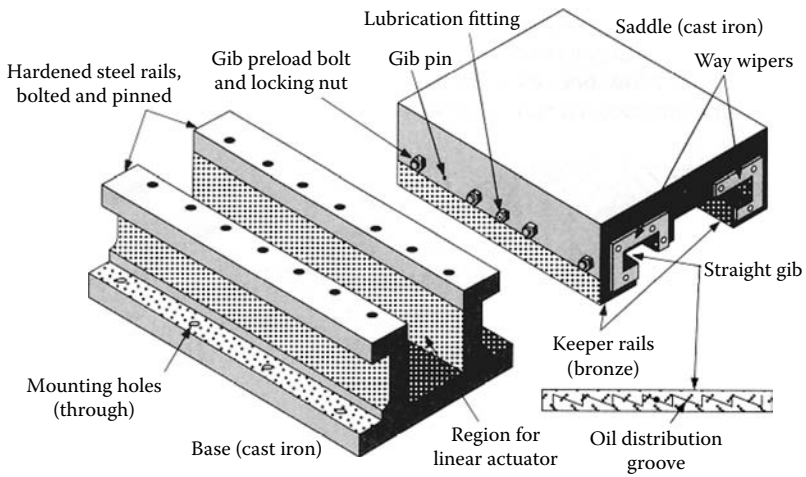


FIGURE 15.8 Example of Dovetail slideway. (From Slocum 1992. With permission.)

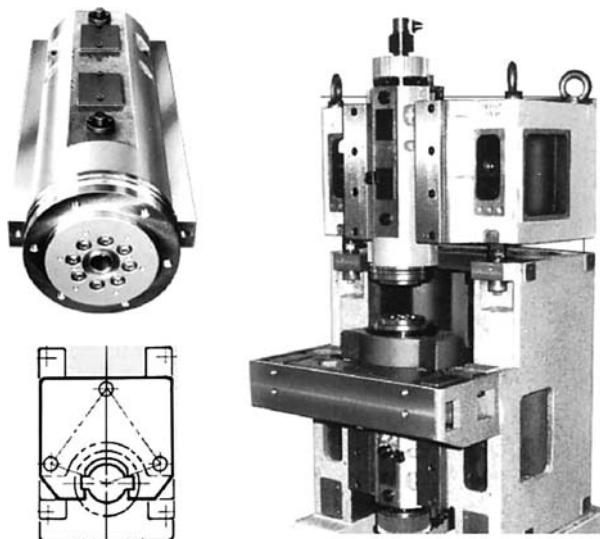
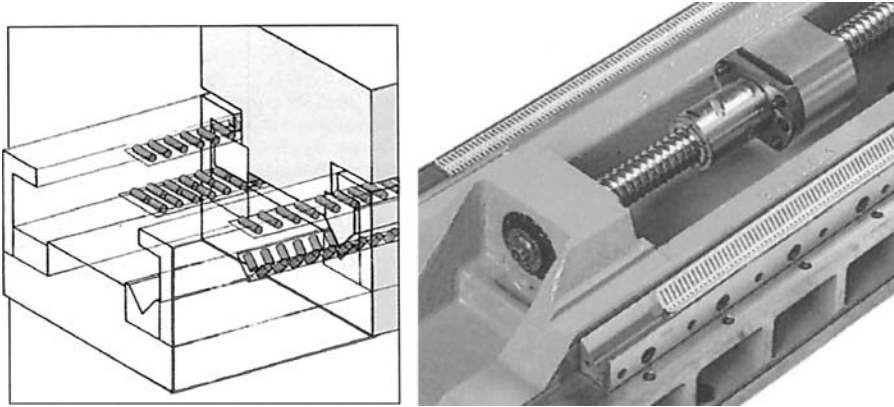


FIGURE 15.9 Koyo machine KVD series vertical spindle surface grinder.



**FIGURE 15.10** Example of Rolling Element slideway. (From Fortuna 1991. With permission.)

Koyo Machine makes use of a square slide version in order to obtain very high stiffness within a confined space for a slide to hold an upper vertical spindle for its superabrasive double-disc grinder [Koyo n.d.] (Figure 15.9). The sliding surface is hardened chrome while the slideway is coated with Turcite (see later).

#### 15.4.5 PLAIN SLIDEWAY MATERIALS

Slideways are traditionally made of cast-iron sliding on cast iron making use of the graphite present as lubricant or on porous brass, especially where gibs are applied. The brass is designed to wear preferentially while providing good lubrication.

The major limitation of these combinations is static friction or stick-slip that can create drive problems with servo errors. One way to reduce this is to use PTFE-based coatings with bronze fillers such as Turcite and Roulon. These have been used extensively, for example, by Koyo [n.d.], Kent [n.d.], Chevalier [2000], and Studer [n.d.]. Under load, the material has a static friction coefficient within 20% of its dynamic friction coefficient of 0.015 [Slocum 1992] (Figure 15.10 and Figure 15.11).

Alternative approaches include hydrostatic slideways and rolling element slideways; and the use of simple ball-bearing, or preloaded, nonrecirculating needle rollers as used by, for example, Fortuna [n.d.] in camlobe grinders in the 1980s and by Mitsui NC thread grinders at about the same time [THK n.d.]. These guideway systems may have less stiffness and damping than plain slideways while still having nonzero stick-slip but they are extremely compact. Rolling element slideways are discussed in more detail later after the discussion of hydrostatic slideways.

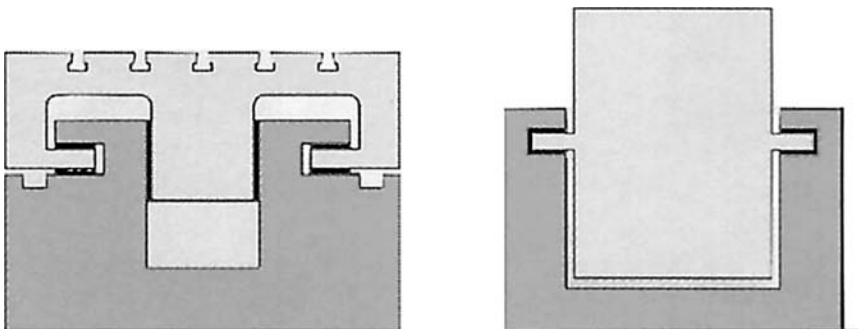


**FIGURE 15.11** Magerle MFP surface profile grinder X-axis (horizontal) and Y-axis (vertical) hydrostatic bearing slideway. (From Magerle n.d. With permission.)

## 15.5 HYDROSTATIC SLIDEWAYS

In high precision, high-production grinders, rolling element slideways tend to have been replaced by advances in hydrostatic bearing design unless there are severe space restrictions.

### 15.5.1 HYDROSTATIC BEARING PRINCIPLE

A hydrostatic bearing is noncontact in that the slide is supported by a film of high pressure oil of the order of 10  $\mu\text{m}$  thick. Stick-slip is therefore eliminated. It functions by producing a continuous flow of high pressure oil through and out of the bearing, the flowrate being controlled by restrictors such as small orifices or capillaries. The control restrictors are necessary to allow the slideway to cope with varying applied loads and maintain a near-constant film thickness. Throughout the bearing surface, small pockets or pads are machined to create areas of high pressure fed by these restrictors and from which the oil flows to the rest of the bearing surfaces before exiting the bearing. The oil is then collected, filtered, repressurized, and recirculated. Information on the operating principles and design of hydrostatic slideways is given by Rowe [1983].

### 15.5.2 PLANE-PAD HYDROSTATIC SLIDEWAY CONFIGURATIONS

As shown in the examples below, opposed-pad hydrostatic ways are used extensively in high-production grinders both in Flat and Vee type configurations, constrained Flat and Vee configurations to handle side force, and square and T constrained ways for vertical and high load normal applications (Figure 15.12–15.14).

### 15.5.3 PLANE-PAD HYDROSTATIC FLOWRATE

For a hydrostatic bearing, the pad pressure is related to the flowrate by [Rowe 1983]

$$q = Ph^3B/\eta$$

where  $q$  = flowrate,  $h$  = film thickness,  $\eta$  = film viscosity, and  $B$  = flow factor (constant).

Due to the cube relationship between flowrate and film thickness, slideway performance is very sensitive to the accuracy of manufacture. Also, the viscosity depends on oil temperature and, hence, flowrate depends on temperature. Chillers are required and oil must be filtered to  $<3 \mu\text{m}$ .

### 15.5.4 HYDROSTATIC SLIDEWAY MATERIALS AND MANUFACTURE

Generating the necessary tolerance on any slideway system can be expensive and time consuming. The ways are either cast into the base and ground and/or are scraped, or the base is ground and ways bought “off-the-shelf” are bolted on. Grinding a base requires a significant investment in capital equipment

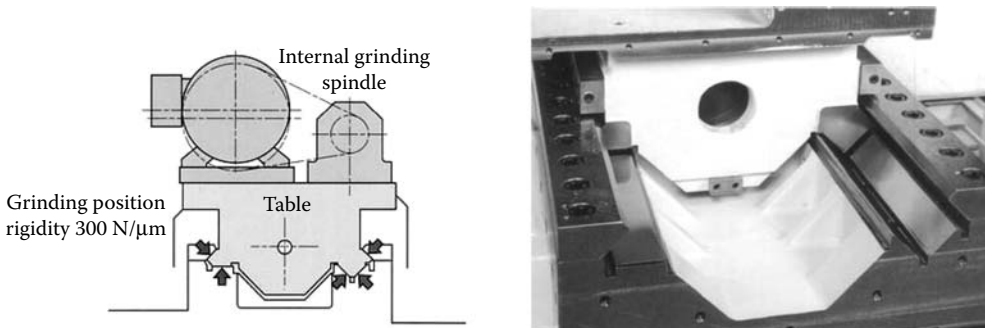


**FIGURE 15.12** Five-way restrained Z-axis hydrostatic slide on an Okuma GI 10 internal grinder. (From Okuma 2000. With permission.)

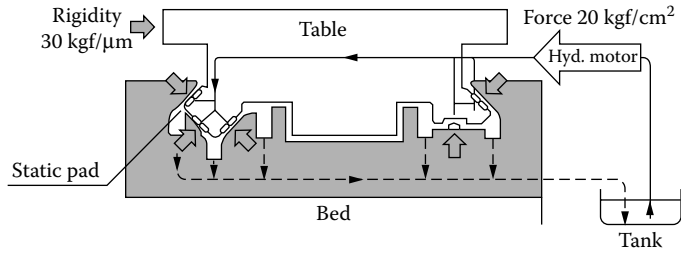


**FIGURE 15.13** Five-way restrained X-axis hydrostatic slide on an Okuma GC-super33 high-speed cam grinder. (From Okuma 1998. With permission.)

for a slideway grinder while scraping is particularly skilled and labor intensive and may still be necessary for preparing the base. Low friction coatings are added in many cases to the surface as insurance in case of a loss of hydrostatic pressure. The ways can still act as plain bearings to avoid damage.

Alloys such as Moglice have been developed that are low friction castable materials that require only a master to produce a finished surface. An example of its use is on the X- and Z-axes of the Bryant UL2 grinders [Bryant 1995] using roundway hydrostatic designs (Figure 15.15).

**15.5.5 ROUND HYDROSTATIC SLIDEWAYS**

Round hydrostatic slideway designs have been available since the 1960s, but it was the use of replication methods to control film thickness that resulted in slides that could move accurately and smoothly at up to 46 m/min (1,800 in/min). Danobat [1991] has also used round hydrostatic bearings in the Z-axis internal grinding slideway of its 585 Universal grinder.

**15.5.6 DIAPHRAGM-CONTROLLED HYDROSTATIC SLIDEWAYS**

A simple double diaphragm valve design was developed by Rowe [1969, 1970] for hydrostatic slideways and for hydrostatic journal bearings. Designs of this type have been successfully implemented in various machine tools and give very high bearing stiffness.

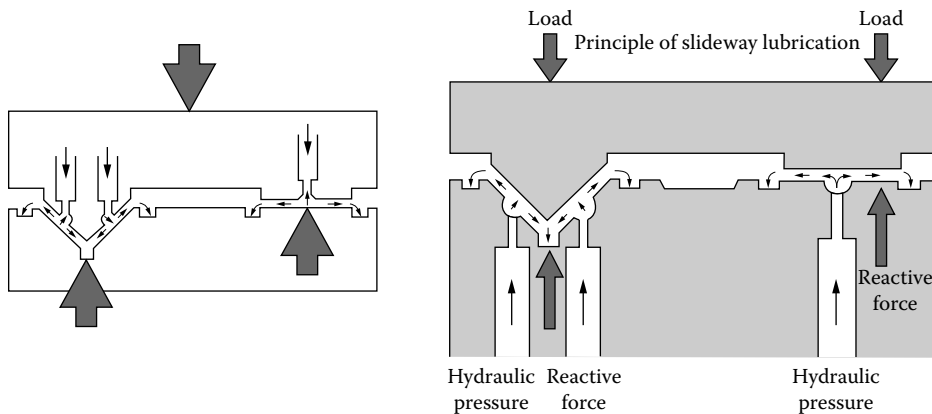


**FIGURE 15.14** Cylindrical grinder examples of hydrostatic Flat and Vee ways. (From Shigiya 2 n.d., Toyoda 1994. With permission.)

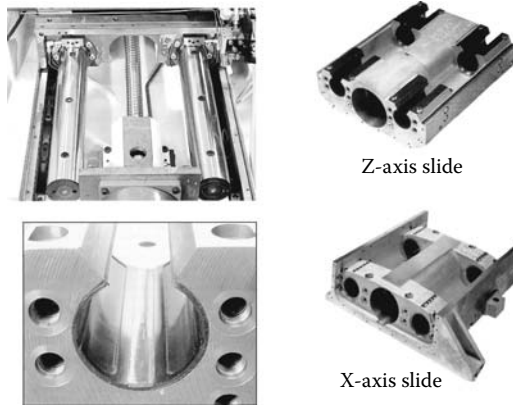


**FIGURE 15.15** Bryant UL2 hydrostatic round slideway designs.

The pressures at the individual pads can nowadays be controlled using ultrasensitive pressure membrane monitors and computer algorithms that regulate and optimize the flow and pressures. The method increases the stiffness and also reduces the oil demand of the system: this, in turn, reduces heat generation. The approach has been reported to be common on cylindrical, gear, and crankshaft grinders in Europe [Anon. 1999].

### 15.5.7 SELF-COMPENSATING HYDROSTATIC SLIDEWAYS

In addition to the shear damping base design, Slocum [1992] and Weldon [Hallum 1994] developed a self-compensating hydrostatic bearing design for use on their Model 1632 cylindrical grinder (Figure 15.16).

A gear pump (1) provides vibration-free fluid delivery to the self-compensating pads (2). The fluid enters the pad through ports at the edge of each and flows to collector grooves at the center that act as a feedback source for the bearing pads (3). There are two travel paths for the fluid (4): one from the lower self-compensating pad to the upper bearing pad and a similar one from the upper self-compensating pad to the lower bearing pad. As a load is applied over a compensation pad, the pad restricts fluid to the opposing bearing pad and, hence, directs additional fluid to the bearing pad opposing the load. The beauty of this system is that it is insensitive to manufacturing errors in the bearing gap and insensitive to dirt because there are no small-diameter passages. Typical port size is 3 mm. It even permits the use of low-viscosity water-based coolants as the fluid medium.

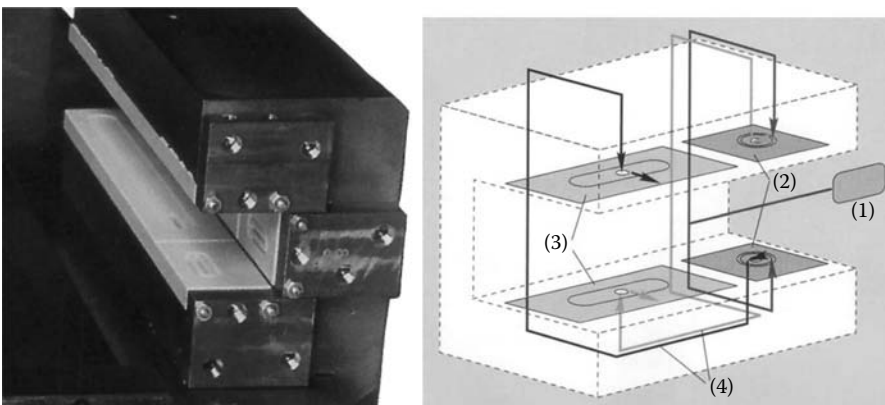


**FIGURE 15.16** Opposed pad hydrostatic slideway bearings. (Courtesy of Weldon Solutions. With permission.)

This type of slideway, supplied by New Way Machine Components Inc., has also been incorporated in machine design by Torrington's Advance Machinery Center [Sotiropoulos 1998].

## 15.6 RECIRCULATING ROLLING ELEMENT SLIDEWAYS

Slideways employing recirculating rolling elements were the salvation of the machining center manufacturers as a means of reducing manufacturing costs while increasing speed for high-precision circular interpolation with CNC controls. They also virtually eliminated stick-slip ( $\mu = 0.001$  to  $0.003$ ) and accompanying loss of motion, without the need for expensive hydrostatic way designs. They were light and allowed much faster acceleration and deceleration than plane sliding bearing ways with less energy and buildup of heat. Plane sliding bearings are limited to 20 to 25 m/min while rolling element bearing designs can run up to and over 120 m/min.

A grinder axis with rolling element slideways will usually consist of two guideways or rails and four bearing blocks to carry the spindle or work table. The rails come preground with straightness accuracy down to 1  $\mu\text{m}$  or less, which are bolted directly to the machine bed. Usually the machine bed is precision ground; however, mounting can be facilitated on occasion without scraping or grinding of the bed surface by using three-point laser aligning of the rails and then filling underneath with a rigid epoxy. The approach creates 100% contact for good damping and stiffness, although the process can be lengthy.

There are two types of rolling element – ball and roller. Regardless of type, the load is carried by two or more channels filled with bearing elements that circulate through them. Ball bearing slideways can be made more accurately, are slightly less expensive, and can handle faster velocities, accelerations, and decelerations rates than roller slideways. Rollers on the other hand have better damping and stiffness characteristics, and can handle twice the load for the same-sized bearing package. Rollers, however, are more sensitive to alignment errors, and with problems with skew caused by the end of the rollers getting pinched such that only the corners bear the load. For this reason, they are often crowned but this reduces the length of contact and, hence, level of damping.

Rolling element slideways are much more sensitive to crashes than plane slideways and provide less damping especially in the direction of motion where the damping is almost nonexistent. In some cases, additional plane-bearing elements may be added to compensate. Also, the bearings are preloaded by making the balls or rollers slightly larger than the channel, such that they distort increasing their contact area and, hence, damping capacity. The slideways are also very sensitive to contamination and must be kept clean of grinding debris or coolant. This mandates using wiper seals on the sliding trucks and slideway covers.

Truck spacing along the length of a rail should be at least twice the width between the rails and never less than 1:1. For additional stiffness, four or more rails may be used as shown in Figure 15.17. This shows the Y-axis guideway for a 700 series Campbell vertical grinding center with four rails together with stacked two-rail X-axis slides. Note also the oil lubrication lines for each truck.

The three most common suppliers of rolling element slides appear to be Schneeberger, THK, and INA Bearings based on grinders made in or entering the U.S. market.

Schneeberger supplies roller-bearing slides with two sets of opposed, crowned rollers in flat raceways. The geometry of the forces is such that the resultant points far outside the rail for greater stiffness. INA uses three tracks of ball bearings with contact angles optimized to carry compressive and side loads. THK provides primarily recirculating ball-rolling elements because of their greater capacity to cope with system misalignments (Figure 15.18). In some cases, flexible plastic retainer rings keep the balls separated to reduce friction, increase damping, and aid lubrication by carrying the grease.

The selection of a particular type of slide is often dependent on the personal choice of the individual design engineer based more on delivery, price, and technical support. Roller bearings, with their higher load capacity and slightly greater resistance to shock, appear to dominate grinders



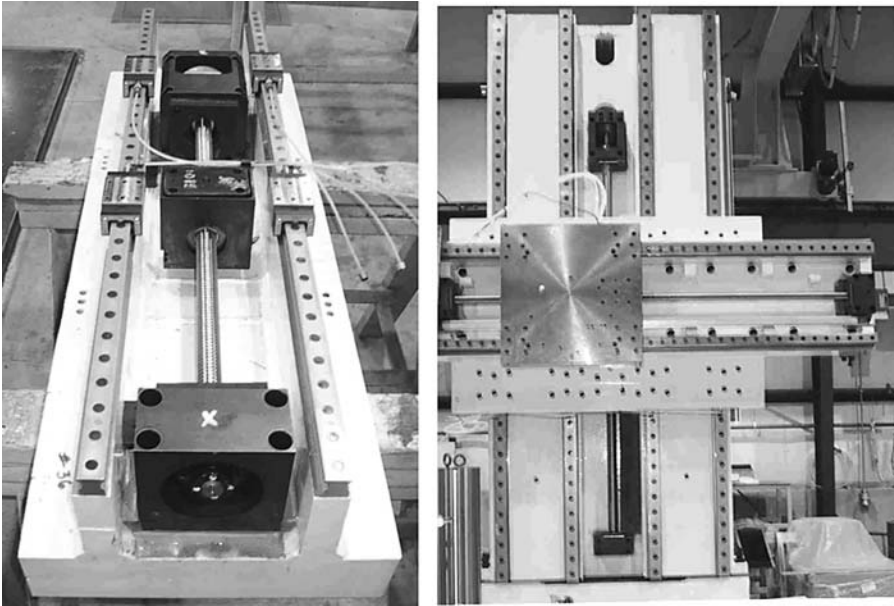


FIGURE 15.17 Campbell 700 series Vertical Grinding Center during construction.

for creep feed grinding, while ball bearings are used more for high speed on hybrid machining/grinding centers.

The slides must be kept well lubricated with a thick oil film to prevent fretting. Grease or slideway oil is used. The simplest greasing method is a manual grease gun as part of standard planned maintenance practice. However, automated grease injection or forced oil lubrication from a central pump is perhaps more reliable. Grease is typically used where there are a lot of short fast movements such as oscillation in internal grinding where an oil film could break down too quickly. Be it roller or ball, the slideways should be run over their full length every so often so ensure a good oil film is maintained. Under normal operations such a system should need lubrication only every 100 km of operation.

It is also recommended that the rails be flash-chromed due to coolant-contamination, even with the best of slideway covers, to prevent corrosion. This is a treatment provided by the rail manufacturer.

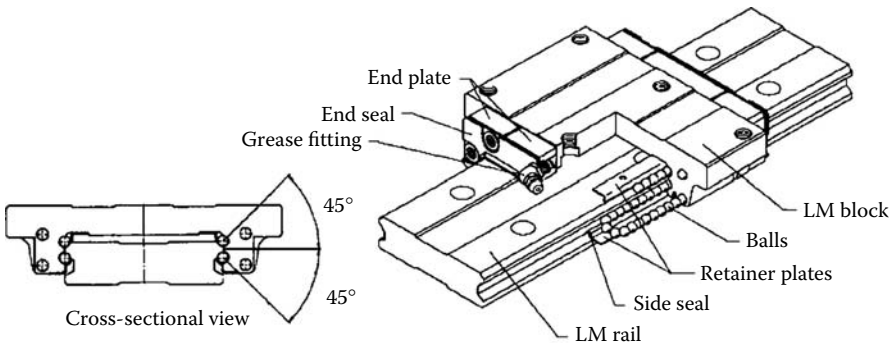


FIGURE 15.18 Recirculating ball rolling element slide system. (From THK n.d. With permission.)

## 15.7 LINEAR AXIS DRIVES AND MOTION CONTROL

### 15.7.1 INTRODUCTION

Motion control is the technology required to drive the carriages on the machine slideways and ensure that the motion is correct. Glancing through any used machinery brochure, it is easy to understand the changes that have occurred in the design of machine tools over the last 25 years. In no area is this more apparent than in linear axis motion control. Prior to about 1980, nearly all machine tools were hydraulically driven; today more than 80% of new machines are driven by servomotors with ballscrews. The driving factors for this have been cost, advances in motor, encoder, and machine control technologies, reduction in the number of mechanical machine components for easier maintenance, and the desire to eliminate hydraulics from machines for heat and vibration reasons.

### 15.7.2 HYDRAULIC DRIVES

A hydraulic drive consists of a cylinder with a piston and rod that slides in and out of it. The force produced is the product of the applied pressure on the piston and the area over which it acts. Manual or servovalves control velocity and position by controlling the flow of fluid in and out of the cylinder. The cylinder can be either single action, often used in opposed pairs, or double action. Hydraulic systems usually offer only medium accuracy and are now most often used in surface grinders with a large range of travel such as the slideway grinder example shown in Figure 15.6.

### 15.7.3 ELECTROHYDRAULIC DRIVES

For precision applications requiring only a short range of motion such as some of the dresser infeed examples illustrated in the previous chapter, electrohydraulic drives are used. These consist of a sealed system with two bellows; a small diameter, long-stroke master connected to a large diameter short-stroke slave. A motor-driven screw compresses the slave bellows and actuates motion of the master bellows. The resolution of the screw motion is increased by the ratio of the master/slave bellows diameter.

### 15.7.4 AC SERVO- AND BALLSCREW DRIVES

Ballscrew and ac servodrives are the basis of most of the current grinders on the market today and led to the elimination of hydraulics. They consist of several components, namely, the recirculating-ball leadscrew, or ballscrew, ballnut, motor, and positional/speed monitoring encoders as illustrated in Figure 15.19.

## 15.8 ELEMENTS OF AC SERVODRIVE BALLSCREW SYSTEMS

### 15.8.1 THE BALLSCREW

A ballscrew (or recirculating ball leadscrew) is at the heart of a controlled linear-motion system. It is a precision-ground hardened steel or stainless steel threaded shaft on which a ballnut rides with rolling contact to provide a positive, high efficiency of transmission and low friction. The ballscrew is manufactured by turning, heat treating, and then finish grinding the thread. In the process of finish grinding, the shaft will “unwind” developing a lead error both cyclic and accumulative. Some of this is compensated in the grinding process but nevertheless there is a residual error (Figure 15.9).

The class of ballscrew is governed by a combination of accumulated lead error and cyclic variation. For a nominal 1-m length, a C0 class would have <8- $\mu\text{m}$  accumulated error and <6- $\mu\text{m}$  variation,

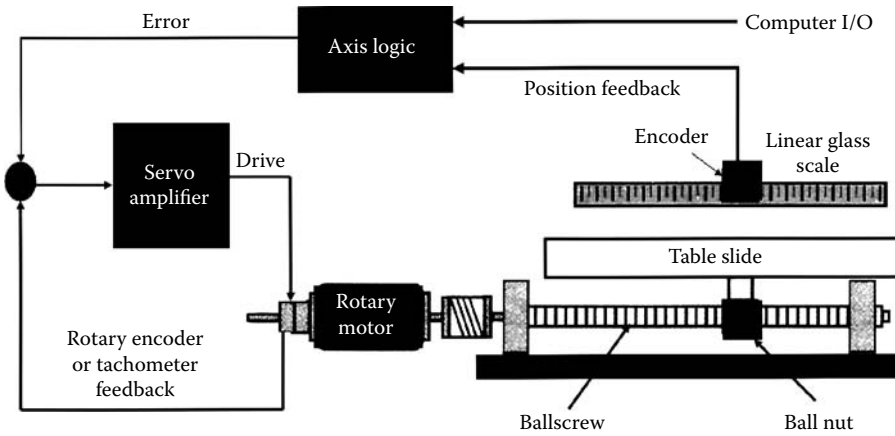


FIGURE 15.19 Typical closed-loop servodrive ballscrew system.

while a C3 class would have  $<21\text{-}\mu\text{m}$  accumulated error and  $<15\text{-}\mu\text{m}$  of variation. Accumulated error can be programmed into modern CNC controls as an offset to correct for the error.

Lower-quality ballscrews are made by rolling the form then heat treating. They are sometimes used on low-cost surface grinders, axes requiring noncritical accuracies, or for materials-handling and peripherals.

Mounting of the ballscrew is somewhat dependent on the speed of operation and personal preference. For grinders, the end coupled to the servomotor is always held fixed using a pair of angular contact bearings. The other end may also be fixed with a similar bearing arrangement or just supported with a plane bearing. Fixing the bearing at both ends provides the greatest stiffness and raises the critical speed at which vibration is induced and is used especially for higher speed requirements. A single fixed end allows for thermal expansion without distortion of the screw (Figure 15.20).

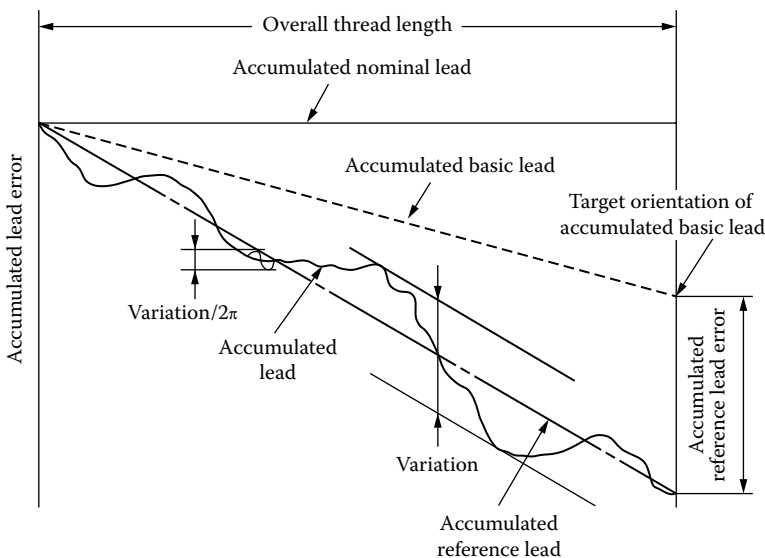


FIGURE 15.20 Ballscrew lead errors. (After THK 1995. With permission.)

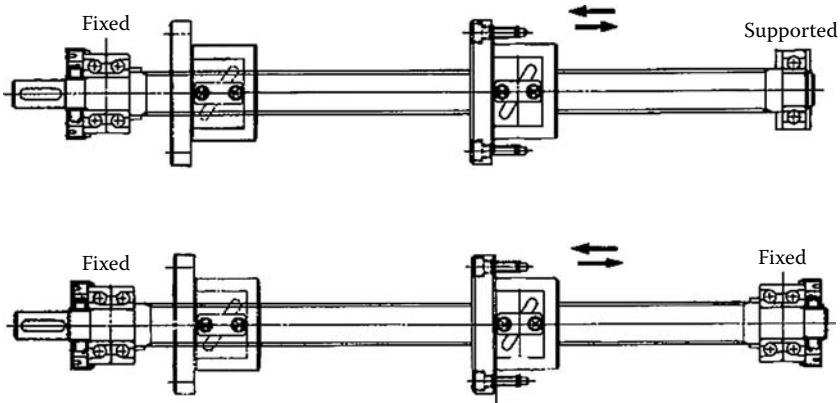


FIGURE 15.21 Ballscrew/nut assembly approaches.

However, heat is also expected to be a greater issue with higher speed. For this reason, screws fixed at both ends for higher speeds are often preloaded axially to allow for some expected thermal growth. Hollow screws are also available through which coolant can be pumped to control thermal expansion.

15.8.2 THE BALLNUT

A ballnut is the other mechanical part of the ballscrew system. Somewhat akin to linear ball-slide systems, ballnuts consist of a nut within which is a recirculating helical track for the bearing balls. There are a number of designs available with varying number of turns and internal or external recirculation of the balls, or with one or two starting points. The selection usually resolves around a compromise of friction, noise, damping, etc. As bearing balls are easily made with high precision, most accuracy problems usually lie in the shaft. Light preload is achieved by the use of slightly oversized balls. Medium to heavy preload, to eliminate backlash, is achieved by the use of two nuts with a spacer between them (Figure 15.22) [THK 1995].

The speed capability of a ballscrew system is related to its DN value, the ball diameter in mm  $\times$  speed in rpm. Values range up to 120,000, which covers the highest speed requirements of most classes of grinder. The current limits of ballscrews for motion accuracy suitable for grinders is

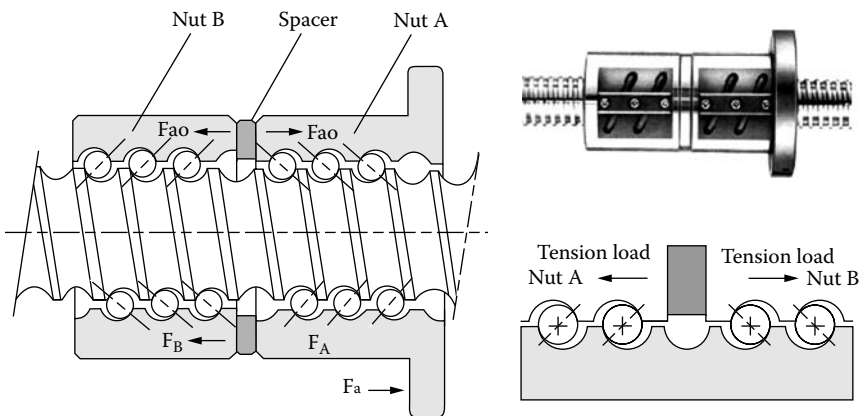
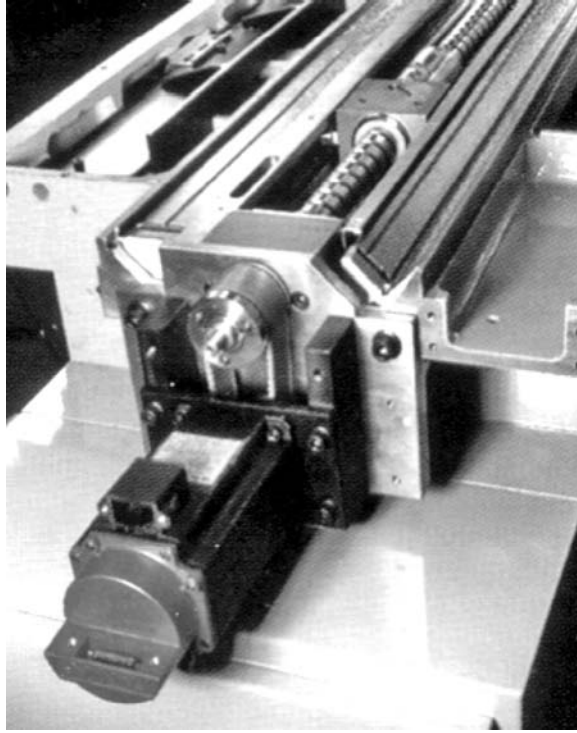


FIGURE 15.22 Preloaded ballnut assembly [THK 1995, with permission] requirement for synchrobel to keep motor below slide surface.



**FIGURE 15.23** An AC servodrive motor in a ballscrew drive system. (Note: the belt drive between the Servo motor/encoder and the ballscrew connection to gain additional table travel. Belts can be the cause of increased maintenance.)

about 40 m/min, although some hybrid machining/grinding centers can achieve 90 m/min and 1 *g* acceleration. Most standard grinders will use ballscrews with a pitch of about 5 to 10 mm and a diameter of at least 35 mm. Higher speed hybrid machining/grinding centers use pitches from 20 to 30 mm.

Special attention should be paid to the mount for the carrier plate to the ballnut and the supporting journal, as any misalignment, in particular, pitch errors, will reduce ballscrew life dramatically. Also, remember when switching from a plane slideway design to a truck and way design where there is a vertical component under gravity, that the full load is now being borne by the nut journal without aid from friction in the slide. The ballnut/ballscrew contact surface can represent >50% of the total friction of the motion resistance. In certain applications such as camlobe grinding where inertia, acceleration, and jerk are key factors to profile accuracy, OEMs such as Landis (Waynesboro, PA) developed a hydrostatic nut design in the early 1990s to reduce friction and eliminate backlash. Instead of metallic contact, the force is transmitted by an oil film between the male screw and the female formed nut. Backlash is reduced to <0.1  $\mu\text{m}$ . The performance of this system has only recently been superseded in some cases by the use of linear motors.

### 15.8.3 AC SERVOMOTORS

Ac servomotors are a class of induction motor modified for servo-operation. It is an asynchronous motor consisting of a stationary ac transformer (stator) and a rotating shorted secondary circuit (rotor) that carries an induced secondary current. The rotor consists of laminated iron cores with slots for conductors. Torque is produced by the interaction of the moving magnetic field and the induced current in the shorted conductors. In a simple induction motor, the speed at which the

magnetic field rotates is the synchronous speed of the motor and is determined by the number of poles in the stator and the frequency of the power supply. For servomotor operation, the stator is wound with two phases (or four) at right angles. The first winding has a fixed voltage supply while the second has an adjustable voltage controlled by a servoamplifier. The great attraction of the motor is its accurate and rapid response characteristics. The motors are available in fractional and integral horsepower sizes and are used in a closed-loop control system in which energy is the control variable. In order to monitor this, the controller must be able to constantly monitor velocity and position. This is achieved through the use of encoders.

#### 15.8.4 ENCODERS

Encoders monitor position and rotation and their derivatives, speed, acceleration, etc. The leading manufacturer is Heidenhain, on whose literature most of this discussion is based [Ernst 1998]. The simplest and most common encoders are rotary encoders mounted directly on the back of the servomotor to monitor the rotation position. The encoder functions on the Moiré principle. The system uses a glass scale or disc because of its transparency and low thermal expansion. The scale has a grating, produced by photolithography, of fine opaque chromium lines of thickness  $C/2$  and spacing  $C$ .

The grating is scanned using a reticule with four windows illuminated by collimated light source. Each window has similar grating lines parallel to the scale. The light passing through each window and the scale is measured by its own photodiode behind.

As the scale moves relative to the windows, a sinusoidal light intensity is produced that is converted to an electrical current. The signal from the four windows is each phase shifted  $90^\circ$ , signal (a) to signal (d) in Figure 15.24. Signal (e) is a reference. Signal (a) and signal (c), and signal (b) and signal (d) are then combined to produce the balanced amplitude signals S1 and S2, which are converted to square wave signal (h) and signal (i). Combination of signal (h) and signal (i) gives a final pulse with a resolution of one fourth of the grating spacing. Further resolution can be obtained via an interpolation circuit. The output is typically 1 V peak to peak.

Rotary encoders can have up to 5,000 radial lines giving 20,000 measuring points per revolution. For a ballscrew pitch of 10 mm this gives a resolution of  $0.5 \mu\text{m}$ . Better resolution can be obtained with interpolation. Rotary encoders function at signal frequencies of 160 kHz to 400 kHz. At 400 kHz with 5000 lines, the maximum table speed allowed corresponds to  $400,000/5000 = 80 \text{ rev/s}$  giving 48 m/min. This speed is acceptable for all normal grinding operations and even some speed stroke grinding applications. Gratings with up to 36,000 lines are available for purely angular positioning. Rotary encoders are also available that have several graduated disks linked by a mechanical transmission that allows them to resolve the number of spindle revolutions and, therefore, the absolute slide position. This negates the need for limit and reference switches but at some loss of resolution.

Rotary encoders are as good if not better at giving feedback on velocity as a tachometer but they are sometimes too remote from the point of grinding to accurately know the position of a slide where it matters. The machine may be too sensitive to thermal variations especially for the resolution required for some high precision applications or the use of CBN. For this reason glass, linear scales are placed next to the slides for positional reading with feedback direct to the programmable multiaxis controller (PMAC). In many cases, if the material for the scale carrier has the same expansion as the workpiece, the thermal effects of the scale and workpiece compensate each other. A standard linear encoder with a period of  $20 \mu\text{m}$  has accuracy of the order of  $3 \mu\text{m/m}$ . As such, this allows measuring steps of  $0.5$  to  $1 \mu\text{m}$ .

The units come "sealed" but nevertheless they should be carefully guarded from coolant and contamination. It is common to mount them under the same slideway guards used to protect the linear guides.

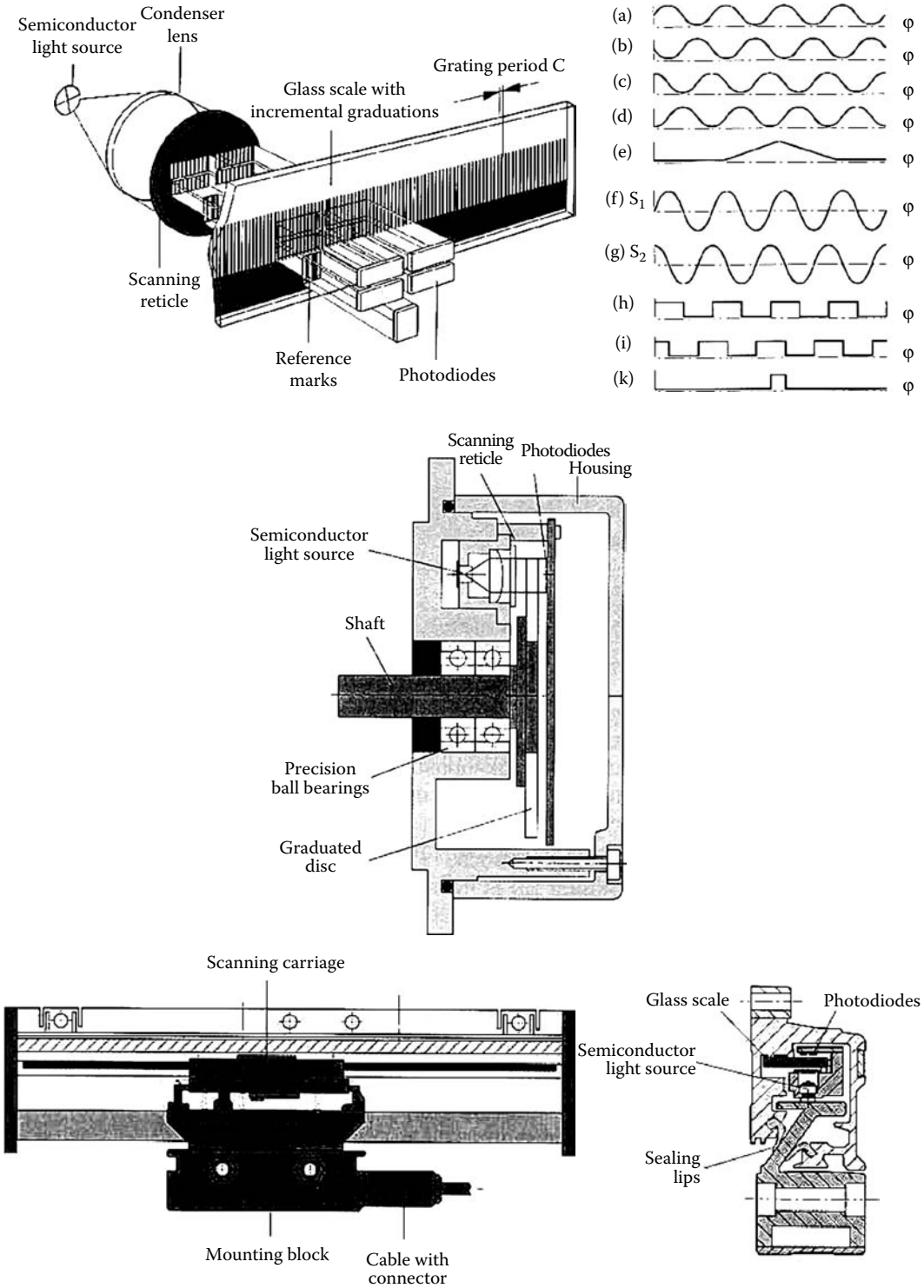


FIGURE 15.24 Examples and operation of linear and rotary encoders. (From Ernst 1998. With permission.)

### 15.8.5 RESOLVERS

Machines built prior to about 1990 may have a resolver, in place of an encoder, based on the inductive measuring principle or “Inductosyn.” In this case a scale and slider consist of two staggered or zigzag conductive strips. An alternating current is passed through the slider and the inductive current measured in the scale circuit. Resolvers of this type are much less accurate than modern encoders and more sensitive to temperature changes.

## 15.9 LINEAR MOTOR DRIVE SYSTEMS

### 15.9.1 INTRODUCTION

Linear motor systems started to make an impact on machine tools in the late 1990s for specialist applications such as CNC crank-pin grinding and camlobe grinding [Landis 1999]. More recently, several OEMs such as Danobat (Deba, Spain), have designed machines for speed-stroke grinding with speeds up to 250 m/min and acceleration/deceleration of 5 *g*. These are based on the superior speed, reduced friction, and inertia obtainable with linear motors.

Linear motors have many advantages. They consist of a single moving part eliminating the ballscrew with its inherent backlash, pitch errors, and compliance. That combined with low inertia and zero friction give a much faster response time and higher accelerator/decelerator rates. The reliability is far greater than a ballscrew while requiring much less maintenance. The system can also run either at low speeds for creep feed grinding or extremely high speeds for speed stroke grinding all with submicron accuracy. In conjunction with direct control through the PMAC via a suitable linear encoder, it is possible to control, position, velocity, and acceleration, which is key for cylindrical grinding of nonround parts.

Linear motors do have disadvantages. First and foremost is cost; the price of a linear motor is still significantly higher for a given power than servodrive systems. However, this is offset to some extent by a faster assembly time into the grinder. The motors generate a lot of heat, especially at high speed, which must be dissipated through internal cooling. The magnets are very high strength and will attract metal swarf unless well guarded or sealed. Linear slides are not commonly used on vertical axes because a counterbalance or brake must be supplied in the event of a power failure. In fact, even for horizontal axes, a capacitor or auxiliary power supply is normally provided to control the axes in the event of a power loss.

Linear motors, like most technologies, had initial teething problems. The slider winding is embedded in epoxy, which is prone to attack by water vapor and allows water to gradually eat its way into the winding and eventually short them. Where linear motors have been applied, the closest attention has been paid to slideway guarding. Many OEMs have tested their first linear motor-driven grinders in the laboratory for several years running prototype production under a range of conditions prior to offering linear motors commercially.

Until very recently, linear motors were still a niche drive for very specific machine movement requirements. If such drives are under consideration it is recommended that the potential buyer confirm with the machine tool builder that they have a successful track record of at least 2 to 3 years.

### 15.9.2 A LINEAR MOTOR SYSTEM

Figure 15.25 shows a typical closed-loop linear motor drive system. An ac linear induction servomotor is essentially a rotary motor that has been laid out flat (see Figure 15.26). It consists of a track containing rare earth (e.g., samarium/cobalt) high-density permanent magnetic strips embedded in epoxy and fixed to the machine base, and a slider assembly made up of a laminated steel structure with conductors wound in transverse slots. The slider is supported by a pair of linear bearings—ideally, hydrostatic



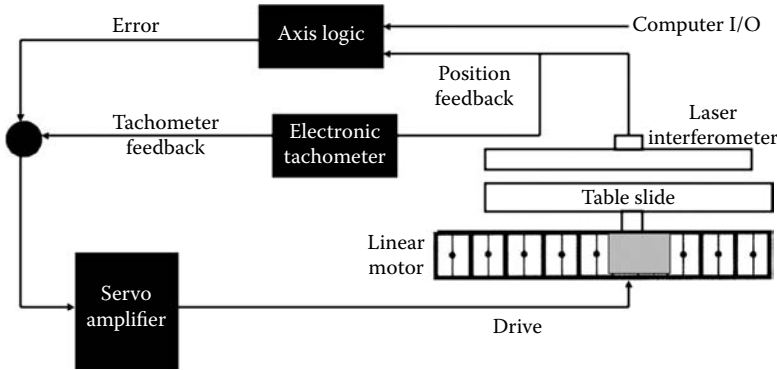


FIGURE 15.25 A closed-loop control system using linear motor drive.

bearings. Thrust is developed by the ac current in the motor conductors interacting with the permanent magnetic field.

### 15.9.3 LASER INTERFEROMETER ENCODERS FOR LINEAR MOTOR DRIVES

Linear motors demand fast positional monitoring response made possible by using linear encoders based on laser interferometry. The simplest form using a homodyne laser is illustrated in Figure 15.27. A laser beam, L, is split by a neutral beam splitter, N, into two beams. The measuring beam strikes the measuring reflector, MR, which is returned in a parallel path where it passes through a  $\lambda/4$  reticule, V, where a portion of the beam is delayed to create a circularly polarized wave. The reference beam is reflected by the reference reflector such that the two beams meet again at the neutral beam splitter and interfere. Further polarizing beam splitters, PT, put the interfering waves into quadrature measured by the four photodiodes, P, resulting in two electrical signals phase shifted by  $90^\circ$ . These signals are then converted into two square wave signals with eight crossover

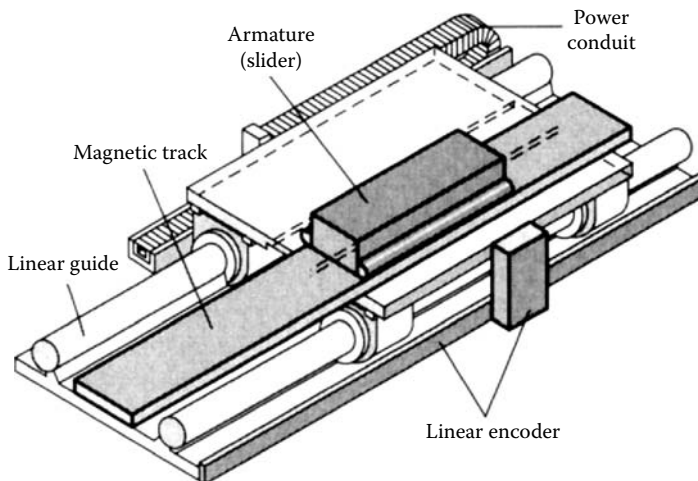


FIGURE 15.26 Elements of a linear motor drive system.

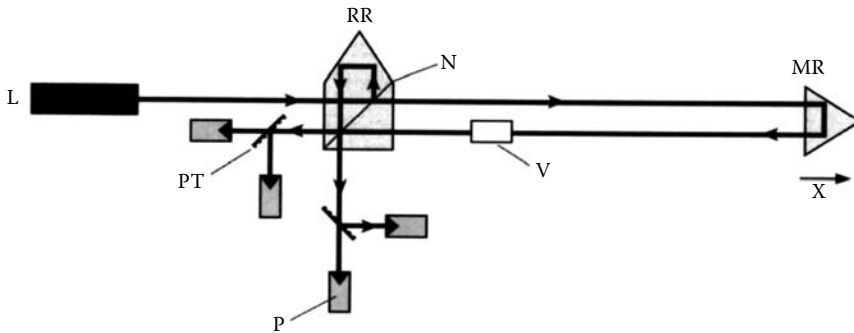


FIGURE 15.27 Principle of the laser interferometer. (From Ernst 1998. With permission.)

points per wavelength of light giving an accuracy of about  $0.08 \mu\text{m}$ . An interpolation circuit can increase sensitivity by a further order of magnitude.

Heterodyne laser systems are also available that use two almost identical wavelengths. Compensation is also possible for temperature, humidity, and air pressure. Fortunately, the clean conditions required for linear motor operation also make conditions unusually suitable for a grinder application and for laser interferometers.

## 15.10 SPINDLE MOTORS AND GRINDING WHEEL DRIVES

Spindle design and selection can be categorized by the type of wheel and operation into:

- Large wheel applications using conventional wheels
- Small wheel applications limited by burst speed and dynamic issues in grinding
- High-speed grinding
- Specialty applications

In many cases, one area overlaps with another, especially where a machine tool builder either standardizes components from one model to another or offers flexibility from upgrading the machine design to handle more than one of the previously mentioned categories.

## 15.11 DRIVE ARRANGEMENTS FOR LARGE CONVENTIONAL WHEELS

### 15.11.1 ROLLING ELEMENT SPINDLE BEARINGS FOR LARGE WHEELS

Rolling bearings have increased in accuracy and reliability over recent decades as closer control has been achieved of materials and manufacturing tolerances. This has allowed rolling bearings to replace hydrodynamic bearings as the choice for many larger-wheel machines to achieve relatively cool running. Rolling bearings have always been more common for smaller high-speed spindles. However, rolling bearings are still subject to wear and eventually need to be replaced. For machines involved in continuous production, it is important to have a program of planned maintenance and replacement in place.

If a machine tool with rolling bearings is to be moved or transported, it is absolutely essential to seek expert advice on care of the bearings. The bearings must be carefully supported and locked to prevent transmission of vibration through the bearings during transport or handling. Failure to heed

this warning will lead to brinelling (indentation of the bearing tracks) and possible complete destruction of the bearings. Subsequent grinding performance will show vibration marks on the workpieces and the bearings will fail after a short running period.

The commonest grinder in the field uses a conventional grinding wheel of 175 mm (7) diameter or larger limited to wheel surface speeds between 32 m/s (6,500 ft/min) and 42 m/s (8,500 ft/min). This leads to a wheel spindle speed requirement <4,600 rpm, a maximum spindle power requirement of about 3 KW/cm (10 hp/in.) of wheel width, and a maximum runout specification of 2  $\mu$ m (80  $\mu$  in.).

Most spindles consist of a cartridge design with the wheel arbor supported by a minimum of two pairs of ABEC 7 or 9 (ISO class 4 or 2) angular contact ball bearings with grease-packed lubrication. Forced-oil lubrication may be used for higher loads or speeds. The spindle is driven by either a simple dc brush or ac synchronous fixed speed motor or, for variable speed, a synchronous multipole induction motor. For reasons of space restraints, the spindle is usually coupled to the motor by a V-belt drive in a back-to-back configuration as shown in Figure 15.28. The design is well established and robust but is prone to problems of belt slippage and balance issues and requires regular maintenance.

For higher load and stiffness requirements such as centerless grinding, the number of angular contact bearings is increased, as in Figure 15.29 [Royal Master 1996]. In addition, when increasing the number of bearing pairs, some are replaced by roller bearing for increased radial stiffness while maintaining angular contact bearings for axial thrust stiffness as shown in the example from Micron [n.d.] (Figure 15.30).

Roller bearings provide better stiffness and damping than ball bearings. They are also less sensitive to temperature than other bearing systems to be discussed below. Another important factor, especially then buying imported machines, is that ball and roller bearings are readily available locally and easy to maintain and service.

Hollow roller bearings have proved of particular interest, certainly in the United States, to rebuilders of surface and centerless grinders. Sold under the trade name Holo-Rol [ZRB 1998], these are high-stiffness roller bearings where each roller is a tube. The hollow rollers act as shocker absorbers and reduce vibration without loss of stiffness. Bearings for use in, for example, the Cincinnati 220-8 centerless grinder each have a stiffness of 4.47 m lbf/in., four times that of a comparably sized ball bearing pair.

Where possible, belt drive designs have been replaced by direct drive motors in which the motor shaft is also the spindle shaft. This dramatically reduces vibration and maintenance issues

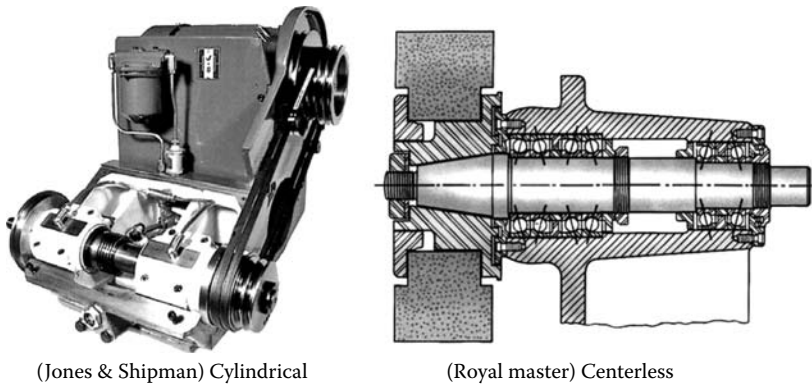


**FIGURE 15.28** Typical wheel spindle arrangement for large conventional wheels. Cylindrical [Jones & Shipman (with permission)]; Centerless [Royal Master (with permission)].

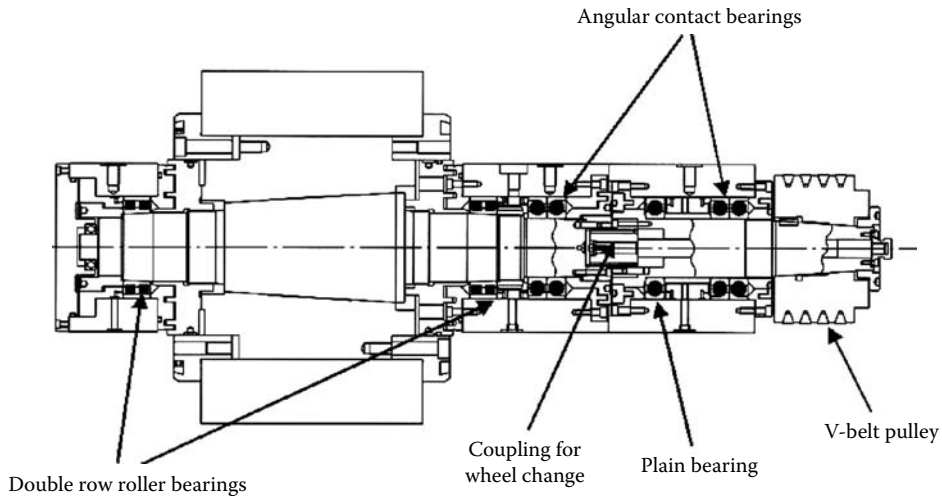


**FIGURE 15.29** Heavy-duty wheel-spindle arrangement with V-belt drive. (From Micron n.d. With permission.)

(Figure 15.30). However, it is an essential requirement that an integral motor is capable of running at the required speed range for the range of wheel sizes to be employed.

### 15.11.2 HYDRODYNAMIC SPINDLE BEARINGS FOR LARGE WHEELS

To improve damping characteristics, part finish, and wheel roundness, a number of Japanese machine tool builders, in particular, have revisited the use of hydrodynamic spindle bearings [Shigiya 2 n.d., Okuma n.d., Toyo n.d., Kondo 1998]. Hydrodynamic bearings were popular in older grinding machines due to their reliability, good accuracy, and long life. The long life of a properly designed hydrodynamic bearing is because the bearing is only subject to wear on start-up, before the oil film is established, and on stopping. However, hydrodynamic bearings create a significant quantity of heat leading to elevated machine temperatures. It is, therefore, important to allow

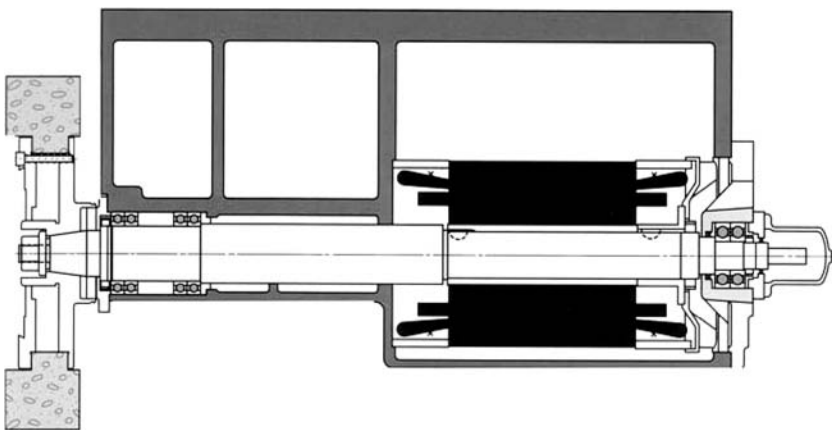


**FIGURE 15.30** Wheel spindle arrangement including an integral motor. (From Mattison n.d. With permission.)

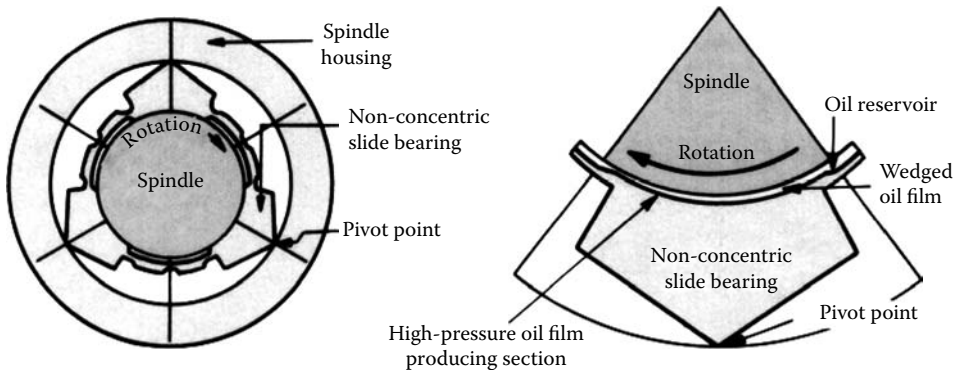


FIGURE 15.31 A multiwedge hydrodynamic bearing arrangement. (From Okuma n.d. With permission.)

machines with hydrodynamic bearings to warm up for a few hours to achieve close size tolerances in continuous production runs.

A modern hydrodynamic bearing is not a simple sleeve bearing but relies on the creation of a wedge by having two surfaces rotating relative to each other with different radii of curvature. Between the two surfaces is low-viscosity spindle oil. Adjacent to each surface, this fluid does not move relative to that particular surface. Consequently, a certain amount of fluid will be constantly dragged into the wedge. The amount entering will be greater than the amount permitted to leave because of the wedge shape resulting in a tendency to try and compress the fluid creating a pressure in the film between the surfaces. The pressure gradient that exists is such as to cause equal quantities to pass each point in the bearing [Dayton 1949]. The point of highest pressure may be up to four times the average pressure over the bearing.

The hydrodynamic bearing design as adopted for a grinding spindle is best described by Kondo [1998]. The bearing is made of hardened steel lined with babbitt metal and consists of three bearing surfaces and three elastic areas. The areas of elastic deformation provide adequate passage for the flow of fluid through the bearing with good temperature control. The clearance gap is 8 to 12  $\mu\text{m}$  and generates a wedge dynamic pressure of 80  $\text{kgf}/\text{cm}^2$ . Kondo claims a precision of 1  $\mu\text{m}$ .

The shape of the bearing surfaces is better illustrated by Okuma [n.d.] as shown in Figure 15.31. The hydrodynamic bearing illustrated is to provide radial support. There is also a wedge-shaped hydrodynamics thrust bearing near the wheel to minimize axial deflection.

This is perhaps more clearly illustrated in Figure 15.32, which is a bearing arrangement for a Toyo outer diameter grinder for bearing inner races. The runout claimed by machine tool builders for hydrodynamic spindle bearing designs range from  $<1 \mu\text{m}$  to  $0.2 \mu\text{m}$ . Hydrodynamic spindles are also supplied by Danobat [n.d.], Kellenberger [n.d.], Monza [1998], and Weldon [1998], among others. One feature in common to most is their use in cylindrical or centerless grinders in a very competitive market where roundness, finish, and chatter elimination are critical. Hydrodynamic bearings do not require a lot of the ancillary equipment and are lower cost than the alternative, hydrostatic bearings.

### 15.11.3 HYDROSTATIC SPINDLE BEARINGS FOR LARGE WHEELS

For applications demanding the greatest stiffness, damping, and power handling requirements with minimal runout, many machine tool builders choose hydrostatic bearings. A hybrid hydrostatic bearing can provide greater load support than many hydrodynamic bearings of the same diameter and can withstand crashes better than other bearing types; a significant issue when using steel-cored CBN wheels! The other major advantage of hydrostatic bearings is that, when properly tuned,

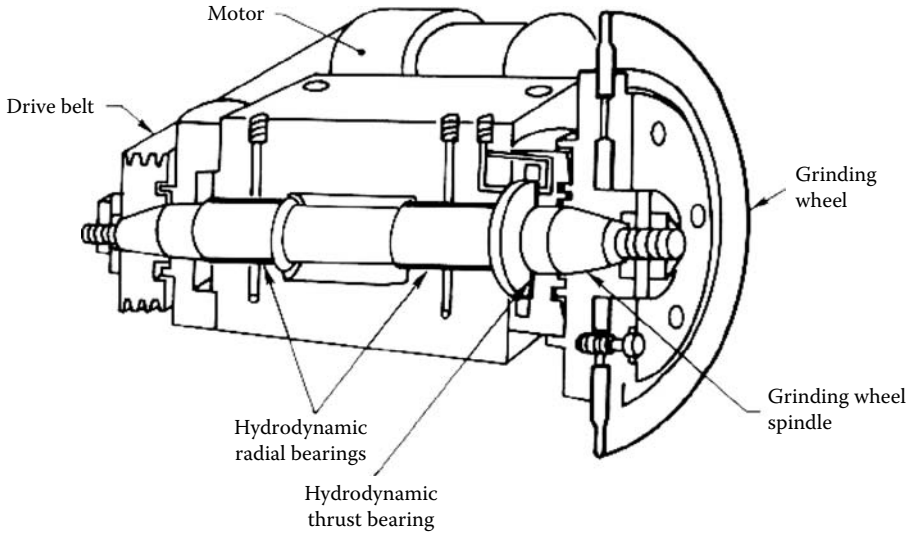


**FIGURE 15.32** A hydrodynamic grinding wheel bearing arrangement. (Based on Toyo n.d. With permission.)

the averaging effect of the bearing will improve running truth by over an order of magnitude relative to the accuracy at which the individual components were machined [Aleyaasin, Whalley, and Ebrahimi 2000]. Radial errors of  $<0.5 \mu\text{m}$  throughout the life of the spindle are typical [Aronson 1995]. For this reason, hydrostatics have become common, if not the standard, for applications such as camshafts [Landis 1996a] and crankshafts [Landis 1996b], roll grinding [Elgin n.d., Waldrich Siegen 1996], some centerless grinders [Koyo 2 n.d.], and several standard cylindrical grinders [Paragon n.d.].

Rotary hydrostatic bearings are built in a similar fashion to their linear counterparts with metered fluid under pressure fed to a series of bearing pads. There are usually two radial or journal bearings with four opposed pads in each and either two axial thrust bearings or an axial thrust and additional oil-filled chamber behind the journal bearing and pressurized by it [Montusiewicz and Osyczka 1997].

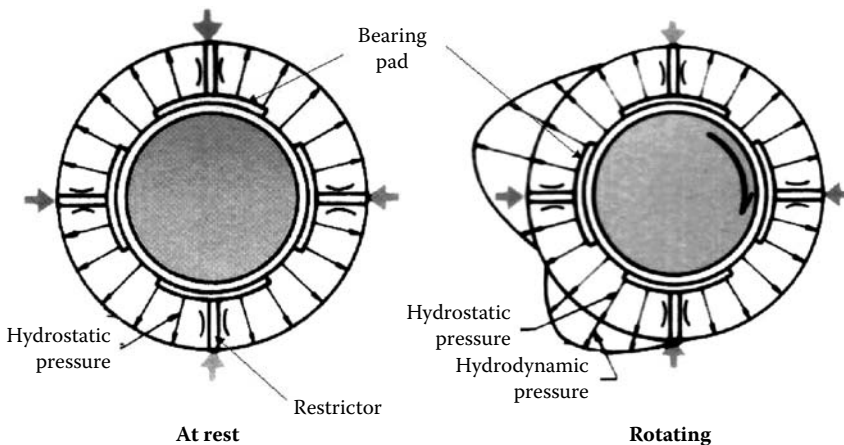


**FIGURE 15.33** Toyoda Stat hybrid hydrostatic bearing. (After Toyoda 1994. With permission.)

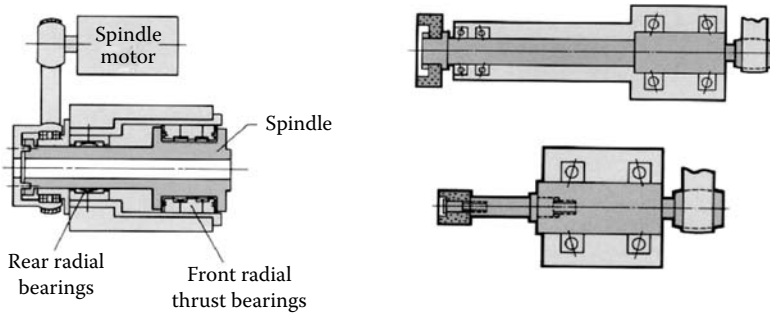


**FIGURE 15.34** Examples of bearing arrangements for small wheel spindles. (From Danobat 1991. With permission.)

At rest, the bearing is purely hydrostatic but as the spindle rotates, fluid will be dragged into the narrow space between the pads generating additional hydrodynamic pressure. While some drag is inevitable and provides additional support at lower speeds, it can lead to instability and excessive heat at higher speed unless flowrate, pad widths, and depths are selected carefully. The principles of hybrid hydrostatic/hydrodynamic bearings were developed by Rowe [1983] who provided design charts for load-bearing capacity and criteria for stable operation. Recessed and plain hybrid hydrostatic designs have been established [Rowe, Koshal, and Stout 1977, Rowe and Koshal 1980, Rowe et al. 1982, Koshal and Rowe 1980, Ives and Rowe 1987].

Several Japanese machine tool builders design spindles specifically to incorporate the effect into “hybrid” hydrostatic spindles [Toyoda 1996, NTC 1999]. Whereas a pure hydrostatic spindle might need 1,000 psi oil pressure, a hybrid bearing might need only 300 psi for the same stiffness. The disadvantage is that the center of rotation will change with spindle speed and oil viscosity [Aronson 1995].

The major disadvantages of hydrostatic bearings, in general, are in the manufacturing and ancillary equipment requirements and their associated costs. The bearings require an oil pump, collection, and recirculation system with filtration to  $<5 \mu\text{m}$ , and a chiller to hold the oil to ambient temperature. Hydrostatic spindles tend to be limited to about 750,000 DN due to heat generated by fluid shear, although bearing temperatures can be kept low by optimization of flowrate to remove unwanted heat [Rowe 1970].

## 15.12 DRIVE ARRANGEMENTS FOR SMALL WHEEL SPINDLE UNITS

### 15.12.1 INTRODUCTION

The problems with spindles designed for small wheels is somewhat different to those for larger wheels in that nearly all wheel bond types, including most superabrasives, are limited by bond strength to operating in the speed range of 35 to 60 m/s. Taking 100 mm (4) diameter as the cutoff for this discussion, the limitations are in flexibility to handle a wide range of wheel diameters and maximum wheel speeds for very small wheels as those used in, for example, the fuel injection industry. The operating range under consideration is therefore 6,000 to 200,000 rpm.

### 15.12.2 ROLLING BEARING SPINDLES WITH BELT DRIVE FOR SMALL WHEELS

The simplest and oldest designs of spindles are grease-packed, angular contact-bearing spindles, belt-driven similar to the larger cylindrical wheel counterpart discussed above except the bearings

are always at least ABEC 7 or 9 (ISO class 4 or 2) and the belts are multiribbed. Spindle nose runout is maintained at 2  $\mu\text{m}$  or better. Grease-packed bearings are capable of running up to about 30,000 rpm [Bryant 1986] or 500,000 DN [Nakamura 1996]. Similarly, belt drives are available up to about 30,000 rpm [Bryant 1986], although the preferred limit is nearer 10,000 rpm [Aronson 1998]. With variable speed control, this arrangement provides a compact flexible arrangement for dedicated internal and universal grinders performing internal and face grinding with conventional wheels in sizes in the range of 100 mm down to 25 to 50 mm in diameter.

### 15.12.3 HIGH-SPEED SPINDLES FOR SMALL WHEELS

For speeds faster than 30,000 rpm, various design considerations need to be incorporated.

#### 15.12.3.1 Direct Drive Motors

Use of direct drive ac asynchronous induction motors with frequency converters are mostly used to eliminate the need for belts. The drive will usually have a closed loop tachometer, thermistor monitored temperature control, and overload protection [Precise n.d.]. Spindle horsepower curves need to be closely married to the rpm requirements as each drive will have a particular operating range in terms of rpm and torque. Controls are now available that can extend the constant horsepower range over a much wider speed range. Bryant [1992], for example, provides just two spindles to cover the entire range from 8,000 to 70,000 rpm.

#### 15.12.3.2 Dynamic Balancing of High-Speed Spindles

Dynamic balancing of all rotating components and *in situ* balancing to better than 1.2 mm/s displacement is critical to spindle life and grind quality [Gamfior n.d.].

#### 15.12.3.3 Oil-Mist Lubrication for High-Speed Spindles

Oil-mist lubrication to replace grease packed bearings can increase the DN value of steel ball-bearings from 500,000 to 1,000,000. Oil mist lubrication requires an oil-mist source and a compressed air source (Figure 15.35). The air needs to be carefully dried to prevent rusting of the spindle and must be filtered to 5  $\mu\text{m}$  or better to prevent contamination of the bearings. The oil-mist at a pressure of about 1 bar provides positive air displacement to the unit, which, coupled with a labyrinth seal, prevents coolant ingress. Also note, even with the current oil-mist systems, when the spindles are run over extended periods of time a long length of pipe connection should be used (>1 m) to facilitate air-oil mixing.

#### 15.12.3.4 Adjustment of Bearing Preload for High-Speed Spindles

Bearing preload needs to be carefully controlled and understood. Insufficient preload leads to low stiffness while excessive preload leads to higher temperature rise and even seizure. As rotational speed increases several factors cause an increase in preload:

- Centrifugal force from the balls
- Hydrodynamic pressure from the oil lubricant
- Thermal expansion from temperature differences due to frictional heat generation causes a temperature gradient between the inner and outer ring
- Thermal expansion of the balls
- Expansion of the inner ring due to centrifugal force



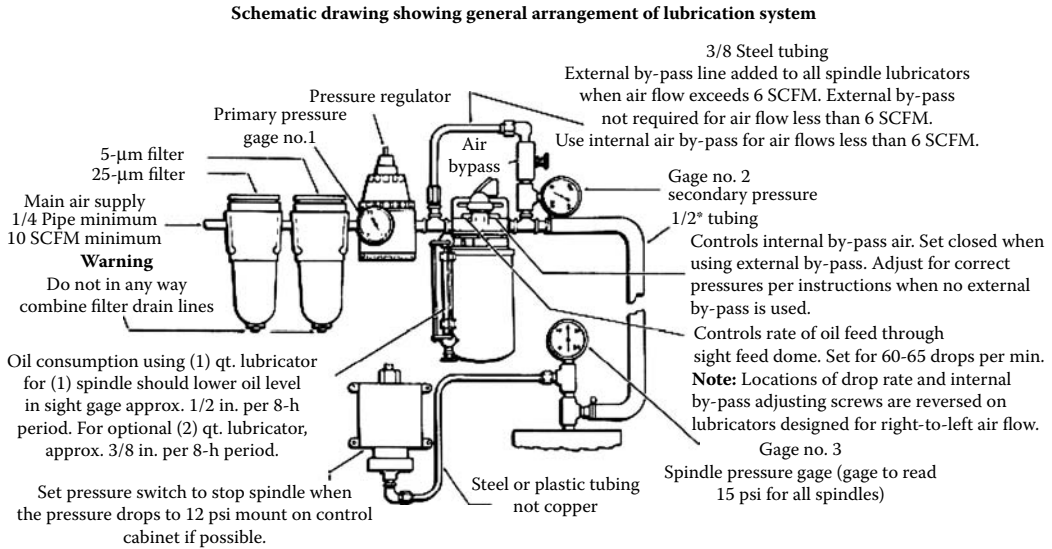


**FIGURE 15.35** Oil-mist lubrication system. (After Bryant Grinders 1986. With permission.)

In addition to affecting preload, thermal effects cause expansion of the spindle arbor leading to axial positional error. To minimize preload effects, several options are available to the machine tool builder as follows.

#### 15.12.4 USE OF CERAMIC BALLS FOR HIGH-SPEED SPINDLES

The first option is the use of hybrid ceramic (silicon nitride) ball bearings. Ceramic balls have a lower density than steel to reduce centrifugal forces; they have lower friction coefficient to reduce frictional heating and lower thermal expansion to minimize the effects of heating. Ceramic is also chemically inert and allows the oil-film to work better and for longer. In many cases, the attraction of ceramics balls is to allow grease-packed lubrication at higher DN values. Hybrid ceramic bearings can be rated for 0.8 to 1.4 m DN when grease packed, or to 2 to 3 m DN with oil-mist lubrication [Nakamura 1996, Aronson 1994, 1996].

#### 15.12.5 LIQUID COOLED HIGH-SPEED SPINDLES

The second option is to liquid cool the spindle by pumping oil through the housing and even injecting cooled oil into the bearings either as a metered oil-air mixture based on monitoring spindle characteristics (i.e., with greater control than a standard oil-mist system) or as a flood jet of oil. The oil-air approach can play a major role in extracting heat from the whole spindle as well as maintaining a positive pressure to the bearings to prevent contamination.

#### 15.12.6 FLOATING REAR BEARING FOR HIGH-SPEED SPINDLES

The third option is to fix the front bearings but allow the rear bearing housing to float in a fluid-film bearing. This allows the radial preload to remain near constant while driving all the axial thermal expansion backward and away from the wheel reference position.

## 15.13 SPINDLES FOR HIGH-SPEED GRINDING

### 15.13.1 INTRODUCTION

Spindle design is not the limiting factor in most high-speed grinding opportunities. As discussed in earlier chapters, wheel speed limitations, dressing, burn, and a host of other factors normally prevent higher speeds before there is a spindle limitation. This is all too clear in, for example, high-speed cylindrical grinding. Current top grinding speeds with CBN wheels is about 200 m/s in actual production. Most of this is focused at the camshaft industry. It may be surprising but there are probably more grinders in countries such as India and Taiwan running at 160 m/s or greater than there are in the United States. This is because car and scooter engines in those countries use cast iron cams whereas U.S. cars require hardened-steel cams because of the higher engine power.

### 15.13.2 SPINDLE BEARINGS FOR HIGH-SPEED GRINDING OF HARDENED STEEL

Hardened steel is much more sensitive to burn than cast iron is and has been limited to grinding speeds under 100 m/s. Even at 200 m/s, a 380-mm wheel rotates at 10,000 rpm, which is within the limits of hydrostatic, hydrodynamic, or ceramic hybrid ball bearing spindles. High wheel speed is used to increase stock removal rates and, therefore, high load capacity is to be expected. For this reason, most high-speed grinders use hydrostatic spindles although Okuma [1998] has optimized its 59-kW hydrodynamic spindle to run 350-mm wheels up to 11,000 rpm. The highly efficient and successful Junker Quickpoint contour grinding process has used an air-cooled grease-packed roller bearing spindle for speeds up to 8,000 rpm or 140 m/s [Junker 1989]. In some cases, it was also belt driven [Junker 1992].

### 15.13.3 SPINDLE BEARINGS FOR HEDG

Grinders for high efficiency deep grinding (HEDG) and superabrasive high-speed grinding with plated wheels have been influenced strongly by machining center design. In many cases, the grinders are, in fact, a multipurpose machining/grinding/drilling center. The wheels are designed around sizes of 125 mm up to 300 mm running at up to 120 m/s. Numerous machine tool companies fall into this category with either a grinding background (e.g., Campbell, Edgetek, Gendron, and Huffman Magerle) or a machining background (e.g., EMAG, Makino, and Mori Seiki). The spindle requirement is, therefore, both speed and flexibility to operate over a range of speeds. Most machine builders use liquid-cooled, ceramic hybrid bearings with ac servomotors operating at speeds 5,000 rpm up to 20,000 rpm. Use of ceramic hybrid bearings allows for larger diameter shafts of 100 mm or greater and, therefore, enhanced stiffness. A similar approach has been taken by the manufacturers of high-production tool grinders that use superabrasive wheel packs in the 100- to 300-mm-diameter range.

### 15.13.4 SPINDLE COOLING FOR HIGH-SPEED GRINDING

It is interesting to note the attention paid by a number of the machine tool builders to how the spindle is cooled. One concern with a demand for flexibility is that to achieve the necessary preload at high rotational speeds may mean a loss of preload at slower speeds. Makino [n.d.] reduces this by injecting chilled oil through the center of the shaft where centrifugal force then injects the oil from the inner to the outer bearing race. The oil is then injected through the housing setting up a temperature gradient from the inner to the outer race and between the bearing and the housing. This temperature difference, combined with the efficiency of core cooling, provides increased thermal stability at higher speeds and allows the bearings to be amply preloaded at rest.

### 15.13.5 SPINDLE BEARINGS FOR VERY SMALL HIGH-PRECISION HIGH-SPEED WHEELS

It is small-diameter wheels that have pushed the limits of spindle design. The fuel injection industry, for example, especially for diesel engines, requires bores as small as 2 mm to be ground to extremely high precision. Current spindle technology is limited to about 200,000 rpm, which is only 21 m/s for a 2-mm wheel. The greatest problems at these speeds are wheel and arbor imbalance, resonance problems, and lack of stiffness of the arbor. Spindles running up to 150,000 rpm are more typical of production currently and these are dedicated to a small range of wheel diameters.

### 15.13.6 ACTIVE MAGNETIC BEARINGS FOR HIGH-SPEED WHEELS

One possible solution to improve stiffness and flexibility in the use of small- and medium-sized wheels is the development of active magnetic bearing (AMB) spindles. AMB spindles have been available since the 1980s [Moritomo and Ota 1986] and a few are in use, certainly in the United States, although their acceptance has been slow.

AMB spindles use a magnetic field to support the rotor. Positional sensors and closed-loop monitoring to a controller constantly controls its position in the field. Originally developed for defense and space applications, AMB spindles have been used at speeds up to 1,000,000 rpm in, for example, centrifuges. For spindle applications, the rotor is levitated by two radial bearings and at least one thrust bearing [Wang et al. 2001]. AMBs are offered at speeds up to 200,000 rpm [IBAG 1996]. Catch bearings are provided in the event of a power loss. One of the big attractions of these spindles is the ability to provide a high power output over a very large range of spindle speeds, which in turn allows flexibility in wheel diameters when grinding a family of different-sized parts. As with any new technology there is a price barrier and learning curve to be overcome before AMB spindles become generally accepted. Certainly the avoidance of oil mist lubrication with its associated environmental issues will be an attraction.

## 15.14 MISCELLANEOUS WHEEL SPINDLES AND DRIVES

### 15.14.1 HYDRAULIC SPINDLE DRIVES

Although much of the interest is in new and emerging technologies, many machines remain in the field built 30 or more years ago. Very often, aspects of an older technology will linger because it has proved such a practical or reliable method. A case in point is the use of gerotor hydraulic motors for dressing spindles discussed in the previous chapter. Hydraulic motors were common wheel drives for applications such as centerless grinding. The motors were compact and had good torque at low rpm. Lidkoping [1998] still offered a state-of-the-art grinder suitable for vitrified CBN wheels with hydraulic piston pump drives on both its grinding and regulating wheels. The hydraulic drive was claimed to give an exact control of wheel velocity.

### 15.14.2 AIR MOTORS AND BEARINGS

The other drive still seen is based on air motors and bearings. Air bearings have very low friction and are, therefore, used for very high speeds. The limitation with air is the load-carrying capacity of the air film. The supply pressures that can be employed are much lower than can be employed with oil. This limits the bearing pressures that can be generated [Rowe 1967].

The most common use for air bearings is in jig grinding. The process is a very low stock-removal process, often carried out dry, with small superabrasive wheels. The workpieces can have deep bores to be ground leading to long, flexible wheel shanks. The torque requirements for the motor are, therefore, low. Moore jig grinders are available with a complete range of air turbine and vane-driven spindles from 9,000 to 175,000 rpm. Similarly, Hauser provides an air spindle for

operations in the range of 80,000 to 160,000 rpm although it also provides direct-drive electric options for slower speeds.

Air bearings in spindles are seen in ultraprecision grinders for specialist applications such as carbide grinding for the die industries with tolerances of  $<0.2 \mu\text{m}$  and surface finishes of  $0.025 \text{ Ra}$  [Pride n.d.]. Many of the grinder manufacturers are focused on the electro-optical and semiconductor businesses and as such are outside the scope of this book but, on occasion, this type of machine is found suitable for ultrahigh precision prototype work.

A case in point is Precitech who manufactures machines for single-point diamond turning or grinding of aspheric surfaces for lenses. The machines are equipped with aerostatic bearing, air-driven spindles for speeds up to 60,000 rpm, although the motor is replaced with a dc servomotor for speeds around 10,000 rpm. With laser interferometer feedback, the machine positional resolution is  $<10 \text{ nm}$ , indicative of the type of low stock removal, high-precision applications where air spindles and bearings are found.

## 15.15 ROTARY DRESSING SYSTEMS

Rotary dressing heads and spindles have become a key feature of modern grinding systems particularly for application with superabrasive wheels. Rotary dressing units are often purchased separately from the basic machine tool. In many cases, dressing spindles are merely an option when buying a new grinder and are only fitted at a later date by end users seeking process improvements. Many older machines were never designed for use with dressing spindles and may need a complete retrofit including modifications to slides, guarding, and machine control programming. Spindle design for these applications is very dependent on available space within the machine as usually it will be replacing a small, simple stationary tool post. In the newest grinders capable of using CBN, the demand becomes more a factor of motor power density and rotational speed to match the higher wheel speeds and dressing forces, and positive crush ratios. Dresser spindle design is a subject that has previously been rather overlooked in books on grinding technology. The following section, therefore, attempts to provide a picture of the overall range of provision and application.

Rotary dressing drives can be basically categorized by their source of power.

### 15.15.1 PNEUMATIC DRIVES

Pneumatic spindles are relatively inexpensive, can run on shop air of 6 to 7 bar (90 psi), and do not suffer from heat problems that would cause significant thermal movement. However, they have low torque or power (or more specifically a low-power density) and are noisy. Larger motors suitable for form roll dressing can require  $3 \text{ m}^3/\text{min}$  ( $100 \text{ ft}^3/\text{min}$ ) of air. In general, their use is limited to internal grinding often in cross-axis dress mode, although even here they are being superceded by electric motors. Where used in uniaxial dress mode (as opposed to a cross-axis configuration) they tend to be equipped with small-diameter cup dressers to limit torque requirements. Speed selection is made by adjustment of airflow.

### 15.15.2 HYDRAULIC DRIVES

Hydraulic drives generally use gerotor pump technology to provide a compact high-power/high-torque motor that has made this style of dresser drive the mainstay of form-roll dressing applications for conventional wheels for the last 30 years. Hydraulic spindles suffer from serious thermal problems as they get hot after only a few minutes, although this can be mitigated by pumping coolant through the housing and/or flooding the exterior of the housing with coolant. Nevertheless, they are not recommended for running continuously for more than 15 min. The other problem with hydraulic motors is that they are generally designed to run counterdirectionally only with a

flow control on the input side of the motor. They can be designed to run unidirectionally using a flow control on the exhaust side of the motor, but this also requires a complete reconfiguration of the spindles design including seals, etc. Since unidirectional dressing is generally limited to newer grinders using advanced abrasives where end users are moving away from hydraulics, hydraulic-powered dressers are almost exclusively used on older grinders for dressing standard alox wheels.

Hydraulic spindles require of the order of 36 bar (approximately 500 psi) and between 19 and 38 l/min (5 to 10 gpm) flow, which should ideally be from a separate closed-loop system filtered to 10  $\mu\text{m}$ . The pressure line from the pump to the spindle should be as short as possible and a minimum of 10 mm (approximately 3/8 in.) diameter. Also the exhaust hose from the motor should never be smaller than the inlet. Speed adjustment is made by use of the flow control. The hydraulics can also provide pressure and lubrication to sleeve bearings used in many of these older spindle designs and as a means of actuating retractable centers for quick roll changes.

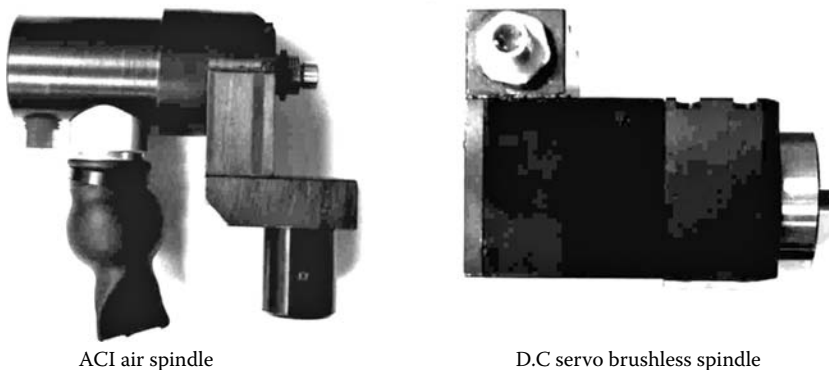
With the trend to eliminate hydraulics on grinders, dresser spindle technology has moved away from hydraulic drives and toward electric drives.

### 15.15.3 ELECTRIC DRIVES

Electric motors can be subdivided into three categories: traditional ac motors, ac servomotors with high-frequency drives popular since the early 1990s, and most recently dc brushless servomotors with high-frequency drives. The trend in these motors is to go to higher and higher power densities so as to be as compact as possible and, hence, give the maximum flexibility both to be fitted into smaller grinder footprints and to provide the additional power required for creep feed and vitrified CBN dressing.

There are numerous advantages to electric drives including the ability to run unidirectional (i.e., in an overrun situation where the grinding wheel tries to drive the dressing tool), a high power and power density, simple speed control, and cleanliness. Motor guarding is more of an issue to prevent coolant access to the windings but this is readily achieved with good rotating seals and/or positive air purging.

The enormous changes that have occurred in the last few years is exemplified in the photographs in Figure 15.36. These show two dressers from Wheel Dressing Inc. (Saint-Gobain Abrasives). The spindle to the left is a model ACI pneumatic spindle designed and in common use for over 25 years specifically for Heald internal grinders; it has a power rating of about 0.05 kW at 20,000 rpm. The spindle to the right is a dc servo brushless electric dresser with a peak power rating of 0.80 kW at 20,000 rpm. Both photographs are at the same magnification.



ACI air spindle

D.C. servo brushless spindle

**FIGURE 15.36** Advances in dresser spindle motor technology. ACI air spindle; dc servo brushless spindle.

**TABLE 15.2**  
**Capacities of Common Dresser Spindle Designs**

Manufacturer	Model	Drive	rpm (max)	Roll Width	Roll Diam	Roll Speed	Power	Application
WDI	ACI	Air	21,000	N/A	63.5 mm	34 m/s	0.05 KW	Traverse
WDI	HCI	Hydraulic	11,500	N/A	28.5 mm	7.5 m/s	0.10 KW	Traverse
WDI	HO 5/8	Hydraulic	3,600	N/A	70.0 mm	7.5 m/s	0.35 KW	Traverse
WDI	ECI	Hydraulic	4,000	25 mm	76.2 mm	7.8 m/s	0.18 KW	Plunge
WDI	HO	Hydraulic	3,600	100 mm	76.2 mm	7.0 m/s	0.35 KW	Plunge
WDI	HI	Hydraulic	2,400	75 mm	100 mm	6.2 m/s	0.45 KW	Plunge
WDI	DFW-AHO	Air	4,000	100 mm	76.2 mm	7.8 m/s	0.30 KW	Plunge
WDI	HHD	Hydraulic	2,300	300 mm	120 mm	7.1 m/s	0.70 KW	Plunge
WDI	DFW-AC	Air	2,400	300 mm	125 mm	7.8 m/s	1.10 KW	Plunge
WDI	DFW-N3	Electric	3,600	300 mm	125 mm	11.1 m/s	0.75 KW	Plunge
Norton	AXH-1464	Hydraulic	20,000	N/A	76.2 mm	39 m/s	0.33 KW	Traverse
Norton	AXH-1440	Hydraulic	4,200	N/A	72.2 mm	8 m/s	0.48 KW	Traverse
Norton	AXH-1416	Hydraulic	4,200	31.75 mm	152 mm	16 m/s	0.48 KW	Plunge
Norton	AXH-1418	Hydraulic	7,450	31.75 mm	152 mm	29 m/s	0.33 KW	Plunge

## 15.16 POWER AND STIFFNESS REQUIREMENTS FOR ROTARY DRESSERS

A review of some commonly available dresser spindles, sold to machine tool builders and as retrofits for grinders previously using single point dressing, gives a good indication of the power requirements and hence stiffness. Table 15.2 lists the capacity of various Wheel Dressing and Norton (Divisions of Saint-Gobain Abrasives) dressing spindles.

The first observation is that the dressers for roll applications tend to operate at speeds around 7 to 8 m/s, which for conventional applications gives a crush ratio of the order of  $-0.2$ . It is also possible to extrapolate guidelines for dresser power requirements for traverse and plunge rotary dressers. It should be noted that spindles handling up to 300-mm-wide rolls will in fact have a series of rolls and spacers and so the diamond-contact width will be considerably less. Based on this, one can estimate approximately 50 W/cm for counterdirectional plunge dressing of conventional wheels, which is four to five times higher than that predicted for a flat roll from Table 15.2 and Table 15.3, but in line with the expected higher power required for profiles and necessary safety factor. Based on this and additional data from the field, the recommendations in Table 15.2 for power requirements can be made.

**TABLE 15.3**  
**Power Requirements for Dresser Spindles by Abrasive  
Type and Dress Application**

Abrasive	Crush Ratio	Application	Spindle Power
Alox	Cross-axis	Traverse—internal grind	50 W
Alox	(-ve)	Traverse—finish grind	100 W
Alox	(-ve)	Traverse—rough grind	250 W
Alox	(-ve)	Plunge	50 W/cm roll width
Alox	(+ve)	Plunge	100 W/cm roll width
CBN	(+ve)	Traverse	150 W
CBN	(-ve)	Plunge	75 W/cm roll width
CBN	(+ve)	Plunge	150 W/cm roll width

Taking these data, estimates can now be made for spindle stiffness requirements and the limits thereof. For example, for a 10-cm-wide roll dressing a CBN wheel might draw up to 1.5 kW running at 25 m/s. This would generate a normal force, based on  $F/F_n = 0.2$ , of up to 300 N. If deflection is to be kept under 2  $\mu\text{m}$ , then the system stiffness must be greater than 150 N/ $\mu\text{m}$  or 1.2 m lbf/in. Precision dressing spindles for form-roll applications have maximum stiffness values in the range of 1 to 2 m lbf/in. (125 to 250 N/ $\mu\text{m}$ ) due to the nature of the bearing designs available and required arbor diameters. However, the sum of the remaining machine components is rarely 1 m lbf/in. except on a small number of specifically designed grinders.

For crush-forming, TVMK [1992] offers a hydraulic unit with a power of only 25 W/cm max, *but* a torque of 10.8 N.m rated for rolls up to 35 mm wide. Since most crush-forming operations occur at roll speeds of 1 to 2 m/s, the normal force created would be expected to be as high as 30 N/cm roll width. This is 50% higher than those for diamond roll dressing conventional wheels with a +0.8 crush ratio, and comparable to the highest dressing forces for CBN wheels indicated above. The advantage of the hydraulic drive is to provide the necessary high torque at low rotational speeds. The results also illustrate why crush forming is uncommon and limited to narrow forms for applications such as thread grinding. Most standard grinders do not have the stiffness capability. Also note, crush forming has a form accuracy of only about 25 to 50  $\mu\text{m}$ , which is an order of magnitude less accurate than diamond roll dressing.

## 15.17 ROTARY DRESSING SPINDLE EXAMPLES

### 15.17.1 INTRODUCTION

Diamond roll dressing was introduced in the 1960s and has been growing in usage until it now represents the commonest dressing method for the majority of profiled and flat grinding applications, and virtually all vitrified CBN applications. Nevertheless, it often remains just an option on new grinders still designed primarily for stationary dressers or a later requirement for retrofitting to existing grinders. Conversion of machines to rotary dressing may require machine modifications including mounting plates, guarding changes, or even additional axes of motion. These axes may be used as controlled infeed motion for the dressing operation or merely to move in to a fixed stop and then after dressing retract in order to clear the dresser from the grind area. Some examples of both dressing spindles and the accompanying infeed systems are illustrated in the proceeding pages [courtesy of Wheel Dressing (Saint-Gobain Abrasives)].

### 15.17.2 DFW-ACI AIR-DRIVEN SPINDLE

Figure 15.36 shows an impellor rotor-driven spindle with ABEC 7 twin ball bearings for radial stiffness and ABEC 7 thrust bearing for axial stiffness. Note, a muffler is required to reduce noise level with air operation. The unit requires dry shop air lubricated and filtered to 5  $\mu\text{m}$ . It was originally designed for Heald internal grinders and is most effective on alox wheels but has been used successfully on small vitrified CBN internal wheels. Since air is compressible, a larger cylinder is required to achieve the same drive stiffness as with a hydraulic cylinder.

### 15.17.3 ECI HYDRAULIC SPINDLE

Figure 15.37 shows a cantilevered hydraulic powered dresser with three pressure-lubricated sleeve bearings for radial stiffness and damping and two ABEC 7 thrust bearings for axial stiffness; used



**FIGURE 15.37** EC1 hydraulic spindle.

with up to 3 diameter by 1 wide rolls typically for traverse dress operations or narrow plunge forms. This hydraulically driven spindle is rated for up to 7,000 rpm although generally runs at 4,000 rpm.

#### **15.17.4 DFW-HI HEAVY-DUTY HYDRAULIC SPINDLE FOR INTERNAL GRINDERS**

This unit shown in Figure 15.38 is a cantilevered hydraulic-powered dresser with three sleeve bearings for radial stiffness and two ABEC 7 thrust bearings for axial stiffness. It is a unit designed for heavy-duty plunge-dressing applications on internal grinders. Rolls can be counterbored to wrap around the spindle to accommodate up to 3 roll widths. This type of layout reduces the cantilever overhang and reduces deflections.

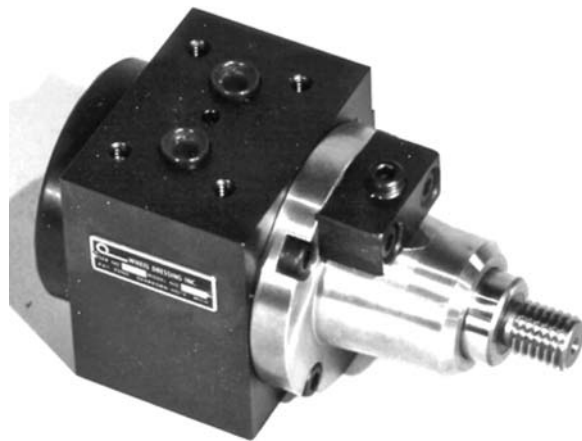


**FIGURE 15.38** DFW-HI hydraulic dresser spindle.





FIGURE 15.39 HO 5/8 hydraulic dresser spindle.

#### 15.17.5 DFW-HO FIVE-EIGHTHS HEAVY-DUTY HYDRAULIC SPINDLE TYPICALLY USED FOR CENTERLESS WHEELS

This unit, shown in Figure 15.39, is an outboard-supported heavy-duty traversing spindle with zero end-play. The outboard support greatly increases the stiffness of the design compared with a cantilever layout. The unit has three sleeve bearings and four thrust bearings with coolant porting for thermal stability. The roll is replaced by removing the end cap where the diamond roll is bolted to a face plate. The dresser is typically used for flat form dressing centerless wheels mounted cross-axis or uniaxially to dress forms and radii. Centerless wheels are wide compared to wheels for most other grinding processes and, therefore, require a heavy-duty spindle.

#### 15.17.6 DFW-HO VARIABLE-SPEED HYDRAULIC DRESSER

The unit, shown in Figure 15.40, is a variable speed, outboard-supported light-duty plunge dresser with pressure-lubricated sleeve and thrust bearings with easy removal of the dresser shaft from the housing for roll replacement. Coolant porting is supplied custom to each unit for the dressing process. The variable speed capability allows a variety of dress conditions for very different wheel grades or diameters.

#### 15.17.7 DFW-HHD HYDRAULIC HEAVY-DUTY PLUNGE DRESSER

Figure 15.41 shows the heavy-duty hydraulic plunge dresser with sleeve and thrust bearings as in the previous example. Custom coolant porting is provided, and easy spindle removal is possible from the housing for roll changes. This unit is typically used for dressing multiple wheel assemblies.

#### 15.17.8 DFW-HTG HEAVY-DUTY HYDRAULIC SPINDLE

The unit shown in Figure 15.42 is a comparable spindle to the DFW-HHD but using two pairs of ABEC 7 angular contact ball bearings to allow the spindle to be used with nonhydraulic drive systems. The housing casting can be custom-made to accommodate up to 500-mm shaft width.



FIGURE 15.40 DFW-HO hydraulic dresser spindle.

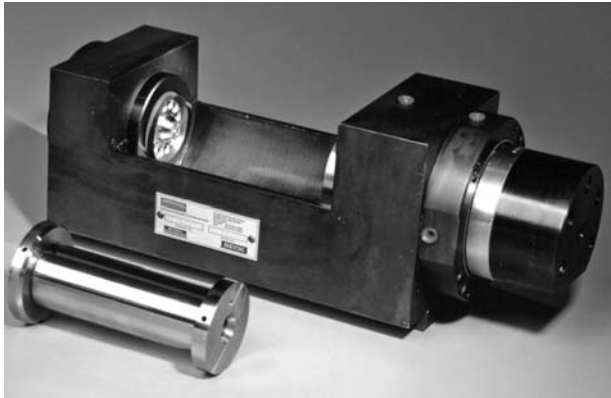


FIGURE 15.41 DFW-HHD heavy-duty plunge hydraulic dresser spindle.

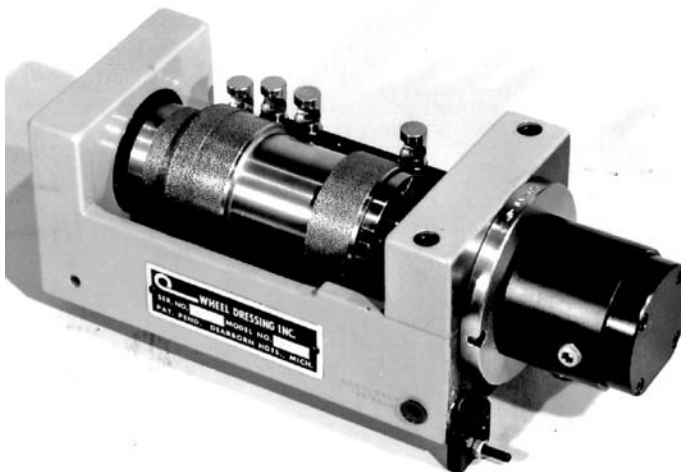


FIGURE 15.42 DFW-HTG plunge hydraulic dresser spindle.

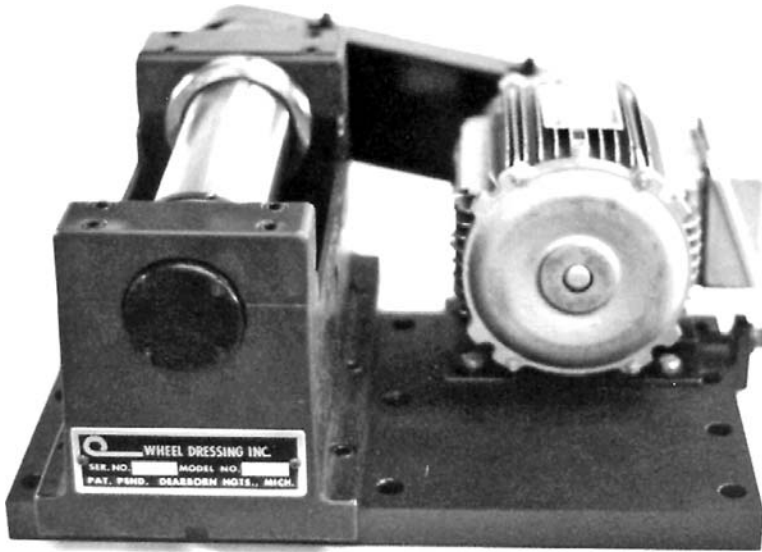


FIGURE 15.43 NTG plunge electric dresser for creep feed grinding.

#### 15.17.9 DFW-NTG BELT-DRIVE SPINDLE

The classic electric, belt-driven dresser shown in Figure 15.43 has an ABEC 7 ball bearing arrangement for table-mounted surface grinders such as creep feed. Air-oil mist porting is required to the bearings while custom porting is provided for dressing. A proximity sensor is often placed on the pulley to confirm spindle rotation. The spindle design can handle up to a 375-mm roll assembly at a fixed speed of up to 3,600 rpm with speed adjustment through changes to the pulley ratio. For the latest grinders with high wheel spindle power and coolant delivery systems the standard electric motor has been replaced by custom ac servo or dc servo motors for variable speed control and better motor sealing as shown in Figure 15.44.

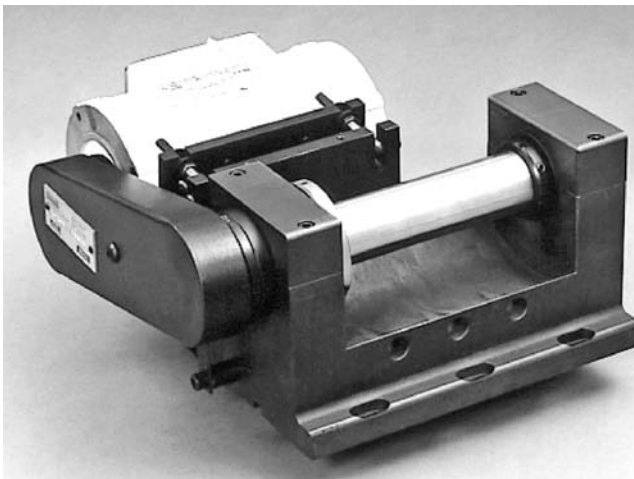


FIGURE 15.44 TG77 upgraded plunge electric dresser.



**FIGURE 15.45** DFW VF45 ac servo HF electric traverse dresser spindle.

#### 15.17.10 DFW-VF44 AC SERVO HF SPINDLE

The ac servo high-frequency motor shown in Figure 15.45 has a peak power of 0.375 kW at 5,500 rpm and a base frequency of 92 Hz. This style of dresser has been the standard for the United States for traverse dressing of vitrified CBN wheels for cylindrical grinding. It is now often fitted with an internal acoustic sensor for touch dressing.

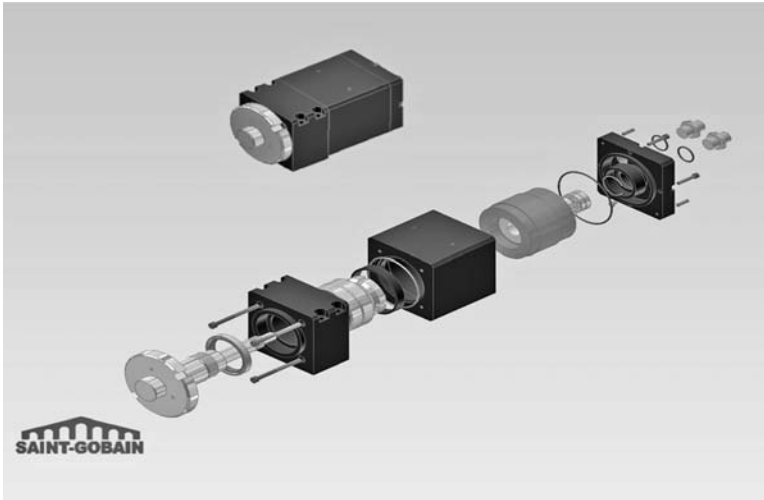
#### 15.17.11 DFS-VS8 DC SERVO VARIABLE-SPEED DRESSER

Figure 15.46 shows a dc brushless servo variable-speed dresser with constant torque and a peak power of 1.3 kW at 6,000 rpm. The spindle is supported on three sets of angular contact bearings including asset for outboard support. The 125-mm-diameter diamond roll has a 35-mm wheel width capacity. It is targeted at heavy-duty traverse applications and form plunge applications with narrow CBN and engineered ceramic seeded gel (SG) wheels. Figure 15.47 shows the unit mounted in a grinding machine for a dressing operation on an SG wheel.

### 15.18 DRESSING INFEEED SYSTEMS

#### 15.18.1 INTRODUCTION

The key to any infeed system is high stiffness and damping, repeatability, and ease of maintenance. The units described below (Courtesy Wheel Dressing Division of Saint-Gobain Abrasives) have proven effective over numerous years in the field. There are a variety of designs combining dresser spindle units and infeed systems varying according to the application and particular features required for the particular application. The following range is described in chronological order from older hydraulic-mechanical compensator designs through dc stepper motors to direct-drive ac servos.



**FIGURE 15.46** DC brushless servoelectric drive dresser spindle.

### 15.18.2 SINGLE HYDRAULICALLY DRIVEN CARRIER

Figure 15.48 shows a single hydraulically oil-lubricated, roundway infeed carrier with mechanical compensation for plunge roll dressing conventional wheels on small cylindrical grinders. Chromed hardened-steel roundways allow more efficient guarding from coolant and abrasive ingress. They also provide excellent damping characteristics. The example shown is equipped with a DFW-HO hydraulic spindle.



**FIGURE 15.47** A postmounted dc brushless servoelectric drive dresser spindle mounted in a grinder dressing on seeded gel wheels.

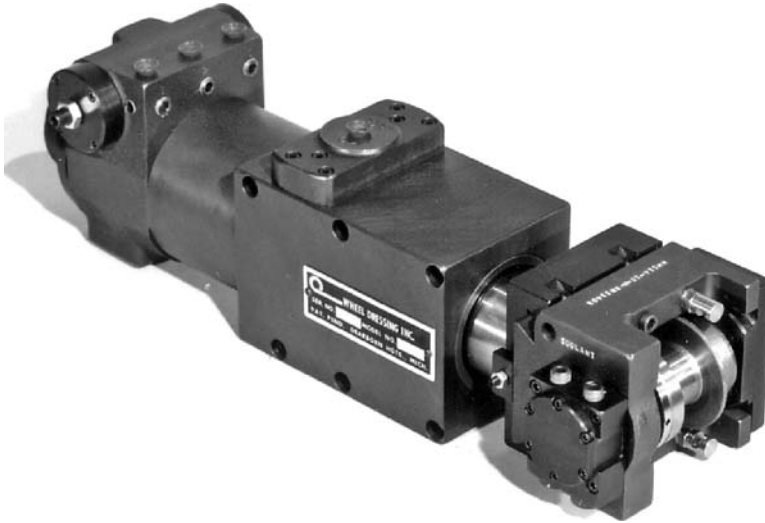


**FIGURE 15.48** Single-barrel hydraulic-driven infeed system.

### 15.18.3 MINI DOUBLE-BARREL INFEED

A mini double-barrel hydraulic-mechanical compensator for medium-sized grinders is shown in Figure 15.49. The system is equipped with a DFW-HO hydraulic spindle.

### 15.18.4 DOUBLE-BARREL INFEED CARRIER

The double-barrel infeed carrier in Figure 15.50 has a hydraulic-mechanical compensator. It is suitable for plunge form dressing on machines such as centerless grinders.

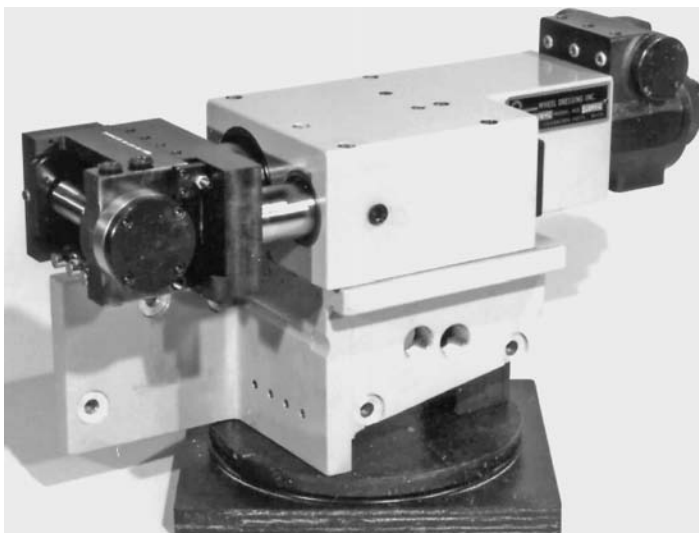


**FIGURE 15.49** Mini hydraulic-mechanical compensated infeed mechanism.

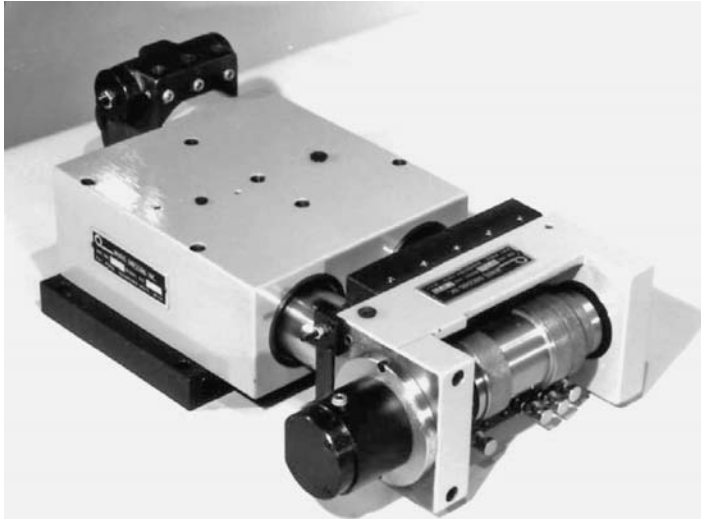


**FIGURE 15.50** Hydraulic-mechanical compensator infeed system.

Figure 15.51 shows an example of a hydraulic-mechanical compensator infeed system with a mounting casting attached directly to the existing platform of a single-point traverse diamond on a Cincinnati centerless grinder.

#### **15.18.5 DOUBLE-BARREL PLUNGE-FORM DRESSER**

Figure 15.52 shows a double-barrel infeed carrier with hydraulic-mechanical compensator for plunge form dressing used on a Cincinnati 480 30° plunge centerless grinder. It replaced a hydrostatic single-point dresser unit and was equipped with a DFW-HHD heavy-duty hydraulic spindle.

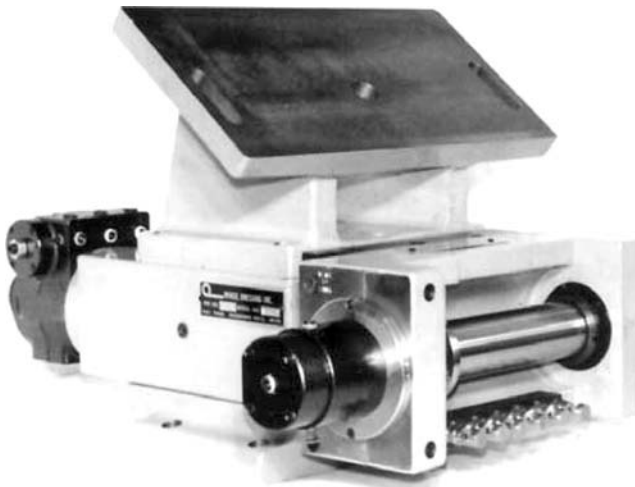


**FIGURE 15.51** Hydraulic-mechanical compensator infeed system for centerless grinder.

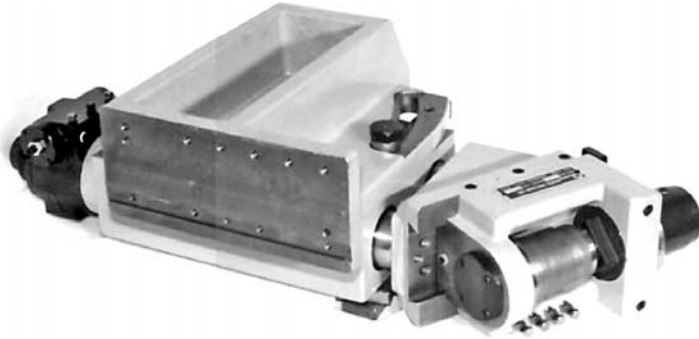


**FIGURE 15.52** Hydraulic-mechanical compensator plunge infeed system for centerless grinder.

### **15.18.6 TRIPLE-BARREL INFEEED CARRIER WITH HYDRAULIC-MECHANICAL COMPENSATOR**

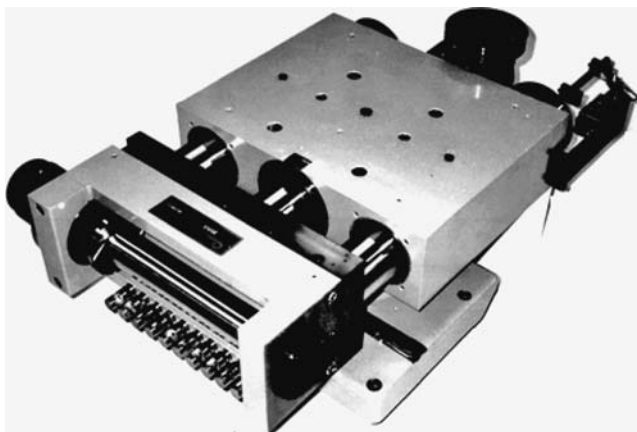
Figure 15.53 shows a triple-barrel infeed carrier for use on large centerless and multiwheel grinders. Custom designs can take up to 20 wide diamond roll assemblies. Note the series of coolant nozzles plumbed through the housing common to all the systems described.

### **15.18.7 STEPPING MOTOR CARRIER**

Figure 15.54 shows a stepping motor and ballscrew infeed compensated double-barrel carrier designed for the SGE-195 bearing grinder. It is equipped with a DFW-HC spindle for quick diamond roll changes.

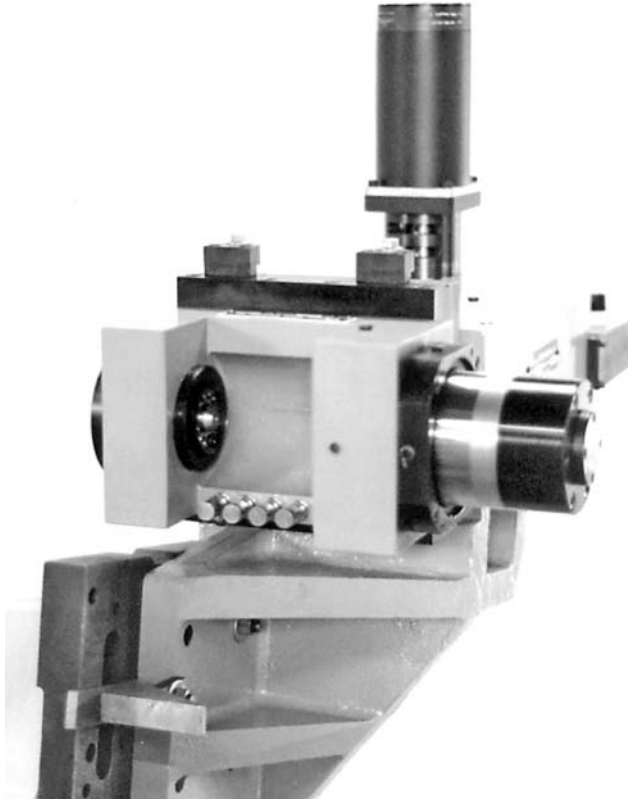
### **15.18.8 STEPPING MOTOR CARRIER FOR A CYLINDRICAL GRINDER**

Figure 15.55 shows a stepping motor and ballscrew infeed-compensation double-barrel carrier suitable for a cylindrical grinder. The carrier is equipped with a DFW-HHD hydraulic spindle.



**FIGURE 15.53** Triple-barrel plunge dresser.





**FIGURE 15.54** Stepper motor/ballscrew infeed double-barrel infeed system.

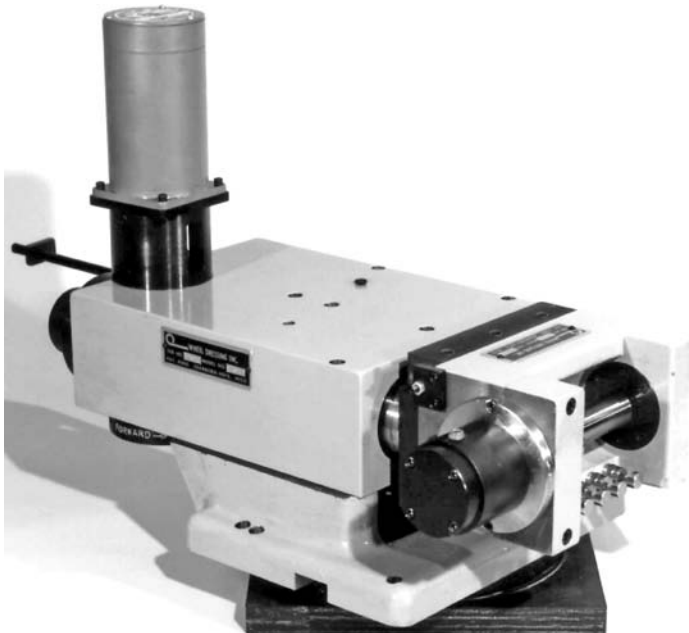


**FIGURE 15.55** Stepper motor/ballscrew infeed system for plunge cylindrical grinder.

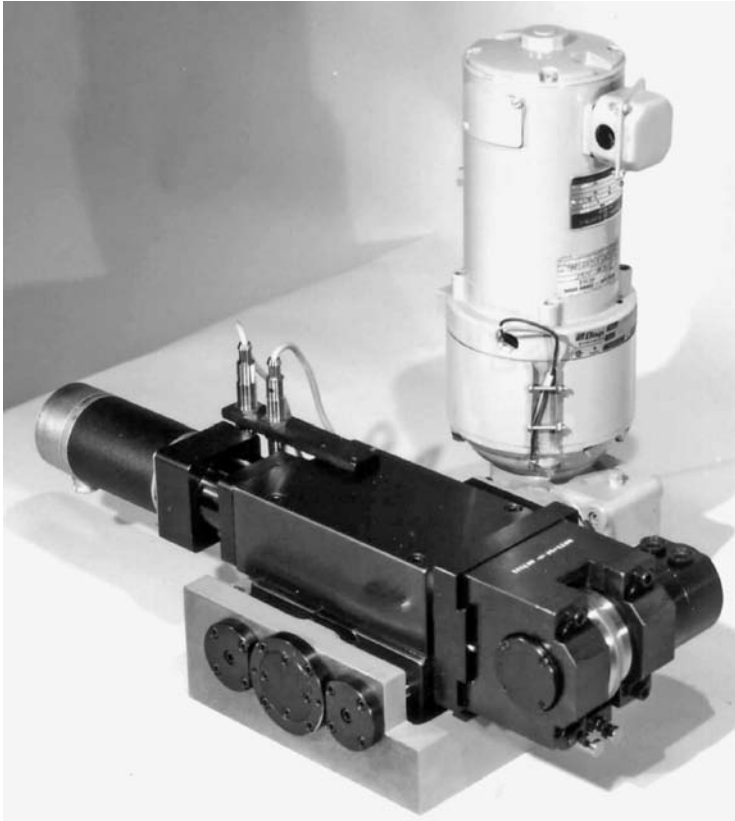


**FIGURE 15.56** Two-axis combination stepper/dc motor traverse dressing system.

### **15.18.9 COMBINATION STEPPER MOTOR AND DC TRAVERSE MOTOR**

Figure 15.56 shows a traverse diamond roll unit with a small double-barrel stepper motor infeed and a dc motor cross-slide and DFW-HTG spindle. This carrier is designed for traverse dressing of CBN and engineered ceramic wheels.

### **15.18.10 PLUNGE-ROLL INFEEED SYSTEM FOR A CREEP-FEED GRINDER**

Figure 15.57 shows a plunge roll infeed system for a Brown & Sharpe (Jones & Shipman) 1236 Hi-Tech creep feed grinder. The dresser is mounted over the wheel on the spindle head. The unit has a servomotor-driven triple-barrel infeed and electric belt-driven spindle assembly. It is equipped with TG angular contact bearing spindle arrangement.

### **15.18.11 SERVMOTOR INFEEED AND DOUBLE-BARREL CARRIER DRESSER**

Figure 15.58 shows a rebuilt Cincinnati 220-8 centerless grinder with a servomotor infeed and double-barrel carrier dresser unit. The spindle has an 8-in.-wide roll capacity.

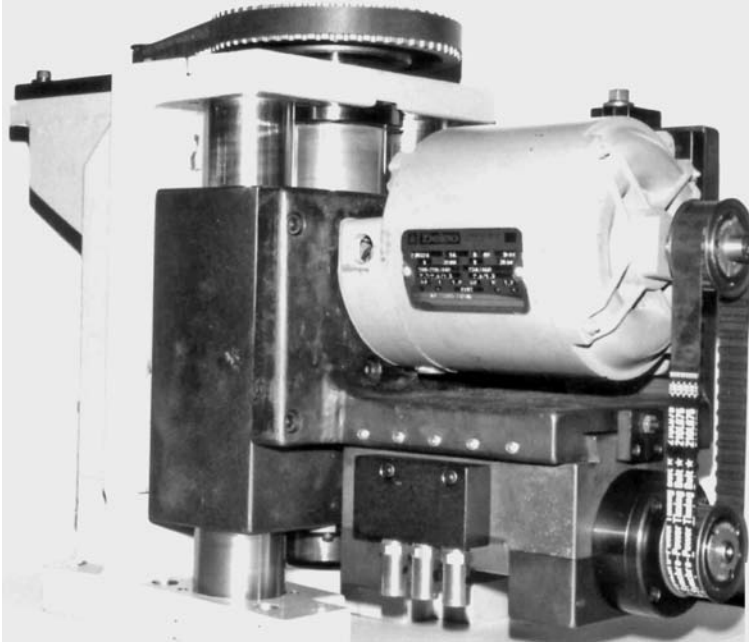


**FIGURE 15.57** Servomotor-driven plunge dresser for creep feed grinding.

#### 15.18.12 TWO-AXIS CNC PROFILE DRESSER

Figure 15.59 shows a two-axis CNC dresser for dressing the OD, radii, and flanks profile for grinding diesel cranks on a remanufactured Landis 4R pin grinder. It is a programmable controller with linear and circular interpolation. The axes are direct-drive servomotor/ballscrew on linear slides to eliminate coupling misalignment and backlash.



**FIGURE 15.58** Rebuilt Cincinnati 220-8 centerless grinder with servo-driven plunge rotary diamond dressing.

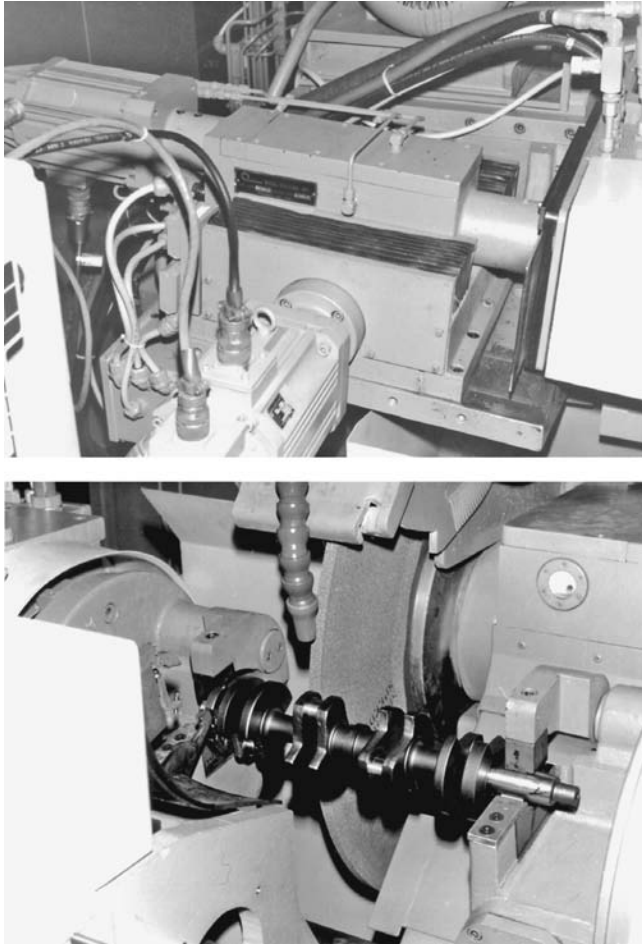


**FIGURE 15.59** Pictures of a Landis 4R crank grinder retrofitted with a two-axis CNC dresser for radius profiling.

Finally, Figure 15.60 and Figure 15.61 provide illustrations of plunge roll dresser spindles *in situ* on two typical grinding applications.

Generation of radii for the bearing industry is still often a problem using circular interpolation of two axes due to the limitations in encoder/ballscrew/control resolution. In many cases, the smoothest radial form is still generated by swiveling about a fixed-radius point. Most grinders in the field are equipped with single-point devices dressing alox or SG-type abrasive wheels, but Nevue [1993] demonstrated these could be readily retrofitted to small rotary devices for dressing CBN wheels.

For the most complex forms, especially in the gear industry, companies such as Normac (Arden, NC) have specialized in compact multiaxis units with accompanying software that can generate and interpolate gear tooth profiles direct from print dimensions. The dresser can be either mounted on the grinder or the wheels dressed offline on a separate machine (Figure 15.62). Offline dressing is common in the tool, thread, and gear-grinding industries. The equipment provided for this range from manual grinders, such as the Junker ARJ 250 example in Figure 15.63, which is designed to generate chamfers, bevels, radii, and other simple shapes, to fully programmable rotary dresser

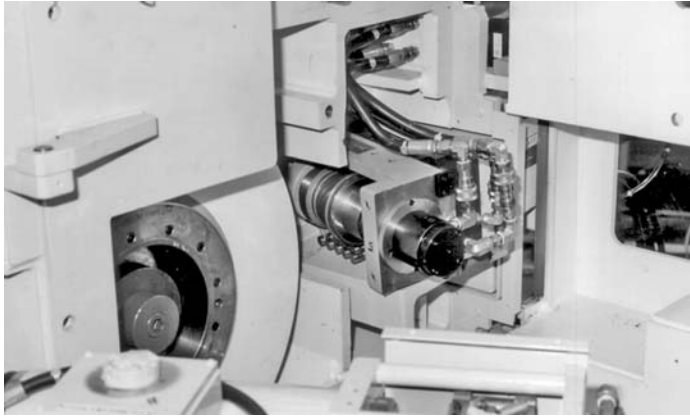


**FIGURE 15.60** Example of dresser mounted in angle-approach for a cylindrical grinder dressing alox wheels. (Courtesy of Landis Grinders. With permission.)

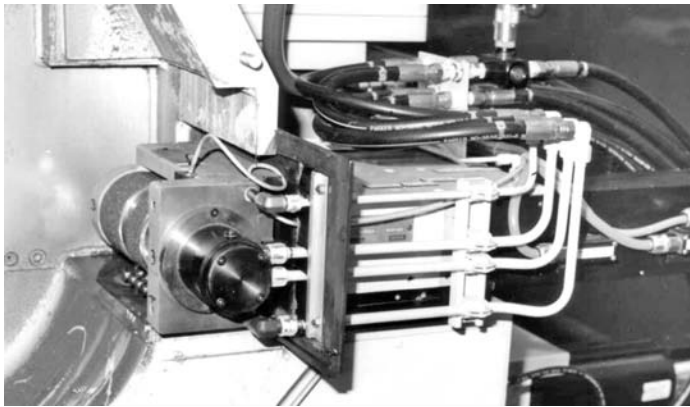


**FIGURE 15.61** Example of dresser mounted in rear of Landis 14RE centerless grinder. (Courtesy of Landis Grinder. With permission.)

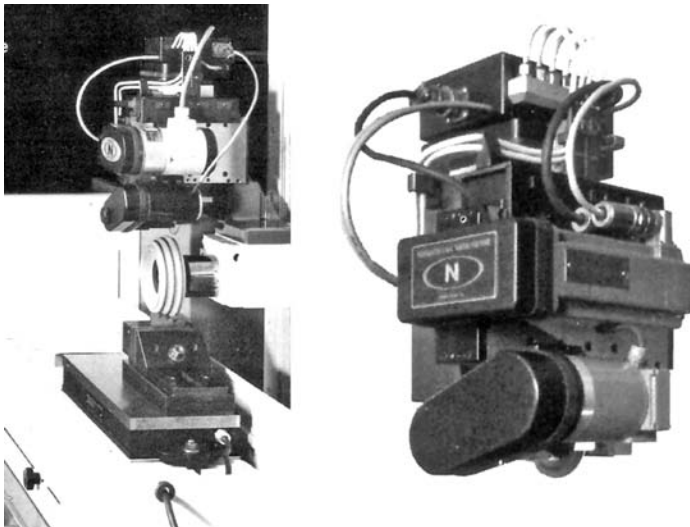


**FIGURE 15.62** Examples of online and offline CNC profiling dressers. (From Normac Grinders. With permission.)

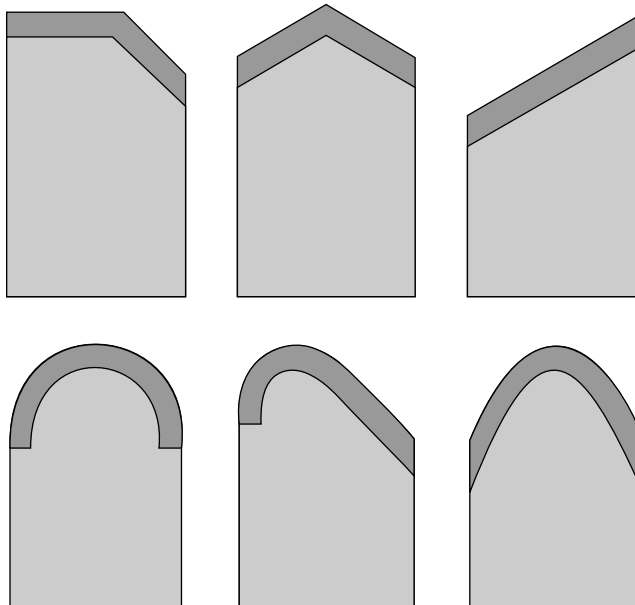


**FIGURE 15.63** ARJ 250 offline dresser. (Courtesy of Max Engineering, Howell, MI. With permission.)

systems with control of X, Y, and C axes in order to maintain the dresser perpendicular to the wheel face for very complex profiles (Figure 15.64) [Orion 1993]. Again, software development is the most critical factor in this technology especially where interpolation of involute forms is involved [Kelly and Smith 1993].

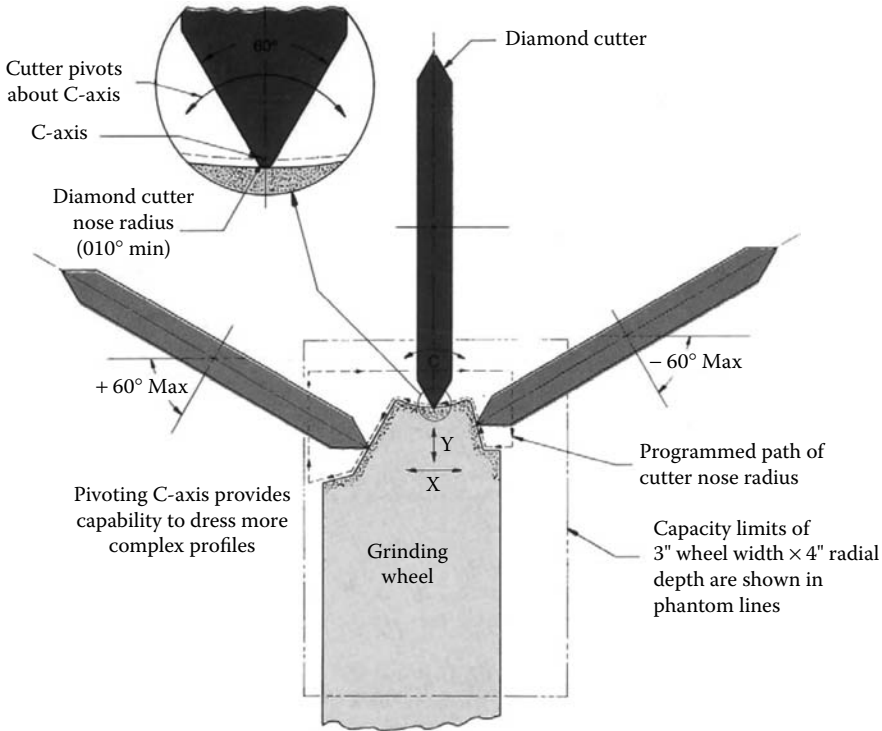


FIGURE 15.64 Orion engineering dresser [Division of Wendt Boart (with permission)] and profiling method.

## REFERENCES

- Acer. n.d. "High Precision Manual/Automatic Surface Grinder Supra Series." Acer Group, Taiwan. Trade Brochure.
- Aleyaasin, M., Whalley, R., and Ebrahimi, M. 2000. "Error Correction in Hydrostatic Spindles by Optimal Bearing Tuning." *Intl. J. Mach. Tools & Mfr.* 40, 809–822.
- Anon. 1999. "Hydrostatics Ready for Prime-Time Machining." *Tooling & Production*.
- Arnone, M. 1997. "Learning the Discipline of Precision Machining—Pt1 Machine Tool Construction, Motion Control." *Mfg. Eng.* 6, 58–64.
- Aronson, R. B. 1994. "Machine Tool 101: Part 3 Spindles & Motors." *Mfg. Eng.* 3, 49–54.
- Aronson, R. B. 1995. "Machine Tool 102: Spindles." *Mfg. Eng.* 3, 99–107, using Landis as reference source.
- Aronson, R. B. 1996. "Spotlight on Spindles." *Mfg. Eng.* 6, 59–66.
- Aronson, R. B. 1998. "Spindles for 2000 and Beyond." *Mfg. Eng.* 7, 106–113.
- Blohm. 1999. Motion #23, March 1999. Blohm Profimat RT p31. Schleifring. Blohm, Hamburg, Germany. Trade Brochure.
- Bryant. 1986. "Standard Wheelheads High-Frequency, Belt-Driven, Accessories High Speed Spindle Systems." Bryant Grinder Corp., Springfield, VT. Trade Brochure.
- Bryant. 1992. "High Speed Range Motorized Spindles." Bryant Grinder Corp., Springfield, VT. Private communication.
- Bryant. 1995. "The Ultraline UL2 High Speed Grinding Machine." Bryant Grinder Corp. Springfield, VT. Trade Brochure.
- Buderus. 1998. "Buderus CNC 335 Machining Center – for Machining Hardened Stock." Buderus Schleiftechnik Asslar, Germany.
- Chevalier. 2000. "FSG-H818CNC, B8818CNC, C1224CNC, High Precision CNC Profile Grinder." Chevalier Machinery, Santa Fe Springs, CA. Trade Brochure.

- Danobat. 1991. "CNC 585 High-Production and Universal Cylindrical Internal Grinding Machines." Danobat, Elgoibar, Spain. Trade Brochure.
- Danobat. n.d. "R1-100-CNC Universal and Cylindrical Grinders." Danobat, Elgoibar, Spain. Trade Brochure.
- Dayton, R. W. 1949. "Sleeve Bearing Materials." *Amer. Soc. Metals* 5-6.
- Den Hartog, J.P. 1956. *Mechanical Vibrations*. Fourth Edition, McGraw-Hill, New York.
- Drake. 2000. "GS:F Flute Grinder." Drake Manufacturing. Akron. Trade Brochure.
- Elb. 1997. "Micro-Cut A Production Machine for Precision-, Profile- & Creepfeed Grinding." Elb-Schliff Werkzeugmaschinen GmbH, Frankfurt, Germany. Trade Brochure.
- Elgin. n.d. "Elgin Traveling Head and Traveling Table Heavy Duty Roll Grinders." S&S Machinery, New York, Trade Brochure.
- EMAG. 1998. "VSC We Also Turn the Drilling Process on Its Head." Emag Maschinenfabrik GmbH, Salach, Germany. Trade Brochure.
- Ernst, A. 1998. *Digital Linear and Angular Metrology*. Verlag Moderne Industrie.
- Fortuna. n.d. "Automated Camshaft Grinding." Fortuna-Werke, Stuttgart Germany. Trade Brochure.
- Gamfior. n.d. "Use and Installation Handbook for Spindles and High-Frequency Spindles." Gamfior S.p.a. Torino, Italy. User Manual.
- Goldcrown. 1993. "GC Series—Precision Centerless Grinding Machines." Goldcrown Machinery (tradename of Landis Machine, Waynesboro). Trade Brochure.
- Hallum, D. L. 1994. "A Machine Tool Built from Mathematics." *American Machinist*, October.
- Hauser. n.d. "Hauser – Your Partner in Grinding." Usach Technologies Elgin, IL. Trade Brochure.
- IBAG. 1996. "IMTS'96 Debut – IBAG Introduces a New Generation of High Speed Machining with Active Magnetic Bearing Spindles." IBAG NA Div of Burnco, Milford, CT. Trade Brochure.
- Ives, D. and Rowe, W. B. 1987. "The Effect of Multiple Supply Sources on the Performance of Heavily Loaded Pressurized High-Speed Journal Bearings." Paper C199/87. *Proc. Inst. Mech. Eng.* (London), Tribology Conference, July.
- Junker. 1989. Junker Grinding Technology. "Quickpoint CNC O.D." Commercial Brochure.
- Junker. 1992. "A New Era in the Field of O.D. Grinding." Erwin Junker Maschinenfabrik GmbH, Nordrach, Germany. Trade Brochure.
- Junker. 1996. "Quickpoint CNC O.D. Single Point Grinding." Erwin Junker Maschinenfabrik GmbH, Nordrach, Germany. Trade Brochure.
- Junker. 1997. "ARJ 250 Dressing Machine." Erwin Junker. Trade Brochure.
- Kellenberger. n.d. "Kel-Universal Grinding Machine for the Highest Demands." Kellenberger Inc., Emslford NY. Trade Brochure.
- Kelly, P.W. and Smith, W. C. 1993. "CNC Grinding Wheel Dressing with Emphasis on Vitrified CBN." 5th International Grinding Conference. Cincinnati, OH SME.
- Kent. n.d. "Precision Surface Grinder KGS-250 Series." Kent Industrial Co, Taiwan. Trade Brochure.
- Kondo. 1998. "Machine Guide." Kondo Machine Works Co. Ltd., Toyohashi City, Japan. Trade Brochure.
- Koshal, D. and Rowe, W. B. 1980. "Fluid Film Journal Bearings Operating in a Hybrid Mode." *Trans. A.S.M.E. J. of Lubr. Technol.* Aug, 103, 558-572. Part 1—Theory, Part 2—Experiments.
- Koyo. n.d. "KVD Series Vertical Spindle Surface Grinder." Koyo Machine Ind., Osaka, Japan. Cat #KVD-9512ET. Trade Brochure.
- Koyo 2. n.d. "Centerless Grinder KC Series." Koyo Machine Ind., Osaka, Japan. Cat #KVD-H608ET. Trade Brochure.
- Landis. 1996a. "Landis® 3L Twin Wheelhead CNC Grinder for Camshafts and Crankshafts." Landis, Waynesboro. Trade Brochure.
- Landis. 1996b. "Landis® 2SE CNC Plain and Eccentric Diameter Shaft Grinders." Landis, Waynesboro. Trade Brochure.
- Landis. 1999. "Linear Motor Wheelfeeds Deliver High-Precision Camlobe and Crankpin Contour Grinding." *Wolftracks* 6, 1, 26. Unova, Cincinnati, OH.
- Lidkoping. 1998. "CG 300 High-Output Precision Centerless Grinding." Lidkoping Machine Tools AB, Lidkoping, Sweden. Trade Brochure #1677, issue 1.
- Magerle. n.d. "Magerle Grinding Systems." Schleifring- Gruppe, Uster Switzerland. Trade Brochure.
- Makino. n.d. "A77 Horizontal Machining Center." Makino Milling Machine Co. Ltd., Tokyo, Japan. Trade Brochure.
- Mattison. n.d. "Horizontal Surface Grinders." Mattison Rockford.



- Micron. n.d. "Twin Grip Centerless Grinder." Micron Machinery Co. Ltd., Yamagata, Japan. Trade Brochure.
- Montusiewicz, J. and Osyczka, A. 1997. "Computer Aided Optimum Design of Machine Tool Spindle Systems with Hydrostatic Bearings." *Proc. Inst. Mech. Eng.* 211 B, 43–51 (spindle design based on Landis-Gendron design).
- Monza. 1998. "Centerless Grinding Machines." Officine Monzeni Spa, Italy. Trade Brochure.
- Moore. 1996. "Moore Precision Jig Grinding Wheels 1996 Edition." Moore Tool Company, Bridgeport, CT. Trade Catalog.
- Moritomo, S. and Ota, M. 1986. "Present High Speed Machine Tool Spindles." *Bull. JSPE* 20, 1, 1–6.
- Nakamura, S. 1996. "High-Speed Spindles for Machine Tools." *Int. J. JSPE* 30, 4, 291–294.
- Nevue, S. R. 1993. "Design and Development of a Diamond Disk Form Truer for CBN Raceway Grinding." M.Sc. thesis, University of Connecticut, Storrs.
- Normac. 1998. "Profilers—CNC Grinding Wheel Profiles & Profiling Centers." Normac Precision Grinding Machines. Trade Brochure.
- Normac. 2000. "CBN-465 Super-Abrasive Wheel Profiling Center." Trade Advertisement.
- NTC. 1999. "Machine Tools for Automotive Industry." Nippei Toyama Corp, Tokyo, Japan. Trade Brochure.
- Okuma. 1998. "GC-Super33 Triple-Speed Cam Grinder." Okuma Corp, Aichi, Japan. Trade Brochure.
- Okuma. 2000. "GI-10N CNC Internal Grinder for Mass Production." Okuma Corp, Aichi, Japan. Trade Brochure.
- Okuma. n.d. "GP-34/44N Plain Cylindrical Grinders." Okuma Corp, Aichi, Japan. Trade Brochure.
- Orion. 1993. "Grinding Wheel Profile Dresser CNC 3 Axes." Orion Engineering Co. Trade Brochure.
- Paragon. n.d. "Universal Cylindrical Grinding Machine." Rong Kuang Machinery Co., Taichung, Taiwan. Trade Brochure.
- Precise. n.d. "Precise High Speed Spindle Systems." The Precise Corporation, Racine WI. Trade Brochure.
- Precitech. 1998. "Precitech Precision." Precitech Precision, Keene, NH. Trade Brochures, reference Nanoform® series of machines.
- Pride. n.d. "Ultra Precision Grinders." Pride Industries Inc., Champlin, MN. Trade Brochure.
- Rowe, W. B. 1967. "Experience with Four Types of Grinding Machine Spindle." *Advances in Machine Tool Design and Research*. Pergamon Press, Oxford and New York. Proceedings 8th International MTDR Conference.
- Rowe, W. B. 1969. "Hydrostatic Bearings." UK Patent 1, 170, 602. (Application 2 2072/66, 18 May 1966)
- Rowe, W. B. 1970. "Diaphragm Valves for Controlling Opposed Pad Hydrostatic Bearings." Proceedings of Tribology Convention, Brighton, and *Proc. Inst. Mech. Eng.* 184 (Pt-3L), 1–9.
- Rowe, W. B. 1983. *Hydrostatic and Hybrid Bearing Design*. Butterworths, Boston.
- Rowe, W. B. 1988. "Advances in Hydrostatic & Hybrid Bearing Technology." IME Tribology Group – Donald Julius Groen Prize Lecture. Proceedings of the Institution of Mechanical Engineers. London.
- Rowe, W. B. and Koshal, D. 1980. "A New Basis for the Optimization of Hybrid Journal Bearings." *Wear* 64, 3, 115–131.
- Rowe, W. B., Koshal, D., and Stout, K. 1977. "Investigation of Recessed and Slot-Entry Journal Bearings for Hybrid Hydrodynamic and Hydrostatic Operation." *Wear* 43, 1, 55–70.
- Rowe, W. B., O'Donoghue, J. P., and Cameron, A. 1970. "Optimization of Externally Pressurized Bearings for Minimum Power and Low Temperature Rise." *Tribology Int.* Aug, 153–157.
- Rowe, W. B., Xu, S. X., Chong, F. S., and Weston, W. 1982. "Hybrid Journal Bearings with Particular Reference to Hole-Entry Configurations." *Tribology Int.* 6 Dec, 15, 6, 339–348.
- Royal Master. 1996. "TG12X4 Centerless Grinder." Royal Master Grinders Inc., Oakland. Trade Brochure.
- Shigiya. n.d. "GPS-30 CNC Cylindrical Grinders." Shigiya Machinery Works, Hiroshima, Japan. Trade Brochure.
- Shigiya 2 n.d. "Cylindrical Grinders – General Catalog." Shigiya Machinery Works, Hiroshima, Japan. Trade Brochure.
- Slocum, A. H. 1992. *Precision Machine Design*. SME Publishing.
- Smith, G. T. 1993. *CNC Machining Technology 3 Part Programming Techniques*. Springer Verlag, New York. pp. 101–124.
- Sotiropoulos, N. 1998. "The Evolution of Grinding Machine Designs and a Look into the Next Generation." *Abrasives Mag.* June/July, pp. 8–10.
- Stadtfeld, H. J. 1995. *Gleason Bevel Gear Technology – Manufacturing, Inspection and Optimization. Collected Publications 1994/95*. The Gleason Works, Rochester, NY.

- Studer. n.d. "All about S21 Lean CNC." Studer Schleifring Group. Trade Brochure.
- THK. 1995. *LM System Ball Screws Catalog #75-1BE*.
- THK. n.d. *LM System – Linear Motion Systems Catalog #75EA*. THK, Yokyo, Japan. Trade Brochure.
- Tobias, S. A. 1965. *Machine Tool Vibration*. Blackie & Son, Glasgow and Bombay.
- Toyo. n.d. "T-235 CNC External Grinding Machine." Toyo Advanced Technologies Co. Ltd., Hiroshima, Japan. Trade Brochure.
- Toyoda. 1994. "GL3A GL3P CNC Cylindrical Grinder." Toyoda Machine Works, Japan. Trade Brochure.
- Toyoda. 1996. "GE3 CNC Cylindrical Grinder." Toyoda Machine Works, Japan. Trade Brochure.
- Tschudin. n.d. "Innovative centerless-grinding machines." Tschudin Systeme, Grenchen, Switzerland. Trade Brochure.
- TVMK. 1992. *Products Guide*. Toyoda Van Moppes Ltd., Okazaki City, Japan.
- Viking. 1998. "Design News Honors Milacron Chief Engineer." *Wolftracks* 5, 2, 12–16.
- Voumard. 2001. "Grinding Machines." Voumard Machines CO SA, La Chaux-de-Fonds, Switzerland. Trade Brochure.
- Waldrich Siegen. 1996. "Worldwide Partners for Intelligent Manufacturing Solutions." Waldrich Siegen, Burbach, Germany. Trade Brochure.
- Wang, X. P. et al. 2001. "Machine Tool Spindles and Active Magnetic Bearings." *Key Eng. Mater.* 202–203, 465–468.
- Weldon. 1991. "Innovative CNC Grinding Technology." Weldon Machine Tool, York. Trade Brochure.
- Weldon. 1994. "We've Struck Gold!" Weldon Machine Tool, York. Trade Brochure. (Note: Shear Damper® is a trademark of Aesop Inc.)
- Weldon. 1998. "P175 CNC Punch Grinder." Weldon Machine Tool, York. Trade Brochure (developed jointly with Tsugami, Japan).
- Yoshida, K. 2000. "Effects of Mounting Numbers of Surface Grinding Machines on Their Rocking Mode Vibrations." *Abrasives Mag.* Jun/Jul, pp. 21–23.
- ZRB. 1998. "ZRB Bearings." Harwington. Trade Catalog.



---

# 16 Surface Grinding

## 16.1 TYPES OF SURFACE GRINDING PROCESS

Terms for grinding were incorporated in an international dictionary for material removal processes by International Institution for Production Engineering (CIRP) after agreement between representatives of a number of countries including from United States, Europe, China, Japan, and Asia [CIRP 2005]. The dictionary gives terms for material-removal processes in French, German, and English and largely incorporates the terms employed in the German standard.

In this handbook, the terms employed are closely aligned with the CIRP dictionary. It allows some flexibility between the general terms derived from general cutting terminology and the more specific terms generally used in grinding. Figure 16.1 is taken from the CIRP dictionary and gives the commonly used symbols for wheel speed, workspeed, depth of cut, geometric contact length, and equivalent wheel diameter.

Surface-grinding processes are classified in Germany according to DIN 8589-11 in terms of the predominantly active grinding wheel surface position and of the table feed motion type. In the case of peripheral grinding, the grinding spindle is parallel to the workpiece surface to be machined. The workpiece material is mainly cut with the circumferential surface of the grinding wheel. In the case of face grinding with axial feed, in contrast, the grinding spindle is vertical to the workpiece surface. In this process, the workpiece material is mainly cut with the face side of the grinding wheel. The table feed motion can be translational or rotary. Figure 16.2 shows the classification of surface-grinding processes according to DIN 8589-11 [DIN 8589]. The reader will find that alternate symbols are used for some terms. Three examples are as follows:

Parameter	Acceptable Symbols			
Grinding wheel speed	$v_s$	or	$v_c$	
Workspeed	$v_w$	or	$v_{ft}$	
Width of grinding	$b_w$	or	$a_p$	or $b_{s,eff}$

## 16.2 BASICS OF RECIPROCATING GRINDING

According to DIN 8589-11, reciprocating grinding is a peripheral longitudinal grinding process with a back-and-forth feed motion, in which the feed motion takes place gradually in small steps with a relatively high feedrate [DIN 8589].

### 16.2.1 PROCESS CHARACTERIZATION

Reciprocating grinding is used for generating plain surfaces of usually large lateral dimensions. The grinding spindle is parallel to the workpiece surface to be machined, the workpiece material being cut mainly with the circumferential side of the grinding wheel. The grinding wheel is fed orthogonally to the workpiece surface by the amount,  $a_p$ , relatively to the workpiece (see Figure 16.3). This direction is in the axial direction with respect to the wheel spindle.

#### 16.2.1.1 Real Depth of Cut

The real depth of cut,  $a_e$ , is the feed relative to the workpiece surface. It is important to recognize that the real depth of cut is not the same as the set depth of cut. This is due to deflections of the

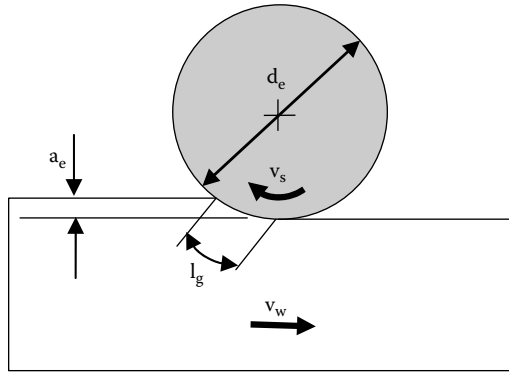


FIGURE 16.1 Wheel speed, workspeed, depth of cut, equivalent grinding wheel diameter, and geometric contact length in grinding. (After CIRP 2005. With permission.)

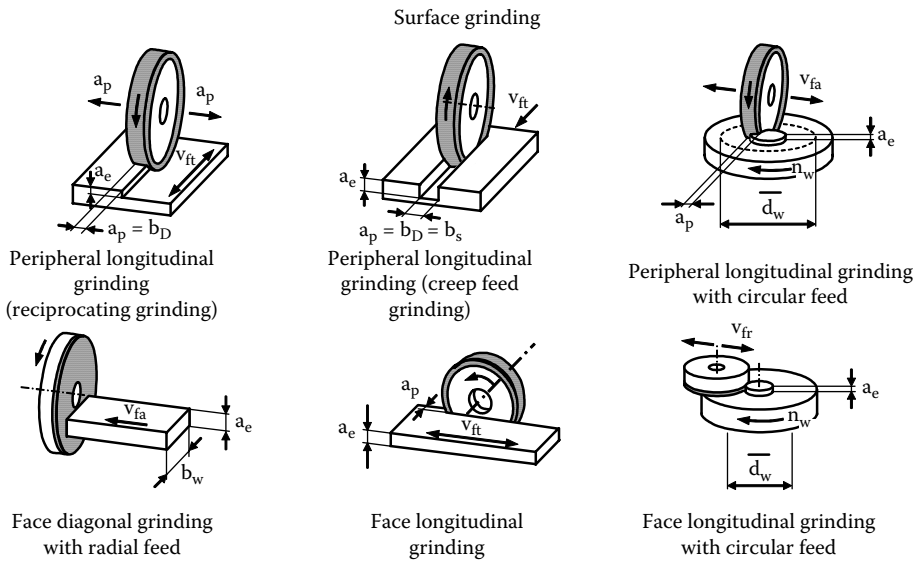


FIGURE 16.2 Classification of surface grinding processes. (After DIN 8589. With permission.)

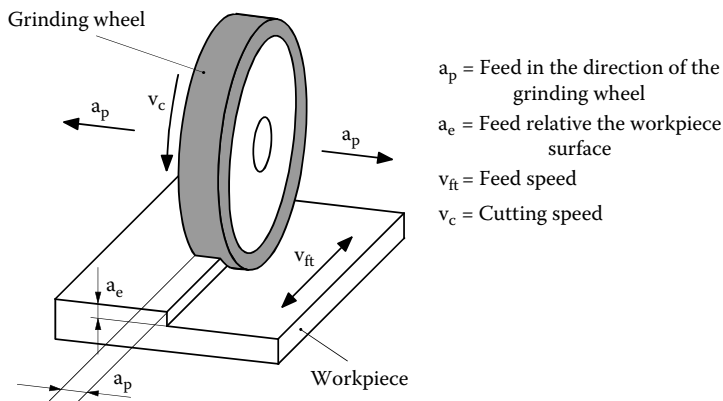


FIGURE 16.3 Longitudinal peripheral grinding.

grinding wheel, of the machine, and due to wheel wear. Grinding performance should always be related to the real depth of cut, otherwise the results will depend very strongly on the particular grinding wheel and the particular grinding machine setup.

In the case of reciprocating grinding, material removal typically takes place at low infeed and a high feedrate with a high number of passes with changing tool engagement and at constant peripheral speed and rotational direction of the grinding wheel. The alternation of up- and down-grinding is inevitable.

### 16.2.1.2 Speed Ratio

As a consequence, the sign of the speed ratio alternates, also due to directional change of feedrate,  $v_{ft}$ , during grinding with synchronous and counterrotation.

$$q = \frac{v_c}{v_{ft}}$$

### 16.2.1.3 Specific Removal Rate

The specific material removal rate  $Q'_w$  for reciprocating grinding is calculated from the product of infeed  $a_e$  and feedrate  $v_{ft}$ :

$$Q'_w = a_e \cdot v_{ft}$$

### 16.2.1.4 Upcut and Downcut Grinding

Differences can be traced back to the progression of cutting-edge engagement. In the case of down grinding, the uncut chip thickness increases directly to the maximum value after the cutting edge is engaged in the material and continuously drops after the cutting edge exits the workpiece. In the case of up-grinding, cutting-edge engagement starts nearly tangentially to the already machined workpiece surface; the uncut chip thickness continuously increases to the maximum value until the cutting edge exits the workpiece. This has consequences for grinding forces, lubrication, and wheel wear particular for deep cuts. These effects are discussed below under creep grinding.

### 16.2.1.5 Nonproductive Time

During machining, there is a considerable amount of nonproductive time. This depends on table speed and acceleration and the nongrinding time can be a multiple of the actual grinding time, that is, the contact time between grinding wheel and workpiece, because of the grinding wheel running beyond the workpiece, and also because of the reversing table motion.

## 16.2.2 INFLUENCES OF GRINDING PARAMETERS ON GRINDING PERFORMANCE

Kinematic parameters and process parameters, as well as the work results, are used for surface grinding process assessment. Table 16.1 shows the relevant assessment values.

### 16.2.2.1 The Influence of Cutting Speed (Wheel Speed)

In the case of reciprocating grinding, the contact length between workpiece and wheel is small and the grinding forces are relatively small. There are only a few cutting edges engaged at the same time; the force on individual cutting edges is accordingly high. By increasing the cutting speed at

**TABLE 16.1**  
**Kinematical and Process Parameters and Work Result in the Surface Grinding Process [Uhlmann 1994(a)]**

Kinematic parameters	Effective cutting edge number $N_{SkinA}$
	Present cutting edge number $N_{Sact}$
	Average chip length $\bar{h}_{ch}$
	Average material removal rate $\bar{l}_{ch}$
	Blunting coefficient $\epsilon_a$
Process parameters and work result	Surface roughness $R_z$
	Single grain force $f_g$
	Grinding force $F_c$
	Contact zone temperature $\vartheta_K$
	Workpiece fringe area temperature $\vartheta_z$
	Edge wear area $A_{sw}$
	Radial wear $\Delta r_s$

Source: From Uhlmann 1994a. With permission.

constant feedrate, the average chip thickness and length are reduced, making the total grinding forces decrease. The thermal stress of tool and workpiece, however, grows if the cutting speed is increased.

### 16.2.2.2 The Influence of Feedrate (Workspeed)

Alongside infeed (i.e., depth of cut), the feedrate considerably affects the total machining time in reciprocating grinding. Increasing the feedrate results in higher average chip thickness and length, and thus in an increase of grinding forces and thermal stress. A repeated start of the grinding wheel to the workpiece and the punctual impact stresses linked with it cause an increase in grinding wheel wear. The surface roughness of the workpiece grows with increasing feedrate. In metal working, feedrates in the range of 25 to 30 m/min are accepted [Spur and Stoelele 1980].

### 16.2.2.3 The Influence of Infeed

Infeed and feedrate (workspeed) crucially determine the total machining time in reciprocating grinding. An increase of infeed increases grinding forces and thermal stress. The workpiece surface roughness decreases with a higher number of engaged cutting edges. In low removal rate grinding, maximum infeeds are recommended in the range of 5 to 10  $\mu\text{m}$  [Spur and Stoelele 1980]. Larger infeeds can be achieved in creep grinding and high-removal-rate grinding.

### 16.2.2.4 The Influence of the Interrupted Cut

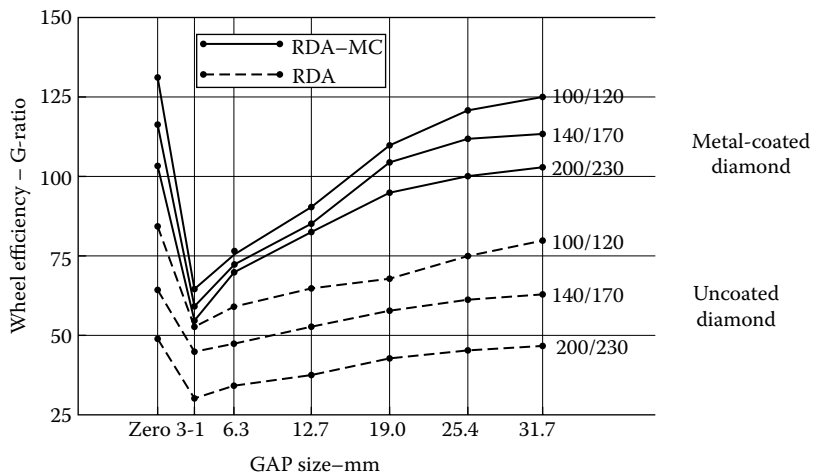
As a result of alternating up- and down-cut grinding, and of frequent approaches to the workpiece, high alternating and impact stresses occur at the grinding wheel in reciprocating grinding. Appropriate grinding wheels and bond materials must be chosen to cope with the additional wear caused by this effect. The abrasive grain must be suitable for alternating and impact stresses and the bond must be capable of holding the abrasive grains firmly in the matrix, even under these conditions. If the bond does not meet this requirement, there will be increased grinding wheel wear and poor surface quality of the workpiece. With higher process forces and temperatures, the risk of displacements between tool and workpiece increases, having negative effects on the work result and on the wheel wear.

### 16.2.2.5 Reciprocating Grinding without Cross-Feed

Reciprocating grinding without cross-feed is employed either for slot grinding or for generating a profile with a preformed wheel. The dresser is usually table mounted and for a conventional wheel may consist either of a simple single point or form block at the end of the slide or of a driven spindle with a form diamond roll. This latter approach is quite common for burn-sensitive components such as nickel-based aerospace components on older grinders using both conventional and plated cubic boron nitride (CBN) wheels.

### 16.2.2.6 Multiple Small Parts

Care should be taken when laying out parts on the table especially when large numbers of small parts are ground together. Where possible, the parts should be butted together. Gaps between parts will cause dropoff of the wheel leading to vibration, force variations, and the other negative effects of an interrupted grind. For example, Hughes and Dean [n.d.] (Figure 16.4) show the impact of spacing when grinding tungsten carbide with resin diamond wheels. Wheel life for a given wheel grade could be varied by a factor 3 depending on the spacing between parts. In the example shown, grit retention was improved by using metal-coated diamond.



**Test parameters**

- Machine: Jones & Shipman model 540 tool room surface grinder
- Wheel type/size: D1A1  $5 \times \frac{1}{4} \times 1\frac{1}{4}$  in.
- Wheel speed: 3,650 rev/min
- Wheel peripheral speed: 24.4 m/s
- Downfeed: 0.025 mm per pass
- Total downfeed per test: 3.0 mm
- Cross-feed: 1.0 mm per traverse reversal
- Table traverse speed: 16 m/min
- Specimen material: ISO grade P 20 tungsten carbide
- Specimen size: 4 pieces each  $101.6 \times 25.4$  mm
- Total specimen area:  $4 \times 25.8 \text{ cm}^2 = 103.2 \text{ cm}^2$
- Coolant: water + Bryto 5 (100:1)
- Coolant flowrate: 3 liters/min
- Number of tests per wheel-gap change: at least 3

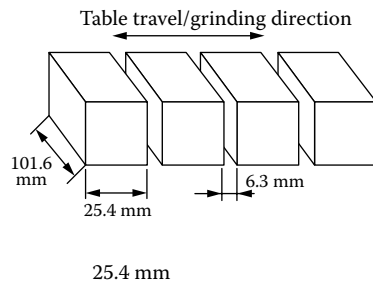


FIGURE 16.4 The effect of part spacing on G-ratio.



### 16.2.3 ECONOMICS

Low thermal, static, and dynamic stresses are advantages of reciprocating grinding, in contrast to creep feed grinding. They allow for a more simple machine design in terms of drive capacity, rigidity, and ancillary units, thus accounting for lower purchase and operating costs. The generally high total machining times are a disadvantage for the workpiece, as well as higher surface roughness of the workpiece (being usually a functional surface), in contrast to creep feed grinding. Considerable secondary processing times are generated by the grinding wheel passing over the workpiece and by the reversing movement of the table.

## 16.3 BASICS OF CREEP GRINDING

### 16.3.1 INTRODUCTION

By means of creep feed grinding, or creep grinding as it is more concisely termed, considerable material-removal rates were achieved with high surface qualities for the first time in the early 1950s. In order to harness the potentials of this grinding process, machines, grinding tools, and grinding technologies were developed [Uhlmann 1994a]. DIN 8589, part 11, defines that in the case of creep feed grinding, the infeed depth must be relatively large and the feedrate accordingly low [DIN 8589]. An extensive description of the process is given by Andrews, Howes, and Pearce [1985].

### 16.3.2 PROCESS CHARACTERIZATION

Peripheral longitudinal grinding (creep feed grinding) forms a negative profile of the grinding wheel in the workpiece, the total grinding stock being cut in one or only a few passes. In this method, the grinding spindle is parallel to the workpiece surface to be machined, the workpiece material being mainly cut with the grinding wheel circumferential side. The grinding wheel is fed orthogonally to the workpiece surface by the amount  $a_e$  relatively to the workpiece (Figure 16.5).

Creep grinding is usually characterized by infeeds  $a_e$  larger than 0.5 mm and feed rates  $v_{ft}$  smaller than 40 mm/s [Uhlmann 1994b]. In metal cutting, infeeds  $a_e$  in the range of 0.1 to 30 mm and feedrates  $v_{ft}$  in the range of 25 to 45 m/s are normal. In contrast to reciprocating grinding, the sign of the speed relation  $q$  does not change.

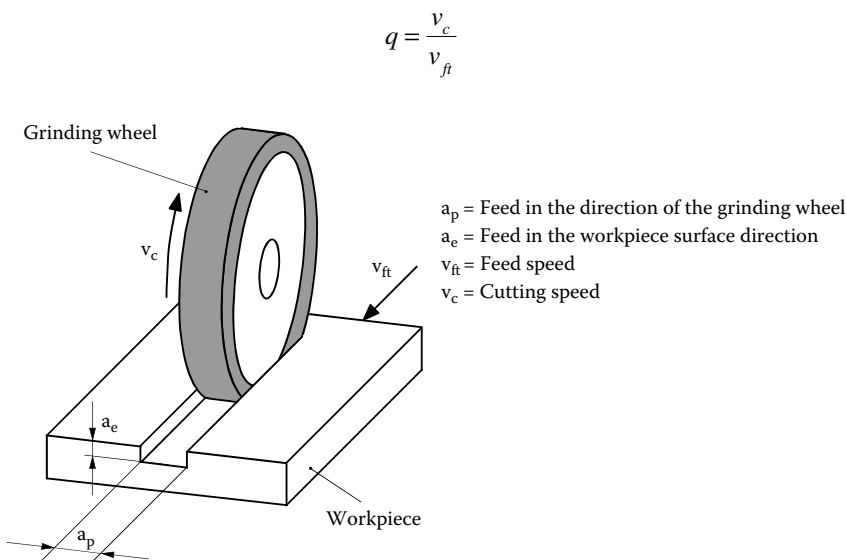


FIGURE 16.5 Creep feed grinding.

If grinding takes place in synchronous rotation,  $q$  is positive; in counterrotation, however, the  $q$  is negative. Through the finishing in one run, the tool-workpiece contact time approximately equals the total machining time. There are no downtimes during the grinding process, as in the case of reciprocating grinding. In the case of machining with diamond and boron nitride grinding wheels, grain protrusion, too, can be a difference between creep feed grinding and reciprocating grinding. If the infeed is larger than the grain protrusion from the bond, the process is called creep feed grinding.

All grinding processes, in which the wheel peripheral speeds are above the usual values of 35 to 45 m/s, can be classified as high-speed grinding. High-speed grinding can be used for the machining of materials such as steels, tungsten carbides, plastics, and ceramics with adapted grinding wheel specification. The advantages of high-speed grinding are higher surface qualities, shorter machining times, little tool wear, and low grinding forces [Minke and Tawakoli 1991].

### 16.3.3 HIGH-EFFICIENCY DEEP GRINDING

High-performance deep grinding, with increased wheel peripheral speed and increased feedrate, is a special case requiring a cooling lubricant supply system adapted in terms of pressure and volume flow capability [Rowe and Jin 2001]. Application limits for high-performance grinding result from wheel safety requirements, that is, the maximum admissible peripheral speeds for grinding wheels. These are approximately 125 m/s for grinding wheels with resin and vitrified bond. In the case of wheel peripheral speeds higher than 125 m/s, mainly CBN grinding wheels with sintered metal or plated metal bond in a metallic base body are used for steel materials. The advantages of high-speed grinding are higher surface quality, shorter machining times, lower wheel wear, and low grinding forces.

Table 16.2 compares typical process values for reciprocating, creep, and high-performance grinding [Minke and Tawakoli 1991]. In the case of creep and high-performance grinding, infeeds in the mm-range reach maximum values of approximately 30 mm. The specific material removal rates in the case of creep feed grinding differ within the range of the conventional values of  $Q'_w = 3$  to 5 mm<sup>3</sup>/(mm/s) [Minke and Tawakoli 1991].

Due to the higher grinding forces in high-performance grinding processes, more demanding requirements are placed on the grinding machine and machine system:

- Rigid concrete or superior stiff structural design
- Robust guiding elements
- Effective spindle drives and mountings
- Use-friendly cooling lubricant and cooling system
- Adapted grinding tools and dressing equipment
- Efficient control equipment

**TABLE 16.2**  
**Process Parameters of Reciprocating, Creep, and High-Performance Grinding Processes**

Set Values	Infeed	Feedrate	Cutting Speed	Specific Material Removal Rate
Process	$a_e$	$v_f$	$v_c$	$Q'_w$
Reciprocating grinding	0.001–0.05 mm	1–30 m/min	20–60 m/s	0.1–10 mm <sup>3</sup> /mm/s
Creep feed grinding	0.1–30 mm	0.05–0.5 m/min	20–60 m/s	0.1–15 mm <sup>3</sup> /mm/s
High-performance grinding	0.1–30 mm	0.5–10 m/min	80–200 m/s	50–2,000 mm <sup>3</sup> /mm/s

### 16.3.4 THE INFLUENCE OF THE SET PARAMETERS IN CREEP FEED GRINDING

The most important setting parameters in creep grinding are cutting speed,  $v_c$ , tangential feedrate,  $v_{ft}$ , and infeed,  $a_e$ . Either up- or down-cut grinding can be set in creep feed grinding. The influence of the setting parameters on the work result will be explained below.

#### 16.3.4.1 The Influence of Cutting Speed $v_c$

Due to the large contact length and large infeed in creep feed grinding, grinding forces tend to be high, which, in turn, lead to high thermal stress in the working zone. High grinding forces lead to machine displacements and thus to dimensional inaccuracies on the workpiece. The grinding forces affecting the machine system can be reduced by minimizing the forces occurring at the single cutting edge during the grinding process. This can be realized by increasing the wheel speeds, which produces a smaller chip thickness and a lower number of active cutting edges. Furthermore, increasing the wheel speed generally results in a reduction of grinding wheel wear and in a lower surface roughness of the workpiece.

#### 16.3.4.2 The Influence of Infeed, $a_e$ , and Feedrate, $v_{ft}$

Machining time in the grinding process is crucially influenced by the infeed,  $a_e$ , and the feedrate,  $v_{ft}$ . An increase of the specific material removal rate by increasing the infeed or the feedrate involves higher grinding forces and elevated thermal stress due to a higher chip thickness [Uhlmann 1994a].

#### 16.3.4.3 The Influence of Dressing Conditions

In the case of creep feed grinding, continuous conditioning may be required during the grinding process. Continuous dressing takes place by separate grinding and profiling devices on the grinding machine. This procedure ensures that the grinding wheel has the necessary sharpness over the whole engagement time, has the desired profile, and sufficient chip spaces are available [Spur, Uhlmann, and Brücher 1993]. A continuously dressed grinding wheel allows for low or constant grinding forces and process temperatures, and favorable wear behavior in the creep feed grinding process. The surface roughness and the condition of the subsurface of the workpiece are positively influenced with respect to the work result.

#### 16.3.4.4 The Influence of Grinding Wheel Specification

Alongside the fully engaged cutting edges, there are additional grain tips engaged, situated deeper, which do not contribute to chip formation but only elastically and plastically deform the workpiece. In contrast to processes with small contact lengths, this occurrence must not be neglected in the case of creep feed grinding because of the large contact length. The friction in the working zone rises, causing higher thermal stress on the workpiece and the tool, as well as higher requirements on the tool drive.

Influencing parameters for the number of active cutting edges are

- Cutting speed,  $v_c$
- Tangential feedrate,  $v_{ft}$
- Infeed,  $a_e$
- Grinding agent concentration (grain number)
- Grinding agent geometry (grain size)

In order to avoid increasing the already high friction in creep feed grinding by additional friction and squeezing processes of the removed chips on workpiece and tool, the safe evacuation of the chips requires sufficient porosity of the bond structure (pores/chip spaces). This additionally counteracts

the clogging of the grinding wheel. High thermal stress requires the transportation of sufficient cooling lubricant to the working zone, which is also aided by larger porosity in the grinding wheel bond. Grinding wheels for creep grinding should be softer than for reciprocating grinding for the same task.

#### 16.3.4.5 The Influence of Up- and Down-Cut Grinding

The process variants up- and down-grinding can be set in the case of creep feed grinding, using the favorable alternative for the particular machining conditions. If the vectors of the cutting and feed motion have the same direction at the contact point of abrasive grain and material, the process is defined as down-grinding. In the case of up-grinding, the vectors of the cutting and feed motion show in different directions [Schleich 1980]. The effect of up-cut or down-cut grinding is discussed further below.

Because of the processes at the cutting edge engagement and the consequent chip formation, down-grinding usually provides smaller surface roughnesses and thus higher-quality surfaces in the case of ductile materials. Due to better surface qualities, lower wear, and smaller grinding forces, down-grinding is recommended and can be traced back to more efficient chip formation of the single cutting edges approaching the workpiece surface with nearly maximum chip thickness. In the case of machining with small material removal rates, this process variant has only little positive effect on the maximum contact zone temperature. In the case of up-grinding, the contact zone temperature drops faster because of better cooling lubricant conditions. There are definitively lower contact zone temperatures during machining with counter rotation with large infeed, high feedrates, and, at the same time, high cutting performances, since the efficiency of cooling lubrication has significant effect here [Uhlmann 1994a].

The machining of metallic materials with creep feed grinding offers a number of advantages in contrast to reciprocating grinding [Spur 1989]:

- Reduced grinding time by 50% to 80% through higher cutting performance
- Lower edge wear leading to good profile stability
- Superior surface qualities
- Smaller single grain forces
- Lower temperatures in the contact zone

#### 16.3.4.6 Process

The chip thickness and thus the cutting force at the single grain are smaller during creep feed grinding than during reciprocating grinding. Additionally, there are no repeat impact loads on the grinding wheel, so that the abrasive grains can be held longer by the bond matrix before the grains are broken out. On the other hand, thermal stress and the total cutting forces are higher (Figure 16.6).

In the case of creep feed grinding, the higher cutting forces require significantly higher static and dynamic rigidity and higher drive performance of the grinding machine and its ancillary units than necessary in the case of reciprocating grinding. The high thermal stress during creep feed grinding does not only represent a high load for tool and grinding machine, but also damages the workpiece material causing cracks and structural changes. Such structural changes do not occur or only to a small extent in the case of reciprocating grinding, being removed with the subsequent pass (Table 16.3).

In the case of reciprocating grinding, the contact zone of tool and workpiece can be easily supplied with cooling lubricant owing to the short length of the contact zone. In the case of creep feed grinding, a much longer contact zone must be wetted, and, because of higher friction, more heat must be discharged. Therefore, the cooling lubricant must be fed with high pressure and volume flow-through nozzles and conducting equipment with defined shapes [Schleich 1980].

	Creep feed grinding	Reciprocating grinding
Infeed $a_e$ (mm)	0.5–30	0.001–0.05
Feed rate $v_{ft}$ (mm/s)	0.1–40	100–500
Speed ratio $q$ (-)	3000–300 000	40–400
Geometrical contact $l_g$ (mm)*	14–110	1.4–4.5
Number of grinding passes	Usually 1	Function of the overall infeed

\*Radius of the grinding wheel  $r_s = 200$  mm

FIGURE 16.6 Differences between reciprocating and creep feed grinding.

**TABLE 16.3**  
**Differences between Reciprocating Grinding and Creep Feed Grinding**

	Reciprocating Grinding	Creep Feed Grinding
Feedrate	High	Low
Infeed	Low	High
Number of tool passes	High	1 (or a few)
Up- and down-grinding	Periodically changing	Adjustable
Secondary processing times	High	Low
Average chip thickness	Larger	Smaller
Average chip length	Smaller	Larger
Average grinding temperature/thermal stress	Lower	Higher
Grinding forces/cutting forces	Lower	Higher
Vertical shape deviation	Smaller	Larger
Surface roughness	Larger	Smaller
Radial wear	Larger	Smaller
Total wear on the grinding wheel	Smaller	Larger
Inclination to chatter	Larger	Smaller

#### 16.3.4.7 Work Results

In creep feed grinding, surface roughnesses are much smaller due to the engagement of a higher number of cutting edges and due to smaller feedrates than in the case of reciprocating grinding. Since the functional surface properties of a workpiece are often important, creep feed grinding has a clear advantage here. This can be traced back to the kinematics of creep grinding. Those grain cutting edges, which do not completely chip off due to their position in the bond or to advanced wear, through plastic deformation, contribute to the smoothing of the workpiece. On the other hand, there are higher forces and thermal stresses that require much higher static and dynamic rigidity and effective driving and ancillary units of the grinding machine. In the case of reciprocating grinding, the number of cutting edges participating in the cutting process is higher in relation to the material volume. Based on the short contact time of grain and workpiece, a different surface is generated. The plastic curl-ups on the workpiece are, unlike in creep feed grinding, not smoothed by the simultaneously engaged neighboring cutting edges but pushed away into neighboring grooves by subsequent chipping processes. This results in temporary coverage of cut grooves by plastically deformed material. These curl-ups additionally increase surface roughness. Due to the stress during the process, these curl-ups do not correspond to the basic material, and there is no material cohesion as in the original state any more. Thus, there is an increased risk of particles detaching from the surface during subsequent use, for example, in the case of sliding bearing surfaces often machined by grinding, and result in component breakdown due to friction and squeezing [Schleich 1980].

#### 16.3.4.8 Grinding Wheels

The selection of the abrasive is mainly based on the properties of the workpiece material and on the secondary conditions during the grinding process, for example, the use of cooling lubricant. The larger creep feed grinding forces and thermal stresses in the working zone, however, require an adjusted bond of the grinding wheel.

In the case of reciprocating grinding, the wheel must absorb the impact stress due to the changing engagement of synchronous and counter rotation and to the high grinding forces at the single grain. In the case of creep feed grinding, impact and single grain forces are lower. In this case, high thermal stresses must be absorbed in the working zone.

A further aspect influencing wheel selection is the chip shape, which is crucially affected by the workpiece material. In the case of reciprocating grinding, there are usually short, thick chips. In contrast, chips are relatively thin and long in the case of creep feed grinding [Uhlmann 1994a]. The combination of abrasive grain/bond must be selected in a way that chips can be easily evacuated from the working zone without additional friction and squeezing on the workpiece and/or clogging of the grinding wheel. Therefore, there must be sufficient chip space available. An open structure of the grinding wheel allows for a significant increase of flowrate in the working zone through the cooling lubricant transport in the pores. This results in an enhanced heat transport, which is of special significance in the case of creep feed grinding.

#### 16.3.4.9 Grinding Wheel Wear

Grinding wheel wear parameters are radial and edge radial wear, the latter usually being much higher during reciprocating and creep feed grinding than radial wear. Edge radial wear is usually higher in the case of reciprocating grinding than during creep grinding [Saljé and Damlos 1983].

The high wear during reciprocating grinding can be partially traced back to the short contact length. The shorter the tool–workpiece contact length at a constant material removal rate, the higher the stress for the single abrasive grain, since there is less time for cutting the material volume than

in creep feed grinding. The material removal rate per grain increases, and thus the sum of cutting forces per grain results in an increased wear. A further factor is the high-impact stresses upon the repeated engagement in the workpiece after reversion. When, for instance, a high-speed steel was ground with an aluminum oxide grinding wheel, the tenfold increase of passes led to a 28% wear growth under otherwise identical conditions [Schleich 1980].

The total grinding forces, however, are usually lower during reciprocating grinding than during creep grinding. While a permanent effective self-sharpening takes place during reciprocating grinding, the large contact length during creep grinding leads to an increasing number of engaged grain cutting edges, the forces rising linearly as a function of the grinding time.

The two processes are further differentiated by the length of grinding path per wheel rotation. Due to the longer grinding path during reciprocating grinding, this process is clearly more sensitive to the grinding wheel out-of-roundness. Radial deviations are characterized by long waves on the workpiece. When certain deviations occur, they usually grow faster in the case of reciprocating grinding [Uhlmann 1994a].

### 16.3.5 REQUIREMENTS FOR CREEP FEED GRINDING MACHINES

The technology of creep feed grinding places special requirements on the design of creep feed grinding machines. This relates to the machine frame and guide ways, feed and grinding spindle drives, and cooling lubricant and dressing devices. Due to higher forces, machine elements such as machine bed, support, table, grinding head, and guide ways are to be designed much more rigidly for creep grinding than for reciprocating grinding machines [VDI 3390]. Furthermore, due to higher thermal stresses, measures must be taken in order to avoid the axial shift of the grinding spindle in the process. Alongside the process-friendly dimensioning of the machine elements, their relative position to each other is also significant. Thus, the force flow through the system should be short and directly counteract geometrical defects on the workpiece. Slide ways, feed drives, and transmission elements must be designed in a way that impact-free motions and positioning accuracies are independent of the selected feedrates and occurring forces.

Grinding spindle drives must be infinitely variable and realize a wide range of cutting speed. Optimized grinding data must be kept constant during the process. In the case of conventional grinding wheels, the rotational speed must be adjusted automatically in order to work with a constant cutting speed in the case of wear-related grinding wheel diameter loss. In favor of minimizing heat propagation in the workpiece, cooling lubricant should be fed synchronously as well as in contrarotation to the grinding wheel.

### 16.3.6 TYPICAL APPLICATIONS

The advantages of creep feed grinding are shorter machining times, lower surface roughness, improved profile, and dimensional accuracy [Minke and Tawakoli 1991]. In industrial mass production, there are two fields of application of creep feed grinding in which high cutting performance and high component quality are required. In mass production, creep feed grinding is used to grind deep grooves with mostly parallel side walls and profiles in tight and deep profile contours and/or for difficult-to-grind materials. In the case of rotor manufacture, up to 30-mm deep slots are ground into the solid, mainly hardened material. A second field of application for creep feed grinding is turbine blade manufacture from nickel-base superalloys. In the case of these workpieces with different profiles, high requirements are placed on geometrical accuracy and surface quality. Moreover, highest demands are made on the absence of heat-influenced workpiece subsurface layers. Creep feed grinding satisfies these work conditions concerning high removal rates and surface quality within the limitations of quickly rising contact zone temperatures [Werner and Minke 1981].

### 16.3.7 ECONOMICS OF CREEP FEED GRINDING

Lower grinding times and high achievable surface quality with a high removal rate argue for creep feed grinding in contrast to reciprocating grinding. In the range of medium to high batches, creep feed grinding is, therefore, more cost-efficient than reciprocating grinding. Grinding machines and ancillary units tend to be expensive resulting from higher thermal, statical, and dynamic stresses and consequent requirements for special machine designs.

The choice of adequate grinding machines is a crucial prerequisite to completely utilize the potential of creep feed grinding. Requirements for economic creep feed grinding of ceramics are as follows [Uhlmann 1994a]:

- High process forces require static and dynamic rigidity, high spindle drive performance, load-independent rotational speed.
- High process temperatures and large contact lengths require cooling lubricant pumps with increased volume flow and pressure, adapted cooling lubricant nozzles.
- High-dimensional accuracy and high forces require high-precision and rigid bearings and guidances, shock-free and precise drives.
- High concentricity and adjustable grinding wheel topography require integrated auxiliary conditioning equipment for diamond grinding wheels.

### 16.4 BASICS OF SPEED-STROKE GRINDING

An innovation of surface grinding driven by the Japanese in the 1980s is a process called Speed Stroke Grinding that involves very high table speeds of 50 to 100 m/min and shallow depth of cuts of the order of 1  $\mu\text{m}$  or less. The interest was initially centered around improved die manufacture and achieving high stock removal rates grinding ceramics while keeping the depth of cut in the ductile grind regime. The earliest work was carried out on Elb grinders using toothed belt drives [Yuji 1990] and on Okamoto grinders [Akinori 1992]. High helix pitch ballscrews and, more recently, the introduction of linear motors have greatly expanded the scope in terms of speed, and acceleration and deceleration rates.

The benefits and drawbacks of the process can be understood by going back to the basic equations relating uncut chip thickness,  $h_{cu}$ , to specific grinding energy,  $e_c$ , force/grit,  $f_g$ , surface finish,  $R_t$ , and mean surface temperature ( $\theta$ ):

$$h_{cu} = \sqrt{\frac{v_w}{v_s} \cdot \frac{1}{C \cdot r} \sqrt{\frac{a_e}{d_e}}}$$

$$e_c \propto \frac{1}{h_{cu}^n} \propto \sqrt{\frac{v_s}{v_w} \cdot C \cdot r \cdot \sqrt{\frac{d_e}{a_e}}}$$

$$R_t \propto \frac{h_{cu}^{4/3}}{a_e^{1/3}}$$

$$f_g \propto h_{cu}^{1.7}$$

$$T_{\max} \propto \sqrt{a_e \cdot v_s \cdot C \cdot r}$$

For a constant stock removal rate, chip thickness increases with workspeed. Consequently, specific energy decreases as table speed increases for constant removal rate, depth of cut, and surface temperature fall, while surface roughness increases and force/grit increases.



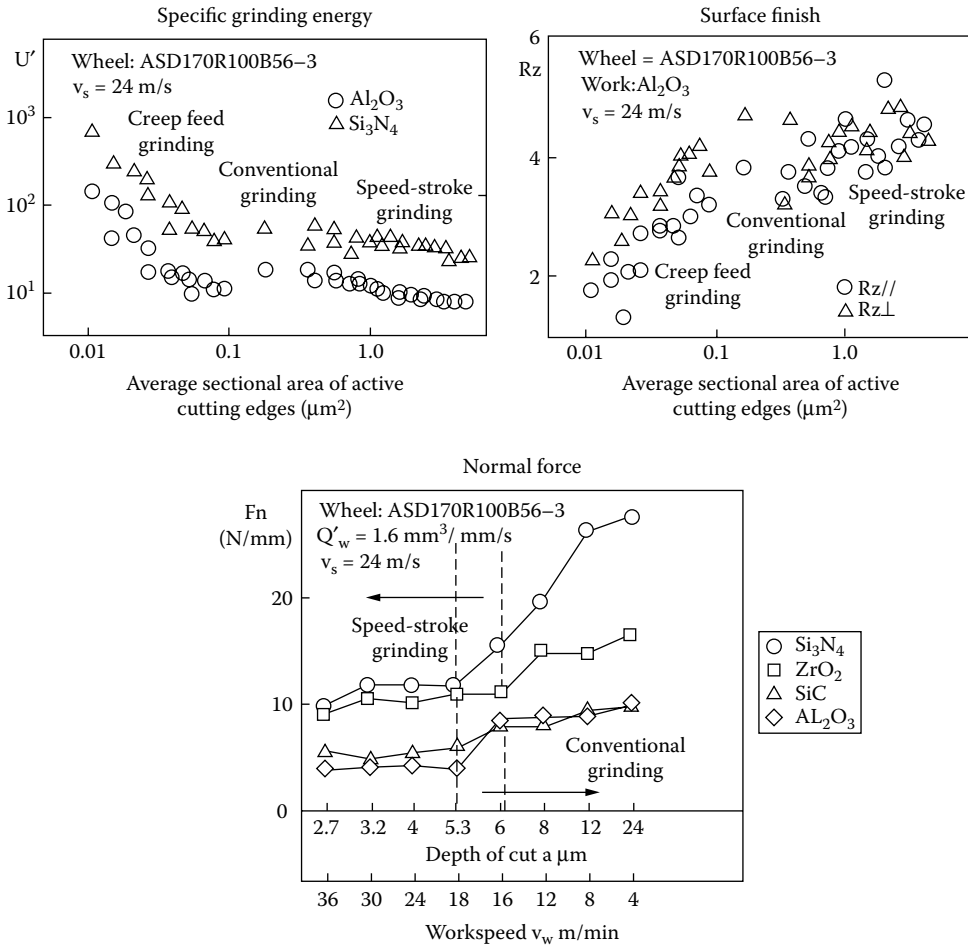


FIGURE 16.7 Process characteristics in speed-stroke grinding.

Speed-stroke grinding, therefore, offers the ability to remove stock faster and with lower forces and less risk of burn, but roughness will be higher and compensation must be made in bond/grit strength for increased force/grit. (Compensation for higher roughness can be made by controlling the process; i.e., switching to a slow table speed for finish grinding). These predictions were demonstrated by Inasaki [1988] in the grinding of alumina and zirconia with resin diamond wheels on a lead screw-driven machine at up to 36 m/min (Figure 16.7).

For the machine tool builder, the primary area of concern for machine design is being able to control the acceleration and deceleration rates without excessive vibration and without overshooting the part so much that the benefits of cycle time are lost (Figure 16.8).

The big advantage of the linear motor is that the pattern of the acceleration and deceleration can be readily adjusted so that forced vibrations can be minimized. Inasaki [1999], for example, demonstrated that a sinusoidal pattern for acceleration and deceleration can successfully suppress wheel head vibration (Figure 16.9).

Wheel grade selection is severely impacted by the effective high level of interrupted cut and high force/grit. Tonshoff, Meyer, and Wobker [1996] reported that wheel wear during speed stroke grinding of alumina was very dependent on bond type. Electroplated and resin bonds showed little

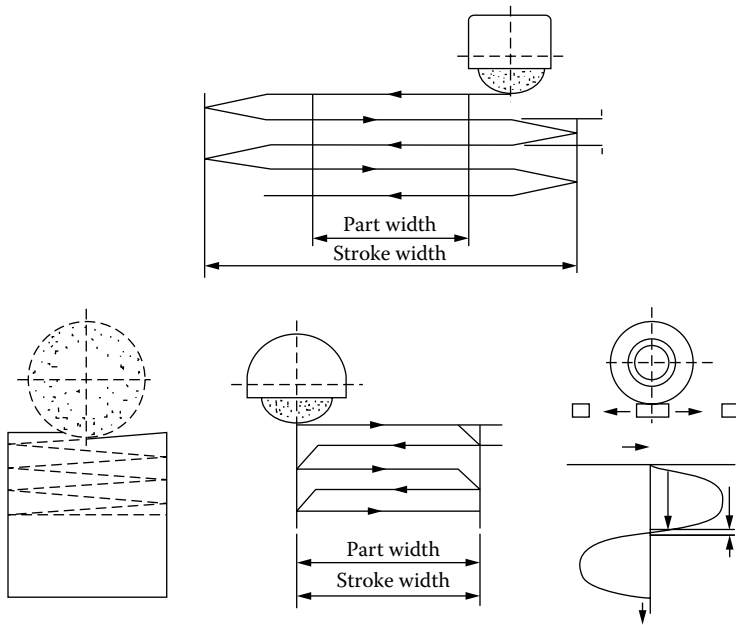


**FIGURE 16.8** Strategies for velocity profiles for speed-stroke grinding.

wear, but metal-bonded wheel wear was significant and vitrified bond wheel wear was dramatic. The differences in wheel wear were postulated to be due to the relative brittleness of the bond in the presence of vibration.

The Jung S320 was one of the first grinders to be offered commercially for speed-stroke grinding targeted at nonstandard punch grinding, slot grinding, and tooling prone to vibration [Motion 2001]. The grinder had a linear motor drive offering 50 m/min at 600 strokes/min and an X-axis position accuracy of 3  $\mu\text{m}$  on 15-mm stroke length.

Danobat designed a machine capable of 200 m/min and a maximum accelerating/decelerating rate of 3 g [Hitchiner 2005]. Speed-stroke grinding is expected to grow in numerous industries as original equipment manufacturers (OEMs) become more experienced in the use of linear magnetic motors.

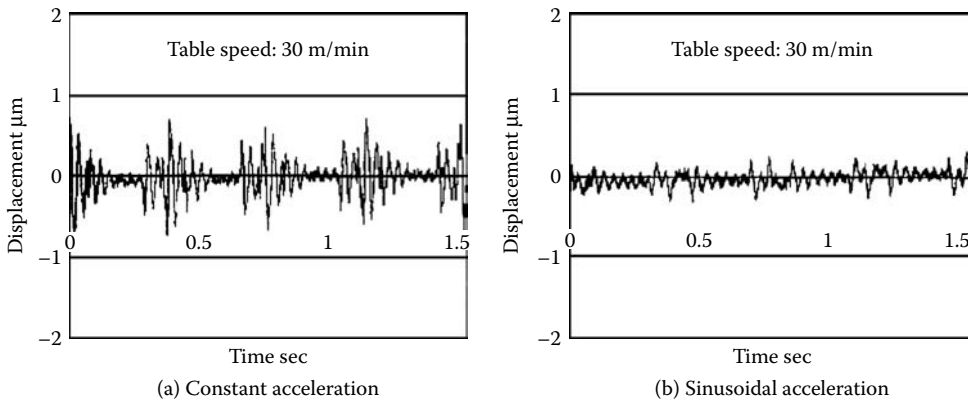


**FIGURE 16.9** Impact of acceleration strategy on machine vibration for speed-stroke grinding. (From Inasaki 1999. With permission.)

## 16.5 SUCCESSFUL APPLICATION OF CREEP FEED GRINDING

### 16.5.1 CREEP FEED GRINDING WITH VITRIFIED WHEELS CONTAINING ALOX AND SILICON CARBIDE

In general, as depths of cut increase so do grinding forces, while uncut chip thickness and, therefore, roughness and force/grit decrease. However, when the depth of cut becomes extreme, that is, greater than 1 to 3 mm maximum grinding temperatures can actually fall. Grinding using a combination of slow table speeds and deep depths of cut defines the creep feed (CF) process. Interest started in this field in the 1950s but reached its zenith from a research viewpoint in the 1970s at the University of Bristol, United Kingdom, driven by the aerospace industry and the need to grind highly burn-sensitive nickel and cobalt-based high-temperature alloys.

The creep feed process was developed using soft (E or F), highly porous conventional wheels at relatively low wheel speed of 15 to 30 m/s to keep frictional heat to a minimum, to limit required coolant pressure, and to limit wheel structural strength. The wheels were dressed using formed diamond rolls. Dressing was at first intermittent during the cycle but it was subsequently found that continuously dressing at infeed levels of 0.2 to 2.0  $\mu\text{m}/\text{rev}$  of the wheel not only maintained the profile but kept the wheel sharp, thus allowing much higher stock removal rates than had previously been seen. This latter process is the familiar continuous dress creep feed (CDCF).

### 16.5.2 COOLANT APPLICATION IN CF GRINDING

Coolant application is absolutely critical to the process. CDCF is usually carried out using a water-based coolant that fills the highly permeable wheel structure when supplied correctly and under sufficient pressure. The coolant then becomes the primary source of heat removal and maintains the part surface at a temperature at or below 130°C, the boiling point of the coolant under the hydrodynamic pressure conditions in the grind [Howes 1990]. The coolant is excellent at maintaining surface temperatures by the efficient removal of heat until the heat flux exceeds the heat capacity of the fluid. At this point, the fluid boils effectively eliminating all benefits of the coolant and temperatures rapidly climb to those experienced in dry grinding (Figure 16.10). The phenomenon is known as “film boiling” [Howes 1990, 1991].

The heat capacity of the coolant is proportional to the bulk temperature of the incoming fluid. As can be seen from Figure 16.10, reducing the incoming coolant temperature by 40°C to 20°C raises the critical power flux by a factor of 2. Similarly, increasing the coolant pressure to an optimum value where the coolant and wheel velocities are matched maximizes the critical power flux.

It is interesting to note that straight oil, due to its lower heat capacity, is less capable of cooling the workpiece and will cause the part surface to be hotter and much more likely to burn [Ye and Pearce 1984]. However, the higher film boiling temperature of the oil (ca. 300°C) is less likely to cause rapid and catastrophic failure of the coolant. Water is the better coolant, unless finish or wheel wear is the overriding issue because of the large capacity of the grinding wheel pores to hold coolant.

#### 16.5.2.1 Film Boiling

The impact of film boiling can be very marked. As the water turns to steam, there is a rapid rise in temperature of the workpiece causing it to thermally expand. This leads to a sudden increase in depth of cut and additional heat generation followed by massive wheel breakdown. The workpiece then cools to leave a series of deep, usually blackened troughs in the surface (Figure 16.11). The effect can often be detected in process by surges in the wheel head spindle power.

#### 16.5.2.2 Coolant Delivery System

Since coolant is such a key factor in continuous dressing (CD) grinding, close attention must be paid to all aspects of the coolant delivery system. Most creep feed applications either have

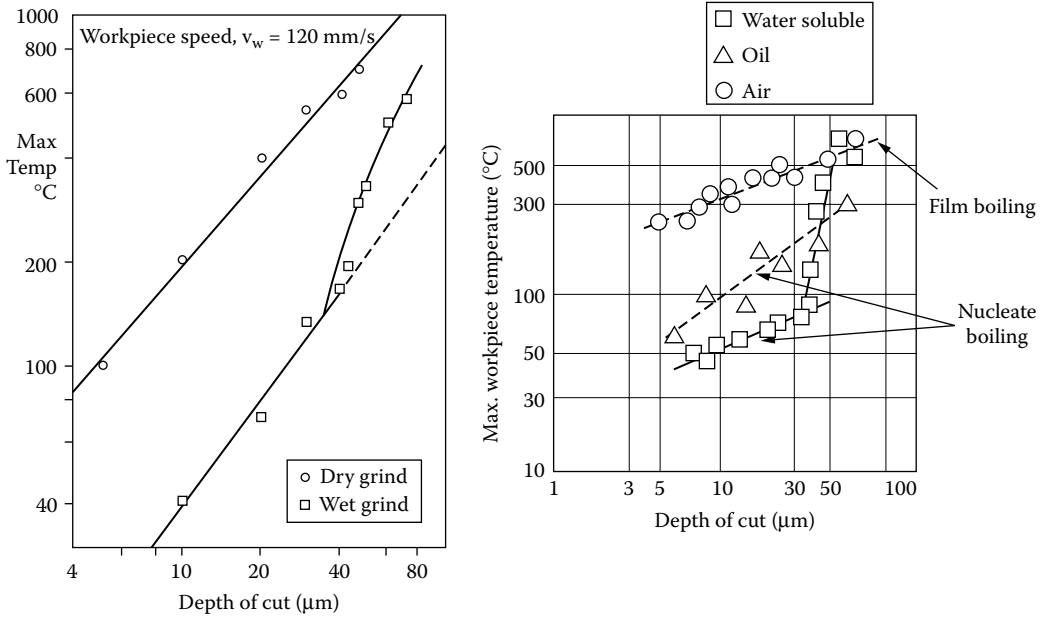


**FIGURE 16.10** Illustrations of the impact that film boiling has on workpiece surface temperatures. (From Howes 1990, 1991. With permission.)

interference with fixtures or other issues that prevent an efficient shoe nozzle from being used. Therefore, coolant delivery must depend on coherent flow nozzle design with sufficient coolant volume and pressure. This discussion is valid for any grind operation where shoe style nozzles cannot be used. Extensive research and consolidation of available information on this subject

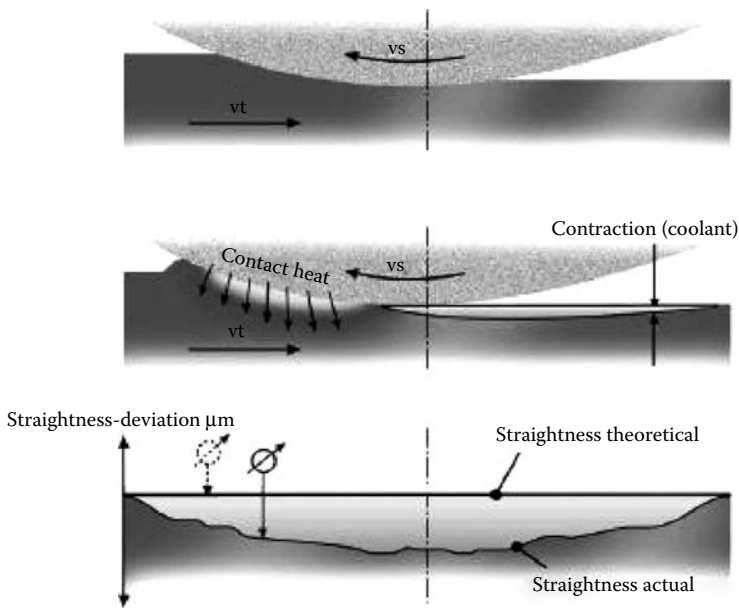


**FIGURE 16.11** Effect of excessive heat generation in the grind contact zone. (From Noichl 2000. With permission.)

carried out by Webster is included in the summary below [Webster, Cui, and Mindek 1995, Webster 2000, Webster et al. 2002].

#### 16.5.2.2.1 Coolant System Capacity

The standard coolant requirement is 1.5 to 2 gpm/hp of grinding power. A good estimation for *minimum* flowrate is therefore to take the spindle horsepower  $\times$  1.5 gpm. For a water-based coolant, at least 10 min is required for settling to allow the release of entrapped air and minimize foaming. This then defines the tank capacity requirement.

#### 16.5.2.2.2 Coolant Pressure

The optimized coolant pressure at the nozzle is such that the coolant velocity matches the wheel velocity. The coolant velocity can be readily calculated from the coolant pressure using  $V = (2\Delta P/\rho)^{1/2}$ , where  $V$  is coolant velocity,  $\Delta P$  is the pressure, and  $\rho$  is the coolant density. Note that calculating the velocity based on the flowrate and the cross-sectional area of the nozzle aperture will always underestimate the velocity as the actual coolant jet cross-sectional area may constrict upon exit depending on the nozzle design. It is always best to measure the pressure as close to the nozzle as possible. With that caveat, Table 16.4 and Table 16.5 give the velocity as a function of pressure together with the associated maximum flow rates for various aperture cross-sectional areas.

#### 16.5.2.2.3 Piping

Values are given in Table 16.6 of pipe diameter against pressure and flowrate. Pressure is to be specified at the nozzle, not at the pump. Piping should be kept as short as possible with minimal bends to avoid head losses. The pipe diameter should also be made as large both to lower head losses but also to keep the flow in the laminar. Webster recommends a velocity of 6 m/s max to keep the Reynolds number of a water-based fluid below the level causing turbulence. This gives the following maximum flowrates for given pipe diameters.

#### 16.5.2.2.4 Nozzle Design

Coolant must be delivered from the pump via the piping, valves, and nozzle at the required pressure to match wheel velocity and in a laminar flow. Any turbulence or entrained air will create dispersion

**TABLE 16.4**  
**Metric Flowrate Chart for a Nozzle with a Coefficient of Discharge of 0.95**

Jet Speed (m/s)	Coolant Nozzle Pressure (Bar)			Flowrate (l/min) for Listed Nozzle Diameters (mm) and Areas (mm <sup>2</sup> )									Area Diam.
	Water	Mineral Oil	Ester Oil	0.8	3.1	7.1	15	28	50	79	113		
	SG = 1.0	SG = 0.87	SG = 0.93	1	2	3	4	6	8	10	12		
20	2	2	2	0.9	3.5	8.1	15	33	57	90	129		
30	5	4	4	1.4	5.3	12	22	49	86	134	193		
40	8	7	7	1.8	7.1	16	29	64	115	179	258		
50	13	11	12	2.2	9.0	20	36	80	144	224	322		
60	18	16	17	2.6	11	24	43	97	172	268	386		
80	32	28	30	3.6	14	32	57	129	229	358	516		
100	50	44	47	4.4	18	40	72	162	287	448	645		
120	72	63	67	5.3	21	49	86	193	344	537	774		
140	98	85	91	6.2	25	56	100	226	401	627	903		
160	128	111	119	7.1	28	64	115	259	458	716	1031		
180	162	141	151	8.0	33	73	129	290	516	805	1160		
200	200	174	186	8.9	35	81	144	323	573	895	1289		

**TABLE 16.5**  
**English Flowrate Chart for a Nozzle with a Coefficient of Discharge of 0.95**

Jet Speed (fpm)	Coolant Nozzle Pressure (psi)			Flowrate (GPM) for Listed Nozzle Diameters (in.) and Areas (in. <sup>2</sup> )									Area Diam.
	Water	Mineral Oil	Ester Oil	.003	.012	.028	.049	.077	.11	.15	.196		
	SG = 1.0	SG = 0.87	SG = 0.93	1/16	1/8	3/16	1/4	5/16	3/8	7/17	1/2		
4,000	30	26	28	0.6	2.4	5.5	9.7	15	22	30	39		
6,000	67	58	62	0.9	3.6	8.2	15	23	33	45	58		
8,000	119	104	111	1.2	4.8	11	19	30	44	59	78		
10,000	187	163	174	1.5	6.1	14	24	38	55	74	97		
12,000	269	234	250	1.8	7.3	16	29	45	65	89	116		
14,000	366	318	340	2.1	8.5	19	34	53	76	104	136		
16,000	478	416	445	2.4	9.7	22	39	61	87	119	155		
18,000	605	526	563	2.7	11	25	44	68	98	134	174		
20,000	747	650	695	3.0	12	27	48	76	109	148	194		
25,000	1,166	1,014	1,084	3.8	15	34	61	95	136	185	242		
30,000	1,680	1,462	1,562	4.5	18	41	73	114	164	223	291		
35,000	2,286	1,989	2,126	5.3	21	48	85	132	191	260	339		
40,000	2,986	2,598	2,777	6.1	24	55	97	151	218	297	388		

causing a rapid loss of momentum and preventing the coolant from overcoming the momentum of air generated by wheel drag—the so-called “air barrier.”

Turbulence can be an inherent problem of the system governed by its Reynolds number (Re), which is defined as:

$$Re = \frac{v \cdot d}{\nu}$$

where

v = fluid velocity

d = diameter of jet or pipe

ν = kinematic viscosity of fluid (10<sup>-6</sup> m<sup>2</sup>/s for water)

The Reynolds number is a measure of flow quality where smaller is less turbulent. Coolant jets are always turbulent. Laminar coolant supply nozzles are rare. Re values in excess of about 2,000 will have turbulence; a value that encompasses virtually all grinding situations. Nevertheless, values up to 100,000 can still give a reasonably constrained flow. The Re value should be improved where possible by chilling the coolant to increase viscosity or by reducing the exit diameter by using several small nozzles. Turbulence and pressure losses can also be generated within the pipes by bends, changes in pipe diameter, or rough surfaces. This can be eliminated

**TABLE 16.6**  
**Maximum Flowrates for 6 m/s Velocity**

Pipe ID (in.)	1/2	3/4	1	1.25	1.5	2	2.5
Flowrate (GPM)	12	27	48	75	109	193	302
Flowrate (1/min)	45	103	183	285	410	730	1140

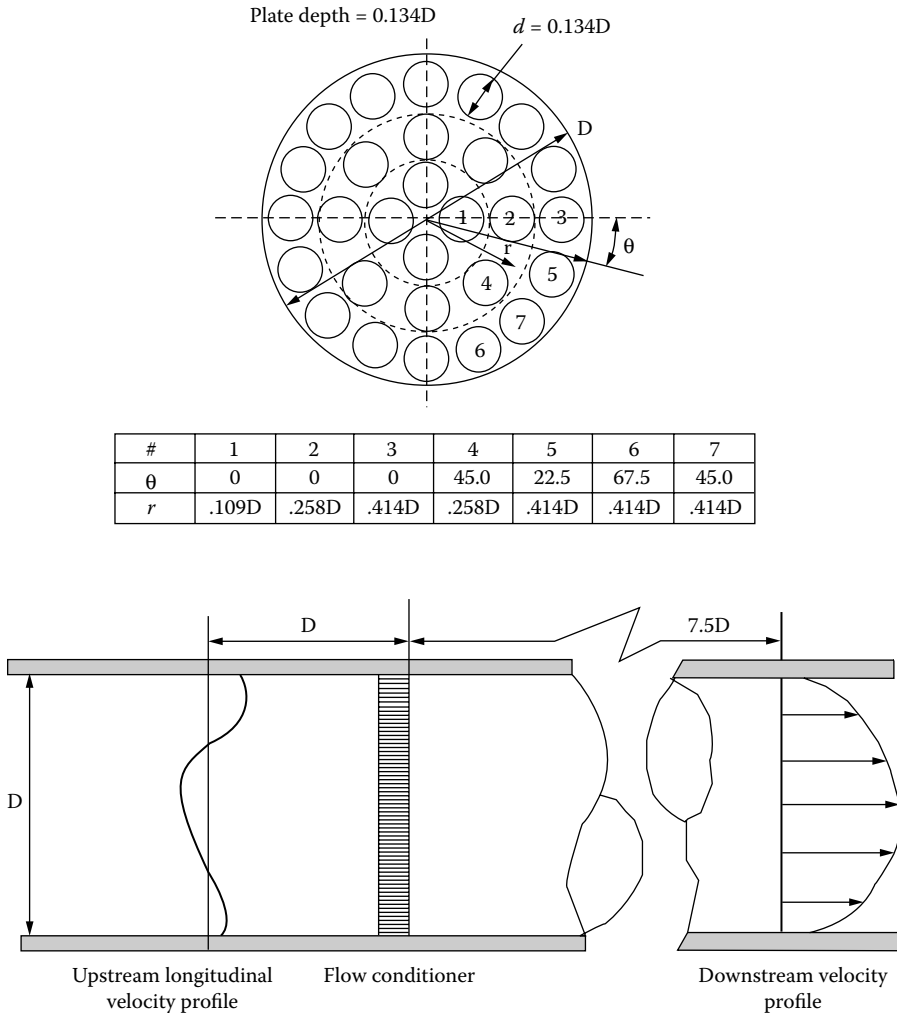
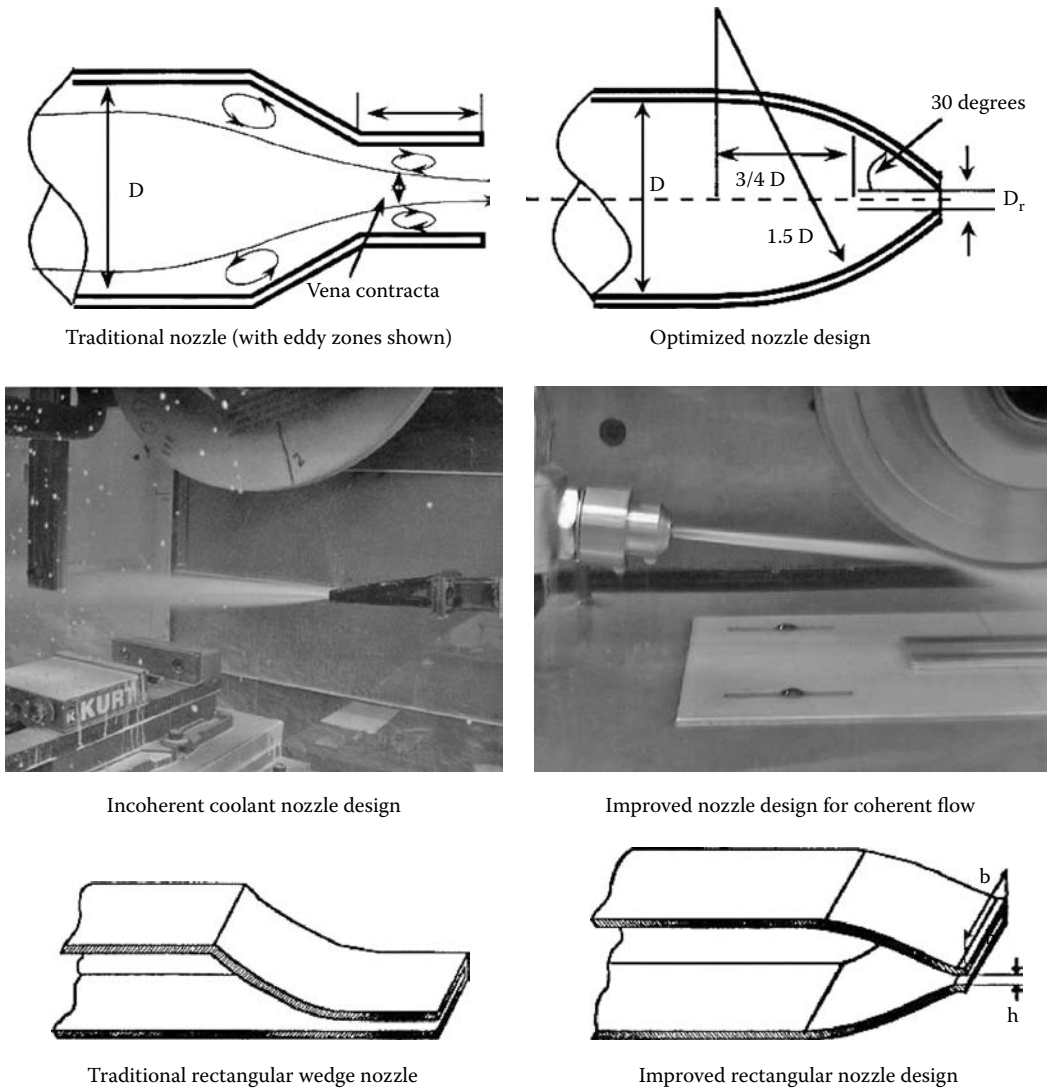


FIGURE 16.12 Mitsubishi flow conditioner. (From Cui 1995. With permission.)

by the use of a flow conditioner just prior to the nozzle system . One very simple style proposed by Webster consists of a Mitsubishi inline flow conditioner, originally designed for creating laminar flow in systems to measure city water supplies as shown in Figure 16.12 Its most important feature is the ability to present a laminar flow to the nozzle entrance with virtually zero drop in pressure.

An optimized nozzle design is as simple as it is effective. The design developed by Webster, Cui, and Mindek at the University of Connecticut to generate coherent jets was based on the 1950 fire hose technology. The beauty of the design is the way it balances all the forces from the coolant such that at the exit all flow is perpendicular to the exit. Ideally this balance is best maintained by using a round opening. However, the design is almost as efficient with a rectangular opening except for some small dispersion effects at the corners as long as the internal profile is balanced (Figure 16.13).

Complex-shaped exit designs to follow the form of the wheel profile should be avoided as they are generally highly dispersing. Instead, several smaller round nozzles can be used far more effectively. When building the nozzles, care should be taken to make sure the inner surface is as smooth as possible and that a sharp edge is maintained at the exit (no nicks).



**FIGURE 16.13** Improvements in nozzle design to achieve more coherent flow.

The concept of using small, round nozzle exits has been taken one stage further by a patented “card key” system whereby quick-change nozzle plates carrying several small, round, internally contoured exits for each required wheel profile can be placed inside a plenum chamber. The system is offered as part of the Field Services Program at Higgins Grinding Technology Center (HGTC), Worcester (Saint-Gobain Abrasives) (Figure 16.14).

Oil coolant has a higher viscosity than water making jet coherency a lot easier. It also offers great benefits in terms of abrasive life (up to 100 × with plated CBN!). However, oil has a range of problems of its own. It is potentially a hazard both environmentally from misting and as a fire risk. It also has a half to a quarter of the thermal conductivity and heat capacity, and is more prone to air entrapment. Gaulin [2002] infers the following coolant system requirements for oil:

Flowrate:	1 gpm/wheel spindle hp
Settling time:	25 min
Chiller capacity:	4,000 BTU/wheel spindle hp



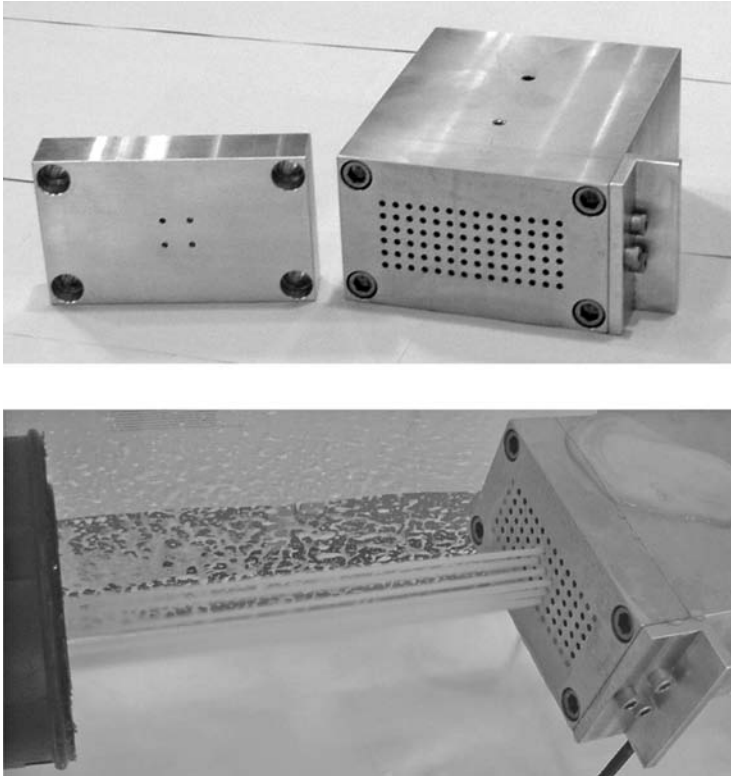


**FIGURE 16.14** Plenum chamber coolant delivery with quick change “card key” nozzle plates. (Courtesy of Saint-Gobain Abrasives. With permission.)

Although the flowrates are actually lower than those for water-based coolant, the settling time and chiller capacity are both approximately triple. The risk of fire is real although somewhat exaggerated. Every oil coolant has a lower and upper explosion limit based on the percentage of oil to air. The limits are typically 0.6% to 7% by volume of oil when the oil can actually be ignited. Flushing the grind area well or throwing down a curtain of oil to flood and knock down misting greatly reduces the fire risk. In the event of a fire there is an overpressure created in the grinder of about 4.5 bar max. So grinders equipped for handling oil should have:

- Good encapsulation to prevent oil or mist from exiting
- An efficient mist extraction system
- A CO<sub>2</sub> fire suppression system
- A spring-loaded flap to release the initial pressure generated from an explosion
- Automatically seal as the CO<sub>2</sub> system kicks in

It is interesting to note that a survey carried out in Germany between 1987 and 1994 found the leading causes of fire were [Ott and Storr 2001]

- Workpiece jammed
- Loss of coolant supply (sensor failure)
- CNC operator error
- Grinding wheel with steel core (e.g., electroplated) lost its coating and generated excess heat from rubbing on the part

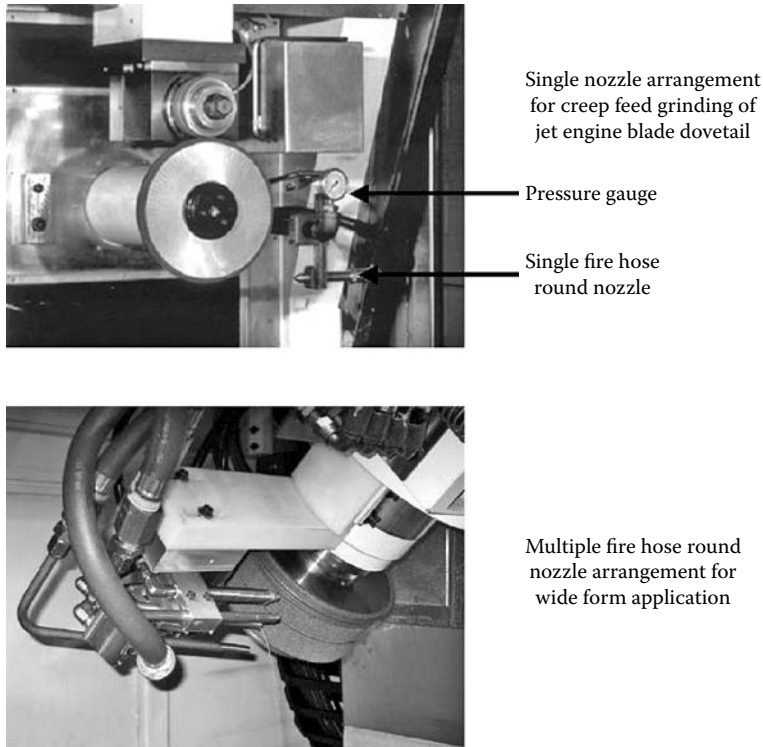


**FIGURE 16.15** Examples of fire hose round nozzle applications.

The impact of oil on the physical size of a coolant can be seen from Figure 16.16. This illustrates a self-contained, compact coolant system designed for a single grinder with a 40 Hp (30 KW) spindle and plated CBN wheels. It consists of a 280 psi (20 bar), 60 gpm (225 l/min) high volume pump, a 1,000 psi (70 bar), 5 gpm (19 l/min) high-pressure scrubber pump, vacuum paper filtration unit, chiller, air-extraction unit, and a coolant tank large enough to allow a 15 min settling time. The system is actually larger than many of the grinders it is designed to supply.

Coolant delivery to creep feed grinding is also a consideration when examining the importance of up- versus down-grinding.

To re-emphasize comments made before, in up-cut grinding, each individual grit experiences a high proportion of its time in contact initially just rubbing or ploughing the workpiece material. This consumes a large amount of energy in friction and elastic and plastic deformation. Only as the grit reaches its exit point does it make a sufficiently deep cutting depth to initiate a chip. In down-cut grinding the chip is almost immediately created suppressing many of the friction losses. In up-grinding the coolant introduced at the point of entry of the wheel acts directly on the newly formed surface. In down-grinding, coolant again added at the point of entry of the wheel must be carried through the grind zone, during which it is heated up before it can react with the newly produced surface [Tawakoli 1993]. In actual production situations, the ease of effectively introducing coolant into the grind for a down-cut grind configuration appears to far outweigh any advantages of the kinematics of up-grinding.

In summary, there are lower grinding forces and power, and a lower risk of burning in down-grinding. Up-grinding, although able on occasion to give longer life, should be reserved for just the last pass in a finish grind mode at  $<50 \mu\text{m}$  d.o.c. and relatively high-table speed to help remove artifacts from the rough grind such as burrs and edge faceting produced by the influence of coolant hydrodynamic force changes.



**FIGURE 16.16** Oil coolant system for use with a 40-Hp grinder operating with plated CBN wheels (pumps, chiller, filter, settling tank, and mist collection). (Courtesy of Campbell Grinders, Spring Lake, MI. With permission.)

### 16.5.3 CONTINUOUS DRESS CREEP FEED

CDCF is characterized by high stock-removal rates. Deep slots with stock levels of the order 10-mm values of  $Q'$  of over 100 mm<sup>3</sup>/mm/s have been reported for both steels and nickel-based materials. However, in actual production due to limited stock levels, access of coolant, or dimensional or thermal stability of the part, the removal rates are generally much lower. For example, Table 16.7 gives some recent case histories of optimized wheel performances from the Radiac Abrasives Web site [2002]. As can be seen, high-removal rates are achieved on relatively burn-insensitive materials and/or large depths of cut. However, where stock amounts are limited especially with burn-sensitive materials, weak clamping, or lack of a heat sink (thin-walled surfaces), removal rates drop precipitously.

CDCF is a higher consumer of grinding wheels and diamond rolls. Remember, the process is consuming the wheel by constantly dressing at a rate of 0.5 to 2  $\mu\text{m}$  per wheel rev! It also requires a high stiffness machine and dressing system. The large amount of abrasive swarf in the system is an additional problem that creates disposal cost and maintenance issues. Nevertheless, to achieve good form accuracy with high stock removal rates and deep depths of cut, it is still a process that is hard to beat.

#### 16.5.3.1 The Viper Process

Several alternatives have been developed using conventional abrasive wheels as alternatives to the CDCF process. The first is the VIPER (Vitrified Improved PERformance) process patented by Rolls Royce [1999] with licenses to various builders of machining centers including Bridgeport and Makino. The VIPER process was developed around multisurface grinding of aerospace components in one clamping where the wheel had to index to several positions. Standard positioning of the nozzle in each case was difficult for clearance reasons and CDCF impossible. The VIPER process uses an indexable nozzle to force coolant at 50 to 70 bar into the wheel structure ahead of its entry into the grind zone [Mohr 2000]. The coolant is then expelled by centrifugal force just at the point

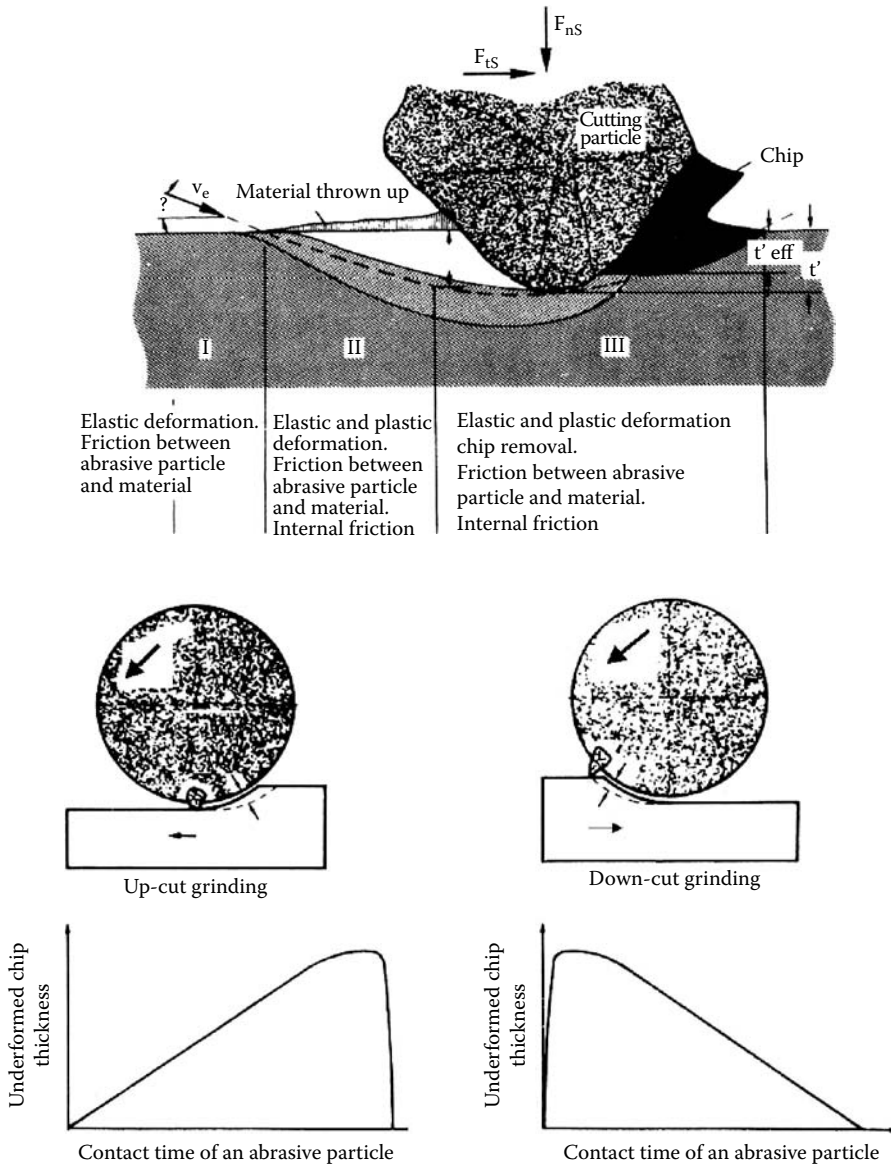


**FIGURE 16.17** Schematic representation of chip formation and chip formation curves for up-cut and down-cut grinding. (After Koenig and Schleich 1982. With permission.)

of grind. Injecting coolant into the wheel ahead of the grind is a common practice and indexable nozzles have been used on grinding/machining centers since the 1980s. However, the novelty of this process is the precise optimized angling of the nozzle to direct the coolant for each operation. An example of the grind process is illustrated in Table 16.8 for grinding aircraft engine blade root forms.

Although a higher stock removal rate can be achieved in the initial rough cut, the wheel breakdown is such that feedrates have to be backed off to maintain form. Part deflection can also be an issue. The components being ground are often quite weak and difficult to hold especially when trying to do a multisurface grind process. Such a process also requires small diameter (<250 mm), ultraporous wheels, which limits life.

**TABLE 16.7**  
**Removal Rates in CDCF**

Component	Material	Dress mode	Wheel Spec	Stock Removal d.o.c. × Feedrate (mm) × (mm/s)	$Q'$ (mm <sup>3</sup> /mm/s)
Connecting rod	Steel 45HrC	CDCF +0.80	RAA542F800VOS	5.7 × 15	85
Pump slot	Steel 58HrC	CDCF +0.80	9RA602F802FVOS	21 × 2.8	60
Blade dovetail	Ni alloy 37HrC	CDCF +0.80	9RA461F850VOS	8.6 × 1.5	13
Vane profile	Rene 37HrC	CDCF +0.80	RAA602E800FVOS	2 × 3.4	6.8
Engine segment	Flame spray Ni	CDCF +0.85	RAA602E800FVOS	1.65 × 1.7	2.8

With the move to grinding and multitasking, several OEMs of machining centers now offer grinding including alternatives to VIPER such as CDCF complete with quick-change wheels and diamond rolls (Makino 2002) (Figure 16.18).

An alternative to this process is the use of extruded ceramic grain wheels, tradename Altos, from Saint-Gobain Abrasives. The latest generations of seeded gel- (SG) based grains (TG and TG2) have increasingly greater length/diameter aspect ratios. As shown in Figure 16.19, the natural packing density decreases steadily as this aspect ratio increases. TG2, for example, has a natural porosity of almost 70%. Even allowing for up to 10% of vitrified bond there is 60% porosity available with high permeability for coolant retention. Furthermore, the bond is concentrated at the crossover points of grains like weld points giving a surprisingly strong structure.

In tests by the author, grinding Inconel 989, typical of land-based gas turbine materials, at 30 m/s and constant 1.25 mm depth of cut in water-based coolant (synthetic), Targa and Altos abrasives generated excessive heat at  $Q'$  values *below* 8 mm<sup>3</sup>/mm/s. However, for  $Q'$  values between 10 to >50 mm<sup>3</sup>/mm/s burn was eliminated, while maintaining a finish <40 micro and a constant G-ratio of 3 to 5. Grinding in oil, the G-ratio increased to 50 with no burn at *any* feedrate up to  $Q' = 50$  mm<sup>3</sup>/mm/s. A similar trend in performance was observed grinding Inconel 718, typical of aeroengine parts. In this case, however, the G-ratio values increased by a factor of 3.

#### 16.5.4 CREEP FEED GRINDING WITH CBN

Creep feed grinding with CBN can be divided quite definitively between plated CBN and vitrified CBN in terms of distinct machine conditions, coolant, and operating parameters.

**TABLE 16.8**  
**Example of Removal Rates in the Viper Process for Grinding Turbine Blade Root Forms**

Pass	Wheel Speed (m/s)	Table Speed (mm/min)	Depth of Cut (mm)	Dressing Depth (mm)	$Q'_w$ (mm <sup>3</sup> /mm/s)
1	35	1,000	1.0	0	16.7
2	35	1,000	0.5	0	8.3
3	35	1,000	0.2	0.2	3.3
4	35	1,000	0.1	0	1.7
5	35	1,000	0.05	0	0.8
6	35	1,000	0.02	0	0.3

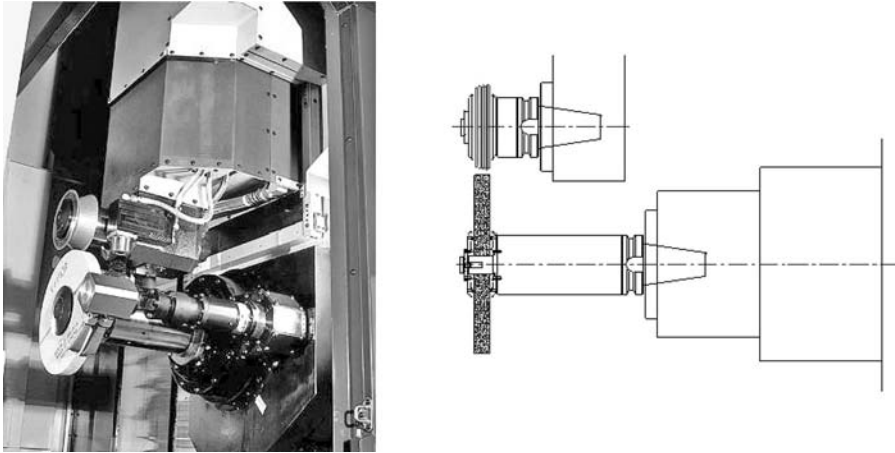


FIGURE 16.18 Makino machining center equipped with CDCF capability on quick-change HSK adaptors.

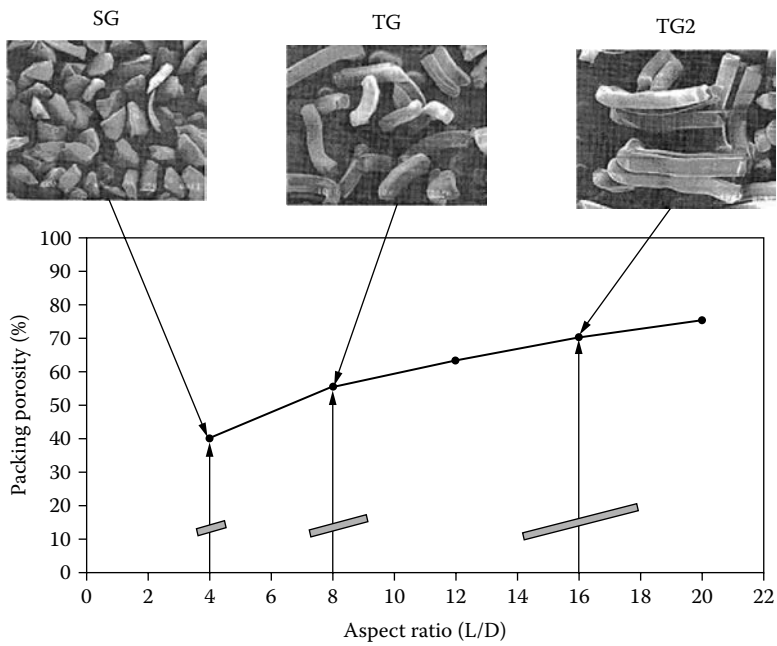


FIGURE 16.19 Large grain aspect ratios of SG and TG wheels.



FIGURE 16.20 Examples of HEDG grinding applications.

### 16.5.4.1 Electroplated CBN

Electroplated CBN wheels consist of a single layer of CBN crystals on a profiled metal hub. As discussed in Chapter 4, this leads to limits on finish and profile tolerances unless the surface is conditioned after plating which adds significantly to the cost. Therefore, the wheels are used more typically in roughing operations and under conditions that maximize life, namely, high wheel speed and oil coolant.

The impact of oil on wheel life cannot be understated. Gaulin [2002] reports a typical life difference between grinding in oil and grinding in water-based coolant of 100:1. Certainly while grinding nickel-based alloys, the author has observed very repeatable data showing 25 to 75 times more life with a good mineral oil compared to the latest synthetic or semisynthetic water-based coolant. Complicated profiles with tight radius requirements may reduce the benefits of oil to some degree, but the improvement relative to water-based coolants is still extreme. In fact, the impact on life is so extreme that the economic use of plated CBN in water-based coolants, certainly as far as the aircraft engine industry is concerned, is very questionable except for small job lots where manufacturing must weigh the wheel cost against the cost of buying expensive formed diamond rolls to dress a bonded wheel and the equipment to utilize them.

The impact of high wheel speed is very similar to that discussed under external cylindrical grinding especially with operation under high efficiency deep grinding (HEDG) conditions. The biggest benefits of plated CBN in HEDG grinding comes about by achieving high stock-removal rates with deep depths of cut and low  $U'$  values while maintaining a modest overall grinding power to keep forces within the range of normal machine stiffness. Not surprisingly, the typical examples seen in the trade literature are narrow slots in, for example, collets, spanners, and pump rotors.

There is one particular application for electroplated CBN wheels that has been the driver for machine design to do HEDG grinding, and that is radial groove grinding of aeroengine components. Many engine components, for example, vanes, nozzles, and casings, require narrow radial slots to be machined in them. Most engines are 500 to 1,000 mm in diameter, which sets the typical range of the slot diameters. Traditionally, these would either be milled with a very small diameter cutter, which is very expensive, or plunge ground with a 2A2 plated wheel of the same diameter as the groove. A 1,000-mm-diameter plated CBN wheel is also both expensive and requires a massive machine to utilize it. An alternative approach is to grind the slot with a small cup wheel of a very precise diameter and dish angle. Figure 16.21 shows the configuration. The groove of depth  $d$  has inner and outer faces defined by radii  $R_1$  and  $R_2$ , respectively. The cup wheel or radius  $r$  is tilted  $\theta^\circ$  from the vertical. The critical part tolerance is usually the outer groove face taper, which must be held to a tolerance of  $\leq 5 \mu\text{m}$ . By comparison, the overall groove width has a tolerance of typically 50 to 100  $\mu\text{m}$ . Simple geometry calculation shows that for a part outer radius,  $R_2$ , the maximum wheel radius to give a theoretical vertical face is given by  $r = R_2 \sin \theta$ . Applying this value of  $\theta$  to the inner wall radius,  $R_1$ , gives a radial difference (taper) between top and bottom of the groove of

$$\begin{aligned} \Delta R_1 &= d^2(1 + \sin^2 \theta) \quad R \gg \Delta R \quad r = R_2 \sin \theta \\ &2R_1 \cos^2 \theta \\ &R_2 > R_1 \end{aligned}$$

If the component tolerancing does not define an outer groove face taper but merely the overall taper from top to bottom of the groove, it is possible to further improve the overall taper by reducing  $\theta$  about  $\pi^\circ$ . It should be noted that  $\Delta R_1$  increases as  $d^2$  but for small changes in angle reducing  $\theta$  produces only a linear relationship of  $\Delta R_2$  with  $d$ . The final adjustment of  $\theta$  is usually done using a 3D CAD design program such as Unigraphics.

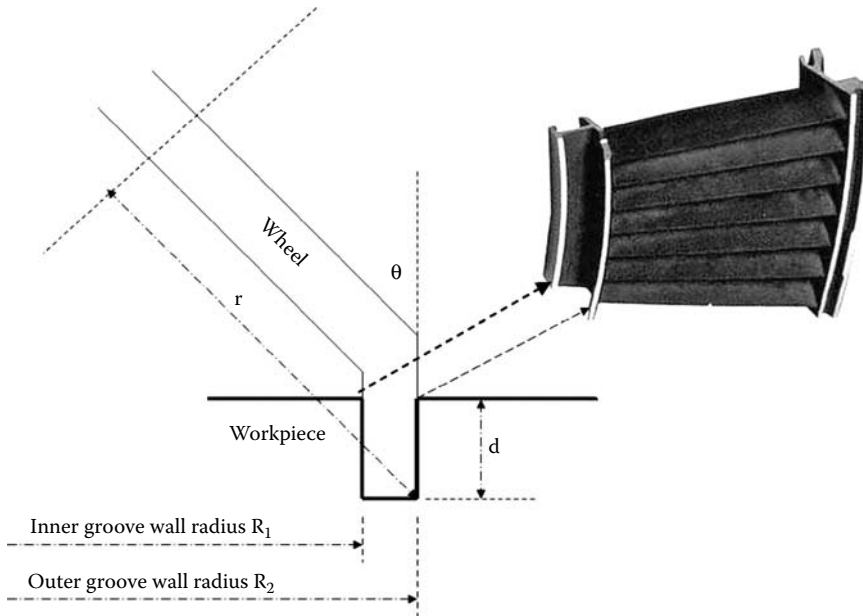


**FIGURE 16.21** Configuration for radial groove grinding using plated CBN wheels.

$\theta$  usually lies in the range of  $10^\circ$  to  $20^\circ$  which defines the wheel diameter in the range of 125 mm to 250 mm. This, in turn, defines the wheel capacity of the machine. Furthermore, the interpolation of the radius requires the coordinated movement of several axes. This has led to purpose-designed grinders such as the Edgetek HEDG grinder (Holroyd Machines, U.K.) (Figure 16.22), but also the adaption of advanced tool and cutter grinders capable of complex, accurate CNC path movements. An example of this from Huffman (Clover, SC) is shown in Figure 16.23.



**FIGURE 16.22** Edgetek HEDG grinder.





**FIGURE 16.23** Huffman high-speed grinder.

Under ideal conditions with deep depths of cut, oil coolant, and high wheel speeds, plated wheels can achieve  $Q' = 100$  to 2,000 depending on the material grindability. However, as with CDCF, conditions are rarely ideal and stock removal rates may be only 10% of those indicated above. For example, grinding Inconel 718 or similar, the maximum stock removal rate in the majority of applications based on burn and wheel life considerations is  $<8 \text{ mm}^3/\text{mm/s}$ .

#### 16.5.4.2 Vitrified CBN

Vitrified CBN has seen a dramatic growth from 1995 in certain key areas of creep feed grinding, especially aerospace alloys and some tool steels. The impact on the grinding of Inconel-based engine components has been particularly dramatic since about 2000 with the introduction of near net shape parts, 6 Sigma and just in time (JIT) manufacturing methods, resistance to the acceptance of oil coolant on the factory floor, and purpose-designed grinders for CBN (see later).

Vitrified CBN grinding of Inconel is incapable, to date, of the removal rates possible with CDCF being limited to  $Q' = 8 \text{ mm}^3/\text{mm/s}$  in water-based coolant for reasons of economics (abrasive cost), but this removal limit is increasing as bond technology improves. Certainly at removal rates of  $Q' < 5 \text{ mm}^3/\text{mm/s}$ , the abrasive cost is often less than half that of conventional abrasives. The abrasive cost against plated CBN grinding in water-based coolant is even more extreme as illustrated in Figure 16.24. This compares the wear of various production specifications of plated CBN with a

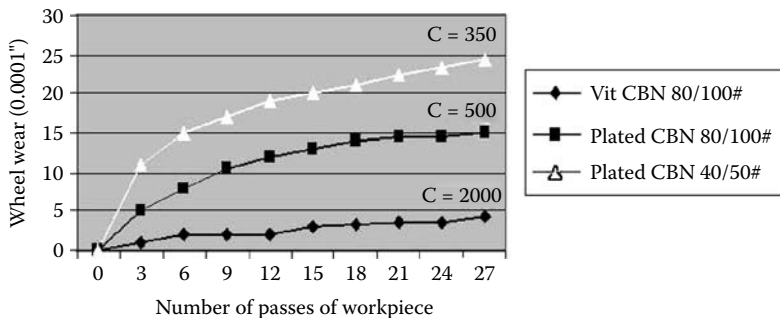


**FIGURE 16.24** Comparison of the wear of vitrified and plated CBN wheels grinding IN 718 in water-soluble oil.

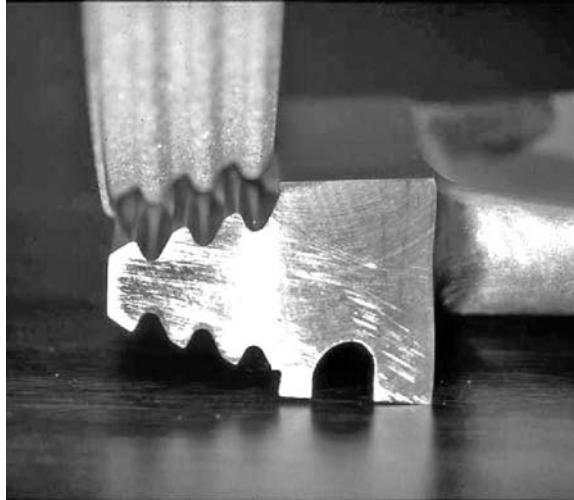


**FIGURE 16.25** Rootform (“dovetail” or “fir-tree”).

standard vitrified CBN production wheel. When the limit of wheel wear is  $<50\ \mu\text{m}$ , typical of most engine component tolerances, plated wheels wear four to seven times faster than vitrified CBN unless the grains are preconditioned as discussed in Chapter 5. At the end of this wear period, the plated wheel must be recoated by the wheel manufacturer, whereas the vitrified CBN wheel can be redressed up to 100 times dependent on layer depth.

Not surprisingly the abrasive cost can be 20 times higher with plated than with vitrified CBN in water-based coolant. However, in oil the life of the plated wheels increases by a far greater factor compared to the increase of vitrified CBN wheel life such that the abrasive costs become almost comparable.

#### 16.5.4.3 Process Selection

The various new and competing technologies, each requiring somewhat different process conditions, require careful consideration of the end users' true needs especially when considering capital

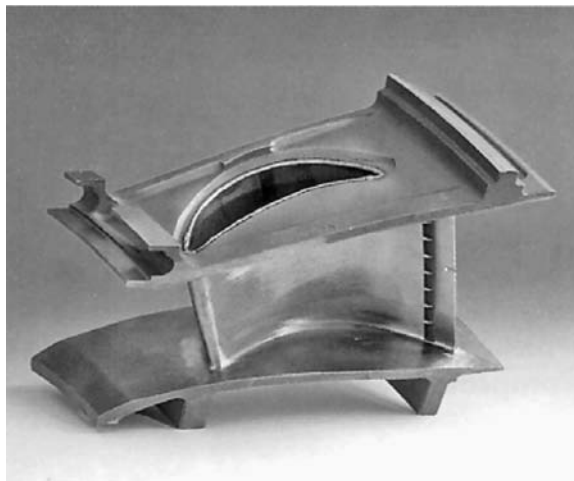


**FIGURE 16.26** Nozzle guide vane grind on aircraft engine blade.

equipment expenditures. This can be readily understood by considering as an example the recent changes in the processing of nickel alloy-based aeroengine components, for example, high temperature blades and vanes.

The choices before a process planner setting up a new production line include the following.

#### 16.5.4.3.1 *Oil or Water for Coolant*

As discussed above oil allows justification of plated CBN and is compatible with TG-based ceramic abrasives. Water-based coolants justify vitrified CBN or CDCF with alox wheels and may permit TG-based abrasives in heavy stock applications.

#### 16.5.4.3.2 *High Volume Batch Production or JIT Cell Manufacturing Concepts*

Traditional manufacturing methods based on CDCF achieve very high production rates in both the aeroengine and land-based gas turbine markets. Extremely complex multispindle machines by OEMs such as Blohm, Elb, and Excello [n.d.] were designed in the late 1970s and 1980s that could grind all the surfaces of a blade in cycle time of the order of a minute. Novel machine design concepts such as opposing twin wheel spindles could grind two opposing faces such as both dovetail forms at the same time to balance the forces at the higher metal removal rates [Salmon 1984]. The output of these machines is still unrivalled but the process was found to have several drawbacks. First, the machines were very complex, some with up to five spindles and over 1,000 control feedback inputs, making them difficult to maintain and requiring a very skilled workforce to maintain them. Second, the processes were geared to high production where change over times could be lengthy. Consequently, large quantities of expensive components would be produced generating a high “work in progress” inventory and total manufacturing times in terms of months. In the 1990s, manufacturing moved toward a JIT strategy in conjunction with a policy for 6 (Six sigma) quality control. This, in turn, led to cell approach for manufacturing where all the equipment to make a part, including CMM inspection and other manufacturing processes such as electrodischarge machining (EDM), were contained within a single cell with a minimal number of operators. Grinders were now much simpler, lower priced, and with tooling designed for quick change over times where necessary. An operator under these conditions could only efficiently function with cycle times of the order of 4 min. The need for CDCF under these conditions was eliminated.

#### 16.5.4.3.3 *Stock Level*

Older casting technology produced casings with very heavy levels of stock up to 10 mm deep making them particularly suited to CDCF. Modern near net shape casting methods have now reduced these stock levels to as little as 1 to 2 mm on many aeroengine components, eliminating the need for a high  $Q'$  operation and making processing much more suited to a CBN solution.

#### 16.5.4.3.4 *Part Holding: Encapsulation or Hard Point Mounting*

Many aerospace components are complex but relatively weak structurally or have reference surfaces that can easily distort. Traditionally, these parts are held by encapsulating them in a low melting alloy. This provides a solid robust structure with clearly defined and rigid location surfaces. However, the mounting and dismounting processes are expensive and add no processing value to the part. With the move toward lower stock levels and the lower  $Q'$  for grinding and its associated forces, end users are implementing hard-point mounting methods where the part is supported on its reference datum points with hardened steel or carbide-tipped pneumatic or hydraulic clamps.

Hard-point mounting increases the processing options available to the end user. The following includes several that are not practical with encapsulation. For example:

- The components can be processed in a series of inexpensive 3-axis grinders with a single grind operation per machine. This can be done either one component at a time (Figure 16.27) or ganged up in series (Figure 16.28).
- The components can be ground on several surfaces in a single clamping on 4- or 5-axis grinders using a combination of tilt and/or rotational axes to present the various grind

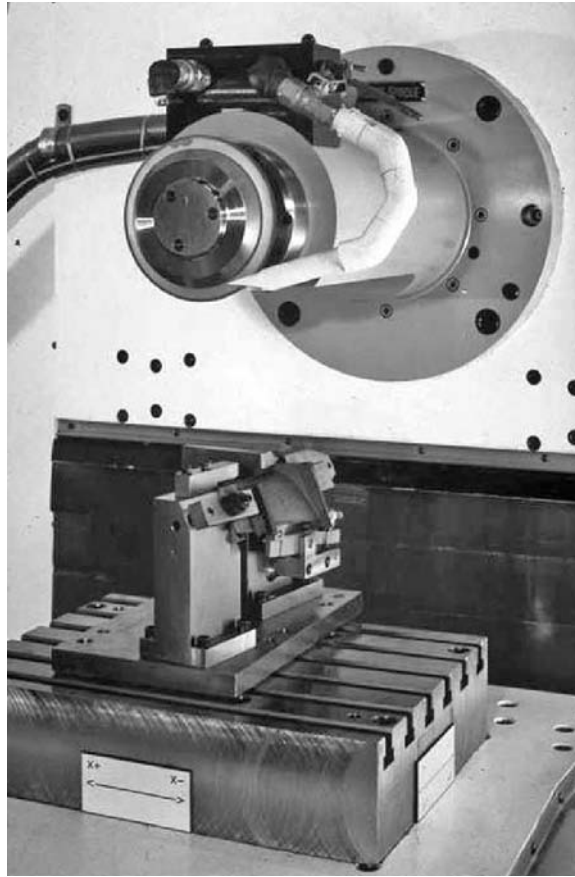


**FIGURE 16.27** Single part fixture.

surfaces in turn to the wheel. The wheel or wheel “pack” (multiple wheel assembly) is designed with a range of diameters and profiles to achieve the clearance to reach and generate the various forms on the part. The design of the fixture is pivotal to the whole process and often extremely complex (Figure 16.29). It can be readily seen that the size of the machine, wheel design, dresser design, and coolant delivery can only be defined once the fixturing is designed. Several companies have specialized in this type of fixturing, working closely with OEMs and wheel makers for turnkey operations.

- Several components can be mounted in a single fixture to present a series of different grind stages. The components are moved progressively from stage to stage taking off one finished blade each time at the final stage and adding one at the initial stage. This approach is most suited to small, easy-to-handle blades on 4- or 5-axis grinders. Fixture design is again critical. For these types of operations in combination with near net shape components, the need for high stock removal rates becomes less critical, as the majority of the cycle time is used for machine indexing. This makes the approach particularly suited to processing using small CBN wheels.

#### 16.5.4.3.5 Selection of Metal Removal Process

One of the most fundamental decisions for the process engineer is to decide which is the most suitable metal removal process. For example, EDM is a relatively slow method for cutting complex forms but

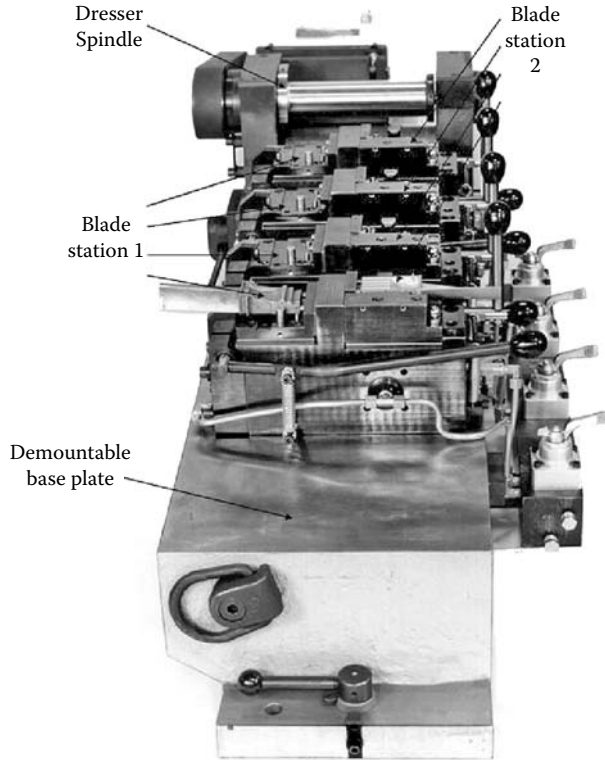


**FIGURE 16.28** Parts ganged up in series.

EDM machines are inexpensive relative to a grinder. Therefore it may be less expensive and more flexible to buy several EDM machines than a single grinder. The decision must be based on capital equipment costs, cycle times, wire/abrasive costs, and tolerances. Milling of nickel-based alloys is very expensive in perishable tooling costs, and with advances in CBN and ceramic wheel technology, manufacturers of land-based engine components are beginning to convert to grinding (Figure 16.32).



**FIGURE 16.29** Engine blade assembly.

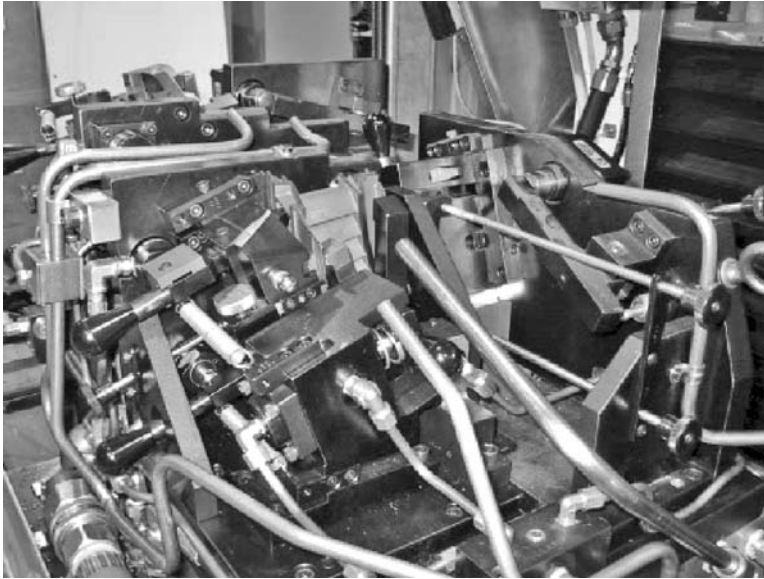


**FIGURE 16.30** Hard-point mounting fixture for nozzle guide vane.

Grinding is also being considered as a replacement for broaching of nickel alloys again due to the high capital and tooling costs, long tool change times, high broaching forces, and floor space required. Burrows et al. [2002] and Aspinall et al. [2002], for example, reported on a study for a consortium including Rolls Royce and SNECMA to replace the broaching of turbine compressor disc root forms with grinding; the root form being first rough ground with Altos wheels then finished ground using small profiled plated CBN pins (Figure 16.33).

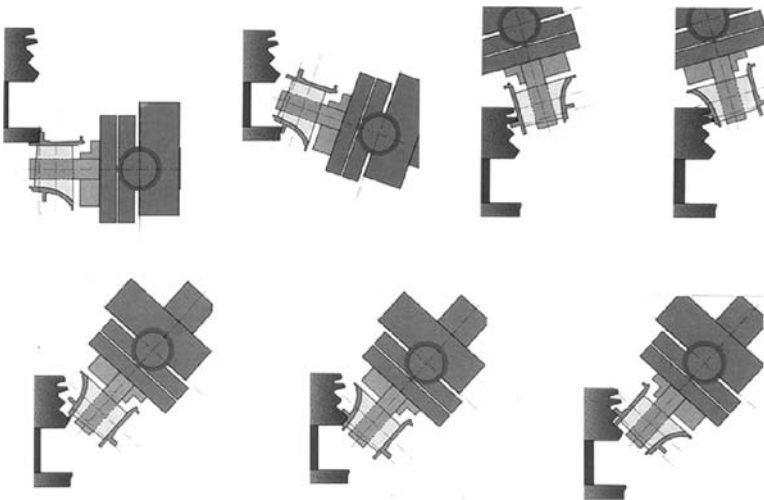


**FIGURE 16.31** Example of multisurface processing of engine component in one fixturing using a profiled wheel pack. (From Blohm n.d. With permission.)

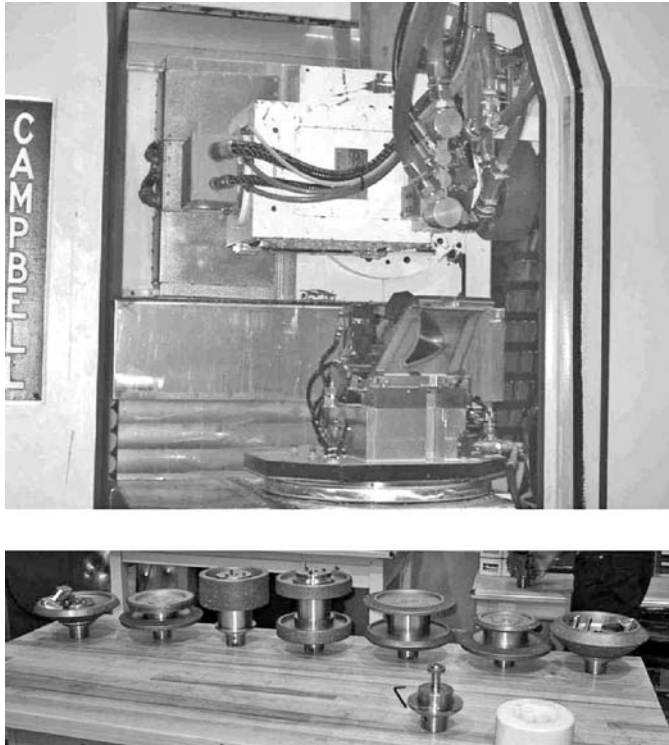


**FIGURE 16.32** Multiaxis machining center for grinding land-based gas turbine buckets with plated CBN wheels to replace milling and HSK automatic wheel changing.

It is interesting to note this study was carried out using a vertical machining center and made significant reference to “multitasking.” The move to multisurface processing of parts in one fixture has demonstrated the benefits in terms of improved tolerances from processing components in a single clamping. However, there is no reason why each metal removal operation must be one of grinding. In multitasking, a machine may be required to do several operations including grind, mill, turn, probe, burnish, and deburr. Machine tools now become much more generic with companies traditionally involved with machining centers offering grinding capability, while manufacturers of grinding machining

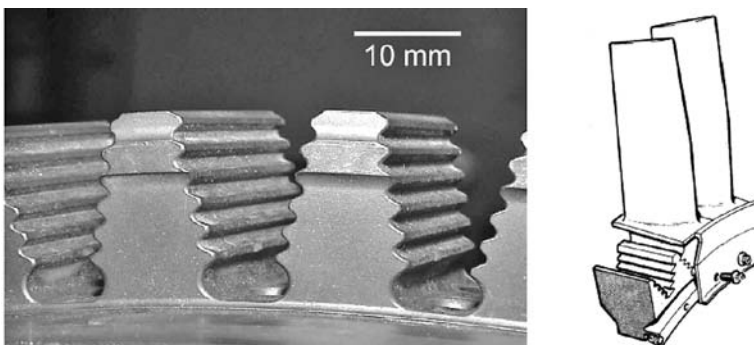


**FIGURE 16.33** Turbine compressor disc root form and sketch showing blade in location. Burrows et al. 2002. With permission.)

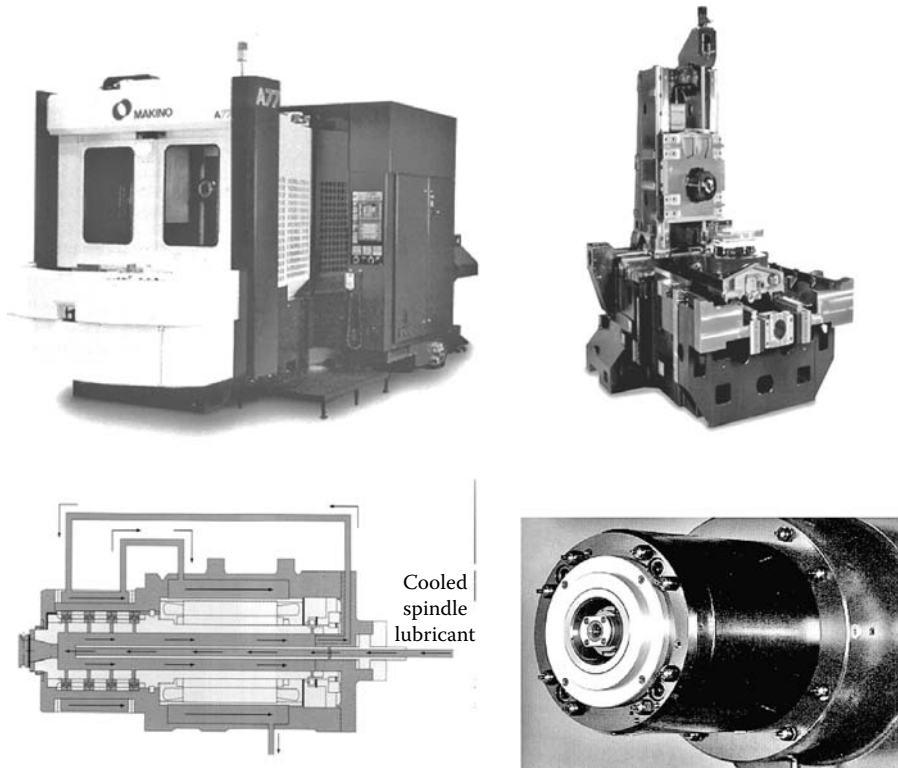


**FIGURE 16.34** Makino A77 grinding center and components.

offer options common to machining centers such as quick-change HSK tooling, milling, and turning capabilities, and a radically different working volume in terms of machine axes movement and reach.

Several of the large manufacturers of high performance machining centers now promote “grinding centers”—machines with structural, drive, and control components, coolant delivery systems, and size control ability comparable or superior to many grinders. On the other hand, manufacturers of high-speed grinders such as Edgetek now refer to their processing as “abrasive machining.” The distinction between a grinding machine and a machining center has become blurred in these instances.

The natural conclusion to this trend is for some end users to attempt to further reduce capital equipment costs by the use of low-cost, mass-produced, vertical machining centers (VMCs) and making modifications to them in-house typically to run plated CBN wheels. This approach has met with some success in application with noncritical tolerances, but the end user should be aware that the stiffness, thermal stability, and repeatability may not be in the same class as a modern grinder and savings in capital equipment may be lost in process development with no guarantee of success as very few VMC manufacturers provide turnkey processes. Attention must also be paid to differences in guarding codes.

With so many options and new technologies to choose from, the selection of the best is difficult. At the current time, the following approaches are being taken by manufacturing:

- High-volume dedicated manufacturers with near net shape parts are converting primarily to vitrified CBN wheels in water-based coolant in combination with hard-point mounting for workholding.
- High-volume dedicated manufacturers with near net shape parts willing to grind in oil are converting to plated CBN in combination with hard-point mounting for workholding.
- High-volume dedicated manufacturers with high stock castings either remain with conventional creep feed wheels in conjunction with traditional CDCF or recent VIPER





Blohm profimat MC



Campbell 950 (Spring Lake, MI, USA)



Jones &amp; Shipman dominator 624



Micron machine (W. Springfield, MA, USA)

**FIGURE 16.35** Examples of compact creep feed grinders.

technology in water-based coolant, or advance ceramic grain wheels in water or oil coolant. The shift to hard-point mounting is slower in these cases because of the higher forces imparted by the higher removal rates that in turn cause part deflection. This is especially a problem when the reference mount points are on thin aerofoil sections.

- Job shop and small-batch manufacturers willing to grind in oil coolant are using predominantly plated CBN with some advanced ceramic grain wheels on simpler form or flat surfaces.
- Job shop and small-batch manufacturers: those unwilling to grind in oil coolant use a combination of conventional alox wheels with CDCF, plated CBN for radial grooves, and occasional vitrified CBN usage as volume justifies.
- Heavy stock castings for land-based engines: manufacturers are moving away from milling to grinding in oil with a combination of advanced ceramic grain (Altos) wheels for roughing and plated CBN for finishing. Existing grind applications with heavy stock on older equipment remain with CDCF technology.

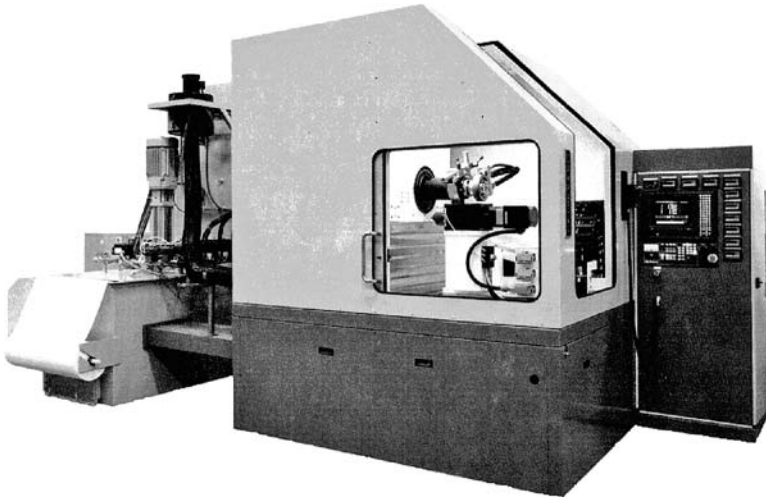


**FIGURE 16.36** Example of 5-axis horizontal spindle grinder for aircraft engine blade multisurface grinding. (Courtesy of Campbell Grinder. With permission.)

Recent developments in machine design have progressed hand-in-glove with the changes occurring in part processing. Dedicated machines for vitrified CBN use small wheels in the range of 8 to 12 (200 to 300 mm) to minimize wheel cost while still maintaining an acceptable range for the dressing crush ratio across a typical 1 depth of form profile.

The working area within the machine is now more a cube to accept the bulky work holding fixture but give free access in all directions. In many cases, this allows a complete downsizing of



**FIGURE 16.37** Example of 5-axis vertical spindle grinder for aircraft engine vane multi-surface grinding.

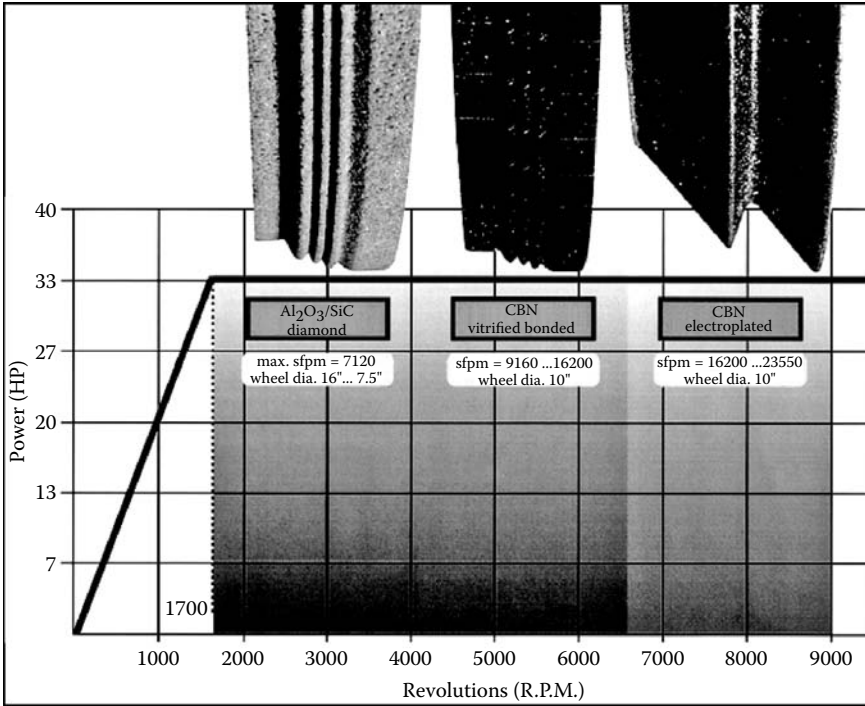


FIGURE 16.38 Power speed combinations for different abrasives.

the machine size, especially width, but with increased stiffness. Several machine tool builders of small, mini, creep feed grinders report machine loop stiffness values in the range of 750,000 to 1,250,000 lbf/in. (130 to 220 N/ $\mu$ m).

Wheel spindle motors must be variable speed with power and torque curve characteristics closely matched to the expected wheel diameter range and types of wheels to be run. This ensures sufficient power over the full life and expected operating speeds of each wheel type. Most ac servomotors have a peak power at a particular rpm and drop off progressively with rpm on either side of this value. Trying to combine different wheel types and diameters, therefore, becomes a compromise. The required wheel speed ranges and diameters for each wheel type are normally as shown in Table 16.9.

It is possible to provide flexibility in order to use a combination of vitrified CBN and regular alox wheels or to use vitrified and plated CBN. In order to provide flexibility with a single machine configuration for all three compromises the power available, some OEMs, such as Blohm [n.d.],

**TABLE 16.9**  
Wheel Diameters against Operating Speed

Bond System	Normal Operating Wheel Speed (sfpm)	Wheel Diameter Range (in.)	Wheel rpm Range
Vitrified alox	4,000–6,500	14–18	850–1,775
Vitrified CBN	6,000–10,000	10–12	1,990–3,820
Plated CBN	9,000–14,000	6–10	3,440–8,910

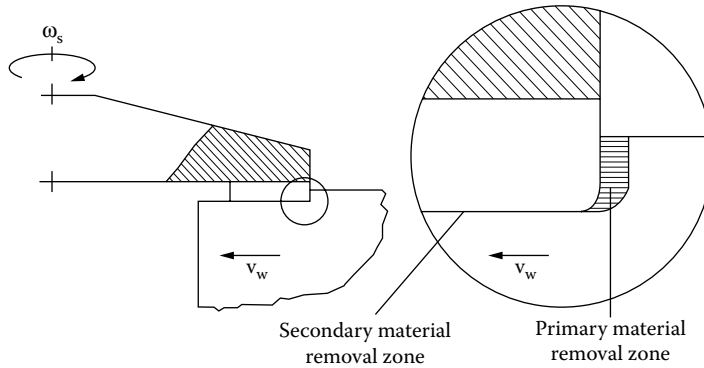


FIGURE 16.39 Material removal in vertical spindle face grinding with horizontal feed.

have developed their spindle technology (Figure 16.39) to extend the range of RPMs over which they can maintain a high level of power. This makes their grinders particularly suitable for the job shop environment by now allowing the use of all the three abrasive types without significant compromise on wheel diameters.

In conclusion, the machine tool industry has undergone major changes over the last 5 years driven by changes in part-processing philosophy and abrasive-wheel technology. This has led at one extreme to dedicated grinders designed in many cases to the processing of a specific part. At the other extreme, machine tools have become ever more flexible both in the use of a greater range of wheel technologies and to encompass multiple metal removal processes.

## 16.6 FACE GRINDING

### 16.6.1 INTRODUCTION

Face grinding is surface grinding using the face of a grinding wheel. Face grinding may be contrasted with the previous examples in this chapter in which grinding was performed predominantly with the peripheral surface of the grinding wheel. Face grinding encompasses a range of processes characterized by a total conformity between the wheel and workpiece. These include segment grinding, double- and single-disc grinding, and double- and single-sided fine grinding. For such a configuration, the standard equation for uncut chip thickness does not apply since  $d_e = \infty$ . Malkin [1989] analyzed vertical spindle face grinding with linear horizontal feed and determined the maximum uncut chip thickness that occurs at the middle of the vertical step (Figure 16.39). For a triangular chip cross section, the chip thickness is given as

$$h_{cu} = \sqrt{\frac{\sqrt{3}}{Cr} \cdot \frac{v_w}{v_s}}$$

where  $v_w$  = table speed,  $v_s$  = wheel speed,  $C$  is the number of active cutting edges per unit area of the grinding wheel surface, and  $r$  is the ratio of width to depth of the triangular chip cross section.

Similarly Malkin [1989] also analyzed face grinding with infeed only (Figure 16.40). In this case, the uncut chip thickness is considered constant and given by

$$h_{cu} = \sqrt{\frac{2}{Cr} \cdot \frac{v_f}{v_s}}$$

where  $v_f$  = infeed and  $v_s$  = wheel speed.

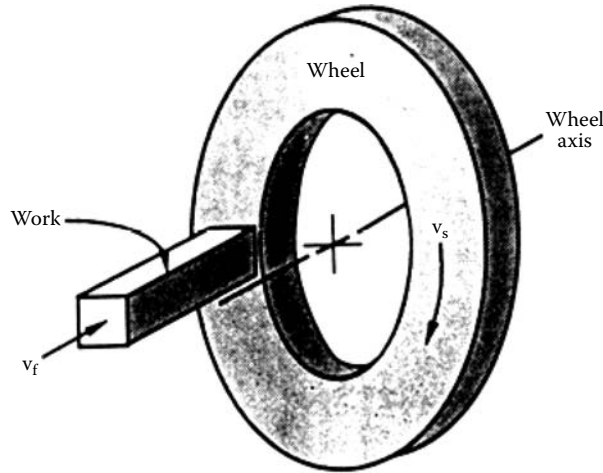


FIGURE 16.40 Face-grinding with plunge feed.

For either configuration or in combination, it is, therefore, possible to predict factors affecting grinding energy and power for the process and by implication burn based on

$$e_c \propto \frac{1}{h_{cu}^n} \propto \sqrt{\frac{v_s}{v_w} \cdot C \cdot r} \cdot \text{or} \sqrt{\frac{v_s}{v_f} \cdot C \cdot r}.$$

$$T_{\max} \propto \sqrt{a_e \cdot v_s \cdot C}.$$

Not surprisingly, conventional wheels for surface grinding are open-structure coarse-grit and friable grain. Superabrasive wheels are low concentration to keep  $Cr$  values low. Wheel speeds are also reduced or in the case of fine grinding as low as 1 to 3 m/s, in part because of the risk of burn but also because the wheels are in shear, which leads to lower burst speeds than in cylindrical grinding.

Heat generation and the associated temperature profiles have been modeled for both linear feed and straight infeed grinding. Lin and Zhang [2001] modeled the temperature field for a cup wheel grinding with linear infeed (Figure 16.41).

They found that the temperature rise is extremely abrupt at the leading edge of the wheel and does not fall away quickly behind. The rise in temperature peaks within 2 mm of the edge of the wheel. The model is based on a simple arc-line heat source. In reality, there will be frictional rubbing from the flat secondary cutting area leading to additional heating. For this reason, where the grind process allows, such as when using highly wear-resistant superabrasive wheels, the width of contact is kept to less than 5 mm and ideally 3 mm.

Spur [1995] calculated the temperature distribution in solid circular components during double-sided fine grinding. Even at low wheel speeds encountered in fine grinding (<4 m/s) quite significant increases in temperature could arise and be focused at specific points.

Such temperature distributions cause differential thermal expansion with the effect that more material is ground off the hottest points on the part and flatness is compromised as the part cools. At higher speeds such as in double-disc grinding, especially of thin parts, coolant starvation can create more catastrophic effects akin to film boiling and resulting in severe burning in often quite localized spots. In high-precision grinding or at high speeds, low heat generation and/or effective coolant delivery is critical.

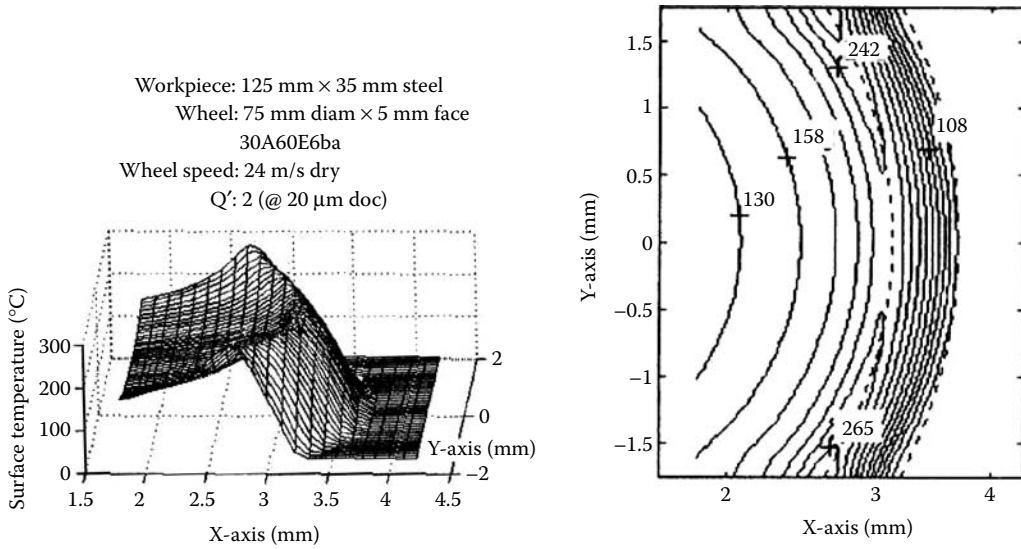


FIGURE 16.41 Temperature distribution in face grinding. (From Lin and Zhang 2001. With permission.)

### 16.6.2 ROUGH GRINDING WITH SEGMENTED WHEELS

Grinding with segments represents the rough, high stock removal end of the flat grinding spectrum. The machine can be very large with powerful motors. The largest recently had a 200-diameter chuck, 117-diameter grinding wheel, and a 600-hp wheel drive custom built for a company to manufacture saws [Anon. 1995].

The majority of segment grinders have rotary tables such as those manufactured in the past by Cone Blanchard and Mattison that offered machines with standard chuck diameters from 20 to 136, spindle motors from 15 to 450 hp, and wheel diameters from 11 to >72. There are still a huge number of these machines in production worldwide with processes that date back to well before 1940 and machine designs that have changed little in the last 20 years [Blanchard 2000, Mattison n.d.]. Wheel speeds are 4,200 sfpm or less. Coolant is delivered to both the outside of the wheel and through the spindle. Table speeds are such that wheel/table rpm will be in the standard range 25:1 to 100:1 to allow adjustment for chatter and burn.

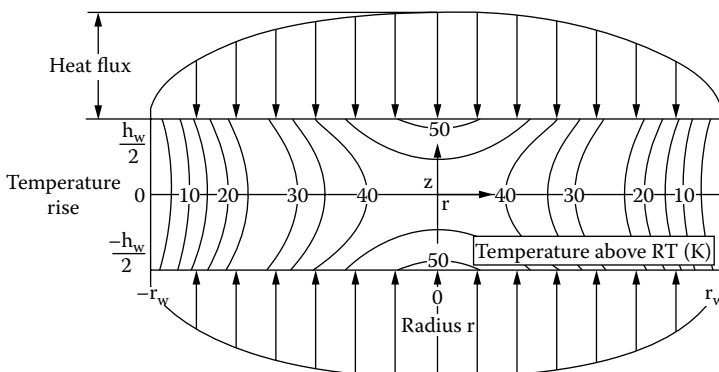
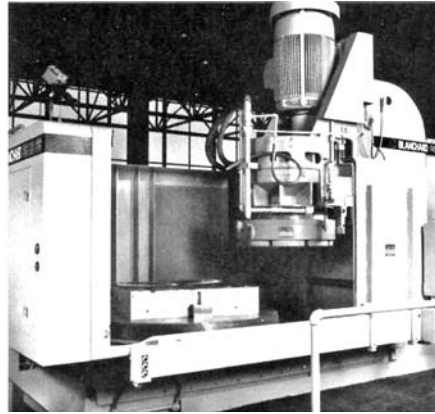
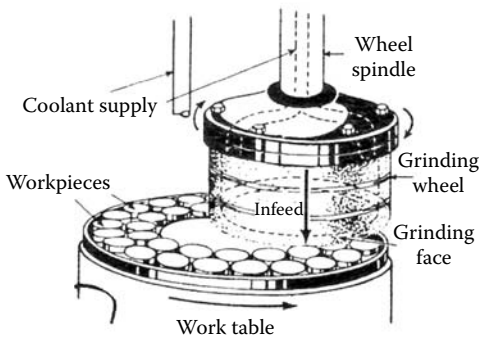


FIGURE 16.42 Temperature rise distribution in double-sided face grinding. (From Spur 1995. With permission.)



**FIGURE 16.43** Vertical spindle face grinding with segmented grinding wheel and rotary work table. (From Reform n.d. With permission.)

With wheel sizes so large, segments are the only practical way of keeping the weight manageable for mounting and demounting. They can also provide additional clearance for coolant access and flushing of swarf. Segments are available in a vast variety of shapes. Some are like pie segments, some form a tongue and groove to lock together, while others are for specific clamping mechanisms. The commonest shapes in the United States are for Blanchard, Cortland, Mattison, and Ferro chucks.

The commonest European grinders seen in the United States are Reform and Goeckel. These machines have linear tables and use smaller segments. They are popular to grind knives for the paper, ceramics, food, and cutlery industries [Reform n.d., Goeckel 1997].

Segments for rough grinding are usually vitrified, highly porous (E–G grades), and contain coarse grit. For the highest metal removal rates, 24#–30# grit is used, which, with an appropriate sparkout, will give a good visual finish (63 RMS). 36#–46# grit is used only for very fine finishes or for grinding difficult materials such as hardened tool steels or some stainless steels. The finest grit sizes available are 180# for the most difficult materials.

Abrasive types are almost exclusively conventional with the exception of some diamond for certain ceramics grinding. CBN is occasionally used, but only for the smallest wheel sizes as the wheel cost is prohibitive. Also, where it is used it is only for fine finish applications as the grit sizes required for roughing (>80#) are not available or cannot be held effectively in the bond (for

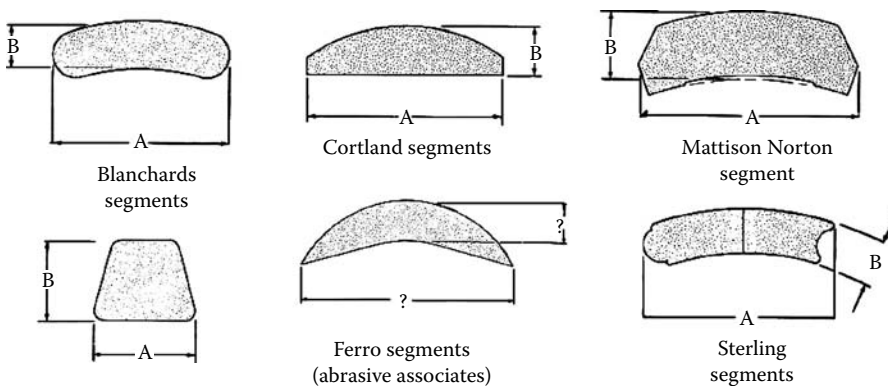


**FIGURE 16.44** Grinding wheel segment shapes.

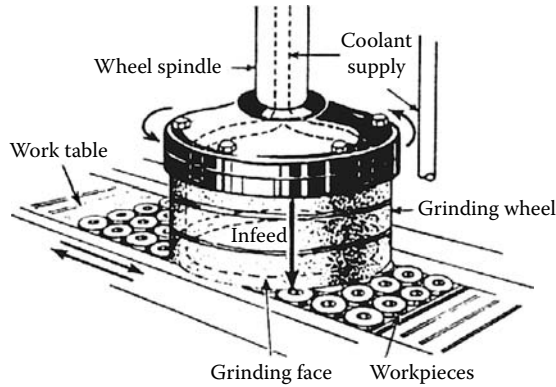


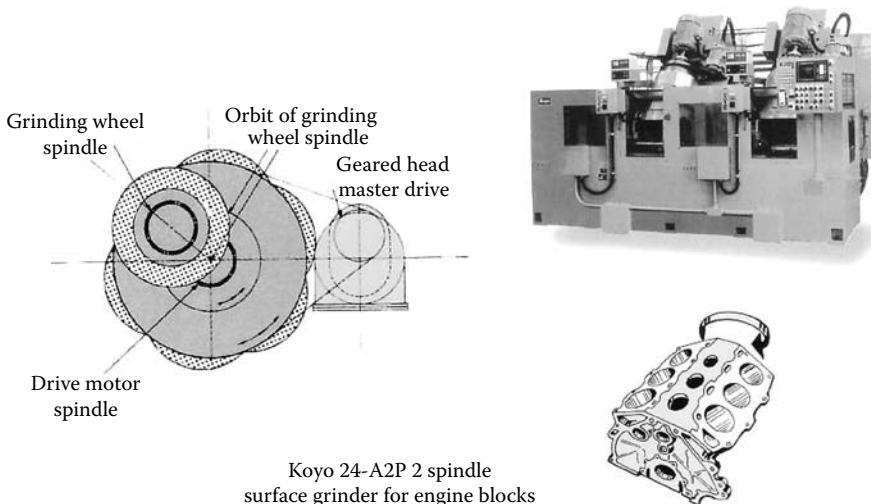
**FIGURE 16.45** Vertical spindle face grinding with linear work table.

the same reason grit sizes coarser than 24# are not used in conventional abrasive segments). The largest wheel noted in the literature is a 22-diameter resin wheel using metal bond segments and resin bond continuous rim CBN at 80# for grinding tool steels [Deming and Carius 1991].

SG is generally offered as an alternative to CBN to improve life and removal rates. Downfeed rates of 0.025 ipm (0.625 mm/min) are reported on D2 steel using SG abrasive in the hardened or unhardened state [Narbut, Stafford, and Tartaglione 1997]. Stock-removal rates are usually determined by monitoring power and burn and by observing wheel wear. Flatness tolerances are in the range of 0.0005 to 0.005 (12 to 125 μm) for general roughing.

With proper grade selection, a wheel should be virtually self-dressing. Diamond-impregnated tools or steel “star cutter” dressers can be used, if required, for initial truing or conditioning purposes.

A lot of rough grinding operations have seen competition from other processes, especially milling and turning. This has led to some interesting shifts back and forth from one process to another. A case in point is the sealing surfaces of engine blocks. This has swung between grinding and lapping, to machining and lapping, then back to grinding or machining only as technology or block design has changed. Currently grinding tooling cost is less than machining and can generate



Koyo 24-A2P 2 spindle surface grinder for engine blocks

**FIGURE 16.46** Koyo inclined head orbital face grinder. (Courtesy of Koyo Machine. With permission.)



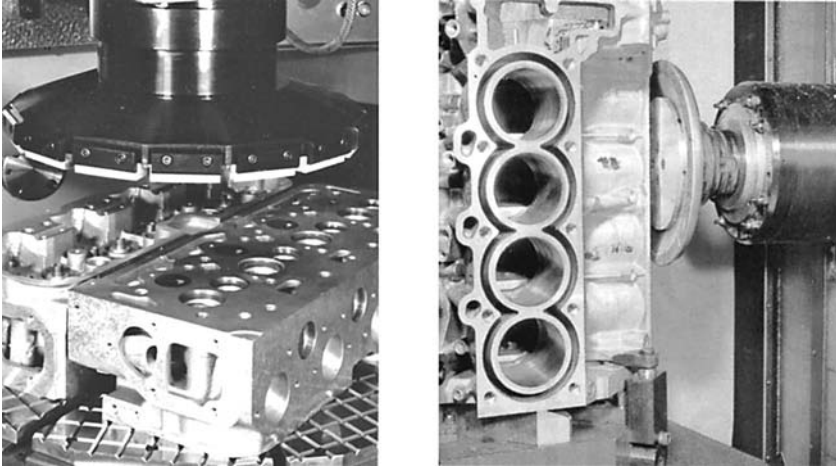


**FIGURE 16.47** Examples of engine block face-grinding setups. (From Sess 1999, Thielenhaus n.d. With permission.)

better sealing surfaces, but machining centers have less capital equipment cost and can have much flexibility for other applications. The industry has, therefore, numerous solutions depending on the tolerances, sealing requirements, and capacity requirements.

Koyo [2001] offers an inclined-head orbital surface grinder to rough and finish grind engine blocks in a production line environment on a single machine. The orbital motion allows the use of a relatively small 355-mm wheel to minimize grinding pressure and part distortion.



**FIGURE 16.48** Examples of small rotary surface face grinders. (From Delta 1997, DCM Tech 1999. With permission.)

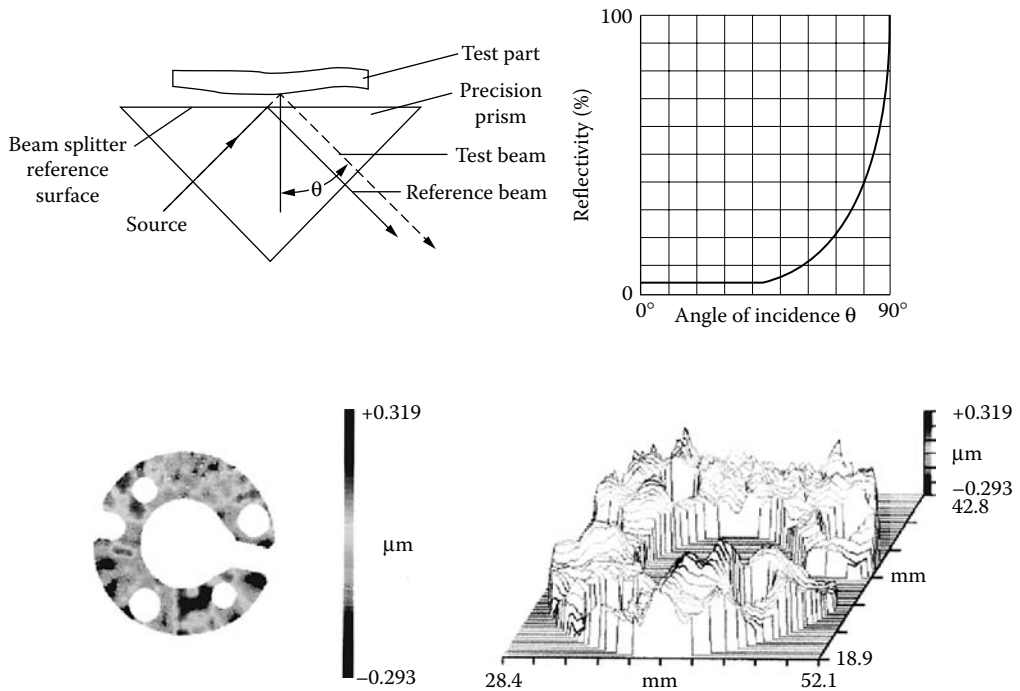


FIGURE 16.49 Flatness measurement by grazing angle interferometry. (From Tropel 1996. With permission.)

### 16.6.3 ROUGH MACHINING/FINISH GRINDING

For manufacturers that choose to rough machine the part, Thielenhaus [n.d.] provides a grinder/superfinisher to microfinish the faces to create a good sealing surface. This is particularly suited for applications such as aluminum cylinder heads with hardened liners that create step problems for machining. The process uses small conventional abrasive segments in a rotating grinding head. Makino [Sess 1999] reported a postmilling process using small high-speed electroplated diamond wheels. A similar combination of turning and electroplated CBN grinding was recently developed to replace double-disc grinding of connecting rods. Three solutions are from machine tool builders with traditions in grinding, superfinishing, and machining, respectively.

### 16.6.4 SINGLE-SIDED FACE GRINDING ON SMALL-SURFACE GRINDERS

This particular type of grinding refers to a range of small inexpensive grinders that use wheels from 18 to as small as 6 for a host of small part applications in tool rooms and small production shops. Typical examples include bearing rings, aircraft parts, punches, dies, seals, inserts, pump components, EDM electrodes, and ejector pins. The wheels may be segments, or more commonly continuous rim, and divided between conventional and narrow rim superabrasive grain. In many ways, this is a continuation of the grinding described in the previous section except using smaller, stiffer machines to obtain tighter tolerances, and with an increased wheel speed range on some models up to 10,500 sfpm (55 m/s). Common machine types in the United States include DCM Tech [1999], Swisher [2000], and Delta [1997].

### 16.6.5 HIGH-PRECISION SINGLE-SIDED DISC GRINDING

The grinders referred to in this section are a further extension of those described above focused at flatness tolerances in the micron and submicron level often in competition with lapping.

**TABLE 16.10**  
**Examples of Face Grinding Applications on Small Rotary Grinders**

Material	Hardness	Part Function	Rate Stock Removal	Tolerance		Surface Fin
				Thickness	Flatness	
A-2	60Rc	Punch	.035/min	.0005	±.0002	20 Ra
A-6	62Rc	Rachet Ring	.018/min	±.0001	±.0002	16 Ra
D-2	60/62Rc	Form Roll Die	.003/min	±.0003	±.0003	24 Ra
M-50	55Rc	Aircraft Brg	.010–.020/min (all four surfaces ground)	±.0001	±.00015	8–10 Ra
T-15	60/62Rc	Form Tool	.020/min	N/A	±.0002	8–12 Ra
4140	50/55Rc	Gear Blank	.070/min	.0005	±.0002	24 Ra
P/M	~55Rc	Hyo Pump	coarse feed/fine feed .050–.010/min	±.0001	.0001	16 Ra
8620	60Rc	Spur Gear	coarse feed/fine feed .100–.020/min	±.0003	±.0003	24–32 Ra
P/M	~50Rc	Hyo Pump Gear	coarse feed/fine feed .040–.005/min	±.00015	±.00015	32 Ra
P/M	~50Rc	Hyo Pump Gear	coarse feed/fine feed .044–.005/min	±.00015	±.00015	32 Ra
Carbide	—	Mechanical Seal	.012/min	±.0002	±.0002	6–10 Ra
Carbide	—	Mechanical Seal	.002/min	±.0001	±.0001	0–1 Ra
ALO <sub>2</sub>	—	Electronic Comp	.030 min	±.0005	±.0005	—
Epoxy	—	Seal	.080/min	±.0005	±.0002	—
Carbon	—	Seal	.080/min	±.0005	±.0002	—
Graphite	—	Disk	.020/min (15 PCS/Chuckload)	±.0002	±.0003	8–12 Ra
1060	55/58Rc	Brg End Plate	.012/min (25 PCS/Chuckload)	±.0003	±.0005	16–24 Ra
1018	Soft	Servomotor Stator	.020/min (8 PCS/Chuckload)	±.0002	±.0002	32 Ra
Magnetic Steel	Soft	Antilock Braking Component	.035 min	±.0005	±.0005	32 Ra
430 Stainless Steel	Soft	Antilock Braking Component	.035 min	±.0005	±.0005	32 Ra
Carbide	—	Insert	.015/min (45 PCS/Chuckload)	±.0002	±.0002	8–12 Ra
Carbide	—	Insert	.001/min (8 PCS/Chuckload)	±.0001	±.0001	0–1 Ra
Bakelite	—	Fuel Control System Component	.020/min (36 PCS/Chuckload)	±.0003	±.0005	32 Ra

Measurement of flatness at the micron level is critical and care should be taken where flatness has been defined by a machine tool builder as to how that value was determined. Use of indicators on a gauge table, linear measurements on Talysurf-style equipment, or counting fringes using an optical flat and monochromatic light source will generally give an overoptimistic value. The most accurate system currently available for general production is based on various grazing angle reflection interferometry technologies with equipment made by companies such as Tropel and Zygo.

The method relies on the interference of light, and the fact that the reflectivity of a rough surface increases dramatically when the light strikes it at a glancing angle allowing inspection of apparently nonreflective surface such as ceramics, plastics, metals, and composite. It is the same

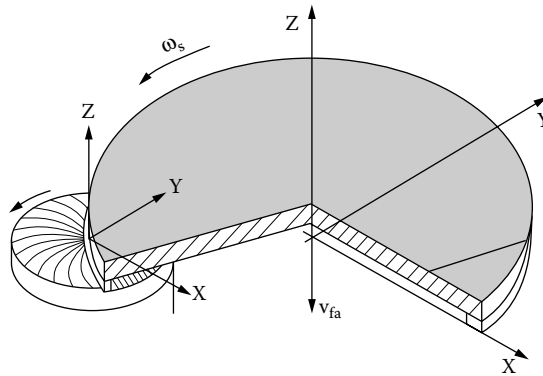


**FIGURE 16.50** Single-disc grinder configuration.

concept as when sunlight strikes water near sunset. The light is reflected much more than at noon. The system uses a laser beam to generate a well column of light, which is divided into two beams by partial reflection at the prism surface. Part of the beam is then reflected off the part where it is then recombined after re-entering the prism creating interference fringes. A camera system then captures data at about 60,000 coordinate points to compile a 3-D image of the test part. The interference pattern is phase shifted by slightly moving the prism and the sinusoidal variation in light intensity is then monitored for each data point. Software then analyzes the phase shift to give the 3-D height map. The system has a resolution of  $0.01\ \mu\text{m}$ , an accuracy of  $0.1\ \mu\text{m}$ , and a range of about  $30\ \mu\text{m}$  in height variation. Image processing time is about 30 s, which is quite sufficient for shop floor process monitoring. Systems are available to handle up to 500-mm parts.

Single-disc grinder technology for the precision steel industries such as automotive components, hydraulics, seals, etc. has been influenced significantly by developments from the semiconductor industry for wafer grinding. To achieve good flatness requires a very stiff machine combined with precision work handling equipment to hold and spin the part, and low grinding forces. Stiffness is achieved by using small wheels with a large spindle bearing to limit cantilever deflection at the wheel edge. Workholders are belt- or gear-driven to spin the part and narrow-faced wheels are used to limit grinding pressure. This naturally leads to the use of superabrasives for wear considerations.

Koyo [2000], for example, has designed a range of single-disc grinders for targeting parts with flatness requirements of the order of  $0.2$  to  $2.0\ \mu\text{m}$  using several combinations of grind methods, grinding either one or two parts at a time or roughing and finishing simultaneously with two wheel heads. In one instance, the author ground hardened-steel cylinders 25 mm in diameter with vitrified CBN wheels and achieved a flatness of  $0.3\ \mu\text{m}$ , finish of  $0.15\ \mu\text{m Ra}$ , stock removal of  $100\ \mu\text{m}$  in 4-s roughing, and a total production rate of 350/hr dressing every 4,000 parts. This was achieved in water-based coolant.

A similar approach, using narrow-face wheels, has been taken by a number of machine tool builders who traditionally specialized in superfinishing. Their processes now often require stock removal, placing them more into a grinding than a polishing regime. Supfina [1996] has reported a machine design for superfinishing of valve tappets. In this case, the tappet face requires a well-defined crown, which is generated again by the use of a small face wheel but with its axis of rotation tilted slightly to that of the part (Figure 16.52).

Research into the use of superabrasive wheels with narrow face widths has resulted in some surprising developments in production grinding in unexpected areas. If the contact width is kept thin enough, the wheel will maintain its flatness indefinitely resulting in grinders using resin or vitrified CBN that do not require dressers. One example is hob grinding; another is “kiss” grinding of thrustwalls on camshaft and crankshafts as a replacement to turning to improve flatness [Hogan 2001].

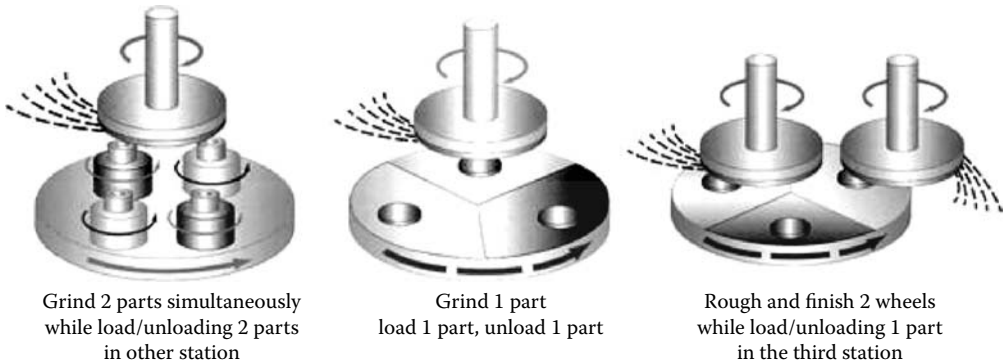


FIGURE 16.51 Grinding strategies for single-disc grinding. (From Koyo 2000. With permission.)

In one example, on crankshafts with Landis 3LB grinders, the author achieved a flatness of  $<4 \mu\text{m}$  with a  $Q'$  of  $40 \text{ mm}^3/\text{mm/s}$  and a G-ratio  $>1,500$ . The CBN wheels ran at speeds up to  $140 \text{ m/s}$  in water-based coolant. The flatness could not be achieved by turning because the chip could not be broken without leaving a raised area.

### 16.6.6 DOUBLE-DISC GRINDING

Double-disc grinding is a high-production, high-accuracy processing for parts with flat and parallel sides. Two opposed grinding wheel discs mounted on separate spindles simultaneously grind opposite and parallel faces on components fed between them by a variety of techniques. Double-disc grinders can be configured in either a horizontal or vertical configuration referring to the axis of wheel rotation. Horizontal grinders are generally used for mid-range part sizes while vertical grinders are used for either very thin or very large parts.

The grinders require extremely high radial and axial stiffness. Most are either designed around a combination of large axial thrust, angular contact, and roller bearing combinations [Daisho n.d., Diskus 1996, Koyo n.d.], or full hydrostatic [Mattison 2 n.d., Kubsh 1998]. The motor drive is

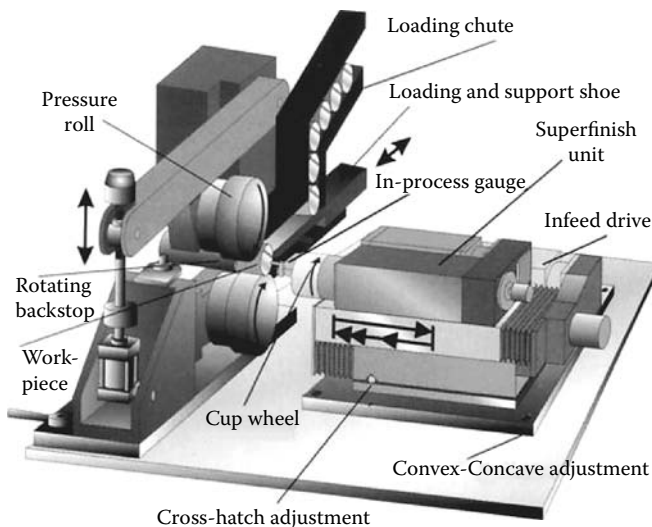
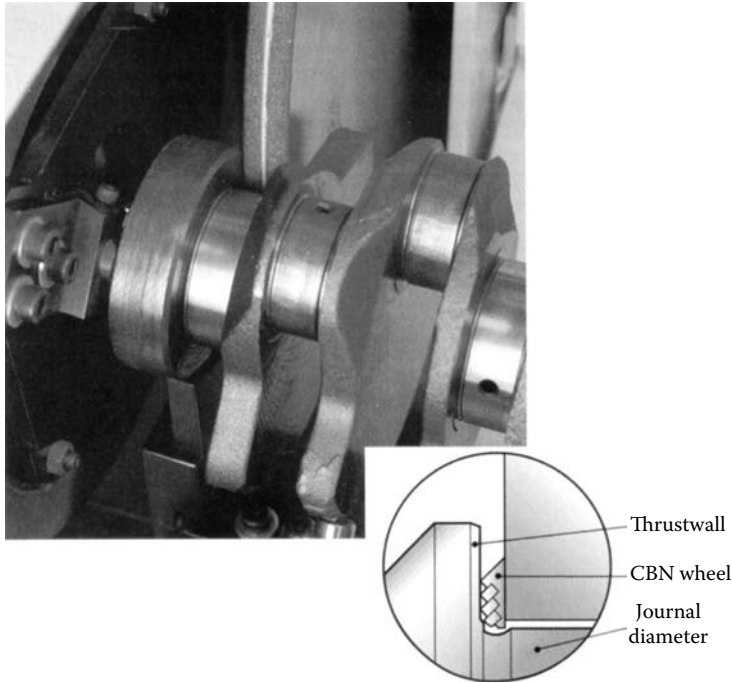


FIGURE 16.52 Superfinishing arrangement for grinding tappets. (From Supfina 1996. With permission.)



**FIGURE 16.53** Face grinding of crankshaft side walls.

usually a synchronous or servo ac belt drive rather than a direct drive because of space limitation of the machine configuration. The spindle shaft and wheel-mounting surface are made from a one-piece steel construction with coolant passed through the center. The wheel is supplied either as an abrasive layer bonded to a steel back plate or as a layer with nuts inserted into the back face, which is in turn bolted to the spindle wheel mounting face. The components of double-disc spindle [Landis Gardner 1989] and wheels are shown in Figure 16.56 and Figure 16.57. Coolant, passed through the center hole, is disseminated over the surface of the wheel with slots while holes relieve the pressure and provide chip clearance and coolant access.

Most wheels for double-disc grinding are resin- or plastic-bonded running at speeds of 35 m/s or less. Resin and plastic bonds can withstand more lateral strain and abuse than other more brittle bonds. Some oxy-chloride bonds are still used with conventional abrasives for the cutlery industry for dry grinding or where cool cutting is critical. Vitrified bond usage has been increasing especially



**FIGURE 16.54** Horizontal spindle double-disc grinder. (Courtesy of Guistina. With permission.)

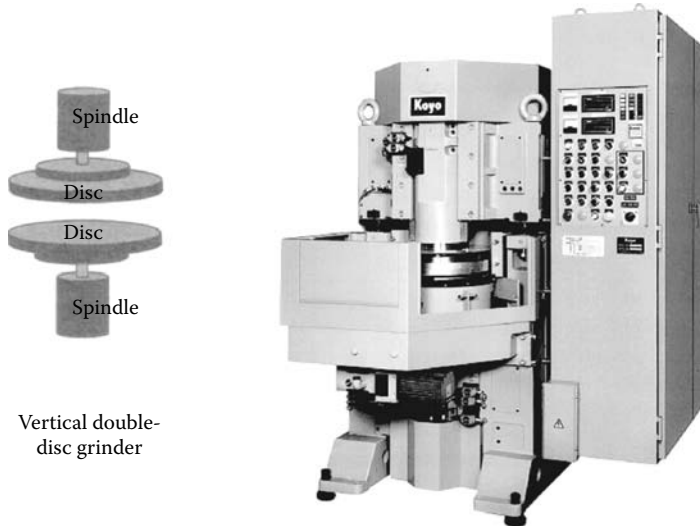


**FIGURE 16.55** Vertical double-disc grinder. (Courtesy of Koyo Grinder. With permission.)

with CBN for finish grinding on small machines specifically designed for using superabrasives. There has also been some interest in the spring grinding industry for electroplated CBN. Anker [1998] reported success in ends grinding of springs dry at 60 m/s on small purpose designed machines using coarse grit ABN 600, although resin-bonded CBN is more common, especially in Japan.

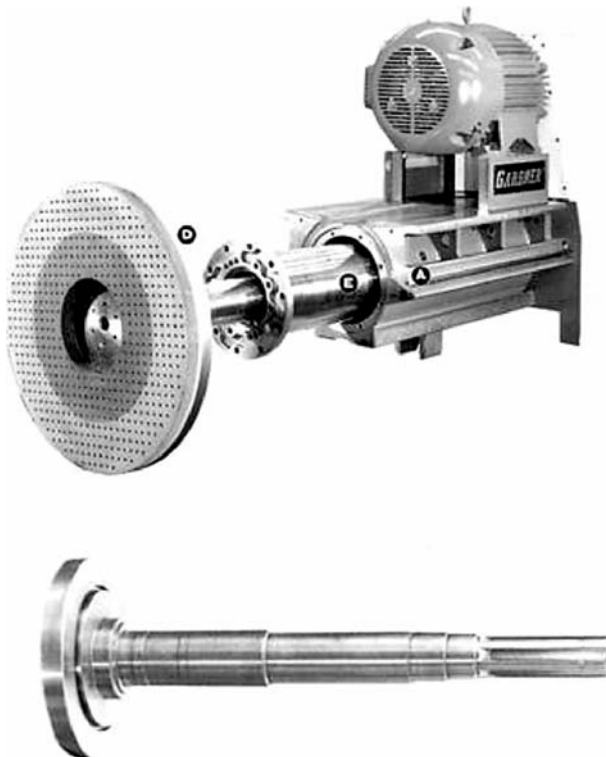


**FIGURE 16.56** Components of a double-disc grinder wheel spindle unit.

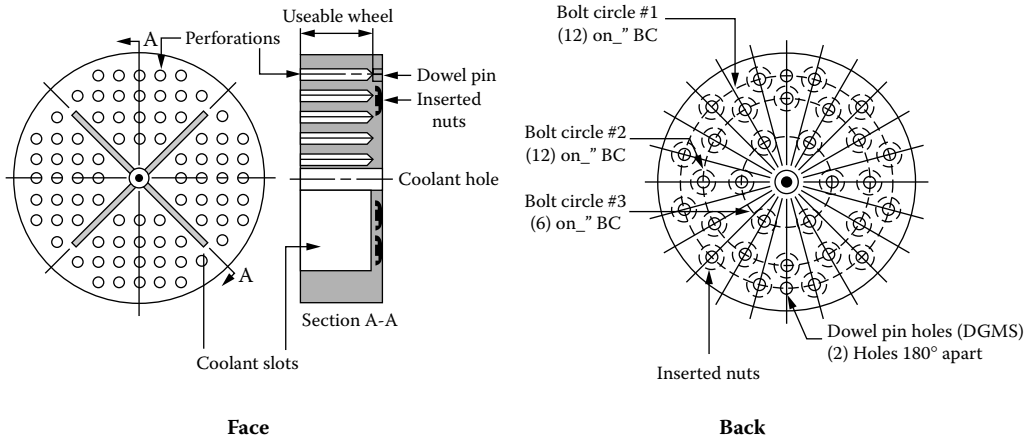


**FIGURE 16.57** Components of a double-disc wheel.

Conventional abrasives still dominate virtually all general roughing processes and commercial-type finishing and semifinishing operations. 16#–36# grit is used for rough grinding, 36#–80# for commercial finishes and tolerances, and 60#–150# for fine finishes and tight tolerances. It is only in this latter category that CBN, in particular, has been competitive with grit sizes in the range of 100#–600#. Deming and Carius [1991], for example, reported good success grinding hydraulic pump vanes on retrofitted Besly double-disc grinders using 30 resin CBN wheels although they note on new dedicated machines the wheel size was reduced to 23.

Since thickness and flatness control is critical, the grinder should be kept in a temperature-controlled room with the coolant chilled to ambient. Some manufacturers even keep workpieces in a coolant bath before grinding so as to stabilize the temperature. With coolant passing through the center of the spindle to remove heat, thermal growth can be held to a minimum. This is further aided by the machine configuration and spindle design inherent in double-disc grinding such that

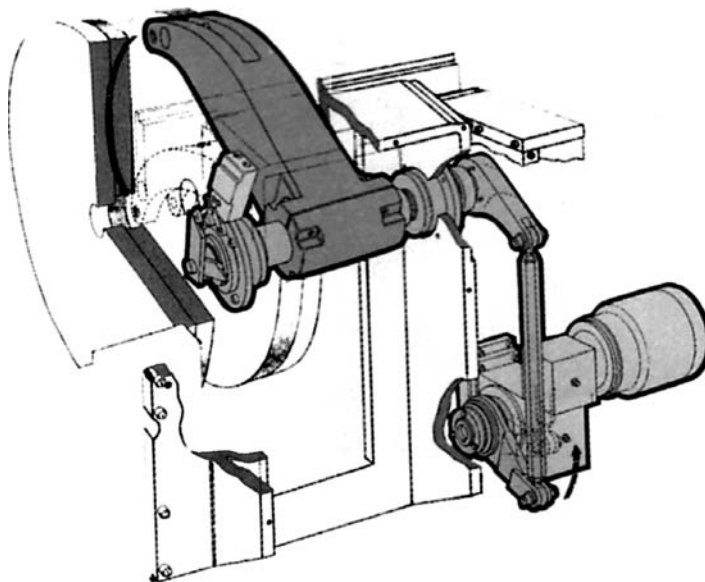


**FIGURE 16.58** Dressing mechanism for horizontal spindle double-disc grinder.



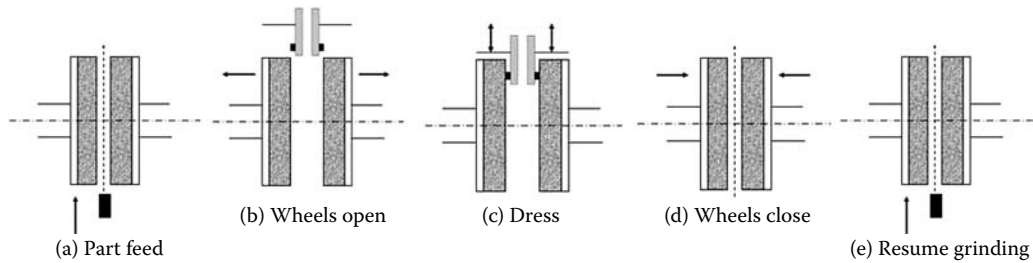


**FIGURE 16.59** Automated dressing cycle for double-disc grinding. (From Mattison 2 n.d. With permission.)

there is a tendency to compensate for thermal growth in the base with growth in the opposite direction for the spindle [Schlie and Rangarajan 1987]. Nevertheless, this is not perfect and compensation must still be added for wheel wear so postprocess gauging is common on precision operations. Timed compensation is more common for commercial tolerance work.

Conventional wheels are dressed using either stationary diamond or star cutter dressers mounted on a powered radial arm dresser that swings between the two wheels dressing both at the same time. The face of each wheel is dressed flat in relation to the spindle alignment regardless of the head setting. For resin and CBN, the radial arm has on occasion been retrofitted with a rotary dresser for truing in combination with either a grit blast-type conditioning process or stick dressing. Resin diamond wheels are almost exclusively dressed using dressing sticks.

There are a variety of techniques for double-disc grinding depending on the stock removal and part tolerance requirements.

Rough grinding with the highest removal rates use through-feed grinding in a shear mode. Through-feed grinding involved feeding the parts supported by rails top and bottom through the center of the wheel. The parts are driven at the entrance of the wheels by belts in contact with the side of the part. Passage through the wheels is driven by contact with the part behind. The wheels are angled with a “head setting” such that the gap between them is narrowest at the entrance where 75% of the stock is removed. Often two or even three grades are used across the face of the wheel to allow for changes in surface footage and prevent burning in the center portion where only rubbing occurs. The wheel wears over time causing a step to move progressively over the wheel face and toward the center.

Higher precision is achieved by progressively grinding using a rotary feed or carousel method. In this case, the wheels are again angled but the maximum clearance is at the exit. The parts are fed in a rotary carrier with pockets that closely match the part shape. Small parts, especially those with a high aspect ratio, are sometimes rotary-fed by a geared-tooth inner ring surrounded by a smooth outer ring.

The calculations for the feed geometry and head settings are relatively straightforward. The carousel should pass over the wheel such that the centerline of the part cuts the inner diameter of the abrasive face. Wheels for rotary grind double disc have a large center hole in order for limited variation in surface footage across the face. Most spindle heads have three or four bolts at pivot points that can be raised up and down and monitored by a portable micrometer. The adjustment can be as simple as a single nut or a series of lockscrews and adjusting screws. There is some debate as to how the stock should be removed. For conventional wheels, the entrance gap should take 20 to 40% of the stock by shear grind with the remainder removed as it passes through the wheels [Doubman and Cox 1997]. For CBN, however, the cut should start about 20 mm into the wheel such that the outer surface of the wheel is kept wear free to just finish grind for flatness.

The wheel should initially be set at zero and then simple geometry allows a ready calculation for how much the entrance and rear pivot points need to be raised in order to equalize stock removal

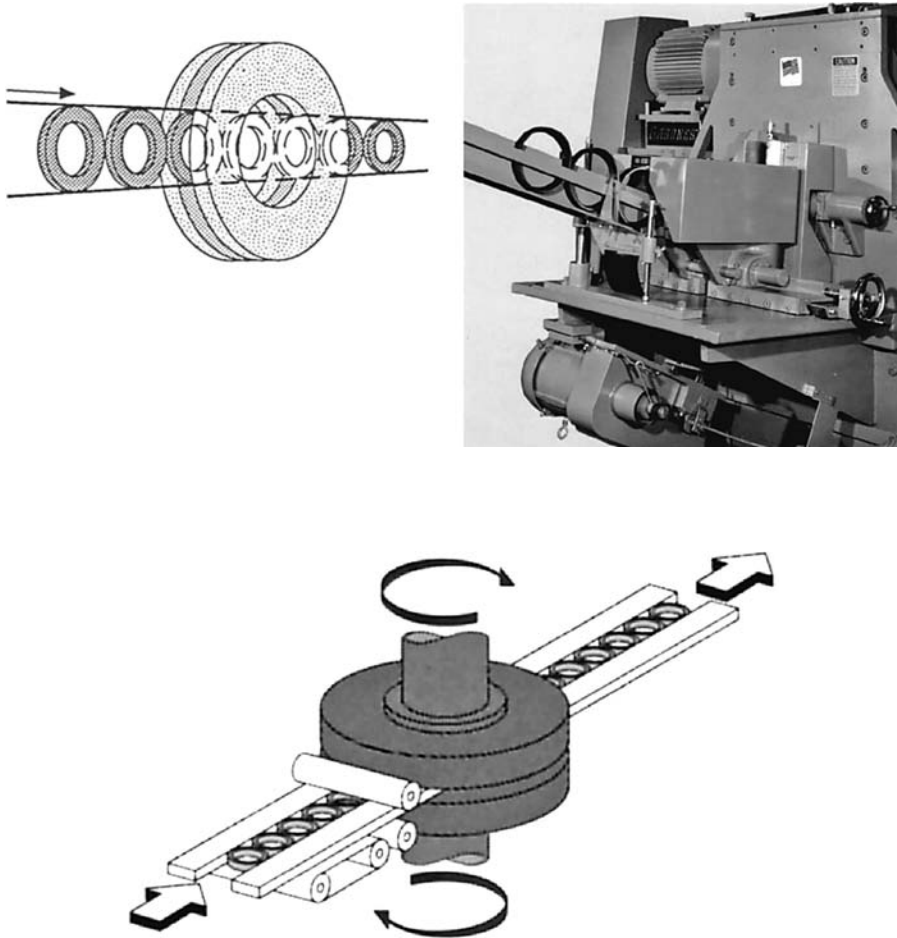
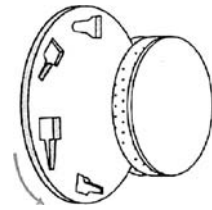


**FIGURE 16.60** Double-disc grinding arrangements. (From Landis Gardner 1989, Diskus 1996. With permission.)

along the whole grind path. The entrance should then be double-checked for clearance with an unground part with the wheels stationary.

Again, two grade wheels are sometimes used. For example, one design by the author uses a combination of coarse grade CBN pellets for rough grinding (for reducing contact area) with a fine grit CBN continuous rim. This increased stock removal capability on one application by a factor 3.

On a vertical disc grinder, the bottom wheel should be set slightly higher than the exit plate. The parts should fit snugly in the carrier. Special attention should be paid in the case of round parts as flatness can be significantly improved if the part is allowed to spin in the holder. The spin is generated by the relative surface footage seen by one side of the part relative to the other. Obviously, the spin can be greatly enhanced by rotating the wheels in opposition but this creates too much wheel wear and can damage the carrier. The wheels are, therefore, rotated in tandem with a small difference in rpm between the two to vary the spin. Excessive spin will cause wear of the carriers that are often made of only mild steel or fiberglass. In some cases, carbide inserts are added to prolong life. The spin is such an issue that it can often be the primary factor governing the selection of coolant. Too high a lubricity can cause the part to lose traction and spin sporadically or even hydroplane. For this reason, double-disc grinding often uses synthetic coolant even with superabrasives.



Rotary carrier (carousel)  
double-disc grinding

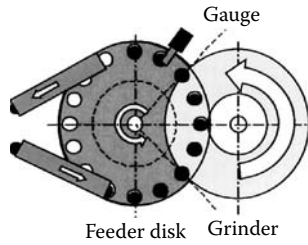
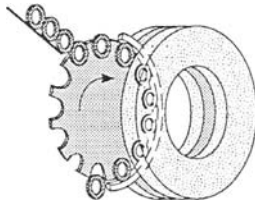
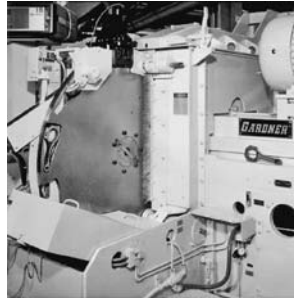


FIGURE 16.61 Rotary and carousel work feeding arrangements.

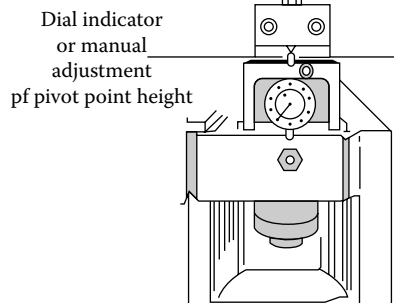
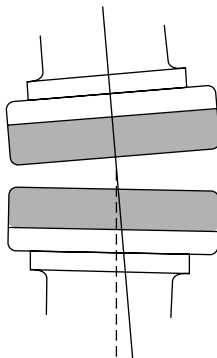
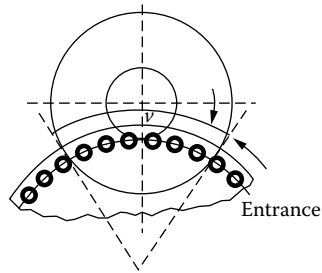
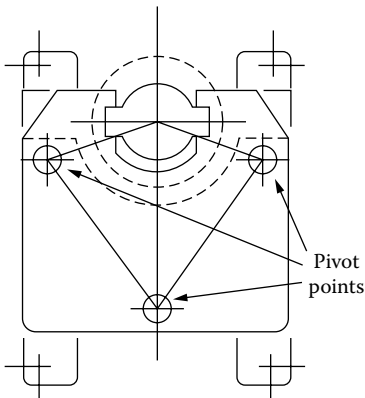
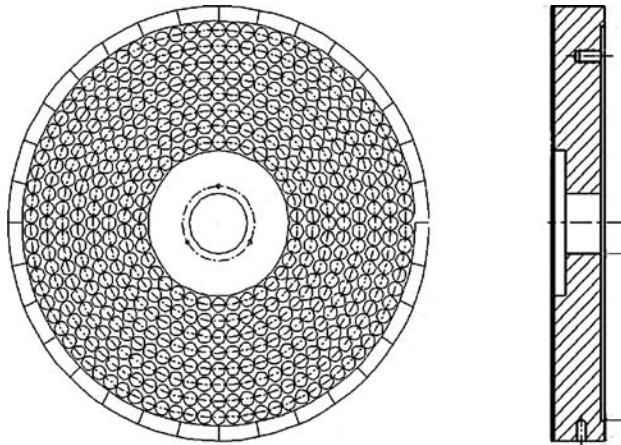


FIGURE 16.62 Three-point adjustment of upper spindle. (From Koyo n.d. With permission.)



**FIGURE 16.63** Two-grade combination pellet and continuous rim superabrasive disc wheel.

Coolant is delivered through the center of the spindle but must be dispersed by means of a baffle or other device to fling the coolant outward. This is made more difficult by the presence of the carrier. For thin parts, the carrier can warp and may well end up being ground on occasion leading to an increased risk of burning.

For the highest precision, through-feed grinders are typically small, compact, and use superabrasives. Examples include the Koyo models KVD 300 (305 mm wheels) and KVD 450 (455 mm wheels). Very few examples exist of larger wheels except for some older references to grinding pump vanes with 23 vitrified CBN [Navarre 1986, Landis Gardner 1989], and for finish grinding of piston rings with 600 mm resin CBN wheels taking 20  $\mu\text{m}$  or less of stock [Buthe et al. 1996]. The problem relates to the difficulty in achieving sufficient stiffness, especially from the cantilever effect that comes into play with the larger diameter wheels as the part exits.

Through-feed grinding, in general, has problems achieving precision tolerances in a single pass with an acceptable cycle time when heavy stock removal is involved ( $>200 \mu\text{m}$ ). The alternative is to infeed the wheel with their faces parallel. Several variations on this method exist. One method is to reciprocate or gun-feed a part between the wheels with linear oscillation. This is particularly effective for controlling wheel flatness when grinding large workpieces.

Alternatives include some form of rotary carrier or swing arm. The carrier may have its own drive mechanism to make the part spin to further improve flatness. Infeed grinding will give the

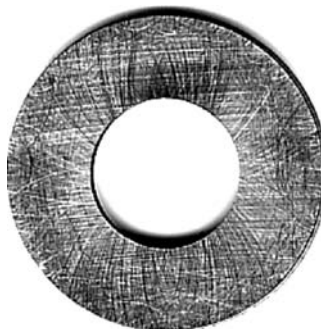


**FIGURE 16.64** Test washer ground with low lubricity coolant.

very best accuracy but at lower production rates. It will also have problems maintaining flatness for prolonged periods of time because of differential surface footage between the outer and inner wheel radii.

The design of the component is important when considering double disc as a processing method. Well-qualified datum surfaces must be provided when trying to control thickness. The surfaces to be ground should be comparable in area, configuration, and stock removal. Otherwise, the stock removed will be uneven or a great deal of trial and error effort must be expended in varying grade and surface footage from one wheel to the other to equalize the removal rates. The face should also be presented to the wheel reasonably flat and parallel. For this reason, the side faces locating in the carriers must also be reasonably square to the surfaces to be ground. There should be no functional surfaces projecting beyond the planes of the surface to be ground. For finish grind operations, the part must be stress relieved, especially for thin parts, to avoid "potato-chip" or "saddle" distortion effects. When through-feed horizontal grinding, the parts need to be in a stable-balanced condition to prevent tipping as they are exiting the wheels.

Typical case history examples from the published literature and trade brochures are given in Table 16.11. Double-disc grinding is limited to tolerances of about 1 to 2  $\mu\text{m}$  for flatness and size and stock levels under 100  $\mu\text{m}$  for high production such as using rotary carrier feed. Slightly better control is possible by infeed grinding but at a considerable cost in cycle time. The best results are again on dedicated machines using small superabrasive wheels.

The limitation on flatness is due to the stiffness of the machine and wheels both in grinding and even in dressing. As stated above, the exit point between the wheels is where the most deflection will occur from being cantilevered furthest from the spindle axis. This is true both for grinding and dressing. Unfortunately, in most cases, the pressure cannot be relieved as in single-disc grinding by reducing the contact width of the wheel.

Resin and many vitrified superabrasive wheels are usually dressed using some form of stick feeder (Figure 16.67).

For larger wheels, the stick pressure becomes the limiting factor for wheel flatness. Koyo has, therefore, developed a contactless dressing process, namely, Electro-Discharge Truing used in conjunction with metal bond diamond wheels. This is reported to double flatness accuracy by eliminating deflection from stick dressing forces.

Double-disc grinding is an important process for the ceramics and semiconductor industry and there is interest here to increase accuracy at high-production rates. One vertical spindle machine design reported by Ueda et al. [1998] involves two novelties. The first is the use of live magnetic bearings to control thickness in conjunction with closed-loop gauging. The second, and perhaps more interesting for its simplicity and general application potential, is to increase the grind length by positioning the parts behind the wheel head. This system grinds electronic filters and oscillators to  $\pm 0.5 \mu\text{m}$ .

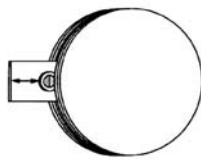
Although spin and reduced wheel-width techniques cannot be used on majority of double-disc grinding applications because of fixturing, there is use of it where only a portion of each surface has to be ground. The most active example currently is brake rotor disc. Grinding is carried out as a finishing operation to improve flatness after turning. The rotors are ground on the outer diameter areas, which means they can be readily held and spun in a work holder. In the 1990s, these were ground using conventional wheels or segments [Anon 1996, Thielenhaus n.d.], but more recently these have been replaced by metal-bonded CBN segments [Daisho 2001] or narrow-faced metal-bonded CBN wheels by machine builders such as Thielenhaus and EMAG. The stock amount varies from 5  $\mu\text{m}$  to 100  $\mu\text{m}$  depending on the turning operation and the material (steel or cast iron). Wheel speeds are low at about 25 m/s or less with blocks but up to 60 m/s with thin-rimmed wheels.

**TABLE 16.11**  
**Examples of Typical Accuracies in Double-Disc Grinding**

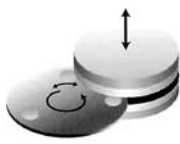
Component	Major Dimension	Stock Allowance	Size	Flatness	<i>l</i> /ism	Finish	Cycle Time	Reference	Year
Compressor cylinder	4.4" diam	.006"	.001"	.0002"	.0002"	25 RMS	18 s	Kibsh	1988
Compressor roller	1.5" diam	.003"	.0002"	.000060"	.000060"	12 RMS	19 s	Kibsh	1988
Compressor vanes	.94" × .16"	.004"	.0002"	.0002"	.0001"	12 RMS	4 s	Kibsh	1988
	.657" × .16"	.009"	.0003"	.0003"	.0002"	12 RMS	4 s	Kibsh	1988
Coil springs	1/8" – 1.25"		.001"		1 degree		1.8 s	Litton	1989
Ferrite seals		.012"	.001"	.00003"	.00003"	20 RMS	1.2 s	Litton	1989
Connecting rod		Rough .0625"					4.5 s	Litton	1989
		Finish .02"	.0002"	.0005"	.0005"	20 RMS	4.5 s	Litton	1989
Circlip		.008"	.001"	.0005"	.0005"	20 RMS	0.72 s	Litton	1989
Aluminum valve part		.020"	.01"	.0015"	.006"	63 RMS	6 s	Litton	1989
Steel washer		Soft .025"	.002"	.001"	.001"	63 RMS	3.6 s	Litton	1989
		Hard .005"	.002"	.001"	.001"	63 RMS	2 s	Litton	1989
Pump rotor			2.5 μm	2.5 μm	2.5 μm	3.2 Ry		Daisho	1998
Cam-ring			2.5 μm	2.5 μm	3.0 μm	0.5 Ra		Daisho	1998
Cylinder			1.2 μm	1.5 μm	1.5 μm	0.5 Ra		Daisho	1998
Drive gear			2.0 μm	2.0 μm	2.0 μm	2.5 Rz		Daisho	1998
Ceramic seal		50 μm		3 μm	3 μm	1.2 Ra	3.5 s	Koyo	c. 1995
Connecting rod		0.3 mm		15 μm	15 μm	3.2 Rz	30 s	Koyo	c. 1995
Compressor roller		50 μm		1 μm	1 μm	1.2 Rz	18 s	Koyo	c. 1995
Bearing ring		80 μm		0.5 μm	0.5 μm	1.0 Rz	0.5 s	Koyo	c. 1995
Aluminum vane		100 μm		5 μm	5 μm	2.5 Rz	8 s	Koyo	c. 1995
Gear		300 μm		2 μm	2 μm	3.2 Rz	10 s	Koyo	c. 1995



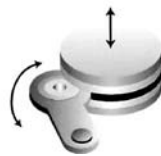
FIGURE 16.65 Test washer ground with high lubricity coolant.



Reciprocating fixture  
double-disc grinding



Rotary infeed  
with oscillation



Swing arm rotary  
infeed method

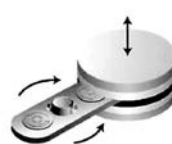


FIGURE 16.66 Examples of feed mechanisms for double-disc grinders.

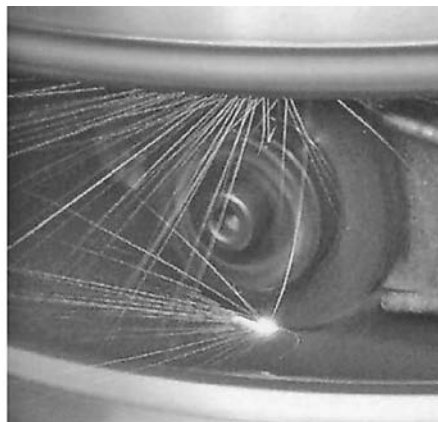
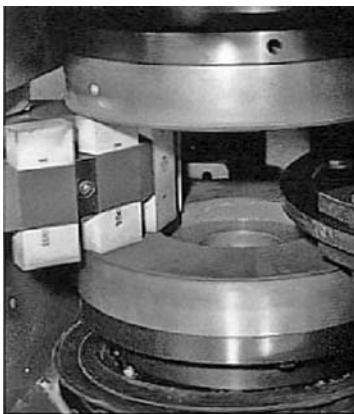


FIGURE 16.67 Comparison of block and electrodischarge truing of superabrasive wheels. (Courtesy of Koyo Machine, Novi, MI. With permission.)

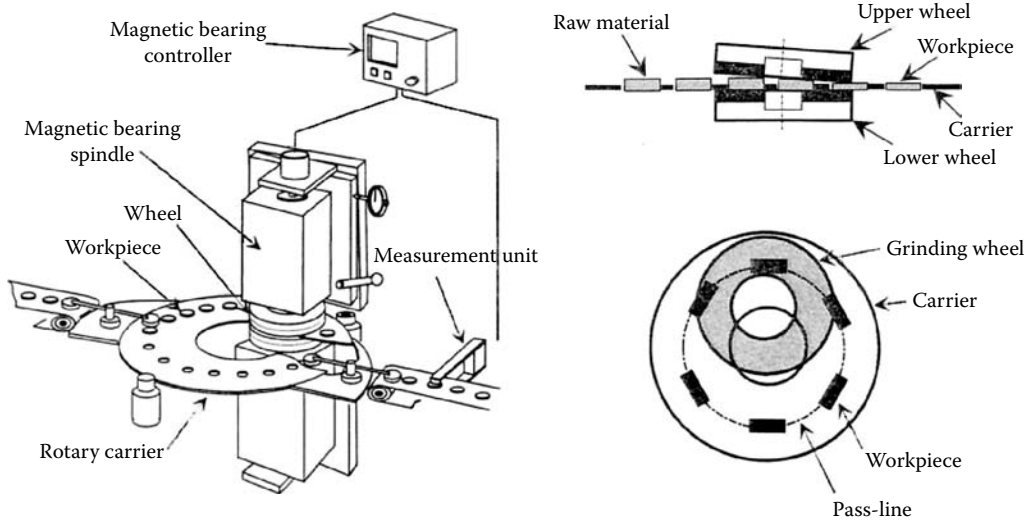


FIGURE 16.68 Double-disc grinder for grinding ceramics. (From Ueda et al. 1998. With permission.)

## 16.7 FINE GRINDING

### 16.7.1 PRINCIPLES AND LIMITATIONS OF LAPPING

Fine grinding, also known as flat honing, low-speed precision grinding, or grinding, with lapping kinematics, refers to a type of grinding being advanced by machine tool builders who previously made lapping machines.



FIGURE 16.69 Examples of alox and superabrasive stone grinding of brake rotor discs. (From Daishi 2001, Thielenhaus n.d. With permission.)



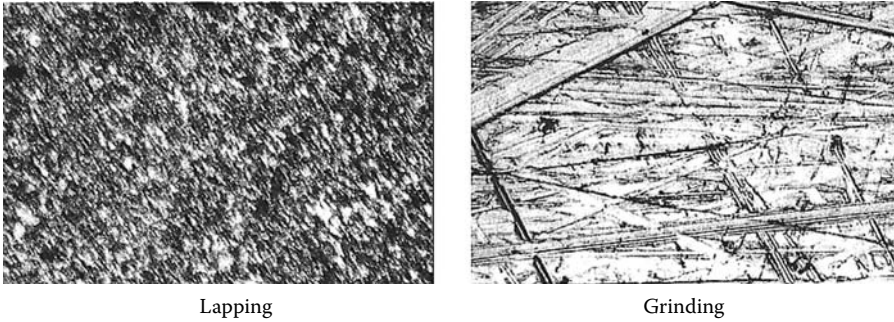


**FIGURE 16.70** Surface textures produced by lapping and fine grinding.

Lapping, using free abrasive slurry, has been the traditional method for achieving micron and submicron flatness. Stock removal occurs as a result of a rolling and sliding of abrasive grains between a lapping plate (single-sided lapping) or plates (double-sided lapping) and the workpiece, resulting in work material compaction, deformation, and finally failure as the material strength is exceeded [Hodge 1992; Schibisch 1997, 1998; von Mackensen 1997]. The process is slow, inefficient in abrasive use, and leaves a dull, pitted surface. The lapping debris must be continually flushed away during processing as the abrasive cannot usually be recycled, leading to high disposal costs. The abrasive slurry must maintain a consistent layer on the plates. Therefore, lapping plate speeds are limited to surface speeds of 1 m/s to resist centrifugal force and prevent heat generation. Perhaps the most problematic issue of all is that the slurry is very dirty and clings to the parts. This creates the need for an additional expensive process of cleaning the finished parts while also producing an unpleasant work environment.

Nevertheless, lapping is a mature and well-developed process in terms of the understanding and control of the kinematics of producing flat surfaces. The more sophisticated lappers use geared carriers to hold the parts, which are driven to describe a planetary motion covering the full surface of the lapping plates as shown in Figure 16.71. The drive mechanism consists of an outer and inner tooth or pin ring; the outer ring is usually fixed while the inner ring rotates to create a series of epicyclic or hypocyclic motions relative to the motion of the bottom plate. The process is discussed in more detail by Ardelt in Appendix 16.1 [Hitchiner, Willey, and Ardelt 2001].

Less sophisticated, single-sided lappers have simple rings to hold them in place and maintain plate flatness (Figure 16.72). The rings rotate by friction created in the process and are moved in and out using simple adjustable arms to prevent the generation of a concave or convex surface.

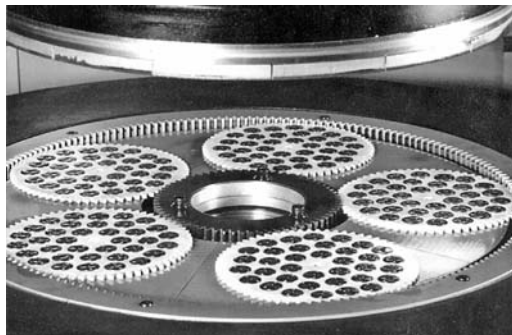


**FIGURE 16.71** Geared fixturing arrangement for a double-sided lapper. (From Melchiorre n.d. With permission.)

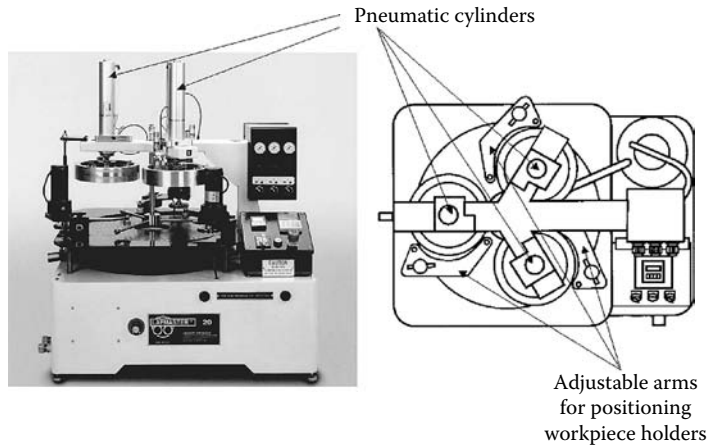


FIGURE 16.72 Lapping machine.

Pressure is applied to the parts either by hand weights, pneumatic pressure, or even, for larger components, just the weight of the part itself.

### 16.7.2 DOUBLE-SIDED FINE GRINDING

As discussed above, the problem with double-disc grinding is generating and maintaining flatness. This is either from the inherent limitation of trying to generate a flat surface while through-feeding into a wedge grind zone, or in the case of the slower infeed methods, maintaining a flat wheel with large differentials in surface footage from the outer to inner diameter.

Lapping kinematics using parallel plates is much better at maintaining wheel flatness and several lapping machine tool builders have taken this concept and made grinders using lapping kinematics together with superabrasive wheels. Although the removal rates are still much lower than a through-feed double-disc grinder, the grind is done in batches with coverage of up to 15 to 20% of the plate area, which can be 100 or more components. Consequently, cycle time/part becomes competitive with other grinding processes while grinding is done under controlled pressure and at low wheel speeds to minimize the risk of thermal damage or distortion.

The earliest efforts were initiated in the late 1970s by OEMs such as Hahn and Kolb using alumina and silicon carbide abrasive. The process was called “flat honing” [Stahli 1998] or “fine grinding” [Anon. 1996b]. This was able to demonstrate the viability of a fixed-abrasive process but wheel wear, and the associated dress time and operator intervention, was often a limiting factor. Although a number of these machines are running very successfully, grinding with superabrasive wheels was subsequently pioneered with European OEMs such as Wolters [2000, n.d.], Stahli [1998], Melchiorre [n.d.], and Modler [n.d.].

Wheel design for fine grinding can take several forms based either on a 100% covered, segmented face with coolant slots or holes, or as pellets (see Figure 16.73). Wheels requiring low coverages use round pellets, while hexagonal pellets are used for packing >90% or to keep gap distances low while grinding small parts. Pellets offer the potential to infinitely vary abrasive coverage across the face of the wheel in order to fine-tune wear. They also provide good coolant access and swarf clearance. However, they are still problematic for small parts and more expensive to fabricate than segmented wheels especially when a high coverage is required.

The wheels are bolted to flanges that have a sophisticated internal labyrinth of coolant channels to control temperature. The coolant itself is fed through holes in the upper wheel. Low-viscosity oil is the coolant of choice, especially in Europe, although some water-based oil has been tried in

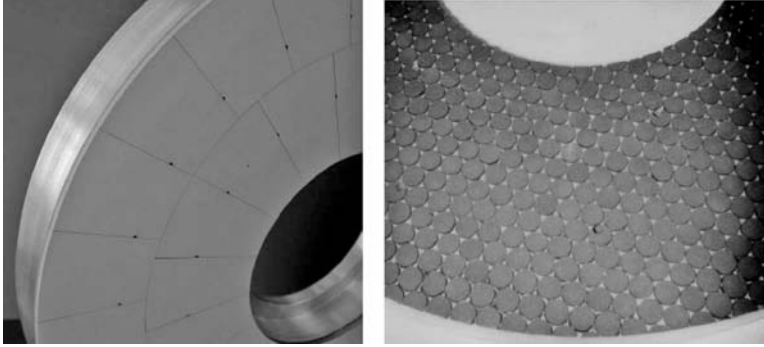


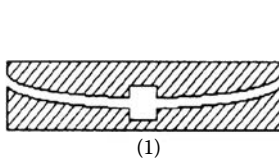
**FIGURE 16.73** Segmental and pellet wheel designs for fine grinding.



**FIGURE 16.74** Peter Wolters Microline double-sided fine grinder.

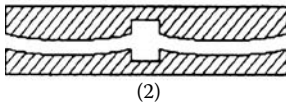


**FIGURE 16.75** Stahli DLM 700 double-sided fine grinder.

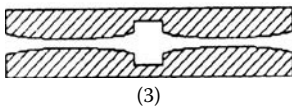


Excessive wear on the bottom wheel with the top wheel conforming over time. Check carrier direction and speed.  
**Actions** (a) Decrease the velocity of the upper wheel.  
 (b) Increase the velocity of the lower wheel.  
 (c) Increase the differential velocity of the carrier and the lower wheel near the wheel inner radius.

For the reverse wear condition reverse the recommendations.



Excessive wear in the ring circle of the carrier. Also excessive wear on bottom wheel.  
**Actions** (a) Reduce number of parts in the center of the carriers.  
 (b) Observe effect of (a) and if necessary then follow the recommendations given in 1/above depending on shape.



Both faces convex. Not enough parts in center of carrier or direction of carrier is being changed too often. If both faces are concave the reverse is true.  
**Action** (a) Adjust part distribution in carriers accordingly.

**FIGURE 16.76** Parameter adjustments for grinding wheel and ring carrier wear. (From Stahl n.d. With permission.)

the United States albeit with reduced wheel life. Wheel speeds prior to about 2000 were for the most part comparable to those used for lapping (1 to 3) m/s. This is, in part, historic but also, in part, to keep heat generation to a minimum with only limited coolant access. More recently, however, speeds have increased significantly with machine tool builders pushing the envelope up to 10 or 15 m/s. In doing so, coolant delivery and regulation have become much more critical as has spindle power, chiller systems, and stiffness.

Spindle horsepower is very dependent on table size and is typically double the power required for lapping because of the higher metal removal rates.

Wheel sizes are large with 700 to 1,000 mm being most common. With the additional power available for grinding, the machine and tooling must be more rigid and rugged to withstand the extra forces. Downfeed systems are predominantly pneumatically controlled [Lapmaster, Stahl,

**TABLE 16.12**  
**Wheel Spindle Power Requirements for Fine Grinding Machines OEM Data from 2000 and Earlier**

Wheel Diameter Range (mm)	450–500	560	650–700	840	900–1,000	1,100–1,200	1,400–1,500	1,800–2,000
Spindle power [Stahli]	3.0 KW		9.5 KW		19 KW	26 KW	32 KW	52 KW
Spindle power [Melchiorre]	3.0 KW		9.2 KW		18.5 KW	22 KW	30 KW	
Spindle power [Modler]			7.5 KW					
Spindle power [Wolters]		(4 KW)	12 KW	(5.5 KW)	16 KW	24 KW		

Source: From OEM, data from 2000 and earlier. With permission.

**TABLE 16.13**  
**Maximum Grind Pressures against Wheel Diameter**

Wheel Diameter Range (mm)	450–500	560	650–700	800–900	900–1,020	1,100–1,230	1,390–1,500	1,800–2,000
Max. Grind Pressure (daN) [Stahli]	300		1,300		2,400	3,200	4,400	7,000
Max. Grind Pressure (daN) [Melchiorre]	300		1,200	1,500	2,500	3,000	3,500	
Max. Grind Pressure (daN) [Modler]			2,000					
Max. Grind Pressure (daN) [Wolters]	250	700	700		1,000	1,000	2,000	3,000

*Source:* From OEM, data from 2000 and earlier. With permission.

and Wolters], but hydraulic [Modler] and mechanical servofeed [Melchiorre] have also been used. The upper wheel head assembly is so heavy that the system is generally providing upward force to keep from allowing the full weight of the head to be applied to the grind. All grinding is carried out under controlled pressure. Pressures are expressed within the industry in “deca Newtons” or daN, where 1 daN = 10 N or 2.25 lb.

Taking the machine design values for pressures and wheel dimensions, together with the fact that the table has a 15 to 20% surface area coverage of components, maximum working pressures for grinding are in the range 7 to 21 N/cm<sup>2</sup> or 10 to 30 lb/in.<sup>2</sup>, which is about double the pressures used for lapping.

Size is monitored in-process by a probe in the center of the spindle assembly and relies on the wheels wearing at submicron levels per load. The ability to monitor size is the limiting factor on cycle time as, in many cases, grinding removal rates can be up to 20 times faster than lapping. With the latest developments in bond technology and machine design, wear rates per load are often 0.2 μm or below.

### 16.7.3 COMPARISON OF FINE GRINDING WITH DOUBLE-DISC GRINDING

The selection of the appropriate technology for generating parts in the flatness range of 0.5 to 2 μm is becoming quite subtle. Technological advances in both processes are accelerating. The view just 5 years ago was that fine grinding held the better flatness but double disc held the better size control. However, with Koyo’s development of EDT dressing of metal bond wheels, flatness can now often be held to <0.5 μm. On the other hand, recent developments in magnetic probes for size control combined with new wheel technology for reduced wheel wear per load has dramatically improved size-holding capability for fine grinding. The drawbacks to fine grinding are that the process is a batch process, which is difficult to fully automate, and the process requires oil coolant. Disc grinding is a continuous feed process, which can be easily automated and runs well in water-based coolants. Fine grinding, due to the number of parts that can be ground simultaneously and the recent increases in wheel speeds and head pressures, probably has a higher throughput. Disc grinding requires constant postprocess gauging to monitor size; fine grinding being a batch process, size is checked just once or twice per load, which can be done manually with minimal labor cost. On the other hand, if there is a size error, the entire batch must be scrapped for fine grinding while it may only be a few parts for disc grinding.

Fine grinding is a technology driven by European machine tool builders, while disc grinding is driven by Japanese machine tool builders, and it is likely that this is influenced by the particular markets that they serve.

**TABLE 16.14**  
**Application Examples for Fine Grinding**

Component	Material	Size (mm)	Stock Amount ( $\mu\text{m}$ )	Removal Rate ( $\mu\text{m}/\text{min}$ )	Rough Grind Time/Part (s)	Flatness ( $\mu\text{m}$ )	$I/\text{fsm}$ ( $\mu\text{m}$ )	Finish ( $\mu\text{m}$ )	Size Control ( $\mu\text{m}$ )	Wheel Spec
bearing plate	bronze	119	330	45	18	<1.5	<2	<0.5 Ra	5	B
bearing race pair	steel 560 HrC	125/70	30	10	9	<1.5	<1.5	0.25 Ra	1.5	B
cam-ring	steel 63 HrC	65	65	10	7	<1.5	<1.5	1.5 Rz	1.5	B
cam-ring	PM 95 HrB	35	150	16	2.5	<1	<1	<0.8 Ra	2.5	B76
cutting tool	M2 62 HrC	75	200	16	14	2.5	2.5	0.15 Ra	2	B46
gear	steel 62 HrC	20	25	7.5	2	<1	<1	<24 Rz	2	B
gear	PM 45 HrC	30.5	43	11	5	<1.2	<1.2	0.18 Ra	1.25	B46
injector plate	steel 61 HrC	20	60	20	2.3	<1	<1	0.15 Ra	1.5	B18/B30
oil pump gear	PM 43 HrC	57	157	20	3.2		<1	<0.35 Ra	1.25	B76
oil pump gear	PM 95 HrB	84	280	35	4.9	<5	<3	0.55 Ra	3	B76
piston ring	90CRMov18	91.5	30	60	0.8	<2	<2	1.8 Rz/0.18 Ra	2	B
piston rod plate	aluminum steel 62 HrC	90 95 $\times$ 75	560 35	135 35	8 33	<1.5 <3	<1.5 <2	<3.7 Rz <2 Rz	10 2	B B
pump plate	PM 70 HrB	89	28	6.6	43	<2.5	<2.5	<0.2 Ra	1.25	B46
pump ring	steel 58 HrC	35	125	15	12	<2	<1	<0.2 Ra	2	B46
pump rotor	PM D39	52	220	25	29	<1.5	<2	2 Rz	2.5	B
pump rotor	PM 52 HrC	44	100	25	3	<1.5	<2	3 Rz	1.5	B
pump stator	PM C11	60	200	40	25	<1.5	<2	2 Rz	2.5	B
slide disc	31CrMo12	136/55	400	28	86	<5	<2	<2.4 Rz	6	B
tappet shim	100Cr6	25	150	25	1–1.5	<2	<2	2 Rz	3	B
thrust-bearing disk	ss1819	200/192	71	10	0	<7	<3	<0.25 Ra	10	B
valve plate	ss1819	100	355	30	3	<40	<2	<0.38 Ra	15	B
valve plate	steel 47 HrC	119	460	45	25	<2.5	<2	<0.6 Ra	2.5	B
seal disc	alumina	42	405	250	0.5	<2	<2	<0.4 Ra	5	D
seal disc	alumina	33/19	405	110	1.1	<2	<2	<0.4 Ra	5	D
seal disc	alumina	37	610	250	1	<2	<2	<0.4 Ra	5	D
seal washer	piezo ceramic	24	18	430	0.03	<1.2	<1.5	0.5 Ra	5	D
slide disc	alumina	23	140	19	6.3	<1	<2	<0.38 Ra	6	D
tile	SiC	63.5	1650	80	68	<5	<5	0.225 Ra	5	D
tool insert	alumina	32	250	16	19	<1	<1	0.25 Ra	2	D

Source: From Wolters 1998. With permission.

## APPENDIX 16.1 LAPPING KINEMATICS

### A16.1.1 INTRODUCTION

Considerable research work has been carried out on grinding with lapping kinematics at the University of Berlin. Dr. Thomas Ardelts has provided detailed information on this research below.

During face grinding on lapping machines, several workpieces are moved simultaneously between two horizontally positioned grinding wheels (Figure A16.1). The parts are fixed in work-piece carriers that are led between two pin circles. This way, characteristic cycloidal path curves are generated between parts and grinding wheels that are similar to the movements in planetary gears. It was found that a variation of the types of planetary movement directly influences material removal rates and driving power and particularly the resulting quality of the produced parts [Ardelt 1999]. As a

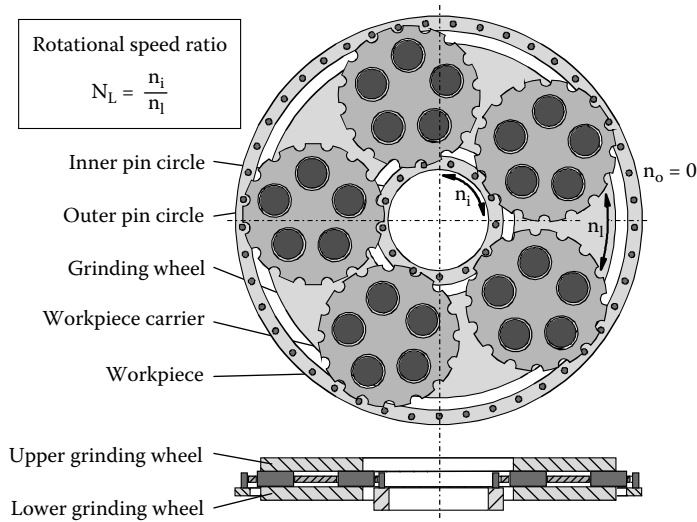


**FIGURE A16.1** Design of a double-wheel lapping or grinding machine. (From Uhlmann 1999. With permission.)

basis of understanding these effects, kinematic possibilities of double-wheel lapping and grinding machines have to be analyzed.

### A16.1.2 KINEMATICAL FUNDAMENTALS

Since the mid-1980s, the Institute for Machine Tools and Factory Management of the Technical University Berlin worked on an analytical description of the relative motions in cycloidal restricted guidance on lapping machines. A model was developed that calculates the profile wear of the lapping wheel as a function of the path curves of the workpieces on the wheels [Spur 1997, Simpfendörfer 1988, Uhlmann 1999].

For all machines with fixed external pin circle, selectable kinematic parameters are the rotational speeds of the lower grinding wheel  $n_l$ , the upper grinding wheel  $n_u$ , and the internal pin circle  $n_i$ . Thus, a description of all path types and velocities related to the lower grinding wheel with the rotational speed ratio

$$N_L = \frac{n_i}{n_l}$$

is possible.  $N_L$  describes unequivocally for a single machine the path type on which the workpieces move relative to the lower grinding wheel. All path types can be covered with different velocities within the scope of the possible rotational speeds of a machine [Ardelt 1999].

### A16.1.3 ANALYSIS OF PATH TYPES AND VELOCITIES

In the following, the connection between rotational speeds and emerging path curves is explained [Ardelt 2000]. This kinematic analysis depends on the diameters of the grinding machine design. In this example, it's done for a machine type Duomat ZL 700 by Stähli Läpp-Technik GmbH, Germany. The outer pin circle of this machine is fixed, whereas the two grinding wheels and the inner pin circle can be driven individually.

Figure A16.2 shows the characteristic path types that a workpiece center point covers as a function of the rotational speed ratio,  $N_L$ . The path types designated with letters are classes, which occur in certain ranges of  $N_L$ . The curves marked with numbers are special cases that arise only at a definite ratio of the two rotational speeds.

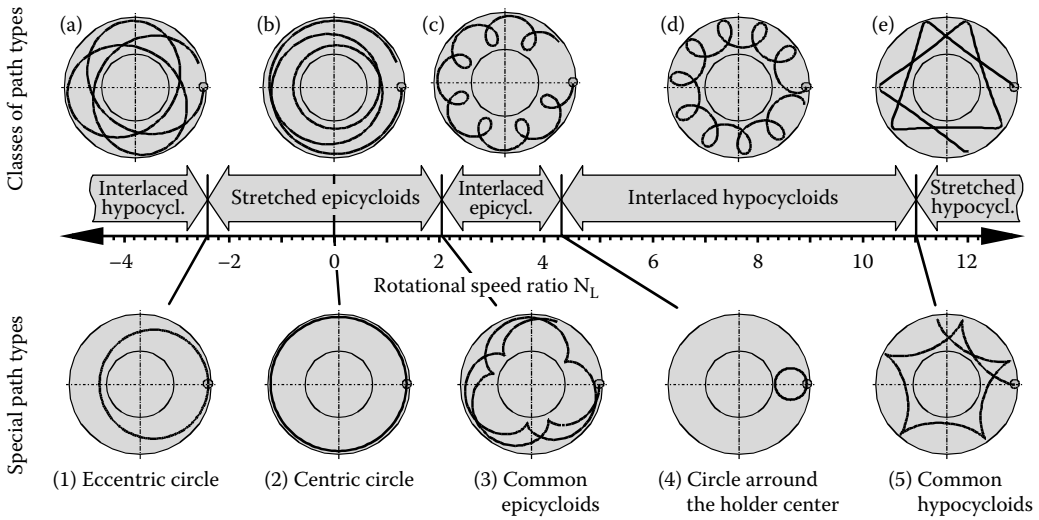


FIGURE A16.2 Path types of the Duomat ZL 700. (From Ardel 2000. With permission.)

At high negative rotational speed ratios, all workpiece points cover stretched hypocycloids (a) on the grinding wheel. These path curves turn into stretched epicycloids (b) at  $-2.39$ . At the transition between these two path types, the parts move on eccentric circular paths around the grinding wheel center (1). Whereas the cyclically recurring shape elements of all path types with  $N_L < 0$  wind around the center of the grinding wheel, tight loops with strong bends emerge at  $N_L > 0$ , repeating themselves on one half of the wheel coating. At a rotational speed ratio of  $2.15$  the stretched epicycloids become interlaced epicycloids (c). At the transition point common epicycloids emerge which show a reversing point in the form of a buckling (3). With increasing rotational speed, ratio circles around the holder center (4) occur which represent the transition point to interlaced hypocycloids (d). At  $N_L = 11.09$  common hypocycloids (5) emerge which turn into stretched hypocycloids (e).

The occurring relative velocities are shown in Figure A16.3. The graph gives the mean path velocity by 100% and the occurring maxima and minima related to this mean value for every rotational speed ratio. The path velocities vary more or less strongly depending on the shape of the curves. The related path velocity  $v'(t)$  given in the diagram is defined as the ratio of the path velocity  $v(t)$  to the

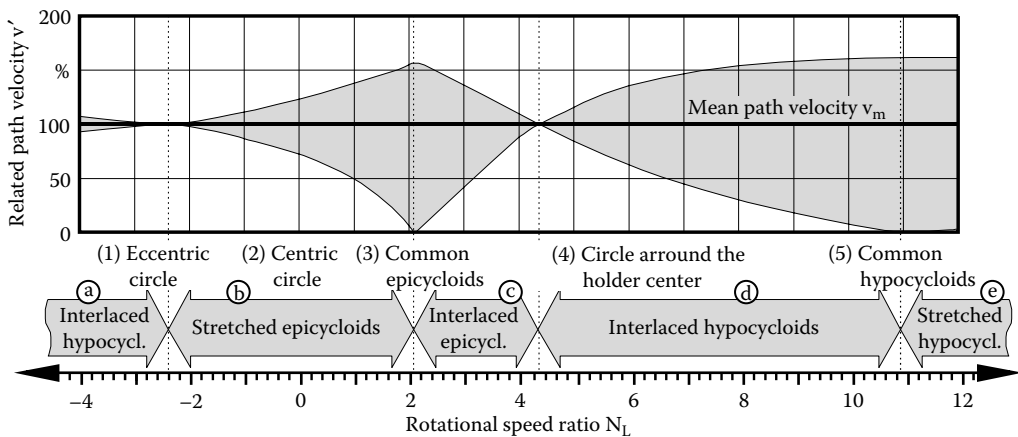
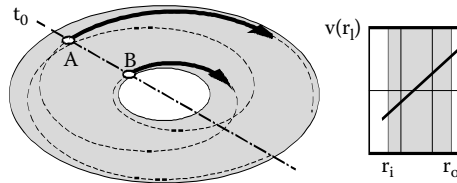


FIGURE A16.3 Related path velocities of the Duomat ZL 700. (From Ardel 2000. With permission.)





**FIGURE A16.4** Path curve sections of two workpieces after a certain grinding time interval. (From Ardel 2000. With permission.)

mean path velocity  $v_m$ . If the lines for minimum, mean, and maximum velocity intersect, the occurring path curves are covered with constant velocity. This effect occurs at  $N_L = -2.39$  and  $4.35$ . As could be seen in the previous graph, circular path types emerge for these two rotational speed ratios. Covering common epi- and hypocycloids at  $N_L = 2.15$  and  $11.09$ , the workpiece points minimum velocity is zero. On these path types, the workpieces are exposed to extreme differences in velocity, which alternately reach a momentary standstill and an acceleration to over 150% of the mean path velocity.

Figure A16.2 and Figure A16.3 demonstrate that the kinematic conditions at equal mean path velocity depend heavily on the rotational speed ratio and thus, on the shape of the path curve. To explain this effect, Figure A16.4 shows two different workpieces moving along a stretched epicycloid path. Along this path curve, the relative velocity increases from the inner to the outer grinding wheel diameter. In a certain grinding time interval  $\Delta t_c$ , workpiece A moves a longer track length than workpiece B does due to their different velocities.

The upper grinding wheel descends simultaneously on all the workpieces. Thus, the achieved workpiece height difference after  $\Delta t_c$  has to be the same for all workpieces. This means that for the mentioned example, in spite of the different relative track length, both workpieces A and B lose the same height. It follows that the angle of grinding grit engagement has to be different for both workpieces, as the velocity vectors in Figure A16.5 show. This effect strongly depends on the type of relative movement and on the distribution of relative velocities as a function of the lower grinding wheel radius.

Different angles of grit engagement may lead to different types of grit wear. It is possible to have one area of the grinding wheel surface working in the self-sharpening range, while another area shows grit flattening and loses its sharpness and grinding ability in short time. To set up stationary grinding processes, it is necessary to have equal microscopic wear conditions on the complete contact area, which can be achieved by analysis of the process kinematics.

**A16.1.4 KINEMATIC POSSIBILITIES OF MACHINES**

The previously shown description of path types during machining on double-wheel lapping and fine grinding machines reveals a very broad range of the rotational speed ratio. This theoretical analysis

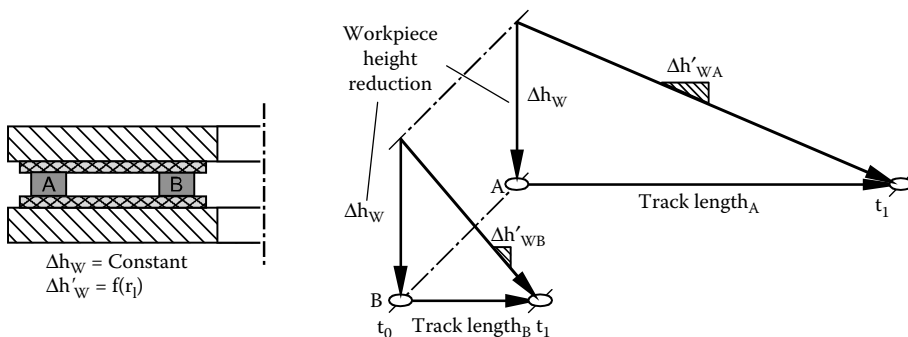


**FIGURE A16.5** Workpiece height reduction. (From Ardel 2000. With permission.)

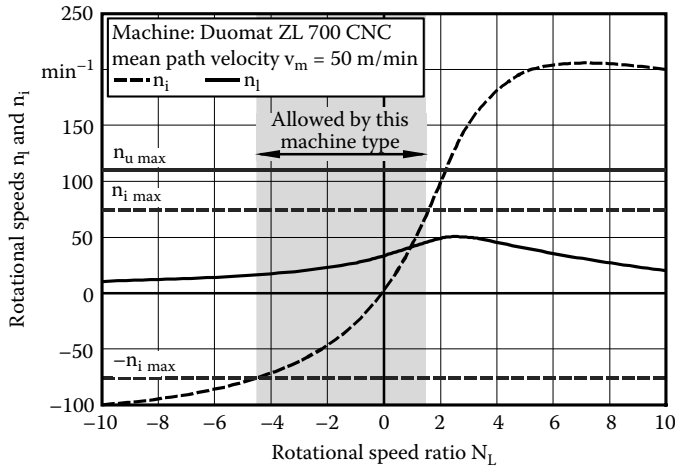


**FIGURE A16.6** Necessary rotational speeds to achieve a mean path velocity of 50 m/min at different rotational speed ratios  $N_L$ . (From Ardel 1999. With permission.)

was carried out, irrespective of the rotational speeds that can actually be set on real machines. Most standard designs permit rotational speeds at the inner pin circle of 50 to 80% of the wheel speed. This means that a rotational speed ratio of 10 can only be reached with 5 to 8% of the maximum wheel speed. This minimum usage of the machine power considerably limits the settable path velocities. To illustrate this fact, for a machine of the type Duomat ZL 700, Figure A16.6 shows the rotational speeds that must be set at the inner pin circle and the lower grinding wheel to reach a mean path velocity of 50 m/min for all rotational speed ratios. The maximum rotational speeds possible are given by the horizontal lines. The perpendicular bar represents the range of settable rotational speed ratios, which is restricted in both directions by the inner pin circle [Uhlmann 1999].

Due to the technological progress in driving technology on the one hand, and knowledge of lapping kinematics on the other, kinematic possibilities of machine systems are constantly expanded and improved. To illustrate this development, Figure A16.7 compares the kinematic possibilities of various generations of the machine family ZL by Stähli GmbH.

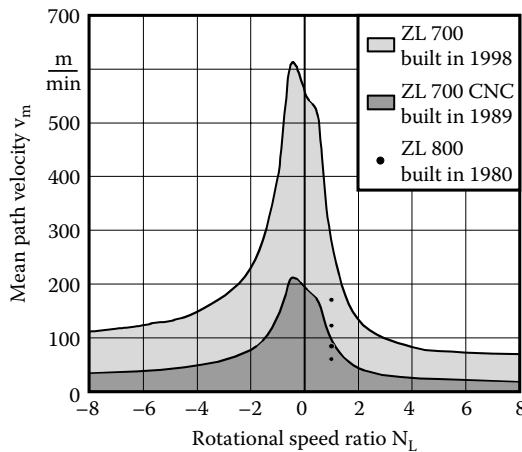


**FIGURE A16.7** Comparison of kinematic possibilities of different double wheel machine designs. From Ardel 1999. With permission.)

For the ZL 800 (built in 1980), the rotational speed ratio between inner pin circle and lower lapping wheel is set firmly by a gearing. Changing the poles at the driving motor serves to realize four different velocities. Freely selectable rotational speeds permit any rotational speed ratios for the design ZL 700 CNC (1989). For the path velocities needed for grinding the range of possible path types is strictly limited. Possible rotational speeds are considerably higher for the ZL 700 built in 1998. Here, both grinding wheels can be driven with up to  $n_{u,l} = \pm 435 \text{ min}^{-1}$ , the inner pin circle with up to  $n_i = \pm 268 \text{ min}^{-1}$ . These rotational speeds allow for mean path velocities  $v_m$  of more than 600 m/min or 10 m/s.

## REFERENCES

- Akinori, Y. 1992. "The Press Industry in Japan." *Puresu Gijutsu* 30, 1, 74–81.
- Andrews, C., Howes, T. D., and Pearce, T. R. A. 1985. *Creep Feed Grinding*. Holt, Rinehart and Winston, New York.
- Anker, A. 1998. "Machining the Ends of Springs with ABN." *IDR* 4, 124–125.
- Anon. 1995. "Huge Rotary Grinder Improves Productivity by 20%." Manual, p. 62.
- Anon. 1996a. "Finish Grinding Improves Quality of Disc Brake Rotors." *Tooling & Production* Dec., 42–46.
- Anon. 1996b. "Fine Grinding Can Be the Answer." *Tooling & Production* June, 45–46.
- Ardelt, T. 1999. "On the Effect of Path Curves on Process and Wheel Wear in Grinding on Lapping Machines. Proceedings." 3rd International Machining and Grinding Conference, Cincinnati, OH.
- Ardelt, T. 2000. "Einfluss der Relativbewegung auf den Prozess und das Arbeitsergebnis beim Planschleifen mit Planetenkinematik." Ph.D. dissertation, TU Berlin.
- Blanchard. 2000. Series of trade brochures on Models 11A-20–42HD/54HD/60HD grinders. Cone-Blanchard Corp, Windsor, VT.
- Blohm. n.d. "Super Abrasive Machining Center." United Grinding Technology, Miamisburg, OH. Trade Catalog.
- Buthe, B., Wilson, E.M. and Boemke, M. 1992. "Double Disc CBN Grinding of Piston Rings." *IDR* 52, 3, 120–124.
- CIRP. 2005. *Dictionary of Production Engineering II, Material Removal Processes*. Springer-Verlag, New York.
- Cui, C. 1995. "Experimental Investigation of Thermo-Fluids in the Grinding Zone." Ph.D. dissertation, University of Connecticut.
- Daisho. n.d. "Daisho Double Disc Grinders DDG Series." Daisho Seiki Corp, Osaka, Japan. Trade brochure.
- Daisho. 1998. "Grind Master V Series." Daisho Seiki Corp, Osaka, Japan. Trade brochure.
- Daisho. 2001. Trade advertisement.
- DCM Tech. 1999. "Industrial Rotary Surface Grinders IG 180M, IG 280M, IG 280 CNC, HB5400 Series." Series of trade brochures.
- Delta. 1997. "Surface Grinding Machines." Delta s.p.a. Cura Carpignano, Italy trade brochure.
- Deming, M. and Carius, A. C. 1991. "Introduction to Superabrasives." Course presented at Superabrasives '91, Chicago, IL. SME.
- DIN 8589, Teil 11, Entwurf (05.2002): Fertigungsverfahren Spanen; Schleifen mit rotierendem Werkzeug; Einordnung, Unterteilung, Begriffe. Berlin, Beuth.
- Diskus. 1996. "Diskus Double Disk Face Grinding Machines Series DDS." Diskus Werke Schleiftechnik, Langen, Germany. Trade brochure.
- Doubman, J. R. and Cox, C. 1997. "Double Disc Grinding in Automotive Parts Manufacturing." *Automot. Mfg. Prod.* Oct., 60–62.
- Ex-Cell-O. n.d. "Grinding Centers XT820/XT285 for Guide Vanes and Turbine Blades." Ex-Cell-O, Eislingen/Fils, Germany. Trade brochure.
- Gaulin, D. 2002. "High Speed Grinding of Difficult to Grind Materials." IMTS SME Conference Proceedings, Chicago.
- Goekel. 1997. "Schleifmaschinen." Goekel Maschinenfabrik GmbH, Darmstadt, Germany. Trade brochure.
- Hitchiner, M. P. 2005. Private communication.
- Hitchiner, M., Willey, B., and Ardelt, T. 2001. "Developments in Flat Grinding with Superabrasives." Precision Grinding & Finishing in the Global Economy. 2001 Conference Proceedings, Gorham, Oak Brook, IL.

- Hodge, J. H. 1992. "Lapping, Honing and Polishing." *ASM Engineered Materials Handbook, Volume 4. Ceramics and Glasses*, ASM International, Materials Park, OH.
- Hogan, B. J. 2001. "Precision Makes Grinding Vital." *Mfg. Engr.* Feb., 42–54.
- Howes, T. 1990. "Assessment of the Cooling and Lubrication Properties of Grinding Fluids." *Ann. CIRP* 39, 1, 313–316.
- Howes, T. 1991. "Avoiding Thermal Damage in Grinding." AES Conference. Sourced from Internet: [www.nauticom.net/www/grind/therm.htm](http://www.nauticom.net/www/grind/therm.htm)
- Hughes, F. and Dean, A. n.d. "Interrupted Cutting of Tungsten Carbide with Diamond Abrasive Grinding Wheels." De Beers IDR publication L16.
- Inasaki, I. 1988. "Speed Stroke Grinding of Advanced Ceramics." *Ann. CIRP* 37, 1, 299–302.
- Inasaki, I. 1999. "Surface Grinding Machine with a Linear Motor Driven Table System. Development and Performance Test." *Ann. CIRP* 48, 1, 243–246.
- Konig, W. and Schleich, H. 1982. "Deep Grinding of High Speed Tool Steel with CBN." *Ultrahard Materials. Application Technology, Volume 1*. P. Daniel, Ed., De Beers Industrial.
- Koyo. n.d. "Vertical Spindle Surface Grinders KVD Series." Koyo Machine Industries, Osaka, Japan. Trade brochure.
- Koyo. 1999. "Koyo Grinders." Koyo Machine Industries, Osaka, Japan. Trade brochure.
- Koyo. 2000. "Koyo R Series Vertical Spindle Type, Rotary Table Type Surface Grinder." Koyo Machine Industries, Osaka, Japan. Trade brochure.
- Koyo. 2001. "Koyo Guide to Machine Tools." Cat # KM-H501ET. Koyo Machine Industries, Osaka, Japan. Trade brochure.
- Kubsh, L. M. 1988. "Disc Grinding: Yesterday, Today and Tomorrow." MR88-593, 3rd International Grinding Conference, Fontana, WI.
- Landis Gardner. 1989. "Horizontal Disc Grinding Machines and Systems." Litton Industrial Automation, S Beloit, IL. Trade brochure.
- Lapmaster. 2000. "Model LFG 12 Dual Face Fine Grinding Machine." Lapmaster International, Morton Grove.
- Lin, B. and Zhang, H. L. 2001. "Theoretical Analysis of Temperature Field in Surface Grinding with Cup Wheel." *Key Engr. Mater.* 202–203, 93–98.
- Litton. 1989. "2V18 @ Vertical Disc Grinders." Litton Industrial Automation, S Beloit, IL. Trade brochure.
- Lutz, G. 1980. Tyrolit Schleifmittelwerke Swarovski, Schwaz, A Zusammenhang zwischen Werkzeugoberfläche, Schnittgeschwindigkeit und Spanform beim Tiefschleifen. *Ing. Dig.* 19, 3.
- Malkin, S. 1989. *Grinding Technology*. Ellis Horwood, New York.
- Mattison. n.d. "Horizontal Surface Grinders." Mattison Machine Works, Rockford, IL. Trade brochure.
- Mattison 2. n.d. "Double Disc Grinders." Mattison Machine Works, Rockford, IL. Trade brochure.
- Melchiorre, n.d. "Melchiorre Fine Grinding, Lapping, Honing, Polishing." Melchiorre S R L, Milano, Italy. Trade brochure.
- Minke, E. and Tawakoli, T. 1991. Hochleistungsschleifen mit CBN-Werkzeugen, in *Wissenschaftliche Zeitschrift der Technischen Universität Otto von Guericke*. Magdeburg, Band. 35, 4.
- Modler. n.d. "Finimat 2000 Automatic Universal Finegrinder." Johann Modler GmbH, Aschaffenburg, Germany. Trade brochure.
- Mohr, H. 2000. "Abgrenzung verschiedener flachschleifverfahren mit ergebnissen beim vollschmitt schleifen." *Moderne Schleiftechnologie*. Seminar April 13. Schwenningen, Germany.
- Motion. 2001. "Speed Stroke Grinding Machine Jung S320." August.
- Narbut, N., Stafford, T., and Tartaglione, J. 1997. "Grinding with Segments." *Cutting Tool Engr.* Dec., 20–30.
- Navarre, N. P. 1986. *CBN and Vitrified Bond: A New Focus*. Machine and Tool Blue Book, October.
- Noichl, H. 2000. "CBN Grinding of Nickel Alloys in the Aerospace Industry." IDA Conference Proceedings Intertech 2000, Vancouver, Canada. July 21.
- Ott, H. W. and Storr, M. 2001. "Grinding Fluids for the Future." Oel-Held GmbH Stuttgart, Germany. Trade technical booklet. See also Ott and Storr. IMTS 2002 paper of same title. September 4, 2002. SME Conference Proceedings. Chicago.
- Pfeiffer, W. and Hollstein, T. 1992. "Einfluß einer Endbearbeitung auf das Festigkeitsverhalten und den Oberflächenzustand," Proceedings Conference, Bearbeitung von Keramik, Symp. der DKG, Fachauschuß Verfahrenstechnik.
- Portmann, F. 1981. "Wirtschaftlichkeit und Produktgüte beim Schleifen." *Technische Rundschau*, Bern, nr. 6.
- Radiac. 2002. "Radiac Abrasives Creep Feed Grinding." Technical data sheets. Salem, IL [cited 29 March 2002]. Available from [www.radiac.com](http://www.radiac.com).

- Reform. n.d. "Schleifmaschinen." Reform Maschinenfabrik Adolf Rabenseifner, Fulda, Germany. Trade brochure.
- Rolls Royce. 1999. Patent EP 0 924 026 A2.
- Rowe, W. B. and Jin, T. 2001. "Temperatures in High-Efficiency Deep Grinding." *Ann. CIRP* 50, 1, 205–208.
- Saljé, E. and Damlos, H.-H. 1983. "Schleifscheibenverschleiß beim Profiplanschleifen – Vergleichende Untersuchungen für das Tief- und das Pendelschleifen." *VDI Zeitschrift* 125, 10.
- Salmon, S. C. 1984. "Abrasive Machining Handbook." Korber AG.
- Schibisch, D. 1997. "Fine Grinding with Superabrasives." *Ceramics Industry*, Dec.
- Schibisch, D. 1998. "Fine Grinding with CBN and Diamond. An Economic Alternative to Free Abrasive Lapping." *Abrasives Mag.* Feb/Mar.
- Schleich, H. 1980. "Flachschleifen mit hohen Leistungen unter Verwendung thermischer Randzonenschädigung." *Technische Mitteilungen <Haus der Technik e.V.>* 73, 11/12.
- Schleifring, K Jung GmbH Göppingen, Germany. Trade publication.
- Schlie, D. R. and Rangarajan, R. S. 1987. "Solving Manufacturing Problems of Today & Tomorrow through Disc Grinding Technology." 25th AES Conference, October 19, Canton, OH.
- Sess, M. 1999. "Machine Tools Are Doing More." *Mfg. Engr.* Nov, 46–53.
- Simpfendörfer, D. 1988. "Entwicklung und Verifizierung eines Prozeßmodells beim Planlappen." Ph.D. dissertation, Technical University Berlin.
- Spur, G. 1989. *Keramikbearbeitung – Schleifen, Honen, Läppen, Abtragen*. Carl Hanser, Verlag München, Wien.
- Spur, G. and Eichhorn, H. 1997. "Kinematisches Simulationsmodell des Läppscheibenverschleißes." *IDR* 31, 2, 169–178.
- Spur, G. and Stöferle, T. 1980. *Handbuch der Fertigungstechnik*. Spanen, Band 3/2. Hanser-Verlag, München.
- Spur, G., Stark, H., and Uhlmann, E. 1986. "Tiefschleifen von Nichtoxidkeramiken mit Diamantschleifscheiben." *Z. Fertigung Automatisierung ZWF/CIM*, 81, 6.
- Spur, G., Uhlmann, E., and Brücher, T. 1993. "Werkstoffspezifische Schleiftechnologie – Schlüssel für erhöhte Prozesslauffähigkeit in der Keramikbearbeitung," in *Jahrbuch Schleifen, Honen, Läppen und Polieren*, Verfahren und Maschinen; 57. Ausgabe, Hrsg.: E. Saljé. Essen, Vulkan-Verlag.
- Spur, G., Funck, A., and Engel, H. 1995. "Problems of Flatness in Plane Surface Grinding." *Trans NAMRI/SME* 23, 97–102.
- Stahli. 1998. "Stahli Flathoning – The Range of Two-Wheel Flathoning and Lapping Machines for Top Quality and High Output." A. W. Stahli Ltd., Biel, Switzerland.
- Stahli. n.d. "Lapping and Flathoning with Two-Wheel Machines." A. W. Stahli Ltd., Biel, Switzerland.
- Stahli, A. W. 2000. "Flat Honing with Diamond and CBN Grinding Discs." *IDR* 1, 9–13.
- Supfina. 1996. "SUPERFINISH for the Engine Industry." Superfina Grieshaber GmbH.
- Swisher. 2000. "Grinding Technology for the 21st Century." Swisher Finishing Systems, Div. Crankshaft Machine Group, Jackson, MI. Trade brochure.
- Tawakoli, T. 1993. "Anforderungen an Kühlschmierstoffanlagen beim Hochleistungsschleifen." *Ind. Diamanten Rundschau* 1, 34.
- Thielenhaus. n.d. "Microfinish® the Economical Precision-Machining Method in the Automotive and Motor Industry." Thielenhaus Microfinish Corp, Novi, MI. Trade brochure.
- Tio, T. H. 1990. "Pendelplanschleifen nichtoxidischer Keramiken." Ph.D. thesis, Verlag Hanser, TU-Berlin.
- Tonshoff, H. K., Meyer, T., and Wobker, H. G. 1996. "Machining Advanced Ceramics with Speed Stroke Grinding." *Ceramics Industry* July, 17–21.
- Tropel. 1996. "Tropel Build on Our Experience." Tropel Corp, Fairport, NY. Trade brochure.
- Ueda, S., Takahashi, M., Nakagawa, T., Inagaki, N., and Yamada, T. 1998. "Development of a High Precision Through-Feed Grinder." *Int. J. Japan Prec. Eng.* 32, 1, 9–12.
- Uhlmann, E. G. 1994a. *Tiefschleifen hochfester keramischer Werkstoffe*, Produktionstechnik. Berlin, Forschungsberichte für die Praxis, Band 129, Carl Hanser Verlag München, Wien.
- Uhlmann, E. 1994b. "Erhöhung der Bauteilqualität und der Wirtschaftlichkeit durch modifiziertes Tiefschleifen," in *Schleifen von Hochleistungskeramik*." Ergebnispräsentation des BMFT-Verbundprojektes, Univ. Kaiserslautern, Kaiserslautern.
- Uhlmann, E. and Ardelt, T. 1999. "Influence of Kinematics on the Face Grinding Process on Lapping Machines." *Ann. CIRP* 48, 1, 281–284.
- VDI 3390 (10.1991): *Tiefschleifen von metallischen Werkstoffen*. Beuth, Berlin.
- von Mackensen, V. et al. 1997. "Fine Grinding with Diamond and CBN." *IDR* 2, 40–43.
- Warnecke, W. 1994. *Schleifen von Hochleistungskeramik*. Verlag TÜV, Rheinland.

- Webster, J. 2000. "Effective Coolant Application in Grinding." IMTS 2000 Conference Proceedings, Chicago.
- Webster, J., Cui, C., and Mindek, R. B. 1995. "Grinding Fluid Application System Design." *Ann. CIRP* 44, 1, 333–338.
- Webster, J., Brinksmeier, E., Heinzl, C., Wittmann, M., and Thoens, K. 2002. "Assessment of Coolant Supply Effectiveness in Continuous-Dress Creep Feed Grinding." Presented to CIRP Aug.
- Werner, P. G. and Minke, E. 1981. "Technologische Merkmale des Tiefschleifens. Erhöhte Schnittkräfte und reduzierte Werkstücktemperaturen –Teil 1." *TZ für praktische Metallbearbeitung* 75, 3.
- Wolters. 1998. "Fine Grinding Applications in the US Market." Peter Wolters trade mailing.
- Wolters. 2000. "Peter Wolters Solutions in Precision Machining." Peter Wolters Werkzeugmaschinen GmbH, Rendsburg, Germany. Trade brochure.
- Wolters 1. n.d. "Microline Perfect Fine Finishing with Electronic-Pneumatic Control." Peter Wolters Werkzeugmaschinen GmbH, Rendsburg, Germany. Trade brochure.
- Wolters 2. n.d. "Peter Wolters Fine Grinding Systems." Peter Wolters of America, Plainville, MA. Trade brochure.
- Ye, N. E. and Pearce, T. R. A. 1984. "A Comparison of Oil and Water as Grinding Fluids in the Creep Feed Grinding Process." *Proc. Inst. Mech. Engr.* 195B, 229–237.
- Yuji, N. 1990. "High Speed Stroke Grinding." *Tsuru Enjinia* 31, 96–101.



---

# 17 External Cylindrical Grinding

## 17.1 THE BASIC PROCESS

### 17.1.1 INTRODUCTION

External cylindrical grinding refers to the grinding of an outer surface of a workpiece around an axis of rotation with the part held between centers. The surface may be a simple straight diameter or stepped, tapered, threaded, or profiled [Marinescu et al. 2004]. The grinder may be configured for a

- Simple plunge operation for straight diameters and complex profiles,
- Angle approach (typically 30° or 45°) for grinding diameters and shoulders without heat damage
- Universal grinders with several spindles on a rotating turret arrangement or a drop-down auxiliary spindle. Universal grinders are designed to allow use in combination with internal and face grinding operations.
- Combination of plunge and traverse operations. On modern CNC grinders these are often “canned” program operations and may be performed with straight, angle approach or special profile wheels. The process has gained special appeal for high-speed grinding with cubic boron nitride (CBN) abrasives although it is not limited to these conditions.

### 17.1.2 WORK DRIVES

In all cases, the part is driven by a work drive. Short parts may be clamped at one end by a chuck or collet. More typically, the parts are held between live or fixed centers and driven by a dog, keyway, or face plate with a locator pin. Longer parts are supported along their lengths by steady rests. Centers are premachined in the part and their location and quality are critical since runout will cause chatter and lead to lobing. Burrs in keyways, used commonly in camshafts, will create major problems where orientation is required.

The workhead design varies greatly from one machine tool builder to another depending on load and sophistication of the equipment. On most standard machines, however, they are ac servo driven at speeds from 10 rpm up to 400 to 1,000 rpm and use hydrodynamic or roller bearing designs. Runout is always held to better than 1.2  $\mu\text{m}$  and in ultraprecision grinders can be held to as tight as 0.1  $\mu\text{m}$ . Ac servodrives allow orientation to be monitored and controlled to seconds, which in turn has allowed original equipment manufacturers (OEMs) over the last 25 years to develop CNC grinding out of round parts such as punches and camshafts. This is discussed in more detail here.

### 17.1.3 THE TAILSTOCK

The tailstock is typically a plain sleeve bearing although linear ball bearings are also used. Most will have taper adjustment capability and hydraulic actuation for automatic load/unload capability. Some tailstocks have spring loading to compensate for temperature changes, while others have coolant ported through them (and the headstocks) for temperature stability.



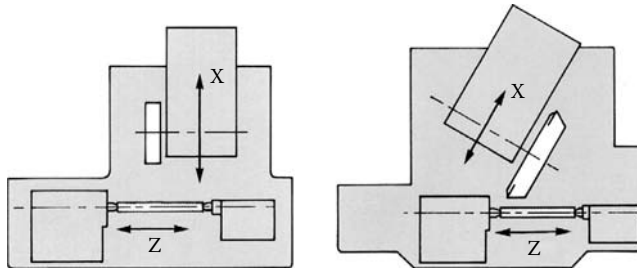


FIGURE 17.1 Machine configurations. (From Shigiya 1996. With permission.)

#### 17.1.4 WHEEL SPEEDS

The vast majority of standard grinders still use conventional abrasives at wheel speeds of 43 m/s or less. The wheel life is relatively long so any benefits from upgrading to CBN have to come from improved cycle time or quality. However, an analysis of about 30 different cylindrical grinders currently on the market reveals the following power capability per unit width of wheel as a function of wheel size and speed (Table 17.1).

Some of the power is required to overcome the inertia of the wheel and flange assembly. So assuming an average power available given by median value for each speed and assuming typical wheel widths between one third and the maximum allowed, the maximum stock removal rates  $Q'$  ( $\text{mm}^3/\text{mm/s}$ ) are also estimated based on hardened steel. These numbers are limited by the system stiffness and cannot be easily increased to justify CBN. The only exceptions, therefore, are grinding very difficult materials such as tool steels or nickel and cobalt-based superalloys where there is a loss of cycle time from dressing, or for very narrow profiles where higher removal rates still remain within the machine stiffness parameters. One area where vitrified CBN is used successfully, for example, at speeds of 60 m/s or less, is groove grinding in transmission shafts.

Since the system can be relatively weak, work/wheel speed ratios are comparable to those for internal grinding; 1:50 for the weakest grinding processes up to 1:150 for stiffer grinding processes. However, the equivalent wheel diameter  $d_e$  always remains under 250 mm (with the possible exception of grinding rolls for the steel industry) and more typically is under 75 mm. Coolant access is, therefore, relatively easy and wheel grades are more a function of material and finish requirement and readily available in wheel makers' specification manuals.

Nevertheless  $d_e$  does have an impact once standard speeds are exceeded. A standard speed for Alox wheels is 43 m/s and this is not just for safety reasons. At speeds up to this value, standard wheel grades can grind parts with the full range of  $d_e$  values using the spindle power provided. However, once 43 m/s is exceeded, the burn level is rapidly exceeded for all but the smallest  $d_e$  value such that by 60 m/s the wheels are limited to  $d_e$  of  $<25$  mm and burn-insensitive workpieces unless the wheel grade and, hence, wheel life are reduced drastically, thus negating much of the reason for higher speeds in the first place.

**TABLE 17.1**  
Wheel Speed, Wheel Diameter, and Power Required per Unit Width

Wheel Speed	350 mm	450 mm	600 mm	$Q'_{\max}$
33 m/s	30 W/mm	60 W/mm	90 W/mm	1.5–4
43 m/s	50 W/mm	100 W/mm	150 W/mm	3–9
60 m/s	100 W/mm	150 W/mm	200 W/mm	4–12

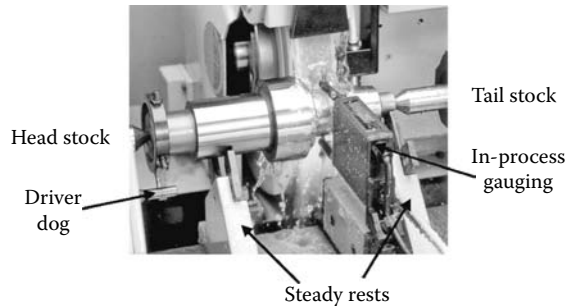


**FIGURE 17.2** External grinding between centers with dog drive and diameter gauging.

Similar effects are seen with vitrified CBN as will be discussed below. The high thermal diffusivity of CBN shifts the wheel speed limit. For example, grinding hardened steel in water-based coolants, the value for CBN is shifted from 43 m/s to 80 m/s. Essentially, machines designed specifically for alox or for CBN abrasives require two quite different wheel-speed ranges although there is a recent approach to use hard-grade vitrified CBN wheels at speeds traditional to alox wheels.

### 17.1.5 STOCK REMOVAL

Part tolerance capability in terms of incoming stock is better than for internal grinding. The stock removed on diameter should be at least three times the roundness specification, six times the straightness specification, and overall twice as much stock on diameter as the total geometry tolerances.

Flat form traverse dressing of alox wheels is usually with a single-point diamond or blade tool mounted on the foot or headstock. Form dressing is again either by interpolation with a stationary or rotary diamond or by plunge roll dressing. The former offers increased flexibility but adds significantly to cycle time. The most accurate forms, particularly in high production applications such as the bearing industry for, for example, twin raceway grinding where truth of radii tolerances are  $<1 \mu\text{m}$ , usually require formed diamond rolls. Radial swing dressers with single-point diamonds are also used.

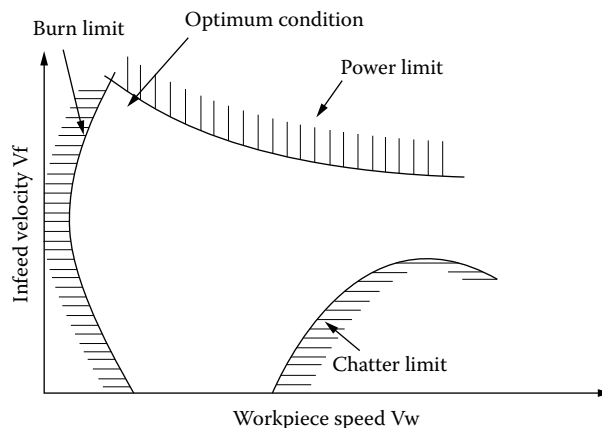


**FIGURE 17.3** Power and process limits in grinding. (From Rowe, Bell, and Brough 1986. With permission.)

### 17.1.6 ANGLE-APPROACH GRINDING

Angle-approach grinding adds complexity to the grinding process. Its benefits are that it allows grinding with the periphery of the wheel, not the side, in order to go from a face to a line contact, and it grinds two surfaces in relation to each other at once. Its major drawbacks are nonuniform wheel wear and increased grinding temperatures relative to a simple outer diameter (OD) plunge, and the fact that dressing is now necessary in two planes. If acoustic emission dress detection is used it must make two independent contacts on orthogonal axes.

The effect of an angle approach is to reduce the equivalent wheel diameter on the face from total conformance to a finite number while making only a small impact on the  $d_e$  for the cylindrical surface. Malkin presents the following formulae for calculating  $d_e$  for face and outer diameter.

$$d_e \text{ (face)} = (\text{wheel diameter})/\sin \alpha \quad \alpha = \text{angle of approach}$$

$$d_e \text{ (OD)} = (\text{wheel diameter})/[(\text{wheel diameter}/\text{part diameter}) + \cos \alpha]$$

Example: Wheel diameter = 450 mm. Part diameter = 25 mm

	$\alpha = 0^\circ$	$\alpha = 30^\circ$	$\alpha = 45^\circ$
$d_e$ (face)	$\infty$	900 mm	636 mm
$d_e$ (OD)	23.7 mm	23.9 mm	24.1 mm

Angle approach requires conventional wheels to be run at no more than 45 m/s, and  $Q'$  values of  $<1$  when removing stock from the face. Much more attention must also be paid to coolant delivery.

### 17.1.7 COMBINED INFEEED WITH TRAVERSE

The final method of grinding is a combination of infeed with traverse. This is a typical operation for long shafts and cylinders. An extreme form is roll grinding for the paper and steel industries. The nature of the wheel wear and the actual  $Q'$  values become less well defined as the wheel is cutting on its leading edge. Since breakdown will be rapid with an alox wheel infeed amounts are kept at  $<15 \mu\text{m}$  on diameter and the wheel cross-fed up to one third (cross-feed one direction only)

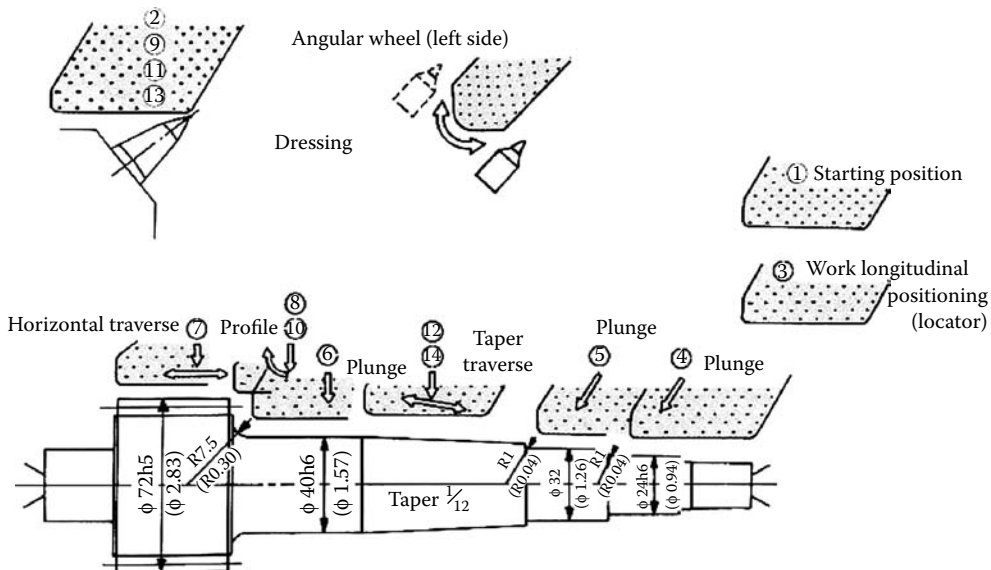


FIGURE 17.4 Combined infeed and traverse for face and diameter grinding.

or one fourth (cross-feed both directions) of its width per revolution of the workpiece. The cutting action is distributed over the feed width with two overlaps at size for finish.

With modern CNC equipment, all the operations described above can be incorporated into grinding many surfaces in a single chucking as illustrated in Figure 17.4 [Okuma n.d.].

## 17.2 HIGH-SPEED GRINDING

### 17.2.1 INTRODUCTION

The last 25 years has seen a dramatic growth in the use of vitrified CBN at wheel speeds of 80 m/s up to as high as 200 m/s in certain key cylindrical applications. Three such applications, camshaft grinding, crankshaft grinding, and peel grinding, will be discussed to illustrate what the technology is and where it is likely to expand. In light of the limitations apparent when grinding with alox wheels at high speed, it is necessary to first review the current theories on heat generation and burn in grinding.

### 17.2.2 ENERGY AND TEMPERATURES IN HIGH-SPEED GRINDING

The starting point to the determination of grinding temperatures is the definition of uncut chip thickness

$$h_{cu} = \sqrt{\frac{v_w}{v_s} \cdot \frac{1}{C \cdot r} \sqrt{\frac{a_e}{d_e}}} \quad h_{cu} \ll a_e$$

where

- $v_s$  = wheel speed
- $v_w$  = workspeed
- $a_e$  = depth of cut
- $d_e$  = equivalent wheel diameter
- $C$  = active grit density
- $r$  = grit cutting point shape factor

$C$  and  $r$  are characteristics of the wheel and how it was dressed. They are usually treated as a single ( $Cr$ ) factor. Uncut chip thickness is a reasonably reliable factor for predicting several grinding variables especially specific grinding energy  $e_c$ :

$$e_c \propto \frac{1}{h_{cu}^n}$$

$$e_c \propto \frac{1}{h_{cu}^n} \propto \sqrt{\frac{v_s}{v_w} \cdot Cr} \sqrt{\frac{d_e}{a_e}}$$

Since  $Cr$  is normally a constant for a given wheel/dress set of conditions some OEMs will use this factor to characterize a given wheel or compare performance from one wheel grade or type to another.  $Cr$  for a plated CBN, for example, is only 20% that of a typical vitrified CBN wheel. Similar predictions can be made for surface roughness,  $R_t$ , and force/grit,  $f'_g$ .

$$R_t \propto \frac{h_{cu}^{4/3}}{a_e^{1/3}} \quad \text{surface roughness}$$

$$f'_g \propto h_{cu}^{1.7} \quad \text{force per grit}$$

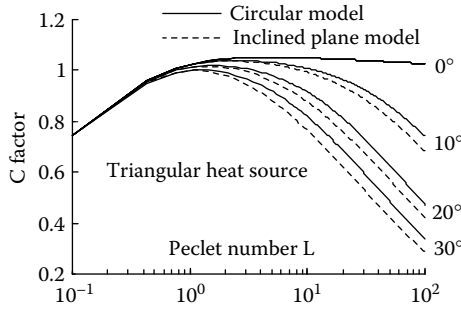


FIGURE 17.5 Factor  $C$  for max temperature. (From Rowe and Jin 2001. With permission.)

Power can be predicted if typical values of specific energy for the particular wheel/material/setup are known. The second and more important step is to determine where the heat goes and what temperatures will be created.

There is an enormous amount of theoretical experimental work on heat and temperature models in grinding as introduced in Chapter 2. Much of this work has been refined and the important factors isolated [Rowe et al. 1996, Rowe and Jin 2001, Marinescu et al. 2004]. The maximum surface temperature depends on the grinding power ( $F'_t \cdot v_s$ ), the grinding speeds, and material parameters. A mean grinding temperature when grinding with coolant is given by

$$T_{\max} = C_{\max} \cdot R_w \cdot \frac{F'_t \cdot v_s}{\beta_w} \cdot \sqrt{\frac{1}{v_w \cdot l_c}}$$

where the thermal parameters in the equation that affect grinding temperature are described as follows.

**17.2.2.1 The  $C_{\max}$  Factor**

The value is approximately equal to 1 for conventional grinding. The value is reduced for deep grinding and at high work speeds, that is, Peclet number,  $L$ . Rowe and Jin [2001] give charts of  $C$  values for maximum temperature  $C_{\max}$  (Figure 17.5) and for finish surface temperature (Figure 17.6).

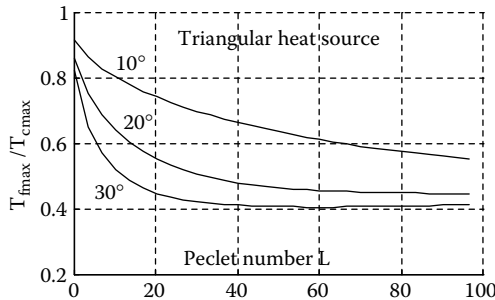


FIGURE 17.6 Maximum temperatures on the finish surface  $T_{f\max}$ , as a fraction of the contact temperature  $T_{c\max}$ . (From Rowe and Jin 2001. With permission.)

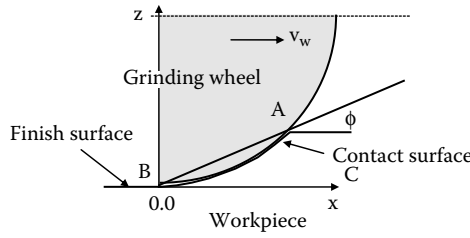


FIGURE 17.7 Contact angle  $\phi$ , contact surface, and finish surface.

**17.2.2.2 Peclet Number  $L$  and Workspeed**

The effect of workspeed is defined by Peclet number  $L$ . Values greater than 5 represent reasonably high workspeed, although much higher values can be achieved and allow cool grinding. Peclet number  $L$  is given by

$$L = \frac{v_w \cdot l_c \cdot \rho \cdot c}{4 \cdot k}$$

where  $k$  = thermal conductivity,  $\rho$  = density, and  $c$  = specific heat capacity of the work material.

**17.2.2.3 Contact Angle  $\phi$**

A large depth of cut and a small wheel diameter lead to a large contact angle (Figure 17.7).

The transient thermal property,  $\beta_w$ , of the workpiece material is given by

$$\beta_w = \sqrt{k \cdot \rho \cdot c}$$

Workpiece heat partition ratio,  $R_w$ , is the proportion of the grinding energy that is conducted into the workpiece.  $R_w$  is a function of the wheel grain conductivity and sharpness and of the transient thermal property. Ignoring for the present, coolant convection and convection by the grinding chips,  $R_w$  approximates to  $R_{ws}$ . Hahn (1962) showed that

$$R_{ws} = \left( 1 + \frac{k_g}{\beta_w \cdot \sqrt{r_0 \cdot v_s}} \right)^{-1}$$

where  $k_g$  is the thermal conductivity of the abrasive grain. Grain sharpness is related to  $r_0$  the contact radius of the grain.  $R_{ws}$  is relatively insensitive to variations of  $r_0$ . Typically,  $R_{ws}$  for conventional grinding varies between 0.7 and 0.9 for vitrified wheels and between 0.4 and 0.6 for CBN wheels. After allowing for heat convected by the coolant and by the chips,  $R_w$  can be greatly reduced below  $R_{ws}$ .

The temperature equation for conventional shallow grinding, can, therefore, be very approximately reduced, for a given wheel/work/machine configuration to

$$T_{max} \propto \sqrt{a_e \cdot v_s \cdot C \cdot r}$$

ignoring heat taken by coolant and chips.

In this case, it follows that increasing wheel speed, increasing depth of cut, or increasing the number of active cutting edges (by, e.g., dull dressing) increases the surface temperatures. However, taking account of heat convected by the coolant and by the chips as follows shows that much lower temperatures can be achieved than would be expected.

#### 17.2.2.4 Heat Convection by Coolant and Chips

In deep grinding, the long contact length allows substantial convective cooling from the grinding coolant. Also, in high-rate grinding with low specific energy, the heat taken away by the grinding chips reduces maximum temperature very substantially [Rowe and Jin 2001]. One of the advantages of high-rate grinding is that specific energy is reduced.

Allowance can be made for convective cooling by subtracting the heat taken away by the coolant and chips as described by Rowe and Jin [2001]. Allowance for convective cooling is essential for creep grinding as shown by Andrew, Howes, and Pearce [1985]. It has also been found important for other high-efficiency deep-grinding processes as employed for drill flute grinding, crankshaft grinding, and cutoff grinding. If allowance is not made for convective cooling, the temperatures are very greatly overestimated.

The maximum temperature equation modified to allow for convective cooling has the form

$$T_{\max} = \frac{F'_t v_s - \rho \cdot c \cdot T_{mp} \cdot a_e \cdot v_w}{\frac{\beta_w \sqrt{v_w l_c}}{R_{ws} C_{\max}} + \frac{2}{3} \cdot h_f \cdot l_c}$$

where  $T_{mp}$  is a temperature approaching the melting point of the workpiece material. For steels, the material is very soft at 1,400°C and this temperature gives a reasonable estimate for the chip convection term.  $h_f$  is the coolant convection coefficient that applies as long as the maximum temperature does not cause the fluid to burn out in the grinding zone. If burnout occurs, the convection coefficient is assumed to be zero. Burnout is a common condition in grinding but should be avoided in creep grinding and for low-stress grinding. Values estimated for convection coefficient when grinding with efficient fluid delivery were 290,000 W/m<sup>2</sup>K for emulsions and 23,000 W/m<sup>2</sup>K for oil [Rowe and Jin 2001].

The contact conditions between the abrasive grain and the workpiece are very different from each other. When an abrasive grain slides against the workpiece, a particular point on the workpiece only contacts the abrasive grain for an extremely short period of time of the order of 1 μs. However, the grain is sliding on the workpiece for a very much longer time, typically 1,000 times longer and of the order of a millisecond.

A key factor for the workpiece, therefore, is transient thermal property  $\beta$ . This term involves both thermal conductivity and heat capacity. Transient thermal property is defined as  $\beta = \sqrt{k \cdot \rho \cdot c}$  and is particularly important for transient heat conduction into the workpiece.

However, the abrasive grain very rapidly achieves its maximum surface temperature, so that the transient thermal property is unimportant. For the abrasive grain, it is thermal conductivity that is important. Pure CBN is known to conduct heat up to 40 times faster than alox. Typically, the value of thermal conductivity for CBN is 5 to 20 times higher than for alox depending on the purity of the CBN. The thermal conductivity of CBN abrasive relative to alox actually lowers temperatures by almost 50% on steels, which is highly significant.

The Specific Grinding Energy,  $e_c$ , is a measure of the input of energy. One factor that can significantly affect its value is coolant. Oil has much better lubrication and will tend to lower this value.

The approximate equation for grinding temperature in shallow grinding makes a number of predictions based on change in depth of cut and wheel speed. First, temperature increases with

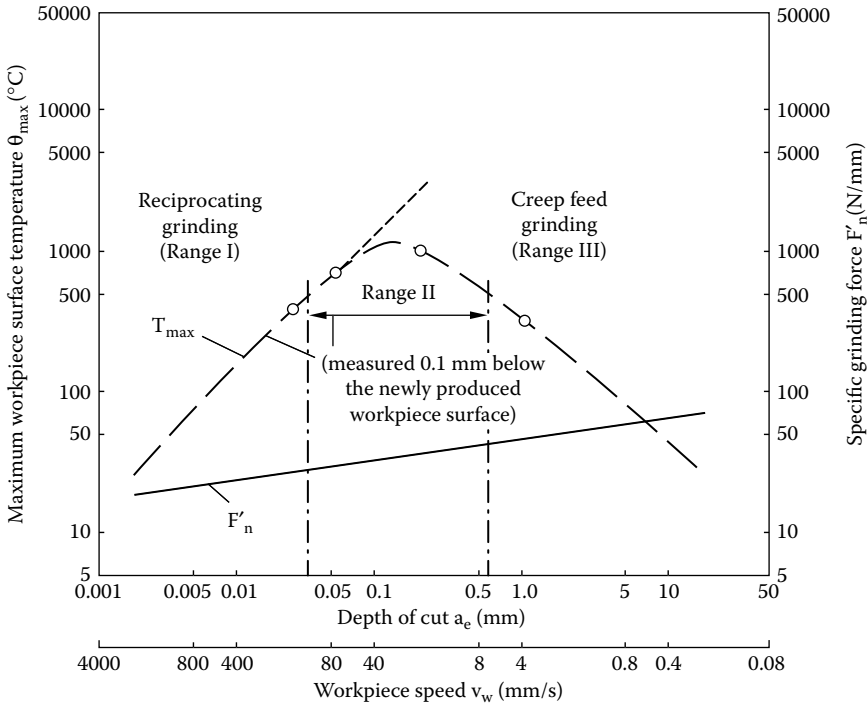


**FIGURE 17.8** Predicted maximum temperatures at constant specific removal rate  $Q'_w$ . (From Werner 1983. With permission.)

depth of cut. The increase is proportional to the (depth of cut)<sup>1/2</sup>. This is a good predictor of temperature at shallow cuts but it was found about 30 years ago that it failed at very deep depths of cut [Werner 1983]. Tawakoli [1993] gives a more accurate trend for temperature in Figure 17.8. Power increases as expected and the approximate shallow grinding prediction of temperature from this is the dotted line. However, in Zone III, with creep feed grinding, it is believed that the contact length becomes so great that the coolant can dissipate over a large-enough area for the temperatures to fall. It should be noted that cylindrical grinding operations very rarely, if ever, get into Zone III. A much more interesting fact is that at very high workspeeds the temperatures should drop dramatically.

The second prediction is that temperature rises with wheel speed. This seems very reasonable in the same way that rubbing your hands faster makes them get hotter from frictional heating. This was also the observation in the grinding industry for most of its history. However, starting in the 1970s, some curious results were obtained from German research suggesting that under certain circumstances if the wheel speed was increased enough the temperatures would actual fall again [Tawakoli 1993]. The explanation given by Tawakoli for this relates to the extremely brief length of time the abrasive grits are in contact with the workpiece. The surface is not in thermal equilibrium. The heat pulse initially spreads out over the surface before penetrating into the workpiece. The heated surface facilitates the removal of the next chip and so reduces the grinding forces. However, before heat can spread down into the surface, the next chip is removed taking the heat with it. The critical wheel speed where these effects start to be apparent is about 100 m/s (Figure 17.9). When the speed exceeds the critical value, rapidly succeeding chip removals reduce the temperature.

It is still not clear whether these observations are for specific operating parameters or a more general effect. The issue gets clouded by problems such as nonoptimized coolant delivery and



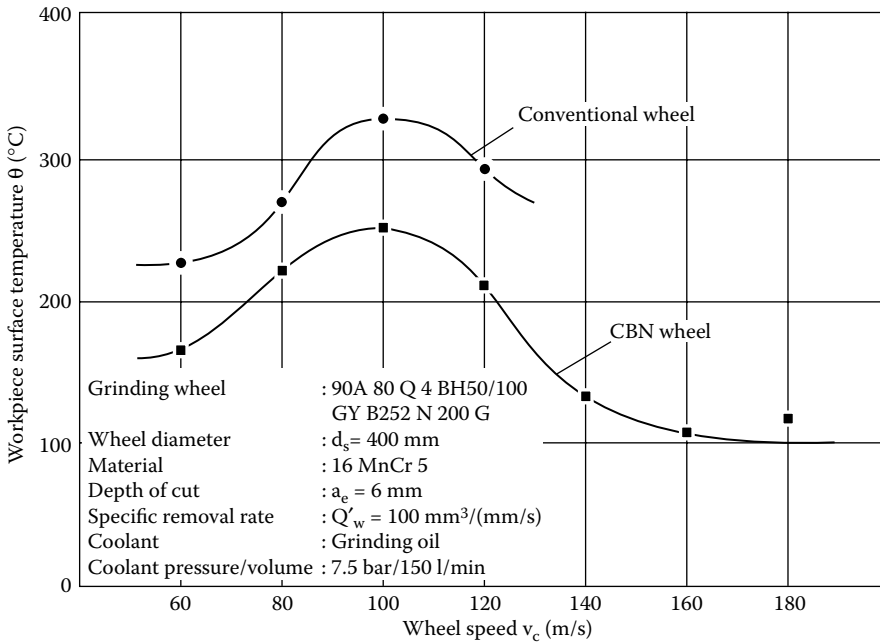


**FIGURE 17.9** Effect of wheel speed on maximum temperatures at constant high removal rate and large depth of cut. (From Tawakoli 1993. With permission.)

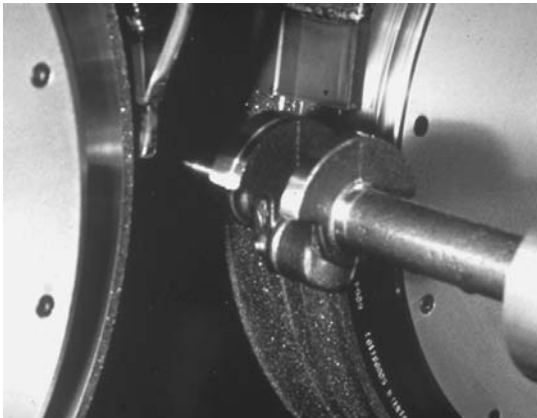
increased machine complexity. It has been found from experience over the last 10 years as more high-speed applications have been investigated that if an application creates burn at <100 m/s then increasing wheel speed does not relieve the problem. However, if a process runs at 100 m/s without burn issues then usually it will also run at 160 m/s. Although most of the data is still anecdotal, it does suggest that the general trend in Figure 17.9 may be correct but that the temperature drop may be a lot less pronounced or even just level off after 100 m/s.

It is also possible to predict what type of applications or conditions are likely to be most successful at very high wheel speeds. The following practical recommendations can be made.

- Grind-burn insensitive material. Wheel speed limits when cylindrical grinding with water-based coolant with vitrified CBN wheels are

Chilled cast iron	>160 m/s
Carbon Steel 30 HrC	>120 m/s
Carbon Steel 60 HrC	<100 m/s
D2 Steel 62 HrC	<90 m/s
Inconel	<70 m/s

- Use oil-based coolant instead of water.
- Use electroplated CBN wheels instead of bonded wheels [smaller  $Cr$ ]. For life as well as for lubrication, these wheels are best used with oil.
- Use very high workspeeds (or very deep depths of cut).
- Use CBN instead of alox.



Grind parameters

Machine : Guhring  
 Wheel speed : 123 m/s  
 Component : Crankshaft  
 Material : Gray cast iron  
 Wheel : Direct plated CBN  
 twin wheel grind  
 Coolant : Oil

Stock removal rate  $Q' = 135-166$   
 Roundness =  $4.5 \mu\text{m}$   
 Roughness  $R_a = 0.75 \mu\text{m}$

**FIGURE 17.10** High-speed crankshaft grinding. (Data courtesy of SGA-Winter. Photo courtesy of GE Super-abrasives. With permission.)

It was perhaps not surprising that one of the very first cylindrical applications to get the industry attention, grinding compressor cranks, met at least four out of five of the optimum conditions (Figure 17.10). Gray cast iron was very easy to grind, it only proved economic to grind in oil, and it used electroplated CBN wheels [Woodside 1988].

The next question that has to be answered when considering high speeds is to determine what the benefits would be to justify the added expense. There has to be higher stock-removal rates, better quality, or lower capitalization/operating costs.

There is a considerable amount of research that has demonstrated that very high stock removal rates ( $Q' > 2,000 \text{ mm}^3/\text{mm/s}$ ) can be achieved with high speed. At these removal rates, the rubbing and ploughing fraction of the specific grinding energy is miniscule and the specific energy decays to an asymptotic level of about  $10$  to  $15 \text{ J/mm}^3$  at speeds of the order of  $120 \text{ m/s}$  and even as low as  $7 \text{ J/mm}^3$  at a speed of  $180 \text{ m/s}$  grinding steel [Rowe and Jin 2001]. For chilled cast iron, the value is  $30 \text{ J/mm}^3$  [Wakuda et al. 1998] (Figure 17.11). Furthermore, both the tangential *and* normal forces are reduced

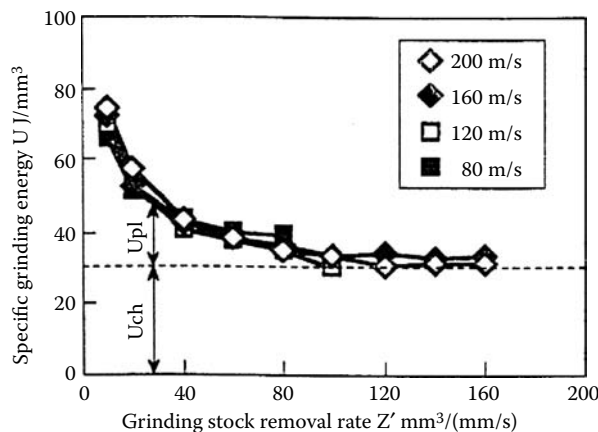


**FIGURE 17.11** Effect of removal rate on specific energy. (From Wakuda et al. 1998. With permission.)

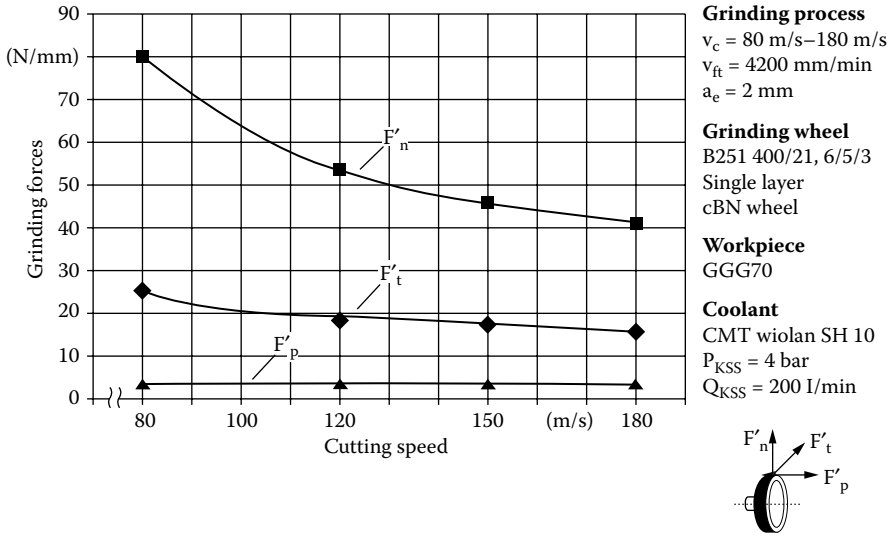


FIGURE 17.12 Effect of wheel speed on grinding forces. (From Toenshoff and Falkenberg 1996. With permission.)

with increasing wheel speed [Toenshoff and Falkenberg 1996]. Potential benefits are, therefore, higher stock removal rates and under the correct conditions or grinding configuration, higher energy efficiency and less pressure on the part (Figure 17.12).

### 17.2.3 COOLANT DRAG AND NOZZLE DESIGN IN HIGH-SPEED GRINDING

A major drawback with higher wheel speeds is the increased demand for nongrind power. This relates, in part, to the increased frictional drag on the spindle. However, a far more significant factor is coolant drag on the wheel.

The whole issue of coolant at high speed is problematic. Direct matching of coolant flow to wheel speed may require supply pressures over 1,000 psi to achieve a coolant velocity of 100 m/s. By 160 m/s the coolant pressure required would be >2,500 psi. Pressures over 1,000 psi will erode vitrified bonds, prevent the maintenance of laminar flow, and create major misting problems. Coolant is, therefore, often applied at low pressure (60 to 150 psi is typical) using a shoe-type nozzle such

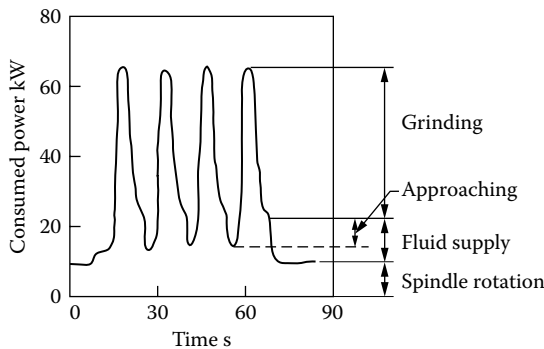
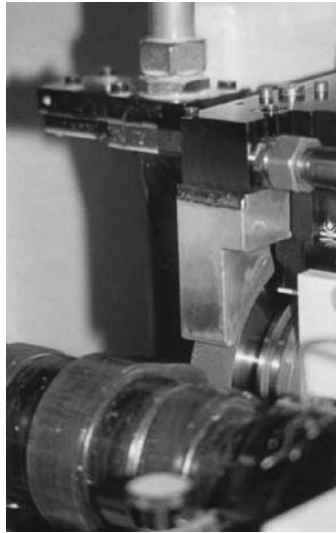


FIGURE 17.13 Power consumption in grinding cast iron camlobes at 200 m/s vitrified CBN wheel. (From Ota 1997. With permission.)



**FIGURE 17.14** Shoe nozzle on Schaudt camlobe grinder for diesel cams. (From UGT 2000. With permission.)

that the wheel accelerates the coolant into the grind zone. If the coolant is applied successfully, this results in large drag forces on the grinding wheel. Once in the grind zone, the coolant also creates enormous hydrodynamic pressure just like a hydrodynamic bearing. This, in turn, creates high normal forces that manifest themselves as profile errors when grinding wide parts at speeds as low as 60 to 80 m/s using vitrified CBN wheels.

At 160 m/s, the force exceeds 20 N/mm wheel width using oil [Brinksmeier and Minke 1993]. The coolant also creates a great deal of resistance for wheel rotation. The combined effects of windage, spindle bearing, and coolant drag at 160 m/s can be as much as 2 kW/mm wheel width [Koenig, Klocke, and Stuff 1997]. This is also confirmed by field experience.

#### 17.2.4 MAXIMUM REMOVAL RATES

Taking both the beneficial and negative impacts of high speed, Table 17.2 gives the maximum stock removal rate as a function of wheel width for a 10-kW spindle.

**TABLE 17.2**  
**Maximum Stock Removal Rates as a Function of Wheel Width**

Wheel Width (mm)	Idle/Coolant (kW)	Grind Power (kW)	$Q'_{\max}$ Steel Electroplate CBN (mm <sup>3</sup> /mm/s)	$Q'_{\max}$ Cast Iron Vitrified CBN (mm <sup>3</sup> /mm/s)
1	2	8	800	270
2	4	6	500	200
3	6	4	300	130
4	8	2	100	60
4.5	9	1	40	20
4.8	9.6	0.4	10	7
5	10	0	0	0

At 160 m/s, to reap benefits from the high speed, the spindle power requirement is a minimum 4 kW/mm of which 50% is actually available for grinding. This has led industry to two options: either use very narrow wheels and get the benefits of low forces (peel grinding) or build high stiffness cylindrical grinders with very large motors (camlobe grinding and crankpin rough grinding).

### 17.2.5 PEEL GRINDING

Peel grinding is an excellent solution to the above analysis and a testament to German research and application in this field. The peel-grinding process is sometimes viewed as turning with a grinding wheel.

Figure 17.15 illustrates the geometry for the simplest version of the process with the wheel axis parallel to the part axis. The entire wheel width is usually no more than 7 mm, especially when grinding in oil. The operation removes the entire stock amount  $z/2$  in a single pass. Roughing occurs over an angled length,  $b_s$ , Schr. of 2 to 5 mm with a spark-out region,  $b_s$ , Ausf. This length can be as little as 2 mm and still hold finish under 2 Rz. This is achieved by using a very high workspeed, up to 10,000 rpm, to obtain a sufficient overlap ratio [Koenig and Treffert n.d.]. The high workspeed also meets one of the criteria above for low burn. For the process to be effective the wheel profile must hold up under high stock-removal rates,  $Q' > 80 \text{ mm}^3/\text{mm/s}$ , which demands oil coolant and high wheel speeds. Initially, metal bond CBN wheels were used but these proved difficult to dress and OEMs have sacrificed some life by going to vitrified CBN for automatic dressing capability. The performance of vitrified CBN bonds has recently increased significantly such that the industry is starting to see successful implementation of the peel-grinding process in water-based coolants.

Numerous OEMs such as Okuma, Overbeck, Gendron, Schaudt, Tecchella, TMW, ITM, and Weldon offer peel grinding in this configuration. Perhaps the biggest proponent, however, has been Junker using a patented Quickpoint process [Junker 1993]. This method greatly reduces the contact length by being able to tilt the wheel at an angle of  $1^\circ$ .

Most applications in the field are currently running at wheel speeds of 90 m/s to 120 m/s.  $Q'$  values are of the order of 50 to 100  $\text{mm}^3/\text{mm/s}$  although accurate definition can be difficult without knowing the exact stable wheel profile. Wheel spindle power ranges from 15 kW to 30 kW depending

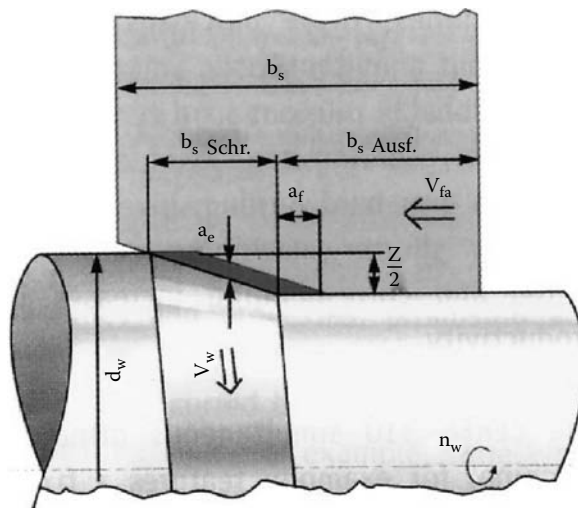
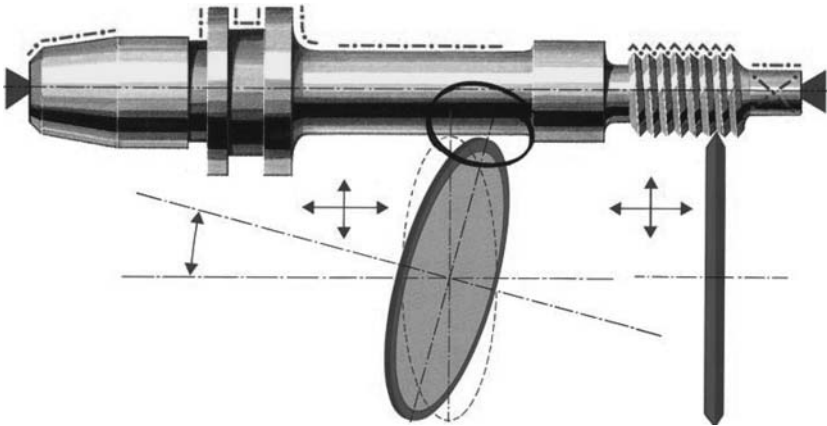


FIGURE 17.15 Wheel profile for parallel contour grinding. (From Lutjens and Mushardt 2000. With permission.)



**FIGURE 17.16** Principle of the Junker Quickpoint contouring cylindrical grind process. (From Junker 1992. With permission.)

on the OEM. In general, for a given grinding power, contour grinding will remove material three times faster with less than a sixth the normal force of conventional plunge grinding.

As reports are now being circulated from end users regarding the performance of the process in actual production, the prognosis is very good. It appears to be highly flexible, allowing fast change over times, and generating improved quality from a consistent grind with low forces. Schultz [1999] from DaimlerChrysler reported that in grinding transmission shafts, peel grinding reduced manufacturing costs by 50% with better and more consistent part quality compared to external plunge grinding with alox wheels. Set-up time was also reduced by 80% because the same wheel could grind a whole family of parts, while machining time was reduced by 45%. Even abrasive costs were reduced by 5%.

There has been resistance in the U.S. market because of the historical requirement for oil coolant. However, at least one application has been developed successfully on Weldon grinders in soluble oil grinding Inconel at 120 m/s and achieving  $Q' = 120 \text{ mm}^3/\text{mm/s}$ . The wheels have to be made wider, reducing some of the low normal force benefits, to allow more wear back of the roughing step while still maintaining a spark-out zone. Finish, size, and roundness appear very stable and independent on spark-out length until a critical minimum value is reached.

With globalization and commonality of processes by larger end users, it is becoming apparent that oil coolant is starting to gain acceptance again in the United States. Improved coolant-handling knowledge from Europe, combined with increasing use of powdered metal for automotive components prone to rusting, are additional drivers. Additionally, as mentioned above, improved vitrified CBN bond technology is permitting economic viability even in water-based coolants.

### 17.3 AUTOMOTIVE CAMLOBE GRINDING

Camlobe grinding has been the leading driver of high-speed grinding over the last 25 years. It is a high-cost process, making up more than 40% of total camshaft manufacturing costs [Wedeniwski 1989]. The operation is very capital-equipment intensive resulting in pressures from end users to reduce cycle times while offering machine tool builders sufficient end sales volume to justify research into innovative processing methods. A flow chart for a modern automotive camshaft manufacturing line is given Figure 17.17.

The finish grinding of the camlobe is one of the most difficult operations in the manufacture of an automotive camshaft. Profiles must be held at micron levels with equally tight timing angles, straightness, and finish requirements. The profiles are defined per degree of part rotation and

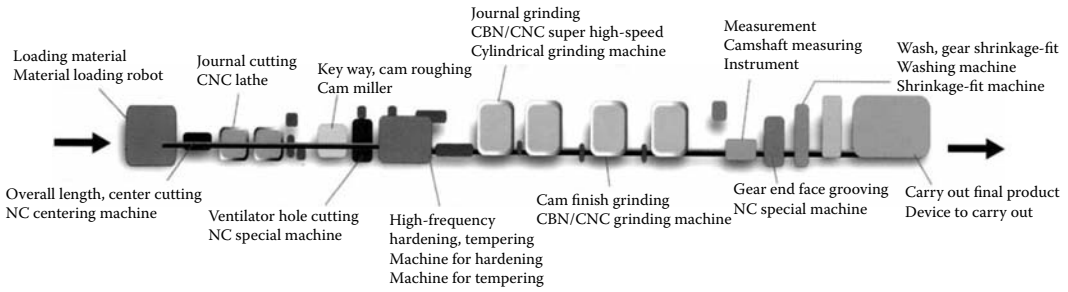


**FIGURE 17.17** Flow chart for a modern automotive camshaft manufacturing line. (From UMS 2002. With permission.)

supplied as a lift table with either a series of length dimensions from the center point or as a deviation from the base circle diameter value. Figure 17.18 provides the terminology for the various features of the camlobe.

There are huge changes in equivalent wheel diameters going from the base circle through the ramp into the flank. On occasion, the flank may even have a “re-entry” or negative radius leading to near total conformance with the wheel,  $d_e \rightarrow \infty$ . Heat generation and burn are constant concerns at points along the flanks where conformance is greatest and/or the coolant is most masked from the grind zone. Thermal modeling of the process presented by Pflager [2002] illustrates the effect (Figure 17.19).

Camlobe grinding has been transformed in the last 25 years. Prior to 1980, all cams were ground on master-cam grinders where the wheel slide movement was controlled by following a rotating template or master-cam. In the late 1970s, ac servo closed-loop systems with CNC controls to the work head were able to control the rotation while maintaining orientation of the camlobe in synchronization with movement of the wheelhead to CNC generate the profile. It was not long after this that machine tool builders realized that the accuracy required for generating cam profiles were the same as those required to implement CBN wheels. The first camlobe grinder reported in the literature designed specifically for CBN was manufactured by Toyoda Machine Works (TMW) and used resin-bonded CBN wheels. One such machine, a TMW GCB7-63, was supplied to Caterpillar about 1980 to grind hardened-steel diesel camshafts [Hanard 1985]. The GCB7 had hydrostatic ways and wheel spindle, CNC profile generation, variable workspeed drive to control stock removal

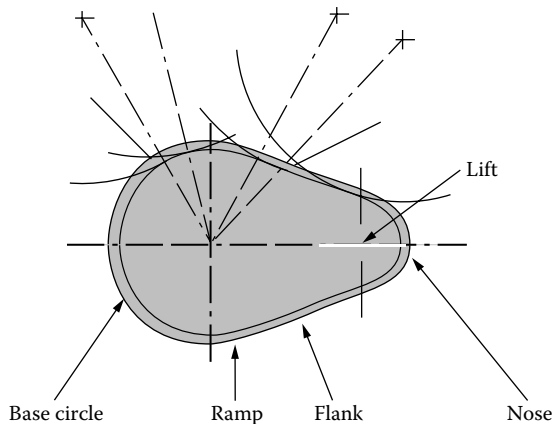


**FIGURE 17.18** Features of a camlobe.

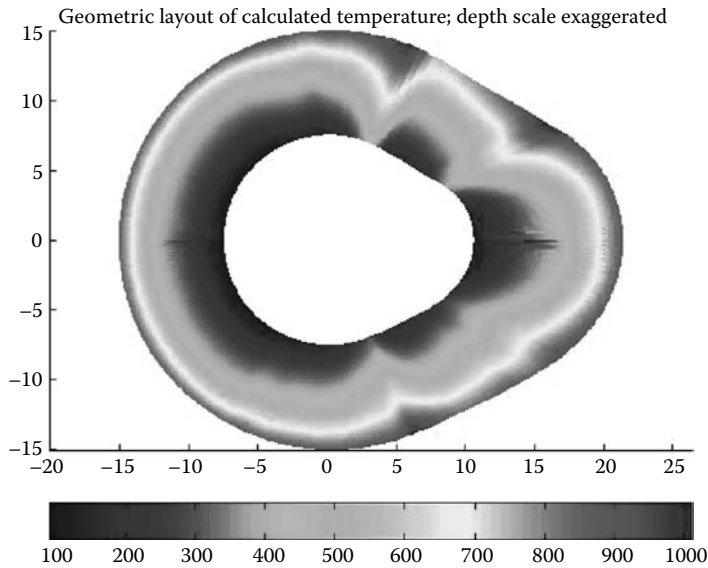


**FIGURE 17.19** Temperature distribution with varying contact conformity (depth greatly exaggerated). (From Pflager 2000. With permission.)

around the camlobe, and an acoustic touch sensor to determine the relative position of the wheel and diamond truer. The wheels were 600 mm in diameter and, being resin-bonded, required a post-true conditioning process using a dressing roll and free abrasive grains. This conditioning process was difficult to control and proved, together with the low resilience of the resin bond, to be the process-limiting factor. The wheel speed was only 50 m/s.

Following the fuel crisis of the 1970s, U.S. automotive manufacturers strived to improve gas mileage by improvements in engine efficiency. One area that was targeted was reduction in engine friction by using a roller rather than a flat tappet to transfer the lift from the camlobe to the valves. Rollers reduced friction but generated higher normal forces that were found to exceed the strength of the cast iron materials in use at the time for camshaft fabrication. This, in turn, forced engine manufacturers to switch to hardened forged steels.

Hardened steel proved to be considerably more difficult to grind than cast iron because it was sensitive to grinding burn due to the formation of untempered martensite, a brittle layer causing spalling and premature cam failure. Steel forgings or assembled cams, despite having only a third the stock of cast iron casting, proved impossible to grind in the hardened state in comparable cycle times to cast iron camshafts.

Two different manufacturing strategies were, therefore, pursued by different engine manufacturers to overcome this problem. Some elected to grind the steel in the soft state, where burn was not an issue, then to heat-treat. This route led to diminished dimensional accuracy due to thermal distortion in the heat treatment. By contrast, Ford Motor Co., for example, demanded grinding in the hardened state and proceeded to develop the technology first by assessing continuous dressing and then by adopting plastic-bonded conventional abrasive wheels. By the mid-1980s, this had become the standard processing route for much of the industry.

In the 1980s, increasing the Environmental Protection Agency's demands for fuel economy, combined with improved emissions, led engine designers to make radical changes to the camlobe. "Re-entry" profiles were designed with concave radii of less than 350 mm in the ramp areas to speed up the rate at which engine valves open and closed. This further increased the risk of thermal damage during grinding because of the increased contact length. It also created a far more fundamental problem: production grinders of the time all used conventional wheels with a usable diameter



range of either 750 to 600 mm or 600 to 450 mm. This was totally impractical to meet production for the new camlobe designs.

In 1984, Suzuki described the first results from a CBN camlobe grinder dedicated to grinding with vitrified CBN wheels. In line with camshafts still made in Japan, the data reported was grinding cast iron. The grinder, a TMW GCH 32, is described in detail by Tsujichi (1988). It had a fixed wheel speed of 80 m/s, this being considered the “state of the art” in high speed at that time. Wheels for this machine had been developed by TVMK, a joint venture between TMW and Unicorn Industries [Hitchiner 1991], and were only 350 mm in diameter to allow the machine to be designed with a small footprint.

In 1985, Ford completed the design for its 3.8 L V6 engine with incorporation of a steel camshaft with the first re-entry (concave) ramp profile. Ford Manufacturing, faced with the capacity issue of a production line making 750,000 cams/year, elected to purchase 16 of the GCH 32 machines and committed themselves to “making them work.” This line was the first major installation of its kind in the world and represented the seminal technological and engineering R&D experiment to determine the viability of CBN for cylindrical grinding [Renaud and Hitchiner 1991].

There was no doubt as to the improvement in quality or ability to make capacity. The main problem was striking a balance between wheel cost/part by using hard grades and eliminating burn by going softer. This was a foretaste of the question of the optimum wheel speed for a given abrasive and application. The solution was to lower the wheel speed from 80 m/s to 60 m/s, which tripled wheel life.

Figure 17.20 gives the abrasive cost/part for the first 9 years of the machine’s installation. After process optimization, the abrasive costs were well below those of conventional wheels grinding a non-re-entry profile cam. The biggest improvements though were in quality.

Some of the achievements listed include:

- 1992 Zero defect award for zero defects reaching assembly lines
- Several Perfect Performance Audits
- Machine uptime of greater than 95%
- Only one camshaft in over 4 million returned from an engine in the field. This was traced to loss of grinder machine power due to lightening and was subsequently eliminated as a potential process problem.
- One operator for 18 machines (two additional grinders installed in 1992)
- One wheelwright for all wheel changes on a two-shift basis; changes scheduled several days in advance (average one wheel/week for the complete line)

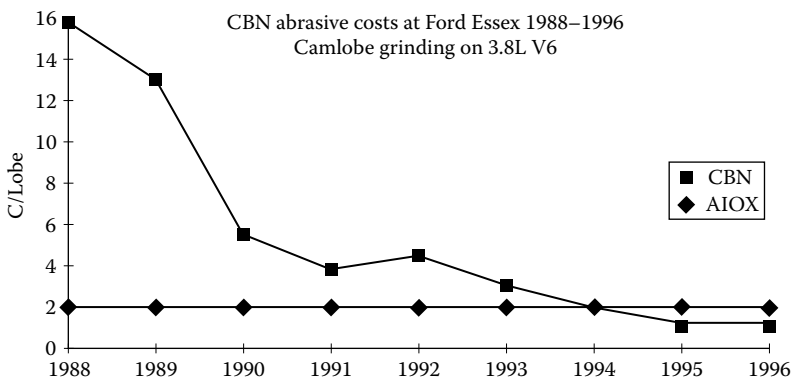
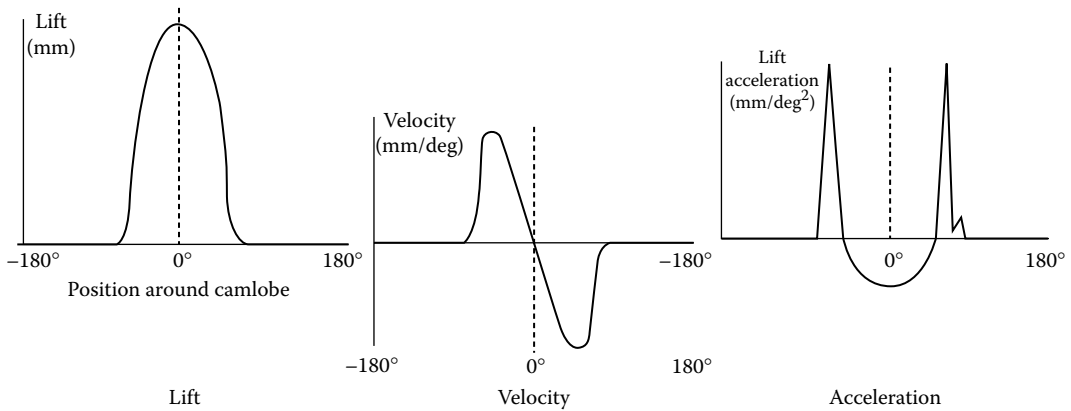


FIGURE 17.20 Reduction of CBN abrasive costs at Ford, Essex 1988–1996.



**FIGURE 17.21** Lift, velocity, and acceleration profiles for 1 rotation of the camlobe. (From Landis 1996. With permission.)

Ten years after 60 m/s was established as the optimum speed for grinding hardened steel with vitrified CBN in water-based coolant, machine tool and wheel technology have improved this to about 90 m/s. They have also tripled stock removal rates from  $Q' = 10$  to  $>30$  mm<sup>3</sup>/mm/s.

In the rest of the world, with the exception of diesel truck engines, most of the camshafts have remained cast iron-based. Consequently they saw far fewer problems using CBN. Also Europe used oil coolant far more frequently. Wheel speeds of 80 m/s to 100 m/s worked well at  $Q'$  values of  $>50$  mm<sup>3</sup>/mm/s. In recent years, with machine tool improvements, these values have now reached as high as  $Q' >180$  mm<sup>3</sup>/mm/s at 160 m/s.

Today there are probably far more grinders in Asia running at 160 m/s grinding scooter, motor cycle, and small car cams than there are in the United States at this speed for all grinding; such is the importance of selecting the right application and material type for high speed grinding.

Grinding camshafts is in large part a geometry problem, or to quote Pflager [2000], “*The problem with cams is that they are not round.*” High-speed grinding with high removal rates requires high workspeeds. The challenge of the machine tool builder is to generate slide movements that can produce these accurately at the required speed.

Machine movements are limited by the dynamics of the machine; namely, its velocity, acceleration, and jerk (rate of change of acceleration) limits, which must be calculated at all points around the lobe. This must be combined with the lift data at each degree and produce a smooth transition-free surface. The angular resolution has, therefore, to be much finer with positional resolution calculated to as many as 10 significant figures. Rotational speeds in older machines were usually limited as much by control computational speeds as machine dynamics.

The workspeed rpm on the base circle is constant and defines the stock removal rate for general definition of process capability. As the wheel moves from the base circle through the ramp to the flank area, the workspeed must reduce rapidly. Since this time is finite due to the inertia of the system, there is a brief period where the contact length and stock removal rate both jump dramatically leading to a significantly higher  $Q'$  value. Although near instantaneous, this can be the life or cycle time-limiting factor for the wheel (Figure 17.22 and 17.23).

The earliest machines were limited to about 100 rpm for workspeed based on computer speed. More recently, workspeeds have increased to over 300 rpm not only by control advances, but also by the use of linear motors to reduce the inertia of the wheel slide. This has allowed a reduction in peak  $Q'$  values and thus pushed up base circle stock removal rate capability. Current  $Q'$  values are typically 20 to 40 mm<sup>3</sup>/mm/s for hardened steel and 70 to 200 mm<sup>3</sup>/mm/s for cast iron.

During roughing the workspeeds are usually set at about 20% over the theoretical limit for maintaining the profile within tolerance. This is to maximize stock removal without thermal damage.

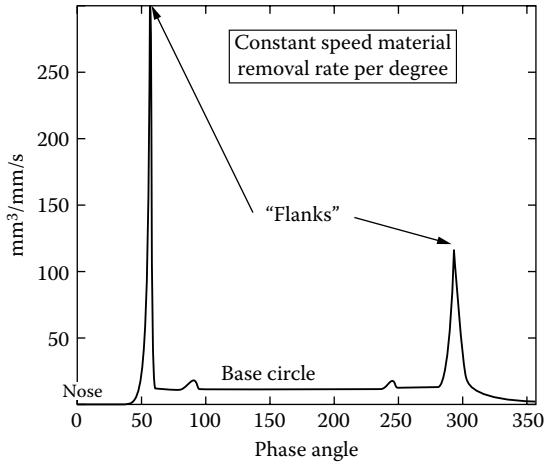


FIGURE 17.22  $Q'$  against phase angle around camlobe at constant work speed.

Finish grind workspeeds are held at 20% below the limit for maintaining profile. The stock amount in finish should be greater than the depth at which thermal damage may have been generated during roughing and is typically 50 to 125  $\mu\text{m}$ .

The sensitivity to burn of the grinding process for hardened steel cams in particular is such that nondestructive inspection methods based on Barkhausen noise have generally been adopted on many production lines [Fix, Tiitto, and Tiitto 1990]. Barkhausen noise is an inductive method that measures the noise generated by the abrupt movement of magnetic domain walls under the application of an alternating magnetic field. When a coil is placed near the sample, the change in magnetization created by the shift in the domain wall induces an electrical pulse. The sum of all pulses from all domain movements within the sample area provides the final signal or Barkhausen noise amplitude (BNA).

The BNA value is sensitive to several factors including the microstructure of the steel, hardness, and surface finish. However, for a given grade of steel kept within the standard limits of the process,

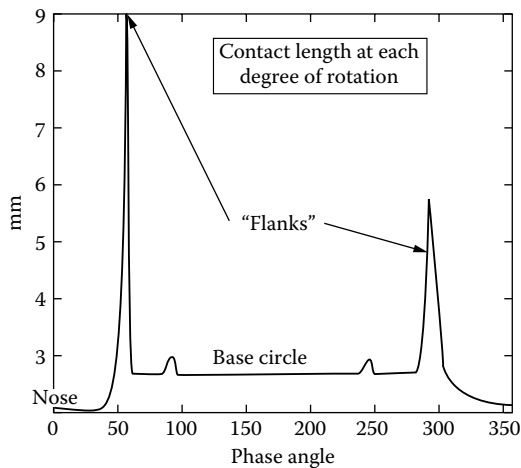
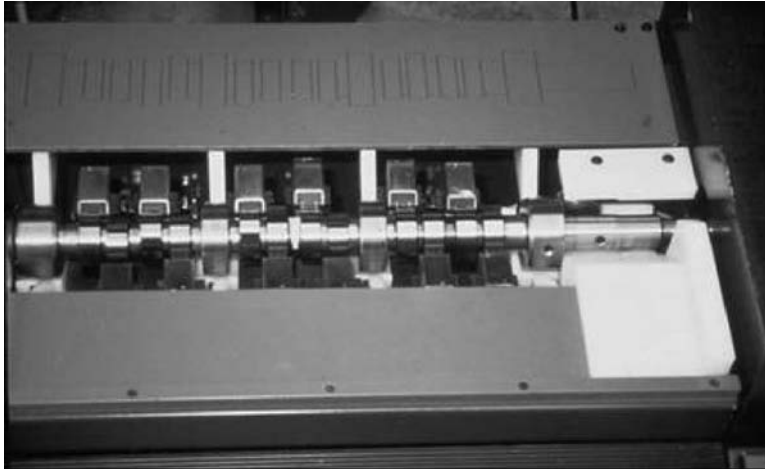


FIGURE 17.23 Contact length versus phase angle around camlobe. (From Pflager 2000. With permission.)



**FIGURE 17.24** Rollscan multihead sensor system from American Stress Technology.

the biggest factor affecting BNA is residual stress. In particular, the relaxation of compressive stress cause by retempering can be detected by an increase in BNA signal. This increase is directly correlated to the severity of the thermal damage so long as the transformation temperature is not exceeded. If the severity of the burn is such that untempered martensite is formed, then the signal actually drops; therefore, the method is primarily for ensuring a process stays in control at a level well below the point that significant softening of the steel occurs.

Figure 17.24 illustrates a Rollscan multihead sensor system from American Stress Technology. The system simultaneously measures all 12 ground lobes of an AISI 1050 steel camshaft. The system must be calibrated by using master cams checked for various levels of burn by Nital etching (Figure 17.25).

The value 50 is nominally set at burn, 45 is the upper process limit, while the process is under control for values less than 40. Figure 17.26 illustrates the change in BNA value on camshafts ground with a vitrified CBN wheel as a function of parts after dress.

In this case, at 80 m/s the chip load was too low and the wheel was glazing leading to increased grinding power. Thermal damage increased such that the wheel had to be dressed after just 30 parts. The signal could also be plotted as a function of angle around the lobe. Figure 17.27 plots the BNA values around a lobe during optimization studies. The initial cycle 1988 with high levels of

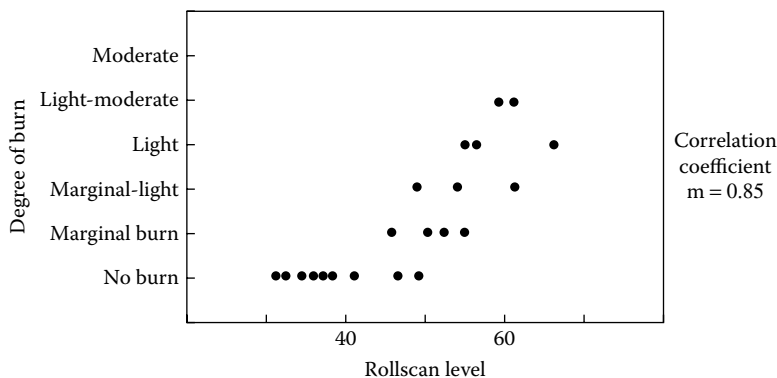


**FIGURE 17.25** Calibration of a Rollscan system for detecting onset of burn.

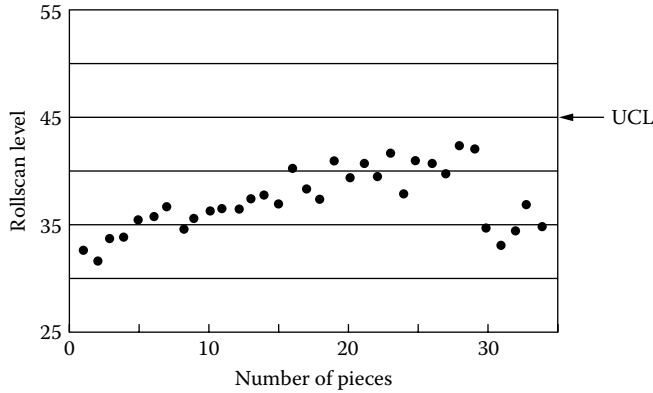


FIGURE 17.26 BNA variation with parts after dress (dress every 30 pieces).

BNA shows peaks in the two ramps as predicted from the temperature analysis in Figure 17.19. This also correlated with Nital etch checks.

Camshafts are inherently weak. They have hollow centers for weight reduction that are pre-ground on the journal surfaces prior to the lobe grind operation. During lobe grinding, the journals are supported by steady rests with flat polycrystalline wear shoes (Figure 17.28).

Any chatter that may have been generated grinding the journals will translate directly to the lobe grind. Furthermore, steady rests are relatively expensive and, therefore, limited to the minimum number to achieve acceptable part quality. Steady rests based on three-point contact may also cause buildup of chatter just as in centerless grinding if incorrectly adjusted. Too hard a wheel grade can readily cause chatter and profile errors from pushoff of the part. Tailstock pressure is applied hydraulically; too little pressure allows the part to bow due to the grinding force while too much will induce bow in the part and create taper. Similar taper problems can be created by incorrect setup of the steady rests. Identification of the root cause is usually achieved by evaluating the change in taper from one lobe to the next.

Camshafts can have up to 16 lobes or more with several in the same rotational phase. This offers the opportunity to grind two lobes at the same time. This concept has been taken further by building

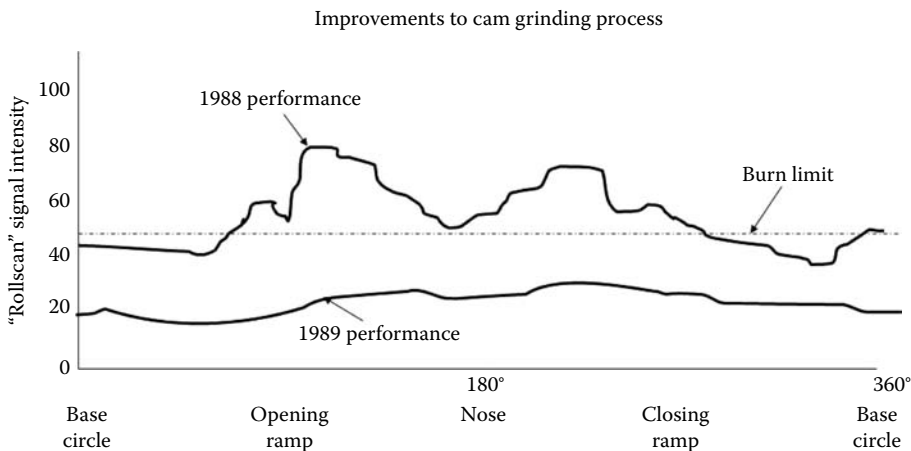
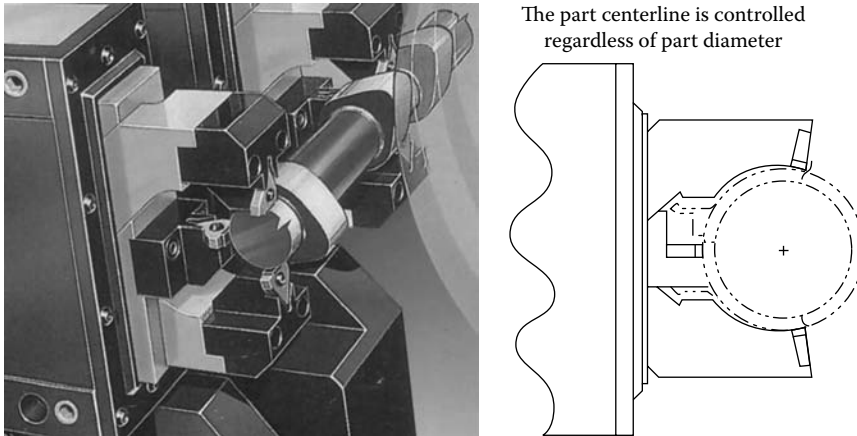


FIGURE 17.27 Rollscan multisensor system and readings.



**FIGURE 17.28** Aerobotech Self-Centering Steady Rest System for camshaft grinding. (From Aerobotech 1996, Anon. 1998b. With permission.)

twin wheel head machines with two independently moving wheel slides. This allows two twin wheel sets with different spacings between the abrasive sections to be used for added flexibility. Up to four lobes with two different spacings can be ground simultaneously (Figure 17.30) [Landis 1996].

Re-entry profiles for most engines for the U.S. market can be ground using wheels of >300 mm. However, smaller engines, especially for the European market, use smaller cams with, therefore, smaller re-entry radii. These have necessitated wheels as small as 50 mm.

For this type of application, an alternative approach has been required: to rough the camlobe using a large plated CBN wheel and to finish and generate the re-entry profile using a small vitrified CBN wheel. The process is carried out in oil coolant to achieve the economics using plated CBN. The wheel speed for the vitrified wheel is limited due to size to <100 m/s. The smaller wheel spindle is on either a vertical slide [Pflager 2002] or a swing-down arm [Schaudt n.d.] to prevent interference with the larger wheel.

These machine configurations created two additional benefits. The first was that since the small wheel was finishing only, it could be specified to produce a lower surface finish than a wheel required to rough and to finish grind. In some circumstances, this allowed the elimination of polishing—a postgrind process using conventional abrasive film and as expensive in terms of consumables as the grinding process itself.

The second benefit related to grinding diesel camshafts. Gasoline camshafts have intake and exhaust lobes; a diesel camshaft has an additional injector lobe, which is typically a different width to the other two types. Diesel camlobes also have extremely stringent straightness specification of <1.25  $\mu\text{m}$ , which is comparable to the break-in depth of a vitrified CBN wheel. When trying to grind all three lobes with one wheel, a step is rapidly formed and the process becomes uneconomic. However, a twin wheel machine with the small auxiliary spindle configured with two vitrified CBN wheels can contend with the different widths.

## 17.4 PUNCH GRINDING

A related, but somewhat simpler, process to camshaft grinding is the grinding of punches for the die and pharmaceutical industries. Profiles for punches are simple radii and straight faces and machine controls are set up with canned programs to generate a given shape with the operator entering a few basic dimensions. Batch sizes are relatively small so flexibility and rapid change over times are critical. Parts are held by the shank in a simple 3- or 4-jaw chuck. Computational

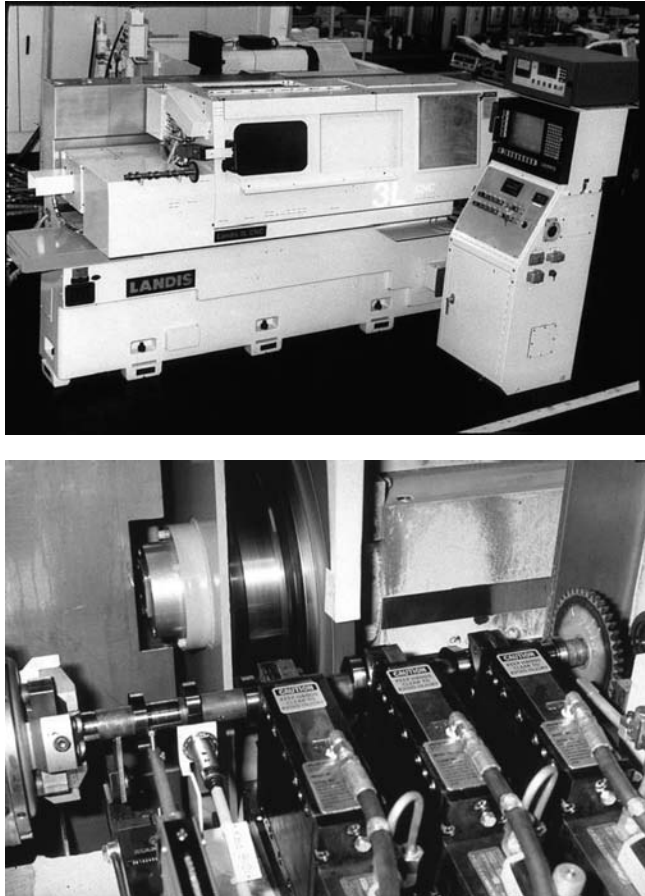


**FIGURE 17.29** Landis 3L CNC single-wheel CBN camlobe grinder.

demands and work speeds, while still demanding, are lower than in camlobe grinders as is the cost of the machine. OEMs include ANCA, Studer, and Weldon.

Most punches are made of tool steel making CBN particularly attractive where punch designs allow a constant wheel corner radius for the blend at the holder end. Cycle times are reduced by 30% [Kampf 2000] or greater over conventional abrasives using wheel speeds of 60 to 80 m/s in water-based coolant.

The problem areas for punch grinding are in holding sharp corners on square punches and holding taper values of 1 to 2  $\mu\text{m}$  parallel and orthogonal to the punch axis as the result of wheel and coolant hydrodynamic pressure. Some errors in profile can be programmed out if they are consistent; others may require prolonged spark-out times if using alox wheels. For CBN wheels, however, the coolant can be switched off almost entirely during spark-out to relieve hydrodynamic effects. The technique is called “trickle” or “dribble” grinding and is even more pertinent to crank pin grinding.

There is also a different strategy required for how stock is removed compared to camlobe grinding. Punches are ordered in very small batches with a requirement to ship within 24 hr. Consequently, the rough stock coming to the grinder usually consists of a basic round, through-hardened billet to limit inventory and maximize flexibility. This can result in up to 30 mm of stock removal on larger parts. An optimized spiral wheel path to the final size is, therefore, key to cycle time reduction (Figure 17.34).

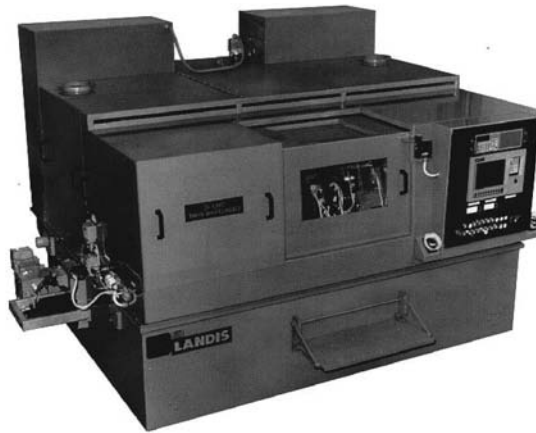
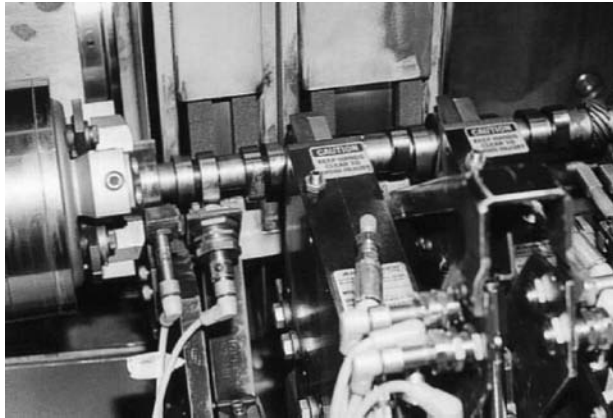


FIGURE 17.30 Landis twin-wheel head camlobe grinder.

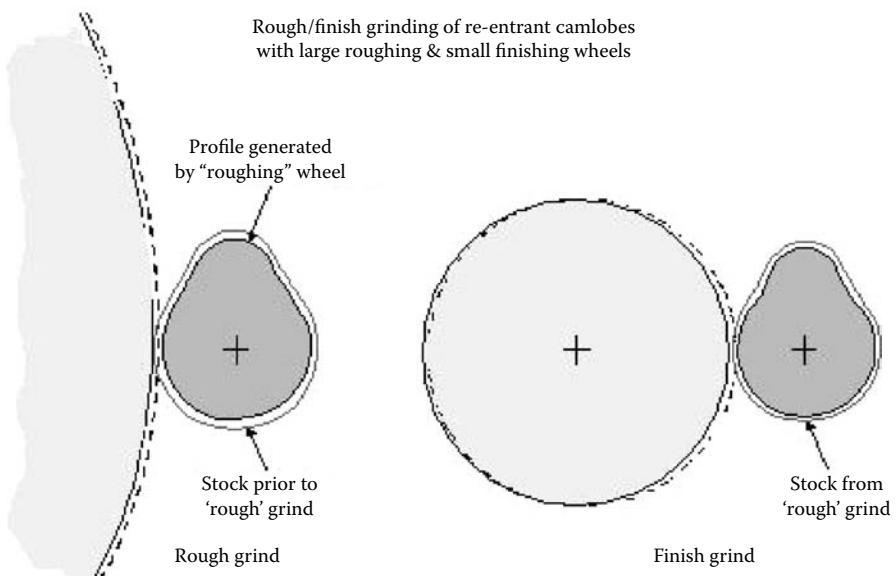
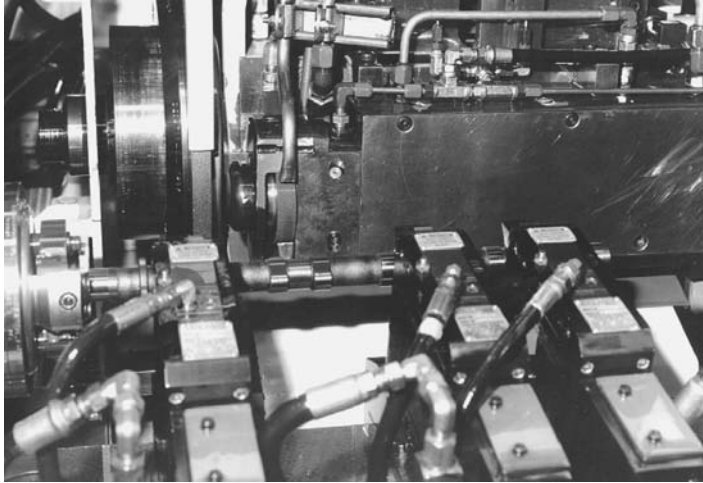


FIGURE 17.31 Large and small grinding wheels compared for re-entrant camlobe.





**FIGURE 17.32** Landis twin wheel camlobe grinder for roughing and finishing re-entry cam profiles. (From Pflager 2002. With permission.)

## 17.5 CRANKSHAFT GRINDING

Whereas camshaft lobe grinding faces difficulties associated with cylindrical grinding, a nonround part at least, all lobes of the component are configured on a common centerline. Finish grinding of crankshaft pins may appear to be a simpler round grind operation but each pin is on a different centerline governed by the “throw” of the crank.

Additionally, the crankshaft is very weak and, hence, easily distorted if overclamped, is unbalanced at grind, and prone to “unwind” if the heat-treat is not carefully controlled. Consequently the first step in designing a grind process for a crankshaft is an FEA analysis of the clamping forces and foot-stock clamping pressures and a subsequent determination of steady or workrest requirements (Figure 17.38) [Pflager 2002].

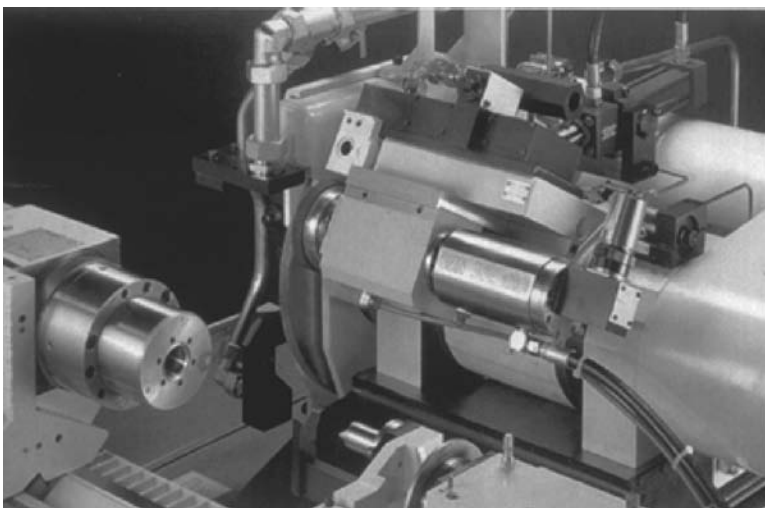


**FIGURE 17.33** Schaudt CF41 CBN twin wheel camlobe grinder for roughing and finishing camlobes with re-entry profiles.

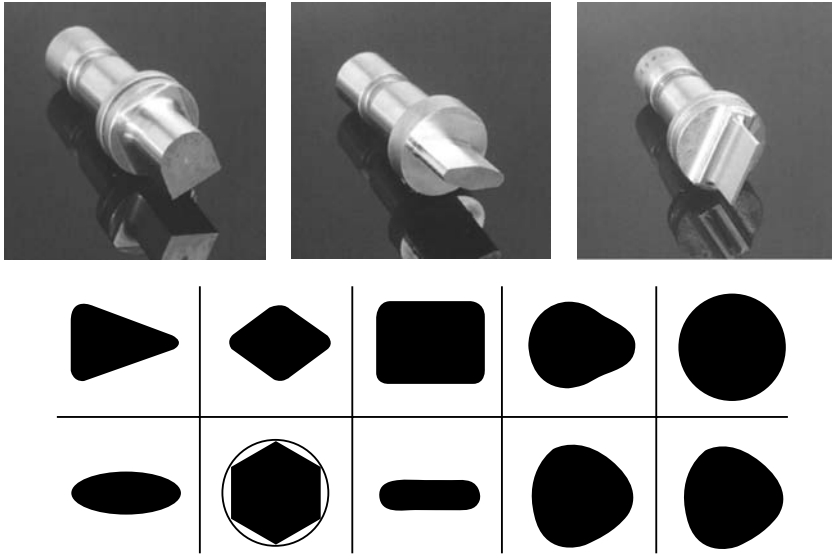


**FIGURE 17.34** Punch profiles. (From Studer 2001. With permission.)

Cranks are made of either nodular iron in the 150 to 250 BHN range for automotive engines or steel surfaces heat treated in the 25 to 40 Hrc range for higher power and diesel applications. Most automotive crank pins are first turn-broached to relieve the sidewalls and leave an undercut at each edge. This undercut is then fillet-rolled, resulting in a finish flat grind with about 1-mm stock performed using vitrified CBN abrasive. For diesel cranks, there is no undercut for fear of generating stress risers and the pin, edge radii, and side walls are all ground. Wheels must be dressed to the exact width and profile. Most of the stock now occurs on plunging the depth of the sidewalls and can be up to 15 mm (Figure 17.39). Special sandwich wheels with split grades are used primarily

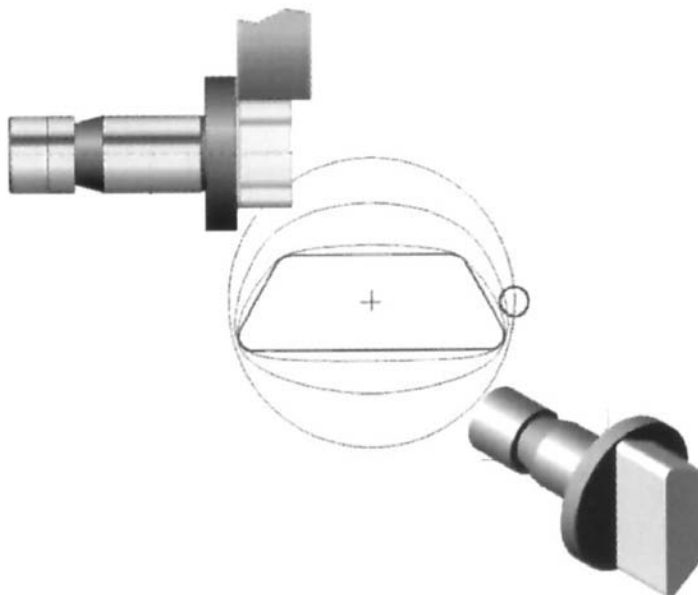


**FIGURE 17.35** Punch grinding strategy. (From Studer 2001. With permission.)

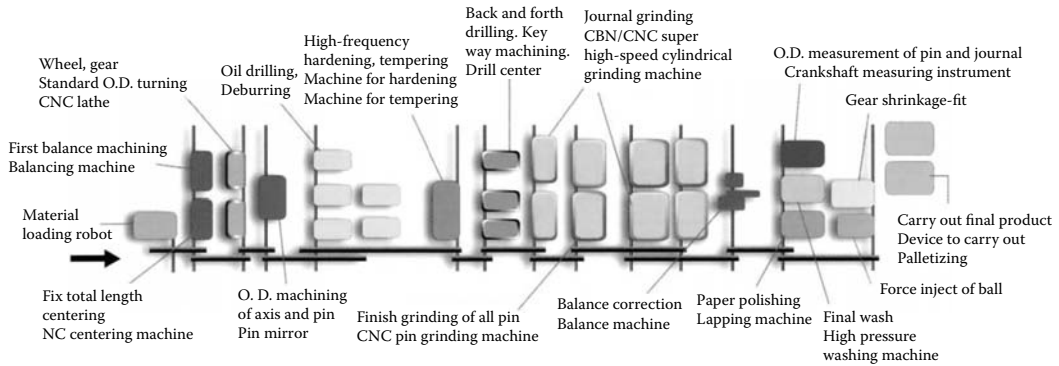


**FIGURE 17.36** Flow chart for a modern automotive crankshaft manufacturing line. (From UMS 2002. With permission.)

with alox/seeded gel combinations although some vitrified CBN applications have been developed recently.

There are several machine design strategies for approaching the issue of grinding each individual pin on its centerline. The traditional method is to use a mechanical chuck to index each pin in turn onto its axis of rotation, and use automatic throw changers to compensate from one crank type to another. The chucks and indexing fixtures are complex, product-specific, and, being mechanical, potentially unreliable. The method loses a significant amount of cycle time for each indexing movement. An alternative approach developed in the early 1990s by Landis for high production, >200,000 cranks/annum, was to use simplified chucking on grinders dedicated to one specific pin [Anon. 1994]. The grinders were set up similar to a transfer line with a load/unload system that moved the crank from one single-pin grinder to the next until all the pins were ground. This reduced cycle time but at the risk that if a grinder had operational problems or required a wheel change then production was lost from all the grinders in the line. Fortunately, the reliability of modern grinder is such that, with proper preventative maintenance, down time from mechanical problems is minimal while CBN technology has pushed wheel life to as great as 3 years.

The introduction of vitrified CBN to crankpin grinding in the late 1980s allowed machine tool builders to completely rethink how crankpins should be ground. The ideal way to grind the crankpins would be with the crankshaft being rotated on the same axis as seen by the engine. This requires the wheel to be moved by the throw amount using a CNC control akin to a camlobe grinder. Such a concept was impossible trying to hold micron-size tolerances over throw lengths of the order of 100 mm with conventional wheels that varied in diameter during their life by 25% and wore microns/pin. However, it became practical with CBN wheels that varied in diameter by only 1% and wore nm/pin.

The process has been termed “CNC contour grinding” [Toenshoff and Falkenberg 1996], “pin chasing” by Naxos Union Emag (2002), or “CNC orbital pin grinding” [Anon. 1998a].

CNC contour grinding offers significant benefits in terms of flexibility, reduced tooling costs; for example, steady rest needs, elimination of complex work chucks, and a smaller machine footprint. Its greatest benefit, however, may be increased quality especially with regards to pin roundness. The standard automotive crankpin tolerance on roundness has historically been 5  $\mu\text{m}$ , but with more stringent 2CpK capability requirements this has now reduced to 2.5  $\mu\text{m}$ . The major source of out-of-roundness in most crankpin grinding operations is created by the presence of oil lubrication holes drilled into surface of the pins. These can be clearly seen in Figure 17.37. These

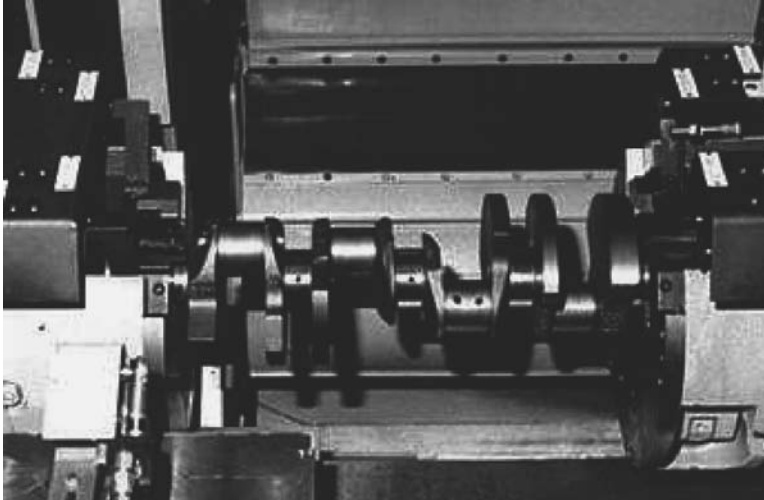


**FIGURE 17.37** Typical crank shaft showing oil lubrication holes in the pins.

holes reduce the wheel/workpiece pressure not only by physically reducing the contact length, but, more importantly, by reducing the hydrodynamic coolant pressure. Depending on the stiffness of the crank, wheel speeds are typically limited to  $\leq 80$  m/s and finish grinding is carried out in “trickle” grind mode to reduce the out-of-roundness down to the order of  $2 \mu\text{m}$ . With traditional grinding methods, this still consumes almost the entire available part tolerance and creates a very discrete and obvious dip in the roundness profile. CNC contour grinding with programmable crankpin angular position capability allows this  $2 \mu\text{m}$  to be compensated for thereby improving overall roundness by 50%.

The drive for increased quality in crankpin grinding has, therefore, led to commonality in machine tool design with camlobe grinding to the point that machine tool builders are now offering a common machine for both applications and with the flexibility to grind mains, too. For example,

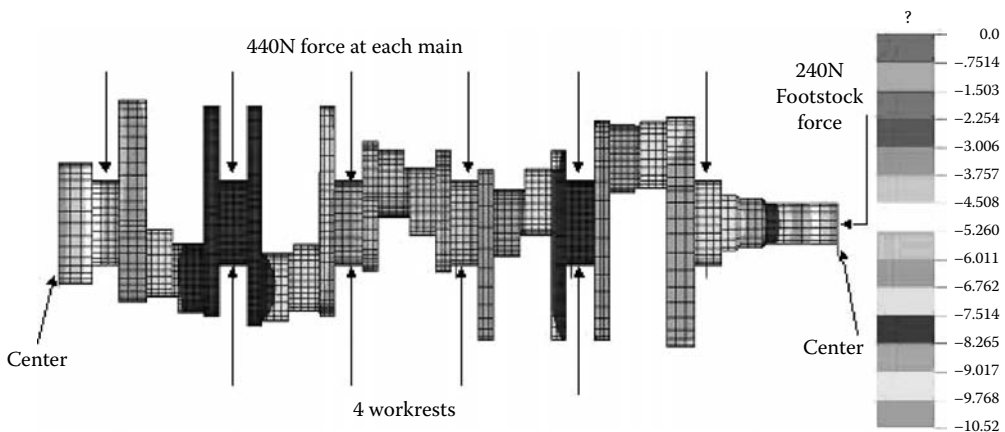


**FIGURE 17.38** FEA analysis of the effect forces on the crankshaft during grinding.

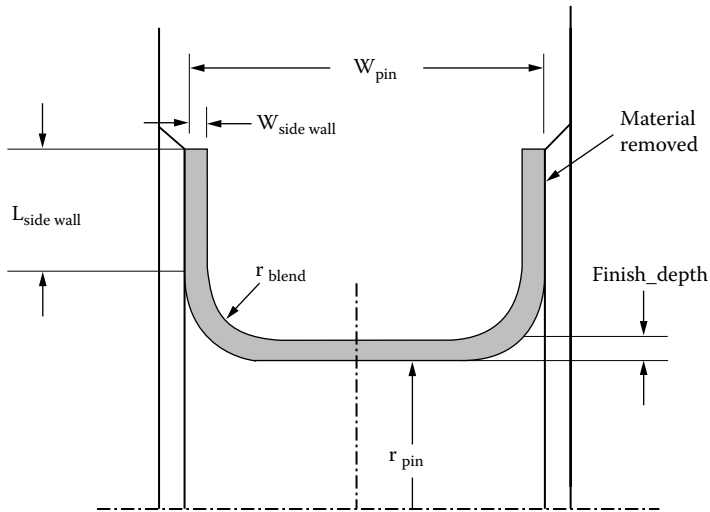


**FIGURE 17.39** Stock removal in diesel crankpin grinding. (From Corallo, Gridley, and Medici 1993. With permission.)

the Landis 3L twin wheelhead nonindexing grinder illustrated in Figure 17.30 can be configured to grind camlobes and/or mains *or* crankpins and/or mains.

Interestingly, the grind process for a dual wheel pin grinder is much more complicated. For a constant workspeed, the instantaneous stock removal rate will vary from a maximum given by  $(\text{rpm}/60) \cdot (\text{stroke} + \text{pin radius}) \cdot \text{infeed}/\text{rev}$  to a minimum given by  $(\text{rpm}/60) \cdot \pi \cdot (\text{stroke} - \text{pin radius}) \cdot \text{infeed}/\text{rev}$ . For a single wheel orbital pin grinder, it is possible to vary the instantaneous workspeed just like in camlobe grinding to even out the removal rate. When dual wheel pin grinding the problem is all the pins are out of phase with each other. This makes optimization of the workspeed more complicated. For a dual wheel arrangement it is also necessary to ensure the two wheel speeds are shifted by 1 to 2% to avoid regenerative chatter.

The most recent developments in crankpin grinding has been to marry together the CNC contour technology with modern plated CBN technology by increasing spindle motor power up to 80 kW and wheel speed up to 160 m/s. In conjunction with increased acceptance of oil coolant from improvements in its handling and containment, rough or “green” grinding has been gaining acceptance as a replacement to turn broaching. Laycock [1996] reported the following maximum stock removal rates for plated CBN wheels rough grinding cam and crank materials in oil:

Soft cast iron	360 mm <sup>3</sup> /mm/s
Soft steel	250 mm <sup>3</sup> /mm/s
Hard steel	200 mm <sup>3</sup> /mm/s

Pflager [2000] confirmed a more general value of >150 mm<sup>3</sup>/mm/s that is over 300% greater than hard turning and 50% greater than soft milling. Giese [1999] reported a plated CBN wheel life grinding pins including the undercuts of 40,000 to 60,000 crankshafts at comparable cycle times to turn broaching. Green grinding eliminated the need for the frequent replacement of carbide cutting tool inserts. Plated CBN has actually proved cost-effective grinding at half the cycle time of turn broaching. Since the machine tool’s cost for a high-speed grinder is comparable or less than the cost of a turn broach [Anon. 2000], green grinding offers significant capital equipment cost savings.

As speed and stock removal rates increase, limitations occur in the maximum power available for grinding. As discussed above, a narrow wheel reduces coolant drag losses making more power available to grind at higher  $Q'$  values and, hence, additional removal rate capability as a result of the lower  $e_c$  values associated with this. Several researchers and OEMs [TMW 1998, Toenshoff et al. 2002] have, therefore, proposed grinding pins and mains in multiple plunges to increase overall stock removal rates and increase flexibility to grind mains and pins of different widths.

## 17.6 ROLL GRINDING

The roll grinding market covers an incredibly broad range of applications from rolls for business machines of just an inch or less in diameter to rolls for the steel industry that can weigh up to 50 tonnes. Workpiece materials include rubber, aluminum, steel, cast iron, ceramics, granite, and exotic metals and polymers. Often finish requirements must be held in a tight band of values, and surface integrity and cosmetic appearance, the elimination of feed lines, are paramount.

The largest areas of use, certainly in abrasive consumption, are the steel and paper industries. Rolls for the steel industry are made of either forged steel (48 to 52 Hrc) or chilled cast iron. Finish specifications and tolerances are driven by whether the rolls are used in hot strip mills or cold strip mills, with the demands for cold strip mills being considerably tighter as they impart the final finish on the rolled steel:

**Hot strip:** 0.002" shape deviation, 0.0020" roundness,  $\leq 40 \mu$ " Ra finish  
**Cold strip:** 0.0005" shape deviation, 0.0002" roundness,  $\leq 10 \mu$ " Ra finish

A typical wheel for a steel roll hot strip application would be 900 mm  $\times$  75 mm and would last about 100 hr grinding 100 to 150 rolls. Typical roll size (50 ton): 750 mm diameter  $\times$  1,800 mm long with 0.25 mm stock on diameter. Most wheels are either conventional resin or occasionally vitrified bonded.

Grinding wheel selection for cold strip rolls is governed by the need to eliminate regenerative chatter. Consequently, very compliant bonds are used such as shellac, resin, epoxy, and even cork abrasive.

Rolls for the paper industry are made from cast iron or chrome steel for general smoothing and calendaring while for some specialty applications, especially for fine paper production, granite and polymer granite are used. Rolls can be up to 1 m in diameter and 12 m long. The shear weight of these in operation creates a sag or bow in the center of the roll that can be a significant proportion of the paper thickness to be smoothed. Consequently, an inverse profile to compensate must be ground in the roll. Surface finish requirements are  $\leq 0.4$  Ra after roughing and  $\leq 0.1$  Ra after finishing.

Most modern machine tools can maintain 1.25  $\mu$ m taper, flatness, and profile on rolls up to 300 tons. Leading OEMs include Waldrich Seigen, Herkules, Pomini, Toshiba, Capco, and Schaudt. Other machines common in the industry include Voith, Farrel, Churchill, Craven, Naxos Union, MSO, and INNSE. Small machines maintain the standard moving carriage design of a typical general-purpose cylindrical grinder, but the large machines for the steel and paper industries have a moving wheel head where the operator moves with the wheel while controlling the process.

A roll grinder consists of up to three independent slides on a massive casting. The whole machine is mounted on a massive isolation pad as in the example in Figure 17.40 of a Pomini machine.

The machine requires an extensive laser alignment upon installation or repositioning to the required accuracy while great care is taken in the design to minimize the effects of thermal movements. Residual repeatable slide errors can be compensated for in modern CNC controls.

The rear axis carries the wheelhead and its primary axes of motion X and Z. All slides are hydrostatic as, in general, is the wheel spindle. Grinders are also equipped with Y and  $U'$  tilt axes

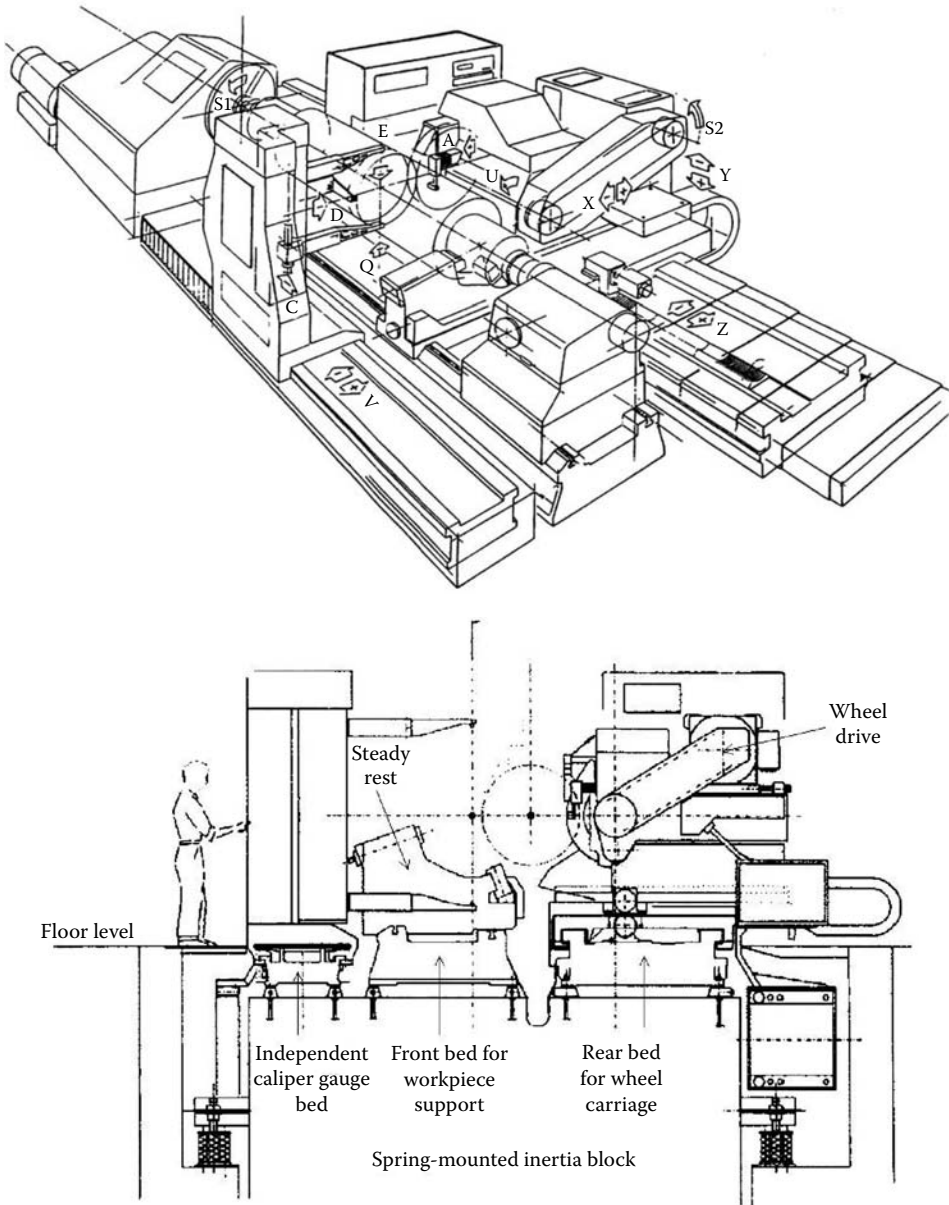


**FIGURE 17.40** Pomini roll grinder general view and cross section. (From Oppenheimer and Grindley 1989. With permission.)

for microswiveling the wheel head. These are required to maintain a normal position against the part when grinding crown profiles in order to minimize feed lines.

All machines are equipped with at least a load monitor for the wheel spindle. On older machines, the operator will constantly infeed the wheel to keep the load constant. On modern CNC machines, the control will either infeed after every stroke or, more typically, at a continuous preset rate during the grind, or adaptively under constant load. This is to compensate for the very significant breakdown of the wheel.

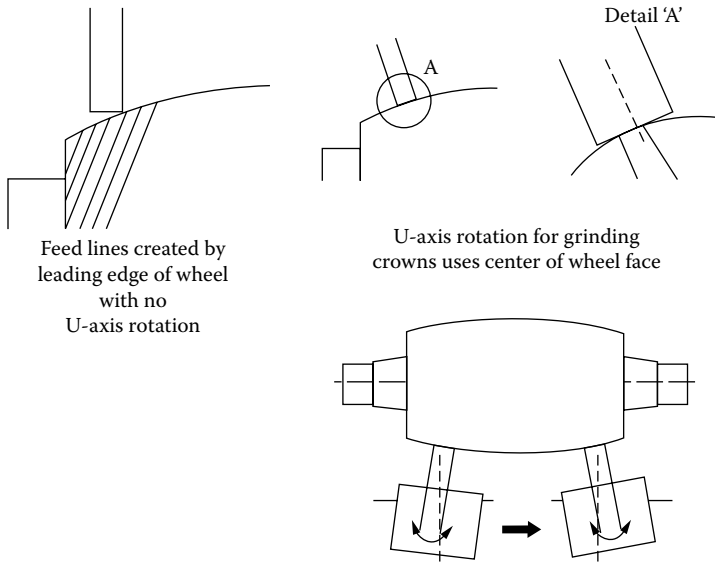


FIGURE 17.41 Roll-grinding using a U-axis wheelhead rotation to generate crown and eliminate feedlines.

The control will also carry out short stroke grinds at certain positions in order to remove excess stock on a new roll or when changing crown (Figure 17.42). All the while the CNC is able to generate a taper, crown, or compound curve shape while compensating for bed error (Waldrich Siegen 1996).

The front or center bed carries the work head drive and tail stock. Being separate and rigid, it allows the isolation of any effect of loading a heavy workpiece. Usually at least one axis of adjustment is available for initial roll alignment and taper correction.

The third carriage carries the gauging equipment — a two-point dimensional measuring caliper with optional Rollscan, eddy current, and finish measuring attachments. A longitudinal V-axis moves the caliper independently of the wheel slide. If a separate carriage is not present, the gauging system rides on the rear carriage with the wheel head.

Older grinders without automatic gauging relied on the operator stopping the grind operation to measure the roll using manual calipers, and then feeding with higher load in those areas with higher stock—a process based on art and experience. Automatic gauging with roundness and shape fed directly into the CNC can now continuously measure and compensate.

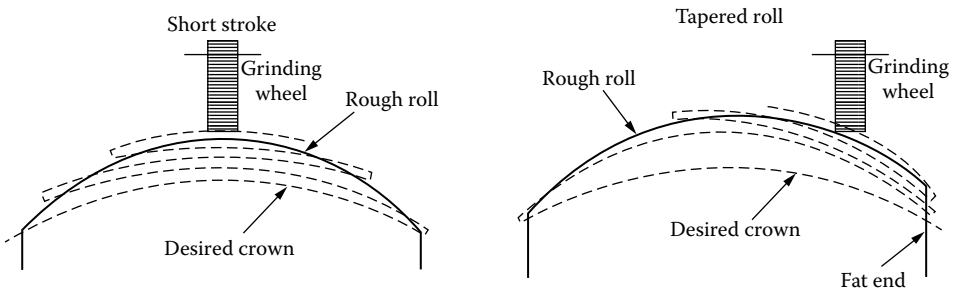


FIGURE 17.42 Short stroke grinding strategies for crown shaping. (From Ehlers 1991. With permission.)



## REFERENCES

- Aerobotech. n.d. Aerobotech Systems, Inc., Madison Heights, MI.
- Andrew, C., Howes, T.D., Pearce, T.R.A. 1985. "Creep Feed Grinding." Holt, Rinehart and Winston Ltd., Eastbourne, U.K.
- Anon. 1994. "Single-Workhead Grinding System for Automotive Crankshafts." Manual. Feb.
- Anon. 1998a. "Single Orbital Crankpin Grinder Replaces Six Dedicated Machines." Manual. Sept.
- Anon. 1998b. "Steady Rest Technology Hold Form in Parts." *Tooling & Production*. June.
- Anon. 2000. "Dagenham Takes a New Turn." *Mach. Prod. Eng.* 7 July.
- Brinksmeier, E. and Minke, E. 1993. "High Performance Surface Grinding—The Influence of Coolant on the Abrasive Process." *Ann. CIRP* 42, 1, 367–370.
- Corallo, V., Gridley, T., and Medici, M. 1993. "Regrinding Rolls for Modern Day Requirements for Size, Shape, Dimension and Finish." 34th MWSP Conference Proceedings ISS-ASME. Vol. 30.
- Ehlers, J. 1991. "Applications of Computer Controls and Display to Roll Grinders." CH2973-6/91/0000. IEEE.
- Fix, R. M., Tiitto, K., and Tiitto, S. 1990. "Automated Control of Camshaft Grinding Process by Barkhausen Noise." *Mater. Evaluation*. 48, 904–908.
- Giese, T. L. 1999. "Grinding It Green." *Tooling & Production*. Dec.
- Hanard, M. R. 1985. "Production Grinding of Cam Lobes with CBN." SME Conference Proceedings, Superabrasives '85.
- Hitchiner, M. P. 1991. "Systems Approach to Production Grinding with Vitrified CBN." 1991 SME Conference Proceedings, Superabrasives '91. MR91-148.
- Junker. 1992. "Junker Quickpoint CNC o.d. Grinding with CBN or Diamond. A New Era in the Field of o.d. Grinding. Erwin Junker Maschinenfabrik GmbH, Nordrach, Germany. Trade brochure.
- Junker. 1993. "Automotive Components Being Ground in High Speed by CBN Grinding Wheels." Erwin Junker Maschinenfabrik GmbH, Nordrach, Germany. Trade brochures.
- Kampf, E. 2000. "Grinding of Form Punches with CBN." *Swiss Qual. Prod.* July.
- Koenig, W., Klocke, F., and Stuff, D. 1997. "High Speed Grinding with CBN Grinding Wheels — Boundary Conditions, Applications and Prospects of a Future-Orientated Technology." 1st French and German Conference on High Speed Machining.
- Koenig, H. C. and Treffert, C., n.d. "High Speed Grinding of Any Contour Using CBN Grinding Wheels." Laboratorium fur Werkzeugmaschinen und Betriebslehre. RWTH, Aachen.
- Landis. 1996. "Landis Windows Based Automatic Workspeed Generation System." Waynesboro, PA. Trade brochure.
- Laycock, M. 1996. "Recent Developments in Camshaft and Crankshaft Grinding." IGT Annual Seminar Bristol, UK.
- Lutjens, P. and Mushardt, H. 2000. "Hard Turning or Grinding." *Eur. Prod. Eng.* July.
- Malkin, S. 1989. *Grinding Technology*. Ellis Horwood, New York.
- Marinescu, I. D., Rowe, W. B., Dimitrov, B., and Inasaki, I. 2004. *Tribology of Abrasive Machining Processes*. William Andrew Publishing, Norwich, NY.
- Naxos Union Emag. 2002. "CBN Kurbelwellen-Schleifmaschinen." Naxos Union GmbH, Fechenheim, Germany. Trade brochure.
- Okuma. n.d. "GP-24N CNC Plain Cylindrical Grinder, GA-24N CNC Angle-Head Cylindrical Grinder." Okuma Machinery Works, Aichi, Japan. Trade brochure.
- Oppenheimer, J. G. and Gridley, T. H., Jr. 1989. "Automatic Roll Grinding in the Nineties." Proceedings of the Aluminum Association. International Aluminum Sheet & Plate Conference. Nashville, TN.
- Ota, M., Ueda, H., and Maeda, M. 1997. "A Cam Grinding Machine Using an Ultra-High Speed and High Power Grinding Wheel Spindle." 1st French & German High Speed Machining Conference.
- Pflager, W. 2000. "High Speed Cam Grinding." IMTS 2000 Manufacturing Conference. SME. Chicago, IL.
- Pflager, W. 2002. "High Speed Grinding in a Mass Production Environment." IMTS 2002 Manufacturing Conference. SME. Chicago, IL.
- Renaud, W. and Hitchiner, M. P. 1991. "The Development of Camshaft Lobe Grinding with Vitrified CBN." SME Conference Proceedings, Superabrasives '91. MR95-163.
- Rowe, W. B. and Jin, T. J. 2001. "Temperatures in High Efficiency Deep Grinding." *Ann. CIRP* 50, 1, 205–208.
- Rowe, W. B., Bell, B., and Brough, D. 1986. "Optimization Studies in High Removal-Rate Centreless Grinding." *Ann. CIRP* 35, 1, 235–238.

- Rowe, W. B., Morgan, M. N., Black, S. C. E., and Mills, B. 1996. "A Simplified Approach to Control of Thermal Damage in Grinding." *Ann. CIRP* 45, 1, 299–302.
- Schaudt. n.d. "CF41 CBN Nockenform-Schleifmaschine" Schaudt Maschinenbau GmbH Stuttgart, Germany. Trade brochure.
- Schultz, A. 1999. "Precision Grinding of Transmission Components Using Modern Grit Materials." Precision Grinding and Grinding with Superabrasives Conference. Gorham Adv. Materials. Chicago, IL.
- Shaw, M. C. 1996. *Principles of Abrasive Processing*. Oxford University Press, U.K.
- Shigiya. 1996. "CNC Cylindrical Grinders GPS-30." Shigiya Machinery Works, Hiroshima, Japan. Trade brochure.
- Studer. 2001. "Motion." Schleifring. August. Trade brochure.
- Suzuki. 1984. "Development of Camshafts and Crankshafts Grinding Technology Using Vitrified CBN Wheels." SME. MR84-526.
- Tawakoli, T. 1993. *High Efficiency Deep Grinding*. Mech. Eng. Publications Ltd., London.
- TMW. 1998. "GL 63M GL 100M." In Japanese. Toyota Machine Works. Aichi, Japan. Trade brochure.
- Toenshoff, H. K. and Falkenberg, Y. 1996. "High-Speed Grinding of Cast Iron Crankshafts with CBN Tools." *IDR* 4, 115–119.
- Toenshoff, H. K., Friemuth, T., and Becker, J. C., 2001. "Next Generation of Crankshaft Production." *Ann. CIRP*.
- Tsujichi, M. 1988. "CNC Camshaft Grinder with Small Diameter CBN Wheel." SME Conference Proceedings of the 3rd International Grinding Conference. Fontana, WI. MR88-609.
- UGT. 2000. "Dana's Long Camshafts Are No Challenge for Schaudt Grinders." *Grind. J.* Summer, 10–11. Miamisburg, OH. Trade brochure.
- UMS. 2002. "United Manufacturing Solutions." UMS Ltd., Nagoya, Japan. Trade brochure.
- Wakuda, M., Ota, M., Ueda, H., and Miyahara, K. 1998. "Development of Ultrahigh Speed and High Power Cam Grinding Machine 1st report — Characteristics of Ultrahigh Speed Grinding of Chilled Casting." *B JSPE* 64, 4, 593–597.
- Waldrich Siegen. 1996. "Worldwide Partners for Intelligent Manufacturing Solutions." Waldrich Siegen. Werkzeugmaschinen, Burbach, Germany. Trade manual.
- Wedeniowski, H. J. 1989. "CBN-Nockenschleifen bei Hochgeschwindigkeit produktiver und ohne Rissbildung." *Werkstoff und Betrieb*. 122, 9, 796–800.
- Werner, G. 1983. "Realisierung niedriger Werkstückoberflächen temperaturen durch den Einsatz des Tief-schleifens." *Trens-Kompodium*. 2, 448–468.
- Woodside, J. 1988. "High-Speed Grinding Proved in Production." *Tooling & Production*. May.



---

# 18 Internal Grinding

## 18.1 INTRODUCTION

Internal grinding is the primary process for the precision finishing of internal surfaces or bores. The bores may be simple cylindrical surfaces or may be surfaces requiring the generation of complex and exact profiles for applications such as bearing and CV joint races or fuel injection seats. Figure 18.1 shows a typical vitrified CBN grinding wheel for internal grinding together with the rotary tool used for dressing.

Most precision internal grinding operations require the capability to hold tolerances on size, roundness, straightness, taper, and cylindricity of the order of 0.5 to 10  $\mu\text{m}$ , but for special applications such as fuel injection the tolerances have become increasingly stringent in recent years to as tight as 0.25  $\mu\text{m}$  or even lower. The majority of the highest volume applications are found in the bearing and automotive industries grinding hardened steel (carbon, alloy, PM, and M50) with relatively small wheels under 100 mm on horizontal spindle grinders with finish requirements under 0.5 Ra. There are also larger diameter applications in specialty bearing and aerospace engine assembly grinding bores up to 1,000 mm more. The largest such parts are usually ground on specialist vertical spindle machines.

Grinding still dominates bore finishing for all the tightest precision tolerance work because of stock-removal capability, accuracy, and cost. However, hard turning is making inroads for finishing larger bores with tolerances  $>2.5 \mu\text{m}$ . It is also becoming more common to see multi-purpose machining centers for applications such as automotive gears that rough turn the bore, rough and finish turn the gear flanges, but then finish grind the bore in the same chucking when tighter accuracy demands. Diamond honing is also gaining favor and is reported to hold good straightness but stock-removal rates are still limited. To be cost effective stock removal must be kept to under 10  $\mu\text{m}$ .

Modern CNC internal grinders provide a great deal of flexibility not only to plunge grind simple bores but also to face grind, profile grind, and even contour grind outer diameters. Multislid machines may even simultaneously grind inner and outer diameters and flanges using two wheels (Figure 18.2 and Figure 18.3).

## 18.2 THE INTERNAL GRINDING PROCESS

In the basic internal grinding process, the wheel is fed perpendicularly into the part usually accompanied by a short-stroke high oscillation along the axis of the wheel. The part is rotated in the opposite direction to the wheel (down grind) in virtually all applications except occasionally in finish grinding with large interrupted cuts if roundness is an issue. The basic internal grinding process is illustrated in Figure 18.4.

Internal grinding is a very weak system where the primary weakness is the wheel mount or quill. This can readily deflect during the grind leading to problems of taper and shape. The grinding conditions are driven first and foremost by the system stiffness and the level of normal grinding force. The key factors to consider are shown here.

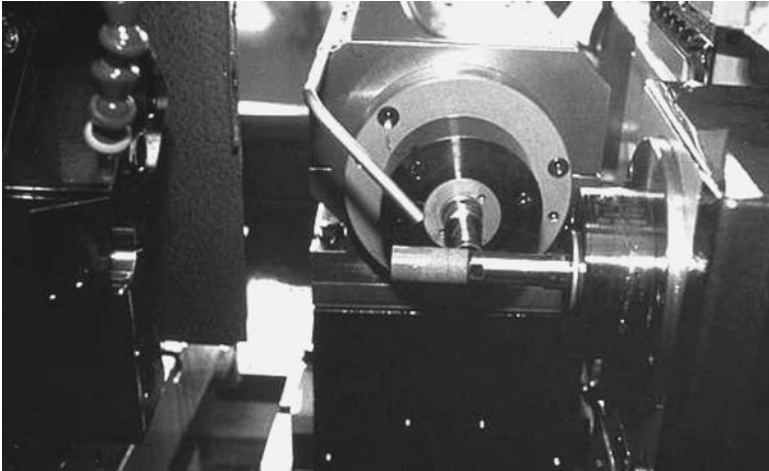


**FIGURE 18.1** Internal grinding machine set up for power steering pump rings showing a vitrified CBN wheel in the dress position.

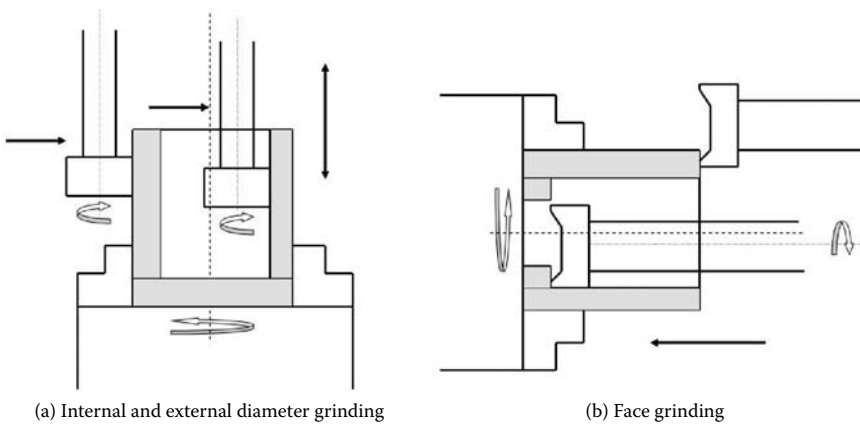


**FIGURE 18.2** Diameter grinding and face grinding operations on an internal grinding machine. (a) Internal and external diameter grinding. (b) Face grinding.

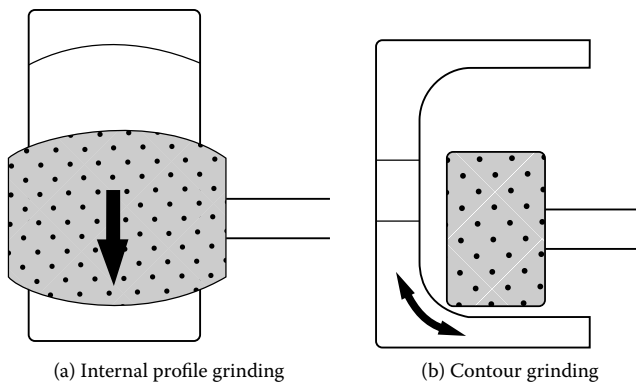


**FIGURE 18.3** Profile grinding and contour grinding operations on an internal grinding machine. (a) Internal profile grinding. (b) Contour grinding.

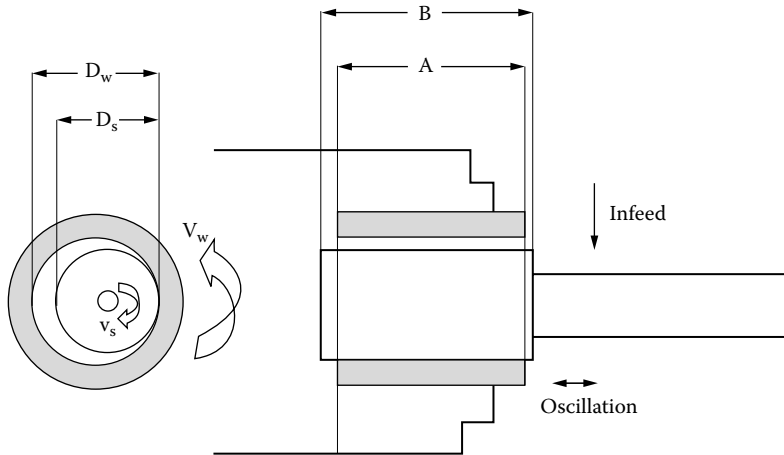


FIGURE 18.4 The basic internal grinding process.

## 18.3 ABRASIVE TYPE

### 18.3.1 GRAIN SELECTION

The first and most important decision in recent years is the choice of whether to use conventional, ceramic, or cubic boron nitride (CBN) abrasive. This will depend on the condition of the machine, dressing capability, and part size. In general, high volume, hardened-steel parts under 15 mm with straight bores, for example, tappet rollers, lifter bodies, fuel injector bores, and small bearings, especially M50 steel aerospace, are usually most cost effective with CBN even on older machines. Between 15 mm and about 50 mm, CBN is becoming more and more common on new equipment. AloX- and SG-based wheels dominate over 50 mm. There are several reasons for this. The first is purely the abrasive cost in the wheel. Small-wheel manufacture carries a high percentage of labor in its cost regardless of abrasive type. For CBN, as the wheel size increases, the cost of abrasive soon dominates and wheel cost becomes proportional to size. With aloX grain, it being much less expensive, the overall manufacturing cost does not increase as rapidly with diameter.

The second issue governing abrasive selection concerns normal force and its relationship to wheel/part conformance characterized by equivalent wheel diameter  $d_e$ , where

$$d_e = \frac{d_w \cdot d_s}{d_w - d_s}$$

The larger the equivalent wheel diameter, the greater the contact length and, hence, the higher the normal force. As  $d_w$  increases, the ratio  $d_w/d_s$  must be reduced to reduce  $d_e$ . Also the grinding pressure must be reduced further by increasing the structure and grit size in the wheel specification. This also improves chip clearance and coolant access. Unfortunately, the range of grit sizes and bond structures available in vitrified CBN systems, which will still allow the necessary high G-ratios to be maintained, is more limited than those for aloX or ceramic wheels. Consequently,  $d_e$  for a CBN wheel is limited to about 150 mm over which the process is compromised either by abrasive cost or cycle time. This will vary by material type: for very difficult to grind materials such as M50 or tool steels, the maximum  $d_e$  value for CBN would be much higher due to gains in productivity by the elimination of dressing, while for simple AISI 52100 plain bearings the maximum  $d_e$  could be nearer 100 mm. Some typical examples of bond specifications for vitrified

**TABLE 18.1**  
**Recommendations for Vitrified CBN Internal Wheels**

$d_s$ (mm)	$d_s/d_w$	$d_e$ (mm)	$Q'$ (mm <sup>3</sup> /mm/s)	Ra ( $\mu$ m)	Specification	Application
5	0.9	50	<1	<0.15	B46 H200 VSS	Fuel injection
10	0.9	90	3	<0.25	B64 I200 VSS	Valve lifters
20	0.85	130	5	<0.40	B91 K200 VSS	UJ cups
30	0.8	150	5	<0.50	B91 K150 VSS	Pumps
50	0.7	165	5	<0.50	B126 K150 VSS	Gear bores
250	0.25	350	3	<0.80	B181 F200 VSS	Aero shrouds

CBN wheels grinding hardened steels are given in Table 18.1. The values for  $d_s$  are for wheels as new and will reduce by up to 20% during use. Bond specifications are based on the Universal (Saint-Gobain Abrasives) VSS bond system. Grades will vary from one wheel manufacturer to another.

For conventional wheels, the range of bond systems is well established by the wheel manufacturers. Table 18.2 provides typical grit size requirements based on  $d_e$  and  $Q'$  values. Again, wheel grade and structure number will vary depending on the manufacturer and grit type.

### 18.3.2 IMPACT ON GRIND CONFIGURATION

The selection of grain type has a significant impact on wheel length. Specifying of the length of an alox or ceramic wheel is based on the recognition that there is a significant level of wheel wear for each part that is ground. The length of the wheel is, therefore, kept short and the wheel oscillates a significant distance past the ends of the part to maintain straightness. The breakdown is sometimes so great that it is often dressed midcycle just prior to finish to re-establish size. Salmon [1984] makes the following general recommendations with reference to Figure 18.5 where the oscillation is a third of the wheel length past both ends of the part.

For CBN wheels, the wear is one hundredth the wear with alox and the goal is to maintain the straightness of the wheel face and avoid excessive edge breakdown. Consequently, the wheel is made about 1 to 2 mm longer than the length of the part and a much smaller oscillation stroke applied such that the wheel normally remains in contact with the full length of the part for all or most of the time. Small adjustments of the end points can be made to adjust for taper and shape in the part. For example, if the back of the part is small then the wheel oscillation end point is moved

**TABLE 18.2**  
**Recommendations for Alox Grit Sizes as Function of Part Size, Roughness, and Stock Removal Requirements**

$d_e$ (mm)	$Q = 1$ (mm <sup>3</sup> /mm/s)	Ra ( $\mu$ m)	$Q = 3$ (mm <sup>3</sup> /mm/s)	Ra ( $\mu$ m)	$Q = 5$ (mm <sup>3</sup> /mm/s)	Ra ( $\mu$ m)
125	150#	<0.15	120#	<0.25	100#	<0.5
250	120#	<0.15	100#	<0.25	80#	<0.5
375	100#	<0.15	80#	<0.25	70#	<0.5
500	100#	<0.15	70#	<0.25	70#	<0.5
750	80#	<0.15	70#	<0.25	60#	<0.5
1,000	80#	<0.15	60#	<0.25	46#	<0.5

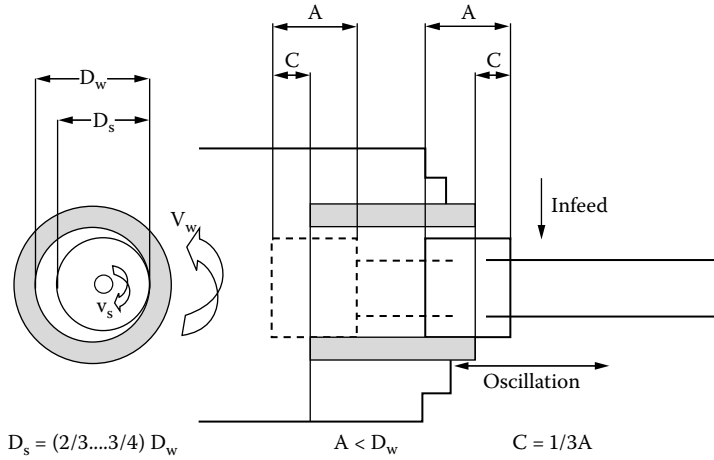


**FIGURE 18.5** Parameters for ID grinding with alox wheels.

farther back past the end of the part such that the wheel contact length is now slightly less than the full length of the part. This gives more time for the wheel to remove metal where the part is small; in addition, the reduced contact length will reduce normal force and quill deflection further improving shape.

Using this method for taper compensation, any residual quill deflection, *if it were constant from part to part*, could be compensated for by adjustment to the wheelhead angle. Unfortunately, the normal forces change significantly both with wheel sharpness after dress and longer term with changing wheel diameter. The machine operator can attempt to adjust for these by either adjustment to the wheelhead alignment or the oscillation end points. This approach is often unacceptable both for the degree of operator intervention and the lack of process control.

### 18.3.4 QUILL DESIGNS FOR CBN

The preferred approach is to ensure that the quill design has been optimized for use with vitrified CBN as illustrated in the Figure 18.6. The quill length should be reduced to a minimum and the

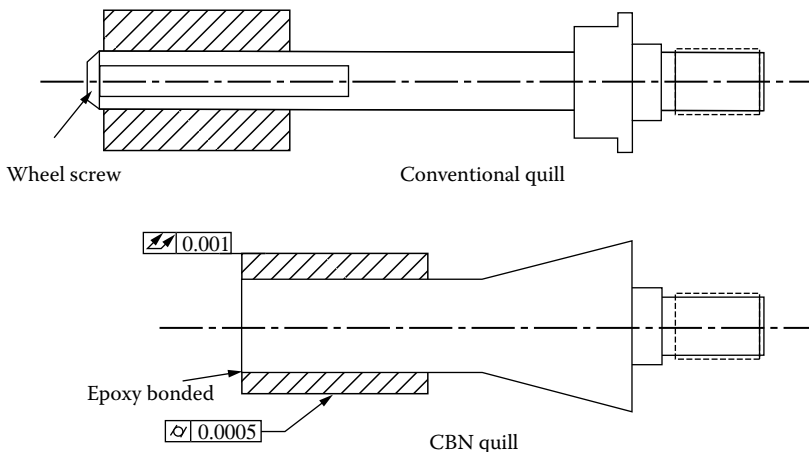


**FIGURE 18.6** Quill design for CBN compared with conventional quills for alox.



mounting diameter increased. The standard wheel screw used for conventional wheels should be eliminated and the wheel glued directly to the quill. This allows the wheel bore size to be maximized (note the lack of stiffness of the wheel bond itself). Stiffer quill materials may also be necessary and several materials are listed above. Carbide is up to four times stiffer than steel but is very brittle and is usually only used for the smallest wheels with very tight tolerances. Molybdenum is twice as stiff as steel and tough but expensive. Ferro-TiC is a less expensive alternative. Tungsten alloys with trade names such as No-Chat and Wolfmet have the same stiffness as molybdenum but cost a third as much. However, they are almost twice as dense and any runout from mistreatment will reduce spindle life.

For a cylindrical bar of radius,  $r$ , and length,  $l$ ,

Material	E	Density
	10 <sup>6</sup> psi	gm cm <sup>-3</sup>
Steel	25–30	8
Titanium	17–27	4
Molybdenum	48–52	10
Tungsten	≈50	19
WC	75–100	13
Ferro-TiC	40–45	6
(Vitrified bond)	4–18	<3)

Discussions with machine tool builders suggest that if the calculated deflection during the rough feed portion of the grind cycle exceeds 80% of part tolerances, then the quill should be redesigned as indicated above. A crude estimate can be made using the equation above by either direct measurement of power or by estimation, that is,

- From spindle power (Assume  $F_n/F_t = 0.33$ )

$$W \text{ (newtons)} = 3 \times \text{Power(watts)} / \text{Wheel speed (m/s)}$$

- From typical values  $Q' = 5 \text{ mm}^3/\text{mm/s}$  and specific energy  $e_c = 60 \text{ J/mm}^3$

$$W \text{ (newtons)} = 3 \times 5 \times 60 \times \text{part length (mm)} / \text{wheel speed (m/s)}$$

Once the CBN wheel length-to-diameter ratio exceeds about 1.5, then increased attention has to be paid to the level of quill deflection. Especially for wheels under 10 mm it may be necessary to resort to a shorter wheel and stroking the bore as with alox wheels.

Quill length can also be a problem. Titanium has been used occasionally for extremely high rpm applications because its low density moves the resonant frequency of the quill above the rotational frequency. However, in general, the gains are relatively small. Figure 18.7 graphs the maximum recommended quill length as a function of spindle rpm. The center line represents steel while the slightly higher line is for titanium, and the lower line is for tungsten.

## 18.4 PROCESS PARAMETERS

### 18.4.1 WHEEL SPEED

As discussed in Chapter 4, wheel speed for internal wheels is limited to 35 to 42 m/s for most conventional wheels and machines, and 60 m/s for vitrified CBN in purpose-designed grinders. Some vitrified CBN wheels are used at up to 80 m/s with special high-strength bonds on steel

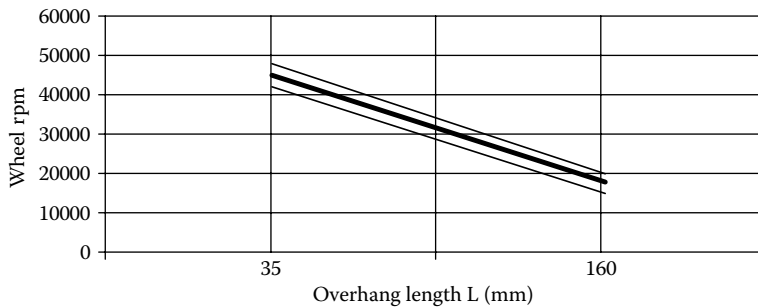


**FIGURE 18.7** Maximum recommended wheel rpm as function of quill length.

cores, and subject to the restraints in Figure 18.7. The practice is generally limited to narrow bearing race applications on specially guarded machines, and where local safety regulations allow. In general, the speed is limited both by bond strength considerations and by coolant hydrodynamic forces. This latter effect can be very deleterious on taper and shape as speed is increased especially for the denser vitrified CBN wheel structures. The pressure is sometimes relieved on long narrow CBN wheels by adding slots along the length of the wheel.

#### 18.4.2 WORKSPEED

Workspeed is usually expressed as a ratio of the work-to-wheel speed (in m/s, not rpms). The value is influenced by dynamic stiffness, onset of burn, and roundness. A typical value would be 1:100 with values as high as 1:50 on stiff grinders for best roundness or 1:150 on weak grinders limited by chatter. As wheel speed increases, the ratio is usually dropped (i.e., the workspeed is increased) to reduce thermal damage. Grinding large bearings for applications such as steel mill workspeeds are limited and the greater risk is chatter. Under these conditions the workspeed velocity is often shifted a few percent every revolution to avoid the onset of regenerative chatter (see also Chapter 8).

#### 18.4.3 OSCILLATION

Oscillation is provided to improve finish, smooth out wheel wear, and adjust for shape. Stroke length is limited to <3 mm typical but is high frequency (up to 20Hz) and fast (up to 1.5 m/min). Oscillation can improve finish Ra and appearance somewhat, and can also reduce spark-out times.

#### 18.4.4 INCOMING PART QUALITY

The incoming part quality is critical. The grind process is often used to “fix” problems earlier in the line and blamed for their deficiencies. The part must come in burr free from any premachining/heat treat process and free of any contamination such as tumbling media used for deburring. (Grit blast media or loose burrs often leave a very characteristic appearance on the wheel face of random pock marks.) On a standard grinder, the out of roundness coming to the machine must be no more than one eighth of the stock amount, while the total geometry error should be no more than about one fourth.

#### 18.4.5 DRESSING

Dressing has been discussed in Chapter 7 for both conventional and CBN wheels. The end user should be aware, however, of the importance of the diamond being on centerline with the wheel. This is especially critical if the wheel is dressed, each part just prior to finishing, for sizing purposes as illustrated in Figure 18.8 [Bryant 1995]. If the diamond is off centerline the wheel will actually

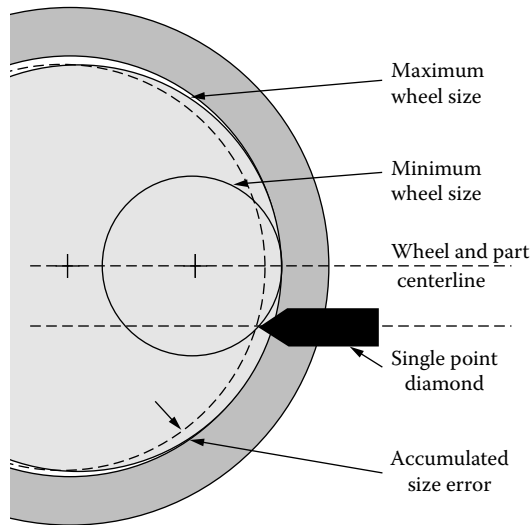


**FIGURE 18.8** The effect on part size of diamond dresser being off centerline.

extend farther by a distance governed by its radius. Consequently, as the wheel gets smaller, this distance will increase leading to the part diameter getting bigger.

When traverse dressing vitrified CBN wheels, attention must be paid to the limitations of the grinder and the dresser spindle. Very few grinders are equipped with acoustic emission (AE) dress sensor technology, yet the dress infeed repeatability is limited by slide repeatability and thermal stability. It is necessary to determine by trial and error a safe total infeed amount to ensure repeatability and also determine the level of wheel wear, if possible. (This may be possible from QC data on size or tracing a coupon of the wheel face.) If the wheel wear is a significant portion of the infeed repeatability, then it is best to make multiple passes at smaller infeed depths to ensure the last pass is at a near constant depth. For example, if the minimum total infeed amount were  $3\ \mu\text{m}$  and the wheel wear were  $1.5\ \mu\text{m}$ , then it would be best to make at least two passes at  $1.5\ \mu\text{m}$  or  $2\ \mu\text{m}$ . However, if the wheel wear were only  $0.5\ \mu\text{m}$  then a single pass at  $3\ \mu\text{m}$  would be stable.

Internal grinding machines are very compact and most have evolved from designs based around single-point diamonds. End users wishing to retrofit an existing machine for rotary dressing have found space for a motorized spindle to be very limited and until the introduction of small high power density dc servomotors, grinders were equipped with air or small ac servo-driven electric dressing spindles with very limited torque. This, in turn, required the dresser diameter to be very small, sometimes only 10 to 15 mm, and often had to be run counterdirectionally. The dresser configuration was usually that of a cup so that even though the dresser wear might be high, the active diameter remained constant to maintain a constant crush ratio. Hydraulic motors offered better torque but had problems of heat generation especially during the prolonged period of new wheel dressing where additional heating would cause thermal errors. Also, industry is now eliminating hydraulics on new grinders where possible to reduce maintenance costs. Fortunately, many of these issues have been overcome with high power density of dc servomotors to eliminate torque deficits, while the use of synthetic needle diamonds in dressing cups and discs has reduced dresser wear.

Plunge roll dressing of alox wheels for internal grinding has been standard for 40 years with hydraulic and electric motorized spindles usually running counterdirectionally. Limitations in available equipment and system stiffness have held back the conversion of such processes to CBN abrasives although this is now changing rapidly.

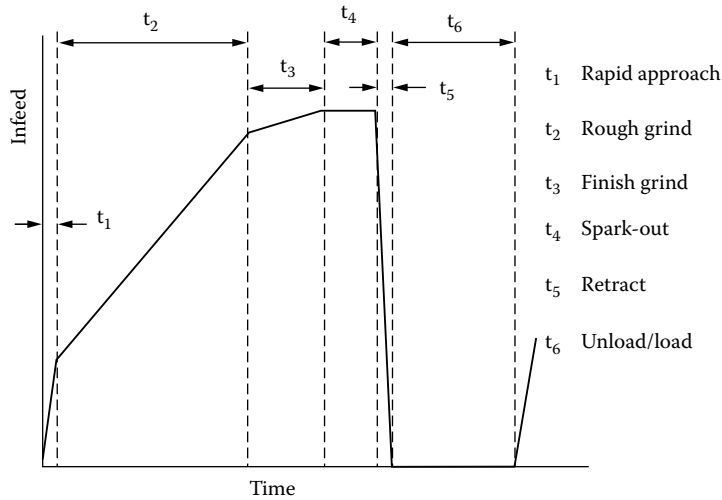


FIGURE 18.9 A typical feed cycle for an internal grinding process.

18.4.6 GRINDING CYCLES

The grind cycle on a standard internal grinder consists of a series of fixed infeed rates and amounts, namely, a rapid approach, rough grind, finish grind (10 to 30  $\mu\text{m}$ ), spark-out, retract, and unload/load. Figure 18.9 graphs the programmed slide moves with time for one grind cycle.

Figure 18.10 illustrates the associated grinding power. There is a rapid climb during roughing leveling off during the finish grind, then going through an exponential decay during spark-out. The spark-out time should ideally be three time constants after which no further material removal or improvement in finish will occur as the threshold force is reached. The graph shows an ideal situation for a part with zero runout entering the grind cycle. In reality, the part will typically have 50 to 100  $\mu\text{m}$  runout and the smooth climb in power during roughing will have superimposed on it rapid oscillations with the frequency of the work rpm. The amplitude of this will reduce but can still often be seen during spark-out demonstrating the level of out-of-roundness still remaining in the part after grind.

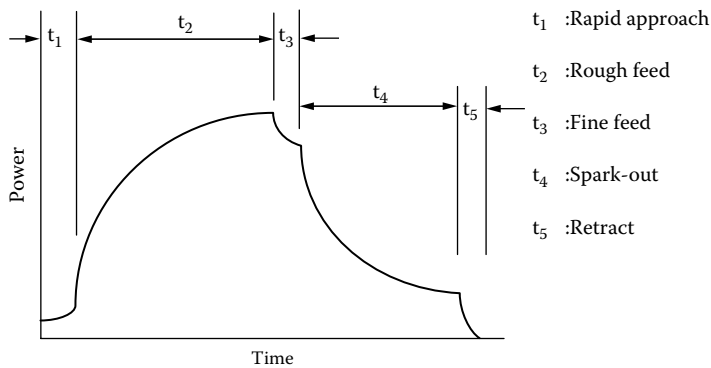


FIGURE 18.10 Variation of power in a typical grinding cycle with set feedrates.

In addition to a superimposed oscillation from runout, any excess stock will show up as a power spike during rapid infeed. Any such spike will be deleterious to wheel life.

#### 18.4.7 AUTOMATIC COMPENSATION OF PROCESS VARIATIONS

A fixed infeed system has major limitations from the inability to adapt to changes in incoming stock or wheel conditions. Much research has been carried out to develop systems to control the system based on force either directly using normal force or indirectly by monitoring power (tangential force).

One of the earliest versions was the Heald controlled force system (CF) pioneered by Dr. Hahn and the Heald Corporation in the 1960s. This applied a controlled normal force from the wheel to the part via a hydraulic ram. By today's standards, the system was relatively crude but highly effective for the appropriate application. Hundreds of these machines are still in production for plain bore applications.

Their use can be problematic when internal plunge profile grinding unless the incoming part preform is well controlled. In bearing manufacture, the race is previously turned in the soft state and then heat treated during which the bearing profile may often distort slightly. To compensate for this, the bearing race is turned to a smaller radius to ensure cleanup after grind. Unfortunately, this leaves excess stock at the two tangent points to the outer diameter. A CF-type process sees only the average force over the whole bearing surface to be ground and will plunge in a rapid approach rate through the excess stock leaving wear steps in the wheel.

In the 1980s, with advances in closed loop ac servo drives, it became possible to closely monitor power. Initially, this was used to detect part contact during rapid approach and to control spark-out times based on decay time constants. The efforts culminated in the 1990s with controlled power grinders such as the Bryant UL2 (Figure 18.11 and Figure 18.12).

In this type of grinder, all the feed points are still fixed but all the infeed rate parameters are now at a fixed power level controlled by a fast-response power monitoring system. The control inputs include a stock load sensor for first contact, rough grind, a rough grind power trip differential for alox wheels (power must drop below a given level at a fixed feed point inner diameter (ID) to allow sufficient relaxation to safely retract the wheel when dressing midcycle), finish grind, and a spark-out power differential (power decays below a given power level). The grinder also takes into account the initial problems of break in for a new CBN wheel. After the initial wheel dress, the first parts are fed at a set percent of full feed power setting and then ramped up at a given percent

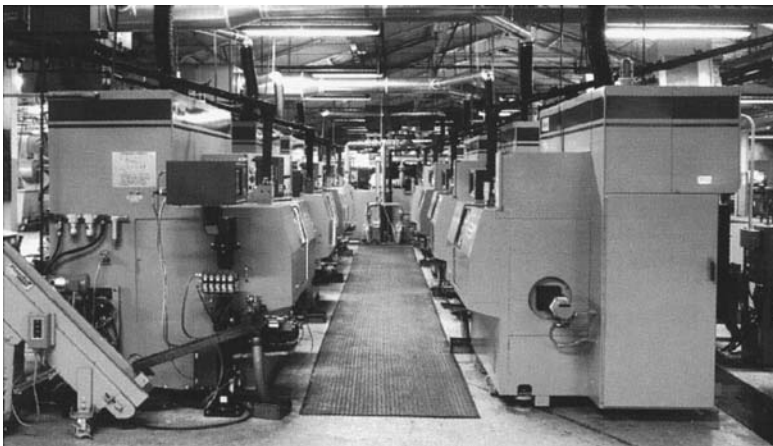


**FIGURE 18.11** First installation of Bryant Grinders for universal-joint cup grinding. (Courtesy of GE Superabrasives. With permission.)

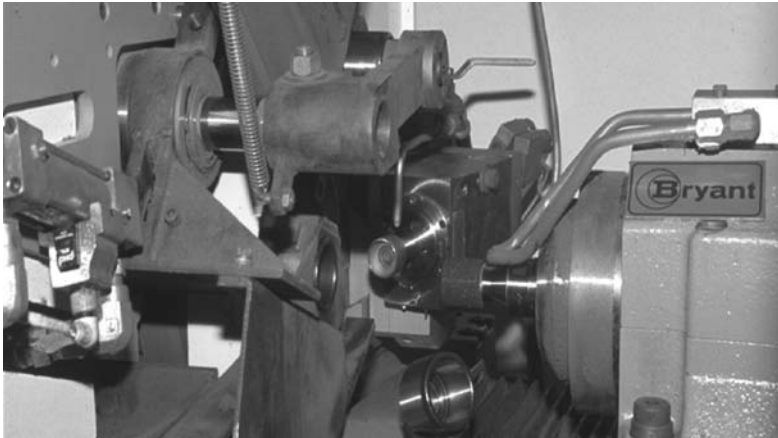


**FIGURE 18.12** Universal-joint cup grinding arrangement. (Courtesy of GE Superabrasives. With permission.)

increment every given number of parts. This prevents loading of the wheel when dull and allows a wheel several grades harder to be used increasing wheel life by up to a factor 5.

As the wheel wears through its life, its diameter can reduce by 20% and significantly affect the grinding conditions in a number of ways. First, the physical amount of CBN becomes less increasing wear and reducing parts/dress. Second,  $d_c$ , and, hence, contact length, is reduced allowing a faster infeed rate for a given adaptive power setting. Fast feedrates will further accelerate the rate of wheel wear. The Bryant UL2 has an equivalent wheel skip decay function option that allows the end user to input a parts/dress algorithm as a function of wheel diameter. This is nonlinear and can vary from, for example, 200 parts/dress for a new wheel diameter to as little as 10 parts/dress at minimum wheel size. In addition, to prevent the wheel getting too sharp and breaking down exponentially, there is CBN adaptive dress trip rate that is set to a given maximum allowed infeed rate. If this value is exceeded, the wheel is automatically dressed.

This system has allowed enormous improvements in CBN wheel life. Adaptive power grinding systems are now available from several machine tool builders either as software integrated into custom controls similar to that described above or as separate control systems that can be added to an existing grinder. In addition, some of the latest CNC controls have options available to control feed to a given power. Its use, though, is limited to a range of wheel sizes from about 6 mm diameter up to 30 mm. Below about 6 mm, the power signal-to-noise ratio is too low to get a clean signal while at diameters greater than about 30 mm the power detection and reaction times are not yet fast enough to prevent loading with harder CBN wheel grades. Linear motor technology is expected to improve on this.

Systems based on normal force offer the ultimate in control as a direct measurement of system deflection. Hahn again pioneered work in the 1990s on direct measurement of normal forces and compensation for quill deflection. In a series of articles, Hahn analyzed the taper deflection problem and proposed a method based on detection of normal force, calculation of quill deflection, and microswivelling of the wheelhead to compensate [Hahn and Labby 1995a, b, Hahn 1997, 2000].

The system deals with the biggest factor that cannot be influenced by adaptive power control, namely, *threshold normal force*. Figure 18.13 plots a typical slide feed cycle for a simple rough grind and spark-out operation together with the actual position of the wheel for a new and used condition. As shown in Figure 18.14, the threshold forces at the end of cycle can be less than half for a worn wheel than a new one. This will result in a significant change in part size and taper over the life of the wheel regardless of spark-out time or roughing infeed rate.

Hahn developed a microangle/force sensing subplate to both measure the force and make the compensation for deflection (Figure 18.15). The system can also measure Work Removal Parameter  $\Lambda (=Q'/F_n)$ , which is a key quantitative measure of wheel sharpness. Although  $\Lambda$  cannot be measured

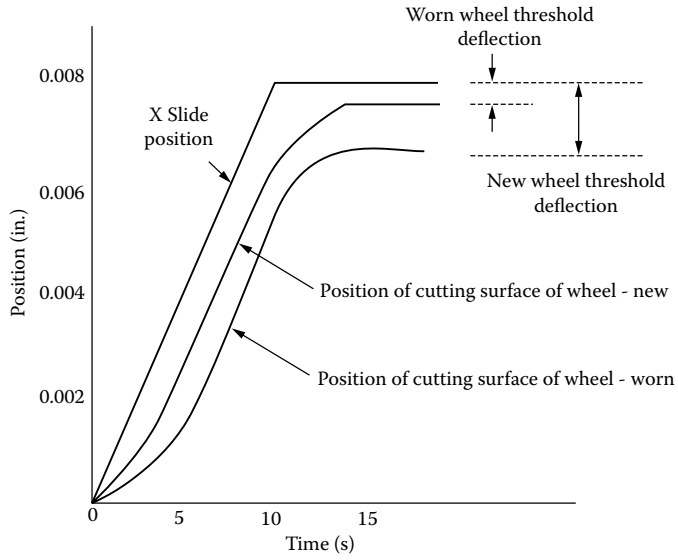


**FIGURE 18.13** Actual position of the grinding wheel surface compared with the feed position due to spindle deflections and wheel wear.

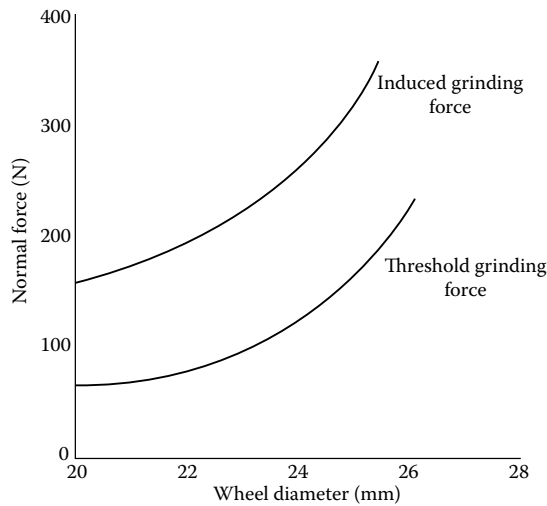


**FIGURE 18.14** Variation of threshold force in a grinding cycle with wheel diameter.

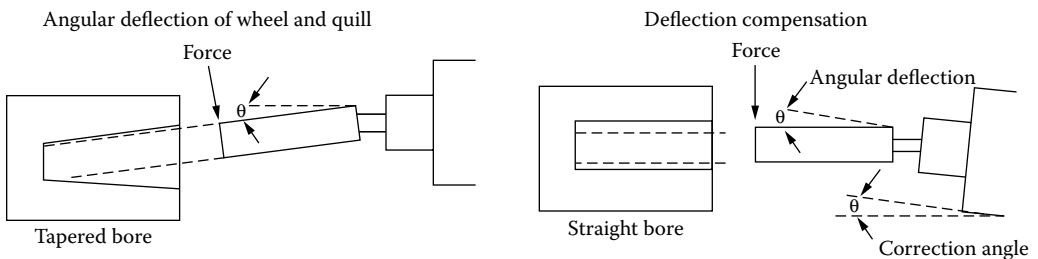


**FIGURE 18.15** Compensation for deflection by adjustment of angle in response to force.

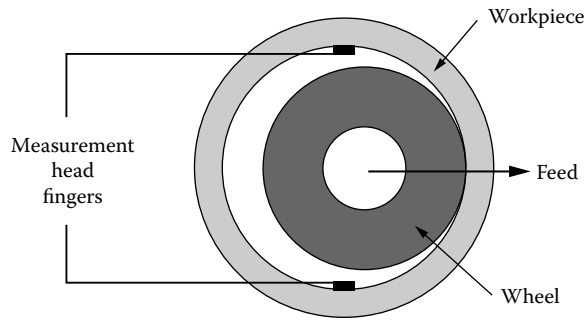


FIGURE 18.16 In-process diameter gauging.

directly using power only, it is a key parameter in determining maximum feedrates in weak systems limited by burn.  $\Lambda$  is especially pertinent to alox wheels that become dull with time after dress and may cause burn if threshold forces are too high.

Having taper compensation based on normal forces also allows faster overall cycle times for weak systems susceptible to chatter. New wheels with relatively large  $d_e$  values can sustain relatively high feedrates without the onset of regenerative chatter. As  $d_e$  is reduced, contact length and regenerative chatter can occur faster. Normally the feedrates and wheelhead position are set to those that are stable for the smallest diameter. With taper compensation, faster feedrates may be used for larger wheels and algorithms applied to gradually reduce rates to those of the fixed infeed grinder as the wheel gets smaller.

Alternate systems based on measuring the physical deflection of a quill using opposed air gauges have reportedly been used in the bearing industry for some years. A system was recently presented by UVA [n.d.] called GPC-PSH, which provides the combination of a sensor in the spindle to measure deflection and a compensating method for swiveling the head. The method is claimed to improve straightness and cylindricity by up to 40% when grinding small fuel-injection components.

Interest in force-controlled grinding is probably much greater than current original equipment manufacturer (OEM) publications and what literature would suggest. Competitive industries such as bearing manufacturers are very secretive with highly skilled research groups; several build their own grinders. The potential for CF grinding was presented in 1988–1990 by Heald in combination with The Torrington Company [Bell et al. 1988, Matson et al. 1990, Vaillette et al. 1991]. These papers focused on several of the aspects of controlled force grinding discussed above. Part of the

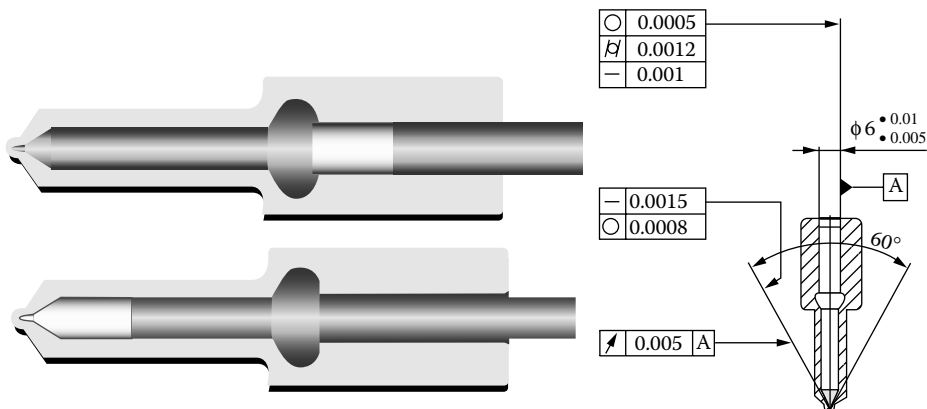
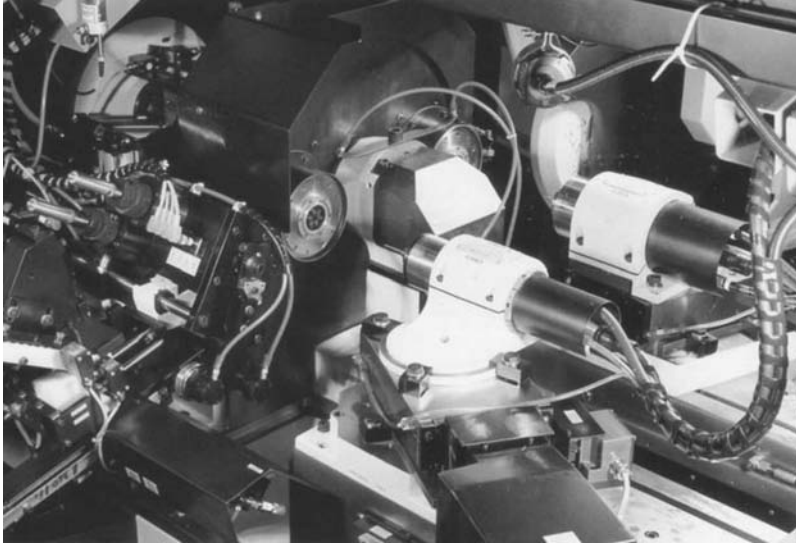


FIGURE 18.17 Example of grinding fuel injector bore and seat. (From UVA n.d. With permission.)





**FIGURE 18.18** Twin wheelhead machine for seat and bore grinding of injector. (From UVA n.d. With permission.)

interest was in how to optimize the use of CBN that was then still quite new, and process optimization by, for example, gap elimination. Another area of research, however, was in the use of  $\Lambda$  to help improve roundness. During rough grinding, once continuous contact has been made between the wheel and part, the level of eccentricity in the part is given by  $(F_{\max} - F_{\min})/K_s$  where  $F_{\max}$  and  $F_{\min}$  are the maximum and minimum normal force, seen in the power consumption plot as a once-per-work revolution spike, and  $K_s$  is the system stiffness. The number of revolutions needed to round the workpiece up to an acceptable running truth is a function of system stiffness and  $\Lambda$ . In the papers referenced, algorithms were used to automatically regulate the feedrates to ensure sufficient revolutions of the workpiece before reaching finished size.

In-process gauging is a common, if somewhat delicate, method of controlling size. Longanbach and Kurfess [1998] reported using in-process gauging for the real-time measurement of out-of-roundness, waviness, or chatter during grinding, which was incorporated into a production grinder.

AE-based sensors have also been applied to internal grinding. Inasaki [1991] reported on an AE sensor water-coupled to the wheel quill as part of an integrated system including power monitoring for developing unattended grinding. AE was used for gap elimination, dressing, and chatter detection. Several machine tool builders offer AE systems as an option for gap elimination and/or touch-dressing CBN wheels, although use of AE for dressing is still limited. Drake [2000] has incorporated the AE sensor in the wheelhead. Studer [2001] has incorporated a ring sensor into the work chuck flange for small wheel applications. EMAG/Reinecker [2001a, b], offer sensory analysis modules that include AE for gap elimination and dressing as well as power-controlled adaptive grinding. Similar options are offered by Toyo [2000] while Okuma [2000] offers AE for touch dressing CBN. Finally, the size of AE sensors has reduced to the point that they can now be fitted inside small dc servo electric dressers.

## 18.5 MACHINE TOOL SELECTION

### 18.5.1 INTRODUCTION

In 1938, in the first edition of *Grinding Wheels and Their Uses*, Heywood wrote: “Internal grinding machines are being improved so rapidly that a machine only a few years old is practically certain

to make the internal grinding operation cost more than it would with a later model.” The most striking fact about this statement is that in the intervening 65 years it is as true as ever!

When selecting a grinder, the end user must be clear on the part dimensions and tolerances, required production rate, and required grinding operations. Some applications require high-volume, dedicated machines while others may have a range of part sizes or require the grinder to do multiple grinding operation not limited to just a single internal grind operation or even just grinding. The following are some examples of common machine types and applications.

### 18.5.2 FUEL INJECTION

Grinding fuel injectors are characterized by very high production requirements, small wheel diameters (2 to 6 mm), limited coolant access, and extremely tight finishes and tolerances. Bore roundness is especially stringent and must be held to  $<0.5 \mu\text{m}$ . Taking the requirement for CpK capability into account, the requirement is nearer  $0.25 \mu\text{m}$ . There is usually a bore grind and an angled seat. For diesel injectors, there are often also faces and combination grinds.

Machine tool builders focused on this industry such as UVA and Bahmuller build modular grinders where the slides and spindle can be easily interchanged or modified thus maintaining flexibility and economics of scale in manufacture. Wheelheads run up to as high as 240,000 rpm [UVA n.d.] but speeds in the range of 140,000 to 180,000 rpm are more standard [Bahmuller 1997, Micron 2000, Okuma 2000, Studer 2001]. Spindle power is  $<3 \text{ kW}$  at these speeds. CBN wheels dominate at around 270#–500# (B76–B36) grit size; and quills are carbide.

There are numerous ways of mounting the wheels. Gluing direct to the carbide by the end user is problematic. Wheels are, therefore, often supplied on wheel screws. However, producing quills in carbide with high accuracy electrodischarge machine-cut internal threads for these to screw into is expensive. Only a few companies such as Hämex Hårdmetallverktyg, Linköping, Sweden can produce to the necessary tolerances. Wheels are, therefore, also sometimes supplied on straight carbide shanks and held in a collet wheel mount.

Getting coolant into the grind zone is difficult. Fortunately, even at the wheel rotational speeds mentioned above, the wheel velocity is still barely 20 to 30 m/s, which limits the risk of thermal damage. Also low viscosity oil, chilled and filtered to  $<5 \mu\text{m}$ , is used almost exclusively. If spray holes exist in the injector tip, it may be fed with coolant from behind the wheel. Many wheel spindles can also provide coolant through the center of the quill, some as high as 120,000 rpm. Specialist wheel companies can produce precision wheels on hollow wheel screws with fine perforations in the wheel face for seat or end grinding to deliver coolant evenly right at the grind point. For new applications, especially grinding at the end of long bores, FEA analysis of the dynamic stiffness and resonant frequencies of the quill is required.

The work drive is the most critical component, for its running truth governs the running truth of the finished part. Aerostatic and angular contact ball bearing drives have been used but the most common are hydrostatic or hydrodynamic. Industry standard for precision is currently  $0.1 \mu\text{m}$ ; speed of rotation is up to 4,000 rpm. Since the workhead is also one of the stiffest parts of the grinder, some OEMs have taken advantage of this and mounted the dressing diamond as a ring around the chuck.

Diaphragm, collet, and jaw chucks are all used for part holding. The primary concern is to avoid distortion of the part and to maintain accurate running truth. The jaws should be regularly ground; the same wheel used as for the bore grinding can grind high-speed steel jaws. Otherwise, dressable vitrified diamond wheels are available for grinding carbide jaws *in situ*.

Most slideways are hydrostatic with ballscrew/ac servo drives accurate to  $0.1 \mu\text{m}$ . The high oscillation/short stroke length required has recently led numerous OEMs to provide linear magnetic motors as options. All state-of-the-art machines have sophisticated CNC controls with a variety of the AE dressing and gap elimination options described above.

Load/unload is carried out with a pick and place arm or gantry as the parts are too small or awkward in shape to load by a gravity-fed method.

**TABLE 18.3**  
**Comparison of Cycle Times from Machine Design Changes**  
**in Last 20 Years**

Grind Step	Pre-1980 m/c	2,000 m/c	Advances
Load/unload	5.0 s	2.0 s	High-speed loaders
Rapid approach	3.0 s	0.5 s	AE/Adaptive grind/CNC
Rough grind	2.5 s	2.5 s	
Dress	1.0 s	0	CBN replaces alox
Finish grind	1.0 s	1.0 s	
Spark-out	3.0 s	1.0 s	Adaptive grind
<b>Total cycle time</b>	<b>15.5 s</b>	<b>7 s</b>	

### 18.5.3 AUTOMOTIVE COMPONENTS (LIFTERS, TAPPETS, UJ CUPS, PLAIN BEARINGS)

This refers to a range of products using wheels in the 5- to 25-mm-diameter range to grind extremely high volumes of components on dedicated grinders. Tolerances now become somewhat relaxed compared with those for fuel injection and fall in the 1 to 5  $\mu\text{m}$  range.

The key to these machines, though, is cycle time, much of which is won or lost in nongrind time. For example, a 20-mm-diameter component with 0.2-mm radial stock can be rough ground at  $Q' = 5 \text{ mm}^3/\text{mm/s}$  in 2.5 s. However, the total cycle time can vary from over 15 s on an old hydraulic/mechanical grinder to less than 7 s on a modern CNC grinder. The savings are in improved load/unload mechanisms, faster slide movements, gap elimination, optimized spark-out times, and ability to use CBN wheels (Table 18.3).

### 18.5.4 MACHINE LAYOUT

The machine design starts with the overall layout of the components. Since only a limited amount of travel is required, the X-axis and Z-axis are on independent slide systems as in the example from Bryant (Figure 18.19) [Koeper 1995]. This allows all the moving components, wheelhead, and workhead close to the machine bed and ballscrews for improved stiffness and thermal stability. Most builders use hydrostatic slides for rigidity and speed (up to 40 m/min) or more recently linear magnetic slides, especially on the Z-axis with the need for high-speed oscillation.

### 18.5.5 WHEEL SPEEDS

Wheel speeds with CBN of 30 to 60 m/s are now readily achievable with available spindles operating at 40,000 to 70,000 rpm with a good torque range. Higher speed spindles are available but these appear to lack the same rigidity, power, or durability. Most modern grinders will maintain a constant wheel velocity as the wheel gets smaller. It is important to check that there is available rpm/torque for the full life of the wheel size and abrasive type especially if planning to use both CBN and alox.

### 18.5.6 WORK-SPINDLE RUNOUT

Workhead spindle runout is held within the range 0.25 to 1.00  $\mu\text{m}$  depending on part tolerances. Speeds can vary within the range of 500 rpm to 3500 rpm depending on the particular application.

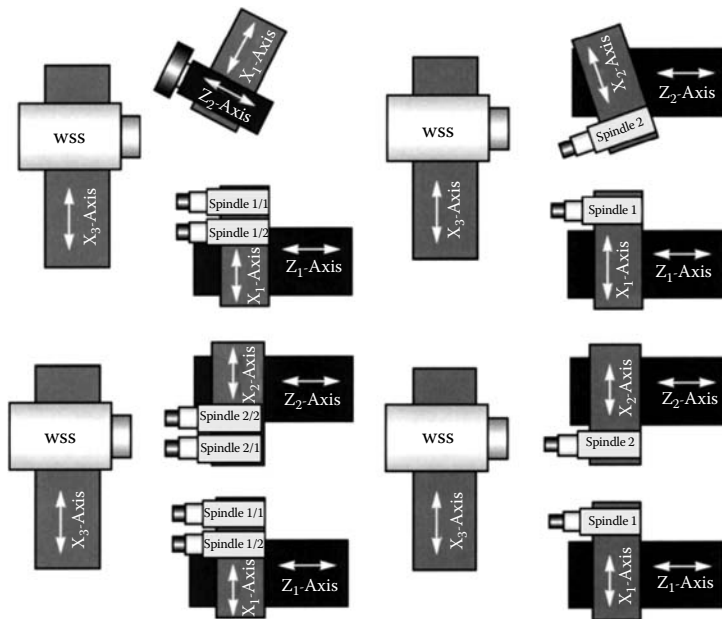


**FIGURE 18.19** Modular machine designs allow for different configurations of multiple grind operations (seats, bores, and faces). (From Bahmuller 1997. With permission.)

### 18.5.7 WORK-LOADING MECHANISMS

The selection of the appropriate load/unload mechanism is a major source of cycle time savings. Options include:

- Through-the-work-spindle loading. Small parts are fed through the workhead into a chuck. Each new part ejects the preceding part that falls or is held by a receiving arm. Grinding resumes as soon as the ground part and receiving arm are clear.
- Linear arm and two-arm loaders. Combination swing and linear motion for front loading. Single-arm version loads only the part being ejected into an unloading chute. Two-arm loader: latest designs use a combination of swing and linear motion with high-speed two-axis ac servo control.
- Flow systems to two-roll and shoe centerless support arrangements. A shoe centerless work support arrangement grinds the ID concentric to the outer diameter (OD). The latest flow or gravity-fed load devices can load/unload in 0.5 s [Toyo 2000, Toyo n.d.]. A gravity-fed loader is used with a simple ejector arm to kick finished parts off the shoes. A variation on this is a two-roller and one-shoe arrangement.

### 18.5.8 COOLANT

Coolant is more likely to be water-based than oil in the United States although the reverse is true in Europe. The difference in performance can be as great as the difference between fixed infeed and adaptive power grinding. For plain bores, coolant is supplied from both the front and back. For blind end applications through-the-spindle coolant is typical.

### 18.5.9 GAUGING

Gauging is standard either as in-process as discussed above or more commonly postprocess using air gauges to measure size, taper, even profile. Typical systems will plot a running performance

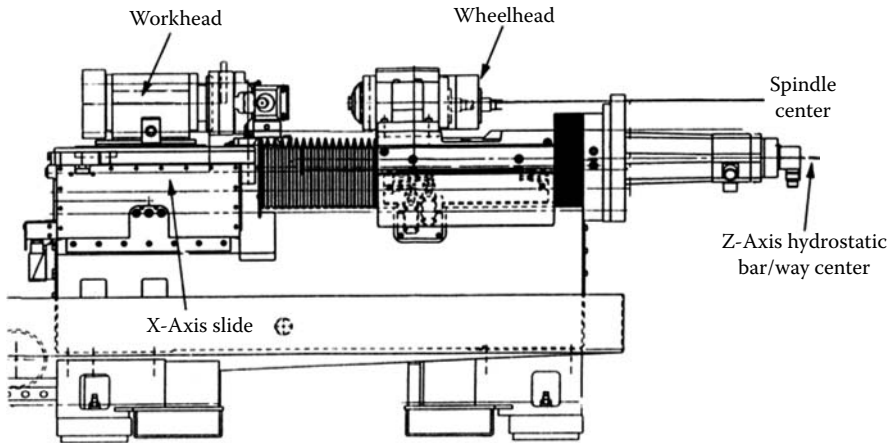


FIGURE 18.20 Bryant UL2 high production grinder configuration. (From Koepfer 1995. With permission.)

statistical process control (SPC) graph and make automatic adjustments on size and sometimes even taper. The systems average out the values of a given number of preceding parts (usually three).

#### 18.5.10 FLEXIBLE MULTIPURPOSE GRINDERS

This refers to a class of grinders that must have the flexibility to perform a range of grinding operations that may also include face and OD grinding in a broad range of parts. Multispindle

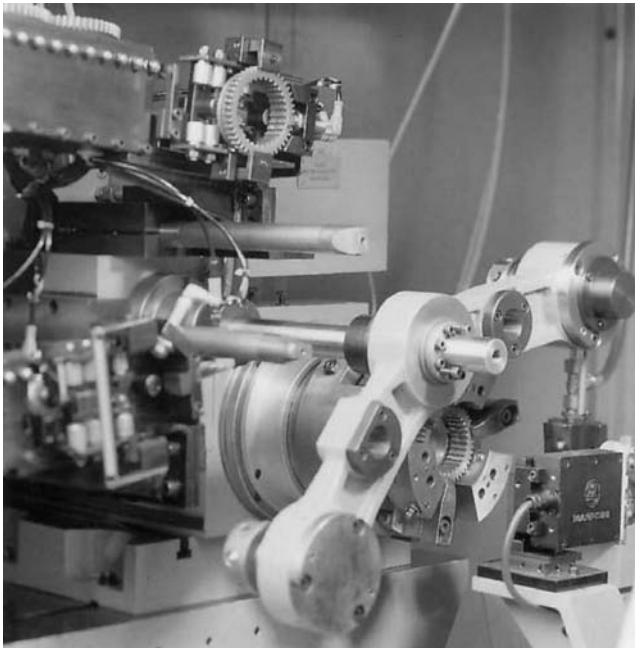
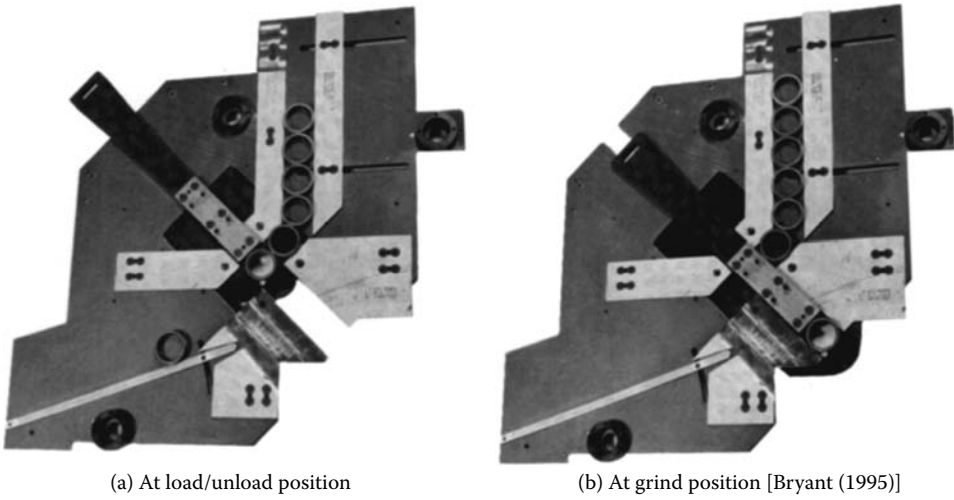
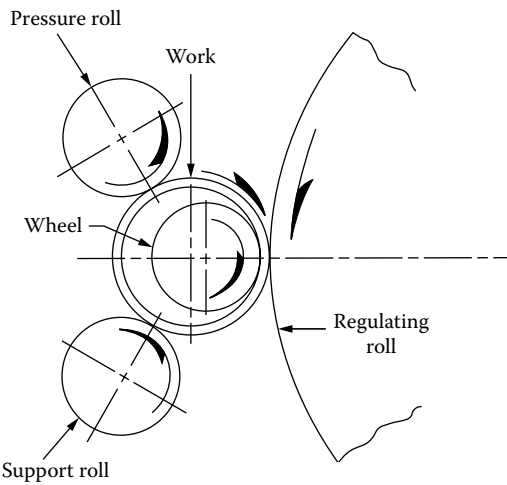


FIGURE 18.21 Swing-arm part loader. (From Danobat 1992. With permission.)



**FIGURE 18.22** Bryant UL2 loader for shoe centerless mode grinding. (a) At load/unload position. (b) At grind position. (From Bryant 1995. With permission.)



**FIGURE 18.23** Two-roll internal centerless grinding machine.

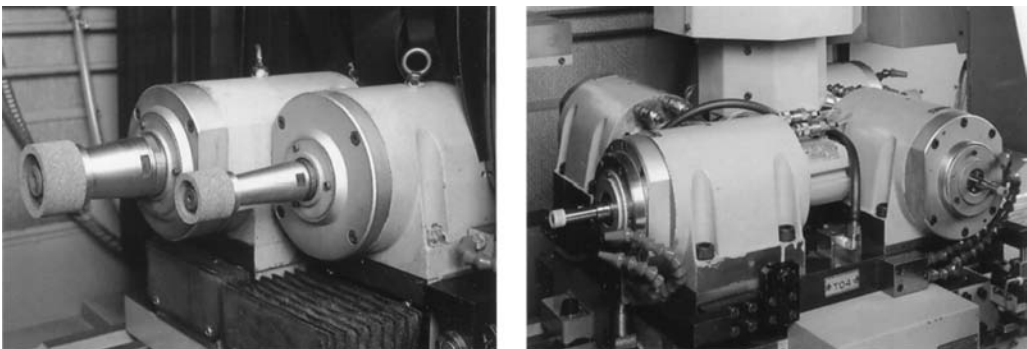


**FIGURE 18.24** Linear and turret spindle arrangements. (From Okuma 1996. With permission.)

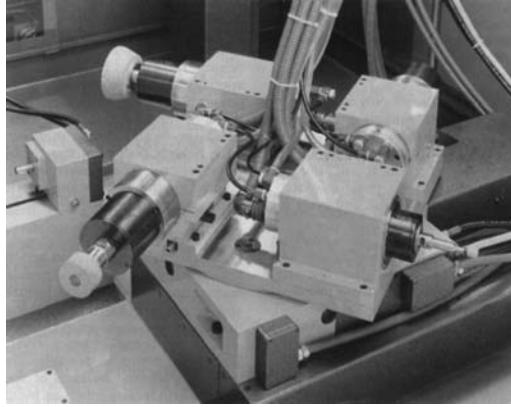


**FIGURE 18.25** Four-spindle turret on Tripet grinder. (From Anon. 1989. With permission.)

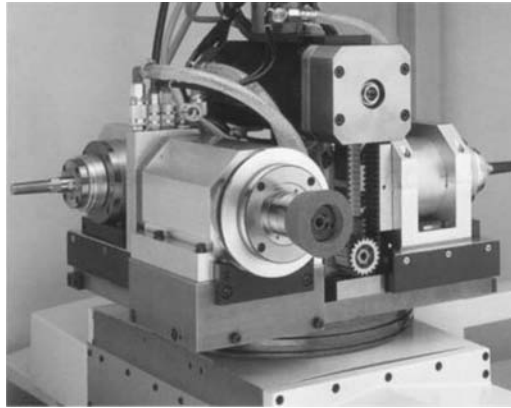


**FIGURE 18.26** Three-spindle turret on Voumard grinder. (From Voumard n.d. With permission.)

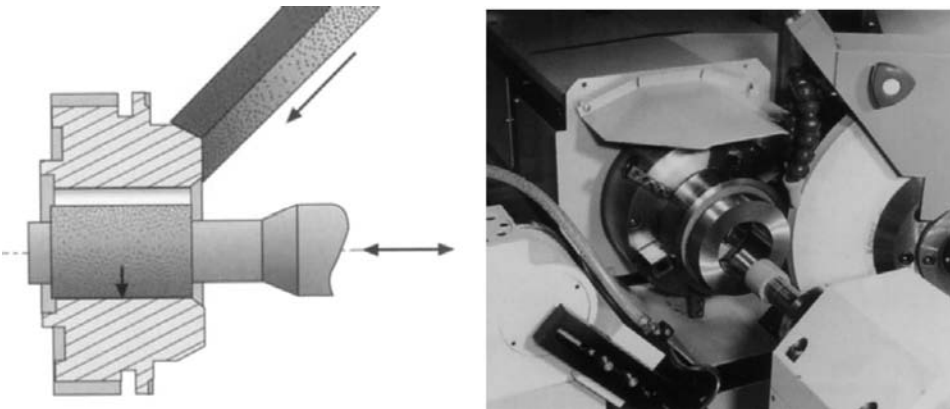


**FIGURE 18.27** Simultaneous grinding of bore and flange. (From BWF. With permission.)

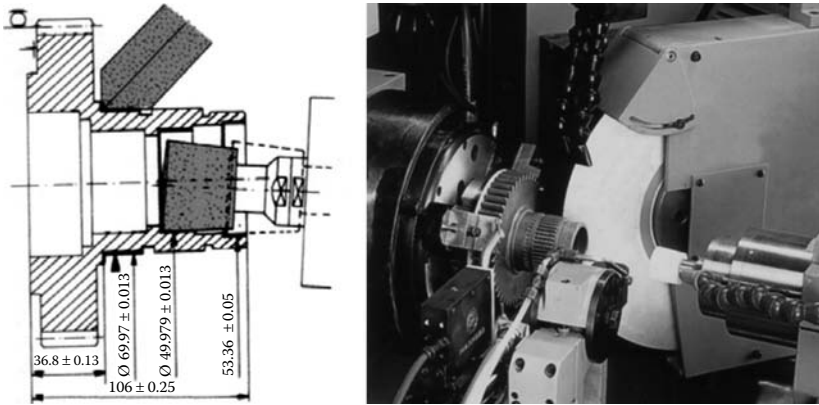


**FIGURE 18.28** Simultaneous grinding of bore, external diameter, and face. (From Danobat 1992. With permission.)

grinders also fall into this category. These can either be assembled on separate linear axes or on turret arrangements that may carry up to four spindles.

More recently, numerous machines have appeared on the market for simultaneously grinding bores and flange/ODs.

Grinder designs will often shift from having independent X- and Z-axis slides to compound slide arrangements to increase the travel range and, hence, range of part sizes. Stacking the axes also allows contouring moves relative to the part *or* dresser. Cycle times are now longer as the slide movements are greater and loading systems have to be flexible or, in many cases, loading is manual. However, they do offer the great advantage to the end user of performing several operations in one chucking.

The last category of machines is the natural result of the consolidation in machine tool manufacturing methods, tighter dimensional tolerancing, and just-in-time (JIT) manufacturing demands. This refers to the combination of machining and grinding in a single chucking. This has been receiving increased impetus since the mid-1990s and has produced some impressive improvements in productivity and capital equipment savings.

Several OEMs have designed vertical spindle machines where the workhead is above the grinding wheel. An example of this from EMAG [2001b] is shown in Figure 18.30. Having the workhead above the wheel allows the part to be loaded by gravity through the spindle into the chuck giving a

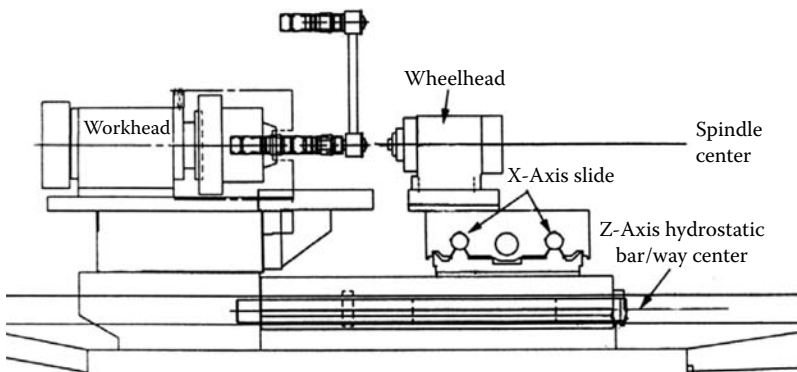


**FIGURE 18.29** Compound slide grinder layout. (From Koepfer 1995. With permission.)





**FIGURE 18.30** Combination grind and turn arrangement with part loading through the vertical workhead. (From EMAG 2001b. With permission.)

load time of 1.5 s. Alternatively, the part is brought on a conveyor into the chuck from below for a load time of about 4 s.

Another example from Campbell uses a conventionally configured vertical spindle grinder for processing gear bores and faces. Originally conceived as a purely grinding operation, the introduction of turning for the gear face reduced cycle time by 70%.

## 18.6 TROUBLESHOOTING

As with any type of grinder when diagnosing problems with an internal grinding process, it is often necessary to go back to basics as for the initial setup of the machine. For internal grinding, the key factor is to ensure there is a straight line of contact between the grinding wheel and the part. There are four principal qualifications:

1. X- and Z-axes must both produce a straight line of motion.
2. The workhead axis must be parallel to the Z-axis.
3. The wheelhead axis must be parallel to the Z-axis and lie in the same plane as the workhead axis.
4. The diamond must lie in the plane established by the wheelhead and workhead axes.

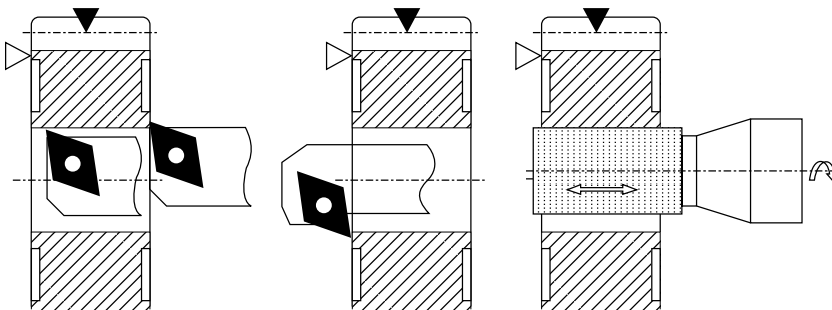


**FIGURE 18.31** Strategy for turning/grinding of gear bore and faces.

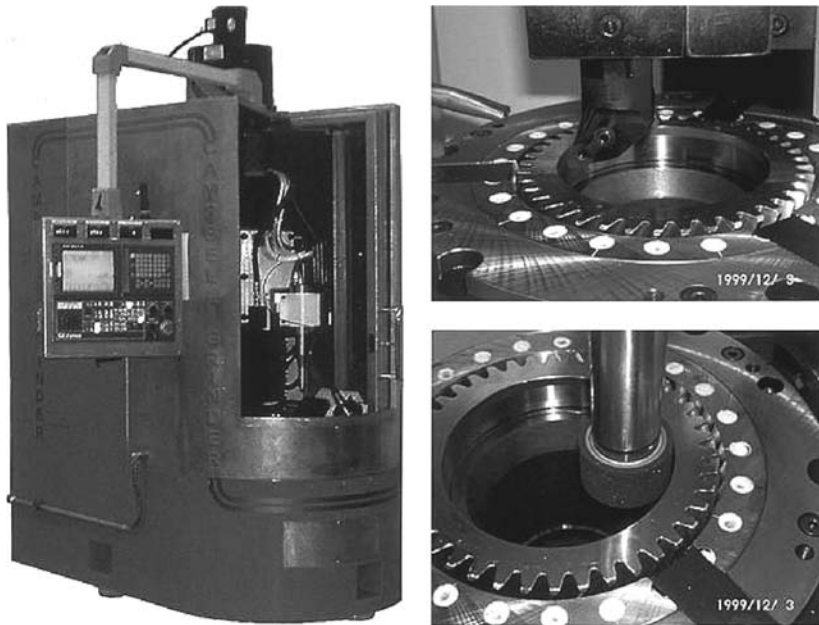


**FIGURE 18.32** Combined grinding and turning machine. (Courtesy of Campbell Grinder. With permission.)

If the X- or Z-axes are not true or are worn the wheel path will not be straight. During dressing, the wheel will be profiled or tapered creating high points in the grind with excessive wear, part taper, and even feed lines. This cannot be corrected by adjusting the wheelhead. A similar problem will occur if the plane of the diamond is incorrect. Bell-mouth is another common problem, which is produced either by worn slides or misalignment of the workhead axis with the wheel path axis. This cannot normally be corrected by reducing the stroke length.

Center height errors were discussed above in terms of the impact on dressing. Another effect is when misalignment of these axes results in the axis of the wheel crossing the centerline of the diamond. In this case, the wheel will be dressed with a hyperbolic shape again resulting in a high point with its attendant problems.

Once these issues are resolved, then the more normal corrective actions can be taken. The most common are

Feed line on workpiece	Dressing problems such as worn or poorly clamped diamond Dresser spindle runout Wheel grade too hard causing loading
Scratching of the part	Wheel too soft or coarse causing grit pullout Poor coolant filtration Wheel speed too slow for wheel grade causing breakdown
Burn	Wheel grade too hard Poor coolant delivery Workspeed too slow Wheel speed too high Wheel infeed rates too high
Wheel glazed	Wheel too hard or too fine Dressing not aggressive enough or diamond is worn

	Too high an oil content in coolant—lower concentration, increase volume (alox wheels)
	Not working the wheel hard enough—increase work and infeed rates
Wheel loaded	Wheel grade too hard or fine
	Dressing not aggressive enough or diamond worn
	Poor coolant/delivery/filtration
	Not working the wheel hard enough—increase work and infeed rates
Bell mouth	Overtravel of wheel
Taper	Wheel breakdown
	Insufficient quill stiffness (CBN—back of part small)
	Wheel not dressed aggressively (CBN—back of part small)
	Incorrect stroke end points for oscillation
Out-of-round bore	Noncleanup
	Overclamping or balance problem with workhead/chuck
	Heat distortion during roughing of face grinding operation
Chatter	Wheel too hard
	Runout or balance issues with quill/wheel/spindle usually after a crash or as wheel bearing fails
	Machine vibrations
	Workspeed too high
	Dresser play, worn diamond
Chipping/cracking	Contamination in incoming parts (shot peen, tumbling media)
	Burrs from turning operation
	Expansion of arbor by temperature curing glue for mounting CBN wheel
	Incorrect rapid approach position for stock level or too high a trip level on gap elimination
	Poor coolant delivery

## REFERENCES

- Anon. 1989. *Anything But the Same Old Grind*. Machine and Tool Blue Book.
- Bahmuller. 1997. "High Precision Internal Grinding with the Modular I-Line." Wilhelm Bahmuller. Pluderhausen, Germany. Trade brochure.
- Bell, W. F. et al. 1988. "Practical Achievement and Monitoring of High Rate Internal Grinding – Part 1 – Machine Instrumentation and Data Acquisition." 3rd International Grinding Conference, Wisconsin. SME MR88-611.
- Bryant. 1995. "The Ultraline UL2 High Speed Grinding Machine." Bryant Grinder Corp, Springfield, VT. Trade brochure.
- Danobat. 1992. "Gear Box – Grinding Machines Gear Grinding." Danobat S Corp, Elgoibar, Spain. Trade brochure.
- Drake. 2000. "GS:1 Internal Grinding System Specifications." Drake Manufacturing, Warren, OH. Trade brochure.
- EMAG Reinecker. 2001a. "Internal Grinder ISA 103 CNC, ISA 102 CNC." Reinecker Karstens Corp., Neu-Ulm, Germany. Trade brochure.
- EMAG Reinecker. 2001b. "VG 110 Vertical Grinding Center, Vertical Turning and Grinding Center." EMAG Maschinenfabrik GmbH, Salach, Germany. Trade brochure.

- Hahn, R. 1997. "Microangling/Force – Sensing Subplate Raises Internal Grinding Precision." *Abrasives Mag.* Dec/Jan.
- Hahn, R. S. 1999. "Trouble Shooting Dressing and Grinding Problems in Precision Internal Grinding Operations." *Abrasives Mag.* Mar/April.
- Hahn, R. S. 2000. "PC-Control Sensors for Production I D Grinding." *Abrasives Mag.* Dec/Jan.
- Hahn, R. S. and Labby, P. 1995a. "Deflection Compensation Stops Bore Taper." *Am. Mach.* June.
- Hahn, R. S. and Labby, P. 1995b. "Normal Force Sensors Raise Internal Grinding Productivity." 1st International Machining and Grinding Conference, Michigan. SME MR95-180.
- Inasaki, I. 1991. "Monitoring and Optimisation of Internal Grinding Process." *Ann. CIRP* 40, 1.
- Koepfer, C. 1995. "Production I D Grinding – Change in the Wind?" *Mod. Mach. Shop* Dec.
- Longanbach, D. M. and Kurfess, T. R. 1998. "Real-Time Measurement for an Internal Grinding System." NAMRC 26, May 19, Georgia. SME MS98-261.
- Matson, C. B. et al. 1990. "Practical Achievement and Monitoring of High Rate Internal Grinding – Part 2 – Evaluation of Collected Data." 4th International Grinding Conference, Michigan. SME MR90-08.
- Micron. 2000. "Super Precision Internal Grinder MIG-101." Micron Machinery, Yamagata, Japan. Trade brochure.
- Okuma. 1996. "GI 20N CNC Internal Grinder." Okuma Corp, Aichi, Japan. Trade brochure.
- Okuma. 2000. "CNC Internal Grinder for Mass Production GI-10N." Okuma Corp, Aichi, Japan. Trade brochure.
- Salmon, S. C. 1984 *Abrasive Machining Handbook*. Korber AG, Germany.
- Studer. 2001. "Process Optimization for Internal Cylindrical Grinding." *Motion* – Trade magazine for Schleifring, Sept.
- Toyo. 2000. T-11L Series CNC Internal Grinding Machines." Toyo Advanced Technologies, Hiroshima, Japan. Trade brochure.
- Toyo. n.d. "T-117 CNC T-157CNC CNC Internal Grinding Machine." Toyo Advanced Technologies, Hiroshima, Japan. Trade brochure.
- UVA. n.d. "UVA U80/U88 for Internal Grinding of Small to Medium Size Workpieces." UVA International AB, Bromma Sweden (includes GPC-PSH system). Trade brochure.
- Vaillette, B. D. et al. 1991. "CBN – Adaptive Grinding." Superabrasives' 91 Conference Proceedings. SME Chicago, IL.
- Voumard. n.d. "Grinding Machines." Voumard Machines Co SA, Jardiniere, Switzerland, Commercial brochure.
- Xiao, G. and Malkin, S. 1996. "On-Line Optimization for Internal Plunge Grinding." *Ann. CIRP*.



---

# 19 Centerless Grinding

## 19.1 THE IMPORTANCE OF CENTERLESS GRINDING

Centerless grinding is used for fast production and high accuracy. The process is best for larger batches where set-up times are small compared to machining time. Small rollers and needles, for example, are machined to close tolerances in quantities of millions by through-feed centerless grinding.

Batch quantities do not need to be large to be cost-effective. Set-up times can be reduced with appropriate set-up fixtures. An advantage of centerless grinding is that center holes are not required for the purpose of location. Location of the workpiece during machining is provided from the newly machined surface itself. This eliminates a production operation and saves cost. It also avoids shape errors associated with out-of-roundness of the center holes. Another advantage is that the workpiece does not need to be clamped to a drive device. This saves time, and accuracy is improved since driving devices are a source of errors.

The range of workpieces and materials produced by centerless grinding is wide. Notable examples include:

- Steel bar stock
- Needles
- Ball and roller bearings
- Bearing rings
- Glass rods
- Plastic rods
- Bottle corks
- Uranium rods
- Formed valve spools
- Axles
- Valve stems

Centerless grinding is used for rapidly cleaning up, roughing, and finish grinding. Workpieces may be straight or formed cylindrical shapes. Workpiece surfaces can be either internal or external cylindrical shapes. The process is often automated with barrel vibration feeders or other devices using sequential pneumatics, hydraulics, or robots. This means that machines can continue production with minimal supervision.

The following list features characterizing the efficiency of the process and factors that make these features possible.

<b>Feature</b>	<b>Associated Factor</b>
Sometimes faster than turning	Wide grinding wheel
Long wheel life	Large-diameter wheel
Fast loading and unloading	Clamping unnecessary
Accuracy	Center errors avoided
Hard materials machined	Very hard wheel grits

## 19.2 BASIC PROCESS

### 19.2.1 EXTERNAL CENTERLESS GRINDING

Centerless grinding is compared with between-centers grinding in Figure 19.1. In center grinding, the workpiece is located on center by means of center holes drilled in the workpiece. In centerless grinding, the workpiece is located on the workpiece perimeter. This can be a significant advantage for achieving part roundness. However, if the set-up geometry is wrong it can lead to poor roundness.

Figure 19.1a shows a plan view of external center grinding. The workpiece is mounted between centers and usually the drive is by a driving dog attached to the workpiece. The rotational speed is controlled by a workhead spindle drive.

This contrasts with the arrangement for centerless grinding shown in Figure 19.1b. In centerless grinding, the workpiece is pushed against the grinding wheel by a control wheel, often known as a regulating wheel. The workpiece is supported underneath by a workrest as in Figure 19.2a.

A control wheel controls workspeed by friction. In normal operation, the workpiece has the same surface speed as the control wheel. The advantage of this is simplicity. The workpiece is pushed into the grinding position with no requirement for clamping. Plunge grinding and through-feed grinding operations may be performed as described in later sections.

### 19.2.2 APPROXIMATE GUIDE TO WORK-HEIGHT

The workpiece center in Figure 19.2a is usually higher than the grinding wheel and control wheel centers. This is because the height of the workpiece is set above center to achieve a rounding action as described later.

An approximate guide to work-center height is

$$h_w = \frac{1}{16} \cdot \frac{1}{\left[ \frac{1}{d_s + d_w} + \frac{1}{d_c + d_w} \right]} \tag{19.1}$$

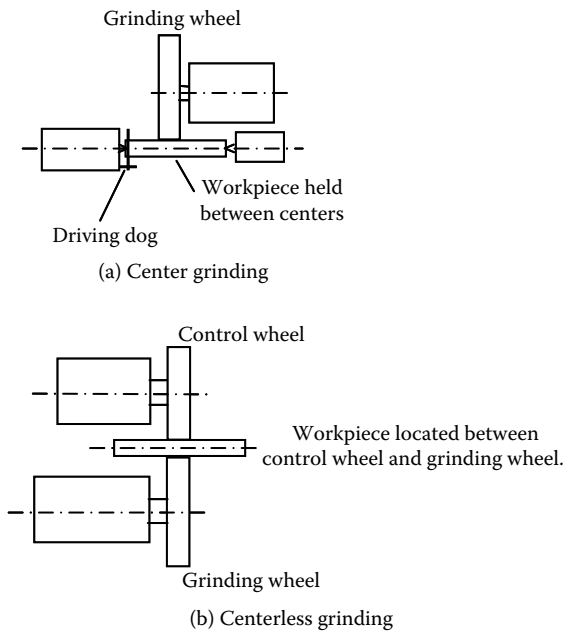
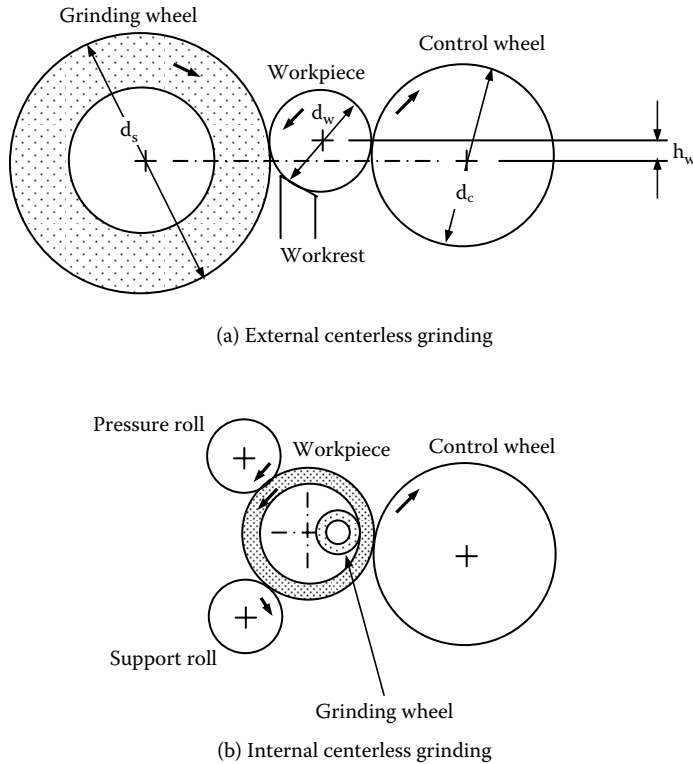


FIGURE 19.1 Workholding in center grinding and centerless grinding.



**FIGURE 19.2** Basic centerless grinding processes.

where  $d_s$  = grinding wheel diameter,  $d_c$  = control wheel diameter, and  $d_w$  = workpiece diameter.

It should be emphasized that Equation 19.1 is only an approximate guide. Detailed guidance on set-up values is given in sections below.

**19.2.3 INTERNAL CENTERLESS GRINDING**

Internal centerless grinding is illustrated in Figure 19.2(b). In the example shown, a control wheel and a support roll locate and support the workpiece. A pressure roll is used to firmly hold the workpiece against the support roll and the control wheel. In this setup, the external diameter needs to be ground prior to the internal diameter. The external surface becomes the reference for concentricity and roundness.

Using the process illustrated, an internal bore can be ground without the need to clamp the workpiece as required in conventional internal grinding.

**19.2.4 SHOE CENTERLESS GRINDING**

Shoe centerless grinding is used for workpieces of short length-to-diameter ratio. Shoe centerless grinding is illustrated in Figure 19.3. Figure 19.3(a) shows an arrangement for external shoe grinding and Figure 19.3(b) shows an arrangement for internal shoe grinding. The workpiece is located axially by a magnetic drive-plate. The workspeed is controlled by the speed of the magnetic drive-plate.

**19.2.5 ROUNDNESS AND ROUNDING GEOMETRY**

The rounding action in centerless grinding depends on the set-up geometry. The set-up geometry is illustrated in Figure 19.4. Angle  $\alpha$  and angle  $\beta$  have a strong effect on rounding action [Dall 1946].



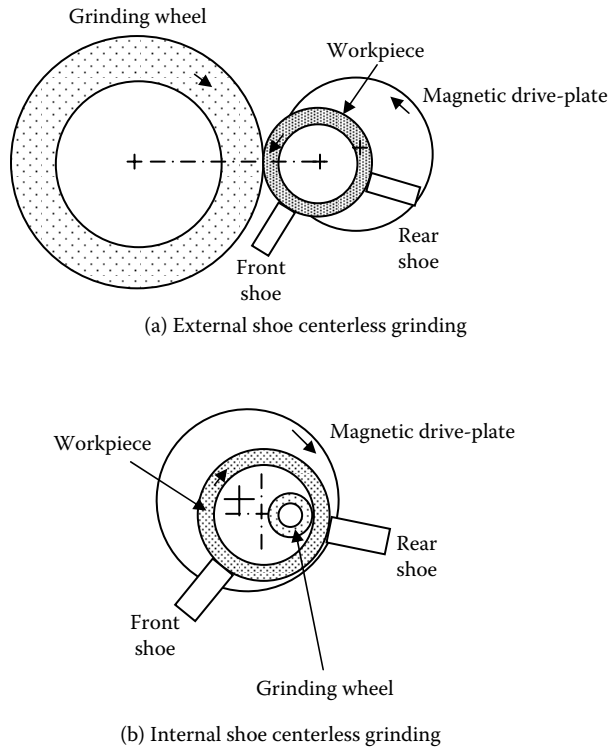


FIGURE 19.3 Shoe centerless grinding.

Angle  $\beta$  is termed the tangent angle. The angles depend on the work-height,  $h_w$ , and the workrest angle,  $\gamma$ , as given below. Good roundness in centerless grinding requires the use of appropriate values of these angles. It is, therefore, advisable to plan a procedure to ensure the required values can be quickly set up and checked. Typical values are

$$\gamma = 30^\circ$$

$$\beta = 6 - 8^\circ$$

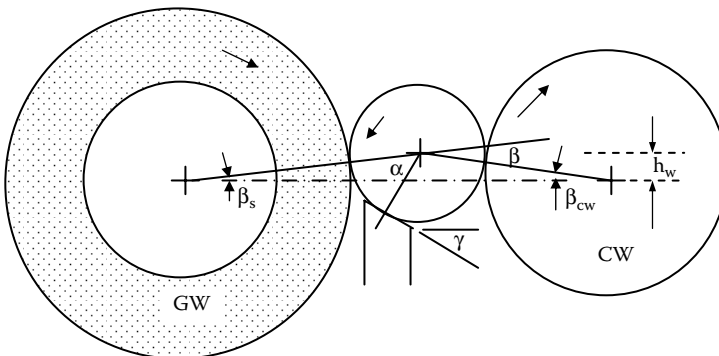


FIGURE 19.4 Rounding geometry.

Angle  $\alpha$  and angle  $\beta$  are related to work-height and workrest angle as follows:

$$\alpha = \frac{\pi}{2} - \gamma - \beta_s \tag{19.2}$$

$$\beta = \beta_s + \beta_{cw} \tag{19.3}$$

where

$$\beta_s = \sin^{-1} \left( \frac{2 \cdot h_w}{d_s + d_w} \right) \tag{19.4}$$

$$\beta_{cw} = \sin^{-1} \left( \frac{2 \cdot h_w}{d_{cw} + d_w} \right) \tag{19.5}$$

The work-height corresponding to a required angle  $\beta$  less than  $10^\circ$  is, therefore, given by

$$h_w = \frac{\beta}{2 \cdot \left[ \frac{1}{d_s + d_w} + \frac{1}{d_{cw} + d_w} \right]} \tag{19.6}$$

where  $\beta$  is expressed in radians.

Centerless grinding conducted under best conditions is extremely accurate. Under nonoptimal conditions, involving vibrations and poor set-up geometry, the process may not produce round work. The analysis of roundness in centerless grinding is discussed in Section 19.10. In summary, odd-order lobing, 3, 5, 7... lobes, is not easily removed with values of tangent angle less than  $4^\circ$ . With larger values of tangent angle, there is a danger of higher order even and odd lobing.

Figure 19.5 illustrates experimental rounding results for tangent angles in the range,  $\beta = 0-10^\circ$  with a  $20^\circ$  workrest and a  $30^\circ$  workrest. The results were obtained by grinding workpieces on which a flat had been previously ground along the length to create a controlled initial error. The depth of the flat was  $9.2 \mu\text{m}$ . The controlled initial error on the workpieces allowed rounding tendencies to be precisely determined for each setup. The optimum range for tangent angle was found to be 6 to  $8^\circ$  with a  $30^\circ$  workrest. Smaller and larger tangent angles reduced the rounding tendency. A  $20^\circ$  workrest led to instability at a  $10^\circ$  tangent angle. The  $30^\circ$  workrest was more stable than a  $20^\circ$  workrest.

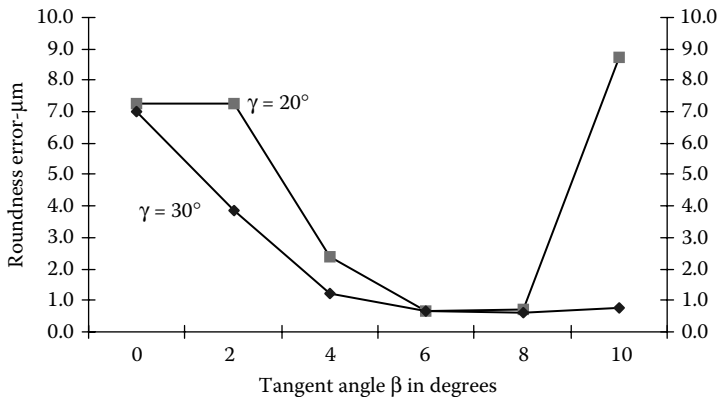


**FIGURE 19.5** Roundness errors measured after grinding a workpiece with a flat; initial roundness error  $9.2 \mu\text{m}$ .

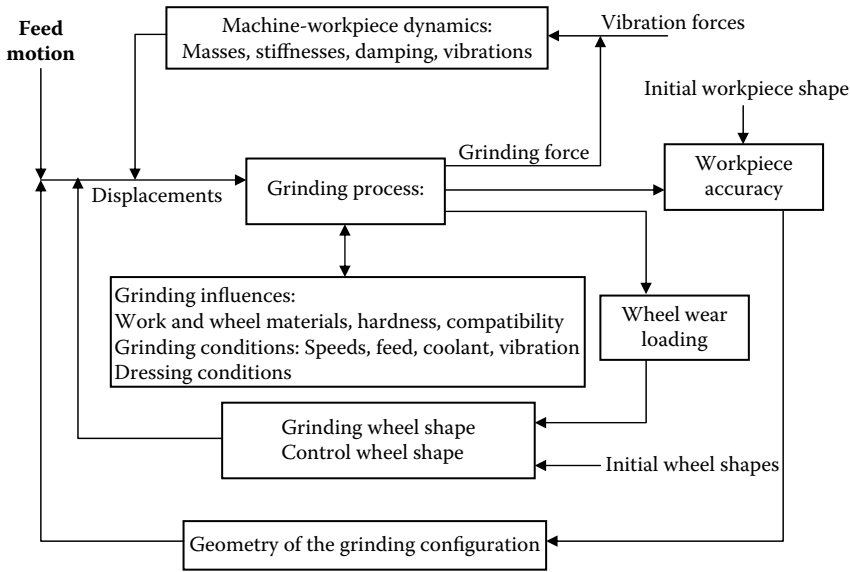


FIGURE 19.6 System interactions and accuracy in centerless grinding.

It has been suggested that low roundness errors can be obtained by varying the set-up angles during the grinding operations [Harrison and Pearce 2004]. For example, a larger tangent angle may be employed for rough grinding to eliminate odd-order lobing and a smaller tangent angle for finish grinding.

### 19.2.6 SYSTEM INTERACTIONS

A machining process is an interaction of geometric, kinematic and dynamic, physical, chemical, and tribological phenomena. It is not necessary to fully understand all these interactions to achieve a satisfactory process, but it is necessary to be aware of the factors that can influence the outcome and seek to determine best practice for each part of the system. For a better understanding of system interactions, the reader is referred to *Tribology of Abrasive Machining Processes* by Marinescu et al. [2004].

Examples of the influences on centerless grinding accuracy are illustrated in Figure 19.6. The input to the process is viewed as the feed motion and the output as workpiece shape and quality. Quality is defined by size, roughness, roundness, straightness, surface integrity, etc. For high accuracy work, there are many factors that determine accuracy and quality. For example,

- Accuracy of the machine setup affects parallelism and size accuracy
- The shape of the grinding wheels affects roundness
- Wheel dressing affects surface roughness
- The composition of the grinding wheel affects grinding forces, process stability, wheel wear, temperature rise, and surface integrity
- Wheel wear affects consistency of size accuracy
- Rounding geometry affects elimination of out-of-roundness (OOR)
- Friction affects speed control
- Process fluid (coolant) affects cooling, flushing, process lubrication, and avoidance of wheel loading
- Machine and workpiece dynamics affect process stability and avoidance of vibrations
- Rotating masses, motors, drive belts, and feed-drives affect forced vibrations.

So far, discussion has been limited to accuracy and quality. There will also be concern for productivity and costs. Productivity is the rate at which goods can be produced to specified quality levels. Productivity and costs are closely related.

An improvement in accuracy capability of a machine is usually accompanied by higher productivity. This is because the manufacturer works to specified tolerances and quality levels. If the machine is capable of better quality, the manufacturer can increase the rate of production and remain safely within tolerances. The manufacturer also seeks to reduce process costs for specified quality levels. This can often be achieved by increasing wheel speed, changing to high-performance abrasives, improved machine structures, improved feed cycles, and improved control systems. The following sections discuss relevant aspects for optimizing system performance.

### 19.3 BASIC RELATIONSHIPS

The basic relationships for parameters such as removal rate, power, and grinding conditions are not in every case the same as for grinding between centers. The basic relationships for centerless grinding are as follows.

#### 19.3.1 DEPTH OF CUT

The real depth of cut at the commencement of grinding is less than expected because of machine and system deflections. With uniform infeed, depth of cut and deflections build up to a steady value. The steady value of real depth of cut is

$$a_e = \frac{v_f}{2 \cdot n_w} = \frac{1}{2} \cdot \pi \cdot d_w \cdot \frac{v_f}{v_w} \quad (19.7)$$

where  $v_f$  is the infeed rate,  $n_w$  is the work rotational speed,  $d_w$  is the work diameter, and  $v_w$  is the workspeed.

It is important to include the factor of one half. This factor arises because feed is relative to the workpiece diameter. As the workpiece diameter reduces, the workpiece center retreats from the grinding wheel so that the depth of cut is halved. The depth of cut is necessary for determination of removal rate.

#### 19.3.2 REMOVAL RATE

The rate material is removed from the workpiece is given by

$$Q_w = a_e \cdot b \cdot v_w \quad (19.8)$$

It is more useful when assessing the overall efficiency of material removal to consider specific removal rate. Specific removal rate is the removal rate per unit width of contact of the grinding wheel.

$$Q'_w = \frac{Q_w}{b} \quad (19.9)$$

#### 19.3.3 POWER

In many cases, power can be measured directly from the machine. If there is provision for measurement of tangential grinding force on a machine, power can be derived from

$$P = F_t \cdot v_s \quad (19.10)$$

where  $F_t$  is tangential grinding force and  $v_s$  is the grinding speed.

### 19.3.4 SPECIFIC ENERGY

The grinding energy to remove a volume of material is a measure of the efficiency of material removal. The specific energy is given by

$$e_c = \frac{P}{Q_w} \quad (19.11)$$

Specific energy is a measure of the difficulty of grinding a work material under particular grinding conditions. Hard materials give rise to higher specific energy than soft materials. Typical values of specific energy range from 10 to 200 J/mm<sup>3</sup> of material removed. Lower and higher values than these are possible. A value of 10 J/mm<sup>3</sup> represents an easy-to-grind material with very efficient grinding conditions. A value of 200 J/mm<sup>3</sup> is typical of many finishing operations at lower process efficiency.

The process engineer, having established a database for particular materials and grinding wheels, uses specific energy to determine machine power requirements and machining rates.

### 19.3.5 CONTACT LENGTH

The total contact length is due to contact force and grinding geometry. Geometric contact length must be added to dynamic contact length according to:

$$l_c^2 = l_g^2 + l_f^2 \quad (19.12)$$

#### 19.3.5.1 Geometric Contact Length

The geometric contact length, based on the undeformed shape of the grinding wheel, depends on the depth of cut.

$$l_g = \sqrt{a_e \cdot d_e} \quad (19.13)$$

where the effective grinding wheel diameter is given in Section 19.3.6.

#### 19.3.5.2 Dynamic Contact Length

Dynamic contact length depends on the force between the grinding wheel and the workpiece in the same way that contact area between an automobile tyre and the road depends on the weight of the automobile. Dynamic contact length is given by Rowe, Morgan, and Qi [1993].

$$l_f = \sqrt{\frac{8 \cdot R_r^2 \cdot F_n \cdot d_e}{\pi \cdot b \cdot E^*}} \quad (19.14)$$

where  $R_r$  is a roughness factor that depends on the roughness of the grinding wheel. Typically,  $R_r$  is of the order of 10.  $F_n$  is the normal grinding force,  $b$  is the width of contact and is usually equal to the width of the grinding wheel or the length of the workpiece.  $E^*$  is the effective modulus of elasticity of the grinding wheel and the workpiece materials. The value is given by

$$\frac{1}{E^*} = \frac{1 - \nu_1^2}{E_1} + \frac{1 - \nu_2^2}{E_2} \quad (19.15)$$

### 19.3.6 EQUIVALENT GRINDING WHEEL DIAMETER

The grinding process is affected by the equivalent grinding wheel diameter. The effective diameter in internal grinding is much greater than in external grinding even though internal grinding wheels are normally much smaller than external wheels. Equivalent diameter is defined as the wheel diameter that gives the same contact condition as in flat surface grinding. The equivalent diameter is based on the relative curvature of the two surfaces in contact.

$$\frac{1}{d_e} = \frac{1}{d_s} \pm \frac{1}{d_w} \quad (19.16)$$

The negative sign applies for internal centerless grinding. Due to the conformity in internal grinding, a softer grinding wheel is required to withstand the increased length of contact and the consequent increase in rubbing contact. The longer geometric contact length increases rubbing wear and tends to cause the wheel to glaze.

### 19.3.7 EQUIVALENT CHIP THICKNESS

Equivalent chip thickness is a measure of the depth of penetration of the abrasive grains into the workpiece. Equivalent chip thickness is given by

$$h_{eq} = a_e \cdot \frac{v_w}{v_s} \quad (19.17)$$

Equivalent chip thickness is the thickness of the layer of workpiece material removed at wheel speed. Since the speed ratio is typically 100, the thickness of the layer removed at wheel speed is approximately one hundredth of the thickness of the layer removed at workspeed. With 0.05 mm depth of cut, equivalent chip thickness is typically 0.5  $\mu\text{m}$ .

In practice, depth of penetration of the abrasive grains into the workpiece varies over a much greater range due to variable spacing between grains, variable depth of grains below the wheel surface, and surface roughness. A rough worn grinding wheel causes much greater grain depths than the same wheel freshly dressed. However, equivalent chip thickness is useful for comparing grain penetration for different grinding operations using a similar abrasive structure.

### 19.3.8 GRINDING RATIO

Grinding ratio is a measure of the suitability of an abrasive for a particular grinding operation. Grinding ratio is defined as:

$$G = \frac{\text{Volume of material removed in grinding}}{\text{Volume of material removed from the grinding wheel}} = \frac{V_w}{V_s} \quad (19.18)$$

Hard work-materials and interrupted cutting operations tend to reduce the grinding ratio. In precision grinding with easy-to-grind materials, a G-ratio of 5,000 or more may be achieved. However, for a difficult-to-grind material operating under adverse conditions, the G-ratio may drop to 1. In adverse conditions, it may be important to increase wheel speed to increase G-ratio.

## 19.4 FEED PROCESSES

### 19.4.1 PLUNGE FEED

In plunge-feed grinding, the workpiece is fed in a radial direction toward the grinding wheel as shown for a stepped shaft in Figure 19.7. In the example shown, the operation simultaneously grinds two diameters. The plunge feedrate,  $v_f$ , is the speed of radial approach.

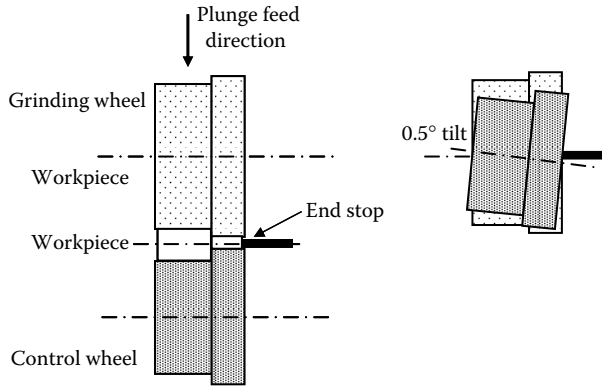


**FIGURE 19.7** Plunge feed of a stepped shaft. The control wheel is tilted 0.5 to 1° to locate the workpiece against the end stop.

Plunge feed may be implemented either through a grinding wheelhead slideway or through a control wheelhead slideway. Larger machines have slideways for both wheelheads for convenience of machine setting. Often, it is convenient to feed the control wheel with both the grinding wheel and the workrest remaining fixed in position. When the feed slide is fully retracted, clearance is created between the control wheel and the workrest. On retraction, the workpiece rolls down the workrest to a chute. This allows ease of workpiece unloading from the machining position. The workpiece can be removed either manually or by an automated device.

A plunge-feed cycle may consist of several phases as illustrated in Figure 19.8. After loading the workpiece, the grinding wheel makes a rapid approach to take up the clearance between the grinding wheel and the workpiece. At a small distance from the workpiece, rapid approach is ceased and speed is reduced to a fast grinding feedrate. The fast feedrate may remove between half and 80% of the stock to be removed. Feedrate is then switched to a slow feedrate in order to improve roundness, reduce roughness, and bring the workpiece close to finish size.

As the feed movement reaches the position for finish size, the feed is stopped and there is a period of dwell. The purpose of the dwell is to allow “spark-out.” During dwell, the process produces sparks for a few seconds or longer due to the elasticity of the machine and grinding wheels. The purpose of spark-out is to allow the deflections of the machine and grinding wheels to spring back and to allow the grinding force to decay to a low level.

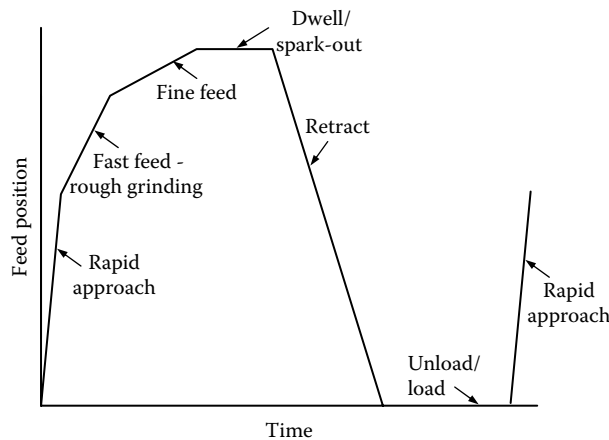


**FIGURE 19.8** A plunge-feed cycle.

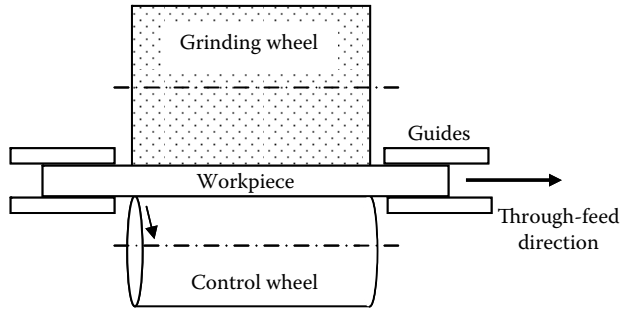


FIGURE 19.9 Through-feed grinding.

Spark-out is very important for size accuracy, roundness, and low roughness. After spark-out, the wheel is smoothly retracted to allow unloading of the workpiece and reloading of the next workpiece.

Intermediate feed-cycle changes and final retraction may be signaled to a computer numerically controlled (CNC) controller using in-process size gauging of the workpieces. A size gauge indicates when a programmed size has been reached and the next phase of the feed cycle is triggered. When the final size has been reached, the system retracts the feed-drive. For this system to work effectively, the system has to establish a relationship between feed axis position and workpiece size. This relationship is set up as part of the initial setting procedure. Usually, automatic compensation will be made for grinding wheel wear and grinding wheel dressing.

An alternative to spark-out is the use of a very fine feedrate. The use of a very fine feedrate ensures that the workpiece reaches finish size without significant delay. The grinding wheel tends to act slightly softer when using a very fine feedrate instead of a dwell.

### 19.4.2 THROUGH-FEED

In through-feed grinding, the grinding wheel is set at a fixed distance from the control wheel as in Figure 19.9. Through-feed is employed for longer workpieces and also for a continuous stream of short workpieces. In most cases, the length-to-diameter ratio of the workpieces is greater than one.

The workpiece is fed between guide plates into the space between the grinding wheel and the control wheel. The axis of the control wheel is inclined at a small angle,  $\Phi$ , to the horizontal so that the axial component of the control wheel speed drives the through-feed motion. The rate of through-feed depends on the angle of inclination of the control wheel.

The surface speed of the workpiece in stable grinding is normally equal to the surface speed of the control wheel. Differences in workpiece and control wheel surface speed are usually negligible. The resultant workspeed,  $v_r$ , can be resolved into two components. By convention, the slowest component of workspeed is termed the feed speed,  $v_f$ , and the fastest component is termed the workspeed,  $v_w$ . The workspeed is, therefore, the circumferential component of the resultant workspeed and the through-feed speed is the axial component.

$$v_w = v_r \cdot \cos \Phi \quad (19.19)$$

The surface speed of the control wheel has a horizontal axial component that provides the axial feedrate of the workpiece otherwise known as the through-feed speed:

$$v_f = v_r \cdot \sin \Phi \quad (19.20)$$

where  $\Phi$  is the angle of inclination and  $v_f$  is the feedrate.



## 19.5 CENTERLESS WHEELS AND DRESSING GEOMETRY

### 19.5.1 THE GRINDING WHEEL

Centerless grinding wheels tend to be larger in diameter and wider than in center grinding. This means there are many more cutting edges available for grinding. Since the cutting action is shared between many more abrasive grains, wheel life between dressing operations tends to be greatly increased. This makes for economic production with little need to interrupt the process for redressing.

Most often, the type of abrasive used for the grinding wheel is vitrified aluminum oxide or silicon carbide. Other types of abrasive may be used, but the vast majority of operations are undertaken with one or other of these two conventional abrasives. These abrasives are inexpensive compared to superabrasives and it is, therefore, reasonable to experiment with different wheels until an optimum wheel specification is achieved. There are many variations of wheel specification and abrasive types used in centerless grinding. The selection of a particular wheel will depend strongly on compatibility with the work material, work-material hardness, the roughness limit, and factors such as size tolerance and risk of thermal damage.

Recent developments in conventional abrasives include monocrystalline grains for greater fracture resistance, sol gel grains that are designed to wear by microfracture while remaining sharp, and high-aspect-ratio grains designed to remain sharp even with heavy wear.

For special operations where extremely high accuracy and low workpiece roughness are required, alternative types of wheel can be used in keeping with modern grinding technology. For example, it is possible to grind ceramics using metal-bond diamond wheels with electrolytic in-process dressing (ELID). For low-temperature grinding of ferrous materials, vitrified cubic boron nitride (CBN) abrasive is increasing in use for center and surface grinding. Vitrified CBN wheels can also be applied in centerless grinding. When using CBN, significant advantages can be obtained but it is important to pay careful attention to CBN grinding technology [Marinescu et al. 2004]. CBN is notable for its natural hardness and high thermal conductivity. Both properties are ideal for grinding.

### 19.5.2 GRINDING WHEEL DRESSING

“Dressing” is a term that commonly includes truing the grinding wheel to achieve a true form and dressing to achieve a suitable cutting edge distribution and sharpness. “Conditioning” is another term used for preparation of a grinding wheel particularly in the case of CBN. Conditioning as a term is used in different ways in different contexts. Conditioning a CBN wheel is often taken narrowly to mean a post-truing operation to open up the wheel surface by using a dressing stick or by machining an easy-to-grind material for a short period prior to grinding workpieces. Conditioning is sometimes used as a general term to include truing and dressing.

Examples of truing a grinding wheel are illustrated in Figure 19.10. The first example shows a truing movement to produce a stepped grinding wheel. The dressing tool is inclined to allow the diameter and the face of the grinding wheel to be trued.

The second example is for through-feed grinding. A small taper is trued on the lead-in area of the grinding wheel to spread the main stock removal over a greater area of the wheel. Without the taper, the main stock removal will be concentrated on the leading edge of the wheel causing rapid wear in this area. It is not absolutely essential to include a lead-in taper because a taper automatically develops as a consequence of rapid wheel wear in the region of rapid stock removal. As wear develops, the taper spreads across the surface of the wheel. However, it is sometimes considered good practice to dress a lead-in taper to provide a more controlled wheel wear process and prevent the possibility of scroll marks from the leading edge of the wheel.

Dressing is primarily important for the accuracy of the grinding wheel profile. Dressing is also important for the effectiveness and economics of the grinding process. Figure 19.11 compares roughness and process power for two different dressing tools. One was a single-point diamond tool.

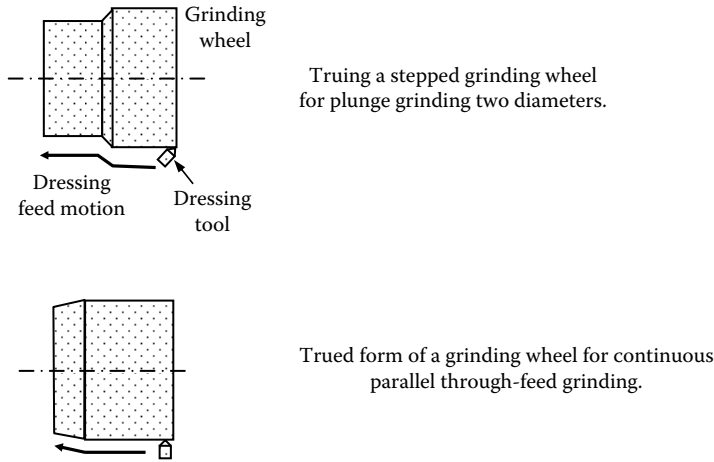


FIGURE 19.10 Examples of dressing operations for plunge and through-feed grinding.

The other was a multipoint impregnated-diamond dressing tool. The two dressing tools give basically similar results although in this example, the sharp single-point diamond yielded lower workpiece roughness after grinding and lower grinding power. A single-point diamond that is allowed to become blunt leads to higher grinding power and poor surface roughness.

The dressing traverse rate is seen to be important. Dressing at a higher rate increases the roughness of the grinding wheel leading to higher workpiece roughness and lower grinding power. This allows faster grinding rates.

### 19.5.3 THE CONTROL WHEEL

The control wheel is usually a rubber bond wheel. The rubber bond allows the regulating wheel to fulfill three important functions. These are to provide sufficient friction for speed control, to provide sufficient flexibility for error averaging, and to provide a surface that can be easily machined to provide accurate positioning. The rubber bond satisfies each of these requirements.

For multidiameter work, the control wheel must be stepped. The step height on the regulating wheel must match the step height on the workpieces to ensure support for the workpiece along an adequate proportion of the length. Normally, support will be provided along the entire length of the workpiece.

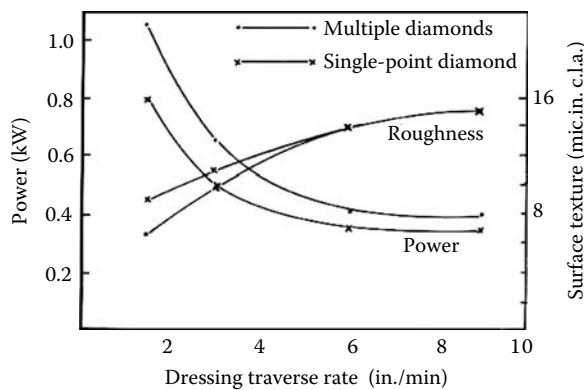


FIGURE 19.11 Effect of dressing traverse rate on power and workpiece roughness.

Angular adjustment of the control wheelhead may be provided in the horizontal plane. This adjustment is convenient for achieving parallel setup and elimination of small workpiece taper errors.

Angular adjustments should also be provided in the vertical plane for provision of an axial feed force. This introduces a further requirement for dressing feed angular adjustments to achieve the necessary control wheel profile as discussed in the next section.

## 19.5.4 CONTROL WHEEL DRESSING

### 19.5.4.1 Dressing Geometry

The axis of the control wheel is inclined at an angle,  $\Phi$ , sufficient to provide traction in the axial direction. A small angle is employed for plunge grinding and a larger angle for through grinding as explained previously. This means the axis of the control wheel is not parallel with the axis of the workpiece. If the control wheel is dressed as a straight cylinder, the angle means there is point contact between the workpiece and the control wheel instead of line contact. Clearly, point contact will not ensure correct positioning of the workpiece parallel to the grinding wheel axis.

Line contact can be ensured between the control wheel and workpiece by dressing the control wheel along the required line of contact. A similar result can be achieved by dressing the control wheel parallel to the required line of contact but directly opposite in the same horizontal plane. This is illustrated in Figure 19.12.

The dressing tool must be set at a height,  $h_d$ , that is related to the work center-height,  $h_w$ . The dressing height is

$$h_d = h_w \cdot \frac{d_c}{d_c + d_w} \quad (19.21)$$

The control wheel is no longer a true cylinder when tilted at an angle,  $\Phi$ , and trued at a height,  $h_d$ . It becomes an hyperboloid. The shape of the control wheel is shown schematically in Figure 19.13. The line of contact corresponds to the line of truing. Truing defines the diameter at each section of the control wheel. As the tool traverses across the control wheel, the height of the tool becomes higher relative to the center of the wheel. This increases the diameter of the wheel. The control wheel becomes larger at the low end of the wheel than at the other and satisfies the requirement that the workpiece is supported on a parallel line of contact with the grinding wheel.

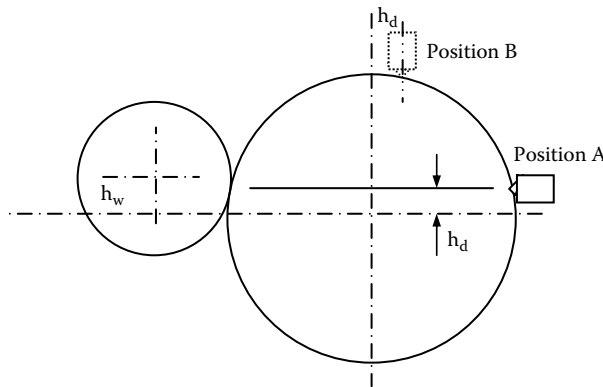


**FIGURE 19.12** The control wheel is dressed at an offset height  $h_d$  to ensure line contact with the workpiece. Dressing may be carried out parallel to the line of contact at Position A or at an angle to the line of contact at Position B.

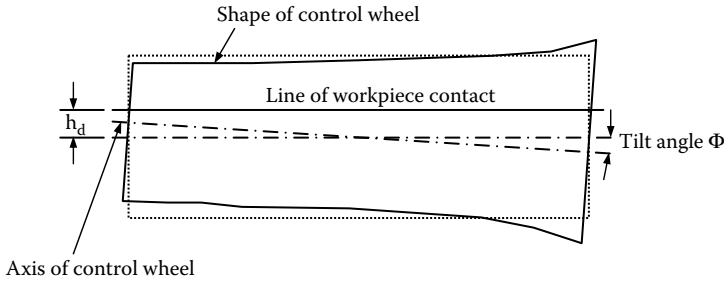


**FIGURE 19.13** The control wheel dressed at an angle and above center.

If the dressing is carried out at Position B in Figure 19.12, it is necessary to make additional adjustments for the angles involved. The dressing slide must be rotated relative to the plane of the line of contact by an angle approximately equal to the angle of tilt. The required rotation is made in a plane parallel to the tangent to the control wheel at the point of contact with the dressing tool. An adjustment is made to the angle for larger diameter workpieces. The dressing angle for Position B as given by Jessup, in the book by King and Hahn [1986], is

$$\Phi_d = \frac{\Phi}{\sqrt{1 + d_w/d_c}} \tag{19.22}$$

**19.5.4.2 Control Wheel Runout**

Hashimoto, Kanai, and Miyashita [1983] demonstrated a major source of errors in centerless grinding is due to runout of the control wheel. To prove this point, the workrest assembly was removed to allow the control wheel to be advanced up to the grinding wheel. By this means, the control wheel was dressed by the grinding wheel with much greater precision than possible by the normal method of dressing.

It was found that roundness errors were reduced from 1.7 to 0.2 μm with high-precision dressing and surface roughness was reduced from 0.32 to 0.12 μm Ra. It was also found that the new dressing method gave the control wheel increased wear resistance. This result has been confirmed by experiments conducted by the author.

**19.6 THE WORKREST**

The support surface of a workrest should be harder than the workpiece. The workrest also has to be tough and capable of withstanding the knocks encountered on the factory floor. The wear-resistant surface of the workrest is selected according to the types of work material ground. For steels, tungsten carbide inserts provide a suitable surface. A typical tipped workrest is illustrated in Figure 19.14.

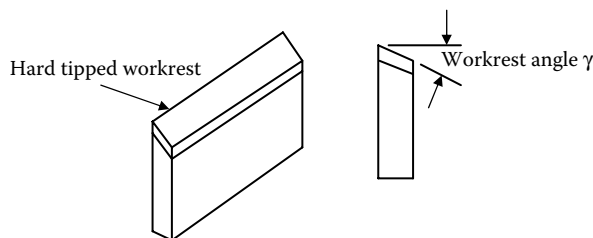


**FIGURE 19.14** A typical workrest.

Formed workpieces require the workrest to be shaped to support the workpiece at more than one position along its length. For example, if the workpiece is stepped, the workrest must also be stepped. The step height on the workrest should correspond to the step height on the workpiece.

The top surface of the workrest is almost invariably angled as shown. The workrest angle,  $\gamma$ , may lie between 0 and 45°. For most work, the angle chosen is 30°. The angle 30° is generally found to give a strong rounding action. A workrest angle of 0° is to be avoided since no rounding action is achieved. The effect of workrest angle is introduced in Section 19.2.5 on rounding geometry.

It is important that the workrest is set horizontal and parallel to the grinding-wheel surface to avoid problems of taper errors on the workpiece and forward ejection of workpieces from the machine.

### 19.7 SPEED CONTROL

For light workpieces, contact with the grinding wheel is sufficient to provide the driving torque to ensure workpiece rotation. A freshly dressed rubber control wheel gives good friction and prevents workpieces from spinning out of control. With sufficient friction, the workrest and the control wheel both resist rotation of the workpiece against the driving torque provided by the grinding wheel. Under these conditions, the workpiece follows the speed of the control wheel.

#### 19.7.1 SPINNING OUT OF CONTROL

With insufficient friction, the workpiece speeds up. This causes the friction coefficient between the workpiece and the regulating wheel to further reduce. The loss of friction causes the workpiece to spin out of control. To avoid this situation, the surfaces of the control wheel and workrest must be clean. Also, the control wheel surface must provide adequate friction. The condition for spinning can be illustrated for the condition illustrated in Figure 19.15 for zero work-height above center.

The grinding wheel exerts a normal force,  $F_n$ , and a tangential force,  $F_t$ . The force ratio may be expressed as a grinding-wheel friction coefficient,  $\mu_{gw}$ . The normal force,  $N_{rest}$ , exerted by the workrest approximately balances  $F_t$ . The frictional force on the workrest is given by the coefficient of friction,  $\mu_{rest}$ , for the two materials under the sliding conditions. Forces on the workpiece balance in the horizontal direction, in the vertical direction, and for rotation. These conditions lead to

$$F_n = N_{cw} + T_{wr} \dots \text{Horizontal forces} \tag{19.23}$$

$$F_t = \mu_{gw} \cdot F_n = N_{wr} - T_{cw} \dots \text{Vertical forces} \tag{19.24}$$

$$T_{wr} = \mu_{wr} \cdot N_{wr} = F_t - T_{cw} \dots \text{Rotational forces} \tag{19.25}$$

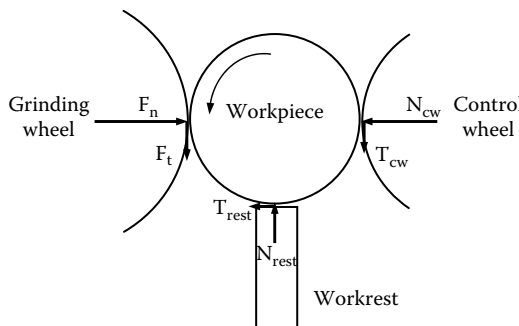


FIGURE 19.15 The forces on a workpiece.

Solving for the normal force on the workrest and the friction force on the control wheel,

$$N_{wr} = \frac{2 \cdot \mu_{gw} \cdot F_n}{1 + \mu_{wr}} \quad (19.26)$$

$$T_{cw} = \frac{1 - \mu_{wr}}{1 + \mu_{wr}} \cdot \mu_{gw} \cdot F_n \quad (19.27)$$

$$T_{wr} = \frac{2 \cdot \mu_{wr}}{1 + \mu_{wr}} \cdot \mu_{gw} \cdot F_n \quad (19.28)$$

$$N_{cw} = \frac{1 + \mu_{wr}(1 - 2 \cdot \mu_{gw})}{1 + \mu_{wr}} \cdot F_n \quad (19.29)$$

For a typical grinding operation, assuming  $\mu_{gw} \approx 0.3$  and a coefficient of friction between workrest and workpiece,  $\mu_{wr} \approx 0.15$ ,

$$F_t = 0.3 \times F_n$$

$$N_{cw} = 0.92 \times F_n$$

$$N_{wr} = 0.52 \times F_n$$

$$T_{wr} = 0.078 \times F_n$$

$$T_{cw} = 0.22 \times F_n$$

The minimum value of the control wheel coefficient of friction for these conditions is

$$\mu_{cw} = \frac{T_{cw}}{N_{cw}} = \frac{0.22}{0.92} \approx 0.24$$

The usual condition is where the workpiece is above center, as in Figure 19.1. The friction on the control wheel becomes even more critical as work-height is increased.

### 19.7.2 FAILURE TO TURN

A different problem can arise with heavy workpieces if there is insufficient control wheel friction to turn the workpiece on contact with the grinding wheel. Heavy workpieces are unlikely to suffer the problem of “spinning.” In fact, heavy workpieces are more likely to suffer the problem of failing to turn at all under the action of the grinding force. If the workpiece fails to turn, the grinding wheel can machine a groove on one side of the workpiece. This situation is potentially dangerous since as the size of the groove increases, the tangential grinding force also increases to the point where the workpiece suddenly starts to rotate, leading to an excessive depth of cut and exceptionally heavy forces on the grinding wheel. It is important that this situation is never allowed to arise since it could lead to wheel breakage. When setting up a grinding process, it is important to check that the workpieces readily rotate and stop the machine if rotation fails to occur.

For heavy workpieces, additional provision must be made to ensure workpiece rotation before contact with the grinding wheel. An additional pressure roll may be employed to push the workpiece

against the control wheel and this may be sufficient. For very large workpieces such as axle shaft housings, it will be necessary to provide an external driving device to grip and rotate the workpiece.

## 19.8 MACHINE STRUCTURE

### 19.8.1 THE BASIC MACHINE ELEMENTS

Main elements of a centerless machine include:

- The machine base and table
- The grinding wheelhead, spindle bearings, and spindle drive
- The control wheelhead, spindle bearings, and spindle drive
- The infeed drive
- The grinding wheel dressing slide and drive
- The control wheel dressing slide and drive
- The workrest slide
- The fluid delivery and return system

The design of the machine must allow the machine

- To accurately position the workpieces in relation to the grinding wheel
- To drive the grinding wheel, control wheel, and workpieces at precise speeds
- To accurately dress the wheels

In this section, aspects of machine design are considered in relation to performance. Results from a conventional machine of the type shown in Figure 19.16 are compared with results from a stiff research machine having the layout illustrated in Figure 19.19. Further information is available in publications by Rowe [1974] and Rowe, Spraggett, and Gill [1987].

### 19.8.2 THE GRINDING FORCE LOOP

Figure 19.16 shows the layout of a very basic centerless machine. In this example, the grinding wheelhead forms part of an integral table and fluid containment tray. There is provision of a slideway

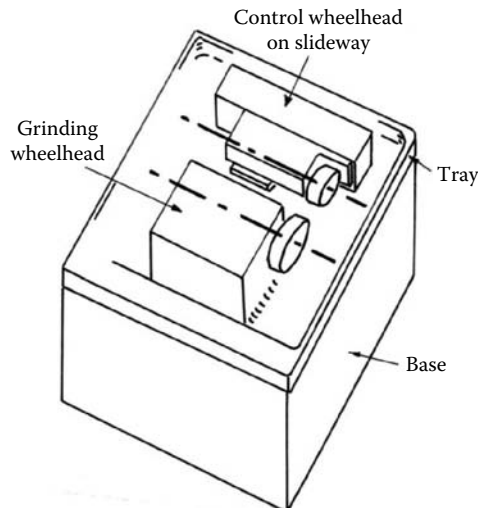


**FIGURE 19.16** The main elements of a centerless machine.

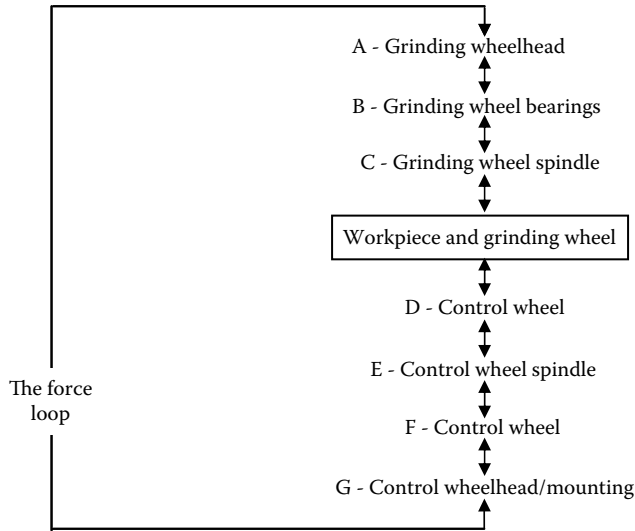


FIGURE 19.17 Constituents of the grinding force loop.

on the table to allow feed of the control wheelhead. No provision is shown to feed the grinding wheelhead nor is provision for angular adjustments to the wheelhead. These features are incorporated into many machines for ease of operation and setup.

Forces in the process cause deflections of the machine leading to the possibility of size inaccuracy and lack of straightness and roundness. Machine design affects both accuracy and production rate since a machine that is more compliant usually has to be operated more slowly to achieve the same accuracy. Often a more compliant machine is incapable of producing the same accuracy as a stiffer and better-designed machine. It is demonstrated below that a stiffer machine reaches the size specification faster than a compliant machine.

The forces in the process are reacted through a chain of machine elements. The overall compliance of the machine depends on the buildup of compliance through the elements in the force loop. The main elements of the loop for the grinding force are shown in Figure 19.17. The compliances of various elements are shown in Figure 19.18. The elasticity of the grinding wheel is not shown, although this is of a similar order of magnitude to the compliance of the control wheel but rather stiffer [Rowe 1974]. Other loops may be constructed for the dressing forces.

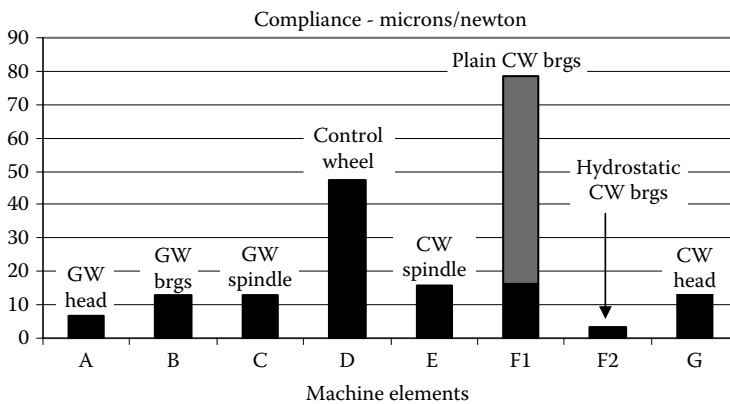
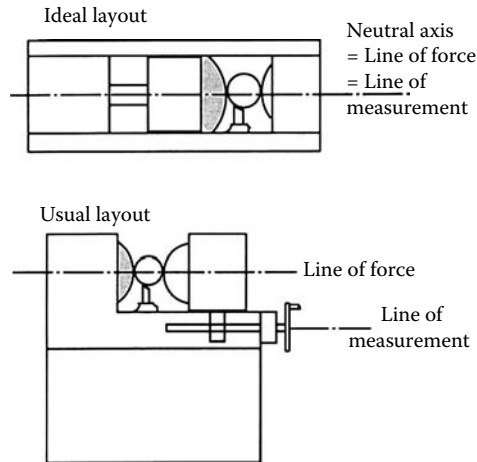


FIGURE 19.18 Compliance of the main elements in the grinding force loop.





**FIGURE 19.19** Design concept for a high-accuracy stiff machine. (From Rowe 1979. With permission.)

Each of the elements in the loop plays a critical role in resisting deflections. In this example, the low-speed plain control wheel bearings are a source of variability and low stiffness under finishing conditions. In addition, the workpiece is also featured in the force loop. If the workpiece is a thin-walled cylinder, the stiffness of the force loop will be greatly reduced.

### 19.8.3 STRUCTURAL LAYOUT

A conventional machine layout constrains the workpiece within a U-section, whereas ideally the workpiece should be constrained within a closed-box layout. This point is illustrated in Figure 19.19. The U-section is inherently subject to deflections in the same manner as a tuning fork. Ideally, a machine should be constructed in a different way designed to resist deflections.

A highly accurate and very stiff research machine was designed and built to demonstrate this point. The layout is illustrated in Figure 19.19. The research machine allowed grinding results to be compared with results from a compliant conventional machine. The structural design was shaped by the following criteria:

- The line of measurement to be coincident with the line of separating force
- The neutral axis for bending to be coincident with the line of force
- The dressing point to be opposite the grinding point on the grinding wheel and opposite the control wheel contact point on the control wheel, that is, along the line of force
- The dressing cam plates to be on the same line of force
- Hydrostatic bearings to be employed for high stiffness and accuracy
- A highly accurate and highly damped feed drive to be provided by a wedge-shaped cam driven between hydrostatic bearings
- The same principles to apply in the plan view. The wheels to be supported symmetrically between the spindle bearings

The resulting wheel-workpiece stiffness was  $3.5 \times 10^7$  N/m, five times greater than the stiffness of the conventional machine. The resonant frequency was increased from 78 Hz to 500 Hz.

The stiff machine gave different grinding results from a conventional machine. Size control and roundness using a similar plunge grinding cycle were improved but the range of workspeeds over which accurate grinding could be achieved was greatly increased as shown in Figure 19.20.

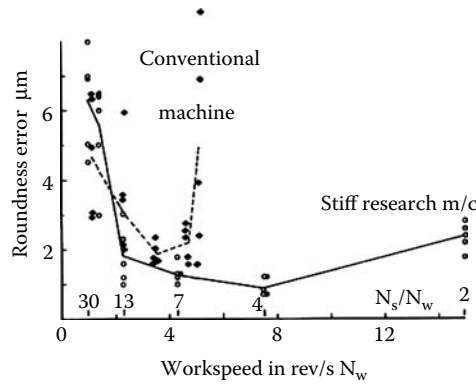


FIGURE 19.20 Effect of machine design on roundness accuracy and operating speed range.

### 19.8.3.1 Low Workspeeds

At low workspeeds, workpiece roundness levels were similar for the two machines and, in fact, higher roundness errors were measured with the stiff machine. The high roundness errors at low workspeeds are partly because there are insufficient revolutions of the workpiece to reduce the roundness errors. Higher roundness errors can result from a stiff machine in some tests due to the rounding process. This aspect is discussed below and also in Section 19.11 and Section 19.12.6 in relation to static compliance.

### 19.8.3.2 High Workspeeds

Results at high workspeeds are in distinct contrast to low speeds. Chatter was experienced with the compliant conventional machine at higher workspeeds, whereas with the stiff machine good accuracy was achieved at much higher speeds. This illustrates that roundness is not only a question of rounding geometry but also of the dynamic performance of the grinding machine. Since production rate is related to workspeed and wheel speed, there is an implication that a dynamically stiff machine allows much higher levels of productivity.

The important point is that vibration levels should be low. Roundness is not simply dependent on static stiffness. In fact, high static stiffness with high-vibration levels worsens roundness. Also, a slow rounding process tends to reduce errors better than a fast process. A compliant machine slows down the rounding process and can, under the right conditions, allow better roundness to be achieved. This was demonstrated by replacing the soft rubber control wheel with a cast iron control wheel. It was found that roundness errors were increased with a stiff cast iron wheel.

## 19.8.4 SPINDLE BEARINGS

The control wheel spindle bearings were the most compliant element in the force loop compliances shown in Figure 19.18. The plain hydrodynamic bearings of the control wheel spindle are shown as Element F1. Plain hydrodynamic bearings are reliable over a long period, but at low speeds they exhibit low and variable compliance. The compliance becomes very high under light loading as when sparking out. This is a serious disadvantage for consistency of grinding. Hydrodynamic bearings are much better at high speeds as when applied in grinding wheel bearings. High-precision rolling elements are better than plain bearings for low speeds, but need to be replaced regularly due to wear. Hydrostatic bearings give improved performance over the speed range having high stiffness, high accuracy, and low wear properties. The disadvantage of hydrostatic bearings is higher cost.

Hydrostatic bearings were substituted for the hydrodynamic control wheel bearings of the conventional machine. The hydrostatic bearings were provided with diaphragm control to improve

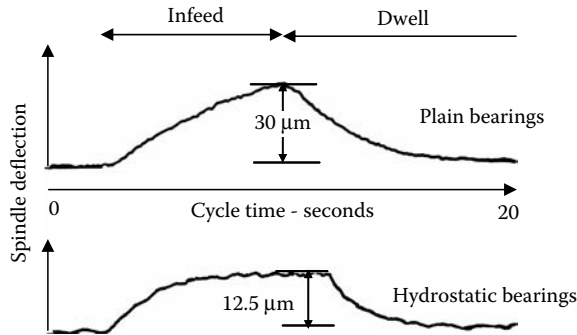


**FIGURE 19.21** Control wheel deflections during a grinding cycle showing the effect of bearing stiffness.

the system stiffness, consistency, and rotational accuracy. The replacement bearings are shown as Element F2 in Figure 19.18. The grinding wheel bearings were also replaced by hydrostatic bearings giving marginally improved stiffness but much-improved rotational accuracy. The result was much better roundness accuracy of the grinding process. The replacement of the control wheel bearings gave much improved size-holding capability. It was possible to achieve a specified size tolerance within a shorter dwell period for spark-out.

Figure 19.21 shows how bearing stiffness affects deflection of the control wheel in plunge grinding for a workpiece 25.4 mm diameter by 50 mm long. The maximum deflections are two and a half times larger with the plain bearings than with the hydrostatic bearings for the control wheel spindle.

Greater deflections of the grinding system require a longer spark-out dwell to reduce the size roundness and surface texture variations. Controlled grinding experiments demonstrate this effect and the results are seen in Figure 19.22.

Size variations are much smaller with the stiff hydrostatic bearings than with the compliant plain bearings. Size variations are reduced to a negligible level in half the dwell period required by the compliant bearings.

Roundness errors also decrease during the dwell period. Stiff hydrostatic bearings reduce roundness errors faster. In later experiments, the grinding wheel bearings were replaced by hydrostatic bearings and the roundness errors were further reduced.

The results for surface texture may seem surprising. Surface roughness reduces during the dwell period as would be expected. However, surface roughness is greater for the stiffer hydrostatic bearings than for the compliant plain bearings. Experience with other machines confirms that stiff systems produce slightly higher surface roughness in grinding. On reflection, this would be expected since a stiffer system imposes greater variations in grain depth than a soft system. A stiff system can produce low roughness but the requirement for low roughness is a system where grain depths are small and uniform. This can be achieved with high-quality small-grain wheels and a low level of vibrations.

Overall stiffness of a system in relation to grinding forces is expressed by the machining-elasticity parameter  $K$ . The parameter  $K$  is the true depth of cut divided by set depth of cut and is explained mathematically in Section 19.11.4. Evaluating  $K$  for the hydrostatic bearing machine and the plain bearing machine gave the following results in controlled grinding experiments:

Plain bearing machine	$K = 0.23$
Hydrostatic bearing machine	$K = 0.44$

In summary, replacing compliant plain wheel bearings by stiff hydrostatic bearings almost doubled the effective system stiffness.

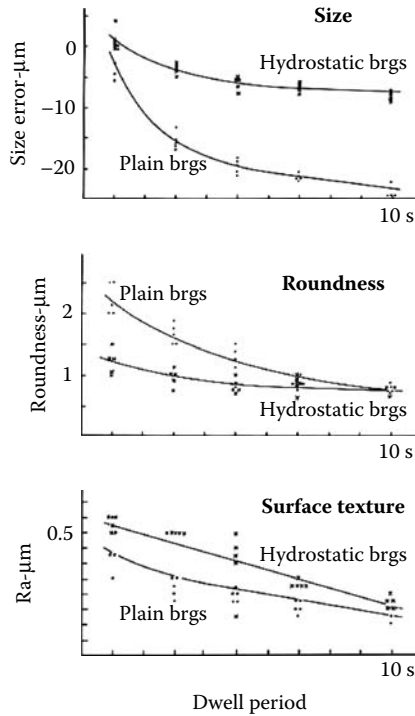


**FIGURE 19.22** Workpiece accuracy with dwell period. Comparing stiff hydrostatic control wheel bearings with compliant hydrodynamic control wheel bearings.

## 19.9 HIGH REMOVAL RATE GRINDING

### 19.9.1 INTRODUCTION

Manufacturers wish to increase grinding rates for several reasons:

- To increase output from each grinding machine
- To increase output by each machine operator
- To reduce cost per part

An experimental investigation of high removal-rate centerless grinding applied to steel and cast iron allowed process limit charts to be defined [Rowe, Bell, and Brough 1986]. These materials are easy-to-grind materials. Limit charts show operating boundaries for infeed rate, workspeed, and wheel speed. Examples are presented below. With large grinding wheels as used in centerless grinding, the rate of wheel wear was low. It was not possible to achieve an excessive wheel wear condition although this might have been possible if more power had been available. The machine employed had a 75-kW motor. The shape of the diagram means there is an optimum point of operation for high removal rate within the region enclosed by the boundaries. This forms the basis of a control strategy.

Characterization of the process is developed by attention to the concept of a “speed effect” and a “size effect.” Results for the speed effect are distinguished and presented separately from results for the size effect to illustrate the differences due to physical effects.

A two-dimensional surface is presented showing the variation of grinding energy with variations in infeed rate, workspeed, and grinding wheel speed. Because speed and size effects are separated on the surface, it is possible to read directly the optimum grinding wheel speed for minimum energy.

## 19.9.2 ROUTES TO HIGH REMOVAL RATE

Some of the key features for achievement of high removal rate are as follows.

### 19.9.2.1 Increasing the Number of Active Grits

The main route to increasing removal involves increasing the number of abrasive grains that remove material within the grinding period. The number of active grits can be increased by:

- Increased grinding wheel diameter
- Increased grinding wheel width
- Increased grinding wheel speed

A larger number of active grits means more material can be removed in a given time. This is because active grits can only remove so much material per engagement. Productivity is, therefore, directly related to the number of grits in engagement per unit time.

### 19.9.2.2 Increasing Removal Rate per Grit

Another route to increasing production rate is to optimize the removal of material per grit engagement. In practice, the material removed per grit cannot be easily determined. This means that overall efficiency of the process and removal rate must be investigated by grinding trials. The effect of grinding cycle parameters on process efficiency is considered further in Section 19.10 on process economics.

Power consumed increases with the number of grits removing material per unit time. Highest removal rate is achieved when removal rate per grit is optimized. If, then, grinding wheelspeed is increased, removal rate per grit is reduced from the optimum value. This reduces efficiency. To optimize removal rate per grit, feedrate must be increased in the same proportion as wheel speed. This restores removal rate per grit to the optimum value and increases overall removal rate. The technique of changing wheel speed and feedrate in a constant proportion maintains kinematic similarity to maintain an optimized process. Ideally, workspeed should also be increased in the same proportion.

### 19.9.2.3 Longer Redress Life

It is important to achieve long wheel redress life. Material removal per grit should be maximum consistent with required quality and consistent with long wheel life between redressing. The large diameter and wide grinding wheels employed in centerless grinding mean that long redress life can usually be achieved more easily than in other grinding processes. Redress life is further explored under process economics. Redress life is strongly dependent on the combined nature of the abrasive, the workpiece material, and the severity of the grinding conditions.

### 19.9.2.4 Improved Abrasive

Subject to achievement of quality levels, harder grits and bonds allow longer redress life and larger stock removal. The bond must not be too hard for the grinding operation and the grits should be sufficiently friable. Otherwise, grits eventually become blunt and are retained if grain forces rise to unacceptable levels. Blunt grits lead to high specific energy and glazed wheels.

Grits that are too weak and a bond that is too soft lead to rapid wheel wear and high surface roughness. An advantage of a soft wheel is that grinding forces tend to be lower than with a hard wheel.

For high wheelspeeds, it is necessary to consider the type of abrasive and wheel design for safe high-speed operation. Superabrasive wheels can be operated at higher speeds than conventional

abrasives. Specialist conventional abrasives are available, designed for speeds up to 140 m/s. These may prove to be the most economic choice for high-speed centerless grinding.

### 19.9.2.5 Grinding Trials

For sustained and repeated batch manufacture, it is worth conducting grinding trials with different wheels and grinding conditions to improve process economics. In this section, effects of grinding wheel speed on grinding rate are considered.

### 19.9.2.6 Improved Grinding Machines and Auxiliary Equipment

Consideration should be given to effects of machine design on grinding rate. Some features to be considered are

- *Machine power.* Many machines have insufficient power and this may frustrate attempts to increase removal rate. The full potential of the grinding wheel and high grinding wheel speed can only be realized if the machine has ample power. Speed and power available at the grinding wheel are particularly important.
- *Variable speed drives.* Variable speed drives allow wheel- and workspeeds to be adjusted to avoid resonant machine conditions. The same requirement applies to rotary dressing tool drives. Highest production rates and best quality are achieved when the machine speeds are adjusted to avoid resonant conditions. In this context, quality levels refer particularly to size, roundness, and roughness. The range of wheel speeds must be sufficient to allow high removal rates.
- *High-speed grinding wheels.* 60 m/s is reasonable for conventional wheels rated up to this speed. Much higher speeds are possible with special purpose wheel designs and superabrasives. High wheel speeds greatly increase the potential for high removal rates while allowing quality levels to be maintained.
- *Machine stiffness.* A high-speed grinding machine needs to be stiffer than a low-speed grinding machine. This implies a sound structural layout and sufficient rigidity. Slideways should allow accurate movement and the feed-drives must allow accurate control and adequate feedrates for grinding and for rapid loading and unloading. Other features to be considered include ease of setup and adjustment of machine settings.
- *Effective fluid delivery.* Fluid delivery assumes increased importance in high-speed grinding. Flowrates and supply pressures must be adequate to ensure transport of fluid into the grinding contact between the grinding wheel and the workpiece. It is only the “useful flowrate” that enters the grinding contact. Only useful flowrate acts to provide process lubrication and ensure cooling at the high-temperature contact interface. The fluid should be delivered as a high-speed sheet of fluid directed as far as possible straight into the grinding contact [Gviniashvili, Wooley, and Rowe 2004].
- *An effective grinding fluid.* The grinding fluid must be chosen for tribological properties of lubrication, cleaning, cooling, material removal, corrosion protection, biocide action, fire risk, and friendliness to the operators and environment. This is a specialist field that requires careful consideration.
- *Dressing equipment.* Dressing slides should be sufficiently rugged and accurate for precise control of dressing operations. The type of dressing tool used is important. Multipoint diamond tools allow greater consistency over a longer period than single-point tools. Diamond rotary tools may be preferred for high grinding wheel speeds, particularly for superabrasive wheels.
- *Wheel guarding.* Wheel failures should be an extremely rare event. However, for high grinding wheel speeds, adequate guarding must contain burst wheels within the guarding enclosure. Wheel guarding must conform to safety regulations.

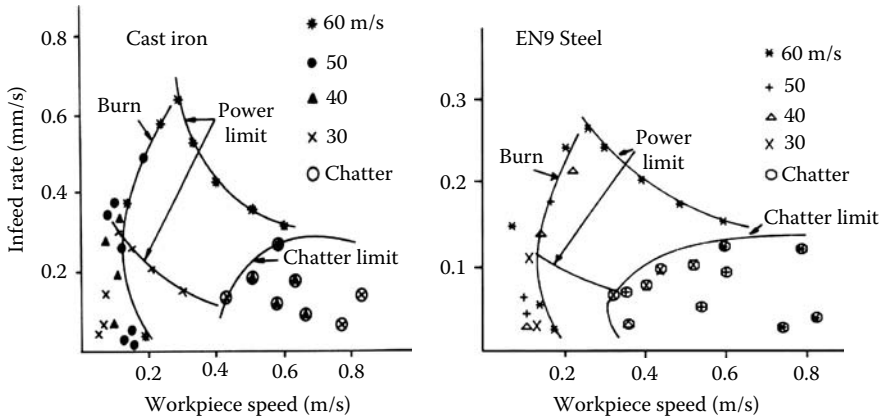


**FIGURE 19.23** Process limits for typical material-machine combinations. 75 kW machine. Workpieces: Gray CI—40 mm diameter by 65 mm long; EN9 — 50 mm diameter by 65 mm long.

### 19.9.3 PROCESS LIMITS

The process limits define the permissible range of speed conditions for stable grinding. Typical process limits are shown in Figure 19.23. Two examples are illustrated for a 75-kW centerless grinding machine. The gray cast iron is an easy-to-grind work material and specific material removal rates were achieved in excess of 40 mm<sup>2</sup>/s. When grinding EN9 steel, the specific removal rate achieved was 20 mm<sup>2</sup>/s. These removal rates were achieved using conventional abrasive wheels at a speed of 60 m/s.

The rate of grinding can be increased up to process limits of maximum machine power available, onset of thermal damage to the workpieces, and chatter. Surface roughness depends primarily on the grinding wheel employed and the dressing process. Initial trials to ascertain the size of the operating area is essential as a first step to process optimization.

The results clearly show the benefits of increasing wheel speed. The removal rates at 60 m/s are more than double the rates achieved at 30 m/s.

An interesting feature of the limit charts is the similarity of the shape for two different materials. This supports the conclusion that these diagrams have general validity.

The charts show that high workspeeds increase the probability of chatter. Low workspeeds increase the probability of burn. Low workspeeds concentrate the process energy in the contact zone for a longer period and so increase the susceptibility to thermal damage. Thermal damage, or burn as it is generally termed, can also give rise to a form of chatter that occurs at low workpiece speeds.

High grinding wheel speeds allow higher infeed rates to be employed for the same grinding forces and thus allow higher removal rates.

#### 19.9.3.1 Effect of Infeed Rate

Material removal rate increases with infeed rate. However, as infeed rate is increased, material removed per grit also increases. This is apparent from the equivalent chip thickness expressed in terms of infeed rate and wheel speed.

$$h_{eq} = \frac{1}{2} \cdot \pi \cdot d_w \cdot \frac{v_f}{v_s} \quad (19.30)$$

Increasing chip thickness leads to higher stresses on the grinding grits causing greater wear and fracture. A consequence is “self-dressing” where the grits maintain or increase their sharpness due to the grinding stresses. This yields the benefit of reducing the energy required to remove a volume of material and produces lower specific energy. The disadvantage of the grit fracture process is higher surface roughness and faster wheel wear. The process where specific energy is reduced due to increased feedrate is termed the “size effect.” The size effect can be explained in several different ways but basically the conclusion is that increased chip thickness or increased volume of material removed per grit reduces specific energy.

Increasing infeed rate, with other parameters constant, tends to increase grinding forces, increase roughness, reduce redress life, and reduce specific energy. The process tends to become more efficient until the optimum chip size is exceeded. Excessive infeed rate leads to high wheel wear, a low grinding ratio, and rapid wheel breakdown.

**19.9.3.2 Effect of Wheel Speed**

Higher wheel speeds allow higher infeed rates to be employed. Increasing wheel speed without increasing infeed rate reduces chip thickness as can be seen from Equation 19.30. In this case, roughness is reduced and grinding forces are reduced although specific energy is increased due to the size effect. The purpose of increasing wheel speed is to allow infeed rate to be increased, thus increasing production rate while maintaining quality levels and process efficiency.

**19.9.3.3 Effect of Workspeed**

Within the stable range, increasing workspeed has a relatively small effect on the process. As workspeed is increased, specific energy is increased as may be deduced from Figure 19.23 and Figure 19.24.

At high workspeeds, the probability of chatter is increased, so there is effectively a maximum workspeed due to the chatter. These results are for a particular workpiece diameter. It is, therefore, necessary to undertake trials for the particular workpieces to be produced. Figure 19.20 shows the chatter limit can be increased by improved machine design to raise the principal resonant frequency.

At low workspeeds, the probability of thermal damage to the workpiece increases. The burn boundary can be moved outward by using a sharper abrasive to reduce the specific energy.

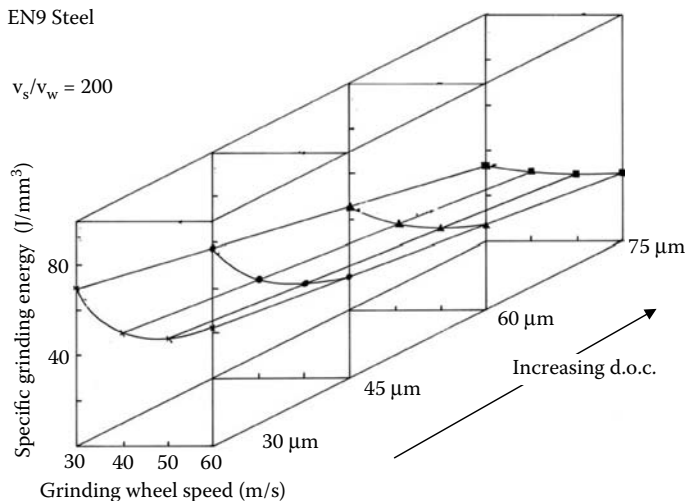


**FIGURE 19.24** Specific energy with increasing depth of cut and wheel speed for constant  $v_s/v_w$ .



**TABLE 19.1**  
**Depth of Cut, Feedrate, and Equivalent Chip**  
**Thickness,  $d_w = 50$  mm Diameter**

Depth of Cut ( $\mu\text{m}$ )	Equivalent Chip Thickness ( $\mu\text{m}$ )	Infeed Rate/Workspeed
30	0.152	0.000386
45	0.224	0.000570
60	0.302	0.000770
75	0.379	0.000965

### 19.9.4 SPECIFIC ENERGY AS A MEASURE OF EFFICIENCY

Specific grinding energy can be considered as a measure of grinding efficiency. A low specific energy implies low energy consumed to remove a given volume of material. Low specific energy allows greater removal rate before meeting the power limit. Since specific energy is proportional to the grinding forces, it usually means that removal rate can be greater before meeting the burn limit and before meeting the chatter limit.

Specific energy reduces with increasing infed rate due to the size effect as discussed previously. An example is shown in Figure 19.24. Table 19.1 shows that the constant speed ratios in Figure 19.24 allow constant depth of cut and constant chip thickness with varying wheel speed.

If grinding wheel speed were increased on its own, the size effect would reduce efficiency. However, the purpose of increasing grinding wheel speed is to allow increased feedrates. By increasing wheel speed and feedrate in direct proportion to each other, the size effect is eliminated. By this means, speed may be increased maintaining depth of cut and chip thickness constant.

It is found that specific energy reduces to a minimum as wheel speed is increased at constant chip thickness and then starts to increase again. This is clearly illustrated in Figure 19.24. Specific energy starts to increase again at higher wheel speeds possibly due to an increased rubbing contribution at higher wheel speed. As feedrate is increased, chip thickness is also increased. This increases the value of optimum wheel speed and suggests that even higher wheel speeds would be an advantage.

Figure 19.24 is typical of grinding processes and suggests an optimum wheel speed applies for particular depth of cut and feedrate conditions. For this example, it appears that the optimum wheel speed is close to 45 m/s at the lower depth of cut and is close to 60 m/s at the higher depth of cut.

## 19.10 ECONOMIC EVALUATION OF CONVENTIONAL AND CBN WHEELS

### 19.10.1 INTRODUCTION

Under particular through-feed centerless grinding conditions, results presented by Koenig and Henn [1982] showed that the minimum cost per part was achieved at removal rates between 1 and 6 mm<sup>3</sup>/mm/s. Increasing or reducing removal rate from this range increased costs. Such results are useful for demonstrating an approach to optimization. In this section, a general approach to optimization is demonstrated.

The following analysis by Rowe and Ebbrell [2004] demonstrates how a systematic approach can allow many different factors to be taken into account leading to large increases in productivity and reductions in costs while maintaining quality levels. The analysis applies for repeated batch manufacture. Costs in grinding can often be reduced by increasing removal rate. However, this is not the only factor and it is necessary to take account of mean cycle time including dwell time for

spark-out and costs related to labor, the grinding machine, grinding wheels, dressing, and maintenance of required quality levels.

As demonstrated in Section 19.9, high wheel speeds allow removal rates to be increased while maintaining quality levels. However, high wheel speeds increase the cost of the grinding machine. Stiffer machines are required. More sophisticated equipment and techniques are required for fluid delivery, dressing, and spindle bearings. Special grinding wheels are required for high speeds and better machine guarding. It is, therefore, necessary to give consideration to costs and benefits of these various aspects. Advantages may be obtained by introducing superabrasive wheels to allow much higher wheels speeds and long redress life.

Redress life results were obtained in grinding between centers using smaller wheels to minimize wheel costs. However, the principles are generally applicable. Repeated batch manufacture is a situation where it is required to maximize production throughput and minimize process costs while achieving specified quality levels.

### 19.10.2 COST RELATIONSHIPS

The following cost analysis takes account of labor cost, machine cost, and abrasive cost. Workpiece quality and redress life are related through the number of parts ground before roughness or roundness tolerance is exceeded.

### 19.10.3 WHEEL COST/PART

$C_s$  is the wheel cost,  $c_s$ , divided by the number of parts produced per wheel,  $N_w$ . The number of parts per wheel is given by

$$N_w = \left[ \left( \frac{d_{s\max} - d_{s\min}}{2} \right) / (r_s + a_d n_d) \right] N_d \quad (19.31)$$

where  $d_{s\max}$  is max wheel diameter,  $d_{s\min}$  is min wheel diameter,  $r_s$  is radial grinding wear per dress,  $a_d$  is dressing depth,  $n_d$  is number of dressing passes, and  $N_d$  is the number of parts per dress. The wheel cost per part is, therefore,

$$C_s = \frac{2 \cdot c_s (r_s + a_d n_d)}{(d_{s\max} - d_{s\min}) N_d} \quad (19.32)$$

Figure 19.25 shows typical wheel cost/part varying with number of parts/dress for alumina and CBN wheels. Redress life has a strong effect using CBN due to initial cost but cost/part may be offset by long redress life. A high wheel speed increases redress life by reducing chip thickness. Wheel cost/part becomes negligible with long redress life.

Initial wheel costs in centerless grinding are higher than in grinding between centers due to the larger diameter and width of centerless wheels. However, redress life is correspondingly increased so that wheel costs are spread over many more workpieces. The wheel costs in Figure 19.25 could be more than doubled in centerless grinding although the wheel cost per part is likely to be reduced.

### 19.10.4 LABOR COST/PART

Labor cost per part,  $C_l$ , is the product of labor rate,  $c_l$ , and total cycle time,  $t_t$ . Labor rate includes general overhead costs other than the cost of the grinding machine. The total cycle time is given by

$$t_t = t_s + t_d / N_d \quad (19.33)$$

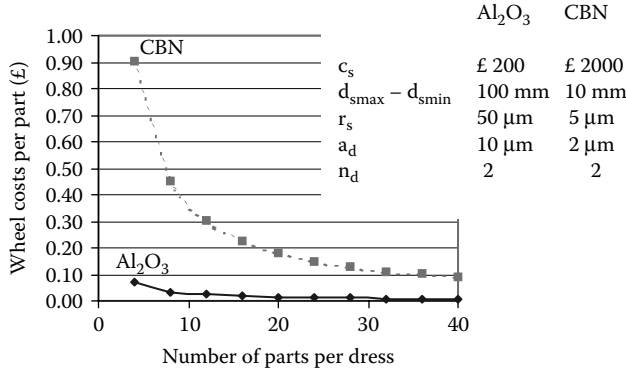


FIGURE 19.25 Dependence of wheel cost per part on number of parts per dress.

where  $t_s$  is the basic cycle time and  $t_d$  is the dressing time. The basic cycle time allows for the diametral stock removal,  $d_{ww}$ , the diametral stand-off,  $d_{ss}$ , and dwell time for spark-out,  $t_{so}$ , so that

$$t_s = \frac{(d_{ww} + d_{ss})\pi d_w}{Q'_w} + t_{so} \tag{19.34}$$

where  $Q'_w$  is specific removal rate and  $d_w$  is the workpiece diameter. Dressing time depends on the wheel width,  $b_s$ , the number of dressing passes,  $n_d$ , and the dressing feedrate,  $v_d$ . The dressing time is

$$t_d = \frac{b_s n_d}{v_d} \tag{19.35}$$

The dressing feedrate depends on the effective width of the dressing tool,  $b_d$ , and the dressing overlap ratio,  $U_d$ . Typically, the overlap ratio should be of the order of 3 to 10. The higher value gives lower roughness but higher grinding forces.

$$v_d = \frac{b_d}{U_d} \times \frac{v_s}{\pi d_s} \tag{19.36}$$

The total cycle time is, therefore,

$$t_t = \frac{(d_{ww} + d_{ss})\pi d_w}{Q'_w} + t_{so} + \frac{b_s n_d}{v_d N_d} \tag{19.37}$$

Multiplying total cycle time by the labor rate gives the labor cost/part as

$$C_l = c_l \left[ \frac{(d_{ww} + d_{ss})\pi d_w}{Q'_w} + t_{so} + \frac{b_s n_d}{v_d N_d} \right] \tag{19.38}$$

Labor cost/part is affected by removal rate, dwell time, number of dressing passes, dressing feed rate, and by number of parts/dress. With many parts/dress, the last term of Equation 19.38 becomes negligible. With several dressing operations per part, the last term becomes large.

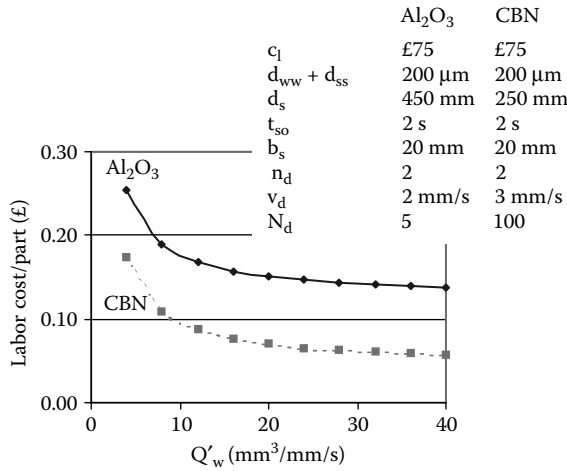


FIGURE 19.26 Dependence of labor cost per part on removal rate.

The labor rate with overheads was based on £75/hr. Figure 19.26 shows high removal rates reduce labor cost/part.

Figure 19.27 shows that redress life can strongly affect labor cost per part. Redress life is particularly important if redress life is short. The effect of dressing cost/part becomes negligible in this example beyond four parts/dress.

19.10.5 MACHINE COST/PART

Machine cost per part,  $C_m$ , is given by the cost of the machine,  $C_{mc}$ , divided by the number of parts,  $N_{mc}$ , produced within the payback time,  $y_t$ . The number of parts produced is

$$N_{mc} = y_t/t_t = y_t/(t_s + t_d/N_d) \tag{19.39}$$

19.10.6 TOTAL VARIABLE COST/PART

The total of the variable costs per part is the sum of wheel cost/part, labor cost/part including an overhead contribution, and machine cost/part. Constant workpiece material cost/part does not affect the selection of process conditions and can, therefore, be left out of this discussion.

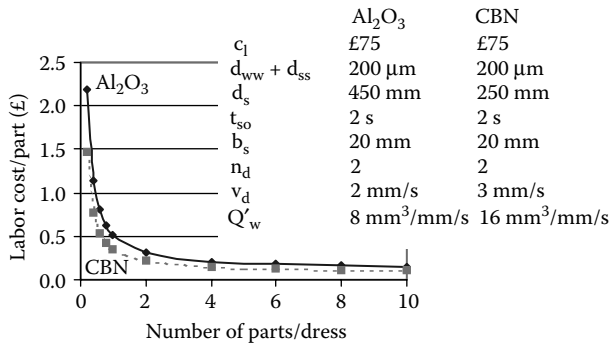


FIGURE 19.27 Dependence of labor cost per part on redress life.

**TABLE 19.2**  
**An L<sub>8</sub>2<sup>7</sup> Experimental Plan**

Trial Parameter	Level						
	A	B	C	D	E	F	G
1	1	1	1	1	1	1	1
2	1	1	1	2	2	2	2
3	1	2	2	1	1	2	2
4	1	2	2	2	2	1	1
5	2	1	2	1	2	1	2
6	2	1	2	2	1	2	1
7	2	2	1	1	2	2	1
8	2	2	1	2	1	1	2

The total cost/part for wheels, labor, and machine is, therefore,

$$C_t = \frac{2c_s(r_s + a_d n_d)}{(d_{s\max} - d_{s\min})N_d} + \left[ \frac{(d_{ww} + d_{ss})\pi d_w}{Q'_w} + t_{so} + \frac{b_s n_d}{v_d N_d} \right] \left( c_l + \frac{C_{mc}}{y_t} \right) \quad (19.40)$$

The number of parts/dress is a factor in all three costs contributing to the total cost. This explains the importance of redress life. Inclusion of machine cost and redress life allows realistic evaluation of high-speed grinding and application of superabrasives.

### 19.10.7 EXPERIMENT DESIGN

To evaluate costs, it is first necessary to determine the effect of grinding conditions on redress life. The effect of long redress life was studied grinding AISI 52100 and the effect of low redress life with Inconel 718. Redress life was defined as the number of parts ground before either roughness of 0.25  $\mu\text{m}$  Ra or roundness error of 1  $\mu\text{m}$  was exceeded. By this means, the specified quality levels are built in to the test procedure. The following procedure allows a comprehensive analysis to be performed with a minimum number of grinding and measuring trials.

An example of an experimental design for a two-level investigation of seven variables using eight trials is given in Table 19.2. In the example shown, four trials are conducted for each value of a parameter. The result for each parameter is the mean value for the combinations of the other parameters shown. In each case, Level 1 represents the low value of a parameter and Level 2 represents the high value. A large number of workpieces are ground for each trial, thus allowing redress life and G-ratio to be assessed.

The investigation was conducted in three stages.

#### 19.10.7.1 Stage 1. Basic Trials

Basic trials were conducted to produce direct-effect charts for specific energy, roughness, roundness, size, and G-ratio. Many factors were varied including wheel speed, workspeed, dwell period, dresser speed, dressing direction, dressing overlap ratio, and dressing depth. Two levels were chosen for each variable. The levels were selected based on experience to give a reasonable span of the operational range. The two-level experiment leads to “direct-effects” charts.

#### 19.10.7.2 Stage 2. Select Best Conditions and Confirm

Best conditions were selected for each grinding wheel by selecting a combination of values from consideration of the effects of each variable on production rate and quality from the direct-effect

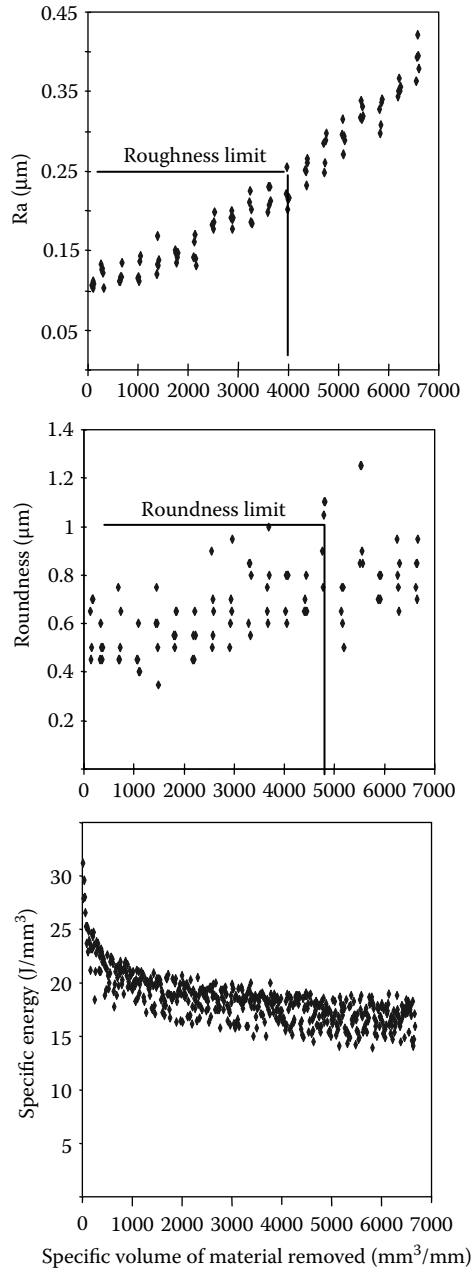


**FIGURE 19.28** Redress life trials in high-speed CBN grinding with 2 s dwell and 20 mm<sup>3</sup>/mm/s removal rate.

charts produced in the basic trials. A combination of values was selected to achieve the quality levels with shortest cycle time. The optimized conditions were validated by confirmation trials.

### 19.10.7.3 Stage 3. Cost Comparisons

Costs per part were evaluated for each grinding wheel using redress life from the trials. Cost comparisons were made based on conditions yielding best results from previous trials.

Figure 19.28 shows typical redress life results. The end of the redress life is indicated when the process no longer yields roughness, roundness, or any other quality parameter within tolerance.

**TABLE 19.3**  
**Wheel, Labor, and Machine Cost Factors**

Wheels Details	All Al <sub>2</sub> O <sub>3</sub>	SG	CBN	CBN
	(45 m/s)	(45 m/s)	(45 m/s)	(60–120 m/s)
$c_s$	£200	£320	£3,000	£1,700
$d_{s\max}$	450 mm	450 mm	450 mm	250 mm
$d_{s\min}$	350 mm	350 mm	438 mm	240 mm
$c_l$	£75	£75	£75	£75
$d_{ww} + d_{ss}$	0.2 mm	0.2 mm	0.2 mm	0.2 mm
$d_w$	40 mm	40 mm	40 mm	40 mm
$b_s$	25 mm	25 mm	25 mm	17 mm
$C_{mc}$	£100,000	£100,000	£100,000	£250,000
$y_t$	1,920 hr	1,920 hr	1,920 hr	1,920 hr

### 19.10.8 MACHINE CONDITIONS AND COST FACTORS

The cost factors used in the evaluation are given in Table 19.3.

A high-speed vitrified CBN wheel was tested on a special-purpose high-speed grinding machine for speeds up to 140 m/s. The results were compared with conventional alumina wheels and CBN wheels tested on a conventional machine at speeds up to 45 m/s.

The special-purpose machine was designed to employ smaller diameter wheels so that wheel costs were lower for the highest wheel speeds. The cost of the special-purpose machine was two and a half times the cost of the conventional machine.

For high-speed CBN grinding, it was necessary to employ a rotary-disk diamond dressing tool with a hydraulic drive. “Touch dressing” was employed to allow very small dressing cuts to be taken. The application of such techniques is essential for the successful application of vitrified CBN. The higher costs have to be justified by increased productivity and lower total cost per part. A 6-month payback period was assumed consisting of 20 working days per month at 16 hr per day.

### 19.10.9 MATERIALS, GRINDING WHEELS, AND GRINDING VARIABLES

#### 19.10.9.1 AISI 52100 Steel

Five grinding wheels were employed for easy-to-grind bearing steel AISI 52100. The wheels are listed in Table 19.4. The medium-speed wheels were larger than the high-speed wheels as indicated in Table 19.3.

A two-level experimental arrangement for eight factors based on an L<sub>16</sub>2<sup>8</sup> array was used to determine the best conditions using high-speed CBN. Other trials were designed to determine best conditions for conventional speeds. Typical values of the parameters are given in Figure 19.29. Further details are available from Ebbrell [2003].

For best results, the following dressing and grinding conditions were selected from the basic trials and confirmed by confirmation trials for AISI 52100:

- *Conventional-speed Al<sub>2</sub>O<sub>3</sub> and SG wheels.* These wheels were dressed using a single point diamond, with  $a_d = 10 \mu\text{m}$ ,  $v_d = 3.18 \text{ mm/s}$ ,  $n_d = 2$ . Grinding conditions were,  $v_s = 45 \text{ m/s}$ ,  $v_w = 20 \text{ m/min}$ , and  $t_{so} = 10 \text{ s}$ . For the basic aluminium oxide wheels, specific removal rate,  $Q'_w = 1 \text{ mm}^3/\text{mm/s}$ . For the SG wheel  $Q'_w = 2.5 \text{ mm}^3/\text{mm/s}$ .

**TABLE 19.4**  
**Grinding Wheels and Machines for Grinding**  
**AISI 52100**

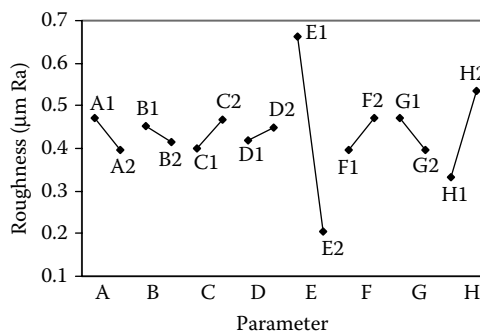
Abrasive Type	Wheel Specification	Wheel Speed (m/s)
Vitrified Al <sub>2</sub> O <sub>3</sub>	A46 K5V	45
Vitrified Al <sub>2</sub> O <sub>3</sub>	A80 J6V	45
Vitrified SG	A60 J8V	45
Vitrified CBN	B91 (Medium speed)	45
Vitrified CBN	B91 (High speed)	60–120

- *Conventional-speed CBN wheel.* The conventional-speed B91 CBN wheel was up-dressed with a rotary disk dresser. The wheel was dressed at a speed,  $v_r = -12.6$  m/s,  $a_d = 2$   $\mu$ m,  $v_d = 3.9$  mm/s, and  $n_d = 2$ . Grinding conditions were  $v_s = 45$  m/s,  $v_w = 26$  m/min,  $t_{so} = 10$  s, and  $Q'_w = 4$  mm<sup>3</sup>/mm/s.
- *High-speed B91 CBN wheel.* The high-speed B91 CBN wheel was dressed at  $v_r = -42$  m/s,  $a_d = 2$   $\mu$ m,  $v_d = 1.7$  mm/s, and  $n_d = 2$ . Grinding conditions were  $v_s = 120$  m/s,  $v_w = 26$  m/min,  $t_{so} = 2$  s, and  $Q'_w = 20$  mm<sup>3</sup>/mm/s.

**19.10.9.2 Inconel 718 Trials**

Three grinding wheels listed in Table 19.5 were each tested using an L<sub>8</sub>2<sup>7</sup> orthogonal array to determine the most favorable conditions.

The aluminum oxide wheel listed having 42% porosity gave better results than a number of other aluminum oxide wheels tested for grinding Inconel 718. The CBN wheels listed also had increased porosity, 40% compared with 35% and showed improved grinding performance for Inconel 718. Porosity was selected based on work by Cai [2002].



Dressing:	A1 = down	A2 = up
Dressing overlap:	B1 = 2	B2 = 10
Dressing depth:	C1 = 2 $\mu$ m	C2 = 10 $\mu$ m
Dressing passes:	D1 = 2	D2 = 10
Wheel speed:	E1 = 60 m/s,	E2 = 120 m/s
Workspeed:	F1 = 36 m/min	F2 = 54 m/min
Finish feed:	G1 = 5 $\mu$ m at 1 $\mu$ m/s,	
Dwell:		G2 = 10 s
Dresser speed:	H1 = 42 m/s	H2 = 72 m/s

**FIGURE 19.29** Direct effects chart for workpiece roughness: high-speed CBN grinding of AISI 52100.



**TABLE 19.5**  
**Grinding Wheel and Machine Combinations for**  
**Grinding Inconel 718**

Abrasive Type	Wheel Details	Wheel Speed (m/s)
Vitrified Al <sub>2</sub> O <sub>3</sub>	A80 J6V	45
Vitrified CBN	B151 (Medium speed)	45
Vitrified CBN	B151 (High speed)	60–120

Best dressing and grinding conditions for the three wheels used for Inconel 718 were

- *Conventional-speed Al<sub>2</sub>O<sub>3</sub> wheel.* The wheel was dressed with a single-point diamond,  $a_d = 2 \mu\text{m}$ ,  $v_d = 1.2 \text{ mm/s}$ , and  $n_d = 2$ . Grinding conditions were  $v_s = 45 \text{ m/s}$ ,  $v_w = 20 \text{ m/min}$ ,  $t_{so} = 10 \text{ s}$ , and  $Q'_w = 2 \text{ mm}^3/\text{mm/s}$ .
- *Conventional-speed vitrified B151 CBN wheel.* The wheel was dressed at  $v_r = -12.6 \text{ m/s}$ ,  $a_d = 2 \mu\text{m}$ ,  $v_d = 1.4 \text{ mm/s}$ , and  $n_d = 2$ . Grinding conditions were  $v_s = 45 \text{ m/s}$ ,  $v_w = 20 \text{ m/min}$ ,  $t_{so} = 10 \text{ s}$ , and  $Q'_w = 2 \text{ mm}^3/\text{mm/s}$ .
- *High-speed B151 CBN wheel.* The wheel was dressed at  $v_r = -42 \text{ m/s}$ ,  $a_d = 2 \mu\text{m}$ ,  $v_d = 8.5 \text{ mm/s}$ , and  $n_d = 2$ . Grinding conditions were  $v_s = 120 \text{ m/s}$ ,  $v_w = 26 \text{ m/min}$ ,  $t_{so} = 2 \text{ s}$ , and  $Q'_w = 2 \text{ mm}^3/\text{mm/s}$ .

**19.10.10 DIRECT-EFFECT CHARTS**

Direct-effect charts are the result of the experimental design described in Section 19.10.7. An example is shown in Figure 19.29. The example is for workpiece roughness in high-speed CBN grinding of AISI 52100. The results clearly show that high wheel speed reduces roughness.

A chart for grinding ratio is shown in Figure 19.30 for the same conditions as in Figure 19.29. Figure 19.30 shows that wear of the grinding wheel is greatly reduced by increasing wheel speed from 60 m/s to 120 m/s. This is correspondingly reflected by longer redress life as indicated in the following cost comparisons.

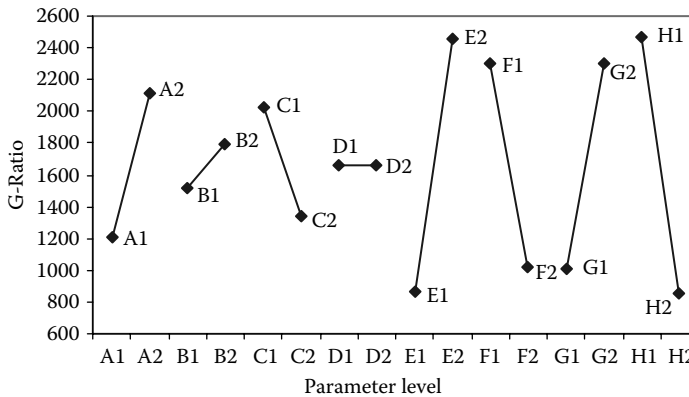


**FIGURE 19.30** Direct-effects chart for grinding ratio. High-speed CBN grinding of AISI 52100 using the same parameters as Figure 19.29.

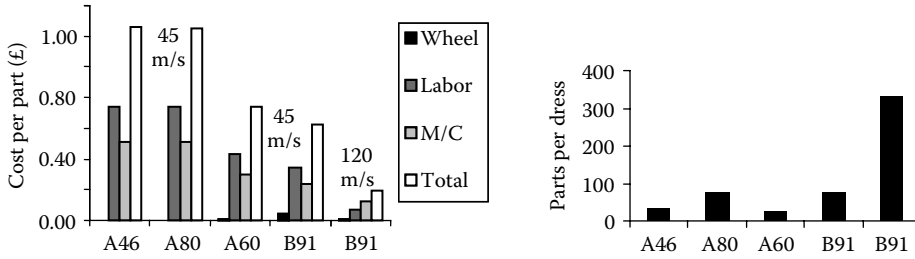


FIGURE 19.31 Comparisons of cost per part and redress life when grinding AISI 52100 with different grinding wheels and grinding conditions.

### 19.10.11 REDRESS LIFE AND COST COMPARISONS

#### 19.10.11.1 AISI 52100

Costs for grinding AISI 52100 were compared for the best conditions found for each grinding wheel and speed condition. The results are presented in Figure 19.31. An A60-SG abrasive designed for high removal rates gave the same quality level and reduced costs compared with conventional alumina abrasives. Vitrified CBN allowed an even higher removal rate at conventional speed further reducing costs and CBN at high speed allowed the highest removal rates and produced the lowest costs.

Costs per part were lower with high-speed CBN despite using a much more expensive machine for this speed. Redress life as indicated by the number of parts ground per dress was also increased using CBN and was further increased at high wheel speed.

#### 19.10.11.2 Inconel 718

Figure 19.32 compares costs/part when grinding Inconel 718 under the best conditions found with different grinding wheels. As with easy-to-grind material, CBN allowed lower costs at conventional wheel speed. However, this was at the same removal rate as used for the alumina wheel. Removal rate could not be increased due to the requirement to stay within tolerances over a reasonable redress life. One part/dress was achieved with alumina and 25 parts/dress with CBN. Using CBN at high wheel speed further improved redress life to 30 parts/dress. This improvement was achieved by limiting removal rate to 2 mm<sup>3</sup>/mm/s for all three conditions.

### 19.10.12 EFFECTS OF REDRESS LIFE

With AISI 52100, redress life was high, so that abrasive cost, dressing cost, and machine cost became negligible compared to removal rate. With high redress life, costs depend primarily on removal rate and

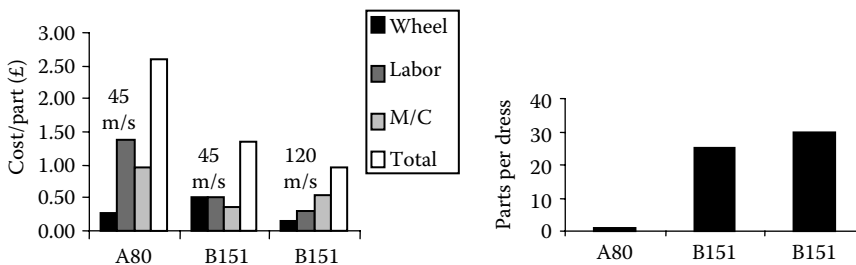


FIGURE 19.32 Comparison of costs per part and redress life when grinding Inconel 718 with different grinding wheels and grinding conditions.

dwelt time. This was also found when grinding at high speed with CBN. Increasing wheel speed allowed removal rates to be increased and dwell time to be reduced while maintaining redress life and quality levels.

However, redress life was short for Inconel 718. In this case, removal rates had to be kept low to allow redress life to be increased. Increasing redress life was the only way to reduce costs. Increasing wheel speed was important to increase redress life.

Figure 19.31 and Figure 19.32 show that high-speed CBN grinding reduces total cost/part for both materials. This is largely due to increased redress life. With AISI 52100, a high redress life was maintained with a high removal rate and short dwell time. With Inconel 718, removal rate had to be kept low to increase redress life. However, high wheel speed also allowed spark-out time to be reduced while maintaining workpiece quality and increased redress life.

### 19.10.13 ECONOMIC CONCLUSIONS

- Vitrified CBN offers advantages at conventional speeds and at high speeds even with a much more expensive machine. This is largely due to longer redress life.
- Increased removal rates are only economic if achieved with long redress life and good quality levels. Long redress life is particularly important in cost reduction for difficult-to-grind materials.
- With high removal rates, long redress life, and short spark-out periods, machine and abrasive costs become negligible.

## 19.11 THE MECHANICS OF ROUNDING

Rounding geometry was introduced in Section 19.2.5. A question of interest is whether centerless grinding is ultimately capable of the highest standards of roundness. In recent years, it has become apparent that achievable standards of roundness are approaching the limits of available measuring machines [Hashimoto et al. 1983].

The question of ultimate roundness is less likely to be posed in this way for most other processes such as cylindrical grinding between centers where the potential achievement of high accuracy tends to be taken for granted and is often assumed to depend only on practical considerations. This may be partly justified although high standards of roundness are often more easily obtained by centerless grinding rather than by grinding between centers where center holes need to be lapped to minimize transmission of shape errors to the cylindrical surface being produced.

### 19.11.1 AVOIDING CONVENIENT WAVINESS

Three- and five-lobe shapes may sometimes persist after centerless grinding. Fortunately, three- and five-lobe shapes may easily be removed by grinding at the correct height above center. Odd order lobing tends to persist with a zero or small value of the tangent angle. Odd order lobing is a constant diameter shape sometimes known as a Gleichdicke shape. A constant diameter Gleichdicke shape can exist and rotate between parallel tangents as provided by the grinding wheel and the control wheel at zero center-height. Gleichdicke deviations from circularity remain undetected by diameter measurement.

An example of a five-lobe shape is shown in Figure 19.33. The large roundness error resulted from grinding a workpiece at a zero tangent angle. The grinding wheel, control wheel, and workrest shapes are superposed on the greatly magnified deviations from circularity of the workpiece. Normally, it is impossible to see roundness errors with the naked eye.

The angle of the workrest has no effect on rounding at  $\beta = 0^\circ$ . This is because any small movements toward or away from the workrest simply cause the workpiece to move vertically up and down the vertical tangent at the control wheel contact point. As the workpiece rotates, the odd-lobe shape is accommodated in the constant distance between the grinding wheel and the control wheel.

Even-lobe shapes are more likely to occur at large values of tangent angle. This situation is also illustrated in Figure 19.33. In the example for  $\beta = 10^\circ$  and  $\gamma = 20^\circ$ , 16 waves are produced,

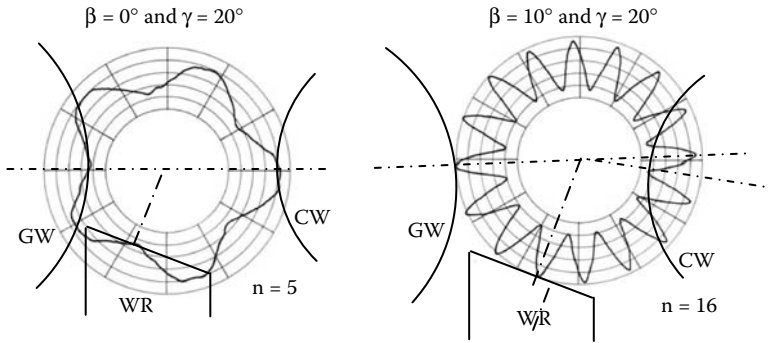


**FIGURE 19.33** Examples of convenient waviness related to the set-up geometry.

that is,  $n = 16$ . An explanation for the susceptibility of this setup to 16 waves can be found by considering the angular pitch of the waviness,  $p = 360/n$ . Each wave in this example is separated by a pitch,  $p = 360/16 = 22.5^\circ$ . Sixteen waves fit neatly so that the waviness is almost unaffected by movement against the workrest. This can be demonstrated as follows.

For  $\beta = 10^\circ$  and  $\gamma = 20^\circ$ , the value  $\alpha \approx 66^\circ$  so that

$$\frac{\alpha}{p} \approx 2.93 \approx 3 \text{ is equal to an integer}$$

Due to the integer relationship, 16 waves are practically unaffected by the contact with the workrest. A peak in contact with the workrest coincides with a peak at the grinding contact. Corrective action due to contact with a workrest is explained in more detail in Section 19.11.2.

Sixteen waves are also unaffected by contact with the control wheel since

$$\frac{180 - \beta}{p} = 7.55 \approx 7.5 \text{ is equal to a half-integer}$$

The implication is that when the crest of a wave contacts the control wheel, the trough of another wave contacts the grinding wheel and there is no corrective action.

It might be expected that  $n = 18$  with  $p = 20^\circ$  would also be a problem for  $\beta = 10^\circ$ , since  $180 - \beta = 8.5 \cdot p$ . This provides exactly the half-integer relationship required for insensitivity to the control wheel contact. However, in this case,  $\alpha \approx 3.3 \cdot p$ , which is well removed from an integer value and is closer to being a half-integer value. The workrest, therefore, has a stronger corrective action on 18 waves than in the previous example for 16 waves.

### 19.11.1.1 Rules for Convenient Waviness

Based on the reasoning discussed before, three conditions can be established. If  $180^\circ - \beta$  gives a half-wavelength,  $360^\circ$  gives a multiple of a whole wavelength, and  $\alpha$  gives a multiple of a whole wavelength, waviness will persist. These three conditions follow.

The number of waves,  $n$ , is an integer.

$$180 - \beta \approx \left( n_1 - \frac{1}{2} \right) \cdot \frac{360}{n} \tag{19.41}$$

$$\alpha \approx n_2 \cdot \frac{360}{n} \tag{19.42}$$

where  $n_1$  and  $n_2$  are other integers.

Miyashita [1965] gave the conditions for convenient waviness as

$$n \cdot \alpha / 180 = \text{even number} \quad (19.43)$$

and

$$n \cdot (180 - \beta) / 180 = \text{odd number} \quad (19.44)$$

Moriya, Kanai, and Miyashita [1994] recommended that  $\alpha/\beta$  should be equal to an odd number to avoid convenient waviness.

It is important to avoid geometry vulnerable to convenient waviness. In the above example, changing the workrest angle to  $30^\circ$  and changing the tangent angle to  $7^\circ$  greatly reduces the risk of convenient waviness. This conclusion can be checked using a spreadsheet or a calculator to check a range of values of  $n$  for near-integer values of  $n_1$  and  $n_2$ .

From a practical viewpoint, it is important to avoid a workspeed that aligns a known source of excitation with a convenient waviness. For example, if  $n = 22$  is a convenient waviness and wheel speed is 20 rev/s, it would be important to avoid a workspeed of 1.1 rev/s since any change in wheel unbalance will directly excite the convenient waviness.

Another practical possibility for reducing roundness errors is to vary the set-up geometry during the grinding operation [Harrison and Pearce 2004]. Perhaps the simplest way to do this is to employ a larger tangent angle for roughing than for finishing. However, it is suggested that if two set-up geometries are employed, both setups should provide a strong rounding tendency.

The analysis of rounding geometries is explored further in Sections 19.12 and 19.13 with reference to process stability.

### 19.11.2 THEORY OF THE FORMATION OF THE WORKPIECE PROFILE

Dall [1946], in the first analytical approach to predicting roundness, used two basic parameters, the tangent angle  $\beta$  and the top workrest angle  $\gamma$  shown in Figure 19.4. He calculated the magnitude of the error reproduced on the workpiece as a result of one already occurring at its point of contact either with the workrest or with the control wheel. The calculations assumed a perfectly rigid machine.

Yonetsu [1959] derived relationships between pregrinding and postgrinding amplitudes of harmonics of the workpiece profile. Theoretical relationships were obtained for the case of a sudden infeed and these were compared with experimental results for infeed made over three revolutions of the workpiece. The theory showed qualitative agreement with the results. Three conclusions reached by Yonetsu were

- Lobed shapes related to odd harmonics below the 11th are better removed with a large tangent angle  $\beta$ .
- Lobed shapes related to even harmonics below the 10th are better removed with a small angle  $\beta$ .
- Other errors are generated, which include even and odd order harmonics that vary with  $\beta$  and it was suggested that these are related to the infeed motion.

Unfortunately the technique is unsuited to a conventional method of stock removal.

Becker [1965] suggested an optimum geometrical configuration for rounding 2, 3, 5, and 7 lobe shapes. This suggestion was reached by investigating a parameter  $s/R$ . The term  $\delta s$  is the difference in the apparent depths of cut when the particular shape is contained in its two extreme positions in the grinding configuration, and  $\delta R = \Delta$  is the roundness error. It was proposed that the larger this parameter is, the greater will be the tendency to remove the shape. On the assumption

that the optimum value of the tangent angle is  $\beta = 6^\circ$ , it was suggested that the optimum workrest angle  $\gamma = 23^\circ$ . Decreasing the workrest angle to  $-10^\circ$  improves the situation slightly for 3 and 5 lobes but worsens the situation for the ellipse and 7 lobes. Increasing the workrest angle is detrimental for 2, 3, and 5 lobes and if over  $35^\circ$  for 7 lobes too. This method enables definite results to be obtained and is simpler than the method of Yonetsu. However, it does not allow an assessment of the final shape to be made nor does it take the elasticity of the machine into account.

The stability of the process was investigated by Gurney [1964]. It was concluded that errors will be generated during the spark-out period and that the stiffer the machine the greater will be the errors. It was also suggested that the grinding wheel may not always remain in contact with the workpiece during the spark-out period.

It was realized in the early days of computers that it would be possible using a mainframe computer to carry out a realistic simulation of the plunge-grinding process taking a number of important factors into account that would otherwise be ignored such as spark-out, machine deflections, vibrations, loss of contact, grinding wheel curvature, and control wheel curvature [Rowe and Barash 1964]. Importantly, by means of simulation, it was possible to show the rate of buildup of regenerated roundness errors. In some cases, a geometric configuration might be theoretically unstable but relatively stable for practical purposes due to the high frequency of the instability and limitations of buildup due to the large arc of contact with the grinding wheel.

The technique revealed several new aspects of the process including some contradictory indications for the effect of machine stiffness. It was, for example, found that work-regenerative vibrations due to geometric instability grew more rapidly with a very stiff machine. However, the elimination of roundness errors in a stable rounding process was usually improved with a stiff machine. It was also possible to explore the introduction of roundness errors due to the plunge-feed process. All these results were verified by experiments and dynamic analysis. The simulation technique and some experimental results are reported here.

Geometric work-regenerative instability was shown to be a special case of more general work-regenerative vibration instability [Rowe 1964]. Other workers such as Richards and Rowe [1972] have since presented stability charts for use in selection of rounding geometry for use in grinding.

Miyashita [1965] analyzed the role of machine vibrations in the generation of workpiece errors. Reeka [1967], following on from Becker, demonstrated the importance of the number of workpiece revolutions in reducing roundness errors.

The rounding process has been analyzed by various workers since, as indicated by the extensive list of references given at the end of the chapter. Extensive results for centerless grinding, either below center or above center, were presented by Johnson [1989].

### 19.11.3 WORKPIECE MOVEMENTS

This discussion deals only with the case of plunge feed, although the analysis has significance also for through-feed.

Figure 19.34 defines position on the workpiece. A line of origin OX can be considered to rotate with the workpiece. Positions on the workpiece surface are defined by the angle from the line of origin. The position A is defined by the angle  $\theta$  so that as the workpiece rotates the angle  $\theta$  increases. When  $\theta = 0$  or  $\theta = 2n\pi$  the line OX is coincident with OA.

In a similar way, Point B at  $\theta - \alpha$  defines the point of contact with the workrest. Point C at  $\theta - \pi + \beta$  defines the point of contact with the control wheel.

If an irregularity on the workpiece arrives at the workrest as shown in Figure 19.34, the center of the workpiece will be displaced. Assuming the workpiece movement is constrained to slide along the tangent of workpiece contact with the control wheel, the movement can be calculated. The workpiece will be pushed away from the workrest at Point B. As a consequence of the movement the workpiece will move away from the grinding wheel at Point A. In this way, an irregularity at Point B gives rise to a further irregularity at Point A. The irregularity can be considered as a local shape error.



The true reduction in radius at the grinding wheel contact point A is  $r(\theta) = R(\theta) - x(\theta)$ , where  $x(\theta)$  is the deflection at the grinding point. Equation 19.45, therefore, becomes

$$r(\theta) = X(\theta) - x(\theta) + K_1 \cdot r(\theta - \alpha) - K_2 \cdot r(\theta - \pi + \beta) \quad (19.46)$$

For the case where  $\beta = 10^\circ$  and  $\alpha = 55^\circ$ , the value of  $K_1$  is approximately equal to 0.2 and the value of  $K_2$  is approximately equal to 0.9. Clearly, an irregularity arriving at the control wheel contact point has a stronger effect than an irregularity arriving at the workrest contact point.

#### 19.11.4 THE MACHINING-ELASTICITY PARAMETER

The machining-elasticity parameter  $K$  is a measure of the springiness of a grinding system. The parameter provides a convenient way to account for elastic deflections of the system due to grinding force. The use of the machining-elasticity parameter works best at frequencies well below the dominant resonant frequency of the system.

$$K = \frac{\text{true depth of cut}}{\text{set depth of cut}} = \frac{a_e}{A} \quad (19.47)$$

Values of  $K$  lie between 0 and 1. High grinding forces and low machine stiffness lead to a low value of  $K$ . A low value might be less than 0.1. Values greater than 0.4 are considered to be high.

It is possible to determine  $K$ , by measuring two stiffness values of the grinding system. This may be demonstrated as follows by considering the relationship between depth of cut and machine system deflections.

The set depth of cut is the sum at any instant of the deflection  $x$  and the true depth of cut  $a_e$ . The value  $K$  can, therefore, be written in the form

$$K = \frac{a_e}{x + a_e} \quad (19.48)$$

True depth of cut and deflection are both approximately proportional to normal grinding force, so that

$$K = \frac{\lambda_0}{k_s + \lambda_0} \quad (19.49)$$

where  $k_s$  is the cutting stiffness and  $\lambda_0$  is the static machine stiffness.

The cutting stiffness depends on workpiece hardness, grinding wheel sharpness, width of cut, and depth of cut. High cutting stiffness leads to high grinding forces. Static machine stiffness includes the combined effect of the grinding wheel, workpiece, and machine structural elements.

A simple alternative method for measuring  $K$  depends on measuring any parameter proportional to depth of cut during “feeding-in” or “sparking-out.” If the grinding machine is fitted with a suitable force transducer or a power-meter capable of showing instantaneous power, the following technique can be used.

In sparking-out, set depth of cut is removed only after a number of revolutions. The rate of decrease of depth of cut depends on the value of  $K$ . If the apparent depth of cut has a value  $a_0$  at the commencement of dwell,  $a_{e1}$  is the real depth of cut in the first half-revolution. The depth of cut diminishes each half-revolution.

$$a_{e1} = K \cdot a_0 \quad (19.50)$$

$$a_{e2} = K \cdot (a_0 - a_{e1}) = (1 - K) \cdot a_{e1} \quad (19.51)$$



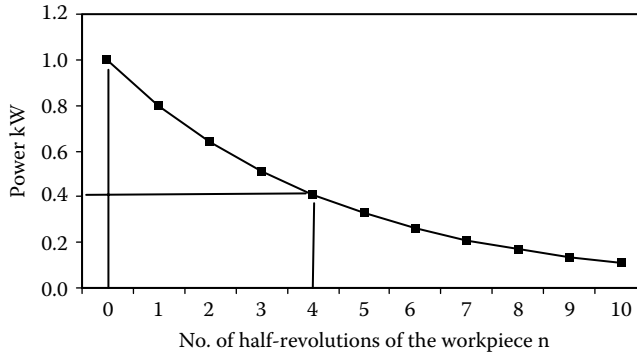


FIGURE 19.35 Power decay during spark-out for  $K = 0.2$ .

After  $n$  half-revolutions

$$\frac{a_{em}}{a_{em-n}} = (1 - K)^n \tag{19.52}$$

If true depth of cut is proportional to grinding power,

$$\frac{P_m}{P_{m-n}} = (1 - K)^n \tag{19.53}$$

The combined effect of grinding force and deflections can be measured by taking the ratio of two values of grinding power separated by  $n$  half-revolutions of the workpiece as illustrated in Figure 19.35.

A typical value of  $K$  for a grinding system is  $K = 0.2$ . This represents a situation where the real depth of cut is one quarter of the total elastic deflections in the system. In this case, the power decays to 0.41 of the starting value after four half-revolutions of the workpiece. The value of  $K$  can be found by plotting the log values of the power decay against  $n$  to obtain a straight line. The slope of the graph is  $\log_e(1 - K)$ .

### 19.11.5 THE BASIC EQUATION FOR ROUNDING

The true depth of cut at any position  $\theta$  is the difference in workpiece radius at that position and the value of radius at the same position one revolution earlier.

$$a_e(\theta) = r(\theta) - r(\theta - 2\pi) \tag{19.54}$$

Similarly, the set depth of cut is the difference between the set reduction in radius at a particular position and the true reduction in radius one revolution earlier.

$$A(\theta) = R(\theta) - r(\theta - 2\pi) \tag{19.55}$$

Substituting Equation 19.45 into Equation 19.55 and from Equation 19.47 and Equation 19.54, the Basic Equation results:

$$r(\theta) = K \cdot [X(\theta) + K_1 \cdot r(\theta - \alpha) - K_2 \cdot r(\theta - \pi + \beta) - r(\theta - 2\pi)] + r(\theta - 2\pi) \tag{19.56}$$

This basic equation with some restrictions may be used to simulate a wide variety of conditions that occur in centerless grinding.

19.11.6 SIMULATION

Simulation is a technique that became popular with the advent of computers. In 1961, it was realized that simulating the process on the Manchester University Mercury computer would make it possible to compare experimental workpiece shapes with predicted shapes and hence discover many important aspects of how the process works [Rowe and Barash 1964]. The technique is reviewed here for its usefulness in explaining the rounding process.

The workpiece circumference is divided into small steps with respect to a radial line of origin. Typically, steps of 1° were sufficient. Initial values of workpiece radius errors were stored for positions around the workpiece. These values represent a set from  $r(-360)$  to  $r(-1)$  when  $\theta = 0^\circ$ . These values, along with any suitable increments for the infeed motion, can be fed into Equation 19.56. The angle theta is increased one step at a time and values calculated for  $r(\theta)$ . These values are stored and represent the developing profile of the workpiece.

It is thus possible to examine the effects of different infeed functions including the importance of the dwell period. Various initial shapes can be investigated as these are a main source of variability between final shapes after grinding. It is even possible to consider the effects of machine vibrations on roundness.

It quickly becomes apparent that restrictions need to be applied to prevent radius increasing. This is the metal replacement restriction and is applied by incorporating a conditional statement. This and other restrictions required are

- *Metal Replacement Restriction.* The value of  $r(\theta)$  is compared with the value of  $r(\theta - 2\pi)$  and replaced by the previous value whenever metal replacement is implied.
- *Grinding Wheel Interference.* With high frequencies and large radius variations from step to step, it is not possible for the shape to be accommodated. This is because the radius of the grinding wheel will interfere with workpiece positions adjacent to the point of contact. This is illustrated in Figure 19.36.

Grinding wheel interference has a practical benefit in grinding in that it limits the development of higher frequency vibrations and has the effect of smoothing the profile. The restriction is applied at nearby positions by calculating the clearance,

$$W_\psi = \left[ \frac{1}{\cos \psi} - 1 \right] \cdot \frac{d_w}{2} \tag{19.57}$$

and the interference,

$$I_\psi = r(\theta) + W_\psi - r(\theta - 2\pi) \tag{19.58}$$

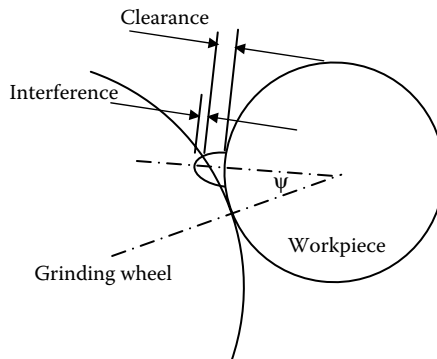
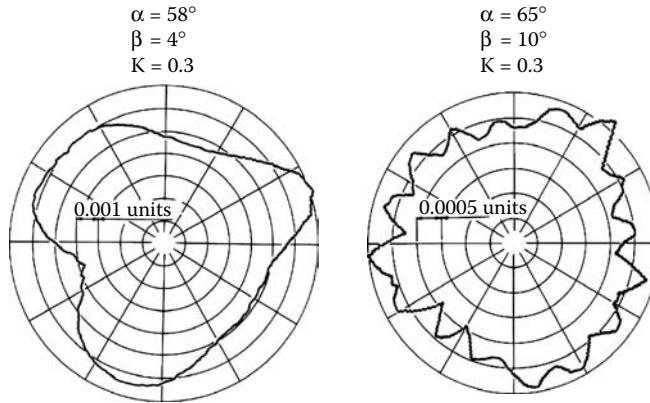


FIGURE 19.36 Grinding wheel interference from positions adjacent to the grinding point.



**FIGURE 19.37** Simulated roundness for a uniform infeed of 1 unit/rev for 45 revolutions.

Modifications only need to be made for positive interference. An amount of material is removed at the adjacent position equal to the interference,  $I_\psi$ , multiplied by the machining-elasticity parameter  $K$ .

- Control Wheel Interference and Workrest Interference Restrictions. Interference at the control wheel and workrest are calculated similarly to the previous example. The largest interference is found and subtracted from the usual term at each contact.

Figure 19.37 shows typical simulation results for a uniform infeed. In both cases, errors due to the infeed are less than 1% of the infeed per revolution after 45 revolutions.

With small values of  $\beta$ , 3 and 5 lobe shapes predominate. Constant diameter shapes can roll between parallel tangents in the same way as a pure cylinder. With zero tangent angles, there is, therefore, no rounding action of odd lobe shapes. With  $\beta = 10^\circ$  and  $\gamma = 20^\circ$ , the rounding geometry is unstable for 16 lobes. The resulting roundness errors are small because there was very little excitation of the instability in the simulation. In practice, roundness errors are very much affected by level of excitation.

Poor roundness will result if the machine resonates at a frequency of instability. The workspeed should, therefore, be set to avoid excitation of an unstable frequency. For this geometry, and a resonant frequency of 72 Hz, workpiece speeds should be avoided in the region of

$$n_w = \frac{72}{16} = 4.5 \quad \text{rev per second}$$

Initial shape errors vary greatly in practice depending on the previous machining process. Effects of initial shape on the final ground shape were investigated using a controlled error. A small flat was machined along the length of the workpiece as described in Section 19.11.7. The workpiece with a flat has a similar effect in grinding to an impulsive force and excites a wide range of frequencies each time the flat passes a contact point.

A series of simulations was performed for a workpiece with a flat. Amplitudes of the workpiece shape harmonics determined by Fourier analysis are illustrated in Figure 19.38. It is seen that 5 lobes predominate at a low tangent angle and even-order lobing at larger tangent angles. At  $10^\circ$ , 16 waves are strongly evident. At  $8^\circ$ , 22 waves appear and also 44 waves. As the tangent angle is increased, the number of even order waves for the predominant harmonic reduces. That is 32 waves, 22 waves, and then 16 waves. Lower numbers of waves tend to present a greater problem than higher numbers of waves. This is because higher frequencies are more likely to be filtered by interference with the grinding wheel, control wheel, and workrest. Higher frequencies may also be smoothed by workpiece inertia.

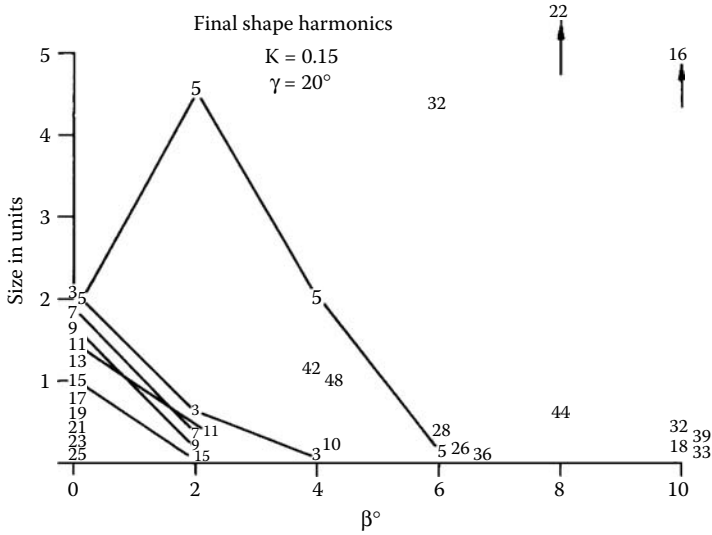


FIGURE 19.38 Simulated grinding of a workpiece with a flat 41 units deep with a 20° workrest.

Figures 19.39 shows simulation results for a 30° workrest. Despite assuming a more compliant system,  $K = 0.08$ , the rounding action was much stronger than in the previous case. The buildup of even-order waviness was less pronounced with the 30° workrest than with a 20° workrest.

19.11.7 ROUNDNESS EXPERIMENTS AND COMPARISON WITH SIMULATION

All roundness problems predicted by simulation were experienced in practice when grinding a workpiece with a flat and sometimes when grinding an initially circular workpiece. The simulation technique was tested by comparison with an experimental shape measured after grinding. The pregrinding shape of the workpiece with a flat is shown in Figure 19.40. The workpiece was then ground to the depth of the flat. That is, the radial stock removed was 57 μm. The postgrinding shape is shown in Figure 19.41.

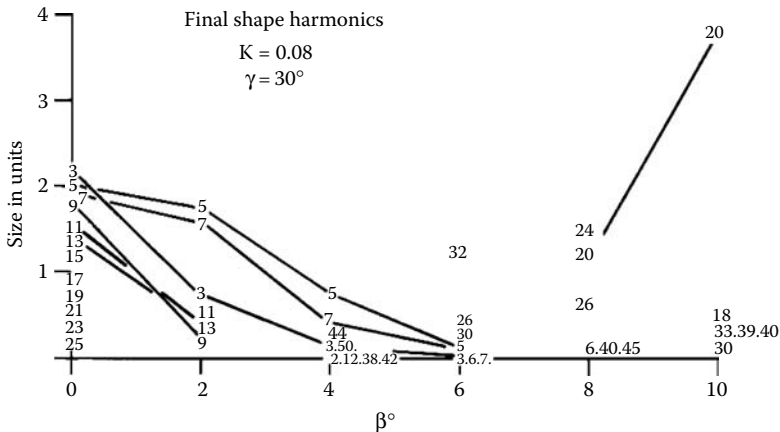
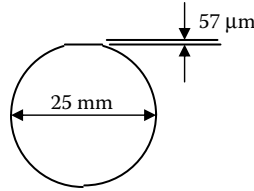


FIGURE 19.39 Simulated grinding of a workpiece with a flat using a 30° workrest.



**FIGURE 19.40** The initial workpiece shape used for experimental determination of rounding effect.

The shape predicted by simulation is shown in Figure 19.41. Agreement with the experimental shape is excellent considering the duration of the grinding cycle over 50 workpiece revolutions. An interesting aspect of the simulation was that it confirmed that the particular grinding setup represented a very compliant system with  $K = 0.08$ . This means the depth of cut at any instant was less than 10% of the deflections.

Good correlation between theory and experiment is obtained when the initial workpiece irregularity is large, so that the effect of initial shape predominates over other effects. Usually, grinding results, when magnified to a high degree, exhibit an almost random spread of shapes and magnitudes reflecting the variety of pregrinding shapes and the buildup of errors on the grinding wheel and control wheel. The advantage of working with a large initial roundness error is that it allows the systematic rounding effect to be clearly seen (Figure 19.5 and Figure 19.42).

Starting with a round workpiece, it might be expected that a perfectly round workpiece should result. Simulation shows that this is not necessarily so. Even with a uniform infeed motion and careful sparking-out, small errors result due to the geometry of the rounding action. With a compliant system and optimum setup of the rounding geometry, errors due to infeed motion are extremely small. Typically, the magnitude of the roundness errors due to the infeed motion was less than two thousandths of the magnitude of the infeed per revolution. This means, for example, that if the depth of cut were  $10\ \mu\text{m}$ , the roundness error would typically be  $0.01\ \mu\text{m}$ . In other words the effect is negligible compared with typical roundness errors ranging in precision grinding from  $0.2$  to  $1.0\ \mu\text{m}$ .

In practice, the best roundness depends on a number of factors including machine vibrations, bearing precision, dressing precision, and wheel wear as outlined in the discussion of the system in Section 19.2.6.

All the roundness problems predicted by simulation were experienced in practice when grinding a workpiece with a flat and sometimes when grinding an initially circular workpiece.

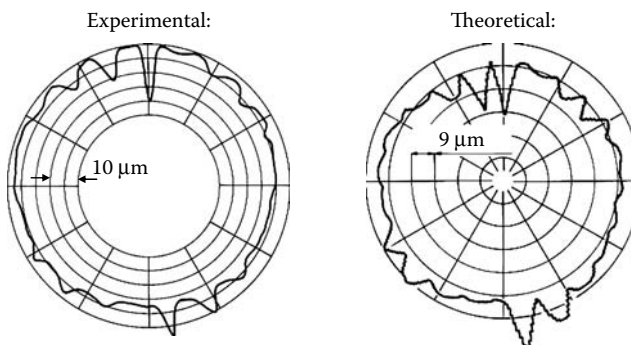


**FIGURE 19.41** Experiment compared with simulation.  $\gamma = 20^\circ$ ,  $\beta = 8^\circ$ ,  $K = 0.08$ . Initial shape: workpiece with flat.

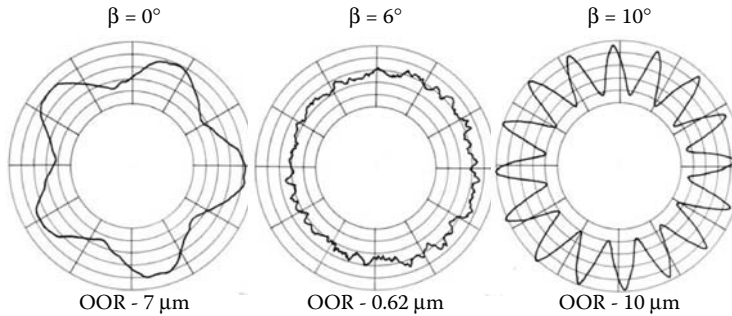


FIGURE 19.42 Experimental roundness resulting from grinding a workpiece with a flat using a 20° workrest.

## 19.12 VIBRATION STABILITY

### 19.12.1 DEFINITIONS

The following definitions are helpful in making distinctions between different types of vibrations that may be experienced in centerless grinding.

#### 19.12.1.1 Marginal Stability

Marginal stability is where waviness neither builds up nor decays as grinding proceeds without direct excitation of the marginally stable frequency. In practice, a linear system excited at a frequency of marginal stability will experience large vibrations only limited by system nonlinearity. Convenient waviness was described earlier in this chapter. Convenient waviness is waviness that can persist and is not corrected by the rounding geometry. Convenient waviness that neither builds up nor decays is termed “marginal geometric stability.”

#### 19.12.1.2 A Stable System

There has also been discussion of the mechanism of rounding. In the case of rounding, it is implied that the system is stable and roundness errors are reduced as grinding proceeds. In a stable system, waviness decays. However, it should be remembered that a stable system produces waviness when there is a source of vibration excitation.

#### 19.12.1.3 An Unstable System

An unstable situation is where waviness and vibration build up as grinding proceeds without a need for direct excitation. If the waviness builds up primarily on the workpiece, the instability is termed “work-regenerative chatter.” Another type of instability is where waviness primarily builds up on the grinding wheel circumference or on the control wheel circumference. This second type of instability is termed “wheel-regenerative chatter.” Wheel-regenerative chatter often builds up slowly with the grinding of successive workpieces so that the instability may not be apparent until a number of workpieces have been ground. The waviness on each succeeding workpiece increases with the waviness on the wheels.

#### 19.12.1.4 Chatter

In machining, an unstable system is said to chatter, since in metal turning and milling, unstable vibrations are characterized by audible vibrations or “chatter.” In grinding, unstable regeneration of waviness and vibrations may occur, but due to a more gentle character the vibrations are not

necessarily audible. The term “chatter” is used to describe regeneration of waviness and vibration due to an unstable system, whether it is audible or inaudible. Chatter should not be confused with forced vibration.

### 19.12.1.5 Forced Vibration

Forced vibrations may occur in stable systems and do not imply chatter or instability. Forced vibrations occur due to the action of the normal machine forces. Examples of forced vibrations are the vibrations forced by grinding wheel unbalance, motor unbalance, uneven belt drives, OOR of the wheel spindles, and cyclic forces due to worn or inaccurate rolling elements in the bearings. Forced vibrations are mostly characterized by a repetitive and constant frequency that can be related to the speed of the offending machine element. It is particularly important to avoid coincidence between a forced vibration frequency and a marginally stable frequency. This situation can usually be avoided by judicious choice of workspeed.

The motivation to analyze stability is the need to design and operate systems for best roundness and to avoid the buildup of waviness due to instability. In principle, most grinding systems will be unstable according to one definition or another. In practice, it is possible to arrive at systems that yield very low roundness errors. Section 9.11 discussed ways to minimize the effect of convenient waviness. Convenient waviness is an example of marginal geometric stability. The following analysis aims to throw further light on problems that may arise and ways to overcome them. Clearly, it is also important to determine where systems may be positively unstable and take measure to avoid this more serious condition.

### 19.12.2 A MODEL OF THE DYNAMIC SYSTEM

The dynamic system is represented in Figure 19.42 [Rowe 1979].

In Section 19.11.3, the geometry relationships were defined in terms of angle. A dynamic system also depends on time and acceleration. Referring to Section 19.11.5, the main relationships in terms of angular position on the workpiece are

$$r(\theta) = X(\theta) - x(\theta) + K_1 \cdot r(\theta - \alpha) - K_2 \cdot r(\theta - \pi + \beta) \quad \dots \quad \text{waviness} \quad (19.59)$$

$$a_e(\theta) = r(\theta) - r(\theta - 2\pi) \quad \dots \quad \text{depth of cut} \quad (19.60)$$

$$x(\theta) = \frac{1}{\lambda(\theta)} F_n(\theta) \quad \dots \quad \text{deflection} \quad (19.61)$$

$$F_n(\theta) = k_s \cdot a_e(\theta) \quad \dots \quad \text{normal force} \quad (19.62)$$

$$r_s(\theta) = C_{sw} \cdot F_n(\theta) + r_s \left( \theta - 2\pi \frac{\Omega_w}{\Omega_s} \right) \quad \dots \quad \text{grinding wheel wear} \quad (19.63)$$

Ideally, control wheel wear and workrest wear should be included in addition to the grinding wheel wear effect. However, these effects are usually much less significant.

Analysis of system stability starts from a general solution of waviness as a function that develops exponentially with time and has complex solutions of the complementary function of the form  $r(t) = c \cdot e^{pt}$ . The roots of the complementary function have the form  $p = \sigma + j\omega$ . The real part,  $\sigma$ , governs the growth rate of the system. A negative value implies a stable decay of the function. A positive value represents an unstable exponentially increasing value. The imaginary part,  $\omega$ , represents frequency. A zero value,  $\sigma = 0$ , corresponds to solutions of the form  $r(t) = c \cdot \sin \omega t$ . This is a waviness condition of marginal stability and constant amplitude.

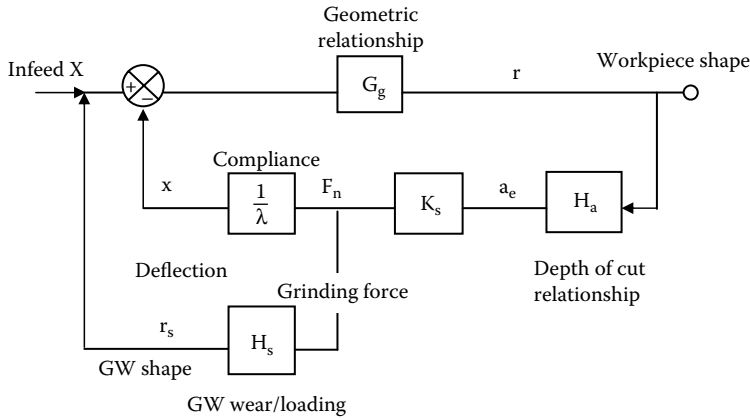


FIGURE 19.43 Representation of grinding as a dynamic system.

If the system has an input function of the form  $u_i = C \cdot \sin \omega t$ , the output of a linear stable system will have the form  $u_o = D \cdot \sin(\omega t + \phi)$  where the amplitude is changed and there is a phase difference between the input and the output sine waves. It is important to realize that a sinusoidal forcing function at a frequency of marginal stability leads to an infinite response. A zero growth rate is, therefore, unstable.

Waviness expressed in terms of angle is  $r(\theta) = c \cdot \sin(2\pi\omega/\Omega) = c \cdot \sin 2\pi n$  where  $\Omega$  is the workpiece speed in radians per second and  $n$  is the number of waves on the workpiece.

Transfer functions give the amplification and phase between the input and output for each block in the system.  $G_g$  gives the amplitude and phase of the wave produced at the grinding point for a sine wave input at the grinding point. Thus, if the feedback produces a workpiece reduction in radius in phase with the existing waviness, the amplitude will tend to grow. If the feedback produces a small reduction in radius in antiphase, the amplitude will tend to decay. A reduction in radius leading or lagging the existing waviness will create a wave that is constantly shifting around the workpiece periphery.

The denominator of a transfer function equated to zero is the characteristic equation of the system or subsystem. The characteristic equation expresses the condition for infinite amplitude response to a sine wave input.

In Laplace form, the transfer functions shown in Figure 19.43 are

$$G_g(s) = \frac{r(s)}{X(s)} = \frac{1}{1 - K_1 e^{-\alpha s} + K_2 e^{-(\pi-\beta)s}} \quad \text{geometric function} \quad (19.64)$$

$$H_a(s) = \frac{a_e(s)}{r(s)} = 1 - e^{-2\pi s} \quad \text{depth of cut function} \quad (19.65)$$

$$\frac{1}{\lambda(s)} = \frac{x(s)}{F_n(s)} \quad \text{compliance function} \quad (19.66)$$

$$H_s(s) = \frac{r_s(s)}{F_n(s)} = \frac{1}{1 - e^{-2\pi s/\Omega_s}} \cdot C_{sw} \quad \text{wheel wear function} \quad (19.67)$$

Work-regenerative stability depends on the main feedback loop in Figure 19.43. The open-loop transfer function for the work-regenerative effect is the product of four terms. The main open-loop



transfer function in this case relates the vibration deflections  $x(s)$  fed back at the grinding point to the prescribed infeed motion  $X(s)$ .

$$\frac{x(s)}{X(s)} = K_s \cdot \frac{1}{\lambda(s)} \cdot G_g(s) \cdot H_a(s) \quad \text{Open-loop transfer function} \quad (19.68)$$

At the limit of stability, the open-loop transfer function is equal to  $-1$ . The open-loop transfer function for limiting stability arranged in terms of angles and number of waves  $n$  is

$$\frac{k_s}{\lambda(s)} (1 - e^{-j2\pi n}) + 1 + K_2 e^{-jn(\pi-\beta)} - K_1 e^{-jn\alpha} = 0 \quad (19.69)$$

The system compliance can be approximated for very low frequencies by writing  $\lambda(s) = \lambda_0$ . This is useful when the waviness corresponds to a frequency well below the principal machine resonance.

A similar open-loop transfer function may be written for the reduction in grinding wheel radius in the wheel regenerative loop.

$$\frac{r_s(s)}{X(s)} = K_s \cdot G_g(s) \cdot H_a(s) \cdot H_s(s) \quad (19.70)$$

Wheel-regenerative vibration builds up waviness on the grinding wheel with increasing duration of grinding. When roundness errors exceed an acceptable level, the grinding wheel must be dressed to restore accuracy.

### 19.12.3 NYQUIST TEST FOR STABILITY

The Nyquist Criterion can conveniently be employed to test for stability. The Nyquist Criterion states that a system will be unstable if the open-loop transfer function encircles the point  $(-1, 0)$  on the negative real axis in a clockwise direction. With a small modification, the test may also be applied to the characteristic equation; the characteristic equation being the denominator of the closed-loop transfer function set to zero. In this case, instability is indicated by encirclement of the origin  $(0, 0)$  instead of the  $(-1, 0)$  point.

It can be seen that the term  $G_g(s) \cdot H_a(s)$  features in both the work-regenerative and the wheel-regenerative loop transfer functions. It is, therefore, important in avoiding instability to ensure that this term is stable. The frequency characteristics of the functions can be explored in the usual way by substituting  $s = j\omega$ .

The following paragraphs explore the stability problem using Nyquist diagrams. Nyquist diagrams are used for simplicity compared to other methods.

### 19.12.4 THE DEPTH OF CUT FUNCTION

The depth of cut function  $H_a(j\omega) = 1 - \cos \omega T + j \cdot \sin \omega T$  is a circle of unit radius centered at the point  $(1, 0)$  on the real axis as the term  $\omega T$  is varied from  $0$  to  $2n\pi$  as illustrated in Figure 19.44. The period  $T$  is related to the workpiece rotational frequency  $\Omega$  expressed in radians per second by  $T = 2\pi/\Omega$ . The number of waves is given by  $n = \omega/\Omega$ , leading to the function  $H_a(j \cdot n) = 1 - \cos 2\pi n + j \cdot \sin 2\pi n$ .

The function has real values at  $0$  and  $+2$ . The real axis represents in-phase depth of cut. The point where the locus crosses the real axis at  $0$  is an integer wave condition where the new wave  $r(\theta)$  is in phase with the old wave  $r(\theta - 2\pi)$  passing the grinding point one revolution earlier. For a constant in-phase amplitude of waviness, excitation of the grinding force is zero. This condition occurs with convenient waviness. Excitation of the force is zero for a large waviness. For integer waves, the compliances and forces have no effect on limiting stability.

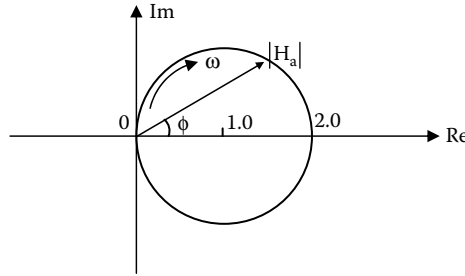


FIGURE 19.44 The frequency characteristics of the depth of cut function.

The point where the locus crosses the real axis at +2 corresponds to the half-integer wave condition where the new wave is exactly 180° out of phase with the old wave. This condition causes a depth of cut amplitude that is double the amplitude of the wave. Instability at frequencies close to this condition corresponds to the harsh nature of chatter experienced in cutting and milling operations. Excitation of the chatter force may be large compared to the case of convenient waviness.

19.12.5 THE GEOMETRIC FUNCTION

The geometric function  $G_g(s)$  as illustrated in Figure 19.45 represents an inner feedback loop in Figure 19.43.

The two feedback terms form circles when varying frequency. The larger circle in Figure 19.46(a) is the control wheel feedback and the smaller circle is the workrest feedback. If the two terms are added, the feedback locus is a spiral of approximate circles varying in size depending on the number of waves. Figure 19.46(b) shows the characteristic equation of the geometric function  $1/G_g(j \cdot n)$  for 16 to 18 waves. Encirclement of the origin indicates geometric instability for 16 waves.

Near the origin, the wave at the control wheel position is in antiphase with the wave at the grinding point. At the workrest, the wave is in phase with the wave at the grinding point as described in the earlier discussion on convenient waviness.

If the locus passes the origin on the negative side, waviness builds up because the feedback adds to the wave at the grinding point. This allows us to define a geometric stability parameter “A.” When A becomes negative the system is geometrically unstable. The parameter A represents feedback to the depth of cut in phase with the waviness. The imaginary part, “-B” represents feedback in quadrature with the waviness. Plotting these two parameters forms the locus  $1/G_g(j \cdot n)$ .

$$\text{Re} = A = 1 + K_2 \cos[n(\pi - \beta)] - K_1 \cos[n\alpha] \tag{19.71}$$

$$\text{Im} = -B = K_1 \sin[n\alpha] - K_2 \sin[n(\pi - \beta)] \tag{19.72}$$

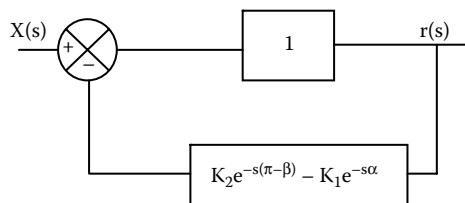
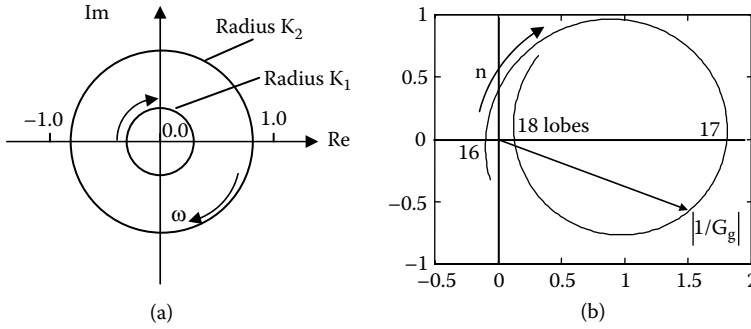


FIGURE 19.45 The geometric function represented as an inner feedback loop.



**FIGURE 19.46** The geometric function  $1/G_g(j\omega)$  for frequencies from 16 to 18 waves.  $\beta = 10^\circ$  and  $\gamma = 20^\circ$ .

The plot in Figure 19.46 is negative for the unstable 16 waves but is slightly positive for the marginally stable 18 waves. The plot indicates a strong rounding tendency for  $n = 17$ .

Figure 19.47 is a plot of the geometric stability parameter,  $A$ , against number of waves over the range of interest. Values are shown for a  $10^\circ$  tangent angle and a  $20^\circ$  workrest angle for up to 32 waves. This plot allows geometric stability at all the frequencies to be investigated. It appears there are several instabilities over the range. The most serious is at 16 waves because the instability coincides with an integer number of waves. The implication of an integer number of waves is that the feedback is exactly in phase with the wave already existing on the surface. It does not matter if the feedback is small because the depth of cut continually adds to the existing waviness instead of reducing it. The system is always unstable in this case even if the machine is rigid. In fact, the buildup of waviness will be faster with a rigid machine since the positive feedback is more strongly imposed through the depth of cut.

Another instability is indicated for approximately five and a half lobes. However, in this case the number of lobes is no longer an integer value. This means the existing waviness must be continually removed and replaced by a new waviness of larger amplitude produced at a new position around the workpiece circumference. In-phase static compliance of the machine or wheel surfaces will reduce the depth of cut and make it difficult for the waviness to grow. Instability for noninteger waviness must be considered together with the force and compliance function as part of a dynamic instability analysis.

We should also be concerned with a local minimum or trough on the geometric stability chart coinciding with an integer number of waves, even if the stability parameter is positive. For example, it can be seen that 18, 20, and 22 waves in Figure 19.46 have troughs on the stability chart. While

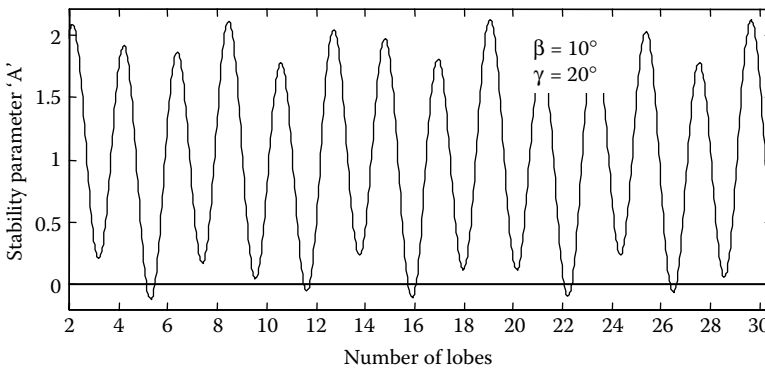


**FIGURE 19.47** Geometric stability parameter “ $A$ ” against number of waves.

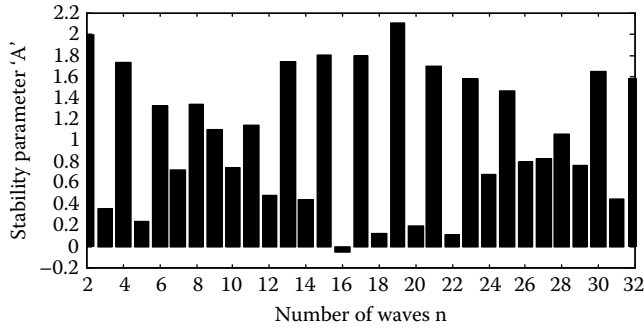


FIGURE 19.48 Geometric stability.  $\beta = 10^\circ$  and  $\gamma = 20^\circ$ .

these numbers of waves are stable, large roundness errors will result if a forcing frequency is allowed to excite these values of waviness.

For the above reasons, geometric stability should be tested for integer-wave values as shown in Figure 19.48. This shows that 16 waves is the only geometric instability up to  $n = 32$ .

Negative values of  $A$  define growth rate as shown in Figure 19.49 for a range of  $\beta$  and  $\gamma$  values. Here the unstable zones are shown for  $n = 3$  to 30 waves. For a tangent angle less than  $5^\circ$ , there is only one area of instability and that is for five lobes having low growth rate. Most of the region is stable. However, a tangent angle less than  $5^\circ$  does not provide a rapid rounding action. Therefore, the tangent angle is usually made larger.

There is a small region at  $\beta = 7.5^\circ$  and  $\gamma = 30^\circ$  that is stable over the whole range up to  $n = 32$ . However, 24 and 26 lobes are only just stable as shown by Figure 19.50. The user can easily construct a range of charts such as Figure 19.50 using a spreadsheet.

In Figure 19.50,  $n = 24$  is only just stable. This may be compared with Figure 19.48 where there is already an instability at  $n = 16$ . The stability indicated in Figure 19.50 is, therefore, more favorable on two counts. There is no absolute instability in Figure 19.50 at an integer number of waves. Also, the first marginal instability is at a higher frequency. This is an advantage because higher frequencies reduce the maximum amplitude of waviness due to interference. This point was explained in Section 19.11.6 with reference to simulation of the process. Some authors refer to the

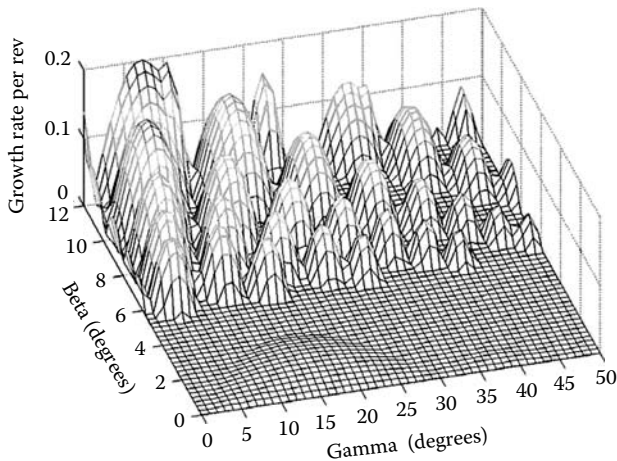


FIGURE 19.49 Maximum growth rate for various  $\beta$  and  $\gamma$ .

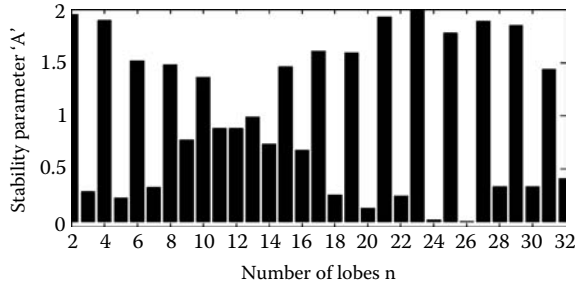


FIGURE 19.50 Geometric stability for  $\beta = 7.5^\circ$  and  $\gamma = 30$ .

interference effect as contact filtering. As explained later, there is also a need to consider workpiece speed in relation to dynamic instability. It will be found that if the first marginal geometric instability occurs at a higher number of waves, a higher workpiece speed may be safely employed.

19.12.6 MACHINE AND WHEEL COMPLIANCES

19.12.6.1 Static Compliance

Static compliance of the machine system is simply the inverse of static stiffness. Static compliance depends primarily on the elasticity of the wheels, bearings, slideways, and machine structure. System behavior, including the effect of static compliance, is similar to the results given by the simulations in Section 19.11. For this case

$$H_a = \frac{1}{\lambda_0} \tag{19.73}$$

the open loop transfer function becomes

$$\frac{x(s)}{X(s)} = \frac{k_s}{\lambda_0} \cdot \frac{1}{1 + K_2 e^{-\alpha s} - K_1 e^{-(\pi-\beta)s}} \cdot (1 - e^{-2\pi s}) \tag{19.74}$$

A high value of grinding force stiffness increases vibration deflections whereas a high value of system stiffness reduces them.

At the limit of stability, Equation 19.74 is equated to zero giving an equation of the same form as Equation 19.69. Figure 19.51 shows the effect of the geometric function modified by static

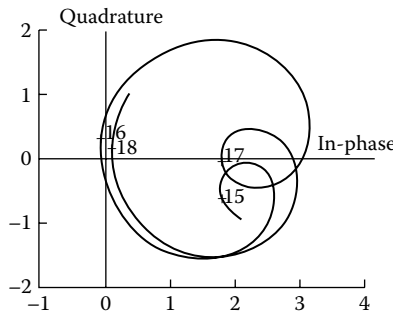


FIGURE 19.51 Modification of  $1/G_g(j\omega)$  by depth of cut and static compliance. Compare with Figure 19.46. Waviness  $n = 14.9$  to  $18.1$ .  $\beta = 10^\circ, \gamma = 20^\circ, k_s/\lambda_0 = 1$ .

compliance and the depth of cut function. The sizes and positions of the circular loops are modified from the values in Figure 19.46 by the depth of cut function. The extent of the modification depends on the magnitude of  $k_s/\lambda_0$ .

It is found that static compliance slightly reduces the growth rate at frequencies close to 16 waves but cannot make the situation stable. The most significant change from Figure 19.46 can be seen from the dimensions on the axes. Due to compliance, the deflections are greatly increased in magnitude.

**19.12.6.2 Dynamic Compliances**

The effect of the frequency response function for machine system compliances can be demonstrated using a second-order single degree of freedom system defined by

$$\frac{\lambda_0}{\lambda(j\omega)} = \frac{\lambda_0 x(j\omega)}{F_n(j\omega)} = \frac{1}{1 - \frac{\omega^2}{\omega_0^2} + \frac{j\omega}{Q\omega_0}} \tag{19.75}$$

where

$$\omega_0 = \sqrt{\frac{\lambda_0}{m}}$$

is the undamped natural frequency.

$$Q = \frac{\lambda_0}{c\omega_0}$$

is the dynamic magnification.  $Q$  is an inverse measure of damping  $c$ .

A frequency response function of a machine is shown in Figure 19.52 for a single mode of vibration. The frequency is expressed in number of waves for a particular workpiece speed by writing  $n = \omega/\Omega$ , as previously. The natural frequency of the machine in this case coincides with 17 waves. This corresponds to a natural frequency of 68 Hz in the tuning fork mode for a workpiece rotational speed of 4 Hz. The machine is lightly damped as indicated by the dynamic magnifier,  $Q = 10$ , a value that corresponds to a critical damping ratio of 0.05. This amplifies the static deflection by a factor of 10 at the resonant frequency.

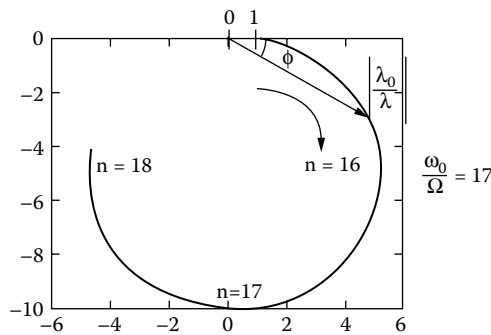


**FIGURE 19.52** Typical 1 d.o.f. frequency response function of machine. Frequency expressed in number of waves. Natural frequency at 17 waves.  $Q = 10$ .

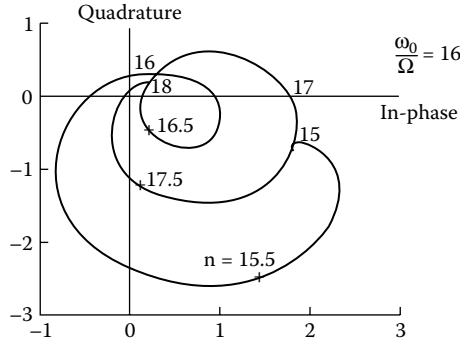


**FIGURE 19.53** Open-loop TF including geometric effects and dynamic compliances for a natural frequency at  $n = 16$  waves.  $\beta = 10^\circ$ .  $\gamma = 20^\circ$ .

The characteristic equation for the grinding process including the dynamic response of the principal vibration mode is

$$\frac{k_s}{\lambda_0} (1 - e^{-2\pi s}) \cdot \frac{1}{\left(1 + \frac{s^2}{\omega_0^2} + \frac{s}{Q\omega_0}\right)} + \frac{1}{G_g(s)} = 0 \tag{19.76}$$

Plotting the characteristic equation of the system for frequencies in the vicinity of the natural frequency for the unstable 16-wave geometry yields Figure 19.53. In this example, the natural frequency is at 16 waves. This result demonstrates the interaction between the large deflections of the machine at the frequency corresponding to 16 waves with the geometric instability at 16 waves. It is seen that frequency at 16 waves remains unstable but the main frequency of the instability is slightly below 16 waves.

Although the static compliance in Figure 19.53 is much lower than in Figure 19.51, the deflections of the dynamic system are much larger due to the resonance. The loop between 17.5 and 18 waves was previously stable with static compliance but has become unstable due to the nearby resonance at  $n = 16$ .

The situation of marginal geometric instability is often made worse by a resonance close to a frequency of marginal instability since resonance increases the probability of vibration amplitudes already in existence independent of the grinding process. These vibrations force a response even if the geometry is stable. The user should, therefore, consider a resonance in the same way as a frequency of forced vibration and avoid a coincidence with a convenient waviness. This may be achieved by adjusting the workspeed.

### 19.12.6.3 Added Static Compliance

It has been shown that the effect of resonance is to destabilize the process. It has also been argued that static compliance can reduce growth rate of regenerative vibration. In this context, we are referring to static compliance that does not contribute toward a resonance. The resonance of a machine is the combined effect of a substantial mass and the supporting stiffness of the structure. However, it is possible to incorporate compliance at the grinding point by making the abrasive structure of the grinding wheel compliant. This does not affect the dominant tuning fork mode of the machine.

If the workpiece has low mass, compliance can also be incorporated at the control wheel surface without affecting the primary resonance. In fact, the soft rubber control wheel fulfills this function.

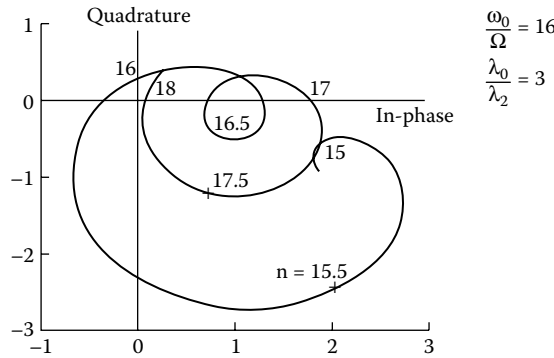


**FIGURE 19.54** Open-loop transfer function of Figure 19.53 modified by added static compliance.  $\beta = 10^\circ$ .  $\gamma = 20^\circ$ .  $k_s/\lambda_0 = 0.1$ .  $\lambda_0/\lambda_2 = 3$ .

An explanation for the stabilizing effect of added compliance is that the frequency response function of the machine is shifted to the right on the real axis. When the machine response function is added to the other terms in the characteristic equation, the shift to the right reduces the probability of enclosing the origin.

Additional static compliance can be demonstrated mathematically by introducing a secondary compliance term  $1/\lambda_2$  into the characteristic equation. Making the secondary compliance three times larger than the basic machine compliance changes the transfer function to that shown in Figure 19.54. This may be compared with Figure 19.53.

$$\frac{k_s}{\lambda_0} (1 - e^{-2\pi s}) \cdot \left( \frac{1}{\left(1 + \frac{s^2}{\omega_0^2} + \frac{s}{Q\omega_0}\right)} + \frac{\lambda_0}{\lambda_2} \right) + \frac{1}{G_g(s)} = 0 \tag{19.77}$$

It can be seen that the additional compliance has stabilized the loop between 17.5 and 18 waves that was previously unstable. However, it is also found that while additional compliance reduces the growth rate at 16 waves, the instability cannot be overcome.

### 19.13 DYNAMIC STABILITY

#### 19.13.1 THRESHOLD CONDITIONS

Substituting  $s = j\omega$  in Equation 19.76, it is possible to solve the characteristic equation to find the unstable limit frequencies and the corresponding limits of grinding force stiffness at the threshold of instability. Noting that  $\omega = n\cdot\Omega$ , the frequencies are given by

$$\left( n \frac{\Omega}{\omega_0} \right)^* = \frac{1}{2Q} \left( \frac{B - A \cdot C}{A + B \cdot C} \right) + \sqrt{\left\{ \left[ \frac{1}{2Q} \left( \frac{B - A \cdot C}{A + B \cdot C} \right) \right]^2 + 1 \right\}} \tag{19.78}$$

where  $A$  and  $B$  are the real and imaginary parts of the geometric function as previously defined and

$$C = \frac{1 - \cos 2\pi n}{\sin 2\pi n} = \frac{\sin \pi n}{\cos \pi n} \tag{19.79}$$



The limiting value is termed  $(k_s/\lambda_0)^*$  and for various values of  $n$  is given by

$$\left(\frac{k_s}{\lambda_0}\right)^* = \frac{\left[\left(n \frac{\Omega}{\omega_0}\right)^2 - 1\right] \cdot A - B \left(\frac{n \cdot \Omega}{Q \omega_0}\right)}{1 - \cos 2\pi n} \tag{19.80}$$

For integer values of  $n$ , stability and instability are independent of the grinding force and stability depends only on geometric stability. For near-integer values of  $n$ , the limiting value of  $(k_s/\lambda_0)^*$  approaches infinity.

For half-integer values of  $n$ , the frequency is given by

$$\left(n \frac{\Omega}{\omega_0}\right)^* = \frac{-A}{2Q \cdot B} + \sqrt{\left\{\left(\frac{-A}{2Q \cdot B}\right)^2 + 1\right\}} \tag{19.81}$$

It is essential to know whether the stable region is for values of  $k_s/\lambda_0$  less than or greater than a limiting value  $(k_s/\lambda_0)^*$ . This can be discovered by checking the phase angle  $\chi$  between the waviness  $r(t)$  and the deflection  $x(t)$ . The system is unstable for  $k_s/\lambda_0 > (k_s/\lambda_0)^*$  if

$$-\frac{\pi}{2} < \chi < +\frac{\pi}{2} \tag{19.82}$$

where

$$\chi = 3 \cdot \pi/2 - \phi - \pi \cdot n \tag{19.83}$$

and

$$\phi = \arctan \frac{n \cdot \Omega / \omega_0}{Q[1 - (n \cdot \Omega / \omega_0)^2]} \tag{19.84}$$

Figure 19.55 illustrates phase relationships between normal grinding force, depth of cut, waviness, and deflection. The sign convention adopted is that a positive grinding force exerted by the grinding wheel on the workpiece gives a positive depth of cut. The workpiece applies an equal and opposite force on the grinding wheel that causes deflection. The deflection lags the grinding force by the angle  $\phi$ . The sign convention for the deflection is based on the assumption that a positive deflection reduces depth of cut.

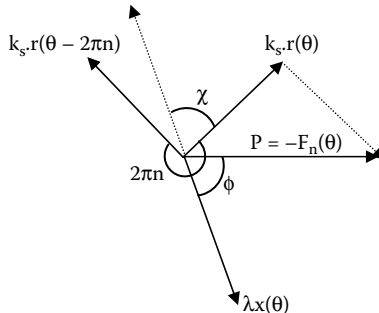
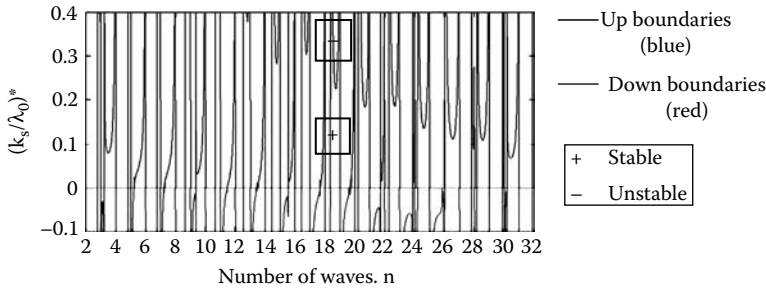


FIGURE 19.55 Vector diagram to determine  $\chi$ .



**FIGURE 19.56** Dynamic stability limits for  $k_s/\lambda_0$ .  $\gamma = 30^\circ$ .  $\beta = 6.5^\circ$ . (Original diagram in color.)

When  $|\chi|$  is less than  $90^\circ$ , deflection increases waviness. This means increasing grinding force increases waviness and the system becomes dynamically unstable.

### 19.13.2 DYNAMIC STABILITY CHARTS

Application of the equations and rules in Section 19.13.1 allows dynamic stability charts to be plotted. The following case study illustrates the application and interpretation of dynamic stability charts. A dynamic stability chart gives the ratio of grinding stiffness to static machine stiffness at the limit of stability. In grinding, it is usually found that increasing this ratio through higher grinding force stiffness or lower machine stiffness makes the process unstable. Conversely, reducing the ratio stabilizes the process. In centerless grinding, it is not possible to make this general conclusion. The following example includes a dynamic stability chart for centerless grinding and explains how to interpret the chart.

Figure 19.56 is a dynamic stability chart for  $\beta = 6.5^\circ$ . Dynamic stability charts are calculated using Equations 19.78, 19.80, and 19.81. The frequency ratio is calculated from Equation 19.78 or 19.81 and the boundary value of stiffness ratio from Equation 19.80. The frequency ratio is

$$\omega/\omega_0 = n \cdot \Omega/\omega_0 \tag{19.85}$$

The frequency ratio is the angular frequency of vibration divided by natural frequency. Since the vibration frequency equals number of waves times angular workspeed in radians per second, frequency ratio can be expressed in terms of number of waves for particular workspeed and natural frequency.

Although the charts are presented in terms of number of waves, it is necessary to remember that the stability limit at a particular point requires the particular workspeed to fulfill the relationship with natural frequency expressed by Equation 19.85.

The dynamic stability chart is presented in terms of number of waves  $n$ . This is necessary since each value of waviness has slightly differing behavior from the neighboring pairs of waviness values. The stability for 16 to 17 waves is different from 18 to 19 waves. The boundaries tend to repeat but are shifted vertically and horizontally.

In practice, dynamic instability is experienced where the product  $n \cdot \Omega$  is close to the natural frequency. This means that dynamic stability problems will not be experienced if the angular workspeed is selected to avoid potentially unstable waviness conditions.

Two sets of dynamic stability boundaries are shown. On the original figure conventional “up” boundaries were shown in blue and unconventional “down” boundaries were shown in red.

### 19.13.3 UP BOUNDARIES

Up boundaries were colored blue in Figure 19.56. Unstable zones lie above the up line and stable zones beneath. An example shows a stable zone marked with a “+” sign and an unstable zone

marked with a “–” sign. Up boundaries were determined by calculating the angle  $\chi$  for each point on the boundary from Equation 19.83 and checking that the point satisfied Equation 19.82.

Up boundaries lie mainly in the top positive region of Figure 19.56 but are occasionally found in the low negative region. Negative boundaries seem irrelevant at first since grinding stiffness and static machine stiffness are always positive. However, the small areas where up boundaries extend into the lower negative region must be avoided. These are up boundaries where if the corresponding speed conditions are applied the process is absolutely unstable. Avoiding the unwanted speed condition is straightforward and is discussed further in Section 19.13.5

#### 19.13.4 DOWN BOUNDARIES

Down boundaries were colored red in Figure 19.56. Unstable zones for down boundaries lie beneath the line and stable zones above the line. Down boundaries indicate unstable zones for increasingly negative grinding forces and stable zones for more positive forces. In a case where a down boundary lies in the negative region of the chart, the system cannot go unstable at the corresponding waviness condition. This is reassuring, since there are large areas of red on the chart. Most of these areas represent areas of absolute stability.

However, there are small areas where down boundaries indicate unstable regions for low positive grinding forces and stable regions for high positive forces. This needs further examination.

An example of a down boundary for low positive grinding forces occurs close to  $n = 26$  suggesting a region affected by poor geometric stability.

The geometric setup  $\beta = 6.5^\circ$  is generally considered to be favorable as this is one of the most stable set-up geometries and is close to  $\beta = 6.4^\circ$ , the setup recommended as optimum by Hashimoto and Lahoti [2004]. Geometric stability for a tangent angle of  $6.5^\circ$  is shown in Figure 19.57 for integer waves. This may be compared with Figure 19.50 for  $\beta = 7.5^\circ$ . In both cases, the waviness  $n = 26$  is only just stable.

Unfortunately, Figure 19.57 does not clarify why the red boundary goes into the positive force domain because the waviness  $n = 26$  is shown as stable. Figure 19.58 is more helpful in this regard, showing geometric stability for noninteger wave numbers.

Figure 19.58 reveals marginal geometric instability at several waviness values. These values correspond precisely with the conditions where the dynamic stability charts show red boundaries in the positive force region. The conclusion is clear. At these values of waviness, it is possible to experience dynamic instability. A further conclusion is that if instability is experienced at one of these waviness values, the grinding force would need to be increased to stabilize the system. This is the opposite of the normal situation in machining where the system is stabilized by reducing the force.

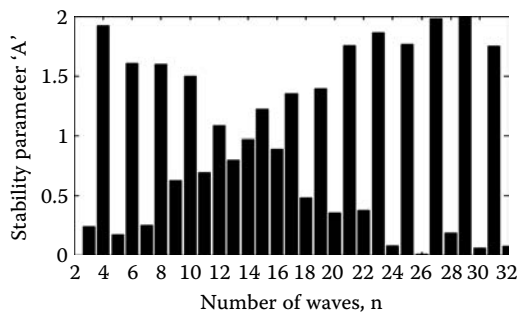


FIGURE 19.57 Geometric stability for integer waves.  $\beta = 6.5^\circ$  and  $\gamma = 30^\circ$ .

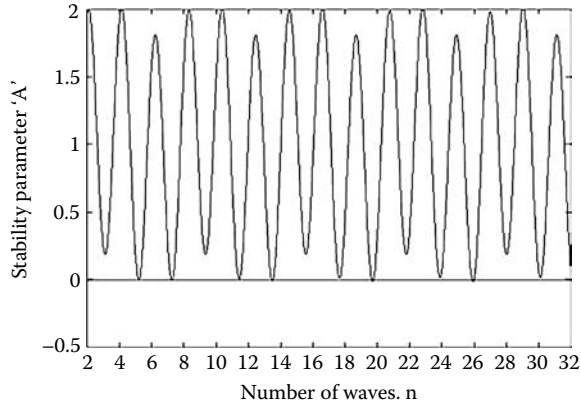


FIGURE 19.58 Geometric stability for fractional waves.  $\beta = 6.5^\circ$  and  $\gamma = 30^\circ$ .

### 19.14 AVOIDING CRITICAL FREQUENCIES

#### 19.14.1 VIBRATION FREQUENCIES AT THRESHOLD CONDITIONS

Figure 19.59 shows a stability threshold plotted against vibration frequency  $\omega$  for  $n = 25.0$  to  $n = 26.1$ . The vibration frequency for a dynamic stability threshold mainly lies just above the natural frequency  $\omega_0$  of the main machine vibration mode.

Figure 19.59 has four distinct zones. These are shown as

- Absolutely stable. 25.0 to 25.8 waves.
- Absolutely unstable. 25.8 to 26.0 waves. Frequency range 1 to  $1.7 \times \omega_0$ .
- Conditional dynamic instability for high forces. Approximately 26.01 waves.
- Conditional dynamic instability for low forces. 26.01 to 26.1 waves.

In this example, it can be seen that care should be taken to avoid frequency ratios  $\omega/\omega_0$  in the range 1.0 to 1.7. For other conditions and number of waves, the range may be even larger.

#### 19.14.2 SELECTION OF WORK ROTATIONAL SPEED

Figure 19.20 shows there is a limiting work rotational speed when dynamic instability becomes a process limit. A compliant machine with a natural frequency of approximately  $f_0 = 76$  Hz gave

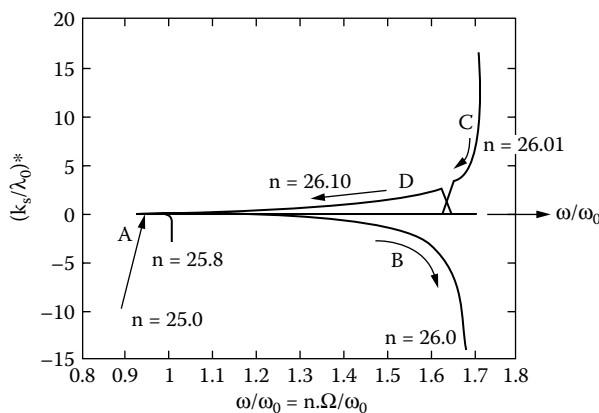


FIGURE 19.59 Vibration frequencies at threshold conditions.  $\beta = 6.5^\circ$ ,  $\gamma = 30^\circ$ .  $n = 25.0$  to 26.1 waves.

instability at work rotational speeds above  $n_w = 4.5$  rev/s. At this workspeed, the number of waves would be expected to exceed  $76/4.5 = 17$  waves.

The results for the very stiff machine presented in Figure 19.20 were for a natural frequency  $f_0 = 500$  Hz. Instability was experienced for workspeeds above 16 rev/s. At this workspeed, the number of waves experienced would be expected to exceed 31 waves.

31 or more waves will be attenuated by contact filtering more than 17 waves. These results explain why a very stiff machine allowed higher workspeeds to be employed and the smaller amplitude of roundness errors when the process became unstable.

If roundness problems are experienced with a particular workpiece diameter, it is necessary to determine the cause of the vibration. Frequency of vibration can be evaluated from the number of waves on the workpiece multiplied by the work rotational speed. This will assist in identifying the source of vibration and workspeed can be chosen to avoid a convenient waviness. If the frequency is identified with a machine resonance, the usual adjustment is to reduce workspeed.

Figure 19.20 shows that at low workspeed there is increased risk of thermal damage. If vibration is associated with a thermal damage condition at very low workspeeds, it is necessary to increase workspeed.

### 19.14.3 SELECTION OF GRINDING WHEEL ROTATIONAL SPEED

Problems can arise in any grinding process when the grinding wheel rotational speed is an integer multiple of the work rotational speed. This is because any wheel runout due to wheel unbalance or other cause will be imposed at the same positions on the workpiece in a repetitive action. For example, if the grinding wheel speed  $n_s = 30$  rev/s and the work rotational speed  $n_w = 3$  rev/s, it is probable that  $n = 30/3 = 10$  waves will be detectable in the work roundness.

For similar reasons, wheel speed should not be allowed to lie at the same speed as the dominant natural frequency. Even direct multiples and submultiples should be avoided.

### 19.14.4 SELECTION OF DRESSER SPEED

The modern practice in precision grinding particularly when using superabrasive grinding wheels is to employ a motorized rotary dressing tool. The tool usually consists of a diamond-faced disc with a narrow cutting edge. A rotary disc is far more durable than a single-point diamond and a precision disc allows excellent rotational accuracy for precision dressing. The runout of the dressing disc is likely to be approximately  $2 \mu\text{m}$ .

Typically, the disc is arranged when dressing to have a surface speed  $v_d = 0.4$  to  $0.8$  times the surface speed of the grinding wheel  $v_s$ . This means the dressing tool has to rotate at high speed for high-speed grinding. The dressing tool assembly must be capable of low vibration operation at these speeds. The dressing tool rotational speed  $n_d$  should not be a multiple of work rotational speed  $n_w$ . For similar reasons, the dresser rotational speed should not be a simple multiple of the grinding wheel rotational speed  $n_s$ .

If it is decided to perform dressing at reduced grinding wheel speed, it is important not to excite machine resonance from the dressing tool system or the grinding wheel drive system.

### 19.14.5 SPEED RULES

Summarizing the requirements outlined in this discussion, the following general rules may be concluded:

- $f_0/n_w$  should not be an integer.
- $n_s/n_w$  should not be an integer.
- $n_d/n_w$  should not be an integer.
- $n_d/n_s$  should not be an integer.

The same principle of avoiding multiple speed relationships that directly affect workpiece roundness can be extended to other machine elements in the system, such as the control wheel, drive motors, and gears.

### 19.15 SUMMARY AND RECOMMENDATIONS FOR ROUNDING

Set-up geometry should provide rapid rounding and avoid convenient waviness.

- Convenient waviness and marginal stability cannot be completely avoided. However, convenient waviness is unlikely to be a problem unless waviness is forced by vibration at the same frequency.
- Static compliance in the system softens the imposition of errors into the workpiece and, hence, makes it easier to achieve low roundness errors.
- Resonant frequencies should be avoided since these amplify vibrations and cause large roundness errors. Resonant vibrations are minimized by well-designed structures and high damping.
- Forced vibrations at a resonant frequency should be avoided. This can be achieved by checking that excitation due to motors, drives, and wheel unbalance are not at a frequency coincident with a dominant machine resonant frequency.
- Sources of forced vibration such as wheel unbalance should not be allowed to excite a frequency of marginal geometric stability.
- Many problems can be overcome by adjusting workspeed. Ideally, a machine should provide a continuously variable range of workspeeds.

### 19.16 PROCESS CONTROL

For the manufacturer producing components by the thousand and the millions, process control assumes great importance. In this situation, it is essential to produce components rapidly and be assured of good quality. It can be wasteful if the process goes out of tolerance, particularly if the situation is not quickly detected. The process control system should, therefore, be able to detect changes that may lead to rejection of parts and take appropriate action.

Basically two different strategies are possible in response to detecting an unacceptable process condition:

- Stop the process and give an alarm.
- Make an adjustment to the operating conditions and continue.

Clearly, the second strategy is preferred to the first.

For flexible manufacture of small quantities, it is difficult to do better than a human operator in control of the process. However, as the drive to reduce costs becomes more important, there is a tendency to automate machines and place a number of machines under the control of one operator.

The relative ease of introducing low-cost automation to centerless grinding for larger batches was mentioned in Section 19.1. There are various levels of automation and the manufacturer will want to base the level of automation on such factors as the need to make frequent changes to produce different components, the frequency of repeat batches, the long-term future for production of such components, and so forth.

The basic levels of automation are likely to include:

- Automated part feeding with bowl feeders, air cylinders, electric drives, and so on
- Automatic size gauging with air gauging, electronic transducers, and so on
- Automated checking of door closure or other safety features
- Automated size compensation using servo drives
- Automated grinding wheel dressing

At the higher levels, automation may be implemented using a CNC machine having appropriate servodrives and measuring scales. A CNC is a system capable of being programmed to produce parts on particular machines. A CNC is given information about the specific machining operation through a part program. The part program allows an operator to feed data about the workpiece shape and the required sequence of operations into the CNC. The CNC gives continuous instructions to servocontrols to position machine axes following the programmed cycle and reads signals from servodrives and measuring devices to ensure the correct positions are achieved. The CNC may also send information about the process to a display screen or to a higher-level computer.

The cost of a CNC machine is much greater than the cost of a manually controlled machine. The decision to change to CNC control will not, therefore, be taken lightly. A CNC that becomes unreliable is a liability and can lead to a machine becoming unusable for long periods.

Before deciding to adopt or reject CNC control for centerless grinding, consideration needs to be given to potential advantages and disadvantages. Potential advantages of a CNC grinding machine are

- Can operate unsupervised for long periods
- Can incorporate control of automation devices and features
- Can incorporate intelligent control for process optimization
- Can in some cases store production data and process data
- Can in some cases communicate with a higher level computer

It should be noted, however, that a low-cost CNC is unlikely to incorporate more than the first of the advantages listed of operating unsupervised for long periods. A more expensive CNC will probably be required to allow integration with a full range of sizing and other equipment.

Some disadvantages of a CNC grinding machine are

- High initial machine cost
- The need for greater reliability of electronic devices over a long working life
- Dependence on a specialized repair service in the event of CNC breakdown

Very little has been published on the application of CNC to centerless grinding machines although several papers have considered optimization and CNC in relation to other grinding processes including Peters 1984 and Toenshoff, Zinnegrebe, and Kemmerling [1986]. More recently, attention has turned to Intelligent Process Control (IPC) based on modern CNC technology [Rowe et al. 1994]. In addition to the direct benefits of reduced manning, intelligent process control offers the potential for

- Sustained removal at maximum rate [Rowe et al. 1986]
- Avoidance of thermal damage [Rowe 1988]
- Accelerated spark-out by overshoot [Malkin 1981]
- Accelerated infeed through digital closed-loop control [Toenshoff et al. 1986]
- Consistent quality and production rate
- Learning strategies for new materials, wheels, dressing conditions, and so on
- Sensing and/or avoidance of chatter
- Feed-forward control of lobing [Frost, Horton, and Tidd 1988]
- Combined grinding and measuring cycles

Figure 19.60 shows a basic scheme for Intelligent Process Control of a Grinding System. The figure is not intended to describe a system currently in existence. It illustrates a framework into which different system developments can be classified. Various aspects that contribute to such a

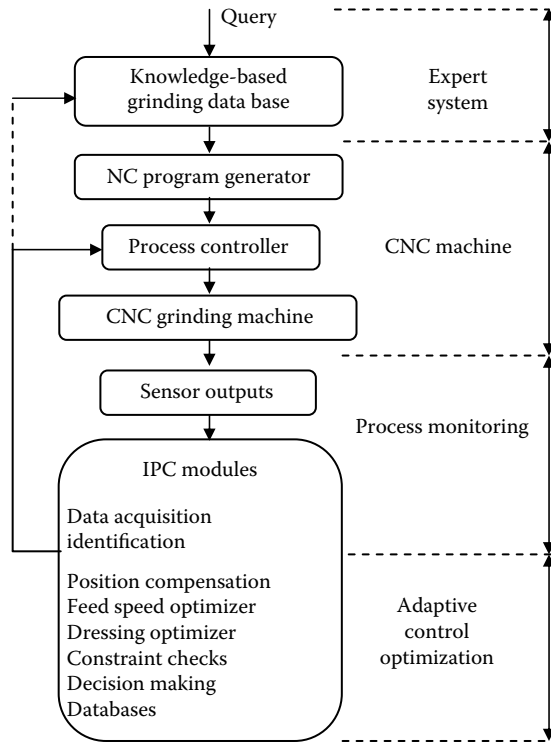


**FIGURE 19.60** Basic scheme for intelligent process control of a grinding system.

scheme have been developed and applied in particular systems as illustrated by some of the references listed above. For further details the reader should refer to Rowe et al. [1994].

The full expert system level illustrated has not yet been commercially developed for grinding, although aspects of such a system may already be incorporated into CNC grinding systems. A prototype expert system was developed and demonstrated that such an approach could be feasible. The operator wishing to machine a new product queried a database for recommendations on feedrate and material removal rate. The system gave advice based on previous products of a similar type or used rules to generate recommendations.

Having decided the basic values to be used for machining the part, these values are entered into the part-program using the part-program generator of the CNC. The process controller then initiates a grinding cycle. The first part is usually machined under close operator supervision to ensure sizing devices are correctly adjusted and change points for the grinding cycle feedrate changes take place at suitable positions.

Size gauging devices are a normal part of the monitoring level. A size reading may be used to trigger a fine feedrate for finish grinding and to trigger the commencement of dwell for spark-out. If the size reading takes place after the workpiece leaves the grinding contact, the size reading may be used to trigger a wear compensation for the infeed movement.

A power-monitoring sensor may be incorporated into the system and can be used in several different ways. If the maximum power reading increases after a number of parts have been produced, it is likely to mean that the grinding wheel has become blunt. This can be used to signal the need to redress the grinding wheel.

If the power reading drops after a number of parts have been produced, it means that the grinding wheel wear has had a self-sharpening effect. This may imply that the grinding wheel is



too soft for the application. However, it may also imply that it is safe to increase feedrate and reduce cycle time. Adaptive Control Optimization is a process where the system varies the feedrate or other parameters to bring the process closer to optimum operation.

Another possibility is to detect potential thermal damage to the workpieces based on the measured power. In this case, feedrate can be limited if the measured power approaches the maximum permissible for avoidance of thermal damage. The application of such a system relies on a process model that allows the onset of thermal damage to be predicted. Several researchers have proposed such systems but the practice lags well behind the theory.

Over the last two decades since the introduction of CNC, grinding process controllers have become increasingly sophisticated. Basic technology for grinding control may be incorporated by the CNC manufacturer. Further specialized technology for grinding may be added by the manufacturer of the grinding machine. In some cases, the machine user may add further specialized technology.

Where centerless grinding is employed for sustained production of batches of components of high precision parts, the greatest priority is likely to be for systematic trials to ensure stable grinding conditions together with high accuracy and high production rates.

By studying the information given in this chapter, the reader will achieve a sound grasp of the fundamental principles required to undertake the development of such a system.

## REFERENCES

- Becker, E. A. 1965. "Krafte und Kreisformfehler beim Spitzenlosen Einstechschleifen." Ph.D. dissertation, T.H. Aachen.
- Cai, R. 2002. "Assessment of Vitrified CBN Wheels for Precision Grinding." Ph.D. thesis, Liverpool John Moores University, UK.
- Dall, A. H. 1946. "Rounding Effect in Centerless Grinding." *Mech. Eng.* April.
- Ebbrell, S. 2003. "Process Requirements for Precision Engineering." Ph.D. thesis, Liverpool John Moores University, UK.
- Frost, M., Horton, B. J., and Tidd, J. L. 1988. "Lobing Control in Centerless Grinding." SME Paper MR88-610.
- Furukawa, Y., Miyashita, M., and Shiozaki, S. 1971. "Vibrational Analysis and Work-Rounding Effect in Centerless Grinding." *Int. J. Mach. Tool Design Res.* 11, 145–175.
- Gurney, J. P. 1964. "An Analysis of Centerless Grinding." *ASME J. Eng. Ind.* Paper 63-wa-26, 87, 163–174.
- Gviniashvili, V. K., Woolley, N. H., and Rowe, W. B. 2004. "Useful Flowrate in Grinding." *Int. J. Mach. Tools Manuf.* 44, 629–636.
- Harrison, A. J. L. and Pearce, T. R. A. 2004. "Reduction of Lobing in Centerless Grinding via Variation of Set-Up Angles." *Key Engineering Materials*. Trans. Tech. Publ., Switzerland, 257–258, 159–164.
- Hashimoto, F. and Lahoti, G. D. 2004. "Optimisation of Set-Up Conditions of the Centerless Grinding Process." *Ann. CIRP* 53, 1, 271–274.
- Hashimoto, F., Kanai, A., and Miyashita, M. 1983. "High Precision Method of Regulating Wheel Dressing and Effect on Grinding Accuracy." *Ann. CIRP* 32, 1, 237–239.
- Hashimoto, F., Miyashita, M., and Yoshioka, J. 1986. "Development of an Algorithm for Giving Optimum Set-Up Geometry for Centerless Grinding Operations." International Grinding Conference, SME Paper MR86-628.
- Johnson, S. P. 1989. "Below-Centre Centerless Grinding." Ph.D. thesis, Coventry Polytechnic, UK and CNAA.
- King, R. R. and Hahn, R. S. 1986. *Handbook of Modern Grinding Technology*. Chapman & Hall, Advanced Industrial Technology Series.
- Klocke, F., Friedrich, D., Linke, B., and Nachmani, Z. 2004. "Basics for In-Process Roundness Error Improvement by a Functional Workrest Blade." *Ann. CIRP* 53, 1, 275–280.
- Koenig, W. and Henn, K. 1982. "Spitzenloses Durchlaufschleifen." *Metalbearbeitung, Part 1 and Part 2*.
- Malkin, S. 1981. "Grinding Cycle Optimization." *Ann. CIRP* 30, 1, 213–217.
- Marinescu, I. D., Rowe, W. B., Dimitrov, B., and Inasaki, I. 2004. *Tribology of Abrasive Machining Processes*. William Andrew Publishing, Norwich, NY.

- Meis, F. U. 1980. "Geometrie und kinematische Grundlagen für das spitzenlose Durchlaufschleifen." Ph.D. dissertation, T.H. Aachen.
- Miyashita, M. 1965. "Influence of Vibrational Displacements of Machine Elements on Out-of-Roundness of Workpiece in Centerless Grinding." In *Memoirs of Faculty of Technology, Tokyo Metropolitan University*.
- Miyashita, M., Hashimoto, F., and Kanai, F. 1982. "Diagram for Selecting Chatter-Free Conditions of Centerless Grinding." *Ann. CIRP* 31, 1, 221–223.
- Moriya, T., Kanai, A., and Miyashita, M. 1994. "Theoretical Analysis of the Rounding Effect in Generalized Centerless Grinding." ASME, *Materials Issues in Machining II*.
- Peters, J. 1984. "Contributions of CIRP Research to Industrial Problems in Grinding." *Ann. CIRP* 33, 2, 1–18.
- Reeka, D. 1967. "Über den Zusammenhang zwischen Schleifspaltgeometrie und Rundheitsfehler beim Spitzenlosen Schleifen." Ph.D. dissertation, T.H. Aachen.
- Richards, D. L. and Rowe, W. B. 1972. "Geometric Stability Charts for Centerless Grinding." *I. Mech. E. J. Mech. Eng. Sci.* 14, 2, 155–158.
- Rowe, W. B. 1974. "An Experimental Investigation of Grinding Machine Compliance and Improvements in Productivity." Proceedings of the 14th International Machine Tool Design and Research Conference, Macmillan, New York.
- Rowe, W. B. 1979. "Research into the Mechanics of Centerless Grinding." *Precision Engineering*. IPC Press.
- Rowe, W. B. and Barash, M. M. 1964. "Computer Method for Investigating Centerless Grinding." *Int J. Mach. Tool Design Res.* 4, 91–116.
- Rowe, W. B. and Ebbrell, S. 2004. "Process Requirements for Cost-Effective Precision Grinding." *Ann. CIRP* 53, 1, 255–258.
- Rowe, W. B. and Koenigsberger, F. 1965. "The Work-Regenerative Effect in Centerless Grinding." *Int J. Mach. Tool Design Res.* 4, 175–187.
- Rowe, W. B., Barash, M. M., and Koenigsberger, F. 1965. "Some Roundness Characteristics of Centerless Grinding." *Int J. Mach. Tool Design Res.* 5, 203–215.
- Rowe, W. B., Bell, W. F., and Brough, D. 1986. "Optimisation Studies in High-Removal Rate Centerless Grinding." *Ann. CIRP* 35, 1, 235–238.
- Rowe, W. B., Miyashita, M., and Koenig, W. 1989. "Centerless Grinding Research and Its Application in Advanced Manufacturing Technology." *Ann. CIRP* 38, 2, 617–625.
- Rowe, W. B., Morgan, M. N., and Qi, H. S. 1993. "The Effect of Deformation on Contact Length in Grinding." *Ann. CIRP* 42, 1, 409–412.
- Rowe, W. B., Pettit, J. A., Boyle, A., and Moruzzi, J. L. 1988. "Avoidance of Thermal Damage in Grinding and Prediction of the Damage Threshold." *Ann. CIRP* 37, 1, 327–330.
- Rowe, W. B., Spraggett, S., and Gill, R. 1987. "Improvements in Centerless Grinding Machine Design." *Ann. CIRP* 36, 1, 207–210.
- Rowe, W. B., Yan, L., Inasaki, I., and Malkin, S. 1994. "Applications of Artificial Intelligence in Grinding." *Ann. CIRP* 43, 2, 1–11.
- Sachsenberg and Kreher. 1939. *Werkstattstechnik und Werksleiter*. 33, 11.
- Schreitmüller, H. 1971. "Kinematische Grundlagen für die praktische Anwendung des spitzenlosen Hochleistungsschleifens." Ph.D. dissertation, T.H. Aachen.
- Stelson, T. S., Komanduri, R., and Shaw, M. C. 1988. "Manual Adaptive Control of a Centerless Grinding Operation." International Conference on Production Research, Tokyo, Preprint 9.2.
- Toenshoff, H. K., Zingrebe, M., and Kemmerling, M. 1986. "Optimization of Internal Grinding by Microcomputer Based Force Control." *Ann. CIRP* 35, 1, 293–296.
- Yonetsu, S. 1959. "Consideration of Centerless Grinding Characteristics through Harmonic Analysis of Out-of-Roundness Curves." Proceedings of the Fujihara Memorial Faculty of Engineering, Keio University.
- Yonetsu, S. 1959. "Forming Mechanism of Cylindrical Work in Centerless Grinding." Proceedings of the Fujihara Memorial Faculty of Engineering, Keio University.
- Yoshioka, J., Hashimoto, F., Miyashita, M., and Daito, M. 1984. "High-Precision Centerless Grinding of Glass as Preceding Operation to Polishing – Dressing Conditions and Accuracy." SME Paper MR84-542.
- Yoshioka, J., Hashimoto, F., Miyashita, M., Kanai, A., Abo, T., and Daito, M. 1985. "Ultra-precision Grinding Technology for Brittle Materials: Application to Surface and Centerless Grinding Processes." ASME, M C Shaw Grinding Symposium, PED.



---

# 20 Ultrasonic Assisted Grinding

## 20.1 INTRODUCTION

A wide variety of applications verify the great potential of high-performance ceramics for components with special requirements. For example, hip joint endoprostheses on aluminum oxide or zirconium oxide bases, components for slide bearings and burners of silicon carbide, as well as ceramic components for roller bearings or valves are made of silicon nitride [Spur 1989, Pattimor 1998, Popp 1998]. Extension of the market share for ceramic components is often opposed by the difficulties of manufacture with respect to achievable component quality and economic efficiency. Manufacturing costs arise mainly in grinding, honing, lapping, and polishing. High costs result from relatively inefficient technologies for machining of brittle-hard materials [Uhlmann 1998]. This demonstrates the need to provide economically efficient machining methods for ceramic workpieces. In addition, there is a lack of suitable strategies for economic manufacture of complex geometries such as bores, holes, grooves, spherical surfaces, and sculptured surfaces [Uhlmann and Holl 1998a].

Although ultrasonic lapping and electrodischarge machining (EDM) processes are suitable for manufacture of these geometries, there are significant disadvantages. Only electrically conductive ceramics such as SiSiC can be machined with EDM methods, and there are technological limits to ultrasonic lapping due to the small material removal rate, the high wear of the forming tools, and unsatisfactory accuracy. Therefore, suitable manufacturing methods for highly accurate and economic machining of ceramic materials have been developed over the past few years. The development of hybrid manufacturing processes on the basis of existing methods opens up new avenues.

In ultrasonic lapping, a forming tool oscillates with ultrasonic frequency and thrusts loose abrasive lapping grains into the surface of the workpiece, thus removing material. Based on this process, ultrasonic action has been superimposed onto conventional machining kinematics in several manufacturing processes over the past few years. In nearly all cases, process results have improved [Drozda 1983, Nankov 1989, Prabhakar, Ferreira, and Haselkorn 1992, Pei, Prabhakar, and Haselkorn 1993, Suzuki et al. 1993, Westkämper and Kappmeyer 1994, Pei and Ferreira 1999].

In industry, ultrasonic lapping and ultrasonic-assisted grinding have been applied so far for finishing brittle-hard materials. Due to high material removal rates and the freedom of geometrical configuration, this method is likely to have a wide range of application possibilities in the future. Figure 20.1 shows the advantage of ultrasonic-assisted grinding in comparison to conventional finishing methods with respect to an increase of the material removal rate in the machining of aluminum oxide through the superposition of grinding kinematics and an ultrasonic frequency.

## 20.2 ULTRASONIC TECHNOLOGY AND PROCESS VARIANTS

Elastomechanical ultrasonic vibration is generated by the transformation of electric energy in piezoceramic or magnetostrictive sonic converters. A voltage generator converts a low-frequency mains voltage into a high-frequency alternating-current voltage. The generated longitudinal vibrations are periodic elastic deformations of the mechanical vibration system in the micrometer range at supersonic frequencies, that is, higher than  $f = 16$  kHz. The sound-generating unit preceding the actual ultrasonic tool or shape-generating counterpart consists of a sonic converter, an amplitude transformer (transforming sections), and sonotrodes [Spur and Holl 1995]. Figure 20.2 shows the design of a vibration system.

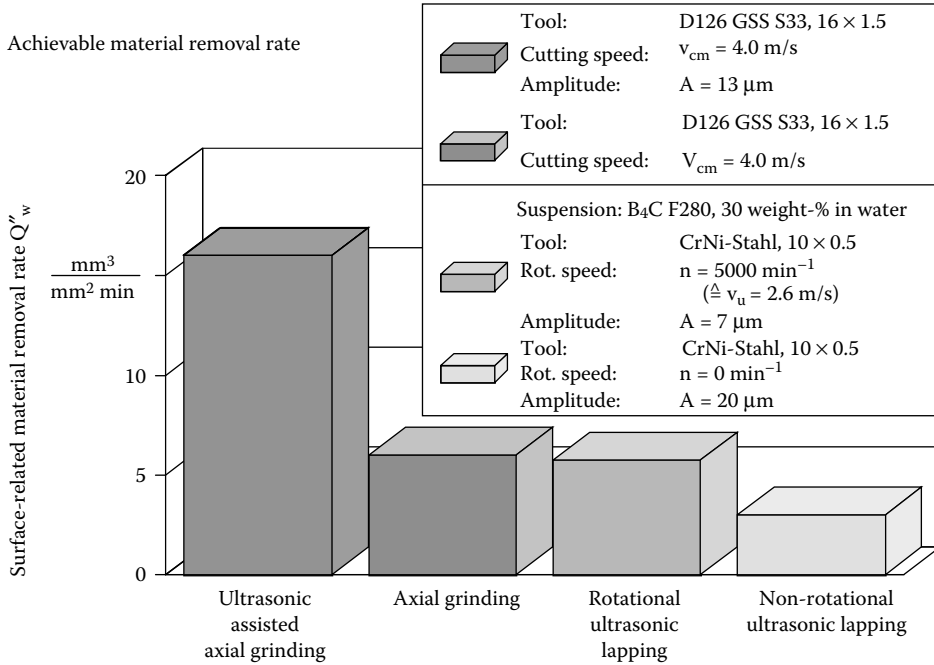


FIGURE 20.1 Achievable material removal rates during the machining of aluminum oxide depending on the applied manufacturing method. (From Carstburg 1993. With permission.)

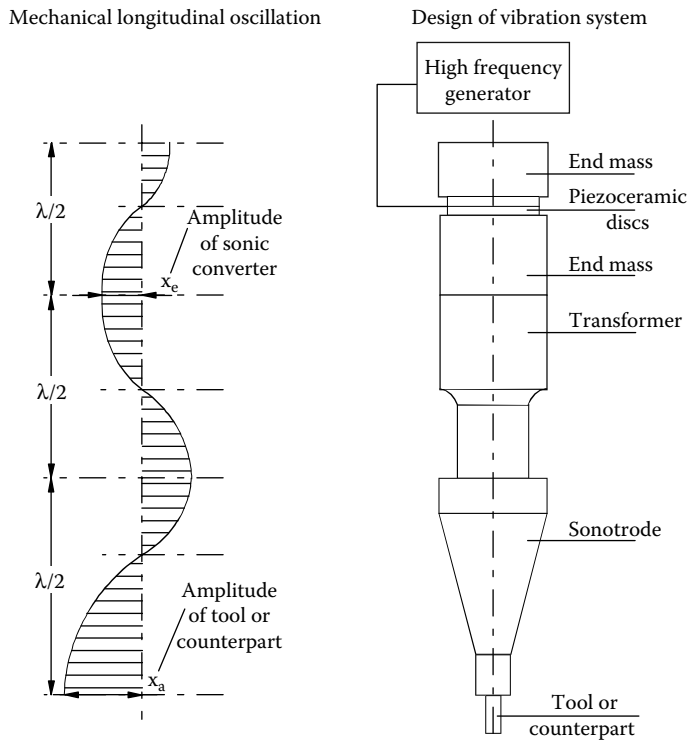


FIGURE 20.2 Design of vibration system and vibration course for the example of ultrasonic lapping. (From Haas 1991. With permission.)

The process of sound generation and transformation should be largely free of losses in order to obtain a high total efficiency of the vibration system. At the same time, it is required to produce maximum vibration amplitude at the sonic converter to reach sufficient amplitude at the effective surface for the machining task. A mainly loss-free increase in amplitude is guaranteed by means of resonance, that is, a vibration with a frequency that corresponds to that of the eigenfrequency of the system. This requires that the geometrical lengths of the single elements must correspond to half the wavelength of the vibration or an integral multiple.

The amplitude of the converter, however, is generally too low for machining. It can be raised to a value sufficient for machining by a subsequent transformer. The sonotrode serves as a tool holder as well as an adaptation to the resonance of the entire vibration system. In addition, there is the possibility to design the sonotrode in a way that allows extra amplitude to be achieved [Haas 1991]. The ultrasonic vibration unit is clamped at the points where vibration nodes occur, because acceleration and amplitude are zero at these points and, thus, normal force freedom predominates.

Electric energy is converted into mechanical vibrations in modern machinery using the piezoelectric effect. It is related to the reversible property of special ceramic materials to deliver electric voltage when affected by external forces. This property is used for the generation of ultrasonic vibration by converting applied voltage into mechanical vibrations. Modern sonic converters usually contain several piezoceramic discs of lead zirconate titanate restricted by two final masses that are mechanically prestressed by a center screwing.

In the course of grinding, ultrasonic frequency can be introduced into the contact zone by the tool as well as by the workpiece. An excitation of oscillation of the workpiece takes place when the dimensions and the weight of the tool do not allow a high-frequency introduction of oscillations with low amplitudes. Depending on the position of the active partners relative to each other and on the direction of oscillations, there are different process modifications that allow the realization of machining tasks (Figure 20.3).

It has been proved that process improvement through ultrasonic superposition can be achieved, particularly where grinding is characterized by constant workpiece-wheel contact. These contact conditions particularly apply to face and cross-peripheral grinding. Moreover, investigations on peripheral grinding showed that the effects resulting from ultrasonic assistance have a more pronounced effect on the work result with increasing contact length [Spur and Holl 1995]. Thus, contrary to creep-feed grinding, hardly any process improvement could be observed in the case of reciprocating grinding.

Process variants of ultrasonic assisted grinding

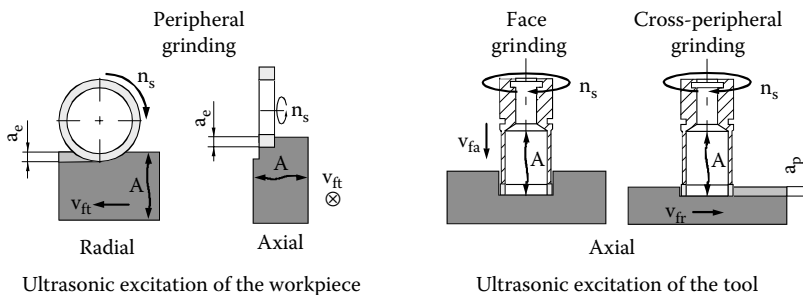


**FIGURE 20.3** Process modifications of ultrasonic assisted grinding. (From Uhlmann and Holl 1998a. With permission.)

### 20.3 ULTRASONIC-ASSISTED GRINDING WITH WORKPIECE EXCITATION

According to the process variant, a supersonic oscillation is superimposed in the contact zone either vertical or parallel to the workpiece surface in addition to the conventional cutting movement. This change in the speed ratios and in the resultant cutting speed leads to functional and wear mechanisms, which are basically different from those of conventional grinding.

### 20.4 PERIPHERAL GRINDING WITH RADIAL ULTRASONIC ASSISTANCE

Material removal and tool wear mechanisms of peripheral longitudinal grinding with radial ultrasonic excitation of the workpiece can be described through the simulation of the engagement of a single grain (Figure 20.4) and through scratch tests [Uhlmann and Holl 1998(b)].

If the feed speed is ignored, the path of a grain making a scratch, without ultrasonics, is described by the segment of a circle. The grain penetrates the material up to the depth of cut of the single grain,  $a_{eG-CON}$ , with a constant wheel speed,  $v_s$ , and a defined engagement angle,  $\alpha_{e-CON}$ . The maximum depth of scratch is reached at the lowest point of the curve. After leaving the surface, the grain has marked a trace of the length  $l_{Rt-CON}$ .

Additional longitudinal workpiece vibration causes significant deviations in a radial direction from the path described before. Depending on how many workpiece vibrations are realized per contact phase, a number of single scratches locally strung together with different scratch depths and lengths emerge instead of a circular scratch. The maximum depth of scratch increases by the value of the amplitude at nominally equal single-grain working engagements. As long as  $a_{eG-CON}$  is smaller than the amplitude, complete contact disruptions occur in each case between the local single-grain scratches. Due to the additional speed component in the radial direction, the grain hits the surface at a larger engagement angle with higher active speed. Each local single-grain scratch is characterized by distinctly shorter contact times and single-grain lengths of scratch, as well as higher single-grain depths of scratch.

Figure 20.5 displays the surfaces of the materials, silicon nitride (SSN), and zirconium oxide ( $ZrO_2$ ) scratched with and without ultrasonic assistance at equal maximum depths of scratch.

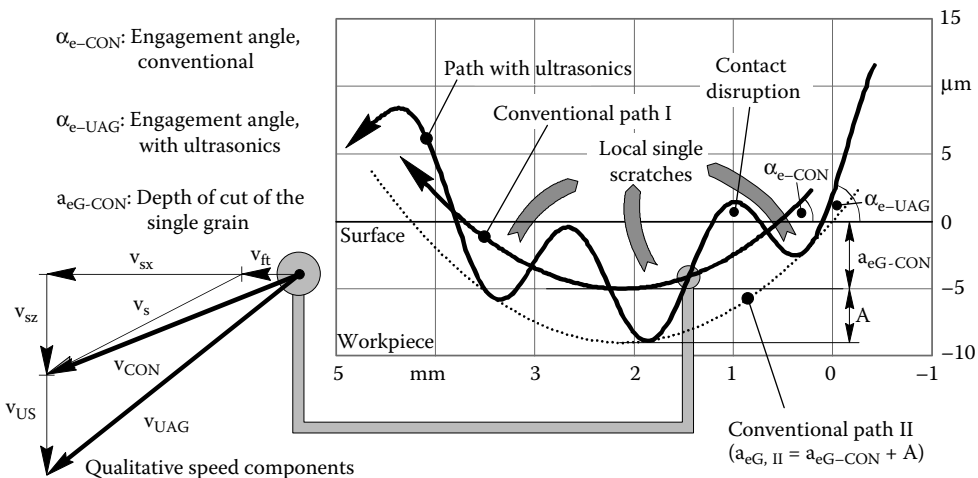


**FIGURE 20.4** Parameters and simulation of the individual grain engagement during ultrasonic-assisted grinding. (From Uhlmann and Holl 1998b. With permission.)

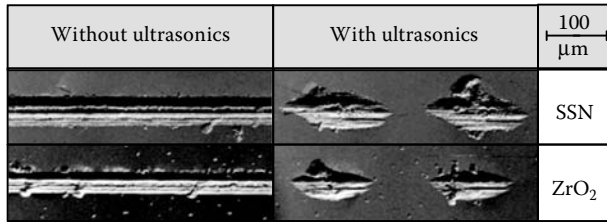


**FIGURE 20.5** Scratches on different ceramics with and without ultrasonics.

The wheel speed of the single-grain diamond was set to  $v_s = 5$  m/s. Scratching without ultrasonic assistance leads to continuous traces, which mainly display areas of plastic deformation on the bottom of the scratch, partly showing traces of other single cutting edges. Processes of material removal occur while the diamond grain moves from right to left, which, due to critical stress conditions, causes radial cracks on the scratch borders that run vertically to the direction of motion. Above this are a number of lateral cracks depending on the  $K_{Ic}$ -value, leading to conchoidal chips of material particles.

Observing the traces generated with ultrasonic assistance it becomes clear that the entire trace is divided into local single-grain scratches. Repeated contact disruptions are due to periodic oscillation of the workpiece as well as superimposed circular movement of the single grain diamonds. The effect of complete liftoff and re-entry into the workpiece surface was similarly noticed for all tested materials. The scratches are primarily characterized by plastic deformations. Lateral crack systems are formed on the right and left borders of the scratches in relation to the depth of indentation, resulting in conchoidal chips.

The effects of ultrasonically assisted grinding cause a higher mechanical load of material and diamond grits. In addition, the time of contact and, hence, the friction effects are distinctly reduced, thus decreasing the thermal loads. However, the degree that mechanical stresses appearing due to material displacement processes in front of the cutting edge are influenced remains unclear.

The theoretical center distance of two local single-grain scratches can be determined by approximation directly from the relation of wheel speed,  $v_s$ , and oscillation frequency,  $f$ . A comparison of theoretical setting conditions with actually generated structures contributed to the verification of the formation of scratch geometries typical for ultrasonics [Spur and Holl 1997].

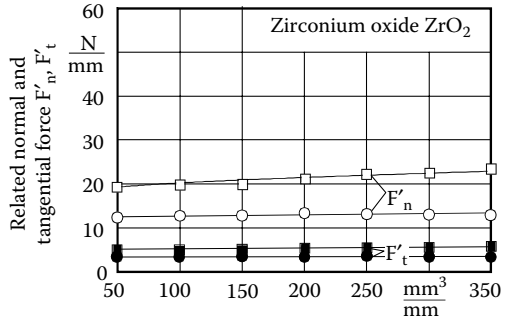
Figure 20.6 shows the resulting normal and tangential forces during creep feed grinding of silicon carbide, zirconium oxide, and aluminum oxide with and without ultrasonics. Ultrasonic assistance leads to a significant reduction of the process forces. Contrary to conventional creep feed grinding, the course of the process course is quasistationary. The ultrasonic superposition leads to higher stresses of the workpiece subsurface and the diamond cutting edges. Without ultrasonic assistance, the diamond cutting edges get flatter in the course of the process, starting from the sharpened state. Thus, the grain strain increases. Above a certain marginal load, the grain parts splinter in big segments or break-off. The grains have not flattened in any of the cases with ultrasonic assistance. Rather, an increase in microsplitting could be observed. If transferred to the grinding process, the microsplitting leads to a continuous generation of sharp single cutting edges. This results in the quasistationary state.

Figure 20.7 shows the integral temperature values in the subsurface of different ceramics during creep feed grinding with and without ultrasonics. The measurement of temperature values was carried out with thermal elements, which were positioned in the subsurface of the workpieces. It becomes clear that the superposition of ultrasonic leads to a significant decrease in temperature.

The contact interruption between wheel and workpiece as a result of ultrasonic oscillation leads to a reduction of engagement times as described above. Moreover, instead of coolant at the contact



Grinding wheel: D126 K+ 8821 JY C50  
 KSS: Lösung 4%, p = 5 bar  
 Cutting speed:  $v_c = 35$  m/s  
 Infeed:  $a_e = 1.0$  mm  
 Feed speed:  $v_{ft} = 300$  mm/min  
 Specific material removal rate:  $Q'_w = 5$  mm<sup>3</sup>/mm/s



■ Convent. creep grinding      ● Ultrasonic assisted creep grinding ( $A_{US} = 4.5$  μm)

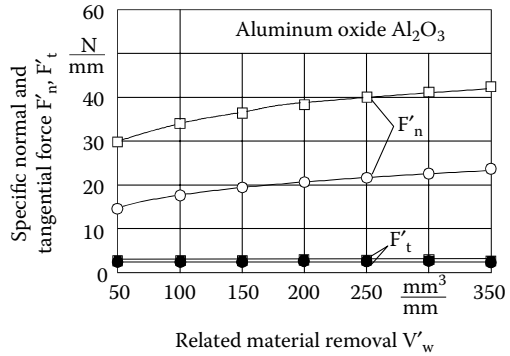
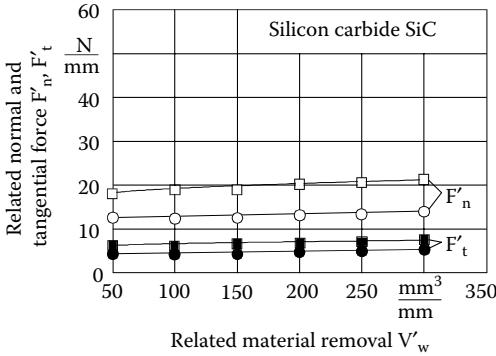
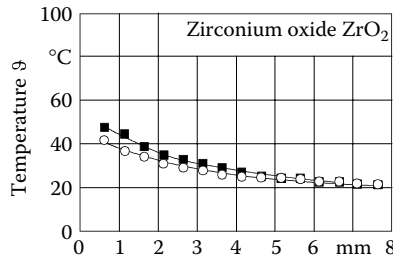


**FIGURE 20.6** Process forces during conventional and ultrasonic-assisted creep feed grinding of different ceramic materials.

Grinding wheel: D126 K+ 8821 JY C50  
 KSS: Solution 4%, p = 5 bar  
 Cutting speed:  $v_c = 35$  m/s  
 Infeed:  $a_e = 1.0$  mm  
 Feed speed:  $v_{ft} = 300$  mm/min  
 Specific material removal rate:  $Q'_w = 5$  mm<sup>3</sup>/mm/s



■ Conv. creep feed grinding      ○ Us assisted creep feed grinding ( $A_{US} = 4.5$  μm)

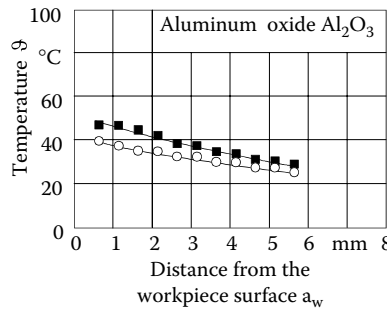
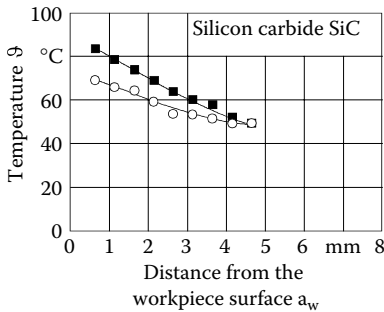


**FIGURE 20.7** Workpiece subsurface temperatures during conventional and ultrasonic-assisted creep feed grinding of different ceramic materials.

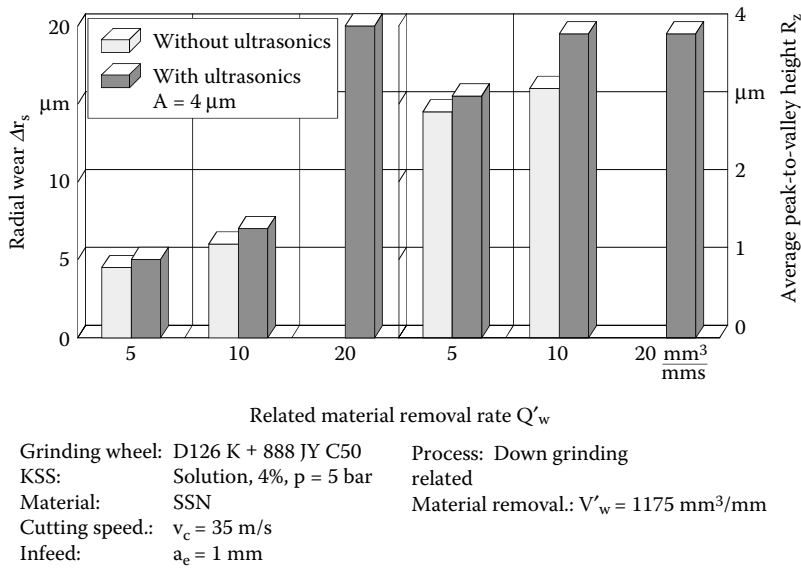


**FIGURE 20.8** Radial wear of the grinding wheel and the surface quality of silicon nitride during conventional and ultrasonic-assisted down grinding.

zone is improved by temporary lifting of one of the active partners and by the removal of chips. The reduction of the friction effects reduce grain flattening and the preferred microsplitting of the diamond grains can be considered further reasons for the decrease of process temperature.

Figure 20.8 shows the radial wear of a grinding wheel and the surface quality of a silicon nitride ceramic. Just as in conventional grinding, radial wear of the grinding wheel increases in grinding with ultrasonics with increasing specific material removal rate. In the case of ultrasonic-assisted grinding, radial wear of the grinding wheel is higher than in conventional grinding. In the case of a material removal rate of  $Q'_w = 20 \text{ mm}^3/\text{mm/s}$ , machining was not possible with a conventional process method due to inadmissible process forces.

Surface roughness also increases with specific material-removal rate in both process variants. In ultrasonic-assisted grinding, surface roughness is higher than in conventional grinding.

### 20.5 PERIPHERAL GRINDING WITH AXIAL ULTRASONIC ASSISTANCE

Peripheral longitudinal grinding with axial ultrasonic assistance is characterized by a periodically changing working direction with continuous cutting edge engagement. The newly created workpiece surfaces have sinusoidal machining marks [Warnecke and Zapp 1995].

Through the superposition of the conventional grinding process with ultrasonic oscillation, there is an additionally arising and constantly changing velocity that is transverse to the cutting speed set on the machine. Since ultrasonic vibration mathematically follows a sinusoidal function, the ultrasonic-related speed fluctuates between zero and a maximum value, determined by the set frequency and amplitude. Hence, the resulting working velocity does not solely occur in the feed direction but, additionally, in the transverse direction. Also, the velocity changes within half a period of ultrasonic oscillation, that is, within 1/44,000th of a second from zero to the maximum value.

The resultant cutting speed leads to a constant change of the stress direction of the diamond cutting edges. Contrary to conventional grinding, the area engaged of the diamond edges is changing.

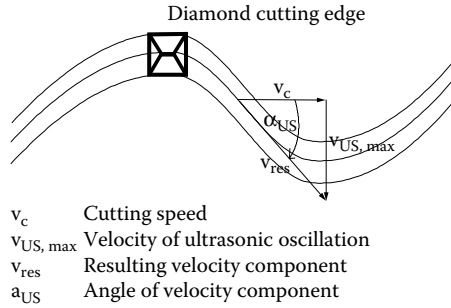


**FIGURE 20.9** Principle of velocity superposition during grinding with axial ultrasonic assistance.

Figure 20.9 shows the principle of the change of the resultant cutting direction as a result of ultrasonic superposition.

In conventional grinding, the machining marks run in the cutting direction. In ultrasonic-assisted grinding with radial excitation, the machining marks are also parallel to the direction of cutting, consisting of individual impact. The vibration in the axial direction causes machining marks transverse to the direction of cutting. Figure 20.10 shows the surface of a silicon nitride workpiece after grinding with axial ultrasonic assistance.

At a cutting speed of  $v_c = 1$  m/s, an ultrasonic frequency  $f = 21$  kHz, and an amplitude of  $A = 4.5 \mu\text{m}$ , the ratio of the amplitude of oscillations and the wavelength is so high that the course of the generated oscillations can be clearly recognized. The infeed was defined at  $a_e = 2 \mu\text{m}$  during these tests.

The creation of surface structures with axial ultrasonic assistance is possible if the tool, the material, and the process parameters are adapted to the requirements. The shape of the formed marks can be specifically set with the choice of the parameters' cutting speed, ultrasonic frequency, and amplitude.

Material:	SSN	Frequency:	$f = 21.27$ kHz	
Cutting speed:	$v_c = 1$ m/s	Amplitude:	$A = 4.5 \mu\text{m}$	
Feed:	$v_{ft} = 86$ mm/min	Infeed:	$a_e = 2 \mu\text{m}$	
Cooling lubricant:	Solution 4%	Grinding wheel:	D46 K + 888JY C50	

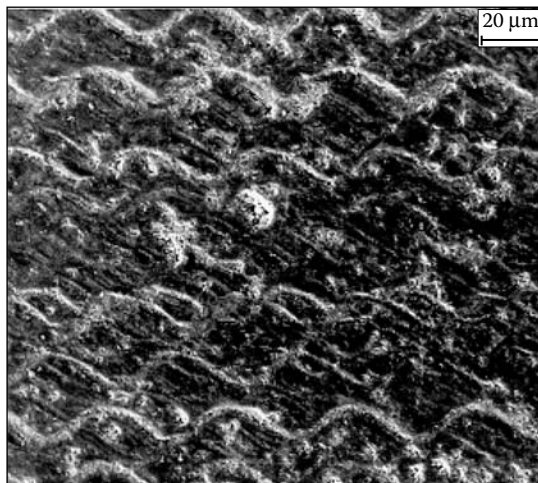


**FIGURE 20.10** Structured surface of silicon nitride.

During the machining with axial superposition of oscillations, process forces are reduced in comparison to conventional grinding. Due to the constantly changing working direction, the wear of the diamonds is clearly smaller. Thus, sharp edge areas of a cutting grain consistently engage in the material, which leads to the reduction of the process forces. As a result of the reduced proportion of friction through the sharper cutting edges, the thermal stresses are reduced as a whole. The contact zone temperature can be reduced, although additional energy is imported to the process by the high-frequency superposition of oscillations [Warnecke and Zapp 1995].

## 20.6 ULTRASONIC-ASSISTED GRINDING WITH EXCITATION OF THE WHEEL

Ultrasonic-assisted grinding with an oscillating wheel is divided into different process modifications. In the case of ultrasonic-assisted cross-peripheral grinding, the feed movement takes place vertically to the tool spindle axis and thus to the generated oscillation. With this process, grooves, gaps, and radii can be machined in brittle-hard materials. The feed movement in the case of ultrasonic-assisted face grinding is, however, parallel to the tool axis. Bores may be machined with this process.

### 20.6.1 ULTRASONIC-ASSISTED CROSS-PERIPHERAL GRINDING

During cross-peripheral grinding, the cutting edge engagement is not interrupted because the peripheral side of the wheel is in contact with the workpiece. Rather, a sinusoidal grain engagement can be observed as a result of the axial oscillation. The engagement at the front face of the wheel takes place according to the movement conditions described for the peripheral longitudinal grinding with radial excitation, leading to local individual engagements.

Figure 20.11 shows the achievable surface topographies and roughnesses after ultrasonic-assisted cross-peripheral grinding of different ceramics. Surface roughness achieved corresponds to values after conventional grinding.

Under certain kinematic conditions, the result of ultrasonic movement vertically to the workpiece surface is a complete interruption of the workpiece-tool contact. On all materials, typical pocket-type surface structures can be observed as an effect of the axial ultrasonic movement. The topography depends on the fracture toughness of the machined material. Bending strengths of components ground conventionally or with ultrasonic assistance are similar, although higher residual compression is imparted to the subsurface of the material through the changed stress in ultrasonic-assisted grinding [Engel and Daus 1999].

Figure 20.12 shows the achievable material-removal rate during ultrasonic-assisted cross-peripheral grinding of different ceramic materials. The feed speed was controlled in the tests by the determination of a maximum process force in the direction of feed. Smaller process forces lead to higher feed speeds and thus to growing material-removal rates. In contrast to ultrasonic-assisted grinding with constant feed speed, this kind of process control prevents inadmissibly high stresses on the tool.

As a result of the ultrasonic superposition of the grinding process, higher material-removal rates can be stated for all investigated materials and used diamond grain sizes of the grinding tools. It can be seen that the diamond grain size is not decisive for the achievable material removal rates during ultrasonic-assisted grinding. There is a correlation between this statement and investigations by Pei and Ferreira [1999], who observed this behavior during the machining of zirconium oxide. It becomes clear that the mechanical properties of the machined material have a significant influence on the machining result.

The surface qualities obtainable are greatly dependent on the characteristics of the machined materials and of the machining process. This can be proved by comparing the surface qualities of ceramics, which were machined with ultrasonic-assisted grinding and plane parallel lapping (Figure 20.13). Excluding the material silicon carbide, the arithmetical mean deviation of samples ground with ultrasonic assistance is slightly above the value established for that of plane parallel lapping.

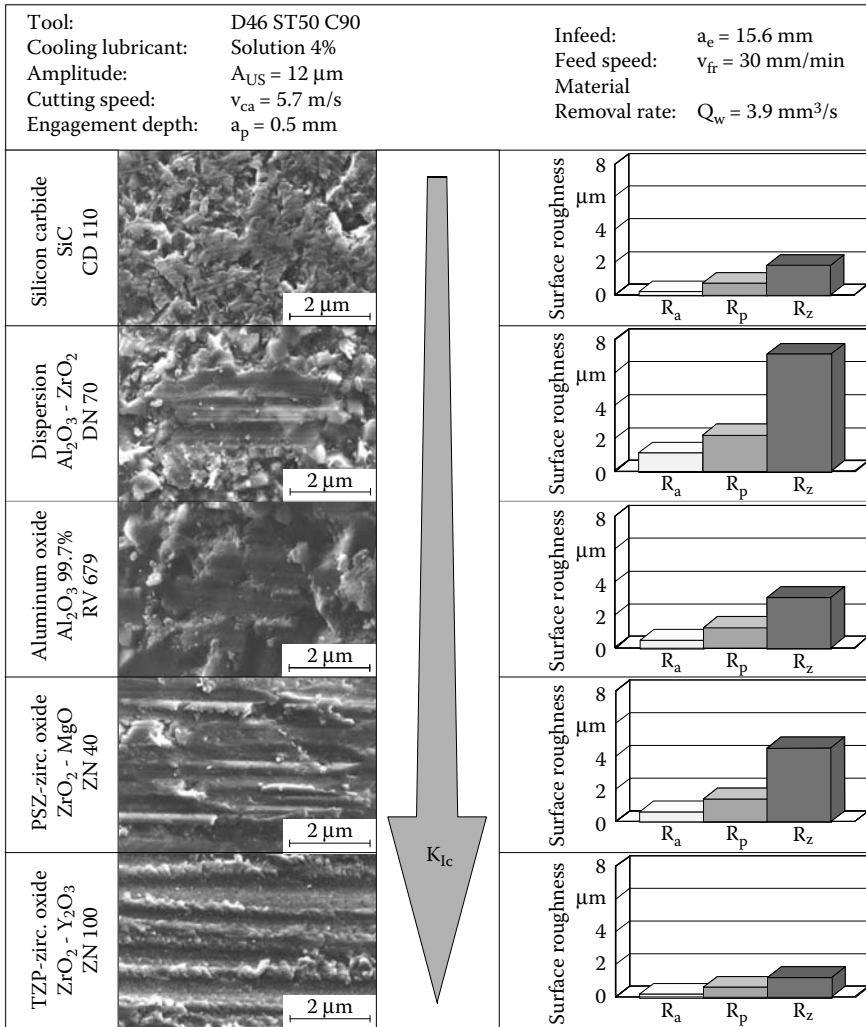


**FIGURE 20.11** Surface topography and roughness of ceramic materials after ultrasonic-assisted cross-peripheral grinding.

For the materials silicon carbide and zirconium oxide (ZN 40) the best surface values were measured during ultrasonic-assisted grinding. Summarizing, the surface qualities obtainable for ceramic materials machined with ultrasonic-assisted grinding can be established at the level of conventional finishing procedures. Despite higher mechanical loads, surface qualities comparable to those of lapping can be achieved.

Bending strengths of ceramic workpieces were investigated for the machining parameters in Figure 20.10. Ultrasonic-assisted grinding gives bending strengths similar to or higher than those of plan-parallel lapping. Moreover ultrasonic-assisted grinding leads to insignificantly higher deviations of bending strengths. These are caused by the alternating load on the workpiece subsurface [Spur et al. 1999].

**20.6.2 ULTRASONIC-ASSISTED FACE GRINDING**

To evaluate the machining process, the development of process forces was analyzed for a path-controlled feed speed. Figure 20.14 illustrates that a grinding operation without ultrasonic assistance

**Material removal rate of peripheral plunge grinding**

Grinding tool: D46...151 St50 C90  
 Cooling lubricant: Solution 4%, p = 5 bar  
 Cutting velocity:  $v_{ca} = 3.1 \text{ m/s}$   
 Depth of engagement:  $a_p = 1.0 \text{ mm}$   
 Infeed:  $a_e = 12 \text{ mm}$   
 Amplitude:  $A = 12 \text{ }\mu\text{m}$   
 Material removal:  $V_w = 720 \text{ mm}^3$   
 Max. process force:  $F_{r,max} = 100 \text{ N}$   
 Tolerable  
 Feed speed:  $v_{fr} = 120 \text{ mm/min}$

□ With ultrasonics    ▨ Without ultrasonics

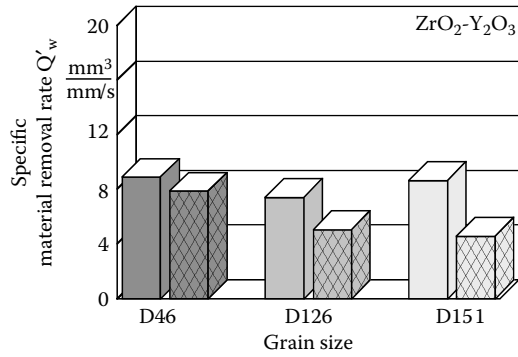
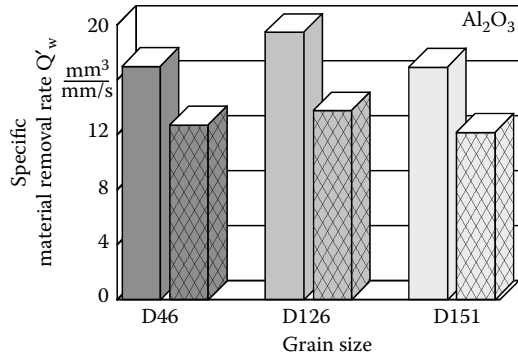
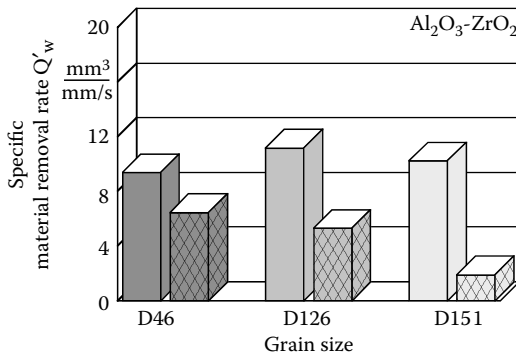


**FIGURE 20.12** Material removal rates during conventional and ultrasonic-assisted grinding of ceramics in relation to the grain size of the tool.

produces a poorer process because rapidly increasing axial forces occur. After a grinding time of  $t_c = 22 \text{ s}$ , the force already reached a value of  $F_z = 240 \text{ N}$ . This level could no longer be tolerated, so the process had to be stopped. A permanent wheel-workpiece contact is responsible for faster blunting of the grinding coating, leading to a strongly reduced cutting ability. This results in an

**Ultrasonic-assisted cross-peripheral grinding**

Grinding tool: D46 ST50 C90  
 Cooling lubricant: solution 4 %  
 Amplitude:  $A_{US} = 12 \text{ }\mu\text{m}$   
 Cutting speed:  $v_{ca} = 5.7 \text{ m/s}$   
 Depth of engagement:  $a_p = 0.5 \text{ mm}$   
 Working engagement:  $a_e = 15.6 \text{ mm}$   
 Feed speed:  $v_{fr} = 30 \text{ mm/min}$   
 Material removal rate:  $Q_w = 3.9 \text{ mm}^3/\text{s}$

**Plane parallel lapping:**

Lapping abrasive: B<sub>4</sub>C F400  
 Rotational speed of the inner pin circle:  $n_i = 64 \text{ rpm}$   
 Rotational speed of the lower wheel:  $n_u = -56 \text{ rpm}$   
 Rotational speed of the upper wheel:  $n_o = 33 \text{ rpm}$   
 Lapping pressure:  $p_l = 0.8 \text{ MPa}$   
 Lapping wheels: Perlitic gray cast iron

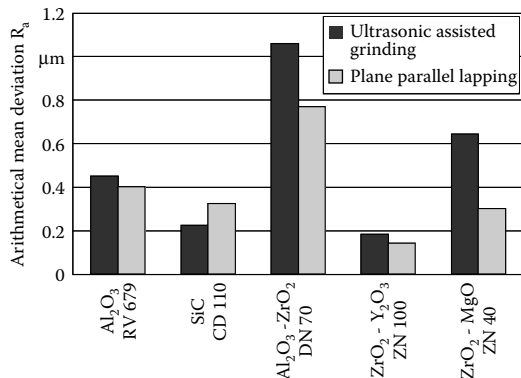


**FIGURE 20.13** Arithmetical mean deviation depending on the material and the machining process. (From Spur et al. 1999. With permission.)

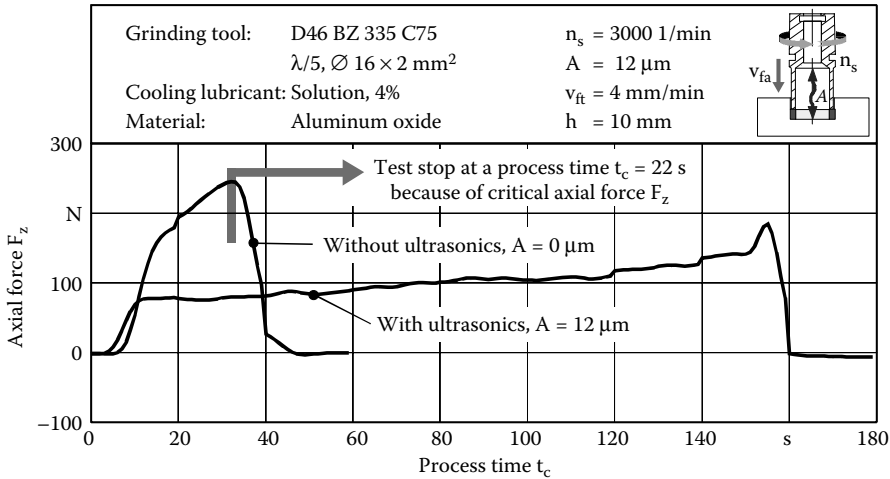


**FIGURE 20.14** Comparison between axial forces during tool-path controlled face grinding with and without ultrasonics.

enormous increase in force if feed speeds are constant. Therefore, economic production of such contours with conventional methods (grinding without ultrasonics) is not possible.

Figure 20.15 shows the influence of ultrasonic oscillations on the process forces during face grinding. The height of the surface-related axial forces depends on the machined material. Alongside fracture toughness, stability and hardness of the material play an important role here.

While the highest surface-related material removal rates of  $Q'_w = 25 \text{ mm}^3/\text{mm}^2/\text{min}$  are achieved for aluminum oxide, they decrease to  $Q'_w = 5 \text{ mm}^3/\text{mm}^2/\text{min}$  during the machining of silicon nitride. A maximum surface-related axial force of  $6 \text{ N}/\text{mm}^2$  was chosen as a critical value. It can be observed in the case of zirconium oxide how the process forces behave in contrast to conventional face grinding. There are similar surface-related axial forces at  $Q'_w = 2.5 \text{ mm}^3/\text{mm}^2/\text{min}$  during conventional

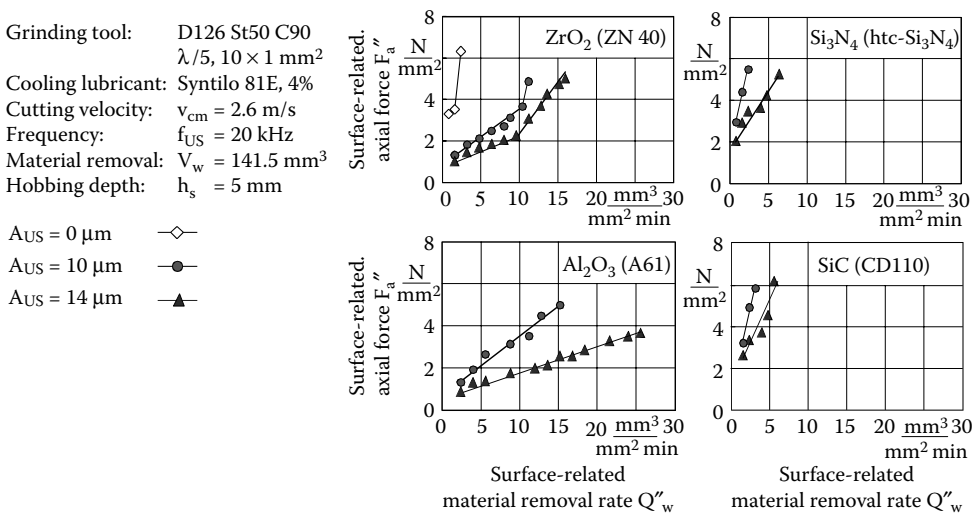


**FIGURE 20.15** Surface-related axial forces during face grinding in relation of the surface-related material removal rate for ceramics. (From Uhlmann 1998. With permission.)

and at  $Q'_w = 15 \text{ mm}^3/\text{mm}^2/\text{min}$  for ultrasonic-assisted grinding with  $A_{US} = 14 \text{ }\mu\text{m}$ . This is a sixfold increase of the material-removal rate.

The influence of the engagement angle  $\alpha_{eUS,max}$  in ultrasonic-assisted grinding described within the scope of the kinematical investigations of the process becomes clear for all four tested materials. The comparison of the effect of two different ultrasonic amplitudes of  $A_{US} = 10 \text{ }\mu\text{m}$  and  $A_{US} = 14 \text{ }\mu\text{m}$  on the process forces shows the influence of the engagement angle  $\alpha_{eUS,max}$ . The reduction of the ultrasonic amplitude leads to a decrease of  $\alpha_{eUS,max} (A_{US} = 14 \text{ }\mu\text{m}) = 32^\circ$  to  $\alpha_{eUS,max} (A_{US} = 10 \text{ }\mu\text{m}) = 24^\circ$ . The result of these kinematical changes is smaller grain acceleration due to the ultrasonics and a reduction of the mechanical, pulsed stresses of the single grains. Basically, these mechanical stresses are the cause of microsplitting of the abrasive grains. In turn, this microsplitting leads to the generation of new sharp cutting edges [Uhlmann 1998].

### 20.7 SUMMARY

Ultrasonic-assisted grinding is a novel finishing process for economic machining of brittle-hard materials. The superposition of the kinematics of the grinding process with ultrasonic oscillations leads to removal and wear mechanisms different from those during conventional grinding. There is microsplitting due to the high stress of the abrasive grains, provoking the constant formation of new sharp edges. The processes are characterized by small process forces with a quasistationary process during the machining allowing an increase of the material-removal rates.

In peripheral grinding with radial ultrasonic superposition, a reduction of process forces of up to 90% could be observed in contrast to conventional grinding with the same specific material-removal rate. At the same time, wear of the grinding wheel as well as surface quality of the machined workpieces increase slightly. In peripheral longitudinal grinding with axial superposition, structured surfaces could be formed and directional machining marks avoided with the help of the kinematics.

In cross-peripheral grinding with axial ultrasonic excitation, complex contours with high specific material-removal rates can be achieved despite the low cutting velocities. At the same time, high surface qualities and shape accuracies can be realized.

In the future, process behavior has to be improved through the definition of harmonized optimum parameters for the ultrasonic oscillation and for the grinding process. Furthermore, wheels have to be designed for the requirements of ultrasonic grinding in terms of the bonds, diamond grain size, and specification.

These results show that ultrasonic-assisted grinding ensures the machining of ceramics in terms of high economic efficiency and component quality. Through the variety of kinematic process variants, it is possible to machine different geometrical elements on brittle-hard materials (Figure 20.16).

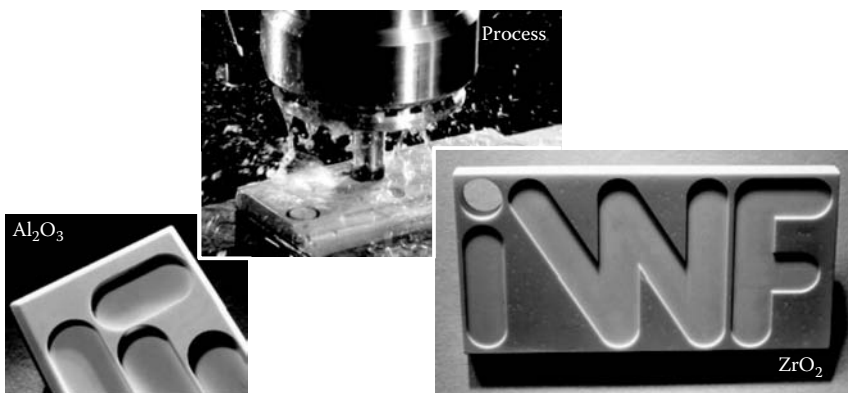


**FIGURE 20.16** Process of ultrasonic assisted cross-peripheral grinding and possible geometrical elements. (From Uhlmann and Holl 1998a. With permission.)



## REFERENCES

- Cartsburg, H. 1993. Hartbearbeitung keramischer Verbundwerkstoffe. Dissertation Technische Universität Berlin, 1993.
- Drozda, T. J. 1983. "Mechanical Nontraditional Machining Processes." *Manuf. Eng.* 91, 1, 61–64.
- Engel, H. and Daus, N.-A. 1999. Veränderung des Wirkmechanismus beim Schleifen durch Ultraschallunterstützung und daraus resultierende Prozeßverbesserungen. Vortrag zum Seminar "Hybride Prozesse der Zerspan- und Abtragtechnik." TU Dresden.
- Haas, R. 1991. Technologie zur Leistungssteigerung beim Ultraschall-schwingläppen. Ph.D. dissertation, RWTH Aachen.
- Nankov, M. M. 1989 "Supersonic Activation or Cup-Shape Diamond Disk Grinding." ISEM-9, Proceedings of the Symposium for Electro Machining. The Japan Society of Electro-Machining Engineers, Nagoya, Japan.
- Pattimore, J. 1998. "Optimisation of Grinding for Cylindrical Silicon Nitride Components for Mass Production." Lecture: "Informativer Arbeitskreis Keramikbearbeitung," IWF Berlin.
- Pei, Z. J., Prabhakar, D., and Haselkorn, M. 1993. *Mechanistic Approach to the Prediction of Material Removal Rates in Rotary Ultrasonic Machining*. Manufacturing Science and Engineering American Society of Manufacturing Engineers, Production Engineering Division (Publication) PED. Volume 64. ASME, New York.
- Pei, Z. J. and Ferreira, P. M. 1999. "An Experimental Investigation of Rotary Ultrasonic Face Milling." *Int. J. Mach. Tools Manuf.* 39, 1327–1344.
- Popp, M. 1998. "Seriengerechte Herstellung von Bauteilen aus Hochleistungskeramik am Beispiel des Keramikwälzlagers." Proceedings: "Karlsruher Arbeitsgespräche 1998," BMBF/PFT, Karlsruhe, 12 und 13.03.
- Prabhakar, D., Ferreira, P. M., and Haselkorn, M. 1992. "An Experimental Investigation on Material Removal Rates in Rotary Ultrasonic Machining." Konferenz-Einzelbericht: Transactions of the North American Manufacturing Research Institution of SME 1992, the 20th NAMRC Conference, Washington State University, Pullman, WA.
- Spur, G. 1989. *Keramikbearbeitung*. München; Wien: Hanser Verlag.
- Spur, G. and Holl, S.-E. 1995. "Ultraschallunterstütztes Schleifen von Hochleistungskeramik," in *Jahrestagung 1995, Kurzreferate*. Deutsche Keramische Gesellschaft, Aachen, Germany.
- Spur, G., Uhlmann, E., Holl, S.-E., and Daus, N.-A. 1999. "Ultrasonic Machining of Ceramics," in *Machining of Ceramics – 2000 and Beyond*. Marinescu, I.D., Ed.
- Suzuki, K., Tochinai, H., Uematsu, T., and Nakagawa, T. 1993. "New Grinding Method for Ceramics Using a Biaxially Vibrated Nonrotational Ultrasonic Tool." *Ann. CIRP* 42, 1, S. 375–378.
- Uhlmann, E. 1998. "Surface Formation in Creep Feed Grinding of Advanced Ceramics with and without Ultrasonic Assistance." *Ann. CIRP* 47, 1, 249–252.
- Uhlmann, E. and Holl, S.-E. 1998a. "Entwicklungen beim Schleifen keramischer Werkstoffe." Vortrag im Rahmen des Seminars, Moderne Schleiftechnologie, am 14 Mai 1998 in Furtwangen, Deutschland.
- Uhlmann, E. and Holl, S.-E. 1998b. "Schwer zerspanbare Werkstoffe ultraschallunterstützt schleifen." *Maschinenmarkt*. 104, 48, S. 34–37.
- Warnecke, G. and Zapp, M. 1995. "Ultrasonic Superimposed Grinding of Advanced Ceramics." Proceedings of the 1st International Machining and Grinding Conference, Dearborn.
- Westkämper, E. and Kappmeyer, G. 1994. "Feiner Abtrag – Anwendungsgerechtes Auslegen von Werkzeugen zum Ultraschallhonen." *Maschinenmarkt*. 100, 30, S. 28–33.

---

# Appendix 1: Glossary

## SYMBOLS

$a, a_p, A:$	Set depth of cut = Programmed depth of cut = Apparent depth of cut.
$a_d:$	Dressing depth.
$a_e:$	Real depth of cut.
$a_e(\theta):$	Depth of cut at position $\theta$ .
$a_{sw}:$	Depth of wheel wear.
$b_{cu}:$	Uncut chip width.
$b_d:$	Active width of dressing tool.
$b_s:$	Contact width on grinding wheel.
$b_w:$	Contact width on workpiece.
$c:$	Damping.
$c, c_b, c_s:$	Costs, labor rate, wheel cost.
$c:$	Specific heat capacity.
$c_p:$	Specific heat at constant pressure.
$c_v:$	Specific heat at constant volume.
$d_{cap}:$	Diameter of capillary.
$d_e:$	Equivalent wheel diameter.
$d_g:$	Grain diameter. Mean grain diameter.
$d_{jet}:$	Fluid jet diameter.
$d_s:$	Diameter of grinding wheel.
$d_{ss}:$	Diametral stand-off.
$d_w:$	Diameter of workpiece.
$d_{ww}:$	Diametral stock removal.
$e_c$ : or $U$ :	Specific cutting energy. Energy per unit volume.
$e_{ch}:$	Energy per unit volume carried away by chips.
$f:$	Frequency in cycles per second.
$f_d:$	Dressing feed per wheel revolution.
$f_n:$	Normal force on a grain.
$f_t:$	Tangential force on a grain.
$h:$	Heat convection coefficient for moving surface. Heat per unit area per degree temperature difference.
$h_{air}:$	Thickness of the boundary layer of air surrounding a wheel.
$h_{cu}:$	Uncut chip thickness.
$\bar{h}_{cu}:$	Mean thickness of uncut chips.
$h_{eq}:$	Equivalent chip thickness.
$h_f:$	Convection coefficient for fluid cooling in contact zone.
$h_{fu}:$	Mean thickness of the useful process fluid layer that passes through the contact.
$h_g:$	Convection coefficient for an abrasive grain.
$h_{jet}:$	Thickness of a uniform jet of process fluid.
$h_p:$	Depth of fluid penetration into the wheel.
$h_{pores}:$	Mean depth of pores at surface of wheel.
$h_{slot}:$	Slot nozzle gap thickness.
$h_w:$	Work-height in centerless grinding.
$h_w:$	Convection coefficient for workpiece.

$h_{wg}$ :	Convection coefficient for the workpiece at a grain contact.
$k$ :	Shear flow stress.
$k$ :	Thermal conductivity.
$k_m$ :	Stiffness of the machine-tool-workpiece system.
$k_s$ :	Normal grinding force per unit depth of cut. (Sometimes termed grinding stiffness.)
$k_w$ :	Thermal conductivity of work-material.
$l_c$ :	Contact length of tool and workpiece. Uncut chip length.
$l_{cap}$ :	Capillary length.
$l_f$ :	Contact length due to force arising from deflection.
$l_{fr}$ :	Contact length due to force for a real surface with roughness.
$l_{fs}$ :	Contact length due to force for a smooth body.
$l_g$ :	Geometric contact length.
$l_{mc}$ :	Length of median crack.
$n$ :	Number of waves.
$n_b$ :	Number of parts per batch.
$n_d$ :	Number of dressing passes.
$n_s$ :	Wheel rotational speed.
$n_w$ :	Workpiece rotational speed.
$p$ :	Angular pitch of waviness.
$p$ :	Pressure.
$p$ :	Normal stress.
$p_p$ :	Pumped pressure.
$q$ :	Tangential stress.
$q$ :	Speed ratio: Wheel speed over workspeed.
$q$ :	Heat flux. Heat per unit area per unit time.
$q_{ch}$ :	Heat flux to chips.
$q_{cu}$ :	Uncut chip aspect ratio.
$q_d$ :	Dressing speed ratio (crush ratio).
$q_f$ :	Heat flux to process fluid.
$q_o, q_t$ :	Mean heat flux. Total heat flux.
$q_s$ :	Heat flux to abrasive.
$q_w$ :	Heat flux to workpiece.
$r$ :	Ratio of chip groove width to groove thickness.
$r_o$ :	Effective radius of wear flat on tip of grain.
$r_g$ :	Effective radius of grain.
$r_s$ :	Radial wheel wear per dress.
$r(\theta)$ :	Reduction in radius at position $\theta$ .
$s$ :	Feed of workpiece per cutting edge.
$s$ :	Laplace operator.
$t$ :	Time.
$t_c$ :	Time of contact of point on workpiece based on real contact length.
$t_c, t_d, t_t$ :	Cycle time per part. Dressing time per part. Total cycle time per part.
$t_g$ :	Time of contact of point on workpiece based on geometric contact length.
$t_{gc}$ :	Time for passage of one grain through the contact zone.
$t_p$ :	Proportion of bearing area at a depth $p$ below highest peak.
$t_o$ :	Machining time.
$t_{so}$ :	Dwell time for spark-out.
$v$ :	Speed of a moving heat source.
$v_c$ :	Cutting speed.
$v_d$ :	Velocity of roll dresser.
$v_{cap}$ :	Mean fluid velocity through capillary.

$v_f$ :	Feedrate or in-feedrate or through-feedrate of workpiece.
$v_{fd}$ or $v_d$ :	Dressing traverse feedrate.
$v_{fe}$ :	Effective feedrate in centerless grinding.
$v_{f.wear}$ :	Rate of reduction of wheel radius due to wear.
$v_{jet}$ :	Fluid jet velocity.
$v_{orifice}$ :	Fluid velocity from orifice.
$v_r$ :	Resultant control wheel speed in centerless grinding.
$v_s$ :	Speed of the wheel.
$v_w$ :	Speed of the workpiece tangential to grinding wheel speed.
$y_b$ :	Thermal boundary layer thickness of the process fluid in the contact zone.
$y_t$ :	Payback time for machine.
$w_{slot}$ :	Width of slot nozzle.
$x(\theta)$ :	Dynamic deflection at position $\theta$ .
$A$ :	Apparent = set depth of cut.
$A$ :	Geometric stability parameter for centerless grinding.
$A_c$ :	Contact area. Overall contact area.
$A_{cu}$ :	Mean cross-sectional area of the uncut chips.
$A_r$ :	Real area of contact.
$B$ :	Brittleness index.
$B$ :	Cutting edge spacing in lateral direction. Mean grain spacing.
$B$ :	Peclet equivalent for inclined band source.
$C$ :	Factor for temperature solution taking account of Peclet number, flux distribution, and geometry.
$C, C_a$ :	Cutting edge density. Number of active cutting edges per unit area.
$C, C_p, C_v$ :	Specific heat capacity. For gases, specific heat at constant pressure or at constant volume.
$C_{stat}, C_{dyn}$ :	Static and dynamic cutting edge density.
$C_a$ :	Area contraction coefficient for fluid jet.
$C_d$ :	Orifice discharge coefficient.
$C_l$ :	Labor cost per part.
$C_m$ :	Machine cost per part.
$C_{me}$ :	Machine cost.
$C_s$ :	Wheel cost per part.
$C_v$ :	Velocity coefficient for orifice or nozzle jet.
$E$ :	Young Modulus of elasticity.
$E$ :	Energy.
$E^*$ :	Equivalent elastic modulus for two bodies in contact.
$E_f$ :	Fracture energy.
$E_p$ :	Plastic flow energy.
$F$ :	Force. Resultant of normal, tangential, and axial forces.
$F^*$ :	Critical load to initiate a crack.
$F_{ij}$ :	Notation used to represent forces on atom "i" from atoms "j."
$F_a$ :	Force parallel to wheel axis.
$F_n$ :	Force normal to wheel surface.
$F'_n$ :	Normal force per unit width.
$F_t$ :	Force tangential to wheel surface.
$F'_t$ :	Tangential force per unit width.
$G$ :	Grinding ratio: Volume of work-material removed divided by wheel wear volume.
$H$ :	Hardness. Brinell hardness.
$H_b$ :	Hardness of material bulk.
$H_m$ :	Momentum power of fluid at wheel speed.

$H_p$ :	Fluid pumping power.
$H_s$ :	Hardness of material at surface.
$H_t$ :	Total pumping and momentum power required to deliver fluid through grinding contact.
$H_v$ :	Vickers hardness.
$H_{RC}$ :	Rockwell hardness.
$K$ :	Machining-elasticity parameter.
$K$ :	Archard-Preston wear coefficient.
$K$ :	Yield shear stress. Flow stress.
$K$ :	Permeability of a wheel.
$K_0[u]$ :	Bessel function of second kind order zero for an argument of value $u$ .
$K_{1C}$ :	Fracture toughness.
$L$ :	Cutting edge spacing in cutting direction.
$L$ :	Peclet number for moving band source.
$M$ :	Mesh number. Measure of grain size based on number of wires used in sieve.
$M'_{air}$ :	Momentum of air boundary layer around wheel per unit wheel width.
$M'_f$ :	Momentum of process fluid.
$M'_f$ :	Momentum of process fluid per unit wheel width.
$N_d, N_w$ :	Number of parts per dress. Number of parts per wheel.
$N_{mc}$ :	Number of parts produced by the machine within payback period.
$P, P_c$ :	Cutting or grinding power.
$P$ -ratio:	Ratio of material volume removed to wheel surface area.
$P'_c$ :	Cutting power per unit width.
$P_c(x)$ :	Probable number of active cutting edges per unit length in cutting direction.
$P_c(z)$ :	Probable number of active cutting edges per unit length in lateral direction.
$P_e$ :	Peclet number for moving band source.
$Q$ :	Dynamic magnification.
$Q$ :	Rate of work material removal.
$Q_f$ :	Flowrate of process fluid.
$Q_{fu}$ :	Useful flowrate. Flowrate that passes through contact zone.
$Q_s$ :	Rate of tool wear.
$Q'_s$ :	Rate of tool wear per unit width.
$Q_w$ :	Rate of work-material removal.
$Q'_w, Q'$ :	Rate of work-material removal per unit width of contact.
$R_a$ :	Measure of average surface roughness.
$R_{ch}$ :	Proportion of total heat taken by chips.
$R_e$ :	Reynolds number.
$R_f$ :	Proportion of total heat taken by fluid.
$R_L$ :	Ratio of real contact length to geometric contact length.
$R_r$ :	Roughness factor. Ratio of contact lengths due to deflection for rough and smooth surfaces.
$R_s$ :	Proportion of total heat taken by abrasive.
$R_t, R_z$ :	Measures of peak to valley roughness.
$R_w$ :	Partition ratio. Proportion of total heat taken by workpiece.
$R_{ws}$ :	Partition ratio for the workpiece-wheel rubbing contact.
$R(\theta)$ :	Set reduction in radius at position $\theta$ , that is, ignoring deflection.
$S_{cu}$ :	Uncut chip surface area.
$S_o$ :	Sommerfeld number.
$T$ :	Tool life or tool redress life.
$T$ :	Temperature.
$T$ :	Time for one work revolution.

$T_d$ :	Maximum wear spot on diamond dressing tool.
$T_{\max}$ :	Maximum value of workpiece background temperature.
$T_{wg}, T_g$ :	Spike (or flash) temperature at a contact between grain and workpiece.
$T_w$ :	Workpiece background temperature in contact zone.
$U_d$ :	Overlap ratio in dressing. Active width of dressing tool divided by dressing feed.
$V_a$ :	Useful volume of abrasive layer.
$V_b$ :	Volume percentage of bond material in an abrasive structure.
$V_{cu}$ :	Uncut chip volume.
$V_g$ :	Volume percentage of abrasive grain in a wheel structure.
$V_p$ :	Volume percentage of air in an abrasive structure. Porosity.
$V_{pw}$ :	Effective porosity ratio at wheel surface. Pore volume/wheel volume at surface.
$V_s$ :	Total wear volume of wheel or tool material removed.
$V_w$ :	Total volume of workpiece material removed.
$W_d$ :	Diamond size (carats).
$X(\theta)$ :	Infeed movement at position $\theta$ .
$\alpha$ :	Feed angle in angle-approach grinding.
$\alpha$ :	Thermal diffusivity.
$\alpha$ :	Angle between wheel and workrest contact.
$\beta$ :	Included tangents angle in centerless grinding.
$\beta$ :	Thermal property for transient heat conduction.
$\beta$ :	Wheel angle in angled-wheel grinding.
$\beta_{cw}$ :	Elevation angle of workpiece from control wheel center in centerless grinding.
$\beta_s$ :	Elevation angle of workpiece from grinding wheel center in centerless grinding.
$\gamma$ :	Top workrest angle in centerless grinding.
$\gamma$ :	Dullness ratio of abrasive grain.
$\gamma$ :	Sharpness ratio of dressing tool.
$\delta$ :	Deflection.
$\chi$ :	Phase angle between waviness and deflection.
$\lambda$ :	Machine system stiffness.
$\lambda_o$ :	Machine system static stiffness.
$\theta_{mp}$ :	Melting temperature of chips.
$\phi$ :	Phase angle between force and deflection.
$\phi$ :	Angle between plane of motion and inclined plane of heat source.
$\phi_{pores}$ :	Porosity of wheel at surface.
$\mu$ :	Friction coefficient.
$\mu$ :	Grinding force ratio.
$\eta$ :	Dynamic viscosity.
$\eta_p$ :	Dynamic viscosity at elevated pressure.
$\nu$ :	Kinematic viscosity.
$\nu$ :	Poisson ratio.
$\rho$ :	Density.
$\sigma_{hs}$ :	Hydrostatic stress.
$\sigma_n$ :	Direct stress.
$\tau$ :	Shear stress or time constant.
$\omega$ :	Frequency in radians per second.
$\omega_o$ :	Undamped natural frequency.
$\Delta, \delta R$ :	Roundness error.
$\Lambda$ :	Stock removal rate parameter. Removal rate divided by normal force.
$\Phi$ :	Control wheel tilt angle.
$\Phi_d$ :	Dressing angle.
$\Omega$ :	Work rotational frequency in radians per second.

## A

<b>Abrasion:</b>	Wearing or machining by rubbing, scratching, or friction.
<b>Abrasion, 2-body:</b>	Wear of one body abraded by another.
<b>Abrasion, 3-body:</b>	Wear of one body acted on by another with free abrasive in the contact.
<b>Abrasive:</b>	Tendency to cause wear. A hard and sharp material that wears a softer material.
<b>Abrasive, conventional:</b>	Hard abrasive mineral grit such as alumina and silicon carbide.
<b>Abrasive composite:</b>	Material consisting of abrasive grains and bond structure.
<b>Abrasive grains:</b>	Hard particles in an abrasive tool that provide the cutting edges.
<b>Abrasive machining:</b>	Machining by an abrasive process such as grinding, honing, lapping, or polishing.
<b>Abrasive medium:</b>	Suspension of abrasive grit in a liquid as used in lapping and polishing.
<b>Abrasive tool:</b>	Tool used for abrasive grinding, lapping, honing, or polishing.
<b>Absorption:</b>	Assimilation of matter from surround into a surface and into the body of the material.
<b>Abusive grinding:</b>	Grinding under conditions which produce severe damage, cracks, or burn.
<b>AC additive:</b>	Anti-corrosion additive.
<b>Accuracy:</b>	Difference between intended value and achieved value.
<b>Acoustic emission:</b>	Process noise produced due to mechanical and metallurgical interactions.
<b>Active cutting depth:</b>	Depth of abrasive surface that actively engages the workpiece surface.
<b>Active layer:</b>	The layer of the abrasive tool that contains the abrasive.
<b>Active surface:</b>	The surface of the active layer that makes abrasive contact.
<b>Additivation:</b>	The adding of additives to a lubricant or process fluid.
<b>Additive:</b>	Substances added in small quantities to modify properties of a lubricant or process fluid.
<b>Adhesion:</b>	Sticking together of two surfaces.
<b>Adhesive loading:</b>	Work-material adhering to tips of abrasive grains of active layer.
<b>Adiabatic:</b>	Process takes place without heat loss or gain within an immediate volume.
<b>Adsorption:</b>	Assimilation of material into close physical-chemical contact with a surface.
<b>Aerostatic bearing:</b>	See air bearing.
<b>AE sensor:</b>	Acoustic emission sensor used to detect wheel contact.
<b>Affinity:</b>	Measure of possibility of chemical reaction between two materials.
<b>AFM:</b>	Atomic force microscopy.
<b>Agglomeration:</b>	Tendency of particles to group together in clumps within a mass.
<b>Air barrier:</b>	Boundary layer of air around a high-speed wheel tending to deflect grinding fluid.
<b>Air bearing:</b>	Aerodynamic or pressure-controlled gas bearing. (See also hydrostatic bearing.)
<b>Algorithm:</b>	Series of statements constituting a calculation routine.
<b>Aloxide, Alox:</b>	Terms sometimes used for aluminum oxide abrasive.
<b>Alumina, Al<sub>2</sub>O<sub>3</sub>:</b>	Aluminium oxide abrasive.

<b>Ambient:</b>	Conditions in the atmosphere surrounding the process.
<b>Amorphous layer:</b>	A thin layer lacking organized structure due to abrasive deformation.
<b>Analytical:</b>	Based on mathematical or logical consideration.
<b>Angle grinding:</b>	The axis of the wheel or the feed motion is angled to the workpiece axis.
<b>Anisotropic:</b>	Material having properties dependent on direction of measurement.
<b>Annulus:</b>	Space or shape between two concentric diameters.
<b>Antifog additive:</b>	Encourages aerosol particles to combine as droplets.
<b>AO additive:</b>	Antioxidation additive used to increase service life of a process fluid.
<b>Apparent contact area:</b>	Total area of contact including spaces between contacts.
<b>Apparent contact pressure:</b>	Normal force divided by apparent contact area.
<b>AR additive:</b>	Antirust additive.
<b>Archard constant:</b>	Coefficient used in Archard-Preston law for wear rate.
<b>Archard law:</b>	Relationship between wear, normal force, hardness, and sliding distance.
<b>Aromatic oils:</b>	Cycloaromatic and mixed structure nonsaturated hydrocarbons.
<b>Arrhenius law:</b>	Relationship for rate of chemical action based on temperature and time.
<b>Asperity:</b>	Sharp edge.
<b>Atmosphere:</b>	Air surrounding a process.
<b>Atp:</b>	Standard atmospheric temperature and pressure.
<b>Austenite:</b>	Gamma phase of low-carbon iron.
<b>Auxiliary processes:</b>	Processes additional to the main abrasive process. For example, fluid delivery, dressing.
<b>AW additive:</b>	Antiwear additive.
<b>Axial force:</b>	Component of force axial to the grinding wheel surface.

## B

<b>Background temperature:</b>	Mean temperature at a point in a region of many flash contacts.
<b>Backlash:</b>	Lost movement on reversal of motion due to clearance in a feed-drive.
<b>Bactericide:</b>	Additive that kills bacteria.
<b>Balancing:</b>	Adding or removing weight to improve wheel balance.
<b>Ballscrew:</b>	Leadscrew with recirculating rolling ball elements.
<b>Band heat source:</b>	Wide heat source having finite length.
<b>Barite, barite:</b>	Barium sulphate, sulphide mineral used for polishing.
<b>Barkhausen Noise:</b>	Electromagnetic technique for detecting subsurface structural changes.
<b>Bauxite:</b>	Impure ore of aluminum and alumina.
<b>Bcc:</b>	Body-centered cubic lattice structure.
<b>Bearing area curve:</b>	Area of solid phase increasing with depth into surface expressed as a fraction.
<b>Bearing steel:</b>	Group of steels used for manufacture of rolling bearing elements.
<b>Bed:</b>	Machine base.



<b>Bell-mouthing:</b>	Internal bore where the diameter at the end is larger than the middle.
<b>Bessel functions:</b>	Mathematical functions used to solve moving heat source problems.
<b>Beta (<math>\beta</math>):</b>	Thermal property for transient heat conduction in a material.
<b>Binder:</b>	Medium for suspension of abrasive particles.
<b>Biocide:</b>	Additive to kill bacteria and improve life of an oil.
<b>Black box:</b>	Unknown system characterized by measuring inputs and outputs.
<b>Blunt cutting edge:</b>	Cutting edge worn to a flat.
<b>Boiling temperature:</b>	Temperature at which grinding fluid rapidly vaporizes producing bubbles.
<b>Bond material:</b>	Material that bonds abrasive grains in a tool.
<b>Bond post:</b>	Bond material joining one grain to another.
<b>Bore grinding:</b>	Grinding an internal cylindrical surface.
<b>Boundary layer:</b>	Region close to a surface. For example, as in fluid.
<b>Boundary lubrication:</b>	Sliding contact with molecular layer of lubricant.
<b>Brake-dresser:</b>	A dressing tool driven by the wheel; speed is controlled by a brake.
<b>Brinell hardness:</b>	Measure of hardness using a standard ball indenter.
<b>Brinelling:</b>	Indentation due to compressive action.
<b>Brittle:</b>	Tendency to fail by cracking fracture.
<b>Brittleness index:</b>	Measure of brittleness based on fracture toughness and Vickers hardness.
<b>BUE:</b>	Built-up edge. Material piled up at leading edge of tool while cutting.
<b>Bulk temperature:</b>	Mean temperature of the whole workpiece.
<b>Burn:</b>	Action of oxidation or material damage due to high machining temperature.
<b>Burnishing:</b>	Smoothing by action of friction.
<b>Burnout, fluid:</b>	The complete drying out of grinding fluid in the contact zone at high temperature.
<b>Burr:</b>	Lip of deformed material extending from edge of cut surface. De-burr is removal of burr.
<b>Bursting speed:</b>	Speed at which a wheel fails due to hoop stresses.

## C

<b>Cam grinder:</b>	Machine for grinding engine camshafts.
<b>Capillary tube:</b>	A tube of large length-to-diameter ratio.
<b>Carat:</b>	Measure of diamond grain size.
<b>Carborundum:</b>	Early name for silicon carbide abrasive.
<b>Carcinogenic:</b>	Tending to lead to cancer in humans.
<b>Cation:</b>	Positively charged ion.
<b>CBN, cBN:</b>	Cubic boron nitride. An extra-hard allotropic form of boron nitride.
<b>CD:</b>	Continuous dressing.
<b>CDCF:</b>	Continuous dress creep feed grinding.
<b>Cementite:</b>	Iron carbide.

<b>Center:</b>	A conical pin that locates in the center hole to hold a cylindrical workpiece.
<b>Center grinding:</b>	Grinding between centers.
<b>Centerless grinding:</b>	Process for grinding without center holes for workpiece support.
<b>Ceramic:</b>	Materials made by firing clays or similar materials. For example, silicon nitride ceramic.
<b>CFD:</b>	Computational fluid dynamics. Type of computer software for fluid flow.
<b>CFRP:</b>	Carbon fiber reinforced plastic.
<b>C-factor:</b>	Temperature factor for heat conduction from a moving source into a workpiece.
<b>Chalk:</b>	Fine white calcium carbonate powder used for polishing.
<b>Characteristic equation:</b>	Denominator of a transfer function set to zero.
<b>Chatter vibration:</b>	Regenerative vibration arising from an unstable machining process.
<b>Chemi-sorption:</b>	Assimilation of a material on a surface by chemical action.
<b>Chip, cross-sectional area:</b>	Cross-sectional area of the uncut chip.
<b>Chip, uncut chip:</b>	Undeformed workpiece material in the path of an oncoming abrasive grain.
<b>Chip aspect ratio:</b>	Ratio of length/width of uncut chip.
<b>Chip length:</b>	Length of the uncut chip.
<b>Chip thickness:</b>	Maximum or mean thickness of uncut chip.
<b>Chip volume, mean:</b>	Volume of material removed divided by number of chips.
<b>Chip width:</b>	Width of the uncut chip.
<b>Chips:</b>	Pieces of material or swarf cut from workpiece.
<b>Chuck:</b>	A type of workholding device for cylindrical parts.
<b>CIRP:</b>	International College/Institution of Production Engineering Research.
<b>Cleaning-up:</b>	Removing a layer of abrasive to remove loading and restore unworn surface.
<b>Climb grinding:</b>	The grinding motion and the workpiece motion are in same direction.
<b>CMC:</b>	Ceramic matrix composite.
<b>CMM<sup>1</sup>:</b>	Chemomechanical machining.
<b>CMM<sup>2</sup>:</b>	Coordinate measuring machine.
<b>CMP:</b>	Chemomechanical polishing.
<b>CNC:</b>	Computer numerical control of a machining system.
<b>Coarse dressing:</b>	Dressing with large dressing depth and large dressing feedrate.
<b>Coated abrasive:</b>	Abrasive applied as a coating to a belt.
<b>Compatibility:</b>	Suitability of two materials to form rubbing couple without severe damage.
<b>Compliance:</b>	Inverse of stiffness. Movement per unit force.
<b>Composite:</b>	Body formed from mixture of two or more materials.
<b>Concentration:</b>	Proportion of a material in a mixture or in a solution. Measure of abrasive in a wheel.
<b>Conditioning:</b>	Process to prepare an abrasive surface for machining. See also dressing.
<b>Conduction:</b>	Transfer of energy through a body. For example, heat conduction.
<b>Conformal contact:</b>	Convex surface contacting within a concave surface.

<b>Constant force process:</b>	Abrasive process controlled by application of constant force.
<b>Contact:</b>	Touching between one body and another.
<b>Contact, grain:</b>	Contact between grain and workpiece.
<b>Contact, wheel:</b>	Contact between wheel and workpiece.
<b>Contact angle:</b>	Half-angle subtended by contact arc at the wheel center.
<b>Contact area:</b>	Apparent area of contact between abrasive tool and workpiece.
<b>Contact area, real:</b>	Sum of grain contact areas with workpiece.
<b>Contact length:</b>	Length of tool and workpiece contact parallel to grinding direction.
<b>Contact length, force:</b>	Contact length due to effect of force and deformation.
<b>Contact length, geometric:</b>	Contact length predicted ignoring roughness, speeds, and deformation.
<b>Contact length, kinematic:</b>	Geometric contact length modified for speed of wheel and workpiece.
<b>Contact length, real:</b>	Contact length including all influences. Also, effective contact length.
<b>Contact length ratio:</b>	Ratio of real contact length/geometric contact length.
<b>Contact mechanics:</b>	Analysis of contact, particular due to elastic/plastic deflections.
<b>Contact pressure:</b>	Normal force divided by contact area. See real and apparent contact pressure.
<b>Contact radius:</b>	Mean radius of the wear flat on an abrasive grain.
<b>Contact surface:</b>	Surface in (apparent) contact area during abrasive machining.
<b>Continuous dressing:</b>	Process of dressing concurrent with grinding.
<b>Contour grinding:</b>	Profile grinding by generation of the required contour.
<b>Controlled feed process:</b>	Abrasive process controlled by application of feed motion.
<b>Control wheel:</b>	Wheel used to control workpiece motion in centerless grinding.
<b>Control wheelhead:</b>	Powered assembly to carry and rotate control wheel.
<b>Convection:</b>	Process of carrying by physical movement. For example, heat carried by motion of fluid.
<b>Convection coefficient:</b>	Convective heat transfer per unit contact area per degree temperature difference.
<b>Convenient waviness:</b>	Nonround shapes that are not corrected in incorrect centerless grinding.
<b>Conventional:</b>	In accordance with traditional or widest practice.
<b>Conventional speed:</b>	Wheel speeds from 20 m/s to 45 m/s.
<b>Coolant:</b>	Grinding fluid.
<b>Corrosion:</b>	Conversion of work-material surface by chemical or electrochemical action.
<b>Corrosion wear:</b>	Removal of material from a surface by corrosion.
<b>Corundum:</b>	Traditional name for aluminum oxide mineral.
<b>Cost:</b>	Price to be paid.
<b>Couette flow:</b>	Flow induced by proximity to a sliding surface. Entrained flow.
<b>Coulomb friction:</b>	Friction force is proportional to normal force.
<b>Covalent:</b>	Electrons are shared by neighboring atoms.
<b>Crankshaft grinder:</b>	Machine for grinding engine crankshafts.
<b>Creep grinding:</b>	Grinding at very low workspeeds and usually with large depth of cut.
<b>Criterion:</b>	Standard for making a judgment. Basis for making a decision.
<b>Critical:</b>	Point at which an abrupt change takes place. For example, critical temperature.

<b>Critical temperature:</b>	Temperature for a change of physical condition. For example, softening.
<b>Cross-axis dressing:</b>	Rotary dressing tool with axis at 90° to the grinding wheel axis.
<b>Cross section:</b>	View of section of body cut through to reveal internal structure.
<b>Cross-sectional area:</b>	Area of a cross section.
<b>Crushing:</b>	Removing a layer of abrasive by applying pressure with a block of softer material.
<b>Crushing-roll:</b>	Roller or disc used for crush dressing.
<b>Crystal:</b>	Solid of regular atomic structure, such as quartz.
<b>Crystalline:</b>	Having an ordered atomic lattice structure.
<b>Cup dresser:</b>	Cup-shaped rotary dressing tool.
<b>Curvature:</b>	Inverse of radius.
<b>Custom:</b>	Designed to suit a particular customer's requirements.
<b>Cut, cutting:</b>	Process of shearing a material. Abbreviation for depth of cut.
<b>Cutoff grinding:</b>	Cutting through material with a thin wheel to remove a slice or slab.
<b>Cutting edge:</b>	That part of an abrasive particle that engages the workpiece.
<b>Cutting edge density:</b>	Number of cutting edges per unit area. Varies with depth.
<b>Cutting edge depth:</b>	Depth of penetration of the grains into the workpiece.
<b>Cutting edge spacing:</b>	Measure of spacing between cutting edges on an abrasive surface.
<b>Cutting edge width:</b>	Measure of the width of the cutting edge in contact with the workpiece.
<b>Cutting force:</b>	Resultant force in cutting process. Vector sum of component forces.
<b>Cutting speed:</b>	Wheel surface speed.
<b>CVD:</b>	Chemical vapor deposition process used to form diamond layer.
<b>Cycle time:</b>	Mean time for the machining of a part.
<b>Cylindrical grinding:</b>	Grinding a cylindrical surface by rotating a workpiece.
<b>Cylindricity:</b>	Measure of deviations from a cylindrical shape.

## D

<b>D'Alembert force:</b>	The reaction experienced when accelerating a mass.
<b>Damping force:</b>	Reaction force proportional to speed.
<b>DBDS:</b>	Dibenzyl disulphide.
<b>Dead center:</b>	Nonrotating work location pin.
<b>Debris:</b>	Small particles of abrasive and workpiece. For example, swarf.
<b>Deep grinding:</b>	Grinding depths of cut much in excess of 0.1 mm.
<b>Deflection:</b>	Movement due to pressure, force, or temperature.
<b>Delamination:</b>	Plate-shaped particles breaking out of surface.
<b>Density:</b>	Mass per unit volume.
<b>Depth of cut:</b>	Instantaneous normal thickness of layer of material to be removed.
<b>Detergent:</b>	Cleansing agent. Additive to oil for cleansing surfaces.
<b>Diamond tool:</b>	Cutting tool using diamond cutting edges.
<b>Dicing:</b>	Cutting into slices.
<b>Diffusion:</b>	Migration of energy or atoms through a material.
<b>Diffusivity:</b>	Thermal property: Conductivity divided by density and specific heat.
<b>DIP-slide:</b>	Used for measurement of bacterial concentration.

<b>Direct stresses:</b>	Tensile or compressive stresses.
<b>Disc dresser:</b>	Disc-shaped dressing tool, usually rotary.
<b>Disc or disk grinding:</b>	Grinding across the face of a disc-shaped wheel.
<b>Dislocation:</b>	Vacancy in a structure. For example, within structure of atoms.
<b>Dispersing additive:</b>	Additive to keep solid particles in suspension in the fluid.
<b>Disturbance:</b>	Change to input value which causes system output to change.
<b>DN value:</b>	Diameter times speed in revolutions per minute.
<b>d.o.c.:</b>	Depth of cut.
<b>Dog drive:</b>	An eccentric pin used to drive a rotating cylindrical workpiece.
<b>Double-side grinding:</b>	Process for simultaneously grinding two sides of a workpiece. Duplex grinding.
<b>Down grinding or down-cut:</b>	The wheel motion and workpiece motion are in same direction.
<b>Dresser head:</b>	Powered assembly to carry and drive rotary dressing tool.
<b>Dressing:</b>	Process to prepare a wheel surface for machining. See also truing and conditioning.
<b>Dressing, continuous:</b>	Process of dressing at the same time as grinding.
<b>Dressing, roll:</b>	Friction or power-driven roll-shaped dressing tool.
<b>Dressing depth:</b>	Depth of cut in dressing operation.
<b>Dressing feedrate:</b>	Traverse/feedrate of dressing tool in dressing operation.
<b>Dressing height:</b>	Offset height of dressing tool relative to grinding wheel axis.
<b>Dressing increment:</b>	Dressing depth.
<b>Dressing lead:</b>	Traverse/feed distance of dressing tool per wheel revolution.
<b>Dressing plate:</b>	Plate dressing tool with diamond grit in the tool cutting surface.
<b>Dressing sharpness ratio:</b>	Dressing depth/dressing width of wedge- or cone-shaped tool.
<b>Dressing speed:</b>	Peripheral speed of a dressing roll.
<b>Dressing stick:</b>	A stick-shaped abrasive tool used to dress a wheel.
<b>Dressing tool:</b>	Tool used for dressing. For example, diamond, fliese, or rotary dressing tool.
<b>Dressing tool-life:</b>	Tool-life of the dressing tool.
<b>Dry machining:</b>	Machining without use of a process fluid.
<b>Ductile:</b>	Tendency to deform by shear without cracking fracture.
<b>Dull:</b>	Blunt. Opposite of sharp.
<b>Dynamic balancing:</b>	Adding or removing weight in two planes to improve couple balance.
<b>Dynamic stiffness:</b>	Usually, stiffness at a particular frequency or less usually, at resonance.
<b>Dynamics:</b>	Analysis of motions including accelerations due to forces.

## E

<b>E:</b>	Young Modulus.
<b>Eccentricity:</b>	Displacement of a center of rotation relative to another.
<b>ECG:</b>	Electrochemical grinding.
<b>ECM:</b>	Electrochemical machining.
<b>EDM:</b>	Electrical discharge machining.
<b>Effective porosity ratio:</b>	Pore volume in active layer divided by total layer volume.
<b>EHL:</b>	Elastohydrodynamic lubrication.
<b>Eigenfrequency:</b>	A particular frequency at which a machine resonates.
<b>Elastic deformation:</b>	Recoverable linear deformation under load.
<b>Elastic modulus:</b>	Material property. Rate of increase of tensile stress with strain in tensile test.

<b>Electrolysis:</b>	Material transfer from an electrode due to electric current and an ionized electrolyte.
<b>Electrolyte:</b>	Electrically conducting liquid used in electrolysis.
<b>Electroplated abrasive:</b>	Abrasive grains attached to tool by electroplated metal.
<b>Element:</b>	A part of a system.
<b>ELID:</b>	Electrolytic In-Process Dressing. Process for metal-bonded wheels.
<b>Emery:</b>	Black abrasive based on corundum with magnetite or hematite.
<b>Empirical:</b>	Deriving from a limited range of measurements. Not based on physics.
<b>Emulsion:</b>	Grinding fluid consisting of a well-dispersed suspension of oil in water.
<b>Emulsion stabilizer:</b>	Surfactant added to resist separating out of the dispersed phase.
<b>Encoder:</b>	Position measuring device based on reading pulses from a rotary or linear scale.
<b>Energy:</b>	Capacity to do work. Measure of work expended.
<b>Energy dissipation:</b>	Transformation of work energy into heat.
<b>Energy partition:</b>	Analysis of energy dissipation to particular heat sinks.
<b>Entrained flow:</b>	Fluid flow induced by parallel sliding of surface. Couette flow.
<b>Environment:</b>	Conditions in surround. For example, atmosphere, noise, temperature.
<b>E.P.:</b>	Extreme pressure conditions as in extreme pressure lubrication.
<b>EP additive:</b>	Extreme pressure additive for process fluid.
<b>EP Wheel:</b>	Electroplated wheel.
<b>EPHL:</b>	Elastoplasto hydrodynamic lubrication.
<b>Equivalent chip thickness:</b>	Thickness of the layer of chips emerging from grinding action.
<b>Equivalent diameter:</b>	Grinding wheel diameter modified to allow for workpiece diameter.
<b>Erosion:</b>	Wear by series of small impacts from gas, liquid, or solid particles.
<b>Error:</b>	Difference between measured value and ideal value. For example, size error.
<b>Error function:</b>	An integral function used in heat transfer calculations.
<b>Esters:</b>	Compounds produced by acid-alcohol reactions with elimination of water.
<b>Exoemission:</b>	Radiation of photons or electrons.
<b>External grinding:</b>	Grinding an external surface particularly for cylindrical grinding.
<b>Extreme pressure (EP):</b>	Extreme pressures as in extreme pressure lubrication.

## F

<b>Face grinding:</b>	Grinding a flat surface using the side face of a grinding wheel.
<b>Fatigue life:</b>	Expected life under a cyclic loading condition.
<b>FCC:</b>	Face-centered cubic lattice structure.
<b>Feed:</b>	An increment of grinding wheel position relative to machined surface, either tangential or normal.
<b>Feed cycle:</b>	A series of feed movements and retractions required to complete a grinding cycle.
<b>Feed per cutting edge:</b>	Distance moved by workpiece in interval between succeeding cutting edges.

<b>Feedrate:</b>	Speed of grinding wheel movement normal or tangential to machined surface.
<b>FEM:</b>	Finite element modeling
<b>Ferrite:</b>	Ductile alpha phase of low-carbon iron.
<b>Ferrous material:</b>	Material containing mainly iron.
<b>Fine dressing:</b>	Dressing with small dressing depth and small dressing feedrate.
<b>Finish surface:</b>	Workpiece surface after grinding.
<b>Firing temperature:</b>	Temperature of vitrification for a vitrified wheel.
<b>Fixture:</b>	Fixed (holding) device.
<b>Flash point:</b>	Lowest temperature at which vapor above a liquid may be ignited in air.
<b>Flash temperature:</b>	Peak temperature at an individual cutting edge/grain.
<b>Flatness:</b>	Measure of deviations from a flat plane.
<b>Fliese:</b>	Diamond-coated wedge-shape tool used for dressing.
<b>Flood nozzle:</b>	Nozzle delivering large volume of fluid at low velocity.
<b>Flow utilization:</b>	Useful flow divided by total flow.
<b>Fluid:</b>	Liquid or gas that can flow.
<b>Flushing:</b>	Displacing swarf by the action of a fluid jet.
<b>Flux<sup>1</sup>:</b>	Flow.
<b>Flux<sup>2</sup>, heat:</b>	Rate of heat flow. For example, heat per unit area per second.
<b>Flux distribution:</b>	Distribution of flux in contact zone. For example, triangular distribution.
<b>FM additive:</b>	Friction modifier additive for process fluids.
<b>Foam depressant:</b>	Additive to promote bubble coalescence.
<b>Fog:</b>	Mist.
<b>Force loop:</b>	The interacting machine elements and workpiece that resist the grinding force.
<b>Forced vibration:</b>	Vibration of constant amplitude due to application of a harmonic force.
<b>Form or profile:</b>	Shape of a section that is not a straight line. Shape that is not a flat surface.
<b>Form dressing:</b>	Dressing a form profile on a wheel with a form tool or by form generation.
<b>Form grinding:</b>	Grinding a form profile with a form tool or by form generation. See generation.
<b>Foundation:</b>	Floor or structure within floor on which a machine is mounted.
<b>Fracture toughness:</b>	Measure of resistance to fracture under impact loading.
<b>Free abrasive:</b>	Loose abrasive grains used in free abrasive processes.
<b>Free radical:</b>	Reactive atom or molecule containing an unpaired electron.
<b>Free surface:</b>	Surface open to the environment.
<b>Friable:</b>	Tending to fracture under compression.
<b>Friction:</b>	Resistance to slip between two sliding surfaces.
<b>Friction coefficient:</b>	Ratio of tangential force to normal force between two sliding bodies.
<b>Friction couple:</b>	The pair of interacting body materials in abrasive contact.
<b>Friction pair:</b>	Friction couple.
<b>Friction polymer film:</b>	Polymer film on work surface formed by friction process.
<b>Friction power:</b>	Power required to overcome frictional drag.
<b>Friction ratio:</b>	Ratio of interface shear stress/shear flow stress of the softer bulk material.

**G**

<b>Garnet:</b>	Crystalline silicate abrasive.
<b>Gauging:</b>	Use of sensors as for in-process diameter measurement.
<b>Gaussian distribution:</b>	Normal distribution.
<b>Gear grinding:</b>	Grinding a gear surface.
<b>Generation:</b>	Producing a shape by compound motions.
<b>Geometrics:</b>	Analysis of points, lengths, lines, curves, and shapes.
<b>Gib:</b>	Tapered strip used to adjust clearance in a slideway assembly.
<b>Glassy bond:</b>	Noncrystalline vitreous bond.
<b>Glazing:</b>	Condition of large wear flats on the abrasive grains.
<b>Gleichdicke shape:</b>	Equal diameter shapes that deviate from round.
<b>GMC:</b>	Glass matrix composite.
<b>Grade, grade letter:</b>	System used to classify hardness of abrasive layer.
<b>Grain, grit:</b>	Abrasive particle.
<b>Grain boundary:</b>	Boundary of grains within a granular structure such as soft steels.
<b>Grain contact:</b>	Touching between a grain and the workpiece.
<b>Grain contact time<sup>1</sup>:</b>	Time a grain is in contact with workpiece.
<b>Grain contact time<sup>2</sup>:</b>	Time a point on workpiece is in contact with a grain.
<b>Grain depth:</b>	Depth of penetration of a grain into the workpiece.
<b>Grain force:</b>	Resultant force on an abrasive grain.
<b>Grain penetration:</b>	Depth of penetration of a grain into the workpiece.
<b>Grain protrusion:</b>	Measure of height of grain tips above surrounding bond.
<b>Grain size:</b>	Measure of the sizes of abrasive grains.
<b>Grating:</b>	Series of parallel wires or lines.
<b>G-ratio:</b>	Volume of material removed divided by volume of grinding wheel removed.
<b>Grindability:</b>	Qualitative or other measure for a material of ease of grinding.
<b>Grinder:</b>	Shop-floor term for grinding machine or operative.
<b>Grind-hardening:</b>	Process proposed for hardening steels from soft state by grinding at high temperatures.
<b>Grinding:</b>	Removal of material from a surface by abrading with a hard rough surface.
<b>Grinding fluid:</b>	Fluid used to lubricate, cool, and flush in abrasive processes. See also process fluid.
<b>Grinding force:</b>	Resultant force in grinding. Vector sum of component forces.
<b>Grinding force ratio:</b>	Ratio of tangential force to normal force.
<b>Grinding power:</b>	Product of tangential force and tangential grinding wheel speed.
<b>Grinding ratio:</b>	Workpiece volume removed by grinding divided by wheel wear volume.
<b>Grinding time:</b>	Part of time spent in grinding.
<b>Grinding wheel:</b>	Cylindrical abrasive tool rotated at high speed in machining.
<b>Grit:</b>	Small hard particle of abrasive. Also Grain.

**H**

<b>Hardness:</b>	Measure of resistance to penetration.
<b>Hardness, hot:</b>	Hardness of a material at elevated temperature.
<b>Harmonic:</b>	Integer multiple of basic frequency.



<b>Headstock:</b>	Machine structure that carries a spindle drive and/or center usually for the work-drive.
<b>Heat:</b>	Thermal form of energy.
<b>Heat conduction:</b>	Transfer of heat through a body due to temperature gradient.
<b>Heat sink:</b>	Where heat goes: heat flows from a hot source to a cool sink.
<b>HEDG:</b>	High-efficiency deep grinding.
<b>Hertz:</b>	Unit of frequency: cycles per second.
<b>Hertzian:</b>	Smooth elastic contact between a sphere and a plane or two spheres.
<b>High speed:</b>	Wheel speeds in excess of 45 m/s.
<b>HLB:</b>	Hydrophile lipophile balance.
<b>Homogeneous, homogenous:</b>	Constant material composition throughout.
<b>Honing:</b>	A cylindrical process using abrasive stones.
<b>Honing stones:</b>	Abrasive blocks inserted in honing tools.
<b>Horizontal grinder:</b>	Grinding wheel axis is horizontal.
<b>Horsepower:</b>	Old unit of power. 746 watts.
<b>HSS:</b>	High-speed steels used for cutting tools.
<b>h-value:</b>	Heat convection value for oil under a standardized condition.
<b>Hv, HV:</b>	Vickers hardness measure.
<b>Hybrid:</b>	Combining two materials, for example, ceramic/steel or modes. For example, hydrostatic and hydrodynamic.
<b>Hydrodynamic<sup>1</sup>:</b>	Usually refers to action of fluid due to surface movements.
<b>Hydrodynamic<sup>2</sup>:</b>	Strict meaning is action due to fluid motion.
<b>Hydrogenation:</b>	Hydrogen reaction used typically to saturate and stabilize a fatty oil.
<b>Hydrostatic bearing:</b>	Load support arranged by pressure-controlled liquid bearing.
<b>Hydrostatic stress:</b>	Contribution to stress system for equal direct stresses, usually compressive.

## I

<b>ID:</b>	Internal diameter.
<b>Image processing:</b>	Techniques for extracting information from surface data.
<b>Impregnated truer:</b>	Dressing tool with small diamonds held in a metal matrix.
<b>Inclined heat source:</b>	Heat source moves in a plane inclined to the workpiece surface.
<b>Infeed:</b>	Feed of the grinding wheel normal to the ground surface.
<b>Internal grinding:</b>	Grinding an internal surface particularly bore grinding.
<b>Interrupted cut:</b>	The wheel repeatedly engages and disengages contact with the workpiece.
<b>Ion:</b>	Electrically charged atom or group of atoms.
<b>Ionic:</b>	Having electrically charged atoms or groups of atoms.
<b>ISO:</b>	International Standards Organisation.
<b>Isotropic:</b>	Material with properties constant in all directions.

## J

<b>Jet:</b>	High velocity fluid stream. Orifice for high velocity fluid.
<b>Jewellers rouge:</b>	Red iron oxide powder used for polishing.

**Journal:** Rotational shaft as in a journal bearing.  
**Junction growth:** Growth of an area of sticking contact.

## K

**$K_{Ic}$ :** Measure of fracture toughness.  
**Kaolin:** Fine white clay made into a paste for polishing.  
**Kinematic similarity:** Uncut chip dimensions remain unchanged.  
**Kinematics:** Analysis of motions, ignoring forces.  
**Kinetics:** Effects or study of rates of action.  
**Kramer Effect:** Exoemission under abrasive conditions.

## L

**Laminar:** Fluid tending to move along steady parallel paths. Nonturbulent.  
**Lap:** An abrasive tool used for lapping.  
**Lapping:** Process of improving form using a lap and abrasive paste/fluid.  
**Lattice:** Structure of directional bonding of atoms.  
**LDA:** Laser-Doppler Anemometry.  
**Leadscrew:** Nut and screw device for transforming rotary motion into linear motion.  
**Limit:** Maximum or minimum permissible value.  
**Limit chart:** Chart showing maximum achievable values of process control variables.  
**Linear motor:** Usual meaning: An electric motor that produces linear motion directly.  
**Liquid:** Intermediate phase on cooling between gas and solid. For example, water or oil.  
**Live center:** Rotating work location center pin.  
**Log, diamond:** Synthetic diamond coated on a prismatic log shape.  
**Longitudinal grinding:** Grinding with a wheel traversing the workpiece length.  
**Losses:** Difference between input and useful output. For example, power losses.  
**Lower bound:** Estimate known to be lower than real value.  
**Lubricant:** Medium such as oil or graphite, which eases sliding between surfaces.  
**Lubricity:** Ability of a fluid to reduce friction other than by its viscosity.

## M

**Machinability:** Qualitative or other measure for a material of machining ease.  
**Machine tool:** A powered machine or system used in part production.  
**Machining:** Production of shape by removal of material from a part.  
**Machining center:** A multitool-head machine, e.g., milling, drilling turning, grinding.  
**Machining conditions:** Process conditions. Values of parameters employed for machining.

<b>Machining-elasticity parameter:</b>	Ratio of real depth of cut to set depth of cut.
<b>Magma-plasma:</b>	Theory of material in energetic state due to intense abrasive deformation.
<b>Magnetic abrasive machining:</b>	Process where magnetism applies force on the abrasive.
<b>Malleable:</b>	Capable of large plastic deformations by pressing and hammering.
<b>Martensite:</b>	Hard brittle phase of carbon dissolved in iron produced by quenching. White phase.
<b>Material removal:</b>	Volume of material removed from workpiece.
<b>Mean:</b>	Arithmetic average of a series of readings.
<b>Mesh number:</b>	Measure of grit size based on number of wires in a sieve. High mesh number yields small grit size.
<b>Metal-bond wheels:</b>	Superabrasive wheels bonded with cast iron or other metal compositions.
<b>MIC value:</b>	Minimum inhibitory concentration of fluid.
<b>Micro-hardness:</b>	Hardness measured with an extremely small indenter.
<b>Microscopy:</b>	Magnified visualization of a surface using one of several physical principles.
<b>Mineral oil:</b>	Natural hydrocarbon oils.
<b>Misalignment:</b>	Deviation from parallelism between two elements.
<b>Mist:</b>	An aerosol dispersion of particles/fluid in the atmosphere.
<b>Mixed lubrication:</b>	Transition between hydrodynamic lubrication and boundary lubrication.
<b>MMC:</b>	Metal matrix composite.
<b>MNIR:</b>	Maximum normal infeed rate.
<b>Model:</b>	Mathematical, physical, or conceptual representation of a structure or process.
<b>Momentum power:</b>	Rate of kinetic energy.
<b>Monocrystal:</b>	Grains constitute a single crystal.
<b>Morphology:</b>	Shape, form, and structure of a body.
<b>MQL:</b>	Minimum quantity lubrication.

## N

<b>Nano-:</b>	Refers to the nanometer order of magnitude. Less than 0.02 $\mu\text{m}$ .
<b>Nano-additive:</b>	Nano-size powders used as additives.
<b>Nano-grinding:</b>	Grinding with nano-size grain penetration.
<b>Nanometer, nm:</b>	1 meter divided by 10 raised to the power 9.
<b>Nanotechnology:</b>	Technology involving machines and processes at the scale of a few nanometers.
<b>Napthenes:</b>	Cycloparaffinic hydrocarbon oils.
<b>Natural fatty oil:</b>	Animal, vegetable, or fish oil.
<b>ND:</b>	Natural diamond.
<b>Neat oil:</b>	Oil not mixed with water. Immiscible oil.
<b>Nip:</b>	Convergent gap at entry to grinding contact zone that creates coolant wedge.
<b>Nodular iron:</b>	Iron containing spherical graphite particles.
<b>Noise:</b>	Unwanted vibration.
<b>No-load power:</b>	Power with grinding wheel rotating but not grinding.
<b>Normal:</b>	1. Perpendicular. 2. Usual.

<b>Normal distribution:</b>	Continuous random distribution with same mean, median, mode. For example, bell curve.
<b>Normal force:</b>	Component of force perpendicular to grinding wheel surface.
<b>Nozzle:</b>	The end of a pipe or hose shaped to direct grinding fluid.
<b>Nozzle, jet:</b>	Nozzle shaped to intensify exit velocity of the grinding fluid.
<b>Nozzle, shoe:</b>	Fluid delivery nozzle shaped to fit snugly around a wheel.
<b>Nyquist criterion:</b>	A statement of a necessary condition for stability.
<b>Nyquist plot:</b>	A graph of amplitude and phase with frequency for an open-loop transfer function.

## O

<b>OD:</b>	Outside diameter.
<b>OEM:</b>	Original equipment manufacturer.
<b>OOR:</b>	Out-of-roundness. Roundness error.
<b>Operator, operative:</b>	Person who operates a machine.
<b>Orbital grinding:</b>	The grinding wheel orbits in addition to rotating.
<b>Organic<sup>1</sup>:</b>	Having biological origins.
<b>Organic<sup>2</sup>:</b>	Based on or related to carbon compounds.
<b>Oscillating:</b>	Motion to and fro, usually for short distances.
<b>Overlap ratio:</b>	Contact width of dressing tool/feed per revolution of wheel.

## P

<b>Padding:</b>	Solids added to bond mixture to modify the effective hardness of an abrasive layer.
<b>Paraffinic oil:</b>	Linear or ramified saturated hydrocarbons.
<b>Particle:</b>	Small part, fragment, grit, or grain.
<b>Partition ratio:</b>	Energy to a heat sink divided by total heat energy.
<b>Passivation:</b>	Slowing corrosion due to inhibitor or protective layer.
<b>Passivator:</b>	Additive to prevent catalytic reaction.
<b>Paste:</b>	Thick mixture of abrasive particles in liquid or wax.
<b>PCBN, PcBN:</b>	Polycrystalline cubic boron nitride.
<b>PCD:</b>	Polycrystalline diamond.
<b>Pearlite:</b>	Eutectoid phase of carbon in iron.
<b>Pelet number:</b>	Dimensionless speed parameter for moving heat sources.
<b>Peel grinding:</b>	Deep cylindrical traverse grinding with high workspeeds and wheel speeds.
<b>Pendulum grinding:</b>	Shop-floor term for forward and back traverse grinding. Reciprocating grinding.
<b>Peripheral grinding:</b>	Grinding with the periphery of the wheel. See, for instance, face grinding.
<b>Permeability:</b>	Measure of the ability of fluid to diffuse through a material.
<b>pH:</b>	Measure of acidity/alkalinity. Acids have pH less than 7.
<b>pH-meter:</b>	Alkalinity meter.
<b>Physi-sorption:</b>	Layers bonded by Van der Waals weak forces.
<b>Pick-up:</b>	1. Scuffing. 2. A sensor.
<b>Pitch error:</b>	Error in spacing of gear teeth at the pitch circle diameter.

<b>Plain:</b>	Smooth, lacking in features, nonrecessed.
<b>Plane:</b>	A flat section of space.
<b>Plasma:</b>	Hot ionized gas.
<b>Plastic deformation:</b>	Nonrecoverable deformation by ductile shear within a material.
<b>Plateau honing:</b>	Removing the peaks of the machining marks to form plateaux.
<b>Plated wheel:</b>	A grinding wheel having a single layer of abrasive bonded to the core by plating.
<b>Ploughing, plowing:</b>	Grooving a surface without loss of material.
<b>Ploughing energy:</b>	Cutting energy less chip energy and sliding energy.
<b>Plunge dressing:</b>	The dressing tool is fed directly into the grinding wheel.
<b>Plunge grinding:</b>	The grinding wheel is fed directly into the workpiece.
<b>PMC:</b>	Polymer matrix composite.
<b>Pneumatic:</b>	Using air as the power source.
<b>Poiseuille flow:</b>	Flow induced by a pressure gradient.
<b>Poisson distribution:</b>	A discrete distribution. Alternative to binomial distribution.
<b>Polishing:</b>	Use of a conformable pad and an abrasive to smooth a surface.
<b>Polycrystalline:</b>	Many small closely packed crystals form the grains.
<b>Pore:</b>	A small hole or channel in a structure. Space between grains in a wheel.
<b>Pore loading:</b>	Abrasive layer with work-material loaded into pores.
<b>Porosity:</b>	Measure of air or pores in a structure.
<b>Potential energy:</b>	Energy having the potential to do work. For example, pressure or height energy.
<b>Potential function:</b>	Model of variation of potential energy. For example, between atoms.
<b>Preston equation:</b>	Alternative source of Archard equation.
<b>Primary shear zone:</b>	Zone of primary shear between workpiece and chip.
<b>Process:</b>	Action or sequence of actions or operations.
<b>Process conditions:</b>	Specification of speeds, feeds, tools, fluid, and all conditions of the process.
<b>Process fluid:</b>	Liquid or gas used to lubricate, flush, and cool an abrasive process.
<b>Process limits:</b>	The maximum permissible values of operating speeds for a process such as grinding.
<b>Process monitoring:</b>	Continuous measurement of any characteristic such as size or power.
<b>Profile:</b>	See form.
<b>Profile grinding:</b>	Grinding a form on a workpiece with a form tool or by generation.
<b>Profilometry:</b>	Techniques for measuring shape or surface texture.
<b>P-type corrosion:</b>	Corrosion with passivated progression.
<b>Pumice stone:</b>	Porous volcanic abrasive used for scouring and polishing.
<b>Pumping power:</b>	Power required to deliver a flow from a pump.
<b>Punch grinding:</b>	Grinding of punches.

## Q

<b>Quadrature:</b>	At 90 degrees orientation.
<b>Qualification:</b>	Measurement/proof of quality.

<b>Quality:</b>	Term used for attributes such as fitness for purpose, roughness, durability.
<b>Quartz:</b>	Hard crystalline silicon dioxide colorless rock.
<b>Quasi-:</b>	Almost but not exactly the real situation.
<b>Quill:</b>	Internal grinding spindle and wheel mount.
<b>R</b>	
$R_a, R_z, R_t$ :	2-D measures of surface roughness.
<b>Rake angle:</b>	Rake angle is between workpiece normal and leading cutting-tool face.
<b>Range:</b>	Difference between minimum and maximum values. For example, cutting edge depth range.
<b>Rare earth element:</b>	Elements of the lanthanide series.
<b>Real contact pressure:</b>	Normal force divided by real contact area.
<b>Real depth of cut:</b>	Actual depth of cut taking account of wheel wear and deflections.
<b>Recess:</b>	Well or pool within a bearing land to spread fluid pressure.
<b>Reciprocal grinding:</b>	Successive forward and back traverse grinding.
<b>Redress life:</b>	Machining time between dress and redress of a wheel.
<b>Redundant energy:</b>	Energy consumed in nonuseful deformation.
<b>Rehardening:</b>	Heating of hardened surface to transformation followed by quenching.
<b>Rehbinder Effect:</b>	Strength reduction due to adsorption of fluid molecules onto material surface.
<b>Removal rate:</b>	Volume rate of material removal from a workpiece.
<b>Repeatability:</b>	Range for series of repeated measurements. For example, sizes or positions.
<b>Replica, surface:</b>	A molded impression of a surface.
<b>Residual stress:</b>	Stress that remains in a material after load is removed.
<b>Resinoid wheel:</b>	Wheel having abrasive grains in resin-based bond.
<b>Resonance:</b>	Large vibrations experienced at a resonant frequency.
<b>Retro-fit:</b>	Equipment added subsequently after a machine has been supplied.
<b>Reynolds number, Re:</b>	Dimensionless parameter increases with ratio of inertia forces to viscous forces.
<b>Ringling:</b>	Acoustic test for flaws in a wheel from sound of a sharp tap.
<b>RMS, rms:</b>	Square root of the mean of the sum of the squares of the differences from the mean.
<b>Roll grinding:</b>	Grinding of large rolls.
<b>Roll-dresser:</b>	Dressing tool in form of roller or disk.
<b>Rolling:</b>	Motion without sliding, as of roller on plane.
<b>Rolling bearing:</b>	Load support on ball or roller elements.
<b>Roots:</b>	Conditions for a maximum amplitude of a dynamic system.
<b>Roughness:</b>	Measure of microdeviations in height of a surface.
<b>Roughness factor:</b>	Ratio of contact lengths due to normal force for rough and smooth contact.
<b>Rounding:</b>	Process of improving roundness.
<b>Roundness, error:</b>	Measure of deviations from a circle. Out-of-roundness.
<b>Roundway:</b>	Round guideway.
<b>Rubbing:</b>	Sliding of one surface on another with frictional contact.

**Rules of mixture:** Rules for properties of a mixture related to element properties.  
**Runout:** Error of circular motion.

## S

**SAE52100:** A bearing steel specification.  
**Sanding:** Sandpaper smoothing of wood or similar material.  
**Scratch:** A groove made by dragging a sharp hard tool along a surface.  
**Screw grinding:** Grinding a screw surface by rotation and axial feed of a workpiece.  
**Scuffing:** Welded workpiece material on tool pulls material out of the workpiece surface.  
**SD:** Synthetic diamond.  
**Secondary shear zone:** Zone of shear between chip and cutting face of tool.  
**Seeded gel, SG:** A tough alumina abrasive produced from alpha-phase chemically precipitated crystals.  
**Segmented wheel:** Wheel with a number of pieces or segments of abrasive layer attached to a holder.  
**Seizure:** General meaning is the welding together of two rubbing elements.  
**Self-dressing:** Self-sharpening. Grinding process wear that provides new sharp cutting edges.  
**Self-excited vibration:** Vibration that builds up when forced.  
**Self-sharpening:** Tendency of grains to produce sharp edges when worn edges fracture.  
**SEM:** Scanning electron microscopy.  
**Sensor:** Measuring device or transducer used to sense a process variable.  
**Servomotor:** Variable speed motor with feedback control for speed or position.  
**Set depth of cut:** Depth of cut ignoring wheel wear and deflection errors.  
**Setup:** Geometry, speeds, and conditions for grinding.  
**Shallow grinding:** Grinding depths of cut less than 0.1 mm.  
**Sharp cutting edge:** Pointed cutting edge.  
**Sharpness:** Measure of angularity or narrowness of cutting tip.  
**Shear:** Plastic sliding within a material acting like a pack of cards.  
**Shear strain rate:** Rate of plastic sliding/thickness of sheared zone.  
**Shellac abrasive:** Abrasive grains held together in a shellac resin bond.  
**Shoe centerless grinding:** Blocks are used for radial location of the workpiece.  
**Shoe nozzle:** Nozzle that fits around the wheel periphery.  
**SI:** Systeme International d'Unités. International system of units.  
**Siccative, siccativator:** Drying agent.  
**Side grinding:** Grinding with the side of the wheel. Face grinding.  
**Silica, SiO<sub>2</sub>:** Silicon dioxide. Occurs naturally as quartz.  
**Silicon carbide, SiC:** A hard bluish-black abrasive.  
**Simulation:** Step-by-step imitation of a process over a short time period.  
**Single-point dressing:** Dressing with a single-point tool such as a single diamond.  
**Sintering:** Process of forming solid by partial fusing of compacted powder.  
**Size effect:** Tendency for reduced specific energy with larger chip size.  
**Slide, slideway:** Machine element for guiding sliding motion.

<b>Slideway grinder:</b>	Long-bed machine for grinding slideways.
<b>Sliding:</b>	Relative movement of two surfaces in tangential direction.
<b>Sliding energy:</b>	Component of energy proportional to sliding area of grains.
<b>Sliding heat source:</b>	Heat source that moves parallel to the workpiece surface.
<b>Slip line field:</b>	Lines of maximum shear stress in a plastic field.
<b>Slot nozzle:</b>	Nozzle having a large gap width-to-thickness ratio.
<b>Slurry:</b>	Dense suspension of powder in a liquid.
<b>Soap<sup>1</sup>:</b>	Product of hydrated oxides and fatty acids.
<b>Soap<sup>2</sup>:</b>	Metallic salt of a fatty acid.
<b>Sol gel:</b>	An alumina abrasive produced from composite phase chemical precipitation.
<b>Solid lubricant:</b>	Lubricant in the form of a lamellar solid such as graphite.
<b>Solution:</b>	Mixture formed of material dissolved in a liquid or solid.
<b>Spacing length:</b>	Cutting edge spacing in direction of grinding.
<b>Spacing width:</b>	Cutting edge spacing in lateral direction.
<b>Spark-out:</b>	Period of dwell while depth of cut decreases.
<b>SPC:</b>	Statistical process control methods.
<b>Specific:</b>	Particular form of a parameter. For example, Sp. Force = force/unit width.
<b>Specific energy:</b>	Energy per unit volume of material removed.
<b>Specific energy in chips:</b>	Energy per unit volume of material removed carried within chips.
<b>Specific energy in fluid:</b>	Energy per unit volume of material removed carried within fluid.
<b>Specific energy in wheel:</b>	Energy per unit volume of material removed carried within wheel.
<b>Specific energy in workpiece:</b>	Energy per unit volume of material removed carried within workpiece.
<b>Specific force:</b>	Force per unit width of grinding wheel contact with workpiece.
<b>Specific heat capacity:</b>	Specific heat: Heat per degree temperature rise.
<b>Specific power<sup>1</sup>:</b>	Power per unit width of grinding wheel contact with workpiece.
<b>Specific power<sup>2</sup>:</b>	Power per unit area of contact.
<b>Specific power<sup>3</sup>:</b>	Power per unit volume removed.
<b>Specific removal rate:</b>	Removal rate per unit width of contact.
<b>Specific wear rate:</b>	Wear rate per unit width.
<b>Specific wear resistance:</b>	Inverse of specific wear rate.
<b>Speed ratio:</b>	Ratio of surface speed of wheel to surface speed of workpiece.
<b>Speed-stroke grinding:</b>	Grinding with high workspeeds of the order of 1 m/s.
<b>Spike temperature:</b>	Temperature at a grain contact. Also flash temperature.
<b>Spindle power:</b>	Power required to drive the main wheel spindle.
<b>Spinel:</b>	Any of a group of hard glassy minerals.
<b>Spinner:</b>	A workpiece that accelerates and spins out of control in centerless grinding.
<b>Spray:</b>	Application of jet or shower of particles, usually liquid.
<b>SSD:</b>	Single synthetic diamond.
<b>Stability limit:</b>	The condition when a small disturbance neither builds up nor decays.
<b>Stainless steels:</b>	A group of corrosion steels containing a high chromium content.
<b>Static deflection:</b>	Movement due to a steady applied force.
<b>Statics:</b>	Analysis with steadily applied forces. See, for instance, Dynamics.



<b>Stepper motor:</b>	Motor that controls position in small steps.
<b>Stick-dressing, sticking:</b>	Use of a "soft" abrasive stick to open/clean a superabrasive wheel surface.
<b>Sticking friction:</b>	Friction due to tangential shearing of a material.
<b>Stiffness:</b>	Resistance to movement: Rate of force divided by movement.
<b>Stochastic:</b>	Acts randomly according to some statistical distribution.
<b>Stock removal:</b>	Normal, radial, or diametral reduction of workpiece dimension.
<b>Stone:</b>	1. A gem. 2. An abrasive tool.
<b>Stress:</b>	Local ratio of force per unit area. For example, shear stress, tensile stress.
<b>Stribeck curve:</b>	Graph of friction coefficient against Sommerfeld/Hersey number.
<b>Structure number:</b>	Number used to indicate proportions of grit and bond volumes in an abrasive layer.
<b>Stylus measurement:</b>	Profilometry using a stylus contact to sense shape or texture deviations.
<b>Surface finish:</b>	Nonscientific term used to describe surface roughness.
<b>Surface grinding:</b>	Peripheral grinding of a flat surface or a profiled surface. See, for instance, face grinding.
<b>Surface texture:</b>	Measure or nature of surface topography. See roughness.
<b>Superabrasive:</b>	Extra-hard abrasive grit such as diamond or cubic boron nitride.
<b>Superfinishing:</b>	Process for production of very low roughness.
<b>Suspension:</b>	Dispersed particles in a liquid medium.
<b>Swarf:</b>	Material debris and chips machined from workpiece.
<b>Synthetic emulsion:</b>	Emulsion of synthetic oil in water.
<b>Synthetic oil:</b>	Oil produced chemically. For example, silicon oils.
<b>System:</b>	Process that transforms inputs to outputs.

## T

<b>Table:</b>	Machine element on which a workpiece or work fixture is mounted.
<b>Tailstock:</b>	Machine subassembly to support a rotating workpiece at opposite end to headstock.
<b>Talc:</b>	Fine magnesium silicate powder used for polishing.
<b>Tangential force:</b>	Component of force tangential to grinding wheel surface.
<b>TDA:</b>	Thermographic differential analysis.
<b>Temper:</b>	Diffusion process leading to softening and temper colors.
<b>Temper colors:</b>	Colors produced on a surface by oxidation at high temperatures.
<b>Temperature gradient:</b>	Rate of increase or reduction in temperature with increasing distance.
<b>Thermal boundary layer:</b>	A thermally affected layer of fluid near a surface.
<b>Thermal conductivity:</b>	Heat transmitted per degree per unit length of transmission.
<b>Thermal stability (TS):</b>	Temperature above which fluid chemical composition breaks down.
<b>Thermal stress:</b>	Stress in a structure arising due to change of temperature.
<b>Thermocouple:</b>	Temperature measurement device based on junction of dissimilar metals.
<b>Thread grinding:</b>	Screw grinding of screw thread forms.
<b>Threshold grinding force:</b>	Minimum force to achieve chip removal.

<b>Through-feed grinding:</b>	The workpiece is fed between centerless grinding wheel and control wheel.
<b>Tilt:</b>	Deviation from vertical/horizontal plane. For example, control wheelhead tilt.
<b>Tolerance:</b>	Defined as difference between maximum and minimum permissible limits.
<b>Tool:</b>	A cutting part or implement.
<b>Tool life:</b>	Machining time between dress and redress of tool.
<b>Tool steel:</b>	A group of steels used for manufacturing cutting tools.
<b>Topography:</b>	Description of surface shape at macro- or microlevel.
<b>Touch dressing:</b>	Dressing process using 1- to 10- $\mu\text{m}$ micron dressing depth.
<b>Transfer function:</b>	Ratio of output to input for a system usually in Laplace form.
<b>Transitional flow:</b>	The domain between fully laminar and fully turbulent flow.
<b>Traverse:</b>	Linear movement. Fast movement on a slideway.
<b>Traverse grinding:</b>	Grinding with the wheel traversing the workpiece length.
<b>Trial:</b>	Series of grinding operations to evaluate a set of grinding conditions.
<b>Triangular heat flux:</b>	Band heat source: Flux varies linearly from maximum to zero.
<b>Tribo-, tribocontact:</b>	Relating to conditions of abrasive deformation and surface generation in sliding contacts.
<b>Tribocatalytic:</b>	Catalytic effects due to tribocontact conditions.
<b>Tribochemical wear:</b>	Chemical wear accelerated by abrasive action.
<b>Tribochemistry:</b>	Tribological phenomena particularly related to chemical action.
<b>Tribology:</b>	The science of friction, lubrication, and wear of sliding contacts.
<b>Tribomechanical:</b>	Quasitribophysical. Mechanical aspects of tribology.
<b>Tribometer:</b>	Machine to test friction and rate of wear for particular speed, force, and contact condition.
<b>Tribooxidation:</b>	Oxidation mechanism under tribocontact conditions.
<b>Triboplasma:</b>	Material in energetic state due to intensive tribocontact.
<b>Triboreaction:</b>	Reaction under tribomechanical activation.
<b>Tribosimulation:</b>	Testing on a rig replicating the real tribological contact conditions.
<b>Tribosorption:</b>	Assimilation of a material on a surface under tribomechanical action.
<b>Tripoli:</b>	Soft powder of siliceous rock (originally from Tripoli, Libya).
<b>Truing:</b>	Process to produce accurate form required on an abrasive tool.
<b>Turbulent flow:</b>	Moving forward with agitated sideways buffeting motion.
<b>Turret:</b>	Indexable tool-head.

## U

<b>Ultrasonic machining:</b>	Machining by ultrasonic vibration of a tool against a workpiece.
<b>Unbalance:</b>	Eccentric mass on rotating disk causing a harmonic force.
<b>Uncut chip thickness:</b>	A notional thickness of the chips based on grain kinematics.
<b>Uniform heat flux:</b>	Band heat source of constant flux magnitude.
<b>Universal machine:</b>	Machine capable of internal and external grinding.
<b>Up grinding or up-cut:</b>	The wheel motion and workpiece motion are in opposite directions.
<b>UPM:</b>	Ultra-Precision Machining.

**Upper bound:** Estimate known to be higher than the real value.  
**Useful flowrate:** Flowrate of grinding fluid that passes into the contact zone.

## V

**Vertical grinder:** Grinding wheel axis is vertical.  
**Vickers hardness:** Hardness measured using standard diamond shape indenter.  
**Vienna lime:** Powder of calcium and magnesium oxides used for polishing.  
**VI-Improver:** Viscosity index additive used to reduce temperature dependence.  
**VIPER process:** A high-rate process developed by Rolls-Royce (Vitrified Improved Performance).  
**Viscous friction:** Friction force is proportional to sliding speed.  
**Vitreous, vitrified:** Glassy phase produced by heating.  
**Vitrification:** Conversion into a glassy form by heating.  
**Vitrified wheel:** Wheel having abrasive grains held together by vitreous bond.

## W

**Waviness:** Surface shape errors having a pattern of undulation.  
**Way:** Slideway or rolling guideway.  
**Wear:** Loss of material from a body by abrasive rubbing and sliding processes.  
**Wear, attritious:** Slow wear evidenced by a polished surface.  
**Wear, fracture:** Removal of parts of a body by cracking and breakage.  
**Wear, microfracture:** Removal of very small parts of a body by small localized cracks.  
**Wear flat:** Plane worn area on the tip of an abrasive grain formed by rubbing.  
**Wear rate<sup>1</sup>:** Wear volume per unit time.  
**Wear rate<sup>2</sup>:** Wear depth per unit time.  
**Wear ratio:** Inverse of grinding ratio.  
**Wheel:** Disc that rotates on a spindle. Abbreviation for grinding wheel.  
**Wheel flange:** Plate used to clamp wheel on hub.  
**Wheel hub:** Adaptor, arbor used to mount wheel on a spindle.  
**Wheel loading:** Tendency for softened workpiece material to adhere to the wheel surface.  
**Wheel speed; Usual:** tangential surface speed of wheel. Sometimes: rotation speed.  
**Wheelhead:** Powered spindle assembly and headstock to carry and drive grinding wheel.  
**Wheel-regenerative chatter:** Self-excited vibration caused by buildup of waves on the wheel.  
**Wheel-work partition:** Division of energy at workpiece and grain contacts.  
**White layer:** White layer of workpiece at surface due to mechanical or thermal effects.  
**Width of cut:** Width of grinding wheel contact with workpiece.  
**Work material:** Workpiece material.  
**Work partition ratio:** Proportion of heat conducted into workpiece in contact zone.  
**Workblade, workplate, workrest:** Plate to support workpiece in centerless grinding.

<b>Workblade angle:</b>	Angle of top surface of workblade.
<b>Work-hardening:</b>	Tendency for shear stress to increase with plastic shear strain.
<b>Workhead:</b>	Powered spindle assembly and headstock to locate and drive workpiece.
<b>Work-height:</b>	Height of the workpiece axis above the grinding wheel axis in centerless grinding.
<b>Workpiece:</b>	The part to be machined.
<b>Work-regenerative chatter:</b>	Self-excited vibration caused by buildup of waves on the workpiece.
<b>Workrest:</b>	Plate used to support workpiece in centerless grinding. Also Workplate or Workblade.
<b>Workspeed:</b>	Tangential speed of workpiece parallel to wheel speed.
<b>Wurtzite:</b>	A form of crystal structure as in wurtzitic diamond or boron nitride.

## X

<b>XRD:</b>	X-ray diffraction technique used for measuring residual stresses.
-------------	-------------------------------------------------------------------

## Z

<b>ZDTP:</b>	Zinc-dialkyl-dithio-phosphates. AW additive for lubricating and process fluids.
<b>ZTA:</b>	Zirconia-toughened alumina.



# Appendix 2: Notation and Use of SI Units

Quantity	Notation	Unit	Notation
<b>Base units</b>			
Mass	[M]	kilogram	kg
Length	[L]	meter	m
Time	[T]	second	s
Electric current		ampere	A
Thermodynamic temperature	[K]	kelvin	K
Amount of substance		mole	mol

Supplementary Units	Unit	Notation	Equivalence
Celsius temperature	celsius	C	—
Angle	radian	rad	—
Frequency	hertz	Hz	[T] <sup>-1</sup> (or cycles/s)
Force	newton	N	[M][L][T] <sup>-2</sup>
Pressure and stress	pascal	Pa	[M][L] <sup>-1</sup> [T] <sup>-2</sup> (or N/m <sup>2</sup> )
Energy, work, heat	joule	J	[M][L] <sup>2</sup> [T] <sup>-2</sup>
Power	watt	W	[M][L] <sup>2</sup> [T] <sup>-3</sup> (or J/s)
Kinematic viscosity	stoke	St	[L] <sup>2</sup> [T] <sup>-1</sup> (or 10 <sup>-4</sup> m <sup>2</sup> /s)
Dynamic viscosity	poise	P	[M][L] <sup>-1</sup> [T] <sup>-1</sup> (or 1 Pa.s = 10 P)
Atomic distances	ångström	Å	[L] (or 10 <sup>-10</sup> m)
Thermal conductivity	—	—	[M][L][T] <sup>-3</sup> [K] <sup>-1</sup> (or W/mK)

## USE OF UNITS

- Units should be associated with numbers.
- Units should not be associated with symbols.
- Equations should be stated without units since any set of consistent units is equally valid.
- Equations should not contain conversion factors for inconsistent units.

## EXAMPLES OF CORRECT AND INCORRECT PRACTICE

$$F = m.a \quad \dots \quad \text{CORRECT}$$

The above equation is simple and elegant. It works with any set of consistent units such as SI or British Engineering units.

$$F = m.a / 32.2 \quad \dots \quad \text{WRONG}$$

The second equation is incorrect and messy. It does not work with consistent SI or British Engineering units. To make the equation work requires that each symbol must be associated with a particular inconsistent unit. This is poor practice and leads to mistakes.

It is equally important that numbers must be associated with units. 1 lb is not the same as 1 slug. Failure to specify units with numbers can lead to extremely expensive disasters as discovered after a failed Mars mission.

When values are inserted into an equation in order to calculate the value of an unknown, it is important that a consistent set of units is employed. The SI system ensures consistency when using base force, length, mass, and time units.

Some examples of consistent sets used in engineering are listed below. Other engineering quantities can be expressed in terms of these units, thus ensuring consistency. Some examples of equivalence in SI units are given above. Some conversion factors between SI and British units are given below.

System	Force	Length	Mass	Time
SI	N	m	kg	s
British Engineering Units	lbf	ft	slug	s
Alternative British Units	lbf	in.	lbf in. <sup>-1</sup> s <sup>2</sup>	s
British Physical Units	pdl	ft	lb	s

### FACTORS FOR CONVERSION BETWEEN SI UNITS AND BRITISH UNITS (VALUES ROUNDED)

Mass: 1 kg = 2.205 lb = 0.06848 slug = 0.8218 lbf in.<sup>-1</sup>s<sup>2</sup>

Length: 1 m = 3.281 ft = 39.37 in.

Temperature rise: 1 K = 1 C = 1.8 F = 1.8 R

Force: 1 N = 7.233 pdl = 0.2248 lbf

Volume: 1 m<sup>3</sup> = 1,000 liters = 61,020 in.<sup>3</sup> = 35.32 ft<sup>3</sup>

Pressure: 1 bar = 0.1 MPa = 14.5 lbf.in.<sup>-2</sup>. 1 N.m<sup>-2</sup> = 0.000145 lbf.in.<sup>-2</sup>

Density: 1 kg.m<sup>-3</sup> = 0.06243 lb.ft<sup>-3</sup> = 0.001939 slug.ft<sup>-3</sup> = 0.00001347 lbf.in.<sup>-4</sup>.s<sup>2</sup>

Energy: 1 J = 0.7376 ft.lbf = 8.851 in.lbf

Power: 1 W = 0.7376 ft.lbf.s<sup>-1</sup> = 8.851 in.lbf.s<sup>-1</sup>

Thermal conductivity: 1 W.m<sup>-1</sup>.K<sup>-1</sup> = 0.0141 lbf.s<sup>-1</sup>.R<sup>-1</sup>

Heat transfer coefficient: 1 W.m<sup>-2</sup>.K<sup>-1</sup> = 0.003172 lbf.in.<sup>-1</sup>.s<sup>-1</sup>.R<sup>-1</sup>

Kinematic viscosity: 1 m<sup>2</sup>.s<sup>-1</sup> = 10<sup>4</sup> St = 10.76 ft<sup>2</sup>.s<sup>-1</sup> = 1550 in.<sup>2</sup>.s<sup>-1</sup>

Dynamic viscosity: 1 N.s.m<sup>-2</sup> = 10 P = 1,000 cP = 0.000145 lbf.s.in.<sup>-2</sup> = 0.000145 reyns

Gem size: 1 metric carat = 2 × 10<sup>-4</sup> kg

---

# Index

## A

### Abrasives 6, 75–102

- Aluminum oxide 75, 76–80, 97, 356, 424, 425, 444, 455, 506
- Bond 103–127
- Ceramic 80–82
- Coated 86, 345
- Cubic boron nitride 45, 75, 93–98, 104, 108, 115, 206, 366, 370, 384, 385, 419, 423, 424, 425, 434, 439, 454, 456, 463, 506
- Diamond 75, 82–93, 114, 271, 345
- Natural 82, 91
- PCD 87, 115
- Synthetic 82
- Grains, grit. See Grain, Grit Characteristics.
- Silicon carbide 75, 97, 356, 506
- SG 75, 80–82, 366, 385, 444, 455

### Accuracy 484

- Alignment 290, 447, 474, 475, 497, 501
- Axis errors 290
- Bearing ratio 15
- Flatness 389, 398, 403, 405
- Form 106
- Gauging. See Grinding Process Capability and Monitoring.
- Grind pattern 15, 16
- Lead errors 300
- Limits 511
- Lobing (See roundness and waviness) 483
- Peak count 15
- Profile 192
- Radius 419
- Repeatability 9
- Roughness 11–16, 105, 157, 208, 224, 238, 257, 276, 351, 353, 354, 421, 475, 491, 500, 510, 513, 555, 558
- Roundness 185, 419, 453, 459, 466, 467, 476, 481, 499, 500, 510, 516, 522, 543
- Run-out 185, 417, 468, 493
- Size 185, 453, 500, 510
- Straightness 356, 419, 453, 456, 476
- Tolerance 368, 389, 393, 400, 406, 453, 458, 485
- Waviness 516, 528, 529

## C

- Compliance** See system stiffness
- Conditioning** See dressing
- Coolant** See fluids
- Costs** See grinding parameters
- Cycles** See grinding cycles

## D

### Dressing 127–167, 267, 273, 394, 419, 459, 475, 490, 492, 498, 503, 543

- Brake 161, 273
- Conditioning 127, 160, 163, 164, 217, 240, 273, 490
- Continuous 156, 192, 364, 433
- Cooling 129
- Cross-axis 149, 151
- Crushing 122
- Depth 127, 131, 137, 140, 142
- ELID 267, 271, 272, 278, 280
- Feedrate 127, 130, 131, 140, 150, 158, 508
- Force 156
- Form/ Profile 132, 142, 150, 152, 155, 158
- Height 492
- Overlap ratio 127, 130, 140, 508
- Scaif angle 129
- Speed
  - Dressing speed ratio 138, 139, 142, 542
- Time 162
- Tools 127, 274
  - Cup 141, 149, 460
  - Disk 139, 460, 512
  - Impregnated 135, 141, 147, 491
  - Plate 135
  - Roll 140, 150, 159, 160, 460
  - Single-point 128, 132, 460, 491
  - Stick 127, 163, 273, 394, 490
- Tool-life 10, 144
- Touch-dressing 144, 147, 158, 241, 512
- Traverse 127, 137, 491
- Truing 127, 273, 274, 279, 490
- Wear 131

## E

**ELID** See Dressing and Grinding Processes.

## F

### Fluids and coolants 195–217, 372, 469, 503

- Air barrier 204
- Additives 197, 198, 199, 200, 211, 212
- Emulsion 196, 206, 208, 209, 213, 356, 368, 422, 424, 476
- Environment 201
- Esters 197, 212
- Explosions, Fires 203, 362
- Filters 203
- Fluid force 14, 429
- Lubrication 34, 199, 201, 206, 211, 313
- Mineral oil 197, 206, 208, 209, 213, 356, 362, 368, 424, 426, 439



Minimum Quantity Lubrication 201, 202, 205  
 Nozzles 203–206, 210, 243  
   Flood 204, 210, 243  
   Jet 204, 243, 358, 361  
   MQL 205  
   Shoe 204, 243, 428  
   Slot 361  
 Power 428, 429  
 Properties 196, 197, 198, 199  
 Requirements 195  
 Supply 202, 203, 205, 242, 349, 351, 356, 358, 362,  
   366, 397  
 Synthetic 197, 209  
 Unbalance 53  
 Velocity 204, 428  
 Viscosity 197, 212, 361  
**Force** See System force and Grinding force

## G

### Grain, grit characteristics

active grain density 12, 19, 421  
 active surface roughness 144  
 contact time 424  
 flats 19, 112, 187, 423  
 force 12, 189, 349, 353, 354, 421  
 hardness 6, 90, 97, 187, 271  
 protrusion 39, 189, 191, 279  
 size 79, 98–99, 100, 104, 456  
 shape 12, 23, 25, 78, 81–96, 120, 187  
 spacing 25, 82, 156  
 speed 556  
 wear 90, 96, 185–195

### Grindability 207, 257

### Grinding chips 33, 257, 353

Shape parameters  
   aspect ratio 257  
   cross-sectional area 30, 278  
   length 29, 277  
   thickness 29–32, 349  
   volume 277

### Grinding Contact

Contact angle 423  
 Contact length 486  
   Geometric 18, 29, 277, 349, 486  
   Dynamic/Deformed 18, 486  
   Real 18  
 Surface  
   Contact surface 423  
   Finish surface 423  
 Time 424

### Grinding Feed Cycle 460, 461, 488, 500

Finishing 462  
 Plunge 462  
 Roughing 462  
 Spark-out 17, 462, 489, 521  
 Through-feed 489  
 Time 10, 11, 468, 507

### Grinding parameters 9

Costs 247–255, 485, 506  
 Coolant 201, 248

Dressing tool 248  
 Inspection 248  
 Filter 248  
 Labor 248, 507  
 Machine 249, 312, 509  
 Tooling 247  
 Wheel 248, 434, 455, 507  
 Depth of cut 11, 20, 341, 347, 425, 485, 528, 530, 531  
   Real 341, 347, 521  
   Set 341, 521  
 Equivalent chip thickness 12, 487, 504  
 Equivalent diameter 11, 29, 418, 420, 455, 487  
 Feed, feed-rate 344, 346, 485, 489, 504  
 Forces 14, 114, 157, 201, 206, 208, 210, 220, 244,  
   349, 428, 463, 494, 497, 557, 560  
 Force ratio 14  
 G-ratio 17, 18, 174, 211, 257, 345, 366, 455, 487,  
   510, 514  
 Infeed 344, 346, 349  
 Interrupted cut 344, 354  
 Oscillation 459  
 P-ratio 18  
 Power 13, 132, 220, 222, 405, 418, 422, 429, 446, 461,  
   466, 467, 485, 491, 521  
 Productivity 167, 485, 497  
 Redress life 10, 168, 502, 511, 515  
 Removal rate 12, 210, 343, 347, 366, 370, 427, 429, 435,  
   485, 501, 504, 550, 555, 559, 560  
 Specific Grinding Energy 12, 221, 222, 353, 354, 421,  
   424, 427, 486, 505, 506, 510  
   Chips 20  
   Fluid 20  
   Wheel 20  
   Workpiece 20  
   Total 12, 20  
 Speed ratio 30, 343, 349, 418  
 Stock removal parameter 17, 257, 463  
 Tangent angle 482, 518, 527, 533  
 Through-feed angle 489, 492  
 Uncut chip thickness 11, 343, 353, 381, 421  
 Upcut and downcut 343, 349, 351, 363, 364  
 Wheel-speed 343, 426, 428, 435, 445, 458, 505, 541, 542  
 Work-height 482, 483  
 Work-rest angle 482, 483, 493, 527, 533  
 Workspeed 344, 425, 459, 489, 494, 499, 505, 541, 542

### Grinding Processes

Angle-approach 417, 420, 472  
 Bore 453, 472, 473  
 Cam 146, 164, 249, 250, 251, 417, 430, 431  
 Crankshaft 146, 234, 252, 389, 390, 427, 430, 442, 444  
 Center 480  
 Centerless 308, 479–549  
   Plunge 487  
   Through-feed 489  
   Shoe 471, 481, 482  
 Contour 444, 453, 454  
 Cut-off 20  
 Cylindrical 6, 29, 170, 171, 417–453  
 Creep-feed 346, 356, 366, 425  
 Deep 188, 422  
 Double-side 390

Drill-flute 20  
 ELID 278, 280  
 Face 6, 208, 381, 454, 473  
 Fine 251, 401  
 Gear 222, 234, 236  
 HEDG 315, 347, 368, 370  
 High-speed 209, 252, 347, 421, 427, 501  
 Internal 150, 170, 188, 248, 417, 453–479  
 Multitasking 252, 366, 453, 473, 474, 475  
 Orbital 385  
 Peel 430  
 Peripheral 6, 341  
 Plunge 417  
 Profile 234, 248, 417, 425  
 Punch 439  
 Reciprocating 289, 341, 345, 349  
 Roll 418, 447  
 Slideway 291  
 Speed-stroke 353  
 Superfinishing 387, 390  
 Surface 6, 29, 170, 274, 341–417  
 Traverse 171, 178, 417  
 Ultrasonic 549–559  
 Universal 417  
 Vertical 292, 298, 474  
 Viper 364, 365, 374–376, 384, 391

**Grinding process capability and monitoring**  
**217–247, 545**  
 Acoustic emission 223, 224, 230, 241, 242, 460, 466  
 limit chart 419, 501, 504  
 monitoring 223, 448, 545  
 optimization and compensation 217, 233, 462, 463, 464,  
 465, 543  
 sensors 217–247, 303, 419, 436, 465, 469, 545  
 trials 503  
 simulation 519, 523

## H

**Heat** See Thermal characteristics

## M

**Machinability** See Materials and properties

**Machine tool structures and elements**  
**285–341, 469, 498, 505**

Axes 290, 473  
 Base, bed 285  
 Bearings  
 air, aerostatic 316, 467  
 hybrid 312  
 hydrodynamic 309, 467, 499  
 hydrostatic 293, 294, 310, 311, 467, 498, 499  
 magnetic 316, 398  
 plain 293  
 rolling 293, 297, 298, 307, 314, 467, 499  
 Control wheels 491  
 Dressers 127–167, 317  
 Cup 141  
 Disk 139, 140  
 Drives and motors, 299–316, 353

Infeeds 325–336  
 Roll 140  
 Rotary 138, 317–325  
 Foundations 288  
 Guideways 290–298  
 Lead-screws 299  
 Requirements 352  
 Sensors See Grinding Process Capability and Monitoring  
 Slideways 290–298  
 Spindles 307, 313, 315, 352, 353, 380, 381, 383, 393,  
 457, 467, 499  
 Tailstock 417, 438  
 Turret 471, 472  
 Wheel-head 307, 313, 315  
 Work-head and work-drives 417, 419  
 Work-rest 439, 481, 493,

## Materials and Properties 257–267

Alloys 13, 263, 352, 368, 374, 426, 458, 513  
 Burrs, 257, 459  
 Ceramics 42, 209, 267–285, 549, 553  
 Deformation  
 Brittle 31, 35, 38, 274, 276  
 Cracks 235, 476  
 Cutting 31, 36, 276, 364  
 Ductile 32, 38, 39, 257–267, 276  
 Elastic 42, 367  
 Plastic 32, 276, 364  
 Ploughing 31, 364  
 Smooth contact 174  
 Rough contact 18, 174, 486  
 Density 458  
 Diffusion 186  
 Ductile 257–267  
 Elastic modulus 18  
 Granite 288  
 Hardness  
 Knoop 188, 262  
 Mohs 271  
 Irons 13, 92, 258, 426, 433, 435, 443  
 Machinability 207, 257  
 Monocrystalline silicon 38  
 Polymer matrix composite 288  
 Steels 13, 92, 259, 260, 389, 426, 433,  
 435, 512  
 Stress  
 Impulse 187, 224  
 Residual 212, 220, 235, 257

## S

### System characteristics 167–185, 484, 528, 529

Compliance(s), stiffness(es) 14, 169, 172, 173, 175, 179,  
 182, 497, 498, 503, 534, 535, 536  
 Damping 71, 172, 175, 180, 182, 287, 498, 535  
 Deflection(s) 175, 185, 464, 500, 521, 528  
 Force(s) 528  
 Machining-elasticity parameter 500, 521  
 Natural frequencies and resonance 169, 170, 176, 524,  
 535, 541  
 Stiffness - See also compliances  
 Roots 176, 177, 528

Transfer functions 529–536  
 Vibration 167, 519, 550  
   Chatter 71, 132, 167, 191, 466, 476, 519, 527  
     Frequency 176, 528, 538, 542  
     Growth rate 178, 528, 533, 535  
     Wheel regenerative 168, 172, 173, 176  
     Work regenerative 168, 172, 176, 519  
   Stability 169, 176, 527  
     Limit 169, 170, 175, 528, 530, 537, 539  
     Parameter 532  
   Forced 71, 167, 168, 528  
   Phase 529, 538  
     In-phase 536  
     Quadrature 536  
   Resonance. See Natural frequencies and resonance.  
   Suppression 167, 178, 180

## T

**Temperature 18–21, 187, 200, 201, 206, 222, 226, 228, 355, 421, 422, 433, 553**

Background 19  
 Boiling 356, 424  
 Chip melting 20, 32, 424  
 Damage 222, 224, 232  
 Finish 422  
 Maximum 422, 424, 425, 426

### Thermal

Conduction 41  
   C-factors 19, 422  
 Convection 19, 422  
   h-factors 20  
 Damage 20, 222, 224, 225, 232, 236, 252, 418, 436, 465, 475, 504  
 Heat flux 41, 222  
 Partition ratio 19, 423  
 Peclet number 423  
 Properties 92, 98  
   Beta ( $\beta$ ) 19, 423, 424  
   Conductivity 19, 423  
   Density 19, 423  
   Diffusivity 419  
   Specific heat capacity 19, 423  
 Stress 38, 118, 208, 212, 349, 557

### Thermocouple 227

**Truing** See Dressing

## U

**Units** See Appendix

## V

**Vibration** See System characteristics

## W

**Wear 90, 96, 105, 185–195, 528, 555**

Abrasive 185  
 Adhesive 185  
 Break-out 189  
 Corrosion 187

Cracks 186, 275  
 Deposition 191  
 Flat 186, 555  
 Fracture 111, 143, 185, 186, 223  
 Micro-fracture 112, 143, 186, 188, 555  
 Rate 174, 212, 456, 528  
 Tribochemical 186

### Wheel 45, 492

Abrasive depth 57  
 Balancing 49–54, 179, 223, 313  
 Bond 103–127  
 Bond life 61, 103, 189, 191, 354, 391  
 Bursting 54–59  
 Clamping 62  
 Compliance/stiffness 73, 169, 174, 175  
 Control and regulating 481, 491, 492  
 Conventional 46, 58, 108  
 Cup 368  
 Damped 72  
 Diamond 271  
 Failure 59  
 Geometric interference 170, 523, 542  
 Glazing 112, 191, 437, 475, 502  
 Grade 9, 109, 116, 438  
 High-speed 45, 54, 64  
 Life 9, 10, 11, 370, 435, 437, 446, 560  
 Loading 463, 476  
 Lubricated 113  
 Metal-bond 122, 126, 272, 279, 398  
 Mounts 53, 61, 64, 68  
 Plated 45–46, 66, 103, 251, 252, 368, 371, 426, 439  
 Porosity 112, 118, 366, 513  
 Reinforced 55–56  
 Resin 118–122, 271, 391, 433  
 Roughness 27  
 Run-out 168, 351, 468  
 Self-dressing  
 Segmented 56, 59, 146, 383  
 Shapes 45  
 Sharpness 185, 463, 557  
 Specification 46, 109, 117, 120  
 Speed 11, 45, 54, 60, 65, 183, 348, 378, 418, 425, 426, 445, 467, 468, 503, 542  
 Speed rating 60  
 Stresses 54  
 Structure 109, 116  
 Stiffness, compliance 169, 174, 175  
 Tolerances 48  
 Topography 24, 25, 28, 130, 189, 192, 217, 224, 229, 231, 241  
 Unbalance 168  
 Vitriified 108–118, 271, 370, 431  
 Wear 111, 104, 185–195, 210, 217, 351, 352, 354, 434, 454, 456, 463, 528, 555

### Work

Feeding and holding 394, 396, 398, 467, 469, 470, 471, 479, 480, 543  
 Speed 11, 19, 168, 183, 425, 430, 435, 459, 468  
 Spinning 494  
 Work-height 480, 482, 483  
 Work-material 13, 14

## **Other Related Titles**

*El-Hofy, Fundamentals of Machining Processes: Conventional and Nonconventional Processes*  
0849372887

*McGeough, Micromachining of Engineering Materials*  
0824706447

*Boothroyd/Knight/Faulkner, Fundamentals of Machining and Machine Tools, Third Edition*  
1574446592

Grinding offers capabilities that range from high-rate material removal to high-precision superfinishing, and has become one of the most widely used industrial machining and surface finishing operations. Reflecting modern developments in the science and practice of modern grinding processes, the **Handbook of Machining with Grinding Wheels** presents a broad range of abrasive machining technologies with a focus on the fundamental concepts and practical applications.

Written by an international team of experts unrivalled in their experience and standing in the field, this comprehensive reference takes a unified approach to abrasive machining that emphasizes the underlying physical principles and how this knowledge can best be applied to solving new grinding problems. Coverage is split neatly into two main sections, with the first dedicated to basic concepts such as grinding parameters, removal mechanisms, abrasive characteristics, and economic efficiency. The remainder of the book addresses applications, including grinding of ductile and brittle materials, grinding machines, and surface, cylindrical, internal, centerless, and ultrasonic-assisted grinding.

*Tracing the changing role of modern industrial grinding, this book...*

- Presents a comprehensive and detailed survey of conventional and cutting-edge grinding technologies
- Builds a strong understanding of the physical processes underlying various grinding operations
- Combines the expertise and experience of renowned experts from Germany, Japan, the United Kingdom, and the United States
- Supplies numerous diagrams and photographs to illustrate the concepts
- Includes a glossary of terms and an appendix on units and conversions

Reflecting the diverse research and industrial experience of the authors, the **Handbook of Machining with Grinding Wheels** combines theoretical and practical information into an authoritative and convenient reference source. It will help deepen knowledge and sharpen problem-solving skills applied to practically any industrial grinding challenge.



**CRC Press**

Taylor & Francis Group  
an informa business

[www.taylorandfrancisgroup.com](http://www.taylorandfrancisgroup.com)

6000 Broken Sound Parkway, NW  
Suite 300, Boca Raton, FL 33487  
270 Madison Avenue  
New York, NY 10016  
2 Park Square, Milton Park  
Abingdon, Oxon OX14 4RN, UK

DK4115

ISBN 1-57444-671-1

